CONF-961107-- Abstr.

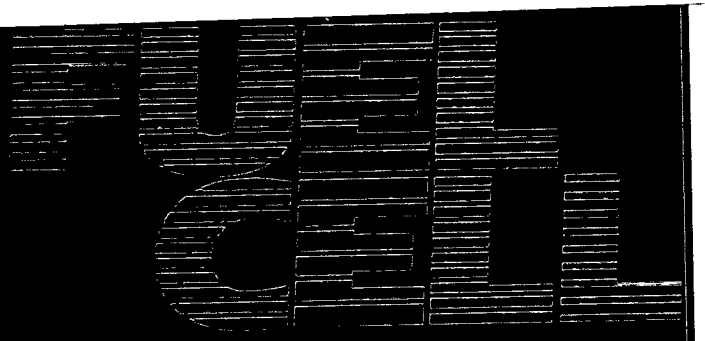

Program and Abstracts

November 17 - 20, 1996
Orlando, Florida

In Cooperation with

UNITED STATES
U. S. Department of Energy
Defense Advanced Research Projects Agency
Electric Power Research Institute
Federal Transit Administration
Gas Research Institute
National Aeronautics and Space Administration
U. S. Army Corps of Engineers

JAPAN
Fuel Cell Development Information Center
New Energy and Industrial Technology Development Organization

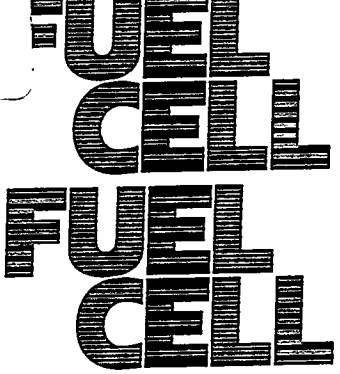

1996 Fuel Cell Seminar

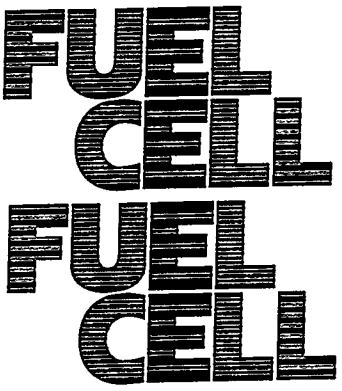

Sponsored by the Fuel Cell Seminar Organizing Committee

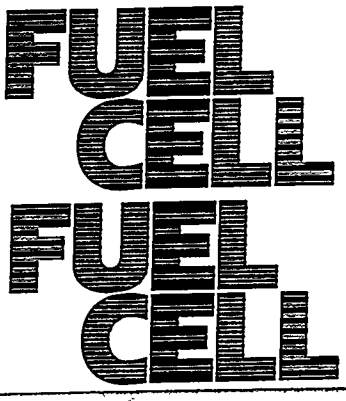

210 items

FUEL CELL

Program and Abstracts

1996 Fuel Cell Seminar

November 17 — 20, 1996
Orlando, Florida

Seminar Coordinated by:
COURTESY ASSOCIATES, INC.
Washington, D.C.

PREFACE

The members of the Fuel Cell Seminar Organizing Committee welcome you to the 1996 Fuel Cell Seminar.

This year's meeting highlights the fact that fuel cells for both stationary and transportation applications have reached "The Dawn of Commercialization". Sales of stationary fuel cells have experienced steady growth over the past two years. Phosphoric acid fuel cell (PAFC) buses have been demonstrated in a number of urban areas. Proton-exchange membrane (PEM) fuel cells are on the verge of revolutionizing the transportation industry, as demonstrated by Ballard's PEMFC buses, the Daimler-Benz NECAR II, the Energy Partners' Gator, and the frenzy of activity in the U.S., Europe, and Japan on development of fuel cell vehicles. These activities and many more will be discussed during the three-day seminar.

This seminar will provide a forum for the exchange of information among people from the international fuel cell community who are engaged in a wide spectrum of fuel cell activities. Discussions addressing research and development of fuel cell technologies, manufacturing and marketing of fuel cells, and experiences of fuel cell users will take place through oral and poster presentations. For the first time, the seminar will include commercial exhibits, further evidence that commercial fuel cell technology has arrived. The Fuel Cell Seminar Organizing Committee invites professionals worldwide, who are concerned about energy and environmental issues, to join the international fuel cell community in welcoming the dawn of fuel cell commercialization at the 1996 Fuel Cell Seminar.

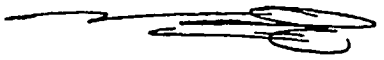

Pandit Patil, Chairman
1996 Fuel Cell Seminar
Organizing Committee

ACKNOWLEDGEMENTS

The organizers of the 1996 Fuel Cell Seminar express their gratitude for the generous support received from the following organizations:

Ballard Power Systems, Inc.
9000 Glenlyon Parkway
Burnaby, British Columbia
CANADA V5J 5J9

Delphi Energy and Engine Management Systems
World Headquarters
P.O. Box 1360
Flint, Michigan 48501-1360

E. I. du Pont de Nemours & Company
Experimental Station
Wilmington, Delaware 19898

Energy Research Corporation
Fuel Cell Engineering
Fuel Cell Manufacturing Corporation
3 Great Pasture Road
Danbury, CT 06813

Ford Motor Company
P.O. Box 2053
Dearborn, MI 48121

Fuji Electric Company
1-12-1 Yurakucho Chiyoda-ku
Tokyo 100 JAPAN

Hitachi, Ltd.
Power Group
4-6 Kanda Surugadai, Chiyoda-ku
Tokyo 101 JAPAN

IHI
Fuel Cell Project Department
3-1-15 Toyuso, Koto-ku
Tokyo 135 JAPAN

International Fuel Cells
ONSI Corporation
195 Governor's Highway
PO BOX 1148
South Windsor, CT 06074

M-C Power Corporation
8040 South Madison Street
Burr Ridge, IL 60521-5808

Mitsubishi Electric Corporation
Energy Technology Department
Tsukaguchi-Honmachi 8-1-1 Amagasaki
Hyogo, 661 JAPAN

Sanyo Electric Company, Ltd.
1-1 Dainochi Higashi-machi
Moriguchi, Osaka 570 JAPAN

Toshiba Corporation
Fuel Cell System Division
1-1-6 Uchisaiwai-cho, Chiyoda-ku
Tokyo 100 JAPAN

ALPHABETICAL EXHIBITOR LISTING

American Methanol Institute
800 Connecticut Ave., NW #620
Washington, DC 20006
202-467-5050
FAX 202-331-9055
The American Methanol Institute Works to Encourage the Development of Methanol Fuel Cell Technologies
Booth # 2

ElectroChem, Inc.
400 W. Cummings Park
Woburn, MA 01801
617-938-5300
FAX 617-935-6966
Fuel Cell Power Source and Accessories
Booth # 16

Electric Power Research Institute
3412 Hillview Ave.
PO BOX 10412
Palo Alto, CA 94303
415-855-2521
FAX 415-855-8501
The Electric Power Research Institute — Products and Services
Booth # 18 & 19

Emprise Corporation
830 Franklin Court
Marietta, Georgia 30067-8939
770-425-1420
FAX 770-425-1425
Various Fuel Cell and Hybrid Vehicle Test Facilities
Booth # 9

Energy Partners, Inc.
1501 Northpoint Parkway, Suite 102
West Palm Beach, FL 33407
407-688-0500
FAX 407-688-9610
PEM Fuel Cell Power Systems & PEM Fuel Cell Powered Vehicles
Booths # 11 & 12

Energy Research Corporation
1634 Eye Street, N.W., Suite 900
Washington, DC 20006
202-737-3232
FAX 202-737-7337
2.8 MW DFC Power Plant (Model) and ERC R&D items
Booth # 10

ETSU
Harwell,Oxfordshire OXll ORA
UNITED KINGDOM
44-1235-433510
FAX 44 1235 432817
The United Kingdom Department of Trade and Industry Advanced Fuel Cells Programme
Booth # 8

W. L. Gore & Associates, Inc.
PO Box 1100
Elkton, MD 21922
410-392-3300
FAX 410-398-6624
GORE-TEX Expanded PTFE Products; GORE-CARBEL Carbon Composite Electrodes; GORE-SELECT Fluoroionomer Composite Products
Booth # 1

ALPHABETICAL EXHIBITOR LISTING

Lynntech, Inc.
7610 Eastmark Drive, Suite 105
College Station, TX 77840
409-693-0017
FAX 409-764-7479
Fuel Cell Test System, Model 2110
Booth # 6

M-C Power Corporation
8040 South Madison Street
Burr Ridge, IL 60521
630-986-8040
FAX 630-986-8153
Molten Carbonate Fuel Cell Power Plants
Booth #15

ONSI Corporation
195 Governors Highway
South Windsor, CT 06074
203-727-2348
FAX 203-727-2216
200 Kilowatt Fuel Cell Power Plant
Booth # 14

Praxair, Inc.
16130 Woodinville-Redmond Road # 7
Woodinville, WA 98072
206-487-1769
FAX 206-487-1859
Multi-Component Ceramic Oxide SOFC Powders — Electrolyte: Yttria-Stabilized Zirconia & Cerium Gadolinium Oxide; Anode: Nickel/Yttria-Stabilized Zirconia; Cathode: Doped Lanthanum Manganite and Cobalt; Interconnect: Doped Lanthanum Chromite
Booth # 13

Scribner Associates, Inc.
1415 West Leigh Drive
Charlottesville, VA 22901
804-977-5521
FAX 804-977-5546
Fuel Cell Loads and Test Systems
Booth # 7

SOFCo
1562 Beeson Street
Alliance, Ohio 44601
330-829-7822
FAX 330-829-7293
Planar Solid Oxide Fuel Cell Technology. Liquid Hydrocarbon Fuel Reforming Technology.
Booth # 5

US Department of Energy
PO Box 880
Morgantown, WV 26507
304-285-4747
FAX 304-285-4469
Morgantown Energy Technology Center's Fuel Cells Display
Booth # 20 & 21

Westinghouse Electric Corporation
Science & Technology Center
1310 Beulah Road
Pittsburgh, PA 15235
412-256-2022
FAX 412-256-2002
Tubular SOFC Bundles
Booths # 3 & 4

PROGRAM AND TABLE OF CONTENTS

SUNDAY, NOVEMBER 17, 1996

3:00 pm- 6:00 pm	Registration	*Tamiami Lounge* *Convention Center*
3:00 pm- 5:00 pm	Presenters Practice Room Open	*Ft. Lauderdale Room* *Convention Center*
3:00 pm- 5:00 pm	Guest Hospitality Room Open	*Key Largo Room* *Convention Center*
5:00 pm- 7:00 pm	Welcoming Reception	*Exhibit Hall*

MONDAY, NOVEMBER 18, 1996

7:30 am- 8:30 am	Presenters Breakfast (Monday Presenters only)	*St. Petersburg/Sarasota Rooms* *Convention Center*
7:30 am- 5:30 pm	Presenters Practice Room Open	*Ft. Lauderdale Room*
7:30 am- 5:00 pm	Registration	*Tamiami Lounge*
7:30 am- 9:00 am	Continental Breakfast	*Tamiami Louge*
8:00 am- 5:00 pm	Guest Hospitality Room Open	*Key Largo Room*
9:00 am- 12:00 Noon	SESSION I	*Cypress Ballroom* *Convention Center*
9:00 am- 9:15 am	Opening Remarks Chair: Dr. Pandit Patil U.S. Department of Energy Office of Advanced Automotive Technologies	
9:15 am- 10:00 am	Keynote Address **Fuel Cell Technology Commercialization Challenges** The Honorable Mary L. Good Under Secretary for Technology U.S. Department of Commerce	
10:00 am- 10:15 am	Refreshment Break	*Tamiami Lounge*

MONDAY, NOVEMBER 18, 1996

10:15 am- **10:50 am**	**Fuel Cells for Automotive Applications** Byron McCormick Managing Director Delco Propulsion Systems	*
10:50 am- **11:25 am**	**Stationary Power Fuel Cell Commercialization Status Worldwide** Mark Williams Product Manager, Fuel Cells U.S. Department of Energy-METC	1
11:25 am- **12:00 Noon**	**Commercial Aspects of Fuel Cells** William E. Cratty Sales Director, Fuel Cells Equitable Resources, Inc.	*
12:00 Noon- **1:00 pm**	**Luncheon**	*Florida Hall* *Exhibit Hall*
	SESSION II-A	
1:15 pm- **4:20 pm**	**POWER PLANT APPLICATIONS** **& DEMONSTRATIONS I** Chair: Mark Williams USDOE/METC Co-Chair: Kazuhiko Takasu NEDO	*Casselberry/Orlando Hall* *Convention Center*
1:15 pm- **1:25 pm**	**Opening Remarks**	
1:25 pm- **1:45 pm**	**Activities Dedicated to FCPP Commercialization at Toshiba** S. Ikeda, J. Ozono and N. Sato, Toshiba Corporation, Tokyo, JAPAN	4
1:45 pm- **2:05 pm**	**Construction and Start-Up of a 250 kW Natural Gas Fired MCFC Demonstration Power Plant** R. Figueroa, San Diego Gas & Electric, San Diego, CA, J. Carter, J. Otahal and R. Rivera, San Diego Gas & Electric, San Diego, CA, J. Scroppo, R. Laurens, M-C Power Corporation, Burr Ridge, IL,	8
2:05 pm- **2:25 pm**	**1000kW On-Site PAFC Power Plant Development and Demonstration** T. Satomi and S. Koike, Phosphoric Acid Fuel Cell Technology Research Association (PAFC-TRA), Osaka, JAPAN and R. Ishikawa, New Energy and Industrial Technology Development Organization (NEDO), Tokyo, JAPAN	12
2:25 pm- **2:45 pm**	**Questions and Answers**	

*Abstract not available at time of publication.

MONDAY, NOVEMBER 18, 1996

MONDAY, NOVEMBER 18, 1996

MONDAY, NOVEMBER 18, 1996

MONDAY, NOVEMBER 18, 1996

MONDAY, NOVEMBER 18, 1996

MONDAY, NOVEMBER 18, 1996

POSTER P1C — Manufacturing and Operating Experience

POSTERS P1D — PAFC R&D

MONDAY, NOVEMBER 18, 1996

5:30 pm-7:30 pm	**Exhibits Open (Posters Remain Open Until 6:30 pm)**	*Exhibit Hall*
7:30 pm-9:30 pm	**Manufacturers Reception**	*Poolside 2 Hibiscus Court*

TUESDAY, NOVEMBER 19, 1996

7:30 am-8:30 am	**Presenters Breakfast** (Tuesday Presenters only)	*St. Petersburg/Sarasota Rooms*
7:30 am-5:30 pm	**Presenters Practice Room Open**	*Ft. Lauderdale Room*
8:00 am-5:00 pm	**Registration**	*Tamiami Lounge*
8:00 am-9:00 am	**Continental Breakfast**	*Tamiami Lounge*
8:00 am-5:00 pm	**Guest Hospitality Room Open**	*Key Largo Room*
	SESSION III-A	
9:00 am-12:05 pm	**TRANSPORTATION APPLICATIONS I** Chair: Jon Leonard SCAQM Co-Chair: Mark Hoberecht NASA	*Casselberry/Orlando Hall*
9:00 am-9:10 am	**Opening Remarks**	

TUESDAY, NOVEMBER 19, 1996

TUESDAY, NOVEMBER 19, 1996

*Abstract not available at time of publication.

TUESDAY, NOVEMBER 19, 1996

*Abstract not available at time of publication.

TUESDAY, NOVEMBER 19, 1996

TUESDAY, NOVEMBER 19, 1996

TUESDAY, NOVEMBER 19, 1996

*Abstract not available at time of publication.

TUESDAY, NOVEMBER 19, 1996

SESSION IV-A

2:15 pm-5:20 pm **MARKET DEVELOPMENT** *Casselberry/Orlando Hall*

Chair:
John O'Sullivan
EPRI

Co-Chair:
Masahiro Watanabe
Yamanashi University

TUESDAY, NOVEMBER 19, 1996

TUESDAY, NOVEMBER 19, 1996

5:00 pm- 5:20 pm	**Questions and Answers**	
5:30 pm- 8:30 pm	**Reception and Exhibition**	*Exhibit Hall*

WEDNESDAY, NOVEMBER 20, 1996

7:30 am- 8:30 am	**Presenters Breakfast** (Wednesday Presenters only)	*St. Petersburg/Sarasota Room*
7:30 am- 5:30 pm	**Presenters Practice Room Open**	*Ft. Lauderdale Room*
8:00 am- 5:00 pm	**Registration**	*Tamiami Lounge*
8:00 am- 9:00 am	**Continental Breakfast**	*Tamiami Lounge*
8:00 am- 5:00 pm	**Guest Hospitality Room Open**	*Key Largo Room*
	SESSION V-A	
9:00 am- 12:05 pm	**MANUFACTURING & OPERATING EXPERIENCE** Chair: Dan Rastler EPRI Co-Chair: Patrick Davis USDOE	*Casselberry/Orlando Hall*
9:00 am- 9:10 am	**Opening Remarks**	
9:10 am- 9:30 am	**PC25™ Product and Manufacturing Experience** E. Hall, W. Riley, and G. Sandelli, ONSI Corporation, South Windsor, CT and E. Hall, International Fuel Cells Corporation, South Windsor, CT	529
9:30 am- 9:50 am	**Status of MCFC Stack Development at Hitachi** S. Takashima, T. Kahara, M. Takeuchi, Y. Amano and T. Yoshida, Hitachi, Ltd., Ibaraki, JAPAN	532
9:50 am- 10:10 am	**Balance of Plant for SOFC Experiences with the Planning, Engineering, Construction and Testing of a 10 kW Planar SOFC Pilot Plan** K. Klov, Statoil Research Centre, Trondheim, NORWAY, P. Sundal, T. Monsen and A. Vik, Prototech as, Fantoft, NORWAY	536

WEDNESDAY, NOVEMBER 20, 1996

SESSION V-B

9:00 am- 12:05 pm	**TRANSPORTATION APPLICATIONS II** Chair: Steve Chalk USDOE Co-Chair: Shang Hsiung FTA	*Kissimmee/St. Cloud Hall*

WEDNESDAY, NOVEMBER 20, 1996

WEDNESDAY, NOVEMBER 20, 1996

WEDNESDAY, NOVEMBER 20, 1996

WEDNESDAY, NOVEMBER 20, 1996

*Abstract not available at time of publication.

WEDNESDAY, NOVEMBER 20, 1996

SESSION VI-A

2:15 pm-5:20 pm **FUEL CELLS - THE FUTURE** *Casselberry/Orlando Hall*
Chair:
Marvin Warshay
NASA

Co-Chair:
Diane Hooie
USDOE

2:15 pm-2:25 pm **Opening Remarks**

2:25 pm-2:45 pm **Lightweight Pressure Vessels and Unitized Regenerative Fuel Cells** 743
F. Mitlitsky, B. Myers and A. Weisberg, Lawrence Livermore National Laboratory, Livermore, CA

2:45 pm-3:05 pm **Hydrogen Fuel Cells in Chemical Industry: The Assemini Project** 747
G. Caserza, T. Bozzoni, Ansaldo CLC s.r.l., Genova, ITALY, G. Porcino and A. Pasquinucci, Enichem s.p.a., Milano, ITALY

3:05 pm-3:25 pm **The Low-Temperature Partial-Oxidation Reforming of Fuels for Transportation Fuel Cell Systems** 750
R. Kumar, S. Ahmed and M. Krumpelt, Argonne National Laboratory, Argonne, IL

3:25 pm-3:45 pm **Questions and Answers**

3:45 pm-4:00 pm **Break** *Tamiami Lounge*

WEDNESDAY, NOVEMBER 20, 1996

SESSION VI-B

2:15 pm- 5:20 pm	**POWER PLANT APPLICATIONS & DEMONSTRATIONS II** Chair: Mike Binder U.S. Army Corps of Engineers Co-Chair: Bill Taylor U.S. Army Construction Engineering Research	*Kissimmee/St. Cloud Hall*

WEDNESDAY, NOVEMBER 20, 1996

STATIONARY POWER FUEL CELL COMMERCIALIZATION STATUS WORLDWIDE

Dr. Mark C. Williams
Fuel Cells Product Manager
U.S. Department of Energy
Morgantown Energy Technology Center
Morgantown, West Virginia USA

Abstract

Fuel cell technologies for stationary power are set to play a role in power generation applications worldwide. The worldwide fuel cell vision is to provide powerplants for the emerging distributed generation and on-site markets. Progress towards commercialization has occurred in all fuel cell development areas. Around 100 ONSI phosphoric acid fuel cell (PAFC) units have been sold, with significant foreign sales in Europe and Japan. Fuji has apparently overcome its PAFC decay problems. Industry-driven molten carbonate fuel cell (MCFC) programs in Japan and the U.S. are conducting megawatt (MW)-class demonstrations, which are bringing the MCFC to the verge of commercialization. Westinghouse Electric, the acknowledged world leader in tubular solid oxide fuel cell (SOFC) technology, continues to set performance records and has completed construction of a 4-MW/year manufacturing facility in the U.S. Fuel cells have also taken a major step forward with the conceptual development of ultra-high efficiency fuel cell/gas turbine plants. Many SOFC developers in Japan, Europe, and North America continue to make significant advances.

Introduction

Fuel cell technologies for stationary power are set to play a significant role in power generation applications worldwide. The worldwide fuel cell vision is to provide powerplants (<20 MW) for the emerging distributed generation and on-site markets. Fuel cells have also taken a major step forward with the conceptual development of larger, advanced, ultra-high efficiency fuel cell/gas turbine plants (50-100 MW) for industrial and traditional customers. These remarkable fuel cell/gas turbine plants promise in excess of 70 percent efficiency. Fuel cells are under consideration for use in many distributed power applications. Fuel cells address important technical and environmental customer needs, such as: (a) Low emissions, (b) premium power quality and uninterruptable power supply applications, (c) efficiency (even in small sizes and part-load), (d) low noise, (e) high-quality by-product heat, (f) modularity, (g) unmanned operation, (h) fuel flexibility, and (i) the highest possible reliability. Progress towards commercialization has occurred in all fuel cell development areas. In the U.S., Japan, and Europe, the programs continue to receive the support of governments, industry, and institutes, and work is carried out at industrial locations, manufacturer sites, and at supporting laboratories and universities.

PAFC Status

In the U.S., the Department of Defense/Department of Energy Climate Change Fuel Cell Program has resulted in both national and international awards. Eighteen U.S. projects and 19 foreign projects have been selected. Additional awards under the program are expected in 1997. Around 100 ONSI PAFC units have been sold, with significant foreign sales in Europe and Japan. In Japan, Osaka Gas and Tokyo Gas are

continuing to demonstrate and test a significant number of fuel cells. Osaka Gas, alone, has tested 49 fuel cell units, totaling 6800 kilowatts (kW's). Osaka Gas has indicated that the ONSI units it has tested have experienced less than 10 percent degradation in 40,000 hours.

Fuji, Toshiba, and Mitsubishi are continuing development in Japan, and some of their fuel cells are being evaluated in Japan and Europe. The 5-MW PAFC test at Amagasaki is expected to be completed by 1997. According to Osaka Gas, Fuji has apparently overcome its PAFC decay problems.

MCFC Status

Industry-driven MCFC programs in Japan and the U.S. are conducting MW-class demonstrations, which are bringing the MCFC to the verge of commercialization. In the U.S., Energy Research Corporation attained 2 MW's at its demonstration in Santa Clara, California. M-C Power plans startup of a 250-kW demonstration at the Miramar Naval Air Station in San Diego, California, by December 1996. Two manufacturing capabilities of 2-17 MW/year have been established in the U.S. The stated objective of the U.S. MCFC Program is to develop a packaged, commercializable MCFC product and to bring a multifueled, integrated, simple, low-cost, modular, market-responsive MCFC powerplant to the marketplace.

In Japan, IHI, Toshiba, Mitsubishi, Hitachi, and Sanyo are continuing MCFC development. Some developers have completed 100-kW tests and are now working on issues in 20-40-kW stacks through the Ministry of International Trade and Industry and the New Energy and Industrial Technology Development Organization. In 1998, Hitachi and IHI will be testing a combined 1-MW pressurized, external reforming MCFC plant near Osaka. Mitsubishi is planning a 300-kW demonstration in the near future. In Europe, ECN and Ansaldo are continuing stack development and testing in MCFC.

SOFC Status

Many SOFC developers in Japan, Europe, and the U.S. continue to make significant advances. In the U.S., in the tubular SOFC area, Westinghouse, working with Ontario-Hydro, has tested an SOFC at 15 atmospheres pressure. In addition, Westinghouse will begin testing of a 100-kW SOFC plant in the Netherlands in 1997. Westinghouse continues to set performance records and has completed a 4 MW/year manufacturing facility in the U.S.

In the U.S., SOFC planar development continues at ZTEK, Allied-Signal, SOFCO, and TMI. ZTEK completed several thousand hours testing on a 1-kW planar SOFC design. SOFC power density feasibilities of 2.0 watts per square centimeter appear feasible. Emphasis in SOFC planar remains on solving design issues and establishing performance.

In Europe and Japan, development continues on both tubular and planar designs at many locations by many developers. MHI, one leading Japanese developer, is working on both tubular and planar designs. MHI should complete 10-kW tubular and 5-kW planar tests in 1996. Siemans plans to complete a 20-kW test in 1996 and a 100-kW test by 1998.

Fuel cells have also taken a major step forward with the conceptual development of larger, advanced, ultra-high efficiency fuel cell/gas turbine plants for industrial and traditional customers. Westinghouse, ZTEK, and others are working to integrate the fuel cell and gas turbine into an ultra-high efficiency powerplant. The SOFC appears to be particularly integratable with the gas turbine.

ACTIVITIES DEDICATED TO FCPP COMMERCIALIZATION AT TOSHIBA

Shin-ichi Ikeda, Jiro Ozono, and Nobuaki Sato
Fuel Cell Systems Division
Toshiba Corporation
1-6 Uchisaiwai-cho, Chiyoda-ku, Tokyo 100, Japan

1. INTRODUCTION

The present line-up of fuel cell power plants (FCPPs) at Toshiba consists of 11MW FCPP for pressurized operation, 1000kW on-site FCPP and 200kW on-site FCPP. In these, an 11MW FCPP installed at Goi Power Station of Tokyo Electric Power Company (TEPCO) is providing valuable experience through more than 20,000 cumulative hours of operation. Also, a 1000kW on-site FCPP, which Toshiba manufactured under the joint program of NEDO and PAFC Technology Research Association, has cumulative operation of 7,500 hours.

Toshiba, however, believes that the 200kW on-site FCPP is the leader in the commercialization of phosphoric acid FCPP. This paper therefore presents the development status of 200kW power plants and our strategic considerations for full commercialization of PC25 type 200kW FCPP.

2. DEVELOPMENT OF 200kW PC25 FCPP

In 1990, IFC (a subsidiary of UTC in which Toshiba has significant interest) and Toshiba formed ONSI as a subsidiary of IFC, which focuses on on-site power plants. Toshiba has since performed E&D and business activities under strong cooperation with IFC/ONSI. As the first step, Toshiba cooperated closely with IFC/ONSI in developing ONSI's 200kW PC25™A FCPP. Toshiba shared in the development and manufacturing of the reformers and electrical system assemblies for PC25 model A units.

Now, a total of 104 units of 200kW PC25 FCPP delivered by ONSI or Toshiba are showing excellent average operating availability of 95%. Most of the plants are showing stable characteristics in cell voltage, as shown in Figure 1. Three units have cumulative operating time exceeding 30,000 hours, and 29 units have exceeded 20,000 hours. Continuous generation in excess of 6 months has been achieved in 29 cases. In April, 1996, the PC25 fleet has accumulated one million hours of service world wide.

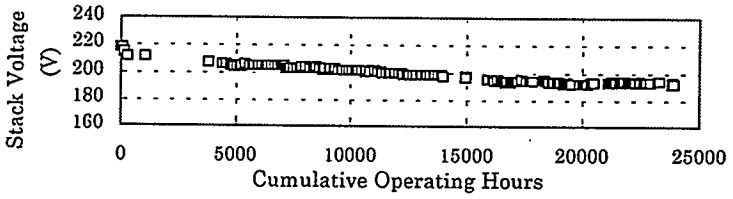

Figure 1. Typical cell voltage change at a PC25A

Succeeding the PC25 A and its modified PC25 B, the most advanced design, PC25 model C (Figure 2), has been developed as a commercial product, and the first production unit was shipped in November, 1995.

Major features of PC25 C are as follows:

- Maintaining the excellent baseline power plant design and characteristics of the preceding model, PC25 A
- Remarkable reduction of size, weight and cost
- Improvement of plant installability and maintainability

The specification for the 200kW PC25 C is shown in Table 1. The 22 units of PC25 C have been shipped to many destinations in U.S., Japan and Korea ; these are now being placed in service. Initial operation has shown good performance. Seven units have been shipped to Japan for Tokyo Gas Company, Osaka Gas Company and Toshiba's factory. A PC25 C at the Torishima site of Osaka Gas, which was the first PC25 C production unit has cumulative operating time more than 2,000 hours. For reference, a prototype PC25 C unit which is installed at the IFC/ONSI plant has recorded cumulative operation time more than 10,000 hours as of the end of August, 1996.

Table 1. Specification of PC25 C

Net AC Efficiency [%LHV]		40
Heat Efficiency [%LHV]		41
Volume	Width [m]	5.5
	Depth [m]	3.0
	Height [m]	3.0
Foot Print [m2/kW]		0.08
Package Weight [ton]		18.2

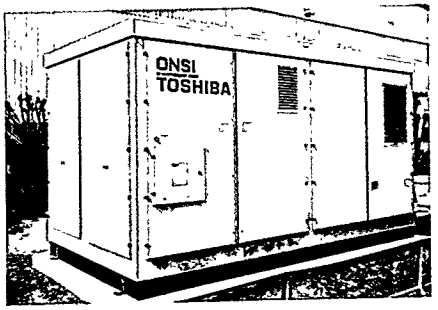

Figure 2. PC25 C 200kW FCPP

3. PROMOTION TO COMMERCIALIZATION

Fuel cell customers demand reliable and high quality energy output at a competitive price. To meet this demand, Toshiba will focus on the three factors ; product reliability, cost reduction, and maintenance and servicing.

(1) Product Reliability

We believe that Toshiba, IFC and ONSI have established the reliable technologies necessary for manufacturing the 200kW on-site FCPP as a commercial product.

As mentioned above, PC25 FCPPs installed at various locations in the world so far are establishing excellent operating records. In addition to the experience from field operation, Toshiba has focused on verifying the stability of cell characteristics during long term operation, since we recognize the customer's concern with durability of cell performance over a cell life of 40,000 hours. For example, Toshiba has performed several teardown inspections and examinations to evaluate the integrity of cell stack assembly observing the interim state of the CSA components which had been operated for an extended period. Key factors affecting cell life, such as carbon corrosion, loss of electrolyte and catalyst sintering, have been evaluated. To date there have been no indications of wear out or life limitation.

This knowledge has strengthened our confidence that long term cell stability will be achieved.

(2) Cost Reduction

While the production cost of PC25 C has been reduced by about 50% in comparison with the preceding model, further cost reduction of FCPP is required for market expansion in the future. Since the reliability of PC25 FCPP is being proven, we believe that cost reduction is the most important factor to be pursued. Cost reduction of FCPP will be accomplished in two ways ; technical innovation and increase of production rate (mass-production effect).

With regard to technical innovation for cost reduction, Toshiba and IFC/ONSI will continue to perform joint activities focusing on cell stack, reformer and inverter, as well as ancillary system improvements.

In order to strongly pursue the mass-production effect, Toshiba and IFC/ONSI have strategically agreed that manufacturing of all PC25 FCPPs contracted by Toshiba or IFC/ONSI with customers should be concentrated into IFC/ONSI. This enables IFC/ONSI to make mass-procurement of materials/components from outside venders and also improve productivity at IFC/ONSI's factory, contributing to cost reduction.

The above strategy is based on the strong cooperation between Toshiba and IFC/ONSI. That is, with respect to sales by Toshiba, these parties will act as one body and IFC/ONSI's factory functions as if a part of Toshiba's, while Toshiba will take the full responsibility to its customers for all aspects of transportation, supervision of installation / trial operation, service and warrantee for any FCPPs to be contracted by Toshiba. In order to smoothly perform the above formation, Toshiba has assigned engineers to work at IFC/ONSI, and a Toshiba manager is acting as a vice president of IFC.

(3) Maintenance and Servicing

Toshiba is making efforts to provide the maintenance support system required to achieve customer satisfaciton. In the spring of 1996, Toshiba established a local service center in the Osaka area to promptly make a diagnosis of problems using a Remote Diagnostic Terminal (RDT). Also, Toshiba will open a training school so that customers can gain practical experience in the operation and maintenance of FCPP and learn troubleshooting.

4. DEVELOPMENT OF VARIOUS APPLICATIONS

To expand the market with making full use of advantages and flexibility of FCPP, Toshiba is developing various kind of applications for on-site power plant. Some examples are presented as follows :

(1)Direct Current Supply System :
A part of DC power from the cell stack can be supplied to DC loads directly or through DC/DC converter.

This system will be attractive for the site where both of AC and DC power sources are required such as chemical process facility, water purifying plant, and DC power source for electronics applications.

(2)Application to Various Fuel Sources :
While natural gas is a prime fuel for FCPP, it can be operated using various fuel sources, such as LPG, kerosene and naphtha. Digester gas which is generated at sewage disposal plants is another alternative fuel source. (See Figure 3)

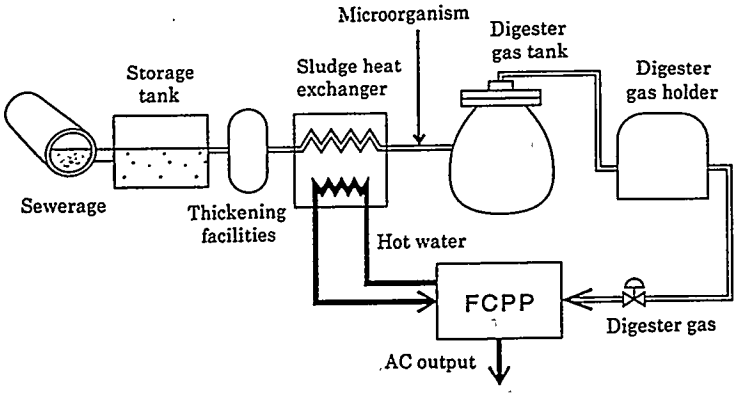

Figure 3. Schematic of Digester Gas Utilization

(3)Application as UPS Function :
FCPP can be a premium power source in place of conventional UPS (Uninterruptible Power Supply) to supply lower cost power with high quality and reliability to any important loads such as computer facilities.

(4)Steam Supply System :
FCPP can supply heat in the form of steam in 170℃, which is generally utilized as an energy source of absorption chiller to produce cold water for air conditioning or as heat source to boiler feed water.

5. SUMMARY

The operating record of the PC25 C fleet continues to show the superior characteristics of the PAFC FCPP and operating times have increased significantly since the last fuel cell seminar. Introduction of the PC25 C demonstrates the continued improvement of this product characteristics.

The potential world wide market for FCPPs is very large and a variety of applications are possible. In cooperation with IFC/ONSI, Toshiba will aggressively pursue the activities required to provide high quality and cost competitive PAFC power plants to the market in Japan and other Asian countries, so that the PC25 FCPP will be widely recognized as an efficient and premium power source with benign emission profile.

CONSTRUCTION AND START-UP OF A 250 KW NATURAL GAS FUELED MCFC DEMONSTRATION POWER PLANT

R. A. Figueroa, J. Carter, R. Rivera, and J. Otahal
San Diego Gas & Electric
San Diego California

J. A. Scroppo and R. M. Laurens
M-C Power Corporation
Burr Ridge, Illinois

San Diego Gas & Electric (SDG&E) is participating with M-C Power in the development and commercialization program of their internally manifolded heat exchanger (IMHEX®) carbonate fuel cell technology. Development of the IMHEX technology base on the UNOCAL test facility resulted in the demonstration of a 250 kW thermally integrated power plant located at the Naval Air Station at Miramar, California.

The members of the commercialization team lead by M-C Power (MCP) include Bechtel Corporation, Stewart & Stevenson Services, Inc., and Ishikawajima-Harima Heavy Industries (IHI). MCP produced the fuel cell stack, Bechtel was responsible for the process engineering including the control system, Stewart & Stevenson was responsible for packaging the process equipment in a skid (pumps, desulfurizer, gas heater, turbo, heat exchanger and steam generator), IHI produced a compact flat plate catalytic reformer operating on natural gas, and SDG&E assumed responsibility for plant construction, start-up and operation of the plant.

The focus of this paper is the participation of a utility, a prospective customer of the product, with the technology developer in coordinating the construction and start-up of the thermally integrated demonstration power plant at a NAS Miramar. We wish to acknowledge the cooperation and assistance of LtCdr. R. Fahey and Mr. J. Gray of NAS Miramar Staff Civil Engineering, Capt. Corbett and Mr. J. Thomas of Public Works Center, and the Commanding Officer of the NAS Miramar Base, Capt. Rollins for their support in making this project a reality.

Construction of a demonstration / proof of concept plant requires the usual coordination between designers, engineers, and technologists. These plants are usually expected to be constructed in university campuses, research institutes, or in a designated host site at utilities. When a proof of concept project is installed at an end user site, project coordination becomes more complex and expectations for success are elevated beyond that of a test. SDG&E took on the role of coordinating the host site activity with the construction and start-up of this project.

SDG&E's participation was primarily to gain experience with a new technology product and to provide utility experience in the start-up process. The thermally integrated power plant at Miramar is a proof of concept, also referred to as the product development test (PDT,) of the IMHEX technology. This is the forerunner of a commercial design for the market entry product by M-C Power by the year 2000.

Demonstration Plant Description and Location:

The PDT plant is located within the NAS Miramar base nearly 15 miles north-east of down town San Diego. The plant includes an improved design of the fuel cell stack, a pressurized process system using the thermal energy to improve cycle efficiency, a skid mounted package with the balance of plant, and an innovative flat plate natural gas reformer by IHI. The plant is contained in a 40 by 80 square foot area and it consists of three main parts: the fuel processor (reformer), the balance of plant (BOP) skid, and the fuel cell stack. Auxiliary equipment includes a nitrogen

gas storage tank and vaporizer, air compressor, and boiler feed water make-up system, which are separate from the BOP skid. It is anticipated that in a commercial plant, the auxiliary equipment will be part of the BOP skid or eliminated. The electrical equipment and control system is within a control room and electrical room, which would be reduced to cabinet size equipment in a commercial product.

Objectives:

The objectives of the PDT test are:

- Determine plant component performance
- Prove that the BOP can be constructed using proven commercial equipment
- Applicability of the product simulating a distributed generation system at an end user site.
- Demonstrate the practicality of building, operating and maintaining power plants with non-specialized work force, which is not the normal operating procedure for an electric utility.

Coordination and Planning:

Construction of the 250 kW PDT plant was an integrated process between six different entities: M-C Power, Bechtel Engineering, Stewart & Stevenson, IHI, The U.S. Navy, and SDG&E. Each group had individual responsibilities, MCP to deliver the fuel cell, Bechtel to deliver process design and construction packages for the mechanical, instrumentation, and electrical contracts including control system design and specifications. Stewart & Stevenson incorporated the BOP into a skid-mounted unit, and SDG&E was the site coordinator providing, civil engineering and design, construction management, plant start-up, and operation. The Navy provided information on utilities on the selected site at NAS. Although IHI was perceived as a vendor of the reformer, coordination was required to ensure the compatibility of the reformer with the process design and transportation of the reformer to the site.

Planning for construction began with site definition and permitting. Site definition included negotiations with the Navy to install the project within the NAS facility followed by site selection. The permits were primarily from the Navy to meet environmental and safety requirements. Since the installation was within a Federal installation, a construction permit from the city was not required. We did however, submit construction drawings to the San Diego Navy Civil Engineering South West Division for their approval. Additional permits were required from the local pollution control district, the DOE environmental department, and the Navy's environmental group within the NAS facility. The PDT project was issued an exception by the San Diego Air Pollution Control District. DOE and NAS issued a categorical exclusion from an Environmental Impact Report.

Construction of the PDT plant began in May 1995 and was completed in September 1996. Figure 1 is a photograph of the near completed plant at the time this paper was issued. Site preparation and civil construction was complete in November 1995 followed by mechanical and electrical construction which began in February 1996. To optimize the available resources, SDG&E electrical crews worked in parallel with the mechanical and civil contractors to expedite the construction process. We experienced some delays in construction due to field design changes.

Plant Commissioning and Start-up:

Although the PDT plant is 250 kW net, the commissioning process was quite similar to commissioning larger conventional power plants. The entire system was divided into subsystems

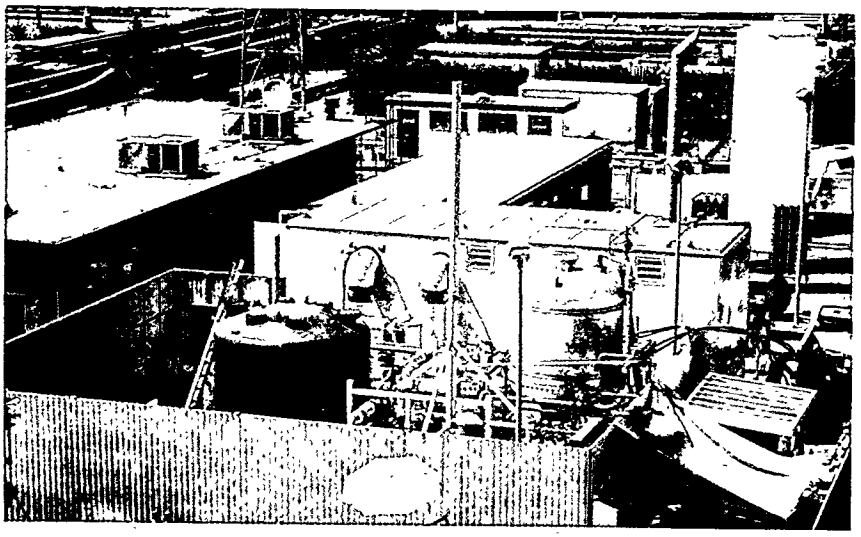

Figure 1. 250 kW PDT Fuel Cell Plant, NAS Miramar

and operators and commissioning personnel were assigned areas of responsibility for each subsystem to ensure safety was the top priority. The commissioning of the subsystems were to be done to the maximum extent prior to initiating a coordinated plant operation.

At the time this paper was issued, we completed checkout of three of six subsystems and were in the process of verifying the operation of the turbo charger subsystem. Figure 2 is a process flow diagram of the plant. Prior to subsystem checkout, all field terminations were verified and the Bailey control system was commissioned. SDG&E lead the commissioning team, which included M-C Power, Bechtel, and Stewart & Stevenson. The commissioning process was performed with experienced SDG&E personnel in process engineering, instrumentation, electrical, operations, controls, and shop personnel.

SDG&E elected to play a unique role in this project as a team member and commissioning lead to ensure that utility procedures were followed and to gain experience with the carbonate fuel cell technology. Part of the process include troubleshooting and resolving technical issues during commissioning period. These issues fall into the following categories:

- Unanticipated limits of pre commercial technology
- Process design interface
- Equipment and system specification integration
- Equipment procurement coordination
- Equipment performance deficiencies
- Construction errors
- Operational procedures deficiencies

During our troubleshooting process, we encountered some BOP system design issues that needed resolution in the field. One example of this is field modifications of the turbocharger loop, which

was not able to achieve self sustaining operation because the performance requirements were not met. Additional engineering and equipment modifications were required to ensure that proper flow and temperature conditions were delivered to the turbocharger system.

Benefits of SDG&E Participation:

By participating in the PDT project, SDG&E was able to improve the success of the PDT project by utilizing experienced power plant engineering, operations, maintenance, and craft personnel. In addition, we were able to use the existing support infrastructure of vendors, suppliers, and services to get quick turn-around of supplies and materials needed in the construction and commissioning process. Throughout the construction and commissioning process, SDG&E was able to provide a user's perspective on process design and solutions to field problems. In addition, we were able to contribute to the adaptation of standard operating procedures and safety considerations. The experienced power plant personnel provided a perspective of looking at the fuel cell as a generating facility rather than a research exercise.

The anticipated benefits to SDG&E include a perspective of how to accommodate a product such as a carbonate fuel cell as part of its operations in a restructured electric utility industry, the potential applications a fuel cell product as distributed generator at customer sites, and the potential impact on the electric distribution system. Fuel cells provide one more option to the utilities' portfolio of distributed generation technologies to consider in their implementation plans. However, when SDG&E initiated its support for the M-C Power technology, electric industry restructure was far from a thought. But as we approach the operation of the PDT plant, the utility business environment is fluid and full of uncertainties.

Conclusion:

The coordination during construction and start-up of the different participants was a challenge. The results to-date however, have been very positive. Throughout the construction and subsystem pre-testing we've had no loss of time due to accidents. The non-specialized work force consisting of technicians, craftsmen, and operators have worked very well. Although we've experienced some setbacks in schedule, we have not identified an insurmountable roadblock to prevent a successful operation of the PDT plant.

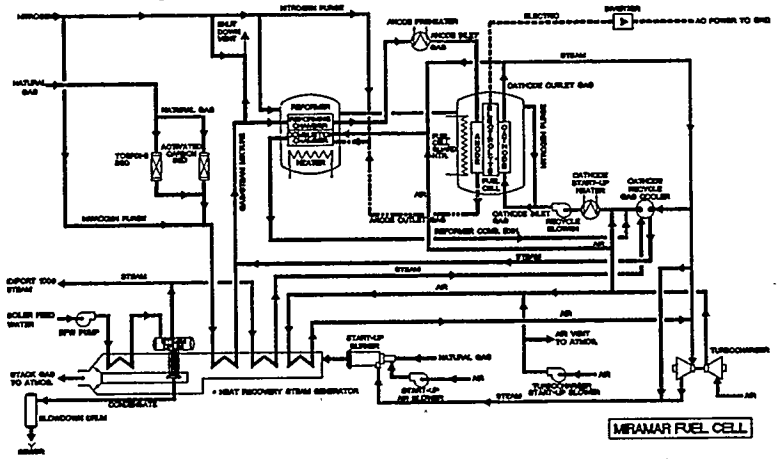

Figure 2. Process Flow Diagram for 250 kW IMHEX Fuel Cell Plant at NAS Miramar

1000kW ON-SITE PAFC POWER PLANT DEVELOPMENT AND DEMONSTRATION

Tomohide Satomi , Shunichi Koike
Phosphoric Acid Fuel Cell Technology Research Association (PAFC-TRA)
3-3 , 3-chome, Tenjinbashi, Kita-ku, Osaka 530, Japan

Ryou Ishikawa
New Energy and Industrial Technology Development Organization (NEDO)
1-1, 3-chome, Higashi-Ikebukuro, Toshima-ku, Tokyo 170, Japan

INTRODUCTION

Phosphoric Acid Fuel Cell Technology Research Association (PAFC-TRA) and New Energy and Industrial Technology Development Organization (NEDO) have been conducting a joint project on development of a 5000kW urban energy center type PAFC power plant (pressurized) and a 1000kW on-site PAFC power plant (non-pressurized).

The objective of the technical development of 1000kW on-site PAFC power plant is to realize a medium size power plant with an overall efficiency of over 70% and an electrical efficiency of over 36%, that could be installed in a large building as a cogeneration system.

The components and system integration development work and the plant design were performed in 1991 and 1992. Manufacturing of the plant and installation at the test site were completed in 1994. PAC test was carried out in 1994, and generation test was started in January 1995. Demonstration test is scheduled for 1995 and 1996.

SYSTEM CONFIGURATION

The 1000 kW on-site PAFC power plant is being developed as a cogeneration system that can be installed in a large building in an urban setting, and the following concepts were identified as the development and design targets:

- For installation in large building complex in urban setting (on-site type) ;
- For supplying electrical power and thermal energy (to be especially efficient in supplying the energy for air-conditioning of large buildings) ;
- Compact and well-integrated configuration for easy transportation to and installation ;
- Highly reliable and durable.

Table 1 summarizes the main target specifications for this plant, and Figure 1 shows the system flow diagram of this plant. Simplicity and high-reliability were given high priorities in developing and designing the basic system configuration.

To meet the targets, a plant design was considered that can produce waste heat recovery in the form of high-temperature (170℃) steam so that building's air-conditioning demand be supplied efficiently with an absorption chiller while achieving the target electrical efficiency. The semi-indirect steam output system was developed that combines direct steam generation by a steam separator and a heat exchanger type steam generator.
And the steam recovery efficiency was improved by lowering the reforming steam/carbon ratio and by using heat exchange between the fuel cell coolant and the supply air.

A package skid method was adopted for the integration of the plant equipment so that the equipment can be manufactured and assembled in factories, then packages can be installed and combined simply at the site, and the plant can be easily transported over land and carried into the installation site. The plant completed has overall dimensions of 12.5 m in width, 8 m in depth, and 3.6 m in height (height is 3.2 m except for cell stack and reformer) and footprint of 100 m^2(0.1m^2/ kW), thus achieving the compactness target.

Table 1. Target Specifications of 1000 kW Plant

	Specifications
Rated output	1,000kW (AC-net)
Efficiency(HHV)	Electrical; 36 %
	Thermal ; ≧ 35 % Steam ; ≧ 20 % Hot water ; ≧ 15 %
	Total ; ≧ 71 %
Fuel cell stack	Operating pressure; Atmospheric
	Operating temperature; 205 ℃
	Number of fuel cell stacks; 2 stacks
	Cell size ; ca. 1m^2
	Current density; 250 mA/cm^2
Reformer	1,000kW class, Multi-tube type
Foot prints	≦ 0.1 m^2/kW
Fuel	Natural gas , Pressure : 0.7 kg/cm^{2}G

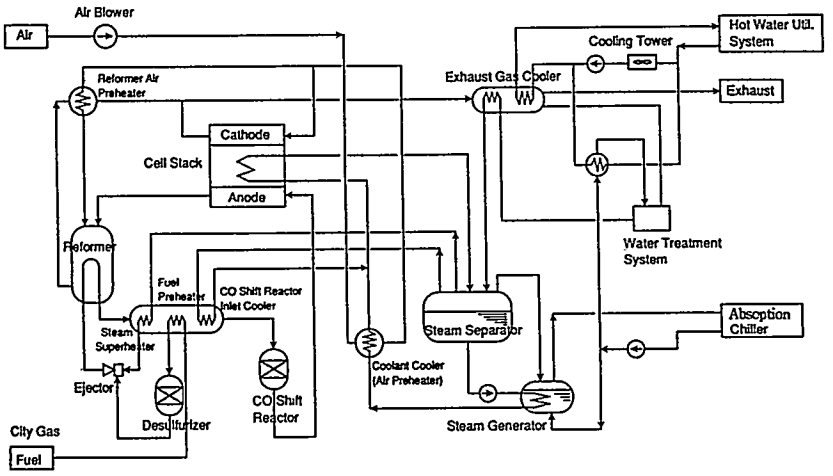

Figure 1. System Flow Diagram of 1000 kW Plant

CHARACTERISTICS OF KEY PLANT COMPONENT

(1) Fuel cell

To achieve high performance and compactness, large, 1 m square class high-performance fuel cell capable of generating 250 mA/cm^2 at atmospheric pressure were selected.

The fuel cell package consists of 2 fuel cell stacks (414 cells/stack), and these stacks are arranged closely with symmetrical configuration of gas manifold. This arrangement can achieve approximately 24% less foot print than the conventional independent two cell stack configuration.

(2) Reformer

The multi-tube type reformer which has 30 reforming tubes inside a vertically positioned cylindrical vessel was developed and employed. To improve heat recovery by high-temperature steam, a reforming system that can minimize the amount of steam necessary for reforming process was developed. This has enabled achievement of a steam/carbon ratio of 2.5 at the rated power level.

(3) Inverter

The inverter has been down-sized 40% compared to a conventional GTO-based unit by using IGBT devices in the main circuit. A self-exciting voltage type PWM control method was selected and a current control function was developed and integrated which allows stable operation even when monentary voltage drop occurs.

PROGRESS OF DEVELOPMENT WORK

The development of this plant began in 1991. The elemental technologies development and the design phase was performed in 1992 and 1993. Manufacturing of the system component equipment and packaging were completed in 1994. The completed system component packages were carried into and installed at the test site. Figure 2 shows how the installed plant looks.

After each package, excepting the cell stack, was installed, the PAC testing was performed from August to December of 1994 to verify the static characteristics of the process system including the reformer and to make control adjustments on start, stop, load change, etc. The series of testing showed that the plant can operate at a methane conversion ratio of at least 93% under the rated capacity and at other parameters exceeding the design levels, proving that the plant has a good control characteristic.

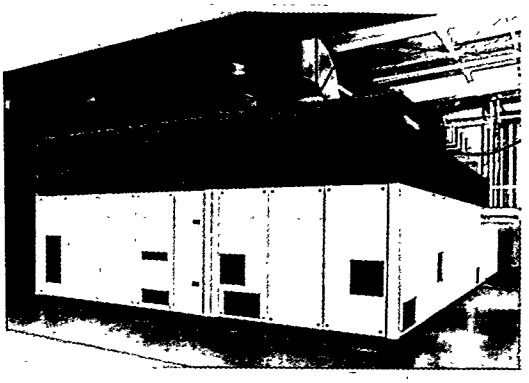

Figure 2. External View of 1000kW Plant

Upon completion of the PAC testing, the cell stack was installed in December 1994 and the power generation adjustment test was begun from January 1995. Initial power generation was successfully conducted in February, and the 1000kW rated power output was achieved in March. And the plant had passed a Governmental inspection in May. Table 2. summarized the operation records as of the end of July 1996, and Figure 3 shows the plant load characteristic data after 1500 hours of operation. The cell stack voltage in the initial power generation stage is higher than the design values, so that the electrical efficiency at the rated power level of 38% or higher and steam recovery efficiency of over 20% were respectively achieved. This is very good performance for an atmospheric pressure type plant. Figuer 4 shows the operation history of the cell stack voltage. The rate of voltage decay except the initial power generation stage is less than 2μV/h. on average, and the characteristics of cell stack has been above the targeted curve during operation.

Table 2. Operation Records of 1000kW Plamt

Items	Record
Initial power generation	Feburuary 28, 1995
Rated output attained	March 7, 1995
Passing Gavernmental inspection	May 11, 1995
Cumulative electric power generated	8,005 MWH
Cumulative generation hours	7,667 hours
Maximum continuous operation	3,247 hours
Cumulative frequency for generation	21 times

As of the end of July 1996

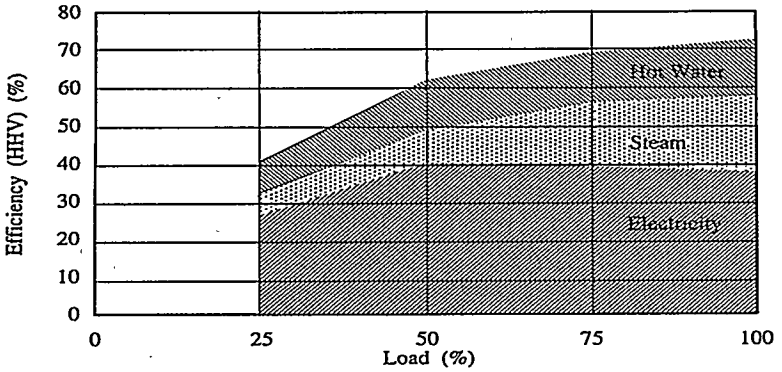

Figure 3. Load Characteristics of 1000kW Plant

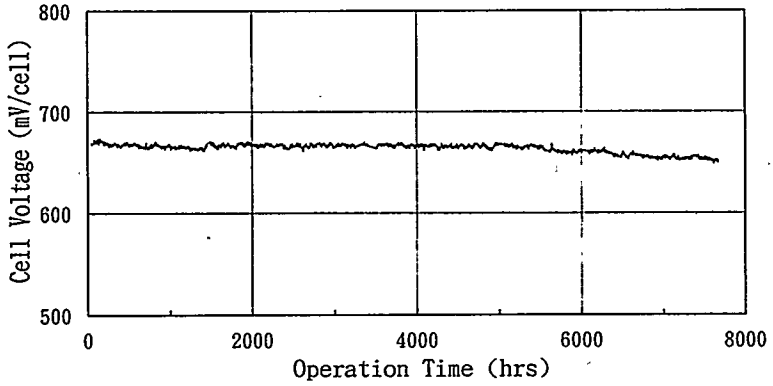

Figure 4. Operation History of Cell Stack Voltage

CONCLUSION

From now through fiscal 1996, demonstration testing and evaluative studies are scheduled in order to promote the commercialization of 1000kW on-site PAFC power plant through demonstration of operating characteristics, reliability, durability, etc.

STARTUP, TESTING, AND OPERATION OF THE SANTA CLARA 2MW DIRECT CARBONATE FUEL CELL DEMONSTRATION PLANT

A. J. Skok, A. J. Leo, (203) 778-1323
Fuel Cell Engineering Corporation
3 Great Pasture Road
Danbury, CT 06813

T.P. O'Shea (408) 246-0831
Santa Clara Demonstration Project
1601 Civic Center Dr., Suite 202A
Santa Clara, CA 95050

INTRODUCTION

The Santa Clara Demonstration Project (SCDP) is a collaboration between several utility organizations, Fuel Cell Engineering Corporation (FCE), and the U. S. Dept. Of Energy aimed at the demonstration of Energy Research Corporation's (ERC) direct carbonate fuel cell (DFC) technology. ERC has been pursuing the development of the DFC for commercialization near the end of this decade, (1) and this project is an integral part of the ERC commercialization effort. The objective of the Santa Clara Demonstration Project is to provide the first full, commercial scale demonstration of this technology. The approach ERC has taken in the commercialization of the DFC is described in detail elsewhere(2). An aggressive core technology development program is in place which is focused by ongoing interaction with customers and vendors to optimize the design of the commercial power plant. ERC has selected a 2.85 MW power plant unit for initial market entry. Two ERC subsidiaries are supporting the commercialization effort: the Fuel Cell Manufacturing Corporation (FCMC) and the Fuel Cell Engineering Corporation (FCE). FCMC manufactures carbonate stacks and multi-stack modules, currently from its production facility in Torrington, CT. FCE is responsible for power plant design, integration of all subsystems, sales/marketing, and client services. FCE is serving as the prime contractor for the design, construction, and testing of the SCDP Plant. FCMC has manufactured the multi-stack submodules used in the DC power section of the plant. Fluor Daniel Inc. (FDI) served as the architect-engineer subcontractor for the design and construction of the plant and provided support to the design of the multi-stack submodules. FDI is also assisting the ERC companies in commercial power plant design.

PROJECT DESCRIPTION

The project involves the design, construction, and testing of a 2MW DFC demonstration power plant in the city of Santa Clara, California. The site for the plant is located at 1255 Space Park Drive in Santa Clara. The site is owned by the City's Electric Department and is immediately adjacent to the Scott Receiving Station, a 115/60kV switching station on the City electrical system. The plant occupies a portion of the site, measuring approximately 150 feet by 150 feet.

The power plant uses 16 fuel cell stacks, each rated at 125kW. The stacks were fabricated and assembled into four 4-stack modules in FCMC's Torrington facility and truck shipped to the Santa Clara site, where they were installed into the two 1MW modules which comprise the DC power section of the plant. The key plant design specifications are listed in Table 1.

POWER PLANT OPERATION

Construction of the balance of plant (the power plant systems not including the fuel cell submodules) was complete in June 1995. In place of the fuel cell submodules, spool pieces had

Nominal Capacity	2 MW
Plant Rating, Net AC	1.8 MW
Heat Rate (LHV) at Rated Power	6850 Btu/kWh
Maximum Emissions at Plant Rating	
SO_x	0.003 lb/MWh
NO_x	0.0004 lb/MWh
CO_2	845 lb/MWh
Noise	60dB(A) at 100ft
Availability	90%
Startup Time, Cold Start Rated Power	40 hours
Ramp Time, Standby to Rated Power	30 minutes
Reactive Power	+/- 1.67 MVAR

Table 1 SCDP Design and Performance Criteria
Performance Target-Based on Commercialization Objectives

been installed connecting fuel cell inlet and exit lines. This allowed the system to be tested without the fuel cell stacks in a series of balance of plant (BOP) pre-test activities. The BOP pre-test effort identified and corrected a number of BOP deficiencies and the required modifications were made to resolve all issues by the end of the pre-test period. The submodules arrived at the site over the period of November 1995 through February 1996. As the units were delivered they were stored in a laydown area adjacent to the power plant.

Once all four units had been delivered, and the BOP pre-test effort had been successfully concluded, the four submodules were installed in the plant. Figure 1 shows the completed power plant after the stack submodule installation.

The power plant acceptance test period has been initiated, beginning with the initial plant start-up, which includes some electrode and matrix conditioning steps which are unique to the first plant heatup. The initial startup demonstrated that the conditioning operation can be controlled sufficiently

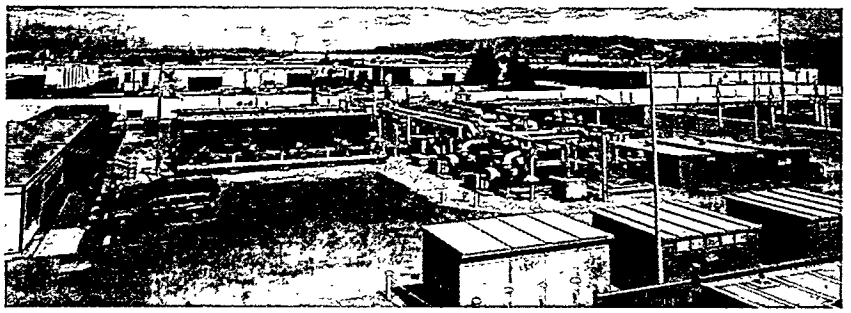

FIGURE 1
THE SANTA CLARA DEMONSTRATION PLANT
The Test Program has begun and the Plant has produced its Rated Power Output.

to allow the start-up of multiple-stack systems. The initial open circuit voltages for the sixteen stacks were equal to within 0.5%, with stack voltages of 251+/-1 Volt (See Figure 2). The successful conditioning of these 16 stacks simultaneously was a significant project milestone. A period of tuning and adjusting the AC/DC inverter control system followed the conditioning operations. While the inverter had been extensively tested during the BOP pre-test activities, this final tuning was required because it had not been operated with the fuel cell stacks. After the initial tuning was completed, the initial grid connect was made at a power level of 200 kW. In the initial phase the PCU was deliberately tripped to verify that the power plant system could ride through inverter trips as the inverter was adjusted further. Once that was completed the power ramp was continued, and on the afternoon of May 2, 1996 the plant reached the design level 2.0 MW gross AC, delivering 1.8 MW net AC to the Santa Clara electric system(See Figure 3).

This initial phase of power plant operations was approached in a conservative manner, focusing on characterizing the plant operations while minimizing operational risks. Two of the auxiliary burners in the system - which are meant to be shut down during normal operations - were kept running in order to minimize the impact of a trip caused by the inverter or any of the BOP equipment. This approach was maintained as the plant was ramped to and above the rated power level. Within these limitations the highest efficiency achieved by the power plant was 43.6% (7820 Btu/kWh LHV). This was achieved at a power output of 1.93 MW net AC to the grid. Throughout the ramp to this higher power level, the stack performance exceeded the projection used in the plant design calculations, indicating that the target efficiency of 6850 Btu/kWh is achievable, once supplemental natural gas use is stopped.

Beginning approximately 520 hours into the plant operation, intermittent anomalies were observed in some of the stack voltages. In order to determine the cause of these events, the power plant was shut down and cooled to ambient temperature for inspection. The cause was determined to be parasitic electrical currents, caused by a breach of the electrical isolation between the fuel cell stacks and the gas distribution piping. FCE has completed the process of cleaning or replacing the damaged dielectric piping. As of the writing of this paper, the power plant restart was in progress.

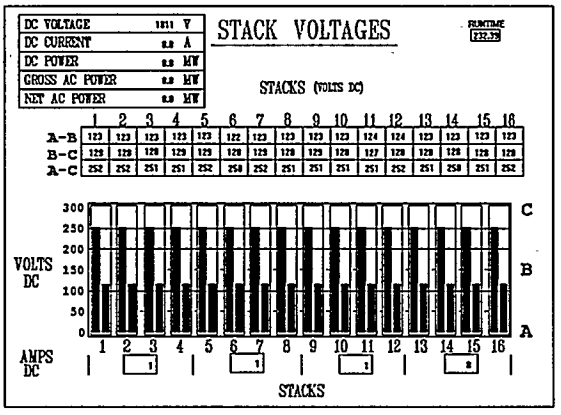

FIGURE 2 OPEN CIRCUIT STACK VOLTAGES
The 16 stacks had very uniform open circuit voltages.

CONTINUED PLANT OPERATION

After the power plant restart has been completed, the acceptance test effort will resume. The acceptance test includes a total of 1000 hours system operation, during which time the plant performance is measured against the design criteria described above. Following the completion of the acceptance test, an additional 9000 hours of endurance testing is planned.

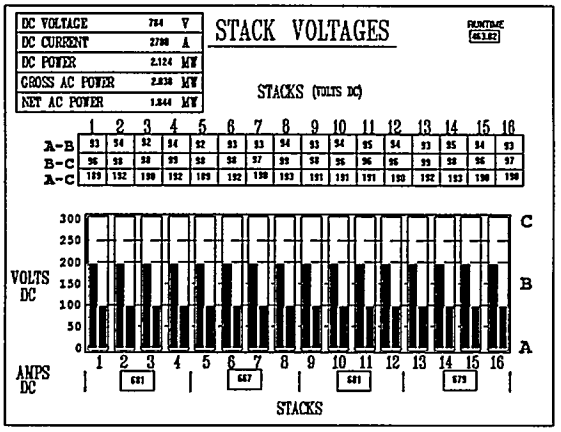

The SCDP project has already begun to meet its objectives. The work to date has demonstrated that a megawatt scale DFC plant can be configured using truck-shipped multistack submodules, and that a multiple stack system can be started and operated with excellent performance and uniformity among the stacks. The power plant has already met its rated power design criteria, and demonstration of the remaining criteria is planned as the plant operation is continued.

FIGURE 3 RATED POWER PLANT OUTPUT
Stack Performance was uniform at 1.8 MW net AC Power.

ACKNOWLEDGMENTS

The design and fabrication of the fuel cell stack modules was done with U.S. Department of Energy support through Morgantown Energy Technology Center (METC), under Cooperative Agreement DE-FC21-92MC29237. The guidance and support of the METC Contracting Officer's Representative, Mr. Thomas J. George, has been greatly appreciated.

The design and procurement of the balance of plant and the construction and testing of the complete system has been supported by the Santa Clara Demonstration Participants. The participants in the SDCP are as follows: City of Santa Clara, City of Los Angeles Department of Water and Power, City of Vernon, Electric Power Research Institute, National Rural Electric Cooperative Association, Sacramento Municipal Utility District, and Southern California Edison Company. Salt River Project (SRP) and the Northern California Power Agency (NCPA) are also supplying some project funding through a consortium agreement with the City of Santa Clara. EPRI has also provided funding beyond its SDCP participant share to support early design and optimization efforts in the project. ERC/FCE is also contributing funding to the project. In addition, the California Energy Commission has provided funding to the City of Santa Clara to support the balance of plant pre-test activities.

REFERENCES

(1) D. Glenn, et al.; DFC Commercialization: This Is It. *Fuel Cells: Programs and Abstracts 1996 Fuel Cell Seminar. November 1996.*

(2) H. Maru, et al.; Direct Fuel Cell Project Design Improvement. *Fuel Cells: Programs and Abstracts 1996 Fuel Cell Seminar. November 1996.*

ARGE DFC - A EUROPEAN APPROACH TO MCFC COMMERCIALIZATION

Peter Kraus, Gerhard Huppmann
MTU Friedrichshafen GmbH
D-81663 München

Dr. Andreas Heiming
Ruhrgas AG
Halterner Str. 125
D-46284 Dorsten

Dr. Kim Aasberg-Petersen
Haldor Topsoe A/S
Nymollevej 55
DK-2800 Lyngby

The largest European program for the commercialization of the molten carbonate fuel cell technology is carried out by the European Direct Fuel Cell Consortium (ARGE DFC). The consortium consists of the following companies:

- MTU Friedrichshafen GmbH (Germany), within the DaimlerBenz Group responsible for off-road propulsion and decentralized energy systems.
- Haldor Topsoe A/S (Denmark), a plant engineering company and specialist for catalytic processes
- Elkraft A.m.b.A. (Denmark), one of the countries two utility companies
- Ruhrgas AG (Germany), the largest German gas company
- RWE AG (Germany), the largest German electrical utility company

MTU acts as a consortium leader. The company shares a license and technology exchange agreement with Energy Research Corporation of Danbury, Connecticut.

Three Phases of Development

Established in 1990, the ARGE DFC has set up a comprehensive 10 year program to bring the MCFC from a laboratory technology to a marketable power plant. The overall program volume will be approx. 100 Million $ to be spent between the years 1990 and 2000. The program is divided into three phases. The first phase (1990-6/1994) can be entitled *basic technology development*. The second period (7/1994-12/1994) is a *product development* phase. The upcoming third phase (1998-2000) will see *field testing* of a number of pilot plants leading gradually into commercialization by the turn of the century.

Achievements of Phase I

In the beginning of our program the work of the ARGE DFC focused on cell technology. Based on the cooperation with ERC we concentrated on finding solutions for material and corrosion problems that limit MCFC life. Improvements in this field were usually tested in small scale 7 x 7" single cells and ministacks. Experience with larger stacks was obtained by the operation of a 3 kW 2 x 3' internal reforming stack in our laboratories in Ottobrunn and a 7 kW 2 x 3' internal reforming stack at the ARGE's test facility operated by Elkraft in Kyndby, Denmark.

The most important result of our Phase I *cell technology* work is the development of stabilization methods for nickel oxide cathodes that reduce the NiO dissolution in the electrolyte by a factor of approx. 4, bringing about cathode lifetimes well beyond 40.000 hours.

In parallel to the cell development, the MCFC technology was qualified for the application with coal gas and other syn-gases in a comprehensive experimental program.

The ARGE's work in *MCFC system design* came to a turning point in 1992 when we realized that conventional system designs do not hold the promise for competitive power plants. As a rule of thumb the fuel cell stack contributes only one third to the cost of the overall system. In a standard configuration the cost of conventional components would keep the system too expensive, even if the cost of the fuel cell stack itself could be reduced to zero (1).

Optimization by Simplification and Integration - the Hot Module Concept
In essence we have found that

- system designs for small to medium scale MCFC power plants have to be as simple as by all means possible. System costs are greatly influenced by this simplification.
- System costs remain prohibitively high even for simplified systems, if these designs are built in a conventional plant engineering manner. Only a high degree of mechanical, thermal, and pneumatic integration promises sufficiently low system cost.
- Intelligent mechanical and pneumatic integration can solve critical fuel cell problems completely, e.g., differential cell pressure.

These findings have led us to the invention of an innovative design approach characterized by the term Hot Module (Fig. 1). A Hot Module combines all the components of an MCFC system operating at similar temperatures and pressures into a common thermally insulated vessel. A typical configuration contains the MCFC stack, a catalytic burner for the anode tail gas and a cathode recycle loop including mixing-in of fresh air and anode exhaust. The cell stack is resting in a horizontal position on the fuel-in manifold, thus providing excellent gas sealing by gravity forces. On the top of the stack the gases exiting from the anodes are mixed into the cathode recycle loop together with fresh air supplied from the outside. The mixture is transported through a bed of combustion catalyst located on top of the mixing area and blown back to the cathode input by the cathode recycle blowers on the top end of the vessel. No gas piping or sealed cathode manifolds are necessary. For start-up, an electrical or gas fired heater is arranged along the cathode input of the stack.

The Hot Module is complemented by a fuel processing system of a similar high degree of mechanical integration. All heat exchangers necessary for preheating of the fuel gas and evaporation of the reforming water are integrated into a common duct supplied with the cathode exit of the Hot Module. The reactors for the desulphurization and preconversion of higher hydrocarbons in the fuel gas are skid mounted alongside this duct to form a compact unit finding its place at one end of the cylindrical stack module. The other end of the stack module is taken by an electrical and electronics compartment containing the control electronics and a state-of-the-art efficient liquid cooled IGBT inverter. The whole arrangement is truck transportable and intended to be installed within buildings as well as in the open.

ARGE DFC Product Development Targets
In the current second phase of our program the ARGE DFC concentrates on the development, qualification and demonstration of a Hot Module power plant with one fuel cell stack of 280 kW. In parallel, R&D work in cell technology is proceeding towards longer lifetimes. Our target is to qualify the cell components for lifetimes up to 40.000 hours. The cell technology work is complemented by a manufacturing technology program for full scale cell components.

Hot Module Power Plant Qualification

In 1995 a first full scale mockup of an integrated fuel cell module was built and tested at room temperature. It consists of all the components of a Hot Module, the cells being substituted by dummy plates of identical dimensions and flow resistance. This *Cold Dummy* was used for mechanical and flow tests and proved the feasibility of the mechanical and pneumatic integration concept. In this year a *Hot Dummy* of the fuel cell module has been tested to prove the mechanical and pneumatic behavior at full operating temperatures of 650°C.

Construction of the first real fuel cell module with the same design starts in the last quarter of 1996. It will go into operation as a complete system in spring 1997 at the Ruhrgas facilities located in Dorsten at the northern end of the Ruhr area. After extensive testing and optimization the plant will be ready for demonstration towards the end of 1997.

Things to Come

After successful test of the Hot Module system demonstrator the ARGE DFC plans to sell a number of precommercial *Field Test Units* into key applications in industrial and commercial cogeneration. This *third phase* of the ARGE's program is intended to generate operational experience on the side of the supplier and confidence into this new technology on the side of the customer, paving the way into commercial application of our innovative product concept.

Acknowledgments

The development of the MCFC technology towards market application is performed jointly by the ARGE DFC. cf. Introduction. Programs underlying this report have been funded by the German Federal Minister for Education and Research, as well as by the European Community. The responsibility for the contents of the publication is with the authors.

1. P. Kraus, "Systems' optimization: achieving the balance," J. of Power Sources. Vol. 49 (1994), No. 1-3, pp. 53-60,

ARGE DFC

Direct Fuel Cell Hot Module

mtu FRIEDRICHSHAFEN

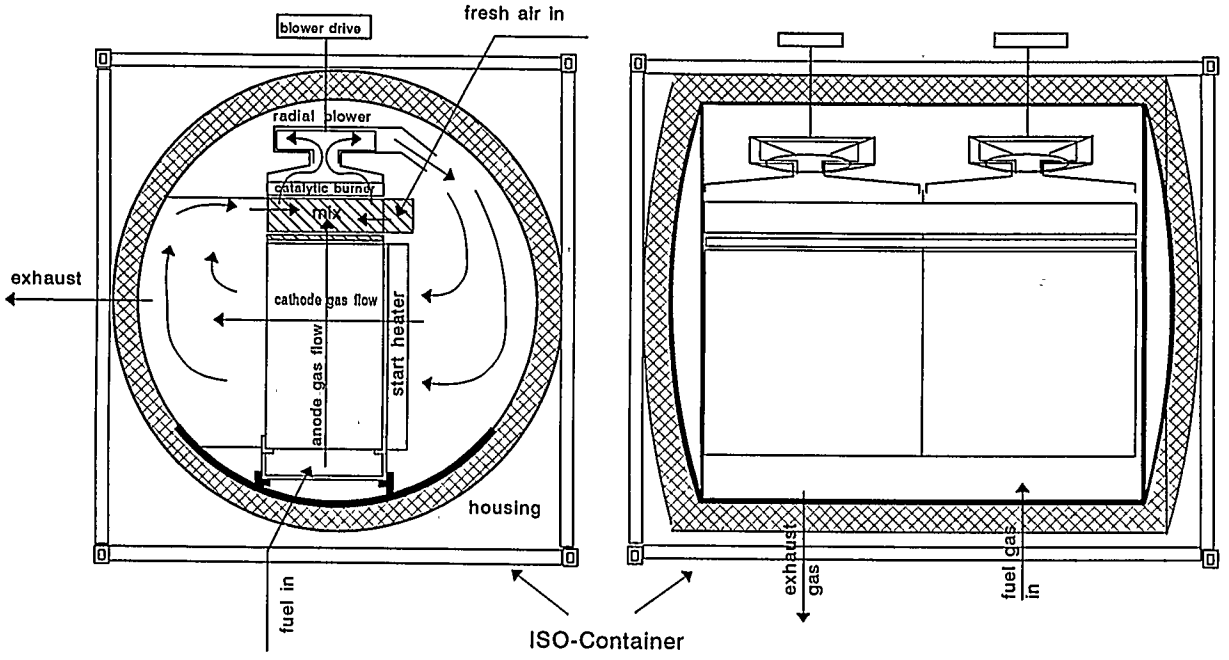

Figure 1: Hot Module Principle

Orland1 8/96

PROGRESS AND PROSPECTS FOR PHOSPHORIC ACID FUEL CELL POWER PLANTS

Leonard J. Bonville, Glen W. Scheffler and Murdo J. Smith
International Fuel Cells Corporation
South Windsor, Connecticut 06074

International Fuel Cells (IFC) has developed the fuel cell power plant as a new, on-site power generation source. IFC's commercial fuel cell product is the 200-kW PC25™ power plant. To date over 100 PC25 units have been manufactured. Fleet operating time is in excess of one million hours. Individual units of the initial power plant model, the PC25 A, have operated for more than 30,000 hours. The first model "C" power plant has over 10,000 hours of operation. The manufacturing, application and operation of this power plant fleet has established a firm base for design and technology development in terms of a clear understanding of the requirements for power plant reliability and durability. This fleet provides the benchmark against which power plant improvements must be measured.

PC25 Power Plant Development Progress

As the first PC25 power plants were entering service, IFC began an aggressive development program to improve the design and manufacturing processes of the power plant to reduce its size, weight and cost. In addition, this on-going development program has addressed the simultaneous goals of improved performance, durability, and reliability. Development progress has been sustained at a compounded rate of 10 percent per year since the late 1980's. This development progress is illustrated in Figure 1 which shows the significant reductions in power plant weight and volume achieved since the initial prototype model was built. These improvements to date are reflected in the PC25 C design which is a one-third reduction in size and weight when compared to the PC25 A.

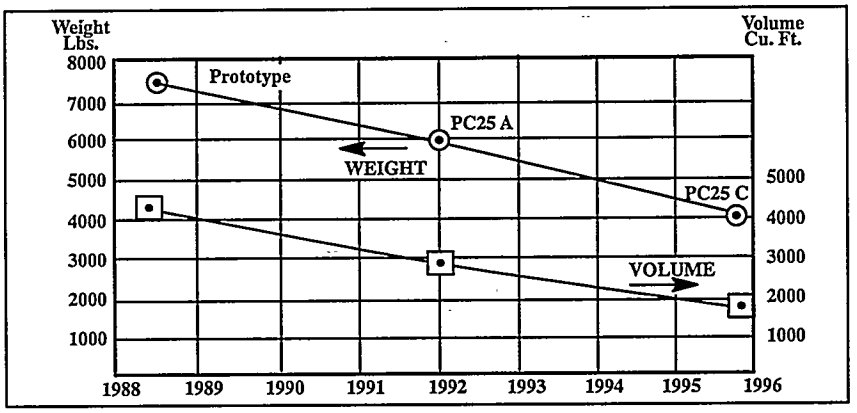

Figure 1: PC25 Power Plant Weight and Volume Improvement

The advances in the PC25 design resulted from improvements in each of the major components; cell stack, fuel processor, power conditioner and ancillary systems. Figure 2 compares the PC25A and PC25 C cell stacks. The height of the stack has been reduced by 20 percent contributing together with processing improvements to a dramatic reduction in stack manufacturing cost. Even further reductions in stack cost and size have been defined under a recent cell component development program sponsored through the Defense Advanced Research Projects Agency (DARPA) and administrated by the U.S. Army Construction Engineering Research Laboratories and parallel efforts funded by IFC and Toshiba. These programs focused on reducing the manufactured cost of the cell stack assembly and resulted in thinner, lower-cost cathode substrate, separator plate and cooler configurations. Incorporation of these advanced components will lead to an additional 12-inch reduction in stack height and significant cost reduction.

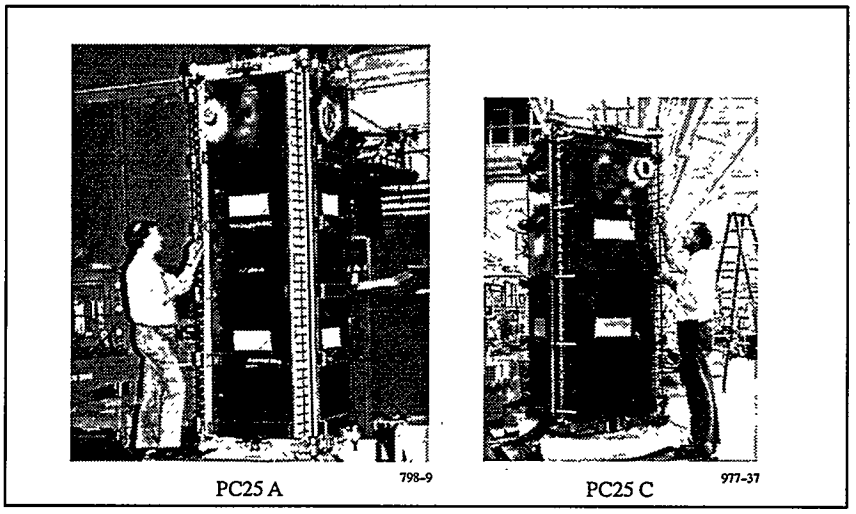

Figure 2: PC25 C Cell Stack Improvement

The fuel processing system has been simplified and its size has been reduced. The capability for operation on propane has been developed. The combination of the reformer size reduction with the reduced stack height provides an overall reduction of 18 inches in power plant height for the PC25 C. Further reformer improvements are being developed in other programs discussed below.

The advent of high capacity Insulated Gate Bipolar Transistors (IGBT) has simplified the power conditioner. Figure 3 compares the electrical system of the PC25 A and PC25 C power plants. The electrical system for the PC25 C is only one third the size of that for the PC25 A. Alternative topologies combined with higher rated IGBT's, presently becoming commercially available, are anticipated to lead to further cost reductions.

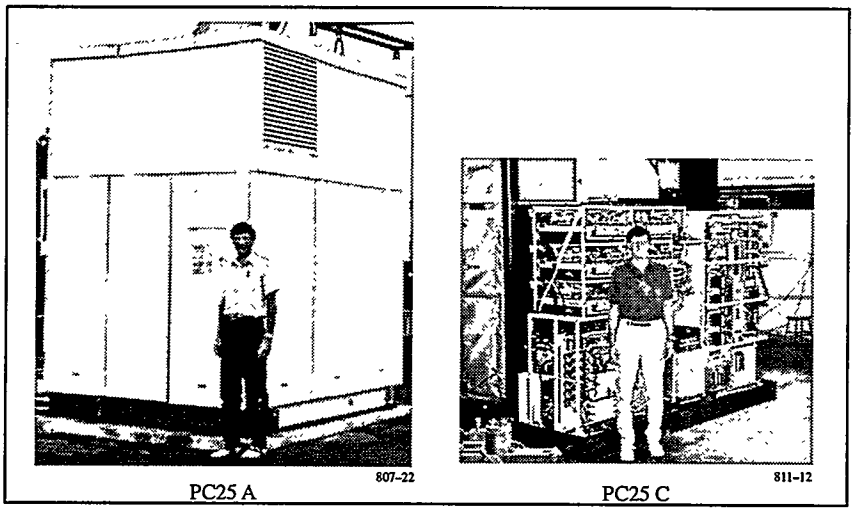

Figure 3: PC25 C Electrical System Improvement

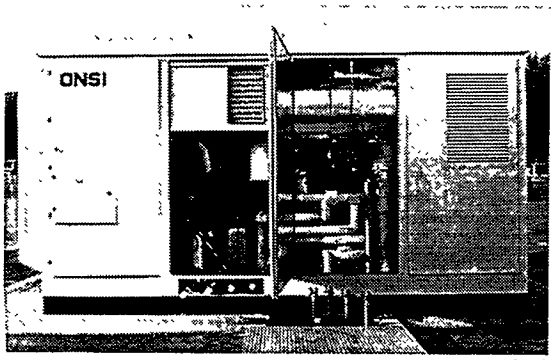

The ancillary components also represent a significant power plant cost element. Reductions in their cost have been addressed through value engineering, including supplier participation, to identify integration opportunities which eliminate components or reduce their size. Figure 4 shows the improved component accessibility designed into the PC25 C.

Figure 4: Improved Component Accessibility

Application Expansion Combined With Technology Extension

Specific application improvements in phosphoric acid fuel cells are illustrated by two on-going development programs; a program sponsored by Georgetown University through the U.S. Department of Transportation to develop a 100-kW power system for a transit bus and a DARPA funded program to develop a 100-kW Mobile Electric Power (MEP) system operational on logistics fuel.

The Georgetown University bus application has specific weight and volume requirements for a dc system that are one-fourth those of the PC25 C and requires multiple start-stop cycles. Methanol is the specified fuel. Significant advances in cell stack and fuel processing technologies are necessary to meet these requirements. A conceptual power plant design is shown in Figure 5. Using the technology base from the PC25, IFC has designed an advanced cell configuration of small planform area with increased performance. An advanced 32-cell stack under test is shown in Figure 6. This cell stack operates at higher power density and and has lower weight per unit area than the PC25 C cell stack. Figure 7 compares the 100-kW compact methanol reformer with the PC25 natural gas reformer. This compact reformer has been tested on methanol and natural gas and scales to less than 50 percent of the PC25 reformer at a 200–kW rating.

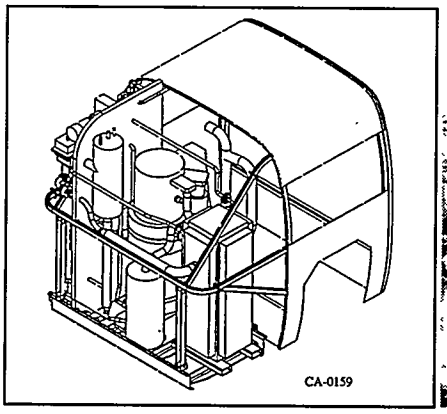

Figure 5: 100 kW Bus Power Plant Concept

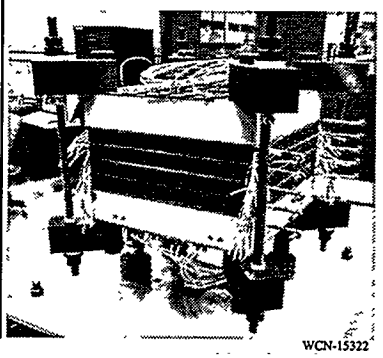

Figure 6: Advanced Cell Stack

Although some of the advancement in characteristics are associated with the transportation design requirements, significant portions of this technology improvement are readily transferable to the PC25 leading to future cost reduction.

The 100-kW MEP power plant concept is shown in Figure 8. The broader military application requires use of logistic fuels. The MEP program is focused on developing a fuel processing system with logistics fuel capability including JP-8 and DF-2. An advanced, auto-thermal reformer has been designed. A full-size module of this design was successfully tested with over 3500 hours of stable operation demonstrating greater than 98 percent conversion on JP-8 fuels containing 100, 800 and 3000 ppm sulfur. Figure 9 shows the module mounted in the test stand. Post-test teardown and inspection showed no evidence of carbon deposits. A complete 100-kW assembly will be built and tested early in 1997.

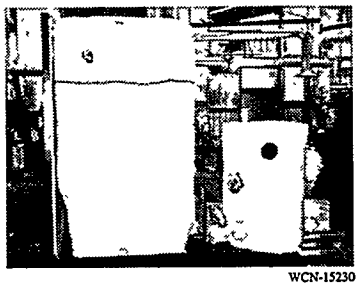

200 kW 100 kW

Figure 7: PC25 C Reformer Compared To Advanced Bus Design

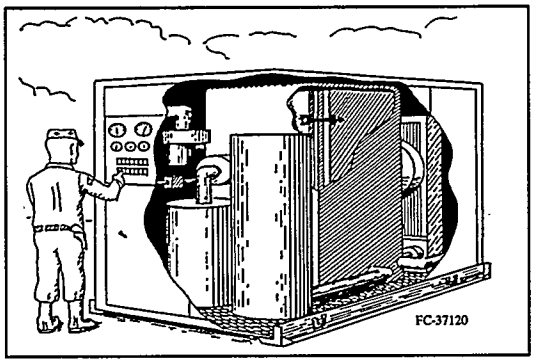

Figure 8: Diesel Fueled MEP100 kW Power Plant Concept

Figure 9: Logistics Fuel Reformer Under Test

Acknowledgements

IFC wishes to thank the U.S. Department of Energy, Georgetown University, U.S. Army Construction Engineering Research Laboratories, Defense Advanced Research Projects Agency and Toshiba Corporation for their continued support of our PAFC power plant development programs.

ADVANCES IN TUBULAR SOLID OXIDE FUEL CELL TECHNOLOGY

S.C. Singhal
Westinghouse Electric Corporation
Science & Technology Center
1310 Beulah Road
Pittsburgh, PA 15235

INTRODUCTION

The design, materials and fabrication processes for the earlier technology Westinghouse tubular geometry cell have been described in detail previously (1). In that design, the active cell components were deposited in the form of thin layers on a ceramic porous support tube (PST). The tubular design of these cells and the materials used therein have been validated by successful electrical testing for over 65,000 h (>7 years). In these early technology PST cells, the support tube, although sufficiently porous, presented an inherent impedance to air flow toward air electrode. In order to reduce such impedence to air flow, the wall thickness of the PST was first decreased from the original 2 mm (the thick-wall PST) to 1.2 mm (the thin-wall PST). The calcia-stabilized zirconia support tube has now been completely eliminated and replaced by a doped lanthanum manganite tube in state-of-the-art SOFCs. This doped lanthanum manganite tube is extruded and sintered to about 30 to 35 percent porosity, and serves as the air electrode onto which the other cell components are fabricated in thin layer form. These latest technology cells are designated as air electrode supported (AES) cells.

In addition to eliminating the calcia-stabilized zirconia support tube, the active length of the cells has also been continually increased to increase the power output per cell. The active length has been increased from 30 cm for pre-1986 thick-wall PST cells to 150 cm for today's commercial prototype AES cells. Additionally, the diameter of the tube in longer length AES cells has been increased from 1.56 cm to 2.2 cm to accommodate larger pressure drops encountered in longer length cells. The power output of such an AES cell is 210 W at 1 atm pressure and 280 W at 10 atm pressure at 1000°C and 85% fuel (89% H_2 + 11% H_2O) utilization.

The fabrication of PST cells involved three electrochemical vapor deposition (EVD) steps, one each for the doped $LaCrO_3$ interconnection, the yttria-stabilized zirconia (YSZ) electrolyte, and the Ni-YSZ fuel electrode. Though EVD provides very high quality thin films (2), it requires capital intensive equipment making the process rather expensive. Investigations on alternate processing techniques have been underway at Westinghouse for several years to replace one or more EVD steps with a more cost-effective approach. The interconnection is now deposited by plasma spraying calcium aluminate containing lanthanum chromite powder over porous, doped lanthanum manganite air electrode tube; calcium aluminate facilitates densification during plasma spraying and subsequent heat treatment. These interconnections have a thermal expansion coefficient much better matched to that of the electrolyte than the previously-used EVD Mg-doped lanthanum chromite interconnection. Plasma spraying of interconnections has now been implemented in the manufacturing of all AES SOFCs. This has resulted in reduced

process cycle time, increased yield, and a major reduction in cell fabrication cost. The materials and fabrication processes for the state-of-the-art AES cells are summarized in Table 1.

Table 1. Materials and fabrication processes for state-of-the-art AES cells.

Component	Material	Thickness	Fabrication Process
Air electrode tube	Doped $LaMnO_3$	2.2 mm	Extrusion-sintering
Electrolyte	$ZrO_2(Y_2O_3)$	40 μm	EVD
Interconnection	Doped $LaCrO_3$	85 μm	Plasma spraying
Fuel Electrode	Ni-$ZrO_2(Y_2O_3)$	100 μm	Slurry spray-EVD

CELL PERFORMANCE

A large number of AES cells with plasma sprayed interconnections have been electrically tested for up to about 9,000 h with little performance degradation. The performance degradation has decreased from about 0.5% per 1,000 h for PST cells to less than 0.2% per 1,000 h for AES cells. Also, the change from PST cells to the AES cells has resulted in a power density increase of about 33%. In addition to improved performance, the AES SOFCs have shown the ability to thermally cycle to room temperature for over 100 times without any mechanical damage or performance loss.

Westinghouse in conjunction with Ontario Hydro Technologies has also tested AES cells at pressures up to 15 atmospheres on both hydrogen and natural gas fuels. Operation at elevated pressures yields a higher cell voltage at any current density due to increased Nernst potential and reduced cathode polarization, and thereby permits higher stack efficiency and greater power output. With pressurized operation, SOFCs can be successfully used as replacements for combustors in combustion turbines; such integrated SOFC-combustion turbine power systems are expected to reach efficiencies approaching 70% (3).

INVESTIGATIONS IN PROGRESS TO FURTHER REDUCE CELL COST

Elimination of one of the cell components (calcia-stabilized zirconia support tube) and replacement of one EVD step by plasma spraying (for depositing interconnection) has resulted in a major reduction in the cost of the AES cells and the cost of electricity ($/kW) produced by using such cells. Investigations are underway to further reduce the cost of these cells by reducing the cost of materials used in SOFCs and replacing another EVD step (for depositing fuel electrode) by a more cost-effective sintering approach.

Over 90% of the weight of an AES cell is that of the doped lanthanum manganite air electrode tube. Presently, the air electrode material is synthesized using high purity component oxides such as La_2O_3 and MnO_2. Over 70% reduction in the cost of air

electrode raw materials is possible if mixed lanthanides are used instead of pure lanthanum compounds to synthesize the air electrode powder. AES cells have now been fabricated using air electrode powder synthesized using mixed lanthanides. The performance of an initial cell with air electrode fabricated using mixed lanthanides at 400 mA/cm^2 was only about 8% lower, primarily due to non-optimized processing conditions and a slightly higher resistivity of the mixed lanthanides air electrode material. Further adjustments in the composition of the air electrode material synthesized using mixed lanthanides are expected to result in lower air electrode resistivity and a cell performance equivalent to that of cells using high purity air electrode material synthesized using pure lanthanum oxide.

Investigations to deposit Ni-YSZ fuel electrode by a non-EVD process have also shown great promise. Deposition of a Ni-YSZ slurry over the YSZ electrolyte followed by sintering has yielded fuel electrodes that are equivalent in electrical conductivity to those fabricated by the EVD process. Cells fabricated with only one-EVD step (sintered fuel electrode, plasma sprayed interconnection, and EVD electrolyte) have shown electrical performance equivalent to those of the two-EVD steps (plasma sprayed interconnection, EVD electrolyte, and EVD fuel electrode) cells. In fact, the sintered fuel electrode polarization is even lower than the already very low (7-15 mV) EVD fuel electrode polarization. This is believed to be due to a larger contact area and a greater number of electrochemically active sites at the electrolyte/sintered fuel electrode interface. This fuel electrode sintering process is currently being scaled up for cell manufacturing.

In the very near future, the AES cell production process will use EVD for only the electrolyte. The EVD process deposits very thin (20 to 40 μm thick), gas-tight electrolyte film over the porous air electrode, reliably, uniformly, and in acceptable cycle time. Nonetheless, deposition of the YSZ electrolyte film by a non-EVD technique such as colloidal/electrophoretic deposition of YSZ over porous air electrode tube followed by sintering is also being investigated.

AES CELLS IN SOFC POWER GENERATION SYSTEMS

AES cells have been tested in two 25 kW systems, each consisting of 576 50-cm active length cells (with EVD electrolyte, EVD fuel electrode, and plasma sprayed interconnection). One system was operated at the Southern California Edison Company's Highgrove Generating Station, under a program with the U.S. Department of Defense's Advanced Research Projects Agency (ARPA). This system was successfully operated for 5,582 h before the project completion. During this time, the system endured five thermal cycles to room temperature, produced up to 27 kW on three different fuels (natural gas, DF-2 diesel, and JP-8 jet turbine fuel), and showed no evidence of performance degradation.

The other system, built for a consortium of Osaka Gas and Tokyo Gas, is still under operation and has passed 8,800 h (>1 year) of successful operation on natural gas without

any performance degradation. During this period, the unit has achieved 25 kW of power output and has endured five thermal cycles to ambient temperature.

A 100 kW SOFC power generation system is presently being built for delivery to a consortium of Dutch and Danish utilities (EDB/ELSAM). The system utilizes state-of-the-art AES cells (2.2 cm diameter, 150 cm active length) with plasma sprayed interconnections.

SUMMARY

State-of-the-art air electrode supported SOFCs have exhibited significant improvements in performance, reliability, and ability to sustain thermal cycles, over previous tubular design. This has been confirmed by successful operation of two 25 kW power generation systems employing such cells. In addition, very significant cost reductions have been achieved by adopting non-EVD processes in cell production; further reductions in materials and processing costs will be realized when the programs currently underway are proven successful and are implemented in cell manufacturing.

ACKNOWLEDGMENTS

Westinghouse acknowledges the guidance and assistance of Mr. William Smith, Project Manager, Office of Product Technology Management, Morgantown Energy Technology Center, U.S. Department of Energy, in the course of the Cooperative Agreement spanning the period from December 1, 1991 through November 30, 1996.

REFERENCES

1. S. C. Singhal, "Recent Progress in Zirconia-Based Fuel Cells," in Proceedings of the Fifth International Conference on the Science and Technology of Zirconia, edited by S.P.S. Badwal, M. J. Bannister, and R.H.J. Hannink, Technomic Publishing Company, Lancaster, PA, pp. 631-651, (1993).

2. U. B. Pal and S. C. Singhal, "Electrochemical Vapor Deposition of Yttria-Stabilized Zirconia Films," J. Electrochem. Soc., Vol. 137, pp. 2937-2941, (1990).

3. W. G. Parker and F. P. Bevc, "SureCELL™ Integrated Solid Oxide Fuel Cell/Combustion Turbine Power Plants for Distributed Power Applications," in Proceedings of the 2nd International Fuel Cell Conference, New Energy and Industrial Technology Development Organization, Kobe, Japan, pp. 275-278, (1996).

STATUS OF-SOFC DEVELOPMENT AT SIEMENS

W. Drenckhahn, L. Blum, H. Greiner
Siemens AG, Power Generation Group
Freyeslebenstr. 1, 91058 Erlangen, Germany

The Siemens SOFC development programme reached an important milestone in June 1995. A stack operating with hydrogen and oxygen produced a peak power of 10.7 kW at a current density of 0.7 A/cm² and was running for more than 1400 hours. The SOFC configuration is based on a flat metal separator plate using the multiple cell array design. Improved PENs, functional layer and joining technique were implemented. Based on this concept, a 100 kW plant was designed.

The SOFC development at Siemens has been started in 1990 after a two years preparation phase. The first period with the goal of the demonstration of a 1 kW SOFC stack operation ended in 1993. This important milestone was finally reached in the begin of 1994. The second project phase with the final milestone of a 20 kW module operation will terminate at the end of 1996. This result will form a basis for the next phase in which a 50 to 100 kW pilot plant will be built and tested.

The planar design of the Siemens high-temperature fuel cell combines metallic and ceramic materials and allows high power densities.
A fuel cell stack consists of two metallic end plates and several bipolar plates containing channels which direct the process gases to the electrochemically active elements. A main task has been to adapt the thermal expansion coefficient of the metallic plate to that of the electrolyte made of 8YSZ and at the same time attaining high corrosion resistance. These goals have been reached with a new metal alloy called $CrFe5Y_2O_3$1, which has been developed together with an Austrian partner, Metallwerke Plansee. This metallic bipolar plate has good electrical conductivity making it especially well-suited for high current densities, and produces a very uniform temperature distribution due to its good thermal conductivity (1). Its high mechanical strength at elevated temperatures permits the manufacture of large plates as well as large-volume stacks consisting of numerous individual cells.

A characteristic of the Siemens design is the multiple cell array concept (2) which depends on the manufacture of large plates as mentioned above. It allows the arrangement of several ceramic single cell elements (so-called PENs) in parallel in one layer. By this measure larger electrode areas can be realized in one stack. The actual bipolar plate has dimensions of 260 x 260 mm². This allows the placement of 16 PENs of the size 50 x 50 mm² in parallel in one layer. The total electrode area per layer is 256 cm².

On the anode side, a Ni-grid works as functional layer to provide good electrical contact. For this purpose $LaCoO_3$ is used on the cathode side. This perovskite is applied by wet spraying of a powder with a certain grain size by an air brush method. This results in a deformable layer compensating the thickness differences of the large number of parts which have to be assembled in one layer in parallel as well as in series.

Decreasing the internal cell resistance, mainly by reduction of the polarization losses at the electrode/electrolyte interfaces, has led to improved cell behaviour with a power output of 0.9 W/cm² (current density of 1.2 A/cm² at a cell voltage of 0.75 V, reacting hydrogen and air at 950 °C). Using a mixture of hydrogen with 50 % water vapour a power density of 0,6 W/cm² was reached. This power output is reduced by about 45 %, if the operating temperature is lowered to 850 °C. The different current-voltage relations are illustrated in fig. 1.

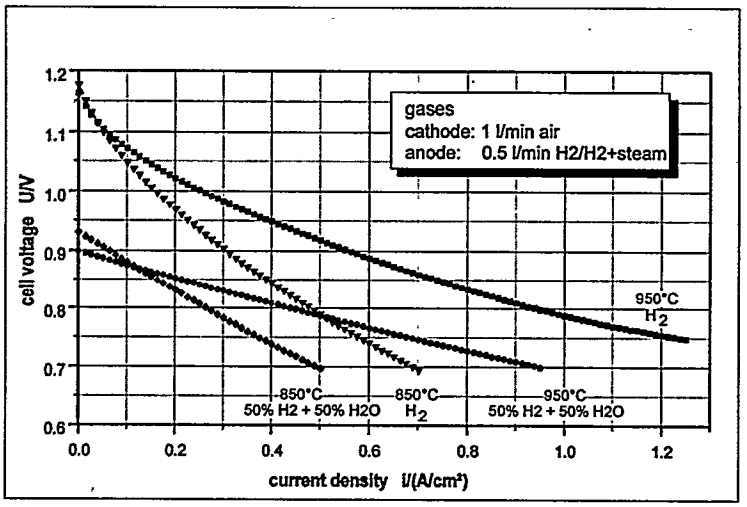

Fig. 1: I/U Curves of Improved Cells with Different Gases, at 850 and 950 °C

Parallel to the improvement of current-voltage relations, also the long term behaviour has been investigated. Changes in electrode preparation and micro structure resulted in degradation rates of less than 2 % in 1000 hours, tested at 950 °C in ceramic housing in H_2/H_2O-atmosphere of 1:1. At 850 °C no degradation could be observed over a period of 4500h. In a first long term test at 850 °C in a metallic housing, a degradation rate of 2 % per 1000h was observed during 2000h of operation. First tests at 950 °C, using a protective layer against chromium evaporation showed similar degradation rates as tests in ceramic housings (3).

A very important step towards manufacturing of bigger stacks has been the transfer of the PEN manufacturing from laboratory scale to a pilot plant. In this plant, 30000 electrolytes of the size 50 x 50 mm² or 10000 parts of the size 100 x 100 mm² can be manufactured per year. The capacity of screen printing and sintering of electrodes is slightly higher. This means PENs for a module up to 100 kW power (operating with air and 80% fuel utilization) can be manufactured per year. The production of PENs with the size 100 x 100 mm² has been started in the beginning of 1996.

Based on the design described above, in June 1995 a stack with 80 cell layers has been assembled, each layer consisting of 16 parallel PENs, which means 1280 PENs with a total electrode area of about 2 m². The stack had dimensions of 260 x 260 x 260 mm³, including end plates.
After brazing and anode reduction the stack performed well. The open circuit voltage of the stack was 104 V. The mean voltage of a single layer was 1.3 V, which indicates that all PENs have been sealed gas tight to the bipolar plates. The initial loading of the stack showed a power output of 10.7 kW (corresponding stack voltage 60 V, mean cell voltage 0,75 V ± 50 mV) at 950 °C and gas utilisation of 50 %. Further loading of the stack was limited by the electrical equipment of the test stand. Operating with hydrogen and air gave a power output of 5.4 kW. The power output at 850 °C was still 4.1 kW. The used PENs were of an older type than described above. The different current-voltage relations of the stack are plotted in fig. 2.

After a number of different I/U-measurements, the stack was operated at constant load of 200 - 300 mA/cm² for 1000 hours at 850 °C. During this time, the stack showed a relatively high degradation rate and compared to the initial performance a power loss of 19 % was observed at the designed load of 270 mA/cm². Afterwards, a thermal cycle of 950 °C/RT/950 °C was run without serious damage to the stack.

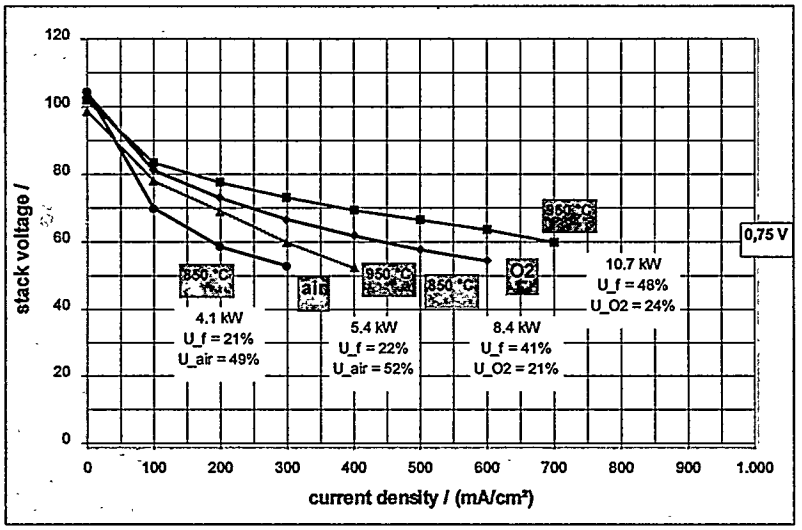

Fig. 2: I/U Curves of 10 kW Stack

Based on these results a 20 kW system was designed and built. It is suited for the operation with hydrogen and air (with the possibility to shift to oxygen).
It will be a self-sustaining system down to a power output of about 10 kW. Therefore, the heat loss to the environment was reduced to about 4 kW. The test facility is designed in a manner that 4 stacks can be operated in parallel. It is controlled by a stored programme computer. Fuel gas flow is adjusted proportional to the load and the air flow regulated so as to keep the max. stack temperature constant. The gases are preheated by the hot waste gases in specially designed recuperative heat exchangers. The plant will be put into operation at the end of August 96. Then the integration and test of the stacks will follow.

The design described above is used as a basis for the layout of bigger stacks and modules.
The design and manufacturing of bipolar plates of the size 360 x 360 mm² has been started, implementing 9 PENs of the size 100 x 100 mm² with a total electrode area of 729 cm² in one layer.
Based on this, it is planned to build up a 50 to 100 kW module consisting of 25 kW stacks till end of 1998. This results in stacks with a height of about 0.5 m.
Investigations on system behaviour and system calculations have led to a flow scheme of a 100kW combined heat and power plant with an electrical efficiency of about 50% and a total

efficiency above 90% (fig. 3). These values are based on the use of air and natural gas with internal reforming.

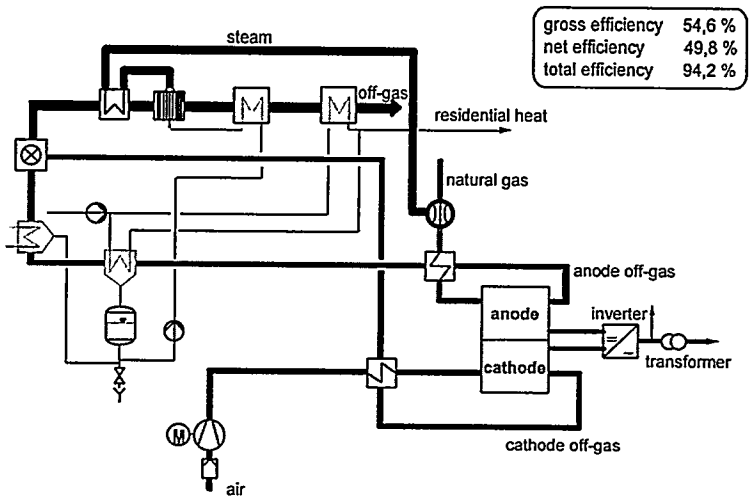

Fig. 3: Flow Scheme of a 100 kW CHP Plant with Heat Recovery

Conclusions

The test results described above proved the feasibility of manufacturing and operating larger stacks based on the multiple cell design using metallic bipolar plates.
The development of PENs with high power density shows the potential of this SOFC technology. The aim must be to reach these values as near as possible under real operating conditions and to further improve the long term stability.
High electrical and system efficiencies can be attained, even for plants with a power output of 100 kW. This represents a great advantage compared to existing technologies.

Acknowledgements

The European Community (research contract JOUE-CT-92-0105), the German Ministry of Education, Research and Development (BMBF) and the MWMT of Nordrhein-Westfalen are greatly acknowledged for financial support.

References

1. H. Greiner, T. Grögler, W. Köck, R. Singer, Chromium Based Alloys for High Temperature SOFC Applications, 4th International Symposium on SOFC, 1995
2. H. Greiner, E. Ivers-Tiffée, W. Wersing, European Patent 0 425 939 B1
3. E. Fendler, R. Henne, R. Ruckdäschel, H. Schmidt, Protecting Layers for the Bipolar Plates of Planar SOFCs Produced by VPS, 2nd European SOFC Forum, 06-10 May 1996, Oslo/ Norway

DEVELOPMENT STATUS OF PLANAR SOFCs AT SANYO

Yasuo Miyake, Yukinori Akiyama, Takashi Yasuo,
Shunsuke Taniguchi, Masataka Kadowaki and Koji Nishio

New Materials Research Center, SANYO Electric Co., Ltd.
1-1, Dainichi-higashimachi, Moriguchi City, Osaka 570, Japan
Telephone: +81-6-900-3553 (Direct)
Facsimile: +81-6-900-3556
E-Mail: n99miyake@yd000.a1.sanyo.co.jp

Hirokazu Sasaki

New Energy and Industrial Technology Development Organization (NEDO)

ABSTRACT

A 2 kW class combined cell stacked module (182 cm^2 × 4× 17) was examined. An output power of 2.47 kW and output power density of 0.20 W/cm^2 were obtained at the current density of 0.3 A/cm^2.

The temperature uniformity is an important factor to develop large scale SOFC modules. Therefore, in this 2 kW class module. one cell was divided into four smaller unit cells to decrease temperature difference across these cells. Moreover, an internal heat-exchanging duct was arranged to spend the surplus heat effectively in the middle of the module.

As for the basic research, the followings were investigated to improve thermal cycle characteristics. One was to adopt a silica/alumina-based sealing material in order to absorb the thermal expansion difference between the electrolyte and the separator. Deterioration was quite small after 12 thermal cycles with a 150 by 150 mm single cell. The other was to use a heat-resisting ferritic alloy as a separator in a 50 by 50 mm single cell in order to decrease the thermal expansion coefficient of the separator. High performance was obtained for 2000 hours at 900 ℃ in an endurance test and deterioration was quite small after a thermal cycle.

EXPERIMENTAL

Module

Figure 1 shows the schematic diagram of the combined cell stacked module. The single combined cell consisted of four unit cells, and active electrode area of each unit cell was 182 cm^2. A 2 kW class combined cell stacked module (182 cm^2 × 4× 17) was examined. The each size of the electrolyte (3 mol% Y_2O_3 partially stabilized ZrO_2) was 150 mm × 200 mm × 0.2 mm^t. A heat-resisting alloy (Inconel 600) was used for the separators. The separators were 350 mm × 350 mm in size. A

form of a gas flow, which consisted of an inner manifold, a counter-flow and an oxidant gas flow with side exhaust, was adopted to the combined cell as well as a 1 kW class module[1]. An internal heat-exchanger duct was arranged at the center in order to decrease the temperature differences within face of combined four unit cells. The temperature profile was measured by thermocouples inserted into the separators. A mixture of 8 mol% Y_2O_3-stabilized ZrO_2 (8YSZ) and NiO was used for the anode material. It was applied to the electrolyte by screen printing and sintered for 2 hours at 1300 ℃. A mixture of $La_{0.9}Sr_{0.1}MnO_3$ (LSM) and 8YSZ was used for the cathode. It was applied to the electrolyte and sintered for 4 hours at 1100 ℃. A mixture of LSM and La_2O_3 was applied to the cathode similarly to form the cathode second layer.

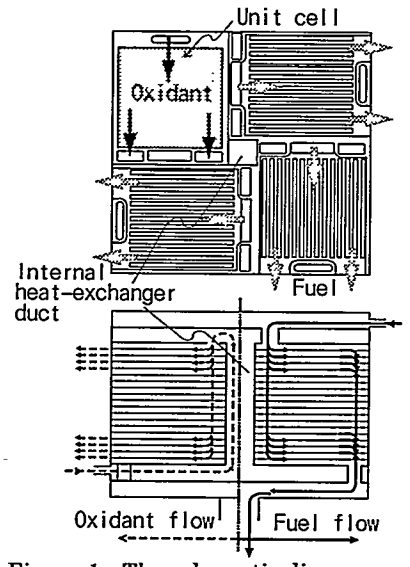

Figure 1 The schematic diagram of the combined cell stacked module

Thermal cycle test of the single cell

Thermal cycles were carried out for a 150 by 150 mm single cell using different sealing materials. A silica/alumina-based sealing material was adopted in order to absorb the thermal expansion difference between the electrolyte and the separator. A heat-resisting alloy (Inconel 600) was used for the separators.

Endurance test of ferrite alloy separator

In order to improve the thermal cycle characteristics, a ferrite alloy was examined for the separator material because its thermal expansion coefficient is smaller than that of nickel-based alloys. A heat-resisting ferrite alloy containing a small amount of rare earth metals was used for the separator and a 50 by 50 mm single cell test was carried out at 900 ℃.

RESULTS AND DISCUSSION

Module

Figure 2 shows V-I and power characteristics of this module. The fuel utilization (Uf) and the oxidant utilization (Uox) were 15 % and 30 % at 0.3 A/cm^2, respectively. An output power of 2.47 kW and output power density of 0.20 W/cm^2 were obtained at the current density of 0.3 A/cm^2. The output power density was equivalent to that of the 1 kW class module (160 cm^2 × 30) which was previously reported[1)2)]. It was therefore considered that the combined cell structure was effective for higher output power SOFC modules, because there was no reduction of

output power density by adopting this structure.
Good performance was obtained up to Uf = 80 % of operation for a single combined cell, so the uniformity of the gas distribution was confirmed.

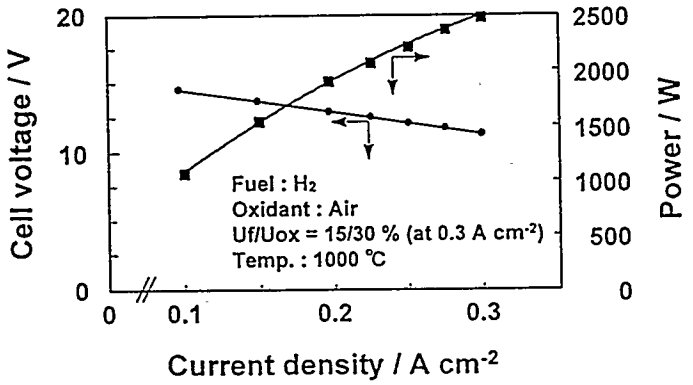

Figure 2 V-I and power characteristics of the module

Thermal cycle test of a single cell

Figure 3 shows the thermal cycle characteristics of single cells using silica/alumina for sealing materials. Deterioration of the V-I characteristics after 12 thermal cycles was quite small. A substantial improvement of the thermal cycle characteristic was observed by employing silica/alumina for sealing.

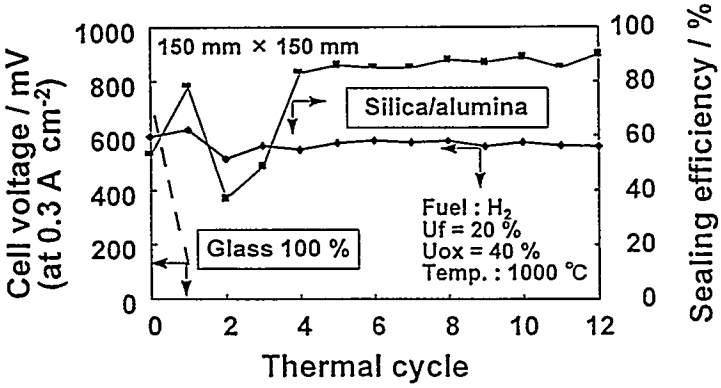

Figure 3 The thermal cycle characteristics of single cells using silica/alumina for sealing materials

Endurance test of ferrite alloy separator

Figure 4 shows the result of the cell endurance test with the heat-resisting ferrite alloy separator. High performance was obtained for 2000 hours at 900 ℃. Thus, the ferrite alloy is expected to serve as a separator material for high-performance SOFCs.

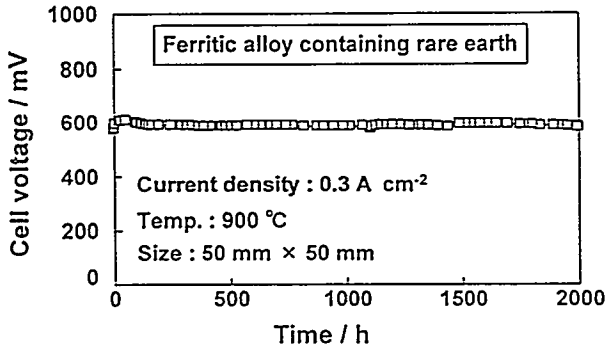

Figure 4 The result of the cell endurance test with the heat-resisting ferrite alloy separator

SUMMARY

(1) An output power of 2.47 kW and output power density of 0.20 W/cm² were obtained with the combined cell stacked module.
(2) Cell performance deterioration was quite small after 12 thermal cycles using a silica/alumina-based sealing material for a 150 by 150 mm single cell.
(3) High performance was obtained for 2000 hours at 900 ℃ of operation using the heat-resisting ferrite alloy separator in a 50 by 50 mm single cell.

ACKNOWLEDGMENT

Part of this work was performed as an R&D project of the New Energy and Industrial Technology Development Organization (NEDO) under the New Sunshine Project of the Agency of Industrial Science and Technology, MITI.

REFERENCES

1) Y. Miyake, T. Yasuo, Y. Akiyama, S. Taniguchi, M. Kadowaki, H. Kawamura and T. Saito, Proceedings of the 4th International Symposium on Solid Oxide Fuel Cells (1995) p.100.
2) M. Kadowaki, Y. Akiyama, T. Yasuo, S. Taniguchi, H. Kawamura, Y. Miyake and T. Saito, Proceedings of the 35th Battery Symposium in Japan (1994) p.323.

ALLIEDSIGNAL SOLID OXIDE FUEL CELL TECHNOLOGY

Nguyen Minh, Kevin Barr, Patrick Kelly, and Kurtis Montgomery
AlliedSignal Aerospace Equipment Systems
2525 West 190th Street
Torrance, CA 90504-6099

INTRODUCTION

AlliedSignal has been developing high-performance, lightweight solid oxide fuel cell (SOFC) technology for a broad spectrum of electric power generation applications. This technology is well suited for use in a variety of power systems, ranging from commercial cogeneration to military mobile power sources. The AlliedSignal SOFC is based on stacking high-performance thin-electrolyte cells with lightweight metallic interconnect assemblies to form a compact structure. The fuel cell can be operated at reduced temperatures (600° to 800°C). SOFC stacks based on this design has the potential of producing 1 kW/kg and 1 kW/L. This paper summarizes the technical status of the design, manufacture, and operation of AlliedSignal SOFCs.

STACK DESIGN

The AlliedSignal SOFC stack design is a flat-plate concept that places ceramic cells in a compliant metallic housing. In this design, single cells are connected in electrical series via metallic fins and interconnects (interconnect assemblies). Metallic fins and interconnects are made from thin cross-section foils. The fins, attached to the interconnects, form flow channels for fuel and oxidant gases. A crossflow version of this design is schematically shown in Figure 1.

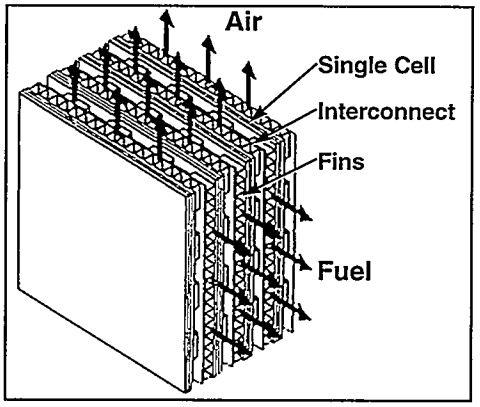

Figure 1 Stack Design

This design has two key features:

- Single cells used in this design contain supported thin electrolytes. Thin electrolytes reduce component weight, improve cell performance, and minimize internal resistance, allowing efficient operation at reduced temperatures. The advantages of reduced-temperature operation include wider choice of materials, longer cell life, increased reliability, and potentially reduced fuel cell cost.
- The metallic interconnect assembly, made from thin foils, is designed to provide sufficient compliancy to minimize thermal expansion mismatch stresses and form a compact, lightweight structure.

This stack design has the potential of having low material and manufacture costs and can produce high power densities while maintaining high efficiency at reduced temperatures.

STACK FABRICATION

AlliedSignal has developed a simple and cost-effective process for fabricating multicell stacks.

(i) Thin-electrolyte cells are made by tape calendering. Tape calendering is a conventional ceramic forming method that involves squeezing a softened thermoplastic polymer/ceramic mix between two rolls to produce a continuous sheet of material. The tape calendering process for fabricating thin-electrolyte cells involves progressive rolling (calendering) of green (unfired) ceramic tapes to form a thin electrolyte (1 to 10 μm thick) on an anode support. The electrolyte/anode bilayer is fired at elevated temperatures to remove the organics. The cathode is then applied on the sintered bilayer to produce a complete cell.

(ii) Metallic interconnect assemblies are fabricated by conventional stamping and joining techniques.

Figure 2 shows as an example a photograph of a typical thin-electrolyte cell fabricated by tape calendering. A photograph of a five-cell stack incorporating thin-electrolyte cells and metallic interconnect assemblies is given in Figure 3.

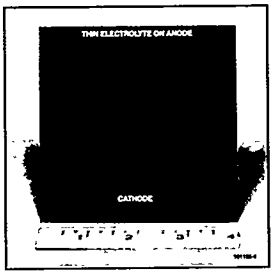

Figure 2 Thin-Electrolyte Cell

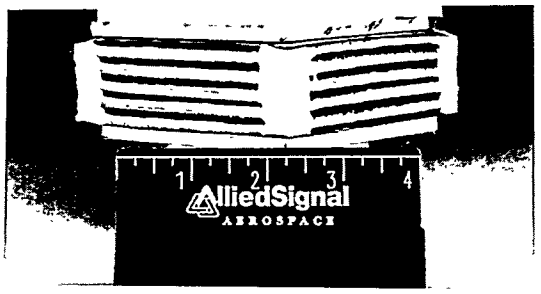

Figure 3 Five-Cell Stack

This fabrication process has several important advantages: simplicity, scalability, and cost effectiveness. In addition, the process is material-independent, thus providing fabrication versatility. Furthermore, the process can be designed for high-volume production using available commercial equipment.

STACK PERFORMANCE

Numerous multicell stacks have been assembled and performance tested. Several have been thermal cycled without significant structural degradation. Figure 4 shows performance curves of three two-cell stacks (footprint area of 25 cm^2) tested with hydrogen fuel and air oxidant at about 800°C. These stacks produced a maximum power of about 25 W with the power density of about 650 mW/cm^2 at 800°C.

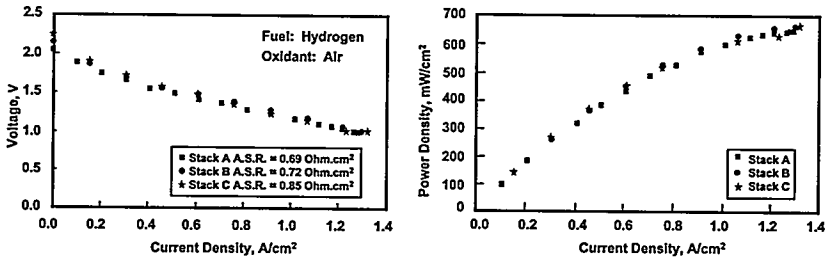

Figure 4 Performance Curves of Two-Cell Stacks

Figure 5 shows voltage/current density and power curves of a five-cell stack (footprint area of 100 cm²) obtained at 800°C. This stack produced peak power of about 270 W at 800°C and 185 W at 700°C, corresponding to power densities of 600 mW/cm² and 410 mW/cm², respectively. This is the best stack performance reported to date at reduced temperatures. Although the design has not been optimized, stack power densities achieved are exceeding or close to the goals of 1 kW/kg and 1 kW/L (Figure 6).

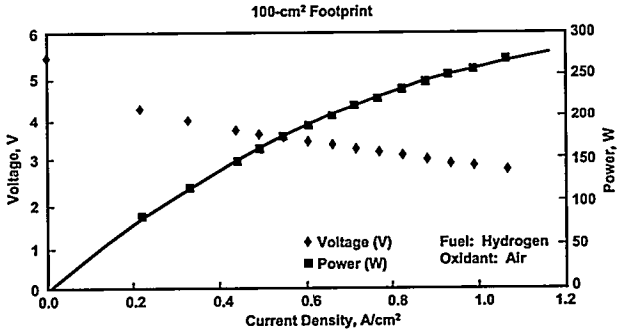

Figure 5 Performance of Five-Cell Stack

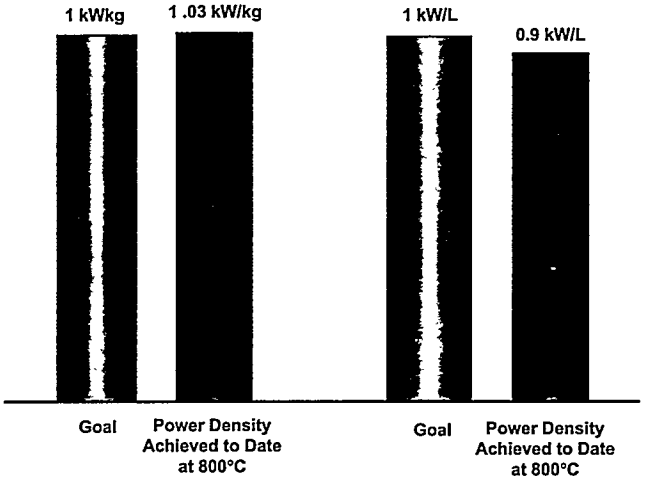

Figure 6 Stack Power Densities

ACKNOWLEDGEMENTS: This work is supported in part by Gas Research Institute (GRI) under Contract 5092-260-2568 and Defense Advanced Research Projects Agency (DARPA) under Contract MDA972-94-C-0029.

TECHNICAL PROBLEMS TO BE SOLVED BEFORE THE SOLID OXIDE FUEL CELL WILL BE COMMERCIALIZED

C. Bagger[1], N. Christiansen[2], P.V. Hendriksen[1], E.J. Jensen[2], S.S. Larsen[2], M. Mogensen[1]

[1] Materials Department, Risø National Laboratory, P.O.Box 49, DK-4000 Roskilde, Denmark

[2] Haldor Topsøe A/S, Nymøllevej 55, DK-2800 Lyngby, Denmark

1. INTRODUCTION

The problems which must be solved before SOFC-systems are competitive with todays power production technology are of both technical and economical nature. The cost of SOFC stacks at the 25 kW level of today is about 30,000 ECU/kW /1/ and it is bound to come down to about 500 ECU/kW. The allowable cost of a SOFC system is anticipated to be around 1500 ECU/kW.

As part of the Danish SOFC program (DK-SOFC) a 0.5 kW stack was built and tested during the second half of 1995 /2/. Based upon the experience gained, an economic analysis has been made. The tools required to approach an economically acceptable solution are outlined below.

2. ECONOMIC ANALYSIS

The Danish 0.5 kW SOFC stack was built according to the Bipolar Flat Plate SOFC (BFP-SOFC) concept. 50 cells, each with an active area of 50 cm^2, produced the targeted 0.5 kW with an overall area specific internal resistance (ASR) of 1 $\Omega \cdot cm^2$ at 1000°C. Cheap ceramic techniques with a potential for upscaling had been selected for the technological development. The 8x8 cm electrolyte was tape cast from high purity zirconia (8 mole% yttria) to a sintered thickness of 160µm. 5-10µm composite electrode layers with La(Sr)MnO_3(LSM) /3/ and NiO /4/, respectively, were deposited by spray painting of ceramic slurries and sintered. Current collecting layers were made from LSM by tape casting and from NiO/YSZ by spray painting. Ceramic interconnects were fabricated from La(Sr)Cr(V)O_3(LSCV) /5/ by uniaxial pressing and sintering at high temperature. The plates were machined with diamonds to give suitable surfaces and cross flow gas channels. The stack was assembled from quality controlled 10-cell substacks.

Based upon the fabrication experience of the first stack, costs were calculated to 3,000-10,000 ECU/kW, depending on the area specific internal stack resistance. The lower limit of the fabrication cost corresponds to 0.4 Ωcm^2. The materials cost, including actual losses during the various fabrication processes and components rejected by quality controls, constitutes ~50% (Fig. 1). The remaining 50% are the cost of capital and manpower in a pilot plant with a total production capacity of 2 MW SOFC stacks per year. In spite of the low-cost ceramic techniques chosen, the stack cost requires a reduction of more than 10 times before it is of commercial interest (500 ECU/kW). A number of tools are available for reduction:

1. Redesign of identified high-cost elements
2. Cheaper materials where acceptable
3. Reduction of the number of components in the repetitive unit of the stack
4. Reduction of losses during fabrication
5. Automation of the production

The interconnect is by far the most expensive individual stack element. The requirement of gas tightness implicates low materials porosity and the presence of gas channels makes the stack ele-

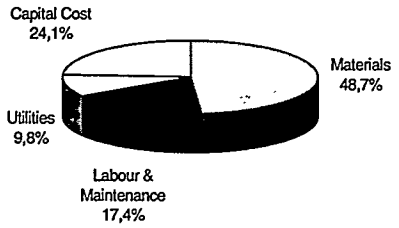

Fig. 1. Distribution of present stack fabrication cost

ment the most voluminous one, altogether maximizing the consumption of the relatively costly lanthanum chromite. The thickness and the layout with channels in cross flow configuration limit the range of applicable ceramic shaping techniques. Increasing demands to planarity minimizes in-plane resistance losses in the electrodes but introduces expensive mechanical grinding after sintering. Reduction of the interconnect element cost clearly requires reconsideration of the design, leading to a lower complexity of the element.

Materials of high purity are usually used for the development of new materials and components in laboratory scale. Commercialization, however, necessitates determination of the importance of purity to enable substitution of frequently used materials with cheaper ones. The cost of pure lanthanum compounds is high. The relatively high content in a stack (Fig. 2) makes the use of much cheaper lanthanide mixtures desirable, and a substitution seems to be acceptable in current collecting elements /6/. The cost of yttrium stabilized zirconia is high, too, when the content of silica, which is detrimental to ion conductivity, is to be kept at a low level. Additions to YSZ which may neutralize the effect of Si in cheaper zirconia are desired.

Generally, losses were high during the laboratory scale fabrication of the stack elements. Mass production and automation will of course reduce the waste fraction somewhat, but losses are to a significant extent inherent to the individual ceramic technique (cut-away green tape, slurry remnants). It is therefore important to establish recycling of waste in the fabrication processes.

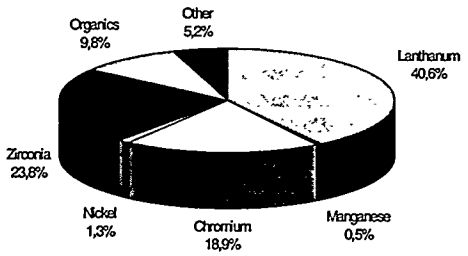

Fig. 2. Distribution of present materials cost

A stack cost reduction factor of 3 may be realized as a result of identified possible improvements of the technology. The relative cost distribution in Fig. 3 shows that materials cost is reduced below 25% of the total, while capital investment cost increases to above 40%.

3. TECHNICAL ANALYSIS

Although a stack ASR of ~1 Ωcm^2 is a reasonable value in the present international context, the value needs improvement to reduce stack volume/kW. The ASR of the individual cells of the standard production was 0.3-0.4 Ωcm^2. Allowing for the resistance of the interconnect, a stack ASR of 0.4-0.5 Ωcm^2 may be realised. This result was actually met by one of the 10-cell substacks constituting the stack. Analysis of stack performance /2/ showed, that the main performance problem was related to dimensional instability of the LSCV interconnect in reducing atmosphere, and the inability of the sealing glass to accommodate the resulting relative in-plane movement between cells and

interconnects. Gas mixing obviously was a main problem, leading to a reduction of the active fuel cell area. Current interrupt measurements showed that for stack sections with less satisfactory performance an increased area specific resistance could be attributed to in-plane current conduction in the thin electrodes.

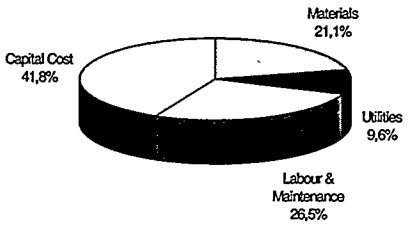

Fig. 3. Assessed distribution of stack fabrication cost after planned optimizations

The performance analysis clearly shows, that the pO_2-related dimensional instability exhibited by the LSCV interconnect cannot be tolerated in high performance stacks. It is necessary to intensify the research for ceramic interconnect materials with much better dimensional stability in reducing atmosphere. Metallic interconnect is an alternative to ceramics, but reduced temperatures are required. The increase in electrode overpotential with decreasing temperatures, however, necessitates further electrode development in order to reach the ASR achieved at higher temperatures.

Few materials have been identified as potential candidates for metallic interconnect, and all have high chromium contents. Oxidation and volatilization of Cr_2O_3 influences ASR and cathode performance adversely, necessitating further development. The presently most advanced metallic interconnect material uses dispersed yttria to reduce the oxidation rate /7/. Fabrication of Cr_2O_3 based alloys usually requires relatively expensive powder metallurgical processes and the presence of yttria boosts the cost of the complex shaped component further due to machining problems.

Cofiring - in the sense of simultaneous sintering of adjacent layers - is often mentioned as a means of reducing the number of sintering steps. Cofiring which includes sintering of the electrolyte membrane is difficult, because sintering temperatures much below 1300°C of YSZ will result in incomplete sintering; cofiring of the YSZ with NiO-based anodes at temperatures above 1300°C may affect the bend strength of the electrolyte adversely assumably due to NiO dissolution in the electrolyte layer, and cofiring with LSM based cathodes at temperatures even below 1200°C may result in the formation of zirconates. The latter prevents full densification of the electrolyte and will affect cathode performance adversely. Cofiring of Ni-based anodes and Cr based interconnect materials at relevant temperatures may also lead to undesired reactions. However, simultaneous firing of non-adjacent layers, e.g. anode and cathode sintering on the two sides of an already sintered electrolyte is a means for reduction of the overall number of sinterings.

Probably, a commercialized SOFC will be fuelled with natural gas. If todays standard anode, the Ni-YSZ-cermet, is exposed to natural gas, carbon precipitation will occur and the anode will be destroyed. Therefore, steam reforming is necessary. The economic calculations show that it is very important to avoid external reforming units which will add to the cost of the SOFC-system (balance of plant). As Ni is a good steam reforming catalyst, internal reforming is in principle possible. However, at 1000°C the endothermic reforming process will be too fast resulting in unacceptable steep temperature gradients at the fuel inlet. Consequently, it is necessary to develop anodes which are either more suitable for internal reforming than todays standard, or preferably able to facilitate direct oxidation of the methane in prereformed natural gas /8/. Prereforming of natural gas will always be necessary to remove hydrocarbons of two or more carbon atoms to avoid carbon deposition in the gas preheating tubes. Natural gas usually contains a few per cent (~5%-10%) of C_2's or higher hydrocarbons.

4. CONCLUSION

An economical analysis of stack fabrication costs, based upon the experience gathered from the first Danish 1/2 kW stack shows, that if an area specific internal resistance of 0.4 Ωcm^2 may be achieved, the stack may be fabricated at 3000 ECU/kW. The fabrication is based upon simple ceramic techniques. This cost is already a major reduction compared to the price published by the European Community /1/ of 30,000 ECU/kW. A number of tools have been identified for further reduction of the stack price: (i) redesign of costly components, (ii) utilisation of cheaper materials where acceptable, (iii) reduction of the number of different components in the stack, and (iv) reduced losses in a highly automated, large scale production. Calculations excluding (iv) show that a reduction to ~1100 ECU/kW is possible. This, however, requires further technological development of the shaping of selected components. More than 40% of the 1100 ECU/kW is capital cost and less than 25% is materials cost. A significant further reduction of the cost towards the assumed commercialisation limit of 500 ECU/kW will have to address a general reduction of the internal stack resistance, as this factor will influence all fabrication costs in the desired direction.

Technically the dimensional instability of the interconnect has to be focused upon, because single sided material expansion during pO_2-changes on the anode side during service will lead to sealing problems and detachment of contacts between the individual stack elements. Presently available metallic interconnect materials are not directly applicable, partly because of high materials cost and high cost of shaping, partly because of the requirement of lower operation temperatures to reduce oxidation and Cr_2O_3 poisoning of electrodes. Finally, it is mandatory that an anode either with an adjusted internal reforming rate or with the ability of direct methane oxidation is developed.

ACKNOWLEDGEMENT

This work was supported by the Danish Energy Agency and ELSAM.

REFERENCES

1. European Commission (1995). A ten year fuel cell research, development and demonstration strategy for Europe. Separate document from the European Commission's Directorate General XII and XVII.
2. Bagger, C., Juhl, M., Hendriksen, P.V., Larsen, P.H., Mogensen, M., Larsen, J.G. and Pehrson, S. (1996). Development and testing of a Danish 0.5 kW SOFC stack. In: Proc. 2nd European Solid Oxide Fuel Cell Forum, 6-10 May 1996, Oslo, Norway. Edited by Bernt Thorstensen, p. 175-184.
3. Bagger, C., Kindl, B. and Mogensen, M. (1995). Solid Oxide Fuel Cell, European patent, pending, no. 94908982.5
4. Bagger, C. (1992). Improved production methods for YSZ electrolyte and Ni-YSZ anode for SOFC. In: Program and Abstracts of 1992 Fuel Cell Seminar, November 29 - December 2, Tucson, Arizona, 241-244.
5. Carter, J.D. (1996). A sintering acid for doped lanthanum chromite. European patent, pending, no. 94923682.2.
6. Singhal, S.C. (1996). Status of solid oxide fuel cell technology. In: These proceedings.
7. Köck, W., Martinz, H.-P., Greiner, H. and Janousek, M. (1995). Development and processing of metallic Cr based materials for SOFC parts. In: Solid oxide fuel cells IV. Edited by M. Dokiya, O. Yamamoto, T. Tagawa and S.C. Singhal, p. 841-849.
8. Mogensen, M., Kindl, B. (1994). Solid state fuel cell and process for the production thereof. European Patent 0571494 and US Patent 5, 350, 641.

DEVELOPMENT OF LOW TEMPERATURE SOLID OXIDE FUEL CELLS

W.T. Bakker, R. Goldstein
Electric Power Research Institute
3412 Hillview Avenue
Palo Alto, CA 94303

Introduction

The historical focus of the electric utility industry has been central station power plants. These plants are usually sited outside urban areas and electricity was delivered via high voltage transmission lines. Several things are beginning to change this historical precedent. One is the popular concern with EMF as a health hazard. This has rendered the construction of new lines as well as upgrading old ones very difficult. Installation of power generating equipment near the customer enables the utility to better utilize existing transmission and distribution networks and defer investments. Power quality and lack of disturbances and interruptions is also becoming increasingly more important to many customers. Grid connected, but dedicated small power plants can greatly improve power quality. Finally the development of high efficiency, low emission, modular fuel cells promises near pollution free localized power generation with an efficiency equal to or exceeding that of even the most efficient central power stations.

Solid oxide fuel cells (SOFC) are especially attractive for small installations, i.e., 100Kw. However, the present ZrO_2 based fuel cells must operate at about 1000°C due to the relatively low conductivity of Yttria doped zirconia. This requires use of costly ceramics or expensive metal alloys for interconnects (bipolar plates), and balance of plant components such as seals, ducts and heat exchangers. The life of SOFC is also limited at 1000°C due to interdiffusion of elements between electrodes and the electrolyte. Operating a SOFC at 650-800°C, will completely eliminate performance degradation due to interdiffusion and allow the use of inexpensive stainless steels for interconnects and balance of plant.

For the above reasons, EPRI is supporting several projects supporting the development of SOFC's capable to operate below 800°C. These projects fall into 3 broad categories: 1) Reduce the thickness of the electrolyte to reduce its resistivity. Calculations show that a 10μm thick ZrO_2 base electrolytes will have a lower resistance at 800°C than standard tape cast 150μm electrolytes at 1000°C. 2) Use of more highly conducting electrolytes. Both doped CeO_2 (Ceria) and doped $LaGaO_3$ are being studied. 3) Improve the efficiency and decrease the overpotentials at the electrodes. Projects in the three areas are briefly described below.

Results

1. Thin ZrO_2 Base Electrodes

Projects in this area carried out at LBNL and the University of Utah. Both projects use colloidal dispersions to cast a thin film of Yttrium stabilized Zirconia (YSZ) electrolyte on a porous Ni-ZrO_2 cermet anode. The thickness of the electrolytes produced at LBNL is generally less than 10 μm, while those produced at the U of Utah are in the 10-20 μm range. Single fuel cells using a strontium doped lanthanum manganite cathode and platinum current collectors were prepared and showed excellent I-V performance in the 700-800°c temperature range. Table 1 and Figure 1 show some of the data produced by LNBL. Efforts to build small stacks are underway.

Table 1 Performance of Thin Film SOFC at 650-800°C

Temperature (°C)	Power Density (mC/cm^2)	Voltage (V)	Current Density (mA/cm^2)
650	140	0.51	280
700	350	0.51	710
750	575	0.48	1250
800	1935	0.43	4500

2. Alternate Electrolytes

There are several electrolytes, which have a considerable higher ionic conductivity than YSZ. The most well known and studied electrolyte is doped CeO_2. A problem with CeO_2 is that it is partially reduced to Ce_2O_3 on the anode side, which induces electronic conduction. This in turn will reduce the open circuit voltage and thus reduce efficiency. However, Prof. Riess[1] has shown that a small amount of electronic conductivity can be tolerated, provided the fuel cell is operated close to its maximum power output. Therefore, a project to study the use of CeO_2 electrolytes has been conducted at Ceramatec. Earlier problem with deterioration of performance with time were overcome and stable performance in single cells in excess of ten thousand hours has been demonstrated. Ceria electrolytes appear to be very compatible with the selected electrode materials, resulting in very flat I-V curves. Thus, the performance of Ceria based fuel cells at 700-800°C is similar to that of Zr O_2 based fuel cells at 1000°C, when operated at 0.6V. This is shown in Figure 2.Efficiency losses due to electronic conductivity are small at 700C or lower.

At the University of Texas at Austin, Prof. Goodenough and his associates have studied the ionic conductivity of doped La GaO_3. When using both cation and anion substitution, a composition with an ionic conductivity of 0.08-1.0 S/cm^2 at 800C was obtained. No electronic conductivity was present even at anode environments (H_2 - 3% H_2O). Single cell experiments showed an OCV near theoretical and a maximum power density of about 350 mW/cm^2. This is much lower than theoretically possible, mainly due to a large anode overpotential.Work on improved electrolyte/electrode compatibility is in progress.

3. Single Component Solid Oxide Fuel Cells

The highest degree of compatibility between electrolyte and electrodes is obtained when all are made of the same base material, i.e., ZrO_2. To achieve the required electronic conductivity and electro catalytic properties, appropriate dopants must be found. The problem is being studied by Prof. W. Worell at the University of Pennsylvania. At present Tb doped ZrO_2 is being studied for the cathode and Ti doped ZrO_2 for the anode. Figure 3 shows that the performance loss at 820°C of a cell with a Tb doped zirconia is considerably lower than that of a conventional LSM cathode. Performance of the TiO_2 doped zirconia anode was about the same as that on Zr_2O_2 - Ni Cermets, which have already a very low overpotential. However, it is expected that debonding between anode and electrolyte will be improved. Scaleup of the technology is planned for next year.

References

1. I. Riess, "The Use of Mixed Ionic/Electronic Conductors in Fuel Cells," Solid State Ionics, 52 (1992) 127-134.

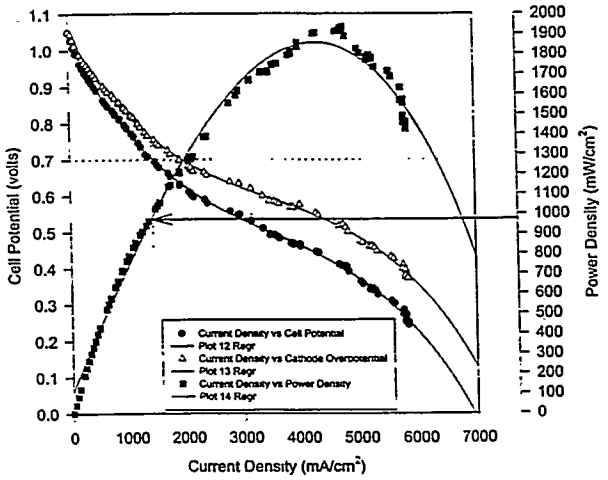

Figure 1. Performance of Thin Film SOFC at 800°C.

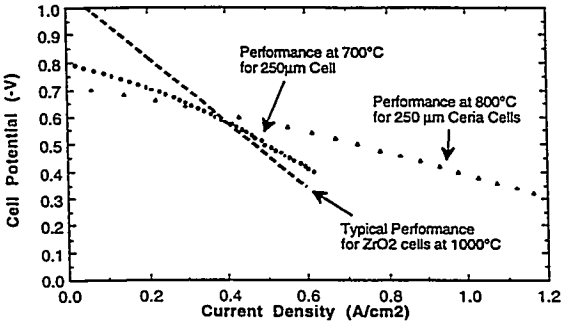

Figure 2. Comparison of Ceria and ZrO_2 SOFC's.

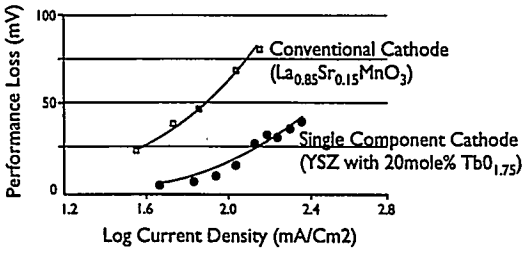

Figure 3. Performance Loss at Cathode of SOFC at 820°C.

DEVELOPMENT OF 1000kW-CLASS MCFC PILOT PLANT

M.Ooue, H.Yasue
MCFC Research Association
87-2 Kamesaki-shinden-asake
Kawagoe-cho, Mie 512 JAPAN
K.Takasu, T.Tsuchitori
New Energy and Industrial Technology Development Organization

1. ABSTRACT

This pilot plant is a part of the New Sunshine Program which has proceeded by the Agency of Industrial Science and Technology of the Ministry of International Trade and Industry.
MCFC Research Association is entrusted with the development of the pilot plant, and constructing it at Kawagoe site.
Following items will be verified by this pilot plant operation.

a. Development of 250kW class stack and confirmation of stack performance and decay rate.
b. System verification such as basic process, control system and operation characteristics, toward commercialization.
c. To get design data for demonstration plant.

2. DEVELOPMENT TARGET

The development targets of this pilot plant are shown in Table 1.

Item	Target
Power Output	1000kW (AC)
Power Generation Efficiency	45%(HHV)
Fuel	LNG
Operation Hours	5000Hr
Stack Decay Rate	1%/1000Hr
Environmental effect	less than regulated value

Table 1. Development Targets

3. BASIC CONCEPT FOR DESIGN

a. System Flow

Process flow sheet of the 1000kW pilot plant is shown in Fig. 1.

b. System configuration

The 1000kW pilot plant's major components are stack, reformer, cathode blower, heat recovery system, electric equipment, control, and utility facilities. Two kinds of fuel cell stacks are used and 4 stacks of 250 kW class in total are connected with two 500kW class inverter. Each 500kW unit has a cathode blower and it can be operated independently. All other equipments are one for this pilot plant. Specification of each components are as follows.

(a) Fuel Cell Stack

Two 250kW cross-flow type stack and two 250kW parallel-flow type stack are used for this pilot plant. By the investigation of the influence of operating temperature on voltage decay rate, the operating temperature of the stacks was modified to be lower than the initial design value.

(b) Reformer

We apply a catalytic burner to the reformer, because the heat value of anode outlet gas is low. Steam / carbon ratio (S/C) for reforming is planned to be 3.5 with allowance to avoid carbon formation and deposition inside the cell.

(c) Cathode Blower

We apply magnetic bearing to the cathode blower for high efficiency under 640 °C.

(d)Heat Recovery System

The heat recovery system is consist of the turbine compressor and the heat recovery steam generator (HRSG).

The turbine compressor has an auxiliary combustor to secure power, that is necessary for the plant start-up and to maintain amount of steam produced by the HRSG.

(e) Electric Equipment

The PWM control type inverter is used to obtain high efficiency and to reduce harmonic distortion. A large capacity IGBT is applied for the inverter device.

(f) Control

The plant is controlled by two operators in the central control room.

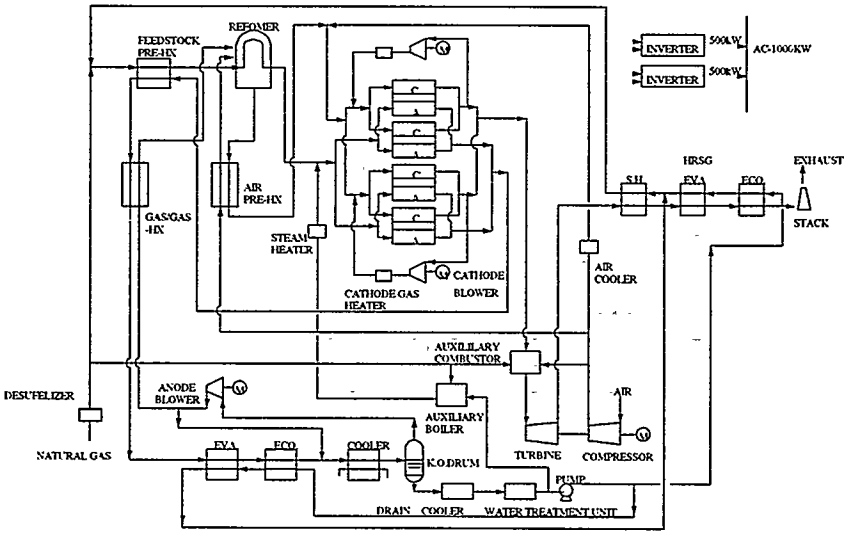

Fig.1 1000kW pilot plant System Configuration

Component	Specification
Fuel cell stack A	250kW x 2, Cross flow type, Cell area 1.20m^2
Fuel cell stack B	250kW x 2, Parallel flow type, Cell area 1.02m^2
Reformer	2-stage catalytic combustion, 18 tubes
Cathode blower	Radial type, Magnetic bearing
Turbine compressor	T: Axial x 2-stage, C: Radial x 2-stage
Heat recovery steam generator	Smoke tube boiler
Anode blower	Radial type
Inverter	500kW x 2, PWM control

Table 2. Specifications of major components

(g) Utility facilities and others

The control air supply line has a back-up line of nitrogen in order to keep operation reliability and safety.

4. PLOT PLAN

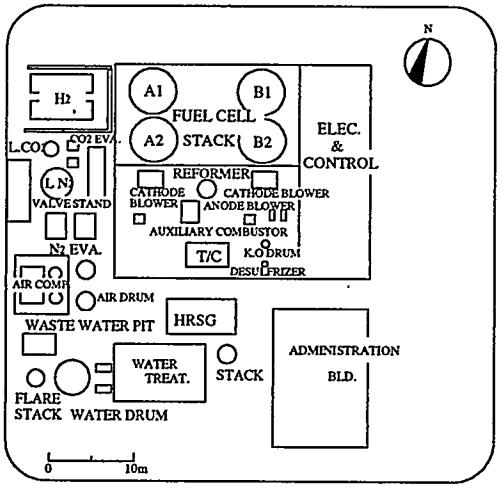

This pilot plant is constructing in Kawagoe Thermal Power Station of Chubu Electric Power Company. The plot plan is shown in Fig. 2. The size of the site is 39.4m x 35.5m. Main components of the pilot plant is placed indoor, except HRSG.

Perspective view of 1000kW pilot plant is shown in Fig. 3.

Fig.2 Plot Plan of 1000kW Pilot Plant

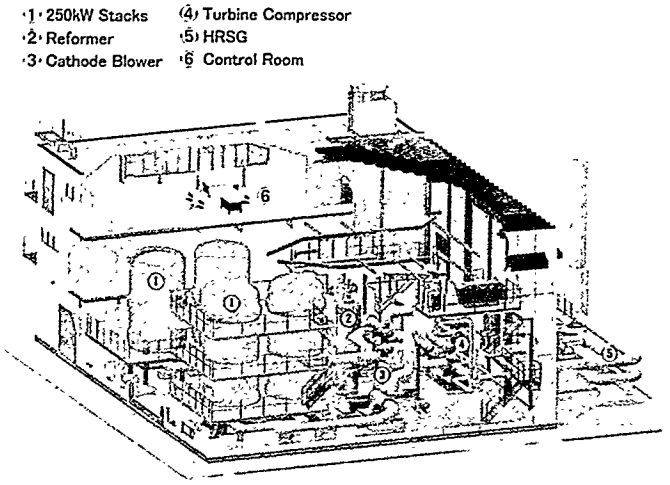

Fig. 3 Perspective view of 1000kW pilot plant

5. SCHEDULE

Development schedule for 1000kW pilot plant is shown in Fig. 4.
In November 1996, the building work of the Kawagoe site will be finished. The plant equipments fabrication will be finished in FY 1996, and they will be installed and adjusted in FY1997. The PAC test will be carried out in FY 1998. And the operation will be carried out in FY 1999.
At present, every equipment are being fabricated by makers. And the Kawagoe MCFC test center is preparing for the equipment installation and PAC test.
The recent photo of the Kawagoe site is shown in Fig. 5.

Fiscal Year	1993	1994	1995	1996	1997	1998	1999
Design							
Equipment Fabrication							
Building							
Equipment Installation							
PAC test							
FC Stack Fabrication & Installation							
Operation							
Evaluation							

Fig. 4 Development Schedule for 1000kW Pilot Plant

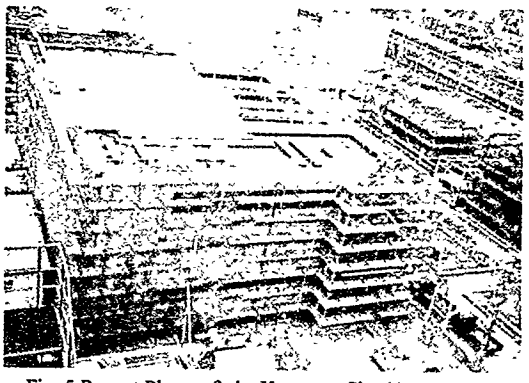

Fig. 5 Recent Photo of the Kawagoe Site (August,1996)

INTEGRATING FUEL CELL POWER SYSTEMS INTO BUILDING PHYSICAL PLANTS

J. Carson
KCI Technologies, Inc.
Hunt Valley, MD 21030

This paper discusses the integration of fuel cell power plants and absorption chillers to cogenerate chilled water or hot water/steam for all weather air conditioning as one possible approach to building system applications. Absorption chillers utilize thermal energy in an absorption based cycle to chill water. It is feasible to use waste heat from fuel cells to provide hydronic heating and cooling. Performance regimes will vary as a function of the supply and quality of waste heat. Respective performance characteristics of fuel cells, absorption chillers and air conditioning systems will define relationships between thermal and electrical load capacities for the combined systems. Specifically, this paper develops thermodynamic relationships between bulk electrical power and cooling/heating capacities for combined fuel cell and absorption chiller system in building applications.

The absorption cycle

Absorption chillers use water vapor at high vacuum as the refrigerant. For discussion, point 1 in the cycle would be the low pressure refrigerant as saturated liquid at approximately 40F. The refrigerant enters the evaporator and removes heat from the working fluid - chilled water - to provide the latent heat for transition to saturated vapor. At point 2, the refrigerant enters the absorber, where it comes into contact with the absorbent - a salt solution with a high affinity for water. The solution is then compressed through a pump and passed to the generator where waste heat effectively boils the refrigerant off to a superheated state at point 3. Once the superheated vapor leaves the generator, it passes through the condenser - point 4 - and the cycle again resembles more conventional refrigeration cycles.

Table 1
Refrigerant Properties

Cycle Pt.	P(PSIA)	T, F	State	h	
1	0.122	40	Sat. vapor	1,078.9	BTU/LB
2	1.354	190	Vapor	1,143.5	BTU/LB
3	1.354	112	Sat. liquid	~80	BTU/LB
4	0.122	40	Throttled	~80	BTU/LB

Table 1 represents state properties of the refrigerant of some typical absorption machines currently available. These machines normally employ an ammonia or lithium bromide solution as the absorbent. Because of the toxicity of ammonia, absorption chillers usually use the lithium bromide solution. During compression and heating, the solution is nominally 54 percent by weight lithium bromide. Once the refrigerant has been "boiled off" in the generator, the remaining solution is 59 percent by weight lithium bromide. When considered from the absorbent side of the cycle, it is essentially a regenerating solvent cycle, where the "strong liquor" absorbs refrigerant in the absorber to become a "weak liquor" and then is regenerated in the generator to become again the "strong liquor." Table 2 contains the performance characteristics for the model used in the analysis.

Table 2
Model Chiller Operational Parameters

Generator vacuum	70 mm Hg (1.354 PSIA)
Evaporator vacuum	6 mm Hg (0.122 PSIA)
Mass fractions	
"Strong" liquor	59%
"Weak" liquor	54%
Generator heat	
Steam	340F, 28 PSIA
Hot water	260F supply (THWS)
	210F return (THWR)

Tables 1 and 2 define the model absorption chiller used in the analysis. Mass and heat balances show that the specific effective heat input Q_R is 15.73 MBTUH/ton cooling, for a coefficient of performance of 0.763. Mass flow rates for the "weak" and "strong" liquors are 141.6 LB_m/HR/ton and 129.6 LB_m/HR/ton, respectively. These flows result in 12 LB_m/HR/ton refrigerant flow.

System Analysis

This analysis treats the cases of molten carbonate fuel cells (MCFCs) and solid oxide fuel cells (SOFCs), because they represent technologies nearer to the market. In both MCFC and SOFC models, anode gas is oxidized in a catalytic burner. The oxidized anode gas and cathode gas are then used to pre-heat incoming fuel and oxidant streams. After the preheat heat exchangers, the streams are combined and pass on to the waste heat recovery system. The waste heat stream is then exhausted, although in the MCFC variant, make-up CO_2 for the cathode is recovered prior to exhaust.

The following are mass balances for the catalytic oxidation of anode gas in MCFCs and SOFCs, respectively:

$$(1+4U_F)CO_2 + 4(1-U_F)H_2 + (4U_F+m-2)H_2O + 2(1+Y)(1-U_F)O_2 + 7.52(1+Y)(1-U_F)N_2 \rightarrow (1+4U_F)CO_2 + (4+m-2)H_2O + 2Y(1-U_F)O_2 + 7.52(1+Y)(1-U_F)N_2 \quad (1)$$

$$4(1-U_F)H_2 + (4U_F+m-2)H_2O + CO_2 + 2(1+Y)(1-U_F)O_2 + 7.52(1+Y)(1-U_F)N_2 \rightarrow (4+m-2)H_2O + 2Y(1-U_F)O_2 + 7.52(1+Y)(1-U_F)N_2 + CO_2 \quad (2)$$

In each equation, U_F is the fuel utilization factor, m is the steam to carbon ration and Y is excess air. The mass balances account for internal reforming. high temperature shift and power reactions. Table 3 contains performance parameters for model MCFC and SOFC power plants. Applying these parameters to equations (1) and (2) defines the compositions of the respective anode gas streams.

Table 3
Operational Parameters for Model Fuel Cells

	MCFC	SOFC
T	1660R	2290R
P	1 Atm.	1 Atm.
U_F	0.75	0.75
U_{OXI}	0.60	0.60
E_{elec}	~50%	~45%
m	2.5	2.5

Following oxidation, anode gas temperature is:

$$T_{ga_1} = \frac{n_{H_2} MW_{H_2} HHV_{H_2} - Q_{LOSS}}{\sum n_i MW_i C_{P_i}(T)} + T_{ga_o} \qquad (3)$$

Calculated values for Q_{LOSS} in equation (3) resulted in theoretical combustion efficiencies in the low 70 percent range. Oxidized anode gas and cathode gas exhausting at stack temperature contain the available waste heat. Most systems will use these streams to preheat incoming fuel, feed water and oxidant. This analysis accounted for the preheat losses and then combined the two streams. Having arrived at a single stream of waste heat, the capacity and heating water flow rate for a hot water generated chiller per megawatt of electricity are:

$$\frac{N}{\dot{W}} = \frac{3.412x10^6 \xi C_g (T_g - T_{HWR})}{HHV_F E_{elec} \dot{Q}_R} \frac{Tons}{MW} \qquad (4)$$

$$\frac{\dot{V}}{\dot{W}} = \frac{N\dot{Q}_R}{500 C_{P_{HW}} (T_{HWS} - T_{HWR})} \frac{GPM}{MW} \qquad (5)$$

Where C_g is the product of gas mass flow rate and specific heat;"xi" is heat exchanger effectiveness.

For steam generated chillers, the mass and heat balances are modified to account for latent heating of steam. The conventional heat balance between gas and steam as it is superheated requires:

$$C_g (T_g - T_x) = \dot{m}_{stm} (h_s - h_f) \qquad (6)$$

Where T_x is the so-called pinch point, typically 50 - 70R above saturated steam temperatures. Values for h_s and h_f are enthalpies of steam vapor and saturated liquid, respectively at 28 PSIA. Therefore, steam rate and chiller capacity are:

$$\dot{m}_{stm} = \frac{3.412x10^6 C_g (T_g - T_x)}{HHV_F E_{elec} (h_s - h_f)} \qquad (7)$$

$$\frac{N}{\dot{W}} = \frac{\dot{Q}_{G_{stm}}}{\dot{Q}_R} = \frac{[h_s - (h_f + h_{fg}x)]\dot{m}_{stm}}{\dot{Q}_R} \frac{Tons}{MW} \qquad (8)$$

The factor x is the quality of steam leaving the chiller generator. Table 4 is a performance schedule for the three configurations of

fuel cell-absorption chiller system: MCFC with hot water generation; MCFC with steam generation, and SOFC with steam generation. Heating performance assumes a 90 % efficiency in hydronic heating generator.

Table 4
Bulk Cogeneration per MW Electrical Output at Full Power

	MCFC-HHW	MCFC-Steam	SOFC-Steam
Anode gas oxidation eff., excess air	0.74 Y= 2.0	0.74 Y=2.0	0.70 Y=2.0
T, waste gas	1240R	1240R	1514R
Mass flow, waste gas	17078PPH	17078PPH	14851PPH
Waste heat recovery efficiency	0.65	T_x = 766R	T_x = 766R
Generator mass flow	89 GPM (HW)	2173 PPH (Steam)	3498 PPH (Steam)
C_g BTU/R-LB_m fuel	15.934	15.934	14.63
Q_c	1258 MBTUH	1835 MBTUH	3961 MBTUH
N/MW	105 Tons	117 Tons	251 Tons
Hydronic flow	56.6 GPM	83 GPM	179 GPM
Heating	1132 MBTUH	1652 MBTUH	3583 MBTUH

Design Issues

Relationships between bulk electrical and thermal capacities at steady state operation for the proposed system have been developed, but several important design issues are not treated in this analysis. Transient behavior and turn down ratio are two important performance problems. With relatively long start up times and low turndown ratios, the first generation of fuel cells may not be suited for the application for many types of building. The ratios of bulk capacities, as well, indicate that thermal capacities may be insufficient to match electrical capacities in many applications. Thermal design for the integrated system will significantly affect the amount of waste heat available for cooling. One factor would include internal vs. external reforming; an external reformer would augment the waste heat from the fuel cell. Another significant design issue would be accommodating respective thermal and power capacities vs. load requirements across the operational envelope. This will probably involve a low temperature cooling system with circulating pump and cooling tower to trim excess thermal capacity and to dissipate secondary heat, eg., from the absorber. Some systems might schedule tandem heating and cooling during milder weather as a method for utilizing excess thermal capacity. The major factor in performance, though, is preheat of fuel, feed water and oxidant. An optimized design would probably employ two stage cooling with cathode gas cooling incoming oxidant and then supplying the first stage of heating to the chiller. Oxidized anode gas would preheat fuel and feedwater and then supply second stage heat.

SPECIAL CONSIDERATIONS ON OPERATING A FUEL CELL POWER PLANT USING NATURAL GAS WITH MARGINAL HEATING VALUE

Moses L. Ng and Chien-Liang Lin
Energy and Resources Laboratories
Industrial Technology Research Institute
Chutung, Hsinchu County, Taiwan
Republic of China

Ya-Tang Cheng
Power Research Institute
Taiwan Power Company
Shu-Lin, Taipei County, Taiwan
Republic of China

INTRODUCTION

In realizing new power generation technologies in Taiwan, a phosphoric acid fuel cell power plant (model PC25B, ONSI Corporation) has been installed in the premises of the Power Research Institute of the Taiwan Power Company in Taipei County of Taiwan. The pipeline gas supplying to the site of this power plant has a high percentage of carbon dioxide [1] and thus a slightly lower heating value than that specified by the manufacturer. Because of the lowering of heating value of input gas, the highest output power from the power plant is understandably less than the rated power of 200 kW designed. Further, the transient response of the power plant as interrupted from the Grid is also affected. Since this gas is also the pipeline gas supplying to the heavily populated Taipei Municipal area, it is conceivable that the success of the operations of fuel cells using this fuel is of vital importance to the promotion of the use of this power generation technology in Taiwan. Hence, experiments were set up to assess the feasibility of this fuel cell power plant using the existing pipeline gas in this part of Taiwan where fuel cells would most likely find useful.

EXPERIMENTAL METHODS

A baseline study of measuring the important parameters of the operation of the power plant under steady state has been performed on different power output from the fuel cell power plant. These parameters will be seen as important indicators showing the state of the power plant in returning to stable operations after disturbances impose on the power plant. To minimize influence from the Grid in achieving the steady state operations, the power plant was put on Grid Independent mode of operation and the output was connected to an electric heater capable of consuming variable wattage from 0 to 200 kW. Data were collected only after long time of operations of the power plant under the same designated power output.

When experiencing disturbance from the Grid during Grid Connected mode of operations, the output from the power plant disconnects from the Grid and the power plant goes to Idle mode of operations. If and when the disturbance from the Grid clears, the power plant will try to resume the original output level and reconnects to the Grid under Grid Connected mode of operations [2]. To simulate this situation, the power plant was put to Idle mode of operations for quite some time to achieve the steady state status. The output level was then programmed to the designed value and the power plant was abruptly changed to Grid Connected mode of operations. Data of importance were then recorded manually in intervals of 10 seconds since the computer code for automatic data acquisition was not available from the manufacturer. The experiments on transient response from the power plant can be concluded after the vital parameters returns to their respective values at steady state operations of similar output levels.

RESULTS AND DISCUSSION

A sample from the pipeline natural gas supplying to the plant site was analyzed and the results were listed in Table 1 against the specification of fuel gas furnished by the manufacturer. It was found that the pipeline gas in use matched most of the specification except in excess carbon dioxide thus lowering the heating value. The results of the steady state operation characteristics of the power plant using this pipeline gas under Idle mode of operation as well as at 100, 125 and 150 kW output are listed in Table 2. Most of the operation characteristics agreed with those specified by the manufacturer, except in the slightly lower electrical efficiency at the respective output levels. In a separate study [3], it was found that the excess content of carbon dioxide, which acts as inert in fuel cells, lowered the energy conversion efficiency.

The results in transient response of the gross and net power output, the reformer temperature and the opening of the steam ejector of the power plant on a step change from steady Idle mode of operation to the specified rated power output are illustrated in Figures 1 to 3 respectively. It can be seen that the output power, especially the net output power responded almost immediately to the power level on the step change, whereas the longest time for the gross output power to settle was within 5 minutes. However, the reformer temperature took longer time in the range of 20 minutes to reach their respective steady state values. The transient response in the opening of the steam ejector valve ZT010 show an unusual behavior of 20% more opening before finally reaching their respective steady state values. This is important especially in the range of output level close to its rated capacity since the power plant will be automatically shutdown in the wide opening of this ejector valve in more than 5 seconds [2].

In the course of performing the steady state experiments, it was found that the fuel cell power plant could be gradually stepped up from the Idle mode of operation to output power of 150 kW at intervals of 25 kW. However, the same increment of 25 kW from 150 kW to 175 kW prompted the power plant to shutdown automatically, as reasoned above. At smaller increments of 5 to 10 kW, the output power of the power plant could be increased to 195 kW after observing the important parameters, especially the opening of the ejector valve, of the power plant reach their steady state values at respective output power. Hence, the steady state measurements of the important parameters of the power plant such as those listed in Table 2 becomes a significant guide in the operations of the fuel cell power plant. In addition, the opening of the steam ejector valve becomes the bottleneck of the operations of the fuel cell power plant both in determining the maximum power output and their rate of increase.

CONCLUSIONS

(1) The use of pipeline gas of excess carbon dioxide content on the operation of an on-site fuel cell power plant may lower the energy conversion efficiency and reduce the maximum output power.

(2) In operating an on-site fuel cell power plant, it is crucial to monitor the opening of the steam ejector, as it may cause unscheduled shutdown of the power plant. In using fuels of marginal heating value, the rate of increase of output power should be limited to avoid automatic shutdown of the power plant due to full opening of the steam ejector, especially when the net output power is close to the rated capacity of 200 kW. In such cases, the opening of the steam ejector corresponding to the similar levels of the output power under steady state conditions can be used as a guide in determining the rate of increase of the net output power of the fuel cell power plant.

ACKNOWLEDGMENTS

This study is co-sponsored by the Energy Commission of the Ministry of Economic Affairs of the Republic of China and the Taiwan Power Company.

REFERENCES

1. Chinese Petroleum Corporation, private communications.
2. *PC25B On-Site Fuel Cell Power Plant- Service Manual,* FCR-12966, ONSI Corporation, South Windsor, Connecticut, (1994).
3. Moses L. Ng, C. L. Lin and Y. T. Cheng, "Operations of an On-Site Fuel Cell Power Plant with Natural Gas of Excess Carbon Dioxide", (in preparation).

TABLE 1 Specification and Analysis of Pipeline Gas

Constituent	Specification, max.	This Study
Methane	100	81.56
Ethane	10	4.63
Propane	5	1.53
Butanes	1.25	0.56
Pentanes, Hexanes, C_6+	0.5	0.07
Carbon Dioxide	3	11.23
Oxygen	2.5	-
Nitrogen	4.0	0.42
Total Sulfur, ppmv	30 max/6 avg.	3.06
Ammonia, ppmv	1	-
Chlorine, ppmv	0.05	-
Supply Pressure, cm aq.	10 - 36	22.5
High Heating Value, kcal/m^3	8,720 (min)	8,610

TABLE 2. Steady State Operation Characteristics of the Fuel Cell Power Plant

	Rated Capacity, %			
	Idle	50	62.5	75
1. Output Power, kW				
.net	1.0	104.2	126.2	154.2
.gross	56.8	121.1	141.4	169.0
2. Stack Current, amp	253.0	565.0	675.1	840.0
3. Stack Voltage, volt	230.8	217.2	214.2	207.4
4. Fuel Consumption, m^3/h	18.8	38.3	46.0	57.4
5. Burner Air Flow, kg/h	93.6	143.6	170.7	209.1
6. Steam Water Separator Temp, °C	188.2	180.3	179.6	175.5
7. Reformer Temperature, °C	815.4	827.5	846.4	874.2
8. Steam Ejector Opening, %	22.4	33.4	42.7	70.1
9. Reformer Efficiency, %	74.6	80.4	80.0	80.3
10. Electrical Efficiency, %	0.7	37.4	37.3	36.7

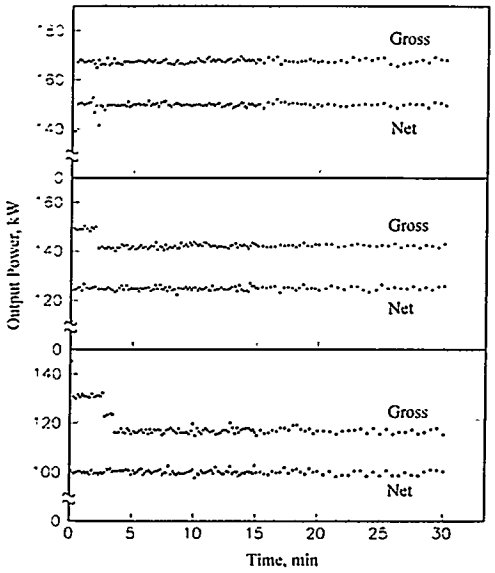

Figure 1.
Transient Response of the Fuel Cell Power Plant in Net and Gross Output Power

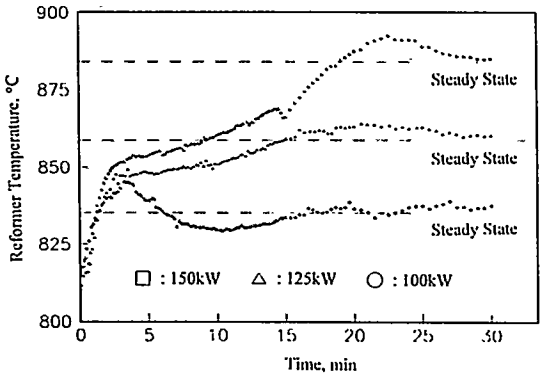

Figure 2.
Transient Response of the Fuel Cell Power Plant in Reformer Temperature

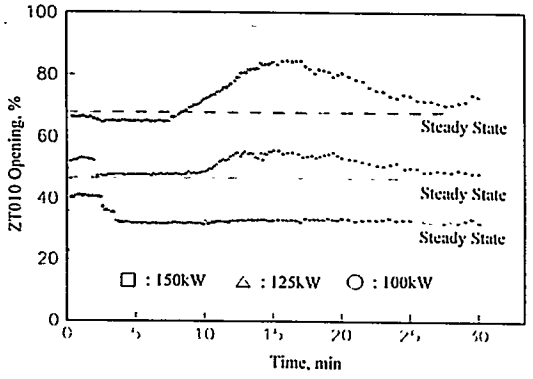

Figure 3.
Transient Response of the Fuel Cell Power Plant in Steam Ejector Opening

DEVELOPMENT OF A 200kW MULTI-FUEL TYPE PAFC POWER PLANT

Tetsuo Take, Yutaka Kuwata, Masahito Adachi, and Tsutomu Ogata
NTT Integrated Information & Energy System Laboratories
3-9-11, Midori-cho, Musashino-shi, Tokyo, 180 Japan

INTRODUCTION

Nippon Telegraph and Telephone Corporation (NTT) has been developing a 200 kW multi-fuel type PAFC power plant which can generate AC 200 kW of constant power by switching fuel from pipeline town gas to liquefied propane gas (LPG) and vice versa. This paper describes the outline of the demonstration test plant and test results of its fundamental characteristics.

DEMONSTRATION TEST PLANT

A main flow diagram of a 200 kW multi-fuel type PAFC power plant which was used for demonstration tests is shown in Fig. 1. The plant was made by partially reconstructing a 200 kW PAFC power plant for pipeline town gas. An LPG supply unit and fuel switching equipment were added to the plant. Start-up and power-generation control programs for LPG and a fuel-switching program were added to a controller in the plant, too. The quantity of the pipeline town gas, LPG, and steam supply is automatically controlled by regulating the open rates of the control valves for pipeline town gas and LPG, and the ejector for steam. When the plant generates power using either pipeline town gas or LPG, both

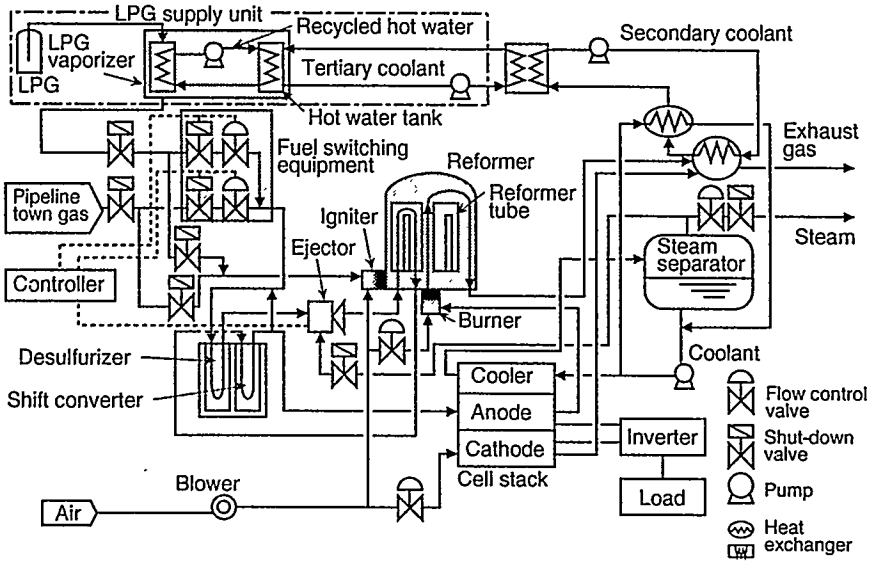

Fig. 1 Main flow diagram of a 200kW multi-fuel type PAFC power plant

control valves are always regulated matching the plant output at that time to avoid shut-down of the plant caused by a transitional shortage of fuel in fuel switching. Fuel switching from pipeline town gas to LPG is carried out by opening the shut-down valve in the LPG supply line and then by closing the shut-down valve in the pipeline-town-gas supply line.

Pipeline town gas and LPG are steam-reformed to form hydrogen, which is necessary for the fuel cell reaction, in the same reformer. Steam reforming of LPG requires much more steam than steam reforming of pipeline town gas to avoid carbon deposition when a conventional Ni-Al_2O_3 catalyst bed is adopted in a reformer. In the developed multi-fuel type PAFC power plant, it is impossible to supply steam which is sufficient to suppress carbon deposition in steam reforming of LPG. A double-layer catalyst bed is therefore adopted in the reformer of this plant. Figure 2 shows the function of the double-layer catalyst bed. The new catalyst bed consists of a Ru-Al_2O_3 catalyst layer located at the gas-inlet side of the catalyst bed and a Ni-Al_2O_3 catalyst layer located at the gas-outlet side of the catalyst bed. This double-layer catalyst bed is designed so that LPG is steam-reformed completely on the Ru-Al_2O_3 catalyst layer. On a Ru-Al_2O_3 catalyst, carbon deposition does not occur in steam reforming of LPG even when the steam supply is suppressed and the steam-to-carbon ratio (S/C) is decreased to 2.0. The methane which forms by the methanation reaction on the Ru-Al_2O_3 catalyst layer is steam-reformed on the Ni-Al_2O_3 catalyst layer. Carbon deposition in steam reforming of LPG can be therefore suppressed by adopting the double-layer catalyst bed.

Waste heat from the plant was utilized to vaporize LPG. The tertiary coolant was supplied to the hot water tank in the LPG vaporizer. The recycled hot water in the vaporizer was then heat-exchanged for this tertiary coolant and heated up. LPG was vaporized by heat-exchange for this recycled hot water.

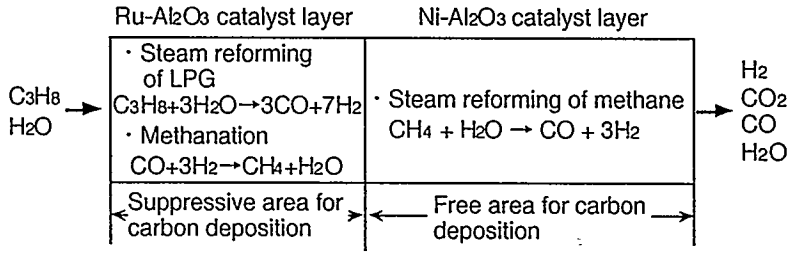

Fig. 2 Function of the double-layer catalyst bed

START-UP CHARACTERISTICS

When the developed 200 kW multi-fuel type PAFC plant was started up from a cold

state by pipeline town gas and LPG, the reformer top-tube temperature and the cell-stack coolant temperature reached 760℃ and 182℃ for 4 hours from the beginning and the start-up of the plant finishes in both cases.

CONSTANT POWER-GENERATION CHARACTERISTICS

The constant power-generation test results at AC 200 kW power generation are shown in Table 1. The fuel-cell DC output power, the average cell voltage, the current density, and the reformer top-tube temperature are almost constant in spite of the kind of fuel. The quantity of the steam supply for steam reforming of LPG is increased compared with that for steam reforming of pipeline town gas. However, it can be controlled below the maximum steam-supply level of the plant by adopting the double-layer catalyst bed in the reformer (Fig. 3). The shift converter and desulfurizer temperatures are almost constant in spite of the kind of fuel.

Table 1 Constant power-generation characteristics at AC 200kW

Fuel	Pipeline town gas	LPG
Fuel-cell DC output power	232.4 kW	230.4 kW
Average cell voltage	0.652 V	0.647 V
Current density	201.0 mA/cm²	200.7 mA/cm²
Quantity of fuel supply	49.2 Nm³/h	22.8 Nm³/h
Quantity of steam supply	127.7 Nm³/h	214.0 Nm³/h
Reformer top-tube temperature	793.9 ℃	792.9 ℃
Methane conversion	89.4 %	94.7 %
CO conversion	97.6 %	99.2 %
Hydrogen utilization	80.4 %	77.8 %
Oxygen utilization	53.9 %	54.4 %

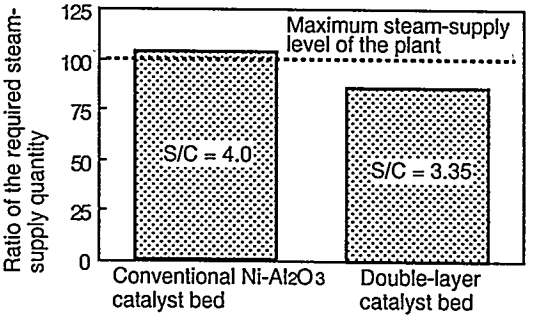

Fig. 3 Comparison of the quantity of steam for steam reforming of LPG at AC 200kW power generation

FUEL SWITCHING CHARACTERISTICS

Figure 4 shows the fuel-switching test results at AC 200 kW power generation. Despite the fuel switching from pipeline town gas to LPG and vice versa, the fuel-cell DC output power and the AC output power remain constant. The fuel and steam supply is automatically controlled to form a fixed quantity of hydrogen in the reformer, to maintain constant output power at AC 200 kW, and to suppress carbon deposition. The steam supply is increased transitionally to avoid steam shortages when the fuel is switched. The reformer top-tube temperature is

changed by fuel switching for 5-6 minutes but is stabilized after that. The fuel-switching test results at the partial output-power generation are similar to those at AC 200 kW power generation.

LPG VAPORIZATION CHARACTERISTICS

22.0 Nm³/h of LPG is vaporized by utilizing exhaust heat from the plant only for the heat source of the LPG vaporizer at AC 200 kW power generation.

8.4kW of the parasite-power consumption is decreased by heating up the recycled hot water in the LPG vaporizer with the tertiary coolant instead of an electric heater located at the hot water tank when power is generated at AC 200 kW by LPG. The fuel-cell DC output power at AC 200 kW power generation by pipeline town gas and that by LPG are therefore almost the same.

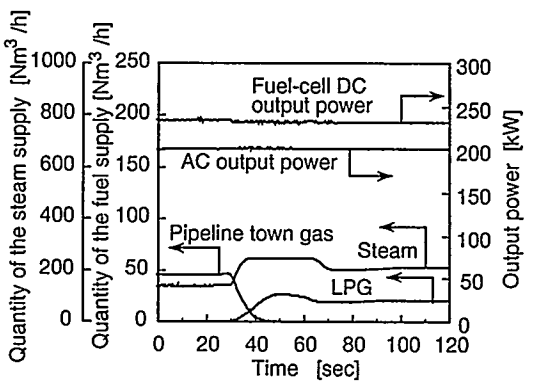

(a) Pipeline town gas → LPG

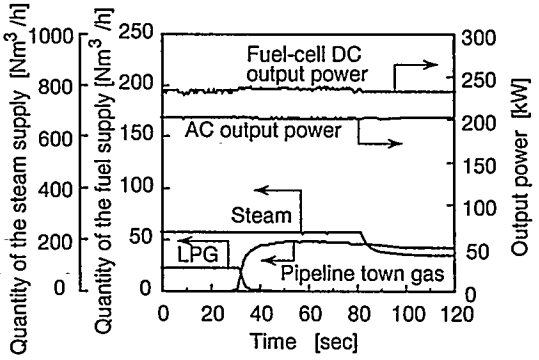

(b) LPG → Pipeline town gas

Fig. 4 Fuel switching characteristics

CONCLUSIONS

The developed 200 kW multi-fuel type PAFC power plant can be started up and can generate constant power at AC 200 kW by pipeline town gas and LPG. In this plant, constant power generation at AC 200 kW can be continued by switching fuel from pipeline town gas to LPG and vice versa, and 8.4 kW of the parasite-power consumption for the LPG vaporizer can be decreased by using exhaust heat from the plant when power is generated at AC 200 kW by LPG.

OPERATION RESULT OF 40kW CLASS MCFC PILOT PLANT

H. Saitoh, S. Hatori, M. Hosaka, H. Uematsu

Ishikawajima-Harima Heavy Industries Co., Ltd.
(IHI)
3-1-15, Toyosu Koto-ku, Tokyo 135 JAPAN

Introduction

Ishikawajima-Harima Heavy Industries Co., Ltd. developed unique Molten Carbonate Fuel Cell (MCFC) system based on our original concept.
To demonstrate the possibility of this system, based on MCFC technology of consigned research from New Energy and Industrial Technology Development Organization (NEDO) in Japan, we designed 40kW class MCFC pilot plant which had all equipments required as a power plant and constructed in our TO-2 Technical Center.
This paper presents the test results of the plant.

1. Test objectives

The main objectives of this test plant are to verify the following items in our concept.

1) Start-up and Shut-down operation within allowable differential pressure limits of stack.
2) Cathode / anode differential pressure control method without high-temperature valves.
3) Emergency shut-down operation within allowable limits of stack.
4) High fuel utilization and high power generation efficiency.

2. Plant Description

The view and process flow diagram of this test plant are shown in Figure 1 and 2 respectively.
In our system, both cathode and anode exhaust gas fed to a reformer combustor, and sensible heat of cathode gas is used as a part of reforming heat source.
Such cathode gas sensible heat reforming method and series arrangement of stacks for gas flow direction realize high fuel utilization, and then, high power generation efficiency.

3. Test Results

The main results in Process and Control (PAC) test are summarized below.

1) The start-up and shut-down operation were verified.
2) As shown in Figure 3, the results of load change test showed us that load change of 10%/min will be available without high-temperature differential pressure control valves.
3) Figure 4 shows typical data of differential pressure in emergency shut-down test at rating load.

The differential pressure were controlled successfully within allowable pressure limits of stack.

After PAC test we have been performing total plant demonstration test. We have confirmed the applicability of cathode gas sensible heat reforming method and series arrangement of stacks for gas flow direction.

4. Conclusions

We have been operating 40kW class MCFC pilot plant successfully first in the world as external reforming system.
Through design and demonstration test of this plant, the results clearly show that cathode gas sensible heat reforming method and series arrangement of stacks for gas flow direction is an effective way for high fuel utilization and high power generation efficiency, also cathode / anode differential pressure control method without high-temperature control valves is realized by connecting the outlet of both cathode and anode of stack with the inlet of combustion side of reformer directly.
We believe that these test results will accelerate further realization of MCFC power plant.

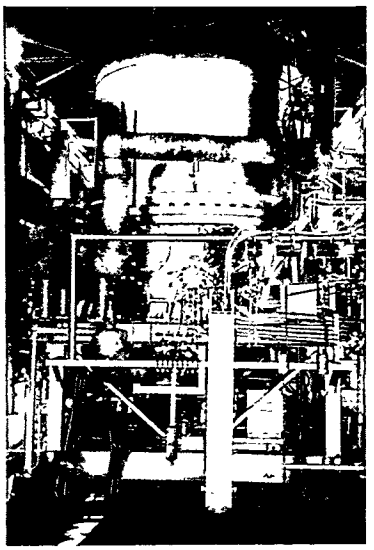

FIG. 1 : VIEW OF 40KW CLASS PILOT PLANT

5. Acknowledgment

This work has been conducted under MCFC technology of consigned research from NEDO(New Energy and Industrial Technology Development Organization) and MCFC Research Association(Technology Research Association for Molten Carbonate Fuel Cell Power Generation System) as a part of the New Sunshine Program of MITI(Ministry of International Trade and Industry). We appreciate their advice and support.

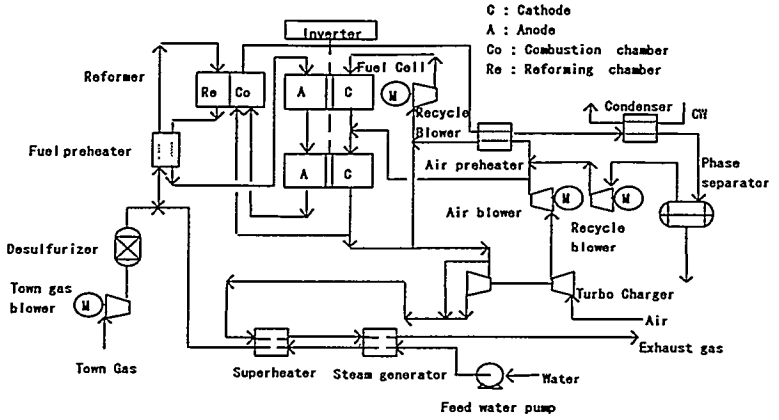

FIG. 2 : PROCESS FLOW DIAGRAM

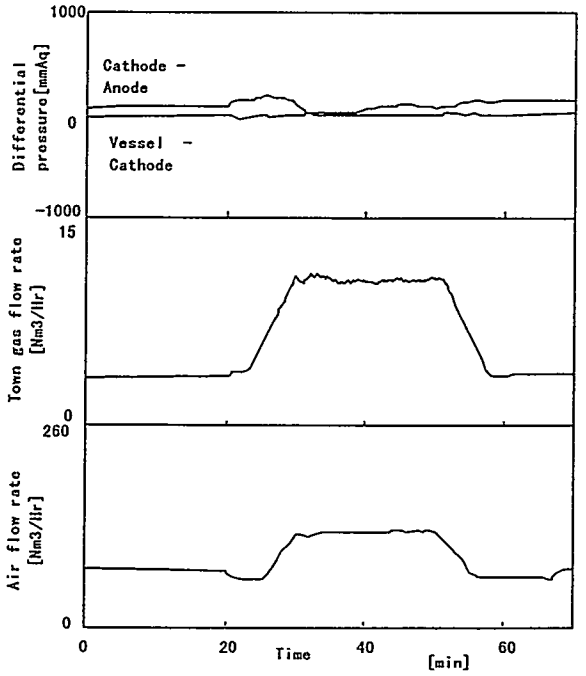

FIG. 3 : RESULT OF 10%/min LOAD CHANGE TEST

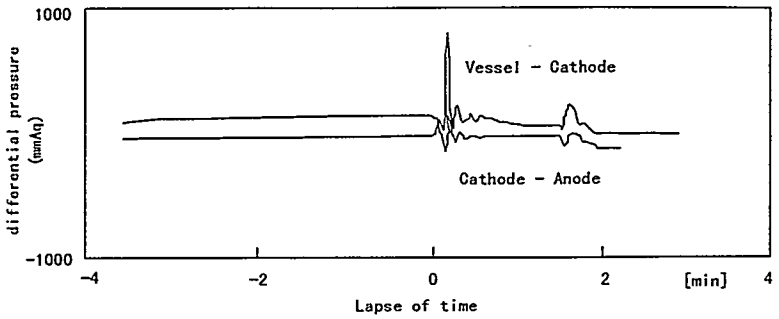

FIG. 4 : BEHAVIOR OF DIFFERENCIAL PRESSURE

TRIAL OPERATION OF A PHOSPHORIC ACID FUEL CELL (PC25) FOR CHP APPLICATIONS IN EUROPE

M. Uhrig, W. Droste and D. Wolf
Ruhrgas AG
D-46284 Dorsten
Germany

INTRODUCTION

In Europe, ten 200 kW phosphoric acid fuel cells (PAFCs) produced by ONSI (PC25) are currently in operation. Their operators collaborate closely in the European Fuel Cell Users Group (EFCUG). The experience gained from trial operation by the four German operators - HEAG, HGW/HEW, Thyssengas and Ruhrgas - coincides with that of the other European operators. This experience can generally be regarded as favourable [1].

With a view to using fuel cells in combined heat and power generation (CHP), the project described in this report, which was carried out in cooperation with the municipal utility of Bochum and Gasunie of the Netherlands, aimed at gaining experience with the PC 25 in field operation under the specific operating conditions prevailing in Europe [2].

The work packages included heat-controlled operation, examination of plant behaviour with varying gas properties and measurement of emissions under dynamic load conditions. The project received EU funding under the JOULE programme.

EXPERIMENTS

The design of the PAFC investigated only allows the electrical output to be preselected, thus permitting power-controlled operation. In CHP in Europe, however, heat-controlled operation is also of considerable significance. In this case, the requirements of the consumer (e.g. a group heating system) in respect of the thermal output to be made available serve as control parameter for the plant.

The amount of heat that can be made available to the group heating system depends, on the one hand, on the preset electrical output and, on the other, on the flow rate of water passing through the fuel cell as well as its supply temperature.

During the trial measurements, thermal output as a function of electrical output based on volumetric water flow rate and return temperature (T_{return}) was determined in extensive series of experiments. This resulted in the curves shown in Fig. 1.

For the purpose of heat-controlled operation, the thermal output made available to the group heating system was measured and served as actual value for a digital controller based on a PI control algorithm. With the aid of this actual value and the set point for thermal output entered manually, the controller determines the corresponding electrical output as the manipulated variable.

In Europe, natural gas comes from various sources. As a result, the gas available to a consumer may have varying properties. Furthermore, LPG/air may be ad-

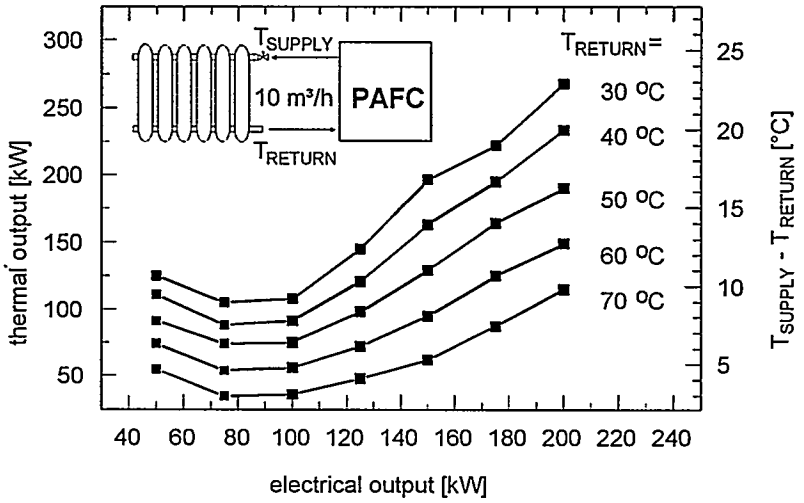

FIG 1: THERMAL OUTPUT VS. ELECTRICAL OUTPUT

mixed for peak-shaving purposes, primarily in winter.

Thus a further priority of the trial operation at Bochum municipal utility were experiments to investigate plant behaviour in the case of LPG/air admixture. For this purpose, a mixing unit was installed which allowed predefined admixture rates. Propane/air with the heating value of natural gas was used.

In another work package, pollutant emissions were measured under various operating conditions.

RESULTS

The time profile of thermal output shown in Fig. 2 demonstrated that heat-controlled operation of a PAFC is possible without any difficulties by using the controller developed by Ruhrgas. The actual value (-2-) excellently follows the set point for thermal output (-3-).

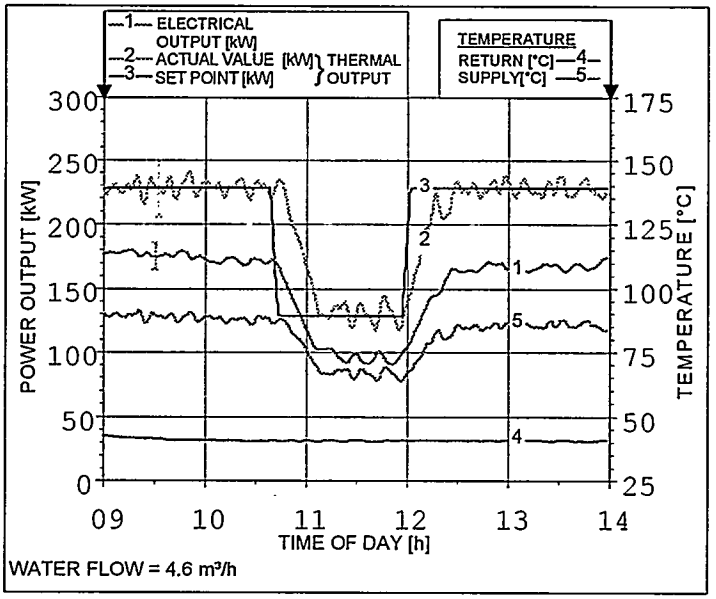

FIG 2: HEAT-CONTROLLED OPERATION: CHANGE OF SET POINT

The experiments on LPG/air admixture were carried out with admixture rates between 5 % and 25 %. It became clear that, with the existing fuel cell design, trouble-free operation using peak-shaving gas over the entire performance range is only possible up to a maximum admixture rate of 15 %.

This is due to the peripheral components of gas treatment, which are not adequately dimensioned for reliable peak-shaving gas operation. This is evident in Fig. 3. It shows the position of the ejector as a function of the electrical output. The ejector controls the admixture of steam for the reforming reaction to produce hydrogen-rich process gas from natural gas. Its dimensions are evidently too small.

This means that, during operation with peak-shaving gas, the maximum ejector position is reached at high outputs and thus leads to plant shutdown.

The results of emission measurements revealed that, in the case of large increases in electrical output, emission peaks may occur in respect of CO and hydrocarbons. However, they drop after a short time and are thus negligible for the overall emissions.

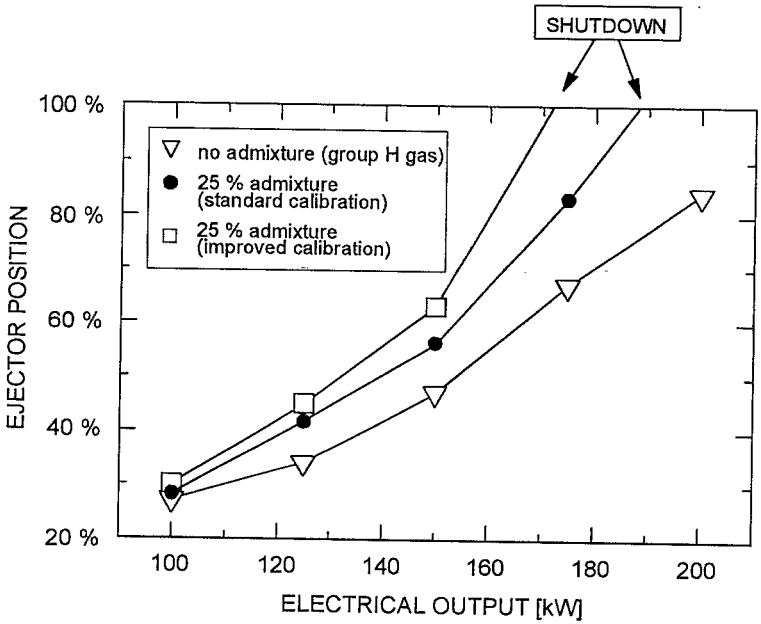

FIG 3: EJECTOR POSITION VS. ELECTRICAL OUTPUT

REFERENCES

[1] Nymoen, H.; Journal of Power Sources, 49 (1994) 63 - 76.

[2] M. Uhrig, H.-J. Kail, W. Mallon, *Cogeneration using fuel cells with changing gas properties,* Proceedings of the 1995 International Gas Research Conference, Cannes (1995).

DYNAMIC SIMULATION OF A DIRECT CARBONATE FUEL CELL POWER PLANT

John B. Ernest
Fluor Daniel, Inc.
Irvine, CA 92698
USA

Hossein Ghezel-Ayagh and Ashok K. Kush
Fuel Cell Engineering,
a subsidiary of Energy Research Corporation
Danbury, CT 06813

Introduction

Fuel Cell Engineering Corporation (FCE) is commercializing a 2.85 MW Direct carbonate Fuel Cell (DFC) power plant. The commercialization sequence has already progressed through construction and operation (Ref. 1) of the first commercial-scale DFC power plant on a U.S. electric utility, the 2 MW Santa Clara Demonstration Project (SCDP), and the completion of the early phases of a Commercial Plant design. A 400 kW fuel cell stack Test Facility is being built at Energy Research Corporation (ERC), FCE's parent company, which will be capable of testing commercial-sized fuel cell stacks in an integrated plant configuration. Fluor Daniel, Inc. provided engineering, procurement, and construction services for SCDP and has jointly developed the Commercial Plant design with FCE, focusing on the balance-of-plant (BOP) equipment outside of the fuel cell modules.

The nature of the next-generation carbonate Fuel Cell power plants is that they will be first-of-a-kind plants, which will follow widely varying loads, with controls automated to run without human intervention. The DFC plant will be highly heat integrated with a very slow thermal response due to the large thermal inertia of the stack itself. These attributes present a compelling case for the use of Dynamic Simulation. Fluor Daniel and FCE have used Dynamic Simulation to address practical issues of process and control design for the past two years.

Dynamic simulation models developed by others have focused on the 2-dimensional temperature details of the stack itself (2, 3), or on the steam reformer (4), or on the separate issue of inverter dynamics, or have taken a theoretical approach to an entire plant based on a simplified BOP (5). Fluor Daniel and FCE have developed a dynamic simulation model of the entire integrated cell stack and BOP for the Test Facility and Commercial Plant and produced results suitable for design. We believe that this effort is broader and has achieved more useful results than all the other dynamic simulations reported in the open literature.

This paper provides a brief orientation to the dynamic simulation technique, its application to FCE's DFC power plant, and the benefits offered by this tool. An illustrative simulation is described and figures show the major plant responses.

The Dynamic Simulation Technique

Dynamic simulation is a process engineering design tool that predicts how a process and its controls respond in time to various process and control changes. In the past, the use of dynamic simulation as a design tool was limited to simple linear modeling techniques for applications such as operator training simulators. Increasingly however, rigorous dynamic simulation with integrated energy and material balances, hydraulics, thermodynamics, and control modeling is being used to design a variety of industrial processes.

Dynamic simulation models must be sufficient to reproduce rigorously the trends in the net performance of the plant equipment and the stability of the control system. This requires much more detail than steady-state models or dynamic models that rely on transfer functions. Fluor Daniel has experience in applying rigorous dynamic simulation to conventional power plants and a variety of other applications from the refining and petrochemical process industries (6, 7, 8).

The dynamic simulation models for the DFC were developed using Aspen Technology, Inc.'s SPEEDUP general purpose dynamic simulation computer program.

DFC Power Plant Dynamic Simulation Modeling Status

Fluor Daniel, in collaboration with FCE, has developed dynamic simulation models for both the Commercial and Test Facility power plants. The Commercial Plant model is based on the data available from the Preliminary design phase. Cases were run which verified this model with two conventional steady-state simulators developed by FCE and Fluor Daniel. Also, a number of simplified transient scenarios were studied. The trends and cause-and-effect relationships predicted by the dynamic simulation model for these simplified scenarios give confidence in the predictions for more realistic cases. The dynamic simulation models will be updated with data from ERC's Test Facility and Commercial Plant design refinements.

DFC Power Plant Modeling Technical Issues

The focus of DFC power plant modeling is on prediction of: control system stability and response; oxidizer operations and cycling; warm-up and cool down time; interactions between the oxidizer, heat exchangers, and stack; the temperature effect on voltage; transient violations of design constraints (none of these can be found by steady-state analysis); and unforeseen problems.

The following characteristics are very important to the dynamic behavior of the DFC power plant: the high degree of heat integration between anode and cathode streams, oxidizer, and DFC stack; the large oxidizer due to startup requirements; the very slow thermal response of the DFC stack; the extensive interactions and constraints on controls; and the extensive control logic, encompassing power generation, standby, startup, and shutdown operations.

Most of the process must be simulated rigorously due to process interactions. For example, to predict accurately the cathode inlet temperature, the dynamic simulation model must predict the heat transfer with the insulated pipes downstream of the oxidizer. However, some physical phenomena can be ignored, such as the fuel treatment system's pressure gradient. The model of the DFC stack includes the temperature, electrical, and gas composition changes due to reforming, shift, anode, and cathode reactions; heat exchange between the cell components and the reformer, anode, and cathode streams; and the current density-voltage-power generation characteristic. The model of the BOP is equally rigorous. Its fuel treatment system includes the natural gas and water/steam flow control valves, preconverter action, and heat exchange. The oxidizer system includes the air supply blower, duct head loss, air flow control valves, thermal burner, catalytic oxidizer, and piping heat exchange and pressure loss. The plant controls include the oxidizer controls, DFC power generation and stack temperature, and master logic.

Figure 1 presents a Block Flow Diagram of the Commercial Plant. Controls and process are of equal prominence.

Simulated Plant Performance

Plant performance is predicted for a wide range of cases: dc power generation rate ramps; control setpoint and mode changes; upsets in gas, steam, air, and auxiliary electrical feeds and thermal burner firing; emergency scenarios; and startup and shutdown.

Figures 2 and 3 present typical simulation results. In this case, the power is being increased from 25% to 100% of rated power, while the oxidizer outlet temperature controller setpoint is raised 100°F at the beginning of the power ramp, then lowered 150°F at the end of the power ramp. The gas flow is set to maintain a fixed fuel utilization. The steam flow is set to maintain a fixed fuel steam/carbon ratio until the flow reaches its maximum.

Figure 2 shows the temperature profile. There are large transients in the oxidizer outlet temperature as the temperature controller follows its setpoint. The temperature is much different at the cathode inlet due to the heat exchange with the intervening pipe. The cathode outlet temperature is still changing long after the power and oxidizer temperature setpoint ramps are complete. Figure 3 shows the stack electrical performance. The major features of Figure 3, the voltage drop and current density increase as the power is increased, could be determined from a sequence of steady-state runs. However, the voltage undershoot and fluctuations are due to the maximum steam flow constraint and controller transients.

Conclusions

Fluor Daniel and FCE have developed dynamic simulation models for both a near-term 400 kW fuel cell stack Test Facility and the preliminary design of FCE's DFC Commercial Plant. These models are already in use and soon will be validated against Test Facility experimental data. The Test Facility dynamic simulation model is able to predict the thermal behavior and control response of the entire power plant. The use of dynamic simulation models in engineering design allows evaluation of system dynamics, equipment design parameters, and control strategies.

Acknowledgment

The design effort described in this paper was supported by the U.S. Department of Energy (Contract No. DE-FC21-95MC31184) and FCE.

References

1. A.J. Leo, A.K. Kush, and M. Farooque, "Development and Demonstration of Direct Fuel Cell System at Energy Research Corporation," IECEC, August 12, 1996, Washington D.C.
2. K. Bolwin, S. Hauff, and W. Schnurnberger, "Dynamic Simulation of Heat Dissipation and Electrochemical Conversion Rates," Fuel Cell Seminar Program and Abstracts, pp. 315-318, Nov./Dec. 1994, San Diego, CA.
3. W. He, R. W. J. Kouffeld, A. Korving, and J. G. M. Becht, "The Dynamic Performance of a Molten Carbonate Fuel Cell in Power Generation Systems," op. cit., pp. 602-605.
4. G. L. Ohl, G. E. Smith, and J. L. Stein, "Dynamic Models of a Methanol to Hydrogen Steam Reformer for Transportation Applications," op. cit., pp. 491-494.
5. W. He, "Dynamic Modeling and Control of Molten Carbonate Fuel Cell Systems," Technische Universiteit Delft, Rept. EV-1754, 10 Jun. 1994.
6. W. E. Kirchmeier, F. M. Faubert, and W. T. Reid III, "Furnace Implosion Study Verified by Trip Test," Instrumentation in the Power Industry, Vol. 20, Proceedings of the Intl. ISA Power Inst. Symposium, pp. 75-91, May 1977.
7. J. B. Ernest and C. A. Depew, "Use dynamic simulation to model HPU reactor depressuring," Hydrocarbon Processing, Vol. 74, No. 1, pp. 72-79, Jan. 1995.
8. C. A. Depew and R. B. Nielsen, "Dynamic simulation for process design," Hydrocarbon Processing, Vol. 75, No. 7, pp. 67-75, Jul. 1996.

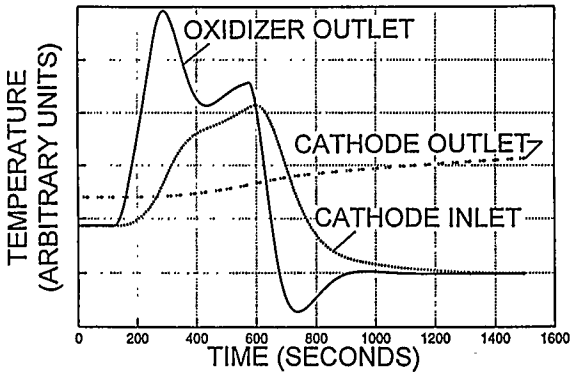

FIGURE 2. OXIDANT GAS TEMPERATURES

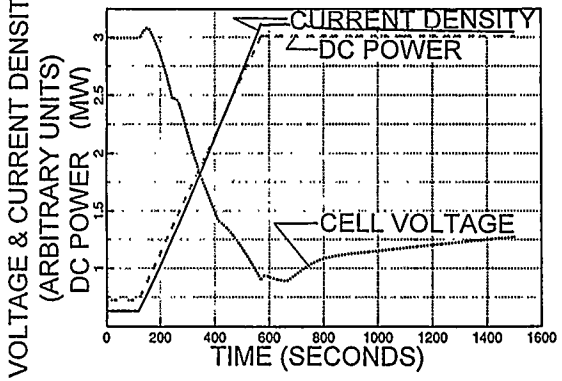

FIGURE 3. ELECTRICAL PERFORMANCE

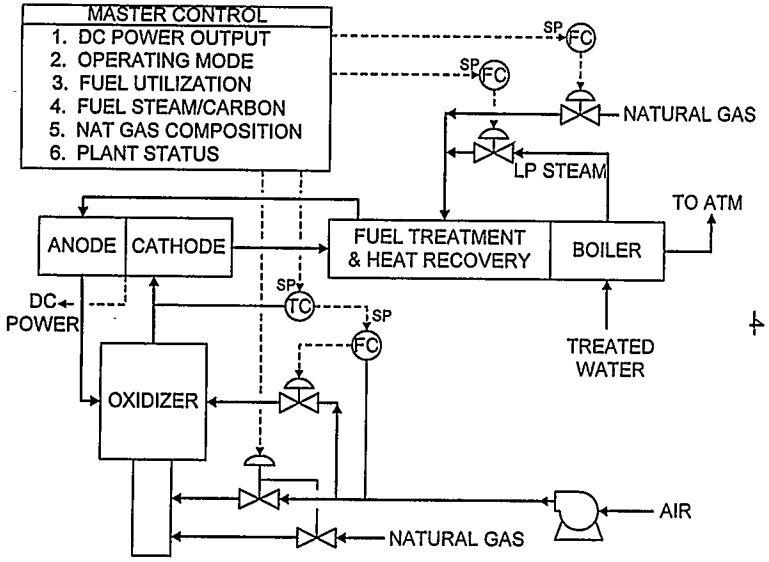

FIGURE 1. BLOCK FLOW DIAGRAM

RESULTS OF 200 KW FUEL CELL EVALUATION PROGRAMS

J. M. Torrey/G. P. Merten
Science Applications International Corporation
San Diego, CA 92121

Dr. M.J. Binder/W.R. Taylor/F.H. Holcomb
U.S. Army Construction Engineering Research Laboratories
Champaign, IL 61826

M.S. Bowers
New York State Energy Research and Development Authority
Albany, NY 12223

Science Applications International Corporation (SAIC) has installed six monitoring systems on ONSI Corporation 200 kW phosphoric acid fuel cells. Three of the systems were installed for the U.S. Army Construction Engineering Research Laboratories (USACERL) which is coordinating the Department of Defense (DoD) fuel cell Demonstration Program and three were installed under a contract with the New York State Energy Research and Development Authority (NYSERDA).

Monitoring of the three NYSERDA sites has been completed. Monitoring systems for the DoD fuel cells were installed in August, 1996 and thus no operating data was available at the time of this writing, but will be presented at the Fuel Cell Seminar.

This paper will present the monitoring configuration and research approach for each program. Additionally, summary performance data is presented for the completed NYSERDA program.

MONITORING APPROACH

The monitoring approach for the two programs are similar. SAIC specified and/or installed the six monitoring systems on the ONSI 200 kW fuel cells. TRC Environmental Corporation performed the emissions monitoring at the three NYSERDA sites. The emissions tests were run at load points from 25% to 100% of rated output in accordance with accepted U.S. Environmental Protection Agency procedures. The monitoring systems specified utilized Campbell Scientific data loggers and a variety of sensors for measuring electric consumption, gas consumption, thermal output, etc.

Data was collected every night via modem and processed at SAIC's offices. NYSERDA and USACERL have access to the database of monitored data. On a periodic basis, a performance summary report is prepared.

NYSERDA PROGRAM

The three New York fuel cells were located at:

St. Vincent's Hospital - Staten Island
Rochester Institute of Technology (RIT) - Rochester
Reifler Cement Company - Buffalo

The St. Vincent's Hospital and RIT sites were monitored for 18 months and Reifler Cement was monitored for ten months. A description of each installation and a summary of operating statistics is provided below.

The fuel cell at St. Vincent's Hospital in Staten Island, NY is configured to operate solely in the grid connected electrical mode. The fuel cell electrical output was fed into the hospital electrical distribution system. There was no sell back of electricity to the electric utility. The fuel cell thermal output was used to heat domestic hot water (DHW) for the hospital and was interfaced with a 1,000 gallon hot water storage tank.

The fuel cell at RIT in Rochester, NY is configured to operate in the grid connected mode only. The fuel cell electrical output was fed into the university's electric grid. There was no sell back of electricity to the electric utility. The fuel cell thermal output was used in an air conditioning reheat system to control humidity in the micro-electronics building which does manufacturing and research on electronic equipment.

The fuel cell at the Reifler Cement Company in Buffalo, NY was configured to operate in both the grid connected and grid independent electrical modes. For the first 8 months, the fuel cell operated in the grid independent mode at an electrical output of 50 kW or less. The fuel cell operated for 10 months in the grid connected mode. During this period, over 60% of the fuel cell electrical output was sold back to the electric utility. The fuel cell thermal output was used to heat process water in the concrete block fabrication and ready-mix processes during the winter months. This allowed the cement plant to extend their operations through the winter at a significant financial benefit.

Operating Statistics for NYSERDA Fuel Cell Program

Description	St. Vincent's	RIT	Reifler Cement
Total Operating Hours (through 4/95)	19,541	11,596	16,692
Monitoring Period	11/93 - 4/95	11/93 - 4/95	7/94 - 4/95
Oper. Hours during Monitoring Period	11,516	11,596	6,282
Electric Capacity Factor (%)	93.5	98.4	90.2
Electrical Efficiency (%)	35.5	35.2	32.8
Thermal Efficiency (%)	37.2	43.1	n/a
Thermal Usage Rate (kBTU/hr)	334	568	314
No. of Forced Outages	20	10	9
No. of Scheduled Outages	4	3	0
Mean Time Between Outages	814	892	709
Longest Time Between Outages	5,592	1,968	1,416
Unadjusted Availability (%)	87.2	88.8	90.1
Adjusted Availability (%)	95.2	93.0	95.6

Fuel Cell Emission Test Results for NYSERDA Fuel Cell Program

Emissions	Specification (lb/MMBTU)	St. Vincent's (lb/MMBTU)*	RIT (lb/MMBTU)*	Reifler Cement (lb/MMBTU)*
NOx	.02	.0036	.0013	.0028
CO	.20	.0036	.0007	.0011
Total Hydro Carbons	.02	.0008	.0008	.0009

* Full Load, Beginning of Life

USACERL/DoD DEMONSTRATION PROGRAM

USACERL is coordinating the installation of approximately 30 ONSI 200 kW phosphoric acid fuel cells at DoD installations. SAIC has installed three monitoring systems at the following locations:

Fort Eustis - Newport New, VA
Kirtland Air Force Base - Albuquerque, NM
Twentynine Palms Marine Corps. Base - Twentynine Palms, CA

The Fort Eustis fuel cell is installed at an athletic facility. The thermal output is used to heat the indoor swimming pool and the DHW used for showers. The fuel cell operates in the grid connected mode and as a back-up power source during electric grid outages.

The Kirtland Air Force Base fuel cell is located at a boiler plant where the thermal output is used to preheat the make-up water for the boilers. The fuel cell operates in the grid connected mode and as a back-up power source during electric grid outages.

The Twentynine Palms fuel cell is located at the Naval hospital on Base. The thermal output is sent to a 1,000 gallon storage tank where it is then used to supply two separate hot water loops for the building. The fuel cell operates in the grid connected mode and as a back-up power source to the hospital during utility grid outages. The existing back-up power provides power to the rest of the building.

The monitoring systems for the USACERL sites were installed in August, 1996 and thus no operating data were available at the time of this writing. In addition to the monitoring systems installed at each of the fuel cells, emissions monitoring will also be performed.

POWER CONVERSION AND QUALITY OF THE SANTA CLARA 2 MW DIRECT CARBONATE FUEL CELL DEMONSTRATION PLANT

A. J. Skok, (203) 778-1323
Fuel Cell Engineering Corporation
3 Great Pasture Road
Danbury, CT 06813

Ramon Z. Abueg (408) 970-3700
Basic Measuring Instruments
3250 Jay Street
Santa Clara, CA 95054

Paul Schwartz (714) 975-3900
Fluor Daniel, Inc.
3333 Michelson Drive
Irvine, CA 92730

Paul H. Eichenberger (408) 984-3158
City of Santa Clara
1500 Warburton Ave.
Santa Clara, CA 95050

M.N. Brodie (604) 488-2107
Fluor Daniel Wright, Ltd.
1075 W. Georgia Street
Vancouver, B.C. V6E-4M7

INTRODUCTION

The Santa Clara Demonstration Project (SCDP) is the first application of a commercial-scale carbonate fuel cell power plant on a U. S. electric utility system.(1) It is also the largest fuel cell power plant ever operated in the United States. The 2MW plant, located in Santa Clara, California, utilizes carbonate fuel cell technology developed by Energy Research Corporation (ERC) of Danbury, Connecticut.(2) The ultimate goal of a fuel cell power plant is to deliver usable power into an electrical distribution system. The power conversion sub-system does this for the Santa Clara Demonstration Plant. A description of this sub-system and its capabilities follows. The sub-system has demonstrated the capability to deliver real power, reactive power and to absorb reactive power on a utility grid. The sub-system can be operated in the same manner as a conventional rotating generator except with enhanced capabilities for reactive power. Measurements demonstrated the power quality from the plant in various operating modes was high quality utility grade power.

POWER PLANT ELECTRICAL SYSTEM

The electrical equipment included in a fuel cell installation has two main purposes. The first function is the adaption of the fuel cell output to suit the requirements at the point of delivery. The second function is the powering of all of the system auxiliaries and controls. The adaption of the direct current produced by the Santa Clara fuel cells into the three phase alternating current required by the utility is accomplished by solid state inverters and transformers with an efficiency approaching 98%. The switching of the current produces harmonics that are only acceptable at very low levels. The present installation uses gate turn off thyristors (GTO's), typical of an industrial drive, with pulse width modulated switching to minimize the lower order harmonics. There are four inverters arranged in pairs. The two inverters in each pair are connected to phase shifted transformers so each pair is electrically independent. The harmonics generated are well known and can be identified as (integral multiples of two times the number of phases) $\pm$ 1 (e.g. a simple three phase bridge produces (nx6) $\pm$ 1 or no.'s 5,7,11,13,17,19 etc.) The magnitude is inversely proportional to the harmonic number. Advantage is taken of these relationships by using two inverters operated with a 30° phase shift to produce a lower magnitude by eliminating (theoretically) the 5th and 7th harmonics. When the total power to be inverted exceeds the capacity of two bridges, consideration can be given to another phase shift to further reduce the harmonics level. The transformers are of "rectifier" construction, with allowance for the harmonics that must be handled. They are also given special attention to minimize the radiated noise for the benefit of the plant neighbors. Control is arranged to regulate the real power

output by controlling both the fuel rate and the electrical output. It is also able to regulate the imaginary power in magnitude and direction either for ± VARs or for voltage control. Protection is provided so that utility disturbance cannot damage the fuel cell installation, by blocking the inverter firing for short periods. Protection is provided for the utility by conventional isolation in case of an overcurrent malfunction. The power conversion equipment was supplied by ABB Industrial Systems, Inc.

TYPES OF POWER QUALITY DISTURBANCES

A power quality problem is any disturbance manifested in voltage, current or frequency deviations which result in failure of equipment. (3) A power disturbance may arise from several sources which include falling tree limbs, lightning strikes, feeder and load switching, operation of non-linear devices, and failure of a power system to maintain synchronous frequency. Power quality is a collection of different event types such as interruptions, rms variations, transients, and harmonics. Voltage sags, which can be caused by faults throughout the electrical transmission or distribution system, are the most serious of these power quality events. They can lead to the undesired shutdown of unprotected critical industrial processing equipment resulting in costly production interruptions. Another power quality phenomena is an oscillatory transient caused by capacitor switching. As more capacitor banks are added for power factor correction, transients during capacitor switching can get magnified. These transients may cause high transient voltages that can cause the malfunction of equipment and protective devices. Harmonic distortion is the non-linear distortion of a system characterized by the appearance in the output of harmonics other than the fundamental component when the input wave is sinusoidal. This is the result of connecting nonlinear loads such as adjustable speed drives, arc furnaces, compact fluorescent lights, and rectifiers. This is dependent on system impedance and the stiffness of the voltage source. Most problems occur when power factor capacitors cause the system to become resonant at a significant harmonic frequency. A harmonic-producing load can affect other loads if significant voltage distortion is caused. The resulting voltage distortion is a function of both the system impedance and the amount of current injected. The fact that the load current is distorted does not always mean that there will be adverse effects on other power consumers. If distortion on the voltage wave form exists, potential results include over-heating of transformers and motors, premature operation of protective devices including fuses, and metering inaccuracies. IEEE Standard 519, (4) specifies limits for harmonic current distortion that can be injected into the system. These limits are shown in Table 1. Values shown are in percent of "average maximum demand load current" and are applicable to twelve-pulse rectifiers.

Table 2. Harmonic Current Limits for SCDP Fuel Cell Power Plant

SCR=ISC/IL	h<11	11<h<17	17<h<23	23<h<35	h>35	TDD
<20%	5.66%	2.83%	2.12%	0.84%	0.42%	7.07%

Total Demand Distortion (TDD) a measure of part load harmonics to full load current is defined as:

$$TDD = \frac{\sqrt{\sum_{h=2}^{\infty} (I_h)^2}}{I_L} \times 100\%$$

Where:
I_h= magnitude of individual harmonic components (rms amps)
h = harmonic order
I_L = maximum demand load current (rms amps) defined above

MEASUREMENT EQUIPMENT

The instrument used to monitor power quality conditions for this project is the BMI (Basic Measuring Instruments) 7100 PQNode. It has the capability to measure rms variations (sags/swells), high speed transients (switching impulse), waveshape faults (capacitor switching), and harmonic distortions (FTT). Any disturbance on a voltage channel automatically cross-triggers all current and voltage measurement channels for a complete three-phase analysis. Voltage sag and swell (rms) disturbance recording is controlled by the following settings: threshold, hysteresis, cycles to trigger (pickup time), cycles to end (dropout time), time interval for Min/Avg/Max computations, and number of time intervals for each record. Voltage impulse disturbance in the 5kHz to 1MHz frequency range are sensed by peak detector circuits. Sub-cycle voltage disturbances are detected by waveshape fault detection circuits. Voltage waveshape fault event data files contain two cycles of captured waveform data, including one cycle of pre-triggered and one cycle of post-triggered waveform. The instrument uses a patented Floating Window Algorithm that captures any distortion on the voltage waveform including sub-cycle events. All disturbance events and steady state data are time and date stamped. Data collected from the instrument can be correlated to operations in the City of Santa Clara's power system grid or operational changes inside the plant.

PLANT POWER QUALITY

The primary power quality issues of an inverter power source are voltage wave form distortion, and current wave from distortion resulting from harmonics. The primary power conversion issues are efficiency and the ability of the power source to operate (ride) through load disturbances of short duration. The fuel cell power plants ability to inject variable amounts of volt-ampere reactive (VAR) power independent of real power increases the concern about voltage wave form distortion. During the operation of the fuel cell power plant, wave forms are continuously monitored. A typical wave form at rated power output is shown in Figure 1. The total harmonic distortion (THD) is 1.15% with the total odd and even components 1.02% and 0.53% respectively. This is excellent quality and well within the IEEE 519 requirements. A trend plot of the voltage harmonics is presented in Fig. 2. This shows the variation in the THD while the fuel cell plant was changing power output and other operating parameters.

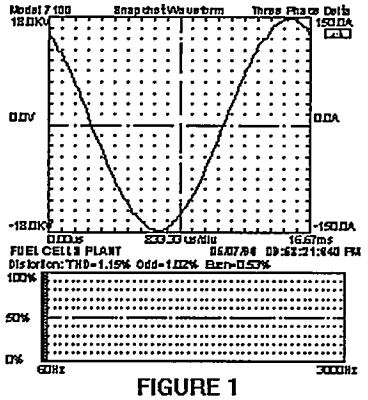

FIGURE 1

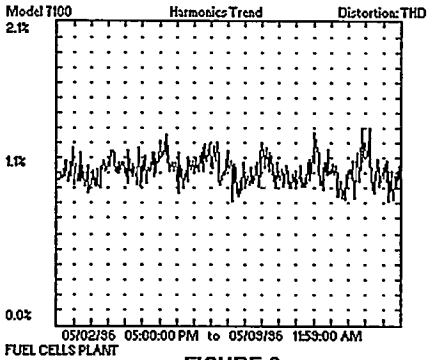

FIGURE 2

While initial data at some of the operating power plant conditions shows compliance to the harmonic limits of IEEE 519, as of the writing of this paper not all plant conditions have been tested and further data is required to fully verify compliance. From an operating stand point, the power plant has proven its capability to ride through short duration grid disturbances without tripping off line. Figure 3 shows a voltage sag on the City of Santa Clara Power System which was caused by an equipment failure. The failure was outside of the City's service area but it had affected the City's grid by causing a voltage sag lasting about 100mSec. On the 12KV feeder to which the plant is connected, the voltage reached a low of about 9.2 KV. This sag caused no upset with the power plant output. Using conventional technology we have demonstrated the fuel cell's ability to produce high quality utility grade power and deliver it to a utility system with high reliability.

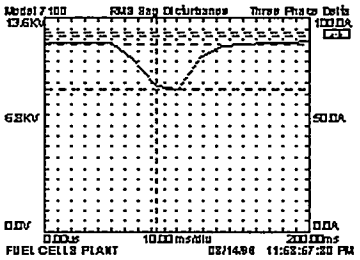

FIGURE 3

ACKNOWLEDGMENTS

In addition to the host utility (the City of Santa Clara), the project is supported by several other utility organizations, including the City of Los Angeles Department of Water and Power, the City of Vernon (CA), the Electric Power Research Institute, the National Rural Electric Cooperative Association, the Sacramento Municipal Utility District, the Southern California Edison Company, Salt River Project, and the Northern California Power Agency. Other funders include Fuel Cell Engineering Corporation (a subsidiary of ERC), the U.S. Department of Energy, and the California Energy Commission. The U.S. Department of Energy, through Morgantown Energy Technology Center, supported the design and construction of the fuel cell stack modules.

REFERENCES

(1) A. Skok, et al.; Startup, Testing, and Operation of the Santa Clara 2MW Direct Carbonate Fuel Cell Demonstration Plant. *Fuel Cells: Programs and Abstracts 1996 Fuel Cell Seminar.* November 1996.

(2) H. Maru, et at.; Direct Fuel Cell Product Design Improvement. *Fuel Cells: Programs and Abstracts 1996 Fuel Cell Seminar.* November 1996.

(3) IEEE Standard 1159-1995; *Recommended Practice for Monitoring Electric Power Quality.* Institute of Electrical and Electronics Engineers.

(4) IEEE Standard 519; *Recommended Practices and Requirements for Harmonic Control in Electrical Power Systems.* Institute of Electrical and Electronics Engineers

MAKING THE GRID THE BACKUP: UTILITY APPLICATIONS FOR FUEL CELL POWER

Sherri L. Eklof
Sacramento Municipal Utility District (SMUD)
Sacramento, CA

SMUD's Advanced and Renewable Technologies (ART) Program (I)

Fuel cells are recognized as a versatile power generation option and accepted component of SMUD's ART Program. SMUD has received wide support and recognition for promoting and implementing fuel cell power plants, as well as other innovative generation, based primarily on technological factors. Current economic and technical realities in the electric generation market highlight other important factors, such as the cost involved to develop a slate of such resources. The goal now is to develop only those select quality resources most likely to become commercially viable in the near future. The challenge becomes the identification of candidate technologies with the greatest potential, and then matching the technologies with the applications that will help to make them successful. Utility participation in this development is critical so as to provide the industry with case examples of advanced technologies that can be applied in a way beneficial to both the utility and its customers. The ART resource acquisitions provide the experience base upon which to guide this selection process, and should bring about the cost reductions and reliability improvements sought.

SMUD's Fuel Cell Experience

In 1994, SMUD completed the installation and energization of two 200 kW phosphoric acid fuel cells (PAFC) within the District's service territory. Both fuel cells are grid-connected with the utility. In the first installation, the fuel cell is sited at the Kaiser Hospital in South Sacramento. The electricity is sent to the SMUD grid while thermal energy is utilized by the hospital for hot water and space heating. The second fuel cell, sited at SMUD's Headquarters Annex building, generates electricity to the grid with no use of the waste heat. Through these two projects, SMUD is gaining experience in the installation, maintenance, and operation of grid-connected fuel cells. SMUD is now looking to move forward in the utilization of fuel cell power in an uninterruptable power supply (UPS) application. Our expectation and hope is to promote a new market niche in which fuel cell power can be used in increasingly cost effective premium power applications.

The UPS Niche

An increasing number of high technology, as well as traditional, businesses are concerned about the reliability and quality of their electricity, as well as an available backup to the normal power supply. The standard UPS design practice is to assume that normal energy needs are supplied from the local utility grid, with backup power during an outage provided by otherwise idle UPS equipment. The fuel cell power plant offers an alternative in which the grid is put in the backup role, with the fuel cell meeting the normal energy needs. This application provides the opportunity for compact, quiet, and efficient fuel cells to fill a new market niche as a cost effective alternative for providing clean and reliable power. To initiate this process, SMUD identifies customers who may be in need of premium power, such as those who are planning either the purchase or replacement of a UPS system. The utility-customer ties are strengthened as SMUD learns more about the energy needs of these customers. Alternatives for meeting premium power needs are discussed, with some customers enthusiastic about the development of a non-polluting source of generation to supply their power.

Premium Power Demonstration Project

SMUD's focus with regards to new technologies is to advance and promote select quality advanced and renewable technologies by demonstration and experience. A current SMUD ART project is the demonstration of a fuel cell in a premium power application, with the fuel cell as the primary source of power and the grid providing the backup. There may be an additional opportunity to expand the utility customer services to include operational support of UPS equipment provided to the customer. The utility-grid configuration which allows operation of the fuel cell power plant independent from the grid during normal system conditions is the Grid-Independent/Grid-Synchronized connection. (II) The fuel cell is synchronized with, but not connected to, the grid. The output of the fuel cell serves the dedicated customer load directly, and responds to load fluctuations. The fuel cell and the customer load are both isolated from disturbances on the grid. A 1/4 cycle static switch will be installed to transfer the load to grid power if the fuel cell shuts down or becomes otherwise unavailable.

Site Selection Factors

The following factors are important to the siting of the Fuel Cell Demonstration Project.

Customer Need - Customers who can benefit most from a premium power application have a strong interest in power quality and reliability, and are generally aware of the potential impacts of grid disturbances. Customers to consider first are those who have approached SMUD looking for help in ensuring their critical loads were consistently met. In this assessment, knowledge of the customer load is essential, with the more critical load best suited to be fed off a fuel cell dedicated to serving it.

Value to the Customer - Cost sharing, in the form of a premium energy rate to be paid by the customer, is an expected and necessary component of this project. It is therefore important to work with customers who both understand the benefit of being fed directly off a fuel cell, and are willing to pay extra for the increased power quality and reliability.

Load Compatibility - With the project output limited to the rating of a single fuel cell, it is important to match the magnitude of the dedicated load to the capability of the fuel cell, which tracks loads well up to 200 kW. A high load factor is desirable.

Thermal Energy Use - A site-specific consideration is whether or not thermal energy from the fuel cell is to be utilized, and in what application. This factor is important in defining the project scope, cost, and benefits.

Customer Site Evaluations

Various project sites have been, and continue to be, considered by SMUD for locating a fuel cell power plant in a UPS application. The factors listed above have been a guideline in this evaluation.

Medical Facility

Positron Emission Tomography (P.E.T.) is a sophisticated medical procedure used in examining and imaging the heart, brain, and other organs. Through this process, a cyclotron converts non-radioactive elements into positron-emitting radioactive isotopes, which are injected into the patient soon after their production. The radioactive compound is distributed through the body, and the P.E.T. scanner produces shows a video image that reveals information about the chemistry of the organ being examined, useful in diagnosing heart disease, cancerous tumors, and Alzheimer's Disease. (III)

The P.E.T. Imaging Center, located in SMUD's service territory, is a high tech medical facility which performs these tests. The customer has informed SMUD of the criticality of maintaining a continuous uninterrupted source of electric power to their equipment. Loss of power during this medical procedure results in a loss of the test data, requiring a repeat of the test procedure with higher costs and customer inconvenience. With the existing service off the distribution system, the facility has experienced interruptions in power due to disturbances on the grid. The facility baseload is approximately 50 kVA for the main distribution bus, and approximately 100 KVA for the transformer serving the entire building load. The load factor is 30-40%. There are no plans for recovery and use of the thermal energy at this site.

State Agency Computing Systems

There are existing dual utility feeds to maintain continuity of service to the critical computer and HVAC load at this state agency. The critical loads are divided among three static transfer switches, each of which switches between the two utility sources. In addition, an existing UPS consists of batteries to backup the static transfer switch which serves the critical computer load; however, the batteries are old and in need of replacement. Initial site monitoring has shown that this computer load is approximately 400-415 kVA. The load factor is high with little fluctuation around-the-clock. The batteries could be replaced with two fuel cells operating in parallel as the primary feed to the computers. The grid would serve to backup to the fuel cell power plant through a 1/4-cycle transfer switch. Additional monitoring is underway to investigate options for a third fuel cell to serve essential cooling equipment. Heat transfer is an additional option under consideration.

University Computer Center

A university campus computer lab has been considered to be fed off a fuel cell, in order to ensure high quality and reliability to the lab, which operates 24 hours a day. This site also includes a thermal application for recovery heat to heat the campus swimming pool. A downside is that the long distance between the computer lab and the swimming pool results in the thermal sales estimate being insufficient to cover the cost of the heat recovery system.

Administrative Data Center

The computer load at this facility is considered critical due to the great economic impact to the business in the event of a loss of power. To further increase reliability, alternatives are being considered beyond the existing motor generators with battery backup. Since the majority of outages occur on the distribution system, a second utility feed would provide greater assurance that at least one live utility feed would be available. A 12 kV automatic transfer switch (ATS) would tie into the existing service transformers, and transfer between utility feeds as required to maintain service. Fuel cell power to serve the critical load was an alternative solution; however, the magnitude of load (in the range of 800 kW) would require a multiple (four unit) installation.

The P.E.T. Fuel Cell Project

The P.E.T. Imaging Center was selected as the site for development of a demonstration project, with a single fuel cell in a grid-independent UPS-type of premium power application. The customer sees value in an increased level of reliability to ensure continuity of service to their high tech medical test equipment. They are open and interested in the option of a fuel cell power plant to serve their facility. Their strong interest in a increased level of reliability explains their willingness to contribute to the project cost, via a cost sharing plan in the form of an increased energy rate.

The following are current issues associated with this project. Work towards resolution of these issues is ongoing, with fuel cell installation anticipated during the first or second quarter of 1997.

Load Fluctuations

Extensive site monitoring at the site shows high-magnitude fluctuations in the customer load that the fuel cell would be required to handle. Work is ongoing to confirm the tolerance of the inverter in the fuel cell power plant's power module to load fluctuations. It is desirable that the fuel cell serve as much load as possible, while still ensuring that the magnitude and duration of fluctuations in load is within the fuel cell's capability. The source of the load fluctuation has been isolated to the chiller fed off the main electrical panel. While modifications to the chiller unit would reduce the magnitude of spiking seen, it is not yet known whether the reduction would sufficiently reduce the spikes to a magnitude within the fuel cell's tolerance. Further investigation is ongoing in this area.

Point of Interconnection

The two alternative electrical interconnections for the fuel cell are either outside at the 480 V transformer serving the entire building load, or inside the electrical room with possible reconfiguration of the panel. Serving the entire facility at the 480 V transformer is the more desirable option; however, there are a couple of complications which may instead require interconnection at the customer's electrical panel. In the event a determination is made that the fuel cell cannot tolerate the starting current of the chiller, a reconfiguration of the electrical circuits would allow removal of the chiller circuit from the fuel cell. The second complication is due to only two of the three service meters at the site belonging to the P.E.T. Imaging Center, with the third feeding another tenant of the building who may not be willing to pay the premium power surcharge. Either SMUD would agree to apply the standard rate regardless of the increased reliability, or the interconnection in the electrical room would have to be such that the meter in question is not served off the fuel cell.

Cost

A Department of Energy grant to buy down the capital cost of the fuel cell was necessary for project approval, and an application has been submitted. Meanwhile, negotiations are underway with the P.E.T. Imaging Center to agree on a premium power rate to cost-share the project expense. While the fuel cell installation is not in itself cost effective, SMUD views it as a demonstration project which presents the opportunity to gain experience and knowledge in applying a fuel cell to serve a dedicated customer load. The project is to be installed via a turnkey bid with ONSI Corporation based on SMUD specifications.

References

I. "Technology Development in a Competitive Environment," SMUD, Advanced and Renewable Technologies, 1995.

II. "Federal Technology Alert, Natural Gas Fuel Cells," Federal Energy Management Program, U.S. Department of Energy, November 1995.

III. Positron Emission Tomography, Patient Information Guide," Northern California Positron Emission Tomography Imaging Center.

DEVELOPMENT OF A 10 kW PEM FUEL CELL FOR STATIONARY APPLICATIONS

H. Barthels, J. Mergel, H.-F. Oetjen, V.M. Schmidt and U. Stimming
Institut für Energieverfahrenstechnik (IEV)
Forschungszentrum Jülich GmbH
52425 Jülich, Germany

Abstact
A 10 kW Proton Exchange Membrane Fuel Cell (PEMFC) is being developed as part of a long-term energy storage path for electricity in the photovoltaic demonstration plant called PHOEBUS at the Forschungszentrum Jülich.

Description of the System

The conversion of solar energy to electricity by photovoltaic modules is accompanied by an energy management problem with respect to power fluctuations and non-synchronized use. This requires the development of an integrated system that converts electricity into an appropiate energy carrier. The storage of solar energy can be performed by water electrolysis producing pure hydrogen and oxygen. The reconversion of the chemical energy into electricity via a fuel cell seems to be well suitable for the long-term storage path.

The Forschungszentrum Jülich GmbH (Research Centre) operates the PHOEBUS demonstration plant comprising all important components for an autonomous all-year energy supply from solar energy [1]. This plant provides electric energy for the Central Library of the Research Center. The plant has now been operated for two years and the experimental experiences gave important insights into the efficiency and operation of the system and its components (Fig.1). The system configuration shows the sums of annual energy flows on the individual paths and the average annual efficiencies of the individual components. In order to satisfy the requirements of autonomous supply, the incoming solar energy of 280 MWh/a is expected to provide the consumer with 17,6 MWh/a electric energy. Related to the solar-electric input of 28,8 Mwh/a an overall plant effiency of 61 % can be obtained.

For short term electricity storage lead acid accumulators are connected via the DC bus and DC/DC converters to the energy management system. On the long-term energy storage during winter months a hydrogen quantity of 1820 m^3 is required. For that the excess energy of the summer months is converted into hydrogen and oxygen by water electrolysis at 7 bar system pressure and transported via compressors to the high-pressure reservoirs. When solar energy supply is not sufficient, the two gases are reconverted into electricity in the fuel cell, depending on demand, and electric energy is fed into the DC bus.

An alkaline 26 kW electrolyser, equipped with highly efficient cells developed by the Research Centre has been working for more than two years without any problems also under fluctuating solar-specific conditions. An availability of 88 % was achieved.

PEM Fuel Cell Development

In the beginning of the project an alkaline fuel cell of the Siemens BZA 4-2 type has been integrated and reached its full electric power of 6.5 kW with an efficiency of 51 % (refered to the upper heating value of hydrogen), increasing to 57 % at partial load. Experience showed, however, that the alkaline fuel cell system is very sensitive to automatic operation due to its complex design and liquid electrolyte (KOH). Therefore, the development of a PEMFC was already begun in 1994 in cooperation with A.F. Sammer Corp./USA. The objective of this project is to build two low power density 5 kW PEMFC stacks.

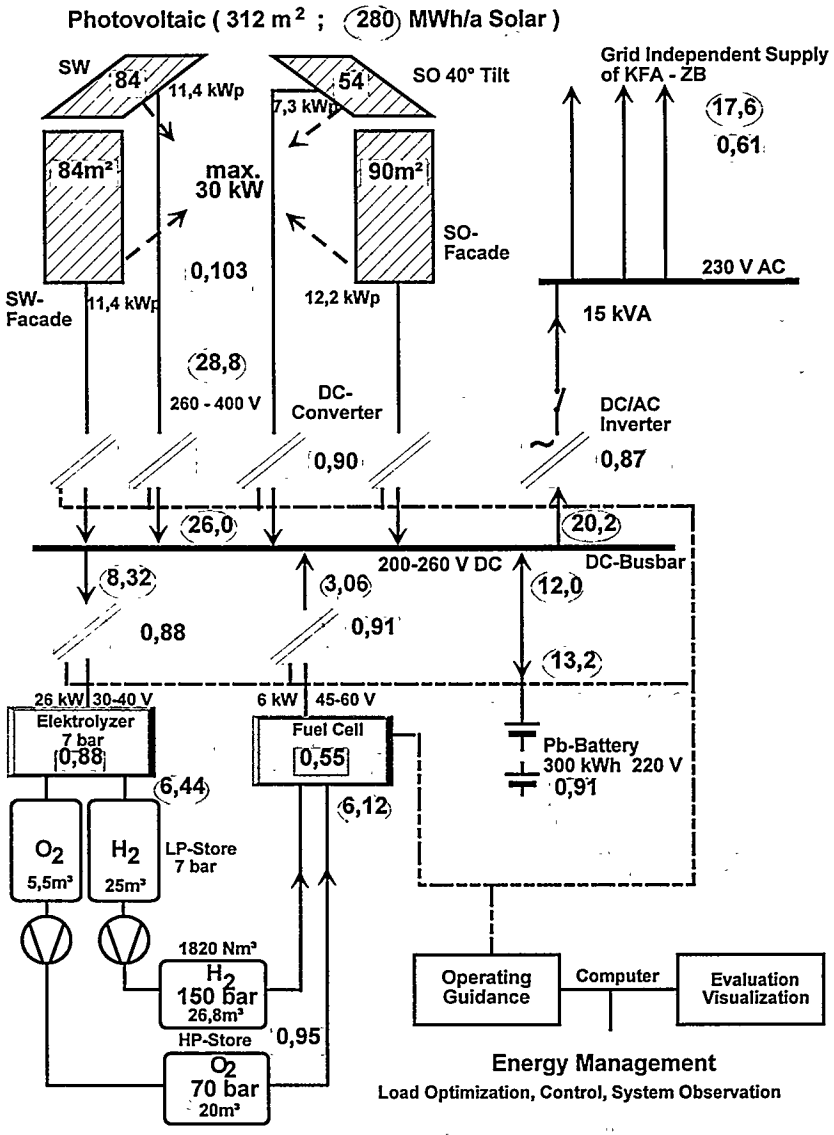

Fig. 1: System configuration of the plant PHOEBUS Jülich with the values of the annual energy sum [ ] in MWh/a on the individual paths and the mean annual efficiency of the individual plant components [ ]

In the present project phase a 2.5 kW stack is currently being tested in Jülich and the characteristics of cell voltage and power density as a function of current density is shown in the Fig. 2. The PEMFC stack having 26 cells with 300 cm^2 electrode area works with pure H_2 (p = 0.4 MPa) and O_2 (p = 0.45 MPa) in dead end operation mode at 70 °C. The Pt loading at the anode was 1.7 mg cm^{-2} and 4.3 mg cm^{-2} at the cathode. The humidification of the cell was performed internally and a special system for draining the product water was developed. This system shows satisfying performance. For an improved version of the stack some new cell components were developed in Jülich. Membrane electrode assemblies (MEAs) were fabricated by hot pressing of gas diffusion electrodes (GDE GmbH, Frankfurt/M, Germany) onto Nafion™117 membranes. The electrodes were impregnated with a Nafion™ solution with a loading of 1 mg cm^{-2}. As electrocatalyst 10 wt % Pt on Vulcan XC 72 was used with a final loading of 1 mg cm^{-2} at each electrode. MEAs were mounted in a four cell stack with the same materials as for the 2.5 kW stack and tested under the same conditions. Fig. 3 shows cell voltage-current density plots for each MEA in the small stack. At 0.7 V cell voltage 0.4 A cm^2 could be obtained which is an improvement of 0.05 A cm^{-2} even at lower catalyst loading compared to the average voltage of the 2.5 kW stack (see Fig. 2).

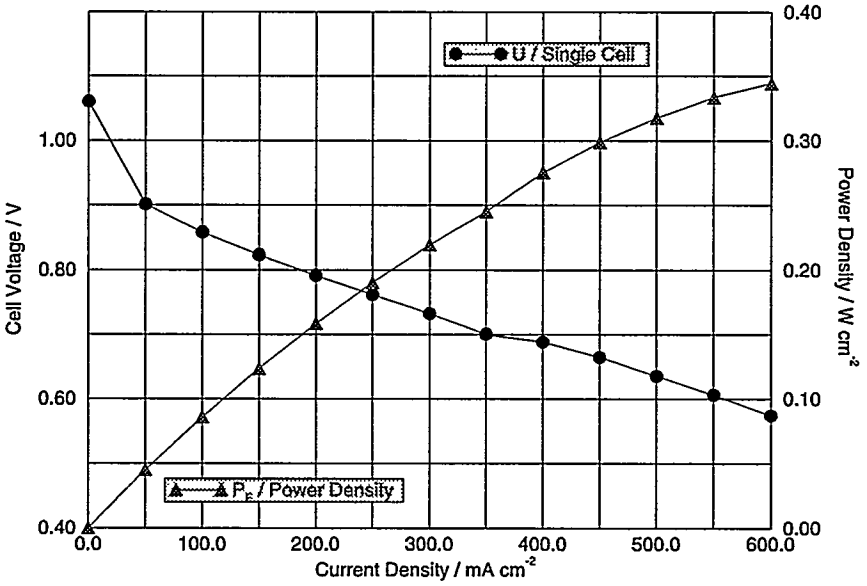

Fig. 2: Average Cell Performance of a 2.5 kW stack

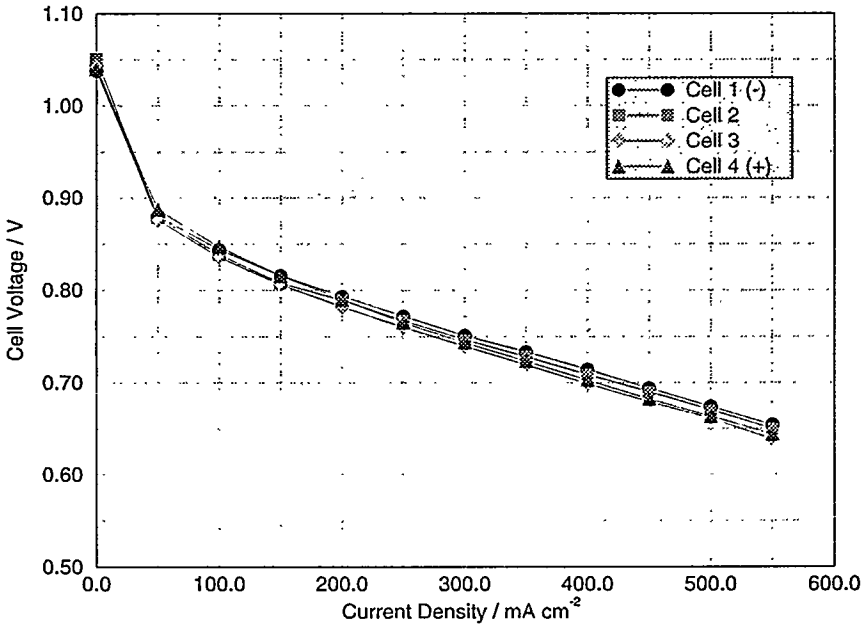

Fig. 3 Single cell performances of a 4- cell stack

Acknowledgement
We thank G. Wolfrum for preparing the MEAs. The project is founded by the Arbeitsgemeinschaft Solar NRW and Ministerium für Wissenschaft and Forschung of the State Nordrhein-Westfalen.

References
[1] H. Barthels, W.A. Brocke, K. Bonhoff, H.G. Groehn, G. Heuts, M. Lennartz, H. Mai, J. Mergel, L. Schmidt, P. Ritzenhoff,
11th World Hydrogen Energy Conference, 23-228 June 1996, Stuttgart, Hydrogen Energy Progress XI, T.N. Veziroglu, C.-J- Winter, J.P. Baselt, G. Kreysa (Eds.), 1996, p. 1005.

DEMONSTRATION OF AN ON-SITE PAFC COGENERATION SYSTEM WITH WASTE HEAT UTILIZATION BY A NEW GAS ABSORPTION CHILLER

Tatsuo Urata
Tokyo Gas Company, LTD.
1-16-25 Shibaura,Minato-ku Tokyo, 105 Japan

Introduction

Analysis and cost reduction of fuel cells is being promoted to achieve commercial on-site phosphoric acid fuel cells (on-site FC). However, for such cells to be effectively utilized, a cogeneration system designed to use the heat generated must be developed at low cost.

Room heating and hot-water supply are the most simple and efficient uses of the waste heat of fuel cells. However, due to the short room-heating period of about 4 months in most areas in Japan, the sites having demand for waste heat of fuel cells throughout the year will be limited to hotels and hospitals.

Tokyo Gas has therefore been developing an on-site FC and the technology to utilize the waste heat of fuel cells for room cooling by means of an absorption refrigerator.

The paper describes the results of fuel cell cogeneration tests conducted on a double effect gas absorption chiller heater with auxiliary waste heat recovery (WGAR) that Tokyo Gas developed in its Energy Technology Research Laboratory (1).

The fuel cell WGAR system

The methods of recovering waste heat from a cell stack cooling system and using it for room cooling being investigated by Tokyo Gas are shown in Table 1. The steam-driven double effect gas absorption refrigerator efficiently uses the waste heat from fuel cells; one unit needs to be installed exclusively for the fuel cell for operation, and other devices are also needed. On the other hand, since the hot-water driven absorption refrigerator has low efficiency and is normally installed jointly with a large double effect gas absorption refrigerator, the investment cost will also increase.

WGAR is equipped with a heat exchanger with auxiliary waste heat recovery in the weak solution line between the high-temperature solution heat exchanger and low-temperature solution heat exchanger of the gas-fired double effect absorption chiller heater. The feature of WGAR are as follows:

1. Fuel cell waste heat is utilized prior to city gas.
2. Since the fuel cell waste heat is not steam but water, the system is simple.
3. Its efficiency is higher than that of a hot-water driven absorption refrigerator.

Tokyo Gas developed WGAR technology in 1994 and revealed it to the makers of gas absorption chiller heaters, and in 1996 commercialized the technology jointly with each of the makers (Sanyo Electric, Hitachi Ltd. and Yazaki Sogyo).

Table 1. Comparison of features of heat utilization methods

Heat recover method	Heat output temperature	Operable chiller heater	Simplicity of system. Required auxiliary equipment
Direct cell cooling water	160 C water/steam	SDAC of ordinary specification	Special absorption chiller heater for fuel cell is needed.
Direct steam	6 k steam	SDAC of ordinary specification	Water treatment equipment for water recovery is added.
Indirect steam	Maximum 5 k steam	SDAC of special specification	Steam generator is added.
hot water	90 C water	WDAC of ordinary specification	It will be installed jointly with a double effect absorption chiller cooler.
hot water	90-120 C water	WGAR	Simple

SDAC=Steam double effect absorption chiller heater
WDAC=Water-driven double effect absorption cooler chiller

Outline of test

The PC25C (made by ONSI-TOSHIBA) equips a high grade heat option that allows the recovery of high-temperature water below 120Åé by exchanging heat with the cell cooling water. WGAR utilizes this waste high-temperature water above 88℃. A cooling capacity device of 150 USRT(527kW) (made by Hitachi) is used in WGAR. The electricity of the fuel cell is connected to the grid. WGAR is used for air-conditioning the main building of the Fundamental Technology Research Laboratory of Tokyo Gas. The test flow is shown in Fig. 1.

Temperature control of the high-temperature water is performed at the inlet of the fuel cell. As the temperature of the high-temperature water rises, heat is discharged by means of a cooling module via a heat exchanger. The temperature in the present test was set at 85℃. WGAR is designed not to perform heat exchange with the waste high-temperature water if the temperature of the waste high-temperature water is low.

The present test was conducted to assess whether operation of the fuel cell is stable even during non-steady state including refrigerator start-up, and to verify the effectiveness of the system.

Test results

Influence of fuel cell on operation

In the present system, the high-temperature water is generated by exchanging heat with the cell cooling water of the fuel cell. The influence of a change in the operating state including start-up of WGAR on the temperature of the cell cooling water of the fuel cell was examined.

As is evident from Fig. 2, the temperature of the high-temperature water dropped during the start-up operation of WGAR, because the heat was taken from WGAR. As for the temperature of the high-

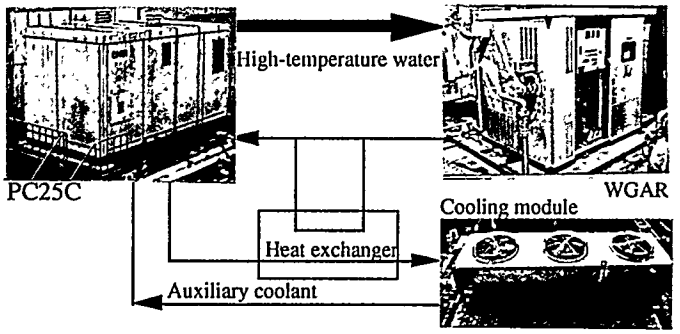

Fig. 1 FC-WGAR Test System

temperature water, the steady-state temperature varies with the solution temperature of WGAR, because the calorie output from the fuel cell is almost constant.

As for the heat output of the fuel cell, a slight temperature drop is observed in the cell cooling water, but its influence on the operation of the fuel cell may be small. On the other hand, when stopping operation of WGAR, the temperature of the high-temperature water rises, but almost no temperature variation was observed in the fuel cell cooling water.

Also, the measurements taken during operation suggested that the operation of WGAR has no adverse effect on the fuel cell.

Heat output efficiency of fuel cell

As for the high-temperature water heat efficiency of PC25C (LHV, high-temperature water of fuel cell inlet temperature: 85℃), a result exceeding 20% of the design value at 200 kW electric output was obtained (Fig.3). When all heat is used in WGAR, the utilization efficiency of the energies of electricity and heat added together was shown to be higher than 60%.

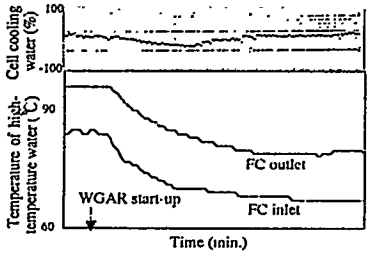

Fig. 2 Temperature changes in high-temperature water and cell cooling water during start-up of WGAR
(The range of temperature change in the cell cooling water during ordinary operation is assumed to be 100%)

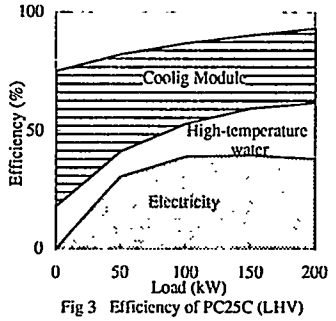

Fig 3 Efficiency of PC25C (LHV)

Test results of WGAR

A test to evaluate the effectiveness of this system was started in the summer of 1996. The data for two days when the atmospheric temperature and the room-cooling load were almost equal are shown below.

Figure 4 shows the fuel cell waste heat input and gas consumption while using fuel cell waste heat. Figure 5 shows gas consumption where fuel cell waste heat was not used. The variation of atmospheric temperature and the room-cooling load were in similar condition.

Room-cooling load is about 60% of the rated load of WGAR, waste heat is used prior to city gas, and all of the fuel cell waste heat is used. The reduction in city gas consumption was 360Mcal/day, and the reduction ratio was 17%.

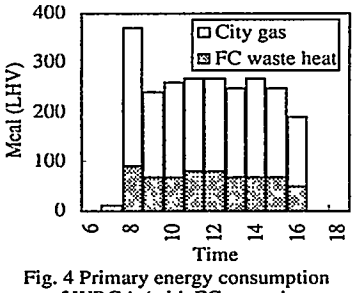

Fig. 4 Primary energy consumption of WRGA (with FC waste heat recovery) (August 13, 1996)

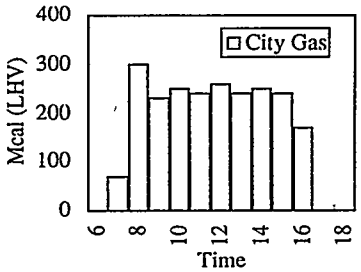

Fig. 5 Primary energy consumption of WRGA (without FC waste heat recovery) (August 14, 1996)

Conclusion

Demonstration tests of cogeneration in which the high-temperature waste heat of fuel cells is utilized in WGAR proved the stability and effectiveness of the system. Tokyo Gas will actively study the introduction of this system.

References

1. Hiroshi Kojima, "Development of gas absorption chiller heater with auxiliary waste heat recovery", international gas research conference, 1996.

OPERATING A FUEL CELL USING LANDFILL GAS

C. E. Trippel, Northeast Utilities Service Company
J. L. Preston, Jr., and J. Trocciola, International Fuel Cells
Dr. R. Spiegel, U.S. Environmental Protection Agency

An ONSI PC25™, 200 kW (nominal capacity) phosphoric acid fuel cell operating on landfill gas is installed at the Town of Groton Flanders Road landfill in Groton, Connecticut. This joint project by the Connecticut Light & Power Company (CL&P) which is an operating company of Northeast Utilities, the Town of Groton, International Fuel Cells (IFC), and the US EPA is intended to demonstrate the viability of installing, operating and maintaining a fuel cell operating on landfill gas at a landfill site. The goals of the project are to evaluate the fuel cell and gas pretreatment unit operation, test modifications to simplify the GPU design and demonstrate reliability of the entire system.

In 1992, the EPA contracted with IFC to design and build a landfill gas pretreatment unit (GPU) that would allow landfill gas (LFG) to be used by a fuel cell. Upon successful demonstration of the GPU, the fuel cell was installed at the Penrose Landfill in Los Angeles to demonstrate the system operation. The energy recovery system operated for approximately 3 months, concluding operations in February 1995. In order to verify operation on a different composition LFG and in different climatic conditions, the energy recovery system was shipped to the East Coast. Discussions between all parties resulted in the Town of Groton landfill being chosen as a site to continue operation of the fuel cell and GPU system. The fuel cell and GPU are currently owned by the EPA. CL&P is the funding source for the project and providing the engineering, design, and construction for the installation as well as the operation and maintenance for the 12-18 month demonstration period. IFC is providing technical expertise for the operation of fuel cell and GPU system. The Town of Groton is providing the site, the collected LFG and operation of an existing landfill gas flare at no cost to CL&P.

The LFG is collected from a 45 acre closed landfill. Based on the estimated volume of solid waste in the Groton landfill, a calculated 204 million cubic feet of LFG would be produced annually. Prior to the installation of the fuel cell system at Groton, the LFG was collected and burned in a flare at a rate of approximately 400 cubic feet per minute (cfm). The fuel cell system uses a maximum of 80 standard cfm of landfill gas while the remaining gas continues to be burned by the flare. Where landfill gas is emitted into the atmosphere without recovery and use, methane has a global warming potential much greater than that of carbon dioxide. Some of the non-methane constituents of LFG, such as hydrogen sulfide, are odoriferous and potentially harmful to the environment.

The fuel cell emissions are primarily water vapor and carbon dioxide. Emissions of NO_x and SO_x, which result from the combustion of LFG, are virtually eliminated. Due to its higher efficiency, the quantity of CO_2 emitted from the fuel cell is less than the amount created through combustion conversion electrical generators such as the combustion turbine and internal combustion engine. A comparison of typical emission rates is as follows:

	Typical Emission Rates (lbs/kWhr)		
	Combustion Turbine	Internal Combustion Engine	Fuel Cell
NOx	0.00153	0.00092	0.00001
SO_2	0.00017	0.00012	0
CO_2	1.96	1.37	0.96

System Description at the Groton Landfill

The LFG is collected from the closed and capped landfill through a series of wells and is drawn out of the landfill by the flare blower. This keeps about a 6 inch water column vacuum on the collection system. A landfill gas compressor draws landfill gas from collection header and compresses the gas to 40 psig for use in the GPU. Two hydrogen sulfide (H_2S) absorbers, using activated carbon as the absorbing medium, are installed on the suction side of the compressor to remove the H_2S from the gas stream prior to compression. A moisture separator prior to the H_2S absorbers removes any bulk moisture present in the gas. The H_2S absorbers are installed in a parallel/series arrangement where normal operation is in series but either absorber can be removed from service while the other is in service. This is useful for carbon change out during operation or testing the removal effectiveness of an individual absorber.

The gas is discharged from the gas compressor and into the GPU where moisture and VOC's including sulfides and halogenated compounds are removed. The GPU has dual clean up trains so when one train is in service cleaning the gas the other is being regenerated with a portion of the cleaned gas. The regeneration gas, in the quantity of 25 scfm, is combusted in an enclosed flare. The cleanup train consists of an alumina plus mole sieve dryer vessel which removes the moisture from the gas, a carbon vessel which absorbs hydrocarbons and VOC's and a refrigeration unit and heat exchanger which are used to cool the gas to 34° F prior to entering the clean up train. The gas leaves the GPU consisting of methane, carbon dioxide, and trace amounts of nitrogen and oxygen. The dew point of the gas is -20° F. The specific composition of the Groton landfill gas leaving the GPU is as follows:

Methane - 57.1%
Carbon dioxide - 41.0%
Nitrogen - 1.5%
Oxygen - 0.4%

The fuel cell has been modified for operation on landfill gas to accept the higher flow rate required because of the reduced methane content in the landfill gas. These modifications include a larger fuel control valve and fuel control venturi plus resizing of two fixed orifices. Minor modifications were also made to the control settings.

Site Layout

The attached site layout plan shows the equipment configuration. The total site encompasses an area 43 feet wide by 135 feet long and is enclosed by a chain link fence. Located at the south end of the site are the existing landfill gas flare and a newly installed underground storage tank to collect condensate that comes from the landfill with the gas as well as from the GPU. The GPU control room houses the GPU control panel, refrigeration unit purge air compressor, nitrogen bottles for actuating the GPU pneumatic valves and project documentation. The GPU flare is used to combust the regeneration gas. The gas pretreatment unit building is a pre-engineered building with aluminum sided and insulated walls and roof. The space inside the building is considered a Class 1, Division 2 location and all electrical equipment and fixtures are explosion proof. Enclosed in the gas pretreatment unit building is the LFG moisture separator, H_2S absorber vessels, gas compressor, GPU and refrigeration unit. A combustible gas detector is used to monitor the interior atmosphere and ultimately shut down the gas compressor if gas is detected. A compressed natural gas (CNG) bottle rack is required to supply start up burner fuel

for the fuel cell and for the GPU flare. The fuel cell and cooling module are in the standard configuration for a typical installation. A nitrogen bottle rack external to the fuel cell is used to increase bottle capacity and facilitate bottle change out. The switchgear contains the distribution bus and breakers for the fuel cell and all other site equipment. The step up transformer takes the 480 volt power from the fuel cell output and increases it to 13,800 volts for use on the utility grid. The equipment and site layout are designed for unmanned operation. Remote data monitoring of the fuel cell and GPU controller will be utilized.

Project Status

Construction was completed in mid June 1996 and system start up and testing is in progress at the time of the submittal of this extended abstract in late August 1996. Prior to start up of the fuel cell, the GPU was started and operated for 200 hours and gas quality suitable for fuel cell operation was verified. Operation of the fuel cell at the Groton site on landfill gas has been achieved with an output of 165 kW obtained to date. The power generated is enough to supply over 100 homes and is fed into the local utility grid.. Continued testing and refinement of the system is expected to achieve a continuous net fuel cell output of 140 kW.

Conclusion

The operation of fuel cells on landfill gas presents an opportunity to use a waste gas that is harmful to the environment to generate electricity more cleanly and efficiently than other methods currently used. The use of other bio gases, such as from waste water treatment plants and livestock wastes, in fuel cells is possible as a result of the work performed using landfill gas as a fuel. This project brings bio gas conversion using fuel cells one step closer to commercial application.

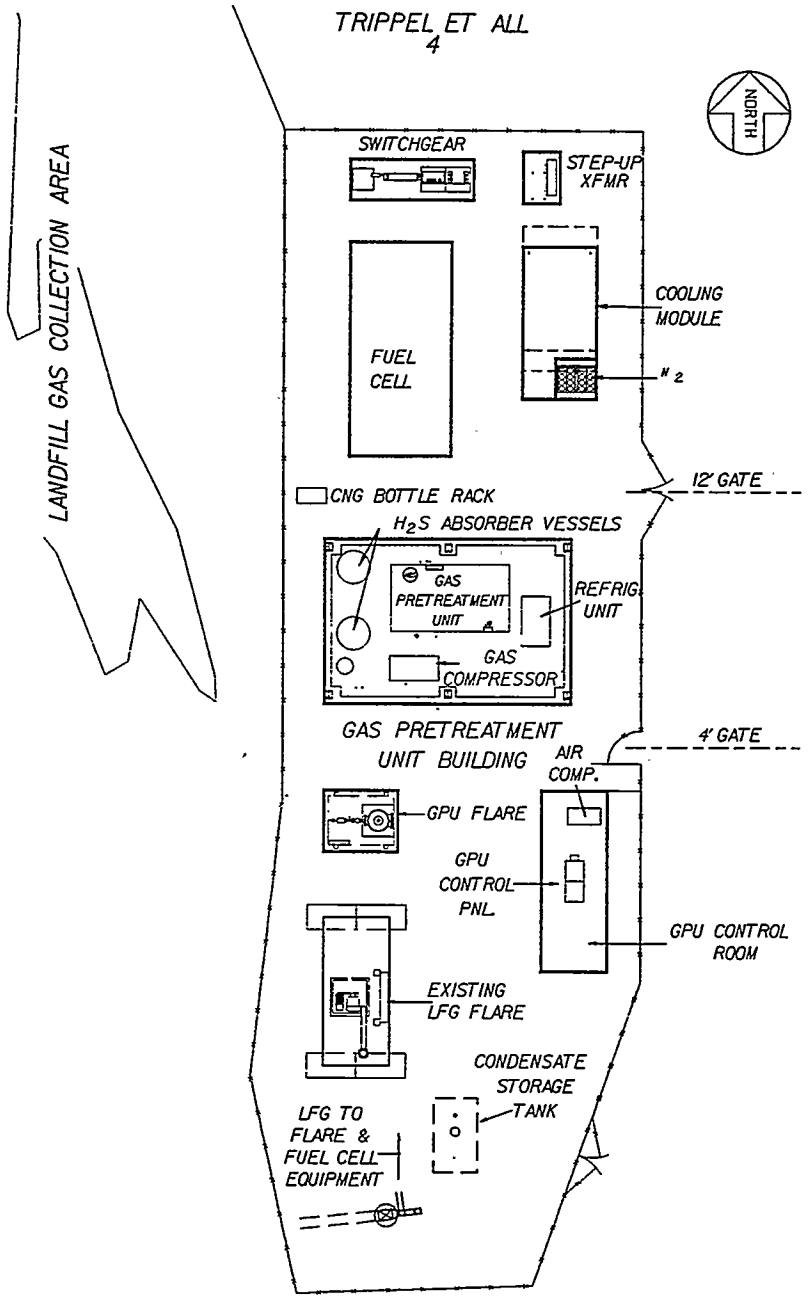

GROTON FUEL CELL SITE LAYOUT

ELECTRICAL POWER SYSTEMS FOR DISTRIBUTED GENERATION

Thomas A. Robertson and Steven J. Huval
Stewart & Stevenson Services, Inc.
Houston, Texas

ABSTRACT

"Distributed Generation" has become the "buzz" word of an electric utility industry facing deregulation. Many industrial facilities utilize equipment in distributed installations to serve the needs of a thermal host through the capture of exhaust energy in a heat recovery steam generator. The electrical power generated is then sold as a "side benefit" to the cost-effective supply of high quality thermal energy.

Distributed generation is desirable for many different reasons, each with unique characteristics of the product. Many years of experience in the distributed generation market has helped Stewart & Stevenson to define a range of product features that are crucial to most any application. The following paper will highlight a few of these applications. The paper will also examine the range of products currently available and in development. Finally, we will survey the additional services offered by Stewart & Stevenson to meet the needs of a rapidly changing power generation industry.

SIGNIFICANT FEATURES FOR DISTRIBUTED GENERATION

Power generation systems must offer a broad range of power outputs and operating characteristics to meet the various needs of prime power, peaking, peak shaving, and continuous base-load operation. As well, they should be natural gas fueled for economy and offer dual fuel capability for areas subject to gas curtailment. Systems must exhibit fuel efficiency, low emissions, and low noise to avoid difficulty in permitting; in short, designed to be a "good neighbor". Portable or transportable systems allow for cost-effective relocation as power needs change. Full-load factory testing avoids initial component failures and inadequate performance. Modular packaging of the main unit and ancillary systems, including controls and switchgear, equates to fast installation with minimal site work to bring power on line quickly, cost effectively, and avoiding extensive site rework. Desirable features of distributed generation also include:

- Unattended operation with full equipment protection and provisions for remote dispatch and supervisory control.
- A small footprint allowing for installation flexibility and parallel construction of permanent generating resources.
- High reliability and availability with first-class service and replacement parts to maximize revenues for customer satisfaction.
- Reduced line losses and disturbances, normally associated with long transmission and distribution systems.
- High quality power suitable for "droop" mode operation in parallel with the local utility, or " Isochronous" operation for isolated bus applications.
- Fast power response for load-following applications.
- Flexible financing or leasing options for short term needs.

TARGET MARKETS FOR DISTRIBUTED POWER

Most applications for distributed power are focused on electric and gas utility installations. Applications in these areas include prime power/base-load, sub-station, compressor, and large commercial equipment.

However, industrial applications present a unique set of requirements and opportunities for distributed power. For many industrial and chemical process plants, the total power consumption for a grassroots facility or the incremental power required for an expansion is less than 20 megawatts (MW). Added to that fact, are the plants' needs for large volumes of high quality steam and hot water. The results is a nearly ideal fit for a distributed power installation.

Additional benefits can be realized by locating the power generation system "inside the fence" at an industrial or chemical process plant. Support equipment normally associated with power generation systems, such as feed-water treatment systems, plant and instrument air, blow-down cooling water, and fire protection systems, can usually be found in industrial facilities. This equipment can be expanded to support the power generation system, with substantially lower capital expenditure than that required by new, dedicated facilities. Distributed power generation systems can be an economical alternative in such plants.

RECIPROCATING PRODUCTS

Generator sets are readily available in sizes ranging from ten kilowatt (kW) to ten MW, in single- and tandem-drive configurations. Stewart & Stevenson's broad range of power generation products powered by reciprocating engines offer portability, low capital cost, fast installation, reliable operation, and low maintenance. Our packages are built for indoor, outdoor, and extreme climate conditions. Sound attenuating enclosures allow these units to meet the most stringent noise requirements for installation near office areas. Yet, these enclosures maintain unobstructed service access to speed repair and maintenance activities, preserving the inherent high availability of the equipment. Our generator set utilize engines from well-known manufacturers such as Generac, Detroit Diesel, Cooper-Superior, EMD, Waukesha, Ruston, Krupp-MaK, and Mirrlees Blackstone. These units are available in an assortment of flexible fuel systems configurations like: Natural gas, diesel, crude oil, pilot-ignited natural gas (PING), and dual fuel (natural gas/diesel). This assures availability of low cost fuels in virtually any area of the world where is needed.

These units are widely varied for applications in both commercial and military applications. Applications like: standby, blackstart, continuous base-load, cogeneration, peaking, peak shaving, and ships' service. The generator sets are available in trailer-mounted configurations, as well as easily transportable units for conventional pad mounting. These units are ideal for service as temporary power while constructing or repairing your power station. You can even use our generator sets for permanent power, peak shavers, and standby power in parallel with larger power plants.

GAS TURBINE PRODUCTS

Stewart & Stevenson has become the world's leading supplier of power generation system utilizing highly-efficient, reliable, and cost-effective "aero-derivative" gas turbines. As the name implies, these engines derive their primary design characteristics from the airline industry. These engines have benefited from several decades of extensive investment in technology to improve efficiency, reliability, power density, reduced exhaust emissions, and

noise. This resulted in improved cost through volume production and component commonality. The gas turbines are available in sizes ranging from 500 kW to 52 MW.

Utilizing these "state-of-the-art" engines from well-known manufacturers, Stewart & Stevenson has developed a broad range of packaged power systems ideally suited to all aspects of distributed generation. Modular construction and a rigid "single-lift" baseplate with full-load factory string testing assures completion of plant installation in as little as 30 days from receipt of order. This significantly reduces project financing costs and provides almost immediate revenue recognition. The inherent small size and high reliability of the turbine, combined with the maintenance provisions incorporated into all Stewart & Stevenson gas turbine packages, assures minimal interruption of power output and revenues. This high availability and fast service/maintenance turn-around time is essential as distributed generation strive to prove itself as suitable replacement for traditional central power stations and multiple-feed grid interconnects.

Stewart & Stevenson gas turbine packages are installed around the world in virtually every type of application. There are portable and permanent application located on land, offshore platforms, and aboard ships of the U.S. and foreign Navies. These power plants provide reliable power and fuel-efficient operation. Today, there are over 740 Stewart & Stevenson gas turbine systems in operation worldwide.

All Stewart & Stevenson gas turbine equipment packages feature:

- Modular system construction with single-lift unitized package.
- Full equipment enclosure with ample workspace around components: large doors and removable walls for major equipment installation and removal; built-in engine removal equipment.
- Fully redundant ventilation systems, lube oil cooling, and filtration systems.
- Integral fire protection system.
- Oversized high efficiency generator.
- Uniform Building Code Zone Four Earthquake Level design.

FUEL CELL PRODUCTS

Stewart & Stevenson has achieved market dominance in engine driven products by keeping an eye and an open mind. Especially toward new developments that hold the promise of providing a product that better serves the needs of our customers. Often, this requires undertaking a leadership role in developing and applying new technologies. Utilizing our experience in power generation and customer knowledge base, assures new products are properly introduced to the marketplace. The latest example of this "eye-to-the-future" philosophy is our involvement in the development and commercialization of power plants utilizing Molten Carbonate fuel Cells (MCFC).

The IMHEX® Team is a partnership consisting of M-C Power Corporation, the fuel cell manufacturer; The Institute of Gas Technology, the fuel cell technology developer; Bechtel Corporation, the process designer; and Stewart & Stevenson Service, Inc., the system's integrator. Stewart & Stevenson is the exclusive distributor of IMHEX® MCFC power plants. The team is currently working on a 250 kW demonstration unit for San Diego Gas and Electric

Company. Construction is underway at the site, located at the Miramar Naval Air Station in San Diego, California. We have also begun a Department of Energy-sponsored program to produce a commercially viable one MW class power plant by the end of this decade. This technology promises extremely high fuel efficiency and immeasurably low emissions.

Advantages of Fuel Cell Power Plants. While fuel cell power units will contain many of the features common in Stewart & Stevenson's engine-driven products, they also offer advantage that distinguish this technology. A typical fuel cell power system is modular by design, including three basic sub-systems: (1) a fuel processor, (2) a power module (the fuel cell), and (3) the inverter. Many of the fuel cell 's advantages are derived from the inherent benefits of these sub-systems.

Fuel cells offer notable fuel flexibility. Typically, the first stage of the fuel cell system is a fuel processor. Therefore, adapting the fuel cell requires only selecting the appropriate fuel processor. Possible fuels include natural gas, landfill gas, digester gas, coal-derived gas, bio-gas, alcohols, methanol, and low methane gas.

The heart of the power unit the fuel cell also is the source of most significant advantages. The electrochemical operation of the fuel cell frees it of the limitations of the Carnot Cycle. The result is a very high efficiency: 45 to 70 percent (LHV, or low heating value) simple cycle efficiency and 70 to 90 percent (LHV) in cogeneration configurations. The fuel cell's efficiency is only marginally affected by temperature and part-load extremes.

Most significantly, the quiet and clean operation of the fuel cell simplify siting and permitting issues. Natural gas fuel cell power plants have a blanket exemption from regulations in California's South Coast Air Quality Management District, producing less than one audible decibels (dBA) at 30 feet. The result is flexibility in site selection with desirable features, such as:

- Indoor or outdoor installation, at or near load points.
- Fully dispatchable, remotely controlled, and unattended operation.
- Compatible with a phased-construction approach.

The final stage of the fuel cell power unit is the inverter. Since the fuel cell's output is direct current, an inverter is required to interface the power unit to an alternating current utility grid. However, the addition of solid-state system improves power quality by eliminating voltage fluctuations and reducing harmonic.

SALES AND SERVICE

Many customers have an immediate need for power. This is especially true with a cash/credit shortage brought on by the tough business climate of the last decade. This is when equipment leasing may provide an attractive options.

Stewart & Stevenson, in conjunction with General Electric Credit Corporation, has recently announced a program to make our gas turbine equipment immediately available for short or long term lease arrangements. This makes it even more practical to install "temporary" power means of delaying costly central station construction, or to install permanent generating capacity without the need to seek traditional financing from banks. Similar programs are being introduced or expanded to cover our smaller gas turbine units and our extensive line of reciprocating products.

A PRELIMINARY DESIGN AND BOP COST ANALYSIS OF M-C POWER'S MCFC COMMERCIAL UNIT

T. P. Chen
Bechtel Corporation
San Francisco, CA 94105

M-C Power Corporation plans to introduce its molten carbonate fuel cell (MCFC) market entry unit in the year 2000 for distributed and on-site power generation. Extensive efforts have been made to analyze the cell stack manufacturing costs. The major objective of this study is to conduct a detailed analysis of BOP costs based on an initial design of the market entry unit.

Major Facilities of the Unit

The design capacity chosen for the market entry unit is 1 MW. The unit is designed for 3 atm pressurized operation. It is totally self-contained, requiring only import of natural gas and a small amount of water. This design effort was very detailed, down to the sizing of each pipe and valve.

The cost analysis is based on a low production volume of 20-50 units per year. The purpose is to determine whether the fuel cell unit can meet the cost goal without the benefit of mass. Essentially, the cost estimate has no factored costs derived from similar project experience. Price quotes were obtained from equipment vendors and materials suppliers. An isometric of the 1 MW market entry unit is shown in Figure 1.

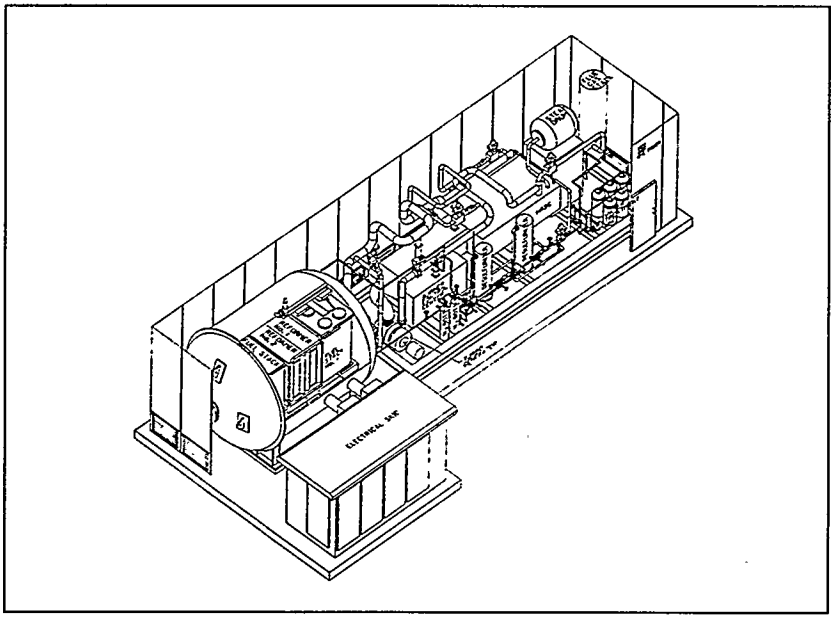

Figure 1: Isometric of the 1 MW market entry unit

The unit basically consists of three packaged skids which require minimum field assembly at the customer's site. The fuel cell skid includes two 300-cell stacks, two IHI plate reformers, and a housing vessel. The reformers convert natural gas into hydrogen and carbon monoxide as the stack fuel feed.

The process skid contains a heat recovery steam generator (HRSG), a turbogenerator, two nitrogen bottles, two desulfurization bottles, six demineralizer bottles, and two BFW pumps. The turbogenerator supplies compressed air as the stack oxidant feed and generates additional power by expanding the stack hot exhaust gas. A high frequency generator which rotates at the same high speed (40,000 rpm) as the turbine-compressor is used. It produces about 10% of the total power output. The expanded gas from the turbogenerator flows to the HRSG where waste heat is recovered to: (1) preheat the compressed air feed to the stacks, (2) preheat desulfurized natural gas from the desulfurizers, and (3) generate steam for the reformers. The HRSG is equipped with an auxiliary burner and the necessary burner control center to provide startup heat for the fuel cell unit. The BFW pumps deliver boiler feed water from the demineralizers to the HRSG. The nitrogen bottles provides purge gas during startup and shutdown and pressurized gas to operate the stack bellows. Most of process pipes are located on top of the HRSG to minimize plot area and pipe support structure requirements.

The electrical skid contains a power conditioning unit and a system control unit. The power conditioning unit has an inverter to convert the stack DC power into AC power. It also has a rectifier-inverter to adjust the turbogenerator high frequency power to standard 60 cycles. The system control unit is a simple industrial-size PC-based system geared for unattended operation of the fuel cell unit.

Each skid is sized within the height, length, and width limits for shipping. The unit is designed with maintenance in mind. Equipment requiring frequent service or replacement, such as the turbogenerator, nitrogen bottles, desulfurizer bottles, demineralizer bottles, and BFW pumps on the process skid, is easily accessible. The fuel cell vessel is oriented so that one vessel head does not face other skids and can be freely lifted open to pull out the stacks and reformers for repairs and other services. The only utility required by the market entry unit is 2 gpm raw water. No cooling water, nitrogen (for normal operation), boiler feed water, and compressed air are consumed.

Plant Performance

The energy conversion of the natural gas feed at full load operation and 60 F design ambient temperature is shown in Figure 2. The overall electric efficiency is very high, 54.4% based on HHV and 60% based on LHV. These efficiencies take into account conversion losses in the power conditioning unit. Because the current design is geared toward maximum power production, the

Figure 2

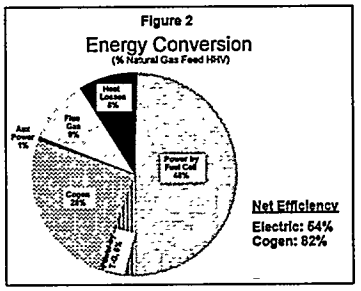

HRSG flue gas temperature is hot enough only for cogeneration of hot water. The recoverable heat corresponding to a 100 F final flue gas temperature is 28% of the total energy in the natural gas feed. The total thermal efficiency, including both power and hot water generation, is 82% on a HHV basis.

In the fuel cell unit, only the boiler feedwater pumps and control valve motors require minimal power. The total required auxiliary power is negligible and is one of the major reasons that the overall electric efficiency is so high.

Figure 3 shows the fuel cell unit is capable of turning down to approximately 30% load and still maintaining a reasonable electric efficiency close to 35% at this minimum load. The corresponding cogeneration efficiency is 67%. The amount of energy available for hot water production, which is the difference between the electric and cogeneration efficiencies, actually increases as the load is reduced. The fuel cell unit is sized for 60 F temperature. At both lower

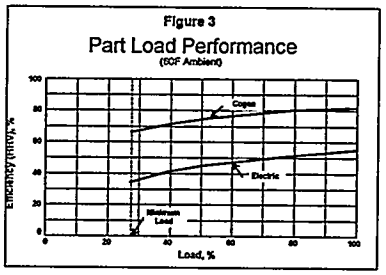

and higher ambient temperatures, the power output is reduced as limited by equipment size. The output is derated by about 8% at -20 F and 2% at 110 F.

The electric and cogeneration efficiencies are plotted as a function of ambient temperature in Figure 4. The efficiencies at -20 F are lower than those at 60 F because the colder air reduces the energy input to the fuel cell unit. The electric efficiency at 110 F is also lower than at 60 F because the additional energy brought in by the hotter air, as limited by equipment size, is not utilized for power generation. In addition, more power is required to compress the hot air. The additional energy in the hot air is transferred to the HRSG flue gas. As a result, the cogeneration efficiency is higher than at 60 F.

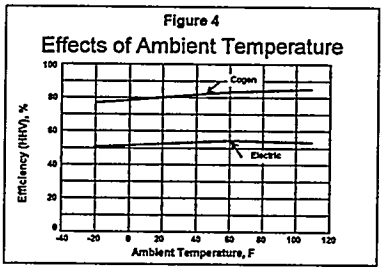

Plot Area Required

The footprint required by the 1 MW market entry unit is compared to a standard tennis court in Figure 5. The 0.75 ft^2/kW requirement is very small, and five such units can fit into an area of the size of a tennis court.

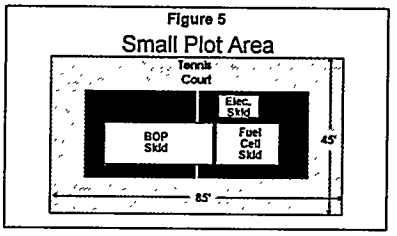

Total BOP Cost

The estimated BOP cost based on the first quarter, 1995 pricing, is shown in Figure 6. The 1 MW unit in the 20-50 units/year production range has a BOP cost of about $1,000/kW, which is the generally accepted cost goal for a successful market entry. A sensitivity study was conducted to determine the economy of scale if the power output were increased to 4 MW. In the 4 MW unit, the fuel cell skid and process skid consist of two parallel trains while the electrical skid has a single train. The increase in capacity from 1 MW to 4 MW reduces BOP costs by approximately 25%.

Figure 6

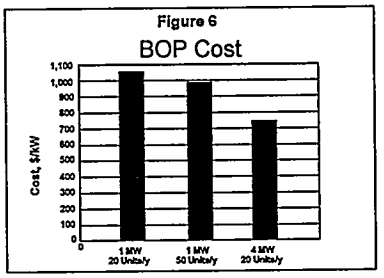

This study has not incorporated any design optimization. For example, the 3 atm system operating pressure was arbitrarily chosen without rigorous tradeoff analyses. The individual BOP components, such as the HRSG and inverter, have not gone through detailed mechanical design and packaging analysis. Additional design optimization efforts could yield significant benefits including further reduction in BOP costs, increased efficiencies, and an even smaller footprint.

Major BOP Cost Components

The major BOP cost components, as shown in Figure 7, are reformers, fuel cell vessel, turbogenerator, HRSG, control valves, process skid assembly labor, and power conditioning unit.

Figure 7

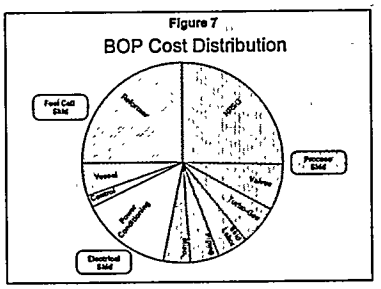

The horizontal fuel cell vessel design has significantly cut down the cost of this equipment. For the turbogenerator, the key issue is not to reduce the cost but to ensure that the projected cost can be achieved. The turbogenerator developer needs to work very closely with component and parts suppliers to determine the optimum design and manufacturing process. The HRSG design and cost estimate has not been optimized for the small-scale applications for fuel cell units. There should be ample opportunity to further reduce the HRSG cost, physical dimensions, and weight. Due to ever-improving electronics. the power conditioning unit has the highest cost reduction probability.

HIGH PRESSURE OPERATION OF TUBULAR SOLID OXIDE FUEL CELLS AND THEIR INTEGRATION WITH GAS TURBINES

C. Haynes, W.J. Wepfer
Georgia Institute of Technology
Atlanta, GA 30332

Fossil fuels continue to be used at a rate greater than that of their natural formation, and the current byproducts from their use are believed to have a detrimental effect on the environment (e.g. global warming). There is thus a significant impetus to have cleaner, more efficient fuel consumption alternatives. Recent progress has led to renewed vigor in the development of fuel cell technology, which has been shown to be capable of producing high efficiencies with relatively benign exhaust products. The tubular solid oxide fuel cell developed by Westinghouse Electric Corporation has shown significant promise. Modeling efforts have been and are underway to optimize and better understand this fuel cell technology. Thus far, the bulk of modeling efforts has been for operation at atmospheric pressure. There is now interest in developing high-efficiency integrated gas turbine/solid oxide fuel cell systems. Such operation of fuel cells would obviously occur at higher pressures. The fuel cells have been successfully modeled under high pressure operation and further investigated as integrated components of an open loop gas turbine cycle.

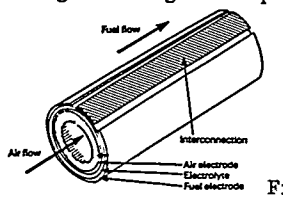

Figure 1

Air electrode supported-tubular solid oxide fuel cells, shown in Figure 1, developed by Westinghouse, have considerable design merit. The solid electrolyte eliminates problems typically associated with liquid electrolyte fuel cells. The tubular design allows for an innovative manufacturing technique and safer performance at the high operating temperatures of approximately 1000° C. Finally, the lack of a support tube significantly decreases the concentration polarization at the cathode (air electrode).

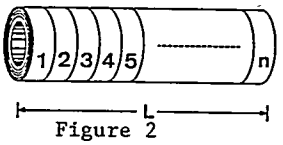

Figure 2

Modeling of fuel cell performance was based on the slice-by-slice, axial marching technique employed by Kanamura, et.al. (1). As illustrated in Figure 2, the fuel cell is divided into a preset number of subdivisions. Each slice may be viewed as a "minicell", with a given current, i_n, flowing from slice anode to cathode. All the slices have the same potential difference, ΔV, between cathode and anode. The governing electrochemical equation for each slice is :

$$\Delta V = \mathcal{E}_n - \Delta V_{pol,n} \qquad [1]$$

where $\mathcal{E}_n$ is the thermodynamic, equilibrium potential; and $\Delta V_{pol,n}$ is the overvoltage due to activation, concentration and ohmic irreversibilities. The equilibrium potential was obtained via the Nernst equation :

$$\mathcal{E}_n = -\Delta G^\circ/nF - R_u T/nF^* \ln \{\Pi f_{prod,n}^{v,prod} / \Pi f_{reac,n}^{v,reac}\} \qquad [2]$$

where "- ΔG^{o}" is the standard Gibbs free energy decrease, "nF" is the charge transferred per reaction and "f" is fugacity. The fuel stream was an ideal gas mixture of hydrogen and steam; the oxidant stream was air. The overall reaction was hydrogen being oxidized to water.

$$H_2 + 1/2\ O_2 \Longrightarrow H_2O \qquad [3]$$

The Nernst equation [2] simplifies to :

$$\mathcal{E}_n = - \Delta G^{o}_{\text{steam formation}}/2F - R_u T/2F * \ln \{p_{H2O,n}/ p_{H2,n}\ p_{O2,n}^{1/2}\} \qquad [4]$$

The ohmic irreversibility was the dominant irreversibility for these fuel cells operating at a high temperature (minimizing activation polarization) and utilizing no support tube (minimizing concentration polarization). The ohmic losses were routinely greater than 90% of polarization losses.

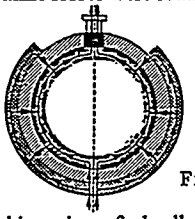

Figure 3

The ohmic loss calculated in a given fuel cell slice was based on Ohm's Law:

$$\Delta V_{n,ohmic} = i_n * R_n \qquad [5]$$

where R_n is the resistance of the slice to current flow. This calculation of resistance was based on the "transmission line" model (3). The proposed current path in a given slice is shown in Figure 3. Each half of a cell slice behaves as a resistor in parallel with the other half. Excellent correlation was obtained between model predictions and empirical results.

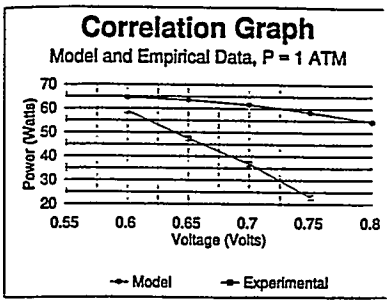

Figure 4(a)

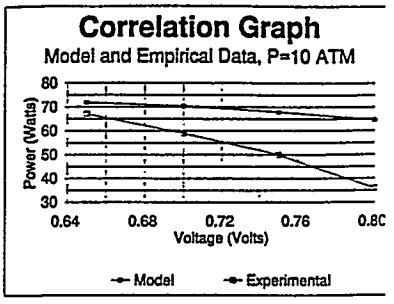

Figure 4(b)

The primary simplification used in the model is isothermal operation. It has been shown that non-isothermal modeling generally gives superior results (4),(5). For this reason the present attempt at modeling higher pressure operation of fuel cells was carefully done within a range of conditions such that results could be compared to published data and verified. For the air electrode supported tubular solid oxide fuel cell, of 50 cm length, Westinghouse published data on 85% fuel utilization of a hydrogen-steam mixture entering the fuel cell with six times the stoichiometric amount of air. Operation pressures ranged from 1-10 atmospheres (2). The fuel cells were operated at a nominal temperature of 1000° C. Emphasis is placed on the word "nominal", because there were temperature gradients present; however, near peak power, as can be seen in Figures 4(a)and 4(b), there was excellent agreement between isothermal model results and the empirical results. Bessette (4) indicates such good correspondence at peak power conditions. Fortunately such close compliance with field data is at current densities corresponding

to peak fuel cell power, because these are the conditions under which fuel cells are expected to operate, even as components in larger energy systems.

Air electrode supported-tubular solid oxide fuel cells have shown increases in power production capability over the previous designs due to the lack of a support tube. As well, high pressure operation of fuel cells has an increase in performance beyond that of Nernst potential consideration (2), because of decreasing polarization with higher pressure. Based on these factors, an investigation was made as to the thermodynamic merit of integrating an air electrode supported-tubular solid oxide fuel cell stack within an open loop Brayton cycle. The following Figure 5 is a flow diagram of the envisioned cycle.

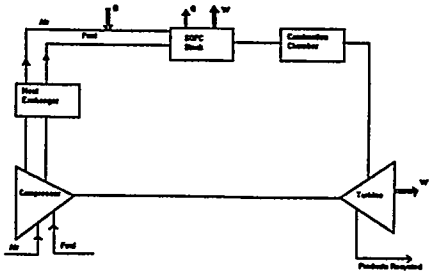

Figure 5

Fuel (89% H_2 , 11% H_2O) and air are compressed to the fuel cell operating pressure and heated as necessary before entering the cell stack. Both streams then pass through the fuel cell stack . Oxidation of the fuel is completed in the combustion chamber, whereupon the product gases expand through the prime mover. Usage of a fuel cell - gas turbine cycle would provide power and high quality heat to the plant. The system shown in Figure 5 was modeled and analyzed with the following simplifications. Compressor and turbine efficiencies are 75% and 80%, respectively, due to their expected size ranges. The fuel cells operate isothermally at 1000°C. Based on the earlier comparisons to experimental data (2), fuel cells were operated at peak power conditions, corresponding to 85% fuel utilization and six times stoichiometric air. These conditions showed the best match between the isothermal model and actual results. In this preliminary study, thermal and performance effects of fuel cell stack geometry were not considered. The 15% of unoxidized fuel leaving the fuel cell is combusted in an adiabatic combustion chamber so that the mixture reaches an adiabatic flame temperature of 1344 K (well below the state-of-the art material limits for turbines). The hot exhaust products from the turbine may be fed back to the hydrogen production section where, after deaeration, the remaining steam can be reused (e.g. steam reformation of methane). The independent variable of interest was operation pressure, ranging up to ten atmospheres. The dependent variables of interest were net power (per fuel cell) of the cycle, thermal efficiency and a modified thermal efficiency. Thermal efficiencies were defined as:

$$\eta = \text{Net power} / (LHV_{FUEL} + \text{Sensible Heat to Gas Flows}) \quad [6]$$

$$\eta_{modified} = \text{Net power} / (LHV_{FUEL} + \text{Sensible Heat to Gas Flows - Fuel Cell Heat}) \quad [7]$$

The modified thermal efficiency accounts for the high quality heat rejected by the fuel cells. Notice that both efficiencies account for the extra heat needed by the gas flow streams. This is particularly important when considering the needed preheating of air before entering the fuel cell stack.

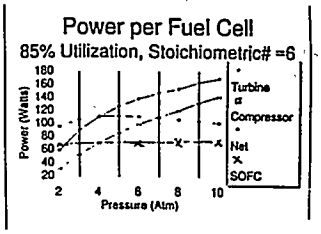

Figure 6

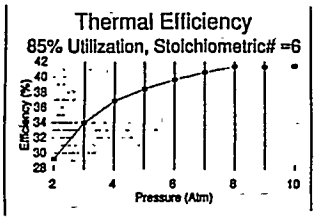

Figure 7

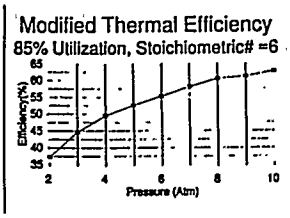

Figure 8

Figure 6 shows the net power per fuel cell going through a maximum. From two atmospheres to ten atmospheres, mass flow rate increased slightly above 5%, and the power per solid oxide fuel cell increased 10%. As well, for a reversible Brayton cycle, performance improves with increasing pressure ratio. Thus, one might expect a monotonic increase in net power, but due to the building influence of turbomachinery inefficiency (25% for the compressor and 20% for the turbine) at higher pressures, backwork, the ratio of compressor work to turbine work, becomes an increasing factor (it goes towards unity as pressure increases).

The system efficiencies measured in Figures 7 and 8 do not go through maxima, because even with net work decreasing, the sensible heating needed for the fluid streams leaving the compressor decreases enough to overcompensate the loss in net power. This decrease in sensible heating is again due to turbomachinery. The increase in irreversibility with higher pressure ratios manifests as larger stream temperatures leaving the compressor. As well, for the modified thermal efficiency, high quality waste heat increases with increasing pressure.

The thermal efficiencies have evident trends. The modified thermal efficiencies are consistently 15-20% higher than the electric thermal efficiencies. This emphasizes the importance of considering the high quality heat rejected from the fuel cell stack. Note that the gain in both thermal efficiencies, from one operation pressure to the next, drops off increasingly at higher pressures. It is important to further analyze and understand this asymptotic trend of the thermal efficiencies.

REFERENCES

1. K. Kanamura, S. Yoshioka and Z. Takehara, "Temperature Distribution in Tubular Solid Oxide Fuel Cell," Proceedings of the First International Symposium on Solid Oxide Fuel Cells, The Electrochemical Society (High Temperature Materials Division), Proceedings Volume 89-11, 1989.

2. Norman Bessette and Raymond George, " Performance Reliability of Westinghouse's Air Electrode Supported Solid Oxide Fuel Cell at Atmospheric and Elevated Pressures", DENKI KAGAKU, (Accepted March 15, 1996).

3. E.F. Sverdrup, C.J. Warde and R.L. Eback, " Design of High-Temperature Solid-Electrolyte Fuel-Cell Batteries for Maximum Power Output per Unit Volume", Energy Conversion, 13, pp.129.

4. Norman F. Bessette II, "Modeling and Simulation for Solid Oxide Fuel Cell Power Systems", Dissertation, Georgia Institute of Technology, July 1994.

EFFECT OF MICROSTRUCTURE ON THE HIGH TEMPERATURE MECHANICAL PROPERTIES OF $(CeO_2)_{0.8}(GdO_{1.5})_{0.2}$ ELECTROLYTES

N M Sammes and Y Zhang
Centre for Technology,
The University of Waikato,
Private Bag 3105, Hamilton,
New Zealand

INTRODUCTION

CeO_2-based oxides have recently been shown to have great potential as electrolytes in medium temperature solid oxide fuel cell applications, primarily due to their high ionic conductivity [1-3]. Steele et al. [4], for example, have examined a cell of the type:

O_2, $La_{0.6}Sr_{0.4}Fe_{0.8}Co_{0.2}O_3|Ce_{0.9}Gd_{0.1}O_{1.95}|Ni\text{-}ZrO_2$, H_2/H_2O at 715°C.

Gd_2O_3 doped CeO_2 has been reported [5] as having one of the highest oxygen ion conductivities of the ceria-based materials. An ionic conductivity of 8.3 x 10^{-2} s/cm has been reported for $(CeO_2)_{0.8}(GdO_{1.5})_{0.2}$ at 800°C, which is approximately four times that of Y_2O_3-doped ZrO_2, at the same temperature [6].

Although the electrical properties of the material have been examined in detail, very little work has considered the microstructural/property relationships, particularly in relation to the mechanical properties. It is well know that CeO_2-based materials are difficult to densify and attempts have been performed to examine this [7]. Preliminary studies have also been undertaken to examine the effect of sintering on the mechanical properties of the material [8]. In this paper we examine the effect of microstructure on the high temperature mechanical properties of $(CeO_2)_{0.8}(GdO_{1.5})_{0.2}$.

EXPERIMENTAL

$(CeO_2)_{0.8}(GdO_{1.5})_{0.2}$ powder was synthesised from $Ce(NO_3)_3$ (99.9% Janssen) and $Gd(NO_3)_3$ (99.9% Aldrich) using a reverse strike co-precipitation technique. The correct stoichiometric amounts of the nitrates were weighed and dissolved in distilled water and stirred for 20 mins. An aqueous oxalic acid (BDH) solution, with a concentration of 0.05M, was then added dropwise into the precipitant (which had been adjusted to pH 6.7 - 6.9) and stirred at 750rpm. The precipitate was then filtered and washed using distilled water (5x), followed by ethanol washing (5x), drying at 50°C (12 hours) and calcining at 700°C/1hr. Milling was performed using a Retsch centrifugal ball mill S1, with a porcelain jar and partially stabilized zirconia (PSZ) milling media. Milling was performed on the calcined powders for 15min., followed by 12hr. drying.

The calcined powders were fabricated into bars (30 x 10 x 3mm) using a standard die press, followed by isostatic pressing (stansted fluid power ltd FPG 2347) at 200MPa. The samples were then sintered in air at between 1550 - 1650°C/15 hrs. The surfaces and edges of all samples were ground using SiC grinding paper (320# - 4000#) followed by polishing (1μm diamond paste). After polishing, all the samples were annealed at 1000°C/2hr. to remove induced residual stresses. The samples (both powder and sintered bars) were examined using a Philips X-pert powder x-ray diffractometer, from room temperature to 1000°C. Scanning electron microscopy (SEM) and energy-dispersive spectroscopy (EDAX) were performed using a Hitatchi S4000 SEM and a Kevex microanalyser attached to the SEM, respectively. Coated samples were examined using either carbon deposition (for EDAX) analysis or rf sputtered gold. Density measurements were performed using the standard Archimedes method.

An Instron 4204 Universal tensile tester, with IEEE-48 interface controlled by an IBM 386 computer, was used for all the flexure testing. 4-point bend tests were performed using a top cross-head span of 10mm and support span of 20mm. A strain gauge (Instron 2630 - 021) was used in these tests to measure the deflection of the beam. All tests were performed at 0.2mm/min. The high-temperature tests were performed using a specially designed furnace integrated into the Instron tester. All samples were heated at a rate of 200°C/hr. and allowed to stabilize for 2hr. before starting the test. A minimum of 8 samples were examined for each test performed.

RESULTS AND DISCUSSION

It is well known that the particle and agglomerate size and shape affects the sintered density of a fired ceramic material, and thus its mechanical integrity. In this work, the effect of milling and calcination temperature was examined. The fired-ceramics fabricated from un-milled powders contained particles that were angular in shape and produced sintered densities of less than 80% theoretical, while the fired-ceramics produced from milled samples (48 hr. using PSZ as a milling medium) were granular in shape and produced sintered densities greater than 95% depending upon the calcination temperature; as described by Reed [9]. Table 1 shows the effect of calcination temperature on the fired density of the $(CeO_2)_{0.8}(GdO_{1.5})_{0.2}$ sample after sintering milled powder at temperatures ranging from 1550 - 1650°C.

Table 1. The effect of Sintering Temperature on the Percentage Theoretical Density of $(CeO_2)_{0.8}(GdO_{1.5})_{0.2}$ as a function of Calcination Temperature.

	Sintered Density at Calcination Temperature			
Sinter Temperature (°C)	Calcined at 600°C	Calcined at 1000°C	Calcined at 1200°C	Particle size (μm) of fired ceramic
1550	91.3	90.5	87.8	3-5
1600	95.5	95.0	95.0	3-5
1650	97.9	96.5	94.9	15-20, 3-7

The sintered density increases as the calcination temperature decreases. This can be explained as a result of the change in the powder morphology with calcination temperature. With increasing calcination temperature, the powder agglomerates become harder, denser and more angular. This results in a retardation of the particle flow and hence in the plastic deformation during pressing; this produces a more porous sintered ceramic.

Increasing the sintering temperature produces an increase in the sintered density of the material, however the microstructure is also affected. Fig. 1 shows the microstructure of $(CeO_2)_{0.8}(GdO_{1.5})_{0.2}$ sintered at 1600°C/15 hrs., while Fig. 2 shows the microstructure of $(CeO_2)_{0.8}(GdO_{1.5})_{0.2}$ sintered at 1650°C/15 hrs. Fig. 1 indicates that the sample has a regular grain size (approximately 3 - 5μm in size), with a number of closed pores at the grain boundary intersects, which indicates that the sample has reached the final stage of sintering [9]. Fig. 2, however, shows a microstructure containing a mixture of coarse grains (20 μm in size) and fine grains (3-7 μm). The sample contains fewer pores than the sample in Fig.1, but appears to have been oversintered [10].

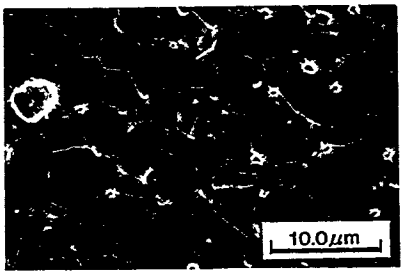

Fig. 1 SEM micrograph of a polished sample of $(CeO_2)_{0.8}(GdO_{1.5})_{0.2}$, sintered at 1600°C/15 hrs.

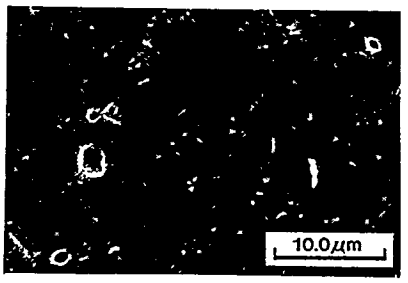

Fig. 2 SEM micrograph of a polished sample of $(CeO_2)_{0.8}(GdO_{1.5})_{0.2}$, sintered at 1650°C/15 hrs.

The room temperature modulus of rupture (MOR) of the samples described in Table 1 was examined, and is shown in Fig. 3. At a sintering temperature of 1600°C, the MOR variation, as a function of calcination temperature, is very small compared to the samples sintered at the other temperatures. This appears to indicate that the powder morphology plays a minor role in the initial fracture mechanism of the sintered sample, and thus the variation can be postulated as being primarily due to the sintering temperature. Under-sintering (at 1550°C, for example) produces a sample with a large number of pores, because it has not yet developed into a fully dense body and may only be in the intermediate stages of sintering [9]. Thus, failure due to the pores can be postulated as being the main fracture mechanism. Over sintering (1650°C, for example) causes a reduction in the MOR via the presence of large grains. The higher temperature also causes the pores to grow via Ostwald ripening, and thus can act as fracture initiation sites. Thus, the optimum sintering temperature for this sample was found to be 1600°C.

The modulus of rupture of $(CeO_2)_{0.8}(GdO_{1.5})_{0.2}$, sintered at 1600°C, was examined as a function of temperature and is shown in Fig. 4.

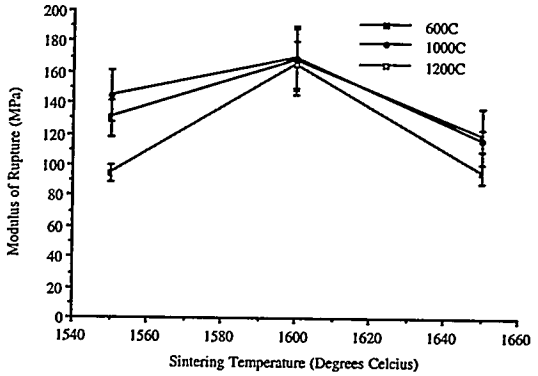

Fig. 3 The modulus of rupture of $(CeO_2)_{0.8}(GdO_{1.5})_{0.2}$ as a function of sintering temperature, at various calcination temperatures.

In general, Fig.4 shows that the modulus of rupture between room temperature and 500°C changes by very little; the increase is possibly an experimental artefact. However, there is an obvious drop in the modulus of rupture between 500°C and 800°C for this particular sample. On examination of the fracture surface at the lower test temperatures, it was apparent that the fracture was due to the extension of flaws and was, therefore independent of temperature, as discussed by Davidge and Evans [11]. At the higher test temperature, the modulus of rupture decreased. At this temperature, various plastic processes (dislocation motion, grain boundary sliding and plastic flow in the second phase) lead to the initial fracture [8]. This is more fully described in [12].

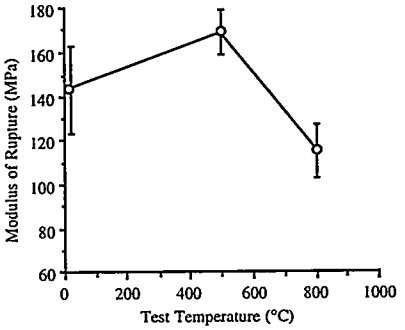

Fig. 4 The effect of test temperature on the modulus of rupture of $(CeO_2)_{0.8}(GdO_{1.5})_{0.2}$

CONCLUSIONS

In conclusion, the fabrication of strong, dense ceria-based electrolytes depends upon the synthesis and fabrication route undertaken. In this work, the optimum calcination temperature, for milled co-precipitated powders, was found to be 600°C, which produced as optimum sintered density of 98% theoretical at a sintering temperature of 1600°C. The sample showed a room temperature modulus of rupture of 165MPa, which is considerably lower than that of yttria-stabilized zirconia, and decreased at temperatures above 500°C.

REFERENCES

1. H.Yahiro, Y.Baba, K.Eguchi and H.Arai, J.Electrochem.Soc., 135, (1988) 2077.
2. S. Hamakawa, T. Hayakawa, H. Yasuda, K.Suzuki, M.Shimizu and K. Takehira, J.Electrochem.Soc., 142, (1995) 159.
3. H. Yahiro, Y. Eguchi, K. Eguchi and H.Arai, J.Appl.Electrochem., 18, (1988) 527.
4. B.C.H. Steele, K.Zheng, N. Kiratzis, R. Rudkin and G.M. Christie in 1994 Fuel Cell Seminar, Courtesy Associates Inc., Washington DC, p481 (1994).
5. T. Kudo and H. Obayashi, J. Electrochem. Soc., 122, (1975) 142.
6. H. Yahiro. E. Eguchi and H. Arai, Solid State Ionics, 36, (1989) 71.
7. C.C. Chen, M.M. Nasrallah and H.U. Anderson, J.Electrochem.Soc., 140, (1993) 3555.
8. N. Sammes, Y. Zhang, G. Tompsett, A.M. Cartner and R. Torrens, Denki Kagaku, 64, (1996) 674.
9. J.S. Reed, *Introduction to the Principles of Ceramic Processing,* J. Wiley and Sons, New York, 1986.
10. G.W. Scherer, J. Amer. Ceram. Soc., 74, (1991) 1523.
11. R.W. Davidge and A.G. Evans, Mater. Sci. and Eng., 6, (1970) 281.
12. N.M. Sammes and Y. Zhang, in Proceedings of the Second European SOFC Conference, p697 (1996).

Improvement of SOFC Electrodes Using Mixed Ionic-Electronic Conductors

Y. Matsuzaki and M. Hishinuma
Fundamental Technology Research Laboratory
Tokyo Gas Co., LTD.
16-25 Shibaura, 1-chome, Minato-ku
Tokyo, 105 Japan

1. Introduction

Since the electrode reaction of SOFC is limited to the proximity of a triple phase boundary (TPB), the local current density at the electrode and electrolyte interface is larger than mean current density, which causes large ohmic and electrode polarization[1]. This paper describes an application of mixed ionic-electronic conductors to reduce such polarization by means of (1) enhancing ionic conductivity of the electrolyte surface layer by coating a high ionic connductors, and (2) reducing the local current density by increasing the electrochemically active sites.

2. Experimental Procedure

Tetragonal yttria-stabilized zirconia (3 mole % Y_2O_3) sheets of 6 cm square and 100 μm thick were used as electrolyte. Sr-doped $LaMnO_3$ (LSM) was used for the air electrode material. $Ce_{0.8}Sm_{0.2}O_{1.9}$ (SDC) was used as a coating material of the electrolyte surface of the air electrode side. To obtain the dense SDC layer, a Ce metallo-organic compound was added to the SDC powder and the mixture was milled by a ball mill. The slurry was then screen-printed on the electrolyte sheet before firing. The fuel electrode was prepared by using the PMSS process[1] which gave high dispersion of the fine YSZ particles in the cermet. Ni-YSZ cermet was typically used for the fuel electrode, but in some cases, CeO_2 was deped to YSZ in the cermet to investigate the effect of it.

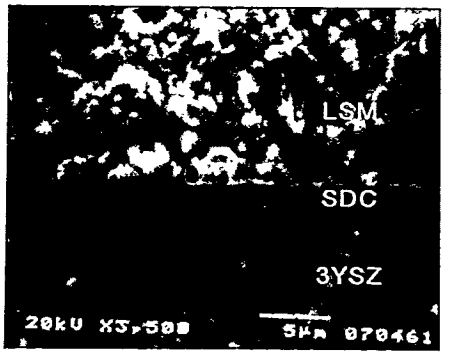

Figure 1 Cross sectional image of the SDC inter-layer prepared at the cathode/electrolyte interface.

3. Effect of SDC layer on the cathode

The ionic conductivity of SDC at 1000°C is 0.35 Scm^{-1}, which is approximately six times

larger than that of 3YSZ[2]. To reduce the overpotential at the air electrode, the SDC layer was prepared at the cathode/electrolyte interface. As shown in the SEM image in Figure 1, the SDC layer is about 5 μm thick and dense. Figure 2 shows the V-I characteristics of three types of single cells. Hydrogen was used as a fuel, and air as an oxidizer. Cell (a) had the Ni-YSZ anode and the LSM cathode. Although cell (b) had the same anode of the cell (a), it had modified cathode with the SDC layer. The SDC layer coating was found to improve cell performance. It was also found through half cell tests that the polarization (IR free) characteristics of the air electrodes were almost same, irrespective of the SDC layer. This suggests that the improvement in performance from cell (a) to cell (b) is due to the reduction in ohmic resistance.

Figure 3 shows the effect of the SDC layer on cell durability. The formation of the SDC layer at the cathode/electrolyte interface is extremely effective in improving long-term stability. SEM observation of aged samples revealed that the air electrode without the SDC layer showed some change in microstructure at the cathode/electrolyte interface, while the air electrode with the SDC layer showed negligible change in the microstructure. This is because of the difference in the reactivity of YSZ and SDC to La_2O_3. The ionic radius of La^{3+} is larger than that of Zr^{4+}, so that La^{3+} can hardly dissolve in ZrO_2, thereby forms $La_2Zr_2O_7$[3),4)] which would causes significant loss in cell performance and change in microstructure. Ce^{4+}, on the other hand, has a larger ionic radius than Zr^{4+}. CeO_2 can thus dissolve La^{3+}, which are considered to work as a dopant as shown in the reaction formula given below, forming O vacancies.

$$La_2O_3 = 2La'_{Ce} + Vo^{\cdot\cdot} + 3O^x_O \quad (1)$$

Accordingly, the air electrode with an SDC inter-layer showed excellent long-term durability and structural stability.

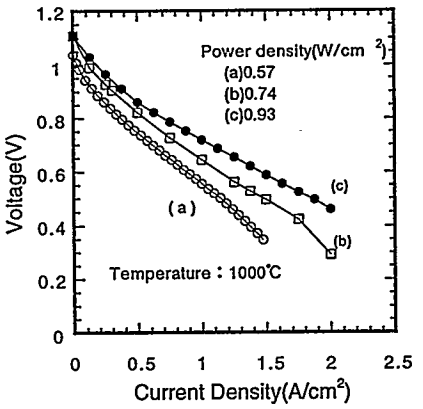

Figure 2

V-I characteristics of single cells with different electrodes: a) LSM cathode and Ni/YSZ anode, b) LSM cathode with SDC inter-layer and Ni/YSZ anode, and c) LSM cathode with SDC inter-layer and Ni/CeYSZ anode.

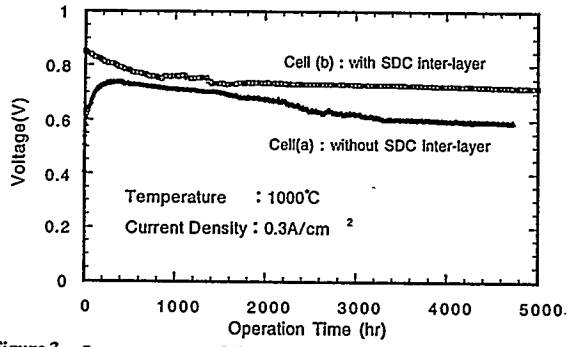

Figure 3 **Long-term test of single cells: a) without the SDC layer, b) with the SDC inter-layer at the cathode/electrolyte interface.**

4. Fuel electrode with a mixed conductor

In order to increase the electrochemically active sites of the fuel electrode, 10 mole % CeO_2 was doped to YSZ in the Ni-YSZ cermet. The doping of CeO_2 causes the YSZ in the cermet to have higher electronic conductivity because the Ce^{4+} ion can be reduced to Ce^{3+} as it is described by the following reaction.

$$Ce^{x}_{Zr} + O^{x}_{O} = 2Ce'_{Zr} + Vo^{\cdot\cdot} + 1/2O_2 \qquad (2)$$

The electrical neutralization condition can be expressed as:

$$[Ce'_{Zr}] = 2[Vo^{\cdot\cdot}] \qquad (3)$$

Applying the law of mass action and substituting equation (3) into equation (2), the $[Ce'_{Zr}]$ is found to be proportional to $(Po_2)^{-1/6}$, where Po_2 is oxygen partial pressure. Therefore, the electronic conductivity of 10 mole % CeO_2-doped YSZ (CeYSZ) increases with reduction of oxygen partial pressure and is expected to have about 1×10^{-1} Scm^{-1} at Po_2 of 1×10^{-18} atm. This value is almost equivalent to the ionic conductivity of YSZ and thus indicates the possibility of CeYSZ particles in the cermet electrode producing the electrochemically active sites as Ni in the cermet plays a roles in the same way. The cell (c) in Figure 2 had the Ni-CeYSZ cermet electrode, whose rest of component materials were same as those of cell (b). Therefore, the improvement seen in the V-I characteristic from cell (b) to cell (c) in Figure 2 was considered to be the result of the increased active sites.

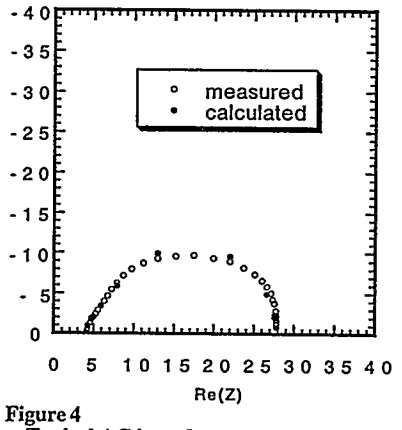

Figure 4 **Typical AC impedance spectrum for a Ni/CeYSZ electrode on a YSZ electrolyte. Closed symbols indicates a fit by the equivalent circuit of Figure 5.**

To investigate the effect of CeO_2 addition to the Ni-YSZ cermet, electrode characteristics were measured by an AC impedance method. A typical AC impedance spectrum of the Ni-CeYSZ cermet electrode is shown in Figure 4. The closed symbol represents calculated values by the equivalent circuit with a finite length diffusion impedance[5] shown in Figure 5. The electrode interface conductivity (σ_e)[6] of Ni-CeYSZ, calculated from the equivalent circuit, is compared in Figure 6 with that of the Ni-YSZ electrode. This clearly indicates that the interface conductivity increased by the addition of CeO_2. The increase in σ_e supports the postulation that the Ni-CeYSZ cermet anode has more electrochemically active sites than does the Ni-YSZ cermet anode.

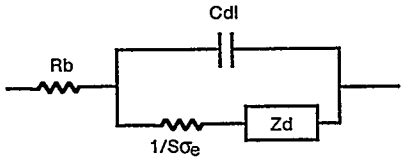

Figure 5 Equivalent circuit used to model AC impedance spectra, where S, σe, Rb, Cdl, and Zd are an effective area of the electrode, an interface conductivity, a bulk resistance, a double layer capacitance, and a finite length diffusion impedance, respectively.

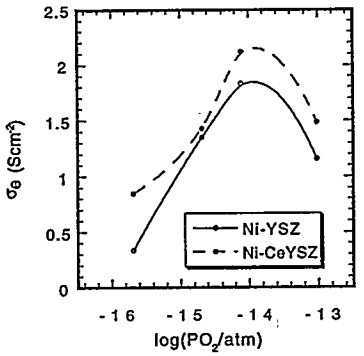

Figure 6 Interface conductivity (1/SRe) of the Ni/YSZ and Ni/CeYSZ electrodes as a function of log(Po_2).

5. Conclusion

Planar type single cells with electrodes modified by mixed ionic-electronic conductors of CeYSZ and SDC were successfully fabricated and tested. An SDC thin layer was made at the cathode/electrolyte interface to reduce the ohmic resistance of ionic current at the interface. CeO_2 was added in the Ni-YSZ cermet anode in order to increase the electronic conductivity of YSZ in the cermet. By these modifications we succeeded in reducing the interfacial overpotential and attained a high power density of 0.93W/cm^2 using hydrogen as a fuel and air as an oxidizer. The SDC inter-layer was also found to be effective in improving the stability of cathode in long term operation.

References

1) Y. Matsuzaki et al., Fuel Cell Seminar Abstract, Tucson, Nov. p-237 (1992)
2) K.Eguchi et al., Solid State Ionics, 52, p-165(1992)
3) O. Yamamoto et al., Proc. of The 1st Int. Symp. on Solid Oxide Fuel Cells., p-242(1989)
4) C. Brugnoni et al., Solid State Ionics, 76, p-177(1995)
5) M. J. Verker et al., J. Electrochem. Soc., 130, p-78, (1983)
6) J. Mizusaki et al., J. Electrochem. Soc., 141, p-1676, (1994)

APPLICATION OF IMPEDANCE SPECTROSCOPY TO SOFC RESEARCH

G. Hsieh and T.O. Mason
Northwestern University
2225 North Campus Drive
Evanston, IL 60208

L.R. Pederson
Pacific Northwest National Laboratory*
P.O. Box 999
Richland, WA 99352

INTRODUCTION

With the resurgence of interest in solid oxide fuel cells and other solid state electrochemical devices, techniques originally developed for characterizing aqueous systems are being adapted and applied to solid state systems. One of these techniques, three-electrode impedance spectroscopy, is particularly powerful as it allows characterization of subcomponent and interfacial properties. Obtaining accurate impedance spectra, however, is difficult as reference electrode impedance is usually non-negligible and solid electrolytes typically have much lower conductance than aqueous solutions. Faidi *et al* and Chechirlian *et al* have both identified problems associated with low conductivity media (1,2). Other sources of error are still being uncovered. Ford *et al* identified resistive contacts with large time constants as a possibility, while Xie *et al* showed that the small contact capacitance of the reference electrode was at fault (3,4). Still others show that instrument limitations play a role (5). Using the voltage divider concept, a simplified model that demonstrates the interplay of these various factors, predicts the form of possible distortions, and offers means to minimize errors is presented.

EXPERIMENTAL

Zirconia powder with 8 mole percent Y_2O_3 (Tosoh Corp., Japan) was isostatically pressed into a cylindrical sample and sintered in air at 1400°C for 2 hours. The sample was 1.7 cm in diameter and 3.0 cm long. Unfluxed platinum paint (Engelhard Corp., NJ) was applied to the flat ends and fired at 900°C to form working (WE) and counter (CE) electrodes. Two small axial holes approximately 1.0 mm in diameter, 0.4 cm deep were drilled into the YSZ sample, one from each end. 0.010" diameter silver wire, terminated in a small bead, was inserted into one hole to form a silver reference electrode (RE). A similarly prepared platinum wire was inserted into the opposite hole to form a platinum reference electrode. Impedance spectra were collected at 570°C using the Solartron 1260 frequency response analyzer (1260 FRA) from 1 MHz to 10 mHz without a potentiostat.

RESULTS AND DISCUSSION

In the three-electrode configuration, a simplified equivalent circuit of the sample and the 1260 FRA is shown in Figure 1. The quantity of interest is Z_{WE}, the true working electrode impedance. Analysis of the circuit shows, however, that the apparent impedance measured by the instrument is not simply Z_{WE}. Because of the voltage divider effect,

* Operated by Battelle Memorial Institute for the U.S. Department of Energy under contract DE-AC06-76RLO 1830

$$Z_{apparent} = \frac{\Delta V}{I} = \frac{Z_{input}}{Z_{input} + Z_{ref}} Z_{WE}$$

where Z_{ref} is the reference electrode impedance and Z_{input} is the input impedance of the instrument. When reference electrode impedance is substantial in relation to the input impedance of the instrument, the magnitude of the apparent impedance will be smaller than the true working electrode impedance. Because this distortion is complex in nature, phase shifts may be introduced in addition to changes in gain.

Since distortions occur when reference electrode impedance is non-negligible in relation to the input impedance of the machine, it is important to know both quantities. The input impedance of the analyzer can be obtained from the manufacturer. For the Solartron 1260 FRA, it is approximately 1 MΩ resistance in parallel with a 35 pF capacitance. External attachments and cabling may increase this input capacitance. Since error gradually increases as reference electrode impedance approaches the instrument input impedance, one needs to define an acceptable tolerance. Conveniently, an acceptable error of 1% corresponds to tolerable reference electrode impedance of approximately 1% the input impedance. Alternatively stated, when reference electrode impedance reaches 1% of the input impedance, measured data will be in error from the true value by approximately 1%. For the 1260 FRA, this 1% tolerable threshold is plotted as the dotted line in Figure 2. At frequencies where reference electrode impedance exceeds this threshold, the measurement is in error by more than 1%. The impedances of the silver and the platinum reference electrodes used in this experiment are also plotted in Figure 2. They were obtained through the procedure outlined by Lagos *et al*, which allows the determination of individual electrode impedances (6).

Note the response of the reference electrodes can be approximated by an equivalent circuit consisting of a charge transfer resistance R_{ct} in parallel with a double layer capacitance C_{dl}, both of which are in series with a contact spreading resistance R_c. Whereas R_{ct} and C_{dl}, which determine the lower frequency response of the electrode, are very dependent on electrode material, the contact resistance R_c determining the high frequency response is more influenced by electrolyte conductivity and contact size. The inverse relationship between R_c and electrolyte conductivity has already been established by Newman (7). Through this spreading resistance, electrolyte conductivity enters into consideration when impedance responses at higher frequencies are of interest. In this experiment, the silver reference has lower spreading resistance because it deforms much more easily than platinum at 570°C and forms a larger contact. Because of the input capacitance in the instrument, the reference electrode impedance eventually exceeds the tolerable threshold at high frequencies, and distortions inevitably occur in the apparent spectra.

As shown in Figure 2, the platinum reference electrode impedance exceeds the threshold level at all frequencies. Thus, according to the voltage divider equation above, it is to be expected that apparent impedance measured with this platinum reference electrode will be in substantial error. It will be much smaller than the true working electrode impedance. Since the impedance of this platinum reference is almost half of the input impedance of the instrument at frequencies where the working electrode arc appears, the magnitude of the apparent impedance is expected to be only 2/3 of the true value. This is in fact what is observed experimentally, as shown in Figure 3. No phase shift was observed. Note that the high frequency intercepts have been shifted along Z' to facilitate comparison. In contrast, the impedance of the silver reference electrode is much lower at the same frequencies, below the tolerable level. Correspondingly, the apparent impedance accurately reflects the true working electrode impedance. Note that there are no tell-tale signs in the platinum reference data that a significant distortion is occurring. Without knowledge of the reference electrode impedance or comparison with the true impedance, data obtained with the platinum reference electrode would appear reasonably correct, however inaccurate, in all aspects.

Although not shown, the high frequency portion of both apparent spectra exhibits an extra capacitive arc above 100KHz. This is also an artifact generated by the voltage divider effect. This distortion modifies the phase angle as well as gain. At this temperature, both the bulk feature and the grain boundary feature of zirconia exist at substantially higher frequencies than the capabilities of the instrument.

SUMMARY

The reference probe is an often overlooked aspect in impedance spectroscopy. Yet a high impedance reference is a major source of errors and distortions. The voltage divider concept was used to generalize and explain the interplay of instrument limitation, electrolyte conductivity, reference resistance and capacitance. A simple experiment on yttria-stabilized zirconia shows that a high impedance reference electrode does indeed produce a large error, and that this error obeys the voltage-divider equation. One solution to minimize this type of error is to carefully select and design a low impedance reference electrode.

ACKNOWLEDGMENTS

This work was supported by the U.S. Department of Energy/Fossil Energy AR&TD Materials Program and the National Defense Science and Engineering Graduate Fellowship. The authors are grateful to Brian Sayers of Solartron Instruments for helpful insights and discussions.

REFERENCES

1. S.E. Faidi and J.D. Scantlebury, "The Limitations of the Electrochemical Impedance Technique in the Study of Electrode Reactions Occurring in Low Conductivity Media," J. Electrochem. Soc., Vol. 136, No. 4, pp. 990-995, April 1989.

2. S. Chechirlian, P. Eichner, M. Keddam, H. Takenouti and H. Mazille, "A Specific Aspect of Impedance Measurements in Low Conductivity Media. Artifacts and Their Interpretation," Electrochimica Acta, Vol. 35, No. 7, pp. 1125-1131, 1990.

3. S. J. Ford, T.O. Mason, B.J. Christensen, R.T. Coverdale, H.M Jennings and E.J. Garboczi, "Electrode Configurations and Impedance Spectra of Cement Pastes," J. Mater. Sci., Vol. 30, pp. 1217-1224, 1995.

4. P. Xie, P. Gu and J.J. Beaudoin, "Contact Capacitance Effect in Measurement of A.C. Impedance Spectra for Hydrating Cement Systems," J. Mater. Sci., Vol. 31, pp. 144-149, 1996.

5. G. Chiodelli and P. Lupotto, "Experimental Approach to the Impedance Spectroscopy Technique," J. Electrochem. Soc., Vol. 138, No. 9, pp. 2703-2711, September, 1991.

6. G.E. Lagos, N. Bonanos and B.C.H. Steele, "Model for the Impedance Analysis in a Three Electrode Solid State Electrochemical Cell," Electrochimica Acta, Vol. 28, No. 11, pp. 1581-1584, 1983.

7. J. Newman, "Resistance for Flow of Current to a Disk," J. Electrochem. Soc., Vol. 113, pp. 501-502, May, 1966.

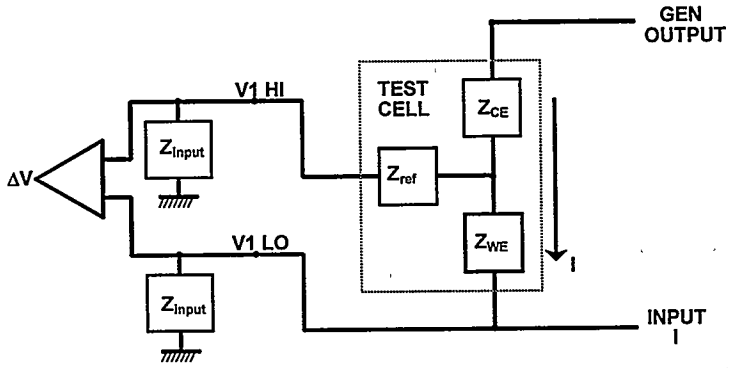

FIGURE 1. Equivalent circuit diagram of a sample and the 1260 FRA, in the three-electrode configuration.

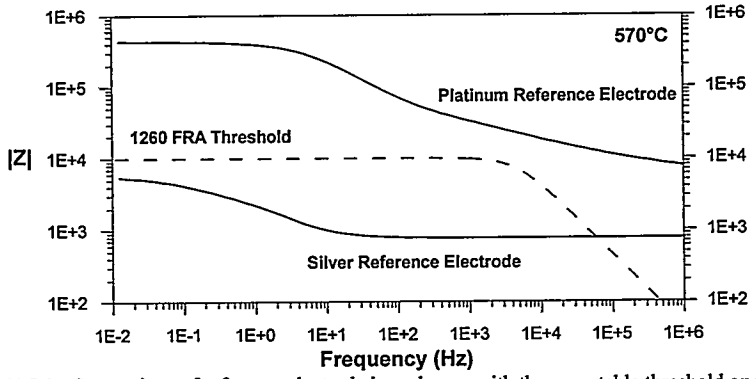

FIGURE 2. Comparison of reference electrode impedances with the acceptable threshold on the Solartron 1260 frequency response analyzer.

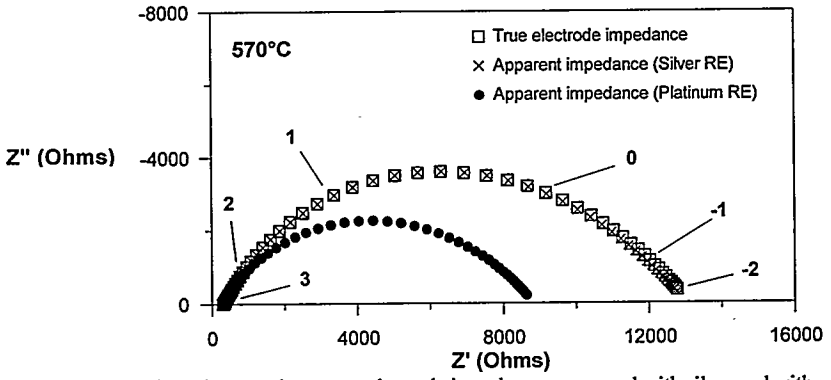

FIGURE 3. True impedance and apparent electrode impedances measured with silver and with platinum reference electrodes. Numbers indicate common logarithm of frequency.

MANUFACTURING OF PLANAR CERAMIC INTERCONNECTS

B.L. Armstrong, G.W. Coffey, K.D. Meinhardt, and T.R. Armstrong
Pacific Northwest National Laboratory*
Richland, WA 99352

INTRODUCTION

The fabrication of ceramic interconnects for solid oxide fuel cells (SOFC) and separator plates for electrochemical separation devices has been a perennial challenge facing developers. Electrochemical vapor deposition (EVD), plasma spraying, pressing, tape casting and tape calendering are processes that are typically utilized to fabricate separator plates or interconnects for the various SOFC designs and electrochemical separation devices (1,2). For sake of brevity and the selection of a planar fuel cell or gas separation device design, pressing will be the only fabrication technique discussed here. This paper reports on the effect of the characteristics of two doped lanthanum manganite powders used in the initial studies as a planar porous separator for a fuel cell cathode and as a dense interconnect for an oxygen generator.

The selection of a suitable fabrication process is highly dependent upon the device design. The raw material properties, such as surface area, particle and agglomerate size distribution, morphology, and minute secondary phases, affect the processing parameters. The influence of the initial powder characteristics on consolidation of ceramics has been well studied (3-5). Armstrong reported on the characteristics of zirconia powders from two synthesis techniques and the effect of those characteristics on consolidation and densification (3). Combustion synthesis yielded hard agglomerates which required ball milling to break down the agglomerate structure to achieve greater than 94% theoretical density. Hydrothermal synthesis provided weakly agglomerated powders in which consolidation and complete densification was dependent upon the pH of the starting suspension and the technique utilized to remove the powder from the suspension. Effects of the raw material properties on fabrication of interconnects was demonstrated by Milliken *et al.* who showed that the sintered density of uniaxially compacted strontium doped $LaCrO_3$ increased with increasing green density (6). The increase in green density was obtained by optimizing isostatic pressure, binder, lubricant, sintering aids, and the reduction of hard agglomerates through ball milling of the starting powder prior to pressing.

EXPERIMENTAL

Material Preparation:
Two commercially available doped lanthanum manganite powders ($(La_{0.8}Ca_{0.2})_{0.98}MnO_3$, hereafter called LCM-20) were evaluated: Powder X (made by a combustion synthesis process) and Powder Y (made by a co-precipitation process). Powder X was calcined at 1000°C for one hour and ball milled for 24 hours to break up hard agglomerates.

Consolidation and Densification:
The powders were mixed with 10 weight percent of total solids of an organic binder system. The resulting mixtures were added to a 50.8 mm ID steel die preheated to 149°C and uniaxially pressed

*Operated by Battelle Memorial Institute for the U.S. Department of Energy under contract DE-AC06-76RLO 1830.

at 8.8 MPa while at temperature. The resulting Powder X and Powder Y discs varied in thickness, averaging 1.975 and 1.414 mms in dimension, respectively. The average thicknesses were normalized to a 10 gram starting weight. After pressing, the Powder X and Powder Y discs were debindered in a three day cycle and heated to the sintering temperature (1150°C and 1450°C, respectively) at a rate of 120°C/hour and held at the selected temperature for two hours in air. The sintered discs were subsequently creep flattened at the sintering temperature for a duration of five hours. All binder burn-out, sintering, and creep flattening studies were made using Lindberg Blue M or Deltech DT-31-FL-10 box furnaces.

Characterization:
Surface areas were measured by a Micrometrics ASAP 2000 BET. Particle and agglomerate size distributions were determined by a Microtrac Series 9200 Full Range Analyzer. Phase was measured using Cu Kα radiation and a Philips Wide Range Vertical Goniometer. Sintered densities were measured with the Archimedes submersion technique using ethanol as the liquid medium. Linear expansion was measured on an Anter Model 1161 dilatometer at a rate of 2°C/minute in air. Elemental analysis was measured using inductively coupled plasma auger electron spectroscopy (ICP AES) and energy dispersive x-ray fluorescence (ED XRF) techniques.

RESULTS AND DISCUSSION

If both powders (X andY) had comparable phase compositions, particle sizes and distributions, surface area and morphologies, it would be predicted that the powders would have similar green densities after pressing and thus similar sintered densities. No differences between Powder X and Powder Y were evident from preliminary x-ray diffraction phase analysis. Phase analysis did not identify any major secondary phases in either powder. Surface area and particle size distribution, however, were indicative of the synthesis methods and varied accordingly. Powder X had a surface area of 6.2 m^2/gm, and the particle size distribution, which was multimodal, ranged from 0.95 to 434.35 μm with a d_{50} at 9.04 μm. This particle size range was reflective of the large, hard agglomerates formed during synthesis and the effect of subsequent milling. Powder Y's surface area was measured at 1.78 m^2/gm. The particle size was monodisperse. The particle size distribution was Gaussian with a range from 2.52 to 15.07 μm with a d_{50} at 5.47 μm.

Further evidence of powder property differences was found in the dilatometric data (Figure 1). The absolute linear shrinkage was measured using bars pressed from both Powder X and Powder Y. The Powder X bar exhibited an expansion at 1250°C whereas the Powder Y bar sintered to complete density at 1450°C without any expansion behavior. This expansion behavior has been observed in lanthanum chromite and strontium doped lanthanum manganite samples when the A/B ratio was approximately 0.90 and when large additions of zirconia (>40 wt%) were mixed in the cathode (7,8). The A/B ratio refers to the cation ratio in the ABO_3 perovskite structure. In addition, this type of expansion can occur in the doped manganites with minor phase additions of silica and alumina. Again, evidence of powder differences was observed in the measured green densities. The Powder Y discs had an average green density of 3.49 gm/cc while the Powder X discs had green densities of 2.5 gm/cc. The low green densities of the Powder X discs were indicative of the large particle sizes, high surface area, and agglomerate morphology. As anticipated from the higher green densities, the linear shrinkage, and the higher achievable sintering temperatures, the Powder Y discs densified to higher sintered densities of 5.8 (92.4% of the 6.27 gm/cc theoretical) versus the 5.04 gm/cc sintered densities (80.4% theoretical) for the Powder X discs. In addition to poor sintered densities, the Powder X discs warped and bowed considerably during sintering and frequently cracked during the process of creep flattening. However, since the Composition B discs did not exhibit any linear expansion during the sintering event, these LCM-

20 discs had minimal warpage and flattened without cracking. A Jet Propulsion Laboratory (JPL) designed separator plate which was characteristic of the as-fabricated discs that were pressed is shown in Figure 2.

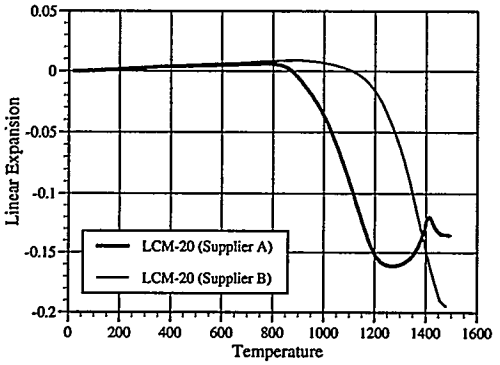

Figure 1: Absolute Linear Expansion of Powder X and Powder Y LCM-20

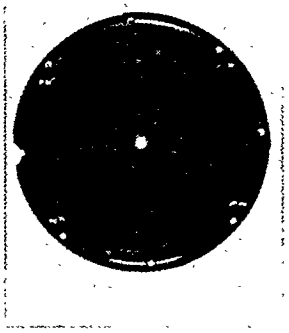

Figure 2: As-Fabricated Doped Lanthanum Manganite Separator Plate (71.8 mm O.D.)

To determine the A/B ratios and whether minor quantities of silica and alumina were present that were not visible in the preliminary x-ray analysis, elemental analysis was measured using ED XRF and ICP AES. The reference used for the ICP AES was a LCM-20 sample synthesized using the glycine nitrate process (GNP). The A/B cation ratios for Powders X and Y were 0.95 and 0.99, respectively (Table 1). The silica content was negligible in both powder samples, however, Powder X had twice the alumina content (0.2 wt%) of Powder Y. Both samples contained trace amounts of zirconia (approximately 0.02 wt%). It is unknown at this time if such trace amounts of alumina and zirconia are sufficient to cause the expansion behavior seen in the Powder X sintering curves or if the alumina contributed to the formation of a glassy, secondary phase. The formation of this glassy phase could seal off the surface of the Powder X discs and subsequently trap the gas evolved during the sintering process.

Table 1: Summary of ICP AES and ED XRF Results

SUPPLIER	ICP AES	ED XRF
PNNL	$(La_{0.784}Ca_{0.216})_{0.979}MnO_3$	$(La_{0.801}Ca_{0.199})_{0.99}MnO_3$
X	$(La_{0.796}Ca_{0.205})_{0.952}MnO_3$	$(La_{0.816}Ca_{0.184})_{1.02}MnO_3$
Y	$(La_{0.799}Ca_{0.201})_{0.995}MnO_3$	$(La_{0.812}Ca_{0.188})_{0.973}MnO_3$

Minor differences in material properties resulting from the initial powder synthesis can have substantial effects on the processing, sintering and ultimately the manufacture of calcium doped lanthanum manganite planar interconnects. Provided the powders and their properties are well understood, inexpensive fabrication is feasible.

ACKNOWLEDGEMENTS

The authors would like to thank the following individuals for their contributions: B.A. Grasher, G.D. Maupin, L.R. Pederson, N.T. Saenz, and J.W. Stevenson.

REFERENCES

1. N.Q. Minh, "Ceramic Fuel Cells," J. Am. Ceram. Soc., Vol. 76, pp. 563-88, March 1993.

2. N.Q. Minh and T. Takahashi, Science and Technology of Ceramic Fuel Cells, pp. 167, 240-293, Elselvier, The Netherlands, 1995.

3. B.L. Armstrong, "Consolidation of Nanomaterials," Materials and Manufacturing Processes, in press.

4. J.A. Mangels and G.L. Messing (eds.), Advances in Ceramics, Vol 9: Forming of Ceramics, The American Ceramic Society, Inc., Columbus, 1984.

5. G.Y. Onoda Jr. and L.L. Hench, Ceramic Processing Before Firing , John Wiley & Sons, Inc., New York, 1978.

6. C. Milliken and A. Khandkar, in Proceedings of The First International Symposium on Solid Oxide Fuel Cells, October 16-18, 1989, Hollywood, FL, S.C. Singhal (ed.), pp. 361-376, Electrochemical Society, Pennington, NJ, 1989.

7. J.W. Stevenson, P.F. Hallman, T.R. Armstrong, and L.A. Chick, "Sintering Behavior of Doped Lanthanum and Yttrium Manganite," J. Am. Ceram. Soc., Vol. 78, pp. 507-12, March, 1995.

8. J.W. Stevenson, T.R. Armstrong, W.J. Weber, in Proceedings of The Fourth International Symposium on Solid Oxide Fuel Cells, M. Dokiya, O. Yamamoto, H. Tagawa, and S. Singhal (eds.), pp. 454-462, The Electrochemical Society, Pennington, NJ, 1995

MECHANICAL PROPERTIES OF LANTHANUM AND YTTRIUM CHROMITES

S.W. Paulik and T.R. Armstrong
Pacific Northwest National Laboratory*
P. O. Box 999
Richland, WA 99352

Introduction

In an operating high-temperature (1000°C) solid oxide fuel cell (SOFC), the interconnect separates the fuel ($P(O_2)\approx10^{-16}$ atm) and the oxidant ($P(O_2)\approx10^{0.2}$ atm), while being electrically conductive and connecting the cells in series. Such severe atmospheric and thermal demands greatly reduce the number of viable candidate materials. Only two materials, acceptor substituted lanthanum chromite and yttrium chromite, meet these severe requirements. In acceptor substituted chromites (Sr^{2+} or Ca^{2+} for La^{3+}), charge compensation is primarily electronic in oxidizing conditions (through the formation of Cr^{4+}). Under reducing conditions, ionic charge compensation becomes significant as the lattice becomes oxygen deficient. The formation of oxygen vacancies is accompanied by the reduction of Cr^{4+} ions to Cr^{3+} and a resultant lattice expansion [1-4]. The lattice expansion observed in large chemical potential gradients is not desirable and has been found to result in greatly reduced mechanical strength [5,6].

Few investigations of the mechanical properties of lanthanum chromite have evaluated the strength in both air and after reduction. Of these investigations, the results are not consistent and comparison of individual results are difficult due to inconsistent sample size, test method and test conditions. Reliable measurements of Young's modulus, Poisson's ratio, and mechanical strength are needed in air and reducing environments so that accurate models can be developed to predict the possible stresses the interconnect may experience in an operating SOFC. Therefore, it is the purpose of this program to measure the mechanical properties of acceptor substituted lanthanum and yttrium chromite to determine the mechanical properties as a function of material chemistry, as well as temperature and atmosphere.

Experimental

$La_{1-x}Ca_xCrO_3$ and $La_{1-x}Sr_xCrO_3$ (x varying between 0.15 and 0.30) powders were synthesized using the glycine nitrate process. Following a 1 hr calcination at 1000°C in air, powders were isostatically pressed into 34 by 34 by 64 mm billets and sintered between 1600 and 1690 °C for 2 to 6 hr. Samples were machined into 3 by 4 by 45 mm military standard 1942B [7] bars. Four-point bend strength was measured (Instron model 1125) in air at 25, 600, 800, and 1000°C using a crosshead speed of 0.508 mm/min on a 20 mm top and 40 mm bottom span. Prior to testing at room temperature, selected samples were exposed to high temperature reducing conditions (1000°C and an oxygen partial pressure varying between 10^{-8} to 10^{-18} atm) for 2 hr using a buffered CO_2/Ar-4%H_2 gas system and cooled to room temperature, maintaining the $P(O_2)$ to approximately 700°C.

Results and Discussion

Table 1 displays the percent theoretical density for the sintered samples. In addition to having low densities, the LCC-15 and LSC samples had pores larger than the grains which will result in lower strengths from a smaller cross-sectional area and large initial flaw size. Both internal and intergranular pores were found in all compositions typical for a liquid phase sintered material. Figures 1 and 2 show the strength as a function of temperature for the lanthanum calcium chromite (denoted LCC, e.g. $La_{0.7}Ca_{0.3}CrO_3$ is written LCC-30) and lanthanum strontium chromite samples, respec-

* Operated by Battelle Memorial Institute for the U.S. Department of Energy under Contract DE-AC06-76RLO 1830.

Table 1: Percent theoretical density of the indicated LCC and LSC compositions.

Composition	LCC-15	LCC-20	LCC-25	LCC-30	LSC-16	LSC-20	LSC-24
% Theoretical Density	86.5±4.5	94.2±1.6	95.7±1.9	97.2±0.5	93.1±1.5	91.6±0.9	91.2±0.7

tively. The room temperature strength of the LCC samples increased with increasing calcium content, which is the result of higher densities and smaller pore sizes. The strength of the LSC samples showed no correlation to the strontium content as samples had similar densities. At elevated temperatures, the strength of the LCC samples decreased with increasing calcium content. Under these conditions, grain boundary-sliding or viscous flow of the grain boundary phases can extend existing flaws leading to decreased strength. [8] The strength of the LSC samples remained unchanged over the entire temperature range. The insensitivity of the porous materials to strength degradation (with temperature) is related to fracture initiated from pores. The pores act as initial flaw sites, and failure occurs via extension of these flaws along the grain boundary. As the temperature increases, the grain boundary surface energy increases, resulting in an increase in the energy necessary to extend the pores along the grain boundary. The resulting increased resistance to pore-crack extension results in constant strength (LSC samples) or even increased strength (LCC-15). This behavior has been observed in UO_2 where fracture occurs by the extension of large pores along the grain boundaries. [8]

Figures 3 and 4 are plots of the room temperature strength as a function of $P(O_2)$ for the treated LCC and LSC samples, respectively. The results indicate both acceptor content and type affect the mechanical perfomance of the material under the reducing conditions. LCC-25 and LCC-30 maintained a constant strength from ambient conditions to a $P(O_2)$ of 10^{-10} atm. As the atmosphere became more reducing, both materials demonstrated a drastic decrease in strength with LCC-30, retaining only 10% of its original strength after exposure to a $P(O_2)$ of 10^{-16} atm. LCC-20 showed similar behavior except the transition $P(O_2)$ was lower (10^{-12} atm) and the material retained 55% of its original strength after exposure to the most reducing condition (10^{-18} atm). The data illustrates that samples with higher acceptor content show a decrease in strength at lower oxygen partial pressures and a greater loss of strength at more reducing conditions. This trend is consistent with the reported isothermal expansion behavior of LCC materials under high temperature reducing conditions. [2-4] Samples exhibited no expansion from ambient air to moderately reducing conditions with the onset of expansion occurring at a higher $P(O_2)$ for compositions with higher acceptor content. Similarly, the magnitude of expansion for a given loss in lattice oxygen was greater in samples with a higher acceptor content. Examining the model [2-4] used to interpret the isothermal expansion behavior can provide insight into the strength behavior. As the lattice loses oxygen and Cr^{4+} ions are reduced to Cr^{3+}, bonds are left unsatisfied and bond lengths increase from the repulsive forces of unshielded neighboring chromium ions. This expansion of the lattice has been documented via x-ray analysis. Armstrong *et al.* [4] measured an increase of 1.3% in the LCC-30 unit cell after reduction in a $P(O_2)$ of 10^{-18} atm at 1000°C. The forces required to rupture the bonds in this lattice, the cohesive strength, should be measurably less than that of a stoichiometric chromite lattice. Examination of fracture surfaces revealed that a transition in fracture mechanism, from intergranular to transgranular fracture, accompanied the decrease in strength. Fracture surfaces from the LCC samples exhibited small amounts of transgranular fracture just prior to the onset of strength degradation. The amount of transgranular fracture increased as the conditions became more reducing and corresponded to the decrease in strength., e.g. LCC-30 showed complete transgranular fracture at 10^{-16} atm. This supports the premise that the combination of oxygen vacancies and longer bond lengths resulted in a weaker lattice; reduced grains (crystallites) are substantially weaker than the unreduced grains and the grain boundaries.

The room temperature strength of the treated LSC samples remained a constant from ambient air to a $P(O_2)$ of 10^{-8} atm. As the treatments became more reducing, however, an increase in strength was observed for all LSC samples, reaching a maximum at 10^{-14} atm. All samples demonstrated intergranular fracture from ambient air to a $P(O_2)$ of 10^{-12} atm. The increase in strength with decreasing $P(O_2)$ can be attributed to an increase in strength of the grain boundary phase or a blunting of pore-grain boundary interfaces, thus limiting the extension of pores near critical size or inhibiting the formation of a critical flaw from several subcritical pores. [8] Similar to the trends observed in the LCC compositions, LSC samples with the highest acceptor content exhibited the greatest reduction in strength as the conditions became more reducing, e.g. LSC-24 retained only 40% of its unreduced strength (~30% of the maximum strength). In contrast, LSC-15 maintained a constant strength from 10^{-10} to 10^{-18} atm at 170% of the unreduced strength. The increase in strength from 10^{-8} to 10^{-14} atm was fairly consistent for all LSC compositions. The data shows that at more reducing conditions, samples with higher acceptor content experience a greater reduction in strength. This trend is consistent with the reported isothermal expansion under high temperature reducing conditions [4]. Relative to the LCC materials, LSC materials with similar acceptor contents display slightly smaller isothermal linear expansion at a given $P(O_2)$ or oxygen deficiency. This corresponds to a smaller lattice expansion at a given oxygen deficiency, i.e. the measured change in the x-ray unit cell volume for LSC-30 after reduction in a $P(O_2)$ of 10^{-18} atm at 1000°C is 0.2%, almost 1/6 of the LCC-30 expansion. [6] This is believed to be due the larger unit cell of LSC materials, which can accommodate oxygen deficiency with less bond lengthening. The cohesive energy in oxygen deficient LSC should remain higher at higher oxygen deficiencies compared to LCC. Fracture surfaces from the LSC samples indicated an onset $P(O_2)$ of 10^{-14} atm for transgranular fracture. An increasing amount of transgranular fracture accompanied the decrease in strength from 10^{-14} to 10^{-18} atm for the LSC-20 and LSC-24 samples, with approximately 60% transgranular fracture for the LSC-24 sample after the 10^{-18} atm treatment. These results are evidence that the loss of lattice oxygen has weakened the lattice but also that the Sr^{2+} ion stabilizes the chromite lattice more than Ca^{2+}.

Conclusions

The strength of the LCC samples decreased with increasing temperature and increased acceptor content. The reduction in strength at elevated temperatures is believed to be caused by a grain boundary-sliding mechanism. The LSC samples showed a constant strength with temperature as failure occurred by extension of the pores along the grain boundaries. The room temperature strength of the reduced LCC and LSC samples was dependent on the $P(O_2)$. Samples with the highest acceptor content showed a precipitous drop in strength after exposure to the most reducing conditions. The loss of lattice oxygen and the reduction of Cr^{4+} to Cr^{3+} resulted in a reduced bond strength in the lattice and a larger bond length. This resulted in a decrease in the cohesive strength of the lattice, and the corresponding decrease in fracture strength as the individual crystals lost mechanical integrity. This was supported by changes in the microstructure (transition from intergranular to transgranular fracture) as the treatments became more reducing.

References

1. S. Srilomsak, D. P. Schilling, and H. U. Anderson, in Proceedings of the 1st Int. Symposium on Solid Oxide Fuel Cells, Hollywood, FL 1989, ed. S. C. Singhal, (The Electrochemical Society, Pennington, NJ, 1989) p. 129.
2. T. R. Armstrong, J. W. Stevenson, P. E. Raney, and L. R. Pederson, in 1994 Fuel Cell Seminar Abstracts, San Diego, CA, (Courtesy Associates 1994) p. 105.

3. T. R. Armstrong, J. W. Stevenson, L. R. Pederson, and P. E. Raney, in Proceedings of the Fourth International Symposium on Solid Oxide Fuel Cells, Yokohama Japan 1995 ed. S. Singhal, (The Electrochemical Society, Pennington, NJ 1995) p. 944
4. T. R. Armstrong, J. W. Stevenson, R. E. Raney and L. R. Pederson, "Dimensional Stability of Doped Lanthanum Chromite in Reducing Environments," submitted J. Electrochem. Soc. 1996.
5. C. Milliken, S. Elangovan and A. Khandkar, in Proceedings of the Third International Symposium on Solid Oxide Fuel Cells, 1993, Edited by S.C. Singhal and H. Iwahara, pp. 335-343.
6. S.W Paulik and T.R. Armstrong, "Mechanical Properties of Acceptor Substituted Lanthanum Chromites," submitted J. Mat. Sci. 1996.
7. G.D. Quinn, F.I. Baratta, and J. A. Conway, "Commentary on U.S. Army Standard Test Method for Flexural Strength of High Performance Ceramics at Ambient Temperature," Army Materials and Mechanics Research Center Technical Report 85-21, Aug. 1985.
8. R. W. Davidge, Mechanical Behavior of Ceramics, pp. 93-103, Cambridge University Press, Cambridge England, 1979.

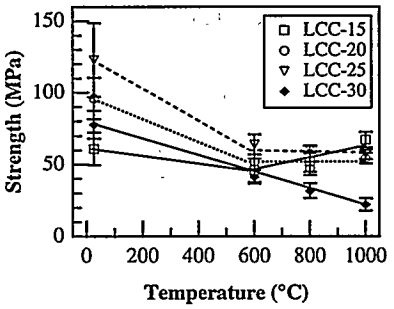

Figure 1. Strength of the LCC compositions as a function of temperature.

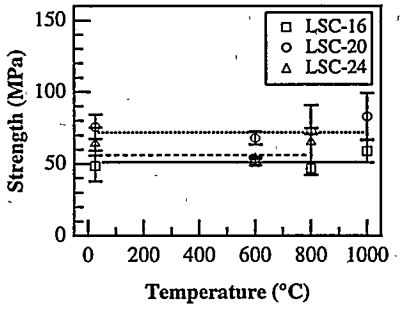

Figure 2. Strength of the indicated LSC compositions as a function of temperature.

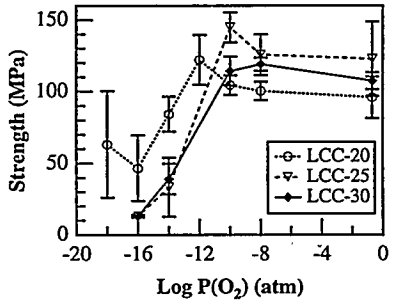

Figure 3. Room temperature strength of the LCC compositions as a function of exposure oxygen partial pressure (1000°C, 2 hr exposure.

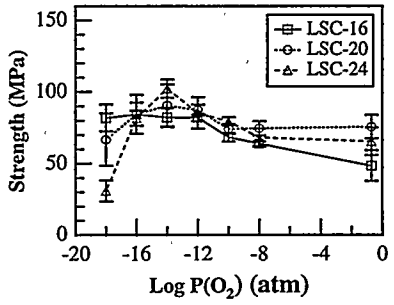

Figure 4. Room temperature strength of the indicated LSC compositions as a function of oxygen partial pressure (1000°C, 2 hr exposure).

Fabrication and Characteristics of Unit Cell for SOFC

Gwi-Yeol KIM, Seung-Wook EOM, Seong-In MOON,
Mun-Soo YUN, and Hee-Chun LIM*

Battery Technology Team
Korea Electrotechnology Research Institute
P.O. Box 20, Changwon, Kyongnam, 641-12O, Korea

*Center for Advanced Studies in Energy and Environment
Korea Electric Power Research Institute
103-16, Munji Dong, Yousung, Taejon, 305-380, Korea

INTRODUCTION

Research and development on solid oxide fuel cells in Korea have been mainly focused on unit cell and small stack. Fuel cell system is called clean generation system which not cause NOx or SOx. It is generation efficiency come to 50-60% in contrast to 40% of combustion generation system. Among the fuel cell system, solid oxide fuel cell is constructed of ceramics, so stack construction is simple, power density is very high, and there are no corrosion problems.

The object of this study is to develop various composing material for SOFC generation system, and to test unit cell performance manufactured. So we try to present a guidance for developing mass power generation system. We concentrated on development of manufacturing process for cathode, anode and electrolyte.

EXPERIMENTAL

Unit cells were fabricated using conventional thick film processing techniques, i.e., doctor blade and screen printing. And we could make planar type unit cell about 7 cm^2 size, using by 8 mol% YSZ electrolyte, perovskite type cathode, and Ni-YSZ cermet anode. As cathode material lanthanum-strontium -manganese perovskite (LSM) of optimized $La0.7Sr0.3MnO_3$ composition was used because of its high electric conductivity and good compatibility with the electrolyte, consisting of zirconia doped with 8 mol% yttria (8YSZ).

A schematic diagram of the fabrication is shown in figure 1. In this fabrication process, electrolyte and anode powders are first mixed with organic binders to form ceramic masses. Anode and cathode slurry were screen printed onto dense YSZ electrolytes and fired at 1400 and 1200°C, respectively.

RESULTS AND DISCUSSION

Figure 2 shows a schematic diagram of the configuration of a unit cell, which consisted of a cell part and a cell holder. The cell holders were made of a heat resistant alloy (Incounel 600) and were used as current collectors and gas manifolds.

Figure 3 shows the I-V characteristic for the fuel cell at 1000°C. The maximum power density is 0.85 W/cm^2 (0.435V, 1.96A/cm^2). The good I-V characteristic implies that both the anode (Ni-YSZ) and cathode ($La0.7Sr0.3MnO_3$) materials are suitable. The open circuit voltage (OCV) obtained from the unit cell is 1.15V.

Figure 4 shows the I-P characteristics of a unit cell for SOFC, for which the YSZ film obtained by doctor blade method was applied. This high power density of SOFC suggests that the Dr.blade method was a very useful method for preparing thin and dense YSZ films for SOFC.

The endurance of a unit cell is evaluated from the result of operating it for more than 510 hours. It is shown in Figure 5. After measuring various characteristics, the unit cell was operated at a constant current density of 150 mA/cm^2.

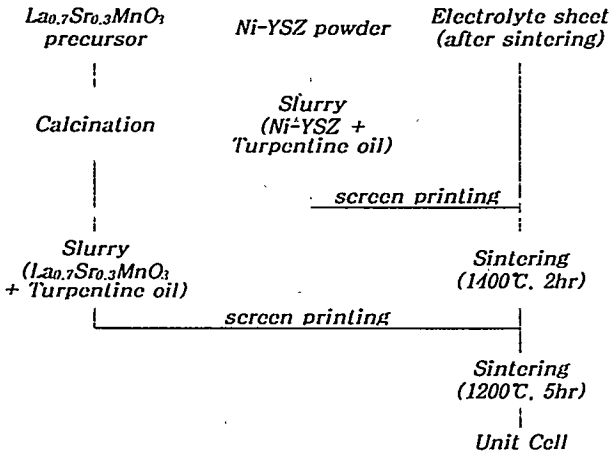

Figure 1. Manufacturing process of SOFC unit cell.

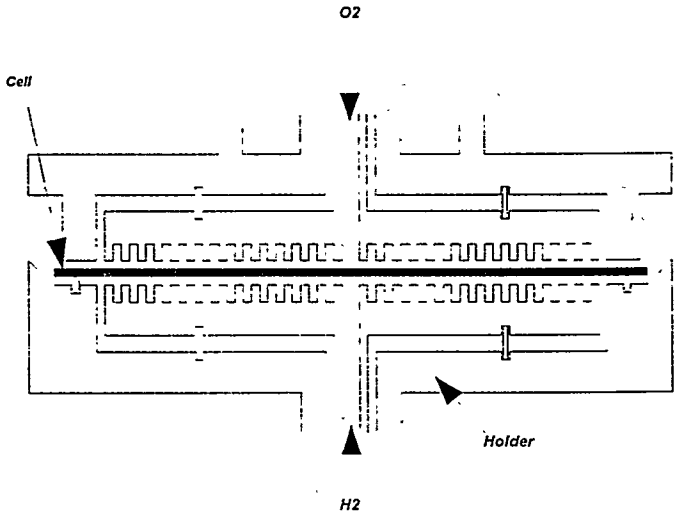

Figure 2. Schematic diagram of the unit cell used for I-V measurements.

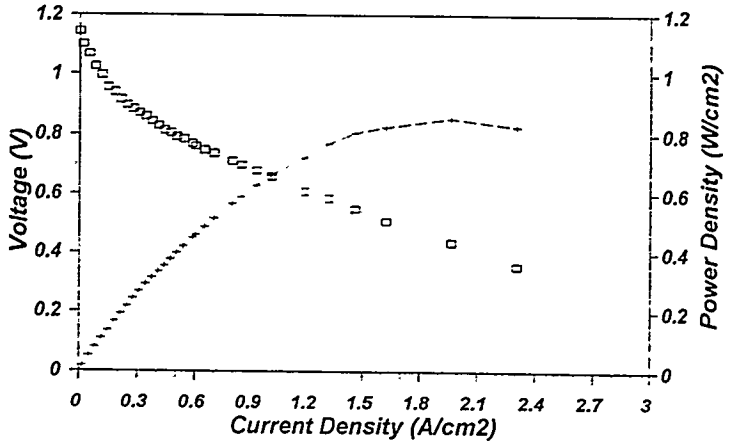

Figure 3. I-V performance of unit cell.

La0.7Sr0.3MnO$_3$/8YSZ/50Ni-YSZ,H$_2$/O$_2$=700/800cc/m,1000°C.

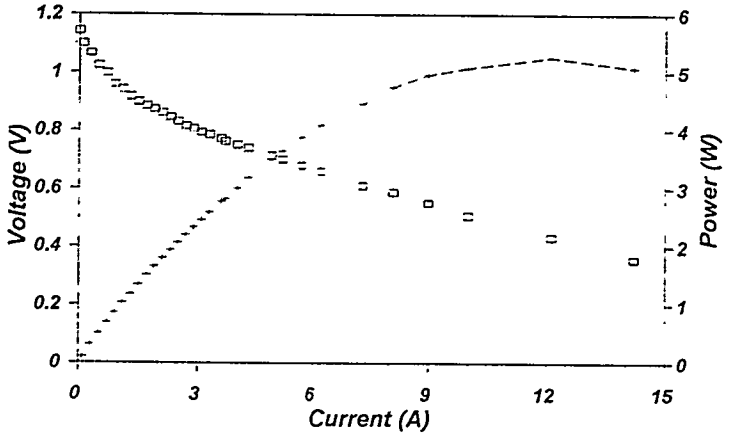

Figure 4. Total electric power of unit cell.

La0.7Sr0.3MnO$_3$/8YSZ/50Ni-YSZ,H$_2$/O$_2$=700/800cc/m,1000°C.

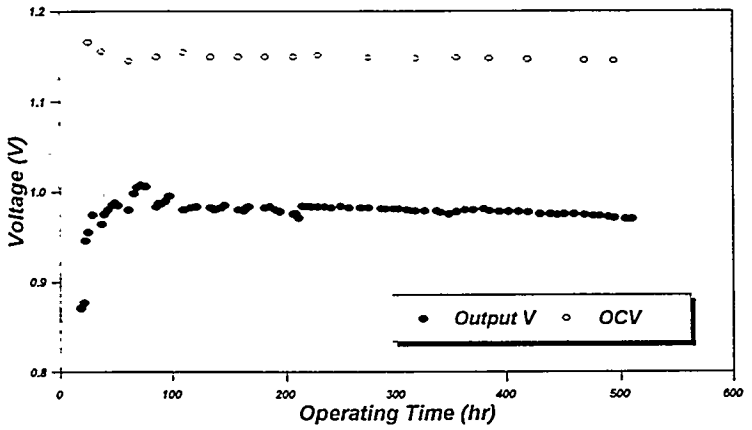

Figure 5. Voltage drop in dependence on operating time.

La0.7Sr0.3MnO_3/8YSZ/50Ni-YSZ,H_2/O_2= 700/8OOcc/m,1000°C at 150 mA/cm^2

CONCLUSIONS

The unit cell of SOFC was fabricated by the use of doctor blade and screen printing method.

It was generated the maximum electric power of 5.2 W at 1000°C with hydrogen and oxygen gas. The current density at the voltage of 0.7 V was 850 mA/cm^2.

The unit cell was operated over 510 hours. Its performance was 0.97V at 150 mA/cm^2 using hydrogen/oxygen.

ACKNOWLEDGEMENT

This study was supported by the Korea Electric Power Corporation.

REFERENCES

1. G.Y.Kim, "A prospect and technical status of Solid Oxide Fuel Cell," KIEE, 43(11), 7-13, 1993.
2. KEPRI, "A Development of Solid Oxide Fuel Cell Technology," KEPRI Report, 93G-T11, Nov. 1995.
3. N.Q.Minh and T.Takahashi, "Science and Technology of Ceramic Fuel Cell," Elsevier, 1995
4. M.Dokiya et al, "Solid Oxide Fuel Cell (SOFC-IV)," Electrochemical Society, 6, 1995

DESIGN AND PERFORMANCE OF TUBULAR FLAT-PLATE SOLID OXIDE FUEL CELL

Toshio MATSUSHIMA, Daisuke IKEDA, Himeko KANAGAWA, Toshiro HIRAI and Atsushi KOMURA(*)

NTT Integrated Information & Energy Systems Laboratories
NTT Advanced Technology(*)
3-9-11, Midori-cho, Musashino-shi, Tokyo, 180 JAPAN

1. INTRODUCTION

With the growing interest in conserving the environmental conditions, much attention is being paid to Solid Oxide Fuel Cell (SOFC), which has high energy-conversion efficiency. Many organizations have conducted studies on tubular and flat type SOFCs (1). Nippon Telegraph and Telephone Corporation (NTT) has studied a combined tubular flat-plate SOFC, and already presented the I-V characteristics of a single cell (2). Here, we report the construction of a stack of this SOFC cell and successful generation tests results.

2. TUBULAR FLAT PLATE SOFC

Figure 1 shows a configuration of a tubular flat-plate SOFC single cell and of a stack. A single cell is fabricated by making a generation part on one side of the tubular flat electrode, which is porous and contains gas channels. Interconnections are also made on the other side of this plate as a thin layer. This design makes it possible to fabricate a very thin electrolyte, because the electrolyte does not need to support the cell. Moreover, current flows perpendicularly in this flat electrode plate through the pillars that connect the two sides of the plate. Consequently, voltage losses in this SOFC cell are low. In the conventional tubular cell, on the other hand, current flows in the thin electrode layers made on the surface of the support tube, and this current flow brings about unacceptable voltage losses.

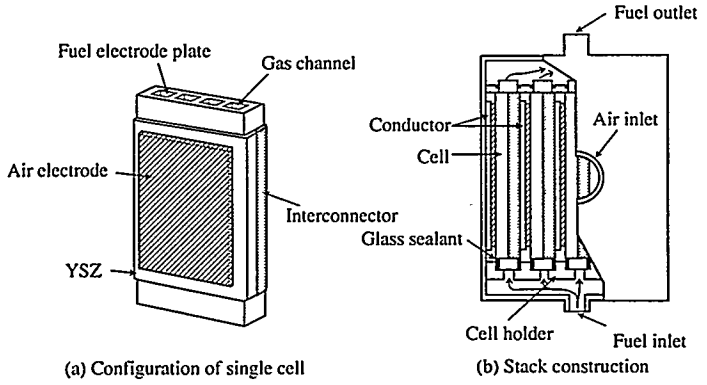

Fig. 1 Proposed tublar flat plate SOFC.
(Fuel electrode plate)

A stack is designed to be fabricated by holding single cells at equal intervals, placing an electrical conductor between cells, and sealing both ends of the cells. A gas-tight seal in the stack can be easily made by these sealing, because there is complete separation of gas inside and outside the plate. Thus, gas sealing is better than conventional flat plate cells. The stack is expected to deliver same characteristics as a single cell , because it can be made without using an interconnection plate,which is usually at least 5 mm thick. Eliminating the interconnection plates will reduce the cost of the SOFC. This is one of the benefits in the commercialization of SOFC.

3. FABRICATION OF SINGLE CELL

A tubular flat plate was made by extrusion, and a single cell was made by fabricating the electrolyte, electrode, and interconnection layers onto that plate. Then, fuel electrode material was applied to the flat plate and electrolyte layer was plasma-sprayed onto it. Air electrode was made on the electrolyte layer by slurry-coating and sintering. The electrode plate, which acts as a cell support, must have good conductivity, porosity, and mechanical strength, so we studied ways to improve of the properties of the fuel electrode, before making cells for the stack.

(1) Properties of fuel electrode

Nickel-zirconia cermet powder was synthesized from nickel oxide and YSZ (Toso: TZ-8Y) by mixing the powders in a ball mill. The characteristics of nickel-zirconia cermets are known to be influenced by the raw material, nickel oxide content and sintering conditions. In order to obtain a cermet with sufficient mechanical strength, we calcined YSZ powder and applied it to the cermets.

Conductivity was measured by the 4-probe method in a hydrogen atmosphere at 1000℃, and porosity was measured by mercury porosimetory and mechanical strength by the 3-point bending test (Japanese Industrial Standard). Gas permeability was measured at room temperature using helium gas.

Figure 2 shows the conductivity of the cermets. Conductivity, which is influenced by the calcination temperature of YSZ, was improved by approximately 10 times. These new cermets show high conductivity evenwhen the nickel oxide content is low. Calcination temperature of YSZ also affects the strength; the strength was lower for a sample synthesized from YSZ calcined at higher temperature.

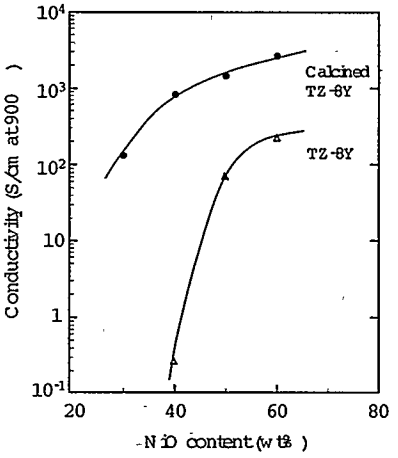

Fig. 2 Conductivity of Ni/YSZ cermets as a function of NiO content.

However, by choosing the appropriate calcination temperature, we obtained a cermet with high strength. Based on this study, we made the flat electrode plate. Several characteristics of the cermets used for the cell are shown in Table 1. As shown in Table 1, the use of the calcined YSZ improved the bending strength by 20%, and also improve pore distribution, and gas-permeability.

Table 1 Characteristics of the cermets

Sample	YSZ powder	NiO (wt%)	Porosity (%) (a)	Mean pore diameter (μm) (a)	He gas permeation coefficient (b)	Conductivity (S/cm) (c)	Mechanical strength (N/mm^2) (d)
Old material	TZ-8Y	60	14	0.22	1.70×10^{-4}	290	100
New material	Calcined TZ-8Y	50	15	0.67	3.60×10^{-4}	1500	123

(a) Measured on as-sintered body.
(b) Measured at room temp. after H_2 reduction (cm^4/g Bsec).
(c) Measured at 1000 in H_2 atmosphere.
(d) Measured after H_2 reduction in accordance with three-point bending test.

(2) Fabrication of single cell

A tubular flat plate was made by extruding the anode material described above. The size of this sintered plate was 40 x 100 x 5 (w-l-t :mm).

The electrolyte and interconnection were deposited as a 200-μm layer by plasma spraying the raw powders. The number of plasma sprays and the spraying distance were carefully selected, because the density of the sprayed layer is related to these conditions. Commercial YSZ powder was used for the electrolyte and $La(Ca)CrO_3$ powder for the interconnection layers. The thermal expansion coefficient of the interconnection was controlled to 10 $x10^{-6}$ (1/K) by varying the ratio of Ca in the powder. The value of this coefficient is almost the same as that of YSZ. The conductivity of interconnection material was 30 S/cm in the ambient atmosphere, and 1 S/cm in a hydrogen atmosphere of at 1000°C. The gas permeability coefficient of the electrolyte layer was $7x10^{-6}$ (cm^4/ g-sec), and that of interconnection was $2x10^{-7}$ (cm^4/ g-sec). An air electrode was made from $La(Sr)MnO_3$ by slurry coating. The air electrode was 50μm thick, and its surface area was 6 cm^2. The external appearence of a single cell is shown in Fig. 3.

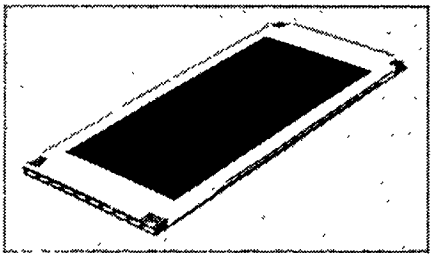

Fig. 3 External appearance of a single tubular flat-plate SOFC cell

4. I-V/P CHARACTERISTICS OF THE STACK

A stack was composed by placing cells in a stack holder made from alumina, and sealing the ends of cells and joints of the holder. Electrical contact between cells was made with a Pt mesh. Generation tests were carried out successfully on this stack at 1000℃ by supplying hydrogen and oxygen gas to each inlet gas manifold. Figure 4 shows the I-V/P characteristics. The open circuit voltage of a single cell was 0.85 V, which is lower than the theoretical value. This is thought to be caused mainly by insufficient density of the YSZ layer. Gas leakage at the side of the single cell might be another cause. Notwithstanding this open circuit voltage, the stack showed faily good characteristics and the voltage loss was small. According to an analysis of the voltage drop, this loss was caused by the resistance of the YSZ layer, and partly by the electrode activity and contact resistance. The maximum output power density of this stack was 0.35 W/cm^2. This power density has proved the usefulness of the concept of the cell and stack of Tubular Flat-Plate SOFC.

In the near future, we expect to improve the density of the electrolyte layer, which should improve the cell characteristics. Then output power of the stack will also be increased by increasing the number of cells.

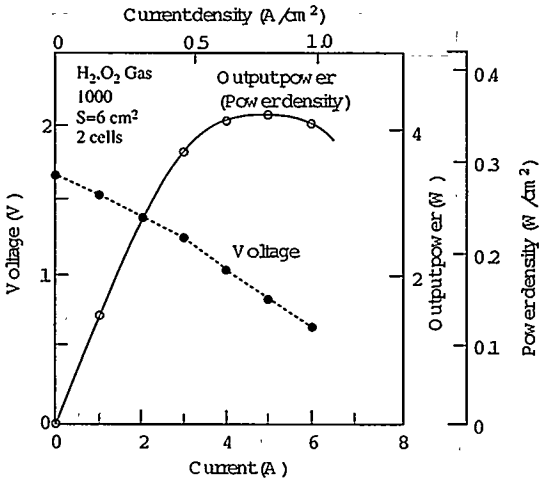

Fig. 4 I-V/P characteristics of the stack.

5. CONCLUSION

A stack of tubular flat-plate SOFC cells was constructed and generated a maximum power density of 0.35 W/cm^2. These results showed the usefulness of the cell design and the fabrication process. We are planning to improve the cell characteristics in the near future, and will also construct a stack with more power and higher power density.

REFERENCES

(1) K. Shinozuka ; Proceedings of 1st International Fuel Cell Conference p.317 (1992)
(2) T. Matsushima, M. Takahashi, T. Ogata ; Abstracts of 1994 Fuel Cell Seminar p.13 (1994)

STUDY ON DURABILITY FOR THERMAL CYCLE OF PLANAR SOFC

Motoo Ando, Kei-ichi Nakata, Shin-ichi Wakayama,
Yoshiyuki Someya , Toshihiko Yoshida
Corporate Research & Development Laboratory
TONEN CORPORATION
1-3-1, Nishi-Tsurugaoka, Ohi-Machi, Iruma-Gun, Saitama, 356, JAPAN

Introduction

TONEN CORPORATION has developed planar type SOFC since 1986. We demonstrated the output of 1.3kW in 1991[1] and 5.1kW in 1995[2]. Simultaneously we have studied how to raise electric efficiency and reliability utilizing hydrogen and propane as fuel[3][4].

Durability for thermal cycle is one of the most important problems of planar SOFC to make it more practical. The planar type SOFC is made up of separator, zirconia electrolyte and glass sealant. The thermal expansion of these components are expected to be the same value, however, they still possess small differences. In this situation, a thermal cycle causes a thermal stress due to the difference of the cell components and is often followed by a rupture in cell components, therefore, the analysis of the thermal stress should give us much useful information.

The thermal cycle process consists of a heating up and cooling down procedure. Zirconia electrolyte is not bonded to the separator under the condition of the initial heating up procedure, and glass sealant becomes soft or melts and glass seals spaces between the zirconia and separator. The glass sealant becomes harder with the cooling down procedure. Moreover, zirconia is tightly bonded with separator below a temperature which is defined as a constraint temperature and thermal stress also occurs. This indicates that the heating up process relaxes the thermal stress and the cooling down increases it.

In this paper, we simulated dependence of the stress on the sealing configuration, thermal expansion of sealant and constraint temperature of sealant glass. Furthermore, we presented SOFC electrical properties after a thermal cycle.

Calculation

<Modeling>

In order to investigate the stress in cell components, we simulated the thermal cycle condition by the Finite Element Method(FEM). As a model we assumed three types of models as shown in figure 1. The cell is made up from $LaSrCrCoO_3$(LSCC) separator, 8mol% Y_2O_3 doped ZrO_2(8YSZ) electrolyte and glass sealant. 8YSZ and LSCC are size of 200mm square. The thickness of the LSCC is 5mm, and 8YSZ is 0.2mm. LSCC separator has several gas channels.

In MODEL 1 simulated 8YSZ and LSCC are tightly bonded at two sides and strained below a constraint temperature. In MODEL 1, thermal expansion of 8YSZ and LSCC caused a thermal stress.

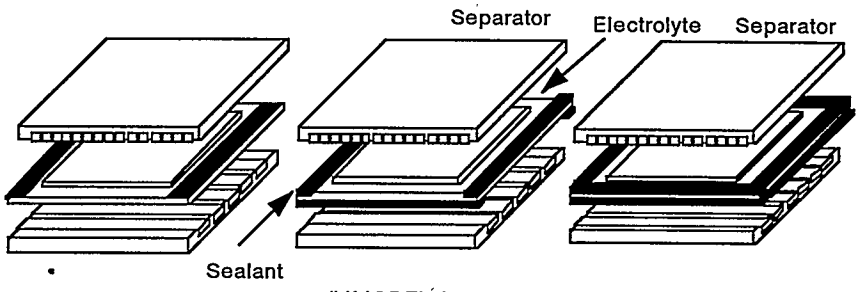

Fig.1 Calculation Model of planer SOFC

In MODEL 2 and MODEL 3, sealant was put at two or four sides of the cell as shown in figure 1(b) (c). We analyzed the cooling down procedure from 1000℃ to room temperature and it is assumed that the thermal stress occurred below a constraint temperature.

Table 1. Conditions of calculation

	sealant	arrangement	constraint temp.
CASE 1	No	MODEL 1	650℃
CASE 2	No	MODEL 1	1000℃
CASE 3	glass 1	MODEL 3	650℃
CASE 4	glass 2	MODEL 3	550℃
CASE 5	glass 2	MODEL 2	550℃

Table 1 shows the conditions of the calculation. Five cases are assumed and calculated. These have different conditions of sealant material, glass arrangement and constraint temperature. Case 1 and case 2 have no glass sealant and are different in the constraint temperature. Case 3 and case 4 have different glasses, and case 4 and 5 have different glass arrangement. As sealant, two types of glass are assumed. The glass 1 is the borosilicate glass. The glass 2 is the soda-lime glass in which fine alumina powder is dispersed to control its viscosity. The thermal expansion coefficient(TEC) and other

Table 2. Parameters of Each Materials

	TEC [$\times 10^{-6}$/K]	Young's modulus [kgf/mm^2]	Poisson's ratio
8YSZ	10.5	20000	0.3
LSC	10.2	7000	0.3
glass 1	3.25	6300	0.2
glass 2	9.9	6900	0.24

parameters of each materials we used are shown in Table 2.

The results of calculation are obtained as the stress distribution in the cell components. Using these results and the mechanical properties of 8YSZ sheets which we measured[4], we roughly estimated the failure probability of the 20 cm square 8YSZ sheets in the cooling cycle. It can be calculated from the equation (1) using Weibull parameter such as 'shape parameter'; m and 'scale parameter'; ξ. Because the main cause of failure in 8YSZ sheet should be surface crack from the fractography.

$$\text{Failure Probability} = \int_A \left(\frac{\sigma}{\xi}\right)^m dA \cdots\cdots\cdots (1)$$

<Results & Discussion>

The results of the calculation are shown in table 3 and figure 2. The table 3 involves five cases and shows the maximum stress in the 8YSZ sheet and the failure probability.

In table 3, the difference of case 1 and case 2 shows that the lower constraint temperature, the smaller the stress occurred and failure probability. But as shown in case 3, even if glass sealant is used and the constraint temperature is lowered, if the glass has a much different TEC such as glass 1, the maximum stress and the failure probability becomes very large. And in the case 4 using glass which has near value of TEC to the other components such as glass 2, the failure probability becomes lower than the case 2. This indicates that constraint temperature and the correspondence of TEC between glass sealant and the other components are essential to the thermal stress.

Table 3 Maximum Stress and Failure Probability of 8YSZ

	CASE 1	CASE 2	CASE 3	CASE 4	CASE 5
σ_{max}[Kgf/mm^2]	5.5	8.6	18.7	5.5	4.7
Failure Probability	5×10^{-8}	1×10^{-5}	4×10^{-2}	1×10^{-8}	5×10^{-9}

Furthermore, as shown in case 5, glass arrangement decreases the failure probability about half. The reason can be explained by the stress distribution shown in figure 2. Figure 2(a) shows the stress distribution pattern of MODEL 1 and MODEL 2. It shows the stress concentrates at the corners of the sheet which are the crossing points of sealant glasses which alternate on either side of the sheet. On the other hand, MODEL 3, with glass arranged at four sides of cell, has a different distribution. In this case, stress concentrates on the boundary between the separator's channels and area constraint by sealant glass. 8YSZ sheet is not constrained at the area of separator's channels, so it shows that stress occurred in 8YSZ sheet concentrates at the boundary of the constraint area.

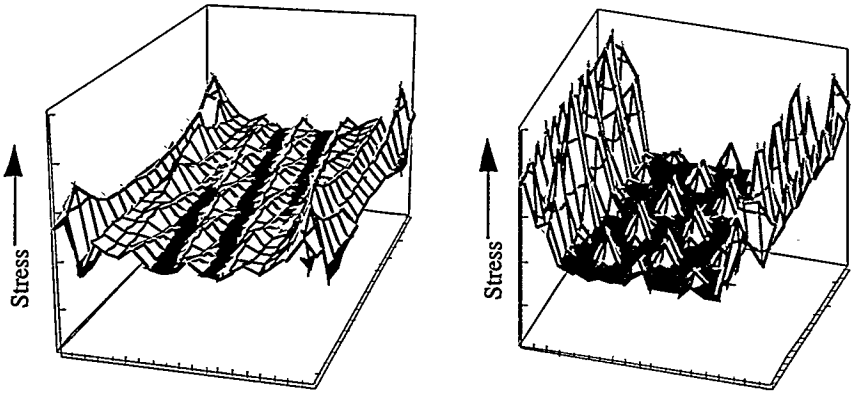

(a)MODEL 1 & MODEL 2 (b)MODEL 3

fig.2 Stress Distribution Pattern in 8YSZ Sheet

These results make the following clear:

(1) Stress accompanied by the thermal cycle is mainly caused by the thermal expansion difference between the sealant material and other components. When this difference is large, it is larger than the stress occurred by the thermal expansion difference between zirconia electrolyte and LSCC separator.

(2) By using glass material as a sealant, it is considered that stress occurs over only a fraction of the cooling cycle. Hence using glass reduces stress more than if a rigid material is used.

(3) Stress concentrates at the boundary of the constraint area.

Therefore the following are important to reduce the stress in thermal cycle:

(a) use glass sealant which have similar thermal expansion to the other components.

(b) reduce the boundary of the constraint area.

Cell Test

From the results of the calculation, we decided the cell structure as case 5 of table 1, and tested it. The cell scale was 20cm square 3 cells stack. As fuel, LPG, reformed with steam was used

at a steam-carbon ratio of about 3.0. Fuel gas and air were supplied by the external manifold of the cross flow structure.

After a thermal cycle from 1000℃ to room temperature, the cell was operated at 1000℃ and performance was measured at several points of fuel utilization.

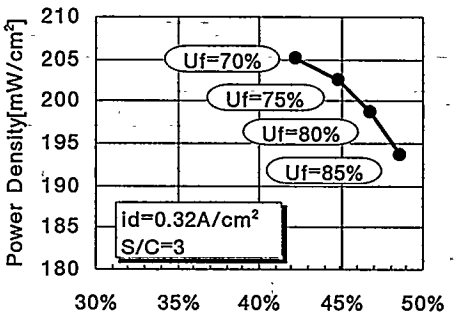

fig.3 Performance of The Tested Cell

The result of cell test is shown in figure 3. It shows the relation of electric efficiency, power density and fuel utilization. After the thermal cycle, this cell was operated at 85% fuel utilization, and it's electrical efficiency was above 45% and power density was about 200[mW/cm²].

This result shows that gas crossing and deterioration of cell property due to rupture of the cell components is little.

Conclusions

In this paper we considered the way to reduce gas crossing and get high efficiency performance of planar SOFC after the thermal cycle, concluding the following;

(1)Stress occurred in zirconia electrolyte is simulated and the ways to reduce it are found.

(2)Over 45% electric efficiency and 200[mW/cm²] power density was obtained after thermal cycle at 20cm square cell

Acknowledgment

This work was partially supported by the Petroleum Energy Center which was subsidized by MITI.

Reference

(1)S. Sakurada and T. Yoshida, The Proceedings of The Second International Symposium on Solid Oxide Fuel Cells, Athens, Greece, p45(1991)

(2)T. Yoshida, A. Tsunoda, Y. Someya, T. Hoshina, H. Seto, H. Koide, S. Wakayama, M. Andoh, I.Mukaizawa, F. Ishizaki, J. Nishimura, N. Ohmori, N. Itoh and K. Nakata, Proceedings of The 9th Gijutsukaihatsukenkyuuseikahappyou, Petroleum Energy Center, p 402(1995)

(3)M.Ando, I.Mukaizawa, H.Koide, Y.Someya, and T.Yoshida, '94 Extended Abstracts of Electrochemical Society of Japan, Yokohama, p251(1994)

(4)Y.Someya, H.Koide, M.Ando, and T.Yoshida, Proceedings of The Fourth International Symposium
on Solid Oxide Fuel Cells, Yokohama, Japan, p86(1995)

(5)T. Hoshina, N. Ohmori, K. Fujimoto, T. Yoshida, Proceedings of The Fourth International Fuel Cell Conference, Kobe, Japan, p247(1996)

MEASUREMENT OF RESIDUAL STRESSES IN DEPOSITED FILMS OF SOFC COMPONENT MATERIALS

T.Kato, A.Momma, S.Nagata and Y.Kasuga
Electrotechnical Laboratory
1-1-4 Umezono, Tsukuba, Ibaraki, Japan

Introduction

The stress induced in Solid oxide fuel cells (SOFC)s has important influence on the lifetime of SOFC. But the data on stress in SOFC and mechanical properties of SOFC component materials have not been accumulated enough to manufacture SOFC. Especially, the data of $La_{1-x}Sr_xMnO_3$ cathode and $La_{1-x}Sr_xCrO_3$ interconnection have been extremely limited. We have estimated numerically the dependences of residual stress in SOFC on the material properties, the cell structure and the fabrication temperatures of the components [1], but these unknown factors have caused obstruction to simulate the accurate behavior of residual stress. Therefore, the residual stresses in deposited $La_{1-x}Sr_xMnO_3$ and $La_{1-x}Sr_xCrO_3$ films are researched by the observation of the bending behavior of the substrate strips. The films of SOFC component materials were prepared by the RF sputtering method, because: (1) It can fabricate dense films of poor sinterable material such as $La_{1-x}Sr_xCrO_3$ compared with sintering or plasma spray method. (2) For the complicated material such as perovskite materials, the difference between the composition of a film and that of a target material is generally small. (3) It can fabricate a thick ceramics film by improving of the deposition rate. For example, Al_2O_3 thick films of 50μm can be fabricated with the deposition rate of approximately 5μm/h industrially. In this paper, the dependence of residual stress on the deposition conditions is defined and mechanical properties of these materials are estimated from the results of the experiments.

Experimental

The sputtering conditions to fabricate the films are listed in Table 1. The thickness of each deposited film was approximately 1μm . $La_{0.9}Sr_{0.1}MnO_3$ and $La_{0.85}Sr_{0.15}CrO_3$ powders were used for the sputtering target. Al_2O_3, the mixture of Al_2O_3 and MgO (SP) whose weight ratio of MgO/Al_2O_3 was 1, and MgO were adopted as the substrates. The surfaces of the substrate strips were polished up to mirror finished and their dimensions were 1mm thick, 10mm wide and 50mm long. Their material properties are shown in Table 2. The crystal structure of the film was determined by X-ray diffractometer (XRD). The composition of the film was measured by energy-dispersive X-ray spectrometer (EDX) and induced coupled plasma spectrometer (ICP). The deflection δ at the center of substrate induced by the deposited film was measured by the Fizeau interferometer. A typical example of the change of its image by the deposition is shown in Fig.1. The residual stress of the film σ was estimated by the following equation [2].

Table1. Sputtering conditions

RF Power /W	300
Target diameter /mm	117
Pressure /10^{-3}Torr	3
Substrate Temp. °C	600~900
gas species	Ar

Table 2. Material properities of substrates materials.

	Young's modulus *E*/GPa	Poisson's ratio ν	Average of coefficient of thermal expansion α / 10^{-6} °C^{-1}			
			600	700	800	900 °C
Al_2O_3	372	0.22	7.3	7.5	7.86	8.13
SP	284	0.24	9.12	9.32	9.59	9.76
MgO	304	0.19	13.1	13.3	13.5	13.7

$$\sigma = \frac{4Eb^2\delta}{3(1-\nu)l^2d}$$

b, l, E, ν, and d denote thickness, length, Young's modulus, Poisson's ratio of the substrate and thickness of the deposited film, respectively.

In general, the residual stresses in thin films consist of thermal stress σ_{th} and intrinsic stress σ_{in} which is produced during the deposition. The thermal stress is caused by the mismatch of thermal expansion coefficients (TEC) between the film and the substrate. Hence, it can be expressed as follows [3].

$$\sigma_{th} = \frac{E_f}{(1-\nu_f)}(\alpha_f - \alpha_s)(T_s - T_r)$$

α_f, α_s denote TECs of a film and a substrate, T_s is the substrate temperature during deposition and T_r is room temperature, respectively.

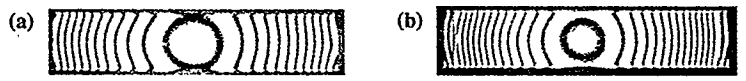

Figure 1. An example of the change of an interferometer image.
a : The surface of the Al_2O_3 substrate before deposition.
b : The surface of $La_{1-x}Sr_xMnO_3$ film on the Al_2O_3 substrate (T_s = 900 °C)

Results and Discussion

XRD patterns of $La_{1-x}Sr_xCrO_3$ and $La_{1-x}Sr_xMnO_3$ films on the three kinds of substrates agree with each other. Crystal structures of both kinds of films were almost cubic. The differences of the atomic ratios between the films and the powder were measured by ICP and EDX. Ratio of La to other atoms in the films slightly increased with the increasing substrate temperature T_s, but the differences are within 5% .

The dependence of the residual stresses in the films on TEC of the substrate is shown in Fig.2. The

plus sign of the residual stress corresponds a tensile stress. All residual stresses of the films on SP and MgO substrates are compressive. Elastic moduli $E_f/(1-\nu_f)$ of $La_{1-x}Sr_xCrO_3$ films and $La_{1-x}Sr_xMnO_3$ films are calculated at 290 GPa and 220 GPa from the dependence of the slope $\Delta\sigma/\Delta\alpha_s$ on the temperature difference T_s-T_r.

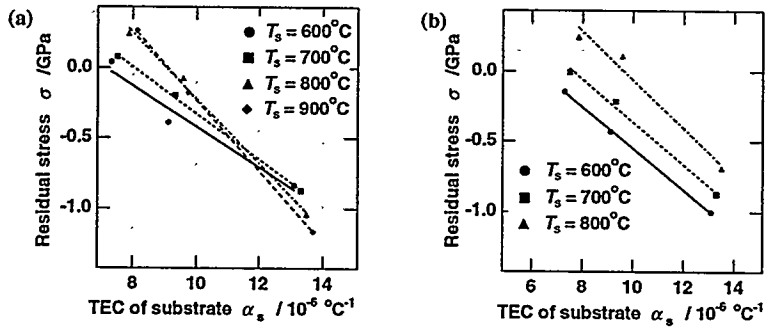

Figure 2. Dependence of residual stress on the TEC of substrate α_s.
a: $La_{1-x}Sr_xCrO_3$ b: $La_{1-x}Sr_xMnO_3$

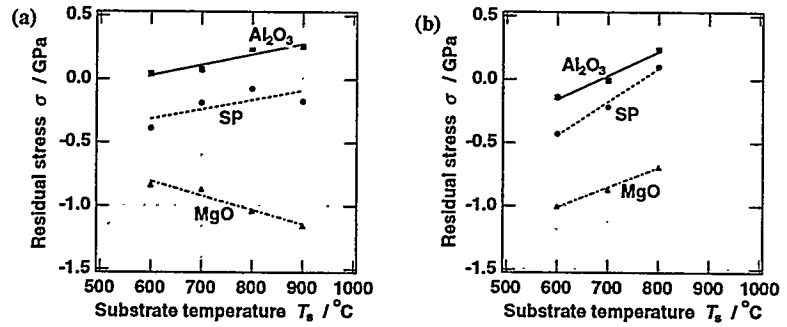

Figure 3. Dependence of residual stress on the substrate temperature T_s.
a: $La_{1-x}Sr_xCrO_3$ b: $La_{1-x}Sr_xMnO_3$

The dependence of the residual stresses in the films on the substrate temperature T_s is shown in Fig.3. Assuming the intrinsic stresses are constant for all kind of substrates within this temperature range, TEC and σ_{in} of the film can be estimated from the $E_f/(1-\nu_f)$ and the dependence of average slopes $\Delta\sigma/\Delta T_s$ on the TEC of the substrate. The result of this estimation is shown in table 3. The difference between TEC of $La_{1-x}Sr_xCrO_3$ films obtained from this measurement and that of balk $La_{1-x}Sr_xCrO_3$ in reductive atmosphere [4] is relatively small. TEC of $La_{1-x}Sr_xMnO_3$ films, which is approximately 1.5 times bigger than that of bulk $La_{1-x}Sr_xMnO_3$ in air [5], shows same tendency as the TEC in reductive atmosphere reported by Mizusaki et al.[6], although the accuracy of measurement and dependence of

Table 3. The estimation of material properities and intrinsic stresses.

	Elastic modulus $E_f/(1-\nu_f)$ /100GPa	TEC (at 700°C) α_f / 10^{-6} °C^{-1}	Intrinsic stress α_{in} / GPa
$La_{1-x}Sr_xCrO_3$	2.9	10	-0.3
$La_{1-x}Sr_xMnO_3$	2.2	19	-1.7

σ_{in} on T_s must be investigate further. The intrinsic stresses of both kinds of films are compressive, especially, the magnitude of σ_{in} in $La_{1-x}Sr_xMnO_3$ films is bigger than σ_{th} in it. These compressive intrinsic stresses prevent the delamination of films from the low TEC substrates such as Al_2O_3 after depositing. For adopting these films for SOFC, It will be necessary to investigate the behavior of films in operating condition further.

Conclusion

$La_{1-x}Sr_xCrO_3$ and $La_{1-x}Sr_xMnO_3$ films were fabricated by RF sputtering method. From the measurement of residual stresses in the films, the elastic moduli, intrinsic stresses and TECs of the both films were estimated. It was clarified that compressive stresses are induced in the films and this stresses prevent the delamination of films from the low TEC substrates.

Reference

1. T.Kato, A.Momma, S.Nagata, Y.Kasuga, "Residual stress analysis of SOFC," Proc. 2nd Int. Fuel Cell Conf., pp461-p464, Feb.1996.
2. P.Jin and S.Maruno, "Evaluation of Internal Stress in Reactively Sputter-Deposited ZrN Thin Films," Japan. J. Applied Phys., Vol.30, No.7, pp1463-1468, 1991.
3. T.Hanabusa, K.Kusaka, K.Tominaga and H.Fujiwara, "Dependence of Substrate and Temperature on Residual Stress in AlN Films Deposited by sputtering," J. Soc. Mat. Sci., Japan, Vol.42, No477, pp627-p633, 1993.
4. N.Sugiura, S.Otoshi, A.Kajimura, M.Suzuki, H.Ohnishi,H.Sasaki and M.Ippommatsu, "Thermal Expansion Properties of A-Site Deficient La(Sr)CrO_3," J. Ceram. Soc. Japan, Vol101, No7, pp769-772, 1993.
5. S.Srilomsak, D.P.Schilling and H.U.Anderson, "Thermal Expansion Studies on Cathode and Interconnect Oxides," Prop. 1st Int. Symp. SOFC, pp129-140,1989.
6. J.Mizusaki, H.Nambu, C.Nakao, H.Tagawa,H.Minamiue and T.Hashimoto, "Relationship of Crystal Structure, Lattice Parameters and Thermal Expansion to Nonstoichiometry in $La_{1-x}MnO_{3+d}$ and $La_{1-x}Sr_xMnO_{3+d}$ Determined by High-temperature X-Ray Diffraction under Controlled Oxygen Partial Pressures," Proc. 4th Int. Symp. SOFC, pp444-453, June, 1995.

CHARACTERIZATION OF CERIA-BASED SOFCs

Rajiv Doshi[1], Jules Routbort[2], & Michael Krumpelt[1]

[1]Electrochemical Technology Program
Chemical Technology Division
[2]Energy Technology Division

Argonne National Laboratory
9700 S. Cass Avenue, Argonne, IL-60439

Solid Oxide Fuel Cells (SOFCs) operating at low temperatures (500-700°C) offer many advantages over the conventional zirconia-based fuel cells operating at higher temperatures. Reduced operating temperatures result in:

- -Application of metallic interconnects with reduced oxidation problems
- -Reduced time for start-up and lower energy consumption to reach operating temperatures
- -Increased thermal cycle ability for the cell structure due to lower thermal stresses of expansion mismatches

While this type of fuel cell may be applied to stationary applications, mobile applications require the ability for rapid start-up and frequent thermal cycling.

Ceria-based fuel cells are currently being developed in the U.K. at Imperial College[1], Netherlands at ECN[2], and U.S.A. at Ceramatec[3]. The cells in each case are made from a doped ceria electrolyte and a $La_{1-x}Sr_xCo_{1-y}Fe_yO_3$ cathode.

Electrolyte Properties

A reduced operating temperature requires using either of a very thin form (about 1μm) of the conventional zirconia electrolyte or a different electrolyte with higher conductivity is. Using a 1-μm-thick electrolyte poses problems in fabrication and in integrity during cycling and operation. A cerium oxide electrolyte doped with a rare earth like gadolinium exhibits higher ionic conductivity in air than the zirconia (fig. 1).

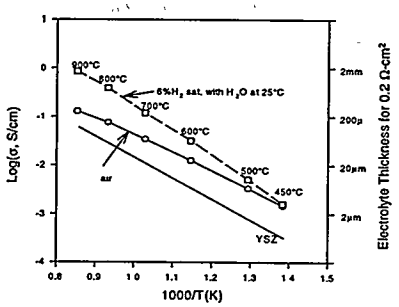

Fig. 1 Conductivity of electrolyte in air and H_2. Required thickness for 0.2 Ω-cm² shown on right.

Unlike zirconia however, ceria exhibits significant electronic conductivity above 500°C in the fuel atmosphere because of the reduction of cerium oxide. The fraction of the Ce^{4+} ions reduced to Ce^{3+} as a function of temperature and oxygen partial pressure (pO_2) is shown in fig. 2. The partial reduction of cerium oxide generates mobile electrons and causes electronic conductivity in the

electrolyte at temperatures above 500°C. Below this temperature the electrolyte remains ionic and can be used as an electrolyte in a solid oxide fuel cell.

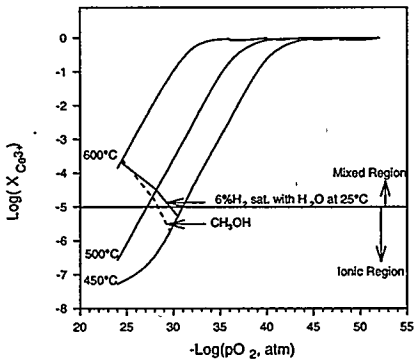

Fig. 2 Fraction of Ce^{4+} ions reduced to Ce^{3+} as a function of temperature and pO_2

Electronic conductivity in the electrolyte is evident from the measured values of the open circuit voltage (OCV) when compared to the Nernst potential as shown in the following table.

Temperature (°C)	Theoretical OCV, mV	Measured OCV, mV
500	1054	995
600	1025	941
700	997	869

Electrochemical Characterization

Figure 3 plots the performance from 500 to 700°C of a cell with the following configuration: *$La_{0.6}Sr_{0.4}Co_{0.2}Fe_{0.8}O_3$ (LSCF) / $Ce_{0.8}Gd_{0.2}O_{1.9}$ Electrolyte / Ni-$Ce_{0.8}Gd_{0.2}O_{1.9}$*

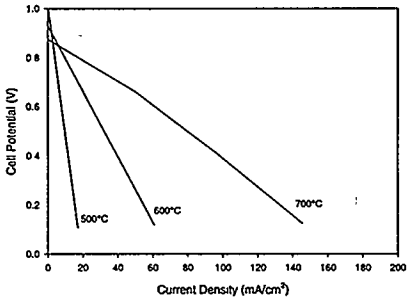

Fig. 3 Cell performance with a 1.2 mm thick electrolyte, LSCF cathode and Ni-cermet anode

It shows that the performance of the cell at 500°C is inadequate. We found that the majority of the voltage losses apart from the electrolyte resistance were at the cathode electrolyte interface. Figure 4 shows the proportion of the voltage loss from the cathode compared to the anode. The electrolyte loss can be reduced by using 10- and 20-μm-thick electrolytes as shown on the right

side of fig. 1. Cathode performance improvement requires either new microstructures or new materials that are more active while being compatible with the electrolyte.

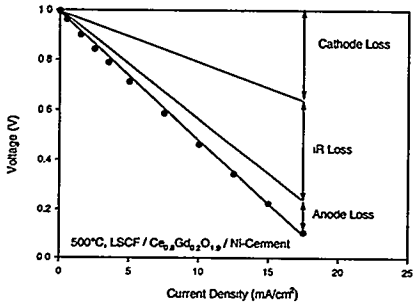

Fig. 4 Voltage losses in the fuel cell showing the large magnitude of the cathode loss

Cathode Properties

The interface resistances of several cathode materials measured by impedance spectroscopy using reference electrodes are shown in fig. 5. Single phase porous cathodes ($La_{0.6}Sr_{0.4}Mn_{0.8}Co_{0.2}O_{3-\delta}$ and LSCF) performed better for materials with an increasing ability to lose oxygen from its lattice when compared to the $La_{1-x}Sr_xMnO_{3-\delta}$ (not shown in figure) cathode used with zirconia-based fuel cells. This presumably stems from an increased ionic conductivity or diffusion while still maintaining electronic conductivity high enough for a cathode.

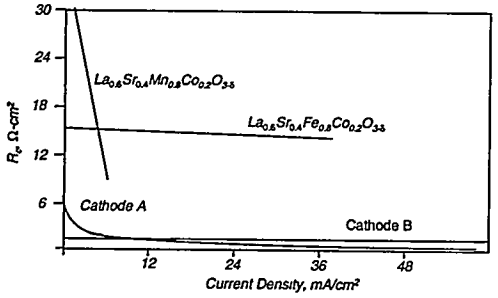

Fig. 5 Interface resistance of cathode electrolyte interface for different cathodes

This hypothesis is supported by the diffusion coefficients of some cathode materials measured on dense samples by isotope (O^{18}) exchange and SIMS which are given in figure 6.

Two phase cathodes performed better still as shown by cathodes A and B in fig. 5. In addition cathode A has the ability to lose oxygen more easily than all other cathodes. This caused an increase in performance with increasing current density.

While the ability of the cathode material to lose oxygen increases the electrode performance for the materials considered, it is also known that this can cause an expansion mismatch with other fuel cell components. It is desirable then to work with materials that exhibit a constant performance at

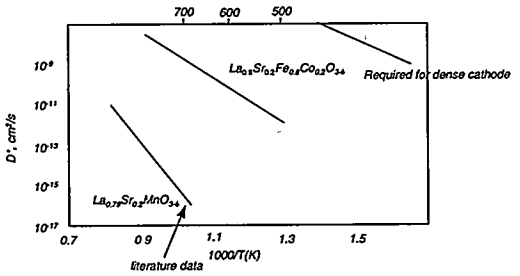

Fig. 6 Oxygen self-diffusion for selected cathode materials

different current densities. Cathode B is such a material with good performance (2.4 Ω-cm^2 at 500°C) however some improvement is still required to achieve values of less than 1 Ω-cm^2.

The performance of a cell with cathode A is shown in figure 7. The OCV was considerably lower owing to significant porosity when the electrolyte was thinner (200 µm). The thinner electrolyte had a reduced resistance, which raised overall performance. Also shown in the figure is a calculated performance curve for a dense electrolyte with negligible thickness.

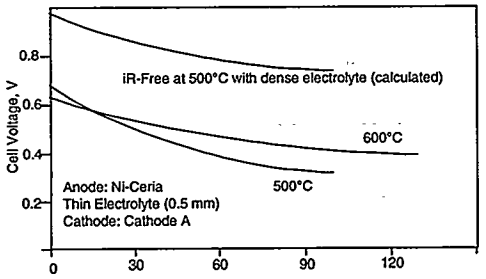

Fig. 7 Cell performance with cathode A. Measured OCV lower due to interconnected porosity.

Cathode performance is also being increased by using improved microstructures. Steele[4] has recently been demonstrated that a thin 1-µm LSCF layer between the electrolyte and a coarser porous thick LSCF electrode exhibited only 0.4 Ω-cm^2 interface resistance.

Conclusions

Cathode performance is being improved by using better materials and/or microstructures. Fabrication of thin dense electrolytes is also necessary to achieve high cell performances.

Acknowledgements

This work is supported by the OTT-DOE under Contract No.W-31-109-ENG-38.

References

[1] M. Sahibzada et.al., Proc. of 2nd European SOFC Forum, Oslo, Norway, May 1996, p687-696
[2] B.C.H. Steele et al., Proc. of the Fuel Cell Seminar, San Diego, CA, Nov. 1994, p479-482
[3] C. Milliken et al., EPRI/GRI Fuel Cell Workshop, Tempe, AZ, Apr. 2-3, 1996
[4] B.C.H. Steele, private communication, July 1996.

IMPROVEMENT OF THE LONG TERM STABILITY IN THE HIGH TEMPERATURE SOLID OXIDE FUEL CELL USING FUNCTIONAL LAYERS

B. Brückner[+], C. Günther[+], R. Ruckdäschel[+], E.Fendler[°] and H. Schmidt[*],
* Siemens AG, Corporate Research and Development, 91050 Erlangen, Germany
+ Siemens AG, Power Generation Group KWU, 91050 Erlangen, Germany
° German Aerospace Research Establishment (DLR), 70569 Stuttgart, Germany

Introduction

In the planar Siemens design of the solid oxide fuel cell a metallic interconnector is used to seperate the ceramic single cells. A disadvantage of the metallic bipolar plate which consists of a chromium alloy (1) is the formation of high volatile Cr-oxides and -hydroxides at the surface at the cathode side. The reaction products evaporate and are reduced at the cathode/electrolyte interface to form new crystalline phases. This process gives rise to long term cell degradation (2). Protective coatings might be successful in preventing the chromium oxide evaporation. The required properties of the protective layers are (I) high electrical conductivity, (II) similar coefficients of thermal expansion to the bipolar plate (III), chemical compatibility to the bipolar plate and cathode material, (IV) a low diffusion coefficient of Cr and (V) chemical stability up to 1223K under oxygen atmosphere.
Furthermore, during operation at 1223K an electrical contact between the metallic plate and the electrodes has to be maintained. This problem could be solved using ceramic layer between the metallic plate and the single cells.

Experimental Procedure and Results

For the deposition of protective coatings the vacuum spraying (VPS) has a high potential, differently doped $LaCrO_3$ powders were used for the coatings. Bipolar plates were first etched in order to remove oxide layers. In combination with a transferred arc a very good adhesion was attained. The effect of the transferred arc is the removal of impurities by gas discharge appearing due to negative polarity of the substrate with respect to the plasma torch (3). Furthermore, some samples were pre-heated just before starting the deposition process in order to increase the adhesion. The structured bipolar plates were deposited in a technical chamber with a robot handled torch and substrate movement which enables the deposition under different spray angles. The high velocity and laminarity of the plasma jet enables the production of very dense and well bonded layer. Phase stability and crystallinity of the layers were checked by x-ray diffraction (XRD) and energy dispersive x-ray analysis (EDX). The microstructure and porosity of the layers were investigated by optical and scanning electron microscopy. Optimizing the substrate pretreatment procedure and the plasma spray process homogenous layers were achieved (fig. 1a) (4,5).

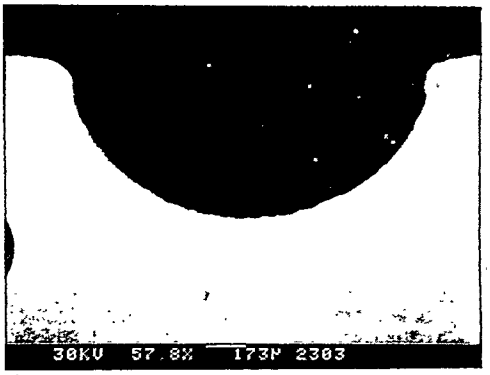

Figure 1 a) VPS-deposition of perovskite layers on a structured bipolar plate

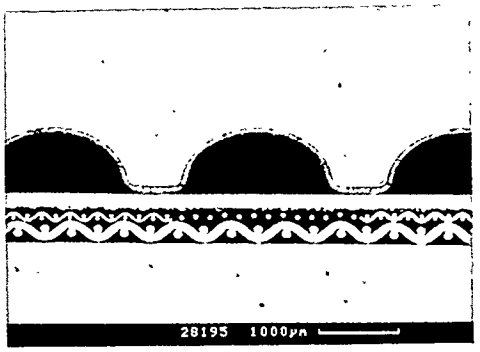

Figure 1 b) Cross-section of a complete stack compound

As contact layer material between the metallic interconnector and the cathode $LaCoO_3$ and Sr-doped $LaMnO_3$ was investigated. The development of these layers was previously published (6). For the deposition of the contact layers an air - brushing technique was used.
A good deformability of this porous layers is required in order to form the electrical contact between the bipolar plate and the cathode during the sealing procedure of the stack.
Pieces of structured bipolar plates (1 cm^2) were coated with several contact layer materials by wet powder spraying. To simulate the weight ratios in a real stack the layers were applied by two different weights, according to mechanical forces of 3.3 and 13 N. Then the test samples were heated with a temperature program that simulates the sealing procedure in a stack. The thickness of the contact layer was measured before and after the temperature treatment. The difference was defined as a measure for the contact layer deformation. Dependent on the weight the layers were deformed by 10% and 20%, respectively. The protecting function of the plasma-sprayed layers was demonstrated with evaporation measurements. The detected chromium content of the investigated bipolar plates coated with $La_{0.8}Sr_{0.2}MnO_3$ were in the range of the detection accuracy. The values for $La_{0.9}Sr_{0.1}CrO_3$ layers on the bipolar plate are the same as for sintered $La_{0.9}Sr_{0.1}CrO_3$ material. No reaction products of evaporated chromium oxides could be detected after annealing coated bipolar plates in contact with cathodes.
Further characterization was maintained by contact resistance measurements and by single cell measurements.
The instrumental set-up of the contact resistance measurements was previously published (7). Two cylinders of bipolar material, 2 mm in diameter each, which were coated with the functional layers, were pressed with the coated area against a sintered sheet of a porous cathode foil. The time dependence of the resistance of this pile was measured by a 4-point technique under operating conditions of a SOFC cathode (1223K, air as ambient gas). For the determination of the contact resistance a constant current of 0.1 A was applied and the voltage drop was plotted as function of time. In each run 8 samples could be measured simultaneously. The time dependence of the contact resistance at 1223K in air of the several investigated layer combinations is illustrated in fig. 2. The gaps in the respective curves are caused by thermic cycles (cooling to room temperature and heating again to operating termperature). The thermic cycles were carried out in order to check the adhesive strength of the layers after this temperature treatment. If $LaCoO_3$ as contact layer was used without any protective layer, a continuos increase of the contact resistance could be observed. After a thermal cycle the contact resistance value increased by a factor of 2. The reason therefore are the different thermal expansion coefficients of $LaCoO_3$ (28 ppm/K) and the bipolar material (11.3 ppm/K) (6), so the temperature treatment leads to a

defoliation of the contact layer. Samples with a protective layer showed a constant low contact resistance over the test period independent of the combination. Even after repeated thermal cycles the contact resistance values remained stable.

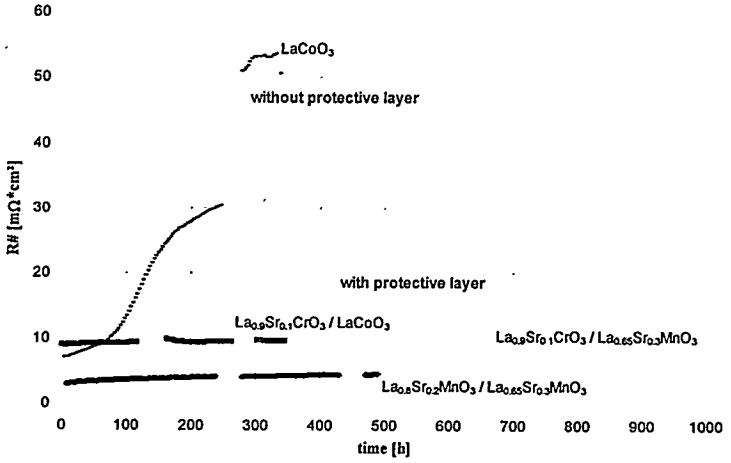

Fig.2: Time dependence of the contact resistance

In single cell housings covered CrFe5 plates were applied as electrical contacts on the cathode side whereas on the anode side a Pt grid was used. The PEN consisted of a 150 mm YSZ electrolyte membrane with a 50 µm $La_{1-x}Sr_xMnO_3$ cathode layer and a 50 µm NiO_2-YSZ anode layer. The electrode area was 16 cm^2. Cell measurements were maintained under galvanostatic conditions at 1223 K in oxygen and dry hydrogen, respectively. Earlier experiments using uncoated interconnector plates resulted in a fast cell degradation caused by a deposition of chromium oxide compounds in the cathode (8). Cells with Sr and Ca doped $LaCrO_3$- or $LaSrMnO_3$ coated interconnectors were stable during 1000 hours of operation (fig. 3).

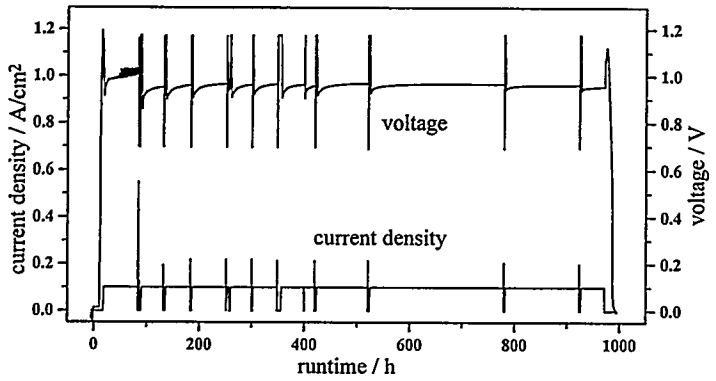

Fig. 3: Cell measurement at 1223K using a $La_{0.9}Sr_{0.1}CrO_3$ covered interconnector plate

Interruptions within the galvanostatic treatment are due to the I/U-characteristic and impedance measurements. By means of SEM and EDS the electrode/electrolyte cross section was investigated with respect to deposited Cr-oxide in the cathode. Cr-compounds could not be detected throughout the cathode. In fig. 1b) a whole stack assemply including a protective and a contact layer is shown.

Conclusion

Using the high velocity torch nozzles designed by the DLR and a careful adaptation of plasma spray parameters succeeded in the production of dense perovskite-type chromite and manganite layers on bipolar plates. The deposition onto structured bipolar plates was a challenge which could be successfully solved by developing a deposition process using a spray robot and by changing the gas channel geometry.
To impede the evaporation of chromium compounds from the interconnector surface and thus the degradation of the electrical performance of the SOFC cathode a protective ceramic layer was developed and successfully tested.
Up to now the VPS technique is the only method of producing reliable protecting layers for the bipolar plate.

References

(1) Köck, W., Martinz, H.-P., Greiner, H., Janousek, M.:''Development and Processing of Metallic Cr Based Materials for SOFC Parts''.

(2) Quadakkers, J., Greiner, H., Köck, W., ''Metals and Alloys for High Temperature SOFC Application''. Proc. of 1st SOFC Forum, Luzern, Switzerland p.525 (1994)

(3) Mühlberger, E., Kremith, R.D.:''System and Method for Plasma Coating'', US-Patent 4 328 257, May 4, 1982

(4) Smith, M.F.: ''An Investigation of the Effects of Droplet Impact Angle in Thermal Spray Deposition'', Proc.7th National Thermal Spray Conf., Boston, USA, p 603 (1994)

(5) Fendler, E., Henne, R., Ruckdäschel, R., Schmidt, H., „Protecting layers for the bipolar plate of planar solid oxide fuel cells produced by VPS", Proc. of 2nd SOFC Forum, Oslo, Norway, p. 269 (1996)

(6) B. Brückner, H. Landes, B. Rathjen, Proceed. of the 3rd Intern. Symp. on Solid Oxide Fuel Cells edited by S.C. Singhal and H. Iwahara, Vol. 93-4, p 641-648, (1993).

(7) H. Schmidt, B. Brückner and K. Fischer, Proc. of the 4th Int. Symposium on Solid Oxide Fuel Cells edited by M. Dokiya, O. Yamamoto, H. Tagawa and S.C. Singhal, Vol. 95-1, p 869 (1995)

(8) Günther, C., Beie, H.-J., Greil, P., Richter, F., „Parameters influencing the Longterm-Stability of the SOFC", Proc. of 2nd SOFC Forum, Oslo, Norway, p. 491 (1996)

EFFECT OF IONIC CONDUCTIVITY OF ZIRCONIA ELECTROLYTES ON POLARIZATION PROPERTIES OF VARIOUS ELECTRODES IN SOFC

Masahiro Watanabe, Hiroyuki Uchida, and Manabu Yoshida
Laboratory of Electrochemical Energy Conversion,
Faculty of Engineering, Yamanashi University
Takeda 4-3, Kofu 400, Japan

INTRODUCTION

Solid oxide fuel cells (SOFCs) have been intensively investigated because, in principle, their energy conversion efficiency is fairly high. Lowering the operating temperature of SOFCs from 1000°C to around 800°C is desirable for reducing serious problems such as physical and chemical degradation of the constructing materials. It is very important to develop high performance electrodes because the electrode reaction rates decrease extremely in such temperature regions.

The object of a series of the studies is to find a clue for achieving higher electrode performances at a low operating temperature than those of the present level. Although the polarization loss at electrodes can be reduced by using mixed-conducting ceria electrolytes *(1)*, or introducing the mixed-conducting (reduced zirconia or ceria) layer on the conventional zirconia electrolyte surface *(2-4)*, no reports are available on the effect of such an ionic conductivity of electrolytes on electrode polarizations. High ionic conductivity of the electrolyte, of course, reduces the ohmic loss. However, we have found that the IR-free polarization of a platinum anode attached to zirconia electrolytes is greatly influenced by the ionic conductivity, σ_{ion}, of the electrolytes used *(5)*. The higher the σ_{ion}, the higher the exchange current density, j_0, for the Pt anode in H_2 at 800 ~ 1000°C. It was indicated that the H_2 oxidation reaction rate was controlled by the supply rate of oxide ions through the Pt/zirconia interface, which is proportional to the σ_{ion}. Recently, we have proposed a new concept of the catalyzed-reaction layers which realizes both high-performances of anodes *(6,7)* and cathodes *(6,8)* for medium-temperature operating SOFCs. From the viewpoints of both fundamental electrochemistry and practical application, it is very interesting to clarify such an effect of σ_{ion} on the polarization of various electrodes. In this paper, we present the interesting dependence of the polarization properties of various electrodes (the SDC anodes with and without Ru microcatalysts, Pt cathode, La(Sr)MnO_3 cathodes with and without Pt microcatalysts) on the σ_{ion} of various zirconia electrolytes at 800 ~ 1000°C.

EXPERMIMENTAL

The solid electrolytes employed were zirconia doped with yttria, ytterbia or scandia. Zirconias with the composition of $(ZrO_2)_{1-X}(Y_2O_3)_X$ (X= 0.03~0.08) and $(ZrO_2)_{0.92}(Yb_2O_3)_{0.08}$ were prepared by the same manner as in ref. 5. Zirconia with the highest σ_{ion}, $(ZrO_2)_{0.89}(Sc_2O_3)_{0.10}(Al_2O_3)_{0.01}$, was also prepared *(9)*. The zirconia specimens will be denoted as 3Y, 4Y, 8Y, 8Yb, and 10Sc, respectively. The relative density of each specimen to the theoretical one was more than 96 %.

The construction of the experimental fuel cell is as described in ref. 6. The anodes tested were porous SDC, $(CeO_2)_{0.8}(SmO_{1.5})_{0.2}$, with and without loading Ru catalysts. The cathodes tested were porous Pt and LSM, $La_{0.85}Sr_{0.15}MnO_3$, with and without loading Pt catalysts. Porous Pt counter electrode was used for each cell. These electrodes were prepared on the zirconia disk by screen-printing method, followed by firing at 1050°C (SDC, Pt) or 1030°C (LSM) for 4 h. Microcrystalline Ru and Pt catalysts were highly dispersed with 0.5 mg/cm^2 on SDC and LSM, respectively, in the same manner as in ref. 6. The projected surface area for each electrode was 0.26 cm^2. Two gold wires for current supply and potential probe were contacted to a gold-mesh current collector attached to each electrode. A platinum wire was wound around the lateral of the electrolyte disk with Pt paste as a reference electrode which exhibited a reversible oxygen potential in air. The anode and cathode compartments were separated by the electrolyte disk and each compartment was sealed by a glass ring gasket.

Hydrogen gas saturated with water vapor at 30°C ($P[H_2O]$ = 0.042 atm) was introduced to the

anode compartment, and oxygen gas at 1 atm was supplied to the cathode compartment. The IR-free polarization characteristics of the electrodes were measured by a current-interruption method at 800~1000°C. The exchange current density, j_0, was determined from the polarization resistance (R_p) in a low overpotential region less than 0.1 V; $R_p = (RT/2F)\, j_0^{-1}$.

RESULTS AND DISCUSSION

As reported previously *(5)*, the ionic transport number for all the electrolytes was confirmed to be unity at 800~1000°C, *i.e.*, no contribution of the electronic conduction. The ionic conductivities, σ_{ion}, decreased in the order, 10Sc>8Yb>8Y>4Y> 3Y in the whole temperature region examined.

SDC Anode The values of $\log j_0$ for H_2 oxidation at the SDC anodes are plotted as a function of $\log \sigma_{ion}$ in Fig. 1. The j_0 at the SDC anodes were much larger than that at Pt anodes *(5)*, and were independent of the σ_{ion} at 900 and 1000°C. At 800°C, however, the j_0 increased linearly with the σ_{ion}. Since these behaviors are quite different from those for the Pt anode *(5)*, the reaction mechanism for the anodic oxidation of H_2 at the SDC/zirconia is completely different from that at the Pt/zirconia. At high temperature in a H_2 atmosphere, SDC is a good mixed conductor *(10)*. The σ_{ion} of the SDC used in the present work is nearly comparable to that of 10Sc-zirconia, and the electronic conductivity σ_e is about one-order of magnitude higher than the σ_{ion}. Therefore, oxide ions may be transported into SDC particles through the entire SDC/zirconia interface, and take part in the anodic oxidation of H_2 at the SDC surface sites;

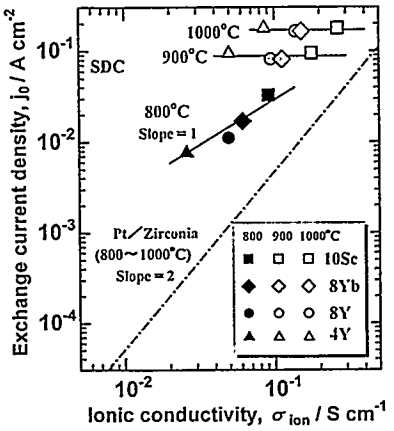

Fig. 1. Plots of the exchange current density j_0 for SDC anodes against σ_{ion} of zirconia solid electrolytes in wet hydrogen ($P[H_2O] = 0.042$ atm).

$$O^{2-}(\text{zirconia}) \rightarrow O^{2-}(\text{SDC}): \quad \text{ion transfer through the interface} \qquad [1]$$

$$O^{2-}(\text{SDC}) + H_2(g) \rightarrow H_2O(g) + 2\,e^-(\text{SDC}): \quad \text{electron transfer at SDC surface} \qquad [2]$$

As described previously *(5)*, the supply rate of O^{2-} to the SDC/zirconia interface is proportional to the σ_{ion} of zirconia electrolyte. When step [1] is fast enough compared to the following step, the j_0 at the SDC must be independent of the supply rate of O^{2-}, or σ_{ion}, and the rate determining step (rds) at the SDC anode is considered to be step [2], which is the case experimentally observed at 900 and 1000°C. This is supported by our previous experimental evidences that the anodic polarization resistance R_p and its activation energy were greatly decreased by loading only a small amount of metal microcalatysts such as Ru, Rh, Ir and Pt onto the SDC particle surfaces at the cell using the 8Y-electrolyte *(6)*. On the other hand, when step [2] is fast enough compared to step [1], the supply rate of O^{2-} into the SDC must control the j_0. The first order-dependence of j_0 on σ_{ion} ($j_0 \propto \sigma_{ion}$) observed at 800°C can be explained by this mechanism if one oxide ion is included in the overall reaction ($n = 2$) at the SDC as written by step [2].

Ru-SDC Anode In order to enhance step [2], Ru-microcrystals were highly dispersed on the porous SDC surfaces where a large part of O^{2-} transported via the SDC/zirconia interface is expected to contribute to the electron transfer reaction.

Figure 2 shows the values of log j_0 for the Ru-SDC anodes as a function of log σ_{ion} of the electrolytes. It must be emphasized that all of the data obtained at different temperatures and different electrolytes fall into a regression line as shown by the solid line, which is parallel to that for the SDC without Ru-catalysts at 800°C (dotted line). The slope of the least-squares fitting line was 1.1 and the correlation factor of the line was 0.97. Thus, the j_0 increases linearly on the Ru-SDC anode with the increase of σ_{ion} in the entire temperature region of 800 ~ 1000°C examined, resulting in the dramatic enhancement of step [2] at the SDC surfaces, while the j_0 on the anodes of SDC alone was leveled-off at 900 and 1000°C due to the insufficient catalytic activity. Therefore, the rds at 900 and 1000°C is shifted from step [2] to step [1] by loading Ru-microcatalysts. The parallel increase in the j_0 at 800°C indicates that the effective surface area increases by the dispersion of Ru-micro-catalysts without changing the rds, *i.e.*, step [1] for both SDC and Ru-SDC. It is very striking that the j_0 on the 10Sc-electrolyte at 800°C is higher than that on 4Y at 900°C, indicating the importance of the high σ_{ion} in electrolytes for low temperature operating SOFCs.

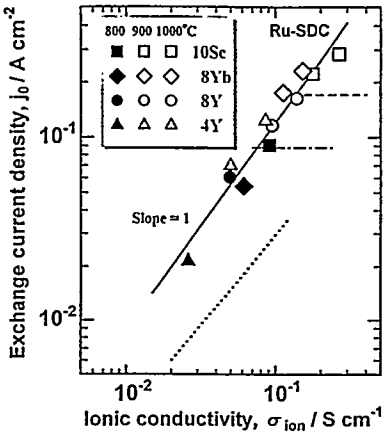

Fig. 2. Plots of j_0 for Ru-SDC anode against σ_{ion} of zirconia electrolytes in wet H_2. Solid line is the least-squares fitting for all the data. The corresponding data for SDC anodes without Ru-catalysts cited from Fig. 1 are indicated by a dotted line (800°C), a dash-dotted line (900°C), and a dashed line (1000°C).

Pt Cathode As shown in Fig. 3, the values of j_0 for oxygen reduction at the Pt cathodes were independent of the σ_{ion} at 900 and 1000°C, but they increased linearly with the increase of σ_{ion} at 800°C. The effective reaction zone for the Pt/zirconia interface is restricted to the portion around the physical triple-phase boundary (TPB) as shown in Fig. 4 (A). The constant j_0 independent of the σ_{ion} at 900 and 1000°C can be well explained when the rds at the Pt cathode is either dissociative adsorption of O_2 or surface diffusion of O_{ad} *(11)*. On the other hand, when the all steps other than step 5 are fast enough, the transport rate of O^{2-} at the interface must control the j_0. The first order-dependence of j_0 on σ_{ion} observed at 800°C can be explained by this mechanism.

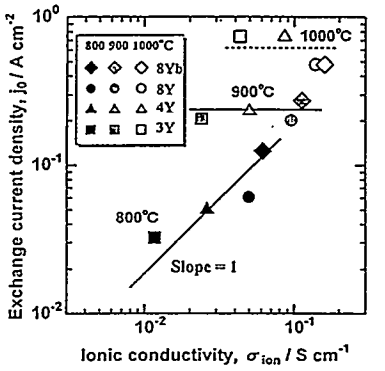

Fig. 3. Plots of j_0 for Pt cathode in O_2 against σ_{ion} of zirconia electrolytes.

LSM Cathode As shown in Fig. 4 (B), the adsorbed oxygen can be ionized at the mixed conducting surfaces of LSM besides TPB-path. The j_0 at the LSM cathodes increased linearly with the increase of σ_{ion} at each temperature, and also increased with elevating the temperature (Fig. 5). This suggests that the rds was apparently mixed with the transport of oxide ions of step 4 and the reaction step 2 and/or 3 in Fig. 4(B).

Pt-LSM Cathode When such surface reactions at step 2 and/or 3 were activated by Pt-microcatalysts dispersed on the surfaces of porous LSM, the j_0 was increased dramatically at 800 and 900°C, depending on the σ_{ion}. As shown in Fig. 5, all the data obtained at different temperatures and different electrolytes fell into a regression line as shown by the solid line. However, the slope of the line was 1.7, which is larger than that expected for the case controlled simply by the ionic transfer step ($j_0 \propto \sigma_{ion}$). We expect that further improvement of the electrocatalytic activity, up to the upper limit purely σ_{ion}-controlled (dotted line), may be achieved on Pt-/LSM below 900°C, since the performances of catalyzed LSM cathodes were found to increase further with decreasing the particle size of Pt-catalysts *(8)*.

The present study reveals that the high σ_{ion} in the electrolyte reduces not only the ohmic loss but also the polarization losses at the anode and cathode. Consequently, the combination of the solid electrolyte having high σ_{ion} and the electrodes consisting of good mixed conductors loaded with microcatalysts is very important to achieve high performance SOFCs which can operate at low temperatures.

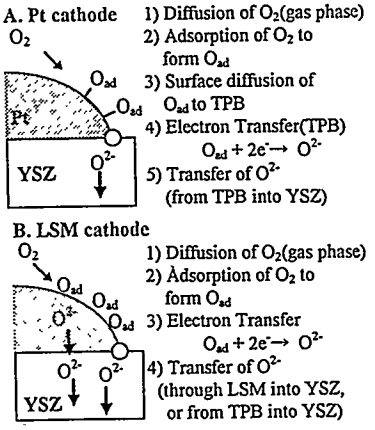

Fig. 4. Schematic illustrations of elementary reaction steps at (A) Pt and (B) LSM cathodes.

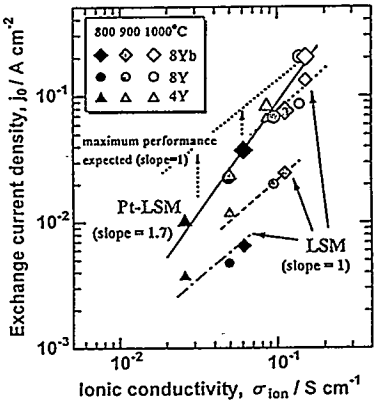

Fig. 5. Plots of j_0 for LSM and Pt-LSM cathodes in O_2 against σ_{ion} of zirconia electrolytes.

REFERENCES

1. T. Takahashi and H. Iwahara, *Denki Kagaku*, 34, 906 (1966); 34, 205 (1966).
2. B. C. Nguyen, T. A. Liu, and D. M. Mason, *J. Electrochem. Soc.*, 133, 1807 (1986).
3. J. L. Shouler and M. Kleitz, *ibid.*, 134, 1045 (1987).
4. P. Van Duk, K. J. De Vries, and A. J. Burggraaf, *Solid State Ionics*, 21, 73 (1986).
5. H. Uchida, M. Yoshida, and M. Watanabe, *J. Phys. Chem.*, 99, 3282 (1995).
6. M. Watanabe, H. Uchida, M. Shibata, N. Mochizuki, and K. Amikura, *J. Electrochem. Soc.*, 141, 342 (1994).
7. M. J. Saeki, H. Uchida, and M. Watanabe, *Catal. Letts.*, 26, 149 (1994); H. Uchida, N. Mochizuki, and M. Watanabe, *J. Electrochem. Soc.*, 143, 1700 (1996).
8. H. Uchida, A. Tsuno, and M. Watanabe, *Denki Kagaku* (English issue), 64, 686 (1996).
9. T. Ishii and Y. Tajima, *J. Electrochem. Soc.*, 141, 3450 (1994).
10. H. Yahiro, Y. Eguchi, K. Eguchi, and H. Arai, *J. Appl. Electrochem.*, 18, 527 (1988).
11. J. Mizusaki, K. Amano, S. Yamauchi, and K. Fueki, *Solid State Ionics*, 22, 313 (1987).

DEVELOPMENT OF OSAKA GAS TYPE PLANAR SOFC

M. Iha, A. Shiratori, O. Chikagawa
H. Takagi and Y. Sakabe
R&D division Murata Mfg. Co., Ltd.
2288 Oshinohara Yasu, Shiga, 520-23

K. Akagi
Fundamental Reseach Lab. Osaka Gas Co., Ltd.
1, Awata-cho, Chudoji Shimogyou-ku, Kyoto, 600

1.Introduction

Osaka Gas Co. has been developing a planar type SOFC (OG type SOFC) which has a suitable structure for stacking (1-3). Murata Mfg. Co. has begun to develop the OG type SOFC stack through joint program since 1993. Figure 1 shows OG type cell structure. Because each cell is sustained by cell holders acting air manifold, the load of upper cell is not put on the lower cells. Single cell is composed of 3-layered membrane and $LaCrO_3$ separator. 5 single cells are mounted on the cell holder, connected with Ni felt electrically, and bonded by glassy material sealant. We call the 5-cell stack a unit. Stacking 13 units, we succeeded 870 W generation in 1993. But the power density was low, 0.11 Wcm^{-2} because of crack in the electrolyte and gas leakage at some cells(4).

Then we concentrated our efforts on developing the fabricating method of the cell without any crack and the unit without gas leakage. As a result, the crack-free cells could be obtained by examining them before unit fabrication using acoustic micrography technique(5). After the units fabrication, the sealant check before stacking is introduced to prevent gas leakage while generating (6).

In this paper, the authors present the performance of single cell, an unit (5-cell stack) and two units (10-cell stack) of which gas tightness are proved with above acoustic technique and sealant check.

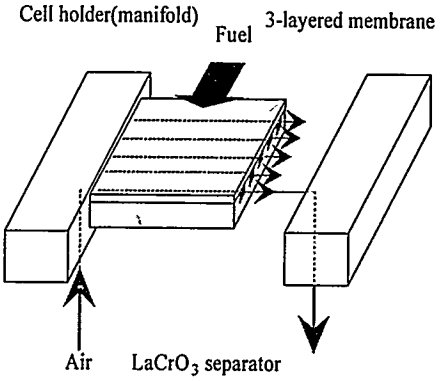

Figure 1 Osaka gas type cell structure

2.Experimental

2.1.Singl cell

8mol% Y_2O_3 doped ZrO_2 (YSZ) were employed for electrolyte. The length of electrolyte membrane was 12 cm × 12cm and the thickness was 300 μm. The materials used for anode and cathode are NiO/YSZ and $(LaSr)MnO_3$/YSZ, respectively. These electrodes powder were prepared in the paste form with vehicles, and screen-printed onto the electrolyte membrane, followed by firing respectively. $(LaSr)CrO_3$ was used for separator, which was bonded to the 3-layered membrane by conductive ceramics bond and glassy material sealant.

The I-V characteristics were measured at 1000 ℃ using H_2 gas humidified by water at 30 ℃ as fuel and air as oxidant gas. The fuel utilization were 40 % and 70 %, and the air utilization was 25% at 36 A ($0.3Acm^{-2}$).

2.2.Units fabrication and measure

Single cells preparing beforehand were bonded to cell holders acting the air manifold. Each cells is connected electrically by Ni felt. The sealant between single cells and manifold was glassy materials, and bonded over the glass transition temperature. 5-cell stack is showed in figure 2. We call this 5-cell stack a unit. After the unit fabrication, gas leakage characteristics of each unit was examined at room temperature by the sealant check technique(6). The crack-free units were then selected.

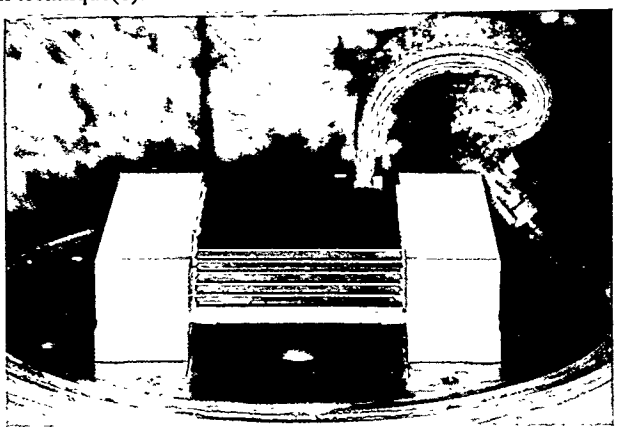

Figure 2 OG type 5-cell stack (a unit)

The performance of crack-free units was measured at 1000 ℃ using H_2 gas humidified by water at 30 ℃ as fuel and air as oxidant gas. The fuel utilization was 20 %, and the thermal cycle characteristics to room temperature was studied.

10-cell stack using crack-free two units was measured at 950 ℃. Fuel utilization was 40% using fuel mentioned above.

3.Results

3.1.Single cell

The I-V/P characteristics are showed in figure 3. The maximum power was 33 W at 40 % fuel utilization, and the power density was 0.27 Wcm^{-2}. Terminal voltage at j = 0.3 Acm^{-2} fell down from 0.703 V to 0.657 V when fuel utilization was changed from 40 % to 70%, the difference was nearly equal to calculated Nernst loss. As a result, the ability of the anode was considered enough to be used at 70% fuel utilization.

Polarization in the electrodes at 0.3 Acm^{-2} was 166 mV. This value was nearly equal to that of polarization which was measured by a current interrupt method using small size

cells (3.14 cm^{-2} of effective electrode area). Consequently, the electrode ability does not decrease if the cell size come large to 120 cm^{-2}.

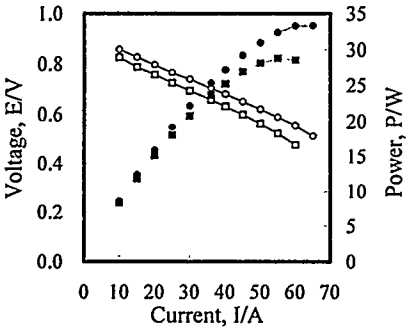

Fig. 3 I-V/P characteristics of single cell

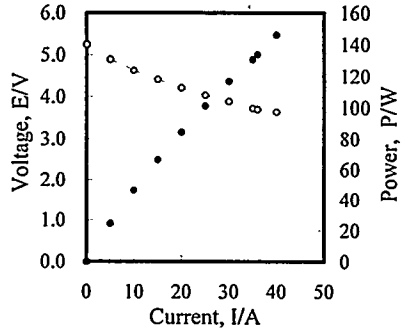

Fig. 4 I-V/P characteristics of 5-cell

3.2.One unit (5-cell stack)

Figure 4 shows the results of 5-cell stack (one unit). The maximum power was 146 W (the power density was 0.24 Wcm^{-2}). There was fuel gas leakage at the portion of the fuel inlet to the stack. So, apparent fuel utilization was 20 %, but substantial fuel utilization may be 40 % in consideration of pressure loss between inlet and outlet in the cell.

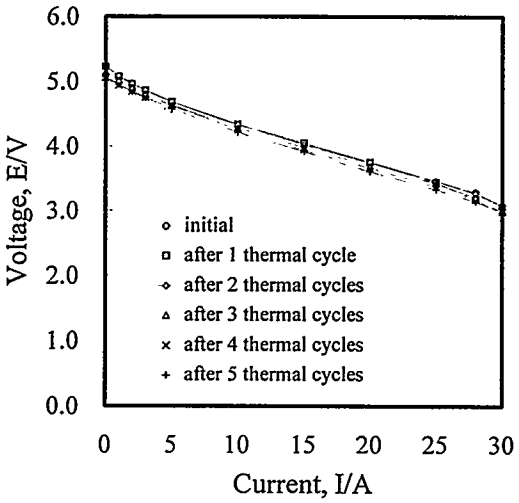

Fig. 5 I-V characteristics after thermal cycles

Figure 5 shows I-V characteristics after performing five thermal cycles to ambient temperature. Degradation of the stack performance can be scarcely observed.

3.3 Two units (10-cell stack)

The performance of 10-cell stack using two units is showed in Figure 6. The maximum power was 294 W (the power density was 0.25 Wcm^{-2}), and terminal voltage at 0.3 Acm^{-2} was 6.88 V. Since the power density was comparable to that of single cell, the decrease of the stack performance by assembling single cells was considered small.

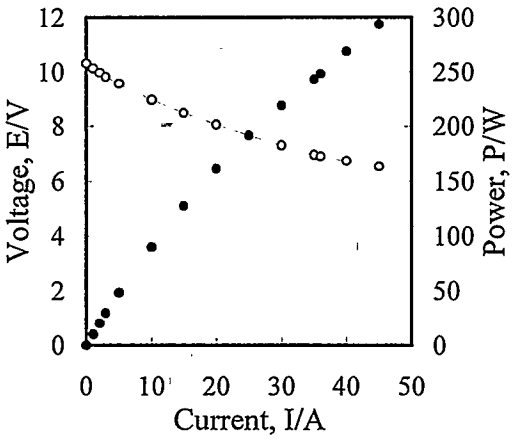

Fig. 6 I-V/P characteristics of 10-cell stack

4.Conclusion

OG type cell stack appear its good thermal cycle performance, and there is little decrease of the power density if they are stacked to 10 cells. Because each cell are connected electrically by Ni felt, the load of upper cell does not put on the lower cells, and thermal stress by deformation of each cells while the stack are heated and cooled may be released. That attribute the good performance of the cell stack.

5.References

(1) K.Akagi, Proc. of the 34th Battery Symp. in Japan, Hiroshima,pp.167-168(1993)
(2) K.Akagi, Extended Abstracts of the 2nd Symp. on SOFC in Japan, Tokyo, pp.33-36(1993)
(3) K.Akagi et al. Proc. of The 1st FCDIC Fuel Cell Symp., Tokyo, pp.300-303(1994)
(4) A.Shiratori et al. Program and Abstracts of Fuel Cell Seminar in SanDiego CA, pp.37-40(1994)
(5) A.Shiratori et al. Proc. of the 4th Interntl Symp. on SOFC, pp.255-263(1995)
(6) K.Akagi et al. Proc. of the 2nd IFCC in Japan, Kobe, pp.239-242(1996)

DEVLOPMENT OF COFIRED TYPE PLANAR SOFC

Hiroaki Taira, Sadaaki Sakamoto, Hua-Bing Zhou, Hideaki Nakai,
Syuuichi Towata, Hiroshi Takagi and Yukio Sakabe
R & D Division, Murata Manufacturing Co., Ltd.
Yasu-gun, Shiga 520-23, Japan
Tel: 0775-87-5111, Fax: 0775-87-1923

INTRODUCTION

We have developed fabrication process for planar SOFC fabricated with cofired anode/electrolyte/ cathode multilayers and interconnects [1-5]. By cofiring technique for the multilayers, we expect to reduce the thickness of the electrolyte layers, resulting in decrease of innerimpedance, and achieve low production cost. On the other hand, the cofiring technique requires that the sintering temperature, the shrinkage profiles and the thermal expansion characteristics of all component materials should be compatible with the other [6]. It is, therefore, difficult to cofire the multilayers with large area.

Using the multilayers with surface area of 150cm^2, we fabricated the multiple cell stacks [5]. The maximum power of 5x4 multiple cell stack (5 planes of cells in series, 4 cells in parallel in each planes 484cm^2 effective electrode area of each cell planes) was 601W (0.25Wcm^{-2}, Uf=40%). However, the terminal voltage of the multiple cell stack decreased by the cause of cell cracking, gas leakage and degradation of cofired multilayers. This paper presents the improvements of cofired multilayers, and the performance of multiple cell stacks with the improved multilayers.

CELL DESIGN

The schematic design of Murata's multiple cell stack is shown in Fig. 1. Four cofired multilayers with surface area of 150cm^2 are connected in parallel in the same interconnect plane. An effective area in each plane was 400cm^2. These four multilayers in the same plane are sandwiched by current collectors and interconnects. For the interconnects materials, we used Ni-Cr alloy or $LaCrO_3$ ceramics. The material used for the electrolyte is Y_2O_3 stabilized ZrO_2. The materials used for the anode and cathode are Ni/YSZ cermet and $(La,Sr)MnO_3$, respectively. The doctor blade technique was used for forming the thin green anode, cathode and electrolyte films. These green ceramics films were cut into desired sizes and laminated as green bodies to form multilayers. The green multilayers were then cofired below 1400℃ and sintered into a rigid structure. The thickness of multilayer is 300μm.

FABRICATION PROCESS

By manipulating the material composition, powder characteristics and firing condition, the mismatch of sintering shrinkage profiles and the thermal expansion characteristics of anode, cathode and electrolyte materials were minimized to achieve good flatness of multilayer surfaces. In this study, we fabricated multilayers with surface area of 150, 225 and 400cm^2. Using multilayers with surface area of 150cm^2, we constructed the multiple cell stacks. The materials of current collectors were almost same as those of electrodes. The grooves of Ni-Cr alloy and $LaCrO_3$ ceramics interconnects were fabricated by a machining process. A composite sealing material was composed of glass and ceramics. The sealing area was increased to prevent gas leakage compared with the previous stack testing, so that the effective electrode area of each cell planes decreased from 484cm^2 to 400cm^2.

PERFORMANCE

IMPROVEMENT OF COFIRED MULTILAYER

In order to improve the reliability of cofired multilayer, we investigated effect of cofiring temperature and composition , synthesis temperature of cathode on reliability of multilayer [2]. As a result, the elevation of cofiring temperature and optimization of composition and synthesis process of cathode for the elevated temperature were effective to improve the reliability of cofired multilayer. The single cell testing was practiced with the multilayers cofired at the different two temperatures. The gross surface area of each cell was 150cm^2 and the effective electrode area was 120cm^2. The tests were performed in an electric furnace at 1000 ℃. Hydrogen gas saturated by water at 30 ℃ was used as the fuel gas. The cell A was cofired at lower temperature, and the cell B was done at higher temperature. Maximum power densities of the cell A and the cell B were 0.31Wcm^{-2} and 0.27Wcm^{-2}, respectively. The inferiority of power density of the cell B was due to the increase in anodic and cathodic polarization resistivity. The results of endurance test were shown in Fig. 2. On the contrary, the degradation rate of terminal voltage (at 0.3Acm^{-2}) of the cell A was higher than that of the cell B (4.2 and 0.19mVh^{-1}, respectively). The superior reliability of multilayer cofired at high temperature seems to be caused by the stable microstructure of electrodes under the operation. It means that the higher cofiring temperature results in the stronger bonding among particles which constitute electrodes.

MULTILAYERS WITH LARGE SURFACE AREA

Cofiring the multilayers with large surface area (up to 400cm^2) was tried to suppress the production costs. By minimizing the mismatch of sintering shrinkage profiles of anode, cathode and electrolyte materials, we achieved to fabricate the good flatness of multilayers with surface area of 225 and 400cm^2. Fabrication process of these multilayers was improved one (type B). The I-V/P characteristics were shown in Fig. 3. The maximum power density of these cells with surface area of 225 and 400cm^2 were 0.23Wcm^{-2} and 0.22Wcm^{-2} respectively. These values were lower than that of multilayers with surface area of 150cm^2 (0.27Wcm^{-2}). Small size cells (30mmϕ) were cut from multilayers with the surface area of 400cm^2 and 150cm^2. Those small size cells were tested to reveal that the inferior power density was due to the multilayers themselves or not. I-V characteristics of those cells were shown in Fig. 4. This figure shows that the characteristics of those small cell cut from multilayers surface area of 400cm^2 were almost equal to that of surface area of 150cm^2. It means that inferiority of power density of single cells with large multilayers was not due to the multilayers, probably to current collection.

STACK PERFORMANCE

The performance of 5x4 multiple cell stacks using multilayers of type B were investigated with Ni-Cr alloy or $LaCrO_3$ ceramics interconnects. The other testing conditions were same as those of single cell. The I-V/P characteristics of the stacks are shown in Fig. 6 and 7. The maximum power of the stacks with alloy and ceramics interconnects were 465W (0.23Wcm^{-2}) and 472W (0.24Wcm^{-2}), respectively (Uf=40%). The results of alloy and ceramics interconnects were scarcely different. To estimate the long-term reliability, the stacks were operated for 500h.

During the testing, some multilayers were broken down. The degradation rate of terminal voltage except the broken multilayers were $0.39mVh^{-1}$ with alloy interconnects and $0.00mV\ h^{-1}$ with ceramics interconnects. For the stacks with alloy interconnects, the Cr ions were detected in the cathode adjacent to the interconnects. The diffusion of Cr ions seems to increase the polarization resitivity of the cathode. The gradual increase of polarization resitivity was considered to result in the degradation of the stack with alloy interconnects.

SUMMARY

(1) In order to improve the long-term reliability of cofired multilayers, the elevation of cofired temperature and optimization of composition and synthesis process of cathode for the elevated temperature were effective. The elevation of cofiring temperature decreased the power densities of cofired multilayers. On the contrary, the degradation rate of terminal voltage of the multilayers cofired at higher temperature was superior to that of the multilayers cofired at lower temperature.
(2) By minimizing the mismatch of sintering shrinkage profiles of anode, cathode and electrolyte materials, we achieved to fabricate the good flatness of multilayers with surface area of 225 and $400cm^2$. Due to the increase in current collecting resitivity, the maximum power densities of large size multilayers deteriorated. But, polarization characteristics of these large size multilayers were almost equal to those of multilayers with surface area of $150cm^2$.
(3) The multiple cell stacks were fabricated with cofired multilayers and Ni-Cr alloy or $LaCrO_3$ interconnects. The maximum power of 5x4 multiple cell stack (5 planes of cells in series, 4 cells in parallel in each planes, $400cm^2$ effective electrode area of each cell planes) were 465W ($0.23W\ cm^{-2}$) and 472W ($0.24Wcm^{-2}$), respectively (Uf=40%). The degradation rate of terminal voltage of the stack with ceramics interconnects was lower than that of the stack alloy interconnects.

ACKNOWLEDGMENT

A part of this work was performed as R&D program of New Energy and Industrial Technology Development Organization (NEDO) under the New Sunshine Project of Agency of Industrial science and Technology, MITI. We would like to express our thanks to NEDO and MITI for their assistance.

REFERENCES

[1] H. Takagi, S. Kobayashi, A. Shiratori, K. Nishida and Y. Sakabe, Proceeding of The 2nd International Symposium on SOFC, Athens, pp.99-103 (1991).
[2] A. Shiratori, S. Kobayashi, H. Taira, Y. Sugimoto, S. Sakamoto, H. Takagi and Y.Sakabe, Proceedings of The International Fuel Cell Conference, Makuhari, pp.297-300 (1992).
[3] H. Takagi, H. Taira, A.Shiratori, S. Kobayashi, Y. Sugimoto, S. Sakamoto and K. Tomono, Proceeding of The 3rd International Symposium on SOFC, Honolulu, pp.738-743 (1993).
[4] H. Takagi, H. Taira, S. Kobayashi, S. Sakamoto and K. Tomono, Proceeding of The 1994 Fuel Cell Seminar, San Diego, pp392-395 (1994).
[5] H. Takagi, H. Taira, S. Kobayashi, S. Sakamoto and K. Tomono, Proceeding of The 4th International Symposium on SOFC, Yokohama, pp120-128 (1995).
[6] N. Q. Minh, C. R. Horne, F. Liu, P. R. Staszak, T. L. Stillwagon and J. V. Ackeren, Proceeding of The International Symposium on SOFC, Miami, pp307-316 (1989).

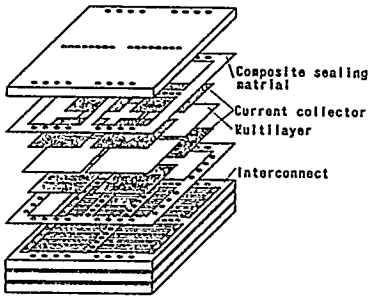

Fig.1 Schematic design of Murata's planar SOFC

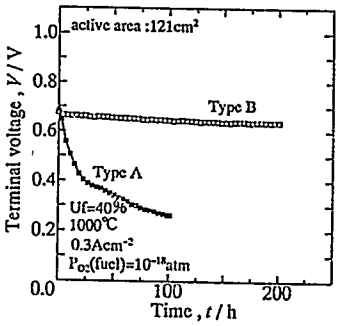

Fig. 2 Endurance test result of single cells

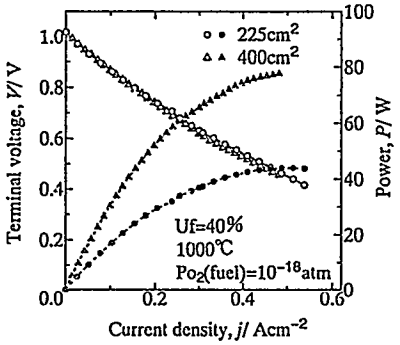

Fig.3 I–V/P characteristics of large–size cells

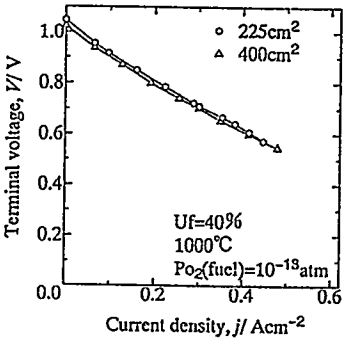

Fig.4 I–V characteristics of small–size cells cut from large–size multilayers

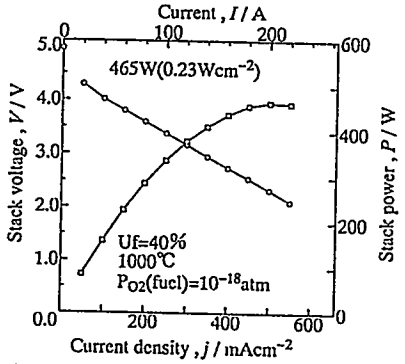

Fig. 5 I–V/P characteristics of 5x4 multiple cell stack with Ni–Cr alloy interconnects.

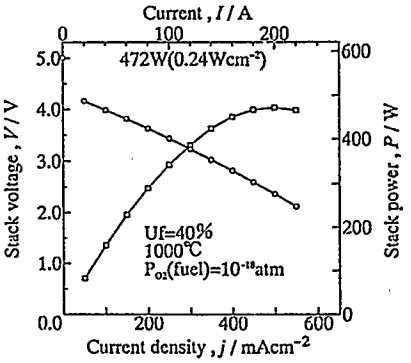

Fig. 6 I–V/P characteristics of 5x4 multiple cell stack with $LaCrO_3$ interconnects.

POWER GENERATION CHARACTERISTICS OF TUBULAR TYPE SOFC BY WET PROCESS

H.Tajiri, T.Nakayama,
Kyushu Electric Power Company , Inc.
2-1-47, Shiobaru, Minami-ku, Fukuoka 815, Japan
M.Kuroishi, A.Ueno, M.Aizawa
TOTO Ltd.,
2-8-1, Honson, Chigasaki-shi, Kanagawa 253, Japan
K. Eguchi, H.Arai
Graduate School of Engineering Sciences, Kyushu Univ.
6-1, Kasugakoen, Ksuga-shi, Fukuoka 816, Japan

INTRODUCTION

The development of a practical solid oxide fuel cell requires improvement of a cell performance and a cell manufacturing technology suitable for the mass production. In particular tubular type SOFC is thought to be superior in its reliability because its configuration can avoid the high temperature sealing and reduce the thermal stress resulting from the contact between cells. The authors have fabricated a tubular cell with an air electrode support by a wet processing technique, which is suitable for mass production in improving a power density (1).To enhance the power output of the module, the Integrated Tubular-Type (ITT) cell has been developed. This paper reports the performance of the single cells with various active anode areas and the bundle with series-connected 9-ITT cells with an active anode area of 840 cm^2 .

EXPERIMENTAL

The fabrication procedure of the cell is summarized in Table 1. Cathode-supported tubular cell structure was employed to reduce the cell resistance. Every cell component was prepared by the wet ceramic process. The support tube was made from the $(La,Sr)MnO_3$ powder by an extrusion process and sintering. $(La,Ca)CrO_3$ powder was synthesized through thermal decomposition of the nitrate mixture and then the resultant slurry was coated to form an interconnector stripe. The YSZ electrolyte thin film and Ni+YSZ anode thick film were also prepared by slurry coating process.

Generation performance of the single cells with various anode areas from 28 to 280cm^2 and that of the ITT cell bundle was evaluated using H_2+11%H_2O as a fuel and air as an oxidant at 1000℃. Long-term generation test and thermal cycle property were evaluated for the single cell.

RESULT AND DISCUSSION

Figure 1 shows the typical generation performance of the single cells with the active anode area of 200-450 cm^2. The diameter and active length are 13 and 700 mm for the 200 cm^2-cell, 16 and 700 mm for the 280 cm^2-cell, and 21 and 900 mm for the 450 cm^2-cell, respectively. The maximum power was 60 W at the current density of 0.6 A cm^{-2} for the 200 cm^2-cell , 75 W at 0.49 A cm^{-2} for the 280 cm^2-cell, and 125 W at 0.47 A cm^{-2} for the 450 cm^2-cell.

Figure 2 shows the long-term stability for the cell with the active area of 28 cm^2 (the diameter and active length are 21 and 50 mm) at 0.3 A cm^{-2}. In this test, three times of shut-down due to outage of the testing device had occurred but the degradation of the cell performance resulting from the thermal cycle to room temperature was not observed.

Long-term stability has been evaluated for the cell with the active anode area of 450 cm^2 at a constant current density of 0.2 and 0.3 A cm^{-2}. Figure 3 shows a typical result. The degradation rate was fairly low.

For the practical use of SOFC, the cell should be sustainable against operational thermal cycles or emergency outages. Thermal cycle test consisting of ten times cooling below 200℃ and twenty times cooling to 600℃ were carried out for the 450 cm^2-cell. Figure 4 shows a typical result of generation performance before and after the thermal cycle test. The degradation from 1.5 to 3.0 % was observed for I-V characteristics, but the reason for this degradation is now under investigation.

Practical SOFC should be assembled into a module for increasing power output. Therefore it is important to develop the cell structure suitable to manufacturing the cell bundle. We have been developing an Integrated Tubular-Type (ITT) cell which has a monolithic structure consisting of parallel-connected three tubular cells. Figure 5 shows the appearance of the ITT cell. A bundle with 9 series-connected ITT cells (the active area of each ITT cell was 840 cm^2) was tested. Figure 6 shows I-V and I-P characteristics of the bundle. The open circuit voltage was ca. 8.63 V which was almost equal to the theoretical value. The maximum output power was 1020 W at 0.22 A cm^{-2}. The mean generation performance of the bundle is about 15 % lower than the performance expected from that of the single cell. Further investigation and development, for example control of the fuel gas flow through the channels of the cell bundle , are required to further improve the cell and bundle generation performance.

REFERENCE

1. K. Tachibana, H. Nakashima, H. Nishiyama, M. Aizawa, K. Eguchi and H. Arai, Proceedings of the 4th International Symposium on SOFCs, The Electrochemical Society, Inc., (1995), pp.208-215

Table 1. Component, material and fabrication process of the cell

component	material	fabrication method
cathode tube	$(La,Sr)MnO_3$	extrusion molding
interconnector	$(La,Ca)CrO_3$	slurry coating
electrolyte	YSZ	slurry coating
anode	Ni/YSZ	slurry coating

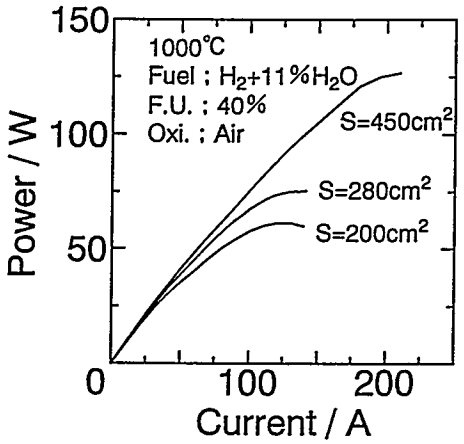

Figure 1. I-P characteristics of the single cells with active anode areas of 200, 280 and 450 cm^2.

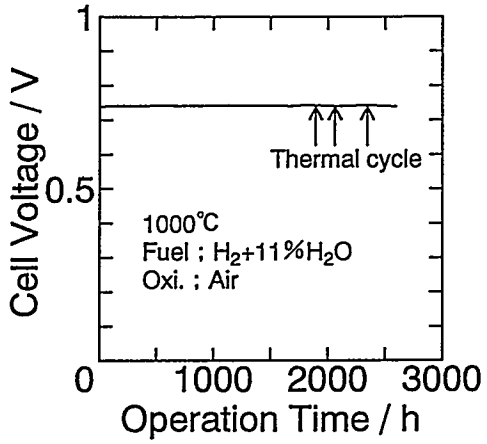

Figure 2. Long-term stability of the cell with an active anode area of 28 cm^2 at current density of 0.3 A cm^{-2}.

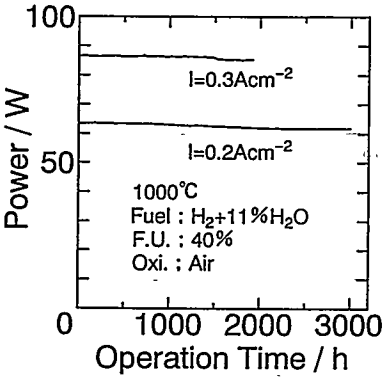

Figure 3. Long-term stability of the 450 cm^2-cell at current density of 0.2 and 0.3 A cm^{-2}.

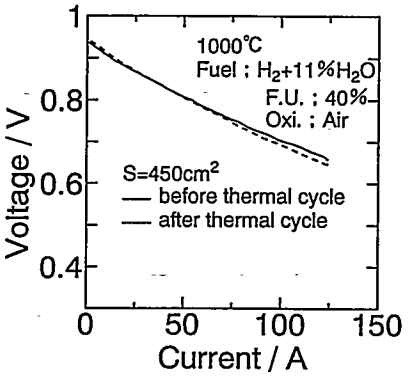

Figure 4. I-V characteristics of the 450 cm^2-cell before and after thermal cycle treatment.

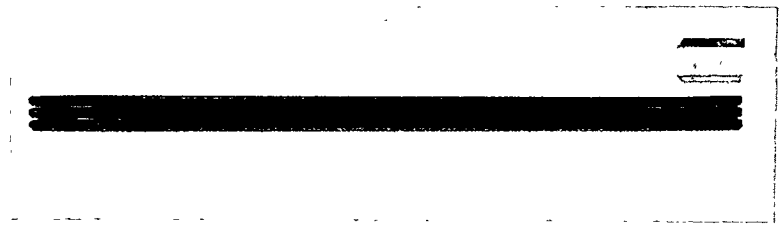

Figure 5. The appearance of Integrated Tubular-Type (ITT) cell.

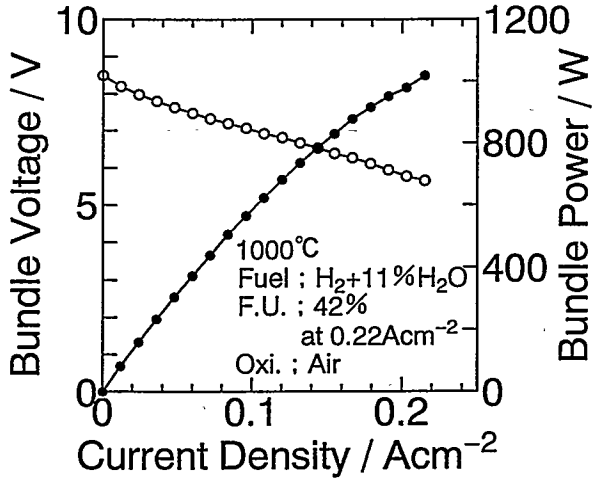

Figure 6. I-V and I-P characteristics of the bundle with 9-ITT cells with an avtive anode area of 840 cm^2.

REALISATION OF AN ANODE SUPPORTED PLANAR SOFC SYSTEM

H.P. Buchkremer*, U. Diekmann**, L.G.J. de Haart***, H. Kabs****,
U. Stimming*** and D. Stöver*
*Institut für Werkstoffe der Energietechnik, **Zentralabteilung Technologie,
***Institut für Energieverfahrenstechnik, ****Programmleitung SOFC
Forschungszentrum Jülich GmbH, D-52425 Jülich, Germany

Introduction

Lowering the operating temperature of SOFCs to below 800 °C potentially lowers production costs of a SOFC system because of a less expensive periphery and is able to guarantee sufficient life time of the stack. One way of achieving lower operating temperatures is the development of new high conductive electrolyte materials. The other way, still based on state-of-the-art material, i.e. yttria-stabilized zirconia (YSZ) electrolyte, is the development of a thin film electrolyte concept.

In the Forschungszentrum Jülich a program was started to produce a supported planar SOFC with an YSZ electrolyte thickness between 10 to 20 µm. One of the electrodes, i.e. the anode, was used as support, in order not to increase the number of components in the SOFC. The high electronic conductivity of the anode-cermet allows the use of relatively thick layers without increasing the cell resistance. An additional advantage of the supported planar concept is the possibility to produce single cells larger than 10x10 cmxcm, that is with an effective electrode cross area of several hundred cm^2.

Materials and Component Manufacturing

NiO-YSZ substrates, with a standard composition of 44 wt% Ni, were manufactured by a Coat-Mix® process. The YSZ electrolyte layer was applied on the pre-sintered anode substrate by vacuum slurry coating. After sintering at 1400 °C, a gas tight electrolyte layer of approximately 15 - 20 µm thickness was formed. The thickness of the substrate was in between 1.5 and 2.0 mm. The substrates were manufactured as large as 25x25 cm^2. A composite cathode layer ($La_{0.65}Sr_{0.30}MnO_3$/8YSZ) of typically 40 µm was finally applied on the electrolyte by Wet Powder Spraying®. A detailed description of the component manufacturing is published elsewhere [1,2].

Metal ODS-alloy plates (94Cr5Fe1Y_2O_3; Plansee AG, Austria) were used as interconnectors and end-plates. Gas channels were mechanically machined into the plates in a cross-flow configuration. Contact layers in order to decrease the electrical resistance at the interface electrode/interconnector were applied to both the anode and cathode side of the interconnector during stack assembly. A composite glass was used as sealing material [1].

Initial Cell and Stack Performance

Single cells and stacks were tested using humidified hydrogen as fuel gas and dry air as the oxidant gas. Fig. 1 shows the initial performance of a 10-cell (10x10 cm^2) stack at 950 and 800 °C. At 950 °C and 7.0 V stack voltage (i.e. 0.7 V per cell) a current density of 420 mA/cm^2 was reached. This corresponds to a power density of 0.28 W/cm^2. The fuel utilization was 37% at this current density. Lowering the operating temperature to 800 °C the current density decreased to around 270 mA/cm^2 at the the same stack voltage of 7.0 V (0.20 W/cm^2) [3].

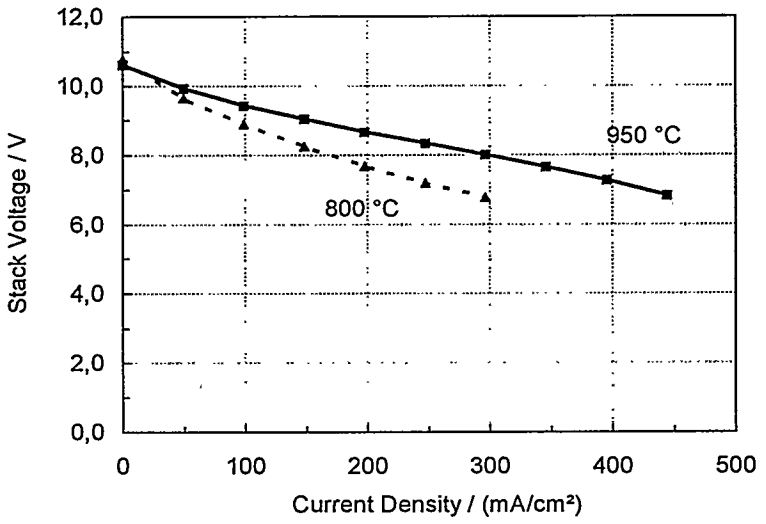

Figure 1. Performance of a 10-cell (10x10 cm²) stack with humidified H_2/air at 950 °C and 800 °C.

The separate cells in the stack showed an almost uniform potential distribution, differences not exceeding ±20 mV. The area (81 cm² per cell) specific resistance amounts 0.73 Ω•cm² at 950 °C and 1.05 Ω•cm² at 800 °C.

A single cell as large as 25x25 cm², with an effective electrode area of 576 cm² was also manufactured and tested with humidified H_2 and air using metallic endplates for current collection. At 950 °C and a working voltage of 0.7 V a current density of 300 mA/cm² was reached, corresponding to a power density of 0.21 W/cm². The area specific resistance was 1.00 Ω•cm² [3].

Both the 10-cell (10x10 cm²) stack and the single cell (25x25 cm²) showed at 950 °C a rapid decrease of the performance, which is most likely due to Cr-oxide deposition in the cathode region, the Cr originating from the unprotected interconnector and endplates used.

Improved Cell and Stack Performance

Materials innovations with respect to the metallic interconnector, the glass-ceramic sealant and the anode substrate facing the electrolyte layer have a pronounced effect both on the performance as well as on the stability of the cells and stacks. These investigations were conducted using small short-stacks, each containing 2 cells of 5x5 cm² with an effective electrode area of 16 cm². As an example Fig. 2 shows the performance of such a 2-cell (5x5 cm²) stack as function of the

operating temperature. At the working voltage of 1.4 V (0.7 V per cell) the current density reached 1,195 mA/cm² at 954 °C and 475 mA/cm² at 811 °C. Corresponding power densities are 0.84 W/cm² and 0.33 W/cm², respectively. In comparison with the results obtained for the 10-cell stack this means an improvement in power density by a factor of 3 at 950 °C and 1.7 at around 800 °C. The difference in these factors is caused by a difference in the temperature dependence of both stacks, for which no clear explanation can be given yet.

Fig. 3 shows the time dependent performance of same the 2-cell (5x5 cm²) stack. After the initial recording of the current-voltage characteristics shown in Fig. 2 during the first 32 hours of operation, the stack was operated at 800 °C at 313 mA/cm² for a period of 357 hours. The stack voltage remained constant at around 1.64 V (0.26 W/cm²) without showing any noticable degradation. A failure in the gas supply system caused irreversible damages to the stack.

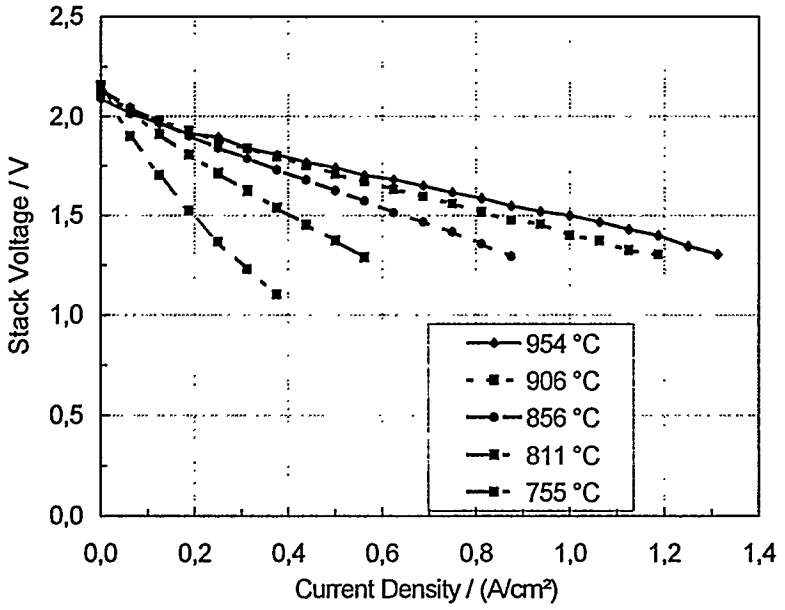

Figure 2. Performance of a 2-cell (5x5 cm²) stack with humidified H_2/air as function of operating temperature between 954 °C and 755 °C

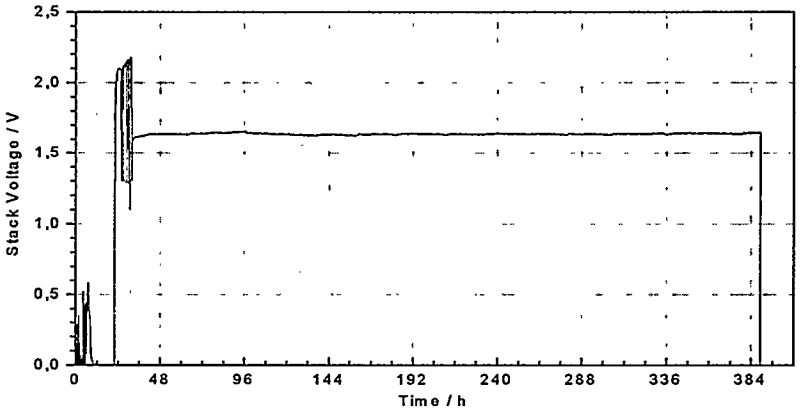

Figure 3. Time dependence of the performance of the 2-cell (5x5 cm^2) stack starting at 32 h at 800 °C under constant load (311 mA/cm^2) with humidified H_2/air.

References

[1] H.P. Buchkremer, U. Diekmann and D. Stöver, "Components Manufacturing and Stack Integration of an Anode Supported Planar SOFC System", in: Proc. 2nd Europ. SOFC Forum (B. Thorstensen, Ed.), pp. 221-228, U. Bossel, Morgenacherstrasse 2F, CH-5452 Oberrohrdorf, Switzerland, 1996.

[2] R. Wilkenhöner, W. Malléner, H.P. Buchkremer, Th. Hauber and U. Stimming, "Cathode Processing by Wet Powder Spraying", in: Proc. 2nd Europ. SOFC Forum (B. Thorstensen, Ed.), pp. 279-288, U. Bossel, Morgenacherstrasse 2F, CH-5452 Oberrohrdorf, Switzerland, 1996.

[3] L.G.J. de Haart, Th. Hauber, K. Mayer and U. Stimming, "Electrochemical Performance of an Anode Supported Planar SOFC System", in: Proc. 2nd Europ. SOFC Forum (B. Thorstensen, Ed.), pp. 229-235, U. Bossel, Morgenacherstrasse 2F, CH-5452 Oberrohrdorf, Switzerland, 1996.

Acknowledgements

The authors would like to thank all members of the SOFC-Substrate-Concept Team for their technical support and helpful discussions.

$LaCrO_3$-DISPERSED Cr FOR METALLIC INTERCONNECT OF PLANAR SOFC

Rak-Hyun Song, Dong Ryul Shin and *Masayuki Dokiya
Korea Institute of Energy Research, P.O.Box 103, Yusong, Taejon, 305-600, Korea
*National Institute of Materials and Chemical Research, 1-1 Higashi, Tsukuba, Ibaraki 305, Japan

INTRODUCTION

In the planar SOFC, the interconnect materials plays two roles as an electrical connection and as a gas separation plate in a cell stack. The interconnect materials must be chemically stable in reducing and oxidizing environments, and have high electronic conductivity, high thermal conductivity, matching thermal expansion with an electrolyte, high mechanical strength, good fabricability, and gas tightness(1). Lanthanum chromite so far has been mainly used as interconnect materials in planar SOFC(1,2). However, the ceramic materials are very weak in mechanical strength and have poor machining property as compared with metal. Also the metallic materials have high electronic conductivity and high thermal conductivity.

Recently some researchers have studied metallic interconnects such as Al_2O_3/Inconel 600 cermet(3), Ni-20Cr coated with (LaSr)CoO_3(4), and Y_2O_3- or La_2O_3-dispersed Cr alloy(5). These alloys have still some problems because Ni-based alloys have high thermal expansion, the added Al_2O_3, Y_2O_3 and La_2O_3 to metals have no electronic conductivity, and the oxide formed on the surface of Cr alloy has high volatility. To solve these problems, in this study, $LaCrO_3$-dispersed Cr for metallic interconnect of planar SOFC was investigated. The $LaCrO_3$-dispersed Cr can be one candidate of metallic interconnect because $LaCrO_3$ possesses electronic conductivity and Cr metal has relatively low thermal expansion. The content of 25 vol.% $LaCrO_3$ was selected on the basis of a theoretically calculated thermal expansion. The thermal expansion, electrical and oxidation properties were examined and the results were discussed as related to SOFC requirements.

EXPERIMENTAL

Figure 1 shows a manufacturing process of 25 vol.% $LaCrO_3$-dispersed Cr(25LC). The pure Cr metal was used as a reference material and manufactured by using the same process as 25LC. The 25LC was prepared by mixing metal Cr and $LaCrO_3$ powders in high energy milling machine for 24 h with organic substance that include polyvinyl butyral and isoprophyl alcohol, followed by sintering under Ar atmosphere with 1 vol.% H_2 for 1 h at 1500 °C that was measured by optical pyrometer. The sintered samples were a disk type of diameter of 10 mm and thickness of 3 mm. Their densities were calculated from volume and weight. The thermal expansion was examined by using a dilatometer between room temperature and 1000 °C. The electrical conductivity was measured at room temperature by HP 4338A Milliohmmeter, and the Kelvin Clip Leads of HP 16005C, D were used as probes. The oxidation tests were carried out in air at 1100 °C, which is higher than normal operation temperature of 1000 °C in SOFC for an acceleration condition. During oxidation test, the samples were maintained at 1100 °C for 20 h and at room temperature for 5 h, which was defined as 1 cycle of the oxidation data.

RESULTS AND DISCUSSION

The relative density was determined by percentage of a sample density and a theoretical density. The relative densities of Cr metal and 25LC were 97 and 95 %, respectively. Thus the sintered sample is considered to satisfy a gas tightness condition in a cell stack. The ac electrical conductivity was measured at a frequency of 1 kHz by four probe method. The Cr metal and 25LC had ac conductivities of 3.63×10^4 and 0.92×10^4 S/cm at room temperature, respectively. Also the

conductivity of Plansee's DUCROLLOY(Cr5Fe1Y_2O_3) was estimated using the same method for comparison. Its ac conductivity was 1.06×10^4 S/cm, which is lower than the reported dc conductivity of 3.4×10^4 S/cm(5). This may be considered to be due to a difference of a measurement method and a contact resistance of the used probes. Nevertheless, the 25LC indicated high conductivity like DUCROLLOY. This means that the 25LC is able to be used as an interconnect material from the viewpoint of electrical conductivity.

Thermal expansion of composite body can be calculated by Turner's and Kerner's models(6). Figure 2 shows the calculated thermal expansion coefficient(TEC) of Cr alloy at 1000 °C as a function of $LaCrO_3$ content. A TEC of about 25 vol.% $LaCrO_3$ at 1000 °C is compatible with that of 8mol% yttria-stabilized zirconia(8YSZ) because, although an average TEC of 8YSZ in the range of room temperature and 1000 °C is 10.5×10^{-6} m/m.K, 8YSZ at 1000 °C has a TEC of 12.5×10^{-6} m/m. Figure 3 shows the measured thermal expansion curves of 25LC and 8YSZ between room temperature and1000 °C. These seem to be reasonably in good agreement on the whole.

Figure 4 shows the oxidation behavior of the 25LC and the pure Cr metal. The 25LC is much more resistant to oxidation in air than the pure Cr. The oxidation rate of the 25LC decreased slowly with increasing number of oxidation cycle, whereas that of the pure Cr increased with number of cycles and then decreased after 4 cycles. From optical microscopy, a delamination of the oxide scale formed at the surface of the 25LC was not found and thus the decreased oxidation rate during oxidation test is considered to be due to an evaporation of the surface oxide. On the other hand, the oxide scale in the Cr metal was spalled, which is thought to be a main reason of the decreased oxidation rate after 4 cycles.

CONCLUSION

The 25 vol.%$LaCrO_3$-dispersed Cr was sintered at 1500 °C under Ar atmosphere with 1 vol.% H_2, which had a relative density of 95%. Its electrical conductivity satisfies a SOFC requirement. The measured thermal expansion of $LaCrO_3$-dispersed Cr was well fitted to that of 8mol.% Y_2O_3-stabilized ZrO_2 electrolyte. Also the oxidation tests show that the $LaCrO_3$-dispersed Cr is very resistant to oxidation in air. These results demonstrate that $LaCrO_3$-dispersed Cr is a useful material for metallic interconnect of planar SOFC. The future works will be focused on the examination of the microstructure and the effects of alloy elements to improve the materials properties.

ACKNOWLEDGEMENT

This work was performed under an international cooperation program between Korea Institute of Energy Research, Korea and National Institute of Materials and Chemical Research, AIST, Japan. Japanese work is under the New Sunshine Project of AIST.

REFERENCES

1. M. Dokiya, T. Horita, N. Sakai, T. Kawada, H. Yokokawa, B. A. van Hassel, and C. S. Montross, "Interconnector Chemistry," pp. 33-41, Proc. the 14th Risø Intern. Sym. Mater. Sci.: High Temperature Electrochemical Behavior of Fast Ion and Mixed Conductors, Eds. F. W. Poulsen, J. J. Bentzen, T. Jacobsen, E. Skou and M. J. L. Østergård. Risø Nat. Lab., Roskilde, Denmark, 1993.
2. N. Q. Minh and T. Takahashi, Science and Technology of Ceramic Fuel Cells, pp. 165-198, Elsevier, Amsterdam, 1995.

3. H. Seto, T. Miyata, A. Tsunoda, T. Yoshida, and S. Sakurada, "Cermet for Interconnection of SOFC," pp. 421-427, Proc. 3rd Intern. Sym. SOFC, Eds. S. C. Singhal and H. Iwahara, The Electrochemical Society, 1993.
4. T. Shiomitsu, T. Kadowaki, and T. Ogawa, "The Influence of (LaSr)CoO_3 Coatings on the Electrical Resistance of Ni-20Cr Alloys in High Temperature Oxidizing Atmosphere," pp. 850-857, Proc. 4th Intern. Sym. SOFC, Eds. M. Dokiya, O. Yamamoto, H. Tagawa, and S. C. Singhal, The Electrochemical Society, 1995.
5. W. Kock, H.-P. Martinz, H. Greiner, and M. Janousek, "Development and Processing of Metallic Cr Based Materials for SOFC Parts," pp. 841-849, ibid., 1995.
6. W. D. Kingery, H. K. Bowen, and D. R. Uhlmann, Introduction to Ceramics, 2nd ed., pp. 603-606, John Wiley & Sons, New York, 1976.

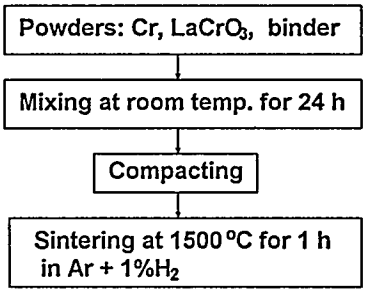

Fig.1 Manufacturing process of 25 vol.%$LaCrO_3$-dispersed Cr.

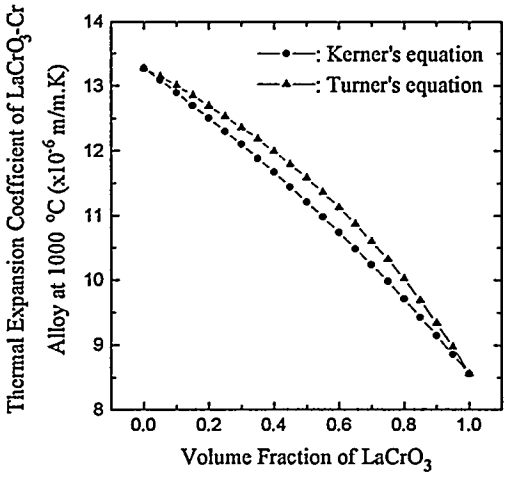

Fig.2 Thermal expansion coefficient of $LaCrO_3$-Cr alloy at 1000 °C as a function of volume fraction of $LaCrO_3$.

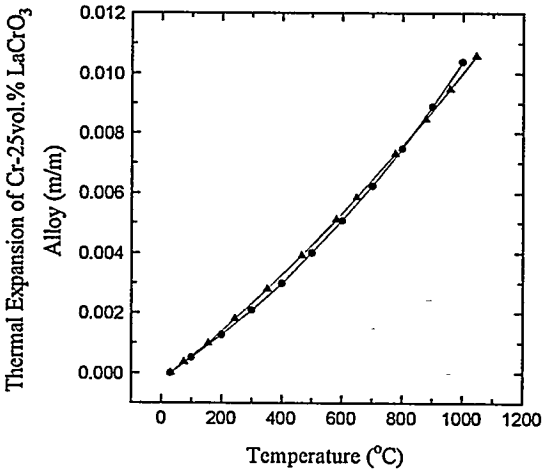

Fig.3 Thermal expansion of 25 vol.%$LaCrO_3$-dispersed Cr(●) and 8 mol% yttria-stabilized zironia(▲)

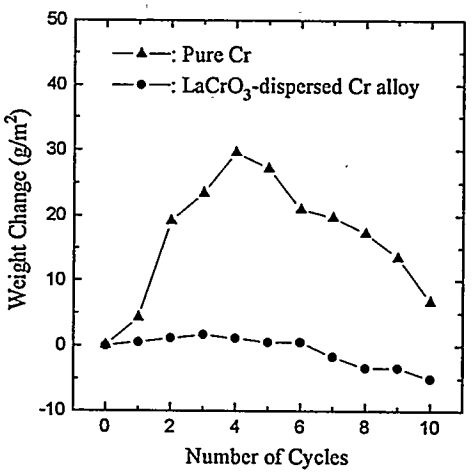

Fig.4 Cyclic oxidation behavior of pure Cr and 25 vol.%$LaCrO_3$-dispersed Cr in air(20 h at 1100 °C/5 h at room temperature).

ZTEK'S ULTRA-HIGH EFFICIENCY FUEL CELL/ GAS TURBINE SYSTEM FOR DISTRIBUTED GENERATION

Michael Hsu, Daniel Nathanson
Ztek Corporation
460 Totten Pond Road
Waltham, Massachusetts 02154
Tel 617-890-5665
Fax 617-890-3731

Dale T. Bradshaw, Don R. Stephenson
Tennessee Valley Authority
1101 Market Street
Chattanooga, Tennessee 37402
Tel 423-751-4631
Fax 423-751-2463

Rocky Goldstein
Electric Power Research Institute
Palo Alto, California 94303
Tel 415-855-2171
Fax 415-855-2295

INTRODUCTION

Ztek's Planar Solid Oxide Fuel Cell (SOFC) system has exceptional potential for utility electric power generation because of: simplicity of components construction, capability for low cost manufacturing, efficient recovery of very high quality by-product heat (up to 1000°C), and system integration simplicity. Utility applications of the Solid Oxide Fuel Cell are varied and include distributed generation units (sub-MW to 30MW capacity), repowering existing power plants (i.e. 30MW to 100MW), and multi-megawatt central power plants.

A TVA/EPRI collaboration program involved functional testing of the advanced solid oxide fuel cell stacks and design scale-up for distributed power generation applications. The emphasis is on the engineering design of the utility modules which will be the building blocks for up to megawatt scale power plants. The program has two distinctive subprograms: Verification test on a 1kW stack and 25kW module for utility demonstration. A 1kW Planar SOFC stack was successfully operated for 15,000 hours as of December, 1995. Ztek began work on a 25kW SOFC Power System for TVA, which plans to install the 25kW SOFC at a host site for demonstration in 1997. The 25kW module is Ztek's intended building block for the commercial use of the Planar SOFC. Systems of up to megawatt capacity can be obtained by packaging the modules in 2-dimensional or 3-dimensional arrays.

The Ztek SOFC Power System Technology offers to TVA the benefits of clean, low cost electricity resulting from low capital cost and ultra high efficiency. In addition to the potential for competitive low cost of electricity, the following additional benefits apply: Maximum Megawatt Capacity per Distributed Site; Maximum Use of Renewable Fuels when Landfill Gas and Biogas are utilized; High Power Quality; Low NOx, SOx and HC Emissions; and Ease of CO_2 Capture.

The above leads to significant utility benefits like Customer Service and Retention, Distributed Generation Service, Response to Global Warming Concerns, and Repowering Opportunities.

FUEL CELL/GAS TURBINE BOTTOMING HYBRID SYSTEM

Ztek is proceeding on development of an ultra-high efficiency hybrid system of its Planar SOFC with a gas turbine, realizing shared cost and performance benefits. The gas turbine as the Balance-of-Plant was a logical selection from a fuel cell system perspective because of: 1) the high-power-density energy conversion of gas turbines; 2) the unique compatibility of the Ztek Planar SOFC with gas turbines; and 3) the availability of low-cost commercial gas turbine systems. A Tennessee Valley Authority/Ztek program is ongoing, which addresses operation of the Advanced Planar SOFC system and design scale-up for utility power generation applications.

The advanced SOFC Fuel Cell/Gas Turbine hybrid approach discussed here, **Figure 1**, is potentially capable of reaching electrical **efficiencies above 70%(LHV), or heat rate of less than 4800 BTU/kWh (LHV).** This alternative has the distinct advantage of being applicable over a wide range of plant capacities, from sub-MW to multi-MW. Ztek's planar SOFC, which operates at 1000°C, has patented features which enhance direct integration with a gas turbine. This approach is based upon applying Ztek's Planar ATI® SOFC as a Combustor And Recuperator Replacement for Advanced Turbine System (**CARR-ATS**). The SOFC will replace the combustor section, and displace the need for a recuperator for efficiency enhancement. Integrating Ztek's patented technology, therefore, can provide increased system efficiency and capacity with reduced NOx emissions.

Assessments revealed the ability to obtain performance with Pressurized SOFC/Gas Turbine Hybrid systems which surpass performance that can be achieved by either a Stand-Alone Gas Turbine or a Stand-Alone Fuel Cell. **Figure 2**, SOFC/Turbine Hybrid System Combined Efficiency, illustrates the predicted maximum system efficiency (LHV) as a function of gas turbine efficiency, considering the fuel cell efficiency from 50% to 55% (LHV). The maximum combined system efficiency ranged from 64% to 71%, for gas turbine efficiencies of 25% to 35%. This hybrid system approach has the benefit of utilizing gas turbine equipment which has already reached an economic scale consistent with the utility industry. The gas turbine industry can in turn benefit by the improved efficiency and environmental performance of the hybrid system. Ztek, applying its patented technology, is uniquely capable of formulating hybrid systems of its Planar ATI® SOFC with gas turbines which can achieve ultra efficient system performance.

SOFC/GAS TURBINE SYSTEM FOR DISTRIBUTED GENERATION

The incentives and justification for the pressurized operation of the Ztek Advanced SOFC integrated with gas turbine bottoming systems are: the physical and chemical stability of its fuel cell components; structural compatibility with operation at high

pressures; compact integration; higher surface power density provision of the fuel cell; and availability of high temperature exhaust gas. For verification of this integrated technology, a development program of the SOFC/Gas Turbine hybrid system, **Figure 3**, is being initiated, leading to a demonstration of integration with a nominal combined capacity of 250kW in the time frame of 1998-1999. This effort addresses a technology enhancement to the SOFC modules developed for atmospheric operation, which applies to stand-alone or SOFC/Steam Turbine hybrid systems. The complementary components sharing in the SOFC/Turbine integration assures accomplishing the system price target of <$1000/kW.

SUMMARY

In conclusion, the gas turbine represents a cost effective resource for the Balance-of-Plant in the fuel cell system, because of its energy conversion performance and the availability as off-the-shelf equipment. The advanced thermal integration features of the Ztek Planar SOFC uniquely facilitate the hybrid system integration with a gas turbine. With the hybrid system integration, the Ztek Planar SOFC and gas turbine can mutually enhance the favorable characteristics of cost, efficiency, package flexibility, and environmental performance for distributed generation.

Studies of near-term applications of Ztek's SOFC technology, by year 2000, indicate that systems in the capacity range of sub-MW to 10MW offer ultra-high efficiency of more than 70% for pressurized SOFC/Gas turbine systems. Ztek plans to provide Distributed Generation products to customers at a system price below $900/kW. It is expected that the Cost-of-Energy of these units can approach 4 Cents/kWh.

The Ztek Planar Solid Oxide Fuel Cell Technology has been developed under cost sharing of corporate funds and contracts with the Tennessee Valley Authority, the Electric Power Research Institute, the U.S. Department of Defense and the U.S. Department of Energy.

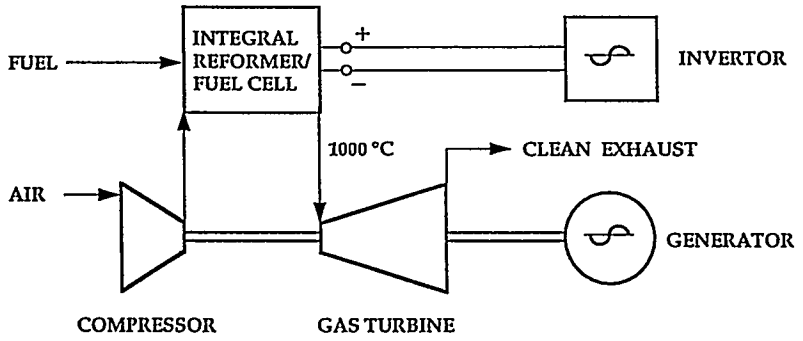

FIGURE 1 SOFC/TURBINE HYBRID INTEGRATION

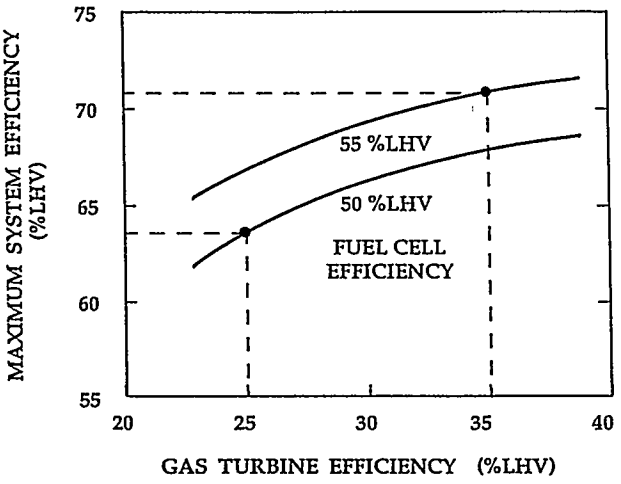

FIGURE 2 FUEL CELL/TURBINE COMBINED EFFICIENCY

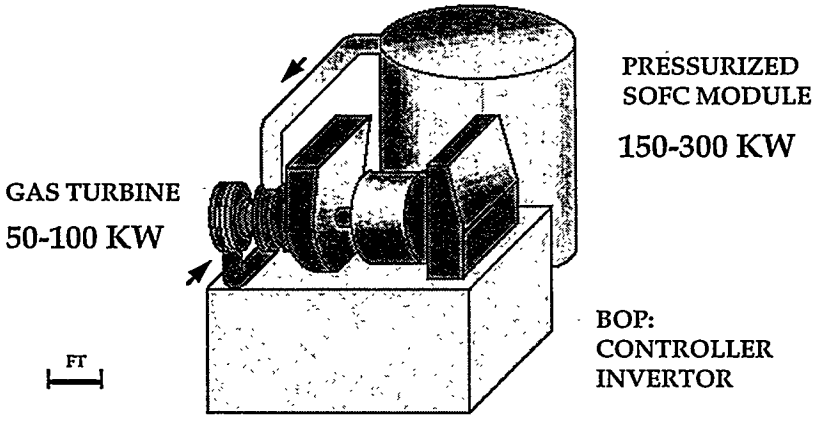

FIGURE 3 SOFC/GAS TURBINE HYBRID SYSTEM DEMONSTRATION

STATUS OF THE TMI SOFC SYSTEM

Robert C. Ruhl, Ph.D., Michael A. Petrik, and Thomas L. Cable, Ph.D.
Technology Management, Inc.
9718 Lake Shore Boulevard
Cleveland, Ohio 44108

PROTOTYPE STATUS

TMI has completed preliminary engineering designs for complete 20kW SOFC systems modules for stationary distributed generation applications using pipeline natural gas [sponsored by Rochester Gas and Electric (Rochester, New York) and EPRI (Palo Alto, California)]. Subsystem concepts are currently being tested.

SYSTEM FEATURES

- Pipeline natural gas is used directly with no sulfur removal required.
- Cooling systems use ambient air and do not require external supplies of makeup or cooling water.
- Indoor or outside installation.
- Grid-connected or grid independent operation.
- Load-following from 0 to 100% of rated net AC output.

DESIGN CRITERIA

TMI design goals have been to achieve lowest product life cost while maintaining a simple system for highest reliability. Other optimization goals have been stable electrical performance, minimal physical size, low NOx emissions.

Balance of plant includes: air filters, air blower, natural-gas compressor, fan-cooled condenser assembly, water pump, inverter, catalytic fuel reformer, high-temperature heat exchangers, stacks, sensors, controls, insulation, and miscellaneous other components, all housed in a single indoor/outdoor enclosure. Optional accessories will include a grid interface box and a heat recovery module (for cogeneration applications).

SYSTEM SPECIFICATIONS

Selected specifications for the 20 kW system are summarized as follows:

Fuel:	Pipeline natural gas at 2 in w.c. minimum
AC Power Output:	0-20 kW continuous; 208Y/120 VAC, 60 Hz, 3 phase
Maximum Current:	65 A rms per phase (23.4 kVA to balanced load)
Grid Connection:	Normally interconnected. Capable of stand-alone operation during grid outages. Will load-follow or export power as desired.
Ambient Conditions:	Outdoor or indoor
Optional Heat Recovery:	Water heating to 160°F. Maximum of 18000 BTU/hr.
Emissions:	Less than 3 lb/GWh NOx. Undetectable particulates, CO, organics
Noise Level:	Less than 65 dbA at 3 feet
Size:	26 inches square by 78 inches tall

Weight:	Approximately 1000 pounds
Current Harmonics:	Less than 4% total at rated load, grid interconnected Easily meets IEEE-519
Maintenance:	Air filter cleaning while operating Once per year preventative maintenance (6-hour outage)
Parallel Operation:	Any number of system modules.
Dynamic Response:	1% to 100% output: less than 4 sec. 100% to 1% output: less than 2 ms.
Efficiency:	At 100% output: 44% net AC output/natural gas HHV At 70% output: 49% At 40% output: 50% At 20% output: 45% At 10% output: 31%

The TMI SOFC/STACK

The basic TMI SOFC was designed to overcome problems associated with high-temperature operation and for low cost manufacture using available fabrication techniques. A key characteristic of the patented design (Fig. 1) is the use of porous, non-sintered, particulate electrodes. Non-sintered particulate electrodes eliminate problems caused by coefficient of thermal expansion mismatches at the interfacial boundaries. This allows the use of metal separators and substitution of materials optimized for electrical and other catalytic properties - (such as sulfur tolerant electrodes) rather than for thermal expansion properties. Porous electrodes support the metal separators, which allows use at higher temperatures since creep concerns are eliminated. Radial gas flows do not require external manifolds and allows for improved thermal management.

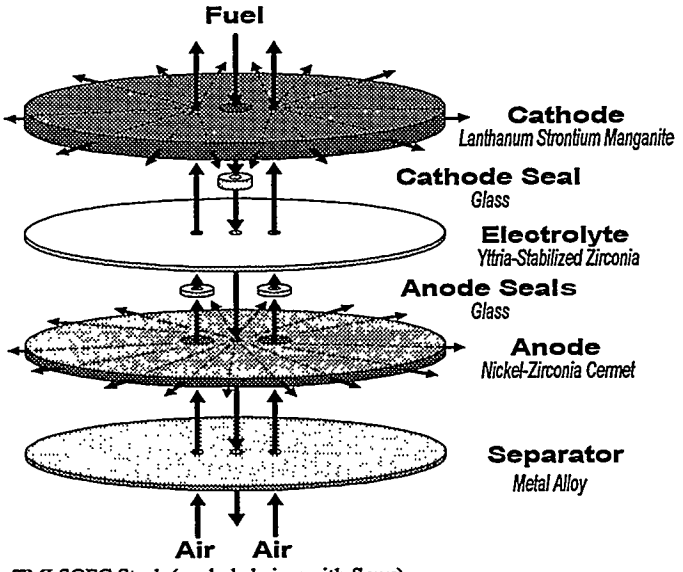

Figure 1. TMI SOFC Stack (exploded view with flows)

- Individual cells are currently at near-commercial size and performance (approximately 55 mm diameter by 1.5 mm thick at over 100 mW/cm^2) and operates between 900°C and 1000°C.
- Commercial stacks will be about 320 cells (for 120 and 208 VAC models) and operate at close to 90% electrochemical fuel utilization on reformed natural gas. Target stack life is 3 to 5 years.
- Over 500 stack tests (plus thousands of single-cell tests) have been performed to date with some stacks exceeding first-generation commercial performance assumptions.
- Stacks have been operated on military logistic fuels containing up to 0.3 wt%S.

SCHEDULE

Development of complete alpha prototype systems is now underway with full system field testing scheduled to begin within the next three years and beta field testing thereafter. Planned natural gas models will range from 1 kW (at 120/240 VAC) to 250 kW (at 480Y/277 VAC) net output.

PRICE

Market entry prices for small scale systems will range between $1500 to $5000/kW (in 1996 dollars). As production volumes and learning curves increase over time, prices will decline to below $1000/kW.

MODIFYING ZIRCONIA SOLID ELECTROLYTE SURFACE PROPERTY TO ENHANCE OXIDE TRANSPORT

Bor Yann Liaw and Steven Y. Song
Hawaii Natural Energy Institute, SOEST, University of Hawaii
2540 Dole Street, Holmes Hall 246, Honolulu, HI 96822, USA

ABSTRACT

Bismuth-strontium-calcium-copper oxide ($Bi_2Sr_2CaCu_2O_8$, BSCCO) is known for its high T_c superconducting behavior and mixed conducting property. The applicability of similar high T_c cuprates for intermediate-temperature solid oxide fuel cell (SOFC) application has been studied recently. We investigated the electrochemical behavior of several Ag|BSCCO|10 mol% yttria-stabilized zirconia (YSZ)|Ag and Ag|YSZ|Ag cells using complex impedance spectroscopy. A highly uniform and porous microstructure was observed at the interface of the YSZ and BSCCO. The ionic conductivity determined from the Nyquest plots in the temperature range of 200-700°C agrees with the values reported in the literature. The specific resistance of the BSCCO|YSZ interface was also determined to be lower than those of the conventional manganite electrode, suggesting that BSCCO seems attractive for cathode applications in SOFC.

INTRODUCTION

Yttria-stabilized zirconia (YSZ) is a typical electrolyte material used in SOFC. To generate useful power from the cell, the electrolyte must exhibit a sufficiently high conductivity. To achieve such a condition, the YSZ-based cell typically has to be operated around 1000°C. Such a high operating temperature often causes degradation and compatibility problems among cell components, affecting SOFC's cell life and commercialization potential. There is a desire to reduce the operating temperature of SOFC to below 800°C (1) to simplify the SOFC design and improve the cell efficiency. To operate SOFC at intermediate temperatures, the choice of electrodes and interconnect would be most likely different from the high-temperature system. Oxide transfer kinetics at the electrode is often the rate limiting step at intermediate temperatures. Conventional electrode materials such as Pt or Sr-doped La manganites are not sufficiently effective in catalyzing transfer kinetics at these temperatures. New electrode materials therefore have to be sought.

Bismuth-strontium-calcium-copper oxide ($Bi_2Sr_2CaCu_2O_8$, BSCCO) has been studied recently as high T_c superconducting materials (2). Similar materials have been studied for SOFC applications (3) since they all exhibit mixed conductivities at intermediate temperatures. Their potential as an oxide conducting electrode material is therefore worth exploring. Here we report the preparation, microstructure, and electrochemical behavior of the BSCCO electrode on 10 mol% YSZ.

EXPERIMENTAL ASPECTS

The 10 mol% yttria-stabilized zirconia were prepared by our collaborators in the Advanced Materials Program in the Australian Nuclear Science and Technology Organization (ANSTO) in the form of sintered and polished circular pellets. The YSZ powder was obtained from TOSOH, Japan. The YSZ powder was first pressed uniaxially with a 0.5 ton of force in a 10 mm diameter die to form pellets. They were then isostatically pressed under 200 MPa to form green body. The pellets were sintered at 1400°C in air for 2 hours, air cooled, followed by polishing with 1 μm diamond paste on both sides of the pellets to the desired thickness, ranging from 0.5 to 2.0 mm.

The $Bi_2Sr_2CaCu_2O_8$ (BSCCO) electrode was prepared separately by solid state reaction. The starting materials were Bi_2O_3, $SrCO_3$, $CaCO_3$ and CuO. They were thoroughly mixed and heat treated under the following conditions: 820°C for 12 hours; 820°C for 12 hours (repeated); and, 840°C for 12 hours; to obtain the final composition. The repeated sintering and grinding procedure was to ensure a complete reaction and high degree of homogeneity. The BSCCO electrode

was coated on one side of the YSZ pellets. The BSCCO powder was first mixed with an organic binder (ethyl cellulose), a lubricant (glycerol) and a solvent (ethanol) to form a paste. A layer of the BSCCO paste (approximately 500 μm thick) was applied to the YSZ pellet surface and allowed to dry for 12 hours. The dried samples were then processed by the following steps: The sample was heated at 150°C hour^{-1} to reach 890°C. The sample was then held at 890°C for 4 hours before subjected to a cooling at 300°C hour^{-1} to room temperature. The sintering at 890°C was able to partially melt the BSCCO compound, creating an effective bonding with YSZ.

Metallic silver made from an in-house silver paste was sintered either onto BSCCO as the contact bonding material or onto YSZ as the counter electrode. The electrical contact was made by attaching a thin Ag foil (0.025 mm thick) on each side of the pellet with a Ag wire (0.25 mm in diameter). The silver paste was made from fine metallic silver powder (1 μm in particle size) and the same organic additives used in the preparation of BSCCO. The following process was used in binding Ag to the cell: The cell assembly was heated at 60°C hour^{-1} to 880°C, held at that temperature for 4 hours and then cooled at 300°C hour^{-1} to room temperature. Each Ag contact area is approximately 8 mm in diameter, giving an apparent surface area of about 0.5 cm^2.

Two different cell configurations were constructed for complex impedance measurements: Type (A)– three cells with the Ag|BSCCO|YSZ|Ag configuration. One used a 0.5 mm thick YSZ pellet and the other two 1.0 mm. Type (B)– one cell with the Ag|YSZ(0.5 mm)|Ag configuration. The conductivity was determined by complex impedance spectroscopy between 200 and 700°C in the frequency range of 10 mHz to 1 MHz using a Solartron 1260 frequency response analyzer. All the measurements were carried out in air inside a temperature-controlled chamber.

The microstructure of the BSCCO|YSZ interface was characterized by scanning electron microscopy (SEM, Zeiss 962) and the chemical composition by energy dispersive x-ray fluorescence spectroscopy (EDAX, Oxford Instruments Link ISIS system) using one of the Type (A) cells. The Ag contact on the BSCCO electrode was removed to allow SEM examination.

RESULTS AND DISCUSSION

Microstructure Characterization: The SEM images show that the BSCCO-covered area is divided into two zones with visible morphological differences: namely a central zone (approximately 15% of the total area) and a rim zone, as shown in Figure 1.

In the central zone, the EDAX analysis reveals that the composition is primarily a combination of Zr, Bi, Sr, Ca, Cu and O. On the surface of this nominal composition, there are many needle-shaped objects, typically 10 μm in diameter and 200 μm long. These whiskers have a nominal composition of $YCuO_2$, suggesting that yttria close to the interface region has reacted with the partially-melted BSCCO to form $YCuO_2$. Zirconia was rejected to the bulk BSCCO.

In the rim zone, we found a noticeable amount of almost spherical or ellipsoidal objects, typically 100-200 μm in diameter or length. EDAX spectra show that these objects are CuO. Underneath these objects is the most interesting feature at the interface. As shown in Figure 2, most of the rim zone was covered by a uniform but highly porous microstructure. The porous microstructure consists of rectangular crystals with a grain size distribution in the 0.5-2 μm range. EDAX spectra indicate that the composition of the crystals is predominantly Zr, Sr, Ca and O. The lack of Cu and Y in the porous microstructure agrees with the existence of CuO in the rim zone and $YCuO_2$ in the central zone, indicating a significant Cu and Y segregation at the interface.

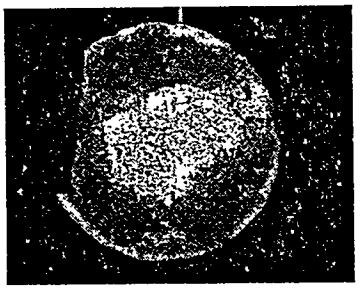

Figure 1: SEM surface morphology of a BSCCO-coated YSZ sample showing contrast between the rim and central zone.

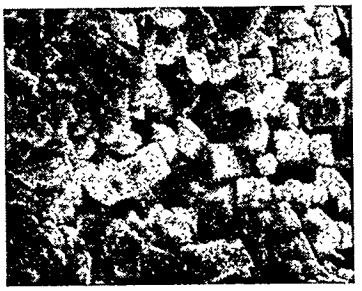

Figure 2: A highly uniform, porous microstructure in the rim zone showing a narrow particle size distribution of 0.5-2.0 μm.

Complex Impedance Spectra: The complex impedance spectra obtained from two types of cell were used to derive kinetic properties of each system. A typical Nyquest plot was shown in Figure 3, comparing the results from the two types of cell at 300°C. Similar to those reported in the literature, the spectrum from the Ag|YSZ|Ag cell contains three semicircles: From the high frequencies, the first semicircle represents the contribution from the bulk conductivity; following by the second semicircle for the grain boundaries and the third for the Ag|YSZ interface. The spectrum from the BSCCO-coated cell, although similar in shape, exhibits some differences: The first semicircle seems to be smaller than that of the previous cell. Since the YSZ pellets were all prepared at the same time from the same composition and heat treatments, one would expect the bulk conductivity having the same value. The difference is therefore possibly attributed to the variation in the aspect ratio. If the assumption is valid, the second semicircle of the BSCCO-coated cell is then apparently larger than that of the cell with only Ag contact. From the asymmetric shape of the second semicircle of the BSCCO-coated cell, we conclude that the impedance contributions from both grain boundary and the BSCCO layer are convoluted in this semicircle. The differences in the second semicircles allowed us to calculate the specific resistance of the BSCCO layer.

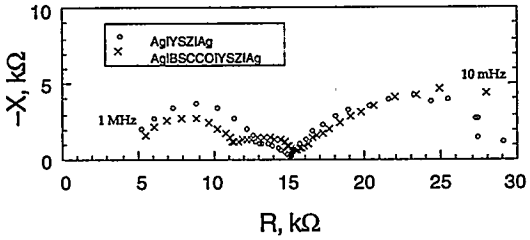

Figure 3: Nyquest plots of the Ag|YSZ|Ag and Ag|BSCCO|YSZ|Ag cells in air at 300°C.

Kinetic Properties: From the Nyquest plots, similar to those shown in Figure 3, we can determine the bulk and grain boundary conductivity of the YSZ samples. The conductivity values obtained from various samples are consistent with those reported in the literature, as shown in Figure 4, including the conductivity data reported by Badwal (4) on 10 mol% YSZ polycrystalline samples (of 92% theoretical density). Our conductivity values are slightly higher than Badwal's, possibly due to either a higher density or variations in the aspect ratio.

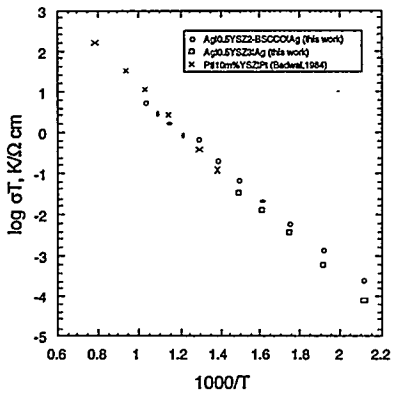

Figure 4: Ionic conductivity of the YSZ samples compared with Badwal's data (4).

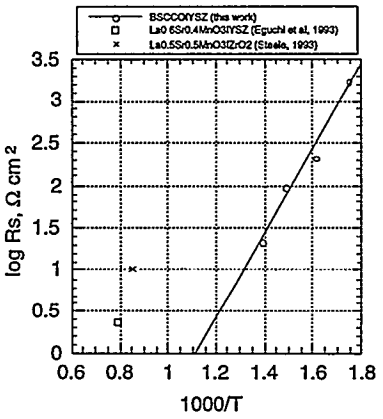

Figure 5: Specific resistance of the BSCCO layer as a function of reciprocal temperature.

The specific resistance of the BSCCO derived from the second semicircle is shown in Figure 5 as a function of reciprocal temperature. Typical specific resistance values of manganite cathode used in SOFC, such as $La_xSr_{1-x}MnO_3$ (5) are also included in the figure for comparison. The smaller resistance of the BSCCO layer than those of the manganites indicates that the BSCCO could be an attractive cathode material for SOFC applications.

CONCLUSION

Our study using complex impedance spectroscopy indicates that the specific resistance of the BSCCO|YSZ interface is quite low, suggesting that BSCCO could be an interesting material for SOFC cathode application.

ACKNOWLEDGMENT

We would like to thank the financial support from the New Energy and Industrial Technology Development Organization (NEDO) in the Ministry of International Trade and Industry (MITI) of Japan under the International Joint Research Program. We would also like to thank Drs. Janusz Nowotny and Zhaoming Zhang in ANSTO and Professor Nobuyasu Mizutani in Tokyo Institute of Technology for providing YSZ pellets and fruitful discussions in this work.

REFERENCES

1. N.Q. Minh, in Science and Technology of Zirconia V, ed. S.P.S. Badwal et al, Technomic Publishing Co., Lancaster, PA, 1993, pp. 652.
2. H. Maeda et al, Japan J. Appl. Phys. 27, pp. L209, 1988.
3. D.J. Vischjager et al, Solid State Ionics, 40/41, pp. 810, 1990.
4. S.P.S. Badwal, J. Mat. Sci., 19, pp. 1767, 1984.
5. K. Eguchi et al, in Science and Technology of Zirconia V, ed. S.P.S. Badwal et al, Technomic Publishing Co., Lancaster, PA, 1993, pp. 694; and B.C.H. Steele, ibid., pp. 713.

DEVELOPMENT OF 10kW SOFC MODULE

N. Hisatome and K. Nagata
Nagasaki Shipyard & Machinery Works
Mitsubishi Heavy Industries, Ltd.
1-1, Akunoura-machi, Nagasaki 852, Japan

S. Kakigami
Electric Power Development Co., Inc.
6-15-1, Ginza, Chuo-ku, Tokyo 100, Japan

H. Omura
Electric Power Development Co., Inc.
1-1, Yanagisaki-machi, Wakamatsu-ku, Kitakyushu 808-01, Japan

ABSTRACT

Mitsubishi Heavy Industries, Ltd. (MHI) has been developing tubular type Solid Oxide Fuel Cells (SOFC) since 1984. A 1kW module of SOFC has been continuously operated for 3,000 hours with 2 scheduled thermal cycles at Electric Power Development Co., Inc. (EPDC) Wakamatsu Power Station in 1993. We have obtained of 34% (HHV as H_2) module efficiency and deterioration rate of 2% per 1,000 hours in this field test.

As for next step, we have developed 10kW module in 1995. The 10kW module has been operated for 5,000 hours continuously. This module does not need heating support to maintain the operation temperature, and the module efficiency was 34% (HHV as H_2).

On the other hand, we have started developing the technology of pressurized SOFC. In 1996, pressurized 1kW module has been tested at MHI Nagasaki Shipyard & Machinery Works. We are now planning the development of pressurized 10kW module.

INTRODUCTION

MHI has been developing SOFC since 1984. From 1986 to 1989, elementary technologies of tubular type SOFC stacks and module were developed with Tokyo Electric Power Co. (TEPCO). In 1989, TEPCO, EPDC and MHI developed 1kW SOFC module, and in 1991 we operated the 1kW module for 1,000 hours at EPDC Wakamatsu Power Station. And in 1993, EPDC and MHI have developed the advanced type 1kW module and operated it for 3,000 hours successfully.

And in 1996, we have developed a 10kW module, which can be operated without heating support. The 10kW module have been operated for 5,000 hours continuously.

DEVELOPMENT OF TUBULAR TYPE CELL STACK

We have applied the spray coating method to the tubular type SOFC. The cell stack has 15 cells connected in series, and the stack length is 500mm.

The overview of stacks is shown in Fig. 1. Fig. 2 shows the structure of the stack. Main materials of films and film thickness are shown in Table 1. Most of films of this stack has

been produced by atmospheric plasma spray coating method. However electrolyte film is produced by low pressure plasma spray (LPS) coating method, because it needs gas tightness.

We have been making efforts to improve cell performance. Major improvements are as follows;

1) Optimization of the spray conditions
2) Quality control of each material
3) Optimization of the cell configuration

Fig. 3 shows the example of I-V characteristics. Tests were conducted at 900 °C, atmospheric pressure, using hydrogen as fuel and air as oxidant. MHI's cell-stack can be operated over 80% fuel utilization and the maximum efficiency reached 40% at the current density at 200 mA/cm^2.

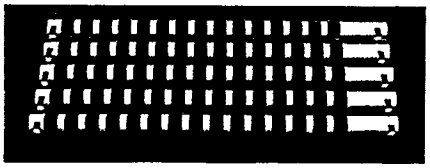

Fig. 1 Appearance of Tubular Type SOFC

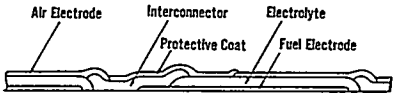

Fig. 2 Tubular Cell Configuration

Table 1 Materials and Film Thickness

Structure Film	Materials	Film Thickness
Fuel Electrode	NiO/YSZ	80~100μm
Electrolyte	YSZ	100~150μm
Air Electrode	$LaCoO_3$	150~200μm
Interconnecter	$NiAl/Al_2O_3$	100~150μm
Substrate Tube	CSZ	Outer Diamater 21mm

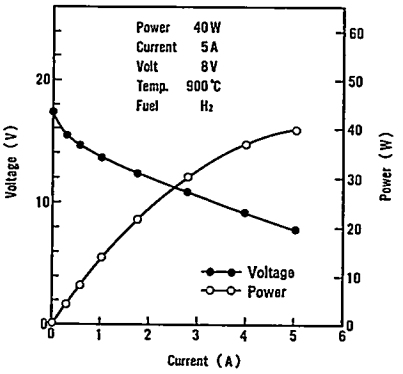

Fig. 3 Example of Cell Performance

DEVELOPMENT OF 10kW MODULE

EPDC and MHI designed and fabricated a 10kW module in 1995. This module mainly consists of four parts, that is fuel plenum, spent fuel plenum, reactor chamber and air preheater. This module structure is same as the 1kW module. Fig. 4 shows the structure of the 10kW module, the specifications are shown in Table 2.

We have adopted a pendant stack structure for relaxation of thermal stress and easy maintenance of stacks. Fuel is fed from the top of the module and introduced to the fuel plenum,

distributed to each cell-stack through injection tubes and utilized for the cell reaction. The spent fuel is exhausted through spent fuel plenum.

Air is heated by air preheater, and is fed to a reactor chamber. Spent air is exhaust through the air exhaust tube, and its heat is exchanged to cold air in the air preheater. Current collectors are made of metal and arranged in plenums with reducing atmosphere; one is in the fuel plenum, the other is in the spent fuel plenum.

The performance curve of the 10kW is shown in Fig. 5. The maximum power output was 12kW and the efficiency was 34% at 80% fuel utilization. Fig. 6 shows module power output through this test. Total operation time was 5,066 hours and module power output was stable over all operation conditions. The deterioration rate was about 1 $\sim$ 2% per 1,000 hours.

Table 2 Specifications of 10kW Module

Power Output	12.0kW D.C.
Open Circuit Voltage	415V
Operation Voltage	229V
Operation Current	52.5A
Number of Stacks	504
Operation Temperature	900℃
Operation Pressure	Atmosphenc Pressure
Outer Size of Module	1500mm Diameter 1750mmHeight

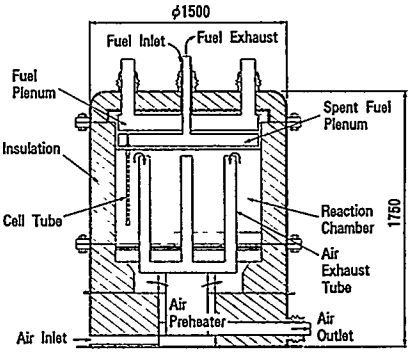

Fig. 4 Structure of 10kW Module

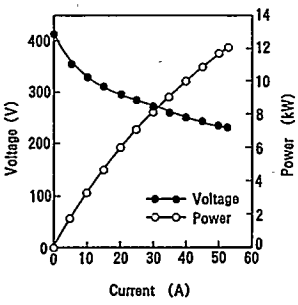

Fig. 5 Performance Curve of 10kW Module

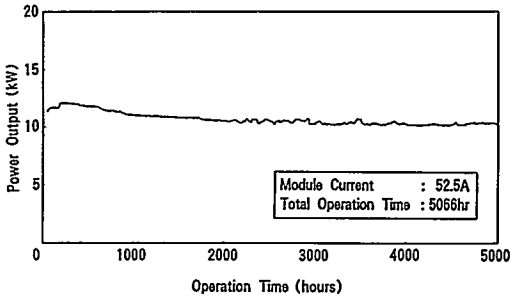

Fig. 6 Operation Results of 10kW Module

PRESSURIZATION

It is necessary to pressurize SOFC module for realizing high efficiency SOFC plant, combined with gas turbine. EPDC & MHI have started developing of pressurizing technologies of SOFC since 1995.

Main technical points are follows;

- Evaluation of the stack performances at pressurized condition
- Establishment of system control technologies

We have developed pressurized 1kW module in 1996. Table 3 shows the performance data of the 1kW module, and Fig. 7 shows the appearance of the pressurized 1kW module. In this test we have confirmed the improvement of module performances by pressurization. And we are now planning the development of a pressurized 10kW module as for next step.

Table 3 Performance Data of 1kW Module

	Atmospheric	Pressurized
Operating Pressure	0atg	5atg
Operating Temperature	900℃	←
Number of Stacks	48	←
Operating Voltage	115V	34.3V
Operating Current	10A	52.5A
Power Output	1.15kW	1.80kW
Fuel Utilization	60%	←
Air Utilization	10%	←
Max. Efficiency (at 200mA/cm²)	33.6%	38%

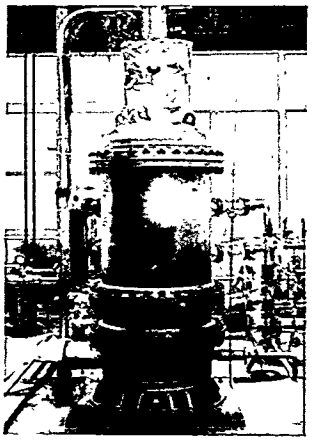

Fig. 7 Appearance of Pressurized 1kW Module

CONCLUSION

EPDC and MHI have developed 10kW module and have operated it for 5,000 hours successfully. Our future target is commercialization of coal gasified SOFC combined cycle. We will accelerate on our SOFC R & D project to realize our target in early future.

REFERENCES

1. T. Saishoji, S. Kakigami, A. Hasimoto and N. Hisatome, "3,000 hrs Operating Test of Tubular Type SOFC 1kW Module", The 1st FCDIC Fuel Cell Symposium Proceedings, Fuel Cell Development Information Center, Tokyo, Japan (1994), pp.290-293.
2. Y. Yamauchi, Y. Yoshida, N. Hisatome and F. Nanjo, "SOFC Development Status of Mitsubishi Heavy Industries", in Fuel Cell Seminar Abstracts, Courtesy Associations, Inc., Washington, DC, (1994), pp.639-642.
3. N. Hisatome, K. Nagata, T. Saishoji and S. Kakigami, "DEVELOPMENT OF TUBULAR TYPE SOFC", in PROCEEDINGS OF THE FOURTH INTERNATIONAL SYMPOSIUM, The Electrochemical Society, Inc., New Jersy, USA (1995), pp.216-220.

STRUCTURE↔PROPERTY RELATIONSHIPS IN SOLID OXIDE FUEL CELLS

W. Huebner, D.M. Reed, and H.U. Anderson

Department of Ceramic Engineering
University of Missouri - Rolla
222 McNutt Hall
Rolla, MO 65401

I. INTRODUCTION

The electrode reactions are a major cause of the energy losses in SOFC's, and limit their use to higher temperatures, typically 800-1000°C. The electrode reactions have received much attention aimed at better understanding the electrode kinetics and mechanisms, but are still very primitive in their basic understanding. The electrode microstructure and its corresponding reactivity has commonly been studied by DC and AC impedance techniques. A common method of examining electrode reactions employs surface-mounted reference electrodes, although this technique often limits the experiment to examination of one electrode. In this study a new technique has been developed of utilizing a Pt voltage probe placed internally into the electrolyte to measure the I-V and impedance spectra of both electrodes operating under cell conditions. Unlike surface mounted electrodes which need to be concerned with distance and dimensions of reference electrodes with respect to working and counter electrodes the internal Pt voltage probe is centered internally at a known depth within the electrolyte and between corresponding electrodes.

The internal Pt voltage probe has been used in this research program to investigate the microstructure ↔ property relations in solid oxide fuel cells (SOFC's) in order to better understand the mechanisms involved in cell performance. The aim is to fabricate SOFC's with controlled microstructures utilizing $La_{1-x}Sr_xMnO_3$ (LSM), yttria stabilized zirconia (YSZ), and Ni-YSZ composites as the cathode, electrolyte, and anode, respectively. Ideally, the electrode materials would be tailored for an increased reaction rate (grain size $\leq$ 1 μm), be stable with time (> 10,000 h), have a thermal expansion match to YSZ ($\alpha \approx 11 \times 10^{-6}$/°C), show limited chemical interaction with the electrolyte, and show no degradation in electrical performance. This paper describes just a few of the starting powder characteristics, electrical conductivity and overpotential measurements, and resultant microstructures as a function of processing conditions (i.e. powder calcination temperature, and annealing temperature) and composition for the electrolyte and cathodes.

II. EXPERIMENTAL PROCEDURE

Single Cell Fabrication

The YSZ electrolyte used in this investigation was self supporting, and the cathodes were applied via screen printing onto a pre-sintered dense electrolyte. The commercially-available YSZ (Zirconia Sales of America Inc.) is a fully stabilized (8 mole % Y_2O_3), co-precipitated powder. This particular powder was chosen because of its low cost, ~$70/kg, low impurity content and low densification temperature, ~1400°C. The YSZ powder had a primary particle size of approximately 250 nm and a corresponding BET surface area of ~ 8.0 m^2/g. YSZ powders were initially dried at 150°C to remove any physically bonded water and then mixed with a commercially available binder system from Ferro Corp, B73210. The slip was ball-milled with ZrO_2 media for 24 - 48 h until the powder was well dispersed. The slurry was tape cast; green thicknesses were ~ 50-75 μm. Circular samples of 2 inch diameter were cut out of the tape and a Pt voltage probe (38 mm long x 0.3 mm wide) was screen printed onto the YSZ tape. Six tapes were stacked and laminated at 3000 psi for 10 min at 70°C in such a way as to place the Pt probe in the center of the fired specimen. The thermal processing schedule for binder removal and densification of the YSZ laminates was 0.5°C/min to 350°C, hold for 1 h, 3°C /min up to 1450°C, hold for 2 h, and then cool at 3°C/min. Sintered electrolytes were 3.2 cm in diameter, and 200 μm thick.

$La_xSr_{0.2}MnO_3$ ($0.7 \leq x \leq 0.79$) compositions were synthesized by the liquid mix technique using $La_2(CO_3)_3$, $SrCO_3$, and $MnCO_3$ as standardized raw materials. The carbonates were dissolved in HNO_3, ethylene glycol, citric acid and water in glass beakers. Heating resulted in the formation of a polymeric precursor solution which was then oxidized at ~300°C. The powder was vibratory milled dry for 4 h with ZrO_2 media, then calcined in MgO crucibles at temperatures of 800 - 1200°C in increments of 100°C. Soak times for all calcinations was 4 h. The powders were vibratory milled again using the same conditions as described before. Powder crystallinity, phase, and surface area were characterized using X-ray diffraction and BET techniques as a function of calcination temperature. The electrode powders were mixed with a commercial resin solution,

BX018-16, from Ferro Corp using a three roll mill. The cathode compositions were screen printed onto dense YSZ electrolytes and sintered at temperatures between 1200°C and 1400°C in 100°C increments for a 1 h hold, with a heating and cooling rates of 3°C/min. A primary goal of this investigation was to vary the grain size and porosity of electrode microstructures and the their impact on electrode performance, therefore powders were calcined and sintered at various temperatures. Cathodes were porous, exhibited grain sizes on the order of 1μm, and gave resultant dimensions of 0.635cm x 0.635cm and ~ 20μm thick.

A Pt grid (0.2 mm line width and 0.2 mm spacing between lines) was screen printed on the electrodes for cell performance experiments to act as a current collector but also to allow gas diffusion to the electrode/electrolyte interface.

Electrical Characterization

Electrical characterization of single cells utilizing the internal Pt voltage probe was investigated to simultaneously separate the losses attributed to each component (anode, electrolyte, cathode) and their interfaces (cathode/electrolyte and anode/electrolyte) during cell operation. The cell performance studies were focused on the reaction kinetics at the interfaces whereas DC conductivity measurements were performed to investigate the resistive losses of each component as a function of time, composition, and preparation condition. Electrochemical (I-V) measurements were carried out using a five electrode configuration which allowed for separation of anode and cathode overpotentials during operation. I-V behavior was performed on both half cells and complete cells using an Anatronics Current/Voltage Control Fuel Cell Testing Module, a Keithley Model 196 Microvolt Meter, and a Fluke 27/FM Multimeter. The Fuel Cell Testing Module was placed in the voltage control mode thus enabling the desired cell voltage and corresponding current to be measured

III. RESULTS AND DISCUSSION

A typical cell with a single Pt voltage probe buried into the center of the electrolyte (100 μm from the cathode and anode) is shown in Figure 1. The Pt probe is ~ 5 μm thick and 200 μm wide. Since all electrolytes had thicknesses of 200 μm and cathodes and anodes had electrode areas of 0.4 cm^2, the resistive loss associated with the electrolyte (82 mV at 1000 mA/cm^2) was used as a baseline for all cell experiments.

Effect of LSM Calcination Temperature on the Electrode Reaction

$La_{0.79}Sr_{0.2}MnO_3$ (LSM) powders were calcined between 800 and 1200°C in increments of 100° for 4 h, prepared as pastes, screen printed onto YSZ electrolytes, and densified at 1200°C. The initial overpotential (η) - current density (j) results for $La_{0.79}Sr_{0.2}MnO_3$ (LSM) powders which were calcined between 800 and 1200°C are shown in Figure 2. All powders calcined below 1100°C show a similar electrochemical response with the 800 and 900°C calcinations showing the best performance (~ 60 and 80 mV at 1000 mA/cm^2). The lower calcination temperatures have a smaller particle size and would therefore be expected to contain more reaction sites (TPBs) for the oxygen reduction reaction to occur. The opposite would be true for the 1200°C calcination temperature. Although the samples are sintered onto the YSZ electrolyte at the same temperature, their still is the tendency for the lower calcination temperatures to initially have a smaller particle size (more TPBs). The sintering of the LSM onto the electrolyte is constrained even at 1200° due to the densified YSZ support, this is also enables porosity to be introduced into the cathode microstructure. All sintering occurs in the z-direction rather than the x-y plane, therefore there is no change in the area of the electrode before and after sintering.

Measurements were again performed on all samples after 24 h of operation. Powders calcined at 800 and 900°C were not stable with time and resulted in higher overpotentials. Powders calcined at temperatures ≥ 1000°C were stable within the 24 h time frame. Figure 3 illustrates the η - j behavior of samples calcined at 800, 900 and 1000°C as a function of time. The sample calcined at 800°C had the largest change in the overpotential and was comparable to the sample calcined at 1200°C (~ 170 mV at 1000 mA/cm^2). The 900°C sample also increased its overpotential but to a smaller extent (~ 100 mV at 1000 mA/cm^2). This can be explained by the

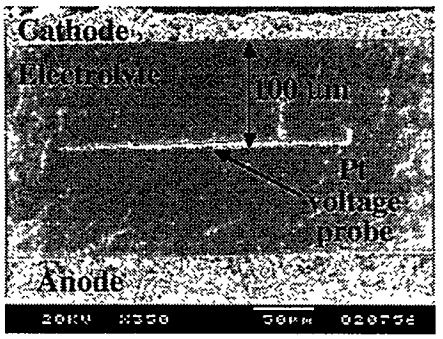

Figure 1. Typical cell with an internal Pt voltage probe.

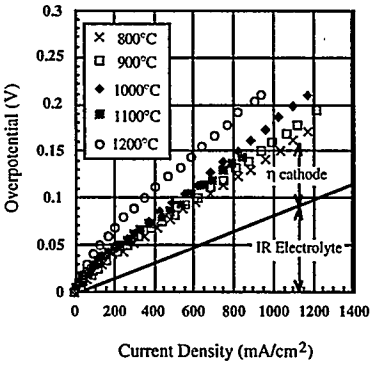

Figure 2. Initial η-j relations of the $La_{0.79}Sr_{0.2}MnO_3$ composition sintered on the electrolyte at 1200°C and calcined at various temperatures.

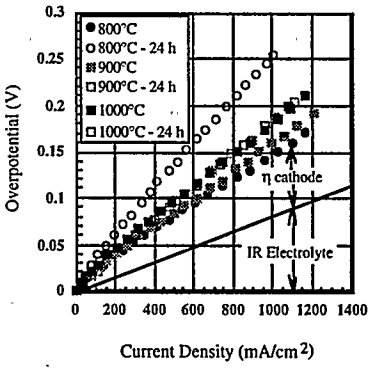

Figure 3. η-j relations initially and after 24 h of operation for the $La_{0.79}Sr_{0.2}MnO_3$ compositions sintered on the electrolyte at 1200°C and calcined at 800, 900, and 1000°C.

powder further coarsening during operation which would give rise to a larger contact area and a reduced number of TPBs. The smallest particles are expected to have the highest driving force for densification which may explain the largest change in the electrochemical results for the 800°C calcination. Higher calcination temperatures (≥1000°C) may also show similar behavior for operation times greater than 24 h.

Effect of Composition and Sintering Temperature on Cathode Performance

The compositions studied were $La_{0.79}Sr_{0.2}MnO_3$ (1% excess Mn), $La_{0.75}Sr_{0.2}MnO_3$ (5% excess Mn), and $La_{0.70}Sr_{0.2}MnO_3$ (10% excess Mn) calcined at 900°C for 4 h then sintered on the YSZ electrolyte at temperatures between 1100-1400°C. Figures 4 and 5 are η-j plots of the three compositions sintered onto the YSZ electrolyte 1200 and 1400°C. Clearly the 1200°C firing condition yields a large variation for the compositions, the 10 % excess Mn shows an extremely small overpotential (~ 40 mV at 1000 mA/cm^2). The 5% excess Mn composition also shows a lower overpotential (~ 80 mV at 1000 mA/cm^2) than the near stoichiometric sample (~ 105 mV at 1000 mA/cm^2). Because the grain sizes for the cathodes were observed to be very similar, this cannot be used as the basis for the large variation in the electrochemical behavior. X-ray diffraction on bilayers was performed to see if a second phase (i.e. $La_2Zr_2O_7$) could be detected at

the interface. The XRD patterns for the three compositions annealed at 1200°C showed the same diffraction peaks corresponding to the YSZ and LSM phases except for the $La_{0.79}Sr_{0.2}MnO_3$ sample which had an extra peak at ~28.5°, corresponding to the 100 % intensity line of the $La_2Zr_2O_7$ phase. Therefore, the addition of excess Mn is effective in decreasing the pyrochlore phase formation at the interface at higher temperatures (≤ 1200°C).

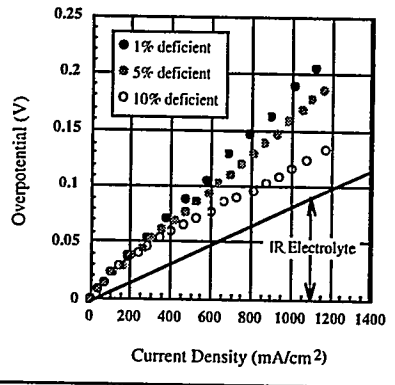

Figure 4. η-j relations of the LSM compositions calcined at 900° and sintered at 1200°C.

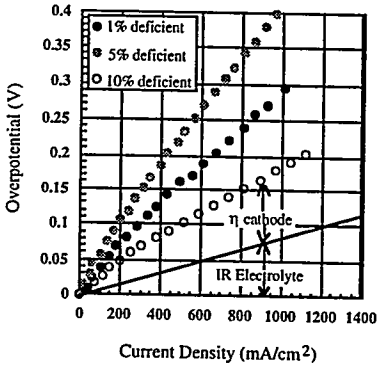

Figure 5. η-j relations of the three LSM compositions calcined at 900°C and sintered at 1400°C.

The overpotential results for the three compositions fired at 1400°C are shown in Figure 5. The 1 % and 10 % excess Mn compositions show a consistent trend with the lower sintering temperatures, namely, that the overpotentials are larger due to both a larger grain size and an increased reaction at the interface. The overpotential values for the 1 and 10 % excess samples at 1000 mA/cm^2 are ~ 210 and 100 mV. The 5 % excess sample has a very high overpotential (~ 320 mV at 1000mA/cm^2), and is not consistent with the previously observed trends. Some possible explanations could be that the sample was cracked or improperly sealed which allowed the mixing of the fuel and oxidant which could reduce the oxygen pressure in the cathode chamber. Another possible explanation is that the sample has not equilibrated within the 24 h period.

IV. CONCLUSIONS

- Increasing the particle size of the $La_{1-x}Sr_xMnO_3$ cathode results in higher overpotentials, but lends long term stability at 1000°C. Increasing the cathode firing temperature increases the overpotential, although the microstructure remains fairly constant. Although 800°C yields the best initial results, after 24 h of operation the overpotential climbs sharply. We have found that 1000°C gives the best performance/stability combination. At 1 A/cm^2, the cathodic overpotential is ≈0.1 V, which is very good
- Nonstoichiometric $La_xSr_{0.20}MnO_3$(x=0.70, 0.75, and 0.79) cathode compositions exhibit the best properties. Previously-summarized results showed that A-site deficient compositions exhibited the lowest overpotentials. To further explore this effect, we completed a series of studies using these compositions fired on at temperatures of 1100, 1200, 1300 and 1400°C. In all instances, 1200°C was the optimum, with the x=0.70 composition being the best. It has an overpotential of only 0.04V at 1 A/cm^2. SEM analyses indicated no second phases or interdiffusion is detectable. Longer time studies are underway.

Acknowledgment

The authors would like to thank the Department of Energy and the Gas Research Institute for their financial support.

MANUFACTURE OF SOFC ELECTRODES BY WET POWDER SPRAYING

R. Wilkenhöner, L.G.J. de Haart *, W. Malléner, H.P. Buchkremer

Forschungszentrum Jülich GmbH, D-52425 Jülich, Germany
Institut für Werkstoffe der Energietechnik
* Institut für Energieverfahrenstechnik

ABSTRACT

The reproducible and commercial manufacturing of electrodes with enhanced electrochemical performance is of central importance for a successful technical realization of Solid Oxide Fuel Cell (SOFC) systems. The route of electrode fabrication for the SOFC by Wet Powder Spraying (WPS) is presented. Stabilized suspensions of the powder materials for the electrodes were sprayed onto a substrate by employing a spray gun. After drying of the layers, binder removal and sintering are performed in one step. The major advantage of this process is its applicability for a large variety of materials and its flexibility with regard to layer shape and thickness. Above all, flat or curved substrates of any size can be coated, thus opening up the possibility of "up-scaling" SOFC technology.

Electrodes with an enhanced electrochemical performance were developed by gradually optimizing the different process steps. For example an optimized SOFC cathode of the composition $La_{0.65}Sr_{0.3}MnO_3$ with 40% 8YSZ showed a mean overpotential of about -50 mV at a current density of -0.8 A/cm^2, with a standard deviation amounting to 16 mV (950°C, air). Such optimized electrodes can be manufactured with a high degree of reproducibility, as a result of employing a computer-controlled X-Y system for moving the spray gun. Several hundred sintered composites, comprising the substrate anode and the electrolyte, of 100x100 mm^2 were coated with the cathode by WPS and used for stack integration. The largest manufactured electrodes were 240x240 mm², and data concerning their thickness homogeneity and electrochemical performance are given.

EXPERIMENTAL

Table 1 Starting powder *(* agglomerated)*

Powder Composition	NiO	TOSOH 8YSZ	$La_{0.65}Sr_{0.3}MnO_3$
Particle size Crystallite size	0.3	~30 µm * 25 nm	10 to 20 µm * < 200 nm
Particle shape	spherical	spherical	spherical
Company	Baker, USA	TOSOH, J	Forschungszentrum Jülich, G

The characteristics of the starting powders are presented in Table 1. Lanthanum-Strontium-Manganese perovskite (LSM) with the optimized composition $La_{0.65}Sr_{0.3}MnO_3$ was used as electroactive cathode material because of its high electric conductivity and enhanced compatibility with the electrolyte (8 mol% Yttria Stabilized Zirconia, 8YSZ) (1,2). A mixture of 8YSZ- and NiO-Powder was used for the anode. After reduction to nickel the nickel amount was 40 vol%, disregarding the porosity. The powders, which were agglomerated in the initial state, had to be deagglomerated and stabilized to prevent reagglomeration in the spray suspensions. Otherwise, the desired fine electrode microstructure - a maximum of particle fineness and a porosity of about 30% - cannot be achieved. Deagglomeration was obtained by milling the spray suspension which consisted of the powder, a suitable dispersant and a carrier (ethanol, water or mixtures thereof) for at least 24 hours until the particle size was less than 1 µm. We used high molecular weight polyelectrolytes as dispersants, which stabilizes the powder particles sterically and also electrostatically in hydrous solvents due to

their dissociation. These dispersants also act as binders for the green coating. Their stabilizing effect was verified immediately after milling. Therefor the viscosity of the spray suspensions was measured with a rotation viscosimeter (Haake RV20).
Wet Powder Spraying has been successfully applied for several applications (3,4). The suspension is sprayed on the substrate by means of a paint gun. Part of the carrier evaporates during the spraying process. Due to the remaining carrier present, the viscosity of the suspension remains low for a sufficient period of time so that local variations in the layer thickness can be compensated by flow processes. After complete drying binder bridges are formed between the particles and towards the substrate ensuring sufficient green strength. Removal of the binder and sintering may be performed in one step. Because of the higher viscosity and density of the powder suspensions compared to paints, the spray gun had to be modified so the spray jet could be varied and reproducibly adjusted for each powder suspension. A computer-controlled X-Y system was installed to guide the gun during spraying ensuring high reproducibility. The required coating area is achieved by masks covering the uncoated areas of the substrate. Layer thickness can be varied by the spray parameters, and by superposing several layers. The minimum thickness depends on the powder particle size. SOFC-Cathodes 90x90 mm^2 and 240x240 mm^2 were produced for the SOFC concept of Forschungszentrum Jülich, which is described elsewhere (5). Overlapping spraying has been applied. Spraying is performed continuously while the gun advances and retreats. The microstructure was evaluated by applying the line intersection method on SEM micrographs. For this purpose, the intercept lengths of at least 50 particles per phase were averaged for each specimen. The thickness of the unsintered coatings was measured with a 3-d coordinate measuring system, and plastic foils with 100±1 µm thickness were used as substrates. By means of impedance spectroscopy and potentiodynamic current-potential-tests, the electrochemical performance of the electrodes was determinated. A schematic diagram of the cell design for the electrochemical measurements can be found in (6).

RESULTS AND DISCUSSION

The major goals of anode development are not only to increase the initial electrochemical performance, but to increase their long-term stability. One mechanism of anode degradation is the coarsening of the microstructure due to sintering of fine nickel particles to large particles. This coarsening can be prevented by a continuous 8YSZ-skeleton or framework in the microstructure, which limits the space for the growth of coarse nickel particles. To achieve such 8YSZ-framework inside the anode, deagglomeration and stabilization, as well as homogenization of the initial powders in the spray suspension are of major importance. Best results were achieved by milling the initial powder (56% NiO with 22% 8YSZ as recieved and 22% 8YSZ pre-calcined at 1300°C for 2 hours) together with the solvent and the dispersant for 48 hours in a ball mill. This powder preparation leads to a homogeneous distribution of nickel- and 8YSZ-particles in the microstructure. Table 2 documents the main manufacturing and microstrucural features of such an anode, the averaged current-potential-curve of which is given in Fig. 1. Due to the formation of a continous and fine 8YSZ-framework in the microstructure, the anode showed an enhanced long-term stability. A galvanostatic long-term test was performed for 300 hours (950°C, 0,2 A/cm^2). The measurement started immediately after the anode had reached the working temperature. The increase of the overpotential was less than 9% per 1000 hours.
By optimizing powder preparation and suspension stabilization, powder particles with less than 1 µm could be successfully processed for cathode manufacture, so the required fine cathode microstructure could be achieved. Further optimization was performed concerning

the content of electrolyte material in the cathode, the sintering conditions and the layer thickness. A detailed report about this optimization is given in (7). The manufacture and microstructure of the optimized cathode is characterized in Table 2. A mean overpotential of about -50 mV was measured at a current density of -0.8 A/cm^2 at 950°C in air. The standard deviation, which was calculated from more than 30 measurements, was 16 mV or 32%. The electrochemical activity was stable for at least 100 hours at -0.2 A/cm^2. The fineness and homogeneity of the microstructure is presented in Fig. 2.

Table 2 Manufacturing and microstructural features of WPS-Electrodes
(*1* bottom layer onto the electrolyte, *2* top layer)

Layer	Composition [wt.%]	Powder [µm]	Sintering (3h) [°C]	Thickness [µm]	Porosity [%]	d_{Pore} [µm]	$d_{Partikel}$ [µm]
CATHODE *1*	60% LSM *40% 8YSZ*	0.27 *0.22*	1200	8 - 13	26	1.2	1.3
CATHODE *2*	LSM	0.9	1200	~30	52	2.2	2
ANODE	56% NiO *22% 8YSZ as recieved* 22% 8YSZ pre-calcined	0.3 *0.22* < 16	1400	~32	41	1.8	1.8 } 1.6

Table 3 Thickness of a 'green' cathode 240x240 mm^2 in size

Average value	Standard deviation	Maximum deviation
69.4 µm	3.9 µm	± 9.3 µm

For the SOFC-Concept of Forschungszentrum Jülich, the sintered composite comprising of a thick anode and a thin-film electrolyte up to 250x250 mm² had to be coated with the cathode and then used for stack integration. Table 3 documents the constancy of the coating thickness for such large cathodes. In order to verify the homogeneity of the electrochemical activity, 10 electrolyte foils with 19.5 mm diameter were distributed in the coating area and subjected to standard coating. The results of their electrochemical measurements are given in Fig. 3. All specimens are within a certain scatter. For -0.8 A/cm^2 the standard deviation is 8 mV and the maximum deviation 13 mV. This deviation is also strongly influenced by the inaccuracy of the electrochemical characterization. As a result of the inaccuracy, the microstructure can be regarded as homogeneous over the entire coated area.

SUMMARY

In this paper the potential of Wet Powder Spraying for the production of SOFC electrodes was demonstrated. Anodes and cathodes with an excellent initial electrochemical performance and an enhanced long-term stability could be manufactured with high reproducibility. The outstanding advantage of this process is its ability to coat flat or curved substrates of any size so that SOFC technology can be "up-scaled" to any size. Cathode manufacture was demonstrated for sizes up to 240x240 mm^2, with a maximum deviation in layer thickness of about ±13% and a constant electrochemical activity, so that the microstructure can be assumed as homogeneous.

REFERENCES

1 E. Syskakis, B. Robens, A. Naoumidis, 'Structural and High Temperature Electrical Properties of $La_YSr_XMnO_3$ Perovskite Materials', Journal de Physique IV, Colloque C7, Supplement au Journal de Physique III, "Euromat", Vol. 3, Nov. 1993 1429ff

2 G. Stochniol, E. Syskakis, A. Naoumidis, 'Chemical Compatibility between Strontium-Doped Lanthanum Manganite and Yttria-Stabilized Zirconia', J. Am. Ceram. Soc. 78 [4] (1995) 929ff
3 A. Ruder, H.P. Buchkremer, H. Jansen, W. Malléner, D. Stöver, 'Wet Powder Spraying - a Process for the Production of Coatings', Surface and Coatings Technology 53 (1992) 71ff
4 M. Fübi, H.P. Buchkremer, D. Stöver, 'Wet Powder Spraying - a new PM-Route for Processing Fiber Reinforced MMC's', Proceedings of the World Congress PM'94: Paris 6.-9.6.1994, 483ff
5 H.P. Buchkremer, U. Diekmann, L.G.J. de Haart, H. Kabs, U. Stimming and D. Stöver, 'Realisation of an Anode Supported Planar SOFC System', this conference
6 J. Divisek, L.G.J. de Haart, P. Holtappels, Th. Lennartz, W. Malléner, U. Stimming and K. Wippermann, 'The kinetics of electrochemical reactions on high temperature fuel cell electrodes', J. Power Sources 49 (1994) 257-270
7 R. Wilkenhöner, Th. Hauber, U. Stimming, W. Malléner, H.P. Buchkremer, 'Cathode Processing by Wet Powder Spraying', Proceedings of the '2. European SOFC Forum', Oslo, Norway, 6.-10.5.1996,

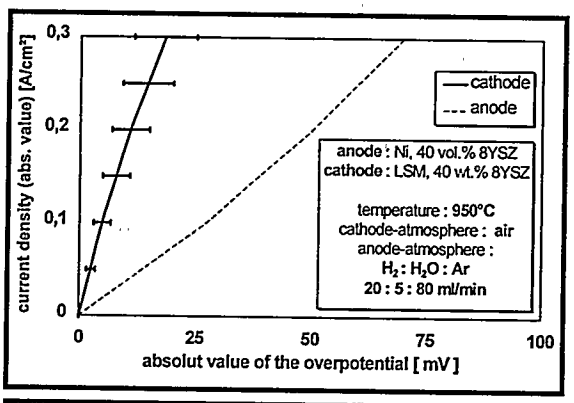

Figure 1

Electrochemical performance of SOFC-anodes and cathodes manufactured by WPS

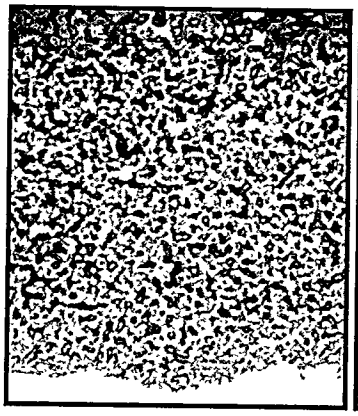

Figure 2 Microstructure of a double-layered SOFC-cathode (dark pores, dark gray LSM, light gray 8YSZ)

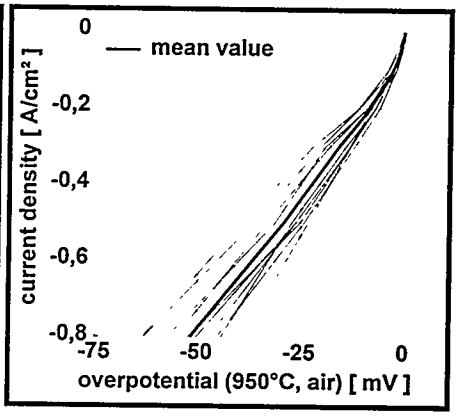

Figure 3 Electrochemical activity of 10 cathodes distributed in the 240x240 mm^2 coating area

STATUS OF SOFCo SOFC TECHNOLOGY DEVELOPMENT

R. Privette, M.A. Perna, K. Kneidel
SOFCo, a Babcock & Wilcox/Ceramatec Co.
1562 Beeson St, Alliance, Ohio 44601

J. Hartvigsen, S. Elangovan, A. Khandkar
SOFCo, 2425 South 900 We
Salt Lake City, Utah 84119

SOFCo, a Babcock & Wilcox / Ceramatec Research & Development Limited Partnership, is a collaborative research and development venture (formed in 1994) to develop technologies related to planar, solid-oxide fuel cells (SOFCs). SOFCo has successfully demonstrated a kW-class, solid-oxide fuel cell module operating on pipeline natural gas. The SOFC system design integrates the air preheater and the fuel processor with the fuel cell stacks into a compact test unit; this is the platform for multi-kW modules. The cells, made of tape-cast zirconia electrolyte and conventional electrode materials, exhibit excellent stability in single-cell tests approaching 40,000 hours of operation (see Figure 1). Stack tests using 10-cm and 15-cm cells with ceramic interconnects also show good performance and stability in tests for many thousands of hours.

Included in these efforts has been a program aimed at lowering operating temperatures of SOFCs. This has several advantages related to long-term stability and lower balance-of-plant costs. Under a program sponsored by the Electric Power Research Institute, SOFCo is evaluating ceria-based SOFCs operating in the temperature range of 650° - 800°C. Optimized cells that maximize ionic conductivity and stability in fuel conditions have led to stable operation for extended durations (see Figure 2). Also, stacks with zirconia electrolyte show stable performance (see Figure 3).

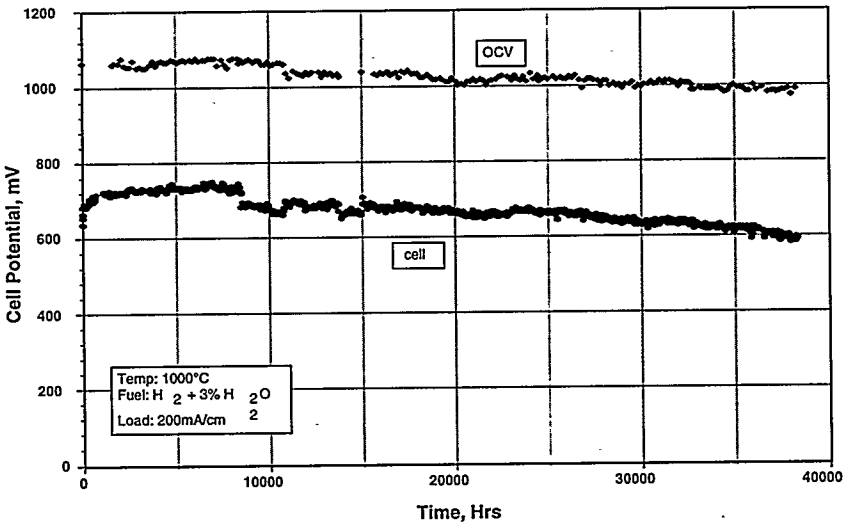

Figure 1: Endurance of SOFCo planar SOFCs

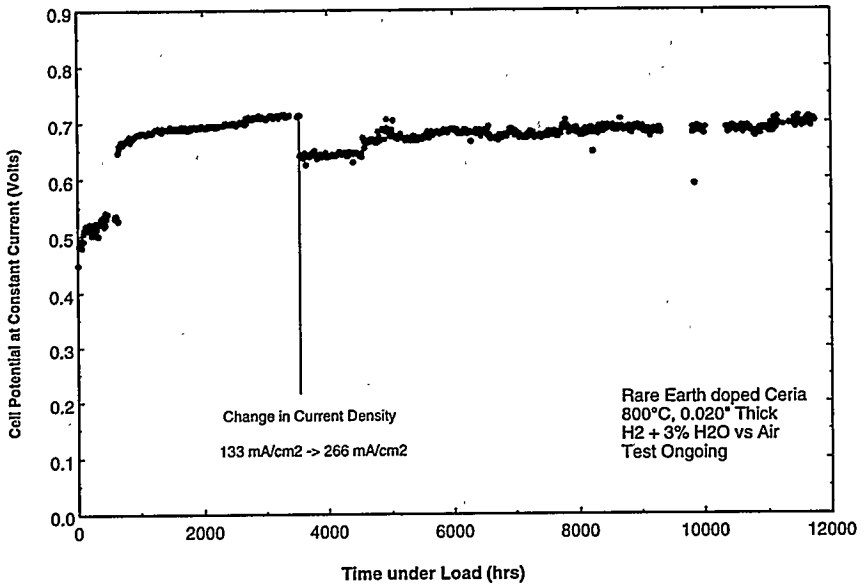

Figure 2: Endurance of low-temperature SOFCo planar SOFCs

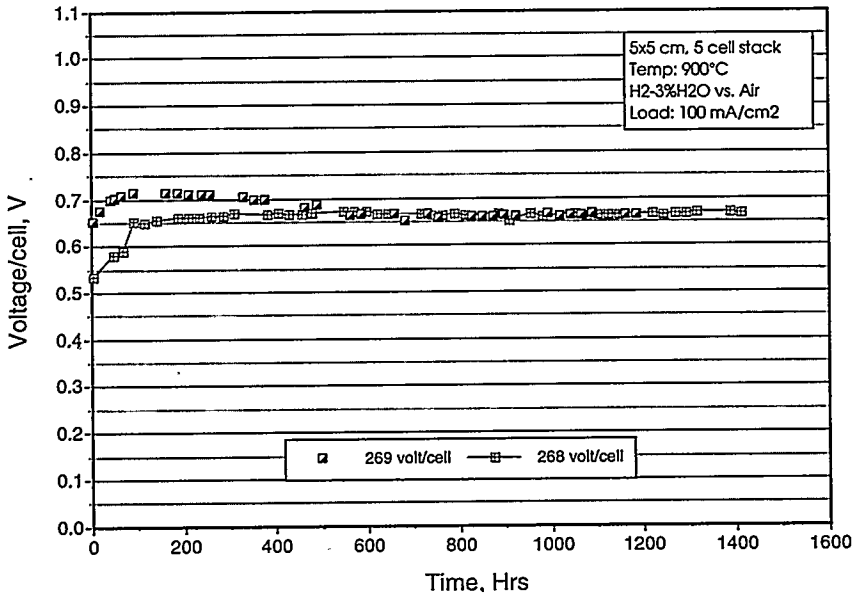

Figure 3: Performance of SOFCo planar SOFC stacks

In addition to natural-gas-fired systems, SOFCo is also currently developing compact, multi-kW fuel cell generators that operate on liquid fuel oil (diesel, JP-8, for example). In conjunction with the U.S. Defense Advance Research Projects Agency and the U.S. Army, SOFCo has recently achieved a first-of-a-kind demonstration of a planar SOFC stack operating on JP-8 logistic fuel. A partial oxidation fuel processor operating at 1 bar was used to convert the liquid fuel to a hydrogen-rich gas. The small size and fuel flexibility of systems based on this technology enable a wide range of mobile and remote power system applications and represent a significant advance in SOFC system technology.

Liquid fuel processing was demonstrated through partial oxidation of the sulfur-laden (500 ppm by weight) military logistic fuel at temperatures exceeding 1100°C, steam-to-carbon ratios of about 1.6, and fuel equivalence ratios of approximately 2.6 (actual fuel-to-air ratio divided by the stoichiometric fuel-to-air ratio). Figure 4 shows the JP-8 fuel conversion efficiency during the 100-hour test of the unit (higher heating value of CO + H_2 + CH_4 products divided by the higher heating value of the feed stock). Extensive work was performed to characterize the product gas composition under a variety of operating conditions. Hydrocarbon speciation, sulfur analysis, and soot formation were considered. Operating conditions were chosen to maximize net system efficiency.

Recent demonstrations of liquid-fueled systems were carried out in a new SOFC system test facility designed and built at the Babcock & Wilcox Research and Development Division's Alliance (Ohio) Research Center. The facility is capable of testing systems using liquid fuels (diesel, JP-8, gasoline), hydrogen, and other bottle gases. Figure 5 shows a schematic of the test facility. A combination of automatic and manual controls

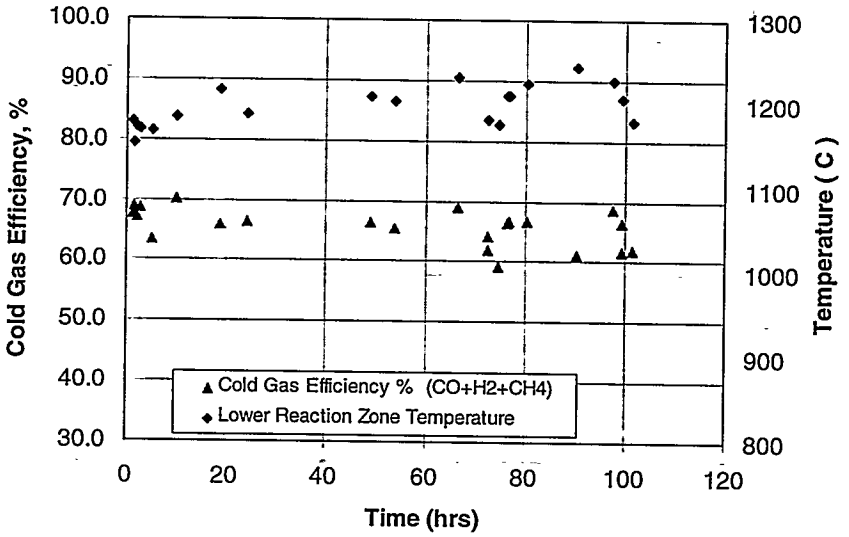

Figure 4: Logistics fuel conversion efficiency

allows significant operational flexibility while maintaining the capability of unattended test operation. Instrumentation is included to record system temperatures, pressures, flow rates, current, voltage, and power. This facility will be used to optimize systems incorporating thermal and physical integration of the generator components in support of SOFCo's ongoing product development activities.

SOFCo continues to develop new programs focusing on larger demonstrations, longer endurance, better performance, and lower cost. It is expected that SOFCo's first new products will incorporate and benefit from the research and development being performed today.

ACKNOWLEDGMENT

Portions of this work are sponsored by the U.S. Army Research Office. The content of the information does not necessarily reflect the position or the policy of the U.S. Government, and no official endorsement should be inferred.

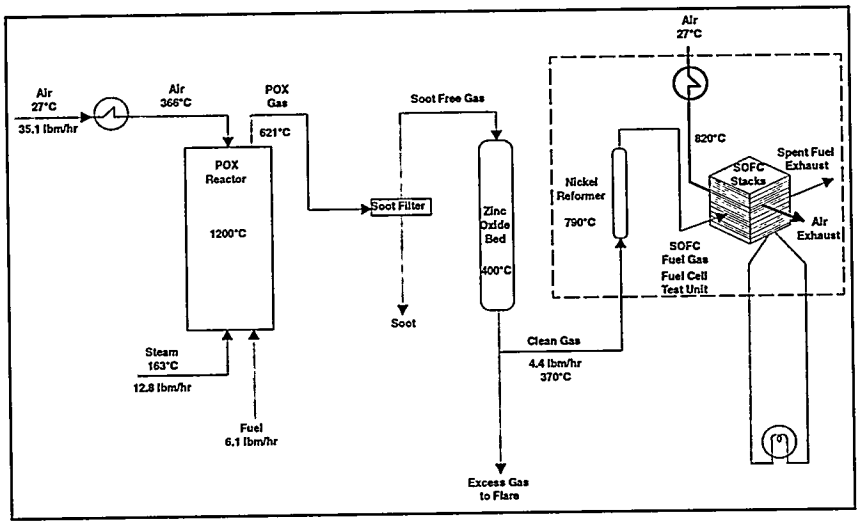

Figure 5: SOFCo system test facility schematic

IMHEX FUEL CELL REPEAT COMPONENT MANUFACTURING CONTINUOUS IMPROVEMENT ACCOMPLISHMENTS

L. A. Jakaitis, V. J. Petraglia, E. S. Bryson, J. F. Czerwien,
G. H. Garcia, K. Katsman, E. B. Petersen, S. L. Woods
M-C Power Corporation
8040 South Madison
Burr Ridge, Illinois 60521 U.S.A.
Phone 708.986.8040 Fax 708.986.8153

INTRODUCTION

M-C Power is taking a power generation technology that has been proven in the laboratory and is making it a commercially competitive product. There are many areas in which this technology required scale up and refinement to reach the market entry goals for the IMHEX® molten carbonate fuel cell power plant. One of the primary areas that needed to be addressed was the manufacturing of the fuel cell stack. Up to this point, the fuel cell stack and associated components were virtually hand made for each system to be tested. M-C Power has now continuously manufactured the repeat components for three (3) 250 kW stacks.

M-C Power's manufacturing strategy integrated both evolutionary and revolutionary improvements into its comprehensive commercialization effort. M-C Power's objectives were to analyze and continuously improve stack component manufacturing and assembly techniques consistent with established specifications and commercial scale production requirements. Evolutionary improvements are those which naturally occur as the production rates are increased and experience is gained. Examples of evolutionary (learning curve) improvements included reducing scrap rates and decreasing raw material costs by buying in large quantities. Revolutionary improvements result in significant design and process changes to meet cost and performance requirements of the market entry system. Revolutionary changes often involve identifying new methods and developing designs to accommodate the new process. Based upon our accomplishments, M-C Power was able to reduce the cost of continuously manufactured fuel cell repeat components from the first to third 250 kW stack by 63%. This paper documents the continuous improvement accomplishments realized by M-C Power during IMHEX® fuel cell repeat component manufacturing.

APPROACH OVERVIEW

M-C Power's approach was to analyze and develop improved stack component manufacturing techniques consistent with established specifications and commercial-scale production requirements. The approach was broken down into four major efforts. The first was the process and technology improvement program. M-C Power formed an Advanced Technology Group to lead this effort. They worked closely with M-C Power's Manufacturing and Engineering Departments as well as IGT and other subcontractors to develop concepts which significantly improved performance and durability and reduced manufacturing cost of the fuel cell stack. Much of this effort involved optimizing current manufacturing processes. These activities resulted in most of the "evolutionary" manufacturing improvements.

The second major effort in M-C Power's approach was to develop comprehensive manufacturing process descriptions. These descriptions include all of the process specifications, component formulations, production equipment requirements and procedures needed to continuously produce molten carbonate fuel cell stacks. This description pulls all of the technical know-how together and formulates it into a detailed set of "instructions" which were used to produce the product. This process helped to identify many of the ideas and concepts that resulted in the evolutionary improvements.

The third effort involved developing the procedures and evaluation system to control and monitor the production processes. This function is important to achieving a cost effective product. It is the link between the manufacturing goals and the actual manufacturing results. Heavy use of statistical process methods was employed during this phase.

The fourth effort was to conduct a Manufacturing Cost Study which would be used to analyze labor and material costs for internally manufactured and externally procured items to develop a total stack cost. Areas that had the highest impact on total cost were targeted for improvements first.

MANUFACTURING PLAN

The major task under this plan was to identify processes which required improvements in technology, design and cost. The principal objectives were to produce and define objectives and strategies that would satisfy both functional and physical requirements at a cost that is compatible with commercialization. The design must be manufacturable at a cost that will permit the item to be introduced competitively in the marketplace.

Objectives

In order to achieve the principal objective, consideration was given to the following areas:

1. To maximize -
   a. Simplicity of design,
   b. Use of economical materials that will satisfy the functional requirements,
   c. Use of economical manufacturing tooling , methods and procedures,
   d. Standardization of materials and components,
   e. Ease of assembly,
   f. Ease of inspecting and testing the product, and
   g. Maintainability of design

2. To minimize -
   a. Critical processes variation,
   b. Generation of scrap and waste,
   c. Procurement lead time,
   d. Special manufacturing tests and inspection procedures,
   e. Limited availability or high cost materials, items and processes

3. To evolve from project management to process management.

4. To modify designs so that they were easier to produce.

Strategy

The plan incorporated producability requirements not only during the conception and development of the process, but also during the production phases and throughout all of the manufacturing runs. The intent of this phase was to:

1. Identify customers's needs and values.
2. Establish price/volume and cost goals.
3. Specify product requirements.
4. Examine function vs. cost tradeoffs.
5. Prepare initial design, test cost viability.
6. Determine final product design and release for manufacture.

Plans

To support our goals and objectives, a plan was implemented to:

1. Identify and quantify component and unit operations which required improvement.
2. Establish Bills of Materials.
3. Define Change Control Procedures.
4. Address the transition required and implement the continuous improvement activities to move MCFC stack manufacturing processes from research and development orientation to commercial scale operation.
5. Alter current project-oriented manufacturing techniques to incorporate more efficient "Flow-Line" and "Work Cell Concepts"

Results

Throughout the three major MCFC Stack manufacturing runs, M-C Power:

1. Developed Manufacturing Resource Techniques to control through-put and quality.
2. Established a Documentation Base to include elements of the Base-line Product Design and Processes.
3. Established and managed under Change Control, a Single Data Base for Designs, Specifications, Master Inspection Plans and other product and process requirements.
4. Defined Methodology and procedural mechanisms for adoption of improved technology.
5. Developed requirements for On-Line Quality, Operator Training, Process Capability Studies and Statistical Process Control.

Production staffing and assignments were adjusted to achieve a two-shift mixing and tape casting capability, a three-shift sintering capability, and a two-shift cutting capability. Procedures were developed to maximize process throughput, while minimizing work-in-process inventory. The impact that this had on the production experience was to increase process yields, as "downstream" problems were identified in a timely manner. To prevent hidden, downstream quality problems, component tape casting runs were treated as lot quantities of one (1) and no additional mixes/casts were performed until components from the previous lot were completely processed. This operational change reduced the work-in-process between each lot to zero (0), thus allowing for process analysis to be completed and improvements to be implemented prior to the next lot. In most cases it was found that the fabrication of the components in large batch sizes necessitated altering and adjusting processes and procedures to address fabrication issues and problems previously unknown. Data collection procedures and reports were developed to accommodate the large manufacturing runs.

Flow diagrams were established identifying the inputs and outputs of each operation. To determine what improvements were required, each step of process was evaluated as to its cause and effect on quality (first pass yields), efficiency (production output and throughput) and effectiveness (cost per unit). After each manufacturing run, Manufacturing Analysis reports were generated, documenting all aspects of the production run.

To control the total quality of parts , a production 'pull' system was used to balance the line between tape casting and sintering. Manufacturing was treated as one continuous process with operations in series, instead of separate and individual processes, i.e. the output of the previous operation is the input to the next operation. Tape casting batch quantities were based upon the quantity of parts that could be processed through the furnace, this minimized the amount of Work-in-Process (WIP) between the two operations. No new lot was manufactured until the previous lot had been completed. Since each component is inspected after each operation, this allows defects to be analyzed

and corrective actions implemented prior to the manufacturing of the next lot. Elimination of causes of defects increased yields and maximized throughput. To maximize yields, variables were controlled. In conjunction with daily feedback, a multi-variate analysis was performed to identify man, machine, method, materials and environmental variables that affected the process.

After identifying bottle neck operations, work in process characteristics (queue size and wait time), general flow through the manufacturing plant was established. Steps were taken to eliminate bottle necks by identifying and eliminating sources of variations (root cause analysis), obtaining new and improved equipment in these areas, and implementing ways to increase process throughput.

Figure 1 shows significant progressive throughput improvements during the first three manufacturing runs.

250 kW STACK	UNOCAL	PDT-1	PDI-1
MFG. CYCLE RATE (RATIO)	1	0.42	0.32

Figure 1. Mfg. Cycle Rate Ratio

Manufacturing Cost Study

To complement the manufacturing analyses, M-C Power initiated a manufacturing cost study. The manufacturing cost study allowed the "interactive" evaluation of reductions in process waste, increased yields, reduced startup and setup times, and higher through-put rates and their effects on total plant capacity and costs. Additionally, the effect of raw material cost changes, part planform and thickness variations, part count adjustments and staffing/equipment assignments, were readily evaluated. The manufacturing cost study was used to evaluate the material, direct labor, and overhead costs associated with the fabrication of IMHEX® molten carbonate stack assemblies. The elements of the manufacturing cost study were used to determine (by Pareto Principle) where the best return on technology investment is to be found.

The manufacturing cost study provided valuable insight into the present manufacturing capabilities of M-C Power. Facility assumptions and staffing assignments were made allowing the evaluation of manufacturing capability and at the same time, showing the allocation of cost among the various stack components. Figure 2 shows progress cost savings during the first three manufacturing runs.

250 kW STACK	UNOCAL	PDT-1	PDI-1
MFG. COST (RATIO)	1	0.51	0.37

Figure 2 Stack Mfg. Cost Analysis

Conclusions

Based upon the identification and implementation of continuous improvement activities, M-C Power:

1. Reduced repeat component manufacturing cycle time by 68%.
2. Reduced repeat component cost by 63%.
3. Identified the key areas which need to be improved in order to reach commercialization goals.

INFLUENCE OF IMPURITY GASES AND OPERATING CONDITIONS ON PAFC PERFORMANCE

K. Hirai, N. Iwasa, M. Suzuki, O. Okada
Osaka Gas Co., Ltd.
4-1-2, Hiranomachi, Chuo-ku, Osaka 541, JAPAN

M. Matsumoto
Kobe Works, Mitsubishi Electric Corporation
1-1-2, Wadasaki-cho, Hyogo-ku, Kobe, Hyogo 652, JAPAN

INTRODUCTION

On-site Phosphoric Acid Fuel Cell (PAFC) Cogeneration system is installed at various test sites, such as at underground parking lot, within chemical plant premises and near urban streets. Since in the current PAFC system, cathode air is supplied to the cell with no particular pre-treatment, impurity gases in the air might influence on cell performance.

We have investigated the influence of various impurity gases in the cathode gas, on sub-scale single cells, and have found that NO_2, SO_2 and toluene affect negatively on cell performance. The results of these experiments and the conceivable mechanism of these effects on cell degradation are reported.

We have also investigated the influence of other operating parameters, such as temperature, current density, fuel utilization on cell performance. From these experiments, we have found that operating temperature is a significant factor, which mainly determines cell voltage decline rate. The results of sub-scale single cell tests and a short-stack verification test are also reported.

EXPERIMENTAL

The sub-scale single cells (manufactured by Mitsubishi Electric Corporation) with $100cm^2$ active electrode area were used in this study.

In these experiments, simulated reformed gas (SRG), which consists of 80% H_2, 19% CO_2 and 1% CO, was used for the anode gas. Cathode air is supplied from air compressor with test impurity gases.

The cell temperature is controlled at 185 ℃ with electric heater. Air utilization and fuel utilization is 50% and 80% respectively. Flow rates of fuel and air were controlled with mass-flow controllers, and adjusted precisely with a gas chromatography. Generated current was controlled with a DC electric load, and maintained at prescribed current density. Operating conditions are listed in Table 1.

Table 1 SUB-SCALE CELL OPERATING CONDITIONS

ITEM	CONDITIONS
CELL SIZE	100cm2
PRESSURE	1 ata
TEMPERATURE	185℃ (170-210℃)
CURRENT DENSITY	300mA/cm2 (100-300mA/cm2)
AIR UTILIZATION	50%
FUEL UTILIZATION	80%
FUEL COMPOSITION	H2 80%, CO2 19%, CO 1%

Table 2 INFLUENCE OF IMPURITY GASES

IMPURITY	VOLTAGE LOSS	POISONING
NO2	-45mV @10ppm -20mV @1ppm	restorable
NO	no influence	
SO2	-5mV @10ppm -20mV @40ppm	restorable
CH4	no influence	
C7H8	-4mV @10ppm	restorable

RESULTS AND DISCUSSION

(1) INFLUENCE OF IMPURITY GASES

Cathode impurity gases, such as NO_2, NO, SO_2, CH_4 and C_7H_8 (toluene) were introduced in the air, and influences on cell voltage were examined. These results were summarized in Table 2.

(a) NOx

In adding 10ppm NO, voltage loss is negligible even in the long-term test. Whereas, in the case of NO_2, obvious cell voltage drop was observed. Fig. 1 shows the influence of NO_2 in the air on cell performance. Various concentrations of NO_2 were added repeatedly on the same cell.

Cell voltage drop depends on NO_2 concentration and added duration time. It became more than 40mV with 100ppm for about 50 hours, about 45 mV with 10ppm for about 1,000 hours, and about 20mV with 1ppm for about 700 hours.

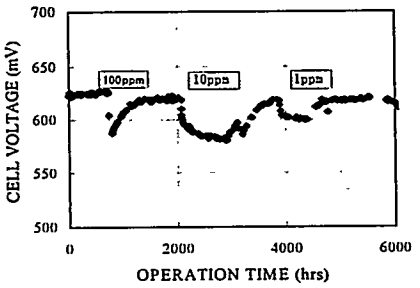

Fig.1 INFLUENCE OF NO2 ADDITION

On terminating NO_2 addition, cell voltage recovered gradually to the initial voltage.

Overall cell voltage decline rate became about 3mV/1,000h, which is normal value at this temperature. This result indicates that NO_2 poisoning is not permanent but temporary.

In our other experiments, it is found that NO_2 adsorbs on the Pt-Alloy catalyst, it reduces active surface area for oxygen reduction, and consequently causes cell voltage drop. In voltage recovering process, this adsorbed NO_2 is probably reduced into N_2, and then is released from cathode.

$$2NO_2 + 8H^+ + 8e^- \rightarrow N_2 + 4H_2O$$

Cell voltage drop at 0.1ppm NO_2 was not observed on another cell. Considering the environmental standard, which requires less than 50~70ppb NO_2, the effect of NO_2 in the air is negligible in practice. However, this influence is so significant that air inlet of PAFC should be kept enough distance from air exhaust outlets of gas engine and gas turbine. In addition, air has to be ventilated sufficiently at indoor parking lot.

(b) SOx

When introduced SO_2 concentration is less than 1ppm, sizable cell voltage drop was not observed. On the other hand, in adding 40ppm SO_2, cell voltage drops by about 20mV within 30 minutes. However, in terminating SO_2 addition, cell voltage recovers to the previous value also within 30 minutes. This result indicates that SO_2 adsorbs physically on the surface of cathode catalyst, but it can be released quite easily from its surface.

(c) TOLUENE

Painting of floors, walls and piping near PAFC unit is a common work at field test sites. Therefore, we investigated the influence of toluene (C_7H_8), a common solvent of paint. It was revealed that toluene affects adversely on cell performance, and this process also occurs quickly like the case of SO_2. However, in this case, toluene seems to be combusted on cathode catalyst. In our other experiments, it is verified that catalyst combustion occurs at as low as 180℃.

Therefore, solvents like toluene have to be removed by the active carbon filter, or it would be better to shut down PAFC unit for safety during paint works.

(2) INFLUENCE OF OPERATING CONDITIONS

Osaka Gas Co., Ltd. has been operating more than 42 units of PAFC cogeneration system. In addition to field operation, we are also investigating the influence of operating parameters, such as temperature, current density, fuel utilization and load change by using these sub-scale single cells. Although real influence should be verified on short-stacks or real cell stacks, sub-scale single cell tests are effective to survey operating parameters respectively.

(a) TEMPERATURE

We examined the influence of operating temperature at 170, 185, 215℃. Fig.2 shows the relationship between operating temperature and cell voltage decline rate. As operating temperature increased, cell voltage decline rate increased exponentially.

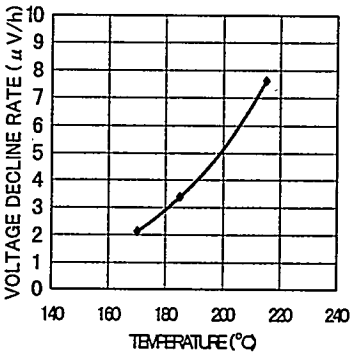

Fig2 INFLUENCE OF TEMPERATURE

(b) CURRENT DENSITY

We also examined the influence of current density at 100, 200, 300 mA/cm^2. Although at lower current density higher cell voltage decline rate was expected because of higher cell voltage, lower cell voltage decline was observed at low current density in reverse. Considering our small number of tested cells, it cannot be concluded that higher current density has an adverse effect on cell performance. However, it can be said that lower current density as low as 100 mA/cm^2 does not accelerate cell degradation.

(c) OTHER OPERATING CONDITIONS

The cell life test under higher fuel utilization at 94% did not show increase of cell voltage decline rate. In real cell stacks, fuel utilization influences more severely due to larger distribution of current and hydrogen concentration, but this result suggests the possibility of higher electrical efficiency PAFC system.

Load change from 150 mA/cm^2 to 300 mA/cm^2 are applied to the sub-scale cell more than 1,000 times, but sizable difference from normal condition was not observed either.

(3) LOW CURRENT DENSITY AND LOW TEMPERATURE PAFC

(a) SHORT-STACK TESTS

The cell life of PAFC is said to be mainly dependent on following three factors,

1) Sintering of Electrocatalyst
2) Flooding of Electrode
3) Loss of Electrolyte (Phosphoric Acid).

If operating temperature is lowered, catalyst sintering and corrosion of carbon material and PTFE will be eased quite obviously. Since loss of electrolyte depends on the vapor pressure of phosphoric acid, lowering temperature is expected to extend the life of electrolyte exponentially.

Although lowering temperature is considered to accelerate corrosion of carbon material due to lower concentration of phosphoric acid, our experiments on sub-scale cells indicate that above mentioned factors are more dominant in determining cell degradation.

In general, current density itself is supposed not to influence on cell

Table 3 SHORT-STACK SPECIFICATIONS

CURRENT DENSITY	150mA/cm2
NUMBER OF CELLS	20
ACTIVE CELL AREA	4,000cm2 class
FUEL UTILIZATION	80%
AIR UTILIZATION	60%
FUEL	13A Reformed Gas

degradation on sub-scale single cells. However, in real cell stacks, as current density increases, average cell temperature also increases due to increase of generated heat.

Therefore, we fabricated the short-stack with large cells, which are developed for on-site 200kW system, and have been operating this short-stack at lower current density than that of 200kW system. Although the temperature of cooling water remains same, the average cell temperature is reduced by approximately 15℃, if current density decreases from 300 mA/cm^2 to 150 mA/cm^2 .

Operating conditions are summarized in Table 3, and the time course change of cell voltage is shown in Fig. 3.

Operation time is still less than 5,000 hours, but very small voltage decline is observed even at the initial stages. It can be expected to achieve cell life extension by reducing current density.

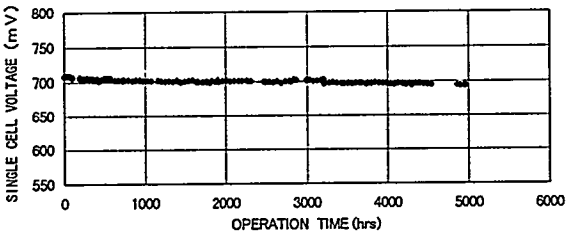

Fig3 SHORT-STACK SINGLE CELL VOLTAGE

(b) SYSTEM EVALUATION

As current density decreases, cell voltage increases and consequently higher electrical efficiency can be obtained. In this system, since current density is lowered to 150 mA/cm^2, it is possible to increase electrical efficiency up to 45% (LHV) by adding minor system design modification. Low Current Density PAFC system has following merits and demerits over conventional PAFC.

MERITS	DEMERITS
① Longer Cell Life by Lowering Average Temperature	① Higher Initial Manufacturing Cost
② Higher Electrical Efficiency	② Lower Heat Recovery
	③ Heavier System Weight

According to our feasibility study of Low Current Density PAFC, if system manufacturing cost is lowered up to $3,000/kW (manufacturing cost of cell stack assembly is estimated 1/3 of total system cost), merits of cell life extension and electrical efficiency increase, exceed demerits of initial cost increase and steam recovery decrease.

CONCLUSIONS

We had following conclusions through our sub-scale single cell tests and a short-stack verification test.

① Cathode impurity gases, such as NO_2, SO_2, toluene have an adverse effect on cell performance. However, considering admissible concentrations of those impurity gases, no pre-treatment will be required under normal conditions.

② Because NO_2 has a striking influence on cell performance at such low concentration as 1 ppm, inlet of supplied air has to be installed properly.

③ From parameter surveys on single sub-scale cells, operating temperature is a significant factor, which mainly determines cell degradation rate.

④ Lowering operating temperature appears effective to extend cell life from short-stack tests.

⑤ From results of our feasibility study, Low Current Density PAFC becomes more profitable on account of longer cell life and higher electrical efficiency, if cell manufacturing cost becomes less than $ 1,000/kW.

Estimation of current density distribution of PAFC by analysis of cell exhaust gas

S. Kato, and A. Seya
Fuji Electric Co.,Ltd.
7 Yawatakaigan-dori Ichihara-shi 290, Japan

A. Asano
Fuji Electric Corporate R&D.,Ltd.
2-2-1 Nagasaka Yokosuka-shi 240-01, Japan

INTRODUCTION

To estimate distributions of current densities, voltages, gas concentrations, etc., in phosphoric acid fuel cell (PAFC) stacks, is very important for getting fuel cells with higher quality. In this work, we have developed a numerical simulation tool to map out the distribution in a PAFC stack. And especially to study current density distribution in the reaction area of the cell, we analyzed gas composition in several positions inside a gas outlet manifold of the PAFC stack. Comparing these measured data with calculated data, the current density distribution in a cell plane calculated by the simulation, was certified.

EXPERIMENTAL

Analysis of cell exhaust gas

Configuration of the short stack used in this work is as follows: the electrode area of 2000cm^2 (square shaped), the gas cross flow type, the construction of 6cells/cooler, the average current density of 300mA/cm^2 (the load current of 600A), the average cell temperature of 190°C, the operating pressure of atmosphere. To obtain the exhaust gas from gas channel, sampling tubes were put into the outlet gas manifold as shown in Fig.1. Gas compositions were measured in dry base under several operating conditions with changing temperature distribution of cooling plate, oxygen utilization and hydrogen utilization. The temperature distributions of cooling plate are shown in Fig.2. In the case1, temperature distribution was uniform, in the case2 and the case3, there were some tendency along with air flow.

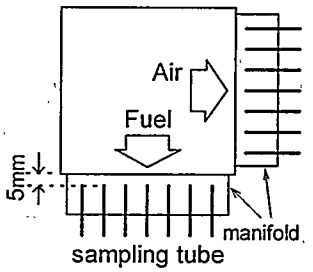

Fig.1 A schematic diagram of an apparatus for gas sampling.

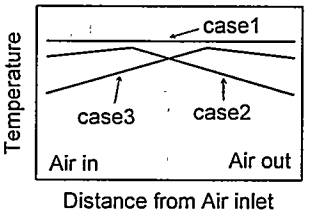

Fig.2 Temperature distribution of cooling plate.

Method of simulation

The algorithm of the present simulation is schematically shown in Fig.3 where Vcell is the stating cell voltage, $J(x,y,z)$ the current densities, $PH2(x,y,z)$ and $PO2(x,y,z)$ the hydrogen and oxygen concentrations, respectively, $T(x,y,z)$ the temperature, ΔP_{fuel} and ΔP_{air} the pressure losses through the fuel and air channels respectively [1]. The model stack consists of 6cells, and each cell was divided into 400 elements (20×20) for the finite difference method. The feature of our simulation is that the analysis is based on actual *V-I* output characteristics of a small area (approximately 3cm^2) PAFC. To cover the variation in a

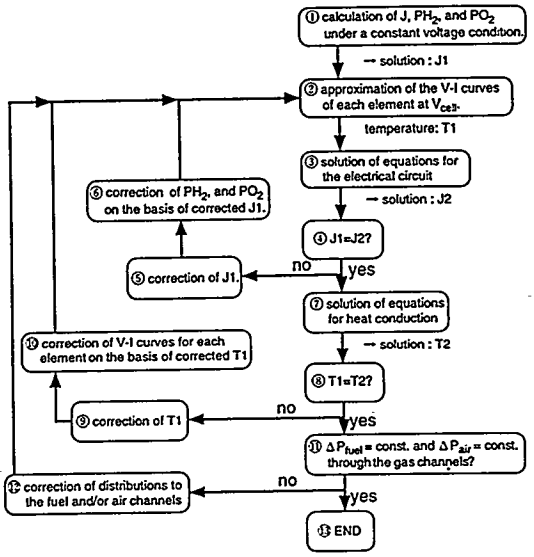

Fig.3 Algorithm of simulation.

PAFC stack, the *V-I* characteristics are taken under a wide range of various conditions. In the measurement, both flow rates for fuel and air are so determined that the gas velocities over the small cell are equal to those in a large area fuel cell stack. Due to the high flow rates for the small cell, the hydrogen and oxygen concentrations are practically uniform over the electrode.

RESULT AND DISCUSSION

Variation of cell exhaust gas composition

Fig.4 shows characteristics of hydrogen concentration deviation at the fuel outlet with three temperature distributions of cooling plate. In case1 with uniform temperature distribution of cooling plate, a minimum value of hydrogen concentration appeared near the air inlet area. It suggests that current density is large at the area where is high oxygen concentration. When temperature at the air outlet area of cooling plate is lower than case1, the hydrogen concentration near the air inlet position decrease (case2). On the other hand, when temperature near the air inlet area is lower, the hydrogen concentration near the air inlet position increase (case3). These results suggest that the temperature distribution of cooling plate influences temperature distribution of cell, and it causes variation of current

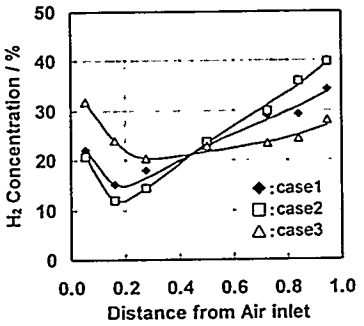

Fig.4 Measured hydrogen concentration at the fuel outlet with various temperature distribution of cooling plate. The average current density is 300mA/cm^2, the hydrogen and oxygen utilization are 80% and 50%, respectively, and hydrogen concentration is 65% at the inlet.

density.

Fig.5 shows the characteristics of hydrogen concentration deviation at the fuel outlet under various oxygen utilization in the case1. The hydrogen concentrations near the air inlet area decrease as oxygen utilization increasing. It suggests that deviation of oxygen concentration in the reaction area becomes larger with higher utilization of oxygen, then current density increase at the area where the oxygen concentration is relatively high. Fig.6 shows the characteristics of oxygen concentration deviation at the air outlet under various hydrogen utilization. The oxygen concentration slightly changes as hydrogen utilization changing.

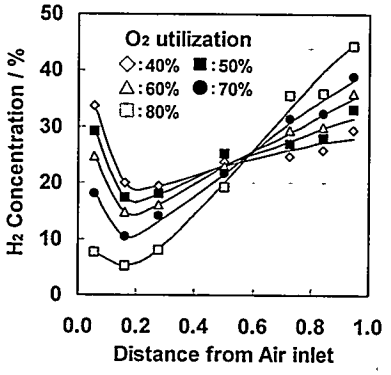

Fig.5 Measured hydrogen concentration at the fuel outlet under various oxygen utilization. The average current density is 300mA/cm^2, the hydrogen and oxygen utilization are 80% and 40-80%, respectively, and hydrogen concentration is 65% at the inlet.

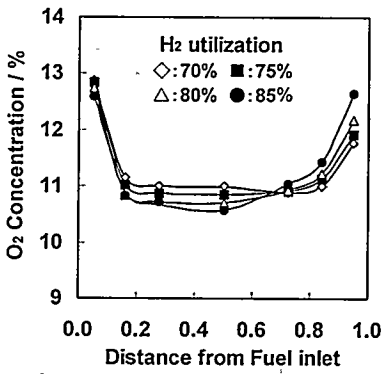

Fig.6 Measured oxygen concentration at the air outlet under various hydrogen utilization. The average current density is 300mA/cm^2, the hydrogen and oxygen utilization are 70-85% and 50%, respectively, and hydrogen concentration is 65% at the inlet.

Simulation

Calculated results of hydrogen concentration deviation at the fuel outlet compare with measured value under oxygen utilization of 50 and 70% in Fig.7. The calculated results almost correspond with the measured one. Fig.8 shows the contour plots of the distributions of current density over the middle (No.3 and 4) cells of the 6-cell-stack, which were calculated under oxygen utilization of 50 and 70%, hydrogen utilization of 80%, average current density of 300mA/cm2, and hydrogen concentration of 65% at the inlet. The current density varies in the range of 250-360mA/cm^2 over the electrode under oxygen utilization of 50%. Under oxygen utilization of 70%, the range of the current density expands into 230-380mA/cm^2.

CONCLUSION

1) In the case of cross flow cell, a minimum point of hydrogen concentration exits near the air inlet area.
2) Temperature distribution of cooling plate influences current density distribution.
3) Hydrogen concentration near the air inlet area decrease as oxygen utilization increasing. On the other hand, oxygen concentrations change little as hydrogen utilization

changing.

4) Calculated results of hydrogen concentration deviation at the fuel outlet almost correspond with the measured results.
5) Calculated result shows that current density varies in the range of 250-360mA/cm^2 over the electrode under oxygen utilization of 50%. Under oxygen utilization of 70%, the range of the current density expands into 230-380mA/cm^2.

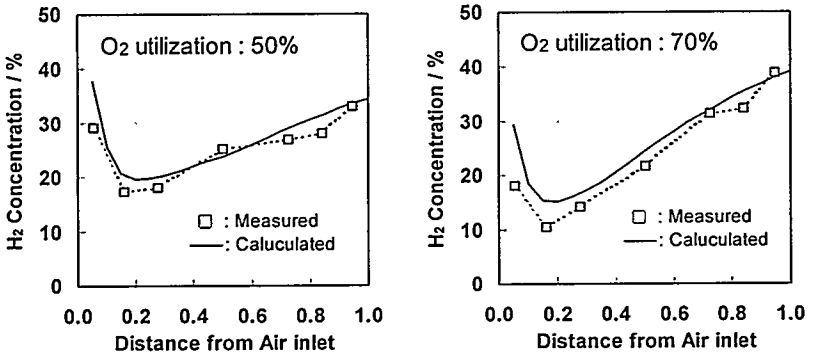

Fig.7 Measured and calculated hydrogen concentration at the fuel outlet. The average current density is 300mA/cm^2, the hydrogen utilization is 80%, and hydrogen concentration is 65% at the inlet.

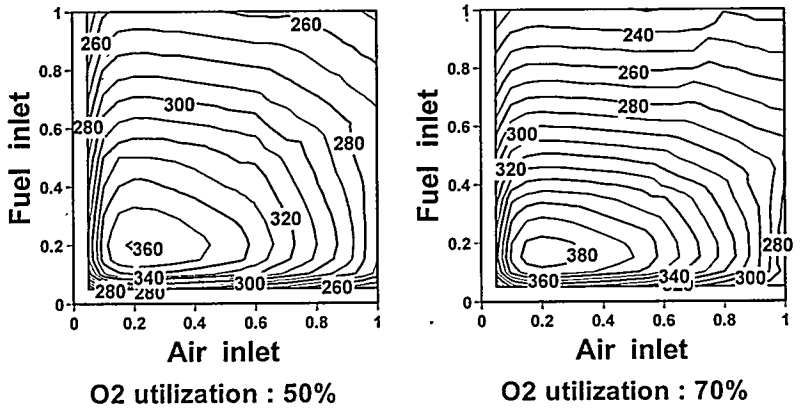

Fig.8 Distribution of current density over the middle cells. The average current density is 300mA/cm^2, the hydrogen utilization is 80%, and hydrogen concentration is 65% at the inlet.

REFERENCES

[1] A.Asano et al , *Denki-Kagaku*, Vol.64, No.6, pp.443-448 (1996)

ACID DISTRIBUTION IN PHOSPHORIC ACID FUEL CELLS

I. Okae, A. Seya, M. Umemoto
Fuji Electric Co.,Ltd
7 YawataKaigan-dori Ichihara-shi Chiba 290, Japan

Introduction

Electrolyte acid distribution among each component of a cell is determined by capillary force when the cell is not in operation, but the distribution under the current load conditions had not been clear so far.

Since the loss of electrolyte acid during operation is inevitable, it is necessary to store enough amount of acid in every cell. But it must be under the level of which the acid disturbs the diffusion of reactive gases. Accordingly to know the actual acid distribution during operation in a cell is very important.

In this report, we carried out experiments to clarify the distribution using small single cells.

A phenomenon of acid transfer

To estimate the acid distribution among components of a cell, the acid fill level (AFL) of each of them was measured. The AFL is defined as the ratio of the volume of absorbed acid to the total pore volume of each component.

When the AFL is measured after cell operation in general, the measured values represent the acid distribution determined almost by capillary forces of each component. It is not necessarily the distribution during operation, because it takes many minutes or some hours to disassemble the cell into each parts. And no descriptions concerning the time of disassembly can be seen in the papers which deal with the acid distribution in a cell [*e.g.* 1]. Therefore we used a special holder and simple structure cells which could be disassembled into each component within extremely short time, thus measured the acid distribution of the load conditions.

Figure 1 shows the single cell used in this study. Each catalytic layer of cathode and anode (A-Cat & F-Cat) was supported by porous carbon substrate (A-Sub & F-Sub). Effective area of each electrode was 3cm^2, and the ribbed plates (A-RP & F-RP) made of porous carbon were set for reactive gases at upper and lower of each electrode.

The weight of every component was measured in advance. In this experiment, the acid

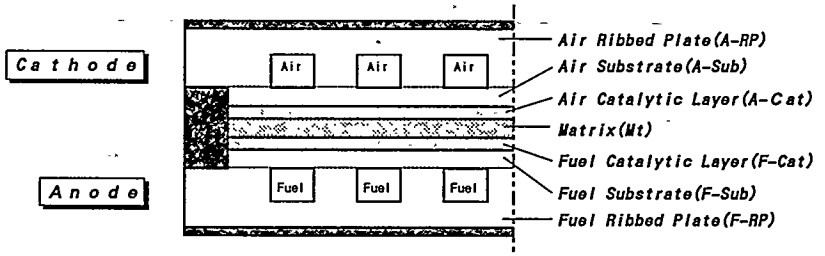

Fig.1. Configuration of the single cell

was loaded only in matrix and in each electrode (it means in both Cat and Sub), not in each RP, at the fabrication of the cell. The cells were tested for 16 hours under two conditions written below. After the test, the cells were disassembled within extremely short time, and the AFL of each component was measured by the weight changes of them.

Condition 1: Open circuit with reactive gases

Condition 2: Current load of 300mA/cm^2.

Figure 2 shows the weight changes of acid in each component, *i.e.* subtracted values of the initial weights from the final weights. Figure 3 shows the AFL after this test.

In the condition 1, the acid in A-Sub and F-Sub decreased almost the same weights, and the acid in A-RP and F-RP increased which approximately corresponded to the loss weights of each Sub. The weight changes of acid in the catalytic layers and the matrix were few. The distribution of the acid between each component was equal to the estimated balance based on the pore size distribution of each component.

In the condition 2, the weight gain of A-RP decreased to 18% of that of condition 1, and that of F-RP increased on the contrary about 1.5 times. Moreover, the acid decrease of A-Sub was greater than that of F-Sub ; the AFL of A-Sub decreased in the vicinity of 0%.

From the results mentioned above, under open circuit condition, the acid was distributed according to the capillary force of each component, regardless of electric potential level or the kinds of gases in each electrode. But when the cell was operated, the acid which was initially loaded in A-Sub and which had been absorbed in A-RP in condition 1 was

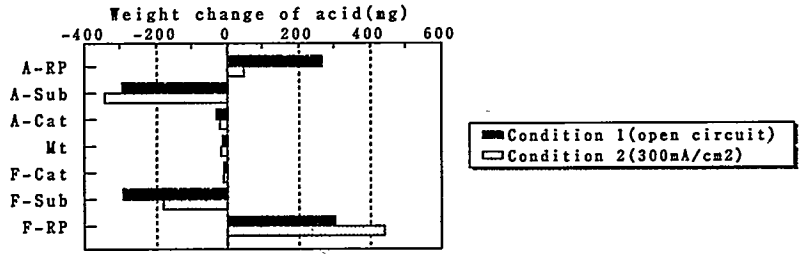

Fig.2. Weight change of acid in each component
(After 16 hours test, at 190℃, PH2/PO2=100%/21%)

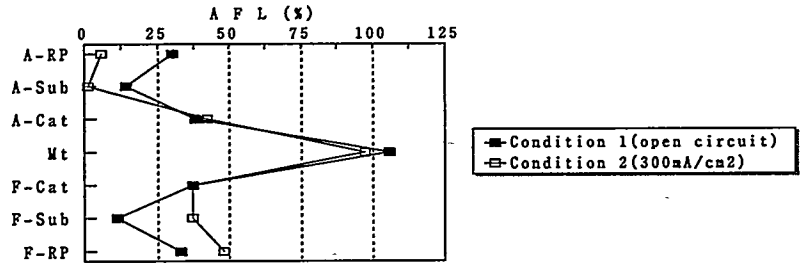

Fig.3. Final Acid fill level(AFL) of each component
(After 16 hours test, at 190℃, PH2/PO2=100%/21%)

transferred to the direction of anode. Consequently a driving force that transfers the acid toward anode exists in a cell during the cell operation.

Tanuma *et al.* conducted an investigation [2] concerning this force, and it was concluded to be electroosmotic pressures generated in the catalytic layers.

The relation between the driving force and current density

To investigate the relation between the acid driving force and current density, the same configuration cells as figure 1 were used. For this experiment the F-Sub was wet-proofed with PTFE dispersion. The purpose of this treatment was to make the difference of the driving force emphasize against the current density. A-RP was loaded with the acid of about 35% AFL at the fabrication of the cell, but not loaded in F-RP. After operating conditions of 150, 300, 600mA/cm^2 for two hours respectively, the AFL of each component of the cell was measured in the same method as the previous section.

The weight of F-RP increased in every current density condition, that means the driving force at these current densities is stronger than the acid repellency force of F-Sub.

Figure.4 shows the correlation between the AFL of both RP and the current density. The AFL of F-RP linearly increased with the increase of the logarithm of current density, and the AFL of A-RP decreased to the contrary of that of F-RP. These findings indicated that the intensity of the driving force increased with the increase of current load.

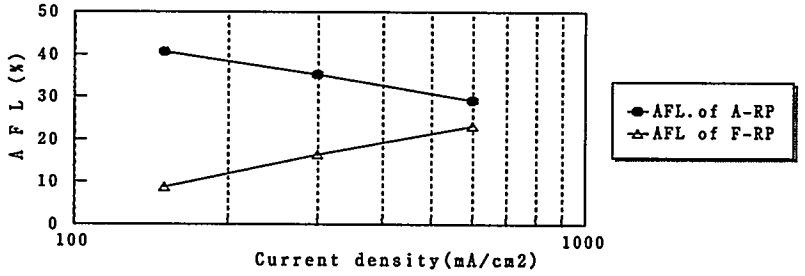

Fig 4. Relation between current density and AFL
(After 2 hours operation, at 190℃, PH2/P02=100%/21%)

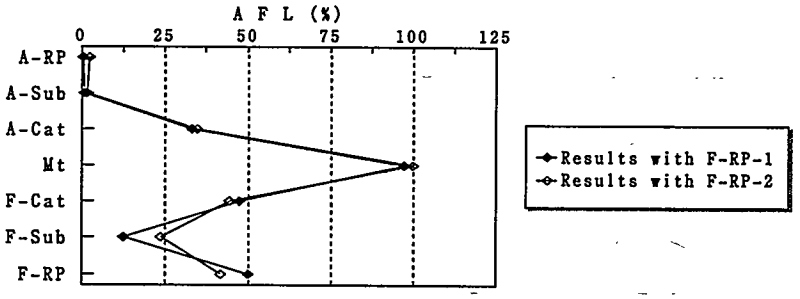

Fig.5. Final AFL of each component
(After 100 hours operation at 600mA/cm2, 190℃, PH2/P02=100%/21%)

The Relation between the driving force and capillary force

In this section also were used the same configuration cells as the figure 1. Both A-Sub and F-Sub were not wet-proofed, and in A-RP was loaded acid of 17% AFL at the fabrication of the cell, not loaded in F-RP. Two kinds of F-RP were prepared for this test ; the pore size of one F-RP (F-RP-1) was much smaller than that of each Sub, and that of the other one (F-RP-2) was bigger than that of F-RP-1 but a little smaller than that of each Sub. Two kinds of cells which used these F-RP were operated for 100 hours at 600mA/cm^2 (enough conditions to attain equilibrium state of acid distribution) and then the AFL of each component was measured.

Figure 5 shows the final AFL after this operation. In both cases, the AFL of catalytic layers scarcely changed, that was, the capillary force which was composed by the particles of catalyst was stronger than the driving force. Same results were obtained under the load conditions of 300 and 150 mA/cm^2 operation. Also the AFL of matrix didn't change and remained approximately 100%. It meant the capillary force of matrix was stronger than the driving force in the cell.

The AFL of RP and Sub were as follows. When the F-RP-1 was used, the AFL of F-Sub decreased to about 12%. Meanwhile with the use of F-RP-2, AFL of the F-Sub was about 24%. It is noted that these balances of the AFL between F-RP and F-CP was approximately in accordance with the balance which could be estimated by the pore size distribution of Sub and RP. Consequently the driving force was generated neither in F-Sub nor in F-RP.

On the other hand, the acid loaded in A-Sub and A-RP was transferred to anode and the AFL decreased almost to 0% in either case of F-RP-1 and F-RP-2. These results were also the same when operated at 300 and 150mA/cm^2. Hence the driving force was stronger than the capillary force of A-Sub and A-RP.

Conclusion

We have revealed the dynamic distribution of electrolyte acid during a cell operation ; the acid loaded in A-RP and A-Sub is transferred to anode by a force other than the capillarity. The strengths of the driving force depends on the current density. In general the force is stronger than the capillary force of Sub and RP, but weaker than that of catalytic layers and matrix. The driving force is generated neither in F-Sub nor in F-RP.

These results are useful for the design of phosphoric acid fuel cells.

Acknowledgment

The authors are sincerely grateful to Mr. Harashima and Mr. Sugiyama for their useful suggestion, and to Mr. Tadano for his great assistance in the experiments.

References

(1)T.Mori , *et al.* *J. Electrochem. Soc.* ; vol. 135, 1104 (May 1988)

(2)R.Tanuma and H.Nishihara, "Electroosmotic electrolyte transport in phosphoric acid fuel cells" The 2nd International Fuel Cell Conference, February 5-8, 1996, JAPAN.

DEVELOPMENT OF PORTABLE FUEL CELLS

K.Nakatou, S.Sumi and N.Nishizawa
Sanyo Electric Co.,Ltd.
1-1 Dainichi-higashimachi,Moriguchi City
Osaka 570, Japan

INTRODUCTION

Sanyo Electric has been concentrating on developing a marketable portable fuel cell using phosphoric acid fuel cells(PAFC). Due to the fact that this power source [1,2]uses PAFC that operate at low temperature around 100 °C , they are easier to handle compared to conventional fuel cells that operate at around 200 °C , they can also be expected to provide extended reliable operation because corrosion of the electrode material and deterioration of the electrode catalyst are almost completely nonexistent. This power source is meant to be used independently and stored at room temperature. When it is started up, it generates electricity itself using its internal load to raise the temperature. As a result, the phosphoric acid (the electolyte) absorbs the reaction water when the temperature starts to be raised (around room temperature). At the same time the concentration and volume of the phosphoric acid changes, which may adversely affect the life time of the cell. We have studied means for starting, operating PAFC stack using methods that can simply evaluate changes in the concentration of the electrolyte in the stack with the aim of improving and extending cell life and report on them in this paper.

EXPERIMENTS

A 250W portable fuel cell (hereafter referred to as the power source) was used for the experiments. 30 cells with 190 cm^2 of active electrode area were used in the stack. The supply and removal of water from inside the stack can be calculated by measuring the amount flow, temperature and humidity of the reactive gas supplied to the stack and the exhaust from the stack. However, when weight changes in the stack are measured from when this power source is being stored until it is started up, operated and stopped, it is thought that the amount and rate of water accumulated in the stack and the amount and rate of exhaust from the stack can be calculated with greater ease and more accuracy. Figure 1 shows the method used in the experiment. The power source was placed on an electronic balance. Weight data and power source operation data were sent to and recorded in a computer. Fuel hydrogen was supplied to the stack through a tube from a hydrogen gas cylinder. The concentration and volume of the phosphoric acid were calculated in the following manner.

(1) The amount of the phosphoric acid when the stack was assembled was used for the amount in the stack.
(2) The temperature and humidity of the atmosphere around the stack was measured immediately before it was started up, and the initial phosphoric acid concentration value was calculated from the relationship[3]between the steam pressure and concentration of the phosphoric acid water solution.
(3) It was assumed that all weight changes were the result of the phosphoric acid absorbing and releasing the water.
(4) It was assumed that only the phosphoric acid within the active electrode area absorbed and released water.
(5) It was assumed that concentration of the phosphoric acid in each component of the electrode was uniform.

RESULTS

Figure 2 shows the progress of the stack current, temperature, weight, concentration and volume

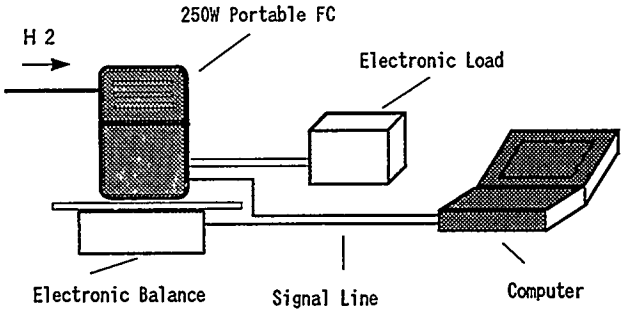

Figure 1 Schematic illustration of experiments

of the phosphoric acid calculated from changes in the weight of stack after the power source has been started and operated with a 100% load for about one hour. Weight changes were plotted as the difference from the weight when the power source was first started up, or 0. From these weight changes, it was found that water was being stored inside the stack until the stack's temperature reached 85 °C . Between 85 °C and 95 °C , the rate of water absorption and removal was equal, and when the temperature exceeded 95 °C , the removal rate exceeded the absorption rate. The initial phosphoric acid concentration was 90% and reached its lowest of approximately 80% 13 minutes after the power source was started up. At the same time, phosphoric acid's volume reached its highest level of approxmately 0.8cm ^{3} /g, a 20% increase over the initial volume. It was found that 50 minutes after power source was started up, the weight was equal to the initial value, and all the water that had been accumlated in the stack had been removed outside the stack. Using these start up and operation patterns, the average cell voltage fell at a rate of approxmately 0.1mV/cycle·cell (more than 700 cycles), yielding a favorable result. When considering applications as a potable power source however, it may be used in a variety of ways, and with varying frequency. Therefore, stack durability and reliability must be established to allow it to meet a variety of operation modes. As an example of these studies, Figure 3 indicates the weight changes when the load on this power source varies.

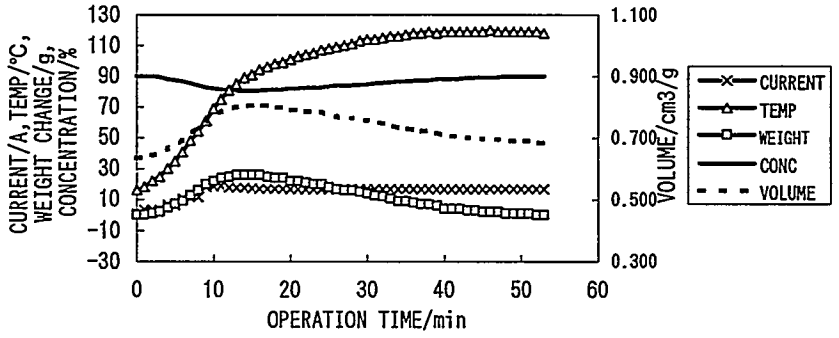

Figure 2 The progress of the stack's data

The controlled temperature was the same for each load. It was found that when the power source is operated in such a manner, its weight decreased in accordance with the reduction of the load. In the same manner, the concentration of the phosphoric acid increased and the volume was reduced the more the load reduced. Figure 4 shows the results when the controlled temperature is changed to maintain the same stack weight regardless of the load. The stack weight could be maintained at a relatively even level by setting the controlled temperature to

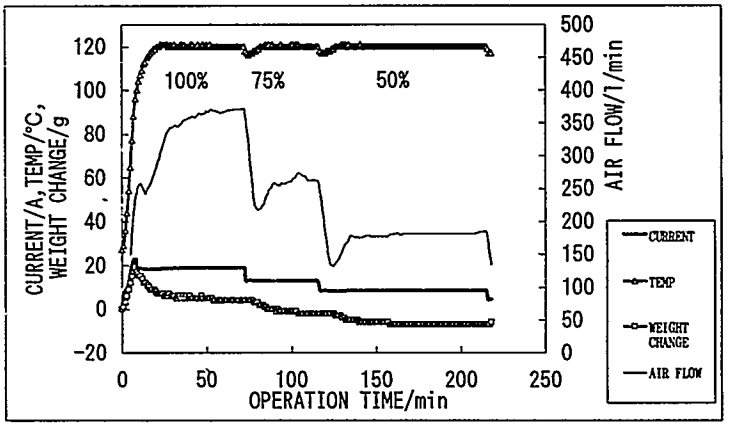

Figure 3 Weight change in the case of control method A

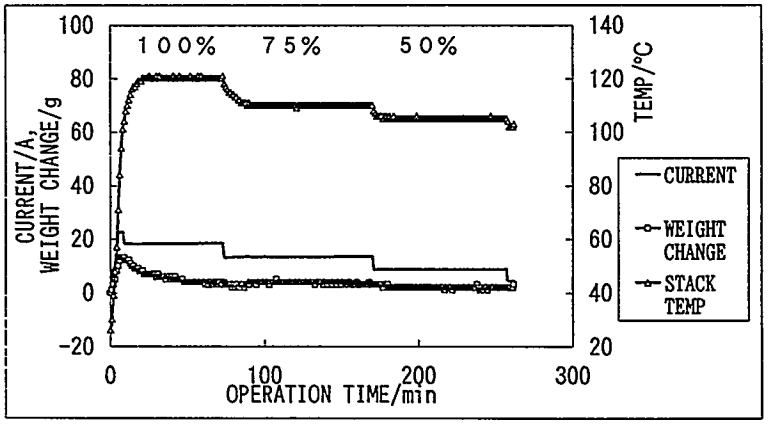

Figure 4 Weight change in the case of control method B

120 °C when the load was 100% , 110 °C when it was 75%, and 105 °C at 50%. Figure 5 shows the lifetime cycling characteristics at a 50% load both when the controlled temperature is maintained for each load (control method A), and when it is changed according to the load (control method B). Cycles 0 to 150 reflect data when control method A was used with a 100% load. During this time, the cell's voltage dropped at a rate of approximately 0.1mV/cycle·cell. At a 50% load using control method A, it became fairly large at approximately 0.3mV/cycle·cell, and recovered to approximately 0.1mV/cycle·cell at a 50% load using control method B. These results show that phosphoric acid concentration and volume changes must be controlled as far as possible in order to increase the lifetime of cells. In other words, the importance of controlling changes in the weight of the cell became clear.

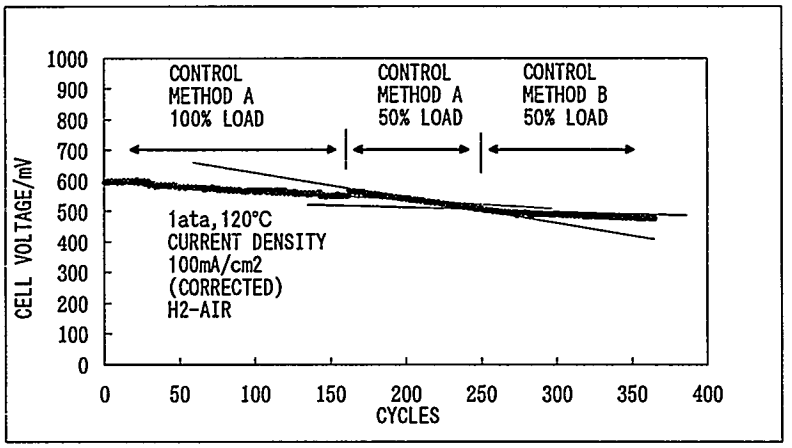

Figure 5 Lifetime cycling characteristics using control method A and B

CONCLUSIONS

A simple technique (weight measurement method) was studied for evaluating the behavior of phosphoric acid when a portable fuel cell is started up and operated. Use of this weight measurement method made it clear that an operation method that maintains the phosphoric acid's weight is effective. These studies resulted in prospects for attaining increased lifetime for portable fuel cells when used in a variety of conditions. SANYO will continue its pursuit of improved portable fuel cell reliability.

REFFERENCES

[1]A.Watanabe, N.Nishizawa, T.Itou, SANYO TECHNICAL REVIEW, Vol.26,No.1, 18(1994).
[2]K.Nakatou, K.Shindou, N.Nishizawa and M.Tsutsumi, The 2nd FCDIC Fuel Cell Symposium Proceedings, 82(1995).
[3]MacDONALD.D.I.et.al."Density, Electrical Conductivity and Vapor Pressure of Phosphoric Acid" Journal of Chemical and Engineering Data,Vol.14, No.3, July(1969).

EVALUATION OF THE PERFORMANCE DEGRADATION AT PAFC INVESTIGATION OF DEALLOYING PROCESS OF ELECTROCATALYSTS WITH IN-SITU XRD

Noriyuki Nakajima[1], Hideaki Miyoshi[2], Kunihiro Nishizaki[3], Takashi Kitai[4], Hiroyuki Uchida[5] and Masahiro Watanabe[5]

Cooperative Research and Development Center, Yamanashi University

Takeda 4-3, Kofu 400, Japan

1; Fuji Electric Co., 2; Mitsubishi Electric Co., 3; Tokyo Gas Co.,Ltd., 4; Toshiba Co., 5; Yamanashi University

INTRODUCTION

As a complementary research project to the demonstration project of 5MW and 1MW PAFC plants, the mechanism and rate of deterioration of the cells and stacks have been studied from 1995 FY, with the objective of establishing an estimation method for the service life-time of the cell stacks. This work has been performed in the Basic Research Project, as part of that project on PAFC's, selecting four subjects (Electrocatalysts degradation, Electrolyte fill-level, Cell material corrosion, Electrolyte loss) as the essential factors relating to the life-time. In this study, the effect of temperature and potential on the dealloying process of electrocatalysts was examined in H_3PO_4 electrolyte with X-ray diffraction measurement.

EXPERIMENTAL

In order to monitor the degradation level at the alloy-electrocatalysts during the anodic polarization under N_2 atmosphere in H_3PO_4 electrolyte at elevated temperatures, a specially designed cell was prepared (see Fig. 1).The cell had a window covered with a polyimide film for X-ray diffraction. The electrocatalyst used was Pt-Co-Ni alloy(ca.2/1/1 gross atomic ratio),supported on carbon black(CB). The alloy-electrocatalysts loading on CB was 20 weight

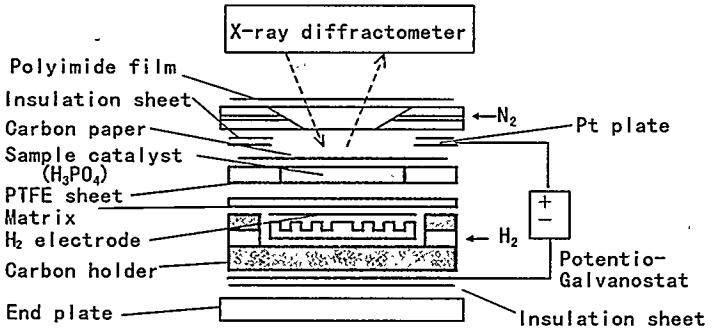

Fig. 1. An apparatus for a corrosion test cell with In-situ X-ray diffraction measurement.

percent Pt. A paste was prepared with the alloy-electrocatalysts and 100% H_3PO_4. The paste was sandwiched between thin carbon papers and mounted in the window side of the cell as a working electrode(WE). A conventional H_2-gas-diffusion electrode and a SiC matrix filled with H_3PO_4 were employed as the counter electrode and the electrolyte layer, respectively. In-situ x-ray diffraction measurement was carried out to monitor the degradation level at the alloy-electrocatalysts during the anodic polarization.

In order to evaluate the effect of temperature and potential on the corrosion of the alloy-electrocatalysts , the WE was polarized at a potential of 0.7 or 0.9V in N_2 atmosphere at elevated temperatures(200,240°C) for 48 hours. The humidity was controlled to keep the concentration of H_3PO_4 constant at 100%.

RESULTS AND DISCUSSION

In-situ X-ray diffraction measurement — Typical in-situ X-ray diffractograms of alloy-electrocatalysts during the anodic polarization are shown in Fig.2. The "as-received" electrocatalysts showed a broad peek around 41.6°, which corresponds to (111)-diffraction of Pt [Co・Ni] alloy phase. With increasing the corrosion time, the peak intensity of the original alloy decreased and the another peak intensity at 40.0°, assigned as *d*(111) of pure-Pt, became stronger. This indicates that the dealloying of electrocatalyst occurred within a few hours at 0.9V at 240°C. Since the shape of the peak became sharp with time, the corrosion process also induced a growth of Pt particles. Thus, the in-situ XRD is very useful to know the time-course of the degradation process of electrocatalysts.

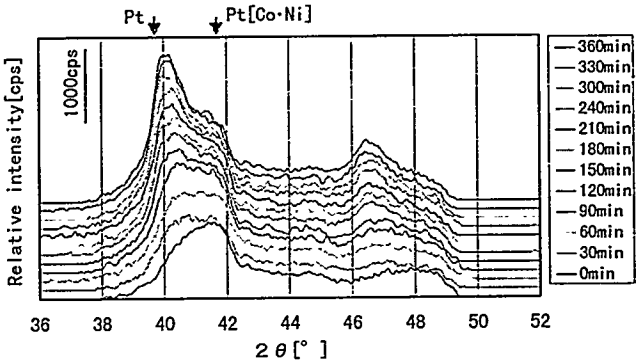

Fig. 2. Typical In-situ X-ray diffractograms of alloy-electrocatalysts during the anodic polarization (240°C, 0.8 mA/cm^2, *ca.* 0.9V)

Effect of temperature and potential for corrosion of the alloy-electrocatalysts —Considering that the main peak between 36° and 44° of the corroded electrocatalyst consisted of three components, Pt[Co•Ni], Pt_3[Co•Ni] and Pt, the observed peak was deconvoluted into three peaks. In order to evaluate the changes in the composition of the alloy during the corrosion process, the relative integrated intensity of each component was determined. The crystallite size for each component was also calculated using Scherrer's equation (Table1). As shown in Fig.3, the relative intensity of Pt[Co•Ni] decreased significantly at 200°C by the anode polarization at 0.7 or 0.9V for 48h. At 240°C, this original alloy phase was almost disappeared. Concomitantly, a formation of pure Pt was accelerated with raising temperature or potential. On the other hand, the relative intensity of Pt_3[Co•Ni] was almost constant independent of the temperature and the potential, indicating that Pt_3[Co•Ni] phase is stable compared with other alloy phases. This is also supported by the results shown in Table 1 that the crystallite size of Pt_3[Co•Ni] was not so changed during the corrosion process at 200°C or 240°C although it increased to some extent at the initial stage.

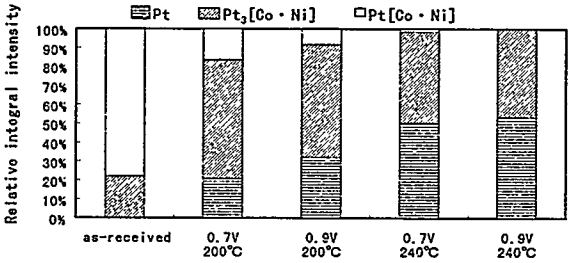

Fig. 3 Phase changes in supported alloy particles with the treatment conditions of different temperatures and potentials for 48 hours.

At 200°C, the crystallite size of Pt increased from 72 Å to 93 Å, i.e., 1.3times, with increasing the potential form 0.7V to 0.9V. The same increase in the potential (0.7→0.9V) at 240°C resulted in the growth of the Pt crystallite size from 91 Å to 127 Å, i.e., 1.4 times. At a given potential, the crystallite size of Pt at 240°C was larger than that at 200°C. The effect of temperature elevation from 200°C to 240°C at a given potential is approximately equivalent to that of potential from 0.7V to 0.9V at a constant temperature for the corrosion process. On the other hand, the crystallite size of Pt[Co•Ni] at

Table 1. Crystallite size changes in different phases on supported alloy catalysts treated under different temperatures and potentials for 48 hours.

Phase	Crystallite size(Å)				
	as-received	200℃		240℃	
		0.7V	0.9V	0.7V	0.9V
Pt[Co・Ni]	53	69	105	111	–
Pt_3[Co・Ni]	48	61	66	70	62
Pt	–	72	93	91	127

200°C increased especially at 0.9V. However, as described above, the relative intensity of Pt[Co•Ni]decreased significantly. Therefore, it is considered that fine particles of Pt[Co•Ni] were dissolved predominantly leaving large-sized one (>100Å) undissolved.

Chemical analysis of content for Pt, Co, and Ni in the alloy-electrocatalysts —The Pt, Co and Ni contents in the corroded electrocatalysts were analyzed by ICP(see Fig.4). It is noteworthy that large amounts of both Ni and Co components were dissolved even at the temperature of 200°C and at the potential of 0.7V,i.e., normal operating condition of PAFC except that the atmosphere was N_2. An elevation of temperature form 200°C to 240°C also resulted in a loss of these components. However, the Pt contents of all specimens were approximately constant. Therefore Pt dissolved from alloy could be deposited again as pure Pt particles. The redeposition of Pt might cause an increase of the crystallite size of Pt as shown in Table 1.

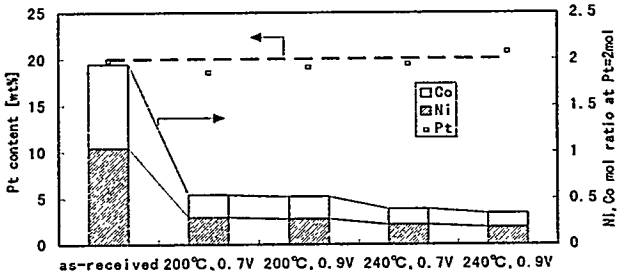

Fig.4. Chemical analysis of content in corrosion process for the alloy-electrocatalysts.

CONCLUSION

The dealloying process of Pt-Co-Ni alloy(ca.2/1/1 gross atomic ratio)supported on CB were investigated at the different of temperature and potential in H_3PO_4. Even at the corrosion condition of 200°C,0.7V for 48h, the Co and Ni component decreased appreciably. Fine particles of Pt[Co•Ni] seemed to be dissolved predominantly leaving large-sized one (>100Å) undissolved. Pt_3[Ni•Co] phase was found to be relatively stable. The Pt in the alloy was dissolved and deposited again as large-sized pure Pt particles during the corrosion process.

These electrocatalysts of various degradation levels are currently subjected to electrochemical measurements in order to examine effects of the degradation of electrocatalysts on the cell performances (see abstract by Nishizaki et al in our group).

ACKNOWLEDGMENT

This work has been supported by the Ministry of Education, Science and Culture, NEDO and PAFC-TRA.

EVALUATION OF THE PERFORMANCE DEGRADATION AT PAFC EFFECT OF ELECTROLYTE FILL-LEVEL ON ELECTRODE PERFORMANCE

Takashi Kitai,[1)] Kunihiro Nishizaki[2)], Noriyuki Nakajima[3)], Hideaki Miyoshi[4)],
Hiroyuki Uchida[5)] and Masahiro Watanabe[5)]
Cooperative Research & Development Center, Yamanashi University
Takeda 4-3, Kofu 400, Japan
1; Toshiba Co., 2; Tokyo Gas Co. Ltd., 3; Fuji Electric Co., 4; Mitsubishi Electric Co.,
5; Yamanashi University

INTRODUCTION

As a complimentary research project to the demonstration project of 5MW and 1MW PAFC plants, the mechanism and rate of deterioration of the cells and stacks have been studied from 1995 FY, with the objective of establishing an estimation method for the service life-time of the cell stacks. This work has been performed in the Basic Research Project, as part of that project on PAFC's, selecting four subjects (Electrocatalysts degradation, Electrolyte fill-level, Cell material corrosion, Electrolyte loss) as the essential factors relating to the life-time. In this report, we will exhibit the effect of the electrolyte fill-level on the electrode performances.

EXPERIMENTAL

An electrolyte-exchangeable single cell was designed for this research. First, the cell temperature was raised to 200℃ with electrolyte being exchanged to concentrated (105%) phosphoric acid. At 200℃, I-V characteristics and oxygen-gain were measured under hydrogen/air and hydrogen/oxygen gas flow. After that, cell temperature was lowered to 25℃ with electrolyte being exchanged to diluted (45%) phosphoric acid. At 25℃, the surface area of supported catalyst and the double-layer current of carbon black support were measured by using cyclic-voltammetry (CV) before and after masking Pt surface with CO poisoning (Fig.1), respectively. By repetition of above operations, the electrolyte fill-level was substantially enhanced. Electrode performance at different electrolyte fill-level was investigated, being monitored the electrolyte fill-level by the double-layer current [1]. Pore distribution of electrode and amount of filled electrolyte in electrode were measured by using Hg-porosimeter and chemical analysis with ICP, respectively.

RESULTS AND DISCUSSION

The relationship between the double-layer current (Idl) which corresponds to the electrolyte fill-level and the oxygen-gain which corresponds to the diffusion-polarization was shown in Fig.2. As the double-layer current increases, the oxygen-gain decreases first. During this process, the fill-level was proceed to an appropriate level. As the double-layer current increases more, the oxygen-gain shows a minimum value, then increases. During this process, the fill-level exceeds the

appropriate level. So, the electrodes at high gas-diffusion loss-level (oxygen-gain=121mV, or Idl=4.5mA/cm^2) and at low gas-diffusion loss-level (oxygen-gain=91mV, or Idl=3.7mA/cm^2), were investigated regarding the dependency of the performances upon the electrolyte fill-levels, respectively. Results were shown in Fig.3. In the case of electrolyte fill-level (vs. total pore volume), the fill-level of the electrode at high gas-diffusion loss was much higher than that of low gas-diffusion loss. For the detail discussion, the electrolyte fill-level was measured, combined with the measurement of pore size distribution, i.e., electrolyte distribution into the primary and secondary pores. The primary pores concerned to be formed between the primary CB particles and acting as reaction sites, and secondary pores to be formed between the CB agglomerates and acting as gas-networks, respectively [2]. At high gas-diffusion loss electrode, the electrolyte fill-level of secondary pores (70%) was extremely high in comparison with that of primary pores (45%). On the other hand, at low gas-diffusion loss electrode, the electrolyte fill-level of the secondary pores was very low (16%), in spite of the electrolyte fill-level of the secondary pores (44%) being equal to that of high gas-diffusion loss electrode. As indicated above, it was clarified that the electrolyte fill-level of the primary pores acting as reaction sites is independent to gas-diffusion loss, and the electrolyte filling to the secondary pores acting as gas-networks inhibits gas diffusion to reaction sites, resulting in an increase of gas-diffusion loss. It was also clarified that the utilization of platinum clusters was constant (45%) at these electrodes.

CONCLUSION

At different diffusion-polarization electrodes, the electrolyte fill-level and distribution were investigated. The major results are listed below.

a) Electrolyte filling to the primary pores is related to utilization of Pt clusters only, and is independent to gas-diffusion loss.

b) Electrolyte filling to the secondary pores inhibits gas diffusion to reaction sites, and brings an increase of gas-diffusion loss.

c) Preferable electrolyte fill-level is clarified, i.e., ca. 3.7mA/cm^2 in the double-layer charging current or ca. 16% of electrolyte fill-level in the secondary pores.

ACKNOWLEDGMENT

This work has been supported by the Ministry of Education, Science and Culture, NEDO and PAFC-TRA.

REFERENCES

1) M. Watanabe et al., Denki Kagaku, 64, 460(1996).

2) M. Watanabe et al., J. Electroanal. Chem., 195, 81 (1985).

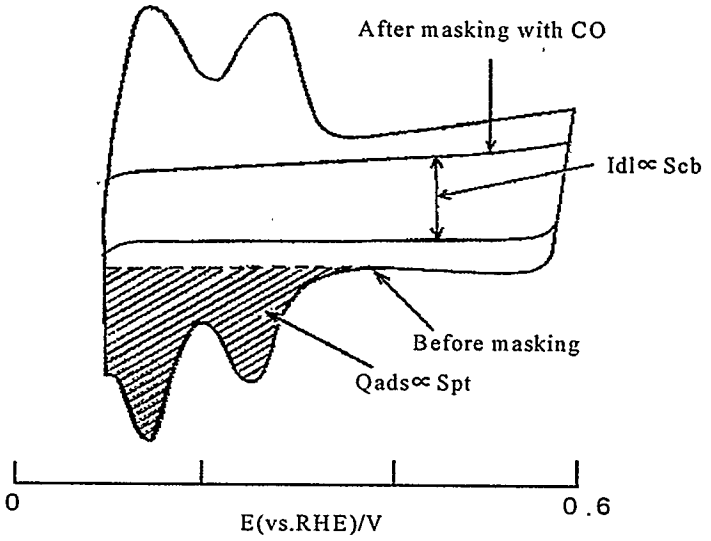

Fig.1. Example of CV

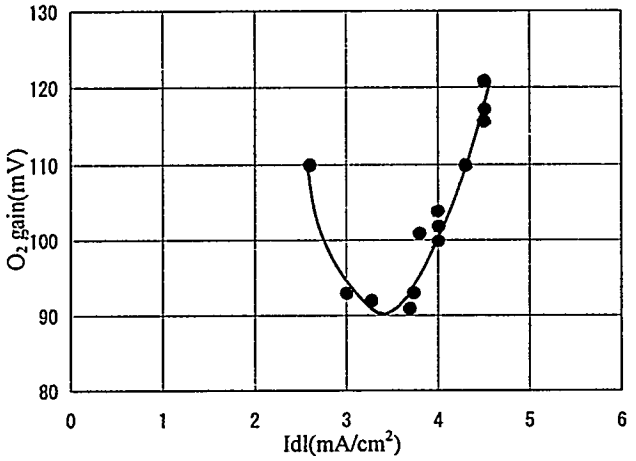

Fig.2. Idl vs. O_2 gain

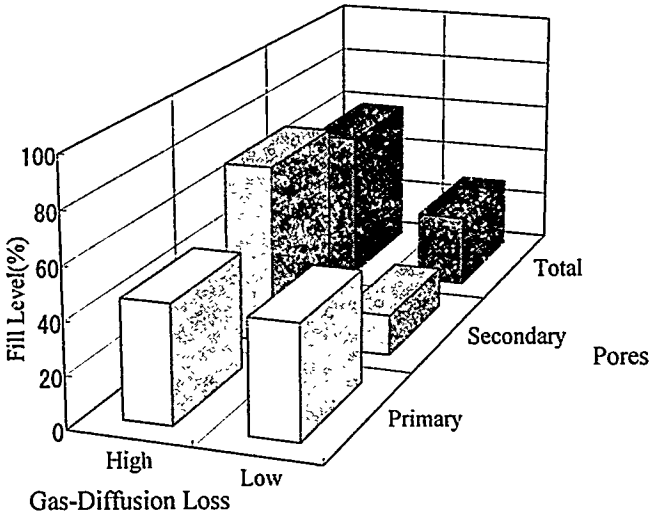

Fig.3. Electrolyte Fill-Level

EVALUATION OF THE PERFORMANCE DEGRADATION AT PAFC EFFECT OF CATALYST DEGRADATION ON ELECTRODE PERFORMANCE

K.Nishizaki[1], T.Kitai[2], N.Nakajima[3], H.Miyoshi[4],
H.Uchida[5] and M.Watanabe[5]
Cooperative Research & Development Center, Yamanashi University,
Takeda 4-3, Kofu 400, Japan
1; Tokyo Gas Co. Ltd., 2; Toshiba Co., 3; Fuji Electric Co., 4; Mitsubishi Electric Co.,
5; Yamanashi University

INTRODUCTION

Aiming commercialization of Phosphoric Acid Fuel Cell (PAFC) power plant, many researches and developments have been contributed. Over 20000 hours operations have been demonstrated by many PAFC power plants. But there is no effective method for the estimation of lifetime of electrochemical cells without a practical long-term operation.

Conducted by New Energy and Industrial Technology Development Organization (NEDO), cooperative research projects aiming development of PAFC lifetime estimation method have started since 1995 FY in Japan. As part of this project, this work has been performed to clarify basic phenomena of the performance degradation at PAFCs jointly by Yamanashi University, Phosphoric Acid Fuel Cell Technology Research Association (PAFC-TRA) and PAFC manufacturers (Toshiba Co., Mitsubishi Electric Co, Fuji Electric Co.).

Among several main causes of the cell performance degradation, effects of catalyst degradation (reduction in metal surface area, dealloying, changes in catalyst support) on PAFC cathode performances are discussed in this work.

EXPERIMENTAL

To clarify the effect of the degradation of catalysts themselves on the electrode performance or the life-time, catalysts in different degradation states prepared by electrochemical treatments of same mother catalysts under different conditions were examined in gas-diffusion electrodes loaded them.

1) Preparation of catalysts in different degradation states

The mother catalyst was an as-received Pt/Ni/Co catalyst (ca. 2/1/1 gross atomic ratio) supported on a carbon black (CB) (ca. 100m^2/g). The loading at the catalyst was 20 percent (w/o) in platinum weight.

The paste of catalysts mixed with phosphoric acid (ca.105%H_3PO_4) was sandwiched between the two sheets of carbon paper (thickness=0.1mm) and was mounted into a SiC matrix type cell as a working electrode. Before electrochemical treatment, catalysts were held at 120℃ with air flow humidified at room temperature for 14 hours which was a similar condition to the initial electrolyte filling in practical PAFCs. Electrochemical treatments were performed in the cell apparatus controlled at different temperature and

potential conditions for 48 hours. A gas diffusion electrode, which is same as a conventional PAFC anode, served both as reversible hydrogen reference electrode (RHE) and counter electrode. The concentration of phosphoric acid electrolyte was controlled at 100%H_3PO_4 by humidification.

2) Characterization of prepared catalysts

The electrochemical metal surface area (S_{pt}), double layer current (I_{DL}) under CO poisoned condition, which corresponds to surface area of the CB support wet with electrolyte [1], were measured by using cyclic voltammetry (CV). S_{pt} was calculated from the amount of charge of hydrogen adsorption peak in CV assuming 210 μ C/cm^2. I_{DL} was defined as a width (mA/mg-C) of CV at 450mV vs RHE in a double layer region under CO poisoned condition. Potential sweep rate was 50mV/s.

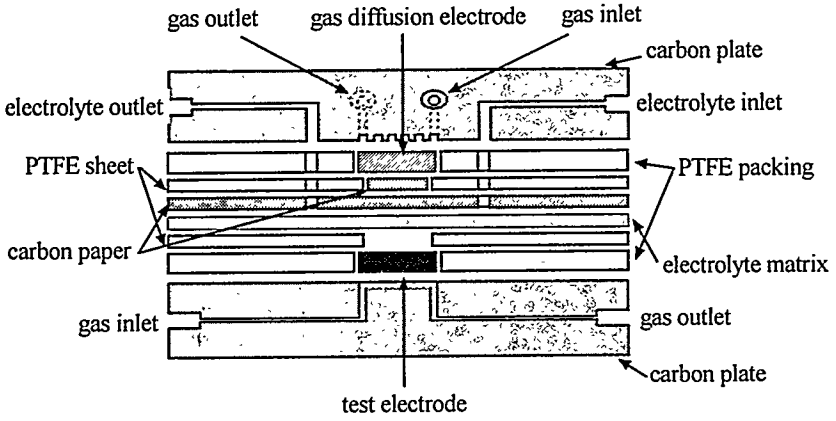

Fig.1 Structure of electrolyte-exchangeable cell

The CV measurements were performed in 45% H_3PO_4 using an electrolyte exchangeable cell (Fig.1). The catalysts sandwiched between a carbon paper wet-proofed with polytetrafluoroethylene (PTFE) (gas side) and a SiC electrolyte matrix attached with a non-wet-proofed carbon paper (electrolyte side) was set as a test electrode. A gas diffusion electrode (same as conventional PAFC anode) was used as a counter electrode. RHE connected to the electrolyte outlet was used as a reference electrode.

X-ray diffraction analysis (XRD) were performed to determine the average crystalline sizes of each phase of Pt[Co•Ni], Pt_3[Co•Ni] and Pt.

3) Evaluation of electrode

The degraded catalyst was fabricated into a PTFE-bonded catalyst layer on the carbon paper substrate wet-proofed with PTFE. Each electrode had a constant platinum loading of 1.0mg/cm^2 and about 38 w/o PTFE for carbon support.

By using electrolyte-exchangeable cell mentioned above, the electrode performances (I-V characteristics and oxygen-gain) were measured in about 100% H_3PO_4 at 200℃. Then I_{DL} and S_{pt} were measured by using cyclic voltammetry (CV) in 45% H_3PO_4 at 25℃ in order to know the electrolyte fill-level and the catalyst utilization.

During the repetition of these measurements, a performance was changed with the increase of the electrolyte fill-level from starved level to appropriate level and subsequently to excessive level.

RESULTS AND DISCUSSION

1) Metal surface area

Table 1 shows the values of surface area determined by electrochemical method for catalysts degraded under various conditions.

Table 1 Metal surface areas of catalysts treated under different temperatures and potentials for 48 hours

Temperature (℃)	Potential (V vs RHE)	Metal surface area (S_{pt}) (m^2/g-Pt)
before electrochemical treatment*		68
200	0.7	35
200	0.8	43
200	0.9	32
220	0.7	32
240	0.7	22
240	0.9	20

*after holding at 120℃/air for 14hours in H_3PO_4 (ca.100%)

The specific surface area of the catalyst was decreased significantly by the treatment with a relatively mild condition of 200℃ at 0.7V. At higher temperature or higher potential condition, that is severer condition, surface area became lower value. XRD of the catalysts under such a condition indicated that large-sized (ca.100Å) Pt particles were formed accompanied by a dessolution of fine Pt[Co・Ni] alloy particles (see abstract by Nakajima et al in our group).

2) Carbon black support

Fig.2 shows the values of I_{DL}, which corresponds to surface area of CB support, for various electrochemical treatment conditions.

While I_{DL} decreased gradually with elevated temperature at 0.7V, it increased appreciably with temperature at 0.9V. These results suggest that corrosion mechanism of CB support at 0.9V differs from that at 0.7V. For example, by the corrosion at 0.9V, the surface of the CB might be roughened or the hydrophilic property of the CB might be increased.

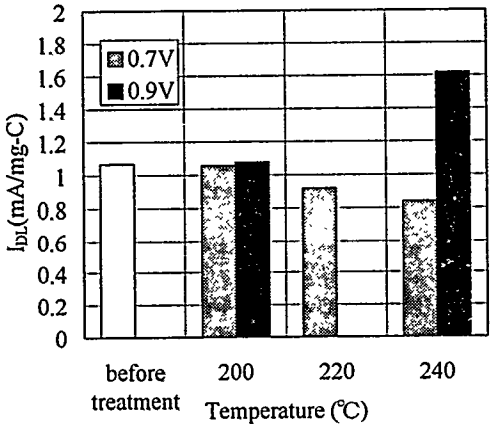

Fig.2 Double layer current (I_{DL}) changes in catalysts
treated under different temperatures and potentials for 48hours

3) Electrode performance

Table 2 shows the preliminary results of electrode performance measurements for electrodes with catalysts before and after electrochemical treatment.

Table 2 Performances of the electrode

electrode	Terminal voltage (mV at 300mA/cm^2, Air)	O_2 gain*** (mV)	I_{DL} (mA/cm^2)	S_{pt} (Pt-cm^2/cm^2)
A*	563	100	4.0	137
B**	551	96	3.7	141

*: electrode A with catalysts before electrochemical treatment
**: electrode B with catalysts treated at 200℃/0.9V
***: voltage difference between O_2 and air at 300mA/cm^2

The terminal voltage of the cell using the degraded catalyst was lower by 12mV than that with the original one, although both catalysts had a similar S_{pt}.

Measurements of other electrodes are currently being conducted to clarify the effect of catalyst degradation on electrode performance.

ACKNOWLEDGMENT

This work has been supported by the Ministry of Education, Science and Culture, NEDO and PAFC-TRA.

REFERENCES

1) M.Watanabe et al., Denki Kagaku (English issue), 64, 460 (1996)

EVALUATION OF THE PERFORMANCE DEGRADATION AT PAFC EFFECT OF OPERATING CONDITIONS ON ACID LOSS

Hideaki Miyoshi[1], Noriyuki Nakajima[2], Takashi Kitai[3], Kunihiro Nishizaki[4], Hiroyuki Uchida[5] and Masahiro Watanabe[5]
Cooperative Research and Development Center, Yamanashi University
Takeda 4-3, Kofu 400, Japan
1; Mitsubishi Electric Co., 2; Fuji Electric Co., 3; Toshiba Co.,
4; Tokyo Gas Co. LTD., 5; Yamanashi University

INTRODUCTION

As a complimentary research project to the demonstration project of 5MW and 1MW PAFC plants, the mechanism and rate of deterioration of the cells and stacks have been studied from 1995 FY conducted by NEDO, with the objective of establishing an estimation method for the service life-time of the cell stacks. As part of this project, this work has been performed to clarify basic phenomena of the performance degradation at PAFCs jointly by Yamanashi University, PAFC-TRA and PAFC manufacturers.

The acid loss into exhaust gases is one of life limiting factors in PAFCs. To design the cells of long-life, it is important to estimate the phosphoric acid loss and to contrive ideas eliminating it. With the objective of obtaining basic data for simulating the acid loss in the large size cells, the effect of the operating conditions on the acid loss into exhaust gases has been studied experimentally by using a single cell with an active electrode area of $100cm^2$.

EXPERIMENTAL

The acid loss into exhaust gases of the anode and cathode has been measured by condensing it in cold traps, as shown in Figure 1, and analyzing the amounts with ICP as a function of the operating conditions. The conditions studied are operating temperature, utilization of reactant gases or current density. Based on the amount of cumulated exhaust gasses and the weight of water condensed, the concentration of phosphoric acid in the exhaust gasses was calculated.

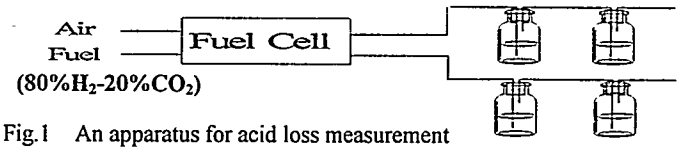

Fig.1 An apparatus for acid loss measurement

RESULTS AND DISCUSSION

1) Effect of the current density at a constant utilization of each anode and cathode reactant gases

Figure 2 shows the effect of the current density on the acid loss rate into the exhaust gases at 220℃. The acid loss rate at the anode and cathode increases with an increase of the current density and the loss into the cathode exhaust gas account for ca. 80 -85% of the total acid loss. Figure 3 shows the effect of the current density on the concentration of phosphoric acid in the exhaust gases. The concentration in the cathode exhaust gas is nearly constant in the region of 50-400 mA/cm^2 but that in the anode varies with current density. Under a constant utilization of each reactant gas, the volume of reactant gases decreases with decreasing current density. So, the increase of the concentration of phosphoric acid in the anode exhaust gas in the low current density region (50-100 mA/cm^2) is ascribed to the low mean linear velocity (see Figure 4). However, it is noteworthy that a difference of the concentrations in the exhaust gases of the anode and cathode in the region of a small linear velocity even though the velocity is the same.

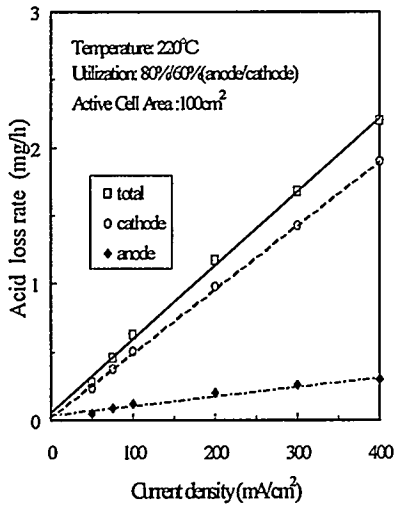

F ig.2. Effect of the current density on the rate of acid loss into exhaust gases

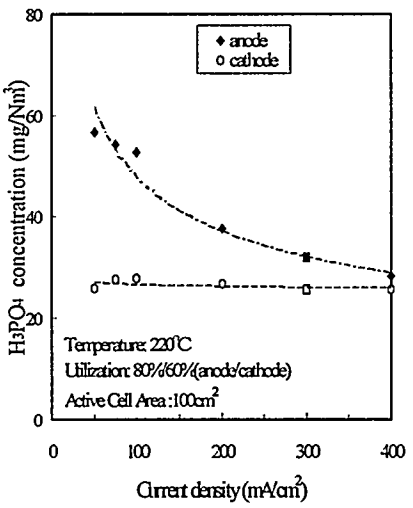

Fig.3. Effect of the current density on H_3PO_4 concentration in exhaust gases

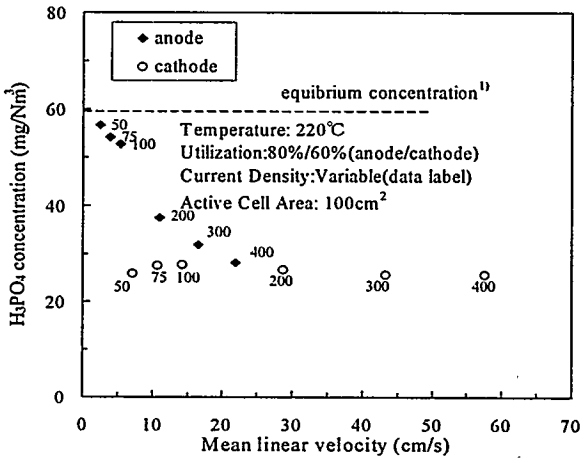

Fig.4. Effect of the mean linear velocity on H_3PO_4 concentration in exhaust gases

2) Effect of the operating temperature on the acid loss at a constant current density

Figure 5 shows the effect of operating temperature on the acid loss rate at 300 mA/cm^2. The acid loss of the anode and cathode increases exponentially with an increase of operating temperature.

The concentration of phosphoric acid in the anode and cathode exhaust gases also increases exponentially, but they are smaller than the equilibrium concentration estimated from Brown's data[1] as shown in Figure 6. Difference between the experimental data and the equilibrium data could be explained by the fact that the concentration of the phosphoric acid in the exhaust gases is affected by the mean linear velocity.

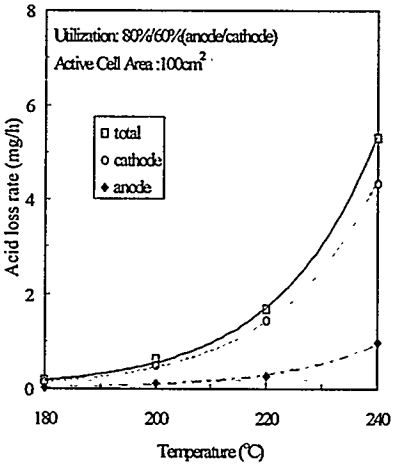

Fig.5. Effect of the operating temperature on the rate of acid loss into exhaust gas

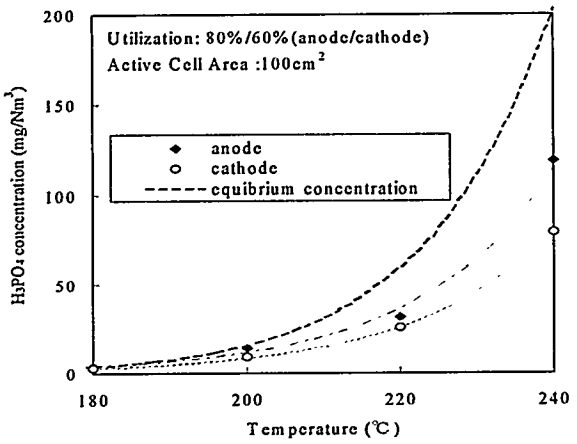

Fig.6. Effect of the operating temperature on H_3PO_4 concentration in exhaust gases

CONCLUSIONS

The major results on the acid loss studied experimentally by using the single cell with the active electrode area of 100 cm^2 are summarized as follows:

(1) The concentration of phosphoric acid in the cathode exhaust gas is nearly constant in the region of 50-400 mA/cm^2 but that in the anode varies with current density.

(2) The concentration of phosphoric acid in the exhaust gases increases exponentially with increase of operating temperature, but they are smaller than the equilibrium concentration estimated from Brown's data.

(3) The concentration of phosphoric acid in the anode exhaust gas is affected by the mean linear velocity, and it reaches nearly to the equilibrium concentration with lowering the mean linear velocity.

ACKNOWLEDGMENT

This work has been supported by the Ministry of Education, Science and Culture, NEDO and PAFC-TRA.

REFERENCES

1) E. H. Brown et al, Industrial and Engineering Chemistry, Vol. 44, 615, (1952)

DEVELOPMENT OF THE ELECTRIC UTILITY DISPERSED USE PAFC STACK

Hiroshi Horiuchi, Ikuo Kotani
Kobe Works, Mitsubishi Electric Co.
1-1-2 Wadasaki-cho Hyogo-ku, Kobe 652 Japan

Isamu Morotomi, Masaru Ogawa, Osamu Yamanishi
Technical Research Laboratory, Kansai Electric Power Co.
11-20 Nakoji 3-chome,Amagasaki,HYOGO 661 Japan

INTRODUCTION

Kansai Electric Power Co. and Mitsubishi Electric Co. have been developing the electric utility dispersed use PAFC stack operated under the ambient pressure. The new cell design have been developed, so that the large scale cell ($1m^2$ size) was adopted for the stack. To confirm the performance and the stability of the $1m^2$ scale cell design, the short stack study had been performed.

EXPERIMENT

The short stack design was optimized by simulation calculation[1),2)], and the life test with some perturbation have been performed. The operation condition of short stack show in Table 1. The short stack was composed with four different cell designed blocks, for the purpose of selecting the proper design, and the each cell designed block's performances have been evaluated respectively during the short stack test[2)]. The short stack test was started since March 1994, the cumulative operation time have reached over 10,000h. Twice extraction of parts from the stack for the purpose of interim inspection have been done during the life test.

The diagnostic tests[3)] for evaluating the variety of the each cell characteristic parameters have been carried out regularly. The operation condition of diagnostic test for the cell characteristics show in Table 2.

The load perturbation test have also done to investigate the influence of the load operation mode on the cell life performance. Figure 1 shows the load pattern of the weekly perturbation, full power load in weekday and standby load in weekend. Figure 2 shows the load pattern of the daily perturbation, full power load in day time and standby mode in night.

Table 1. The standard operation condition of short stack.

ITEM	STATE
Current density	$300mA/cm^2$
Size of electrode are	$8,000cm^2$ class
Cell numbers	20 cells
Gas utilization	Fuel 80%, Air 60%
Fuel gas composition	Humid mixed gas(H_2:80%,CO_2:20%)
Operation temperature	200°C

Table 2. The operation condition of diagnostic test for the cell characteristics.

ITEM	Current density	Air utilization	Fuel utilization
Reacting activity	$75\text{-}300mA/cm^2$	60%	80%
Cathode gas diffusion	$300mA/cm^2$	50-70%	70-90%
Anode gas diffusion	$300mA/cm^2$	60%	80%

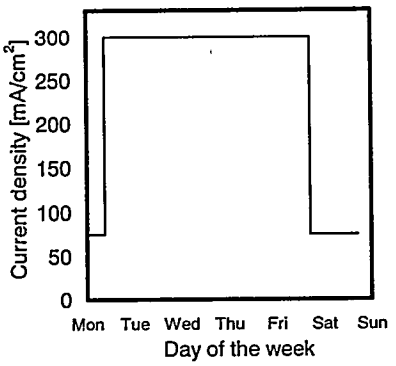

Fig.1 Pattern diagram
(weekly load perturbation)

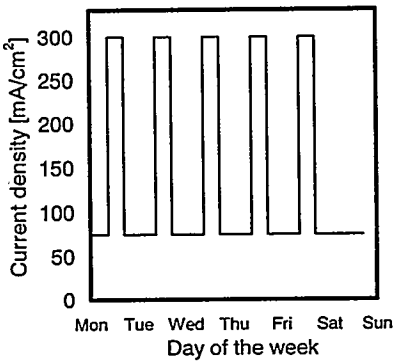

Fig.2 Pattern diagram
(daily load perturbation)

RESULTS AND DISCUSSION

(1)Variety of cell performance

Figure 3 shows the typical designed block's life performance. In the initial term, the start-stop operation had been carried out repeatedly to improve the electrolyte adsorption into the electrode catalyst layer, and the performance decay rate shows the larger value, 5.9mV/Kh. After then, the stable life performance about 2mV/Kh have been obtained. The two points of the parts extracting from the other block show in Fig.3 respectively, the interrupted performance decay happened at that time. It is considered that, in order to release the fastening the stack and the fitting state of each cell elements interfaces would be varied, internal resistant might be increased, or the daily start-stop operation, for the initial dealing with the new exchanged cell block, might be influenced. Because of excepting these points influences, the performance decay rates are estimated on the interval term during the points. For the purpose of consideration of the influence of start-stop, the cumulative count of start-stop are also plotted in Fig.3. Although it seem that larger decay rates are shown in the term of many start-stop operated, it has been remained the much obscure phenomena on these term yet and the test which would be manifest of these have been carrying out.

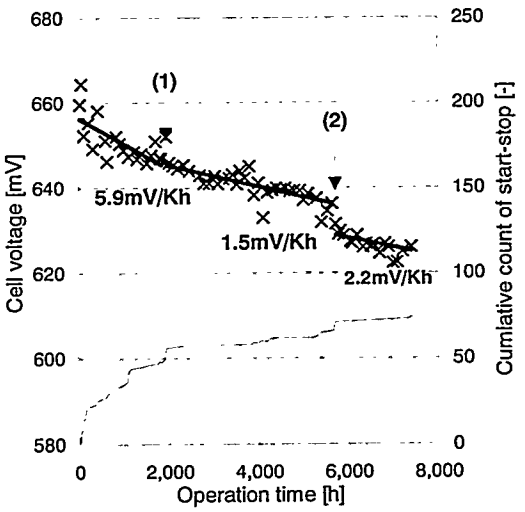

Fig.3 Life performance characteristics

(2)Variety of the cell characteristic parameters

The variety of reacting activity defined by the light load(75mA/cm^2) performance show in Fig.4, the performance decay showed about 30mV from initial to 8,000h. The decay range has been shown equal to the rate load decay shown in Fig.3, and the performance decay rate could be explained to cause only by the decay of reacting activity.

The results of the diagnostic test to evaluate the cathode gas diffusive state by the varying air utilization operation, shows in Fig.5. The plotted values are standardized with the cell performance changing range divided by the unit range of the air utilization. So that the values seem scarcely changed in whole testing term, the cathode diffusive state has been confirmed to change little. Although the results are abridged, it has been also confirmed to change little of the anode diffusive state.

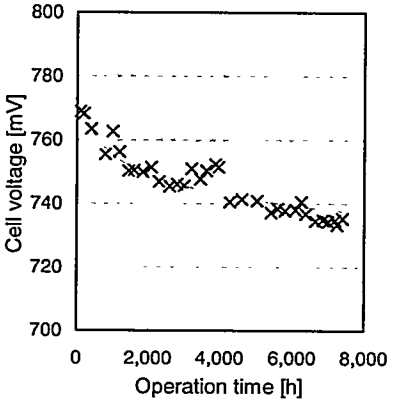

Fig.4 Results of the diagnostic test (variety of the light load performance)

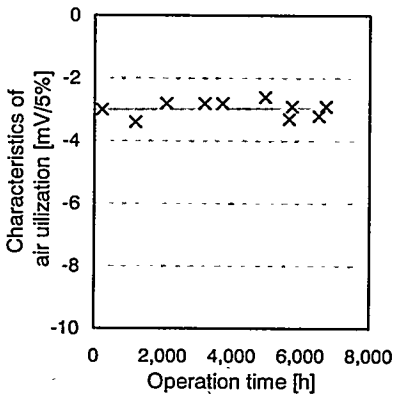

Fig.5 Results of the diagnostic test (variety of cathode diffusive state)

(3)Influence of the perturbation

Figure 6 shows the results of weekly load perturbation test, the decay rate showed 2.9mV/Kh in this term. As for the decay rate of daily load perturbation test were less than weekly one,1.4mV/Kh,shown in Fig.7. The supposed reasons are follow.

- Because of the motive force on the electrolyte moving from cathode to anode by the ionic mobility during rate load(high current density) operation, the electrolyte adsorbed in the cathode would be got out and the electrode effective surface area and cell performance must be reduced.
- In the standby(low current density) operation, the motive force would become so weaker that the moved electrolyte would be recycled back to cathode and be adsorbed again, and cell performance must be recovered.
- It is considered that daily perturbation would be often recovering the cell performance, the appeared decay rate might be seemed lower.
- Although the decay rate of the daily perturbation is seemed lower than weekly's as in the short term, the low rate(1.5mV/Kh) has been obtained in the continuous operation term until then, thus the reducing of the cell performance with the electrolyte moving would be settled down and the influence would be reduced during the long term operation.

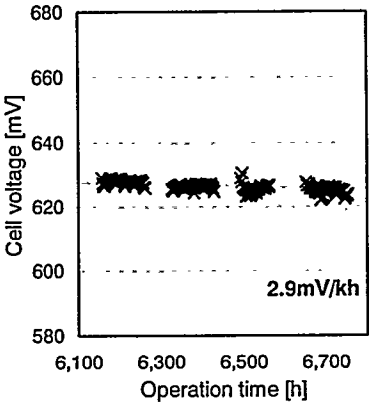

Fig.6 Results of load perturbation test (weekly load perturbation)

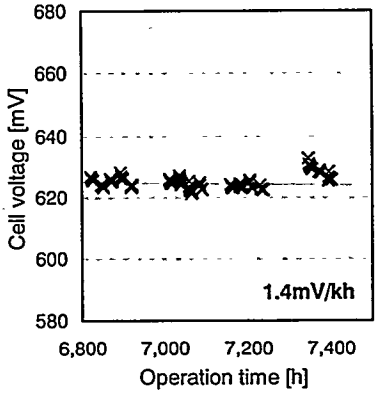

Fig.7 Results of load perturbation test (daily load perturbation)

Optimizing the stack design by these results of the short stack study, 500kW stack have been made and started to demonstrating operation since this year.

References

1)Y. Matsumoto, T. Matsuoka, Y. Takuma and H. Horiuchi
Proceeding of 5th Annual Conference of Power &Energy Soc. IEE. Japan, July(1994).
2)H. Horiuchi, M. Matsumoto, M. Ogawa and K. Hotta
J. Denki Kagaku , 64, 449(1996)
3)H. Horiuchi, T. Otani, I. Morotomi, M. Ogawa and K. Hotta
Proceeding of 7th Annual Conference of Power &Energy Soc. IEE. Japan, Aug.(1996).

DEVELOPMENT OF ON-SITE PAFC STACKS

K. Hotta, Y. Matsumoto, * H. Horiuchi, * T. Ohtani
Kansai Electric Power Co., Amagasaki 661 JAPAN
* Mitsubishi Electric Corp., Kobe 652 JAPAN

PAFC(Phosphoric Acid Fuel Cell) has been researched for commercial use and demonstration plants have been installed in various sites. However, PAFC don't have a enough stability yet, so more resaearch and development must be required in the future.

Especially, cell stack needs a proper state of three phases (liquid, gas and solid) interface. It is very difficult technology to keep this condition for a long time.

In the small size cell with the electrode area of 100cm^2, gas flow and temperature distributions show uniformity. But in the large size cell with the electrode area of 4000cm^2, the temperature distributions show non-uniformity. These distributions would cause to be shorten the cell life. Because these distributions make hot-spot and gas poverty in limited parts.

So we inserted thermocouples in short-stack for measuring three-dimensional temperature ditributions and observed effects of current density and gas utilization on temperature.

For measurement, we used a short-stack shown in table 1, and measured on experimental conditions shown in table 2.

Table 1. Specification of short-stack

Operating Pressure	Ambient Pressure
Electrode Area	4000 cm^2 class
ELectrode Form	Rectangular (F:A=2:1)
Cell Number	24 cells
Cooling Composition	6 cells / cooler
Cooling Water Temp.	170 ℃
Supplied Gases	
Anode	H_2 :80% CO_2 :20%
Cathode	Air

Table 2. Experimental Conditons

No.	Variable Item	Constant Item
①	Current Density 100, 150, 200, 250, 300 (mA/cm^2)	Air Utilization = 60% Fuel Utilization = 80%
②	Air Utilization 50, 60, 70 (%)	Current Density = 300 mA/cm^2 Fuel Utilization = 80%
③	Fuel Utilization 50, 60, 70, 80, 90 (%)	Current Density = 300 mA/cm^2 Air Utilization = 60%

The subject part for measurement is 3P (13C ~ 18C) shown in Figure1, and fit up twenty-five thermocouples on a cell shown in Figure2 respectivery.

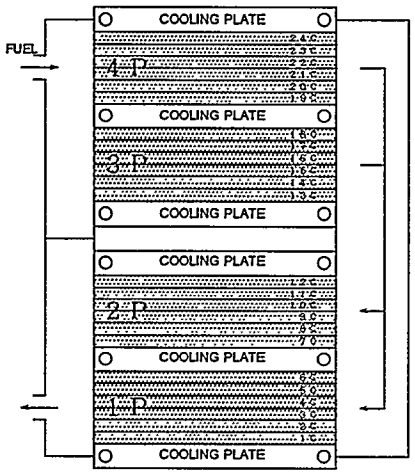

Figure 1 Composition of Short-stack

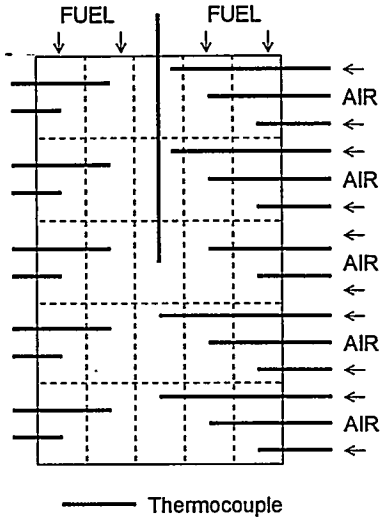

Figure 2 Mesurement Points on a cell

① Current Density

Figure 3 shows the effect of current density on temperature distribution. Temperature is rising remarkably together with the ascent of current density. The rising rate was about 10 °C /100mA cm $^{-2}$. And the distribution among cells varied tiny at light load, but at high current density, this one varied widely and generated the big hot-spot on center cells in a part.

② Air Utilization

Figure 4 shows the effect of air utilization on temperature distribution. Temparature is rising together with the ascent of the air utilization, and the hot-spot moved to the air inlet area. The rising rate was about 1 ~ 2 °C /10%.

③ Fuel Utilization

This distribution was the same result with the air one, but hot-spot didn't moved.

By these measurement, it became clear that the current density had an effect on temperature. Table 3 shows relationship between current density and maximum temperature.

Table 3 Current Density and Maximum Temperature

Current Density (mA/cm2)	100	150	200	250	300
Maximum Temp. (°C)	185	190	200	205	210

On this table, Maximum temperature reached to 210 °C at 300mA/cm ^{2} . Too high temperature might be shorten the cell's life, but all of electrode in the stack don't react enough, because three-dimensional distributions exist. In the near future, how to flatten these distributions will be a target to develop for commercial use on PAFC.

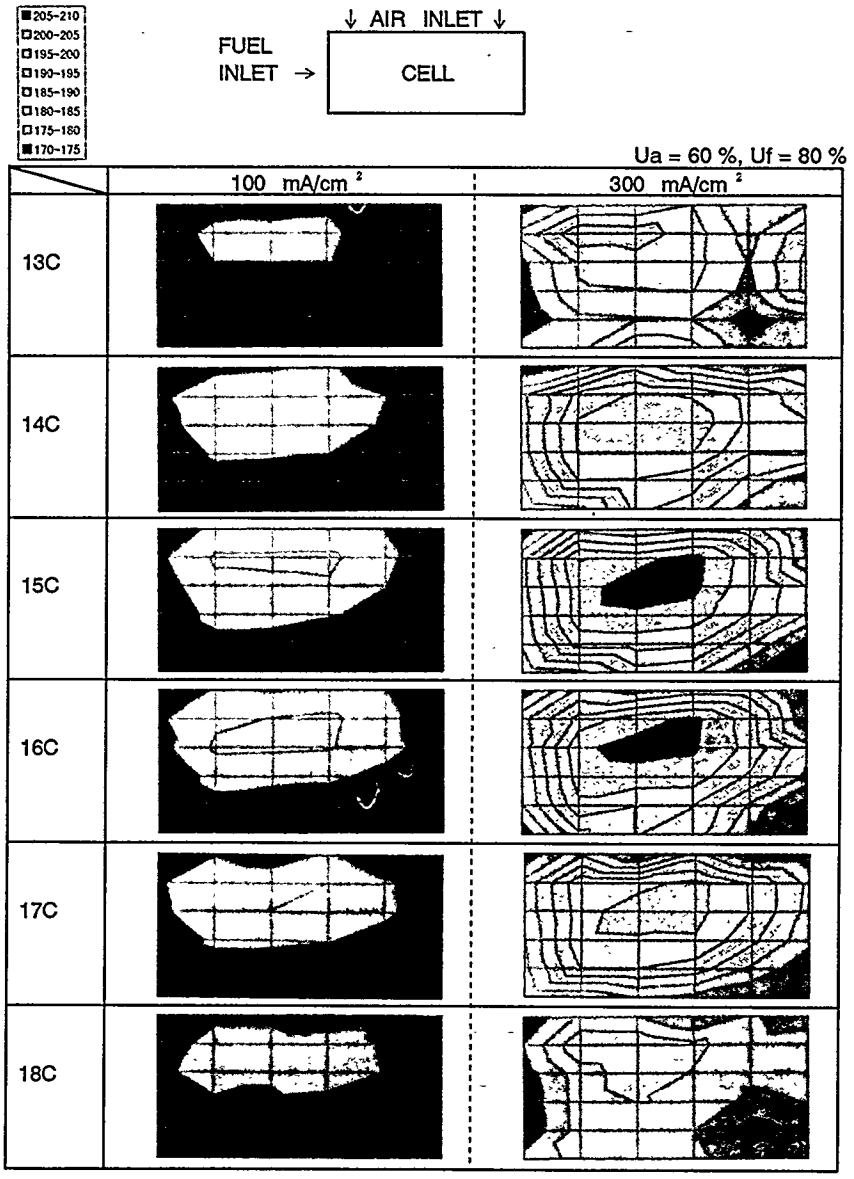

Figure 3 Temperature distributions of each cell at 100, 300 mA/cm ^{2}

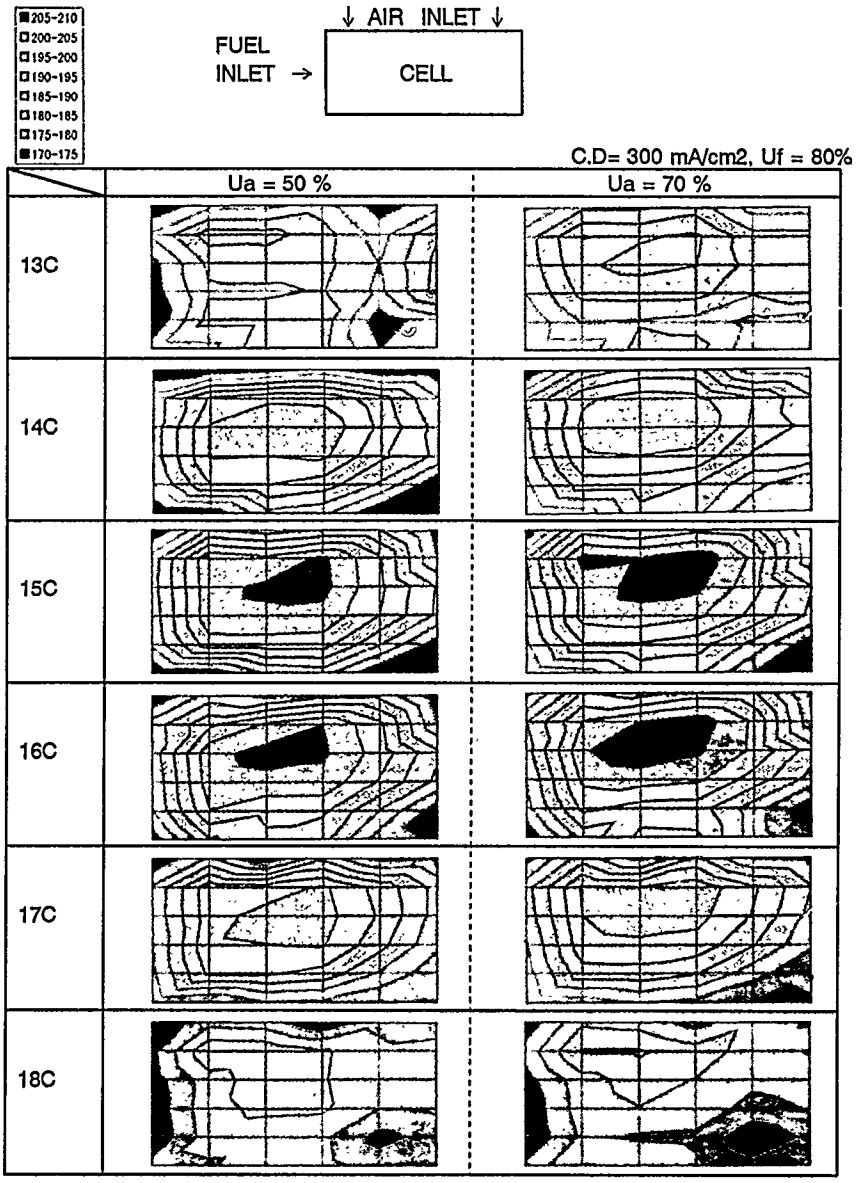

Figure 4 Temperature distributions of each cell at 50, 70% air utilization

EVALUATION OF THE ELECTRODE PERFORMANCE FOR PAFC BY USING ACID ABSORPTION, ACCELERATION AND AC-IMPEDANCE MEASUREMENT

Chang-Soo Kim, Rak-Hyun Song, Byung-Woo Choi, Dong Ryul Shin and Soo-Hyun Choi
Korea Institute of Energy Research, P.O.Box 103, Yousung, Taejon, KOREA

INTRODUCTION

In PAFC, the degradation on cathode electrode caused by carbon corrosion[1], platinum dissolution[2] and growth[3] is especially severe. An acceleration test is a good technique for evaluating the degradation of electrode performance, because it does not need long time. Coleman et al[4] used thermal cycling and on-off cycling as an acceleration test. Song et al[5] showed that hydrogen shortage decreased the electrode performance more rapidly than that of air shortage in gas shortage test. Honji et al[6] reported that the rate of coarsening of Pt particle is rapid in open circuit potential and this is one of major causes on the performance degradation of electrode. The cathode performance has been studied by using acid absorption, acceleration and ac-impedance measurements as functions of the polytetrafluoroethylene(PTFE) contents and sintering temperatures of the electrode.

EXPERIMENTS

To investigate the PTFE effect in the electrode, PTFE content was varied in the range of from 25 to 65 weight percent at the sintering temperature of 350℃. To investigate the sintering temperature effect in the electrode, temperature was varied in the range of from 310 to 390 ℃ and PTFE content was 45 weight percent.

Phosphoric Acid absorption on electrocatalyst layer and the cathode polarization are measured in 190℃ phosphoric acid. When the temperature of electrolyte is heated from room temperature to 190℃, the acceleration time is defined as the 0 hour. The 24 hour acceleration test is defined as the condition when the electrode is placed in open circuit potential for 24 hours under 190℃.

RESULTS AND DISCUSSION

Acid absorption in electrocatalyst layer with PTFE contents is shown in Fig.1. Acid absorption in electrocatalyst layer is increased with increasing time and saturated after 10 hours. Acid absorption in electrocatalyst layer is increased rapidly in the case of low PTFE contents like 25 wt.%. In the case of high PTFE contents like 65 wt.%, the slow rate of acid saturation in electrocatalyst layer is observed. But both cases are saturated within 10 hours.

In phosphoric acid fuel cell, carbon corrosion in electrocatalyst layer and the loss of PTFE film are produced continuously with increasing operation hours. The loss of PTFE film leads to decrement of hydrophobicity in electrocatalyst layer, phosphoric acid can be penetrated continuously into electrocatalyst layer. When the electrocatalyst contacts with phosphoric acid electrolyte, carbon corrosion and loss of PTFE film start in electrocatalyst layer. The corrosion of carbon is more severe when the electrocatalyst layer is placed at OCP. During acid absorption test, acid absorption rate decreases with increasing acid absorption time.After acid absorption arrived at saturation, the increased weight of electrocatalyst layer by acid absorption is same as its weight loss by carbon corrosion and loss of PTFE loss. Therefore the acid absorption is apparently shown to be saturated.

Electrode performance as a function of PTFE contents is shown in Fig.2. With increasing PTFE contents, the performance of cathode increases in the low PTFE region but decreases in the high PTFE region. In medium point of PTFE the electrode has maximum performance. The PTFE content that shows maximum performance in the variation of acceleration time is shifted from 35 wt.% to 45 wt.% of PTFE content with increasing of acceleration time. In the case of low PTFE

content, the acid absorption rate is higher than that of high PTFE content and also the absorbed acid quantity is also increased with decreasing PTFE content. So, in the initial stage of acceleration test, three phase reaction boundary is easily formed in the low PTFE content region and the good performance is shown in relatively low 35 wt.% PTFE. In Fig. 2, the electrode of low PTFE content is rapidly degradation with increasing acceleration test time. In 25 and 35 wt.% PTFE contents the electrode performance is rapidly lowered. This means that the electrode of low PTFE contents is easily flooded with increasing acceleration test time. In the case of PTFE content more than 45wt.%, the performance of the electrode increases slightly in 5 hour acceleration test than that of in 0 hour acceleration test, but the performance is decreased in 24 hour acceleration test.

Fig. 3 shows the electrode performance at $0.7V_{RHE}$ sintered at various temperatures. As stated above, the electrode sintered at 350°C showed the highest performance and it had current density of 305 mA/cm^2 at 5 hrs of acceleration test. Electrode performance may degrade rapidly by flooding due to carbon corrosion and loss of PTFE although it has high initial performance. To the contrary, the electrode having low initial performance may have long life if it has high wetproofing ability to the electrolyte. In other words, when the wetproofing ability is too high, flooding by electrolyte will be little but the electrode performance will decrease because of insufficient formation of 3 phase interface.

Figure 4 presents the measured impedance in Nyquist representation for the unwetted Pt/C electrode specimen subjected to 250, 300, 350, 450, 500 and $550mV_{RHE}$ in 1M H_2SO_4 solution. One does not observe the constant phase element (CPE) appearing due to a porous structure of the electrode which has a theoretical slope of 45° in the high frequency range of the Nyquist plot, indicating that the electrolyte does not infiltrate into the narrow pores of the unwetted Pt/C electrode. Thus, oxygen reduction occurring on the surface of the unwetted Pt/C electrode mainly contributes to the resulting cathodic current of the ac-impedance response. For the unwetted Pt/C electrode subjected to potentials from 250 to 550 mV_{RHE} (Fig. 4), one high frequency capacitive arc and one low frequency inductive arc are observed. The occurrence of the low frequency inductive arc indicates that oxygen reduction proceeds via formation of intermediate states on the unwetted Pt/C electrode specimen. The magnitude of the overall impedance increases with decreasing overpotential for oxygen reduction.

The Nyquist plots for oxygen reduction on the pre-wetted Pt/C electrode specimen subjected to 250, 300, 350, 450, 500 and 550 mV_{RHE} in 1 M H_2SO_4 solution are shown in Fig. 5. In contrast to the unwetted Pt/C electrode specimen, the impedance spectra obtained from potential range from 250 to 550 mV_{RHE} consist of the CPE with a slope of 45°, one high frequency capacitive arc, and on low frequency capacitive arc. The appearance of the CPE in the high frequency range indicates that the electrolyte infiltrates into the narrow pores of the pre-wetted Pt/C electrode specimen. Considering that the overall impedance value of the pre-wetted Pt/C electrode specimen is smaller by three orders in magnitude than that of the unwetted Pt/C electrode specimen, oxygen reduction occurring within the narrow pores mainly contributes to the resulting cathodic current of the ac-impedance response. The inductive to capacitive transition in impedance spectra with pre-wetting treatment implies the change in mechanism and kinetics of oxygen reduction.

CONCLUSIONS

From the investigation of acid absorption, half cell polarization experiment through acceleration and ac impedance measurement with the electrode fabricated by varying the PTFE content and sintering temperature, the following conclusions are drawn:

1. The PTFE content that shows maximum performance is shifted from 35 wt.% to 45 wt.% of PTFE content with increase of acceleration time. In the case of low PTFE content, the acid absorption rate is higher than that of high PTFE content and also the absorbed acid quantity is also increased with decreasing PTFE content.

2. The optimum condition of sintering temperature is 350℃. When the sintering temperature is lower than 350℃,the performance of electrode is rapidly decreased and the phenomena is closely related with poor formation of PTFE film and microstructure concerned acid absorption.

3. From the analysis of ac-impedance measurement, the impedance spectra change from a capacitive arc and an inductive arc to two capacitive arcs, as depletion of the dissolved oxygen within narrow pores markedly appears. It is indicative of changes in mechanism and kinetics of oxygen reduction on the electrode in 1M H_2SO_4 solution at room temperature.

ACKNOWLEDGMENT

This work is supported by the Ministry of Trade, Industry and Energy, Korea.

REFERENCE

1. G. A. Gruver, J. Electrochem. Soc., 125, 1719 (1978)
2. P. Bindra, S.J. Clouser, and E. yeager, J. Electrochem. Soc., 126, 1631 (1979)
3. J. Aragane, T. Murahashi, and T. Odaka, J. Electro. Soc. 135,844 (1988)
4. A.J. Coleman, A. A. Adams, J. A. Jocbstl, and G. W. Walker, Power Source Conference, 29th, 9-13 (1980).
5. Rak-Hyun Song, Chang-Soo Kim, Byung-Woo Choi, Dong-Ryul Shin, Soo-Hyun Choi, Hwahak Konghak, 31, 6, 735-743 (1993).
6. A. Honji, T. Mori, K. Tamura, and Y. Hishinuma, J. Electrochem. Soc., 135(2) 355-359 (1988).

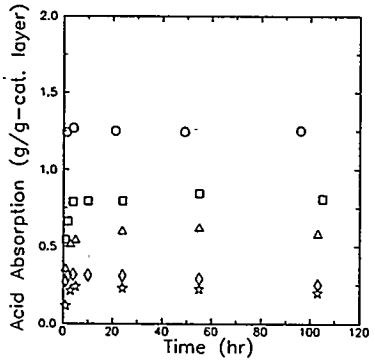

Fig.1. Acid absorption in electrocatalyst layer with variation of 25wt% (○), 35wt% (□), 45wt% (△), 55wt% (◇), and 65wt% (☆) of PTFE contents.

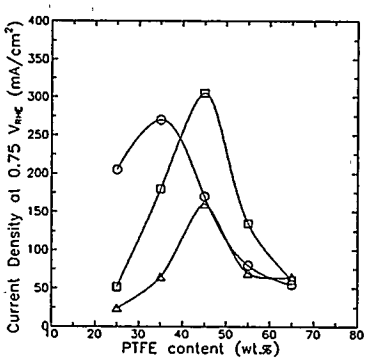

Fig.2. Current density (mA/㎠) of cathode at 0.75VRHE as a function of PTFE contents in the electrocatalyt layer. Reaction gas is oxygen. Accelcration test time are 0 hour (○), 5 hour (□), and 24 hour (△).

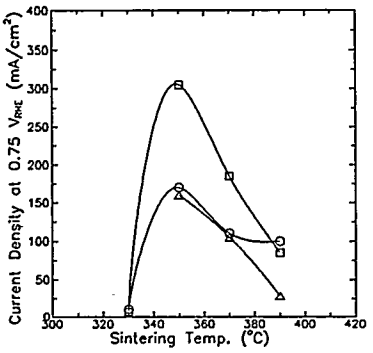

Fig.3. Current density (mA/㎠) of cathode at 0.75 VRHE as a function of sintering temperature. Reaction gas is oxygen. Acceleration test time are 0 hour (○), 5 hours (□), 24 hours (△).

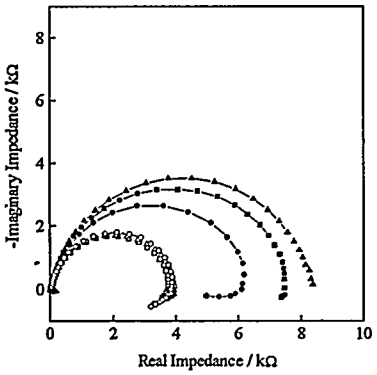

Fig.4. Nyquist plots for oxygen reduction on the unwetted Pt/C electrode subjected to various applied potentials of: 250 mV_{RHE}, ○;300 mV_{RHE},□;350 mV_{RHE},; 450 mV_{RHE},●; 550 mV_{RHE}, ■; 550 mV_{RHE}, ▲ in 1M H_2SO_4 solution.

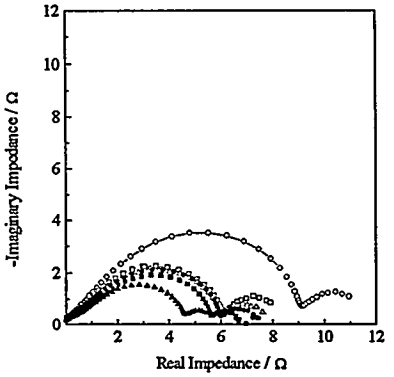

Fig.5. Nyquist plots for oxygen reduction on the pre-wetted Pt/C electrode subjected to various applied potentials of: 250 mV_{RHE}, ○;300 mV_{RHE},□;350 mV_{RHE}, ; 450 mV_{RHE}, ●; 500 mV_{RHE}, ■; 550 mV_{RHE}, ▲in 1M H_2SO_4 solution.

BREAKING DOWN THE BARRIERS TO COMMERCIALIZATION OF FUEL CELLS IN TRANSPORTATION THROUGH GOVERNMENT - INDUSTRY R&D PROGRAMS

S. G. Chalk
Office of Transportation Technologies
U.S. Department of Energy
Washington, D.C.

S. R. Venkateswaran
Energetics, Inc.
Columbia, Maryland

PEM FUEL CELLS FOR AUTOMOTIVE APPLICATIONS

PEM fuel cell technology is rapidly emerging as a viable propulsion alternative to the internal combustion engine. Fuel cells offer the advantages of low emissions, high efficiency, fuel flexibility, quiet and continuous operation, and modularity. Over the last decade, dramatic advances have been achieved in the performance and cost of PEM fuel cell technologies for automotive applications. However, significant technical barriers remain to making fuel cell propulsion systems viable alternatives to the internal combustion engine. This paper focuses on the progress achieved and remaining technical barriers while highlighting Government-industry R&D efforts that are accelerating fuel cell technology toward commercialization.

GOVERNMENT - INDUSTRY R&D PROGRAM

The U.S. Department of Energy (DOE) is spearheading an ambitious, cost-shared, Government-industry R&D program with the goal of developing highly efficient, low or zero emission, automotive fuel cell propulsion systems utilizing conventional and alternative fuels. The near-term objective of the program is to validate fuel cell power systems by the year 2000 that are:

- Greater than 51 percent energy efficient at 40-kW maximum power;
- More than 100 times cleaner than U.S. Environmental Protection Agency (EPA) Tier II emissions;
- Capable of operating on gasoline, methanol, ethanol, natural gas, or hydrogen.

Longer-term objectives (by year 2004) are to validate fuel cell propulsion systems that meet consumer expectations, i.e., have competitive costs with internal combustion engines and equivalent or better performance, range, safety, and reliability.

A major driver for the Transportation Fuel Cell Program is the Partnership for a New Generation of Vehicles (PNGV), which has selected PEM fuel cells as one of three primary propulsion candidates for achieving the goal of tripling automobile fuel economy (80 miles per gallon [mpg] mid-size sedan). Vehicle systems analyses have been performed to establish a matrix of technological approaches. Figure 1 illustrates the approximate "design space" for possible alternative approaches

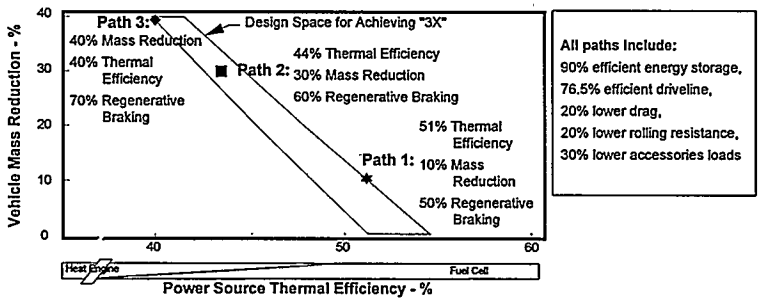

Figure 1: Approximate "Design Space" for Achieving 3X Fuel Economy Improvement

to achieving the PNGV goal (1). This figure clearly indicates the particular appeal of fuel cells — their higher efficiencies would lessen the requirement for mass reduction and other vehicle system improvements to meet the PNGV's 80-mpg goal.

To effectively address PNGV requirements and overcome the significant technical barriers facing fuel cells, the *National Fuel Cell Alliance* (see Figure 2) has been established among DOE, industry, national laboratories, and universities. The Alliance provides a mechanism for obtaining industry consensus and recommendations for program direction and it facilitates sharing of government-sponsored fuel cell R&D results among the domestic auto industry. Under this structure, the Big Three U.S. automakers provide technical requirements through the United States Council for Automotive Research (USCAR) and will determine whether the fuel cell technology meets customer expectations. DOE maintains overall management responsibility for the program and contracts with fuel cell developers, component suppliers, and research institutions to conduct the pre-competitive R&D identified by USCAR. Independent teams of the Big Three automakers and fuel cell and component suppliers have formed to apply the results of this research to develop fuel cell vehicles. National laboratories and universities are conducting supporting R&D on enabling technologies (e.g. fuel processing technologies) and advanced concepts (e.g. direct methanol fuel cells). Close coordination is maintained with DOE's Hydrogen Program with respect to fuel reforming and hydrogen production and storage development activities.

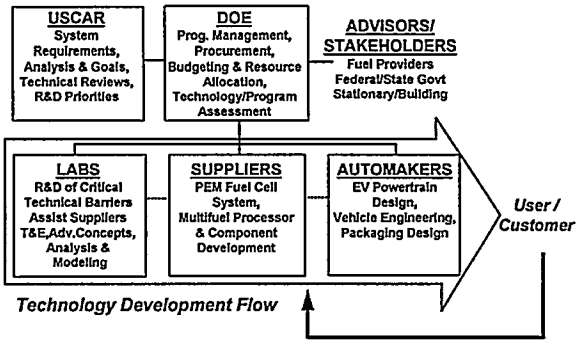

Figure 2: National Fuel Cell Alliance

FUEL CELL STACK DEVELOPMENT PROGRESS

Since 1990, the DOE-industry R&D program has supported PEM stack development by various fuel cell suppliers including Energy Partners, International Fuel Cells, Mechanical Technology, Inc., Analytic Power, Delphi Automotive, and AlliedSignal. These suppliers are focusing on automotive-scale fuel cell power sources, nominally 50-kW.

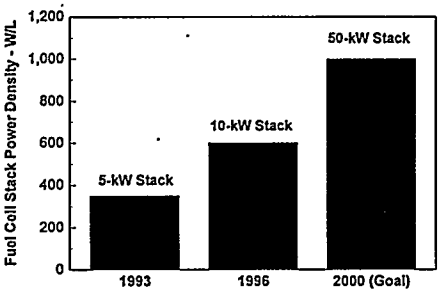

Figure 3: PEM Stack Development Progress (DOE Program)

The DOE programs have achieved significant progress in PEM stack development, as shown in Figure 3 in terms of the stack power density, a key measure of performance and size. The power density of 600 W/L achieved in 1996 (with a 10-kW PEM stack) represents almost a doubling of the levels achieved in 1993 with a 5-kW stack. This increase in power density has been achieved despite an order of magnitude reduction in platinum loading from 4 mg/cm^2 to 0.25 mg/cm^2. The Program has already met the platinum loading goal for the year 2000 at the 10-kW scale in 1996, but not yet at the required scale of 50-kW. Bipolar plates have also become lighter, with some suppliers having changed from graphite to metal plates. DOE is planning a new three-year development program with a stack power density goal of 1000 W/L, by

the year 2000. This will contribute to a PNGV system goal of 350 W/L which includes the heat, water, and gas management systems in addition to the stack. This system power density goal is critical to meeting automotive performance and packaging requirements and will be the key measure of success for the new development program. Looking beyond the year 2000, the next major (and ultimate PNGV) goal is to achieve a system power density of 400 W/L by the year 2004.

FUEL PROCESSING DEVELOPMENT PROGRESS

The overall fuel strategy for DOE's Transportation Fuel Cell Program is shown in Figure 4. The Program seeks to establish a fuel-flexible pathway (to commercialization of fuel cells) that is pragmatic in the near term and capable of using the existing fuel infrastructure while driving toward long-term sustainable energy supplies based on a renewable fuel infrastructure.

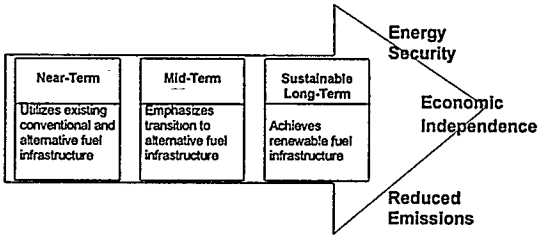

Figure 4: Fuel Strategy for DOE Transportation Fuel Cell Program

Since the near-term strategy emphasizes fuel flexibility, the DOE program is developing fuel-flexible fuel processors that reform gasoline, ethanol, natural gas, and methanol to hydrogen. The state of fuel processor "system" development is currently lagging fuel cell stack development. This is especially true for PEM fuel cells because of reformate gas purity requirements. In terms of transient response time and start-up capabilities, fuel processing technology has not yet been demonstrated at the automotive scale. However, as shown in Figure 5, the DOE program has achieved encouraging progress as of 1996. Fuel processor power density, a key measure of performance and size, exceeds 500 W/L (excluding CO clean-up system and controls). The year 2000 goal for the fuel processor system power density is 600 W/L. Another key parameter for viability is fuel processor system cost. Arthur D. Little, Inc. estimates that a fuel- flexible fuel processor would cost approximately $20/kW, assuming high volume production (2). Further cost reduction is needed.

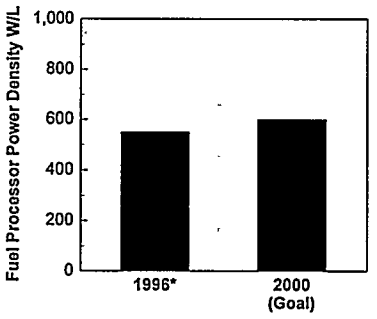

Figure 5: DOE Fuel Processor Development

OVERCOMING REMAINING TECHNICAL BARRIERS

DOE is planning a new three-year development program to address the significant remaining technical barriers to achieving the viability of fuel cell technology in transportation. For the fuel cell power system, key areas include carbon monoxide (CO) poisoning, stack material cost/performance (bipolar plates, membrane electrode assemblies, carbon paper), thermal management, and integrating balance of plant (compressors, humidifiers, heat exchangers, sensors, and controls). For the fuel processor, key challenges include CO cleanup, system integration and efficiency, start-up/transient operation, and thermal management. Hydrogen storage and overall propulsion system integration and validation also require serious attention. Based on priorities and guidance provided by the auto industry, DOE is addressing these barriers by focusing its component development activities on the following:

- CO cleanup devices and CO tolerant fuel cell catalysts;

- Lightweight, low-cost bipolar plates;
- Low-cost, high-volume manufacturing processes and materials for membranes and membrane electrode assemblies; and
- Balance of plant ancillary components such as compact heat exchangers, sensors, and controls.

BREAKING DOWN COST BARRIERS

The present cost of PEM fuel cell systems (projected to high volume production) needs to be reduced to less than $50/kW to be competitive with internal combustion engines. Figure 6 shows the year 2000 and ultimate (year 2004) cost targets for automotive applications established by the DOE-industry program. Breaking down the cost barrier will require choosing appropriate materials (with adequate performance) that are suitable for high volume manufacturing processes. This will be accomplished through the component R&D activities (discussed above) in which both industry and the national laboratories will play key roles. The expertise of the national laboratories with advanced materials and processing techniques will be critical to the success of these efforts.

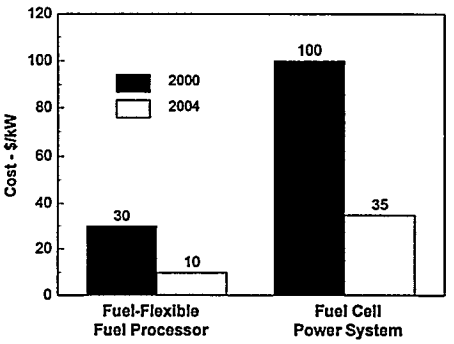

Figure 6: Cost Targets for the DOE-Industry Program

Intelligent system trade-offs between performance, size, and cost will also be required to reduce the costs of the fuel cell power system and fuel processor. For example, initial efforts to increase fuel cell performance have led to the development of high efficiency compressors and expanders. However, this increased performance needs to be evaluated against the added size and cost of the compressor/expander to the total power system. Several developers are now pursuing low or ambient pressure operation of the stack as an option to resolving this trade-off. In the fuel processing area, the total system impact of choices for the type of CO cleanup (i.e., preferential oxidation, filters, etc.) has to be carefully evaluated because of the serious implications for performance, size, and cost.

FUTURE DIRECTIONS

During the next few years, the DOE-industry R&D program will focus on increasing performance and reducing the size of the fuel cell and fuel processor systems. Cost reduction will also be a priority, through component, materials, and processing R&D as well as design trade-offs that might compromise performance and size in favor of simpler, less expensive systems and components. Planned 1997 procurements from the DOE program will target the year 2000 technical goals for the fuel cell and fuel processor systems as well as component R&D to address critical technology barriers prioritized by industry. These efforts will serve to further reduce the risk associated with fuel cell technology in vehicular applications and determine if the promise of affordable, clean, efficient, and reliable fuel cell power systems for transportation will be realized.

REFERENCES

1. "PNGV. Partnership for a New Generation of Vehicles Program Plan," The Government PNGV Secretariat, U.S. Department of Commerce, Washington, DC. Revised November 1995.

2. W. L. Mitchell, J. H. J. Thijssen, J. M. Bentley, and N. J. Marek, "Development of a Catalytic Partial Oxidation Ethanol Reformer for Fuel Cell Applications", SAE Paper # 952761, The Society of Automotive Engineers, 1995.

PEFC R&D TECHNOLOGY AT TOYOTA

Shigeyuki Kawatsu, Satoshi Aoyama and Masayoshi Iwase
Higashifuji Technical Center
TOYOTA MOTOR CORPORATION
1200, Mishuku, Susono, Shizuoka 410-11 JAPAN

1. INTRODUCTION

Fuel cells are being considered as notable new energy sources due to, not only their potential for obtaining high energy conversion efficiencies, but also their environmental sensitive features. These are especially important now that the problems relating to global environmental pollution are regarded as serious social issues. Polymer electrolyte fuel cells (PEFCs) in particular are being pursued due in part to the prospect of realizing timely enhancements to several key characteristics, including size and power. Encouraged by these anticipated improvements, PEFCs are being investigated as promising power generator candidates for hybrid electric vehicles.

The substantial future potential of PEFCs has been noted by TOYOTA, and has motivated extensive R&D activities toward the practical application of PEFCs to hybrid electric vehicles. These R&D efforts include, not only activities on such key areas as performance enhancement, but also extensive attention to a broad range of related concerns, such as cost reduction, reformer development, system integration, durability, reliability and so on. From these diverse tasks, this paper focuses on the issues related to ensuring adequate PEFC performance when reformed fuel is utilized. Recent outcomes of R&D conducted at TOYOTA on this topic will be described.

2. PEFC POWERED ELECTRIC VEHICLE DESIGN

The optimum design of an electric vehicle powered by a PEFC is a hybrid system, consisting of a PEFC and a secondary battery, as shown in Figure 1. The secondary battery plays multiple roles - load leveling against variations in load, power supply for activation of the PEFC and storage of the electric energy regenerated from braking. A PEFC powered hybrid electric vehicle system should be capable of operating in a high energy conversion efficiencies region, and of attaining higher fuel economies than those of an internal combustion engine (ICE) powered hybrid electric vehicle system.

3. FUEL SUPPLY METHOD

When considering the application of a PEFC to an automobile, questions arise on the best method to supply hydrogen fuel to the system. Of the options investigated, onboard reforming offered important merits over direct hydrogen storage, including ease of refueling and the potential to increase vehicle operating range. For vehicle applications hydrogen supplied via steam reforming of methanol was determined to be most appropriate, considering the following features:

1) lower reforming temperature and reduced reforming energy requirements;
2) small amount of by-products to be generated during the reforming process;
3) existence of a relatively well established refueling infrastructure
(with current markets for methanol engine vehicles); and
4) independence from crude oil resources, as methanol is made from natural gas.

4. PEFC OPERATION WITH REFORMED GAS

Theoretically, the reformed gas generated by the methanol steam reforming reaction should be composed of 75% H_2 and 25% CO_2. In practice, however, the gas also contains some residual methanol and a small amount of carbon monoxide (CO). There was some concern at TOYOTA regarding the possible adverse effects that these components - and CO in particular - may have on PEFC performance. It was confirmed that PEFC performance deteriorates markedly, where a platinum (Pt) electrocatalyst is used, if CO concentrations in the reformed gas are even 20ppm. [1]

In order to remain within the size and weight limitations required for the application of PEFCs to

electric vehicles, the prevention of any drop in energy conversion efficiency is essential. This is also important in order to create cost reductions to allow for practical mass production. Therefore, controlling the effects of CO is necessary. As for the appropriate approach for the prevention of CO poisoning, the utilization of a combination of methods appears most practical. This combination would include, installation of shifter and/ or CO selective oxidizer to the reformer, reducing the CO concentrations in the reformed gas to a given level, and modification of the PEFC anode electrocatalyst, providing an appropriate level of CO tolerance in the PEFC. In other words, it is vital for successful CO control to establish well-balanced measures in both the reformer and PEFC itself.

5. INVESTIGATION RESULTS

5.1 CO Reduction in the CO Selective Oxidizer

Using a model gas corresponding to that of reformed methanol, the CO selective oxidation performance of various catalysts was evaluated. As shown in Figure 2, the Ru catalyst was found to be capable of reducing CO concentration in a wider operating temperature range and in a wider range of gas flow rates than that of the well-known Pt catalyst widely used for the CO selective oxidizer. These results indicate that, by using the Ru catalyst for the CO selective oxidizer, it is possible to supply reformed gas with a stably low CO concentration, continuously, against the load variations imperative for automobile operation.[2]

Side reactions that occur in the CO selective oxidizer were studied to help to elucidate the reason for the excellent CO selective oxidation characteristics shown by the Ru catalyst. It is known that CO is generated by the reverse shift reaction, as expressed in Equation (1), which occurs in the CO selective oxidizer.[3]

$$H_2 + CO_2 \rightarrow CO + H_2O \quad (1)$$

In order to check the influence of reverse shift reaction, a model gas (CO_2=25%, H_2=75%) not containing CO was humidified and fed, without air, into a CO selective oxidizer. The CO concentration in the out going gas was then measured. It was clearly found that the amount of CO generated with the Ru catalyst was smaller than that with the Pt catalyst, as shown in Figure 3.

Also known to occur in the CO selective oxidizer, where a noble metal catalyst is used, are the methanation reactions expressed in Equations (2) and (3).

$$CO + 3H_2 \rightarrow CH_4 + H_2O \quad (2)$$
$$CO_2 + 4H_2 \rightarrow CH_4 + 2H_2O \quad (3)$$

To check the relationship between the CO and CH_4 concentrations formed, another model gas (CO=0.1%, CO_2=25%, H_2=balance) containing CO was humidified and fed, without air, into a CO selective oxidizer. As the results in Figure 4 indicate, as the catalyst temperature rose, the CH_4 concentration tended to increase while the CO concentration tended to decrease. Additional investigations indicated that these reactions occurred more readily when the Ru catalyst was utilized for CO selective oxidation.[4]

Detailed analysis produced further insight into the reverse shift reaction and methanation reactions, as well as the benefits of Ru utilization. In the case of an oxidizer using the Pt catalyst, CO is oxidized into CO_2, but then a portion reverts back to CO via the reverse shift reaction. Though this reversal also occurs where the Ru catalyst is used, it is to a lesser extent. In addition, with Ru, a portion of the CO generated by reverse shift reaction is converted to CH_4 as methanation reaction occurs. Consequently, the Ru catalyst is capable of producing lower levels of CO at the oxidizer outlet, owing, not only to reduced reverse shift reaction, but also to this CO to CH_4 conversion. Thus, in view of these results, as well as obvious cost advantage over Pt, a compact, low cost methanol reformer, suitable for automotive use, can be devised by the application of Ru to the CO selective oxidizer.

5.2 Prevention of CO Poisoning with Alloy Electrocatalyst

In order to enhance the CO tolerance of the PEFC anode electrocatalysts, the CO tolerances of

several Pt based alloy electrocatalysts were evaluated. Proper alloying of the experimental catalysts were confirmed by means of X-ray diffraction prior to evaluation. Utilizing a Pt cathode electrocatalyst and anode gas containing 100ppm CO the samples were evaluated. Figure 5 shows a comparison of the cell voltage measurements obtained at a current density of 0.4A/cm^2. Only the Pt-Ru electrocatalyst exhibited a higher CO tolerance than the unalloyed Pt electrocatalyst.

Once the Pt-Ru electrocatalyst was identified as superior in CO performance, the alloy ratio was then optimized, as was the active layer thickness and supporting process of the Pt-Ru electrocatalysts. Using the knowledge obtained by these optimization efforts, a new type of Pt-Ru electrocatalyst was prepared, and its performance in the PEFC was evaluated. As shown in Figure 6, cell performance equivalent to that of a Pt electrocatalyst was obtained, and performance similar to that in pure hydrogen was obtained, even with gas containing CO concentrations of 100ppm.[5][6]

5.3 Prevention of the Effects of CO_2

In addition to CO, reformed gas also contains CO_2. The probable detrimental effects on the PEFC, anticipated by the presence of CO_2, were investigated. As a result, two phenomena were found, namely, CO poisoning and CO_2 barrier effect. CO generated from the CO_2 contained in the reformed gas was found to poison the electrocatalyst. [7] Additionally, the CO_2 was found to stagnate around the anode. Due to the greater specific gravity of the CO_2, this stagnation impeded the diffusion of H_2 over the electrode's active layer and lowered performance.

As indicated earlier, the poisoning caused by CO can be successfully averted by the application of a Pt-Ru alloyed anode electrocatalyst to the PEFC. Regarding the control of the CO_2 barrier effect, optimization of the gas flow field shape was found to be the most effective. In other words, by combining the knowledge of electrocatalysts and gas flow fields, it is possible to prevent the adverse effects of CO_2 contained in the reformed gas.[8]

5.4 Prevention of the Effects of Residual Methanol

Because reformed gas was also found to contain some residual methanol, its effects on cell performance needed to be clarified. Cell performance was measured using a model reformed gas containing various concentrations of methanol. It was found that as methanol concentrations increased cell performance decreased. As expected, Pt electrocatalyst poisoning was one of the sources of the deteriorating performance. This poisoning was caused by the dissolution of methanol in the anode, resulting in the formation of poisonous aldehyde. The occurrence of another phenomenon was also confirmed, methanol crossover. Methanol contained in the anode gas permeated into the electrolyte membrane, reaching the cathode and reacting with oxygen contained in the air, thus, lowering the potential of the cathode.

Nevertheless, it was concluded that these adverse effects of residual methanol can be reduced to an acceptable level with the employment of both a Pt-Ru anode electrocatalyst, and optimization of PEFC operating conditions. [9]

6. CONCLUSIONS

As described, extensive knowledge has been gained on electrocatalysts, electrode structures, gas flow fields, PEFC operating conditions, catalysts for CO selective oxidizer, etc. Through the application of this knowledge to the methanol reformer and PEFC, it has become possible to attain cell performance equivalent to that in pure hydrogen when utilizing a methanol reformer and reformed gas in the PEFC system.

TOYOTA is continuing to conduct studies in the various areas mentioned earlier. Further development of the PEFC itself is naturally necessary. However, it will also be vital to enhance overall vehicle and component performance, including that of the secondary battery, to allow the practical adoption of PEFCs in the near future. TOYOTA will continue to aggressively pursue R&D in this field in order to realize the effective use of electric vehicles powered by PEFCs.

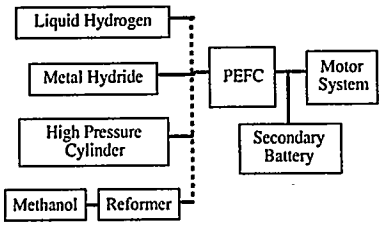

Fig.1 Design of EV Powered by PEFC

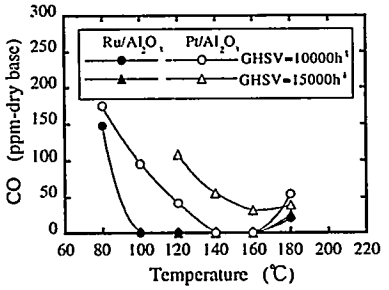

Fig.2 CO Oxidation Performance of Ru and Pt Catalysts

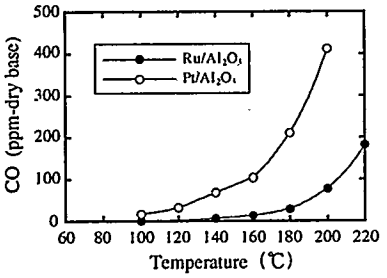

Fig.3 Reverse Shift Reaction of Ru and Pt Catalysts

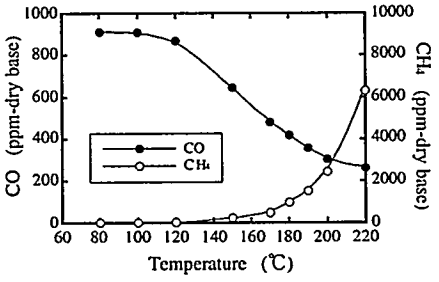

Fig.4 CO Methanation Reaction of Ru Catalyst

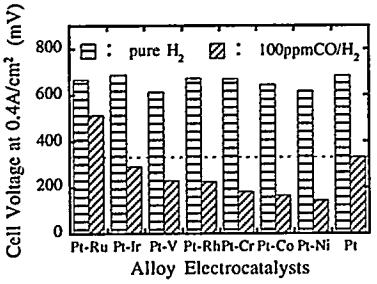

Fig.5 CO Tolerance of Alloy Electrocatalysts

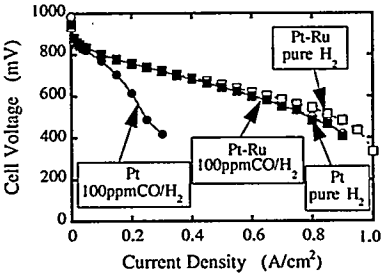

Fig.6 CO Tolerance of Developed Pt-Ru Alloy Electrocatalyst

REFERENCES
1) S. Kawatsu and M. Iwase, Abst. The 35th Battery Symposium in Japan, p.299 (1994)
2) S. Aoyama, Proc. The 2nd FCDIC Fuel Cell Symposium, p.235 (1995)
3) R. D. Sutton and N. E. Vanderborgh, Proc. The Annual Automotive Technology Development Contractors' Coordination Meeting 1992, p.493 (1992)
4) S. Aoyama, S. Kawatsu and M. Iwase, Abst. The 36th Battery Symposium in Japan, p.243 (1995)
5) S. Kawatsu and M. Iwase, Abst. The 36th Battery Symposium in Japan, p.241 (1995)
6) M. Iwase and S. Kawatsu, Proc. The 1st Int. Symposium on Proton Conducting Membrane Fuel Cells, (Proceedings Volume 95-23), p.12 (1995)
7) M. S. Wilson, C. R. Derouin, J. A. Valerio and S. Gottesfeld, Proc. The 29th Intersoc. Energy Convers. Eng. Conf., p.1203 (1993)
8) S. Kawatsu and M. Iwase, Proc. The Electrochemical Society of Japan 1995 Fall Meeting, p.206 (1995)
9) S.Kawatsu and M.Iwase, Proc. The 62nd Meeting of The Electrochemical Society of Japan, p.76 (1995)

FUEL CELL SYSTEMS FOR PASSENGER CARS - OPPORTUNITIES AND REQUIREMENTS

Joachim Tachtler
BMW
D-80788 Munich
Germany

Carl Bourne
Rover Group
Coventry CV4 7AL
United Kingdom

Possible forms of energy for the propulsion of passenger cars

From the point of view of energy density, handling and economy, present-day motor fuels are superior to all known alternatives. The internal combustion engine powered by them satisfies the requirements of customers to an excellent degree.

The search for alternatives can therefore only be justified if emissions can be avoided totally and non-fossil primary energy sources can be used or at least partially our dependence on mineral oil can be reduced.

What was long suspected has been increasingly confirmed, not least by developments at BMW: electricity (stored in batteries) and hydrogen offer the best prerequisites for achieving these goals in the long term. These forms of energy can be produced in sufficient quantities and with relatively little effect on the environment. They promise to produce an absolute minimum of pollutants when used in vehicles.

Natural gas, which is very similar to hydrogen, and hybrid systems, that would compensate for battery risks, could perform a valuable function in the transitional phase.

Significant improvements in the performance of fuel cells

Fuel cells produce electric current direct from chemical fuels, preferably hydrogen. They offer the potential of powering vehicles with electric drive system with an increased operating range. Of the various types of fuel cells, the most interesting for use in passenger cars is the PEM (polymer electrolyte membrane) fuel cell. Today it can already be operated at temperatures between 4 and 80°C. Oxygen, necessary for the reaction, is obtained from pressurized ambient air [1].

For several years, specialists in electrochemistry – also in collaboration with car development engineers – have been trying to make fuel cell technology a useful source of motive power. Considerable improvements in performance have been achieved in recent years. The main motivation for these developments is the high potential efficiency and the possibility of the classification as a "Zero Emission Vehicle" (ZEV), at least if hydrogen is carried on board.

At Solar-Wasserstoff-Bayern GmbH (SWB), a company in which BMW has been an active partner since 1987, tests have been carried out starting in 1990 on various fuel cells for stationary and mobile applications [2]. A ground conveyor vehicle equipped with the first Siemens air/hydrogen fuel cell system will start trials at SWB in Neunburg in late 1996. Siemens has several decades of experience derived from developing fuel cell drive systems for submarines [3].

The energy consumption of the complete fuel cell system is an especially important consideration. Although the efficiency of single cells is theoretically very high, the additional energy for the cooling system, the air compressor and the controller have to be taken into account. It therefore seems more sensible to develop fuel cells that can be operated at low pressures than to aim for high power density at the cost of high pressures. This is made all the more important by the need to use excess air (λ approx. 2). The new Siemens system is particularly interesting, as its maximum operating overpressure is only 0.5 bar.

Besides the need for efficiency and low pollution, fuel cells must prove their worth in everyday use. The critical performance factors are rapid start-up, fast response to changes in power demand, such as we are used to with internal combustion engines, and also reliable operation under all environmental conditions. Temperatures below freezing could be a problem here. There also exists no experience of how fuel cells cope with real conditions such as sustained road induced vibration or long periods at rest.

A significant problem faced by the automotive sector is the issue of cost. Key requirements for the reduction of the production costs - currently several million DM for each fuel cell system - are the development of mass productionable bipolar plates, inexpensive and environmentally compatible membranes and the minimization of platinum in the electrodes. Present fuel cells contain so much platinum that there are not sufficient known world reserves to equip all the vehicles currently in use. The amount of platinum per vehicle must therefore be reduced to the level of present-day exhaust catalytic converters with a similar level of platinum recoverable through recycling.

Zero-emission vehicle with a high range

Although fuel cell technology will probably be initially commercialized for stationary electrical power generation, it is interesting to know that it is now technically feasible to power passenger cars with fuel cells – albeit with certain restrictions. On the subject of this fascinating challenge, BMW presented at the World Hydrogen Energy Conference "Hydrogen '96" its initial study for an experimental ZEV with a range of 1000 km. The vehicle concept is based on a 3 Series BMW with liquid hydrogen tank, fuel cell system and electric motor.

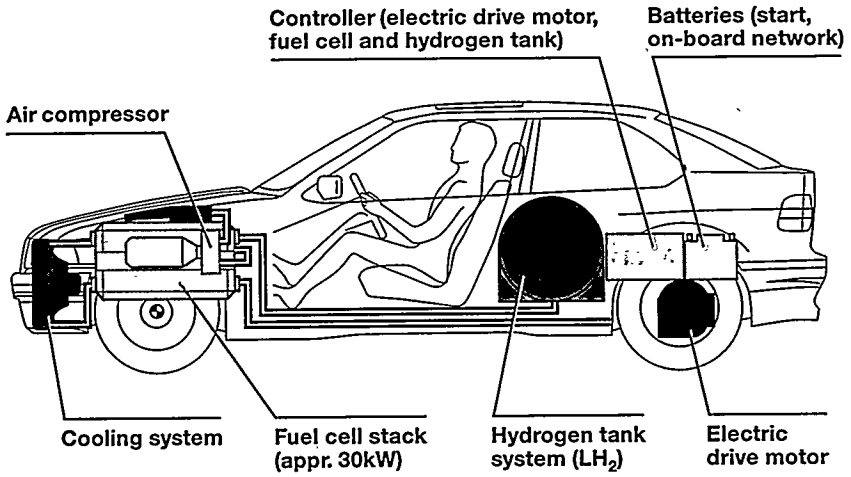

Fig. 1: Basic concept for an experimental "ZEV with a range of 1000 km" [4]

The current state of development of fuel-cell systems leaves several disadvantages: apart from the high costs and low power output, the weight and volume are still too high. Besides the fuel-cell stack and hydrogen supply, the vehicle must also house various auxiliaries needed for operation. Their size is largely determined by the nominal power rating, operating pressure, and maximum operating temperature. For example, the cooling system must be significantly larger than that of an internal combustion engine, owing to the relatively low permissible temperature for the cooling fluid and the reduced quantity of heat which can be dissipated via the 'exhaust'.

Liquid hydrogen (LH_2) was chosen in order to achieve the greatest possible range, but also because of the purity required by PEM fuel cells. LH_2 has a much higher energy density than other forms of hydrogen storage. The alternatives, high-pressure cylinders or metal hydride storage, are so bulky and heavy that they would compromise the vehicle's performance in terms of range, safety and handling to the extent where their use would offer no advantage over conventional battery vehicles. For short-haul traffic, battery vehicles excel themselves through a higher overall efficiency under certain conditions.

The described vehicle concept represents the practical optimum with the available fuel cell technology, taking into account safety and convenience in everyday use. However, the advances made with fuel cells should not let us forget that with the same basic vehicle equipped with conventional technologies at relatively low costs considerably higher payloads and roughly five times the power are achievable, whilst still remaining below emission limits set for the Ultra Low Emission Vehicle (ULEV).

Emission problems with on-board generation of hydrogen

Since there is no existing hydrogen infrastructure and the costs of providing it are high, work is also being carried out on systems for generating hydrogen in the vehicle. Of all the chemical fuels which are liquid at normal temperatures, methanol is the easiest to convert to hydrogen. Experiments with gasoline are also under way, with a view to using the existing network of filling stations. Direct on-board reforming of natural gas would be another way to avoid the energy losses involved in first producing methanol.

The development of the necessary reformer systems for hydrogen production concentrates on its behaviour under start-up and transient loads as well as energy efficiency, but must take also into account the by-products which are produced. Even if no immediate poisoning of the electrodes can be detected, the influence of lowest concentrations of impurities over the life of the fuel cell remains hard to estimate. It is also an open question whether a system consisting of fuel cell plus reformer could meet the requirements to be classified as an "Equivalent ZEV" (EZEV), taking into account the necessary overall assessment of emissions for this classification.

To complement BMW activities, Rover is involved in a joint project funded by the EU to develop a system of steam reforming of methanol suitable for use in vehicles. CJB, the partner responsible for developing the reformer, has been operating a stack of Ballard fuel cells with reformer gas since 1993. The project has also accumulated valuable experience in operating individual cells with deliberately contaminated reactants (air and hydrogen).

Concep studies have shown that a large number of additional components must be taken into account when incorporating fuel cell systems with on-board fuel processing into a car [5]. In addition to the required purification and cooling of the hydrogen gas before it reaches the fuel cell, it may be necessary to use a buffer store to cope with the power transients experienced during vehicle operation. Due to the resulting adverse effect on payload and useful space, together with the many still unanswered questions on reforming, on-board storage of hydrogen will remain the ideal way of supplying fuel cell systems for the foreseeable future.

From natural gas to hydrogen

Since the late seventies, BMW has been working on the use of LH_2 as a fuel for cars. In cooperation with research partners, certification authorities and other manufacturing companies, the experimental vehicles and storage systems have been continuously improved in terms of function, safety, customer acceptance and cost. The cryogenic tanks built into the present BMW experimental vehicles with hydrogen drive system have proved so effective that no insurmountable technical risks can be expected if they were to be put into series production.

In order to accustom today's public to the idea of hydrogen, BMW has decided to take natural gas as an intermediate step. Natural gas consists largely of methane (CH_4). After hydrogen itself, it is the fuel with the highest hydrogen content and its physical properties are similar. Both energy carriers are gaseous at normal temperatures, and are the cleanest fuels.

BMW is the first European manufacturer to offer series-production vehicles powered by natural gas [6]. The 316g compact and 518g touring models, adapted for dual-fuel operation on gasoline or compressed natural gas (CNG), are international trendsetters. The cars meet the strictest Californian emission values and can be considered amongst the circle of cleanest cars in the world.

Outlook

Efforts to reduce the carbon content of motor fuels will open up opportunities for new technologies, not just in the field of energy but also in that of motive power. In addition to the versatile spark-ignition engines and besides fuel cells, gas turbines could also become an interesting alternative, so long as their transient behaviour can be improved while retaining the fuel efficiency.

In terms of efficiency and emissions, fuel cell systems are promising not just for passenger cars but also for commercial vehicles and stationary generation of electricity. Working together with capable system deliveres, BMW and Rover are contributing to solve the key problems of fuel cell systems for passenger cars, finding a possible route into mass production.

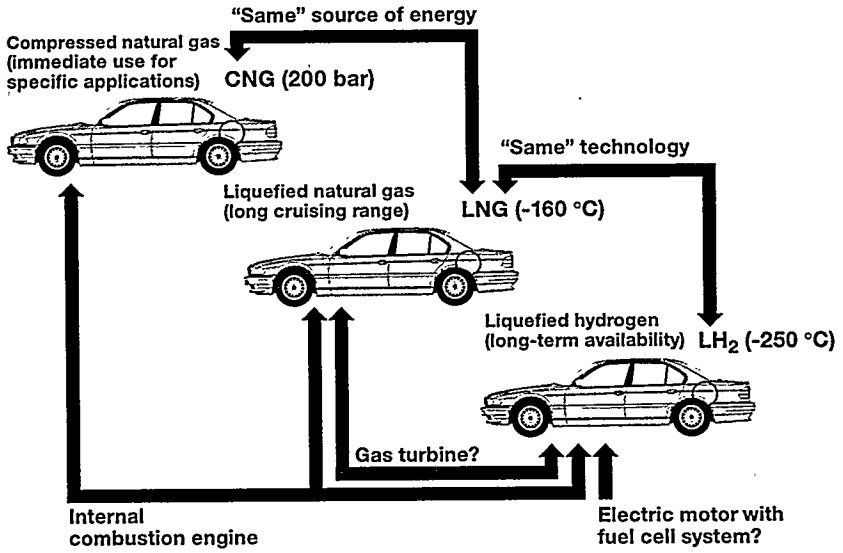

Fig.: 2: From natural gas to hydrogen

References

[1] Ledjeff, K. (ed.): "Brennstoffzellen, Entwicklung – Technologie – Anwendung". C.F. Müller Verlag, Heidelberg, 1995. ISBN 3-7880-7514-7.

[2] Szyszka, A.; Schimpf, G.; Tachtler, J.: "Bisherige Erfahrungen mit einer 6,5 kW elektrisch alkalischen und einer 80 kW elektrisch phosphorsauren Brennstoffzellenanlage im SWB Projekt in Neunburg vorm Wald (Stand Dezember 1991)". VDI Berichte No. 912, pp. 147-161. VDI Verlag, Düsseldorf, 1992.

[3] Straßer,K. ; Löhberg, R.: "Present PEM FC Technology and ist Potential Role within the SWB Program". First European FC Group Workshop, 26.- 27. Juni 1991, Regensburg, Germany.

[4] Braess, H.-H.; Strobl, W.: "Hydrogen as a Fuel for the Road Transport of the Future: possibilities and prerequisites". Proceedings of the 11th World Hydrogen Energy Conference, Stuttgart, 23-28 June 1996, pp. 1373-1404.

[5] Dams, R.; Adams, K.; Bourne, C.; Smith, J.: "Critical Components for Fuel Cell Hybrid Power Trains". Autotech 1995 Conference, Birmingham, UK,October 1995.

[6] Langen, P.: "Pathway to NGV Markets: an automaker's view". Proceedings of the 2nd Annual European NGV Conference and Exhibition, Basle, 8 - 10 May 1996.

FUEL CELLS - FROM THE LABORATORY TO THE ROAD

Matthew H. Fronk
Delphi Energy and Engine Management Systems
Rochester, New York 14602

The PEM Fuel Cell faces stiff competition from existing automotive powerplants and other Hybrid APUs. To be successful, the Fuel Cell will have to demonstrate real customer advantages such as fuel economy and emissions. The PEM technology has an inherent advantage over other powerplants in both thermal efficiency and emission performance, and as such fits in very well with the future regulations that strive to clean up the environment. In addition, it will need to be cost competitive and provide acceptable performance. The majority of development activity on PEM Fuel Cells to date has concentrated primarily in the area of Stack refinement and optimization with improvements coming in higher power densities and higher specific power. To make the Fuel Cell compatible with an automotive environment the entire system will need to be analyzed, understood, and then engineered to work together in an efficient manner.

There are several areas of development that need to be "engineered" for the automotive environment including Fuel Supply, Fuel Cell Stack, Fuel Cell system, and Vehicle System Integration. Each of these areas has several subsystems incorporated within it and as such must be designed from an overall systems level standpoint to insure both proper function along with minimized costs.

The fuel supply system is critical for an automobile. Today's drivers are familiar with pulling up to a pump and putting gasoline or diesel into their tanks at a rate of between 6 and 12 gallons per minute. There are regulations in effect to contain any evaporative emissions and fuel volatility is adjusted seasonally/regionally by the oil companies to insure proper vehicle performance. In addition vehicle manufactures take great measures to insure the vehicles perform at ambient temperatures ranging from -40C to 50C. Customers expect immediate starting with no stalls at any time along with immediate response in all conditions. Modern Electronic Fuel Injection Systems are all capable of delivering this performance.

The PEM Fuel Cell of today has been demonstrated typically with tanked hydrogen since this is the type of "fuel" that the stack needs to consume to produce power. Hydrogen today is not typically available at the local service station in pressures ranging from 200-300bar(3000-4500psi). Hydrogen fueled Fuel Cell automobiles would be difficult to merge into the infrastructure in place both in the U.S., Europe, and Asia. Therefore, another solution is required for the near term. Tanked liquid fuels seem to be the most attractive since they would allow the Fuel Cell to enter the market with existing types of infrastructures. Methanol "cracks" at low temperatures and gives good hydrogen yields, but there are concerns about availability and low temperature performance. Some type of gasoline derivative would be ideal since it is readily available, has known performance in various environmental situations, and can be blended to meet various conditions. It is also much less harsh on Fuel System componentry then methanol.

A gasoline based Fuel Processor would appear to give the Fuel Cell an easier entry into the market, but with this system comes higher temperature operation and lower hydrogen yields. These issues along with the monitoring and transient control of the Fuel Processor "subsystem" are critical to the successful operation and introduction of the Fuel Cell engine. Significant development work needs to continue in the development of Fuel Systems and controls, catalysts,

reactor configurations to speed the system coming on line, and the general area of sensors required for feedback control. Automotive solutions to these problems are required to meet cost and performance targets. Laboratory grade instrumentation cannot be sold with each new vehicle. Successful engineering and production implementation of this subsystem can help insure that this new technology could be accepted by the motoring public.

Once a suitable fuel supply system has been configured that can supply stack quality gas, an analysis of what the Fuel Cell Stack requirements are has to be fully detailed. For the automotive world, cooling with de-ionized water, while working fine in the lab, would have difficulties in March in upstate New York. Likewise the issues of stack freezing and effects on membranes and plates. These are all issues that are being addressed in industry development on a full-scale basis that are typically not addressed in laboratory or academic pursuits.

The stack itself consists of several sub-systems. Examples include the membrane, the membrane electrode assembly, the carbon paper, and the plates. Additionally there exists the need for thermal management, diagnostics, and assembly of the stack itself. Current state of the art membranes are offered by a small number of companies world wide. As the interest in Fuel Cells grows additional new product offering will come from new players in the market. This will help drive the cost down. Similar progress will occur in the areas of the carbon paper and bi-polar plate material. One would hope to see sheet goods that were stampable or highly conductive materials that could be suitable for injection molding. These materials are all aimed at cost reduction and high volume, automotive type manufacturing.

The integration of the Fuel Cell components into a system is the critical issue in making a cost effective replacement for the internal combustion engine that will meet all customer expectations. Issues surrounding Fuel Processor start-up and transient response, sensors and control algorithms, stack start up, air and fuel supply, all need to be engineered and validated with methods similar to what is used in today's automotive powerplants if we are to insure customer acceptability. Many new components in the areas of sensors, compressors, electric motors, and power electronics still need invention and development. It is essential that these items are developed by industry in order that cost, durability, and performance goals are realized.

Once the Fuel Cell powerplant has been properly developed it will then need to be readied for vehicle installation. In order for this phase of development to move forward efficiently, the requirements of the vehicle platform will have had to been incorporated in the development of the Fuel Cell System. There will be many issues to consider depending on the vehicle application. Examples include decisions on Fuel Cell only or a Hybrid configuration, regenerative braking, what fuel, what environmental conditions, and what duty cycle (passenger car or HD). Optimizing fuel consumption and making the vehicle transparent to the vehicle of today with respect to noise, durability, and performance, are all engineering challenges that will need to be addressed by the vehicle manufacturers.

While the engineering required is significant, many of these platform needs have already been addressed in GM's EV-1 and with further and timely development activity focused in the appropriate areas, the Fuel Cell powerplant can become a contender in the automotive community of tomorrow.

DEVELOPMENT OF PEFC FOR TRANSPORTABLE APPLICATIONS

Hideo Maeda, Hisatoshi Fukumoto, Kenro Mitsuda, Hiroaki Urushibata
Masao Enami* and Kazuhiko Takasu*
Advanced Technology R&D Center, MITSUBISHI ELECTRIC Corporation
8-1-1, Tsukaguchi-Honmachi,Amagasaki, Hyogo, 661 Japan
* NEDO (New Energy and Industrial Technology Development Organization)
3-1-1 Sunshine 60, 29F, Higashi-ikebukuro, Toshima-Ku,Tokyo, 170 Japan

Since FY1992, we have been developing PEFC technologies under NEDO's R&D program. High power density and rapid start-up are essential requirements for transportable applications. Also, if reformed gas is used as fuel, the prevention of CO poisoning and improvement of response to loading are essential. In this paper, methods to increase the effective surface area of a cell, start-up and endurance test results, the study of CO poisoning with a pulse electrolyzing method and the demonstration of a hydrogen recovery subsystem are presented.

ENLARGEMENT OF THE EFFECTIVE SURFACE AREA

In order to enlarge the effective surface area, new M&E fabrication technologies named " the three dimensional bonding method[1]"(micro curved cell) and "waved electrode-membrane assembly[2]" (macro curved cell) were developed.

(1) Micro curved cell The schematics and effects of the bonding method are shown in Fig. 1 and 2 respectively. By enlarging the area of the catalyst layer and closing both electrodes, the performance of a micro curved cell is made superior to that of a non-bonded one (only contacting).

(2) Macro curved cell The schematics and effects of waved M&E are shown in Fig. 3 and 4 respectively. The cell voltages of waved M&E are higher than that of flat M&E when oxygen is used, or in a low current density region. It was clear that gas diffusion problems arose, especially at the cathode, when the pitch of the wave was long.

START UP AND DSS CYCLE TEST OF A 1kW CLASS MODULE WITH INT. HUM.

Fig. 5 shows the starting characteristics of a 1kW class module with an internal humidifier (25-cell stack). Full power was obtained within several tens of seconds of starting at room temperature. The power level of the module was stable even when the temperatures changed. An endurance test under the DSS (Daily Start and Stop) mode was also carried out and the results are shown in Fig. 6. Rather stable performance was maintained during over 50 DSS cycles.

STUDY OF CO POISONING

The influence of CO poisoning was studied using the pulse electrolyzing method as shown in Fig.7. The relationship between the CO loss after pulse electrolyzing and the quantity of electricity supplied for several pulse voltages is shown in Fig. 8. It was found that CO loss was reduced according to the quantity of electricity supplied at the pulse electrolyzing. However, the minimum CO losses depended on the pulse voltages. This suggests the existence of absorbed chemical species of carbon monoxide, which requires extremely high potentials to be oxidized.

HYDROGEN RECOVERY SUBSYSTEM

In order to improve the start-up time of the reformer and the response to loading, a

hydrogen recovery subsystem was studied and evaluated. In the subsystem, hydrogen in the fuel exhaust is recovered and stored(purified and compressed) using an electrochemical hydrogen purifier and an electrochemical hydrogen compressor as shown in Fig. 9. The stored hydrogen can be used for heating the methanol reformer(at start-up) or for producing peak power. A hydrogen compression of 100 atm over atmospheric pressure was obtained with a PE electrochemical hydrogen compressor as shown in Fig. 10. The applied voltage needs to be decreased and the current density needs to be increased to improve the system.

CONCLUSION

1) Methods to enlarge the effective surface area microscopically and macroscopically were studied and the results were confirmed.
2) Superior start up performance and stability in the DSS mode were confirmed on a 1kW class module with an internal humidifier when pure hydrogen was used as fuel.
3) The influence of CO poisoning was studied using a pulse electrolyzing method.
4) A hydrogen recovery subsystem of laboratory size was demonstrated.

ACKNOWLEDGMENTS

This work was carried out under contract with the New Energy and Industrial Technology Development Organization (NEDO).

REFERENCES

1. H.Maeda, K.Mitsuda, H.Urushibata, M.Enami and K.Takasu, "PERFORMANCE OF PEFC 1KW CLASS MODULE", Proc. of the 2nd IFCC, 5-08,pp367-370, Feb. 1996.
2. K.Mitsuda, T.Murahashi, Y.Sakamoto and T.Mitsunaga, "ELECTROCHEMICAL SINGLE BATTERY AND METHOD FOR PRODUCING THE SAME", U.S.PAT. 4,981,763 (1991).

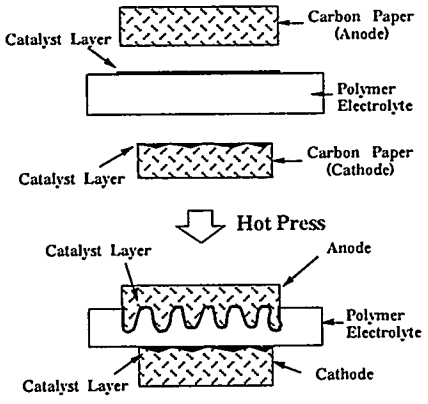

Fig.1. Schematics of the "three dimensional bonding method" (micro curved cell).

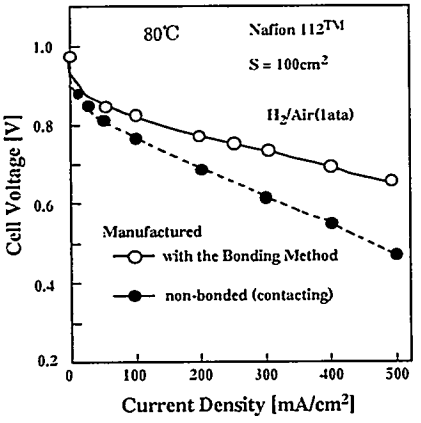

Fig. 2. Comparison of polarization curves for PEFC single cells with and without the bonding method.

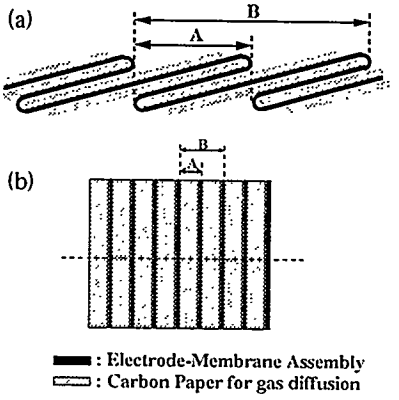

Fig. 3. Schematics of waved electrode-membrane assembly (macro curved cell): (a) cross section, (b) plane

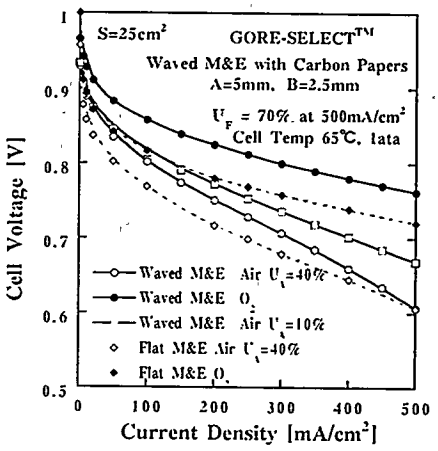

Fig. 4. Comparison of polarization curves for waved M&E and flat M&E.

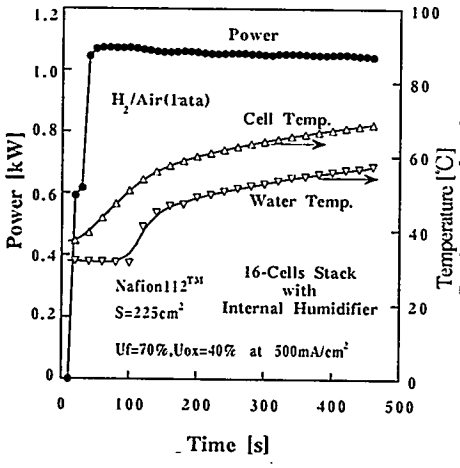

Fig. 5. Start up performance of a 1kW class module.

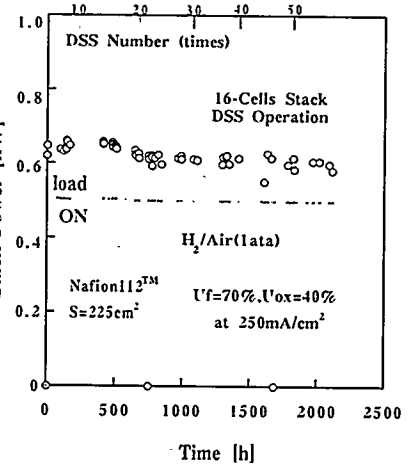

Fig. 6. Endurance test of a 1kW class module in the DSS mode.

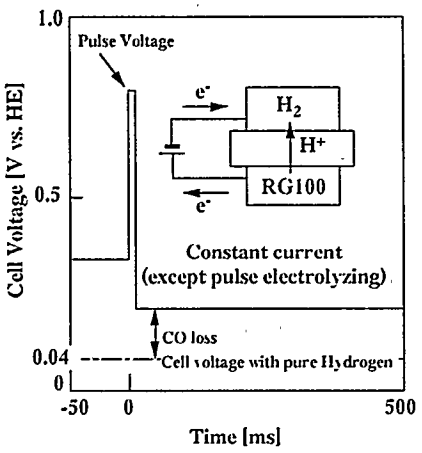

Fig. 7. Schematics of the pulse electrolyzing method.

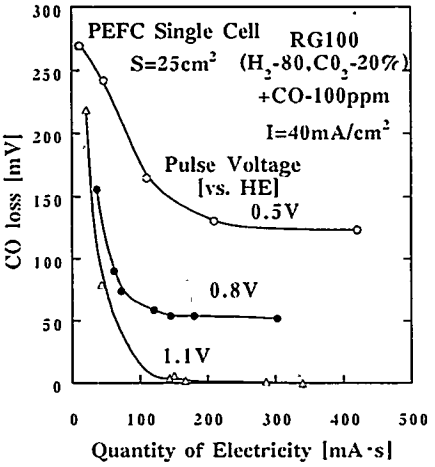

Fig. 8. Relationship between CO loss and the quantity of electricity supplied at pulse electrolyzing.

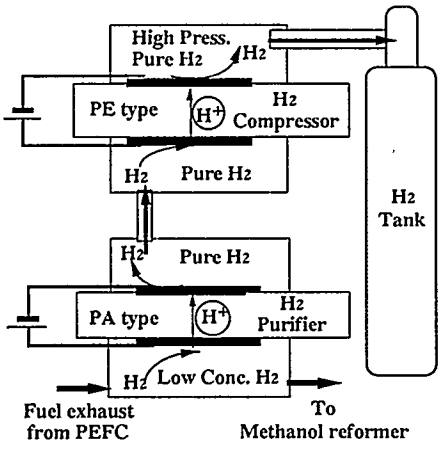

Fig. 9. Schematics of an electrochemical hydrogen purifier and an electrochemical hydrogen compressor.

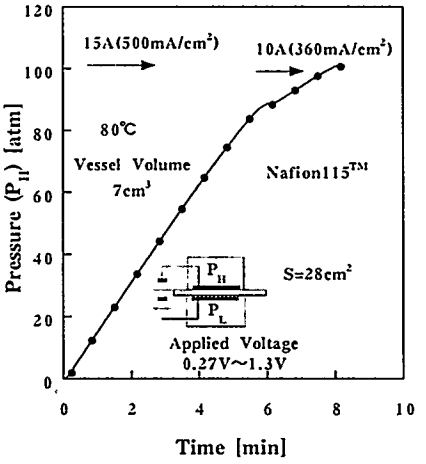

Fig. 10. Pressure changes of a PE type electrochemical hydrogen compressor over time .

HIGH POWER DENSITY FUEL CELL STACK DEVELOPMENT FOR AUTOMOTIVE APPLICATIONS

Ric Pow
Ballard Power Systems Inc.
9000 Glenlyon Parkway
Burnaby, British Columbia
Canada V5J 5J9

Michael Reindl and Werner Tillmetz
Dornier GmbH
department FOEE
D-88039 Friedrichshafen
Germany

Introduction

This paper describes the joint development by Daimler-Benz and Ballard Power Systems of a high power-density fuel cell stack and its demonstration in a 6-passenger Minivan.

Background

The PEM fuel cell is generally recognized as a promising candidate to realize society's objectives of ultra low and zero-emission vehicles. Ballard Power Systems has been working on the development of the PEM fuel cell since the mid eighties, and by 1993 had reached a level of technology represented by the Mk 5 stack. This technology enabled interested parties to get some experience with fuel cell operation and to gather test results. The Mk 5 was not optimized for power density, efficiency, durability, or cost and it was recognized that new generations of fuel cells would be required for commercial applications.

In 1993, Daimler-Benz and Ballard commenced joint development of a high power-density fuel cell stack for the automotive application, which was given the name "Mk 7." The first phase of the program targeted demonstration in a passenger vehicle within 4 years. The objective was to produce technology that is compact enough to power a car, is capable of operating in an automotive environment, and has adequate transient response to fulfill typical automotive duty cycles. The development of the technology to a level where it is commercially competitive with other environmentally acceptable alternatives to the internal combustion engine will be the topic of future phases.

NECAR I

The first task was the integration of the existing Mk 5 technology into a commercially available vehicle, which was given the name NECAR, for New Electric Car. The purpose was to provide a working platform to collect experience in the operation of a motive fuel cell power plant, and learn about the requirements for technology advancement. It also provided assurance that the technology is viable for the application, and that with development, can meet the requirements of the commercial automotive market.

Mk 7 Fuel Cell Stack

The major objective of development of the Mk 7 stack was a dramatic increase in power density. Analysis of practicable fuel cell systems for the car indicates that the power density of the fuel cell stack must be at least five times greater than the Mk 5, which was the state of the art at the beginning of the project. In addition, it was desired that the fuel cell be capable of operating on reformed methanol, in preparation for future applications. The longevity target for the fuel cell was at least 1000 hours to enable demonstration and collect experience. This represents a balance between the need to test large numbers of designs, and operating conditions, and the eventual need for 3000-5000 hours in a commercial product. Other requirements included operation on reduced air and reactant flows, pressures, and humidification to optimize overall system performance, and

operation in an automotive environment. Included are frequent start-up/shut-down, rapid load changes, and vibration/accelerations resulting from both normal operation and impact.

Elaboration of the technology was conducted in four main technical areas; cell development, membrane electrode assembly (MEA), stack engineering, and manufacturing process development.

Cell Development

Work started with investigation and screening of many design concepts, bipolar plate designs, and flow field techniques to increase the specific power output, and reduce the volume and weight of the cell. For example, a new flow field pattern was devised to make optimal use of the envelope area, resulting in an increase of area utilization from about 36% to greater than 80%. Area utilization is defined as the ratio of electro-chemically active area to cell-envelope area. The remaining area is used for fluid headers, seals, and tie-rods. The increase was made possible by a novel cell arrangement. The number of tie-rods was reduced from sixteen to four, the tie-rods were located inside the gas headers, and the flow fields were routed around the headers.

Membrane Electrode Assembly

The MEA development focused on designs to consistently provide good performance, under all operating conditions, using the various fuel gas mixtures for the required lifetime. Many different MEA designs were developed using combinations of a variety of the basic elements (membranes, catalysts, and gas diffusion electrodes).

Designs were initially proven on a 1-cell basis, using beginning-of-life performance as the first screen, and Mk 5 V-I curves as the performance baseline. Promising candidates were run for 1000 hours, to ensure adequate performance stability, and mechanical integrity over the period. Preferred designs were operated in ten-cell stacks to prove operation in the serial configuration, and to give statistical significance to the data.

Stack Design

Using successful designs of cells and MEAs, stack designs were produced. Included are details of the MEA, the bipolar plates, seals, stack endplates, compression hardware, and tooling to enable repeatable manufacture and dependable stack assembly. Success is determined by the ability to produce stacks of approximately 150 cells that give full performance projected from 10-cell stacks.

Manufacturing Process Development

Manufacturing process development was conducted concurrently with the evolution of the design. Early in the program, a study was conducted to review the manufacturing capabilities for the Mk 5 design, and project the suitability to the requirements for the emerging Mk 7 concepts. Considerations included repeatability, reproducibility, tooling requirements, capacities, capabilities, material logistics, and quality plan. A second study culminated in a model for production volumes and cost reduction in various phases. These included laboratory scale, pilot scale, pre-commercial, and finally full commercial production, representing increasing volumes and decreasing costs over the next 15 years.

As concepts evolved to optimize the Mk 7, designs were reviewed regarding manufacturability. Processes for manufacture at the increasing rates were conceptualized. Vendors were sought out and qualified. Processes suitable for the laboratory scale production required during the course of

this project were developed in detail. Suitable tooling was specified and purchased when possible, modified if necessary, or designed and built otherwise. Prototype parts were produced and checked to determine capability and cycle times of the processes, the tooling, and the operators.

Verification of Mk 7 Technology

Many cells, short stacks, and full sized stacks were built and tested during the program. The Mk 7 design has been tested for over 1 million cell-hours. Individual cells and 10-cell stacks have been operated continuously for more than 2500 hours. To date, production has included 17 full sized stacks, dozens of short stacks ranging from 10 to 50 cells, and hundreds of single cells totaling thousands of flow field plates and MEAs.

In addition to electrical performance and durability, many other aspects of the design have been verified. These include long-term compatibility of materials, corrosion resistance, resistance to vibration and impact, exposure to temperature extremes (including freezing), electrical isolation, influence of cycling loads/fluid pressures.

A photo of the Mk 7 side-by-side with the Mk 5 predecessor is shown in Figure 1, and a summary of specifications of the two fuel cell stacks is contained in Table 1.

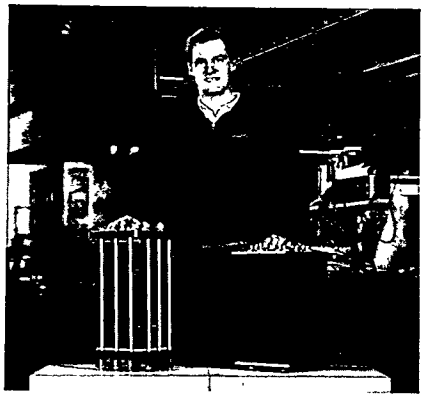

Figure 1: Mk 5 and Mk 7 Fuel Cell Stacks

Specifications	Mk 5	Mk 7
Length (mm)	650	650
Width and Height (mm)	250	250
Volume (liters)	32	32
Weight (kg)	40	40
Number of Cells	35	140
Power (kW)	5	32
Stack Efficiency	47%	55%
Volumetric Power Density (W/l)	156	1000
Gravimetric Power Density (W/kg)	125	800

Table 1: Summary of Specifications - Mk 5 and Mk 7 Fuel Cells

NECAR II

A second fuel cell powered vehicle, based on the Mercedes V-Class Minivan, was assembled. The system (including many improved components) was built around just two Mk 7 stacks, that provided the same power as the twelve Mk 5 stacks in the NECAR I. It proved to be indistinguishable in driveability from a high-quality IC-engined model, except for its quietness, and the lack of any harmful emissions. Average fuel efficiency is up to 40%, compared with 15% - 25% for an IC engine. A photo is contained in Figure 2, and technical specifications highlighting the improvements owing to the development are summarized in Table 2.

Figure 2: NECAR II

Specifications	NECAR I	NECAR II
Base Vehicle	MB 180	MB V-Class
Gross Power (DC Electrical - kW)	50	50
Seating Capacity	2	6
Weight of Powerplant (kg)	1050	300
Top Speed (km/hr)	90	110
Range (km)	156	250

Table 2: Summary of Specifications - NECAR I and NECAR II

The vehicle has been operated for many thousands of kilometers on test tracks and public roads with no major problems. The fuel cells have consistently and reliably provided the full 50 kW for which they were designed. The load is evenly shared from cell-to-cell and stack-to-stack. Adequate power is available to give satisfying performance even from a cold start, and the dynamic response is excellent.

Concluding Comments

The program to develop an automotive fuel cell stack and demonstrate it in a passenger vehicle has succeeded. There is clearly still much to be done in advancing the technology, establishing the required infrastructure, assimilating fuel cell vehicles in production lines of automobile manufacturing companies, and getting it into the hands of consumers. Notwithstanding these challenges, the rapid advancements made in areas where there are justified objections to new technologies for ultra-low and zero-emission vehicles, and the absence of any technical barriers during development are continuing evidence that PEM fuel cell technology may indeed be the route to meeting our society's objectives towards clean mobility.

DIRECT FUEL CELL PRODUCT DESIGN IMPROVEMENT

H.C. Maru (Presenter) and M. Farooque
Energy Research Corporation
3 Great Pasture Road
Danbury, CT 06813, USA
203-792-1460 (phone) 203-798-2945 (fax)
erc!hmaru@attmail.com

INTRODUCTION - Significant milestones have been attained towards the technology development, field testing and commercialization of direct fuel cell power plant since the 1994 Fuel Cell Seminar. Under a 5-year cooperative agreement with the Department of Energy signed in December 1994, Energy Research Corporation (ERC) has been developing the design for a MW-scale direct fuel cell power plant, with input from previous technology efforts (1) and the Santa Clara Demonstration Project (2). The effort encompasses product definition in consultation with the Fuel Cell Commercialization Group, potential customers, as well as extensive system design and packaging. Manufacturing process improvements, test facility construction, cell component scale up, performance and endurance improvements, stack engineering, and critical balance-of-plant development are also addressed. Major emphasis of this product design improvement project is on increased efficiency, compactness and cost reduction to establish a competitive place in the market. A 2.85 MW power plant with an efficiency of 58% and a footprint of 420 m^2 has been designed. Component and subsystem testing is being conducted at various levels. Planning and preparation for verification of a full size prototype unit are in progress. This paper presents the results obtained since the last fuel cell seminar.

PRODUCT DEFINITION AND DESIGN - Requirements for a baseline power plant have been defined based on the ongoing interactions with potential customers, and a survey of pipeline natural gas compositions, water supply quality, grid connection requirements, site conditions and applicable regulations. Stack and balance-of-plant designs have been revised substantially based on the experience gained under the Santa Clara Demonstration Project. It became clear from the Santa Clara design that the power plant footprint was dominated by rectangular fuel cell submodules and associated piping. The basic stack design was, therefore, improved to increase cell size from 6000 cm^2 to 9000 cm^2, and the number of cells in a stack was increased to a maximum (300+), considering the limitations of transportation requirements. The stacks are packaged in a cylindrical containers, and rather than insulating individual stacks, the container itself is insulated. The net result is a significant increase in areal and volumetric power density. Two cylindrical modules with approximately 4m diameter are designed to accommodate 8 stacks of approximately 375kW (DC) to provide 2.85MW (AC) in the commercial power plant. The amount of piping was also considerably reduced, with a net result of a compact power plant. Characteristics of a baseline power plant are summarized in Table 1.

The footprint of this power plant is expected to be 420 m^2 (4500 ft^2) as compared to about 3740 m^2 (40,000 ft^2) in the case of the Santa Clara Demonstration Project. On a m^2/kW basis, this is an order of magnitude reduction in footprint. A pictorial comparison of the commercial design with the Santa Clara demonstration power plant is shown in Figure 1. An installed capital cost update based on budgetary quotes from vendors indicates that projected cost of

$1250/kW (1995 dollars) is achievable with the new plant design. An independent stochastic review using Monte Carlo simulation confirmed that the probability of meeting this goal is high (>75%). Optional features such as operation on peak-shaving natural gas, grid-independent operation and site conditions different from those designed for the baseline plant are also planned to be offered, as shown in Table 1.

Table 1. SUMMARY OF COMMERCIAL DIRECT FUEL CELL POWER PLANT DESIGN CHARACTERISTICS:
An Efficient, Cost Effective and Compact Unit is to be Offered

BASELINE UNIT SPECIFICATIONS	
Plant Rating, Net AC	2.85 MW
Heat Rate (LHV) at Rated Power	6.22 x 10^6 J/kWh (5900 Btu/kWh, 58%)
Footprint	<420 m^2 (<4500 ft^2)
Maximum Emissions at Plant Rating	
Sox	< Detection Limit
No_x	< Detection Limit
CO_2	350 kg/MWh (770 lb/MWh)
Noise	60 dB(a) at 30m
Fuel	U.S. Pipline Natural Gas excepting peak-shaving
Installation	Outdoor
Seismic Rating	UBC Zone 2
Utility Connection	Grid Connected 15 kW breaker-class switchgear
Operation	Unattended

MAJOR OPTIONS

- Peak-shaving natural gas, liquid fuel, and other special fuels
- Seismic Rating: UBC Zones 3 and 4
- "Islanded" operation
- Cogeneration

MANUFACTURING - ERC's wholly-owned subsidiary, Fuel Cell Manufacturing Corporation located in Torrington, CT, has been focusing on scale-up of cell component area and production capability. On a three-shift basis, production capacity with the new 9000 cm^2 cells is expected to be 17 MW/year. The facility has already produced 3MW equivalent stacks. New equipment has been installed for production rate increase as well as quality control. While the capacity and production rates are increased, yields are being increased almost 20%, simultaneously reducing thickness variation by 50%.

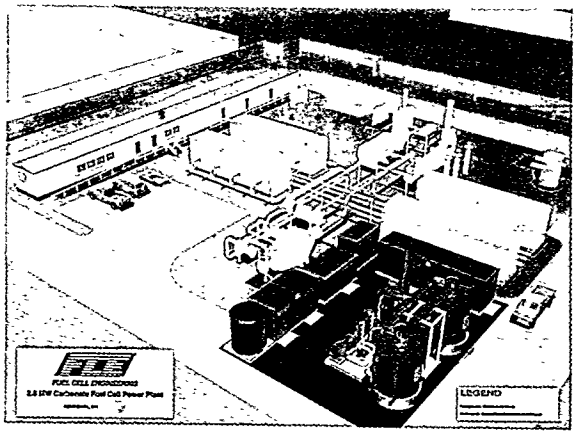

Figure 1. COMPARISON OF COMMERCIAL DESIGN WITH SANTA CLARA DEMONSTRATION POWER PLANT:
An Order of Magnitude Decrease in Footprint (m^2/kW) is Anticipated

Significant cost reductions have been achieved through design changes and weight reductions through close cooperation with ERC and vendor development. A 3-fold reduction as compared with previous design in cell component cost (on \$/m^2 basis) is anticipated. ERC's European technology partner, Motoren-und Turbinen-Union Friedrichshafen GmbH, an affiliate of Daimler Benz, has contributed a significant manufacturing advancement to reduce corrosion protection cost.

TECHNOLOGY DEVELOPMENT AND VERIFICATION - This activity focuses on the improved cell and stack designs to meet performance, endurance and cost goals. The first 9000 cm^2 area subscale stack has already been tested. The results show that the large area cell design can achieve an excellent temperature uniformity. The second subscale stack is getting ready for testing as of this writing. An intermediate-height stack test is planned before testing of the full-height stack in 1997.

Prior to building the full-height stack, a stack simulator has been built for verification of assembly procedures, manifold designs, new light-weight auxiliary hardware and gas flow distribution designs. A photograph of the simulator is shown in Figure 2. The gas flow model and the hydrodynamic experiments were utilized to define tall stack manifold designs for

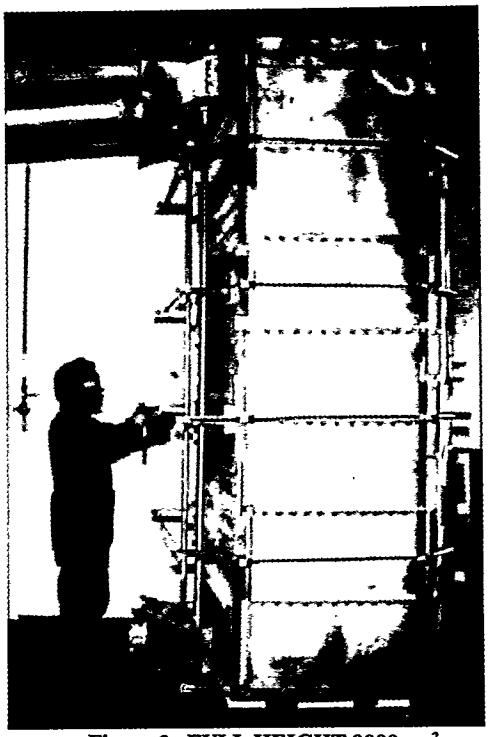

Figure 2. FULL HEIGHT 9000 cm² CELL AREA STACK SIMULATOR: Verified Assembly, Auxiliary Component Designs and Flow Distribution

achieving uniform cell-to-cell flow distribution. Less than 2% flow variation between cells is projected. A fuel cell "module" will contain four full-size stacks. Design of the gas flow distribution system within the module was defined with the help of modeling and cold flow tests. Flow variations between stacks of less than 1% are projected.

Construction of a 400kW subscale power plant for integrated testing of a full-height stack is expected to be completed before the end of this year. The system will also be used to verify critical BOP equipment designs. Significant test experience with diffferent size stacks as well as Santa Clara project has been accumulated. Over 1000 MWh of electricity has been produced, much of it supplied to utility grid.

Demonstration of 2.85MW prototype power plant is planned to be constructed adjacent to ERC's Danbury, CT facilities. Work on environmental and other permitting has been initiated. Construction will begin upon acquisition of necessary permits.

ACKNOWLEDGMENT - The support of DOE and DOD/DARPA for the system and technology development and verification is gratefully acknowledged. The keen insight and support of METC Contracting Officer's representative, Mr. Tom George, is greatly appreciated.

REFERENCES:

1. Farooque, M., et al, "Direct Carbonate Fuel Cell Development", Fuel Cell Seminar Abstracts, Courtesy Associates, Washington, DC, 1994.

2. Leo, T., "Santa Clara Demonstration Status," Advanced Fuel Cells 1996 Review Meeting, Department of Energy, Aug. 20-21, 1996.

STATUS OF MCFC STACK TECHNOLOGY AT IHI

M.Hosaka, T.Morita, T.Matsuyama and M.Otsubo
Ishikawajima-Harima Heavy Industries Co., Ltd.
Tokyo, Japan

1. INTRODUCTION

The molten carbonate fuel cell (MCFC) is a promising option for highly efficient power generation possible to enlarge. IHI has been studying parallel flow MCFC stacks with internal manifolds that have a large electrode area of $1m^2$. IHI will make two 250 kW stacks for MW plant, and has begun to make cell components for the plant. To improve the stability of stack, soft corrugated plate used in the separator has been developed, and a way of gathering current from stacks has been studied. The DC output potential of the plant being very high, the design of electric insulation will be very important. A 20 kW short stack test was conducted in 1995 FY to certificate some of the improvements and components of the MW plant.

These activities are presented below.

2. SPECIFICATIONS OF 250 kW STACK

250 kW stacks will be installed at Kawagoe Power Station in 1998 FY. The 250 kW stack, shown in Fig.1, piles up two 125 kW sub-stacks in series. The sub-stack has 140 cells, that half of the cells, i.e., 70 cells, are making a block on an intermediate holder and the other are under the holder. Each 70 cells' block is compressed by springs instead of air bellow used for past stacks. Two 250 kW stacks and the sub-stacks are electrically connected in series, and generate total of over 500 volts at OCV. Thermal insulation will be set both around the vicinity of stack and outside of the vessel. We plan to monitor the performance every 5 cell instead of every cell as usual, because wiring a great deal of cable in a vessel is difficult and increases the probabilities of causing leakage current. The number of cable is still great and should be much fewer in a future.

3. IMPROVEMENTS OF STACK TECHNOLOGY

(1) Structure of separator

IHI has been adopting internally manifolded stack concept. It is important to keep good contact among cell components for both of effective area and wet seal area including internal manifold. Heights of cell components will change during long term operation at high temperature. To follow the thickness change of cell components, we select soft corrugated plate setting in the separator under wet seal. The soft corrugated plate shown in Fig.2 has elastic and plastic characteristics as shown in the figure. Though the corrugated plate shows relaxation for the first time load cycle, the curve does not change after that. It is sufficient for the soft corrugated plate to follow the component's thickness change. The corrugated plate also keeps strength enough under the high temperature operation by creep analysis.

(2) End cell performance

Most of the full sized stack we have tested before shows that the performances of end cell were usually lower than the other cells. This is mainly caused by the way of taking out load current from terminals of end plate. The current distribution of the end cell is affected by the potential distribution of the end plate, that gathers current from the stack. Fig.3 shows the potential distribution in the end plate, in case of the same current among the terminals. The current distribution vertical to the flow direction in a cell will bring fuel utilization's distribution non uniform among channels in a separator. This distribution reduces the performance, and according to circumstances this increases the decay rate of end cell.

(3) Insulation

Stacks in the plant will produce high electrical potential. Piping, measuring cables, heater plates and holding system connected with stack should be highly insulated not to come about leakage current. Ceramic fiber or glass fiber is usually used as insulating sheet or covering. This material must be taken notice of these lowering electric non-conductance at high temperature. To reduce the probability of occurring leakage current by measuring cables, the cell's potential will be measured by every 5 cell instead of each cell as usual.

4. 20 kW SHORT STACK TEST

The 125 kW sub-stacks for the MW plant will be done pre-treatment and partial generating test at the factory of IHI. Then the stack will be transported by trailer to Kawagoe Power Station where MW plant will be constructed. Therefore the sub-stack should be gotten thermal cycling before operation at Kawagoe.

20 kW short stack was tested to certify cell components that will plan to be used for the 125 kW sub-stack, and to predict the performance of MW plant after thermal cycling. Fig.4 shows the 20 kW stack, which was installed in a pre-treatment vessel at IHI's atmospheric 50 kW stack test stand. The stack had two holding system, one was the current air bellow and the other was spring. To simplify holding system, the air bellow of the stack was removed during the thermal cycling, simulating operation without air bellows at Kawagoe.

(1) Results of test

Stack operating history is shown in Fig.5. Excepting for the hours of the planned thermal cycling, the stack completed a total of 1,793 hot hours with 1,536 hours of on-load operation and generated 26 MWh electric power. Fig.6 shows performance of each cell before and after thermal cycling. There was no effect on stack performance as a result of the thermal cycling. Gas leakage and short current were almost little there.

(2) Prediction of 250 kW performance

The gas composition, being fed to the cathode side in MW plant, have very low concentration of carbon dioxide and oxygen. We usually take data at higher concentration than MW condition. Recently Morita et al. proposed a correlation of cathode overpotential [1], which stands up even if at the low concentration. Fig.7 shows the relation to be good for performances of stacks [2]. The stack showed good performance at simulated MW condition, and got over the planned values. The decay rate of the stack under the simulated continuous operation of MW plant also satisfied them.

5. CONCLUSION

(1) The design of the stack for MW plant has been making a step forward, especially in the concept of soft separator and in the way of gathering current from the stack.
(2) 20 kW short stack test to certificate cell components of 250 kW stack satisfied the planned performance of MW plant.

ACKNOWLEDGMENT

This work has been conducted under a contract from NEDO (New Energy and Industrial Technology Development Organization) and MCFC Research Association (Technology Research Association for Molten Carbonate Fuel Cell Power Generation System) as a part of the New Sunshine Program of MITI (Ministry of International Trade and Industry). We appreciate their advice and support.

REFERENCE

(1) H.Morita, et al., "Analysis of Performance of Molten Carbonate Fuel Cell. Performance Formulation Based on Cathode Reaction Mechanisms", DENKI KAGAKU , 63-11(1995)
(2) A.Matsunaga,et al., "Analysis of Molten Carbonate Fuel Cell Performance", Jun.1996 Japan, The 3rd FCDIC Fuel Cell Symposium Proceedings.

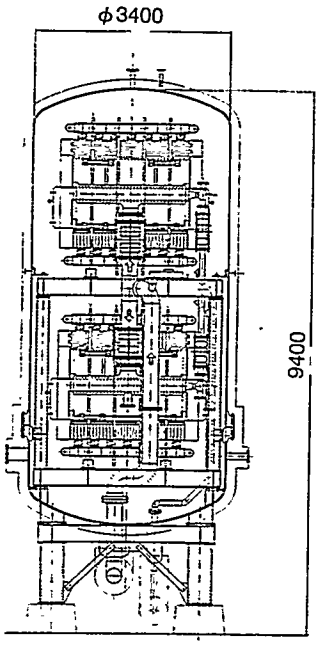

Fig.1 250kW stack

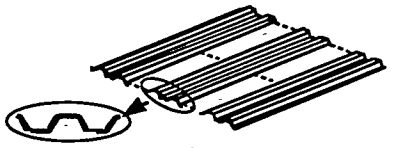

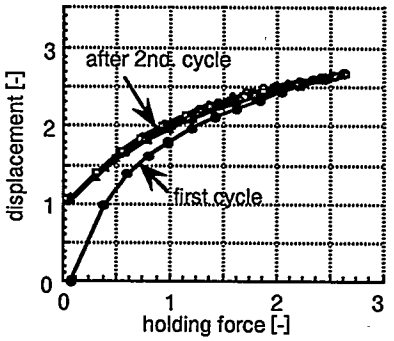

Fig.2 Characteristics of soft corrugated plate

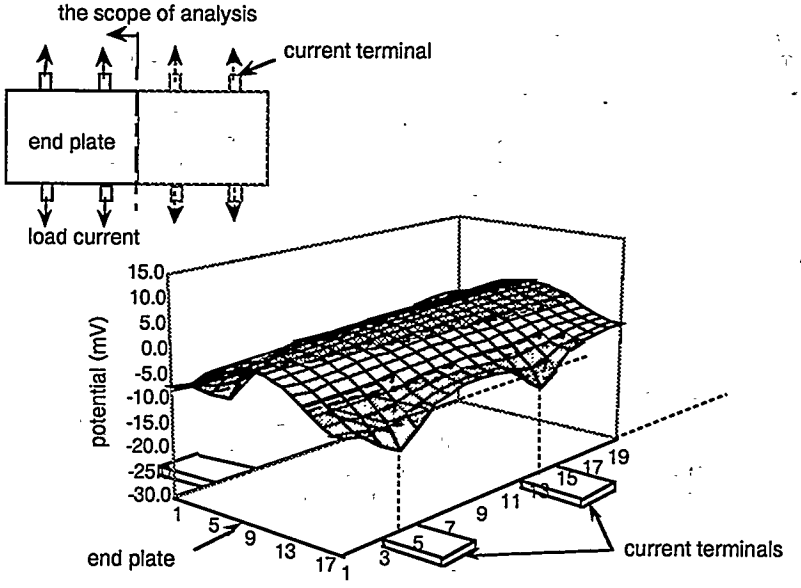

Fig.3 Potential distribution of end plate gathering current from stack

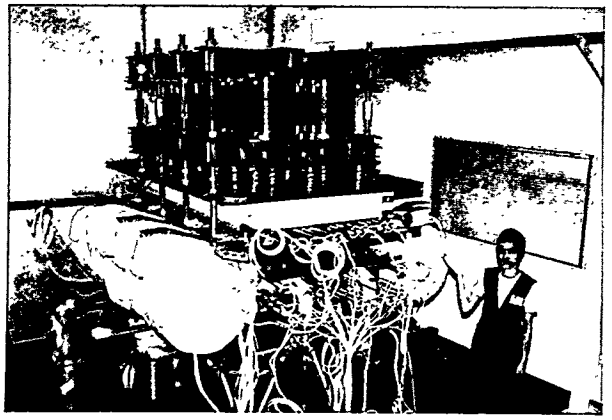

Fig.4 20kW stack

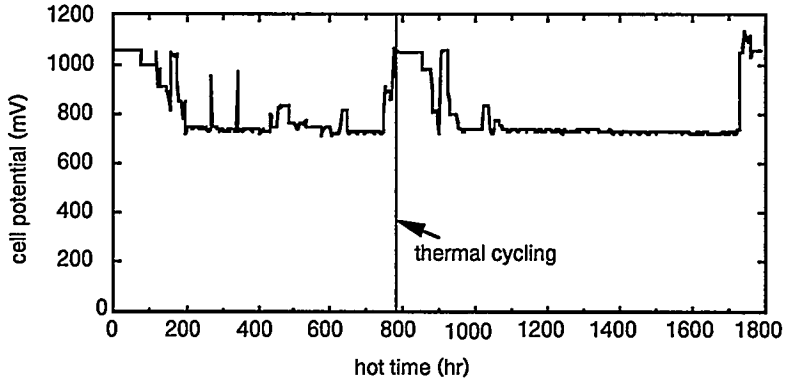

Fig.5 Operating histry of 20kW test

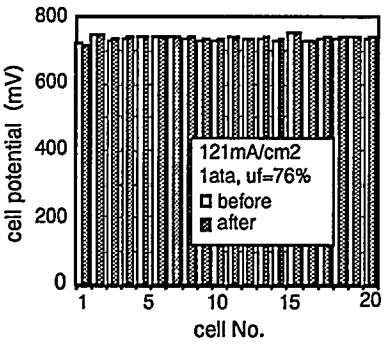

Fig.6 Cell performance of 20kW stack

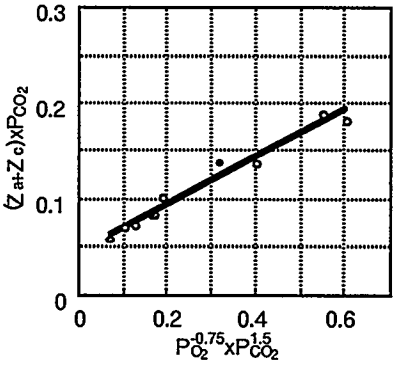

Fig.7 Over pottential for cathode gas composition

DEVELOPMENT OF LARGE SCALE INTERNAL REFORMING MOLTEN CARBONATE FUEL CELL

A. Sasaki, T. Shinoki and M. Matsumura
Mitsubishi Electric Corporation
Advanced Technology R&D Center
1−1, Tsukaguchi−Honmachi 8 Chome,
Amagasaki, Hyogo 661, JAPAN

INTRODUCTION

Internal Reforming (IR) is a prominent scheme for Molten Carbonate Fuel Cell (MCFC) power generating systems in order to get high efficiency i.e. 55−60% as based on the Higher Heating Value (HHV) and compact configuration. The Advanced Internal Reforming (AIR) technology has been developed based on two types of the IR−MCFC technology i.e. Direct Internal Reforming (DIR) and Indirect Internal Reforming (IIR). The outline of development plan is shown in Fig.1.

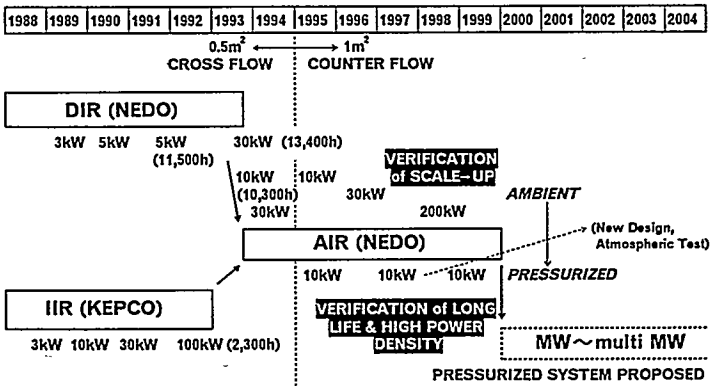

Fig.1 Outline of Development Plan at Mitsubishi Electric Corp.

The main targets of AIR concept are scale−up (1m ^{2} cell, 200kW stack), life elongation up to 40,000hours and high power density (pressurized) operation of IR stacks. Two 10kW AIR stacks of which electrode area is 1m ^{2} have been manufactured and tested, recently. One stack is operated at the atmospheric pressure and another stack is operated at 0.5MPa, which is the first pressurized IR stack in the world. In this paper, the AIR technology for large scale cells is reported laying stress on the performance of these two stacks.

LARGE CELL (1m ^{2}) ADVANCED INTERNAL REFORMING (AIR) STACK DESIGN

The AIR configuration consists of plate reformers piled in every 6 cells and catalyst beds also installed in the anode gas channels. The AIR is elegant scheme in order to reduce the stack cooling duty and to get suitable temperature distributions in the stack.

It is the point to optimize the temperature distribution in order to develop large scale and high power density IR stacks. The temperature distribution dominates performance and life characteristics. It is significant to make energy balance between endothermic reforming reaction and exothermic cell reaction, locally as well as totally in the IR stacks. Triple gas flows i.e. fuel gas (LNG+steam), anode gas and cathode gas are arranged in the 1 dimensional configuration, as for the 1m ^{2} cell IR stacks. Fig.2

shows such AIR stack configuration. The bipolar plate configuration used in the $1m^2$ cell is also shown in Fig. 3. The counter flow scheme is adopted between the anode gas

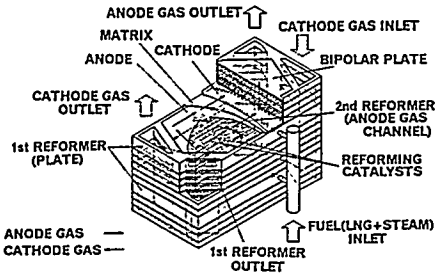

Fig. 2 AIR Stack Configuration

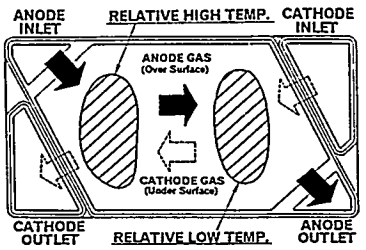

Fig. 3 $1m^2$ Bipolar Plate Configuration

and the cathode gas. This 1 dimensional flow configuration makes the temperature distribution simple in the cell plane, so that the thermal design should be easy and generallized.

$1m^2$ −10kW AIR STACK for ATMOSPHERIC PRESSURE OPERATION

The code name of a $1m^2$ −10kW AIR stack for atmospheric pressure operation is AIR100−1. The specification of AIR100−1 is shown in Table 1 and the situation of installing is also shown in Photo 1.

Table 1 Specification of AIR100−1

Capacity	10kW
Electrode Area	$1m^2$
Electrolyte	Li/K
Reforming	Advanced IR
Cell Number	12
1st Reformers	2 (3−R−6−R−3)
Gas Flow	Counter Flow
Pressure	0.1MPa

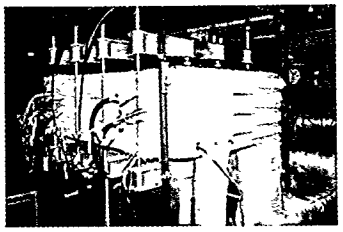

Photo 1 Installation of AIR100−1

The initial performance as the average cell voltage is 0.791V at the current density=150mA/cm^2, when the fuel is the city gas (Japanese code:13A, natural gas) at the steam to carbon ratio=3, the fuel utilization is 80%, the oxidant is Air/CO_2 =70/30 and the oxidant utilization is 30%. This value is higher than data of $0.5m^2$ AIR stacks i.e. 0.78V at the maximum, so that the stack design which uses large cells is satisfactory. The individual cell voltages are shown in Fig. 4. The AIR100−1 stack has been operated stably since February 1996. The operation time is 3,410hours (the power generating time:3,211hours) and the total generated electric power is 39MWh on August 9, 1996. The voltage decay rate is about 5mV/1,000h up to now, including scheduled thermal cycle once.

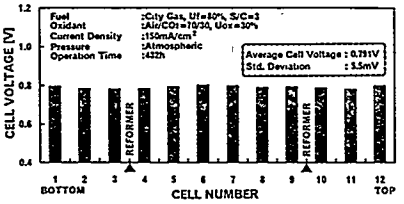

Fig. 4 Initial Performance of AIR100−1

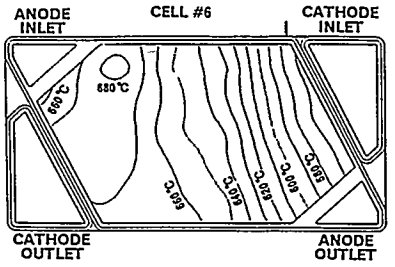

Fig. 5 Temperature Distribution in the Cell Plane of AIR100−1

A typical temperature distribution in the cell plane of AIR100−1 is shown in Fig. 5. The 1 dimensional temperature gradient is almost attained in the direction of the cathode gas flow. The inlet side of the cathode (the outlet side of the anode), where the temperature is relatively low, is utilized to elongate the catalyst life of the 2nd reformer. Furthermore, the cathode gas outlet temperature is the maximum so that it is easy to perform the temperature control of the stack and to recover the exhaust gas energy form the stack. The progress in the thermal design of IR stacks is shown in Fig. 6 and 7. This is the design concept to raise the average operating temperature, keeping the maximum temperature constant and also keeping the cathode gas flow rate decreasing.

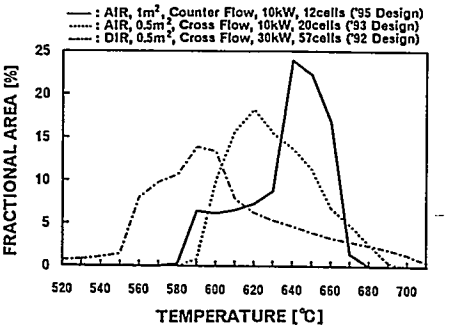

Fig. 6 Progress of Temperature Distributions of IR Stacks

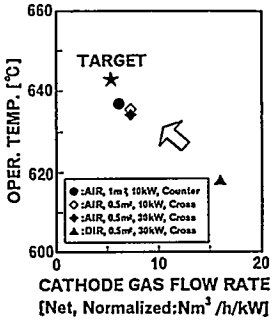

Fig.7 Progress of Thermal Balances of IR Stacks

1m^2−10kW AIR STACK for PRESSURIZED OPERATION

The code name of a 1m^2−10kW AIR stack for pressurized operation is PIR100−1. The specification of PIR100−1 is shown in Table 2 and the situation of installing is also shown in Photo 2. This stack uses Li/Na electrolyte instead of Li/K in order to reduce Ni dissolution at the pressurized operation. PIR100−1 shows 0.851V at 150mA/cm^2, 0.781V at 250mA/cm^2 and 0.745V at 300mA/cm^2, when the fuel is CH_4/H_2O=25/75, the fuel utilization is 80%, the oxidant is AIR/CO_2=70/30, the oxidant utilization is 20% and the operating pressure is 0.5MPa. Fig. 8 shows the i−V curve and Fig. 9 shows the power density. 2.2kW/m^2 as the power density of MCFC stacks is the highest record in the world. PIR100−1 has been operated since March 1996. The operation time is 2,871hours (the power generating time:2,007hours and the continuous 250mA/cm^2 operation time:500hours) on August 9, 1996.

Table 1 Specification of PIR100-1

Capacity	10kW
Electrode Area	1m ^{2}
Electrolyte	Li/Na
Reforming	Advanced IR
Cell Number	8
1st Reformers	1 (4-R-4)
Gas Flow	Counter Flow
Pressure	0.5MPa

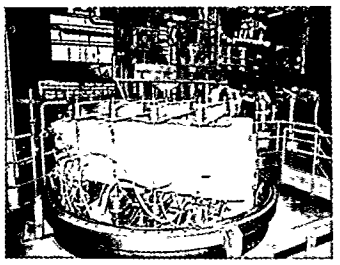

Photo 2 Installation of PIR100-1

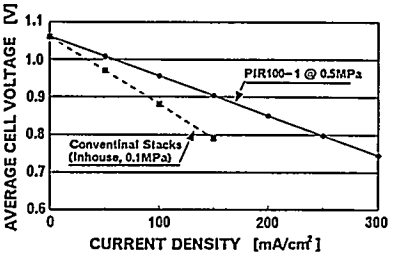

Fig. 8 i-V Characteristcis of PIR100-1

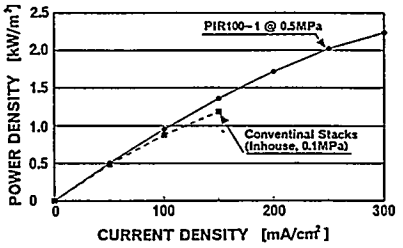

Fig. 9 Power Density Curve of PIR100-1

CONCLUSIONS

The performance of 1m ^{2} AIR stacks is better than those of 0.5m ^{2} AIR stacks. The temperature distribution in the 1m ^{2} cell plane is satisfactory due to 1 dimensional counter flow scheme between the anode gas and cathode gas. A 200kW AIR stack for atmospheric pressure operation has been developed, adopting and checking this AIR design concept. The operation of this 200kW stack is scheduled to be at the Japanese electric utility site in 1999.

The life characteristics of pressurized AIR operation have been also evaluated in parallel with scale-up. The target is to operate the long life and high power density AIR stacks. The IR stack technology will be completed when the scale-up technology by the 200kW development and the long life/high power density technology by the pressurized short stacks fuse into one.

ACKNOWLEDGEMENT

This study has been carried out as a part of the New Sunshine Program of the Agency of Industrial Science and Technology (AIST), Ministry of International Trade and Industry (MITI), under a contract with the New Energy and Industrial Technology Development Organization (NEDO) and in a shared work in the Technology Research Association for Molten Carbonate Fuel Cell Power Generation System. The authors appreciate their advice and support.

Progress of MCFC Stack Technology at Toshiba

M.Hori, T. Hayashi, and Y. Shimizu
Toshiba Corporation
1-6 Uchisaiwai-cho, Chiyoda-ku, Tokyo 100,Japan

Introduction

Toshiba is working on the development of MCFC stack technology; improvement of cell characteristics, and establishment of separator technology. For the cell technology, Toshiba has concentrated on both the restraints of NiO cathode dissolution and electrolyte loss from cells, which are the critical issues to extend cell life in MCFC, and great progress has been made. On the other hand, recognizing that the separator is one of key elements in accomplishing reliable and cost-competitive MCFC stacks, Toshiba has been accelerating the technology establishment and verification of an advanced type separator. A sub-scale stack with such a separator was provided for an electric generating test, and has been operated for more than 10,000 hours. This paper presents several topics obtained through the technical activities in the MCFC field at Toshiba.

1.Cell Technologies

Fig.1 shows the progress of single-cell performances since 1990 at Toshiba. By taking a few countermeasures to restrain the NiO cathode dissolution and the electrolyte loss, great progress has been made in the improvement of cell performance since 1992.

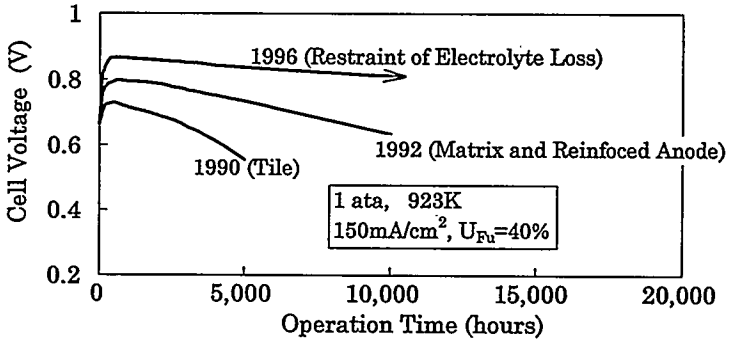

Fig.1 Progress of single-cell performances

1.1 Restraint of NiO cathode dissolution

To restrain the cathode dissolution, Toshiba has discovered three kinds of effective countermeasures; a $LiFeO_2$ layer, an out-of-cell oxidized NiO cathode, and a Li_2CO_3-Na_2CO_3 eutectic electrolyte. Fig.2 shows the Ni amount detected in the electrolyte layers of a conventional cell with *in-situ* oxidized NiO cathode and an advanced cell adopting the countermeasures after holding both the cells in 70Air/30CO_2 at 923K for 50 hours. By taking such countermeasures, the NiO dissolution rate could be reduced to about 1/20. Fig.3 shows the electric generating test results for a single-cell

taking the countermeasures. The test was conducted under the accelerating condition of various CO_2 partial pressures from 0.3atm to 3.0atm. In the figure, the operation time on the horizontal axis was expanded by the accelerating times of CO_2 partial pressures. From the figure, it is estimated that at least 20,000 hours could be expected as the cell life from the NiO cathode dissolution point of view.

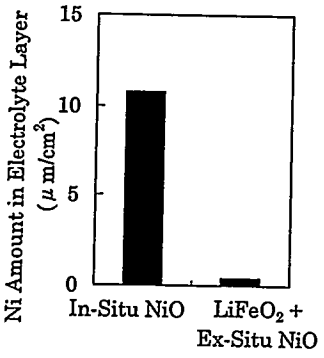

Fig.2 Comparison of Ni amount in electrolyte layers

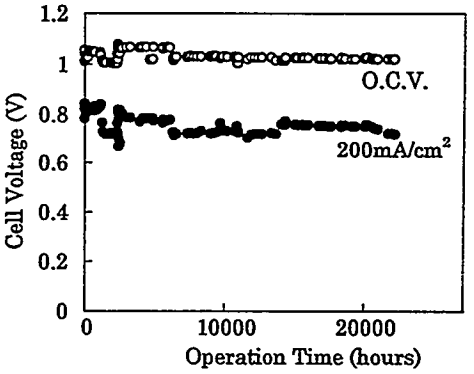

Fig.3 Performance time change of the cell with the countermeasures

1.2 Restraint of electrolyte loss

Toshiba has considered that the electrolyte loss from cells is mainly caused by the particle growth of γ-$LiAlO_2$ adopted as an electrolyte support material, and has examined whether α-$LiAlO_2$ could be applied, in place of γ-$LiAlO_2$, as the electrolyte support material. Fig.4 shows the SEM photographs of γ-$LiAlO_2$ and α-$LiAlO_2$ after holding them in $36Air/16CO_2/48H_2O$ at 923K for 5,500 hours. The particles of α-$LiAlO_2$ didn't grow, while that of γ-$LiAlO_2$ grew. Judging from these results, α-$LiAlO_2$ would be superior to γ-$LiAlO_2$ for the electrolyte support material. In order to verify the stability of α-$LiAlO_2$, an electric generating test is being conducted on a single-cell with α-$LiAlO_2$ as the electrolyte support material. The test result to date is shown in Fig.1 as a performance time change with an additional remark of 1996. Even beyond 10,000 hours, the excellent cell characteristic is being obtained.

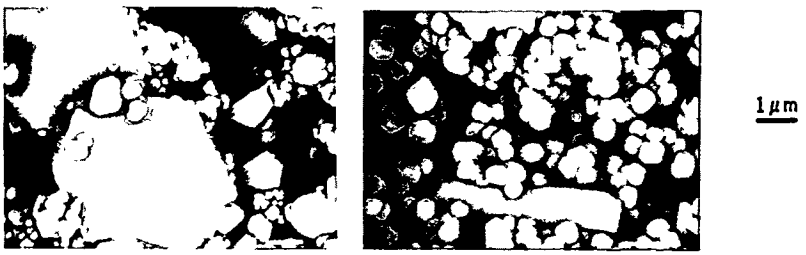

γ-$LiAlO_2$ Matrix α-$LiAlO_2$ Matrix

Fig.4 Particle growth of γ-$LiAlO_2$ and α-$LiAlO_2$

2.Stack Technologies

Fig.5 shows a conceptual illustration of a MCFC stack using the advanced type separator Toshiba has developed. The separator is an internal manifold type, and is flexible configuration. The separator is composed of thin sheets of metal such as 0.3-0.4 mm in thickness. A kind of spring element is incorporated into the edge sealing portions of the separator. The flexible configuration will meet the two important requirements to the separator; electrical contact of cell repeating parts, and reactant gas sealing (wet sealing) along the separator edge.

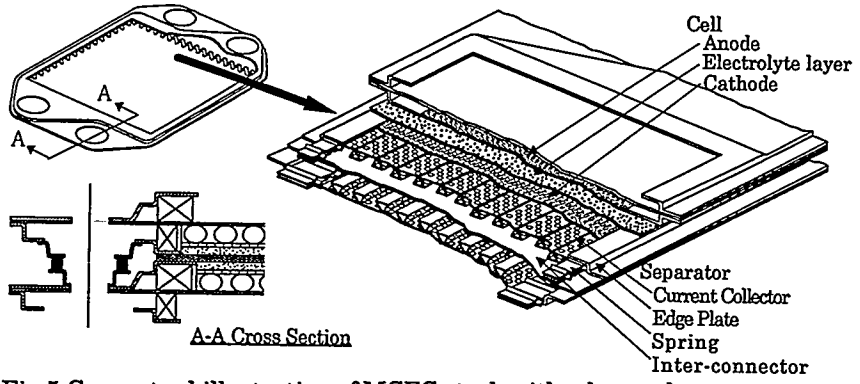

Fig.5 Conceptual illustration of MCFC stack with advanced type separator

To make a preliminary evaluation of the practicability of the advanced type separator, a sub-scale stack, which is composed of three 1200cm² cells and four separators with the flexible configuration, were provided for an electric generating test. Fig.6 shows the test results. Even beyond 10,000 hours, the stack is still being operated and the separators are maintaining their functions.

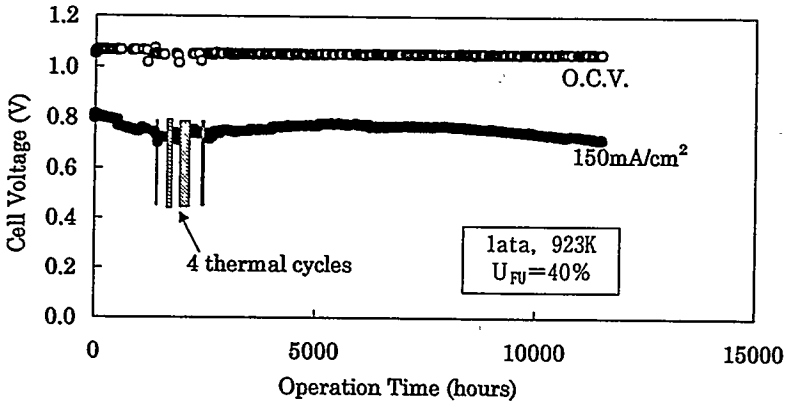

Fig.6 Electric generating test results of a sub-scale stack

3.Manufacturing Process Technologies of Full-sized Parts

Toshiba is proceeding to develop the manufacturing process technologies of full-sized flexible separator, electrodes and α-$LiAlO_2$ matrix. Fig.7 shows the α-$LiAlO_2$ matrix-tape manufactured by a continuous tape caster.

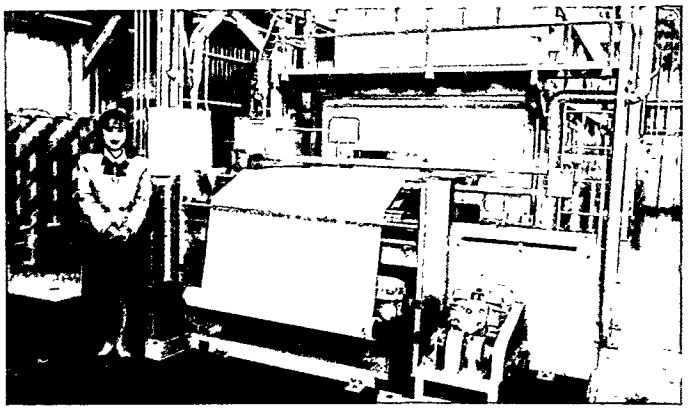

Fig.7 α-$LiAlO_2$ matrix-tape manufactured by a continuous tape caster

4.Full-sized Stack Test for Verification

Incorporating all technical knowledge mentioned above, Toshiba has fabricated a full-sized cell stack. Fig.8 shows the stack mounted on a test stand. The test for evaluating gas leakage will be conducted on this stack soon.

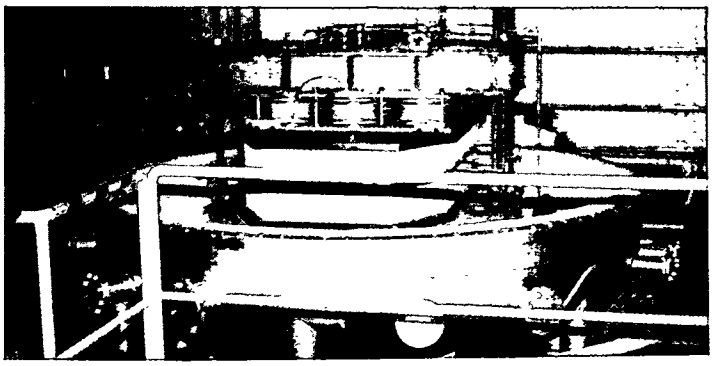

Fig.8 Full-sized stack mounted on a test stand

Acknowledgment

A part of the works was conducted by the MCFC Research Association. The MCFC Research Association was commissioned to do the work by NEDO (New Energy and Industrial Technology Development Organization) as a part of the New Sunshine Program of MITI (Ministry of International Trade and Industry).
We appreciate the advice and support of MCFC R.A., NEDO and MITI.

DEMONSTRATION OF DIRECT INTERNAL REFORMING FOR MCFC POWER PLANTS

*K. Aasberg-Petersen, **P. Simonsen, *P.S. Christensen,
*S.K. Winther, *E. Jørn, *C. Olsen, *E.J. Jensen
*HALDOR TOPSØE A/S, Nymøllevej 55,
DK-2800 Lyngby, Denmark
**Elkraft AmbA, Lautruphøj 5,
DK-2750 Ballerup, Denmark

1. Introduction

The conversion of methane into hydrogen for an MCFC by steam reforming is accomplished either externally or internally in the stack. In the case of external reforming the plant electrical efficiency is 5% abs. lower mainly because more parasitic power is required for air compression for stack cooling [1]. Furthermore, heat produced in the stack must be transferred to the external reformer to drive the endothermic steam reforming reaction giving a more complex plant layout.

A more suitable and cost effective approach is to use internal steam reforming of methane. Internal reforming may be accomplished either by Indirect Internal Reforming (IIR) and Direct Internal Reforming (DIR) in series or by DIR-only as illustrated in Fig. 1. To avoid carbon formation in the anode compartment higher hydrocarbons in the feedstock are converted into hydrogen, methane and carbon oxides by reaction with steam in an adiabatic prereformer [2] upstream the fuel cell stack.

This paper discusses key elements of the design of both types of internal reforming and presents data from pilot plants with a combined total of more than 10,000 operating hours. The project is being carried out as part of the activities of the European MCFC Consortium, ARGE [3].

2. The IIR/DIR-system

Depending upon the operating temperature and the steam-to-carbon ratio 60-90% of the methane fed to the MCFC is steam reformed in the IIR-chambers. The remaining methane must be steam reformed in the anode chamber to reach a high fuel utilization and a high plant electrical efficiency. Catalyst pellets may be used but a more elegant solution allowing easier cell assembly is catalyzed hardware [4] where the surfaces of the cell hardware are covered with a thin layer of steam reforming catalyst. The performance of catalyzed hardware has been demonstrated in the IIR-chambers of a pipeline natural gas (PNG) fuelled 7 kW MCFC pilot plant at Elkraft's facilities in Kyndby with no deactivation as illustrated in Fig. 2.

The catalyst in the anode chamber, whether as pellets or catalyzed hardware, is susceptible to poisoning by alkali resulting in loss of catalyst activity. In the

IIR/DIR system the catalyst in the anode chamber must retain a few percent of its original activity to reach a 95% methane conversion for the lifetime of the fuel cell stack [4]. Data from a PNG fuelled 8 kW pilot plant from 1994 operated at Elkraft's facilities in Kyndby (Kyndby II) show that long catalyst life in the anode chamber can be achieved as illustrated in Fig. 3.

3. The DIR-only System

The stack cost can be substantially reduced by omitting the IIR-chambers and performing the internal reforming only by DIR. However, in this case the amount of catalyst that can be placed in the anode chamber is limited. A large amount of catalyst will result in a severe and stack damaging temperature drop in the anode inlet area during the initial period of operation when the catalyst is highly active. On the other hand, a small amount of catalyst will result in short catalyst lifetime and, thereby, low stack efficiency.

A novel catalytic system which avoids the stack damaging temperature drop while maintaining sufficient catalyst lifetime has been developed. A mathematical model has been derived for the MCFC stack. Model computer simulations were performed to define an optimal catalyst (activity) distribution in the anode chamber. Fig. 4 shows the calculated temperature distribution for a DIR-only MCFC stack at typical start of run conditions. The calculated methane conversion exceeds 99%.

A new type of internal reforming catalyst is used in the anode inlet area. The start-of-run activity of the catalyst has been tuned to match the required activity as defined by the model calculations. Accelerated out of cell experiments in an alkali poisoning reactor indicate that the activity close to stack end-of-life is similar to catalysts used in the anode chamber of the IIR/DIR-system. The calculated temperature profile close to the end-of-life is shown in Fig. 5. The corresponding methane conversion is above 97%.

An 8 kW DIR-only pilot plant experiment for validation of the model is planned at Elkraft's facilities in Kyndby (Kyndby III) during the fall of 1996.

4. Acknowledgements

Part of this work has been supported by the Danish Ministry of Energy and another part by the Joule-Programme of the European Union.

5. References

1. J.R. Rostrup-Nielsen and L.J. Christiansen, Proc. Int. Symp. on Energy and Environment, Helsinki, August, 1991, p. 52.
2. T.S. Christensen, "Adiabatic prereforming of hydrocarbons - an important step in syngas production", Appl.Cat.A: General 138(1996), 282.

3. P. Kraus, A. Heiming and K. Aasberg-Petersen, Proc. this conference.
4. J.R. Rostrup-Nielsen and L.J. Christiansen: "Internal steam reforming in fuel cells and alkali poisoning", Appl.Cat. A: General 126 (1995) 381.

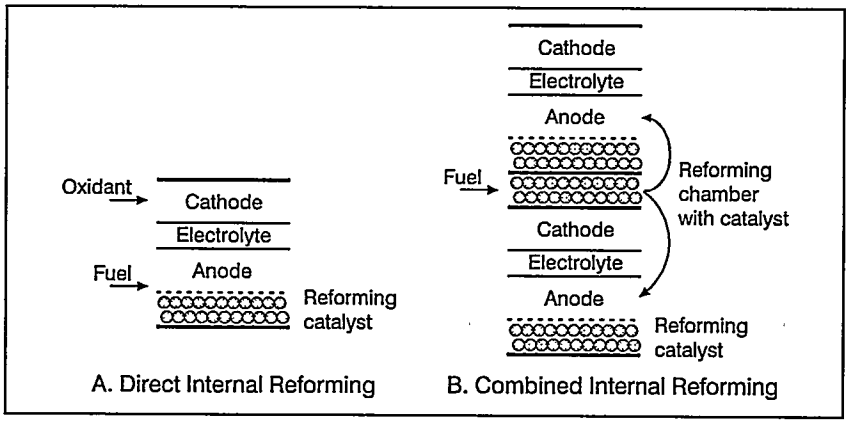

Figure 1: Principles of Internal Steam Reforming.

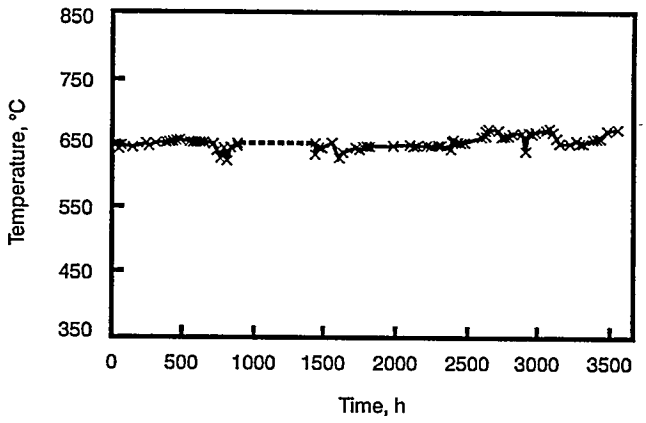

Figure 2: Equilibrium temperature exit IIR-chambers with catalyzed hardware in 7 kW MCFC pilot plant. The constant equilibrium temperature indicates no deactivation. The MCFC stack was delivered by ERC.

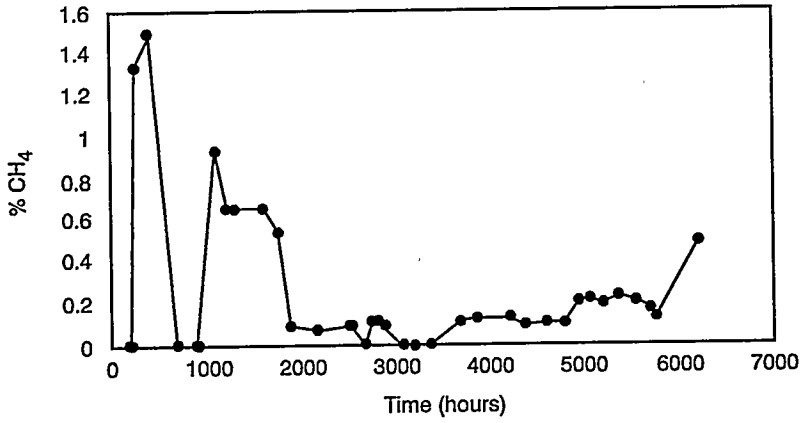

Figure 3: Methane leakage exit anode chamber in 8 kW pilot plant illustrating good performance of the anode chamber catalyst. The plant was at constant load from 2000-6000 hours of operation. The anode exit gas is in chemical equilibrium at the last data point (6200 hours) taken at low fuel utilization. The MCFC stack was delivered by ERC.

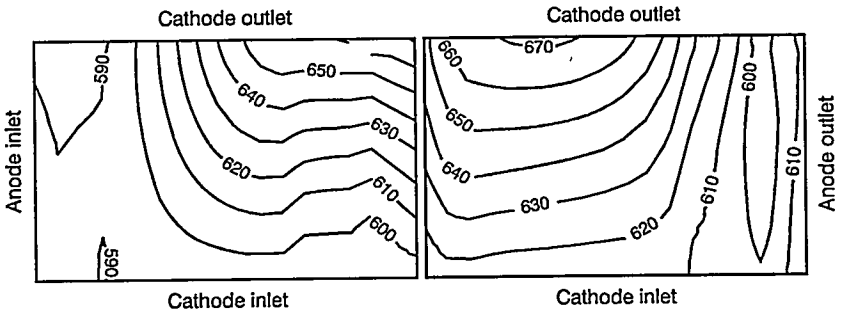

Figure 4: Calculated temperature profile (°C) at start of run conditions.

Figure 5: Calculated temperature profile (°C) close to end-of-life conditions.

STATUS OF THE M-C POWER IMHEX® MCFC COMMERCIALIZATION PROGRAM

René M Laurens*, Joseph A Scroppo, Randy J Petri and Thomas G Benjamin
M-C Power Corporation
8040 South Madison Street
Burr Ridge, IL 60521 U.S.A.
Phone 708.986.8040 Fax 708.986.8153

COMMERCIALIZATION and MARKETING STATUS

Six years ago, M-C Power (MCP) developed a comprehensive business plan to commercialize molten carbonate fuel cell (MCFC) power plants. On an annual basis the plan has been reviewed and modified to adapt to identified end user needs and technological advancements. As a result, product definition kept abreast with marketing requirements. Over the last five years, there was order and reason for subtle shifts in supply, demand, competition and pricing policies. Today, however, traditional market assessment assumptions must be challenged. There is a revolution taking place. The revolution can be summed up in one word... deregulation. Deregulation of the airline industry led to consideration of the natural gas industry. Now that natural gas deregulation is behind us, it is electric power and telecommunications that are receiving attention. Increased emphasis is being placed on achieving market-priced power. The net result will be thinner margins for the seller and the end user. What does this mean for the commercialization of molten carbonate fuel cells ?

The imminent electric market restructuring will create new forces that will move the MCFC market in new directions. First, the energy customer will enjoy a wide range of choices for electric power and services. Efficiency improvement, power quality and on-site generation will be at the top of the purchase menu. Then, creative electric pricing programs will emerge and price indexing will become common. Under mature deregulation, energy options for large industrial and commercial customers will be optimized based on specific customer requirements. Restructuring is likely to cause transmission congestions as participants move away from regulated transmission activities. Transmission congestion within sensitive air basins will provide the opportunity for strategic placement of MCFC power plants. The extremely competitive nature of wholesale power generation suggests that MCFC applications are best suited for placement at or near customer sites. Thus, MCFC power plants can compete in a retail market while exploiting their environmentally benign characteristics.

After the Year 2005, power generation capacity shortages are likely because of retired, stranded generating assets. Mature market electric power pricing in the deregulated environment will only result after restructuring is completely implemented nationwide. This means that full electric price reductions will not occur until around the Year 2005. Considering electric restructuring, the U.S. Department of Energy is predicting stable natural gas prices through the year 2015, increasing by only 1.5 % per year.[1] Although a high fuel gas price enhances the benefits from the high efficiency characteristics of the MCFC power plant, our analyses reveal that four opportunity segments will remain in the deregulated environment. These four market segments are:

Market Segment	Representative Business
1. Commercial facilities	Hospitals, hotels, offices and retails establishments.
2. Industrial manufacturing	Textile mills, paper and allied products, chemicals, glass and primary metals.
3. Off-site power generation	Distributed generation; supports electric distribution system.
4. Opportunity fuels	Landfill gas, sewage treatment digester gas, refineries, petrochemical plants, chemical and allied products.

Hospitals have the most favorable energy use characteristics of any commercial building for on-site cogeneration systems. They are electrical-energy intensive, require significant thermal energy and their energy use pattern is fairly constant- that is, it does not diminish appreciably at night or on weekends and holidays. Additional candidates include: other kinds of health care facilities such as nursing homes and convalescent center, prisons and hotels.

Distributed generation, as presented here, is power capacity that is owned by the electric utility and is classified as distribution assets rather than as a generation asset. The initial distributed generation applications of MCFC's will be in areas where electrical transmission and distribution costs are the highest. Other high priority uses will be areas where a utility can defer or cancel new substation construction or upgrades. During the Years 2000 to 2005, fuel cells could capture as much as 500 MW of capacity.

The primary uses for MCFC's in industrial manufacturing is for cogeneration and manufacturing plant emission reduction. Opportunity fuels in the petroleum refinery, petrochemical and chemical industries include hydrogen and carbon monoxide. Methane from landfills and waste water treatment plants are also considered opportunity fuels.

TESTING and TECHNOLOGY DEVELOPMENT

Full-area, short height stack testing. Short height, full-area stack testing is conducted to verify stack design changes or qualify components used in full height prototypes. MCP conducted one full-area, short height test (MCP-7) to qualify the components for the Naval Air Station (NAS) Miramar demonstation. The principal objectives of the test were to verify: 1) performance of the components, 2) the effect of increased negative fit up, 3) the effect of integrated feed rails towards reducing the cell pressure drop, and, 4) unattended stack test operation. A brief summary of the results obtained is given below.

Performance- Figure 1 contains typical MCP-7 polarization data. The polarization was conducted at 1 atm and 75% fuel utilization at 160 mA/cm^2, using system gases (simulated cathode recycle power plant gases). The test duration was 2,369 h with 1,050 h of steady state operation on simulated power plant gases. The average power produced on system gases at 1 atm equates to 19.6 kW (~1 kW/cell) at 160 mA/cm^2.

Fit up- Negative fit up is used to ensure good seal pressure in the gas manifold area while maintaining the ability of the rail to follow cathode creepage. A potentail drawback was that internal resistances may increase; however, data collected showed this was not the case. In fact, we noted a slight improvement, or reduction of resistance by 3.4%, over previous data.

Figure 1. MCP-7 Polarization

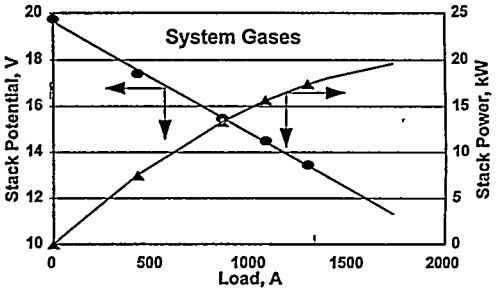

Integrated feed rail- Previous plate designs used pressed/machined pieces to distribute reactant gases. A total of ten (10) feed rails were used; manufacturing was costly and time consuming. Integration of the feed rails into the main plate not only reduced plate cost but provided the added benefit of reduced cell face pressure drop. Data collected during MCP-7 revealed a 5% reduction in pressure drop when compared with other short height stacks for a wide range of cathode flows.

Unattended operation- To meet low operating cost and remote siting capabilities an MCFC-based power plant must operate unattended. The MCP test facility control system was improved to enable this type of operation. During MCP-7, the facility operated 1,300 h in this mode and responded well to both scheduled and unscheduled power outages and other simulated tests.

Prototype testing. We completed the construction of our second prototype 250 kW full height stack. The first stack-- installed at Unocal's Fred Hartley Research Center -- was not successful. Consequently, MCP stopped manufacturing of the Miramar stack and conducted an extensive review of its component manufacturing, assembly, conditioning, transportation, field installation and startup procedures. While the stack produced 80 kW in the acceptance test facility (ATF), the review team identified that the most probable causes for the lack of stack performance were the in-field oxidation of the anodes and loss of clamping pressure. In addition, the team identified 48 issues where improvement was needed. The great majority of these were implemented. A summary of the significant changes made to ensure the success of the NAS Miramar stack is presented below:

Manufacturing- Modified procedures yielded much improved component tolerances. In general, the manufacturing teams achieved tolerances of $\pm$ 2 mils on components with areas in excess of 10,000 cm^2.

Assembly- A comprehensive three-dimensional, finite element, thermo-mechanical stack asembly model was completed. The model enables stack engineers to evaluate the effect of stacking tolerances on gas sealing requirements and active area contact forces. The model was validated via a series of live stack assembly tests of from 50 to 250 cells that were instrumented with a real-time strain gauge system as well as pressure sensitive film. The computer simulations and live assembly tests confirmed that force distribution plates are needed to realize good gas seals and electrical contact. The verified model was then used to specify the number, spacing and thickness of these force distribution plates. Figure 2 shows the assembled Miramar stack; a total of 9 such "intermediate", or force distribution plates were used.

Figure 2. NAS Miramar 250 kW Stack

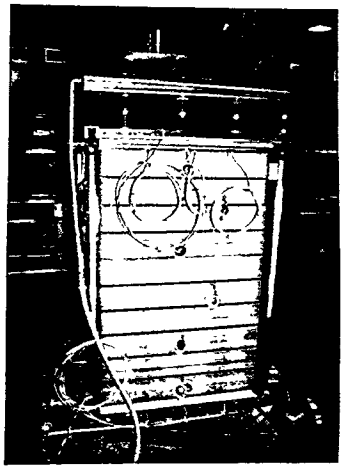

Conditioning- Several bench scale tests were made to validate the procedures to be used for conditioning the Miramar stack. Redundant equipment and instrumentation were added to the acceptance test facility to enhance its reliability. The actual conditioning process for the NAS Miramar stack was uneventful. We met the 200 hours goal set for on-load operation in the ATF, with over 150 hours of operation at 25% load; using simulated power plant gases set at 60% fuel utilization. The maximum power output was 104 kW for a six hour period. The maximum load could not be sustained due to facility cooling limitations. To prevent loss of clamping pressure after stack conditioning -- a key recommendation made by the review team-- a redundant spring clamping system was installed.

Transportation and Field Assembly- Figure 3 shows the power module leaving the MCP manufacturing facility. The procedures used for transportation of the NAS Miramar stack were identical to those used for the Unocal stack. Confirmation testing after stack arrival at Miramar revealed no adverse effects due to transportation. The field stack assembly was completed on schedule and the power module is ready

for integration after the startup test(s) are completed on the balance of plant (BOP) equipment. Redundant stack height measurement systems, another key recommendation made by the review team, were installed and verified by MCP engineers.

Figure 3. NAS Miramar power module

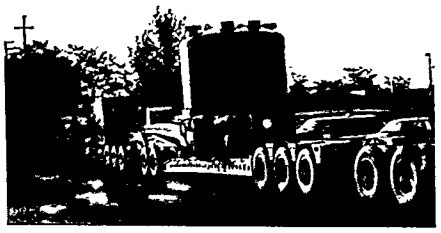

Market Entry Component Development. To achieve market entry performance, life and cost requirements, MCP has modified the existing cell package components using a continuous improvement approach. Particular emphasis was placed on the development and scale up of a sodium-based electrolyte and a Ni dissolution resistant cathode.

For example, the IMHEX team completed a very successful series of bench scale tests using first and second generation stabilized cathodes. Detailed results for the solid solution cathodes are given elsewhere.[2] Here, a brief description of the results obtained from a new, second generation stabilized cathode are given. The test completed 10,000 h of operation, including more than a year on load with simulated power plant system gases. The cell operated at 3 atm pressure at a voltage of 763 mV at 160 mA/cm^2, with flows set for 60% fuel utilization. There was no discernable decay. The on-load lifegraph is shown in Figure 4.

Figure 4.

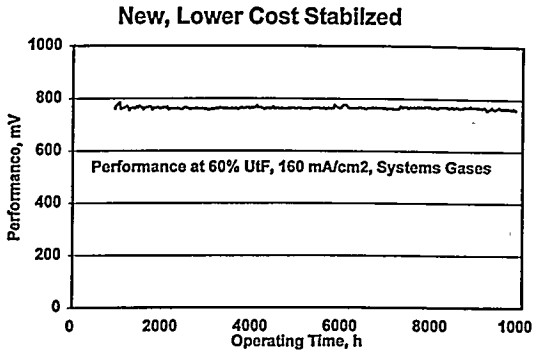

The new cathode in this test is projected to be 6%less expensive to produce than the current state-of-the-art NiO cathode and 69%less expensive than the first generation stabilized cathodes. In addition, the lower cost stabilized cathode is easier to manufacture, with higher production yields and increased strength in the sintered state.

CONCLUSIONS and FUTURE OUTLOOK

The MCP marketing and product development efforts have been described. The business plan clearly establishes a preferred commercialization path-- adjust to an ever changing utility industry and fit the key entry areas. Technically, we are positioning ourselves for these new market entry areas via the development and readiness for full-scale testing of new components that meet the performance and life goal requirements. Thus, MCP is ready to meet the challenges of an exciting and ever-changing utility industry future.

REFERENCES

1. Annual Energy Outlook 1996: with Projections to 2015, DOE/EIA-0383(96), January 1996.
2 "Effect of Pressure on Performance & Endurance of MCFC's", Sishtla, C., et al, 1994 National Fuel Cell Seminar, pg 400.

ANSALDO PROGRAMS ON FUEL CELL VEHICLES

Bartolomeo G. Marcenaro and Flavio Federici
Ansaldo Ricerche Srl
Corso Perrone 25
16161 GENOVA - ITALY
Tel. +39-10-6558427
Fax. +39-10-6558104
marcen@ari.ansaldo.it

The growth in traffic and the importance of maintaining a stable ecology at the global scale, particularly with regard to atmospheric pollution, raises the necessity to realise a new generation of vehicles which are more efficient, more economical and compatible with the environment.

At European level, the *Car of Tomorrow* task force has identified fuel cells as a promising alternative propulsion system.

Ansaldo Ricerche has been involved in the development of fuel cell vehicles since the early nineties. Current ongoing programs relates to:

- Fuel cell bus demonstrator (EQHHPP BUS) Test in 1996
- Fuel cell boat demonstrator (EQHHPP BOAT) Test in 1997
- Fuel cell passenger car prototype (FEVER) Test in 1997
- 2nd generation Fuel cell bus (FCBUS) 1996-1999
- 2nd generation Fuel cell passenger car (HYDRO-GEN) 1996-1999

EQHHPP FC BUS
This project, first announced during 1992 Fuel Cell Seminar, concerns the realisation of a demonstrator of a full size urban bus (12 m) powered by SPFC fuel cells. The bus is conceived as a *laboratory vehicle* , where all components are laid out on the passenger compartment for ease of access during tests.

The construction has been finished early this year and operational tests are being performed at Ansaldo premises. Tests on the road are scheduled early 1997 in the Italian city of Brescia.

The project has accumulated over one year delay due to technical problems on some components.

EQHHPP FC BOAT
A small passenger boats (20 m) is being converted to fuel cell by using the same concept of the EQHHPP fuel cell bus.
The generator is being installed and tests are scheduled for 1997 on Lake Maggiore (Italy)

FEVER (Fuel cell Electric Vehicle for Efficiency and Range)
A European Commission Joule II project, aimed at developing a fuel cell passenger car, namely a Renault LAGUNA, powered by SPFC fuel cell.
The target is a high efficiency vehicle with a range of about 500 km, to be tested from spring 1997.

FC-BUS
The concept developed for the EQHHPP FC BUS is to be engineered into a urban bus without loosing any passenger capacity.
Taking advantage of the new Fuel Cell stacks developed for the FEVER project, a 50 kW generator, fed by gaseous hydrogen, will be installed in the engine compartment of a standard NEOPLAN N4114 urban bus.
The project started May 1996 and will end April 1999.

HYDRO-GEN
A further development of De Nora's SPFC stacks is the main objective of this project. A 12-15 kW stack operating at very low pressure is to be developed and subsequently installed on a Peugeot minivan. A special hydrogen tank will be developed for operation at 700 bars.
The project, launched on January 96 will last 48 months.

The following table summarises the programs and involved partners

	FC TYPE	FC POWER	TOTAL POWER	FUEL	RANGE	PROJECT MANAGER	PARTNERS
EQHHPP BUS	SPFC (De Nora)	8 x 5kW	120 kW	LH2	300 km	ANSALDO	DE NORA (I) MESSER GRIESHEIM (D) ASM-BRESCIA (I)
EQHHPP BOAT	SPFC (De Nora)	9 x 5kW	120 kW	LH2	200 km	ANSALDO	DE NORA (I) MESSER GRIESHEIM (D)
FEVER	SPFC (De Nora)	3 x 10kW	30 kW	LH2	500 km	RENAULT	ANSALDO (I) DE NORA (I) ECOLE DES MINES (F) VOLVO (S) AIR LIQUIDE (F)
FCBUS	SPFC (De Nora)	5 x 10 kW	150 kW	GH2	300 km	ANSALDO	NEOPLAN (D) DE NORA (I) SAR (D) AIR LIQUIDE (F) UNIV. OF GENOA (I)
HYDRO-GEN	SPFC (De Nora)	30 kW	30 kW	GH2 @ 700 bar	> 300 km	PEUGEOT	ANSALDO (I) DE NORA (I) SOLVAY (B) CEA (F) RENAULT (F)

PERFORMANCE EVALUATION OF 1 KW PEFC

Hideaki Komaki
Ishikawajima-Harima Heavy Industries Co., Ltd.
2-1-1 Toyosu, Koto-ku, Tokyo 135, Japan

Syozo Tsuchiyama
The Shipbuilding Research Association of Japan
Senpaku Shinko Bldg., 1-15-16 Toranomon, Minato-ku,
Tokyo 105, Japan

This report covers part of a joint study on a PEFC propulsion system for surface ships, summarized in a presentation to this Seminar, entitled "Study on a PEFC Propulsion System for Surface Ships", and which envisages application to a 1,500 DWT cargo vessel. The aspect treated here concerns the effects brought on PEFC operating performance by conditions particular to shipboard operation. The performance characteristics were examined through tests performed on a 1 kW stack and on a single cell (Manufactured by Fuji Electric Co., Ltd.). The tests covered the items (1) to (4) cited in the headings of the sections that follow.

Specifications of the stack and single cell are as given in Table 1, and the conditions applied for the tests on both stack and single cell in Table 2.

Table 1 Specifications of stack and single cell

	Stack	Single cell
Output	1.1kW	14 W
Voltage	11 V	0.7 V
Current	100 A	20 A
Number of cells	16	1
Electrode surface area	250	50 cm^2
Fuel	Hydrogen	Hydrogen, simulated reformate gas
Oxidant	Air	Air

Table 2 Conditions commonly adopted for all tests

Temperature	73°C (346 K)
Pressure	0.2 MPa abs.
Fuel utilization	75% at 400 mA/cm^2
Air utilization	25% at 400 mA/cm^2

(1) Static characteristics

On both stack and single cell, the V-I characteristics were determined with parametric changes brought on such factors as temperature, pressure, fuel and air utilization, and compositions of fuel and of oxidant.

The effects on the V-I characteristics brought by changes in temperature proved to be as shown in Figs. 1 and 2, which indicate highest cell voltage to be derivable at around 73°C.

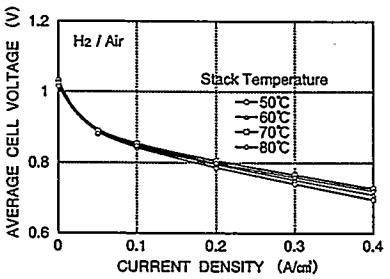

Fig. 1 V-I characteristics obtained under different stack temperatures

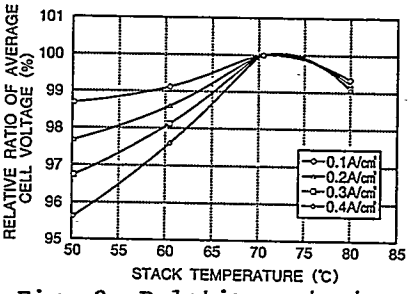

Fig. 2 Relative output voltage as function of stack temperature

From the data acquired on static characteristics, empirical formulas have been derived for correcting output voltage, as reproduced below.

$$V=V_{BASE}+\triangle V(i)+\triangle V(P)+\triangle V(T)+\triangle V(C)+\triangle V(A)+\triangle V(HC)$$

$\triangle V(i) = \beta_{IR}(i_2-i_1)$ $\quad \beta_{IR} = -0.380\text{mV/mA/cm}^2$ $(200\text{mA/cm}^2 < i < 400\text{mA/cm}^2)$

$\triangle V(P) = \beta_P \ln(P_2/P_1)$ $\quad \beta_P = 57\text{mV/kg/cm}^2$

$\triangle V(T) = \beta_T (T_2-T_1)$ $\quad \beta_T = 1.59\text{mV/℃}$ $(T \leqq 73℃)$

$= -0.69\text{mV/℃}$ $(T > 73℃)$

$\triangle V(C) = \beta_C \ln(Y_{O2}/Y_{O1})$ $\quad \beta_C = 102$ (taking account of steam partial press.)

$\triangle V(A) = \beta_A \ln(Y_{H2}/Y_{H1})$ $\quad \beta_A = 49$ (at 400mA/cm²)

$\triangle V(HC) = \beta_{HC}(T-T_C)$ $\quad \beta_{HC} = 1.5\text{mV/℃}$ $: 0 \leqq (T-T_C) \leqq 12.5℃$

$= 9.6\text{mV/℃}$ $: 12.5℃ < (T-T_C) \leqq 25℃$

where V : Cell voltage [mV]
i : Current density [mA/cm^2]
P : Pressure [kg/cm^2 abs.]
T : Stack temperature [°C]
Y_H : Molecular fraction of hydrogen
Y_O : Molecular fraction of oxygen
T_C : Dew point of cathode inlet air [°C]

β : Voltage correction coefficient

1 : Reference condition.
2 : Operating point
IR : Current density
HC : Cathode dew point

(2) Changes of load

The 1 kW stack was used for tests covering load increase/decrease, sharp load lowering/rising, overloading, and repeated loading.

The test on sharp load lowering/rising——simulating the conditions occurring upon crash-stop astern maneuver——yielded the results reproduced in Fig. 3, where load was lowered at a rate of 18%/s and raised at 3%/s. Figure 4 shows the result of repeated loading test, in which the current was 10 times lowered from rated level down to 25% and raised again at intervals of 20s. The output power is revealed to have well followed the changes of current (i.e. of load).

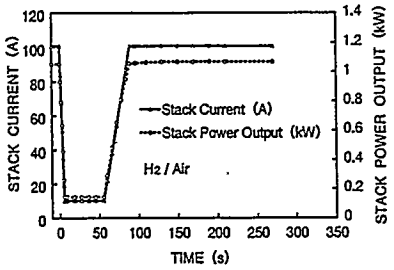

Fig. 3 Results of sharp load lowering/rising test

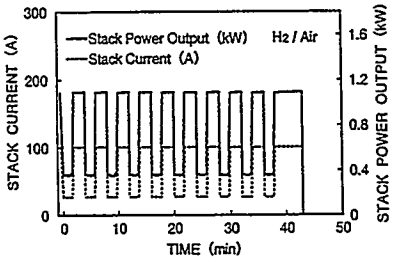

Fig. 4 Results of repeated loading test

(3) Operation of stack in inclined position

Hull inclination and pitching/rolling motions being indispensably required to be taken into account in shipboard operation, this factor was considered in a test in which the stack was operated at positions inclined in the four directions and at 5° intervals to the maximum angles indicated in Fig. 5. It proved that stack performance was the most adversely affected when the inclination placed the air exhaust manifold on the under side. For practical application of the PEFC to ship propulsion, there is need to devise a means of letting the generated water freely flow out with the stack inclined to angles up to 30°.

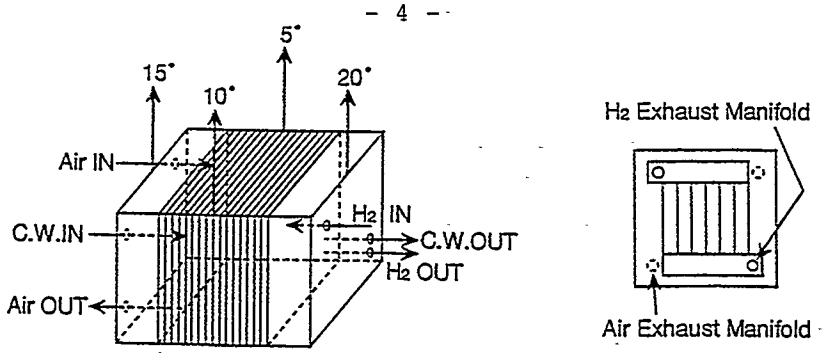

Fig. 5 Maximum allowable angles of stack inclination

(4) Effect of salinity

For evaluating the effect on fuel cell brought by the presence of salinity in the sea air, the single cell operating performance was measured after impregnating for a prescribed duration a membrane electrode assembly in water containing salt in parametrically varied concentrations. Test results are presented in Fig. 6, where 120mg/300ml salt concentration corresponds to the total quantity of salt entering a single cell upon operation for 100 h at 50% air utilization rate in sea atmosphere (containing 30 mg salt/m^3) in heavy sea.

The foregoing data indicate the necessity of passing the air supplied to cell through a filter of 99.3% salt removal efficiency, in order to prevent lowering of cell output voltage by the salinity of marine atmosphere during the course of cell life (40,000 h). This requirement is based on the supposition that heavy seas continue ininterrupted during 40,000 h and that all the salt entering the cathod is trapped in the membrane electrode assembly.

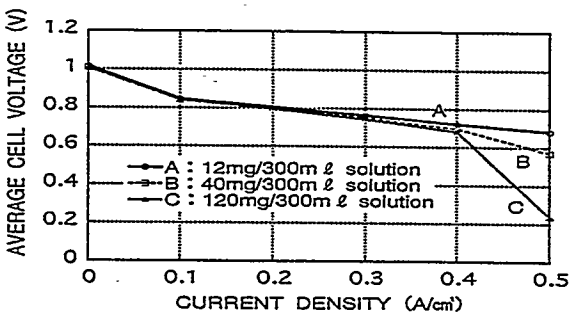

Fig. 6 Results of salinity effect test

EXPERIMENTAL INVESTIGATION ON A TURBINE COMPRESSOR FOR AIR SUPPLY SYSTEM OF A FUEL CELL

Masayasu Matsuda
Sumitomo Heavy Industries, Ltd.
19 Natsushima-cho, Yokosuka 237, Japan

Syozo Tsuchiyama
The Shipbuilding Research Association of Japan
1-15-16 Toranomon, Minato-ku, Tokyo, 105, Japan

This report covers part of a joint study on a PEFC propulsion system for surface ships, summarized in a presentation to this Seminar, entitled "Study on a PEFC Propulsion System for Surface Ships", and which envisages application to a 1,500 DWT cargo vessel. The aspect treated here concerns a study on the air supply system for the PEFC, with particular reference to system components.

AIR SUPPLY SYSTEM CONCEIVED FOR THE ENVISAGED SHIP

With the view to providing high PEFC operating efficiency over a wide range of loading, as well as to ensuring versatile load-following capability, the air supply system conceived to equip the envisaged ship is devised to seek:-

- Enhancement of PEFC generating efficiency through pressurized fuel cell operation (use of air compressor)
- Retrenchment of compressor power at low load (compressor delivery flow rate and pressure controlled to follow variations in fuel cell load)
- Enhanced utilization of surplus hydrogen in the off-gas (use of an auxiliary combustor installed immediately upstream of turbine)
- Enhanced utilization of exhaust heat (turbine compressor equipped with generator-motor).

The generator-motor referred to above is connected to the compressor shaft through reduction gearing, and serves as generator during excess turbine output, and as motor during shortages of same.

ALTERNATIVE AIR SUPPLY SYSTEMS EVALUATED

To serve in selecting the best combination of devices for the fuel cell air supply system, a comparative evaluation was made of the alternatives cited in Table 1, applying the criteria of space occupied, weight, operating efficiency and controllability.

The comparison was made under the common condition of not controlling the turbine inlet temperature (except for the "Turbine Compressor Only" alternative). Particular weight was attached to availability of auxiliary power source to supplement compressor driving power shortage under partial load, in view of the relatively low temperature of the heat source, i.e. exhaust heat from fuel cell and from methanol reformer.

Among the alternatives evaluated, that of "Turbine Compressor with Generator-Motor" has proved to promise the highest operating efficiency, combined with compact equipment size, as noted in Table 1. It is envisaged to adopt this combination as ultimate choice of air supply system.

EXPERIMENTAL SETUP

For the purpose of verifying air supply system controllability, an experiment on system components was conducted on the motor-driven blower + turbine compressor alternative, which alternative was chosen on account of its permitting various experimental conditions to be more easily set. A 2-stage rotary motor-driven blower was used, combined with a single-stage centrifugal automobile turbocharger driven by single-stage radial turbine. The system capacity was set at approximately 1/10 of that for the envisaged actual ship. The experimental equipment is schematized in Fig. 1.

In the experiment, the following key items were examined, which are of interest in common with the turbine compressor + generator-motor alternative envisaged as ultimate choice.

- To verify the operating stability of this system
- To determine the operating characteristics of the respective control systems, and to identify problems calling for solution
- To verify the controllability of the respective control systems under changes of load and of turbine inlet temperature
- To verify the starting characteristics and effect of startup load reduction provided by the compressor bypass line.

Air supply flow rate was controlled by regulating the 1st-stage blower revolution.

Controllability of the air supply system was evaluated for the following alternative control methods:

(1) Without pressure control

Compressor delivery flow rate alone was controlled, and delivery pressure was left to follow its course. With no regulation intervening between turbine and compressor, all throttling loss is eliminated, to contribute toward raising the operating efficiency. The uncontrolled delivery pressure has proved to vary with such factors as the temperatures of environment and of turbine.

(2) Control of fuel cell outlet pressure

The control valve (V2 in Fig. 1) installed at fuel cell outlet was regulated to control the fuel cell outlet pressure. Closing this valve proved effectively to prevent dropping of fuel cell pressure upon such occurrences as abrupt lowering of turbine inlet pressure caused by turbine temperature decrease during operation under constant fuel cell load. It was further ascertained that the valve also provides a similar adjusting function upon lowering of turbine flow rate.

(3) Regulation of fuel cell bypass line flow rate

The rate of air supply to fuel cell from compressor delivery was adjusted by regulating the fuel cell bypass line control valve (V3 in Fig. 1). In practical application, this action is to be brought to play in partial load operation, when required to reduce the air supply to fuel cell to a level below minimum blower delivery rate.

Proper functioning of this action has been verified.

(4) Regulation of turbine bypass line flow rate

The turbine bypass line control valve (V4 in Fig. 1) serves to regulate the flow to turbine and lower the turbine inlet pressure. This action has proved to prevent abrupt rise of turbine inlet pressure upon such occurrences as turbine temperature rise during operation under constant fuel cell load. It has further been ascertained that the valve also provides a similar adjusting function against rise of turbine inlet pressure with increase of turbine flow rate.

An example of experimental results is shown in Fig. 2, representing a run on turbine compressor startup without use of the compressor bypass line. Further details are to be reported in poster session.

Table 1: Comparative evaluation of alternative air supply systems

		Turbine compr. with gen.-mot.	Motor-driv. blower +Turbine compr.	Motor-driv. compr. +Turbo gen.	Turbine compr. only
Electric Power req'd	High load (100%)	◎ -5 kW(*)	○ 0 kW	△ 10 kW	○ 0 kW
	Low load (50%)	○ 2 kW	○ 2 kW	△ 5 kW	× 30 kW(**)
Flow Control	High load.	○ Compr. rev.	○ Turbine bypass	◎ Compr. rev.	○ Turbine bypass
	Low load	○ Compr. rev.	○ Blower rev.	◎ Compr. rev.	△ Turbine temp.
Space occupied : weight		○	△	×	×

◎:Best ○:Good △:Acceptable ×:Not Good

(*) Power furnished by generator
(**) Heat furnished by methanol

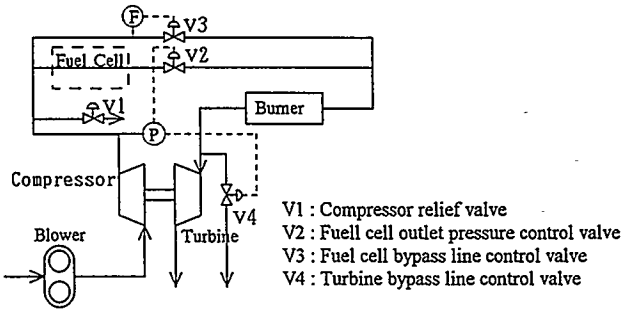

Figure 1: Schematic of experimental setup

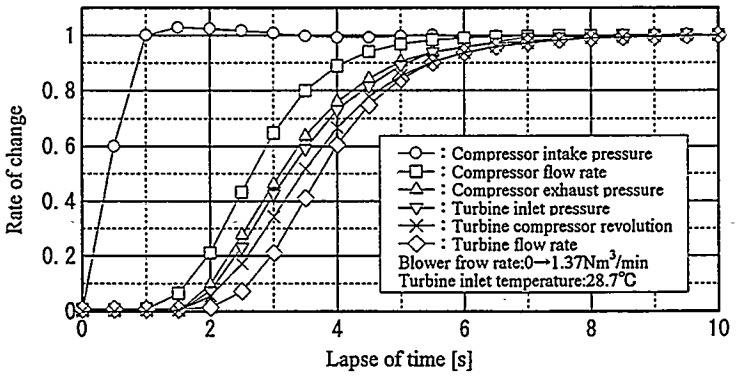

Figure 2: Starting characteristics of turbine compressor

DEVELOPMENT OF A SELECTIVE OXIDATION CO REMOVAL REACTOR FOR METHANOL REFORMATE GAS

Shunji Okada, Yoshiaki Takatani, Seiji Terada
and Shinichi Ohtani
Kawasaki Heavy Industry, Ltd.
1-1 Kawasaki-cho, Akashi, Hyogo-ken 673, Japan

Syozo Tsuchiyama
The Shipbuilding Research Association of Japan
1-15-16 Toranomon, Minato-ku, Tokyo, 105, Japan

This report forms part of a joint study on a PEFC propulsion system for surface ships, summarized in a presentation to this Seminar, entitled "Study on a PEFC Propulsion System for Surface Ships", and which envisages application to a 1,500 DWT cargo vessel. The aspect treated here concernns laboratory-scale tests aimed at reducing by selective oxidation to a level below 10 ppm the carbon monoxide (CO) contained to a concentration of around 1% in reformate gas.

The catalyst chosen was Ru-base, for its high CO removal efficiency with little parasitic reaction. The catalyst was tested on a laboratory-scale reactor corresponding to a 1-kW output PEFC system.

A difficulty encountered in the present tests was heating of the catalyst layer by the exothermic oxidation reaction, and devising a means of ensuring optimum catalyst temperature is a matter calling for further development in practical application. The results of studies to be conducted on such and other subjects are to be incorporated in the design of a 500-kW class marine propulsion fuel cell system.

LABORATORY-SCALE TESTS

For acquiring basic data to serve in selecting catalysts, laboratory-scale tests using a flow-through reactor were conducted at atmospheric pressure on simulated reformate gas.

(1) Temperature-dependent characteristics of catalyst

The dependence on catalyst temperature shown by the CO removal and hydrogen loss characteristics of representative alumina-supported noble metal catalysts proved to be as shown in Fig. 1, where the CO and hydrogen removal efficiencies η_{CO} and η_{H} are plotted against catalyst temperature.

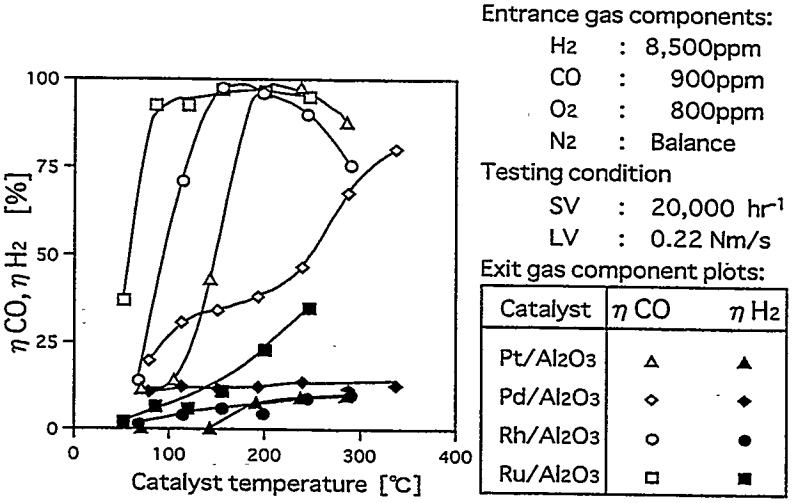

Fig. 1 Temperature-dependent CO removal and H_2 loss characteristics of representative catalysts

The highest CO removal efficiency is seen to have been obtained over a wide temperature range with Ru-base catalyst. As regards hydrogen loss, all catalysts have tended to raise their effectiveness with increasing temperature. In this respect, Ru-base catalyst is at a disadvantage for its diminishing hydrogen at a rapidly rising rate with increasing temperature, thus taking away hydrogen that could serve usefully as fuel.

(2) Parasitic reactions of catalyst

Conceivable parasitic reactions that might be induced by catalyst include reverse-shift reaction, methanation and hydrogen oxidation. To examine such possibility, the temperature-dependent behavior of Ru- and Rh-base catalysts were examined on a simulated reformate gas devoid of CO.

The results, indicated in Fig. 2, reveal that with such gas initially devoid of CO, Rh-base catalyst generates CO by reverse-shift at high temperature. Such reaction is not induced by Ru-base catalyst, but on the other hand, this catalyst generates CH_4 by methanation of CO_2. While CH_4 does not directly detract from PEFC performance, its generation is at the expense of consuming fuel hydrogen, and should thus be minimized.

Entrance Gas Components - CO2 : 1.8%; H2 : 6.0%; N2 : Balance
Testing conditions: SV : 20,000 hr^{-1}; LV : 0.22 Nm/s
Exit gas component plots:

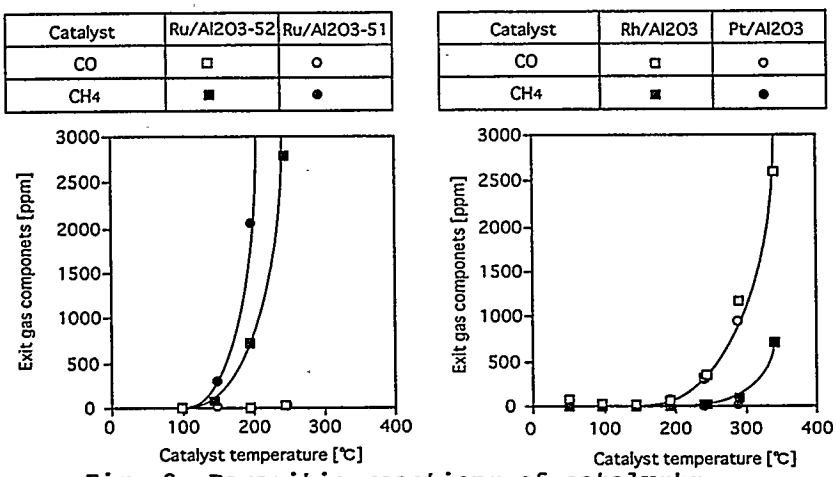

Fig. 2 Parasitic reactions of catalysts verified with gas initially devoid of CO

(3) Tests on reformate gas with reactor corresponding to 1kW output PEFC system

For the purpose of deriving criteria to serve in selecting granular catalysts for removal of CO——which is present in 1 to 2% concentration in gas from actual reformate reactor (H_2:CO_2 = 75/25)——and also for evaluating catalyst performance, tests were conducted on a laboratory reactor corresponding to a 1kW output PEFC system, with results as summarized below.

(3-1) Performance of Ru-base catalyst

The performance of Ru-base catalyst was examined in terms of the reactor exit CO and CH_4 concentrations related to stoichiometric ratio, at different catalyst entrance temperatures.

The plots shown in Fig. 3 are from runs at 100 and 150°C catalyst entrance temperature. Exit CO concentration is seen to lower with increasing stoichiometric ratio up to 3.2, at which point a concentration of 16 ppm has been marked with 150°C reactor entrance temperature. The original CO concentration at reactor entrance was 10,057 ppm, meaning that the catalyst performed at a CO removal efficiency n_{CO} of 99.84%.

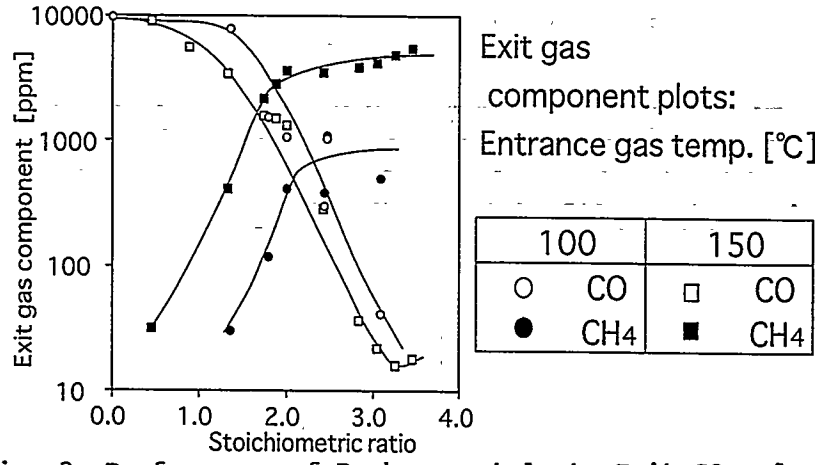

Fig. 3 Performance of Ru-base catalyst: Exit CO and CH4 concentrations vs. stoichiometric ratio

If a CO converter were installed downstream of the reformer to reduce the CO concentration below 7,000 ppm before entering the reactor, the target CO concentration of 10 ppm could well be realized at reactor exit.

The influence of differences in catalyst temperature was insignificant in the range covered (100 - 150°C).

(3-2) Effect of temperature on catalyst performance

The selective oxidation process involves exothermic reaction, which makes it important to ensure a uniform temperature distribution through the catalyst bed. For this reason a comparison was made between two alternative arrangements: (a) filling the reactor with catalyst only; (b) diluting the catalyst with inert (glass) beads to disperse the generated heat.

The results revealed the catalyst diluted with 6.3-fold volume of glass beads to have effectively served to spread the heat. In the present experimetal setup, a thermostat was used as heat source, but no means was provided for actively removing the generated heat. Hence, the catalyst temperature exceeded 250°C in the leading catalyst layer, which for this reason could only remove less than 90% of the CO.

A possible solution to the above difficulty may be the adoption of a heat exchanger type reactor to remove heat, in combination with catalyst dilution.

PERFORMANCE OF CATALYSTS FOR CO REMOVAL BY METHANATION

Hitoshi Oshiro, Kiichi Nagaya and Koichi Mitani
Hitachi Zosen Corporation
2-2-11 Funamachi, Taisho-ku, Osaka 551, Japan

Syozo Tsuchiyama
The Shipbuilding Research Association of Japan
1-15-16 Toranomon, Minato-ku, Tokyo, 105, Japan

This report forms part of a joint study on a PEFC propulsion system for surface ships, summarized in a presentation to this Seminar, entitled "Study on a PEFC Propulsion System for Surface Ships", and which envisages application to a 1,500 DWT cargo vessel. The aspect treated here concerns an experiment in reducing by methanation to a level below 10 ppm the CO that is contained to around 1% in reformate gas.

EXPERIMENTAL SETUP

To precede application test with actual CO removal equipment for verifying practical performance, the present experiment was undertaken using the equipment shown in Fig. 1 to determine (1) the methanation rate for obtaining basic data on catalysts, and (2) catalyst performance using reformate gas under conditions close to practical application.

(1) Methanation rate

Catalysts tested :

Three Ni-Al_2O_3 base methanation catalysts obtained obtained from market
Catalyst A (20 to 24% Ni)
Catalyst B (14 to 17% Ni)
Catalyst C (20% Ni, 4 to 6% CaO)

Reaction temperature :
Varied in three steps 200, 225 and 250°C

Reaction pressure :
Varied in three steps 2, 3 and 5 kgf/cm^2 abs.

Subject gases tested:

99% H_2 - 1% CO mixture
99% H_2 - 1% CO_2 mixture
99% H_2 - 1% CO + steam mixture
99% H_2 - 1% CO_2 + steam mixture

Quantity of catalyst applied : 1 ml

(2) Methanation performance of catalyst

Catalyst tested: Catalyst C (3/16" spherules containing 20% Ni, 4 to 6% CaO)
Quantity of catalyst applied : 530 ml
Reaction temperatures: 200, 225 and 250°C
Reaction pressure : 2 kgf/cm^2 abs.
SV : 300, 500 and 1,000 h^{-1}
Subject gas tested :
Reformate gas (generated at 250°C from methanol/water mixture at S/C = 1.55 and 1.7)

RESULTS

(1) Methanation rate

Tests on all three Ni-Al_2O_3 base catalysts proved both reaction rate constants k_{CO} and k_{CO2} to be significantly influenced by the reaction temperature: For this reason, the reaction constants were equated to the inverse value of reaction temperature, recorded in Arrhenius plots. Representative reaction rate equations thus empirically derived were as given below.

- For CO methanation

$$r_{co} = 7.436 \times 10^{13} \cdot \exp(-1.375 \times 10^5 / RT) \cdot p_{co} / (1 + 12.97 \cdot p_{co})^2$$

where
r_{CO} : Reaction rate [mol/(h·g)
p_{CO} : CO partial pressure [kgf/cm^2 abs.]
T : Reaction temperature [K] (200 to 250°C)
R : Gas constant [8.314 J/(mol·K)]

A comparison is given in Fig. 2 between the reaction rate derived by the above equation and corresponding measured data.

- For CO_2 methanation

$$r_{co_2} = 1.063 \times 10^{11} \cdot \exp(-1.094 \times 10^5 / RT) \cdot p_{co_2} / (1 + 66.86 \cdot p_{co_2})$$

where the symbols are the same as for r_{CO}, with all references to CO and co replaced respectively by CO_2 and CO_2.

Calculated and measured values are compared in Fig. 3.

(2) Methanation performance of catalyst

The CO concentration at reactor exit varied with reaction temperature and SV as shown in Fig. 4. Table 1 presents the gas compositions analyzed at reactor entrance and exit, in terms of dry gas content, for the run using S/C = 1.55 methanol/water mixture.

It is seen from this table that reduction of CO below the 10 ppm target value is possible at static condition with reaction at 250°C and SV = 300 h^{-1}.

From the CH_4 concentrations, some CO2 methanation reaction would appear to have occurred, which would consume hydrogen, otherwise utilizable as fuel, beyond the amount necessary for CO elimination, to lower the overall thermal efficiency of this process.

Table 1 CO, Co2, CH2 concentration at reactor inlet/outlet (S/C: 1.55)

Test condition		CO Conc.		CO_2 Conc.		CH_4 Conc.	
SV	Temp.	Inlet	Outlet	Inlet	Outlet	Inlet	Outlet
1000h^{-1}	200℃	1.33%	4040ppm	23.8%	24.3%	—	0.73%
	225℃		1180ppm		24.4%		0.97%
	250℃		297ppm		23.6%		4.30%
500h^{-1}	200℃	1.33%	527ppm	23.8%	24.6%	—	1.97%
	225℃		231ppm		23.7%		4.32%
	250℃		24ppm		23.3%		4.70%
300h^{-1}	200℃	1.28%	471ppm	23.7%	24.3%	—	2.13%
	225℃		231ppm		23.5%		4.35%
	250℃		8ppm		22.9%		4.80%

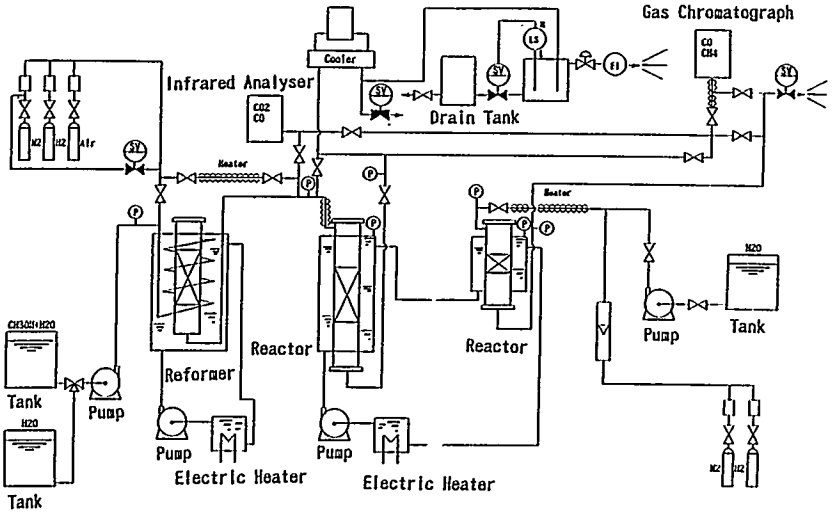

Fig. 1 Flow sheet of equipment

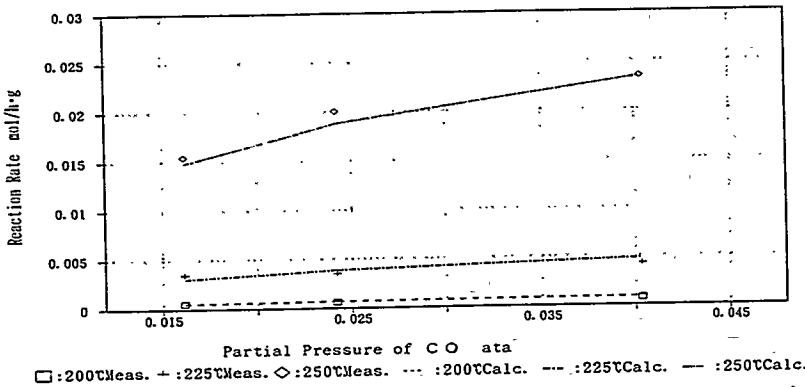

Fig. 2 Reaction rate of CO methanation (Catalyst C)

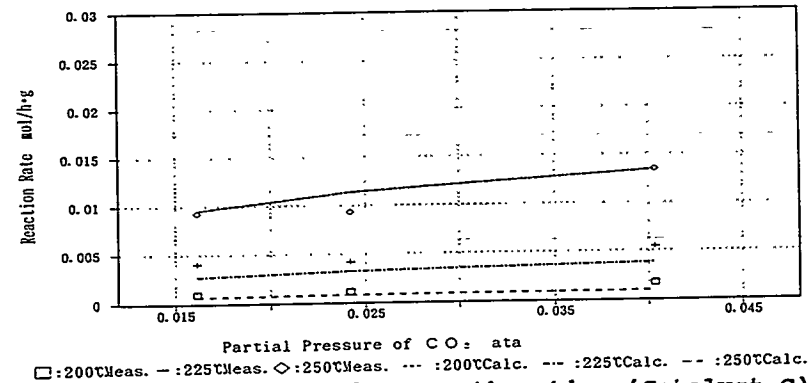

Fig. 3 Reaction rate of CO_2 methanation (Catalyst C)

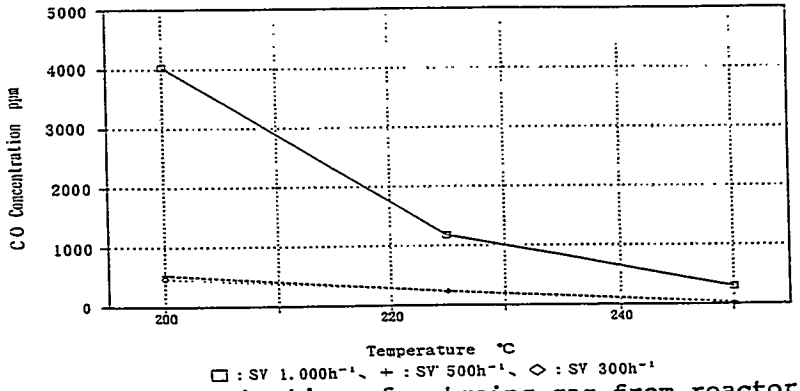

Fig. 4 CO concentration of outgoing gas from reactor (S/C: 1.55)

POWER FEATURE REQUIRED FOR PEFC POWERED ELECTRIC PROPULSION SHIP

Isao Yoshida
Ships & Offshore Structures Planning Dept.
NKK Corporation
2-1 Suehiro-cho, Tsurumi-ku, Yokohama 230, Japan

Masaru Oka
Ship Designing Dept.,
Mitsubishi Heavy Industries, Ltd.
1-1 Akunoura-machi, Nagasaki 850-91, Japan

This report covers part of a joint study on a PEFC system for ship propulsion, summarized in a presentation to this Seminar, entitled "Study on a PEFC Propulsion System for Surface Ships", and which envisages application to a 1,500 DWT cargo vessel. The aspect treated here concerns an analysis of the load-following performance required and estimated of a PEFC system to power the envisaged ship.

The analysis proved that difficulty should be expected of the fuel supply circuit in following with adequate rapidity the sharp changes of load on fuel cell under certain conditions. Further integrated experiments and simulation exercises are currently in progress to further analyze the response characteristics of the fuel supply circuit——particularly of the methanol reformer and gas reservoir——to determine the best measure to be adopted for overcoming the expected difficulty.

MANEUVERING PATTERNS

A vital consideration needing to be made in applying fuel cells as power source for ship propulsion is that, compared with land vehicles, extremely sharp and wide fluctuations of load require to be accommodated. Such load fluctuations are caused under conditions such as:-

- Maneuvering in close waters inside ports
- Actuation of large shipboard machinery such as bow thrusters for berthing and unberthing operations
- Crash stop astern maneuver to avoid collision.
- Propeller racing when it emerges above water in heavy sea.

The conditions cited above would follow the patterns shown in Fig. 1.

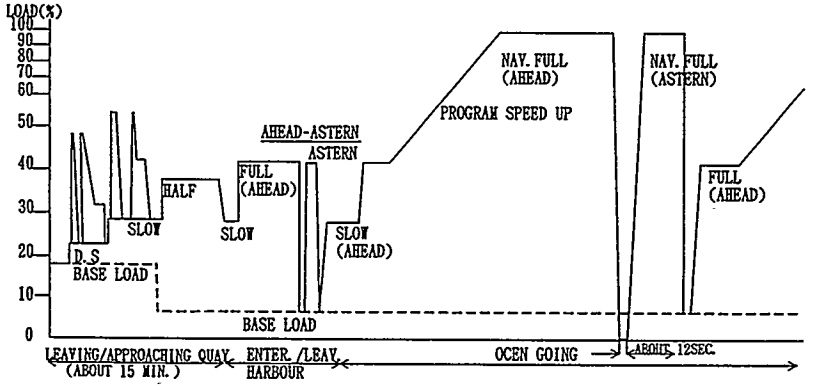

Fig. 1 Maneuvering patterns

LOAD CHANGES OCCASIONED BY VARIOUS MANEUVERS

The changes of load on power source occasioned under the operating conditions cited in the preceding section are modelized in Fig. 2 for the case of crash stop astern maneuver, and in Fig. 3 for propeller racing.

MEASURES FOR ACCOMMODATING LOAD CHANGES

The rates of load change occasioned on the envisaged ship by the conditions referred to above proved to be: ±4.3%/s for bow thruster actuation, - 42.5%/s for crash stop astern maneuver, and + 10.5%/s for propeller racing.

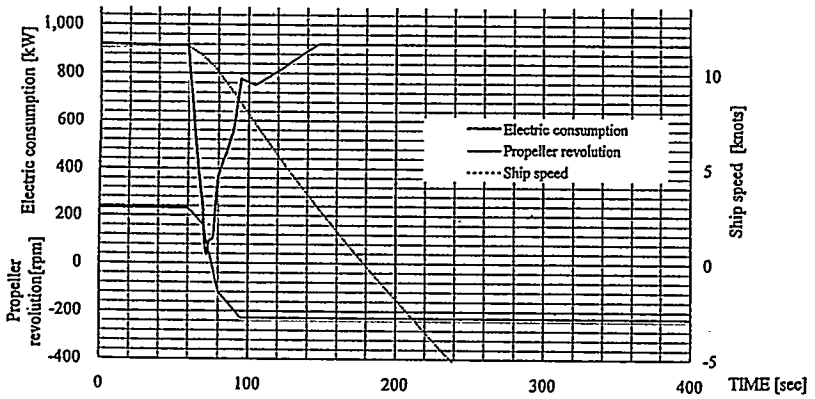

Fig. 2 Load fluctuations estimated to occur upon crash stop astern maneuver

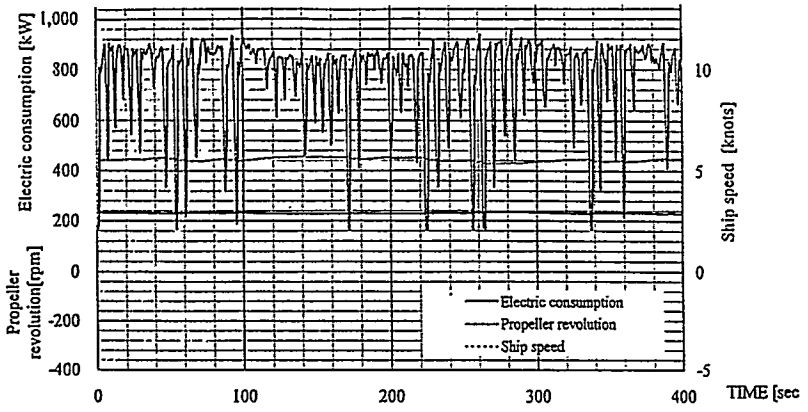

Fig. 3 Load fluctuations estimated to occur upon propeller racing

The present analysis proved the load-following performance of the PEFC system constituents to be as follows:-

(1) The PEFC itself responds extremely rapidly to load changes, which can be followed with almost no time lag.

(2) Air supply to cell is expected to respond with some delay——of the order of several seconds——but this should not cause any problem in actual practice.

(3) Fuel supply can be expected to create some difficulty. As countermeasure, in the case of the maneuvering pattern of Fig. 1:-

For bow thruster actuation during maneuvers of berthing/unberthing and of entering/leaving port, the fuel supply rate would be set to equal the base load plus command power output of bow thrusters or propulsion motors. Abrupt load increases at rates beyond the response characteristics of the fuel supply system would be accommodated by battery discharge; abrupt load decreases would be absorbed by a gas reservoir to be installed on the reformate gas supply line of the fuel cell. Examination is further under way of a means of burning the unutilized anode off-gas in a catalytic combuster and recovering the effluent heat.

- To deal with the abrupt load decrease occurring upon crash stop astern maneuver, constituting the occasion of maximum rate of load change, considering that the limit to fuel supply circuit pressure will preclude resorting to the measure cited above for bow thruster actuation, and in view of the infrequency expected of this maneuver, the possibility is being examined of dealing with the eventuality by burning the excess fuel in a catalytic combuster to be installed in the exhaust duct line of fuel cell and releasing the effluent to atmosphere.

- Load variations accompanying transitions between navigation in confined water and in open sea are to be controlled, independently of the rate at which the command lever is moved, by what is known as "programmed acceleration" and "programmed deceleration", based on the load-following characteristics of the fuel supply circuit.

The arrangement of system control circuitry contemplated for accommodating abrupt load variations is schematized in Fig. 4.

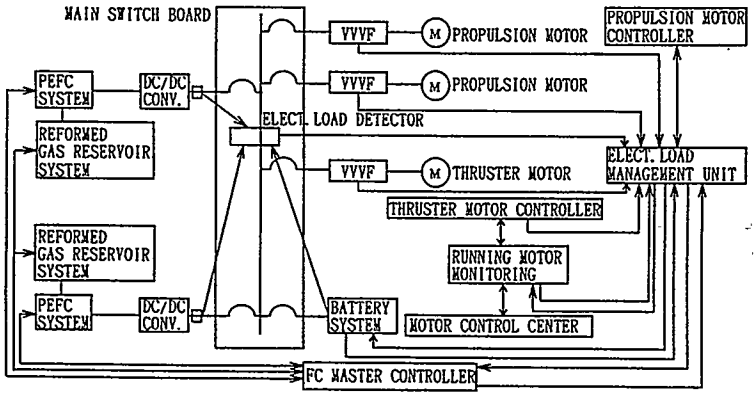

Fig. 4 System control circuitry contemplated for accommodating abrupt load variations

DYNAMIC SIMULATOR FOR PEFC PROPULSION PLANT

Masataka Hiraide, Eiichi Kaneda and Takao Sato,
Mitsui Engineering & Shipbuilding Co., Ltd.
5-6-4 Tsukiji, Chuo-ku, Tokyo 105, Japan

Syozo Tsuchiyama
The Shipbuilding Research Association of Japan
1-15-16 Toranomon, Minato-ku, Tokyo, 105, Japan

This report covers part of a joint study on a PEFC propulsion system for surface ships, summarized in a presentation to this Seminar, entitled "Study on a PEFC Propulsion System for Surface Ships", and which envisages application to a 1,500 DWT cargo vessel. The work presented here focuses on a simulation study on PEFC propulsion plant performance, and particularly on the system response to changes in load.

Using a dynamic simulator composed of system components including fuel cell, various simulations were executed, to examine the performance of the system as a whole and of the individual system components under quick and large load changes such as occasioned by maneuvering operations and by racing when the propeller emerges above water in heavy sea.

SIMULATOR MODEL

The simulation program comprises mathematical models of the PEFC propulsion plant including fuel cell, reformer, turbine compressor, humidifier, steam separator, heat exchangers, evaporators, gas reservoir and propulsion system, as shown in Fig. 1. The models are expressed in differential equations based on material and energy balance equations, combined with algebraic equations. Consideration is also given to the reaction kinetics of the reformer.

SIMULATION

Using the dynamic simulator, the PEFC propulsion plant performance was analyzed on the following items:

(1) Steady-state operation
(2) Open loop responses
(3) Control system performance
(4) Performance under the following conditions:
    (a) Step changes to fuel cell load
    (b) Maneuvering
    (c) Propeller racing
    (d) Bow thruster operation
    (e) Crash stop astern.

Validity of the dynamic simulation program was confirmed by the satisfactory results obtained for steady-state operation under item (1) above; the simulation of item (2) served to find out the characteristics of the load change. The foregoing results were utilized in analyzing the control system performance under item (3). The PEFC system incorporating the control system was dynamically simulated covering the operations cited under items (4)(a) through (e) above.

RESULTS

The results of simulation on the system response to step changes to fuel cell load are shown in Fig. 2, in terms of fuel cell output, methanol flow rate, reformer fuel utilization, PEFC anode pressure and reformer outlet temperature. The case of propeller racing is represented in Fig. 3, in similar terms.

The simulation results shown in Figs. 2 and 3 indicate that, when the load is lowering, the fuel cell output can well follow the change in demand of load. The rise in reformer outlet temperature seen in Fig. 2 upon lowering of load could be eliminated by providing a bypass line from reformer combustion gas line to combustor. Such and other process improvements are currently being brought to the simulation system. The simulator is also being evaluated through comparisons with experimental data. The results can be expected to permit making more detailed analyses of PEFC propulsion plant performance.

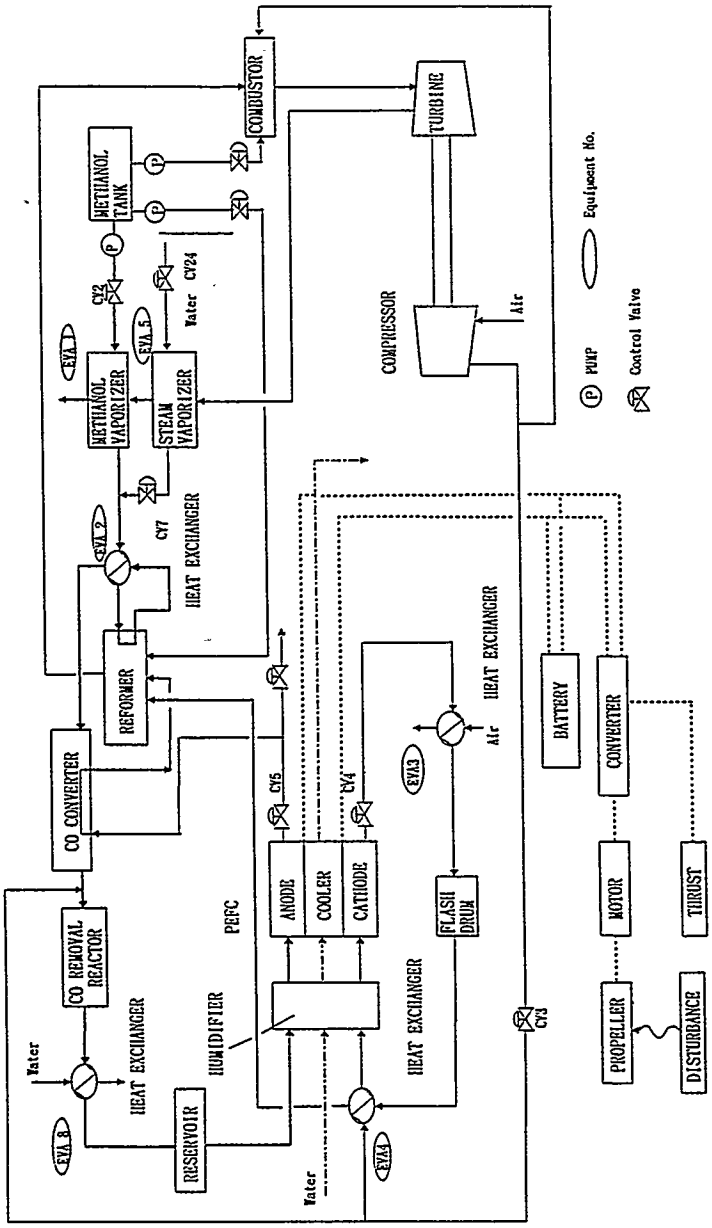

Fig. 1 Scheme of Simulation Model

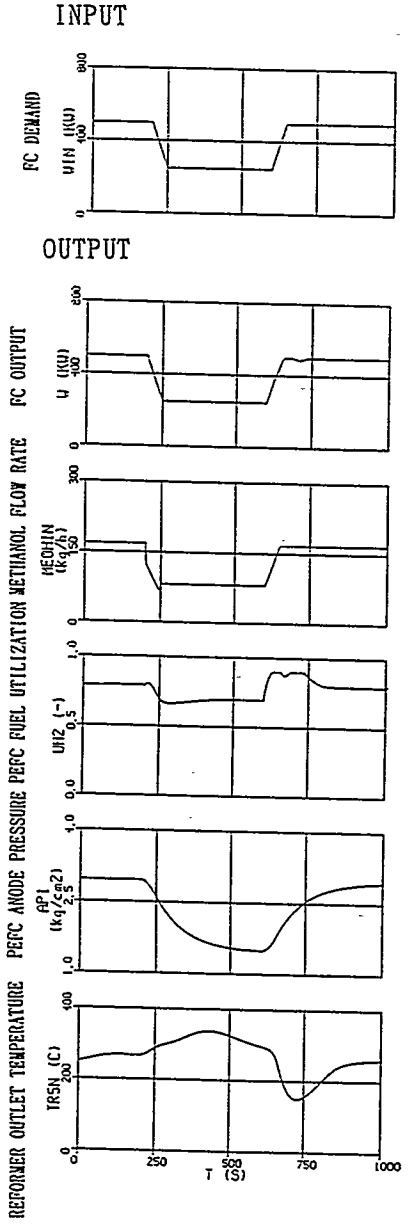

Fig. 2 SYSTEM RESPONSE TO STEP CHANGE IN FUEL CELL LOAD

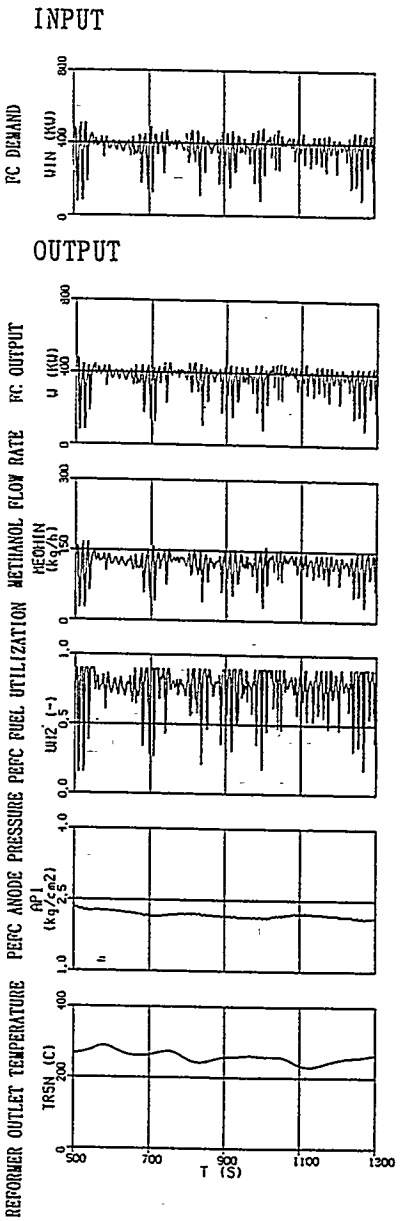

Fig. 3 PROPELLER RACING SIMULATION OUTPUT

AIR-BREATHING FUEL CELL STACKS FOR PORTABLE POWER APPLICATIONS

M. S. Wilson, D. DeCaro, J. K. Neutzler, C. Zawodzinski and S. Gottesfeld
Electronic and Electrochemical Materials and Devices Research Group, MS D429,
Los Alamos National Laboratory, Los Alamos New Mexico 87545

Introduction

Increasing attention is being directed towards polymer electrolyte fuel cells as battery replacements because of their potentially superior energy densities and the possibility of "mechanical" refueling. On the low end of the power requirement scale (ca. 10 W), fuel cells can compete with primary and secondary batteries only if the fuel cell systems are simple, inexpensive, and reliable. Considerations of cost and simplicity (and minimal parasitic power) discourage the use of conventional performance enhancing subsystems (e.g., humidification, cooling, or forced-reactant flow). Thus, we are developing a stack design that is inherently self-regulating to allow effective operation without the benefit of such auxiliary components [1-3]. As such, the air cathode does not use forced flow to replenish the depleted oxygen. Instead, the oxygen in the air must diffuse into the stack from the periphery of the unit cells. For this reason the stack is described as "air-breathing." This configuration limits the ability of water to escape which prevents the polymer electrolyte membranes from drying out, even at relatively high continuous operation temperatures (+60°C). This results in stacks with reliable and stable performance.

This air-breathing configuration assumes a unique stack geometry that utilizes circular flow-field plates with an annular hydrogen feed manifold and the single tie-bolt extending up through the central axis of the stack. With this geometry, the hydrogen supply to the unit cells is radially outward, and the air supply is from the periphery inward. This configuration has several advantages. The entire periphery is free to air access and allows greater heat conduction to enhance cooling. Furthermore, all of the components in the stack (e.g., the flow-fields, seals and membrane/electrode assemblies), are radially symmetrical, so part fabrication is simple and the entire system is potentially low-cost. Lastly, this configuration is compact and lightweight.

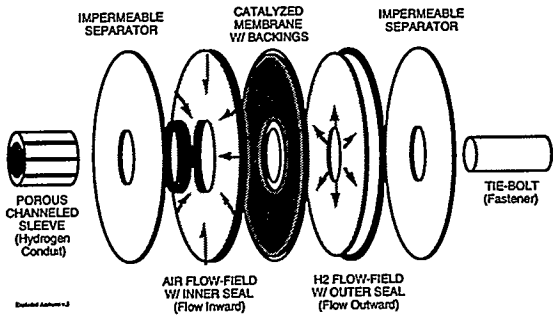

Figure 1. Schematic of the components in a unit cell of the air-breather fuel cell stack.

Air-Breather Stack

Figure 1 depicts the key components of a unit cell for an air-breather stack. Most stacks are 2" (5.1 cm) in diameter with cell active areas of about 13 cm^2, although 1.5" (3.8 cm) diameter stacks with 6 cm^2 active area cells have also been investigated. End-plates (not shown in the figure) compress the collection of unit cells together with the use of a tie-bolt projecting up through the middle. Around the tie-bolt is a porous, channeled sleeve that provides alignment for the unit cell components and a conduit for the hydrogen to reach the inner edge of the hydrogen flow-fields. Hydrogen feed is dead-ended, although provision is made for an initial purge. The reactant flow-fields are typically reinforced carbon paper (e.g. Spectracarb, from Spectracorp,

Lawrence, MA). Seals are located at the inner edge of the air flow-field and the outer edge of the hydrogen flow-field. The flow-fields bracket the membrane/electrode assembly (MEA), which consists of a catalyzed polymer electrolyte membrane sandwiched between two gas diffusion backings from E-TEK (Natick, MA). Stainless steel foil separators, that are typically 0.010" (0.25 mm) thick, prevent the reactants in the back-to-back flow-fields from mixing. In multi-cell stacks, the odd separators are of a larger diameter to provide cooling fins, which gives the stack the appearance of a finned tube.

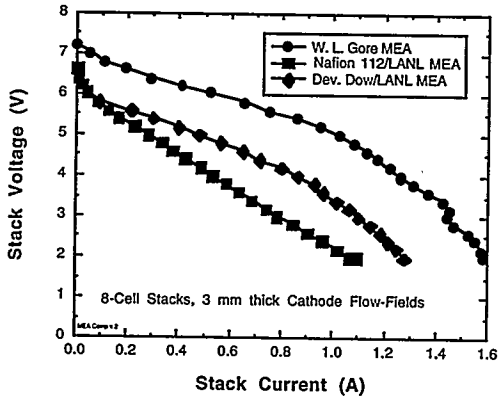

Figure 2. Polarization curves of 8-cell air-breather stacks using a series of different MEAs.

Results

A series of 13 cm^2 active area, 8-cell stacks using the 2" (5 cm) diameter elements and 2.5" (6.4 cm) diameter cooling fins/separators every two cells were assembled and tested using various combinations of flow-fields, MEAs and backings at ambient pressures of 0.75 atm (the laboratory is at an altitude of 7,200 ft or 2,200 m). Not surprisingly, cell performance is substantially affected by the thickness of the cathode flow-field because oxygen must diffuse in from the periphery through this structure. However, while the performance of a single cell air-breather increases with flow-field thickness, more modest thicknesses provide the best performances in multi-cell stacks. Since under continuous operation a multi-cell stack naturally runs warmer than a single cell (ca. 60°C vs. ca. 30°C), too thick of a flow-field allows the cell to dry out excessively. Modeling suggests that the cells suffer once the water partial pressure throughout the flow-field drops below the saturated vapor pressure [3]. A cathode flow-field thickness of about 3 mm is optimal for continuous operation with the 2" diameter 8-cell stacks.

Figure 2 depicts polarization curves for a series of continuously operating 8-cell stacks using different MEAs, one a W. L. Gore catalyzed composite membrane product [4], and the other two MEAs are commercially supplied membranes catalyzed by a process developed at Los Alamos (LANL) [5]. It is readily evident that the W. L. Gore MEA enjoys more than a 100 mV advantage over the other two MEAs, most likely due to an electrode kinetic advantage realized by attaining a higher water content in the catalyst layer. Since the LANL catalyzation process "toughens" the ionomer in the catalyst layer such that it can withstand the rigors of high current density operation, it apparently does not adsorb an appreciable amount of water under the air-breather conditions. Not only is the W. L. Gore MEA quite thin (ca. 20 μm), but it also appears to accommodate substantially more water in the catalyst layer, the combination of which results in improved hydration and performance under these conditions.

Another key component is the gas diffusion backing. 8-cell stacks were operated with and without E-TEK backings and with and without a Teflon treatment. The cells using the backings were clearly superior, as flooding was apparent in the cells with the MEA directly against the carbon paper. The need for a "microporous" backing structure to control flooding has been previously observed in high performance cells [5].

Figure 3 depicts the voltage output of an 8-cell air-breathing stack operating on a portable metal hydride canister at a constant current of 1 A. After coming up quickly, the fluctuations about 5 V are quite small for the first 5 - 6 hours, at which point the hydrogen becomes depleted and some of the cells become starved for hydrogen.

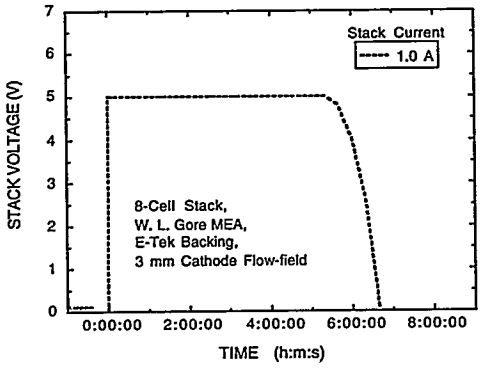

Figure 3. Voltage response (at 1 A) of an 8-cell stack fueled by a portable metal hydride cylinder.

A number of cells have operated for over a thousand hours. Barring seal failures or similar events, performance losses are minimal. Long shut-down periods usually have no effect except on the rapidity of start-up. Upon disassembly, separators made of 304 SS foil typically exhibit some corrosion. The features on the anode sides appear to be a deposit and the cathode sides are pit corroded. The use of 316 SS foils improves the situation, but some effects are still noticeable.

System Energy Densities

At this point, the specific powers we obtain for a roughly 6 to 7 W, 10-cell stack are in the neighborhood of 40 W/kg. In combination with the commercial portable metal hydride supply canisters that we currently use (that are about 0.5 wt% hydrogen), a system specific energy of about 60 Wh/kg is obtained for a 10 W system (Figure 4). If the gravimetric density of the hydride storage would be increased to 1.5 wt% hydrogen (which is within the realm of room temperature metal hydrides), then about 150 Wh/kg could be obtained for a 10 W, 10 hour system. From this point on, increased fuel capacity provides even higher specific energies, which increases the appeal of a system that can use multiple, replaceable fuel canisters. In contrast, the specific energies of conventional batteries are tied to the design, not the total energy capacity, and the best rechargeable batteries (Li-ion) are currently limited to about 110 Wh/kg. As suggested in Figure 4, increases in hydrogen storage density significantly increase the specific energies. Higher levels, such as the 4 wt% hydrogen density depicted in the figure, are easily attainable with chemical hydrides, although the challenge in this case is to develop systems that are low-cost, relatively

benign, and viable for consumer applications. However, if such hydrogen storage systems can be realized, the portable fuel cell will become a formidable competitor for many applications.

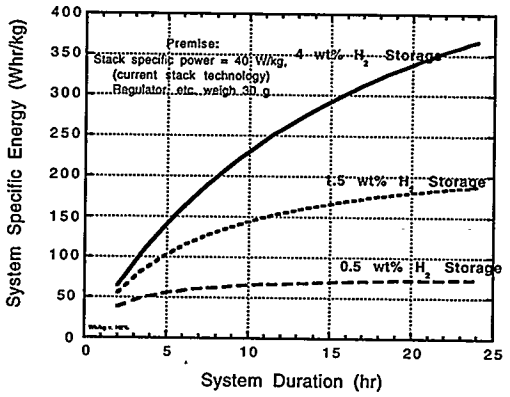

Figure 4. Effect of hydrogen storage density on the specific energy of a 10 W fuel cell system.

Applications

For the immediate future, the use of portable fuel cells will probably be limited to niche applications for technically proficient users (e.g., industry, military, hobbyists, etc.). As such, we have demonstrated the air-breather fuel cells in several different radio-control model cars. The hydrogen storage and "transparent" consumer interface challenges will need to be resolved for truly huge markets such as communications or portable computers. In anticipation, we routinely demonstrate an Apple Powerbook 180 laptop operating on two 10-cell stacks with hydrogen supplied from interchangeable portable cylinders. No cooling fan or auxiliary electronics (e.g. a DC to DC converter) are necessary. Thus, this system (the two 10-cell stacks, a pressure regulator, and a metal hydride canister) could conceivably fit into a roughly 2.5"x2.5"x12" (5x5x30 cm) enclosure. Appropriate modifications of the metal hydride alloy may possibly even eliminate the need for the pressure regulator. Either way, a very simple, potentially low-cost, high energy-density fuel cell system is achieved.

References

1. M. S. Wilson, "Annular Feed Air Breathing Fuel Cell Stack," U. S. Patent No. 5,514,486.
2. M. S. Wilson and J. K . Neutzler, "Annular Feed Air Breathing Fuel Cell Stack," Pat. Pend.
3. J. K. Neutzler, "Development of a Portable, Passive, Air-Breathing, Polymer Electrolyte Fuel Cell Stack," M. S. Thesis, Arizona State University, May 1995.
4. J. A. Kolde, B. Bahar, M. S. Wilson, T. A. Zawodzinski and S. Gottesfeld, "Advanced Composite Polymer Electrolyte Fuel Cell Membranes," in Proton Conducting Membrane Fuel Cells I, Edited by S. Gottesfeld, G. Halpert and A. Landgrebe, The Electrochemical Society Proceedings Series, Vol. 95-23, pp. 193-201, 1995.
5. M. S. Wilson, J. Valerio and S. Gottesfeld, "Low Platinum Loading Electrodes for Polymer Electrolyte Fuel Cells Fabricated Using Thermoplastic Ionomers," Electrochim. Acta, Vol. 40, p. 355, 1995.

DIESEL FUEL TO DC POWER
Navy & Marine Corps Applications

David P. Bloomfield
Analytic Power Corporation
268 Summer Street
Boston, MA 02210

Introduction

During the past year Analytic Power has tested fuel cell stacks and diesel fuel processors for US Navy and Marine Corps applications. The units are 10 kW demonstration power plants. The USN power plant was built to demonstrate the feasibility of diesel fueled PEM fuel cell power plants for 250 kW and 2.5 MW shipboard power systems. We designed and tested a ten cell, 1 kW USMC substack and fuel processor. The complete 10 kW prototype power plant, which has application to both power and hydrogen generation, is now under construction. The USN and USMC fuel cell stacks have been tested on both actual and simulated reformate.

Analytic Power has accumulated operating experience with autothermal reforming based fuel processors operating on sulfur bearing diesel fuel, jet fuel, propane, and natural gas. We have also completed the design and fabrication of an advanced regenerative ATR for the USMC. One of the significant problems with small fuel processors is heat loss which limits its ability to operate with the high steam to carbon ratios required for coke free, high efficiency operation. The new USMC unit specifically addresses these heat transfer issues. The advances in these military programs have been incorporated into Analytic Power's commercial units which are now under test.

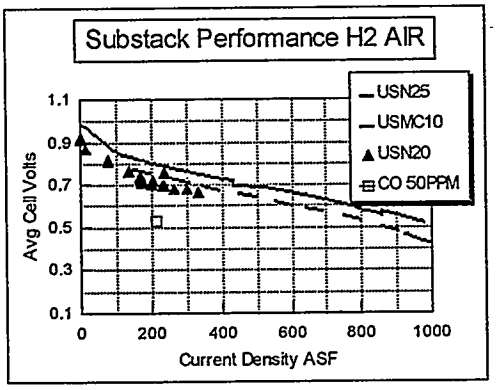

Figure 1 - Baseline Hydrogen Air Performance

Military System Requirements

Fuel cell power plants in military applications must demonstrate fuel flexibility (sulfur bearing diesel and jet fuels) and they must be quick starting. Analytic Power's units now start in about one hour; this time will be reduced to 20 minutes. The power plants must be able to function in a wide range of environmental conditions. USN units must operate in a salt spray environment. Both USMC and USN units must be extremely rugged -- capable of withstanding heavy shock and vibration loads. The missions require good load following capability and a hot standby operating mode. Finally, military units must be compact and lightweight.

PEM Fuel Cells Stacks

The fuel cell stacks built by Analytic Power use W.L. Gore membranes and cathodes. The anodes are catalyzed by Analytic Power using an alloy of Pt/Ru. The USN and the USMC stacks use machined carbon paper flow fields fabricated by Analytic Power. The flow field design is based

on a finite difference model developed jointly by Analytic Power and the University of South Carolina. This flow field design has dramatically improved reactant gas distribution and cell stack performance. The bipolar plates are composite units fabricated from nitrided titanium separator plates, carbon paper flow fields and plastic cell frames with O-ring seals. The stacks are water cooled.

Figure 1 shows the hydrogen/air performance of the USN and USMC stacks tested on reformed hydrocarbons. The upper line is the 10-cell USMC stack performance at 40 psig and 180°F. It is the average of all cells in the stack. Some cells reached 0.6 volts per cell at 1000 ASF. The next line in Figure 1 corresponds to a 25-cell stack built for the USN program. The performance level of this stack is about three times better than previous builds which did not have the new advanced flow fields. The 25-cell stack was operated at about 35 psig and 160°F. The lower temperature accounts for the difference in performance between USN and USMC stacks. The triangular data points were obtained from a 20 cell-USN stack operating between 130°F and 150°F at about 25 psig. The figure also shows a data point which represents the average voltage at 200 ASF when 50 PPM carbon monoxide was admitted into the cell. The average performance at 200 ASF dropped about 200 mv when the stack was exposed to carbon monoxide. As we will show, performance was completely restored by titrating the stack anode gas with air.

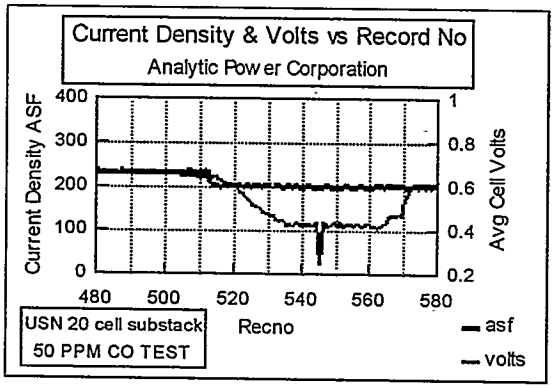

Figure 2 - Current Density & Volts vs Record No.

Figure 2 shows a 20-cell USN substack test on 50 PPM carbon monoxide contaminated gas. The stack was also tested at 100 PPM and 150 PPM levels. Stacks are now being endurance tested on simulated reformate. The figure shows that the average cell voltage drops about 200 millivolts with the cell stack on a 200 ASF load. Figure 3 shows that carbon monoxide admission starts at about record number 490, near the point where performance starts to drop. The 600 records accumulated in the test correspond to about 5.25 hours of testing. Each record number represents about 30 seconds. At record number 565 we started titrating air into the anode. Figure 2 shows that performance recovers completely when air is present in the anode cavities.

Autothermal Reforming Fuel Processor

Figure 4 shows a schematic of the USN fuel processor test stand. All the fuel processor components are mounted in the test stand. Analytic Power developed a simulation program which has proven useful in correlating the experimental data of the fuel processor.

The USN ATR started operation in April of 1995. After about a year of operation on a variety of fuels ranging from jet fuel to diesel fuel, several stainless steel ATR components corroded. The unit was rebuilt with Inconel replacement parts and a new catalyst. Since the rebuild, the unit has attained efficiencies of about 75% on diesel fuel. The design objective is to reach about 82%.

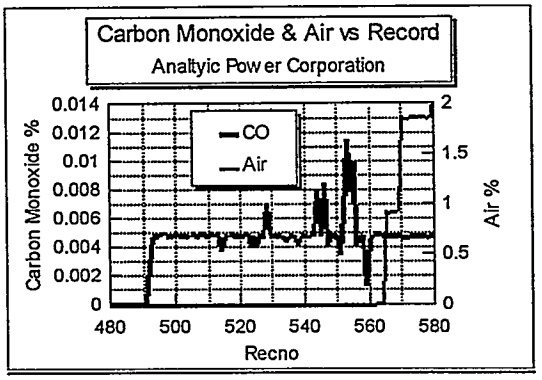

Figure 3 - Carbon Monoxide and Air vs Record No.

The ATR been tested at pressures from 1 to 2.5 atm. Most of our operations have used low steam to carbon ratios because of the heat loss from the ATR. Heat loss limits the ATR's capacity to heat steam and air to partial oxidation temperatures. While the condition can be remedied by elevating the oxygen to carbon ratio, this hurts efficiency. Low hydrogen to carbon ratios in the ATR enhances coke formation, especially at elevated pressure., No coke formation has been experienced at low pressure. Since the ATR was rebuilt and the insulation was replaced, heat loss has been greatly reduced and operation at elevated pressure has been improved. The new USMC ATR design is expected to greatly reduce heat loss.

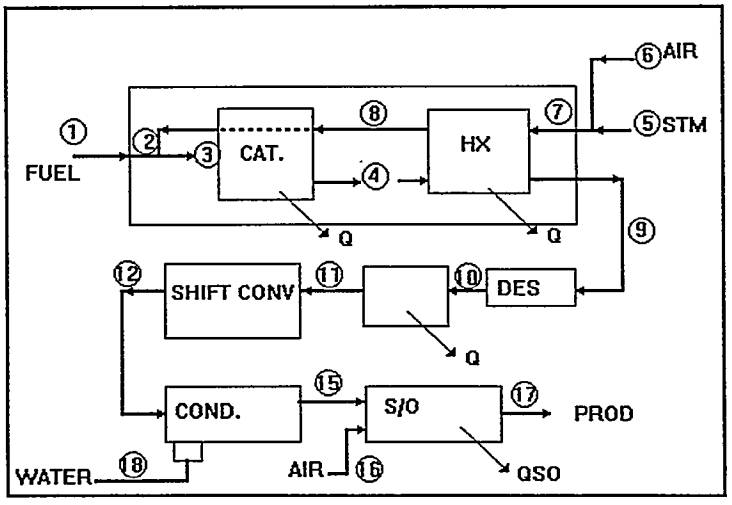

Figure 4 - ATR based Fuel Processor

We are concentrating on selective oxidation to reduce the carbon monoxide level from the fuel processor. Both the USN and USMC cell stacks have been operated successfully on the effluent from a natural gas fuel processor. However, the performance is somewhat erratic because of the relatively high levels of carbon monoxide leaving the selective oxidizer. Our most recent results show improved selective oxidizer performance at temperatures of 350°F rather than the 180 to 250° F which were originally used. The higher temperature necessitates relocating the selective oxidizer from the position shown in Figure 4 to a point between the shift converter and condenser. A sample of the effluent composition at various points in the fuel processor is presented in Table 1. The table shows the gas compositions from a diesel fuel reforming test, analyzed at the ATR or shift converter exit. The gas compositions, which are on a dry basis, were obtained with a gas chromatograph which is part of the USN fuel processor test stand instrumentation.

The oxygen to carbon ratios shown in the table are quite high while the steam to carbon ratios are low. These conditions generally result in a reactor inlet temperature of about 2000°F. The high inlet temperature is required to get high conversions of diesel fuel to carbon oxides. The present system also suffers from a shift converter inlet temperature and, consequently, a high shift converter exit temperature. This results in a high carbon monoxide concentration at the shift converter exit.

Table 1
Fuel Processor Effluent Composition

O_2/C	H_2O/C	% adj. H_2	% adj. N_2	% adj. CO	% adj. CH_4	% adj. CO_2	Sample
0.43	0.71	24.10	59.07	8.31	1.35	7.17	ATR
0.45	1.54	35.47	39.21	14.19	1.51	9.61	ATR
0.45	0.69	35.18	40.30	13.88	1.22	9.42	ATR
0.45	1.62	2.31	56.96	0.90	1.29	38.54	SC
0.46	0.74	1.28	58.07	0.30	1.48	38.87	SC
0.46	0.72	35.99	36.72	1.40	3.21	22.68	SC
0.46	0.74	36.85	37.82	1.05	0.88	23.40	SC
0.46	1.65	32.41	32.96	11.42	0.62	22.59	ATR

The USMC reformer, which is nearing completion, uses a thermally regenerative design and an advanced heat transfer system. This should greatly reduce heat loss from the reactor surface. The USMC fuel processor will also employ separate high and low temperature shift converters.

Acknowledgments
Analytic Power acknowledges the support for this work which has been provided by the U.S. Navy Office of Naval Research and the Strategic Environmental Research and Development Program. Mr. Joseph Woerner of the Naval Surface Warfare Center, Carderock Division is the Technical Contract Officer. The USMC power plant work has been supported by the U.S. Marine Corps, Amphibious Warfighting Technologies. Buck Thomas is the Technical Contract Officer.

FUEL ECONOMY AND RANGE ESTIMATES FOR FUEL CELL POWERED AUTOMOBILES

Margaret Steinbugler and Joan Ogden
Center for Energy and Environmental Studies
School of Engineering and Applied Science
Princeton University, Princeton, New Jersey 08544-5263

While a number of automotive fuel cell applications have been demonstrated, including a golf cart [1,2], buses [2-4], and a van [5], these systems and others that have been proposed [6] have utilized differing configurations ranging from direct hydrogen fuel cell-only power plants to fuel cell/battery hybrids operating on reformed methanol. To date there is no clear consensus on which configuration, from among the possible combinations of fuel cell, peaking device, and fuel type, is the most likely to be successfully commercialized. System simplicity favors direct hydrogen fuel cell vehicles, but infrastructure is lacking. Infrastructure favors a system using a liquid fuel with a fuel processor, but system integration and performance issues remain. A number of studies have analyzed particular configurations on either a system [7-10] or vehicle [11-16] scale. The objective of this work is to estimate, within a consistent framework, fuel economies and ranges for a variety of configurations using flexible models with the goal of identifying the most promising configurations and the most important areas for further research and development.

Configurations considered include a direct hydrogen fuel cell vehicle with no peaking device, a direct hydrogen fuel cell vehicle with a peaking device (battery, flywheel, or ultracapacitor), a fuel cell vehicle operating on methanol steam reformate with peaking device, and a fuel cell vehicle operating on liquid hydrocarbon partial oxidation (POX) reformate with peaking device.

A computer model has been developed to estimate fuel economies and ranges for these vehicles. Inputs to the model include vehicle parameters, a driving schedule, and performance and weight information about vehicle components.

Required vehicle parameters include coefficients of drag and rolling resistance, glider weight, frontal area, and accessory power. Driving schedules currently being considered are the Federal Urban Driving Schedule (FUDS), the Federal Highway Driving Schedule (FHDS), and each of these with their velocities increased by 25%.

Vehicle components include the fuel cell system, peaking devices such as batteries, flywheels, and ultracapacitors, fuel storage, fuel processor, and electric drive motor. The model takes into account the masses, peak power and/or energy storage capabilities of these devices and either sizes the vehicle power train for specified acceleration and hill climbing performance or allows the user to specify component sizes.

For each second of the chosen driving schedule, road load equations are used to calculate the power demanded from (or, via regenerative braking, deliverable to) the power plant. The fuel cell system is considered the primary power source. If it can supply all the power needed, it does so. The peaking device is considered to augment the fuel cell and only delivers power when the power needed to adhere to the driving schedule exceeds the fuel cell system's capabilities. This may occur in a direct hydrogen configuration when the fuel cell system is small; it may occur in an indirect system if the fuel cell system is small or if the fuel processor is unable to follow load transients.

During the simulation, peaking device state of charge and hydrogen consumed by the

fuel cell are tracked. When the driving schedule simulation is completed, total fuel consumed and distance traveled are calculated, resulting in estimates for fuel economy and range.

One broad generalization that can be made is that even with a system as efficient as a direct hydrogen fuel cell powering the vehicle, load reductions (ie, lower mass, drag and rolling coefficients, and accessory power) relative to today's typical midsize cars are necessary to achieve the Partnership for a New Generation of Vehicles (PNGV) 80 mpg goal. For example, a direct hydrogen fuel cell-only vehicle with performance and vehicle characteristics (such as weight and drag coefficient) consistent with today's commercial midsize cars has an estimated combined urban/highway fuel economy of 64 mpg. To achieve 80 mpg via weight reduction alone would require a 35% reduction in curb weight. If drag coefficient could be reduced from 0.35 to 0.30, curb weight reduction needed for 80 mpg would be only 26.5%. Fuel cell vehicles operating on reformate suffer additional losses relative to direct hydrogen vehicles due to reformate quality (hydrogen dilution) and lower hydrogen utilization and may have more difficulty attaining the PNGV goal.

References

1. Showgo Watanabe, Hajime Yamane, Yoshihiro Kirikii, and Yasuake Hasegawa, "Polymer Electrolyte Fuel Cell As Power Source for Electric Vehicles," presented at the Small Engine Technology Conference, Pisa, Italy, December 2, 1993.

2. Keith Prater, "Polymer Electrolyte Fuel Cells: A Review of Recent Developments," *Journal of Power Sources*, Vol. 51, pp. 129-144, 1994.

3. PMR *(Platinum Metals Review)*, "Fourth Grove Fuel Cell Symposium," Vol. 39, No. 4, pp. 160-164, 1995.

4. Jeffrey K. Fisher, "Description and Test Results of the 30-Foot PAFC Transit Bus," presentation, Society of Automotive Engineers Fuel Cells for Transportation TOPTEC, Santa Fe, NM, March 27-29, 1995.

5. Daimler-Benz, "NECAR II-Driving without Emissions," company brochure, 1996.

6. James T. Larkins, "The DOT/Georgetown 40-Foot Advanced PAFC Transit Bus Program," presentation, Society of Automotive Engineers Fuel Cells for Transportation TOPTEC, Santa Fe, NM, March 27-29, 1995.

7. R. Kumar, R. Ahluwalia, H. K. Geyer, and M. Krumpelt, "Modeling of Polymer Electrolyte Fuel Cell Systems," *Preprints of the Annual Automotive Technology Development Contractors' Coordination Meeting*, Vol. II, Dearborn, MI, October 18-21, 1993.

8. Romesh Kumar, "Overview of Fuel Processing Options for Polymer Electrolyte Fuel Cell Systems," *Preprints of the Annual Automotive Technology Development Contractors' Coordination Meeting, PNGV Workshop on Fuel Processing for Proton Exchange Membrane (PEM) Fuel Cells*, Dearborn, MI, October 23-27, 1995.

9. Gordon C. Cheng and Riju Saini, "Fuel Reformer Technologies for Fuel Cell Vehicles," presented at the Society of Automotive Engineers Fuel Cells for Transportation TOPTEC, Diamond Bar, CA, March 10, 1993.

10. J. C. Amphlett, R. M. Baumert, R. F. Mann, and B. A. Peppley, "System Analysis of an Integrated Methanol Steam Reformer/PEM Fuel Cell Power Generating System," *Proceedings of the 27th Intersociety Energy Conversion Engineering Conference*, Vol. 3, pp. 3.343-3.348, San Diego, CA, August 3-7, 1992.

11. Mark DeLuchi, "Hydrogen Fuel-Cell Vehicles," Research Report UCD-ITS-RR-92-14, Institute of Transportation Studies, University of California, Davis, September 1992.

12. Allison Gas Turbine Division, General Motors Corporation, "Research and Development of Proton-Exchange Membrane (PEM) Fuel Cell System for Transportation Applications: Initial Conceptual Design Report," prepared for the U. S. Department of Energy, Office of Transportation Technologies, Report DOE/CH/10435-01, February 1994.

13. Brian James, George N. Baum, and Ira Kuhn, "Technology Development Goals for Automotive Fuel Cell Power Systems: Final Report," ANL-94/44, August 1994.

14. C. E. Thomas, "Overview of Onboard Liquid Fuel Storage and Reformation Systems," Society of Automotive Engineers Fuel Cells for Transportation TOPTEC, Alexandria, VA, April 2-4, 1996.

15. P. L. Adcock, R. T. Barton, C. D. Dudfield, P. J. Mitchell, P. Naylor, and A. Newbold, "Prospects for the Application of Fuel Cells in Electric Vehicles," *Journal of Power Sources*, Vol. 37, 1992.

16. Vas Choudhry, Dennis Humphris, Amit Ghosh, Naum Pinsky, and Michael Wehrey, "Analysis of an Optimal Battery/Fuel Cell Hybrid Vehicle Configuration," *Proceedings of the First Annual World Car 2001 Conference*, June 21, 1993.

DIESEL FUELED SHIP PROPULSION FUEL CELL DEMONSTRATION PROJECT

William H. Kumm
President
Arctic Energies Ltd.
511 Heavitree Lane
Severna Park, MD 21146-1010
Tel 410-987-5454
FAX 410-987-7549

Brief Summary of Paper

The paper describes the work underway to adapt a former US Navy diesel electric drive ship as a 2.4 Megawatt fuel cell powered, US Coast Guard operated, demonstrator. The Project will design the new configuration, and then remove the four 600 kW diesel electric generators and auxiliaries. It will design, build and install fourteen or more nominal 180 kW diesel fueled molten carbonate internal reforming direct fuel cells (DFCs). The USCG cutter VINDICATOR has been chosen. The adaptation will be carried out at the USCG shipyard at Curtis Bay, MD. A multi-agency (state and federal) cooperative project is now underway. The USCG prime contractor, AEL, is performing the work under a Phase III Small Business Innovation Research (SBIR) award. This follows their successful completion of Phases I and II under contract to the US Naval Sea Systems (NAVSEA) from 1989 through 1993 which successfully demonstrated the feasibility of diesel fueled DFCs. The demonstrated marine propulsion of a USCG cutter will lead to commercial, naval ship and submarine applications as well as on-land applications such as diesel fueled locomotives.

DEMIXING AND EFFECTIVE VOLATILITY OF MOLTEN ALKALI CARBONATE MELTS IN MCFCs

Thomas Brenscheidt, Hartmut Wendt
Institut für Chemische Technologie, TH Darmstadt
Petersenstr. 20, D - 64287 Darmstadt, Germany

Introduction:

Since the early investigation of A. Klemm (1), the demixing of the cations of molten binary salt mixtures with a common anion due to the different mobilities of two different cations had been investigated in numerous experiments and the respective results interpreted in terms of structural features of the melts; see for instance (2) and (3). 1-1 electrolytes had been preferentially investigated. Okada also reported investigations on lithium carbonate/potassium carbonate mixtures in the temperature range from 980 to 1070 K, (4). From this investigation it is known, that the heavier potassium cation is faster than lithium in mixtures which are more concentrated in potassium than $x_{K2CO3} = 0{,}32$ (Chemla effect)whereas below this isotachic concentration lithium is faster.

Theory and Prediction:

Charge and mass transfer in the electrolyte of molten carbonate fuel cells is accomplished by the movement of the carbonate anions, which are generated at the cathode and decomposed by release of CO_2 at the anode. Against the steadily moving stream of carbonate anions the cations are migrating - but according to their different mobilities with different velocities. Under steady state conditions the relatively faster cation would accumulate in the catholyte. Steady state conditions for the cations are defined by zero velocities of the summed convective, migrative and diffusive mass transfer:

$$0 = \dot{n}_{(total)} = \dot{n}_{conv} + \dot{n}_{mig} + \dot{n}_{diff} \tag{1}$$

With t_i equaling the so-called internal transfer number of cation i, defined against the background of the anion common to both salts and x_i equaling the mole fraction of the salt $(M_i)_2CO_3$ in the binary mixtures one obtains for the three transport terms

$$\dot{n}_{conv} = -\frac{i}{2}\frac{2}{F}\cdot x_i \quad ; \dot{n}_{mig} = \frac{i}{F}\cdot t_i ; \quad \dot{n}_{dif} f = -\frac{\partial c_i}{\partial_y}\cdot D_i \tag{2}$$

and calculates the steady state balance

$$0 = -\frac{i}{F}(x_i - t_i) - \frac{\partial c_i}{\partial_y}\cdot D \tag{3}$$

With the volumetric concentration of the cation, i, c_i, which is given to a good approximation by $c_i = x_i\rho/\bar{M}$ with ρ equal to the density of the melt and $\bar{M}$ equal to the mean molar weight of the melt one arrives at

$$\frac{dx_i}{dy} = -\frac{i}{F}(x_i - t_i)\cdot\frac{\bar{M}}{\rho}\cdot\frac{1}{D_i} \tag{4}$$

y is the distance of the point of consideration from the outer surface of the fuel cell anode, t_i as the internal transfer number is, defined by the internal mobilities, b_i and b_j of the two cations and by the mole fractions x_i and x_j of the two salts in the binary mixture:

$$t_i = \frac{x_i b_i}{x_i b_i + x_j b_j} = \frac{x_i b_i}{x_i(b_i - b_j) + b_j} \tag{5}$$

A closed solution of diff. equ. (4) is impossible, as the bi, bj values are not constant as the concentrations of the molten mixture changes. According to equ. (4) the sign of the gradient dx_i/dy depends on the sign of the quantity $(x_i - t_i)$ and its magnitude depends also on the current density, i. For $x_K > 0{,}32$, as is demonstrated in fig. 1, the quantity (x - t) calculated from Okada's data for Li_2CO_3/K_2CO_3 melts becomes negative for potassium and as $\partial c_K/\partial y$ is positive, the potassium concentration increases in going from the anode to the cathode, whereas the concentration of lithium decreases correspondingly. Since the lower melting eutectic of the Li_2CO_3/K_2CO_3 system which defines the usual melt composition in MCFCs, has the composition xK = 0,38 we can definitely predict the accumulation of potassium and the depletion of lithium in the cathode. We expect also, that on the anode side of the cell a limiting potassium concentration will be attained that matches the concentration of the isotachotic point if more and more potassium is dragged into the cathode as would be expected as the current density is increased. Relative mobilities in binary molten Li_2CO_3/Na_2CO_3 mixtures are not known. Performing steady state operation of MCFC which make use of this electrolyte and analyzing the steady state distribution of lithium and sodium in these cells would allow to draw conclusions concerning the relative internal mobilities and transference number of both cations.

Results:

(a) Li_2CO_3/K_2CO_3 eutectic: Table 1 collects the chemical analyses of a 340 h experiment performed at 650 °C with a steady current density of 100 mA cm^{-2}.

Table 1

Potassium and lithium contents of MCFC operated for 340 h at 100 mA cm^{-2}

	anode	matrix	cathode
total K/mg	21,2	175	25
total Li/mg	7,0	58	6,3
thickness/mm	0,8	1,1	0,5
mol% Li_2CO_3	64	64	58

It is evident that the greatest part of the electrolyte is contained in the matrix (75 to 80 %) and that almost equal parts of the remaining electrolyte are contained in both electrodes. The ratio m (K)/m(Li) is almost equal in the matrix and the anode (~3) but it increases to 4 in the cathode.

Fig. 2 shows for three independent experiments - two with 100 mA cm^{-2} - one with 150 mA cm^{-2} the mean lithium carbonate mole fraction in the anode, matrix and cathode. Evidently anode and matrix electrolyte exhibit almost the same chemical composition but the catholyte is seizeably depleted in lithium. This effect becomes much more pronounced at higher current densitits. As the current density increases by a factor of 1,5 the concentration difference,

$$\Delta x_{Li_2CO_3} = x_{Li}(matrix) - x_{Li}(cathode)$$

increases by a factor of almost 3, indicating that the current density of a MCFC with Li_2CO_3/K_2CO_3 eutectic melt might become a critical operation parameter.

Table 2

Demixing of Li_2CO_3/Na_2CO_3 eutectic in MCFC

		mole % Li_2CO_3		
Operating time/h	c.d./mA cm^{-2}	anode	matrix	cathode
139	100	56	51	49
69	150	56	54	53
116	150	53	(57)	48

Li_2CO_3/Na_2CO_3 electrolyte: Transference experiments had also been performed with Li_2CO_3/Na_2CO_3-eutectic (52/48 mole/mole). Table 2 lists the analyses of the cell melts in the three different components of a respective lithium-sodium carbonate cell.
Obviously also with lithium/sodium carbonate melts (52/48 mole/mole) depletion of lithium and the accumulation of the heavier sodium is observed in the cathode. But the effect is weaker and the concentration gradient seems to be more evenly distributed across the cell than with lithium/potassium carbonate melts.

Discussion:

Accumulation of heavier alkali cation (K^+ or Na^+) and depletion of Li^+ at the cathode is firmly established. This has several consequences:

(a) the electrode kinetics of oxygen evolution is affected as the solubility of oxygen in the mixed alkali carbonate melts depends on the lithium contents.
(b) The effective volatility of the melt, which is mainly determined by the mole fraction of the more volatile sodium and potassium carbonates respectively is enhanced to some extent according to their increased concentration (9).
(c) At seizeably increased current densities, which are desirable because of the still insufficient power density of MCFCs, the concentration enhancement of potassium cations at the cathode could lead to the crossing of the liquidus/solidus curve with precipitation of lithium carbonate in the anode.
(d) With lithium/sodium carbonate melts demixing is much weaker. This together with the lower nickel oxide solubility and volatility is reason enough to seriously consider Li/Na melts as more appropriate than Li/K melts.

Acknowledgement:

The authors are indebted to Siemens AG, MTU Frieddrichshafen GmbH and the German Federal Ministry of Research and Development for partial support of this investigation.

References:

1. A. Klemm, H. Hinterberger, P. Hoernes, Anreicherung der schweren Isotope von Li und K durch elektrolytische Ionenwanderung in geschmolzenen Chloriden, Z. Naturforsch,. **2a**, 245 (1947)
2. A. Klemm, Ionic Mobilities in G. Mamantov, C.B. Mamantov and I. Braunstein eds., Advances in Molten Salt Chemistry, Elesevier, Amsterdam, 1987, vol. 6, p. 1
3. M. Chemla, I. Okada, Ionic mobilities of nonvalent cations in molten salt mixtures, Electrochim. Acta. **35** 1761 (1990)
4. C. Yang, R. Takagi, K. Kawamura, I. Okada, Internal cation mobilities in the molten binary system Li_2CO_3 - K_2CO_3,, Electrochim. Acta, **32** (1987) 1607
5. O. Böhme, Grundlagenuntersuchungen zur Karbonatschmelzenzelle, Kathode und Matrix, PhD thesis, TH Darmstadt, 1992
6. J.R. Selman and L.G. Marianowski. "Fuel Cells" in Molten Salt Technology, D.G. Lovering ed. Plenum Press, New York and London 1982, p. 332
7. O. Böhme, F.-U. Leidich, H.J. Salge and H. Wendt, Development of materials and production technologies for molten carbonate fuel cells, Intl. J. Hydrogen Energy, **19** 349 (1994)
8. Cheo-cheng'Yang, Rynzo Tagaki, I. Okada, Internal cation mobilities in the molten system (Li-Na)NO_3 and (Na-Cs)NO_3, Z. Naturforsch. **35a**, 1186 (1980)

9 . H. Mohn and H. Wendt, Molecular thermodynamics of molten salt evaporation IV. The evaporation of molten carbonates in atmospheres containing CO_2 and water vapour. Zeitschr. f. Physik. Chemie. **192**, 101 (1995)

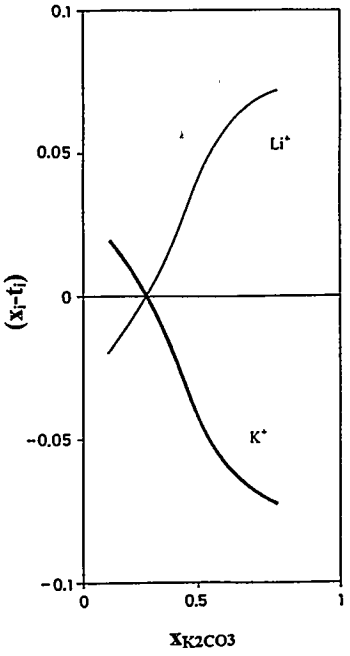

Fig.1: (x - t) for Li^+ and K^+ in molten Li_2CO_3/K_2CO_3 mixtures vs. mole fraction of K_2CO_3

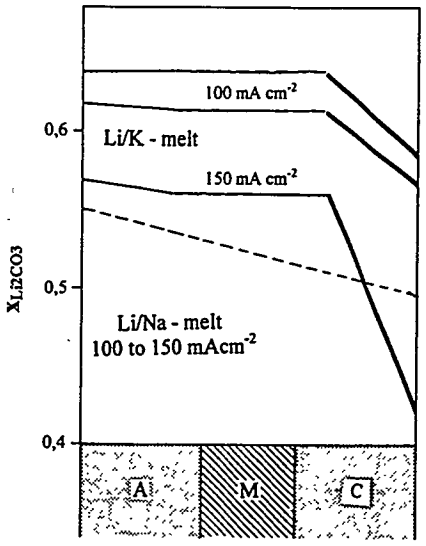

Fig.2: Experimentally determined mole fractions of Li_2CO_3 in MCFC anodes(A). matrix (M) and cathode (C) after400 h of operation at 100 and 150 mA cm^{-2} at 650 °C. Full lines: Li_2CO_3/K_2CO_3 (38/62) and dotted lines: Li_2CO_3/Na_2CO_3 (48/52)

OPERATION CHARACTERISTICS OF A MULTIPLE TYPE MCFC

S Kuroe, T Kamo,
Hitachi Research Laboratory, Hitachi, Ltd.
1-1, Omica-cho 7-chome, Hitachi-shi Ibaraki-ken, 319-12 Japan.
E-mail: kuroe@hrl.hitachi.co.jp
H. Fujimura,
Power and Industrial Systems R & D Division, Hitachi, Ltd.
1-1 Saiwai-cho 3-chome, Hitachi-shi Ibaraki-ken, 317 Japan

and T. Kahara
Hitachi Works, Hitachi Ltd.
1-1 Saiwai-cho 3-chome, Hitachi-shi Ibaraki-ken, 317 Japan

Multiple type structure of MCFC of which the separator of the cell is divided by four element cells has been studied. For the stable operation of this type cell, the effect of gas flow rate and temperature distribution on the cell voltage should be clear.

In order to clarify these characteristics, a small sized mimic model has been made and tested. The flow rate distribution for the four element cells were varied and cell voltage and temperature distribution were measured for each cell. The decrease in cell voltage and the increase in maximum temperature became remarkable when the apparent utilization factor for one element cell became over 100%. The calculated results agreed fairly good with test results.

1. Structure and characteristic of a multiple type cell.

Figure 1 shows a schematic of a single cell of multiple type MCFC. A cathode, an anode, a current corrector and a gas channel were divided into four divided cells except a electrolyte plate. The reaction gases (for both cathode and anode) flows from the center lattice part toward the peripheral regions, and the flow directions of anode gas and cathode gas are perpendicular to each other. Figure 2 shows a schematic of the multiple type cell used for experiments. The size of the cell was 50 cm x 50 cm, and the area of this cell is one-thirteenth of actual cell(100kW class). We called this multiple type cell as M900 stack. M900 stack has 2 cells. They are defined as No. 1 and No. 2 cell from the lower part sequentially. And M900 stack has four manifold(A,B,C,D). At each manifold, flow rate of the reaction gas into each divided cell(A,B,C,D) can be controlled independently.

2. Voltage-time characteristics of the multiple type cell

At first, the cell characteristic under equal flow rate to each 4 divided cells has been measured as a basic characteristic of the cell. Only time dependence of No. 1 cell performance is shown in figure 3, because No. 2 cell showed almost same tendency. Therefore, we indicate only the result of No. 1 cell in this paper. M900 stack was operated continually about 2,000 hours. The performance change until about 1,500 hours was shown in this figure. As for operating

condition, hydrogen/carbon dioxide/steam ratio of anode gas was 72/18/10, and the air/carbon dioxide ratio of cathode gas was 70/30. And the M900 stack was operated in continually under the condition of 150mA/cm^2 load(rated load of the cell), 650℃ operating temperature, 60% fuel gas utilization and 30% oxidant gas utilization. Under various load current condition, cell voltage and internal resistance (alternating current resistance at 1kHz) were measured simultaneously. The alternating current resistance was measured using Milli-ohm meter (HP4231A).

In figure 3, the open circuit voltage showed almost constant value of 1.07 V, and the cell voltage at the rated load showed 0.8 V in early stage, and has a tendency to fall by gradually. The internal resistance showed almost the same during the operation, approximately 0.6 Ω cm^2. The performance decay rate was 0.8% per 1,000 hour.

In figure 4, the relationship between operation temperature and cell performance decay rate is shown, which were obtained by small-sized cells of 100 cm^2 class cell. It is clear that the performance decay rate increased with increasing of temperature. The performance decay rate at 650℃ was approximately 1% per 1,000 hours, and this characteristics was also the same as this M900 stack.

3. The effect of the flow rate distribution on the cell performance

Figure 5 shows the influence of the flow rate distribution on cells performance. This figure shows the results when the rate of fuel gas supply to each divided cells were changed, but the total gas flow rate was kept constant, and the fuel utilization at 40%. The case 1 indicates that the gas flow rate between each divided cells was equal, and the case 2 indicates that the gas flow rate of the divided cell A was increased by 30% than the average, and considerable share was reduced from divided cell B, in other words, the gas flow rate of the divided cell B was considerably reduced. The case 3 indicates that the gas flow rate of divided cells A and B was increased 30% than the average, and flow rate of remaining divided cells C and D were reduced by 30%. Finally, the case 4, the gas flow rate of the divided cell A was reduced by 90% than the average, and remaining divided cells B-D were increased by 30%. The vertical axis of the figure shows a ratio compared with the cell voltage of case 1, *i.e.*, the deviation of the cell performance in the case 2-4 from the uniform gas flow distribution(case 1). And horizontal axis was defined by the following equation that represented a standard deviation of fuel gas flow rate of 4 divided cells.

$$\text{(Deviation of flow rate)} = \Sigma [\{(Qi/Q-1)\}\text{^}2]/4 \quad \cdots (1)$$

Where Qi is the flow rate of the fuel gas to each divided cells and Q is the fuel gas flow rate of the average with all the divided cells, respectively. As a result, the performance change of case 4 was extremely large.

In figure 5, it is also indicated the simulated performance change ratio simultaneously, where the open circle plots were experimental results, and the region of slanted line was a simulated one. From this figure, in spite of the performance loss was within 0.6% when the change of the

deviation of flow rate was within 20%, it was found, that the performance fall became large suddenly as the inclination with deviation of flow rate surpassed approximately 30%. The measured values were settled in the range that were predicted by the calculation. In this figure, the reason why the calculated values had some range, because there were several cases which had different patterns of flow rate distribution at the same deviation of flow rate.

4. Effect of the deviation of flow rate on a temperature distribution in cell

In figure 6, the change of the temperature distribution caused by the deviation of flow rate in four divided cells is shown. In this figure, the isothermal lines were obtained by using interpolation by Lunge Kutta method using the 20 points of measured temperature values. From this figure, the temperature in a divided cell A decreased because the fuel flow rate was decreased (The apparent utilization was high). On the other hand, the temperature increased because the fuel flow rate was increased (The apparent utilization was low) in a divided cell D. These changes can be explained that the electric current was concentrated on a divided cell D by the sufficient gas flow rate and this increased the generation of heat.

5. Conclusion A reduced size cell was produced, and the effect on the cell performances and the temperature distribution with changing the gas supply condition into four divided cells were examined. And we obtained the following results.

(1) The performance decay rate of the reduction model was agreed with which the performance decay rate of the small-sized cells.

(2) Cell performance deteriorated with increasing the deviation of the flow rate gradually, and the performance fall became remarkable when the apparent utilization with the divided cell exceeded 100%.

Acknowledgment

This work was conduced by the MCFC Research Association. The MCFC Research Association was commissioned to do the work by NEDO (New Energy and Industrial Technology Development Organization) as a part of the New Sunshine Program of MITI (Ministry of International Trade and Industry). We appreciate the advice and support of the MCFC R.A., NEDO and MITI.

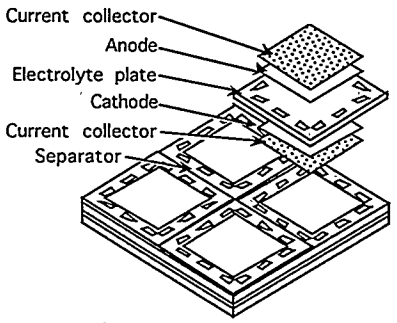

Figure 1 Schematic of Multiple Type MCFC.

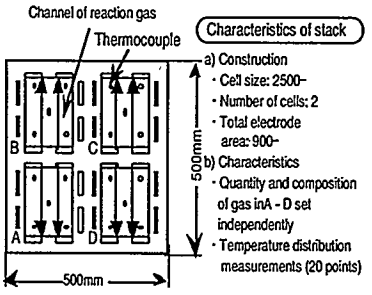

Figure 2 Schematic cross-sectional view of one cell in the Multiple Type MCFC.

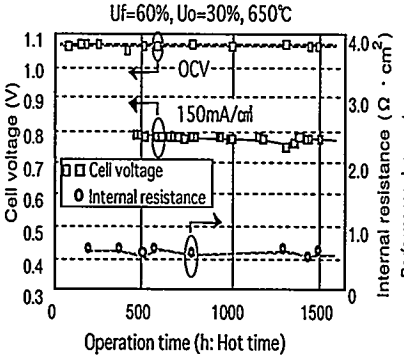

Figure 3 Cell performance change during the operation.

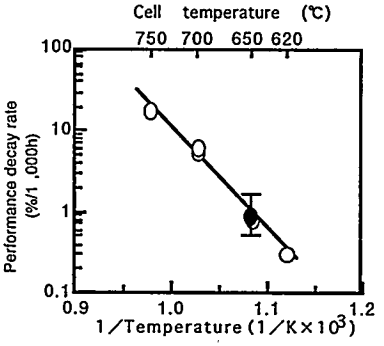

Figure 4 Relationship between operation temperature and cell performance decay rate.

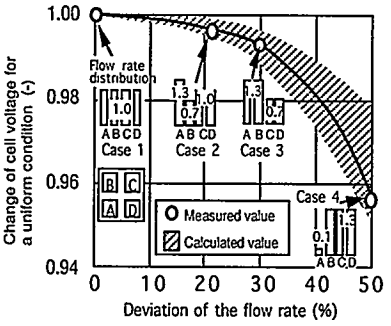

Figure 5 The influence of the deviation of flow quantity on the cell performance.

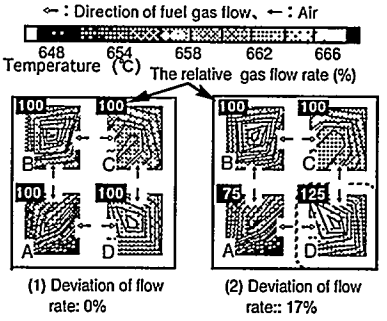

Figure 6 Change of temperature distribution by deviation of flow rate.

MCFC POWER PLANT WITH CO_2 SEPARATION

Noboru Kinoshita
Ishikawajima-Harima Heavy Industries Co., Ltd.
1-15 Toyosu 3-Chome, Koto-ku
Tokyo 135 Japan

Fuel cell power plant has been developed for many years with expectation of high system efficiency. In the meantime the gas turbine combined cycle has shown its considerable progress in improving system efficiency. Fuel cell power plant will no longer be attractive unless it exceeds the gas turbine combined cycle at least in the system efficiency. It is said CO_2 separation could improve the efficiency of fuel cell power plant. IHI has developed the CO_2 separator for fuel cell power plant. This study describes that the CO_2 separator can increase the efficiency of the molten carbonate fuel cell (MCFC) power plant by 5% and the expected efficiency reaches 63 % in HHV basis.

CO_2 SEPARATOR

In general, CO_2 separation is performed by means of absorption, adsorption and membrane. If we want to apply these technologies for the fuel cell plant, we encounters some difficulties. For example, adsorption needs excessive power consumption and absorption requires considerable heat energy while membrane has poor selectivity. IHI has developed the CO_2 separator tailored for the fuel cell plant by improving the liquid absorption technology.(1)

SYSTEM DESCRIPTION

A schematic flow diagram of the MCFC power plant with CO_2 separation is shown in Figure 1. Natural gas fuel is heated by exchanging heat with anode exhaust gas in the heat exchanger E-3, where also a small amount of steam is generated and the anode exhaust recycle stream from the CO_2 absorber T-1 is heated. These streams are combined and further heated in the heat exchanger E-1. The hot fuel gas flows through the anode channels. In the anode chamber, natural gas is reformed to hydrogen and carbon oxides and utilized to produce electricity. The electrochemical reactions provide heat necessary for the endothermic reforming reaction. The anode exhaust gas contains unused fuel such as hydrogen and carbon monoxide. These valuable fuels can be used thoroughly in the fuel cell by means of recycling themselves through the CO_2 separator.

Exhaust gas leaves the anode at 650℃ and flows through the heat exchangers E-1, E-2 and E-3 and is further cooled in E-4 and fed to the CO_2 absorber T-1, where most of carbon dioxide and steam are transferred to the liquid absorbent. The overhead gas which contains 25 vol % (dry) CO_2 after treated in T-1 is compressed by the recycle gas compressor C-3 and heated in E-3. A small portion of this stream is sent to the catalytic burner R-1 to raise the cathode inlet gas temperature. The remainder is recycled back to the anode chamber. The anode recycle gas flow rate is adjusted such that the fuel cell outlet gas temperature is approximately 650℃.

Air is fed to the CO_2 stripper T-2 via the air blower C-1. In the CO_2 stripper, CO_2 and steam are transferred to the air stream. At the top of the stripper, the operating temperature and pressure are approximately 60℃ and 1.23 kg/cm^2 respectively. The overhead gas is compressed by the air compressor C-2 to a sufficient pressure to operate the fuel cell at the pressure of 5 kg/cm^2. The compressor consists of two stages and an inter cooler and is driven by the expander X-1. The compressed gas is heated by exchanging heat with the expander exhaust gas in the heat exchanger E-5. This preheated stream is further heated by exchanging heat with the anode exhaust in E-2 where the high temperature sift reaction takes place to maximize heat recovery from the anode

exhaust. This hot stream is passed over the catalytic burner R-1 then enters the cathode chamber of the fuel cell. The cathode exhaust leaves at 650℃ and enters the expander X-1 to recover energy from the hot stream.

The absorbent leaving the bottom of the stripper T-2 is pumped to the top of the absorber T-1. After absorbing CO_2 and steam in T-1, the absorbent is heated in the inter cooler of the air compressor C-2 and in the heat exchanger E-4 to the temperature of 62℃, then recycled back to the top of the stripper T-2.

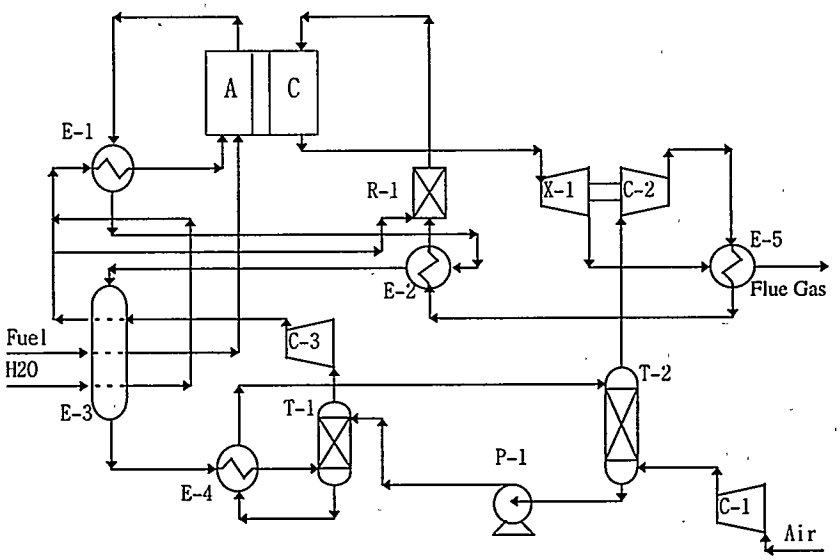

Figure 1: A Schematic Flow Diagram of MCFC Power Plant with CO_2 Separation

PRESSURE

The parametric analysis shown below is based on the power plant size of about 50 MW. At higher pressure the fuel cell performance improves and the size of the CO_2 separator becomes smaller because the flow rate of absorbent decreases. However, as shown in Figure 2, the parasitic power consumption increases especially in the air blower C-1. The power requirement for the

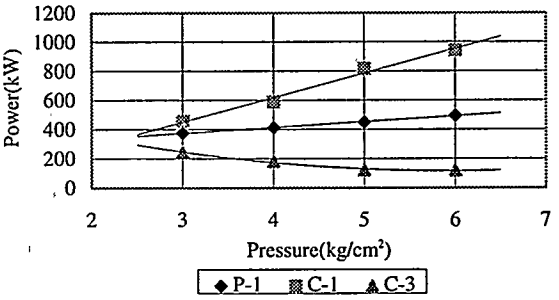

Figure 2: Pressure effects on parasitic power

absorbent pump P-1 increases slightly as the higher head requirement overcomes the effect of the reduced flow rate. The power requirement for the recycle gas compressor C-3 decreases slightly also. As a result of the above considerations, the operating pressure of 5 kg/cm^2 is selected for the fuel cell stack.

TEMPERATURE

The lower is the operating temperature of fuel cell, the longer the fuel cell life is expected. On the other hand, at higher temperatures, the fuel cell performance improves but the increase in costs for equipment and maintenance would offset the performance gains. Therefore, in this study the temperature of 650℃ is selected as a maximum temperature for the fuel cell outlet.

The temperature of absorbent affects largely the design of the CO_2 separator. The performance of the CO_2 separator improves at higher temperature while heat requirement increases due to the increased vaporization of steam in the CO_2 stripper. Also the absorbent will be degraded at higher temperatures. The available heat from the anode exhaust and the inter cooler of the air compressor covers the heat requirement of the CO_2 separator when the operating temperature of the inlet stream of the CO_2 stripper is about 62℃. This temperature is low enough to avoid degradation of absorbent.

CALCULATION BASIS

The system efficiency is calculated on the basis shown in Table 1.

Table 1: Basis for System Efficiency Calculation

Power Plant Size (MW)	50
Inverter Efficiency (%)	98
Machinery Efficiency (%)	
Expander-Compressor	
Expander(adiabatic)	88
Compressor(adiabatic)	85
Mechanical Loss	5
Generator	90
Other Compressors (adiabatic)	80
Pump	75
Motor	90
Heat Loss (Gcal/H)	
Fuel Cell Stack	2-3
High Temperature Piping	1.7
Catalytic Burner	0.4
Other Parasitic Power Consumption (kW)	500

For comparison purpose, the system efficiency of the internal reforming(IR-) MCFC power plant is also calculated on the same basis.

RESULTS

The calculated results are summarized in Table 2 to evaluate the effects of the CO_2 separation. The results shows the system efficiency increases from 58% to 63% by using the CO_2 separator. The considerable improvement of fuel utilization from 82% to 93.6% has greater effect on the

enhancement of system efficiency than the extent of reduction of the excess power generation of the expander-compressor. The reduction of power generated in the expander-compressor is mainly due to the compression work for CO_2 which is transferred from the anode exhaust to the oxidant stream.

Table 2: The effect of CO_2 Separator

	IR-MCFC	w/ CO_2 separator
Fuel Supplied (HHV Gcal/H)	78.413	78.413
Fuel Utilization -Overall (%)	82.0	93.6
Cell Voltage (mV)	805	822
Net Power Output (MW)	53.0	56.7
System Efficiency (HHV %)	58	63
Operating Pressure at Fuel Cell Inlet (kg/cm^2)	3.5	5.0
Power Generated by Expander-Compressor(kW)	2760	0
Flow Rate of Absorbent (m^3/H)	0	2545

The following is the brief specifications of main equipment of the CO_2 separator calculated by using IHI's experimental data. Both towers consist of structured packing.

Absorber T-1	Packing Height (m)	4.0
	Tower Diameter (m)	5.3
	Packing Pressure Drop (mmH_2O)	35
Stripper T-2	Packing Height (m)	8.0
	Tower Diameter (m)	7.0
	Packing Pressure Drop (mmH_2O)	430

SUMMARY

The CO_2 separator is able to improve the system efficiency of the MCFC power plant and the expected system efficiency reaches 63 HHV %. This considerable improvement is mainly due to the increment of fuel utilization. This high value is assured by the peculiar features of the CO_2 separator. The unused valuable fuels in the anode exhaust can be recycled back to the fuel cell once the anode exhaust gets rid of CO_2.

In this study, the effectiveness of the CO_2 separator is shown when it's applied to the internal reforrming MCFC. Alternatively it is possible to apply it to the external reforming MCFC. In this case the system efficiency decreases to about 60% because of a large amount of anode gas recycle at high temperature required to transfer the waste heat from the fuel cell to the external reformer, that needs additional power consumption of the hot recycle gas compressor. Also the anode gas recycle dilutes the anode gas composition and lowers the Nernst potential that leads to the increased size of the fuel cell stack.

REFERENCES

1. N. Kinoshita, "Development of CO_2 Separator for MCFC," Fuel Cell Seminar, Nov/Dec. 1992

AN APPROACH FOR LONGER LIFETIME MCFCS

Masaru Matsumoto, Masahiko Tatsumi, Takuro Hayano, Hitoshi Takeya, Atsushi Miki
MCFC Research Association
3-10-10, Minami-Ohtsuka, Toshima-ku, Tokyo, 170 JAPAN

For entering into commercialization of MCFC power plants in the beginning of the 21st century, we will devote to research for increasing lifetime as long as 40,000 hours with cell performance decay rate of 0.25 %/1000hrs as the target in FY 1999.

This paper will discuss on our approach for longer lifetime MCFCs through electrolyte-loss management and NiO precipitation management as well as micro-structural control of electrodes and matrix plates. Cell voltage decay rate will be estimated by simulation through series of experiments on accelerated conditions.

1. Introduction

MCFC power plants have the high potential for commercialization in competition with thermal power plants. From the technological viewpoint for commercialization, it will depend on cell voltage endurance for long term with appropriate current density under pressurized condition. From the economical viewpoint, it will depend on capital cost as well as system simplicity and reliability.

Several causes will contribute to voltage losses in a practical fuel cell. The cell performance is theoretically decreases from open circuit voltage by Nernst loss, the reaction polarization in anode and cathode, electronic polarization and ion conductive polarization. Open circuit voltage is also decreased by Ni precipitation amount and gas crossover. Each of them will cause output voltage decay during operation.

2. Investigation for Longer Endurance

MCFC stack components consist of porous materials such as anodes, cathodes and matrix plates as well as non-porous materials such as separators and current collectors. Every compartment in MCFC is, indeed, susceptible to suffer severe corrosion. It causes electrolyte loss from matrix, metallic Ni precipitation onto matrix plates and micro-structural degradation of porous materials. They have still limitation from several technical problems for 40,000 hour lifetime in operating conditions. Figure 1 shows major research efforts to be devoted corresponding to endurance time region.

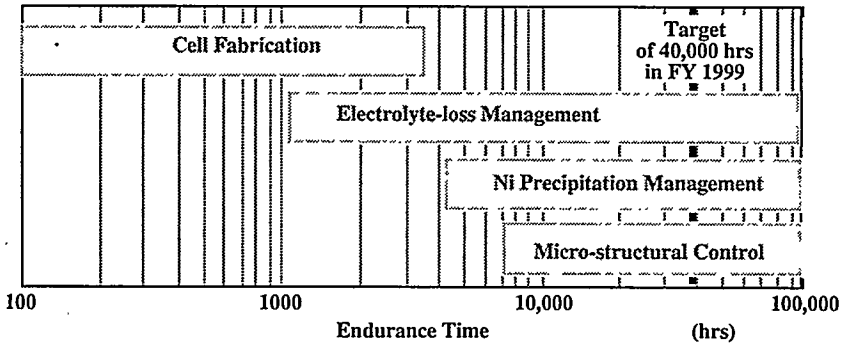

Fig.1 Research Efforts for Longer Lifetime

3. Component Degradation

Alkali carbonates form a highly conductive molten salt with carbonate ions at the high operating temperatures. Cell performance of MCFCs has been improved steadily in recent years. An MCFC stack will still suffer from component degradation including corrosion of each component, Ni precipitation and gas crossover as well as creepage of electrolyte. Figure 2 shows operating principles and degradation phenomena observed as follows;

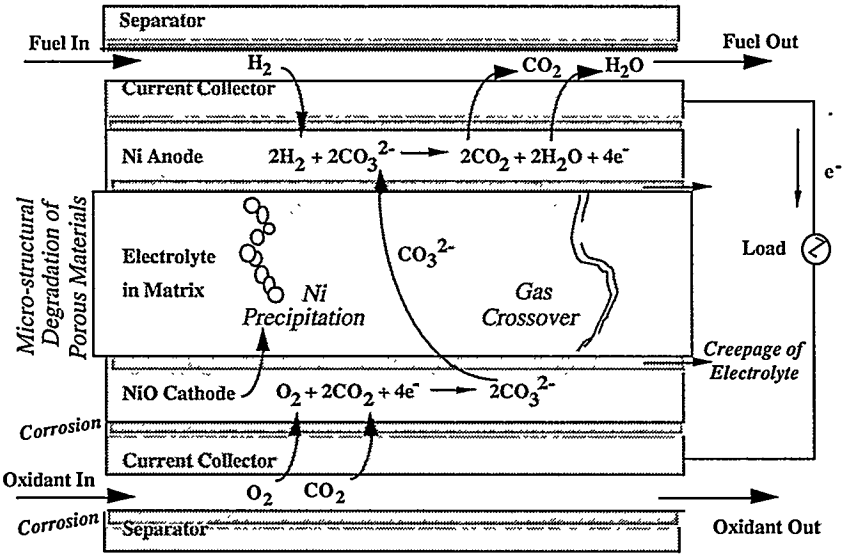

Fig.2 Operating Principle and Component Degradation

4. Performance Decay

A 5 kW external reforming type stack with 1 m^2 active area, for example, has provided performance decay rate of 3 mV/1000hrs with 16,000 hrs under a little lower operating temperature of 617 ℃, whose decay rate is estimated as about 5 mV/1000hrs under standard operating temperature of 650 ℃.

A 20 kW short stack of our state-of-the-art has been also under operation. The gas flow distribution has been well uniformed with internal manifold type. Matrix of porous $LiAlO_2$ has about 1 mm thickness. Anode of Ni-Cr-Al powdered alloy metal has also 1 mm thickness. Cathode is made of in-situ oxidized porous NiO with Mg additives. Performance decay rate of Kawagoe 1 MW pilot plant, scheduled to be operated in FY 1999, has been estimated as 6 mV/1000hrs with initial output of 782 mV from the results.

Generally speaking, overall performance decay rate in present is around 0.5 to 1.0 %/1000hrs and stack life is around 6000 to 7000 hrs from the limitation of Ni precipitation. Several corrosive reactions of each component are induced in molten carbonate during operation.

Figures 3 and 4 show the data published from the world as well as corresponding target of ours as follows;

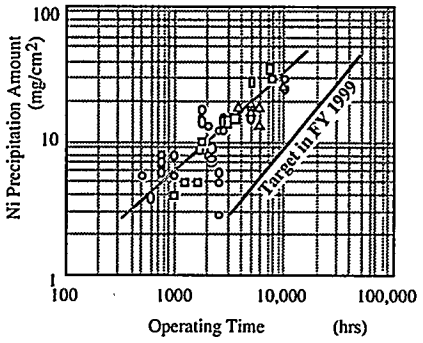

Fig.3 Ni Precipitation Amount during Operation

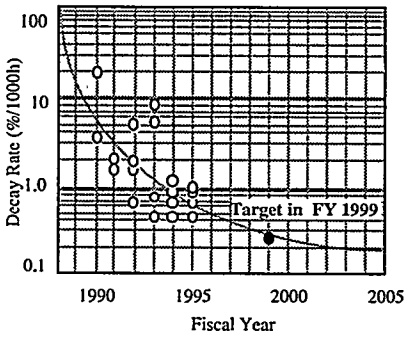

Fig. 4 Decay Rate in Recent Years

Performance decay rate in FY 1999 is targeted as 0.25 %/1000hrs and lifetime is as 40,000 hrs. Table 1 shows target of Ni short-circuit time and performance decay rate in FY 1999 as well as state-of-the-art of them as follows;

Table 1 Performance Decay Rate of State-of-the-art and Our Target

	State-of-the-art	Target in FY 1999
Ni precipitation amount	6 to 7 mg/cm²/1000hrs	1 mg/cm²/1000hrs
Short-circuit time (t_{sc})	6000 to 7000 hrs	40,000 hrs

	State-of-the-art	Target in FY 1999
Overall resistance	0.5 to 1.0 %/1000hrs = 4.0 to 8.0 mV/1000hrs	0.25 %/1000hrs = 2 mV/1000hrs
Reaction resistance in anode and cathode (R_a+R_c)	0.29 to 0.5 %/1000hrs	0.12 %/1000hrs
Electronic resistance (R_e)	0.06 to 0.2 %/1000hrs	0.08 %/1000hrs
Ion conductive resistance (R_i)	0.15 to 0.3 %/1000hrs	0.05 %/1000hrs

5. Estimation of Cell Endurance

Lifetime around 40,000 hrs is, indeed, long time to demonstrate. In order to prospect for newly developed stacks with better performance in shorter investigating period, Central Research Institute of Electric Power Industry (CRIEPI) has just now started to induce equations for estimation of individual decay rates such as reaction resistance in anode and cathode (R_a, R_c), electronic resistance (R_e) and ion conductive resistance (R_i) as well as short-circuit time (t_{sc}) as follows;

$$R_a = A\left(\theta_a(t)\right)\exp\left(-\frac{\Delta H_a}{RT}\right)P_{H_2}^{-0.5}$$

$$R_c = B\left(\theta_c(t)\right)T\exp\left(-\frac{\Delta H_{O_2^-}}{RT}\right)P_{O_2}^{-0.75}P_{CO_2}^{-0.5} + C\left(\theta_c(t)\right)T\exp\left(-\frac{\Delta H_{CO_2}}{RT}\right)P_{CO_2}^{-1}$$

$$R_i = L\,D\exp\left(-\frac{\Delta E_i}{RT}\right)\left(\varepsilon_e\theta_e(t)\right)^{1.5}$$

$$R_e = F + G\exp\left(-\frac{\Delta E_e}{RT}\right)t^{0.5}$$

$$t_{SC} = KL^{1.5}P_{CO_2}^{-1}$$

where L is matrix thickness, θ_a is electrolyte pore-filling ratio in anode, θ_c is electrolyte pore-filling ratio in cathode, θ_e is electrolyte pore-filling ratio in matrix and ε_e is void -space ratio of matrix.

More adequate equations with functions of operating time, temperature and partial pressures will be induced by basic cell operation under series of several accelerated conditions for approximately estimating longer lifetime of cell stacks improved and developed further.

6. Conclusion

MCFCs provide the opportunity for achieving higher system efficiencies operating under higher temperature condition around 650 ℃ because of the nature of electrolyte. Considering about future commercialization of MCFC power plants, we shall continue to devote to our research and development through international information exchange. Such issues including manufacturing cost shall be overcome after achieving our target in FY1999.

7. Acknowledgement

This research for longer lifetime cell has been conducted at New Sunshine Programme Headquarters in Agency of Industrial Science and technology, Ministry of International Trade and Industry. The substantial help and valuable comments on this paper from MITI as well as NEDO are gratefully acknowledged.

8. References

1. K. Tanimoto et al., "Long Term Operation of the 100-cm2 class Single-Cell of MCFC", 2nd IFCC, p. 211, Feb. 1996
2. Y. Mugikura et al., "Shorting by Dissolution of NiO Cathode in MCFC", 2nd IFCC, p. 169, Feb. 1996
3. S. Mitsushima et al., "Modeling of Life for Molten Carbonate Fuel Cells", 2nd IFCC, p. 211, Feb. 1996
4. A. Tsuru et al., "Electrode's Deformation and Cell Performance on MCFC Stack", 2nd IFCC, p. 161, Feb. 1996
5. A. Sasaki et al., "Development of Internal Reforming Molten Carbonate Fuel Cell", 2nd IFCC, p. 131, Feb. 1996
6 M. Tatumi et al., "Current Status and Future Aspect of the Development of Long Life Cell", 2nd IFCC, p. 203, Feb. 1996

ENDURANCE TESTING WITH Li/Na ELECTROLYTE

Estela T. Ong, Robert J. Remick
and Chakravarthy I. Sishtla
Institute of Gas Technology
1700 South Mount Prospect Road
Des Plaines, IL 60018-1804

Abstract

The Institute of Gas Technology (IGT), under subcontract to M-C Power Corporation under DOE funding, has been operating bench-scale fuel cells to investigate the performance and endurance issues of the Li/Na electrolyte because it offers higher ionic conductivity, higher exchange current densities, lower vapor pressures, and lower cathode dissolution rates than the Li/K electrolyte. These cells have continued to show higher performance and lower decay rates than the Li/K cells since the publication of our two previous papers in 1994.(1,2)

In this paper, test results of two long-term 100-cm^2 bench scale cells are discussed. One cell operated continuously at 160 mA/cm^2 for 17,000 hours with reference gases ($60H_2/20CO_2/20H_2O$ fuel at 75% utilization and $30CO_2/70$ air oxidant humidified at room temperature at 50% utlization). The other cell operated at 160 mA/cm^2 for 6900 hours at 3 atm with system gases ($64H_2/16CO_2/20H_2O$ at 75% utilization and an M-C Power system-defined oxidant at 40% utlization). Both cells have shown the highest performance and longest endurance among IGT cells operated to date.

Results and Discussion

IGT Cell-934 operated continuously at 160 mA/cm^2 for 17,000 hours (about 2 years) with reference gases, including one thermal cycle, with a decay rate of 2 mV/1000 hours. It reached a peak performance of 809 mV. Its performance lifegraph is shown in Figure 1. The thermal cycle occurred after about 6000 hours of operation: the cell was cooled down, clamped between flanges,and moved to another test facility where it was restarted. Toward the end of the 17,000 hours operation, cell performance had decreased to about 720 mV due to decreased anode wet seal efficiency and OCV and increased N_2 crossover.

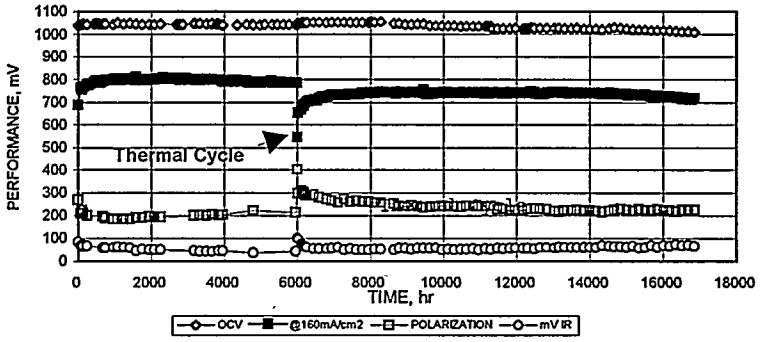

Fiugre 1. Cell-934

Cell-941operated for 6900 hours at 3 atm with system gases at 160 mA/cm^2. It had a peak performance of 765 mV and a decay rate of 3 mV/1000 hours until a cathode overpressure incident occurred at about 5300 hours of operation. Thereafter, the cell decayed more rapidly. Its lifegraph is shown in Figure 2. Post test examination showed that corrosion of the anode wet seal was mild as was the case with the 17,000-hour cell. Wet seal leakage in the latter cell was related to the matrix and not due to wet seal corrosion.

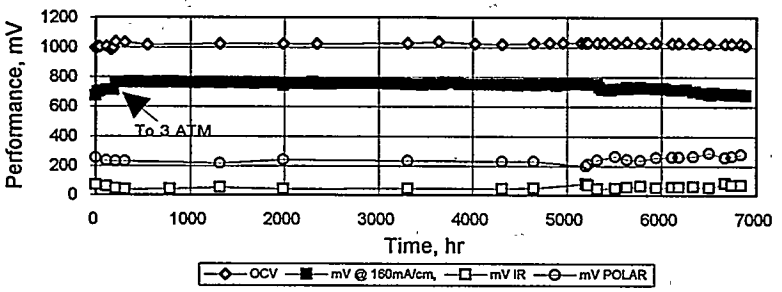

Figure 2. IGT CELL-941

Sensitivity to fuel and oxidant utilizations for Li/Na have been discussed before.(1,2) They are indications of the magnitude of the anode and cathode polarizations and of the uniformity of gas flow distibution across the electrodes. They were determined to be 1.5 mV/%U_f and 0.5 mV/%U_{ox}, respectively. These values are slightly greater than those of Li/K. The performance sensitivity to temperature has also been determined. Although internal resistance (IR) varies with temperature similarly for Li/Na and Li/K, the electrode polarization of Li/Na, especially when a stabilized cathode(SC) is used, was found to decrease at a greater rate with decreasing temperature below 650°C than Li/K (Figure 3). This could be due to poor carbonate distribution in the cell components or to different reaction kinetics.

Carbonate loss from the porous components of Cell-934 was determined to be 3.7 grams or 2.2 g/10,000 hours. This is higher than the loss observed for Li/K electrolyte under similar operating conditions, which was 1.6 g/10,000 hours (Figure 4). White salt deposits on the external surface of the anode flange of Cell-934 were evident indicating carbonate creepage. There were 1.5 grams carbonate accounted from the washings of this cell's hardware, therefore, just 2.2 grams or 1.3 g/10,000 hrs carbonate were unaccounted.

Carbonate loss from the porous components of the 3 atm Cell-941 was determined to be 1.8 grams or 2.6 g/10,000 hours, comparable to that observed for Cell-934. Heavy salt deposits on the external surface of the cell's anode flange were also observed.

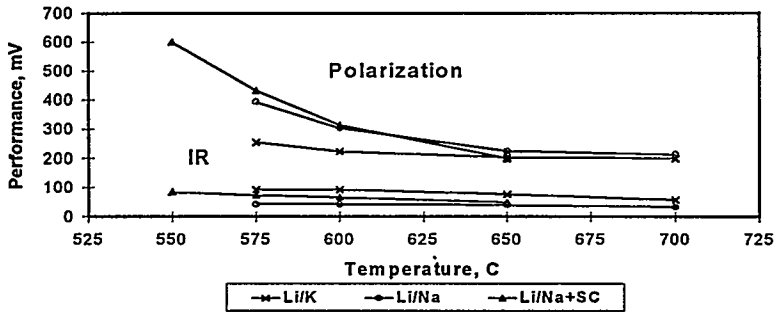

Figure 3. CELL POLARIZATION AND IR vs. TEMPERATURE

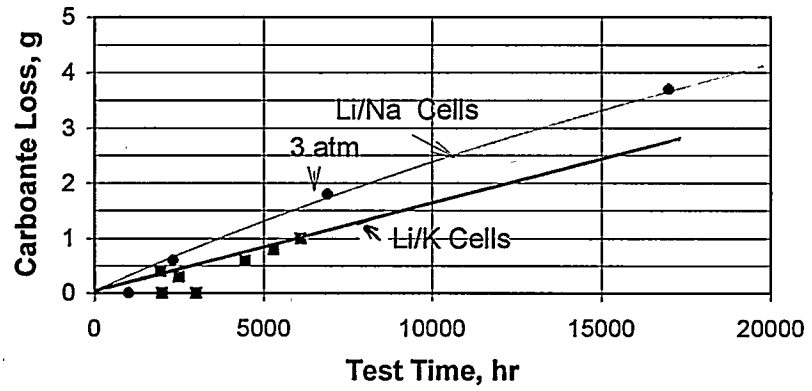

Figure 4. CARBONATE LOSS FROM 94-cm^2 CELLS

The amount of Ni in the matrix was determined to be 17.1 mg/cm^2 for the 17,000-hour cell and 14.6 mg/cm^2 for the 3 atm 6900-hour cell. There was no sign of cell shorting either from the CO_2 analysis of the fuel outlet gases under OCV condition or from the microscopic examination of the matrix cross sections. Although the cathodes of these two cells were stabilized, the observed rates of cathode dissolution are higher than those observed with Li/Na cells with an unstabilized cathode(Figure 5).

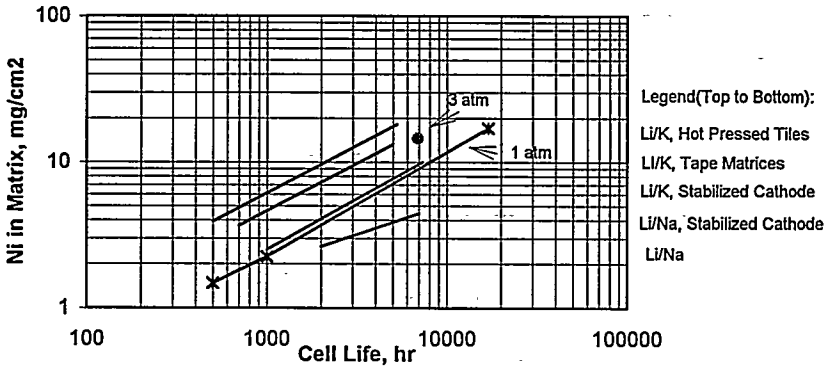

Figure 5. CATHODE DISSOLUTION IN 100-cm^2 CELLS

Acknowledgment

This work was carried out under DOE Contract No. DE-FC21-95MC30133, MCP Subcontract No. MCP-17-IGT. The authors wish to thank Mr. Leonard G. Marianowski, IGT Project Manager, and Mr. Thomas G. Benjamin, M-C Power Project Manager, for their technical guidance and direction.

References Cited

1. C. I. Sishtla, D. Vasil, R. Platon, E. T. Ong, R. J. Remick and R. J. Evans, "Effect of Pressure on Performance and Endurance of a Molten Carbonat Fuel Cell." Paper presented at the 1994 Fuel Cell Seminar, San Diego, California. November 28-December 1, 1994.

2. E. T. Ong, R. J. Remick, and C. I. Sishtla, "Cell Testing of Li/Na Electrolyte." Paper presented at the 1994 Fuel Cell Seminar, San Diego, California. November 28-December 1, 1994.

R&D of MCFC matrix for long term operation

Takashi Nishimura, Yoji Fujita, Hiroaki Urushibata, Akira Sasaki
Mitsubishi Electric Corporation
Advanced Technology R&D Center
1-1, Tsukaguchi-Honmachi 8 Chome,
Amagasaki, Hyogo 661, JAPAN

INTRODUCTION

Long term operation is an essential subject in the commercialization of the Molten Carbonate Fuel Cell (MCFC). Material stability is important for the development of the MCFC, particularly for long term operation. In this paper, the specification and the stabilization of MCFC matrix are investigated, with the aim of producing 40000 hours of operation.

It is common knowledge that matrix thickness has a large influence on shorting time, as shorting is caused by the dissolution of the nickel oxide cathodes (1,2). Therefore, the optimum thickness of a matrix designed for 40000 hours operation without the nickel shorting was sought. The influences of different electrolytes and matrix specifications on the shorting time were measured with accelerated cell tests. The internal resistance of the matrix was also estimated.

Gamma(γ)-lithium aluminate ($LiAlO_2$) powder with a sub-micron particle diameter is commonly used for a raw material of matrix to retain molten carbonate electrolytes. This is because most researchers found that γ -$LiAlO_2$ was the most stable material in the MCFC environment among the three allotropic forms alpha (α), beta (β), and γ (3,4). However, two problems with the stability of γ -$LiAlO_2$ are being vigorously discussed, especially in Japan: particle growth causes decreasing electrolyte retention (5,6), and the transformation of γ to α (6,7). This transformation contradicts the accepted opinion that γ is the most stable form. In this paper, the particle growth and the phase transformation of $LiAlO_2$ are examined with post-test analyses. The influence of matrix degradation on cell performance is also considered.

EXPERIMENT

Accelerated single cell tests have been performed to evaluate the nickel shorting time for three cells with the different electrolytes and matrices. The specifications are shown in Table 1. To accelerate the shorting, thinner matrices (0.5 ± 0.01 mm) were used, and the average partial pressure of the carbon dioxide in the cathode gas ($P_{CO_2\_avg}$) was 1.72 atm. The anode was made of Ni-Al alloy. Lithiated nickel oxide was used for the cathode. The matrix was made of γ -$LiAlO_2$ by tape casting method. A comparison of shorting times of Li/K and Li/Na carbonate was carried out by testing cells *A* and *B* (Table 1). A new matrix which had a structure delaying the shorting time was used with the Li/Na carbonate in cell *C*. Each cell was usually operated at 150mA/cm^2. The operation was continued until the open circuit voltage obviously dropped due to the nickel shorting.

Table 1 Specifications and results of accelerated cell tests

Cell Type	Electrolyte (m/o)	Matrix specification	Shorting time / hours	Coefficient A of eq.[1]
A	Li/K =62/38	Conventional	300	2.06×10^{5}
B	Li/Na=53/47	Conventional	800	5.50×10^{5}
C	Li/Na=53/47	Improved	2050	14.10×10^{5}
Operating pressure: 3atm, Current density: 150mA/cm^2 Matrix thickness: 0. 5 ± 0.01mm Average partial pressure of CO_2 in cathode gas: 1.72atm				

Post-test analyses were performed to estimate the in-cell stability of the $LiAlO_2$ for several

single cells, which were operated for 5000 ~ 20000 hours under the conditions shown in Table 2. The component specifications of these cells were the same as the previous cells used for the accelerated tests with the exception of the matrix thickness. The γ -$LiAlO_2$ powder used for the matrices in these cells has a purity of over 98% (α content < 2%) and a sub-micron particle diameter. After disassembling the cells that were operated, particle diameter and phase composition of the $LiAlO_2$ were examined with a scanning electron microscope (SEM) and an x-ray microdiffractometer. Both examinations were performed at three positions in the cross section of the matrix (near the cathode, at the middle layer, and near the anode) in each cell. The collimator with a 50 μ m ϕ pin hole was used for the x-ray microdiffractmeter measurement.

Table 2 Specifications of cell tests to estimate matrix stabilization

Cell No.	Electrolyte	Gas Utilization Uf/U_{O_2}/U_{CO_2} %	Cathode Gas Composition $O_2/N_2/CO_2$ %	Operation Time hours
LK1	Li/K	40/40/40	15/55/30	5000
LK2	Li/K	40/40/40	15/55/30	15000
LK3	Li/K	80/27/40	10/76/14	20000
LN1	Li/Na	40/40/40	15/55/30	7500
LN2	Li/Na	60/40/80	17/70/17	10000
Operating pressure: Atmosphere, Current density: 150mA/ cm^2 Anode Gas Composition: H_2/CO_2=80/20(50 °C Humidity)				

RESULTS AND DISCUSSIONS

The optimum thickness and IR loss of the matrix

Optimum thickness is the minimum thickness necessary for operating cells for 40000 hours without shorting in this paper. Researchers reported that the shorting time is approximately proportional to the second power of the matrix thickness and the reciprocal of the cathode CO_2 partial pressure (2), as shown in Eq. [1].

$$(\text{Shorting time / hours}) = A \times \frac{(\text{Matrix thickness / cm})^2}{(P_{CO_2\_avg} \text{ / atm})} \quad [1]$$

A of Eq. [1] is the coefficient which depends on the cell specifications. The calculated number of A for various cells is shown in Table 1. The optimum thickness of the matrix can be estimated with Eq. [1] for various operating conditions. Fig. 1 shows the calculated optimum thickness. The $P_{CO_2\_avg}$ was assumed to be 0.5 atm in a 5 atm pressurized condition. These results show that the improvements of electrolyte and matrix structure are very effective for the reduction of matrix thickness.

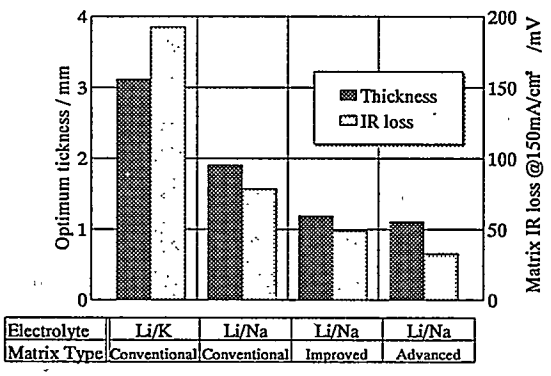

Fig.1 Calculated results of optimum thickness and IR loss of matrices for 40000 hours of operation without Ni-shorting ($P_{CO_2\_avg}$=0.5atm)

The internal resistance (IR) loss of a matrix can be calculated using Archie's equation shown in Eq. [2] (7).

$$(\text{Resistance / } \Omega \cdot \text{cm}^2) = \frac{(\text{Electrolyte volume fraction})^{-B} \cdot (\text{Matrix thickness / cm})}{(\text{Electrolyte conductivity / } (\Omega \cdot \text{cm})^{-1})} \quad [2]$$

The calculated IR loss of the endurable matrices over 40000 hours is also shown in Fig. 1. The empirical number was used as the coefficient B (8), and the current density was 150 mA/cm^2 . As seen in Fig. 1, the IR loss of a matrix with Li/Na electrolyte is below half of that of one with Li/K electrolyte. This is caused by the thinner matrix and high conductivity of Li/Na. In addition, the IR loss of the improved matrix is lower than that of a conventional matrix. The advanced matrix which is shown in Fig. 1 is now being developed to achieve a further reduction of the resistance. This is because the advanced matrix has a higher porosity than the others. From these results, it is expected that the pressurized operation of the MCFC becomes possible with the improvements of the electrolyte composition and the matrix structure, even if the nickel oxide cathode is used.

In-cell stability of the $LiAlO_2$

Fig. 2 shows the results of post test analyses of the maximum particle diameters of $LiAlO_2$ at different positions in the cross section of the matrix. $LiAlO_2$ particles grew near the cathode with passage of time. On the other hand, fine particles were kept at the middle layer even in the cell operated for 20000 hours. There was little influence brought about by differences in the electrolyte and cathode gases on particle growth, although it was reported that particle growth was influenced by the basicity of electrolyte (5).

Fig. 3 shows the α -$LiAlO_2$ content as determined by x-ray diffraction. The transformation of γ to α was remarkable near the cathode where the particle growth was accelerated. These results suggest that there is a relation between phase transformation and particle growth. It was observed that the particle growth was accelerated in out-of-cell tests, when the packing of the matrix was looser (9). This particle growth might be caused by the decrease in packing density due to the phase transformation.

Fig. 4 shows the changes in internal resistance and gas cross-over in the cell operated for 20000 hours. The amount of cross-over didn't increase. This is because of the fine pore layer in the middle of matrix layer which retained electrolyte. However, the resistance increased gradually after 16000 hours. Particle growth causes the cell resistance to increase due to the lowering of electrolyte retention. These results suggest that it is necessary to take some action to inhibit particle growth for longer operation.

REFERENCES

1. H. R. Kunz and J. W. Pandolfo, "The Effects of Nickel Oxide Cathode Dissolution on Molten Carbonate Fuel Cell Life" J. Electrochem. Soc., 139, pp.1549-56, Jun. 1992
2. S. Yoshioka and H. Urushibata, "Simulation of MCFC's Life caused by Cathode Dissolution and Shorting", Extended Abstracts of the 186th Electrochem. Soc. Fall meeting, Vol. 94-2, Maiami Beach, Florida, October 9-14, pp.938-9, 1994
3. P. A. Finn, "The Effects of Different Environments on the Thermal Stability of Powdered Sample of $LiAlO_2$" J. Electrochem. Soc., Vol. 127, No. 1, pp.236-8, Jan. 1980
4. G. H. Kucera, "Thermal Characterization of Lithium Aluminate/Alkali Carbonate Electrolyte Structure", Proceedings of the 11th North American Thermal Analysis Society Conference, New Orleans, Oct. 18-22, pp. 90-94, Oct. 1981
5. H. Sotouchi, Y. Watanabe, T. Kobayashi, and M. Murai, "Mechanism of Crystal Growth of Lithium Aluminate Particles in Molten Lithium and Potassium Carbonates", J. Electrochem. Soc., Vol. 139, No. 4, Apr. 1992
6, K. Tanimoto, M. Yanagida, T. Kojima, Y. Tamiya, and Y. Miyazaki, "Long Term Operation of 100-c m^2 Class Single Cell of MCFC", Proceedings of the 2nd IFCC, Japan, Feb. 5-8, pp. 207-210, 1996
7. P. Delahay and C. W. Tobias, Advances in Electrochemistry and Electrochemical Engineering, Vol. 2 Interscience Publishers, New York, 1962
8. T. Nishimura, J. Hosokawa, H. Urushibata, "Development of Molten Carbonate Fuel Cell -Investigation of Internal Resistance of Electrolyte Matrix", Abstracts of the 34th Battery Symposium in Japan, Nov. 22-24, pp133-4, 1993
9. T. Nishimura, Y. Fujita, H. Urushibata, A. Sasaki, "Study of Particle Growth and Phase Transformation of MCFC Matrix", Abstracts of the 37th Battery Symposium in Japan, Sept. 25-27, 2B11, 1996

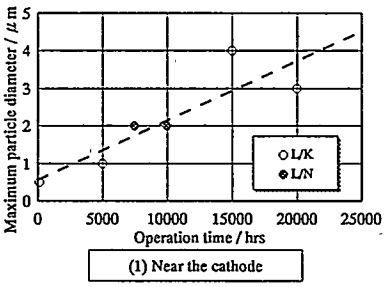

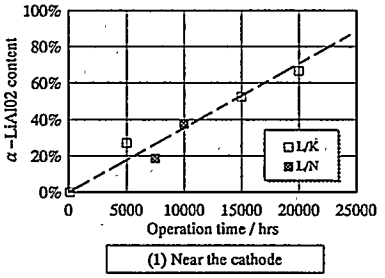

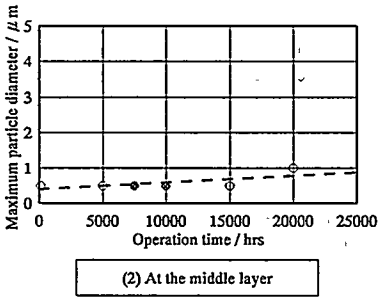

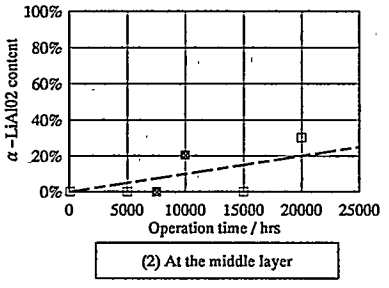

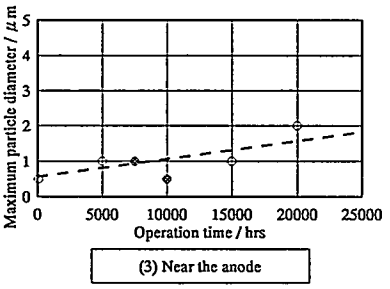

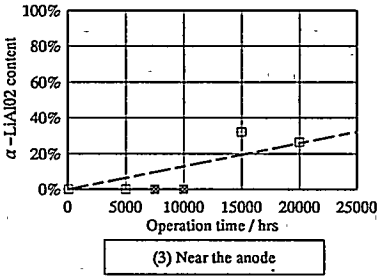

Fig.2 Particle growth over time

Fig.3 Transformations over time

$$\alpha\text{-LiAlO2 content} = \frac{D_\alpha}{D_\alpha + D_\gamma}$$

$D_{\alpha(\gamma)}$: Diffracted Intensity of α (γ)
Detectable Sensitivity > 10%

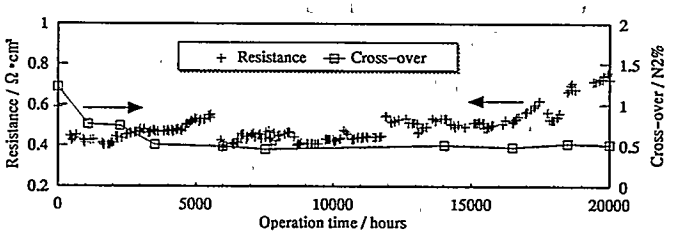

Fig.4 Change of cell resistance and cross-over over 20000 hours of operation

PROPERTIES OF $LiCoO_2$-COATED NiO MCFC CATHODE

S.T. Kuk, *H.J. Kwon, **H.S. Chun, K. Kim
Department of Chemistry, Korea University, Seoul, 132-701, Korea
* Samsung Electronics Co. Ltd., Suwon, 442-742, Korea
** Department of Chemical engineering, Korea University, Seoul, 132-701, Korea

Abstract

PVA-asssisted sol-gel method is useful in producing metal oxides with large surface area at low temperature. We fabricated $LiCoO_2$-coated NiO(LC-NiO) cathode by PVA-asssisted sol-gel method and measured its properties. The electrical conductivity of LC-NiO cathode was measured to be more than 5 times as high as that of NiO and unit cell test showed improved performance. From the SEM images and Raman spectra, we confirmed that the structure of LC-NiO was different from that of NiO. For 250 hours of steady operation of unit cells, the mean voltage of the cells were 0.78V for NiO and 0.85V for $LiCoO_2$-coated NiO at a current density of $150mA/cm^2$.

Introduction

The solubility of NiO cathode in molten carbonate fuel cell(MCFC) electrolyte has been identified as one of the major technical obstacles facing fuel cell commercialization. Lithium cobalt oxide, $LiCoO_2$ was selected as one of the new materials for MCFC cathode because the solubility of $LiCoO_2$ is small and the rate of dissolution into the melt is slower than that for NiO, although the electrical conductivity is lower than that of NiO. So we coated NiO which has higher electrical conductivity with stable $LiCoO_2$ in carbonate and got $LiCoO_2$-coated NiO(LC-NiO) cathode by PVA-asssisted sol-gel method.

The use of PVA greatly suppressed the formation of precipitates from which the heterogeneity stems. Thereby, homogeneity in the composition of the precursor could be attained, eliminating the diffusion barrier. It is speculated that the hydroxy ligands on the PVA interact with, or are complexed to the metal ions, wrapping them and forming cocoons like local structure around the ions. This local isolation would prevent agglomeration of metal components, cutting off the proceeding toward the formation of precipitates. Presumably, this isolation would be conserved until the organic moieties are burned off by being heated. In this study, we measured properties of LC-NiO cathode fabricated by PVA-asssisted sol-gel method and investgated whether LC-NiO cathode had the possiblity as the MCFC cathode.

Experimental

At first, lithium acetate($CH_3COO \cdot Li \cdot 2H_2O$) and cobalt acetate($Co(CH_3COO)_2 \cdot 4H_2O$) were dissolved in water stoichiometrically. Another solution was prepared by dissolving PVA in water. The two solutions were mixed and heated to 60~80°C. Pure nickel electrodes were prepared by tape casting method and the electrodes were coated by viscous (Li,Co)-PVA solution. The electrode

coating used dipping method at atmospheric pressure or at vacuum. After heat treatment at 800°C for 2 hours, the properties of LC-NiO electrodes were investgated by TGA, DSC, SEM, Raman spectroscopy, conductivity measurement, and unit cell test.

Results and Discussion

Figure 1 and figure 2 are TGA and DSC curves, respectively, of various electrodes and the (Li,Co)-PVA solution. The (Li,Co)-PVA solution shows a large weight loss and an endotherimc reaction curve at 50°C~150°C due to water evaporation. The LC-NiO and NiO electrodes show a weight loss and exotherimc reaction curves at 300°C~500°C because of the oxidation of organic materials in the electrodes. At 600°C~800°C, exotherimc reactions of LC-NiO and NiO electrodes are assumed due to the formation of oxides.

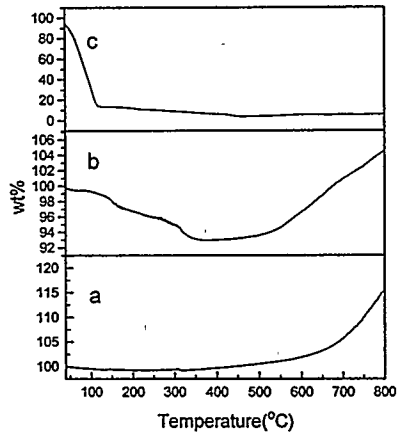

Figure 1.TGA curves of
a) pure Ni electrode,
b) LC-Ni electrode,
c) (Li,Co-PVA)solution.

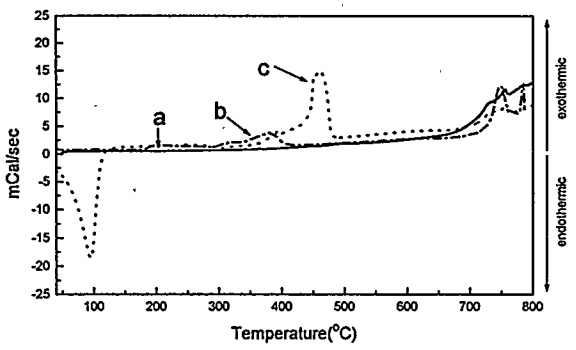

Figure 2. DSC curves of
a) pure Ni electrode,
b) LC-Ni electrode,
c) (Li,Co-PVA)solution.

Figure 3 shows SEM images of NiO and LC-Ni electrodes after heat treatment at 800°C for 2 hours. The surface structure of LC-NiO electrode was different from that of pure NiO electrode.

The structure of NiO electrode shows many micro pores and round-shape particles. On the other hand, the surface structure of LC-NiO electrode shows few micro pores and angular-shape particles.

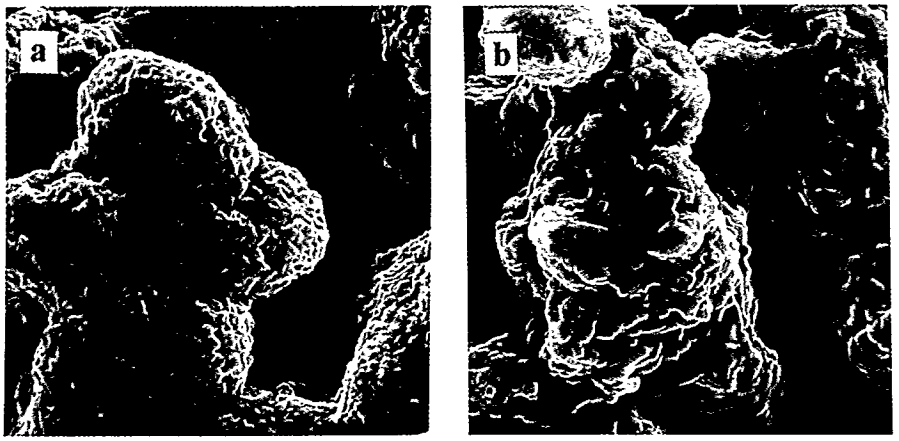

Figure 3. SEM images of a) pure NiO electrode, b) LC-NiO electrode after heat treatment at 800°C for 2 hours.

Figure 4 shows the Raman spectra of various electrodes. The Raman spectra of two LC-NiO electrodes(b, c) were different from that of NiO electrode(a). For $LiCoO_2$, previous Raman spectra show two strong Raman bands at 485 and 597 cm^{-1}. NiO Raman spectra are shown in figure 4. a). However only Raman band was observed at 597 cm^{-1} for two LC-NiO electrodes, which might be due to the lithiation of NiO electrodes.

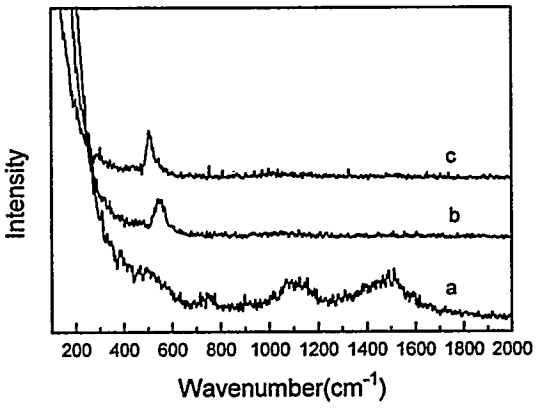

Figure 4. Raman spectra of
a) pure NiO electrode,
b) LC-NiO electrode by dipping at atmospheric pressure,
c) LC-NiO electrode by dipping at vacuum after heat treatment at 800°C for 2 hours.

Table 1. shows the electrical conductivity of various electrodes. The electrical conductivity of LC-NiO cathode was measured to be more than 5 times as high as that of pure NiO.

Table 1. The electrical conductivity of various electrodes.

Electrode	NiO	LC-NiO
Conductivity($ohm^{-1}cm^{-1}$)	3.23×10^{-5}	1.82×10^{-4}

The performance of unit cell using the LC-NiO cathode showed in Figure 5. For 250 hours of steady operation of unit cells, the mean voltage of the cells were 0.78V for NiO(a) and 0.85V for LC-NiO(b) at a current density of $150mA/cm^2$.

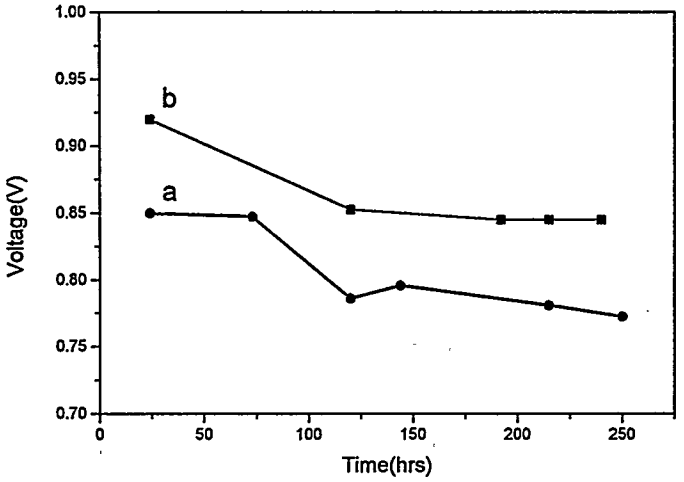

Figure 5. The plots of operation time vs. votage.

Conclusions

We fabricated $LiCoO_2$-coated NiO(LC-NiO) cathode by PVA-asssisted sol-gel method. After heat treatment at 800°C for 2 hours, the SEM image of LC-NiO electrode was different from that of pure NiO electrode and the fact was confirmed by Raman spectra. The electrical conductivity of LC-NiO cathode was measured to be more than 5 times as high as that of pure NiO. For 250 hours of steady operation of unit cells, the mean voltage of the cells were 0.78V for NiO and 0.85V for LC-NiO at a current density of $150mA/cm^2$. The efficiency improvement of LC-NiO cathode cannot be explained yet..

Reference

1. K. I. Ota, "Solubility of Cobalt Oxide in Molten Carbonate," J. Electrochem. Soc., Vol. 142, No. 10, pp. 3322-3326, Oct. 1995
2. H. J. Kwon, S. T. Kuk, H. B. Park, D. G. Park, K. Kim, J. Mater. Sci. Lett. 15, 428, 1996
3. X. Li, H. Zhang, J. Mater. Sci. Engng. B18, 209, 1993
4. H. Taguchi, H. Yoshioka, J. Solid State Chem., 104, 460, 1993

GUIDELINES FOR DESIGN AND DEVELOPMENT OF INDUSTRIALLY RELEVANT MCFC STACKS

A. Torazza(°), A. Dufour(°), L. Giorgi(◊), J. G. Martín(▽), G. Rocchini(⊗), F. J. Simon(*)
(°)Ansaldo Ricerche S.r.l., Corso Perrone 25, I-16161 Genova
(◊)ENEA, Via Anguillarese 301, I-00060 Roma
(▽)IBERDROLA S.A., C/Goya 4, S-28001 Madrid
(⊗)ENEL S.p.A. - CRAM, Via Rubattino 54, I-20134 Milano
(*)Babcock & Wilcox Española, S.A. Fabrica Galindo, S-48510 Galindo - Vizcaya

Introduction

An interesting way of reducing the production costs of the electrical energy by improving efficiency and, at the same time, having a good integration between environment and power plants is offered by the utilisation of the fuel cells operating at high temperatures. From this point of view, Molten Carbonate Fuel Cells (MCFCs) seem to be one of the most promising technologies because of their environmental friendly operation for various fuels and potential low cost. In fact it is well known that the MCFCs overall plant efficiency is typically some 50% and can reach, as a consequence of their high operating temperature, 65% with a bottoming cycle. Moreover MCFCs will be particularly attractive for dispersed power plants of MW size located at user sites. Additional advantages of MCFCs are their good response to base and partial load, short time for plant erection and modularity.

However, the competitiveness of MCFC power plants with respect to the other plant types depends, in a significant way, on the achievement of some basic prerequisites concerning technical, economical and environmental aspects. An important practical problem regards the process simplicity of the overall system and the proper choice of plant components as concerns their performance, reliability, cost reduction and lifetime.
In particular the MCFC stack, which is the key component, still needs improvements to reach high performance during long term operation as well as a close integration with the balance of plant (BoP), which is essential for the effective management of heat and gas flow. Another important goal concerns an easy maintenance and a low-cost replacement of the stack.

Ansaldo Ricerche, also within a technical co-operation with ENEL and ENEA, engaged in the field of MCFCs since the early eighties, Babcock & Wilcox Española, IBERDROLA and their partners are facing the previous problems by taking advantage of their experience concerning the design and construction of a 100 kW MCFC stack which will be tested at the IBERDROLA facility in Guadalix, near Madrid. After this test, the stack will be placed in a 100 kW MCFC prototype cogeneration power plant under erection, at the CISE premises, near Milan. These activities are carried out under two JOULE and THERMIE contracts from European Union (EU). As regards the THERMIE project, CISE is the ENEL representative.

In the frame of its co-operation with Ansaldo Ricerche, the role of ENEL is to support the technology development and assessment through the performance of specific activities concerning the physicochemical characterisation of materials and the operation of laboratory monocells and small size stacks, and to provide basic ideas as concerns the plant type and configuration as well as its operation modalities.

General considerations

At present the main efforts of Ansaldo Ricerche and Babcock & Wilcox Española are addressed to improve MCFC technology, define optimum systems for fuel processing and re-design fuel

cell stacks for application to MW class power plants mainly fuelled with natural gas and consistent with the market opportunities concerning dispersed and on-site applications. However some studies concerning the use of coal gas as fuel are also undertaken [1].

To this aim Ansaldo Ricerche and its Spanish partners defined their roles to reach in a short time and in a cost effective way the target of the joint program [2] according to their actual technological background. From this point of view the activities to be developed have been splitted in such a way that each partner, within its specific roles and expertise, may collaborate in the most important tasks of the joint program. Moreover, IBERDROLA, a Spanish electrical utility, will support some technical choices dealing with the BoP and definition of the basic criteria for connection to the grid and for operation modalities.

Some of the previous activities are performed within a new program partially founded by the EU, lasting three years and mainly focused to the development and assessment of cost effective stack through the re-design of the stack as well as the proper selection of electrode materials and repeat components by performing suitable tests also using one full area short stack.

Stack design

Many experimental activities aimed at supporting the design and construction of the basic stack module concerned the design, manufacturing and testing of several stacks having cells with an useful area of 100, 702 and 6760 cm^2. This program permitted to assess the validity of the present technology, define proper operating conditions and individuate the critical parameters conditioning the integration of the stack in the plant. Useful information about the manufacturing of repeat porous and metallic components were also gained so that it was possible to set up a pre-industrial production line, which permitted to define its running criteria and to evaluate properly the relevant costs and specific problems for mass production.

Actually a sound knowledge has been already obtained to review the basic requirements relating to the plant and stack and concerning the cost reduction, modularity improvement, control simplification, easy maintenance and high reliability. Other important aspects to be considered concern assembly procedures, start-up cycles, gas sealing, impurity tolerability and diagnostic tools.

The present technology for the construction of large size stacks is based on elements having a geometrical area of 0.75 m^2 with a rated power ranging from 50 to 100 kW. Anodes are based on Ni-Cr alloys with a chromium content ranging from 2 to 5% and are formed using proprietary heat treatments under suitable atmospheres concerning debinding, pre-sintering, sintering, chromium pre-oxidation. After the previous operations anodes are filled with a mixture of Li and K carbonates having a proprietary composition. Cathodes, made of nickel, are oxidised in situ during the conditioning phase of stacks, performed using a suitable atmosphere, to give a lithiated nickel oxide structure. The electrolyte matrix, constituted by γ-$LiAlO_2$, is placed in the stack in the green state and is typically made of some layers having an overall thickness less than 1 mm. Particular care is devoted to the selection of the γ-$LiAlO_2$ powders to prevent matrix crack growth and thickness reduction during stack operation. The removal of binders is performed using a proprietary process during stack start-up.

Current collector and gas distributor are constituted by a single piece which is obtained by die forming. This component is carefully controlled to verify the respect of specifications as concerns its height which is very important in order to get a uniform pressure over all the contact region and to reduce significantly the value of the internal resistance. Cathodic current collector and gas distributor are made of AISI 310 S stainless steel. Anodic current collector and

gas distributors have a more complex structure based on a trilayer sheet made of nickel clad AISI 310 S stainless steel. Springs for cathodic and anodic regions are selected to operate properly at a temperature of about 700 °C. Separator plates are made of AISI 310 S stainless steel and the zones of the wet sealing are aluminised according to a proprietary procedure. Besides the filling of the anodes with Li and K carbonates, a further amount, necessary for a correct stack performance, is added in the anodic current collectors using a proprietary procedure. Its amount is determined by applying a mathematical model, validated by several experimental observations, which permits to account for electrolyte losses due to corrosion and decomposition processes and migration under the influence of electrical fields.

The present stack design is based on the external manifolding configuration. The mechanical sealing at the operating temperature is obtained using a suitable assembly of α-alumina, zirconia felt and cloth. The design account also for the slide due to hot stack compaction under the axial mechanical load. External manifolds are properly matched to the stack by a system which assures a nearly constant pressure on the seals. The axial mechanical load is applied through a pneumatic bellow which operates with nitrogen and permits to regulate accurately the pressure during the stack start-up and operation. The use of a pneumatic bellow is very effective to reduce the contact resistance and entity of the gas leakage's through wet seals. A mechanical system becomes active when the value of the axial load is less than a prefixed threshold.

The current practice is to equip stacks with suitable sensors in order to collect the values of several physical quantities such as: cell voltage, internal resistance, cell temperature map, inlet and outlet manifold temperature at different regions and stack compaction versus operation time.

The first prototype of the 0.75 m^2 technology is a stack having 20 cells which will be operated under a pressure of 3.5 bar. This stack will be fed with anodic and cathodic gas mixtures simulating the operating conditions of the 100 kW stack. In fact the cogenerative 100 kW plant utilises heat sensible reforming system to produce hydrogen rich gas from natural gas. At present the stack is in the assembly phase and its operation is planned at middle October, 1996.

Ansaldo Ricerche experience based on single cells and subscale stacks has shown that some critical aspects of the present stack technology which includes also conditioning procedures are: aluminization of separator plate in the wet seal region, stack assembly procedures, stack conditioning cycle and non-repeat metallic parts. It is useful to underline that the previous problems are not of technical nature but mainly arise from an economical point of view because at present some of the previous operation are not cost effective.
In order to move towards the pre-commercial application of plants based on MCFC technology, the following intermediate targets have been fixed for the basic stack module:

- Cell area 0.75 m^2
- Power density 160 mW cm^{-2} at 750 mV/cell
- Operating pressure 3.5 atm
- Decay rate < 2 mV per 1000 h
- Lifetime > 20000 h
- Cost 3000 – 4000 $/kW.

The previous goals are consistent with the technical and economical requirements of a pre-commercial phase and industrial application because the effective commercialisation requires only the improvement of manufacturing facilities for cost reduction and mass production

To reach the previous targets and improve stack design, a guideline handbook with reference to the stack configuration, mechanical load management, cell number, gas manifolding, choice of

materials and/or components, assembly and maintenance procedures will be defined. The influence of the "size-dependent" parameters will be also examined in order to identify and optimise the size of the commercial units. In addition to these activities, Ansaldo Ricerche is starting a specific technical program aimed at defining a new start-up cycle procedures, which should require less tight controls and envisage the possibility of performing such an operation directly on the plant, and at designing improved fabrication technologies of the non-repeat metallic parts in order to face a mass production with a low manufacturing time and effective costs.

Stack configuration will be defined also by using suitable mathematical modelling to support the choice criteria for single block or submodule arrangement. This point is very important as concerns the start-up cycle, performance, reparability and maintenance. The mathematical modelling is also useful to define basic criteria and methodology for the design of new stacks and to select the main parameters affecting their sizing.

As regards the development of effective cathodes, the doped lithium cobaltite will be examined and specifications concerning total porosity, mean pore size, surface specific area, electrical conductivity and stability in molten carbonates will be established. Furthermore an experimental activity concerning anodes stabilised whit aluminium has been started and some specimens have been prepared. The characterisation of their performance on monocells is in progress.

Conclusions

Ansaldo Ricerche experience, concerning single cells and subscale stacks, shows that the present technology seems to be valid for the construction of stacks whit a size of about 100 kW even if the single cell performance as well as the anode and cathode stability can be improved.

Mathematical modelling of stack design and performance is an useful tool to reach the designed target and define the expected performance when the state-of-the-art materials are used. Mathematical simulation is also useful for a correct distribution of the process gases.

At last, a new crossed approach "system-to-stack" and "stack-to-system" has been defined, which should overcome the distortion due to the fact of considering separately the stack development and BoP specifications. This new approach permits a comparative analysis of mutual links of stacks, ancillary devices and BoP equipment by accounting for the use of the proprietary Compact Unit concept and comparing the effectiveness of the different fuel processing systems.

Acknowledgements

Part of the work described in this paper has been performed under the financial support of the European Commission in the framework of the JOULE programmes. The authors thank also International Fuel Cells for its useful technical contributions.

References

1. A. Dufour, A. Torazza, V. Regis, G. Rocchini, E. Hermana; "MCFC Compact Unit and System Improvements for 100 kW - 2 MW Dual-Fuel Demonstration Plant", Conference Paper Power-Gen Europe, Book II, Vol.5, p. 859, Amsterdam, 1995.
2. M. Brossa, A. Dufour, E. Hermana, J. F. Jimenez, F. Sanson, "The European MOLCARE Programme: a 100 kW Demonstrative Plant and Engineering Development of the MCFC Technology", Proc. Fuel Cells Seminar, p.238, San Diego, 1994.

MODELING AND SIMULATION OF NiO DISSOLUTION AND Ni DEPOSITION IN MOLTEN CARBONATE FUEL CELLS

Suk Woo Nam, Hyung-Joon Choi, Tae Hoon Lim, -Hwan Oh, and Seong-Ahn Hong
Korea Institute of Science & Technology
Seoul 136-791, Korea

Introduction

Dissolution of NiO cathode into the electrolyte matrix is an important phenomena limiting the lifetime of molten carbonate fuel cell (MCFC). The dissolved nickel diffuses into the matrix and is reduced by dissolved hydrogen leading to the formation of metallic nickel films in the pores of the matrix. The growth of Ni films in the electrolyte matrix during the continuous cell operation results eventually in shorting between cathode and anode. Various mathematical and empirical models [1-4] have been developed to describe the NiO dissolution and Ni deposition processes, and these models have some success in estimating the lifetime of MCFC by correlating the amount of Ni deposited in the matrix with shorting time.

Since the exact mechanism of Ni deposition was not well understood, deposition reaction was assumed to be very fast in most of the models and the Ni deposition region was limited around a point in the matrix. In fact, formation of Ni films takes place in a rather broad region in the matrix, the location and thickness of the film depending on operating conditions as well as matrix properties. In this study, we assumed simple reaction kinetics for Ni deposition and developed a mathematical model to get the distribution of nickel in the matrix.

Model Development

Ni deposition is known to occur by the following reaction :

$$Ni^{2+} + H_2 + CO_3^{2-} \rightarrow Ni + H_2O + CO_2. \quad (1)$$

Ni^{2+} dissolved from the cathode and hydrogen dissolved at the anode diffuse opposite to each other and react within the pores of the matrix. The Ni deposition process is similar to the one used for the fabrication of inorganic membranes by chemical vapor deposition in an opposing reactants geometry [5,6]. But, transport mechanism of charged species like Ni^{2+} in the electrolyte is somewhat different from gas diffusion in the pores. For simplicity, consider the deposition of Ni in a cylindrical pore of the matrix with an initial pore radius r_o at any axial position z, as shown in Fig. 1. As Ni is deposited on the wall of the pore, the pore radius changes. From the deposition model, we can find the pore radius change as a function of pore axial position and time. The progress of Ni deposition can be characterized by the instantaneous radius calculated from the amount of Ni in the deposit layer using molar volume of Ni (ρ_{Ni}) and molecular weight ($M_{w,Ni}$) :

$$\frac{dr}{dt} = - R_{Ni} M_{w,Ni} / \rho_{Ni} \quad (2)$$

with initial condition :

$$r = r_o \quad \text{at} \quad t = 0. \quad (3)$$

R_{Ni} denotes the formation rate of Ni based on unit surface area of the pore. In this study we assume simple reaction kinetics for Ni formation :

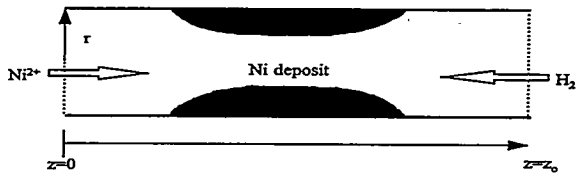

Fig. 1. Cylindrical pore of the matrix for modeling Ni deposition.

$$R_{Ni} = k\ C_{Ni2+}\ C_{H2} \tag{4}$$

and reaction rate for reactant i based on unit pore volume, R_i, can be correlated with R_{Ni} by :

$$R_i = -\frac{2}{r} R_{Ni}. \tag{5}$$

Assuming quasi-steady state for the deposition process, material balance of reactant i in the cylindrical pore gives :

$$-(1/r^2)(J_i\ r^2) = R_i \tag{6}$$

where J_i is the flux of i. Transport of Ni^{2+} through the electrolyte in the matrix pore can be described by diffusion, migration and convection. Since the migration of Ni^{2+} due to the gradient of electric field in the matrix is minor [1], we neglect migration term in J_i. Then flux of species i becomes :

$$J_i = J_{i,\,diffusion} + J_{i,\,convection} \tag{7}$$

with

$$J_{i,\,diffusion} = -D_i\ d\,C_i / d\,z \tag{8}$$

$$J_{i,\,convection} = v\ C_i \tag{9}$$

where D_i denotes an effective diffusion coefficient of i, and v denotes the convective flow rate. Effective diffusion coefficient is correlated with bulk diffusivity (D_i^b) by :

$$D_i = (\varepsilon/\tau)\, D_i^b \tag{10}$$

where τ is tortuosity factor and ε is porosity of the matrix. Since the poroity is a function of pore radius, D_i changes with axial position and time during the deposition. The convective transport takes place by the carbonate ion flow due to the fuel cell reaction in the anode and cathode. The amount of carbonate ion transported from the cathode side to the anode side is proportional to the current density (I/A) and the electrolyte velocity can be expressed as :

$$v = (I/A)\, M_w / (nF\rho)\ (r_o / r)^2 \tag{11}$$

Therefore, flux of Ni^{2+} or H_2 becomes :

$$J_{Ni2+} = -D_{Ni2+}\ d\,C_{Ni2+} / d\,z + v\,C_{Ni2+} \tag{12}$$

$$J_{H2} = -D_{H2}\, d\,C_{H2} / d\,z - v\,C_{H2}. \quad (13)$$

The boundary conditions at both ends of the matrix are :

$$C_{Ni2+} = C_{Ni2+}^{\circ}, \quad d\,C_{H2} / d\,z = 0 \quad \text{at } z = 0 \quad (14)$$

$$C_{H2} = C_{H2}^{\circ}, \quad d\,C_{Ni2+} / d\,z = 0 \quad \text{at } z = z_o. \quad (15)$$

C_{Ni2+} at the cathode-electrolyte interface can be calculated assuming that NiO dissolution reaction :

$$NiO + CO_2 \leftrightarrow Ni^{2+} + CO_3^{2-} \quad (16)$$

is always in equilibrium. Then C_{Ni2+} is proportional to the partial pressure of CO_2 at the cathode that is the average partial pressure of CO_2 determined by the material balance in the cathode for given current density. C_{H2}° can be obtained from the Henry's law using average partial pressure of H_2 at the anode side. The differential equation (2) and (6) together with initial and boundary conditions (3), (14) and (15) were solved by finite difference method. The amount of Ni deposited in the matrix was obtained by integrating the pore radius along the pore axis. The kinetic parameters were optimized so that the evolution of the amount of nickel in the matrix during the cell operation was fitted well to the $3cm^2$-cell data from the literature [1,2].

Distribution of Ni in the matrix

The distribution of Ni in the matrix depends on the operating conditions and matrix properties. We concentrate in this abstract on the effect of gas composition on the Ni distribution. Fig. 2 and Fig. 3 show the distribution of Ni in the matrix at 2,000h as a function of cathode CO_2 partial pressure (P_{CO2}) and anode hydrogen partial pressure (P_{H2}), respectively. The location of Ni deposit moves toward the anode side with increasing P_{CO2}. In addition, the amount of Ni deposited in the matrix increases with increasing P_{CO2}. Similar results were obtained when P_{H2} at the anode side were varied. As P_{H2} decreases, the film location moves to the anode side and Ni distribution becomes broad.

It was found that the amount of Ni deposited in the matrix of a $3cm^2$ cell was higher than the amount found in the bench-scale cell or stack even if the same feed compositions were used [1]. Since $3cm^2$ cell is usually operated at lower utilization, average P_{CO2} and P_{H2} in the $3cm^2$ cell should be higher than those in the bench-scale cell or stack. Since the amount of Ni increases with increasing P_{CO2} and P_{H2} as shown in Fig. 2 and Fig. 3, it is expected that the amount of Ni deposited in the $3cm^2$ cell is higher than that in the bench-scale cell or stack. Furthermore, the simulation results indicate that the thickness of Ni deposit is lower for the $3cm^2$ cell.

Previously, Kasai and Suzuki found from the co-flow type $100cm^2$-cell experiment that the Ni distribution in the matrix was not uniform along the gas flowing direction [7]. For the matrix placed near the gas inlet, Ni was deposited in a narrow region close to the cathode side. On the other hand, Ni deposit was found in a broad region close to the anode side of the matrix near the gas outlet.. These results can be clearly explained in view of the results obtained from the simulation. Since fuel utilization is usually higher than CO_2 utilization in the bench-scale cell experiment, gradient of P_{H2} will be higher along the gas flowing direction. Near the gas inlet, P_{H2} is relatively high and Ni deposition would occur far from the anode side of the matrix. As P_{H2} decreases along the gas flowing direction, the location of Ni deposition moves to the anode side as shown in Fig. 3. The Ni distribution is relatively broad in the matrix near the gas outlet since both P_{H2} and P_{CO2} are low at this location.

References

1. D.A. Shores, J.R. Selman, S. Irani and E.T. Ong, Proceedings of the second Symposium on the MCFC Technology, Electrochem. Soc., Pennington, NJ, p290 (1990).
2. J.B.J. Veldhuis, S.B. van der Molen, R.C. Makkus and G.H.J. Broers, Ber. Bunsenges. Phys. Chem., 94, 947 (1990).
3. H.R. Kunz and J.W. Pandolof, J. Electorchem. Soc., 139, 1549 (1992).
4. Y. Mugikura, T. Abe, S. Yoshioka and H. Urushibata, J. Electorchem. Soc., 142, 2971 (1995).
5. G.R. Gavalas, C.E. Megiris and S.W. Nam, Chem. Eng. Sci., 44, 1829 (1989).
6. Y.S. Lin and A.J. Burggraaf, J. Membrane Sci., 46, 3067 (1991).
7. H. Kasai and A. Suzuki, Proceedings of the second Symposium on the MCFC Technology, Electrochem. Soc., Pennington, NJ, p240 (1990).

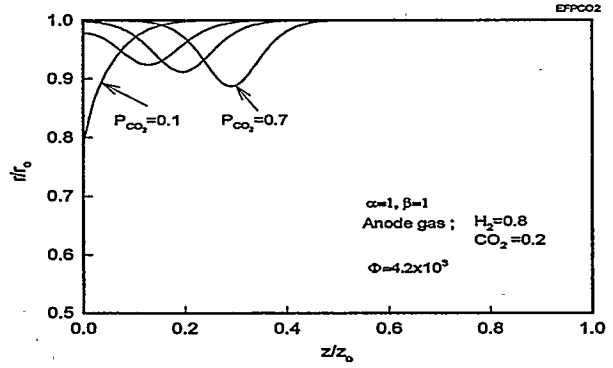

Fig. 2. Effect of P_{CO2} at the cathode on the Ni distribution in the matrix.

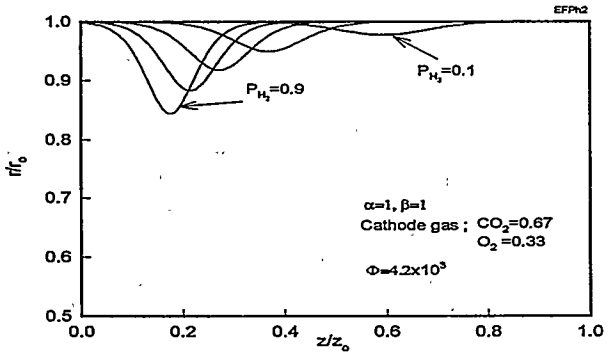

Fig. 3. Effect of P_{H2} at the anode on the Ni distribution in the matrix.

HIGH TEMPERATURE CORROSION OF SEPARATOR MATERIALS FOR MCFC

Masahiro Yanagida, Kazumi Tanimoto, Toshikatsu Kojima,
Yukiko Tamiya, Takashi Asai and Yoshinori Miyazaki
Osaka National Research Institute
1-8-31 Midorigaoka, Ikeda, Osaka 563, Japan

1. Introduction

The Molten Carbonate Fuel Cell (MCFC) is one of promising high efficiency power generation devices with low emission. Molten carbonate used for its electrolyte plays an important role in MCFC. It separates between anode and cathode gas environment and provides ionic conductivity on MCFC operation. Stainless steel is conventionally used as separator/current collector materials in MCFC cathode environment. As corrosion of the components of MCFC caused by the electrolyte proceeds with the electrolyte consumption, the corrosion in the MCFC is related to its performance and life. To understand and inhibit the corrosion in the MCFC is important to realize MCFC power generation system.

We have studied the effect of alkaline earth carbonate addition into carbonate on corrosion of type 316L stainless steel[1]. In this paper, we describe the effect of the temperature on corrosion behavior of type 316L stainless steel with carbonate mixture, $(Li_{0.62}K_{0.38})_2CO_3$, under the cathode environment in out-of-cell test.

2. Experimental

The commercially available type 316L stainless steel (SUS316L) sheet, which is 0.5 mm in thickness, was served as corrosion specimen. Its chemical composition is listed in table 1. The plate was cut into 10 x 20 mm, polished with wet #1000 abrasive paper, washed, degreased by acetone, rinsed with distilled water, and dried. Reagent grade Li_2CO_3 and K_2CO_3, which purity was > 99.0% and > 99.5%, respectively, were served for preparation of mixed carbonate. Mixed carbonate composed of Li_2CO_3 : K_2CO_3 = 62 : 38 (mol%) was melted at 650 °C under pure CO_2 environment, quenched and ground prior to coating. Specimens were coated with the mixed carbonate of 5 mg/cm^2 and hung in an alumina crucible. Corrosion test was carried out under the ambient cathode environment (CO_2/O_2 = 2/1) at 600, 650, 700 °C in out-of-cell. After the corrosion test, weight gain due to corrosion was measured by removing carbonate. In order to investigate the corrosion behavior, tested corrosion specimens after removing deposit by distilled water were analyzed by X-ray diffraction (XRD) and electron probe micro-analysis (EPMA).

3. Results and discussion

Results of weight gain due to the corrosion with time at various temperatures are shown in Figure 1. Though Cr was only detected in all the melts after the test as the element dissolved from the specimen, the amount of dissolved Cr was negligibly small. The weight of all the specimens increases with increasing time in the range from 25 to 500 hours and increasing temperature in the range of 600 to 700 °C. In these ranges, all the weight gains with time follow parabolic rate equation :

$$x^2 = k_p \cdot t$$

where x is the weight gain (mg), k_p the parabolic rate constant (mg^2/h), and t the time exposed (h). These results indicate the corrosion behavior is controlled by diffusion. Hot corrosion cannot be observed in the test at the temperature in the range of 600 to 700 °C.

Results of XRD show that corrosion products on all specimens were identified as lithium ferrite, such as $LiFeO_2$, and $LiCrO_2$. Though no potassium compound was found in the solid corrosion products, K_2CrO_4 were identified in the deposit tested by XRD. Results of EPMA show that corrosion products on all specimens consist of two layer structure, Fe rich oxide as an outer layer and Cr rich oxide as an inner layer. Lithium in the carbonate melt reacts with iron and chromium in the specimen and is fixed in the corrosion products of solid phase. On the other hand, potassium reacts chromium and still exists in the carbonate deposit of liquid phase.

Reference

1. M. Yanagida, S. Baba, K. Tanimoto, T. Kojima, N. Ohtori, Y. Tamiya, T. Asai, Y. Miyazaki and M. Azuma, *DENKI KAGAKU*, **64**, 542 (1996).

Table 1. Chemical composition in wt% of type 316L stainless steel used.

C	P	S	O	N	Si	Mn	Mo	Ni	Cr	Fe
0.022	0.029	0.010	0.0060	0.0262	0.65	1.01	2.14	12.01	17.02	Bal.(67)

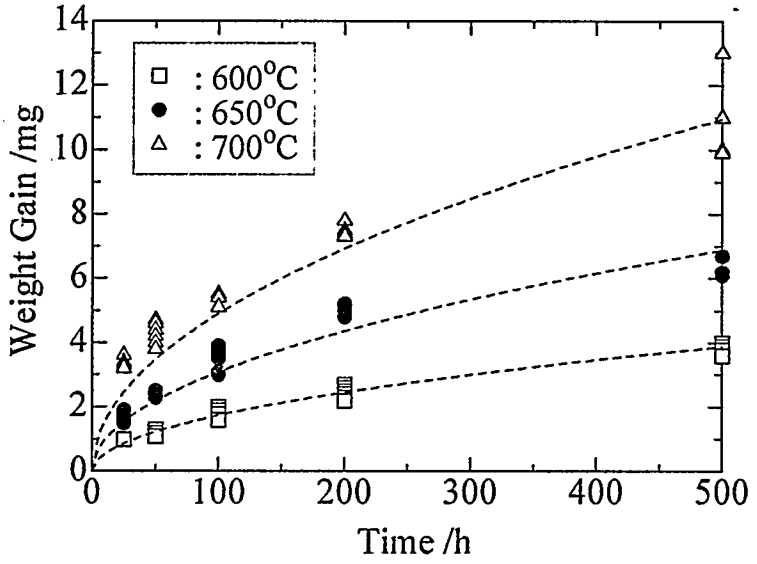

Figure 1: Relationship between weight gain and test duration with 5 mg/cm^2 of molten carbonate, $(Li_{0.62}K_{0.38})_2CO_3$, under 67% CO_2 - 33% O_2 at various temperatures.

PHYSICAL PROPERTIES OF MOLTEN CARBONATE ELECTROLYTE

T. KOJIMA, M. YANAGIDA, K. TANIMOTO, Y. TAMIYA,
T. ASAI, and Y. MIYAZAKI
Osaka National Research Institute
Midorigaoka 1-8-31, Ikeda City, Osaka 563, Japan

1.Introduction

Recently many kinds of compositions of molten carbonate electrolyte have been applied to molten carbonate fuel cell in order to avoid the several problems such as corrosion of separator plate and NiO cathode dissolution. Many researchers recognize that the addition of alkaline earth (Ca, Sr, and Ba) carbonate to Li_2CO_3-Na_2CO_3 and Li_2CO_3-K_2CO_3 eutectic electrolytes is effective to avoid these problems[1]. On the other hand, one of the corrosion products, CrO_4^{2-} ion is found to dissolve into electrolyte and accumulated during the long-term MCFC operation[2]. This would affect the performance of MCFC.

There, however, are little known data of physical properties of molten carbonate containing alkaline earth carbonates and CrO_4^{2-}. We report the measured and accumulated data for these molten carbonate of electrical conductivity and surface tension to select favorable composition of molten carbonate electrolytes.

2.Electrical conductivity

Electrical conductivity would directly affect the output of MCFC in the form of IR loss. The electrical conductivity of molten carbonate was measured using AC two probe technique[3].

The addition of alkaline earth carbonate resulted in decrease of the conductivity linearly with mole fraction of additives. The linear relationship between mole fraction of alkaline earth carbonate and conductivity makes it easy to calculate the conductivity of ternary mixture of Li-Na-alkaline earth and Li-K-alkaline earth from the data of alkali binary carbonate systems as shown in Fig. 1, as an example for $SrCO_3$ addition. These decrease of conductivity by the addition of alkaline earth carbonate may be due to the exchanging conductive alkali cations with less conductive alkaline earth cations, which strongly attract carbonate ions by their double charge.

Molten Li_2CO_3-Na_2CO_3(52:48mol%) added with alkaline earth carbonate by 10 mol% show about 1.3 times higher electrical conductivity than that of conventional molten Li_2CO_3-K_2CO_3 (62:38mol%) electrolyte at 923K. These electrolytes are promising from the viewpoints of not only low solubility of NiO[1], but also higher conductivity.

The addition of CrO_4^{2-} to Li_2CO_3-Na_2CO_3(52:48mol%) and Li_2CO_3-K_2CO_3(62:38mol%) by 3 and 5 mol% was found to decrease the electrical conductivity of mixture as shown in Fig.2, and show less influence upon the conductivity of these mixtures than that of alkaline earth carbonate. Because the addition of CrO_4^{2-} is only exchange less conductive carbonate ion with CrO_4^{2-}.

3.Surface tension

Surface tension would have influence upon gas-electrode reaction site and distribution of electrolyte among the cell components. The surface tension of molten carbonate was measured using maximum bubble pressure technique. The addition of alkaline earth carbonates into any of alkali (Li, Na and K) carbonate and their mixture resulted in the increase of surface tension of mixtures as shown in Fig.3. It is also because of double charged small alkaline earth cations attract carbonate ion stronger than alkali cations.

In the case of CrO_4^{2-} addition, it makes the surface tension of mixture lower as shown in Fig 4. The reason for the decrease of surface tension of mixtures is that larger CrO_4^{2-} ion should have weaker coulombic force than carbonate ion.

4.Conclusion

- The addition of all alkaline earth carbonate to alkali carbonate resulted in increase of the surface tension and decrease of the electrical conductivity of mixtures.
- The addition of CrO_4^{2-} to alkali carbonate resulted in decrease of both surface tension and electrical conductivity of mixtures.
- Molten Li_2CO_3-Na_2CO_3(52:48mol%) added with alkaline earth carbonate is promising from the viewpoint of higher electrical conductivity than conventional molten Li_2CO_3-K_2CO_3 (62:38mol%) electrolyte.

5.Reference

1) K. Tanimoto, Y. Miyazaki, M. Yanagida, S. Tanase, T. Kojima, N. Ohtori, H. Okuyama and T. Kodama, *Denki Kagaku*, 63, 316 (1995).

2)H. Kasai, Y. Hayakawa, H Ukai and S. Yajima, *Denki Kagaku*, 64, 526 (1996).

3) Y. Miyazaki, M. Yanagida, K. Tanimoto, T. Kodama and S. Tanase, *J. Electrochem. Soc.*, **133**, 1402, (1986).

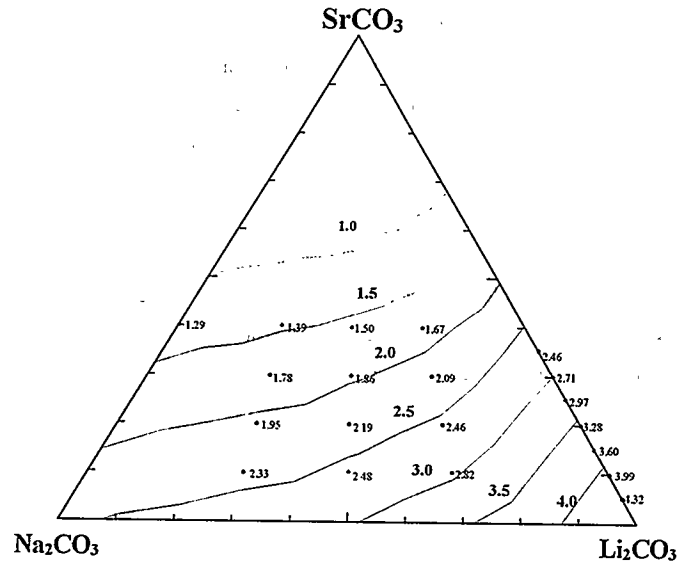

Fig.1 Conductivity (Scm^{-1}) of Li_2CO_3-Na_2CO_3-$SrCO_3$ ternary molten carbonate mixtures at 1073K and calculated contour curves.

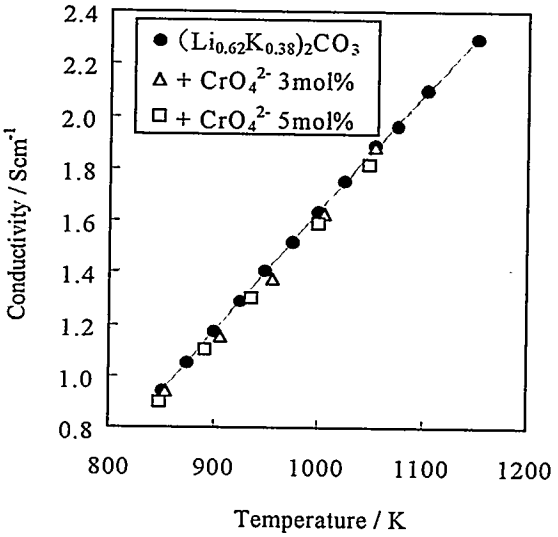

Fig.2 Temperature dependence of electrical conductivity of molten Li_2CO_3-K_2CO_3 (62:38mol%) with/without CrO_4^{2-}.

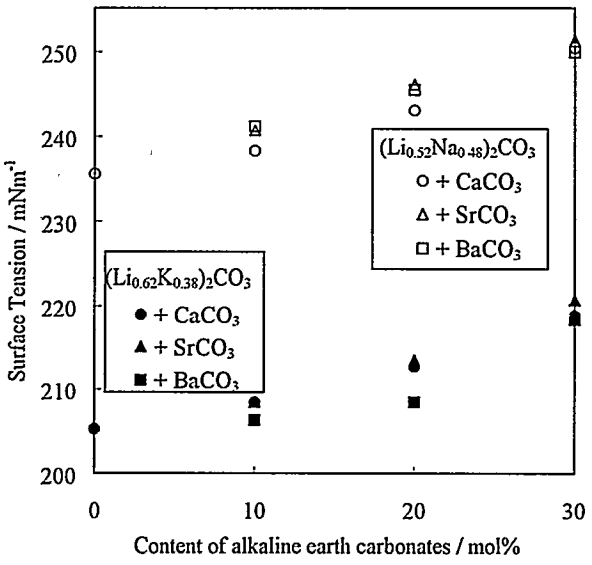

Fig.3 The surface tension of Li_2CO_3-Na_2CO_3 (52:48mol%) and Li_2CO_3-K_2CO_3 (62:38mol%) containing alkaline earth (Ca, Sr and Ba) carbonates at 923K.

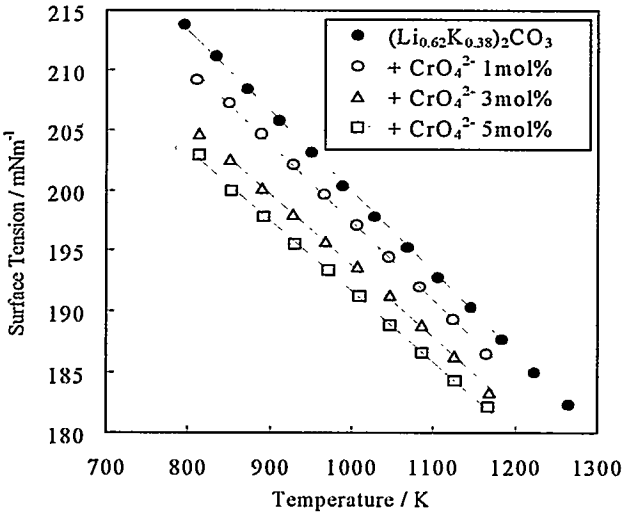

Fig.4 Temperature dependence of surface tension of Li_2CO_3-K_2CO_3 (62:38mol%) with/without containing CrO_4^{2-}.

HIGH POWER DENSITY CARBONATE FUEL CELL

C. Yuh, R. Johnsen, J. Doyon and J. Allen
Energy Research Corporation
3 Great Pasture Road
Danbury, CT 06813, U.S.A.

Carbonate fuel cell is a highly efficient and environmentally clean source of power generation. Many organizations worldwide are actively pursuing the development of the technology. Field demonstration of multi-MW size power plant has been initiated in 1996 (1), a step toward commercialization before the turn of the century. Energy Research Corporation (ERC) is planning to introduce a 2.85MW commercial fuel cell power plant with an efficiency of 58%, which is quite attractive for distributed power generation. However, to further expand competitive edge over alternative systems and to achieve wider market penetration, ERC is exploring advanced carbonate fuel cells having significantly higher power densities. A more compact power plant would also stimulate interest in new markets such as ships and submarines where space limitations exist. The activities focused on reducing cell polarization and internal resistance as well as on advanced thin cell components.

APPROACHES

Cathode and anode polarizations are major voltage loss contributors in a carbonate fuel cell. According to literature (2), the anode polarization is mainly caused by diffusional mass transfer limitation in the pores. The cathode polarization is mixed activation and concentration polarization. Gas accessibility limitation caused by current collector geometry (3) also contribute to the concentration polarization. A mathematical model has recently been used to estimate electrode polarization as a function of electrode porosity, thickness and current collector geometry. Performance data of several 250cm^2 cells were used for model verification. The estimated cathode polarization is about 70 mV for ERC's baseline cathode and cathode current collector, using 5NRS oxidant (12.5%O_2,19.1%CO_2) at 75% CO_2 utilization and 160 mA/cm^2. The modeling results also indicated that gas-phase diffusional polarization (both in-plane and through-plane, as shown in Figure 1, is an important contributor. This conclusion is also verified by diagnostic testing using He carrier gas (3). Therefore, using thinner cathode and adjusting current collector geometry to increase gas accessibility are expected to reduce cathode polarization. Furthermore, the anode polarization was estimated to be >30 mV, using SRNG fuel (73% H_2, 18%CO_2 and 9% H_2O) at 75% fuel utilization and 160 mA/cm^2. Therefore, there may be an additional opportunity of reducing anode polarization by increasing gas accessibility in the porous anode structure. Based on this model simulation, a new current collector design was developed to enhance gas accessibility.

A thinner matrix allows reduction of ionic resistance and increase of power density. However, it requires a high strength to withstand the stress associated with thin component design for compact cells. An advanced robust matrix was developed recently (4). It has significantly increased strength compared to the baseline. With such a matrix, the use of thin components becomes feasible.

Another approach for increasing power density is to use a monolithic cell design. In this design the bipolar plate is dimpled (Figure 2). The active components are manufactured as thin tapes. The perforated anode and cathode current collectors are also dimpled. Since the green tapes are pliable, the components in this assembly are in intimate contact. Therefore, the monolithic design allows using thin flexible components and less number of cell hardware. Due

to the monolithic structure, additional active area is available for current generation. Because of the higher stress associated with the thin-component monolithic design, the use of the robust matrix discussed above is essential.

CELL TESTING

Several thin-component 250cm^2 single cells (planar or monolithic) incorporating advanced matrix and current collector design have been operated. Using a thin robust matrix has reduced cell ohmic resistance by more than 15 mV at 160 mA/cm^2. Figure 3 shows a comparison between constant utilization polarization of planar thin- and normal-thickness matrix designs, showing about 25 mV performance improvement at 160 ma/cm^2 under ERC's standard SRNG/5NRS condition. Using the advanced anode current collector design, about 20-25 mV performance improvement was recorded at 160 mA/cm^2 under same test condition. However, using the advanced current collector design on the cathode side, only a few mV performance improvement can be realized for the normal thickness cathode, predictable by the model simulation. Therefore, for achieving additional cathode performance, a thinner cathode may be desired. In summary, at least 40mV performance improvement can be achieved with the above approaches. Figure 4 shows much increased performance with monolithic cell design, indicating the potential of 400 mA/cm^2 operation. This enhanced performance can be attributed to not only the reduced mass transfer resistance (thinner cathode and special current collector design) but also the additional active area for power generation.

CONCLUSION

Several approaches has been evaluated to enhance performance and power density of carbonate fuel cells. Diffusional mass transfer resistance can be reduced by using thinner electrodes and by enhancing gas accessibility. Thin robust matrix can be used for reducing ionic resistance without compromising gas sealing efficiency. At least 40 mV performance enhancement can be expected by using the above approaches in combination. These improvements need to be translated in commercial-scale hardware.

ACKNOWLEDGEMENT

This effort was supported by the U.S. Department of Energy under Contracts DE-FC21-95MC31184, DE-FG05-93ER81510 and DE-FG05-93ER81512.

REFERENCES

1. A.L. Leo, "Santa Clara Demonstration Status," Proc. Advanced Fuel Cells '96 Review Meeting, Morgantown Energy Technology Center, WV, August, 1996.
2. C. Yuh and J.R. Selman, "Polarization of Molten Carbonate Fuel Cell Electrodes, II. Characterization by AC Impedance and Response to Current Interruption," J. Electrochem. Soc., Vol. 138, No. 2, pp. 3649-3656, December, 1991.
3. H.R. Kunz and L.A. Murphy, "The Effect of Oxidant Composition on the Performance of Molten Carbonate Fuel Cells," J. Electrochem. Soc., Vol. 135, No. 5, pp. 1124-1131, May, 1988.
4. C. Yuh, C. Huang and R. Johnsen, "Carbonate Fuel Cell Matrix Strengthening," Proc. Advanced Fuel Cells '96 Review Meeting, Morgantown Energy Technology Center, WV, August, 1996.

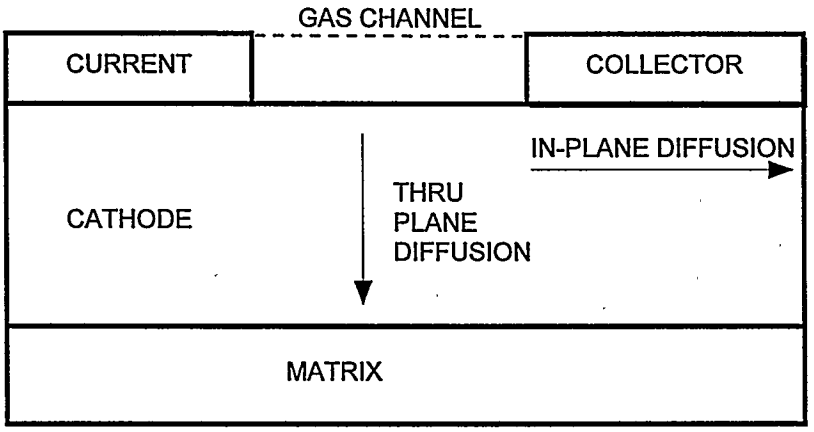

Figure 1. GAS DIFFUSION IN FUEL CELL ELECTRODE:
Both In-plane and Through-plane Diffusion Influence Electrode Performance.

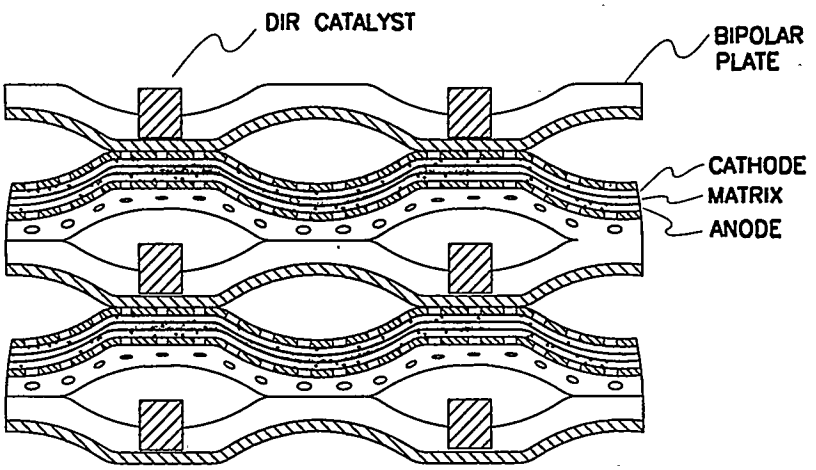

Figure 2. CROSS-SECTIONAL VIEW OF MONOLITHIC FUEL CELL:
Thin Flexible Components Can Be Used in This Design.

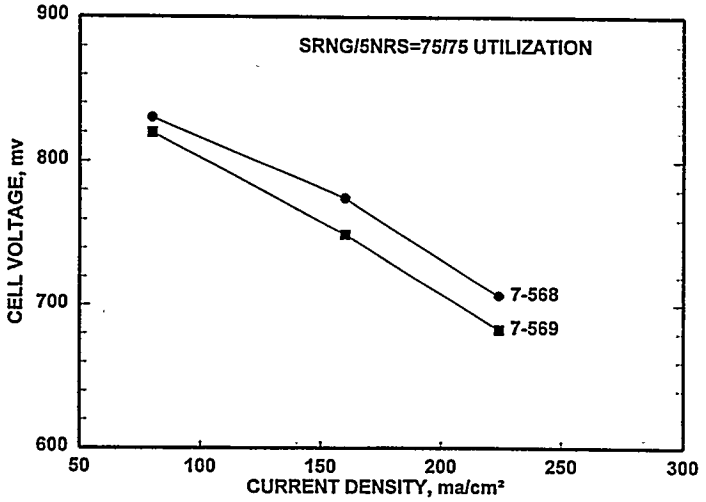

FIGURE 3. CELL PERFORMANCE WITH DIFFERENT MATRIX THICKNESSES: A Thin Matrix in 7-568 Improves Cell Performance by More Than 15 mV.

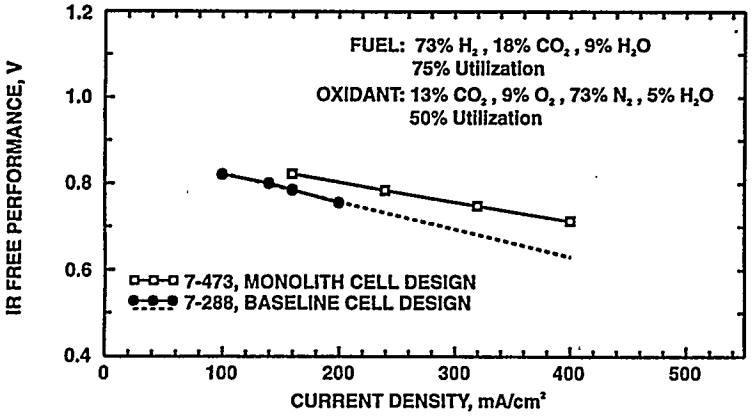

FIGURE 4. HIGH CURRENT DENSITY OPERATION OF MONOLITHIC FUEL CELL: Increased Cell Performance Demonstrated with Thin-Component Monolithic Design.

PRESENT STATUS OF SOME TECHNOLOGICAL ACTIVITIES SUPPORTING THE MOLCARE PROJECT

A. Torazza[o], G. Rocchini[■], M. Scagliotti[•]
[o]Ansaldo Ricerche S.r.l., Corso Perrone 25, I-16161 Genova
[■]ENEL S.p.A. - CRAM, Via Rubattino 54, I-20134 Milano
[•]CISE S.p.A., P.O. Box 12081, I-20134 Milano

Introduction

The development of MCFC stack technology is carried out at Ansaldo Ricerche in the framework of the MOLCARE project (1), a cooperation with Spanish companies under a partial UE funding, while a specific research program concerning the physico-chemical characterization of materials is performed jointly by CISE and ENEL (2). The project includes the development, the construction and the testing of a full scale 100 kW prototype, the assessment of stack technology on subscale stacks, the mathematical modelling of the MCFC based plants and the basic researches. The aim of the basic researches, carried out on single cells, is to improve the effectiveness and durability of both the active and the hardware materials.

The Ansaldo stack technology is based on external manifolding. The full scale 100 kW prototype will be integrated with the sensible heat reformer and other ancillary equipments according to the "Compact Unit (CU)" concept (1). These technical choices stress requirements for manifold gasket configuration, electrolyte migration control, Δp management and porous component compaction.

Stack Technology

The present MCFC technology under development at Ansaldo Ricerche makes use of a green electrolyte matrix, of a nickel cathode, which is oxidised and lithiated in situ during the start up cycle, and of a nickel-chromium anode. A proprietary methodology is used to accomodate proper quantities of lithium and potassium carbonates in each cell.

Subscale stacks having the same active area and an increasing number of cells have been fabricated and operated in the last three years. In particular two stacks of 15 cells with active area of 702 cm^2 were tested at atmospheric pressure at CISE for more than 1600 and 1800 hours of hot time respectively (3). In the latter stack the manifold sealings and electrolyte matrix impermeability to process gases were significantly improved.

In 1996 a stack of 50 cells with the same active area was tested for more than 750 hours of hot time using the Ansaldo Ricerche pressurized facility (fig. 1).

At the end of the start up cycle an average OCV of 1042 $\pm$ 5 mV was noticed at approximately 600 °C (fuel: 25%H_2-9%CO_2-11%H_2O-55%N_2; oxidant: 86%air-14%CO_2). During the operation at atmospheric pressure most of the cells reached the expected performance of 740 mV at a current density j = 158 mA/cm^2 with the fuel utilization U_f = 40%. This cell performance should correspond to a stack power output of 4.1 kW. However, the power output of about 4 kW was obtained, but at 206 mA/cm^2 with U_f = 50% (fig. 2), due to the anomalous behavior of some bottom cells. The stack power output P(j) measured after 600 hours of hot time is shown in fig. 2 together with the voltage V(j) of the cell n. 30 starting from the bottom, which is representative of the average behavior of the properly operating cells.

Gaschromatographic analyses were performed at regular intervals on the process gases and did not evidence cross-over phenomena through the electrolyte matrices.

Post test analyses are now in progress mainly to get information about the electrolyte sharing among the cells and the porous components, and also about the electrode compaction.

In parallel a great effort was devoted to set up the facilities for the fabrication of porous repeat parts (1100 mm width continuous tape casting) and metallic components. A full scale stack assembling area under controlled atmosphere was also set up at Ansaldo Ricerche. The first stack of 20 cells having a useful area of 6760 cm^2 is under construction. It will be tested within the end of this year.

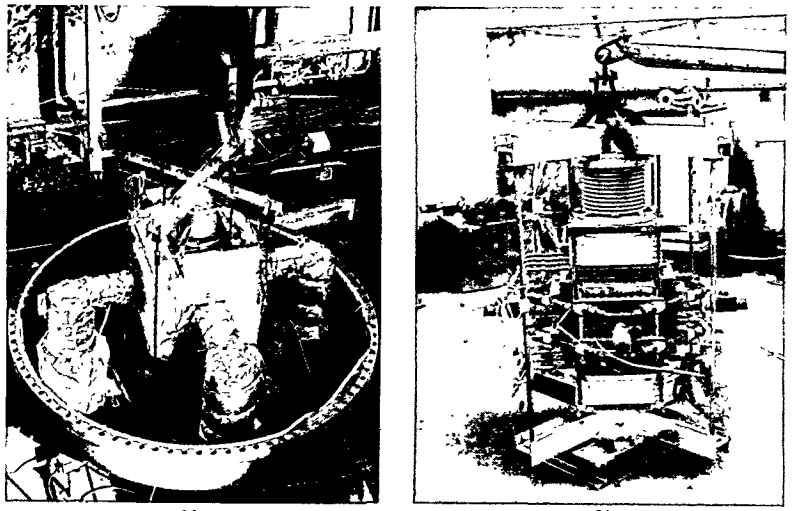

(a) (b)

Fig. 1 - The 50-cell stack tested at the pressurized Ansaldo Ricerche facility in 1996: (a) at the test facility, (b) after thermal insulation removal.

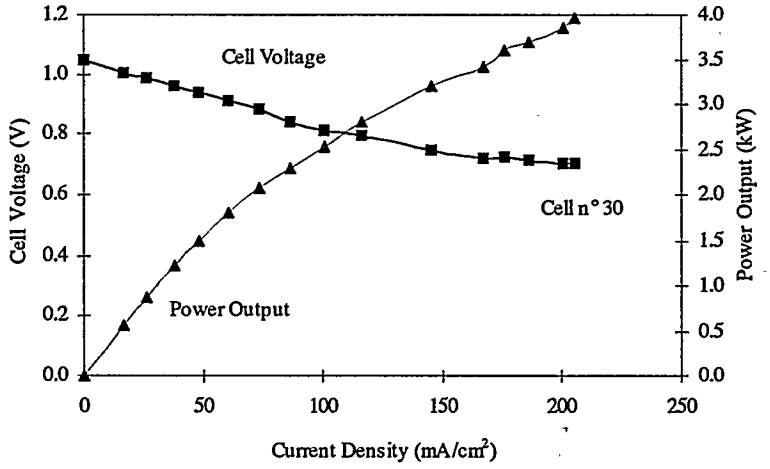

Fig. 2 - Behavior of P(j) and V(j) measured after 600 hours of hot time (U_f= 50% at 206 mA/cm^2) on the 50-cell stack tested at Ansaldo Ricerche facility in 1996.

Bench-scale Single Cell Testing

The basic activities on standard bench-scale single cells are currently being carried out at Ansaldo Ricerche and CISE. Tests of a few thousands hours are performed at atmospheric pressure and in pressurized conditions using square cells having an active area of approximately 50 cm^2. The aim of this experimental program is to optimize porous electrodes and to test protective coatings on current collectors and housing components.

The cells are fed with fuel and oxidant gas compositions similar to those planned for the next full scale stacks and in particular for the first stack of 20 cells of 6760 cm^2.

In the standard conditions of testing (fuel: 35%H_2-23%CO_2-42%H_2O; oxidant: 86%air-14%CO_2; U_{H2}=U_{CO2}=60% at 150 mA/cm^2) cell voltages of 700-710 mV were obtained at 150 mA/cm^2 (fig. 3). When using a 52%H_2-13%CO_2-35%H_2O fuel and a 70%air-30%CO_2 oxidant (U_{H2} = U_{CO2} = 40%) cell voltages exceeding 800 mV were obtained at 150 mA/cm^2 with the present component technology.

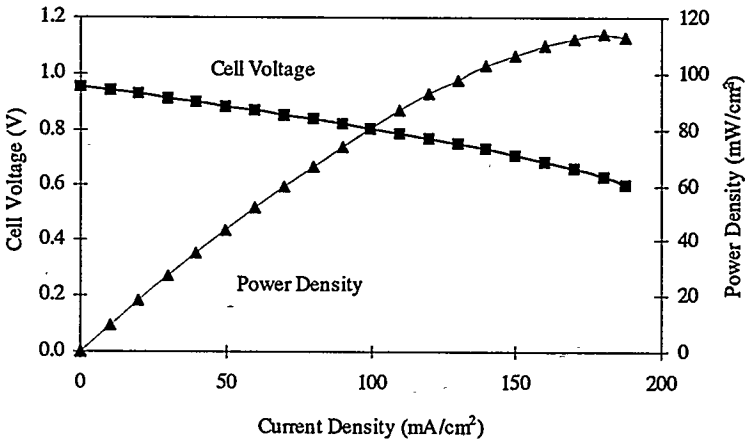

Fig. 3 - Behavior of cell voltage and power density as a function of the current density measured after 277 hours of hot time on the ARI-X33 cell fed with 35%H_2-23%CO_2-42%H_2O fuel and 86%air-14%CO_2 oxidant (U_f = 57% at 150 mA/cm^2).

Materials Characterization

Both the porous electrodes and the protective coatings are characterized before and after the tests in stacks and single cells. This important task is mainly carried out, under the ENEL coordination, at CISE where different diagnostic tools are available including mercury porosimetry, helium pycnometry, electron microscopy, X-ray diffraction, Auger and X-ray photoelectron spectroscopies. At present, the main effort is focused on the careful evaluation of the morphological properties of porous repeat parts, because of their influence on electrolyte sharing and on cell performance.

The combined use of mercury porosimetry, helium pycnometry and SEM image analyses provides useful data to improve the quality and the homogeneity of full scale porous components. Also the chromium distribution in Ni-Cr anodes is under study in order to increase their mechanical stability. Satisfactory results were obtained on nickel coated anodic current collectors and aluminized bipolar plates. The behavior of the shielded slot type anodic current collector made from Ni/AISI310/Ni threelayer was satisfactory both in stack and in single cell runs. Similarly, the effectiveness of the protective coatings in the wet seal area of bipolar plates was demonstrated by the SEM-EDS analyses of the samples of the subscale stacks.
More recently, the experimental methods for the determination of the electrolyte content and the sharing of the electrolyte among the different porous components (anode, matrix and cathode) were set up. Preliminary data have been obtained on the 15-cell stack operated at CISE in 1995 and on the 50-cell stack operated at Ansaldo Ricerche in 1996. These results are useful in order to define proper solutions for the electrolyte management in full scale stacks with external manifolding.

Conclusions

The scaling up approach of the Ansaldo stack technology and the basic research activities on bench-scale cells and material characterization provided satisfactory results.
Some problems faced in the initial phase of cell and stack development were overcome. The new technology is promising because the cell performance is in agreement with literature data.
Finally, further efforts are needed to improve the homogeneity of the cell performance as well as the component stability and durability, even if our data show that cell power densities are already consistent with the final goal of the full scale 100 kW prototype.

Acknowledgements

The authors thank ENEA, Babcok Wilcox Española, Iberdrola, Fabbricazioni Nucleari and International Fuel Cells for their useful technical contributions.

References

1. M. Brossa, A. Dufour, E. Hermana, J. F. Jimenez, F. Sanson, "The European MOLCARE program: a 100 kW demonstrative plant and engineering development of the MCFC technology", 1994 Fuel Cell Seminar, San Diego, p. 238.
2. G. Rocchini, M. Scagliotti, A. Torazza, "Technological and basic activities on MCFC", 1994 Fuel Cell Seminar, San Diego, p. 573.
3. P. Araldi, L. Bigoni, A. Colombo, F. Gariboldi, B. Passalacqua, P. Savoldelli, M. Zappaterra, "Assessment of MCFC stack technology in Italy", 1994 Fuel Cell Seminar, San Diego, p. 570.

PERFORMACE OF NEW 10 kW CLASS MCFC USING Li/K AND Li/Na ELECTROLYTE

Yoshihiro Mugikura, Fumihiko Yoshiba, Yoshiyuki Izaki, Takao Watanabe
Central Research Institute of Electric Power Industry
2-6-1 Nagasaka, Yokosuka-shi, Kanagawa-ken 240-01 Japan
Koh Takahashi, Sei Takashima, and Toshiki Kahara
Hitachi Works, Hitachi, Ltd.
3-1-1 Saiwaicho, Hitachi-shi, Ibaraki-ken, 317 Japan

1. INTRODUCTION

The molten carbonate fuel cell (MCFC) uses generally mixture of lithium carbonate and potassium carbonate (Li/K) as the electrolyte, NiO cathode dissolution is one of serious problems for MCFC life [1]. The NiO cathode has been found to dissolve into the electrolyte as Ni^{2+} ion which is reduced to metallic Ni by H_2 in the fuel gas and bridges the anode and the cathode. The bridges short circuit and degrade cell performance and shorten cell life. Since solubility of NiO in mixture of lithium carbonate and sodium carbonate (Li/Na) is lower than in Li/K, it takes longer time to take place shorting by NiO cathode dissolution in Li/Na compared with in Li/K. The ionic conductivity of Li/Na is higher than of Li/K, however, oxygen solubility in Li/Na is lower than in Li/K. A new 10 kW class MCFC stack composed of Li/K cells and Li/Na cells, was tested. Basic performance of the Li/K cells and Li/Na cells of the stack was reported.

2. EXPERIMENTAL

The stack consisted of 26 cells. The cell area was 2520 cm^2. The electrolyte of six cells, which were located at top of the stack, was $Li/NaCO_3$ (Li/Na=53/47 mol %). Other cells used Li/KCO_3 (Li/K=62/38 mol %). The weight of the separator plate was lighter than of the conventional plates since the separator plate consisted of thin stainless steel plates. Gas follow pattern was cross flow type. In the operation, the maximum temperature in the stack was kept lower than 680 ^0C. The stack was installed in the test facility of CRIEPI, after the initial performance check of the stack with heating up and cooling down processes at Hitachi Works site. The stack was operated at 3 - 7 ata. No gas recycling such as cathode gas recycling was applied.

3. RESULTS

Figure 1 shows effect of pressure on cell performance. The cell performance of Li/Na is lower than of Li/K at 3 ata. However, pressure gain of Li/Na cell is larger than of Li/K cell and is approximately two times larger than of Li/K cell. This pressure gain agrees with the result of small single cell [2]. The maximum output voltage of Li/Na cell is higher than of Li/K cell at pressures higher than 5 ata. Each cell performance of the stack was analyzed by the following new method [3]. Output voltage (V) is determined by following equation using open circuit voltage (E) and

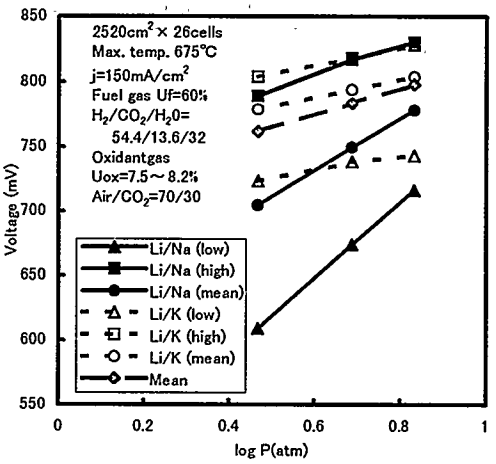

Fig. 1 Effect of pressure on cell performance

Nernst loss (η_{NE}) if anode reaction resistance (R_a), cathode reaction resistance (R_c) and internal resistance (R_{ir}) are propotional to current density (j).

$$V = E - \eta_{NE} - j(R_a + R_c + R_{ir}) \quad (1)$$

E and η_{NE} are calculated using single cell performance model [4]. 650 ^{0}C is assumed as the representative stack temperature in the calculation. In addition, R_{ir} observed at approximately 600 ^{0}C is compensared using the representative temperature. Temperature in the stack is actually not uniform. However, $R_a + R_c$ of each cell of the stack is able to be calculated with good accuracy since $E - \eta_{NE} - jR_{ir}$ in Eq. (1) is changed only within 10 mV by temperature change of 70 ^{0}C since increment of temperature increases $E - \eta_{NE}$ but decreases jR_{ir}. R_a is approximately constant if the fuel gas is reformed LNG [5]. Furthermore, R_c is given by following equation, even if cathode gas composition is changed, since cathode polarization is controlled by super oxide ion and CO_2 diffusion [5].

$$R_c = AP_{O_2}^{-0.75}P_{CO_2}^{0.5} + BP_{CO_2}^{-1} \quad (2)$$

The stack was tested with several cathode gas compositions. $R_a + R_c$ of each cell of the stack was calculated using Eq. (1). Parameter A. B and R_a were determined from dependence of the cathode gas composition. As a result, voltage drops by R_{ir}, R_a and R_c were separated.

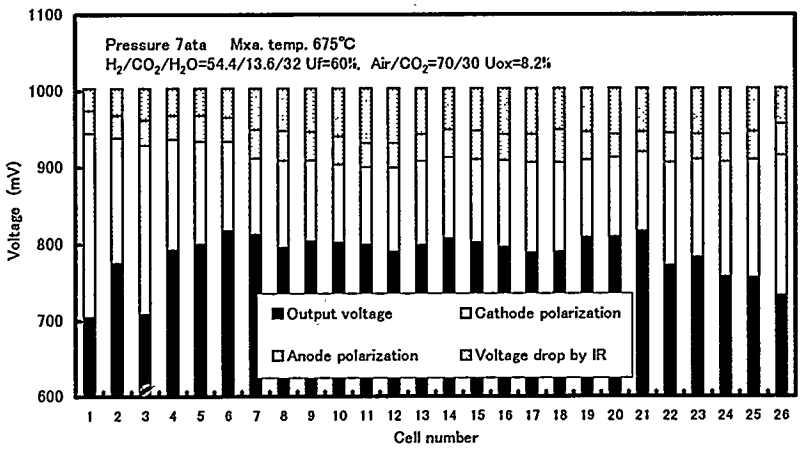

Fig. 2 Analyzed result of each cell performance.

Figure 2 shows analyzed result of each cell performance of the stack. Nernst loss is not shown. Voltage drops by R_{ir} of Li/Na cells (No. 1 - 6) are almost half of these of Li/K cells (No. 7 - 26) since the ionic conductivity of Li/Na is approximately two times larger than of Li/K. Cathode polarizations located top and bottom of the stack are large since temperatures of these cells are lower than of middle cells. Cathode polarization of Li/Na cell (No. 6) is approximately equal to of Li/K cells (No. 7 - 21). Good performance of Li/Na cell at 7 ata is brought by low cathode polarization and low voltage drop by R_{ir}. Anode polarization analyzed by this method agrees with the result of single cell test. The method can analyze each cell performance of the stack with good accuracy.

Figure 3 shows relationship between cell voltages and parameter A. Circles indicate measured cell voltages and squares indicate cell voltages compensated using R_{ir}. There is a obvious relationship between compensated cell voltage and parameter A. Based on the result, it can be

said cell voltage is controlled by parameter A relating to diffusion of super oxide in the electrolyte under this condition. Diffusion of super oxide plays an important roll in the cathode polarization. At lower CO_2 partial pressure, effect of parameter B relating to CO_2 diffusion would be larger. The result suggested that thickness of electrolyte film on the cathode of low performance cell is thicker than of high performance cell or that actual effective cell area for cathode reaction of low performance cell is smaller than of high performance cell.

Figure 4 shows history of the stack performance. Initial stack performance such as pressure gain and fuel utilization characteristics, was measured before 500 h. Since then, the stack has been operated under constant condition. Operation pressure was 7 ata. Cathode gas composition was Air/CO_2=80/ 20 since high CO_2 partial pressure accelerates shorting by NiO cathode dissolution. Both Li/K and Li/Na cells showed stable performance until 1400 h. However, Li/K mean cell voltages began to drop after 1400 h. Shorting by NiO cathode dissolution is assumed to be a cause for dropping of voltage. Anode inlet and outlet gas compositions have been usually analyzed by the gas chromatography in parallel with the operation. Fuel consumption by cell reaction , combustion and methanation was calculated with mass balance between anode inlet and outlet gas compositions. Shorting current density was

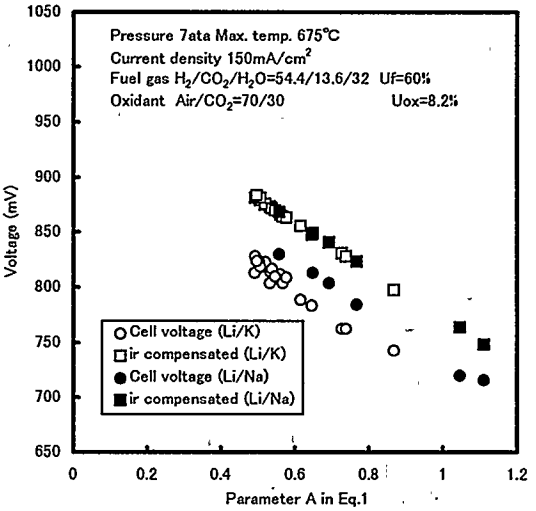

Fig. 3 Relationship between cell voltage and parameter A.

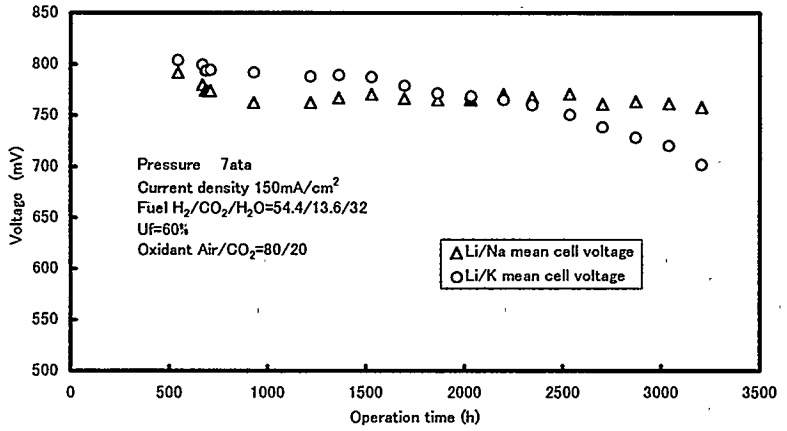

Fig. 4 History of stack performance

calculated from difference between set current density and calculated fuel consumption by cell reaction.

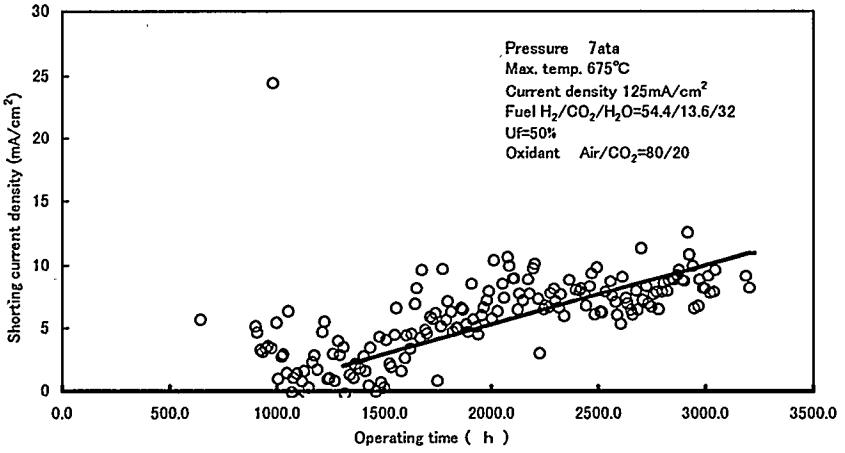

Fig. 5 Shorting current by NiO cathode dissolution

Figure 5 shows history of calculated shorting current density. Short current density began to increase at 1400 h and then gradually increased with operation time. This result agrees with the measured voltage history in Fig. 4. The shorting current would be caused by NiO cathode dissolution. The measured shorting time shows a good agreement with the time calculated by empirical equation [1]. Ni contents of Li/K cells at 1400 h calculated by data of single cells are enough to occur the shorting [6]. However, Ni contents of Li/Na cells are lower than of Li/K cells since NiO solubility of Li/Na is lower than of Li/K.

4. Conclusions

- Each cell performance of the stack is able to be analyzed by new performance analysis method with good accuracy.
- Voltage drop by R_{ir} of Li/Na cell is approximately half of that of Li/K cell from the analysis.
- Diffusion of super oxide and CO_2 plays an important roll in the cathode polarization. It is suggested that thickness of electrolyte film on the cathode of low performance cell is thicker than of high performance cell or that actual effective cell area for cathode reaction of low performance cell is smaller than of high performance cell.
- Shoring by NiO cathode dissolution would take place in Li/K cells at 1400 h. The shorting time agreed with estimated value by empirical equation.

References

(1) Y. Mugikura, T. Abe, S. Yoshioka and H. Urushibata, *J. Electrochem. Soc.* 142, 2971 (1995)
(2) M. Yoshikawa, F. Yoshiba, H. Morita, T. Abe, M. Yamaguchi and K. Iwamoto, The second FCDIC Fuel Cell Symposium Proceedings 289(1995)
(3) Y. Mugikura, H. Morita, Y. Izaki and T. Watanabe, submitted to The 37th Battery Symposium in Japan (1996)
(4) Y. Mugikura, T. Abe, T. Watanabe and Y. Izaki, *Denki Kagaku*, 60, 124 (1992)
(5) H. Morita, Y. Mugikura, Y. Izaki, T. Watanabe and T. Abe, *Denki Kagaku* 63,1053 (1995)
(6) Y. Mugikura, M. Yoshikawa, Y. Izaki and T. Watanabe, , The second International Fuel Cell Conference Proceedings 169 (1996)

Electrolyte Loss In Corrosion of 30Cr-45Ni-1Al-0.03Y-Fe Alloy for MCFC Separator

Katsumi Masamura, Koichiro Ohe, Masahiro Takemura
Materials and Processing Research Center, NKK Corporation
1-1 Minami-Watarida, Kawasaki-ku, Kawasaki, 210 Japan

Introduction

To establish high performance of MCFC, a new high corrosion resistant alloy (30%Cr-45%Ni-1%Al-0.03%Y-Fe) for MCFC separator has been developed[1][2][3][4]. The developed alloy has good corrosion resistance for both anode and cathode environments. On the other hand, one of the main factors to determine the life time of MCFC stack is electrolyte loss. A potential danger of electrolyte loss cased by corrosion of metal components is pointed out. Basic mechanism of electrolyte loss is proposed according to following reactions.

$$Fe + Li^+ + 2CO_3^{2-} = LiFeO_2 + 2CO_2 + 4e^-$$

$$Cr + K^+ + 4CO_3^{2-} = K_2CrO_4 + 4CO_2 + 8e^-$$

High Cr content alloy such as type 310S(25%Cr-20%Ni) has disadvantages in view of electrolyte loss in spite of high corrosion resistance[5]. It is said that the dissolution of Cr ion into electrolyte is detrimental for electrolyte loss, because a mole of CrO_4^{2-} ion combines 2 moles of K^+ ions as K_2CrO_4, while a mole of Fe^{3+} ion combine a mole of Li^+ ion as $LiFeO_2$. To understand the mechanism of electrolyte loss due to corrosion of metal component, the distribution of metal ions in oxide and molten salt were studied.

Experimental

Two types of corrosion tests were conducted. Immersion test was used to determine dissolved metal ions in carbonate. Coating test was used simulating separator surface on which wetted by thin salt layer, to determine the distribution of metal ions in oxide and salt. Conditions of corrosion tests are listed in Table 1.

Four types of alloys (type 304: 18.1%Cr-8.3%Ni, 316L: 16.3%Cr-11.9%Ni-2.5%Mo, 310S: 24.8%Cr-21.4%Ni and the developed ally:30.1%Cr-44.9%Ni-1.0%Al-0.045%Y) were used.

Table 1 Conditions of corrosion test

	Immersion test	Coating method
Temperature	650℃	
Gas composition	30%CO_2-14%O_2-N_2 bal.	
Salt composition	62 mole %Li_2CO_3-38 mole %K_2CO_3	
Amount of Salt	40g	50mg·cm^2
Test duration	205h, 500h	1000h

After corrosion test, the soluble substances of salt were extracted by water and residuals were filtered from the solution. Metal ions (Li, K, Fe, Cr and Ni) of solution and residual were analyzed.

Results and discussion

Effect of Cr content on mass loss by immersion and coated tests are shown in Fig. 1. Mass loss after corrosion tests was reduced with high Cr content for all conditions tested. The developed alloy showed the highest corrosion resistance in both test methods.

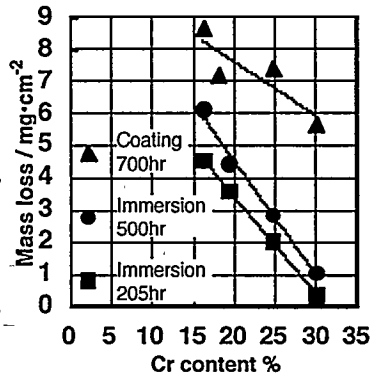

Fig. 1 Effect of Cr content on mass loss after immersion and coating test in molten carbonate at 650°C

Chemical analyses of salt after corrosion test are shown in Table 2 and Table 3. After immersion test, Cr was identified from salt and only a little amount of Fe and Ni were detected. No residuals were found in salt used for immersion test after extraction by water.

In soluble substance, a small amount of Fe and Ni was found but only Cr was identified as alloy element. On the other hand, in residuals, Fe and Ni were determined but Cr was not found for type 304, 316L and 30%Cr-45%Ni alloy. Only for type 310S Stainless steel, a little amount of Cr was identified. This result suggested

Table 2 Metal ion concentration in salt after 205 and 500 hours immersion test at 650°C(%, Original weight of salt was 40g respectively)

	205 hours					500 hours				
	Li	K	Cr	Fe	Ni	Li	K	Cr	Fe	Ni
304	9.10	30.1	0.006	0.002	0.002	9.39	33.8	0.006	0.002	0.002
316L	9.45	30.3	0.005	0.002	0.002	9.33	33.6	0.003	0.002	0.002
310S	9.37	29.6	0.004	0.002	0.002	9.70	32.8	0.010	0.002	0.002
30%Cr-45%Ni	9.05	39.8	0.004	0.002	0.002	10.5	35.4	0.006	0.002	0.002

Table 3 Metal ion ratio of soluble and insoluble substance in salt after coating test for 700 hours at 650°C (mole ratio)

	Soluble substance					Insoluble substance				
	Li	K	Cr	Fe	Ni	Li	K	Cr	Fe	Ni
304	0.29	0.55	0.16	0.0	0.0	0.57	0.0	0.0	0.40	0.02
316L	0.24	0.58	0.17	0.0	0.0	0.54	0.0	0.0	0.43	0.03
310S	0.35	0.24	0.41	0.0	0.0	0.46	0.0	0.04	0.41	0.10
30%Cr-45%Ni	0.37	0.20	0.43	0.0	0.0	0.44	0.0	0.0	0.47	0.10

Li+K+Cr+Fe+Ni=1.00

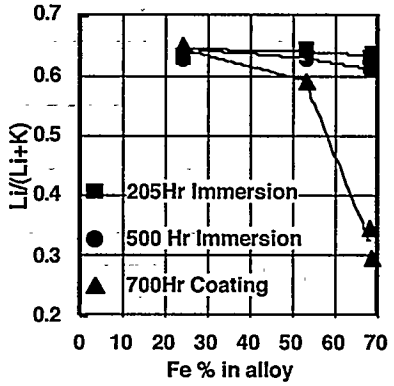

Fig. 2 Effect of Fe content of alloys on Li/(Li+K) ratio after corrosion tests.

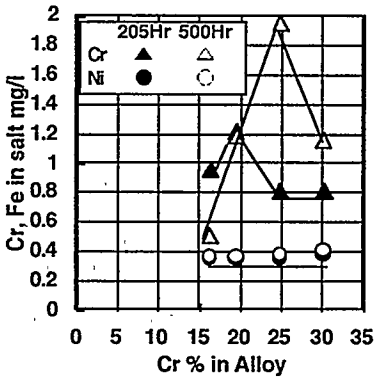

Fig. 3 Effect of Cr content on Cr dissolution into molten carbonate after 205 and 500 hour immersion test at 650°C

that soluble substance is mixture of carbonate and K_2CrO_4. The ratio of Li/Fe of residuals are from 0.94 to 1.42. This fact indicate that main part of insoluble substance is $LiFeO_2$. The insoluble substance was removed oxide formed on surface of materials.

Effect of Fe content in alloys on Li/(Li+K) in salt after corrosion test shown Fig. 2. Original value of this ratio is 0.62-0.64. After corrosion test, Li in salt on type 304 and 316L decreased, because Fe ion was formed solid $LiFeO_2$. In coating test, as the amount of salt was limited, the decrease of Li was drastic for type 304 and 316L stainless steels. On the developed alloy (24%Fe), Li/(Li+K) ratio was not reduced in case of coating and immersion tests. This results suggested that 30%Cr-45%Ni alloy scarcely fixed Li ion in corrosion.

Effect of Cr content on the concentration of dissolved Cr and Fe ions in molten salt were shown in Fig. 3. The concentration of Fe ion was small and independent from alloy composition and test duration. After 205 hours immersion test, the concentration of dissolved Cr ion was almost same for all alloys tested. After 500 hours corrosion test, Cr concentration increased with Cr content of alloy up to 25%, and become small at 30%Cr alloy.

The structure of oxide films after corrosion tests were examined by SEM. The cross-sectional view of oxide films is shown in Fig. 4. For all alloys tested, oxide films had same structure. From EPMA analysis, inner layer is Cr rich oxide. The outer layer is $LiFeO_2$ determined by X lay diffraction. 30%Cr alloy has thin oxide layer and it is mainly Cr rich oxide. Type 304SS and 316L SS has thick oxide layer and its main component was $LiFeO_2$.

Summary

After corrosion test, distribution of metal ions (Fe, Ni, Cr, Li and K) in surface oxide and molten salt was determined.

1. Fe ion is fixed in outer oxide layer formed on surface as $LiFeO_2$.
2. Cr ion is fixed inner oxide layer and dissolved into salt as CrO_4^{2-} ion.
3. Type 304 or 316 stainless steel show poor corrosion resistance and fix Li as $LiFeO_2$. The developed 30%Cr-45%Ni-1%Al-0.03%Y-Fe alloy scarcely fix Li ion, because its high corrosion resistance and small Fe content.

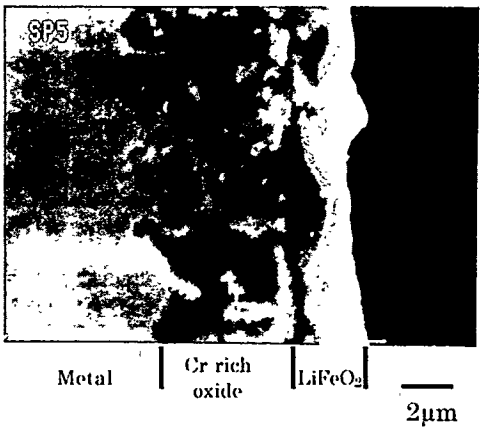

Fig. 4 Cross-sectional view of surface of 30%Cr-45%Ni alloy after coating test for 700hours at 650°C

4. The developed alloy with 30%Cr has high corrosion resistance and its dissolved Cr is as same as type 304 and 316. Amount of dissolved Cr into salt by corrosion is determined by corrosion rate, Cr content of alloy and structure of oxide films. Type 310S Stainless steel containing 25%Cr is not sufficient in view of corrosion resistance and Cr dissolution.

Acknowledgment

This work was conducted by MCFC Research Association and JRCM (Japan Research and Development Center). The MCFC Research Association was commissioned to do the work by NEDO (New Energy and Industrial Technology Development Organization) as a part of New Sunshine Program of MITI (Ministry of International Trade and Industry). We appreciate the advice and support of JRCM, MCFC R.A., NEDO and MITI.

---

[1] T. Shimada, K. Kuriki, M. Yamanouchi, M. Tamura: 1990 Fuel Cell Seminar, p171 (1990)
[2] Y. Kuriki, M. Yamanouchi, T. Shimada, M. Tamura: Proceedings of International Stainless Steel, p408 (1991)
[3] Toru Shimada, Norio Ariga, Jun-ichi Sakai, Katsumi Masamura: The 3rd IUMRS International Conference on Advanced Materials.93, pp. K-44 (1993)
[4] Koichiro Ohe, Toru Shimada, Norio Ariga, Katsumi Masamura: Proceedings of The 2nd International Fuel Cell Conference, pp.181 (1996)
[5] Hiroaki Urushibata: Proceeding of 25th MCFC seminar, pp.55 (1996)

LITHIUM-FERRATE-BASED CATHODES FOR MOLTEN CARBONATE FUEL CELLS

M. T. Lanagan, I. Bloom,† T. D. Kaun,† J. Wolfenstine,† and M. Krumpelt†

Energy Technology Division, Chemical Technology Division†
Argonne National Laboratory
Argonne, IL 60439–4838

Introduction

Argonne National Laboratory is developing advanced cathodes for pressurized operation of the molten carbonate fuel cell (MCFC) at ~650°C [2–5]. To be economically viable for stationary power generation, molten carbonate fuel cells must have lifetimes of more than 25,000 h while exhibiting superior cell performance [6]. In the present technology, lithiated NiO is used as the cathode. Over the lifetime of the cell, however, Ni^{2+} ions tend to transport to the anode, where they are reduced to metallic Ni [7]. With increased CO_2 partial pressure, the transport of Ni increases because of the increased solubility of NiO in the carbonate electrolyte. Although this process is slow in MCFCs operated at 1 atm and a low CO_2 partial pressure (about 0.1 atm), transport of nickel to the anode may be excessive at a higher pressure (e.g., 3 atm) and a high CO_2 partial pressure (e.g., about 0.3 atm). This transport is expected to lead eventually to poor MCFC performance and/or short circuiting.

Several alternative cathode compositions have been explored to reduce cathode solubility in the molten salt electrolyte [2–5,8]. For example, $LiCoO_2$ has been studied extensively [8,9,10] as a potential cathode material. The $LiCoO_2$ cathode has a low resistivity, about 1 Ω-cm, and can be used as a direct substitute for NiO. However, the high material cost may prevent large-scale implementation.

Argonne is developing advanced cathodes based on lithium ferrate ($LiFeO_2$), which is attractive because of its very low solubility in the molten $(Li,K)_2CO_3$ electrolyte [11]. Because of its high resistivity (about 300 Ω-cm), however, $LiFeO_2$ cannot be used as a direct substitute for NiO. Cation substitution is, therefore, necessary to decrease resistivity.

We determined the effect of cation substitution on the resistivity and deformation of $LiFeO_2$. The substituents were chosen because their respective oxides as well as $LiFeO_2$ crystallize with the rock-salt structure.

Experimental

Materials Synthesis and Characterization. Stoichiometric amounts of Li_2CO_3, Fe_2O_3, CoO, NiO and/or MgO were mixed and heat treated at 825°C for 4 h. The powders were pressed into disks and sintered at 1000°C for 4 h. Upon cooling, the phase distribution of the sintered disks was characterized by X-ray diffraction. The relative densities of the pellets were in the range of 60–90%; $LiCoO_2$ had the highest (93% of theoretical) and pure $LiFeO_2$, the lowest (81%). All materials except $LiCoO_2$ had equiaxed grains (0.96–1.43 μm). $LiCoO_2$ had acicular grain morphology (5 × 1.5 μm).

Resistivity and Deformation Rate Measurements. Resistivity was determined using the four-wire, dc, van der Pauw method at 650°C in air. Parallelepipeds (2 × 2 × 4 mm) were cut from

the sintered pellets. The samples were deformed by compression at a constant deformation rate in air at 1000°C.

Cell Tests. Promising materials were tested in a 5 × 5-cm cell with a pressed $(Li,K)_2CO_3$ electrolyte tile. The test cell was operated at 650°C using an O_2-CO_2 gas mixture which simulated pressurized operation at 3–5 atm.

Results and Discussion

Materials. We found that the range of homogeneity for Co-substituted $LiFeO_2$ is limited; several phases are formed during synthesis. All of the diffraction peaks for Mg-substituted $LiFeO_2$ were indexed to a rock-salt structure. Further analysis shows that the lattice parameter increases monotonically with MgO concentration, indicating a complete solid solution (Fig. 1). Fayard found that both CoO and MgO formed complete solid solutions with $LiFeO_2$ [12]. Apparently, Co solubility is affected by differences in synthesis conditions.

Resistivity Measurements. Resistivity results for MgO-substituted $LiFeO_2$ samples show that the minimum resistivity is approximately 100 Ω-cm (at 650°C in air) and appears in the MgO concentration range of 6–12 mol% (Fig. 2). Clearly, the resistivity of Mg-substituted $LiFeO_2$ is too high; lower resistivity values (~1 Ω-cm) are necessary for MCFC cathodes. By using different cation substituents, we lowered the resistivity of a $LiFeO_2$-based material (designated Material 1) to 1.3 Ω-cm at 650°C.

Deformation Rate Studies. Figure 3 shows a log-log plot of the deformation rate *vs* stress at 1000°C for five materials: (a) pure $LiFeO_2$, (b) 12.5 m/o NiO-$LiFeO_2$, (c) 9 m/o MgO-$LiFeO_2$, (d) pure $LiCoO_2$, and (e) 5 m/o Li_2O-NiO. Here, the deformation rate was normalized with respect to grain size and stress to the material density, and it was assumed that the deformation rate is controlled by lattice diffusion. The slope of all curves is close to unity, implying that they all exhibit the same deformation mechanism (e.g., diffusional creep and/or grain boundary sliding). Materials (a) and (d) have higher deformation rates than (e), lithiated NiO; Material (d) has the highest deformation rate. Doping $LiFeO_2$ with NiO or MgO decreases the deformation rate as compared to that of pure $LiFeO_2$. Materials (a), (b), (c), and (d) will compact more than lithiated NiO at 650°C.

Cell Tests. A fibrous cathode of Material 1 was used in a cell test. The cell potential at 160 mA/cm^2 as a function of time is shown in Fig. 4. After an initial break-in period, a constant potential of 850 mV was observed for 1700 h. Polarization experiments showed a small degradation at 1706 h (see Fig. 5). These results show that $LiFeO_2$-based cathodes have good performance and durability at high CO_2 partial pressures.

Conclusions

Several $LiFeO_2$-based materials with cation substitutions were synthesized and characterized. With the proper choice of substituents, the resistivity of $LiFeO_2$ was lowered to about 1 Ω-cm.

The $LiCoO_2$- and $LiFeO_2$-based cathode materials have deformation rates higher than that of lithiated NiO at 1000°C. They will compact more at 650°C. Doping the alternative cathodes decreases their deformation rates.

The $LiFeO_2$-based cathodes exhibit cell potentials which are stable for long periods of time under simulated pressurized operation. $LiFeO_2$-based materials continue to show promise as cathodes for the MCFC.

Acknowledgments

The authors thank H. Wilson Abernathy III, Bryant Polzin, and Ryan Thayer for their assistance in sample preparation. This research was supported under a contract with M-C Power Corporation.

References

1. Faculty Research Participant. Present address: Dept. of Chemical-Biochemical Engineering, University of California, Irvine, CA.

2. A. P. Brown, G. H. Kucera, M. F. Roche, D. D. Chu, and E. Indacochea, "Performance of Alternative Cathodes for Molten Carbonate Fuel Cells," *Fuel Cell Seminar Program and Abstracts*, November 29–December 2, 1992, Tucson, AZ, p. 125.

3. G. Kucera, A. Brown, D. Chu, and E. Indacochea, "Development of Alternative Components for Molten Carbonate Fuel Cells," presented at EPRI/GRI Fuel Cell Workshop on Fuel Cell Technology Research and Development, April 29–30, 1992, San Francisco, CA.

4. J. L. Smith, G. H. Kucera, and A. P. Brown, "Development of Cathode Materials and Structures for the Molten Carbonate Fuel Cell," *Proc. 2nd Symp. on Molten Carbonate Fuel Technology*, J. Selman, D. A. Shores, H. C. Maru and I. Uchida, eds., Vol. 90-16 (Oct. 1990), The Electrochemical Soc., p. 226–ff, and references cited therein.

5. G. H. Kucera and J. L. Smith, "Electronically Conductive Ceramics for High Temperature Oxidizing Environments," US Pat. No. 4,564,567 (January 1986).

6. C. Yuh, M. Faooque, and H. Maru, "Selection of Materials for Carbonate Fuel Cell Use," *Electrochemical Society Extended Abstracts*, Vol. 94-2 (Oct. 1994).

7. N.Q. Minh, "Technological Status of Nickel Oxide Cathodes in Molten Carbonate Fuel Cells," *J. Power Sources*, Vol. 24, pp. 1-19 (1988).

8. L. Plomp, E. F. Sitters, J. B. J. Veldhuis, R. C. Makkus, and S. B. van der Molen, "Performance and Dissolution-Precipitation Behavior of Molten Carbonate Fuel Cell Cathodes," *Proc. Electrochem. Soc.*, Vol. 93-3, pp. 171-185 (1993) and L. Plomp, R. C. Makkus, E. F. Sitters, and G. Rietveld, "Endurance Issues and Materials Development in Molten Carbonate Fuel Cells," *Fuel Cell Seminar Program and Abstracts*, November 28–December 1, 1994, San Diego, CA, p. 164.

9. B. Bergman, E. Fontes, C. Lagergren, G. Lindbergh, A. Lundblad, S. Schwartz, D. Simonsson, and C. Sylwan, "Swedish Research on MCFC," *Fuel Cell Seminar Program and Abstracts*, November 29–December 2, 1992, Tucson, AZ, p. 73.

10. M. Carewska, S. Scaccia, G. Ghidelli, L. Giorgi and E. Simonetti, "Synthesis and Electronic Conductivity of $LiCoO_2$ Materials for MCFC Alternative Cathodes," *Fuel Cell Seminar Program and Abstracts*, November 28–December 1, 1994, San Diego, CA, p. 176 and references cited therein.

11. D. Shores and Y. Qu, "Dissolution of Oxides in Molten Carbonates," *Proc. 3rd International Symp. on Carbonate Fuel Cell Technology*, Electrochem. Soc., Vol. 93-3, pp. 356-367 (1993).

12. M. Fayard, "Sur les Phénomènes Ordre-Désordre dans l'Oxyde Mixte $LiFeO_2$ et sur les Propriétés de ses Solutions Solides avec Quelques Oxydes du Type NaCl," *Annales de Chimie*, pp. 1313-1335 (1961).

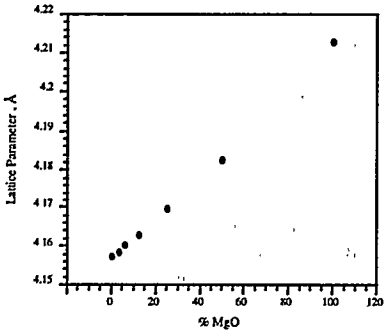

Fig. 1. Effect of MgO concentration on unit cell dimensions.

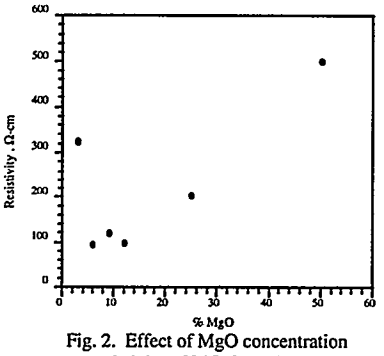

Fig. 2. Effect of MgO concentration on resistivity of $LiFeO_2$ at 650°C in air.

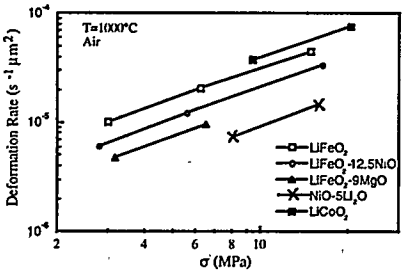

Fig. 3. Grain-size-compensated deformation rate *vs* density-compensated stress.

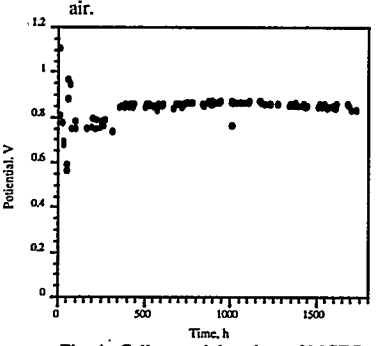

Fig. 4. Cell potential *vs* time of MCFC test cell containing Material 1 cathode.

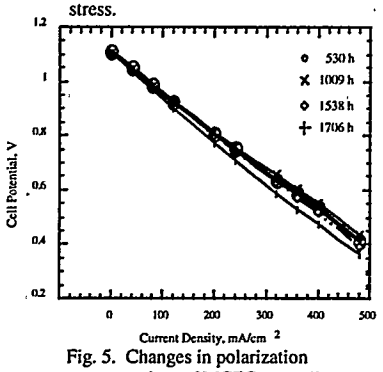

Fig. 5. Changes in polarization curves vs time of MCFC test cell containing Material 1 cathode.

THREE-DIMENSIONAL AND DYNAMICAL PERFORMANCE OF A MOLTEN CARBONATE FUEL CELL STACK

W. He
Delft University of Technology
Faculty of Mechanical Engineering and Marine Technology,
2628 CD Delft, The Netherlands
email: W.He@wbmt.tudelft.nl
Q. Chen
Massachusetts Institute of Technology,
Department of Architecture
Cambridge, MA 02139, U.S.A.
email: Qchen@mit.edu

ABSTRACT

The three-dimensional and dynamic performance of a molten carbonate fuel cell (MCFC) stack operating under load-following modes have been investigated by using dynamic simulation. The major processes with regard to an MCFC's safe and efficient operation in power-generation systems, such as the mass and heat transport, chemical reactions and electrical power generation, are formulated in a three-dimensional, time-dependent form using the computational-fluid-dynamics (CFD) technique. The grid definitions have been explained, and a simple test to determine whether the simulation results being acceptable has been introduced. In this paper, the model performance is demonstrated by applying it to calculate the distributions of current density and temperature under a step change.

INTRODUCTION

The distributions of the crucial parameters, e.g., temperature, pressure, gas concentration and density, in a molten carbonate fuel cell (MCFC) stack have a major impact on its safe and efficient operation. We try to attack the problem by developing a three-dimensional MCFC stack model based on physical laws using the computational-fluid-dynamics (CFD) technique. More specifically, the model has been implemented in the CFD package PHOENICS (CHAM, 1995). The analysis of the distributions under transient conditions is emphasized, futher, this paper is confined to the modeling an MCFC stack without internal reforming. Throughout the paper, the term 'fuel cell' refers to MCFC without internal reforming.

RELATED PHYSICAL LAWS

In order to derive the equations the structure of a fuel cell stack has been simplified. A stack is represented by a series of cells. Each cell contains a unit (including electrolyte, anode and cathode), two half-separators, a layer of fuel gas, and a layer of oxidant gas.

The time constant which is of interest for dynamic modeling should be specified. The time constant for the slowest process, which is significant to stack safe operation under load-following modes, is estimated to be in the range of a few 10^1 to 10^3 seconds (He, 1994). Those processes, with time constants much smaller than a chosen fraction of the slowest process, should preferably be eliminated from the dynamic equations. The time limit selected is 1 second, so the processes with a time constant estimated to be larger than one second are modelled in the form of dynamic equations; other processes are modelled in the form of static equations.

The current density or species concentrations distribution in the fuel and oxidant gas channels is determined by the mass balance equation, including the cell and water-shift reactions. The temperature distribution is determined by the energy balance, including heat transfer, heat generation from both electrochemical cell and water-shift reactions, and heat

generated due to losses in electrodes power generation. Furthermore, the equations of mass balance and heat balance are related to that of momentum. The major differential equations describing the dynamic processes in a fuel cell stack use a series of mass, energy and momentum equations applying to the cell unit, separator, fuel gas and oxidant gas. In addition, auxiliary algebraic and differential equations are provided to calculate the cell electrochemical performance (e.g., cell working voltage), chemical reaction rates, heat-transfer coefficient, the mixture gas physical properties, and also the initial and the boundary conditions.

CFD APPROACH

The computational grid definition is based on a compromise between accuracy and efficiency. One type of grid for a single cell is illustrated in Fig. 1, in which x, y and z respectively represent: the fuel gas channel direction, the stack direction and oxidant gas direction. The height of a cell (in the y direction) has been increased by a ratio of 200:1. The x and z grid have 16 and 8 uniform elements respectively. The x grid is more dense than the z grid because the change of a fuel gas in the cell direction is often more significant than that of an oxidant gas (the utilization of fuel gas is normally higher than that of oxidant gas). In the y direction, there are five zones: two for half-separators and three for fuel gas, cell unit and oxidant gas. There are three grids for each of the two half-separators, nine for cell unit and 15 for fuel and oxidant gas respectively.

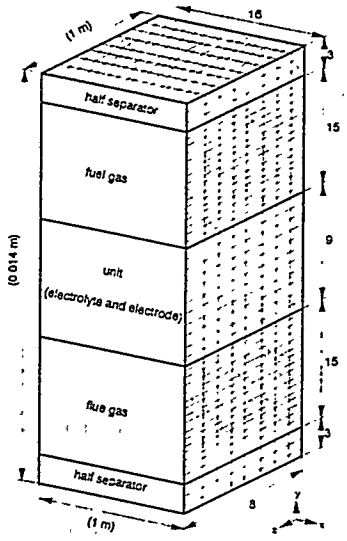

Fig. 1 Dimensions and computational grids for a single cell

Under transient conditions, a time-step grid must also be specified. To ensure convergence of the numerical solution, for a step or ramp change, a fine grid is often required. For example, a +10% step change in voltage can be approximately simulated by 100 grids in a very short interval with a +0.1% step change in voltage taking place in each grid.

STACK CFD PACKAGE TEST

The converged simulation results derived from the stack CFD package must be carefully checked. Under transient conditions, the simulation results at one time-step grid will be used as the initial conditions for the simulation at the next time-step grid, consequently, the computational errors at each time-step grid are accumulated. However, there are no general rules to check the correctness of such simulation results. One simple check procedure which seems effective has been used by the authors. This entails conducting an additional steady state simulation under the final state of the transient condition, then comparing the results between the transient simulation for a large time-step grid and this steady state simulation. If the transient simulation results for a large time-step grid are in agreement with the steady state simulation, the preliminary performance of the stack CFD package is considered to be acceptable.

RESULTS AND DISCUSSION

To evaluate the usefulness of the present fuel-cell model, a fuel cell stack with 5 cells has been selected as an example for demonstration. The characteristics of a stack is described by (He and Chen, 1996). The responses of stack current and temperature distributions to +10% step voltage are discussed. In accordance with the time range considered earlier, the simulation time for the stack response is 7200 seconds, with a relatively dense time-step grid in the beginning and succeeded by a coarse time-step grid. The simulation results are therefore selectively illustrated in the interval of 40 seconds for the current density, and at 120, 3600 and 7200 seconds for the temperature.

Figure 2 (a) shows the response of the current density and temperature that takes place in the separator of cell unit 5. It indicates that the overall current density decreases when the stack voltage increases, which satisfies the voltage-current relation. Between 0 and 80 s, the current density profile changes significantly, but not between 80 s and 120 s. Figures 2 (b) illustrates that the overall temperature decreases. The rapid change in current density between time 0 s and 80 s may result from the rapid response of mass storage and chemical reaction. The slow change of current density from time 80 s to 7200 s may result from the slow response of temperature, where temperature response is determined by energy storage.

CONCLUSIONS

In order to assess the three-dimensional distributions of crucial parameters in a fuel cell stack under transient conditions, a stack model using CFD technique has been described. It has been shown that this method is capable of modeling the chemical and physical processes of a fuel cell stack in three-dimensional, time-dependent form. Furthermore, the grid definitions and the proposed simple test for a stack CFD package seem effective. The simulation-derived distributions of current and temperature under a step change of voltage appear to be reasonable.

ACKNOWLEDGEMENTS

The first author thanks Professor R.W.J. Kouffeld and Professor O.H. Bosgra for the opportunity to perform the investigation.

REFERENCES

CHAM development team, 1995, 'The PHOENICS Reference Manual, TR200', Concentration, Heat and Momentum Limited, London.

He, W. and Chen, Q., 1996, "Three-dimensional simulation of a molten carbonate fuel cell stack under transient conditions", ASME, Annual, Atlanta, USA, Nov. 17-22 (accepted).

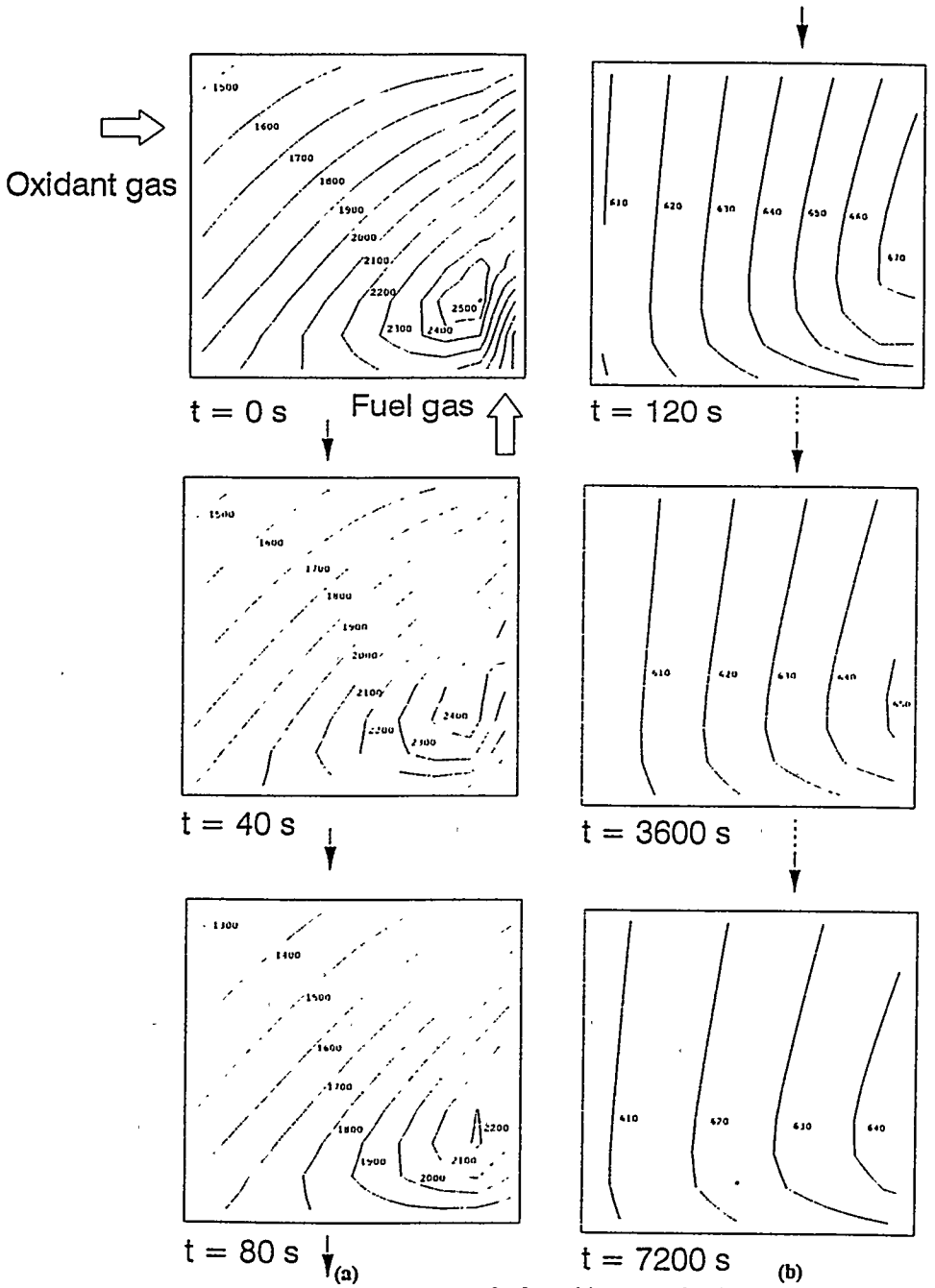

Fig. 2 Distributions under a step change of voltage (a) current density, and (b) temperature

FUEL CELL SYSTEMS FOR A SUSTAINABLE ENERGY PRODUCTION

Timo Kivisaari
Royal Institute of Technology
Department of Chemical Engineering and Technology/
Chemical Technology
S-100 44 Stockholm
Sweden

Introduction

When talking about fuel cell systems for stationary applications, two of the advantages are claimed to be a high inherent efficiency and environmentally favourable characteristics.
It should, however, be obvious to everybody that in order to call an energy production route environmentally benign, it is not enough that just the energy production step itself has a low negative environmental impact, but that all steps involved (e.g. fuel pre-treatment, fuel processing etc.) should be subjected to the same constraints if the overall production process is to be considered environmentally friendly.
In order to evaluate the technical possibilities of a biomass fuelled MCFC unit for stationary applications a system study of a 40 MWe biomass-fired MCFC system is currently carried out at The Royal Institute of Technology, as part of the international co-operation within the IEA Advanced Fuel Cell Programme Annex I, Balance of Plant of MCFC Systems.
In addition to the present work, other recent studies involving biomass and fuel cells can be found in literature [1, 2, 3, 4, 5].

Fuels for fuel cells

The main requirement for a fuel to be applicable for stationary fuel cell use is that is should be possible to gasify in order to be fed to the fuel cell. Therefore the easiest fuels to use in fuel cell power plants are those that in their natural state are gaseous (e.g. natural gas and LNG). The simplicity arises from that fact that the fuels are in the gaseous state at the temperatures and pressures where they are used, and therefore the necessary pre-treatment is limited to removal of impurities followed by catalytic steamreforming, either externally or internally within the fuel cell stack.
Another class of possible fuels are those that in their natural state occur as liquids (e.g. ethanol [6], kerosene and other liquid fuels). Prior to purification and steamreforming an additional step is needed to transfer the liquid fuel into a gaseous state for all of these. Since the fuels characterised as liquids usually have a low boiling point, the transformation can be categorised as evaporation. The use of these fuels will probably be confined to smaller scale stationary systems.
The last, but not less important, category of fuels are the ones that are more or less solid in their natural state (i.e. heavy fuel oils, coals, peat and biomass). Similarly to liquid fuels a phase transformation is needed before the final fuel cleanup. They therefore need to undergo a thermochemical conversion to render a gaseous mixture that can be used in the fuel cell. Since the gasification results in a partial oxidation process of the original solid fuel, no further processing, except for gas purification, is needed if the now gaseous fuel is to be used in an MCFC unit.
When looking at the fuels applicable for larger scale applications, it can be recognised that the only fuel meeting the criterium of renewability is biomass, whereas the others are either manufactured from, or are themselves, fossil fuels. These fuels can therefore only be considered renewable in a multi million year time-span, and the supply is usually considered finite.
In addition to being a renewable fuel, with infinite fuel supply, the use of biomass has another considerable advantage. It does not result in any net production of CO_2 to the atmosphere, at least if coupled with active silviculture. Therefore, the use of biomass as a fuel in an MCFC system will favourably influence the greenhouse effect, resulting in a fuel cell system for a sustainable energy production.

Biomass gasification

As in the case with coal fired MCFC power plants, the first process step of a biomass-fuelled MCFC power plant is the gasification of the primary fuel. The main difference compared to coal systems is the fact that biomass requires a considerably lower gasification temperature than coal. The reason for this is the higher reactivity of biomass under gasification conditions which results in adequate reaction rate and conversion at lower temperatures. Coal requires a gasifier temperature of more than 1000 °C, whereas biomass only needs gasification temperatures in the range of 500 - 1000 °C.

As a result, biomass gasifiers can be operated with air as the primary gasification medium, whereas a coal gasifier requires oxygen for its operation. As a consequence, biomass gasification systems does not need the cryogenic units necessary for the oxygen production which is required in coal gasification.

A major drawback resulting from the, so far, low interest in biomass is that information about contaminant levels acceptable for an MCFC unit are scarce. For coal, on the other hand, there are several continuing evaluation programs related to these issues [7, 8]. To some extent the pollutants are the same and the coal-related data can be used directly, in other cases additional research may become necessary.

Layout of a biomass fuelled-MCFC unit

The flowsheet envisioned for a 40 MWe MCFC power plant with biomass gasification can be seen in figure 1.

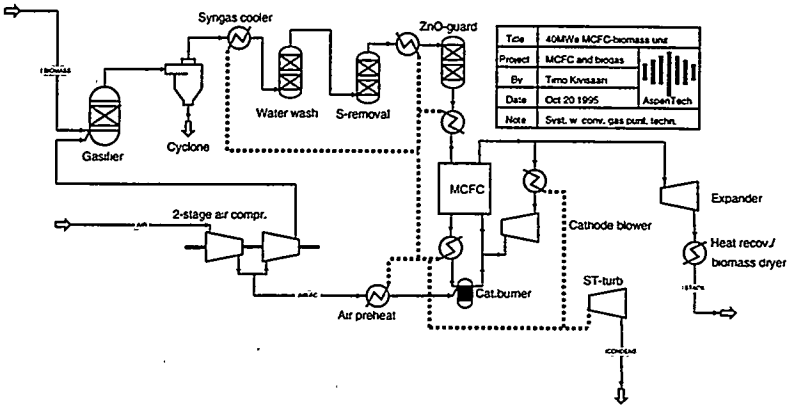

Figure 1. Envisioned layout of a 40 MWe biomass-fired MCFC unit

The first step is the gasifier, where the pressurised thermochemical decomposition of biomass takes place in presence of air. The resulting gas consists mainly of CH_4, CO, CO_2, N_2 and H_2. The dust removal in a cyclone is followed by a syngas cooler where the gas is cooled before subsequent purification. The first step of the purification is a water-wash used to remove ammonia and tars, which is followed by a conventional sulphur removal step (e.g. Selexol™, Purisol™, Rectisol™ etc.). Another possibility would be the utilisation of a high temperature purification technique, but since these are at the development stage, it has been considered safer to study a system with conventional purification.

Depending on the capabilities of the conventional purification, a ZnO bed may become necessary to remove trace amounts of sulphur.
After completed cleaning, the gas is reheated before entering the MCFC anodes.
The spent fuel is mixed with air and passed trough a catalytic combustor. The combusted anode off-gas can then be fed to the MCFC cathodes, thus ensuring adequate CO_2 supply.
Cathode off-gas leaving the fuel cell is divided into two streams, one to be recirculated back to the fuel cell cathodes, and another stream which is passed through an expansion turbine.
The large amount of heat that can be extracted both from the syngas cooler as well as from the expansion turbine effluent can be used for steam generation and additional power production in steam turbines.

Results

A technical assessment of the power plant described above is currently in progress at The Royal Institute of Technology, as part of the international co-operation within the IEA Advanced Fuel Cell Programme Annex I, Balance of Plant of MCFC Systems, and the results of this assessment is to be presented during the 1996 Fuel Cell Seminar in Kissimee, Florida.

Acknowledgements

This work is financially supported by the Swedish National Board for Technical and Economical Development (NUTEK).

References

1. G. Liberati and G. Spazzafumo, "MCFC versus SOFC in biomass gasifier/fuel cell power plants", Abstracts - Fourth Grove Fuel Cell Symposium, 19-22 September 1995, London.

2. S. Kartha, E.D. Larson, J.M. Ogden and R.H. Williams, "Biomass Integrated Gasifier/Fuel Cell Electric Power Generation and Cogeneration", 1994 Fuel Cell Seminar, Program and Abstracts, November 28 - December 1, 1994, San Diego, CA.

3. T. Mäkinen, J. Leppälahti, E. Kurkela and Y. Solantausta, "Electricity produced from biomass by gasification and a solid oxide fuel cell", 8th European Conference on Biomass for Energy, Environment, Agriculture and Industry, 3-5 October, 1994, Vienna.

4. A. Ramsköld, "Biobränslebaserade bränsleceller". Report from Vattenfall Research, Stockholm, 1993.

5. G. Liberati and G. Spazzafumo, "Biomass Gasifier/MCFC Plants - Performance Perspec tives", 1992 Fuel Cell Seminar, Program and Abstracts, November 29 - December 2, 1992, Tucson, AZ.

6. Information available at Energy Research Corporation's Internet WorldWideWeb-page: http://www.ercc.com/fuelcell.html, August 28, 1996.

7. M.C. Wiliams and D.A. Berry, " Overview of the DOE-Funded Fuel Cells Contaminants R&D Program", 1990 Fuel Cell Seminar, Program and Abstracts, November 25 - 28, 1990, Phoenix, AZ.

8. J.H. Hirschenhofer, D.B. Stauffer and R.R. Engleman, "Fuel Cell, A Handbook (Revision 3)", - DOE Report, DOE/METC-94/1006 (DE94004072).

ADVANCED COMPONENT DEVELOPMENT OF MCFC TECHNOLOGY AT M-C POWER

D.S. Erickson, E.J. Haugh, and T. G. Benjamin
M-C Power Corporation
8040 South Madison Street
Burr Ridge, IL 60521

INTRODUCTION

M-C Power Corporation (MCP) was founded in 1987 to commercialize Molten Carbonate Fuel Cell (MCFC) stacks. The first generation of active area cell components were successfully scaled-up from the 100-cm^2 area laboratory scale to continuous production of commercial-area (1-m^2) components. These components have been tested in five commercial-area subscale (20-kW) stacks and one commercial-scale (250-kW) stack. The second 250 kW stack is being installed in the power plant for operation in late 1996 and components have already been manufactured for the third 250-kW stack which is scheduled to go on-line in the middle of 1997.

Concurrent with commercial-area (1-m^2) active component manufacturing has been an ongoing effort to develop and test advanced component technologies that will enable MCP to meet its future cost and performance goals. The primary goal is to lower the total cell package cost, while attaining improvements in cell performance and endurance. This work is being completed through analysis of the cost drivers for raw materials and manufacturing techniques. A program is in place to verify the performance of the lower cost materials through pressurized (3 atm) bench scale (100-cm^2) cell tests.

Bench-scale cell testing of advanced active area components has shown that simultaneous cost reduction and improvements in the performance and endurance are attainable. Following performance verification at the bench scale level, scale-up of the advanced component manufacturing processes to commercial-area has been ongoing in the past year. The following sections discuss some of the performance improvements and reductions in cost that have been realized.

LOWER COST STABILIZED CATHODE

The stabilized cathode was developed to inhibit NiO dissolution which could result in cell shorting at target operational times and pressures for commercial MCFC stacks. Reduced NiO dissolution for cells operated with stabilized cathodes has been demonstrated in several atmospheric and pressurized bench-scale cell tests. The initial version of the stabilized cathode tripled the base cost of the cathode due to raw material processing requirements.

In the past two years, a stabilized cathode has been developed with a base material cost comparable to the unstabilized cathode: the lower-cost stabilized cathode has a raw material cost 6 percent lower than the current state-of-the-art unstabilized cathode, and 69% lower than the initial version of the stabilized cathode. In addition to the reduction in raw material costs, commercial-area manufacturing trials indicate that the lower cost stabilized cathode will have higher production yields than the initial version because of increased strength in the sintered state. Current results indicate further cost reductions are possible.

A 100-cm^2 cell test of the lower cost stabilized cathode with the Li/Na electrolyte system completed 10,000 hours of operation, including more than a year of operation at pressurized systems conditions. The test operated with negligible decay (Figure 1), and was terminated only after repeated uncontrolled thermal cycles to 150 °C which resulted from facility power outages.

Li/Na ELECTROLYTE SYSTEM

The lithium/sodium (Li/Na) electrolyte system is being tested because of its high ionic conductivity which results in higher cell performances observed as a direct result of lower internal cell resistance. The Li/Na electrolyte was utilized in the previously mentioned 10,000 hour cell test which operated at M-C Power with negligible decay (Figure 1). Scale-up of the Li/Na electrolyte to commercial-area tape casting was completed this year and no additional costs were incurred when compared to the Li/K electrolyte. Current development focuses on lowering the electrolyte material costs and increasing manufacturing rates for commercial-area stack testing scheduled for next year.

NEW LOWER COST MATRIX

The lower cost matrix was developed and tested as part of an effort to reduce MCFC stack costs without sacrificing the performance or endurance of the state-of-the-art MCP high performance matrices. Cells operated with the new, lower cost matrix have shown stable performance and endurance at both atmospheric and elevated (3 atm) pressures. A life graph of a 2000 hour cell test of the lower cost matrix on system gases pressurized to 3 atmospheres is shown in Figure 2 . This cell was terminated voluntarily for analysis of the post-test carbonate distribution and cell package characteristics. In addition to a dramatic reduction in raw material cost, the lower cost matrix exhibits an improved in-cell porosimetry with improved carbonate retention properties, and increased resistance to in-cell compaction. Because of these improvements, increased MCFC endurance is expected. Scale-up of the lower cost matrix to commercial-area manufacturing and testing is in progress.

STRENGTHENED ANODE

MCP has begun manufacturing trials and pressurized bench scale cell tests of a strengthened anode. A recent cell test demonstrated a stable performance of ~755 mV for over 2000 hours at 3 atmospheres on systems gases. This cell was terminated after a load device failure. Analysis of the post-test carbonate distribution and package characteristics is in progress. Ongoing work at M-C Power includes optimizing the physical properties (creep resistance and strength characteristics) of these anodes by characterizing the effect manufacturing procedures have on the *in situ* strength.

CONCLUSION

Recent development activities at M-C Power Corporation have demonstrated the ability to lower the total cell package cost while also improving the performance and endurance of the molten carbonate fuel cell commercial stack technology.

ACKNOWLEDGMENTS

This project was funded by the following sponsors: the U.S. Department of Energy, Electric Power Research Institute, Gas Research Institute, and San Diego Gas & Electric.

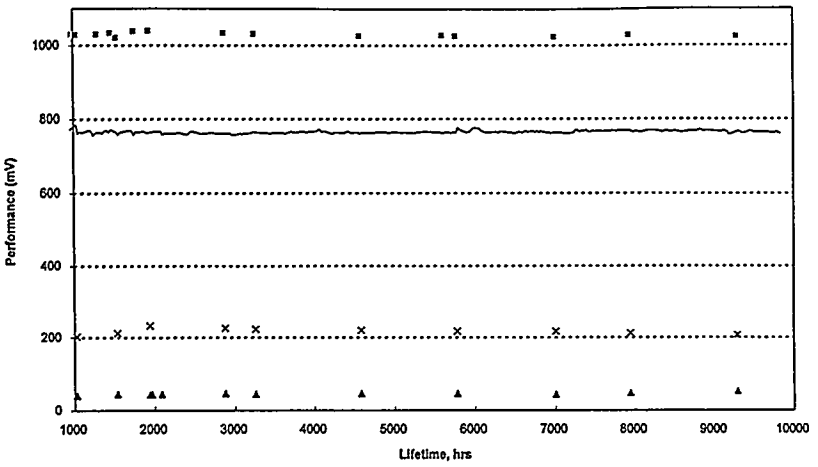

Figure 1. 100-cm² Cell Test Life Graph of Lower Cost Stabilized Cathode and Li/Na Electrolyte.

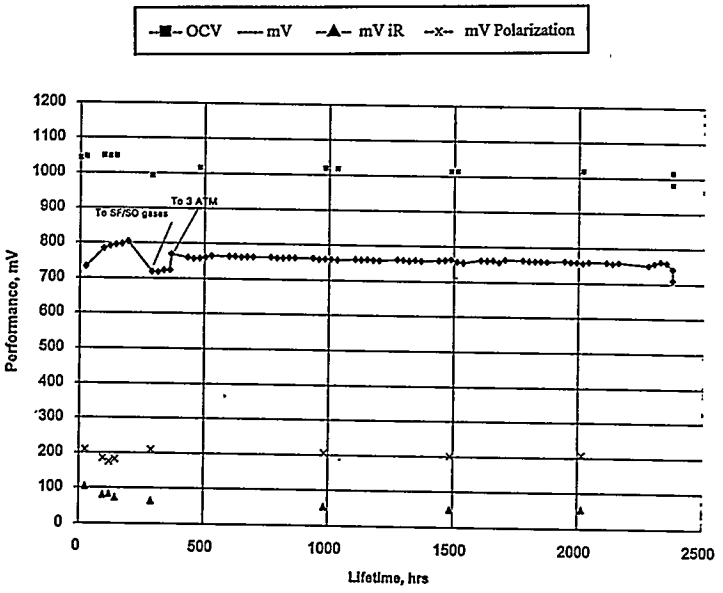

Figure 2. 100-cm² Cell Test Life Graph of Lower Cost Matrix.

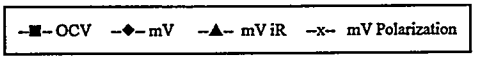

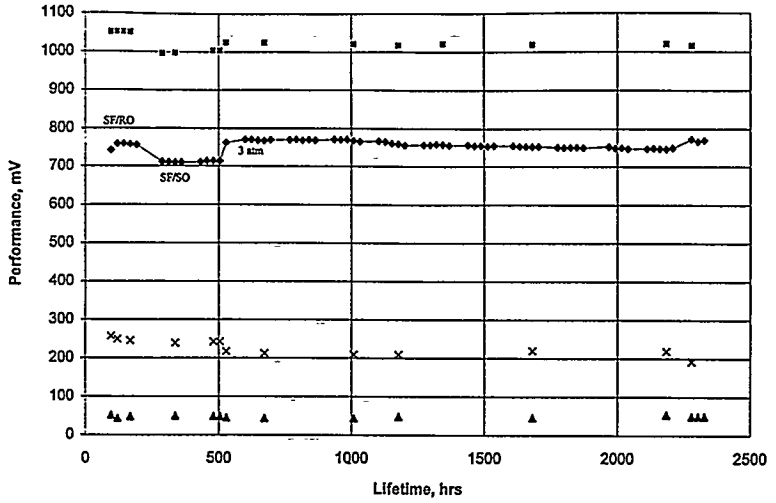

Figure 3. 100-cm² Cell Test Life Graph of Strengthened Anode

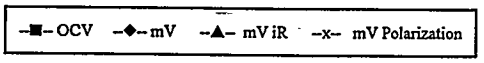

LONG TERM OPERATION OF THE 100-cm^2 CLASS SINGLE CELL OF MCFC

Kazumi TANIMOTO, Masahiro YANAGIDA, Toshikatsu KOJIMA
Yukiko TAMIYA and Yoshinori MIYAZAKI
Osaka National Research Institute
Midorigaoka 1-8-31, Ikeda, Osaka 563, Japan

Abstract

The R&D on Molten Carbonate Fuel Cell (MCFC) is proceeding as one of the New Sun Shine Project sponsored by Japanese government. In ONRI (Osaka National Research Institute), the tested MCFCs were assembled with the state-of-the-art components and operated under the load condition for 40000 hours and 34000 hours. We analyzed the performance reduction.

1. Introduction

The R&D on MCFC in Japan is proceeding as one of the New SunShine Project sponsored by Japanese government. The main target of the second stage started in 1987 is the demonstration of the 1000kW class MCFC power generating system in 1999. ONRI has participated in the research of the alternative materials and the evaluation of material for MCFC. We evaluated the conventional material from the viewpoint of stability by the operation of 100-cm^2 class single cell for up to 40000 hours.

2. Experimental

2-1. Operation

The tested single 100-cm^2 class cell were assembled with the state-of-the-art components, which are shown in Table 1. The normal operation condition is shown in Table 2. We started to operate the two MCFCs in 1991. The cell performances were measured once a day. The cell resistance was measured by using the milliohm meter, 1kHz AC. The carbonates as electrolyte were added at the appropriated time.

In this test the CO_2 supply was accidentally interrupted due to the equipment failure. There was no heat-cycle for both cells. Two cells were kept at the operating temperature, 650 °C. The single cells were operated for 34000 hours and 40000 hours.

2-2. Analysis of degradation of cell performance

The reduction of cell voltage at 150 mA/cm^2 was analyzed to clearify a contribution of life-limting-factor.

Table 1. Materials for tested MCFC

Component	Material
Anode	Ni-Al base alloy
Cathode	NiO
Matrix/ Carbonate	$LiAlO_2$/ Li_2CO_3:K_2CO_3=62:38mol%
Housing	Stainless Steel

Table 2. Normal operation condition

Pressure	Atmospheric
Temperature	650 ° C
Anode gas	H_2/CO_2:80/20 (50 °C Humidify)
Cathode gas	Air/CO_2:70/30
Gas Utilization	40%@150mA/cm^2 (both side)
Normal load	150mA/cm^2

3. Results and discussions

3-1. The long term operation

(a). 40000-hour-operation MCFC

The performance with time was shown in Figure 1. This cell experienced the interruption of CO_2 three times for 40000-hour-operation. Though the first interruption did not influence the cell performance, the second and the third interruption influenced the cell performance positively. It has not been recognized that the CO_2 interruption brought this effect. The anode outlet pipe was closed at 26000 hours due to something entering it. The close of outlet pipe for two days may make the break of gas seal at the part of wet seal..

The reduction of OCV began at 12000 hours. It was due to the short circuit induced by the deposited nickel in matrix. This phenomenon was initiated by the dissolution of NiO cathode. Ota et al. reported that solubility of NiO in carbonate was proportional to the pressure of CO_2[1]. The cathode gas was diluted by the addition of nitrogen after 16000 hours to reduce the dissolution of NiO cathode. After then cathode gas composition was $CO_2/O_2/N_2$:22/11/67. However, OCV gradually reduced during the operation.

The carbonates were added seventeen times during operation. The addition of carbonate reduced the cell resistance and improved the cell

performance until 20000 hours. After that, the addition of carbonate do not maintain the cell resistance The matrix cannot hold the carbonate electrolyte due to the degradation of $LiAlO_2$.

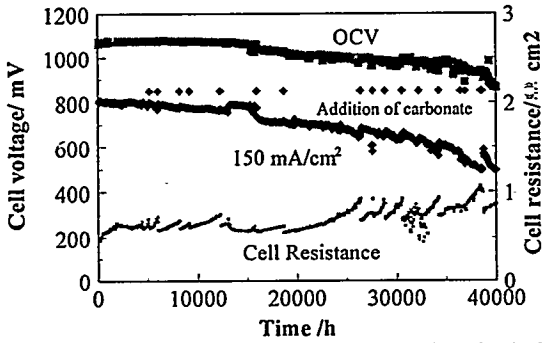

Figure 1. Cell Performance of 40000-hour-operation of MCFC

(b) The 34000-hour-operation MCFC

The performances with time was shown in Figure 2. This cell experienced the interruption of CO_2 twice. Though the first interruption did not influence the cell performance, the second one reduced the cell performance. It has not been clarified that the CO_2 interruption brought these effects and different results with the comparison of 40000-hour-operation MCFC.

The OCV was almost constant until 25000 hours. After then it slightly decreased. The gaschromatography result indicated that gas leakage was not found in operation. The reduction of OCV also was due to the short circuit.

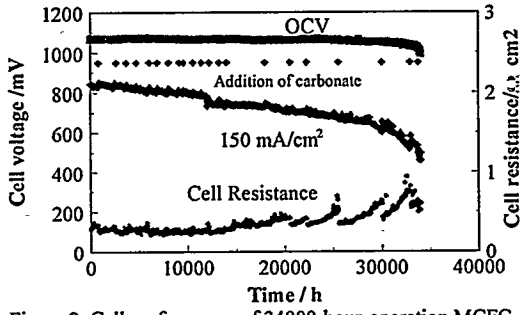

Figure 2. Cell performance of 34000-hour-operation MCFC

(c) Analysis of degradation of cell performance

The cell voltage with time and current density is formulated as follows.

$$E(t,I)=E_0-\Delta E_{n.l.}-\Delta E_{NiO}(t)-(R_a(t)+R_c(t)+R_{ohm}(t))I$$

E_0: theoretical cell voltage, $\Delta E_{n.l.}$: Nernst loss, $\Delta E_{NiO}(t)$: Cell voltage reduction by self shorting, $R_a(t)+R_c(t)$: Non-ohmic polarization, $R_{ohm}(t)$: Ohmic cell resistance.

The reduction of OCV was corresponded to the self shorting by the deposition of nickel. $\Delta E_{NiO}(t)$ was estimated from the profile of OCV with time. Ohmic resistance was estimated by the profile cell resistance with time. We have three different degradation rates. α_1 is the observed degradation rate. α_2 is corrected by subtracting $\Delta E_{NiO}(t)$. α_3 is corrected by subtracting $\Delta E_{NiO}(t)$ and $(R_{ohm}(t) - R_{ohm}(0))$.

$E_1(t,I=150mA/cm^2)=E_0-\Delta E_{n.l.}-\Delta E_{NiO}(t)-(R_a(t)+R_c(t)+R_{ohm}(t))I$
$=E_{1,0}(t=0, I=150mA/cm^2)-\alpha_1 t$----------(1)

$E_2(t,I=150mA/cm^2)=E_0-\Delta E_{n.l.}-(R_a(t)+R_c(t)+R_{ohm}(t))I$
$=E_{2,0}(t=0, I=150mA/cm^2)-\alpha_2 t$ ----------(2)

$E_3(t,I=150mA/cm^2)=E_0-\Delta E_{n.l.}-(R_a(t)+R_c(t)+R_{ohm}(0))I$
$=E_{3,0}(t=0, I=150mA/cm^2)-\alpha_3 t$ ----------(3)

The degradation behaviors of tested MCFCs at operation time were different. We considered three steps for long operation. The degradation rate at third step were higher than those at other steps. The large degradation at third step was caused by the short circuit and the increasing cell resistance. We guess that the difference of 34000-hour-operation MCFC and 40000-hour-operation MCFC was due to the different pore distribution of matrix . It came from the different fabrication process of matrix.

Table 1. Degradation rate of 34000-hour -operation

	1st step	2nd step	3rd step
	0～12000h	12000h～29000h	29000h～34000h
α_1	5	6.1	27.6
α_2	5.1	5.3	20.9
α_3	5.7	3.8	14

Table 2. Degradation rate of 40000-hour -operation.

	1st step	2nd step	3rd step
	0～13000h	16000h～26400h	26400h～38500h
α_1	3.3	5.5	13.4
α_2	3.4	1.1	9.1
α_3	2.2	-2.8	6.8

(unit: μV/h)

4.Reference

1.K.Ota et al, *J.Electrochem. Soc.*, **139**(2), 667(1992).

THE RUSSIAN/AMERICAN FUEL CELL CONSORTIUM

A. Sylwester and R. Baker
Applied Energy Technology Integration
Sandia National Laboratory
P.O. Box 5800
Albuquerque, NM 87185

M. Krumpelt
Argonne National Laboratory
9700 South Cass Avenue
Argonne, IL 60439

BACKGROUND

The United States and Russia discovered a mutual interest in fuel cell development during a series of workshops designed to teach entrepreneurial skills to Russian nuclear weapon scientists and engineers to aid them in converting their skill to peaceful applications.

The proposal for a Russian/American Fuel Cell Consortium was initiated at the third workshop held in Livermore, CA, in May 1994. Representatives from U.S. fuel cell industries, U.S. research institutes, Russian institutes and ministries, and U.S. national laboratories attended, including those from GAZPROM, the Russian natural gas company. GASPROM needs to provide power for telemetry, cathodic corrosion protection of gas lines, and gas line pumping power in remote areas, and estimates that it needs approximately seventy thousand 1.5 to 15 KW plants to do so. Since the workshop, several direct working relationships have developed between the Russian Nuclear Weapon Institutes and the U.S. fuel cell industry.

Together, the Russians and Americans have developed a concept to make the consortium successful: to leverage financial resources by providing a best match of technical resources to solve specific problems in fuel cell power development and to eliminate unknown/unplanned duplication of effort. In this concept, power users would communicate their needs to potential fuel cell manufacturers. Fuel suppliers would report their ability to provide and distribute suitable fuels for utilization by the manufacturers fuel cell plants. The potential fuel cell manufacturers would then inform the scientists and engineers of the technical problems that prevent rapid fuel cell commercialization. Lastly, the scientists and engineers would identify and utilize the proper technical resources to solve these technical problems. An important side benefit of this concept is that it will strongly support defense conversion goals by providing meaningful technical challenges for Russian and U.S. scientists previously engaged in the development of nuclear weapons.

IMPLEMENTATION

The concept is being implemented by means of an agreement between the United States Department of Energy (DOE) and the Russian Federation Ministry of Atomic Energy (MINATOM). This agreement is guided by the principles of the December 1993 Russian/American agreement on scientific and technical collaboration and specifically addresses fuel cell development. The mission and purposes of the consortium are given on the poster. A steering committee composed of representatives from the U.S. and Russian governments national laboratories, and industry prepared the agreement and supporting documents for the consortium. The major supporting documents are those describing the Russian/American Fuel Cell Consortium (RAFCO) Participants and the Project Proposal guidelines. Both of these documents are shown on the poster and are available along with the basic agreement at the RAFCO table.

OPERATION

RAFCO will be operated by a Joint Committee selected from the participants and chaired by two representatives, one from DOE and one from MINATOM. Various subcommittees including the proposal guidance and evaluation committee will support the Joint Committee.

Intellectual property rights are recognized as an important concern and are covered in the agreement and supporting documents. The first cooperative projects to be implemented under the agreement have been identified by the steering committee and will be started as soon as the agreement is in place. A list of these projects in provided on the poster.

FUNDING

Primary funding will come from government sources, with both governments sharing costs. Private industry and other agencies are expected to provide funding for projects meeting their special interests.

RELATED ACTIVITIES

Joint ventures between U.S. industry and Russian entities are expected and encouraged to develop out of RAFCO activities.

CATALYZED DOUBLE LAYER CATHODES FOR HIGH PERFORMANCE AND LONG LIFE MOLTEN CARBONATE FUEL CELLS

M.Bischoff
Motoren- und Turbinen Union Friedrichshafen GmbH; 81663 Munich; Germany

U.Jantsch, B.Rohland
Center for Solar Energy & Hydrogen Research, 89081 Ulm; Germany

$NiO/LiCoO_2$ double layer cathodes (DLCs) were prepared with a thin highly active $LiCoO_2$-layer by a new double layer tape casting/sintering procedure. The resulting metallic porous precursor plates were mounted into the MCFC and heated up by a special procedure to form $LiCoO_2$ from air, Co and Li_2CO_3 in a solid/gas reaction. MCFCs with highly active $NiO/LiCoO_2$-DLCs can operate over prolonged periods of time with a Ni-precipitation which is 10% lower than one finds with state of the art NiO cathodes. According to [1] $LiCoO_2$-cathodes have theoretical life times of more than 100 000 hours at nonpressurized conditions.

MCFCs with new $NiO/LiCoO_2$ double layer cathodes (DLC) were investigated with regard to variable parameters of their microstructure. From the agglomerate model of the porous MCFC cathode, the dependence of the polarization resistance from the radius of the agglomerates and the inner agglomerate surface area was calculated.

Measurements of the pore size distribution by means of a mercury porosimeter have shown that during the first couple of hundred hours of contact with the carbonate melt at 650°C the morphology of the $LiCoO_2$ cathode layer undergoes some change. Originally there is a dual pore structure with large gas pores (radius ≈ 2.5 µm) and small agglomerate pores (radius ≈ 0.01 µm). After treatment with the melt the radius of the large pores was shifted to ≈ 4 µm and the radius of the small pores to 0.3 µm. However, polarization measurements did not shoe any indication that this structural changes had any effect on the electrode polarization.

Cathodes with different agglomerate sizes were prepared to study the influence of the agglomerate diameter on the electrode polarization. Fig.1 shows a SEM micrograph of one of this cathodes and table 1 gives the morphological parameters.

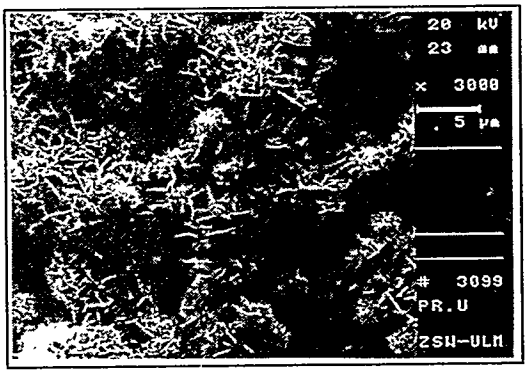

Fig. 1: SEM micrograph of a $LiCoO_2$-cathode

The iR-free cathode polarization versus current density at three different average agglomerate diameters are shown in Fig 2. As expected from the theory, the smallest polarization is obtained, if a cathode with a small agglomerate diameter is used. The iR-free polarization for cathode E3 at 650°C is 30 mV at 100 mA/cm² using a gas composition of 70% air/ 30% CO_2.

Table 1: Morphological parameters of various $LiCoO_2$ cathodes, calculated from pore size distribution measurements [2].

Cathode No	average agglomerate diameter [µm]	exterior surface area of agglomerates [m^2/cm^3]	specific inner surface area [m^2/cm^3]
E1	15.0	0.030	2.06
E2	10.5	0.055	7.80
E3	3.5	0.400	10.40

For the cathode E1, however, which has large agglomerates and a small inner specific area, we obtained 120 mV at 100 mA/cm² for the polarization voltage. The electrode E2 has a high specific inner surface area but an agglomerate diameter which is rather large. This gives a polarization voltage of 50 mV at 100 mA/cm².

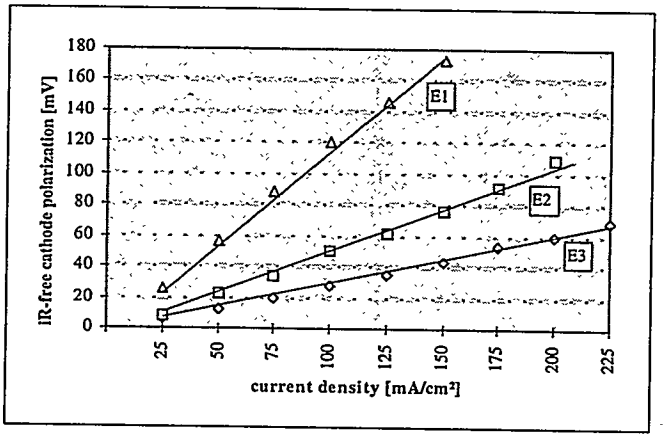

Fig. 2: iR-free cathode polarization versus current density at various average agglomerate sizes

Cells with NiO/$LiCoO_2$-DLCs, which are long term stable under pressure up to 5 bar, were operated at variable oxygen partial pressure. At realistic gas compositions, 650°C and 5 bar total pressure, a cell performance of 245 mW/cm² was obtained. Fig. 3 shows the cell voltage as a function of current density at 1 and 5 bar pressure.

The catalytic activation of the inner surface of the $LiCoO_2$-layer makes it viable, to reduce the operating temperature without a serious performance penalty. Measurements on standard and activated DLC's have shown, that in the temperature range 550°C to 700°C the activation energy with respect to the charge transfer resistance can be reduced from 108 kJ/mol to 60 kJ/mol (see Fig.4).

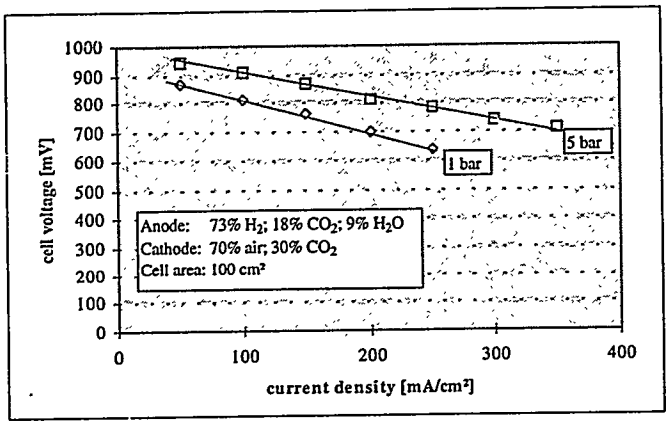

Fig.3: Cell Voltage at constant anode and cathode gas utilization versus current density at 1 and 5 bar pressure with $LiCoO_2$ cathode

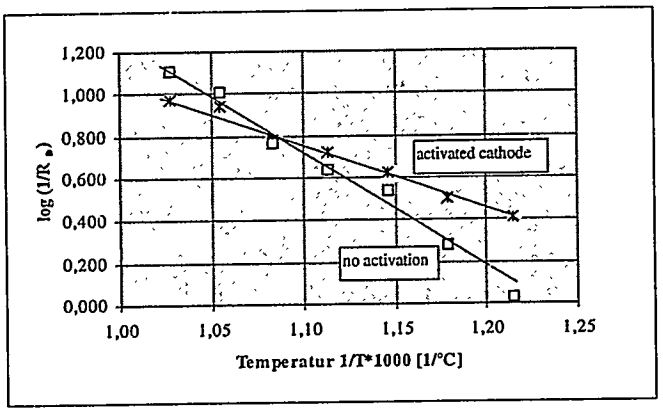

Fig.4: Arrhenius plot with respect to the reciprocal charge transfer resistance showing the activation energy for the activated and not activated cathode

CONCLUSIONS

MCFCs with NiO/$LiCoO_2$-cathodes achieve a high power density at 650°C comparable to that of regular NiO-cathodes provided that the following conditions of the microstructure are given:

- average agglomerate diameter < 3µm
- specific inner surface of agglomerates > 10 m^2/cm^3

[1] L.Plomb, R.C.Makkus, E.F.Sitters, G.Rietveld, „ Endurance Issues and Materials Development in Molten Carbonate Fuel Cell Technology" Program and Abstracts, pp. 164-167, 1994 Fuel Cell Seminar, San Diego, California, Nov.28-Dec.1

[2] B.Rohland, U.Jantsch, „$LiCoO_2$-Cathodes with Optimized Microstructure. One of the Keys for High Performance and Long Life MCFC", Denki Kagaku, Vol. 64, No.6, pp. 519-525, 1996

Acknowledgment:

This work is based on a project supported by the German Federal Ministry of Education, Science, Research and Technology (BMBF) through contract No. 0329173B. The authors wish to express their gratitude for the support received.

DEVELOPMENT OF A NEW ELECTROLYTE MATRIX FOR MCFC

I. Nagashima,K. Higaki, S. Terada,
and T. Suemitsu

Akashi Technical Institute, Kawasaki Heavy Industries, Ltd.
1-1, Kawasaki-cho, Akashi, 673 Japan

Introduction

To prolong the life of cell is one of the most important issues for MCFC to be brought into actual application. In this respect, investigators have been proposing the addition of tungstate salt such as K2WO4 into MCFC electrolyte, which is supposed effectively to reduce the sintering of anode probably by precipitates formed through the reduction of tungstate with dissolved hydrogen near the anode surface (1).
In this research, such effect upon sintering of anode was quantitatively examined by out-of-cell tests and the validity of above assumption for the mechanism was confirmed. Also other effects of tungstate salt addition into electrolyte, such upon corrosion of separator, solubility of cathode, stability of matrix substrates (LiAlO2) were investigated.

Effect on sintering of anode

Fig.1 is an example of the results of 100cm^2 class cell operating test using pure Ni anode with 1.4 weight % K2WO4 addition into electrolyte, which shows more than 10,000 hours operation was possible (1), although 2 to 3 thousands hours operation, at most, was possible in case of no addition of tungstate salt due to sintering of pure Ni anode. Fig.2 is an example of pore volume change of pure Ni anode using electrolyte with/without tungstate salt addition, which was obtained by simulated cell operation with 10cm^2 effective electrode area. It shows that tungstate salt addition into electrolyte has some effect of restricting the microstructural change of the anode. Fig.3, obtained by an EPMA analysis, shows the distribution of W concentration across the anode and the electrolyte matrix after 10,000 hours cell operation. Clearly the concentration of W at the anode portion is higher than that at the matrix portion. This means that tungstate ion ,$WO4^{2-}$, converts into some other insoluble compounds at the anode portion as a sink and the diffusion of $WO4^{2-}$ ion from the matrix portion to the anode portion occurs. Such compound of W is supposed to be formed through the reduction of $WO4^{2-}$ ion by dissolved hydrogen in the electrolyte and to precipitate around the anode particles, accordingly to restrict the sintering of Ni anode.

Effect on the corrosiveness of electrolyte

In general, oxi-anions including carbonate ion tend to dissociate oxide ion, O^{2-}, according to the ambient condition and to affect the basisty of the melts. Tungstate ion, $WO4^{2-}$, is supposed to act similarly and possibly to have some effects on corrosion of separator material by melts or cathode (NiO) dissolution in melts. Fig.4 shows the solubility of NiO vs partial pressure of CO2 in Li/K carbonate system and Li/Na carbonate system both with and without K2WO4 addition and shows that the effect of K2WO4 addition on the solubility of NiO is small. On the other hand, as shown in Fig.5, results of corrosion test using SUS316L test pieces at cathode

ambient shows that K2WO4 addition has some effect on the corrosiveness of the melt and minimum corrosion was attained at 1.4 wt% K2WO4 addition. These could not be explained merely by the basisty of the melt and further investigation is required.

Stability of matrix substrate (LiAlO2)

Phase transition and particle growth of LiAlO2 particle, observed during longer cell operation, is a serious problem to overcome in order to attain more than 40,000 hours of life of MCFC for it causes pore coarsening of porous matrix substrate and less capillary force to retain the electrolyte in its pores (2). Out-of-cell tests, in which LiAlO2 powders were impregnated in melts, were conducted and the effect of various parameters on phase transition and particle growth of LiAlO2, including tungstate salt addition into melt, were investigated. Fig.6 is an example of phase transition of LiAlO2 at CO2 ambient and shows that tungstate salt addition has some influence on the phase stability of LiAlO2. In case of no addition of tungstate salt, increase of α phase and decrease of β phase and γ phase were remarkable, whereas such phase transition were small and especially slight increase of γ phase was observed in case of tungstate salt addition. These mechanism of phase transition and particle growth, including the effects of additives other than tungstate salt, are now under investigation.

Conclusion

Effects of tungstate salt addition into MCFC electrolyte were investigated by out-of-cell tests. Anode sintering was reduced by tungstate salt addition, which was supposed to originate in the precipitation of W containing compounds around the anode particles formed by the reduction of tungstate by dissolving hydrogen. Solubility of cathode (NiO) was not affected by tungstate salt addition but the corrosion of stainless steel was minimum at 1.4 wt% addition. Further, phase transition of LiAlO2 was reduced by tungstate salt addition.

Acknowledgement

This work was conducted under a contract from NEDO (New Energy and Industrial Technology Development Organization) and MCFC Research Association as a part of the New Sunshine Program of MITI (Ministry of International Trade and Industry).
We appreciate their advice and support.

Reference

1.Terada et al., "Development of a New Electrolyte Matrix for MCFC", Fuel Cell Seminar Program and abstracts, pp128-131, Nov.28-Dec.1, (1994)
2.Tanimoto et al., "Long term Operation of 100 cm2 class Single Cell of MCFC", Proc. 2nd IFCC, pp207-210, Fev.5-8, (1996)

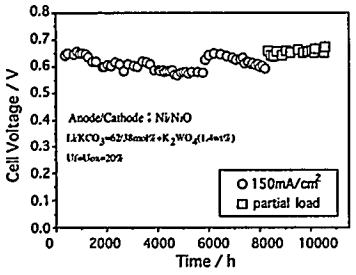

Fig.1 An Example of 100cm² Cell Performance

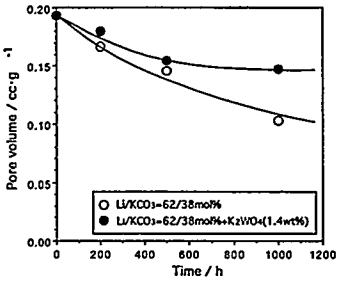

Fig.2 The Influence of Tungstate Addition on Anode Pore Volume

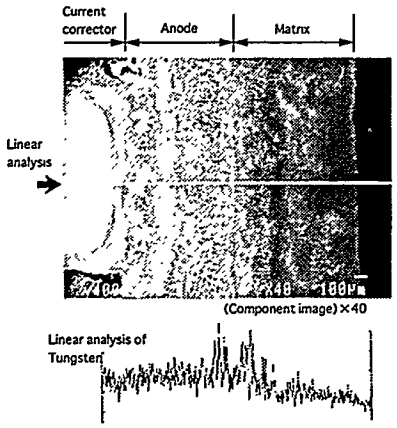

Fig.3 Deposition of Tungsten (After 10000h operation)

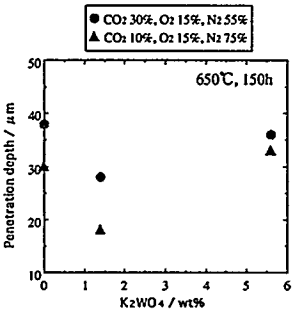

Fig.4 The Influence of Tungstate Addition on SUS316L Corrosion

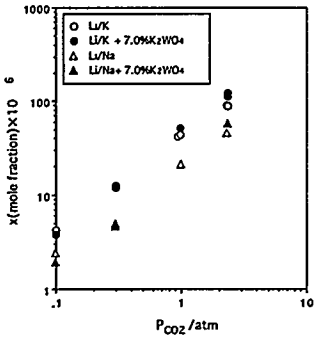

Fig.5 The Influence of Tungstate Addition on Cathode Solubility

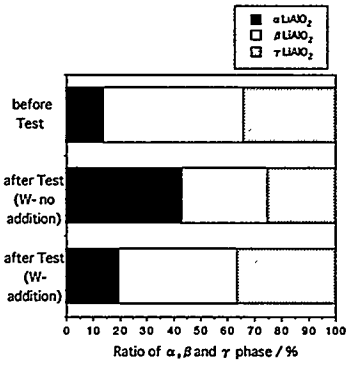

Fig.6 The Influence of Tungstate Addition on Phase Transition of Matrix

<Test condition>
Matrix : HSA-19
Electrolyte : Li/KCO₃(62/38), w/o 1.4wt %K₂WO₄
Temp. : 650℃
Gas : CO₂
Time : 500h

TEST RESULTS OF A 2 kW INTERNAL MANIFOLD MCFC STACK

H.-C. Lim, J-H. Seol, K.-S. Ahn, I.-H. Oh, T.-H. Lim, S.-W. Nam, S.-A. Hong
CASEE, Korea Electric Power Research Institute,
103-16 Munji-dong, Yousung-gu, Taejon 305-308 Korea

Korea Institute of Science and Technology
39-1 Cheongryangri-dong, Seongbuk-gu, Seoul 136-791, Korea

INTRODUCTION

A R&D program on MCFC, of which current target is to establish the fundamental technology through fabricating a 2kW stack with the performance higher than 0.8V at 150mA/㎠, has been started since 1993. The program consisted of two phases : a 2kW class MCFC stack and the test facility will be constructed and operated during the first phase (1993-1996) and then a 100kW MCFC system will be constructed in the second phase(1997-2002) on the basement of first phase results. From this strategy, KEPRI formed the MCFC developing group with Korea Institute of Science and Technology(KIST) and Samsung Heavy Industry (SHI) for fabricating, operating and evaluating of 2kW MCFC stack. This paper presents the results of this first phase program and some of the problems experienced during its operation and fabrication of stack components. Specification of the stack under operation is shown in Table 1.

FABRICATION OF CELL COMPONENTS

As for the electrodes, the metal powders (Ni for cathode and a mixture of 90% Ni and 10% Cr for anodes) were used for making slurries and the slurry was casted into the shape of tape by the tape casting method. After being dried, this green sheet was then dewaxed and sintered in the electric furnace under the atmosphere of $Ar-H_2$ to complete the process. A sintered Ni for cathodes was further oxidized into NiO during the cell operation by an in-situ method. $LiAlO_2$ powders and the mixture of 62 mole % Li_2CO_3 and 38 mole% K_2CO_3 powders were used as the materials for the matrix and electrolyte plate, respectively, which were also fabricated by the tape casting method. To meet the requirement of 1,000㎠ electrode area, the skill of the component enlargement up to 45cm x 42cm in matrix and electrolyte plate and 36 x 31 in electrodes has been established and these large size components have been successfully supplied to be used in the stack. Separator plates consisted of 2 mask plates and 1 center plate. Separator plate had the gas channel of co-flow pattern. Al coating on the wet seal area of the separators was also chosen for its corrosion protection. Plasma spray method for Al coating in the separators was adapted.

STACK SPECIFICATION AND CONFIGURATION

An internally manifolded stack with the electrode area of 1,000㎠ has been designed and fabricated. The components for the stack were fabricated at KIST laboratory and delivered to KEPRI for assembling the stack where the test facility was constructed for operation and evaluation. On the top and bottom, the electric heaters were located for avoiding the heat loss from the stack. The reaction gas supply and the exhaust were equipped at the bottom of stack through the gas manifold. The air cylinder and the load cells located on the top and under the bottom of the stack were used for compressing the stack. More than 50 thermocouples and 20 electric terminals were installed for measuring the temperature, cell voltage and load current in the stack.

Table 1. Specification of a 2 kW stack being operated

Items	Specification
Power output	2.5kW
Cell voltage	0.82V/cell
Current density	150mA/㎠
Electrode area	1,000 ㎠
Cell Number	20 cell
Current collector	Anode : Ni, Cathode : SUS
Separator	SUS 316L
Operating temperature	650℃
Operating pressure	1 atm
Fuel utilization	40%
Reforming method	External
Manifold	Internal

STACK TEST FACILITY

Stack test facility consisted of a gas supplying unit which had a reformer with a catalystic burning system to supply the heat to the reactor, a gas preheating unit and the gas cooling and separating unit. In addition, this system had a data acquisition and control unit which controls the temperature and mass-flow automatically.

STACK PERFORMANCE

Two 2 kW stacks have been tested since this February. First stack(ST-14) was operated more than 1,000 hours but failed in the continuous operation under the load of 150A because of separator defaults. Second stack(ST-17) has been operating for 800 hours (as of writing this paper) without any degradation of

voltage under the 150A electric load. Fig. 1 shows the I-V characteristics of the 2kW stacks ST-14 and ST-17. The fuel and oxidant utilization at 150mA/㎠ were kept 40% in the test and 70% of air and 30% of CO_2 were used as an oxidant gas. It is seen that the OCVs were 21.0 V(1.050V/cell) in stack ST-14 and 21.6 V (1.805V/cell) in stack ST-17 while the voltages at current density of 150mA/㎠ were 14.74V (0.737V/cell) in the stack ST-14 and 16.52V (0.826V/cell) in ST-17, respectively. The corresponding analysis of the voltage loss reveals that the loss composed of Nernst loss, the internal resistance loss, and the electrode polarization. Most of voltage loss came from the electrode polarization and the internal resistance.

Fig. 2 showd the voltage distribution of 20 cells in the stack ST-17. The cell by cell voltage variation during the nomal operation under the load of 150A showed that the voltages ranged from 800 to 860 mV except No.11 cell which had malfunction in the cathode channel. The standard deviation of the cell voltages in the stack ST-17 showed 8.8mV which was less than the previous stack. Thus, uniformity of the cell to cell performance seems to be very good in the stack ST-17.

Fig.3 showes the endurance test results of stack ST-17. The stack is now being operated for 800 hours with the performance of no decay rate, which also turned out a huge progress compared to previous the small stack because of Al coating in the separator's wet-seal area.

CONCLUDING REMARKS

The 2 kw class stack was successfully manufactured and has been operated more than 800 hours. Based on the encouraging test results from this stack, our 2-phase program for construction of a 100 kW stack will be continued. Efforts will be made on the enlargement of components, the long term operation, the development of alternative materials, and so on.

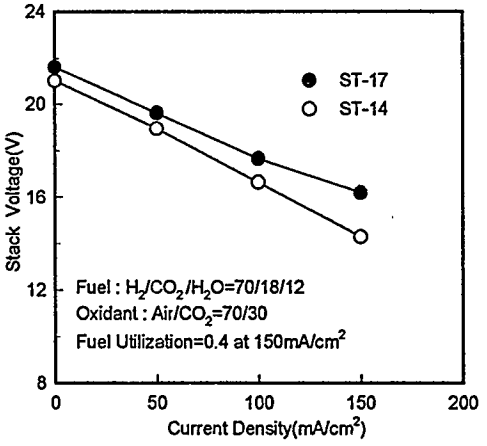

Fig. 1. I-V Characteristics of the Stacks

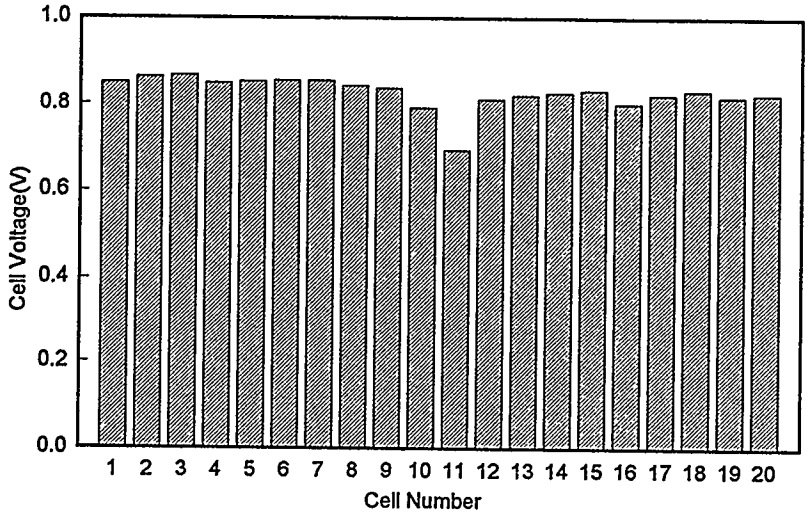

Fig. 2. Distribution of Cell Voltage at the load of 150mA/cm^2 in ST-17.

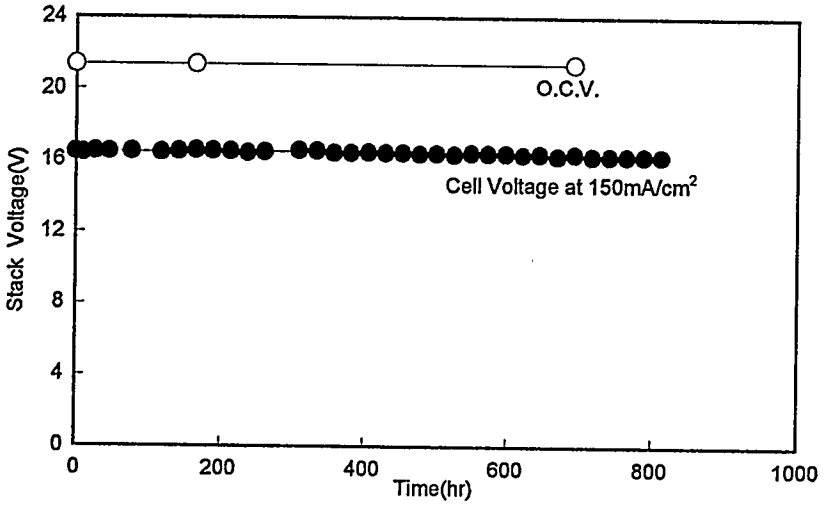

Fig. 3. Cell Performance of ST-17 .

PREDICTION OF TEMPERATURE PROFILE IN MCFC STACK

Kab Soo Lee, Hwayong Kim, Seong-An Hong*, Hee Chun Lim**
Department of Chemical Engineering
Seoul National University
Seoul, Korea.
*Korea Institute of Science and Technology
**Korea Electric Power Research Institute

ABSTRACT

A simple three dimensional model was developed to simulate the temperature distribution and the performance of various flow types of the MCFC stack. The objective of this study was to understand the complicated phenomena occurring in the MCFC stack and to supply the basic data for optimizing the operating condition of the MCFC stack. Assuming that the stack consists of a number of differential elements which have uniform temperature and gas composition, the model was solved by finite difference method. The performance of this model was demonstrated by comparing the calculated value with experimental data of the 1.5kW class co-flow type MCFC stack operated in KIST. This model can be utilized as a simple diagnostic tool in case of the operational abnormality such as the hot spot which often occurs inside the stack.

SYSTEM

The objective system of this study is 1.5kW class MCFC stack composed of 20 unit cells[1]. The effective area of the electrode is 625cm^2. Preheated fuel and oxidant gases are supplied through the internal manifold to the channels of each unit cell.

Because of the complexity of the phenomena in the real system; e. g., mass transport, heat transfer, chemical and electrochemical reactions, etc. adequate simplification by several assumptions is required before the equations are described. The assumptions employed are as follows.

(1) Stack is operating at steady state.
(2) The differential element is at isothermal condition and the gas composition, current density and heat generation rate are uniformly distributed in it.
(3) All gases are ideal and flow in laminar regime.
(4) Operating voltage of the stack is constantly maintained.
(5) Radiative heat transfer is neglected.

EQUATIONS

The relation between operating cell voltage and current can be simply expressed by Ohm's law.

$$V = E - I \cdot (Z_a + Z_c + Z_{IR}) \qquad (1)$$

where, Z_a, Z_c, Z_{IR} are anode polarization, cathode polarization and internal resistance, respectively.

Z_a, Z_c are the function of the gas composition and temperature.

$$Z_a = C_1 \cdot (P_{H_2})^a \cdot (P_{CO_{2,a}})^b \cdot (P_{H_2O})^c \cdot (P_{CO})^d \cdot \mathrm{Exp}\left(\frac{-\Delta E_{a,a}}{RT}\right) \quad (2)$$

$$Z_c = C_2 \cdot (P_{O_2})^e \cdot (P_{CO_{2,c}})^f \cdot \mathrm{Exp}\left(\frac{-\Delta E_{a,c}}{RT}\right) \quad (3)$$

Where, C_1 and C_2 are constants, ΔE is the activation energy. The power index a, b, c, d, e and f were estimated empirically[2]. And Z_{IR} is the function of the gas temperature[3].

E is the equilibrium potential obtained from Nernst equation.

$$E = E^o + \frac{RT}{nF} \ln \frac{P_{H_2} \cdot P_{O_2}^{\,2} \cdot P_{CO_{2,c}}}{P_{H_2O} \cdot P_{CO_{2,a}}} \quad (4)$$

Where, E^o is the standard potential, F is Faraday constant. The equilibrium partial pressure of the anode gases were obtained from the thermodynamic equilibrium constant considering the water-gas shift reaction[4].

By the assumption of the steady state and uniform current in differential element, material balance can be expressed as follows.

$$\frac{\partial M_i}{\partial x} = \frac{I}{nF\Delta x} \quad (5)$$

where, M_i is the mole flow rate of each gas, Δx is the length of unit grid.

Energy balance considering mass transfer and heat loss is,

$$K_j A_j \frac{\partial T}{\partial x} - M_A C_i \cdot \Delta T_i - H_{loss} = -(E - V) \cdot I \quad (6)$$

where, K_j, A_j are the thermal conductivity and the heat conduction area of each direction, C_i is the heat capacity of each gas, H_{loss} is the heat loss from the stack.

PERFORMANCE OF THE STACK

From the co-flow type stack simulation, 1.74kW of power was obtained at a current density of 150mA/cm^2, a somewhat higher value than experimental value of 1.70kW(Figure 1). At this condition it was calculated that the voltage loss of the stack results from Nernst loss by 63mV, electrode polarization by 81mV and IR loss by 80mV, respectively. These values were similar to the experimental values (64mV, 85mV, 79mV, respectively).

The current density profile of the stack was also obtained. Regardless of the type of the gas flow, the profile tended to decrease with the progression of the anode gas flow. This trend was because the current density was more strongly affected by the gas composition than the temperature. However, because of the temperature effect, significant differences of the current density profile existed among the different gas flow type of the stack. The average current density of the stack at the same operating voltage was larger in order of co-flow, cross flow and counter flow.

TEMPERATURE PROFILE

The results of comparison between the calculated temperature and the measured one are illustrated in Figure 2. Even though the former deviates by 1-10℃ from the later, but there exists the similar tendency.

The average stack temperature was 652.2℃ for co-flow type, and 651.7℃, 651.6 ℃ for cross flow, counter flow, respectively. Figure 3 shows the calculated temperature profile in the 10th cell plate of various flow types of the stack. The temperature increased in the gas flow direction. The increasing tendency of the temperature was due to the relatively low temperature(550℃) of the inlet gas, and the gas flow type of the stack heavily influenced on the temperature profile.

CONCLUSION

A three dimensional MCFC stack model of various flow type was developed. This model gave a reasonable prediction of the performance and the temperature profile. According to the simulation results, the co-flow type stack showed a better performance and temperature profile than the cross flow or counter flow type stack.

REFERENCES

1. S.-A. Hong, I. H. Oh, T. H. Lim, S. W. Nam and K. S. Lee, "A Development of 2kW Class Molten Carbonate Fuel Cell Stack", Final Report, KEPCO, 1995.
2. C. Y. Yuh and J. R. Selman, "The Polarization of Molten Carbonate Fuel Cell Electrodes", J. of Electrochem. Soc., Vol. 138, No. 12, P. 3642, 1991.
3. P. G. Glugna and V. J. DeCarlo, "The Specific Conductance of Molten Carbonate Fuel Cell Tiles", J. of Electrochem. Soc., Vol. 129, No. 8, P. 1745, 1982.
4. J. M. Smith and H. C. Van Ness, "Introduction to Chemical Engineering Thermodynamics", 4th ed., McGrow-Hill, New York, 1987.

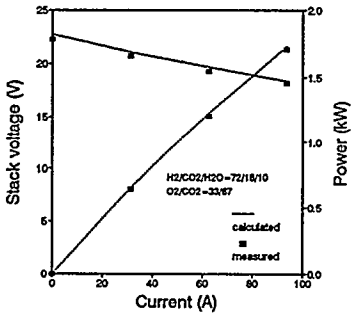

Figure 1. Performance of the 1.5kW class co-flow type MCFC stack.

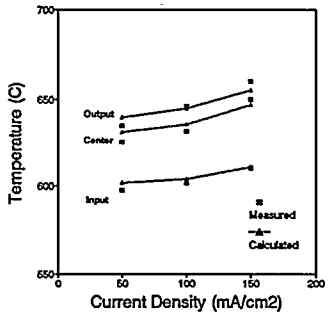

Figure 2. Comparison of the calculated value with the experimental value of the stack temperature.

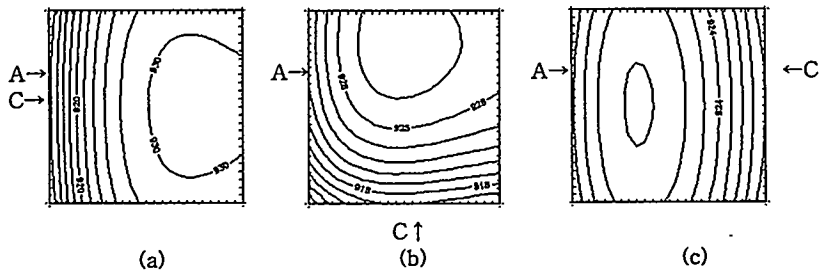

Figure 3. Temperature profile in the 10th cell plate of various flow types of the stack. (a) Co-flow (b)Cross flow (c)Counter flow

DEVELOPMENT OF CU ALLOY ANODE AND SEPARATOR COATED WITH AL-NI INTERMETALLIC COMPOUND

K. Toyokura
The Japan Research and Development Center for Metals
6F No.17 Mori-bldg., 1-26-5 Toranomon, Minato-ku , Tokyo 105, Japan

K. Hoshino
Mitsubishi Materials Corporation
1-297 Kitabukuro-cho, Omiya, Saitama 330, Japan

M. Yamamoto
Nisshin Steel Co., Ltd
4976 Shinnanyo city, Yamaguchi 746, Japan

INTRODUCTION

Anode made of Cu alloy and separator coated with Al-Ni intermetallic compound have been developed for MCFC.

Anode of Ni alloy is usually used. However, the alternative of cost lower than Ni alloy anode should be needed, because Ni is expensive. Cu is attractive as an anode material for MCFC because it is inexpensive and electrochemically noble. However, the creep resistance of Cu is not sufficient, compared with Ni alloy. In this study, strengthening due to oxide-dispersed microstructure has been developed in Cu-Ni-Al alloy with the two-step sintering process.

A wet-seal technique has been widely applied for gas-sealing and supporting of electrolyte in MCFC. Since the wet-seal area is exposed to a severe corrosive environment, corrosion resistance of material for wet sealing is related with the cell performance. Al-Ni plating with post-heat treating for stainless steel has been investigated. Stainless steel substrate was plated with Al after being coated with Ni, then heat-treated at 750 ℃ for 1 hour in Ar gas atmosphere. Due to the treatment, Al-Ni intermetallic compound (mainly Al3Ni2) layer is formed on stainless steel surface. The long-term immersion test was carried out till 14,500 hours in 62mol%Li2CO3-38mol%K2CO3 at 650 ℃ under air-30%CO2 atmosphere, for the purpose of evaluating the corrosion resistance and thermal stability of Al-Ni intermetallic compound layer in actual generating with MCFC.

EXPERIMENTAL

Cu alloy anode

Powder of Cu alloy was made with high pressure water atomization method, and was sieved under 44 μm in diameter. Green sheet was made from the powder with conventional tape casting method. Cu alloy anode was made of the green sheet, which was heated at 700 ℃ in H2 after being heated at 450～1,050 ℃ in air (namely the two-step sintering method involving both oxidation and reduction for the green sheet). Creep test of Cu

alloy anode coated with electrolyte was carried out in a H2-CO2-H2O (79-19-2) mixture gas stream under 5kgf/cm² at 700℃, in order to evaluate the stability of morphology at high temperature. The evaluation was determined by measuring thickness of Cu alloy anode.

Potentiodynamics polarization measurement were performed under anode atmosphere (H2-20%CO2 gas bubbled in Li2CO3-38mol%K2CO3 molten carbonate) at 650 ℃ with the 33%O2-67%CO2/Au reference electrode.

Coated separator

The specimens are shown in Table 1. The chemical composition is given in Table 2. The specimens were electroplated with Al and Ni. There were two kinds of coating thickness in specimens. One is 15μm of Al coating thickness with 5μm of Ni coating thickness (Type A), and another is 10μm of Al with 5μm of Ni (Type B). And coated specimens were heated at 750℃ for 1 hour in Ar gas.

Immersion test in molten carbonate and heat test under air atmosphere were carried out till about 15,000 hours.

RESULTS

Cu alloy anode

Creep tests were performed with Cu-50%Ni-5%Al anode and Cu-30%Ni-5%Al anode in H2-CO2-H2O (79-19-2) mixture gas stream, under 5kgf/cm² at 700 ℃ for 1,000 hours. The result is shown in Figure 1. The result indicates that Cu-30%Ni-5%Al anode has sufficient creep resistance (less than 5% for 1,000 hours), although Cu-30%Ni-5%Al anode has inferior to Cu-50%Ni-5%Al anode in creep resistance in the condition.

Potentiodynamics polarization measurements on Cu, Ni, Cu-30%Ni alloy and Cu-50%Ni alloy were carried out under an anode atmosphere (H2-20%CO2 gas bubbled in Li2CO3-38mol%K2CO3 molten carbonate) at 650℃ with Au reference electrode (under an atmosphere of 33%O2-67%CO2), as Cu-Ni alloy layer is formed on the surface of Cu-Ni-Al anode which is sintered through the two-step sintering process involving both oxidation and reduction. The relation between Ni content in Cu-Ni alloy and potential is shown in Figure 2. The result indicates that the potential becomes higher as Cu content increases in Cu-Ni alloy.

Coated separator

Figure 3 shows cross section of microstructure after immersion test at 650 ℃. The coating is in good adhesion and has good corrosion resistance. No defects such as crack and detach are observed in the coating. Thickness of oxide film formed on the surface of Al-Ni layer is about 5μm after 14,500 hours. This oxide film has a good protection against molten carbonate. Figure 4 shows cross section of microstructure after heat test at 650, 700, 750℃. Coating heated for 10,000 hours is in good adhesion in specimens in both Type A and B, although voids grow near the interface of coating and substrate in Type B specimen.

ACKNOWLEDGMENT

This work was conducted under a subcontract with MCFC Research Association which was commissioned by NEDO (New Energy and Industrial Technology Development Organization) as a part of the New Sunshine Program of MITI (Ministry of International Trade and Industry). We appreciate the advise and support of MCFC research association, NEDO and MITI.

Table1 Plating thickness and heat-treated conditions of Al/Ni-plated materials used in immersion test.

	substrate	plating thickness		heat-treated condition
		Ni (μm)	Al (μm)	
TypeA	SUS310S	5	15	750 1h
TypeB			10	

Table 2 Chemical composition of plating substrate. (mass%)

	C	Si	Mn	P	S	Ni	Cr	Fe
AISI310S	0.06	0.80	1.03	0.02	0.003	19.69	25.67	bal.

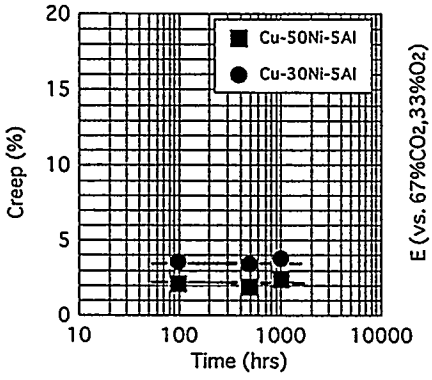

Figure 1 Creep of Cu-Ni-Al anodes

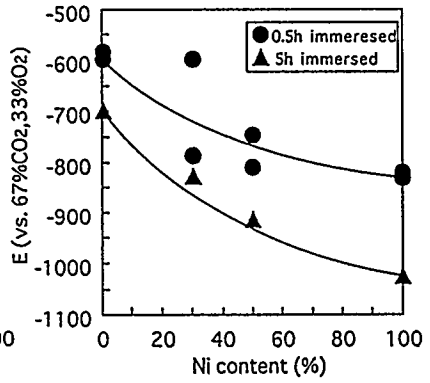

Figure 2 Immersion potential of Cu, Ni, Cu-30%Ni, Cu-50%Ni

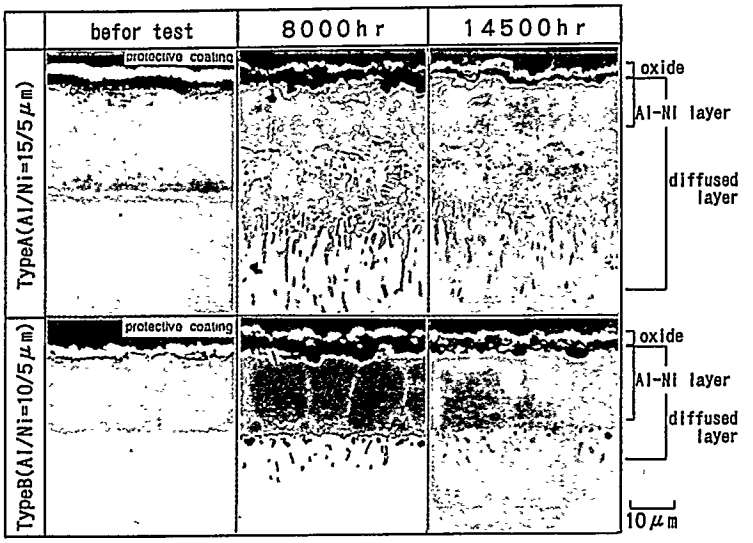

Figure 3 REM images of cross section of surface layers before and after immersion test at 650°C under 70%air-30%CO_2 atmosphere.

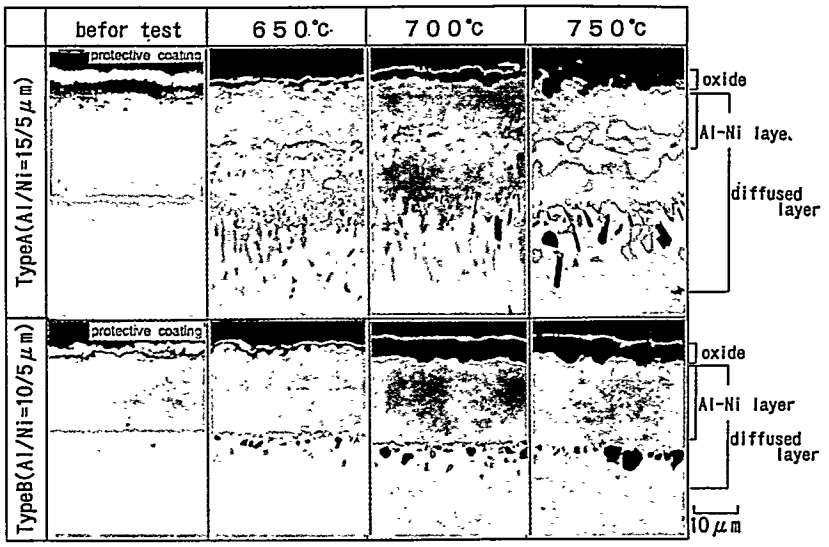

Figure 4 REM images of cross section of surface layers befor and after heating test for 10000hr, under Air atmoshere

EVALUATION ON THE FEASIBILITY OF ETHANOL STEAM REFORMING IN A MOLTEN CARBONATE FUEL CELL

S.Cavallaro **, E. Passalacqua*, G.Maggio *, A. Patti*, S.Freni*
* *Istituto CNR-TAE, via S.Lucia sopra Contesse 39, 98126 S. Lucia, Messina, Italy.*
** *Dipartimento di Chimica Industriale - Università di Messina P.O. Box 29, 98166, Messina, Italy.*

Introduction

The molten carbonate fuel cells (MCFCs) utilizing traditional fuels represent a suitable technological progress in comparison with pure hydrogen-fed MCFCs. The more investigated fuel for such an application is the methane, which has the advantages of low cost and large availability; besides, several authors demonstrated the feasibility of a methane based MCFC [1-2]. In particular, the methane steam-reforming allows the conversion of the fuel in hydrogen also inside the cell (internal reforming configuration), utilizing the excess heat to compensate the reaction endothermicity. In this case, however, both the catalyst and the cell materials are subjected to thermal stresses due to the *cold spots* arising near to the reaction sites MCFC [3].

An alternative, in accordance with the recent proposals of other authors [4, may be to produce hydrogen from methane by the partial oxidation reaction, rather than by steam reforming. This reaction is exothermic ($\Delta H°$=-19.1 kJ/mol H_2) and it needs to verify the possibility to obtain an acceptable distribution of the temperature inside the cell. The alcohols and, in particular, methanol [5] shows the gas reformed compositions as a function of the steam/ethanol molar ratio, ranging from 1.0 to 3.5. The hydrogen production enhances with this ratio, but it presents a maximum at S/EtOH of about 2.0. Otherwise, the increase of S/EtOH depresses the production of CO and CH_4, and ethanol [6] may be a further solution for the hydrogen production inside a MCFC. In this case, also, the reaction in cell is less endothermic compared with the methane steam reforming with the additional advantage of a liquid fuel more easily storable and transportable. Aim of the present work is to perform a comparative evaluation of the different solutions, with particular reference to the use of ethanol.

Thermodynamic approach

Figure 1 shows the values of the Gibbs free energy of formation of the molecules involved in the various processes as a function of the temperature.

As results from this figure, at the cell temperature (T=923 K) the more stable compounds are CO, CO_2 and H_2O; hence, equilibria will be shifted towards the formation of such products. Starting from ethanol or methanol, some methane could be produced. In any case, an appropriate flow of H_2O must be established to prevent coke formation.

Whatever reaction is considered, the immediate use of hydrogen in cell, in accordance with the direct internal reforming (DIR-

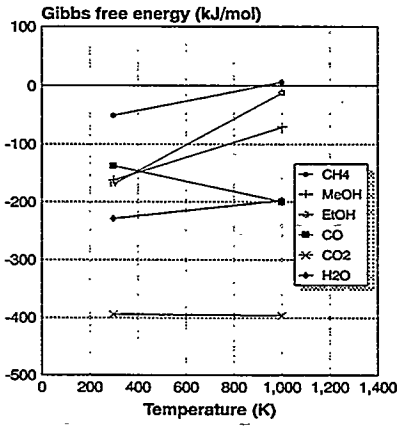

Fig.1: Gibbs free energy of different species vs. temperature.

MCFC) configuration, enhances the fuel conversion for all the equilibria.

The optimal cell operation depends on the amount of heat released or required by the considered reaction. In fact, since the electrochemical cell reaction is exothermic, it could be beneficial to directly utilise, the excess heat in the anodic compartment (DIR-MCFC), to supply the fuel reforming reaction.

The standard hentalpies per moles of H_2 corresponding to the main steam reforming reactions, the partial oxidation and the shift reaction, which occurs contemporaneously on the same catalytic sites, are given as follows:

1. $CH_4 + H_2O = CO + 3\ H_2$	$\Delta H° = 68.8$ kJ/mol H_2
2. $CH_4 + 1/2\ O_2 = CO + 2\ H_2$	$\Delta H° = -19.1$ kJ/mol H_2
3. $CH_3OH = CO + 2\ H_2$	$\Delta H° = 45.0$ kJ/mol H_2
4. $C_2H_5OH + H_2O = 2\ CO + 4\ H_2$	$\Delta H° = 64.0$ kJ/mol H_2
5. $C_2H_5OH + 1/2\ O_2 = 2\ CO + 3\ H_2$	$\Delta H° = 4.68$ kJ/mol H_2
6. $CO + H_2O = CO_2 + H_2$	$\Delta H° = -41.2$ kJ/mol H_2

The reaction 1. is the most endothermic among the considered reactions, it produces the colder spots on the reaction sites. The more exothermic, except the shift reaction 6. which takes place independently from the used fuel, is the methane partial oxidation reaction 2.. The ethanol partial oxidation is almost athermal, while, among the steam reforming reactions, that of methanol is surely the less endothermic.

At last, it is useful to consider also the moles of H_2 produced from a mole of converted fuel, as shown in Tab.I. This parameter is very significative to evaluate the DIR-MCFC plant compactness and to optimize the fuel storage and transportation devices. In the light of such observations, it seemed interesting to focus our attention on the ethanol steam reforming.

Table I: H_2/fuel molar ratio

	CH_4	CH_3OH	C_2H_5OH
Steam reforming	4	3	6
Partial oxidation	3	3	5

Catalysts

The catalysts of more general use for the methane and methanol steam reforming are formed of Ni or noble metals supported on MgO [4]. Although the same catalysts can also work for the partial oxidation reactions, the use of mixed oxides of La and other metals (Fe, Co, Ni, etc.) minimizes the coke formation improving the metal dispersion [7]. The methanol and ethanol reforming have been also studied on mixed catalysts based on Cu [8], which operate with high yields in CO_x at even T is lower than 600 K. Some catalysts, specifically used in the past for the synthesis of the alcohols, are, also, suitable for the decomposition of the ethanol into carbon dioxide and hydrogen. This group comprises catalysts based on Zn, Cr, chromium/manganese/zinc oxides, opportunely doped by alkaline metals. Further examined catalysts, based on $CuO/ZnO/Al_2O_3$ (BASF S3-85), seem applicable to the ethanol steam reforming, but they show lower stability to the molten carbonate fuel cell temperature. At last, catalysts based on silver are still used for the dehydrogenation of the ethanol into acetaldehyde.

The use of an high operative pressure, although not recommended from a thermodynamic point of view, allows the interposition of metallic or ceramic membranes between the catalyst and the anode, reducing in such a way the poisoning of the catalyst due to the electrolyte alkali vapours. The investigation on the employment of membranes, began since the sexties, demonstrated that they are able to catalyze the dehydrogenation of hydrocarbons or the steam reforming reactions, when they supported some appropriate catalysts.

Results and discussion

In Fig.2 are reported the gas reformed compositions as a function of the steam/ethanol molar ratio, ranging from 1.0 to 3.5, that represent the typical behaviour of the selectivity yielded by the ethanol steam reforming reaction. The hydrogen production enhances with this ratio, but it presents a maximum at S/EtOH of about 2.0. Otherwise, the increase of S/EtOH depresses the production of CO and CH_4, because it moves the reaction equilibrium towards a further production of hydrogen. Furthermore, it is opportune to consider that the risk of carbon deposition, on the active catalyst sites, increases heavily when values of S/EtOH lower than 2.0 will be applied. In Fig.3 are reported the polarization curves calculated for a molten carbonate fuel cell with direct internal reforming of ethanol. The curves have been determined considering a flow of ethanol corresponding to a fuel utilization coefficient equal to 75% for a current density of 160 mA/cm^2 and for operational temperature ranging from 873 K to 973 K.

As well as other type of fuel cell, the influence of the temperature on the cell performance is significant also for the determination of the open circuit cell voltage. In fact, this value decreases of about 32 mV/100 K. Anyway, for every considered temperature, the limit current results equal to about 270 mA/cm^2. The operational pressure does not influence the cell voltage. In fact, its increase, unadvisable from a thermodynamic point of view (see above), enhances the electrochemical cell reaction, through a rise in the partial pressure of the reactants. These two effects are compensated and the overall results is a difference of few milliVolts in the cell potential. Thus, a rise in the operational pressure of 1 to 5 atm, produces a detrimental effect for current densities lower than 50 mA/cm^2, while for higher current densities values there is an increase of the cell voltage in the order of 10 mV.

Conclusions

At the present time, various catalysts are available for the ethanol steam reforming, which can be performed at the typical operative conditions of a molten carbonate fuel cell. In addition to the traditional catalysts based on noble metals or Ni/MgO, catalysts based on mixed oxides ($ZnCrO_x$ and $CuO/ZnO/Al_2O_3$) may also be utilized to produce hydrogen from ethanol. However, the endurance of these catalysts at long-term operative conditions and high temperature, and their tolerance in the presence of eventual electrolyte vapours, needs to be verified. Considering the favourable molar ratio between the produced hydrogen and the raw fuel to be reformed, ethanol represents an efficacious alternative to the use of methane to feed fuel cells. The use of membranes separating the anodic compartment from the reforming section is also possible at intermediate or high pressures, since this parameter doesn't heavily affect the overall cell performance.

References

[1] B. Baker, D. Burns, C. Lee, H. Maru, P. Patel, *Internal Reforming for Natural Gas Fuelled Molten Carbonate Fuel Cells*, prep. for GRI Contr. No 5080-344-0302, (1981)
[2] M. A. Rosen, *Int. J. of Hydrogen Energy*, 16, 3, 207, (1991)
[3] S. Cavallaro, S.Freni, R.Cannistraci, M.Aquino and N.Giordano, *Int. J. of Hydrogen Energy*, 181, (1992)
[4] D. Qin, J. Lapszewicz, X. Jiang, *J. of Catalysis*, 159, 140, 1996.
[5] C.J. Jiang, D.L. Trimm, M. S. Wainwright, N. W. Cant, *Applied Catalysis A: General*, 93, 245, 1993.
[6] S. Freni, G. Maggio,S. Cavallaro, *La Termotecnica*,4, 53-59, 1996.
[7] A. Slagtern, U. Olsby, *Applied Catalysis A: General*, *110*, 99, 1994.
[8] H. Agaras, G. Cerrella, M.A. Laborde, *Applied Catalysis*, 45, 53, 1988.
[9] S. Cavallaro, S. Freni, *Int. J. Hydrogen Energy*, 21, in press, 1996.

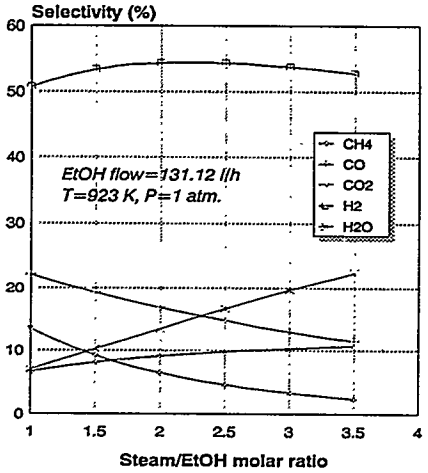

Fig.2: Selectivity of ethanol steam reforming reaction vs. steam/EtOH molar ratio.

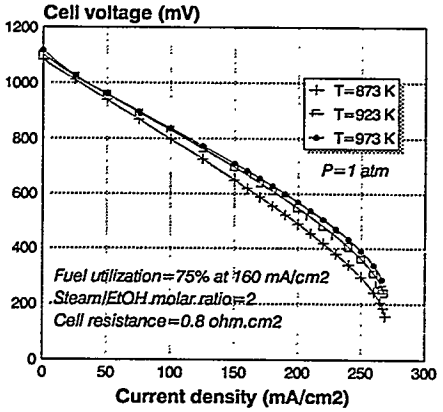

Fig.3: Cell voltage vs. current density at different temperatures

USE OF CERAMIC POROUS MEMBRANES IN MOLTEN CARBONATE FUEL CELLS.

E. Passalacqua, S. Freni, A. Patti and G. Maggio.
Institute CNR-TAE, via Salita S. Lucia sopra Contesse 39, S. Lucia, Messina (ITALY).

Abstract

The diffusion of alkali vapours in the anode compartment of a DIR-MCFC produces the deactivation of the internal reforming catalyst. Sets of ceramic porous membranes purposed to limit the diffusion have been manufactured by different techniques and the influence of the preparation technique and of the preparative variables on the morphological characteristics of the membranes structures has been studied.

Introduction

The direct internal reforming (DIR-MCFC) is one of the most promising configuration of molten carbonate fuel cells. The tendency of the internal reforming catalyst (Ni/Al_2O_3 or Ni/MgO) to react with traces of electrolyte vapours, like KOH, and thus to be poisoned [1-3], limit the complete development of this configuration. Besides of the development of catalysts for internal reforming containing nickel supported on an alkali-resistant support [4,5] or the introduction of a separator plate of Ni/Cu foil, positioned between the catalyst and the anode that permits the hydrogen diffusion but not the passage of carbonate [6], the carbonate transport towards the catalyst can be reduced by interposing, between catalyst and anode a porous ceramic membrane, composed by a wide variety of ceramic materials, like Al_2O_3, ZrO_2, MgO, B_4N, SiC, SiO_2 [7], permeable to hydrogen, that will be a physical limit to the KOH diffusion.

This paper reports some interesting aspects emerging from a wide research carried out on the preparation techniques of the ceramic porous membranes based on material chemically inert to the alkali and thermally stable at the operational temperature of the molten carbonate fuel cells.

Experimental

The techniques of hot-rolling (HR) and tape-casting (TC) were selected to produce the samples of membranes and three different preparation procedures were investigated as a function of the binder and of the technique adopted.

The slurries were produced by dispersing, at room temperature and under stirring, the ceramic powder, plasticizer (polyethylene glycol) and the binder in the solvent. Then the slurries were heated at the solvent evaporation temperature under stirring, until a satisfactory homogeneous dispersion degree was reached. The obtained slips were hot-rolled (T=343 K) or tape-cast to produce green tapes with the desired size and thickness. Following this preparative procedure we have prepared the green tapes with methyl cellulose as binder and aqueous solvent by HR technique (MTC-HR); with MTC and aqueous solvent by TC technique (MTC-TC); and with polyvinylbutyral and non aqueous solvent (trichloroethylene/ethanol) by TC technique (PVB-TC).

Finally the green tapes underwent a thermal treatment cycle at a temperature ranging from 573 K to 1773 K, in an oven under nitrogen flow. The thermal profile of treatment conditions was determined by the thermogravimetric analyses carried out on samples prepared with MTC or PVB as binder by a STA 409 Netzsch simultaneous thermal analyzer in the temperature range between 293 K and 973 K.

The structure of the membrane samples was characterized by measurements of the thickness by means of a thickness gauge and of the hydrogen permeability by applying a pressure drop (Δp) to

the sample.

Furthermore, porosimetric analyses were carried out by the mercury intrusion technique (Carlo Erba Porosimeter Mod.2000), in the range between 0.001 μm and 100 μm. From the porosimetric distribution curves, the total pore volume (Vp), the average pore radius (Rav) and the total porosity (EPS) of the samples were measured.

The capability of some ceramic membranes to resist alkali vapour diffusion in the cell operative conditions (923 K) was verified in simulated conditions. Tests of 150 hours were carried out wherein the porous membranes were placed between alkali doped (with a mixture of Li_2/K_2CO_3) alumina pellets and undoped one, under a nitrogen flow. At the end of each test, the K content was determined by atomic absorption spectroscopy analysis, carried out on an atomic absorption (AA) Perkin-Elmer model 4000 spectrophotometer.

Results and Discussion

Fig. 1 shows the TG profiles for a sample of 2E-3μm green tape. In the range between 293 K and 413 K, the sample presents a weight loss of 0.3%, attributable to the water evaporation. The burn-out of the material starts at 453 K and it is complete at 743 K, with a weight loss of 10.4%.

The main characteristics of the manufactured ceramic porous membranes are summarized in Table I.

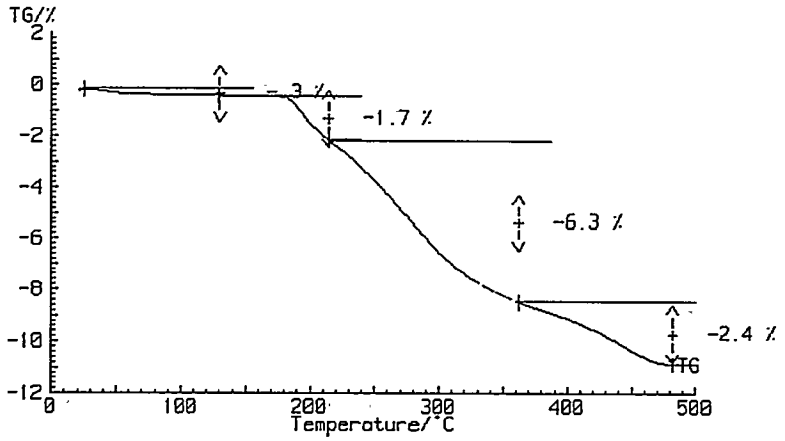

Fig.1- TGA profile for a sample of 2E-3μm green tape.

The TC technique allows a more accurate thickness control and the production of thinner ceramic tapes than the HR one. The porosimetric results show constant Vp (about 235 mm^3/g for Al_2O_3-3μm and 340 mm^3/g for SiC-5μm) as reported in table I. This parameter is independent on the nature of the binder, it appeared to depend mainly on the particle size of the starting

material. In fact, samples prepared with larger particle size (3F-18μm) produce ceramic tapes with large pores and with a drastic lowering of the total pore volume and of the porosity.

The preparation technique could influence the value of the average pore radius. In Fig. 2 are reported the porosimetric curves of two samples of SiC membranes (3H-5μm and 3E-5μm), produced by the same starting powder and firing conditions but with different green preparation method. The HR sample has smaller pores and a more dense structure than the TC one. Moreover, the porosimetric analyses measured, also, a smaller total pore volume for the 3H-5μm sample that is in agreement with the earlier evidence. These differences of the structures could be the effect of the typical pressure exerted by the cylinders on the paste, during the hot rolling procedure.

TABLE I - Main characteristics of some porous membranes manufacture.

Sample--particle size	Mater.	Procedure	Thermal Treatment	Thick. mm	Perm. *	Vp mm^3/g	Rav μm	EPS %
6B-135μm	ZrO_2	MTC-HR	1773 K	1.25	-	177	35.9	41
5E-89μm	MgO	MTC-HR	573 K	0.59	-	151	4.5	27
5D-5/6μm	MgO	MTC-HR	723 K	1.05	-	629	0.12	48
4C-5μm	B_4C	MTC-HR	923 K	1.3	-	295	2.8	39
4D-50μm	B_4C	MTC-HR	923 K	0.96	-	389	7.9	46
3H-5μm	SiC	MTC-HR	1773 K	1.00	0.66	314	1.62	47
3E-5μm	SiC	MTC-TC	1773 K	0.32	3.44	367	2.19	43
3E-5μm 700 h tested	SiC	MTC-TC	1773 K	0.32	-	349	2.02	40
3M-5μm	SiC	PVB-TC	1773 K	0.45	-	344	1.76	45
3F-18μm	SiC	PVB-TC	1773 K	0.37	17.2	62	4.5	16
R2E-3μm	Al_2O_3	MTC-HR	1773 K	0.88	0.15	227	0.54	48
2D-3μm	Al_2O_3	MTC-TC	1773 K	0.29	0.30	248	0.46	44
2E-3μm	Al_2O_3	PVB-TC	1773 K	0.61	0.22	236	0.57	40

* $cc/cm^2 \cdot min \cdot mmH_2O$

To investigate the reliability of these membranes, some of the most promising Al_2O_3 and SiC samples were tested in simulated molten carbonate fuel cell conditions. During the tests the gas pressure drop between the two faces of the membranes, which was continuously checked, did not present any variation, demonstrating that the structure did not change very much.

After the test, the porosimetric analyses, carried out on the samples, indicated that the porosity of the structure decreased from 43 to 40%, also the averaged pore radius (from 2.19 μm to 2.02 μm) and the total pore volume (from 367 mm^3/g to 349 mm^3/g) do not change very much from their initial values. At meantime, the curves of pores distribution of the 3E-5μm samples before and after the test, reported in Fig. 3, show a similar trend without significant differences.

Finally, the post mortem analyses indicated that these membranes have some capability to hinder alkali vapour diffusion; in fact, from spectrophotometric analysis has been seen that there was no potassium detectable beyond the porous membranes, while it has been found on the membranes in amount ranging 0.06 to 1.2 mg/g of membrane.

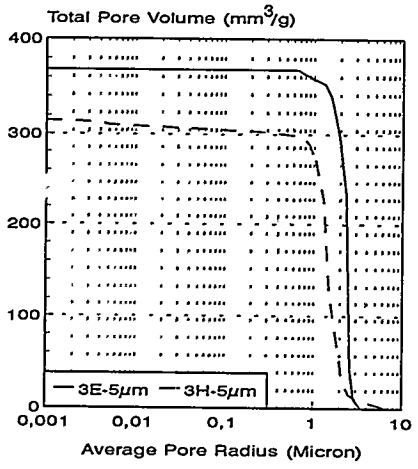

Fig.2 - Porosimetric curves for two SiC samples by HR and TC technique.

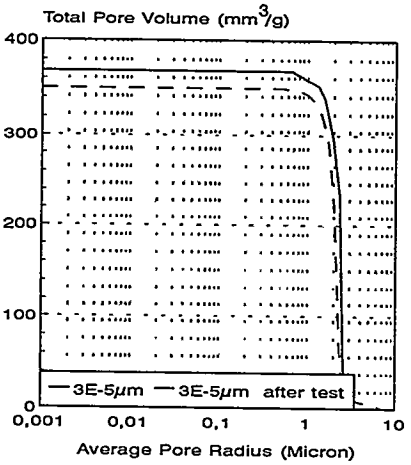

Fig.3 - Porosimetric curves of the 3E-5μm sample before and after the test.

Conclusions

The structural characteristics of the membranes depend on several factors. The use of different binders does not change the porosimetric characteristics if the content of the binder is maintained constant, while the particles size of the starting material influences the total pores volume of the membranes. Some samples (Al_2O_3 and SiC), tested under simulated molten carbonate fuel cell conditions, showed no significant variations in the porous structure characteristics.

This experimental work demonstrates the capability of porous ceramic membranes to control the electrolyte vapour diffusion. However, a further aspect to be investigated in future is the effectiveness of the porous membranes in the cell and the influence of this component on the performance and on the design of the fuel cell system.

References

1. K. Sato, T. Tanaka and T. Murahashi, Proc. 1990 Fuel Cell Seminar, 40-43, Phoenix, Arizona, Nov. 25-28, 1990.
2. S.S. Penner, J.R. Selman, Assessment of Research Needs for Advanced Fuel Cells, DOE/ER 30060-T1, 1985.
3. S. Cavallaro, S. Freni, R. Cannistraci, M. Aquino, N. Giordano, Int. J. Hydrogen Energy, 17, 3, 181-186, 1992.
4. R.J. Selman, Molten Carbonate Fuel Cells (MCFC's), DOE/ER 30060-T1, 11(1-2), 153, 1990.
5. N.Q. Minh, Prpc. 1987 Electrochem. Soc. Conf., vol.87/2, 2169, 1987.
6. L.G. Marianowski and G. Vogel, EP 0257398 A2, 1987.
7. H.P. Hsieh, *Menbrane reactor technology,* AIChE Symposium series, 85, 268, 53-67, (1989).

PERFORMANCE OF AN INTERNAL REFORMING MOLTEN CARBONATE FUEL CELL SUPPLIED WITH ETHANOL/WATER MIXTURE

S. Freni, G. Maggio, F. Barone, E. Passalacqua, A. Patti, M. Minutoli
Istituto CNR-TAE, via Salita S. Lucia sopra Contesse 39, 98126 Santa Lucia, Messina, Italy
tel. 001-90-624230 ; fax 001-90.624247

Introduction

The state of art on the field of molten carbonate fuel cell (MCFC) systems covers many technological aspects related to the use of these systems for the production of electricity [1-2]. In this respect, extensive research efforts have been made to develop a technology using the methane [3-4] based on the steam reforming process, and different configurations have been analysed and their performance determined for several operative cell conditions [5].

However, the operative temperature (T~923 K) of the MCFC, that allows the direct conversion of hydrocarbons or alcohols into H_2 and CO, promotes researches in the field of alternative fuels, more easily transported and reformed compared to methane [6].

In this paper are described the most indicative results obtained by a study that considers the use of water/ethanol mixture as an attractive alternative to the methane for a molten carbonate fuel cell.

Thermodynamics

The thermodynamic balance of the ethanol reforming reaction is represented by the following reactions:

$$C_2H_5OH + H_2O \leftrightarrow 4\ H_2 + 2\ CO \qquad (1).$$

$$CO + H_2O \leftrightarrow H_2 + CO_2 \qquad (2).$$

$$CO + 3\ H_2 \leftrightarrow CH_4 + H_2O \qquad (3).$$

where the last one represents the reaction of steam reforming of methane that will take place simultaneously to these reactions.

The reactions (1)-(3) can be expressed mathematically by equations correlating the equilibrium constants to the molar fractions of the gaseous components and to the total pressure.

Moreover, the equilibrium constants are related to the free energies of each molecule involved in the equilibrium reactions and can be determined, at a fixed temperature, as a function of the inlet moles of ethanol, moles of hydrogen electrochemically converted by the cell, inlet moles of steam. Because of the complexity of the analytical solution a multidimensional globally convergent method [7] for non-linear system of equations has been used to calculate the outlet gas composition.

The equilibrium potential, V, has been determined by the Nernst equation, while the potentials of the cell, operating with production of electricity, have been determined taking in consideration the losses due to the electrodes overpotentials and to the cell resistance.

Then, both electrical and thermal power contributions can be determined as well as the efficiencies of the system The energy balances and the energy efficiencies for these systems, at steady-state conditions, are represented by the following equations:

$$m_f\ h_f + m_o\ h_o = W + Q_u + \sum_w Q_w + \sum_w m_w h_w \qquad (4)$$

$$\eta = \frac{W + Q_u}{m_f h_f} = \frac{W + f\,Q_p}{m_f h_f} \qquad (5)$$

where m is the mass flow, h the enthalpy, W the electrical power released by the cell and Q the thermal power and the subscripts f, o, u, w, p refer to the fuel, oxidant, useful, waste and produced, respectively.

Results and discussion

This analysis starts with the determination of the polarization curve of the molten carbonate fuel cell fed by a mixture of water/ethanol, calculated at the conditions reported in Tab. I. The obtained curve, shown in Fig.1, evidences as the open circuit voltage (OCV) resulted of 1099.9 mV, while the cell limiting current results approximately equal to 280 mA/cm^2.

As evident in Fig. 1, the performance of an ethanol direct internal reforming MCFC has been compared with that of a methane direct internal reforming MCFC, operating under similar conditions. A methane inlet flow equal to 142.5 l/h has been considered, in order to have the same fuel utilization, at any fixed current density, to perform a rational comparison.

The analysis of these data indicates that the ethanol internal reforming configuration gives higher OCV (1099.9 mV vs. 1074 mV) and cell potential (578.0 mV vs. 526.9 mV at 190 mA/cm^2). Besides, the electrical efficiency result higher in the ethanol cell and is equal to 34.2% and 31.9% at 190 mA/cm^2.

Tab.I: operational conditions for the base case

Parameter	*Units*	
Temperature	*K*	*923*
Pressure	*atm*	*1.0*
EtOH inlet flow	*l/h*	*95.0*
Fuel utiliz. (190 mA/ cm²)	*%*	*69.9*
Steam/EtOH ratio		*2.0*
O_2/CO_2 ratio		*0.167/0.2*
Oxidant utiliz. (190 mA/cm²)	*%*	*39.7*
Cell resistance	*Ω cm²*	*0.80*

The curves reported in Fig. 2 give the variations of the anodic gas composition as a function of the current density. From this diagram, it is evident that the production of methane associated to the reaction (3) is not negligible. Thus, at OCV conditions, the methane percentage in the outlet anodic gas composition is 6.4%, but it decreases when the current density increases, and a complete consumption of CH_4 is obtained at current densities greater than 150 mA/cm^2.

The carbon monoxide production, is also relevant and the amount of CO, in the outlet anodic composition, shows a peak localized at current densities close to 25 mA/cm^2, and then decreases for higher current densities.

The steam and carbon dioxide concentrations in the exhaust anodic gas reveal an analogous behaviour: H_2O and CO_2 monotonically increase with the current density, because both are products of the electrochemistry activity of the cell.

Furthermore, at high current densities the carbon dioxide is the main component of the exhaust gases. For instance there is about 60% of CO_2 in the exhaust anode gas, at 260 mA/cm^2.

The percentage of hydrogen produced by the ethanol reforming, at OCV conditions, is 54.3%, and this value quickly decreases when the electricity is released by the cell.

The curve representing the values of the electrical efficiency calculated as a function of the fuel utilisation is reported in Fig.3. The trend of this curve is similar to that of the electrical power density, and presents a maximum values of 34.2%, in correspondence of a fuel utilization equal to 70%. Beyond this value, the efficiency collapses because of the significant increasing of the electrode overpotentials and ohmic losses.

In Fig.4 are shown the curves representing the electrical power density and the thermal power density released by the cell as a function of the current density. This parameter is paramount on the degree of reliability of the examined system to the production of electricity and heat. Thus, the electrical power density curve presents a volcano shaped behaviour with a maximum of 109.8 mW/cm^2, localized at about 190 mA/cm^2.

This curve appears depressed in the region characterized by high values of current density because of a lack of hydrogen. A specular behaviour is evidenced for the thermal power density, calculated assuming that 50% of the waste energy (uncombusted fuel and sensible heat) is recovered (f=0.5).

It appears evident that, in the range of operative temperatures explored, the system can reach levels of efficiency interesting for practical applications. So, an overall efficiency of 66.6% (34.2% is the corresponding electrical efficiency) can be obtained at 190 mA/cm^2 for the cell operating at 923K.

Conclusions

The theoretical calculations, carried out to evaluate the feasibility of an ethanol direct internal reforming molten carbonate fuel cell system to produce electrical energy and heat, indicate some restrictions, but also several encouraging aspects on the utilisation of these systems to this purpose.

So, it appears very interesting to note that the full reforming of the ethanol is reached at the operational conditions, and there is not unconverted ethanol in the exhaust anode gas composition.

In practice, the most convenient values of current density at which the examined system must operate are close to 190 mA/cm^2. At this value of current density, in fact, the maximum of the fuel utilization (~70%) matches with the higher electrical efficiency (34.2% at 923 K and 1 atm) and their values are appreciable for practical applications. But, there is also the evidence that the electrical power released by the cell is limited in the region characterized by high values of current density (>190 mA/cm^2) because of overpotentials and ohmic losses.

Thus, a system operating at 923 K can yield about 109.8 mW/cm^2 at 190 mA/cm^2 that represents an acceptable compromise to limit problems of hardware corrosion and electrolyte vaporisation that shortening the cell life time.

However, another important parameter for evaluating the reliability degree of the examined system to the production of heat and electricity is the value of the electrical efficiency that can be reached. The case of system fed by ethanol presents an acceptable value of electrical efficiency (34.2%), that should be fully compared to those of a MCFC traditional system (32.2% at same temperature), and the same goes for the overall efficiency values calculated with the assumption that the 50% of waste heat is recovered (maxima at 923 K are 66.9% and 64.9% for the ethanol and the methane case, respectively).

The results of this comparison indicate that a cell based on the direct internal reforming of ethanol gives theoretical results that encourage further studies on their applications on the field of the electricity production.

References

[1] S. Freni, M. Aquino, N. Giordano, *J. of Power Sources*, 39, 203 (1992).

[2] S. Freni, M. Aquino, E. Passalacqua, *J. of Power Sources*, 52, 41 (1994).

[3] T. Tanaka, M. Matsumura, Y. Gonjo, C. Hirai, T. Hokada, M. Miyazaki, *25th Int. Society Energy Conversion Engineering Conference*, Reno, Nevada, Vol.3, 201.

[4] K. Joon, L.P. De Vaal, *1994 Fuel Cell Seminar*, San Diego, California. 273 (1994).

[5] S. Cavallaro, S.Freni, R.Cannistraci, M.Aquino and N.Giordano, *Int. J. of Hydrogen Energy*, 17, (3) 181 (1992).

[6] S. Cavallaro, S. Freni, IT. Patent No RM94A000318, (May 25, 1994).

[7] W. H. Press, S.A. Teukolsky, W.T. Vetterling, B.P. Flannery, *Numerical Recipes in Fortran: The Art of Scientific Computing, 2nd Ed.*, Cambridge University Press., (1993).

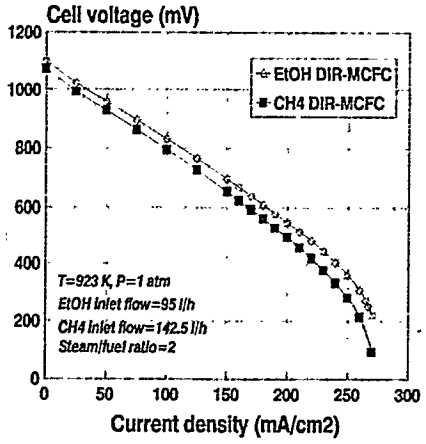

Fig.1: Cell voltage vs. current density. Comparison between ethanol and methane steam reforming.

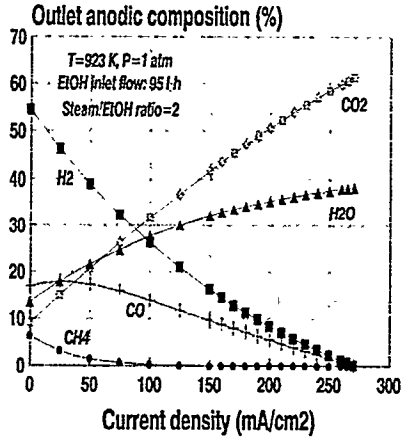

Fig.2: Outlet anode composition vs. current density.

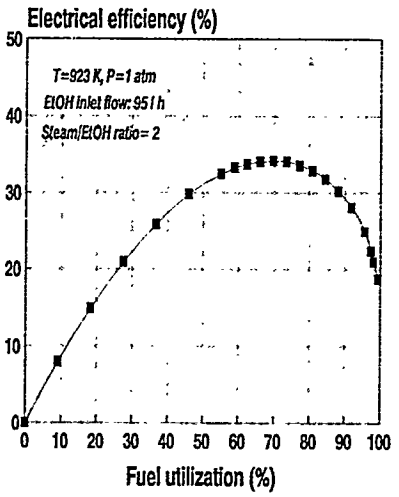

Fig.3: Electrical efficiency vs. fuel utilization.

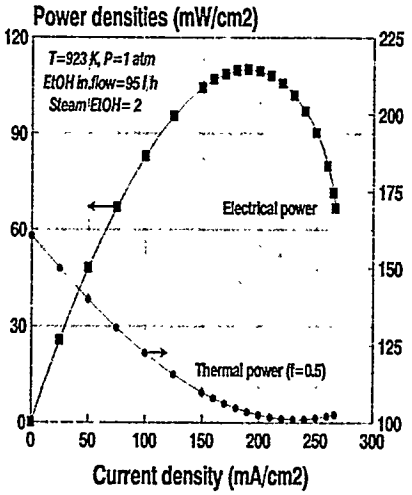

Fig.4: Thermal power density (for f=0.5) and electrical power density vs. current density.

HIGH EFFICIENCY DIRECT FUEL CELL HYBRID POWER CYCLE FOR NEAR TERM APPLICATION

George Steinfeld and Hans C. Maru
Energy Research Corporation
3 Great Pasture Road, Danbury, CT 06810
Tel. 203-792-1460 Fax 203-798-2945

Robert A. Sanderson P.E.
Fuel Cell Systems Consultant
115 Apple Hill, Wethersfield, CT 06019
Tel. 260-563-9823 Fax 860-721-6459

INTRODUCTION -- Direct carbonate fuel cells being developed by Energy Research Corporation can generate power at an efficiency approaching 60% LHV. This unique fuel cell technology can consume natural gas and other hydrocarbon based fuels directly without requiring an external reformer, thus providing a simpler and inherently efficient power generation system. A 2 MW power plant demonstration of this technology has been initiated at an installation in the city of Santa Clara in California. A 2.85 MW commercial configuration shown in Figure 1 is presently being developed. The complete plant includes the carbonate fuel cell modules, an inverter, transformer and switchgear, a heat recovery unit and supporting instrument air and water treatment systems. The emission levels for this 2.85 MW plant are projected to be orders of magnitude below existing or proposed standards. The 30 year levelized cost of electricity, without inflation, is projected to be approximately 5¢/kW-h assuming capital cost for the carbonate fuel cell system of $1000/kW.

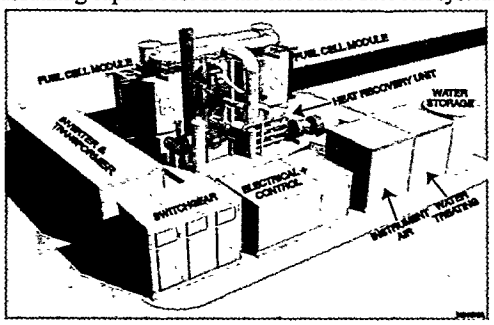

Figure 1. 2.85 MW POWER PLANT:
The Direct Fuel Cell Technology for the Hybrid Cycle

ERC conducted studies of hybrid power cycles in cooperation with the U.S. Department of Energy, Morgantown Energy Technology Center (METC) to identify a higher efficiency economically competitive system. A hybrid power cycle at 200 MW size which generates power at an LHV efficiency in excess of 70% was identified[1]. In these studies the hybrid power cycle had an LHV efficiency of 72.6% and relative insensitivity to ambient temperature compared to a gas turbine combined cycle. In this paper, a near term, simplified 20 MW power plant is describEd utilizing an atmospheric pressure direct carbonate fuel cell/turbine hybrid power cycle. This system utilizes a lower temperature (760°C) heat exchanger and can be implemented by the year 2001.

HYBRID POWER CYCLE DESCRIPTION -- The system includes a direct carbonate fuel cell, a gas turbine, and a steam cycle. Natural gas flows to the fuel cell and the gas turbine. Air flows to the gas turbine and exhaust from the gas turbine flows to the fuel cell. Anode exhaust from the fuel cell is oxidized providing heat to the gas turbine. Cathode exhaust from the fuel cell flows to the steam cycle.

In the system for a 20 MW plant with a hybrid power cycle, shown in Figure 2, about 74% of the methane fuel flows to near atmospheric pressure direct internal reforming carbonate fuel cells. Methane is internally reformed to H_2 at an H_2O/C ratio of 1.5, and fuel utilization in the fuel cell anode is 80%.

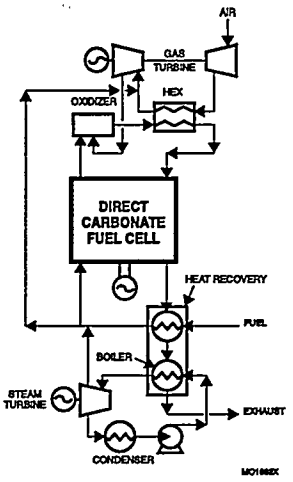

Figure 2. SYSTEM SCHEMATIC OF HYBRID POWER CYCLE:
A Topping Cycle and a Steam Bottoming Cycle

The unreacted H_2 and CO flow to an oxidizer which operates at 761°C. The remaining 26% of the methane fuel is compressed and flows to the gas turbine combustor. The gas turbine compressor delivers air at 10 atm to a heat exchanger which heats the air to 589°C. The heated air then flows to the gas turbine combustor where it is heated further to 982°C before flowing through the turbine. Turbine exhaust containing O_2 and CO_2 flows to the anode exhaust oxidizer. Exhaust from the anode exhaust oxidizer heats the compressed air in the heat exchanger before being recycled to the fuel cell cathode. Exhaust from the cathodes at 670°C flows to the steam bottoming system. The steam bottoming system includes a Heat Recovery Steam Generator (HRSG), steam turbine, condenser and condensate and boiler feed pumps. The steam turbine includes an extraction point for the steam to the fuel cell system. The HRSG includes a reheater for the fuel cell system steam, a superheater, and a boiler. The system also includes a condensate reheater and deaerator, not shown on the simplified schematic. Exhaust leaves the system at 62°C.

PLANT PERFORMANCE -- The performance of the 20 MW plant with a hybrid power cycle was analyzed using CHEMCAD[2] system simulation software with an ERC developed fuel cell model. The results are shown in Table 1. In the hybrid power cycle about 65% of the power is produced by the fuel cell system with its DC/AC inverter, 16 % comes from a generator driven by the gas turbine, and the remaining 19% comes from the generator driven by the steam turbine. There is a 4% loss for pumps and blowers in the system. The overall efficiency of the hybrid power cycle is 65%.

Table 1. 20MW HYBRID POWER CYCLE PERFORMANCE:
Overall Efficiency is 65%

POWER GENERATION	MW
Gas Turbine	3.5
Fuel Cell	14.3
Steam Turbine	4.1
Parasitic Power	-0.8
TOTAL	21.1
NET AC LHV EFFICIENCY	**%**
Fuel Cell	57.2
Fuel Cell & Gas Turbine	52.6
Steam System	35.7
Overall	65.2

EMISSIONS -- A comparison of the NOx between a hybrid power cycle and a gas turbine combined cycle was made on the basis of equilibrium levels predicted from the burners in the two systems at their respective operating conditions. The results showed that

the 20 MW hybrid power cycle is expected to generate 83% less NOx than a 20 MW gas turbine combined cycle.

The emission of sulfur dioxide (SOx) is expected to be only about 1% of the level from a gas turbine combined cycle because the fuel is desulfurized in the process (not shown on the simplified system schematic Figure 2). The contribution of carbon dioxide CO_2 to the atmosphere is expected to be about 24% lower than a gas turbine combined cycle due to the higher efficiency.

COST OF ELECTRICITY -- The 30 year levelized cost of electricity for the 20 MW plant with a hybrid power cycle is estimated at 5.1 ¢/kWh, without inflation, using methods recommended in EPRI TAG[4] . This includes levelized plant cost of 1.4 ¢/kWh, operating and maintenance (O&M) cost of 1.3 ¢/kWh, and levelized fuel cost of 2.4 ¢/kWh.

The 30 year levelized plant cost is based on overall capital cost of 1059 $/kW in 1995 dollars. This overall plant capital cost assumes 1000 $/kW for the fuel cell system. The capital cost for the gas turbine was estimated at 610 $/kW[5] and the steam system at 1260 $kW[5]. The cost of the heat exchanger which transfers heat to the gas turbine compressor exhaust was estimated at 9.5 $/kW compared to 53 $/kW in the 200 MW plant studies[1] based on its lower temperature and heat duty requirements.

The O&M cost includes the fuel cell system O&M cost projected by ERC at 0.8 ¢/kWh including 5 year stack replacement. The combined O&M costs for the gas turbine and steam system is estimated at 0.5 ¢/kWh[3]. The levelized fuel cost of 2.4 ¢/kWh is based on a first year fuel cost of $ 3/MMBTU and a capacity factor of 0.91. The calculated levelizing factor is 1.37[4], an interest rate of 5.3%, no inflation and a fuel escalation rate of 2.5% per year.

COMPARISON WITH A 20 MW GAS TURBINE COMBINED CYCLE -- For perspective on the commercialization prospects for a 20 MW plant with a hybrid power cycle, a comparison was made with a 20 MW gas turbine combined cycle. The comparison addressed issues of performance and cost of electricity. The gas turbine combined cycle selected for the comparison is a commercially available model rated at 18.7 MW. This system is composed of a single gas turbine rated at about 13.4 MW and a 5.3 MW steam turbine. Published[5] heat rate is 6870 BTU/kWh (49.7% LHV efficiency). The 30 year levelized cost of electricity for the 20 MW class combined cycle was estimated at 5.2 ¢/kWh, without inflation, using EPRI TAG[4]. The 30 year levelized plant cost is based on published[5] cost of the commercially available model combined cycle, and estimates of installation and project cost, resulting in an estimated plant capital cost of 954 $/kW. The O&M cost[3] of the combined cycle is in 1995 dollars. The levelized fuel cost of 3.1 ¢/kWh is based on the same assumptions as used to estimate the fuel cost for the hybrid power cycle. A breakdown of cost of electricity is shown in Table 2 in comparison with the hybrid power cycle. As shown in Table 2, the hybrid power cycle COE fuel cost component at $3/MMBTU ($3.163/MMKJ) is significantly less than the fuel cost component for the combined cycle, off- setting the higher plant and O&M COE cost components in the hybrid power cycle. As first year fuel costs increase, the COE cost advantage of the hybrid system increases, as shown in Figure 3. The hybrid power cycle is competitive

Table 2.
HYBRID POWER CYCLE VS.
COMBINED CYCLE LEVELIZED COE

	Hybrid Power Cycle ¢/KwH	Combined Cycle ¢/KwH
Fuel	2.38	3.13
Plant	1.36	1.20
O&M	1.31	0.83
Total	5.05	5.16

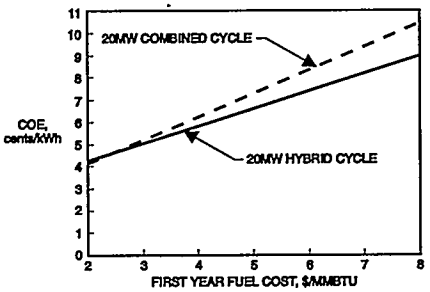

Figure 3. EFFECT OF FIRST YEAR FUEL COST ON COST OF ELECTRICITY:
Hybrid Cycle Provides Significant Advantage at High Fuel Costs

with the combined cycle for 20 MW installations in which the first year fuel cost is above $2.5/MMBTU.

TECHNICAL CHALLENGES -- Near term hybrid power cycle commercialization in a 20 MW size, demonstrating efficiency of 65%, can be achieved with available heat exchanger technology and without anode recycle. For this near term application, attention must be directed to the integration of the fuel cell system with a gas turbine and steam system which have relatively low power output. In addition the gas turbine compressor air is heated external to the gas turbine and then returned to the gas turbine burner for supplementary heating before passing through the turbine. Gas turbine technology must be reviewed in detail with gas turbine suppliers and the gas turbine design modified to accommodate the hybrid power cycle integration requirements. In order to achieve the 72% efficiency promise of the hybrid power cycle, technology and development advancements are needed for heat exchangers capable of 1094°C and pressures up to 400 psig. In addition, an anode recycle at 650°C is required.

CONCLUSIONS -- A 20MW hybrid power cycle for near term application using available technology, including a 760°C heat exchanger, with steam provided from the bottoming cycle steam system rather than anode recycle result in an estimated LHV efficiency of 65%. The NOx emissions are 83% lower than a 20 MW gas turbine combined cycle. The estimated cost of electricity for the near term 20 MW plant with a hybrid power cycle is 5.1 ¢/kWh, which is competitive with a 20 MW combined cycle for installations where the fuel cost is above $2.5/MMBTU.

REFERENCES

1. George Steinfeld, Hans C. Maru and Robert A. Sanderson, "High Efficiency Carbonate Fuel Cell/Turbine Hybrid Power Cycle", 1996 IECEC Conference.
2. CHEMCAD Version 3.0, Chemstations Inc., Houston Texas.
3. EPRI-P-6571-L Technical Assessment Guide, Vol 1, Electrical Supply, Rev 6, Sept. 1989.
4. EPRI-TR-100281 Technical Assessment Guide, Vol 3, Fundamental & Methods - Electrical Supply, Rev 6, December 1989.
5. Gas Turbine World Handbook, 1995 Edition.

MARKET OPPORTUNITIES FOR FUEL CELLS IN ARGENTINA

C.M. Marschoff
Dpt. of Chemical Engineering - University of Buenos Aires
Ciudad Universitaria - (1428) Buenos Aires - Argentina
Jaime Lande and Silvina Espíndola
Jaime Lande & Asociados
Larrea 785 - (1030) Buenos Aires - Argentina

Electricity in Argentina is mainly supplied through the National Interconnected System (NIS) grid, that manages the generation of all medium and large size utilities (thermal, hydro and nuclear) in the country. However, there are still large areas not linked to the NIS: electricity there either comes from utilities that mainly work with diesel groups, or is obtained by individuals from 1-5 kW generators (mostly IC powered, although some wind and solar devices also exist). Finally, in many low-income rural and semi-rural sites, there is no electric generation at all.

In this context, we wish to show that there is an important market niche where fuel cells should be competitive and that this market size justifies a detailed investment analysis. Thus, we have performed economic calculations in three sites, which are representative samples of different structural situations, in which costs of fuel cell produced electricity are compared to presently existing devices. Also, calculations were carried out for use of fuel cells in Antarctica.

Sites with base generation through a diesel group: We have chosen for this case the small town of Bandera Bajada, which was previously studied by one of us (1), and have made the calculations for the present situation at this place. In Table 1 the present cost of electricity is detailed while, in Table 2, the break-even capital cost for fuel cells, which are assumed to work with compressed natural gas, is obtained assuming that book life is 10 years and that the investment would have obtained an 8% interest rate during this time.

Sites where diesel groups work as back-up of other devices: The town of Aluminé, also previously studied and where a micro-hydroturbine is the base generator, was taken as a representative case. Table 3 shows the present electricity production cost for the diesel group and Table 4 gives the obtained results for the case in which diesel groups are substituted by fuel cells fed with natural gas which is now available at this town.

Sites in which electricity is individually generated: The Paraná River Delta region was taken since this is the most important case in the country of this kind of situation. Presently, electricity is produced at most during 4-5 hours per day because of the noise that IC engines produce and, also, because generation costs in this condition are quite large. In this respect it must be pointed out thah some estimations indicate that the real cost of electricity at the Delta is over 1 US$/Kwh (2). If the large amounts of landfill produced methane that exist in this zone are used to feed fuel cells, 40 Kw groups producing

60000 Kwh/year to be distributed among groups of 200-500 neighbours would have a break-even capital cost of 2650 US$/kW.

Fuel cell utilization in Antarctica: Energy needs at scientific bases in Antarctica are presently satisfied by direct combustion of hydrocarbons, mainly gas oil, fuel oil and gasoline. This fact poses two problems: first, the polluting effect of these fuels which must be eliminated in terms of the Antarctic Agreement which has been signed by all nations operating or with interest in that continent; second, the very high cost of fuel transportation makes electricity obtained by the low efficiency diesel generators and IC engines very expensive. Methanol fed fuel cells were chosen as substitute after analysis of different alternative fuels and, if the 6 Argentinian bases electricity generation were carried on by modified PC25 generators, the figures shown in Tables 5-7 are obtained.

These results indicate that there seem to be several market niches in Argentina for fuel cells: diesel generators account for more than 400 MW installed power, a significant number of people is now living on individually generated electricity and more than 50 scientific bases in Antarctica would welcome switching to fuel cell generators. Time seems ripe for a detailed investment analysis on these three areas.

ANNUALIZED CAPITAL COST	2,200 US$/y
FUEL & FUEL TRANSPORTATION	8,320 US$/y
OPERATION & MAINTENANCE LABOUR	29,250 US$/y
SPARE PIECES, ETC.	3,900 US$/y
MISCELLANEOUS	1,800 US$/y
ELECTRICITY COST	76 US$/Kwh

Table 1: Electricity cost at Bandera Bajada where a 40 Kw generator delivers 60,000 Kwh/y

FUEL & FUEL TRANSPORTATION	3,900 US$/y
OPERATION & MAINTENANCE LABOUR	10,300 US$/y
SPARE PIECES, ETC.	2,000 US$/y
MISCELLANEOUS	2,000 US$/y
BREAK-EVEN GENERATOR COST	3,160 US$/Kwh

Table 2: Break-even fuel cell generator cost at Bandera Bajada

ANNUALIZED CAPITAL COST	9,600 US$/y
FUEL & FUEL TRANSPORTATION	80,250 US$/y
OPERATION & MAINTENANCE LABOUR	25,300 US$/y
SPARE PIECES, ETC.	22,800 US$/y
MISCELLANEOUS	6,000 US$/y
ELECTRICITY COST	.36 US$/Kwh

Table 3: Electricity cost at Aluminé for diesel groups generating 400,000 Kwh/y

FUEL & FUEL TRANSPORTATION	3,500 US$/y
OPERATION & MAINTENANCE LABOUR	7,900 US$/y
SPARE PARTS, ETC.	5,300 US$/y
MISCELLANEOUS	3,000 US$/y
BREAK-EVEN GENERATOR COST	2,790 US$/Kw

Table 4: Break-even cost for a 200 Kw fuel cell generator at Aluminé

ITEM	DIESEL ENGINES	FUEL CELLS
Fuel cost	420,000	250,000
Personnel	80,000	--------
Ice-breaker	500,000	--------
Fuel discharge	30,000	--------
Maintenance	20,000	6,000

Table 5: Differential annual operating costs, in US$, for diesel and fuel cell generators in Antarctica

Year	1	2	3	4	5	6	7	8	9	10
Capital	.6	-	-	-	-	.6	-	-	-	-
O & M	.9	.9	.9	.9	.9	.9	.9	.9	.9	.9
TOTAL	1.5	.9	.9	.9	.9	1.5	.9	.9	.9	.9

Table 6: Differential costs for electric generation with diesel engines in Antarctica during the first 10 years (in MUS$)

Year	1	2	3	4	5	6	7	8	9	10
Capital	3	-	-	-	-	-	-	-	-	-
O & M	-	.25	.25	.25	.25	.48	.25	.25	.25	.25
Income	-	.20	.20	.20	.20	.20	.20	.20	.20	.20
TOTAL	3	.05	.05	.05	.05	.28	.05	.05	.05	.05

Table 7: Differential costs for electric generation with fuel cells in Antarctica during the first 10 years (in MUS$). Income results from leasing of free space in the ice-breaker.

REFERENCES

1.- C.M. Marschoff and L. Yanes, National Fuel Cell Seminar, Long Beach, 1988
2.- E.G. Faletty, Private communication

CAN FUEL CELLS COMPETE? A STUDY OF THE COMPETITION

Diane T. Hooie, P.E., Ph.D.
Project Manager
and
Edward L. Parsons
Director

Power Systems Technology Division
U.S. Department of Energy, Morgantown Energy Technology Center
P. O. Box 880
Morgantown, WV 26507 U.S.A.

PHONE: 304-285-4524
FAX: 304-285-4403
E-MAIL: dhooie@metc.doe.com

As fuel cells enter the early stages of commercialization, other manufacturers and packagers of power generation equipment are beginning see fuel cells as potential competition as well as an opportunity to collaborate to increase market share. Most fuel cell market studies, however, portray fuel cells as being able to compete "because the market opportunity is so large." This paper addresses what the competition for fuel cells will be in the power generation/co-generation market segments, how they can collaborate, as well as some of the advantages and disadvantages of each for capturing significant market share. In particular, the advanced gas turbine and tandem cycles will be compared to phosphoric acid, molten carbonate, and solid oxide fuel cells.

DECENTRALIZED CONVERSION OF BIOMASS TO ENERGY, FUELS AND ELECTRICITY WITH FUEL CELLS

Patrick Grimes
Grimes Associates
504 Mountain Avenue
Westfield, NJ, 07090-3036

Introduction

Fuel cells, new processes, advanced equipment and total system approaches will allow biomass to become a larger source of energy to make electricity, fuel and chemicals. These innovative new approaches allow smaller scale operations and allow decentralization of biomass to energy. The pivotal role of biomass will change and expand. Biomass will become a significant near term and a long term energy source.

Traditional biomass processes

More traditional and classical biomass approaches have used large dispersed harvesting of biomass. The harvest is dried locally. The dried solids would be collected and transported over long distances to stockpiles at central locations near or at the electricity producing stations. At the central locations, the dried biomass would be gasified to a hydrogen rich gas. The gas would then be used to fire boilers to produce steam for steam turbine / generators for electricity production. The gas also could be used to fire gas turbine generators. Electrical power would then, under special arrangements, be put into the grid by the local utility companies. The central conversion locations stations were in the low 100's mW range. The thermal quality of the biomass gas fuel is relatively low and special design boilers and turbines are needed to extract the energy.

Fresh biomass has low energy content by weight and volume compared to conventional fuels. Removal of water by drying increases the energy content by weight and volume. Some energy is lost, however, through the release of volatile organics in the drying processes. (The "ashes" from the gasification or biomass processing - potential fertilizers - would be landfilled like conventional fuel ashes and not returned to the fields.) Fermentation and digestion can be used to produce methane gas from biomass and landfills.

Biomass has to be collected from a relatively large area to supply the power plants. The organization efforts required and the economics of long distance transport of low energy content fuels are not attractive. The power plants are

small by utility standards and not appealing. These activities have had a slow growth.

Decentralization

Decentralization is the current new wave of the 90's and will continue. We are steadily moving into the next century - "the Electric Century". Decentralization has brought the need for new and relevant technologies for stationary and mobile power ; for innovative, adaptive and smart control systems ; and for discreet chemical processes in modular form.

There is a decided shift from "Big is Better" to "Small is Beneficial". Small systems can be made from factory produced components and modules. Mass production techniques allow lower costs. The components and modules can be designed to fit together simply at the user. The classical expensive costs of the field erection are minimal or eliminated.

Fuel Cells --Mobile and stationary power plants

Fuel cell powered buses are presently operating with 50 to 100 plus kW power plants and more buses have been ordered. The Military is doing R and D on fuel cell systems to lead to the new silent efficient electric army. Emphasis is on power for the individual soldier and on fuel cell systems which can operate on logistic fuels -- diesel fuel and jet fuel..

Fuel cell electric vehicles, FCEV, are being encouraged by developments in DOT and DOE together with joint industry programs (PNGV) and private developments. The movements toward FCEV will require competitive automotive costs - a few 10's of dollars per kW. Additionally, power conditioning, sensors and controls will increase in reliability and compactness at lower cost.

Present and future stationary power generation is undergoing great changes as the effects of deregulation and subsequent decentralization take place. Traditional utilities because of local regulations find it cheaper to buy power rather than generating power themselves. Today they are buying power through the interconnected power grid from other utilities, from independent power producers and wind / solar electricity producers. The US electric power grid is presently two large east and west electric grids with a few central interconnects. Central

generation stations as "an island" in a region have been absorbed into the .grids. long gone into the giant grids.

Significant amounts of the new power generation is by independent power producers supplying local users with various ratios of electricity and heat.

200 kW fuel cell power plants are being commercialized by ONSI Systems (part of International Fuel Cells). These fuel cell systems are now providing power to hotels, hospitals, office buildings and industries. Associations of utilities are looking to test smaller fuel cell systems as part of powering small subdivisions (25 - 50 kW) or in the basements of private houses (2 - 5 kW). Dispersed power is being produced nearer the customer.

The fuel processor for the 200 kW fuel cell system is now being used by the hydrogen merchant gas industry to supply small scale hydrogen to users.

Biomass conversion

Conversion of biomass R and D activities continue to make progress. Work continues on the standard approaches to improve the conversion percentages and techniques of handling the wastes. New approaches of using super critical water medium in the gasification of wet biomass to hydrogen appear particularly attractive. Decentralization allows consideration of smaller scale converters easing some of the previous constraints on processors.

Advanced gas conversion (AGC) processes are converting natural gas to hydrogen and carbon monoxide (synthesis gas). The synthesis gas is later converted to fuel liquids. These aliphatic hydrocarbon liquids have a high degree of purity. Synthesis gas is a work horse chemical feed stock. Synthesis gas, with modification of the synthesis processes, can make chemicals and/ or supply fuel to fuel cells. Biomass can also equally serve as a source of hydrogen and carbon monoxide for the conversion process.

Summary

Decentralized conversion of biomass to energy fuel and electricity from fuel cells is a productive way of bring biomass to the market place. The necessary system sub components and modules are becoming available. Gasifiers are being improved and new techniques are being brought forward. Fuel cells for stationary

power dispersed power and for vehicle power plants can be readily adapted for the biomass applications. Gas conversion and chemical processing on small scale allow conversion of biomass to concentrated easily stored forms. These forms can be used as fuel or as chemical products.

These developments will be further encouraged and enhanced by the opportunity to make the decentralized systems -- a new market for hardware.

Several scenarios for the decentralized approaches for conversion of biomass to energy, electricity, fuels and chemicals using small gasifiers, converters and fuel cells will be presented.

DISTRIBUTED GENERATION – THE FUEL PROCESSING EXAMPLE

Richard A. Victor
Praxair, Inc.
Tonawanda, New York 14151

Paul J. Farris
Valerie Maston
International Fuel Cells Corporation
South Windsor, Connecticut 06074

The increased costs of transportation and distribution are leading many commercial and industrial firms to consider the on-site generation for energy and other commodities used in their facilities. This trend has been accelerated by the development of compact, efficient processes for converting basic raw materials into finished services at the distributed sites.

Distributed generation with the PC25™ fuel cell power plant is providing a new cost effective technology to meet building electric and thermal needs. Small compact on-site separator systems are providing nitrogen and oxygen to many industrial users of these gases. The adaptation of the fuel processing section of the PC25 power plant for on-site hydrogen generation at industrial sites extends distributed generation benefits to the users of industrial hydrogen.

Industrial hydrogen, although handled in large quantities at refineries, is used in much smaller quantities by nearly all basic industries throughout the world. Presently, hydrogen typically is produced in large plants where substantial and dependable long-term volumes of low-cost feedstock are available from established production processes in heavily industrialized areas. Most customers use hydrogen in the gaseous state. Local low-volume users can get gas delivered in tube trailers which normally operate at ranges less than 200 miles. For the larger volume users and for longer distances, there has been a cost advantage in producing, delivering and storing liquid and converting it back to gas at the point of use. Liquefaction is energy intensive and thus represents a substantial portion of the cost of delivering hydrogen.

Typically, distribution represents more than 30 percent of the overall cost of delivered hydrogen. Therefore, there is considerable incentive to develop low cost, compact systems for on-site hydrogen generation.

Praxair and International Fuel Cells Corporation (IFC) have designed and are marketing small on-site hydrogen generators with capacities of up to 25 million standard cubic feet per month (708,000 cubic meters). A flow schematic of the hydrogen generation system is shown in Figure 1. The plant incorporates a steam reforming system incorporating fuel processing equipment and technology from IFC's PC25 power plants, and compression and hydrogen purification systems designed by Praxair. The purification offgas is recycled to the reforming system to provide energy for the reforming process.

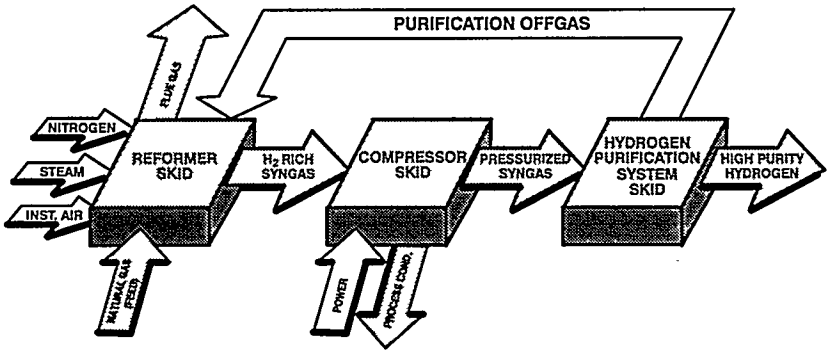

Figure 1: Hydrogen Generation System Schematic

HP-310

The hydrogen generation plants are modular in design and can be scaled to have rated output capabilities ranging from 5,000 to 25,000 standard cubic feet per month. Other features of the plant are listed in the Table. The design features such as automatic, unattended operation, high reliability and low maintenance provide favorable economics for on-site hydrogen generation. The plants are projected to have a significant cost savings over liquid hydrogen deliveries presently used to meet this need.

Table
Hydrogen Generation System Features

- Five plant sizes, from 6,000 to 30,000 cubic feet (160 to 800 cubic meters) per hour
- Compact plot requirements from 1,800 square feet (170 square meters)
- Standard modular design
- Hydrogen purities up to 99.999 percent
- Delivery pressure as needed
- Natural gas or propane feedstock
- Skid-mounted portability
- Automatic, unattended operation
- Low emissions

Two hydrogen generation plants incorporating these technologies are scheduled to begin operation in 1996. Figure 2 shows the first reformer skid being shipped from IFC's facility in South Windsor, Connecticut. This pallet is 10 ft. by 36 ft. and incorporates five (5) PC25 fuel processing units, and a control system which communicates with the overall plant controller to provide start-up, shutdown and normal operation of the reformer section. The control system automatically adjusts the hydrogen rich Syngas output in response to signals from the overall plant controller.

The Syngas is then compressed to feed a pressure swing absorption system which removes impurities, yielding a gaseous hydrogen with a purity level up to 99.999 percent.

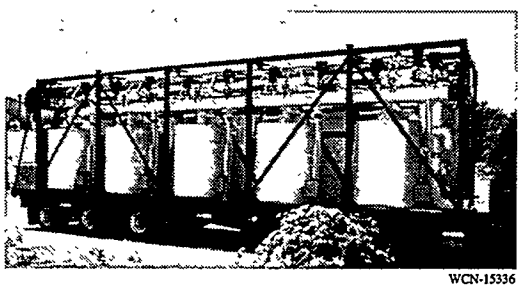

WCN-15336

Figure 2: Reformer Skid

The initial applications of this product are fats/edible oils, glass making, electronics, specialty chemicals and annealing industries. These applications are growing rapidly and have a need for on-site hydrogen in the quantities consistent with the output of the hydrogen generation system.

The hydrogen generation system described in this paper represents a significant step in combining fuel cell technology with advanced gas purification technology to provide dispersed hydrogen generation for use in the growing small hydrogen users' market.

HP-310

DEVELOPMENT OF ADVANCED CONCEPTS FOR DIR-MCFC COGENERATION APPLICATIONS IN THE EUROPEAN MARKET

Peter J. Kortbeek, Ron G. Ottervanger[1] and Andrew L. Dicks[2]

[1]Dutch Fuel Cell Corporation (BCN)
PO Box 1093, 1940 EB Beverwijk, The Netherlands
Tel nr: 31-251-279200; Fax : 31-251-223887; E-mail: sae@euronet.nl

[2]British Gas plc, Research and Technology Division
Ashby Road, Loughborough, Leicestershire LE11 3QU, United Kingdom
Tel: 44-1509-282818; Fax: 44-1509-283144; E-mail: andrew.dicks@bggrc.co.uk

Introduction

Early 1996 a three year (1996 - 1998) joint European project was launched under the name 'Advanced DIR-MCFC Development', aiming at the development of Direct Internal Reforming (DIR) Molten Carbonate Fuel Cell (MCFC) systems for cogeneration applications for the European market. In this project participate: Brandstofcel Nederland BV (BCN), British Gas plc (BG), Gaz de France (GDF), Netherlands Energy Research foundation (ECN), Stork, Royal Schelde and Sydkraft AB. The European Fuel Cell User Group (EFCUG) supports the project as an advisory board.
Whereas the US and Japanese programmes are aimed at large-scale demonstrations of the MCFC technology, this project focusses on the development of concepts and technology, required for MCFC systems that will be competative on the cogeneration market. The project partners provide the essential expertise: from end-user, system engineering, stack development up to fundamental material research.

The 'Advanced DIR-MCFC Development' project

The project involves three levels: 1/ cogeneration market analysis, 2/ system development and 3/ stack and material development. The market analysis provides the essential guidance for system concept studies and MCFC technology development. Tasks at the different levels are carried out in parallel and with strong interaction. The project development plan is shown in the figure below.

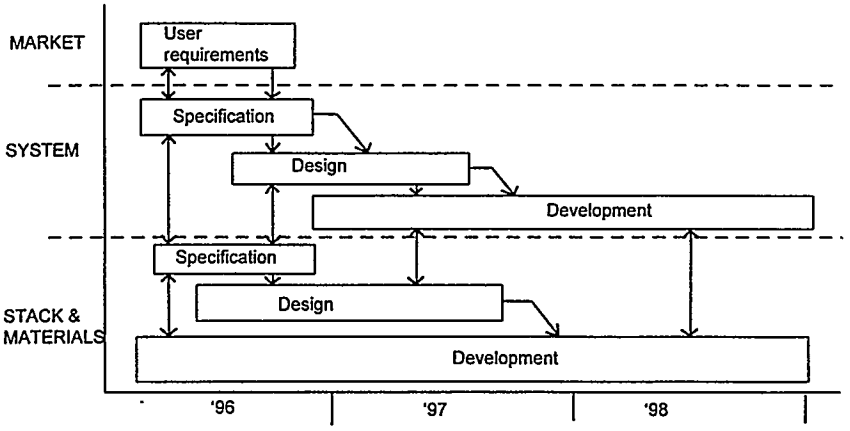

Figure 1: development plan

1/ Analysis of the European cogeneration market

The market analysis, based on in-house expertise, literature surveys and enquiries during the first half of 1996, has revealed important information with respect to the European market demands and the specific end-user requirements for cogeneration systems. This analysis is not a simple task since, within the 15 member countries of the European Union (EU), there exists an enormous diversity both in the structure of the energy market and the availability and usage of primary fuels. To make the situation even more complex, in many countries the energy market is undergoing fundamental changes, which, in general, will transform the structure from strict monopolies to a more open market situation. The diversity in the energy market is also reflected in the market penetration of cogeneration systems. On average, cogeneration accounts for about 7% of the electricity produced in Europe. Penetration of cogeneration in most European countries is in the 1-4% range whereas in a few (the Netherlands, Denmark and Finland) this is substantially higher (30% or above). Although it is generally accepted that cogeneration increases the overall efficiency of energy use substantially, and therefore contributes to lowering the environmental impact of energy production, many barriers prevent its acceptance. Eliminating these barriers will require the efforts of many, both in the markets, institutions and political fields.

This project focuses on the European market for medium sized (0.5-10 MWe), natural gas fuelled, cogeneration systems. Typical technologies that have already penetrated this market segment are gas-engines and gas-turbines which, in general, replace central power/steam boiler systems. Emerging technologies on this market are other fuel cell types like PAFC, SPFC and SOFC. Applications that are attractive for medium sized MCFC systems are:

- light process industry, eg. food processing
- residential applications
- hotels
- hospitals

Particularly attractive features of the hotel and hospital niche market are the steady demand of both power and heat over the year and the consumption of steam for air conditioning.

Other important aspects covered in the present study are 'standards' and 'regulations.' It is considered of vital importance that the system design complies with European, national and local standards and regulations.

Based on the market analysis and user requirements, cogeneration applications will be selected where MCFC systems offer positive benefits compared with competing technologies.

2/ System development

Fuel cell systems are expected to have the benefits of high efficiency at full and part load, high quality of heat, flexibility in heat-to-power ratio and an extremely low environmental impact.

However, these benefits are so far only demonstrated by the 'first generation' demonstration installations, which typically are very complex, voluminous, and expensive. To improve the economics of MCFC systems, the present high capital cost has to be reduced.

Cost reduction of the system is one of the main driving forces for the system design studies carried out in this project. Compared with External Reforming (ER) systems, Internal Reforming (IR) MCFC systems allow for a simpler system layout and lower parasitic power losses associated with stack cooling. Compared with Indirect Internal Reforming (IIR), Direct Internal Reforming (DIR) gives advantages in terms of a simpler design and lower stack cost.

Over the past decade, tools have been developed to model MCFC systems both under steady-state and dynamic conditions. These tools are used in the present project for trade-off studies taking into account a wide variety of system concepts (based on ER and IR stacks), with and without process flow recycling under ambient or pressurised conditions, for the application selected in the market study. From these studies one system concept will be selected, for which a preliminary design will be made, including a cost and economic analysis.

First results show that DIR systems operating at atmospheric pressure in the range up to several MW are more cost effective and have a wider operational window than pressurised systems.

3/ Stack development

A system dedicated internally manifolded DIR stack design is under development in the project. Verification of the design will be carried out in stacks of 0.1 m^2 area up to 2kW output. Improvements with respect to state-of-the-art ECN technology concern the following key issues:

- thermo-hydraulic management
- cell sealing for sustained large differential pressures across the stack
- verification of lifetime to 25,000 hours

In a DIR stack, about 60% of the heat from the electrochemical reaction is absorbed by the endothermic steam reforming reaction. Disadvantages that are often encountered when the heat from an ER stack is removed by the process gas do not occur. On the other hand, in a DIR stack, flow and thermal distribution are more strongly coupled than in the ER case. Modelling of the thermo-hydraulic behaviour is essential for the development of DIR stack design. A 3-dimensional model has been developed in which the main process parameters are taken into account. The model has been validated with experimental data obtained from ER and DIR stack tests.

In the 'first generation' MCFC installations, pressure control was achieved by using hot valves. Such valves are expensive. These valves can be omitted if the stack can sustain differential pressures of the order of 200 mbar. Seals are currently under development to reach this target.

The target for the service life of the stack under system operating conditions is 25,000 hours. This target is a severe challenge for state-of-the-art technology in several areas: cathode dissolution, separator corrosion, reforming catalyst activity and electrolyte management. An improved cathode (based on LiCoO2) and separator coating is currently being developed.

Electrolyte evaporation is reduced by switching the carbonate composition from lithium-potassium to lithium-sodium. Issues affecting the catalyst lifetime are also being studied.

Acknowledgement

The project is funded by the partners, by the European Commission (under JOULE III contract) and, for the Dutch part, by the Dutch Ministry of Economic Affairs and the Dutch Agency for Energy and Environment (NOVEM BV).

AMMONIA SYNTHESIS AND ER-MCFC-TECHNOLOGY - A PROFITABLE COMBINATION?

G.P.J. Dijkema†, J. Vervoort, R.J.E. Daniëls, C.P. Luteijn††
Delft University of Technology
†Faculty of Systems Engineering, Policy Analysis and Management
††Faculty of Chemical Engineering and Materials Science
Jaffalaan 5, 2628 BX Delft The Netherlands

Similar to stand-alone ER-MCFC power systems industrial ammonia production facilities include hydrogen-rich synthesis-gas production. Therefore, integration of ER-MCFC stacks in a conventional industrial ammonia plant was investigated. By preliminary process design calculations three promising process structures were evaluated:

1. ER-MCFC is fed by the ammonia plant's steam-reformer; anode off-gas to firing
2. similar to structure 1; in this case the anode off-gas is redirected to the ammonia process
3. ER-MCFC is fed by ammonia-synthesis purge gas

The results indicate that for options 1 and 3 a return-on-investment for the ER-MCFC of around 8% is achievable at a stack cost of $250/kW and a revenue of 7c/kWh. Option 2 is not profitable, because of the associated reduction in ammonia production. The degree of hydrogen-utilization in the ER-MCFC to be selected for maximum profit varies with the process structure and indicates that there is scope for ER-MCFC stacks which operate at low hydrogen-utilization.

Introduction

External Reforming Molten Carbonate Fuel Cell (ER-MCFC) systems research is primarily focused on the development of stand-alone power systems where an extensive amount of capital-intensive equipment is required in addition to the ER-MCFC-stack. As a consequence the competitiveness of ER-MCFC power systems still remains doubtful, also because economy-of-scale effects are limited compared to cogeneration systems. Incorporation of the MCFC-stack in chemical production processes may offer a market where its potential is fully utilized. More in particular the combination of ammonia production and ER-MCFC technology may be promising for fuel cell technology because industrial ammonia production facilities include hydrogen-rich synthesis-gas production and because ammonia is the world's largest chemical produced.

Ammonia plant description

An industrial ammonia plant based on conventional steam-reforming operated on natural gas comprises [1]:

- a catalytic steam reformer operated at 20-30 bar, and $T_{exit} \approx 780°C$., producing synthesis gas (a mixture of CO, H_2, and CO_2), with a significant amount of unconverted methane;
- secondary reforming with air. By catalytic partial oxidation of the unconverted methane using air the remainder of the feed is reformed autothermally, and the nitrogen required for the ammonia synthesis is fed to the process;
- CO-shift, CO_2 removal and methanation of residual CO;
- ammonia synthesis loop ($P \approx 100$-200bar) composed of a reactor, separator make-up gas and recycle compressor.

Conversion in the two-stage ammonia reactor is 21% per pass. The liquid product is essentially free of impurities and may be sent to storage. The reactor off-gas is recycled. Although stoechiometric for ammonia synthesis, the syngas from the secondary reformer contains some inerts (methane, noble gases); thus a purge from the synthesis-loop is required, which may amount to as much as 5% of the amount of hydrogen produced in the plant, which after hydrogen-recovery is normally fired in the reformer furnace.

Process structures for combinations of ER-MCFC and ammonia technology

In process system design an ER-MCFC-stack may be considered to be a ***multifunctional unit operation*** [2]. Besides producing DC-power and heat at high temperature, the MCFC acts as a H_2- and CO-consumer. It also may add CO_2 to the process gas (by CO-shift and the active transport of CO_2 from anode to cathode), and supply power and heat. The full potential of an ER-MCFC in an ammonia plant is utilized if all these functions are applied for the benefit of the process. Furthermore, the ammonia plant should perform as many of the functions of the ER-MCFC stand-alone power system [2], viz. generation of a hydrogen-rich feed gas, supply of compressed air and CO_2 and utilization of anode-off gas and heat generated.

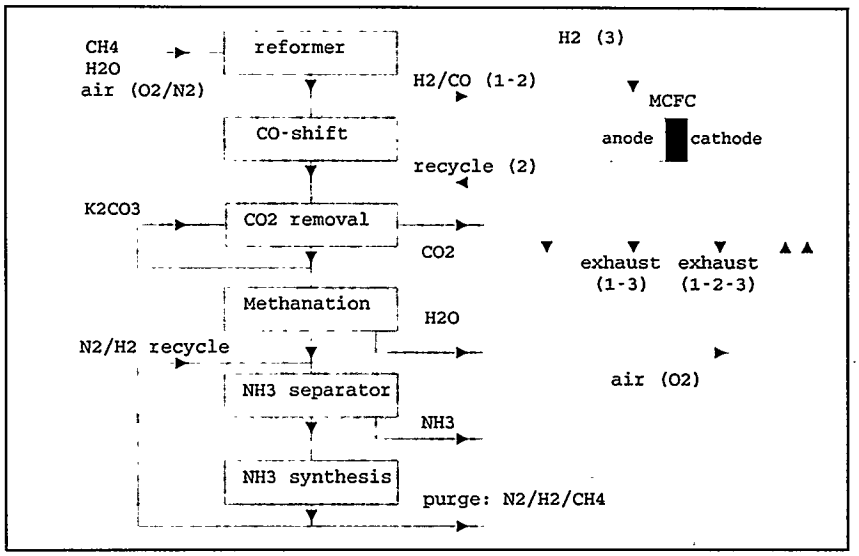

Figure 1: Overview of the process lay-out, depicting the three process structures.

Design objective

The aim was to develop a process structure which results in a clearly demonstrated benefit for ER-MCFC integration in a conventional, world-scale (2000 tpd) ammonia plant [3]. The additional costs for the ER-MCFC should yield a return-on-investment (ROI) greater than 10% [4].

Selection of system structure

From the ammonia plant-description given above it appears that the ER-MCFC feed may be taken from the process after the primary reformer, the secondary reformer or even after CO-shift or the CO_2-removal, or from the ammonia synthesis purge.

There is no reason to select the last option since CO-shift will take place in the ER-MCFC. Selection between the primary and secondary reformer product gas is more difficult: the gas from the primary reformer contains up to 15% unconverted methane, which will be lost for the ammonia process in option 1. The gas is, however, at a suitable temperature (780°C). The gas from the secondary reformer has a high temperature (1100°C), requiring gas-cooling. The methane content is negligible, but the gas is now diluted with nitrogen. Basic mass & energy

balance calculations revealed that MCFC-feed gas from the secondary reformer outlet would be most profitable, together with utilization of the synthesis-loop purge. Use of the synthesis purge gas is obvious, it is also a suitable source for the MCFC [5]. The three process structures evaluated are depicted in figure 1.

Design of the ER-MCFC powerplant

The layout of the ER-MCFC power plant for combination with ammonia production is depicted in figure 2. It is designed for minimum cost and maximum system performance. In all cases CO_2 is taken from the ammonia plant. This stream is freed of any hydrogen and hydrocarbons present by catalytic combustion. Part of the anode off-gas is used to reach a sufficiently high combustion temperature. Air from the secondary reformer air-supply compressor is mixed with the CO_2, pre-heated and sent to the cathode. The presence of this catalytic combustor also allows cold start-up: it may act as a start-up heater. The feed rate, e.g. the sum of the H_2 and CO flow, to the MCFC is the same for the three options. It is set at the amount of H_2 available in the purge stream of the ammonia synthesis loop, which is used to feed the MCFC in option 3. In option 1 & 2 the reformer section is expanded by 10 % to feed an MCFC with an equivalent amount of H_2 and CO. The nominal stack-capacity (at 90% hydrogen-utilization) is approximately 28 MW.

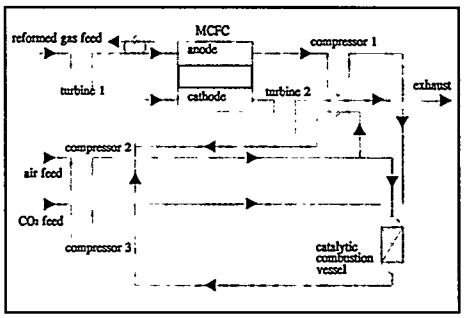

Figure 2: design of the ER-MCFC power plant

Design calculations & design parameters

The design was calculated using the flowsheeting packageAspen-plus™, using the ER-MCFC model developed by Goossens [6]. The ammonia plant model, based on data available from literature, was tuned in such a way that the design and performance of a Dutch ammonia facility was emulated, including its utility system. The MCFC simulation model applied is based on the membrane reactor model available in the Aspen package [6].

Apart from the process structure and ER-MCFC capacity an important design parameter is the hydrogen utilization in the MCFC: the higher the utilization, the more heat is produced in the cell. The only way to remove this heat is to increase flow of air and/or CO_2 to the cathode, which invokes parasitic power consumption. Therefore the MCFC-utilization was optimised. The hydrogen utilization degree was allowed to vary between 50 and 95% in the simulations.

Economic evaluation

It is obvious that option 1 or 2 may provide an economic advantage if power generation has a higher added value than ammonia production per unit syngas produced. In case excess reformer capacity is available which cannot be accommodated in the synthesis loop because of plant bottlenecks there may be significant scope for fuel cell application. In case a novel plant is built, there may be an advantage if the maximum single-train reformer capacity exceeds the maximum single-train ammonia synthesis loop capacity. To emulate the last two cases, a reformer capacity expansion or excess of 10% was used in the calculations.

The results of the economic evaluation have been summarized in table 1. The investment has been estimated assuming the cogeneration plant comprises 4 functional units [7]. The economic performance of the ammonia plant is calculated to be 14.3 % ROI. However, the refrigeration system of the ammonia plant was not accounted for.

In table 1 it is depicted how the combined plants perform. As stated option 2 is not economically feasible due to the redirection of the anode-off gas into the ammonia process, which results in a make-up syngas which contains more inert methane which lowers the ammonia production.
The investment of the MCFC powerplant is estimated at 0.83 Mio $/MWe. Pay-out times of option 1 and 3 are less than 5 years and these options might be profitable (ROI≥10 %), if capital costs for MCFC stacks decrease.

Table 1 : Economic results of three powerplant options

	Power-production (MW)	MCFC conversion (%)	Investment estimate (Mio US$)	ROI (%)
option 1	41.0	75	209	7.0
option 2	29.7	95	214	-3.1
option 3	34.9	75	203	7.0

Concluding remarks

The evaluation shows that cogeneration of power and ammonia may be profitable. Process system integration in this case should, however, be limited to the sharing of syngas producton facilities. Redirection of MCFC off- gases to the process is not attractive because of the reduction in ammonia production. This is caused by the transport of CO_2 to the anode, which leads to an increased level of methane in the ammonia synthesis loop.
This type of cogeneration is only feasible if the return on investment on both products is the same, or in case excess partial process capacity offers reduced marginal investment costs.

This application demonstrates that the optimimum hydrogen utilization in the MCFC is a function of system configuration. The structure proposed for hydrogen- and hydrocarbon removal from CO_2 may offer an interesting option also for stand-alone fuel cell systems. Finally, high pressure operation of the cell would be advantageous in this application. Altogether the results demonstrate that the concept of cogeneration of power and chemicals using process integrated MCFCs needs to be seriously evaluated to develop technology for this promising industrial market.

References

1. J.R. Jennings, "Catalytic ammonia synthesis; fundamentals and practice", Plenum, New York, 1991.
2. G.P.J. Dijkema, C.P. Luteijn and M.P.C. Weijnen, "Process design for combined generation of power, heat and chemicals: process integrated applications of energy conversion systems in chemical plants", Proc. 5th World Congress of Chemical Engineering, Vol. III, pp. 28-34, San Diego, 1996
3. J. Vervoort, R.J.E. Daniels, C.P. Luteijn, G.P.J. Dijkema, "MCFC technology in ammonia synthesis from natural gas; a profitable combination ?", *Inter*duct, Delft, 1996
4. P..J. van den Berg, W.A. de Jong, "Introduction to chemical process technology", Delft, 1979
5 F.A. Frydenlund, EP. 0423177 to Haldor Topsoe, 1993.
6. J.C.J.M. Goossens, "Conceptual design of a fuel cell system for an electrothermal phosphorus process", TwAIO study report, Faculty of Chemical Engineering and Material Science, Delft, 1995.
7. F.C. Zevnik and R.L. Buchanan, "Generalized correlation of process investment", Chem. Eng. Prog., Vol. 59, p. 70-77, feb. 1963.

THE CHEMICAL INDUSTRY, A NOVEL MARKET NICHE FOR FUEL CELLS?

G.P.J. Dijkema[†], J. Grievink[††], C.P. Luteijn[††], M.P.C. Weijnen[††]

Delft University of Technology
[†]Faculty of Systems Engineering, Policy Analysis and Management
Jaffalaan 5, 2628 BX Delft The Netherlands

[††]Faculty of Chemical Engineering and Materials Science
Julianalaan 136, 2628 BL Delft

Abstract
The chemical industry may be seen as a market for fuel cells. Fuel cells can be applied to upgrade by-product hydrogen. Fuel cell stacks may be fully integrated in the process system design to enhance the chemical process performance. In this case the arrangement of stacks is one of the unit operations which the chemical process is composed of. Finally trigeneration systems may be designed to produce chemicals, power and heat simultaneously, as equally important commercial products. Identification of novel market opportunities in the chemical industry can be done by a three-step method. The economic feasibility largely depends on stack lifetime and stack capital cost.

Introduction

The possibility to utilize low-BTU off-gases by implementing fuel cells on-site has been identified as a possible high value application in the fuel cell community [1]. In the chemical industry hydrogen-containing by-product streams are produced in a large number of processes. Also power and heat demand normally are large and on-site cogeneration systems are common in the industry. Thus the situation in the chemical industry seems to be promising for these kind of fuel cell applications.

In addition to by-product hydrogen utilisation ample opportunities for fuel-cell application of a different kind exist in the chemical industry, albeit not suitable for market-entry. These include process-integrated applications of fuel cell stacks [2] and trigeneration processes for the combined production of power, heat and chemicals [3,4]. Below these categories are described and some examples are given for phosphor, methanol and ammonia plants. A general method to identify novel market opportunities for specific options for fuel cell integration in chemical plants and design of trigeneration processes is introduced [4]. This is completed by an assesment of parameters which affect economic feasibility.

By-product hydrogen utilisation

The application of fuel cells to utilize hydrogen-rich process off-gases is rather obvious. Although a patent was issued to Haldor Topsoe for the use of ammonia synthesis off-gas as a fuel for an ER-MCFC [5] and the availability of hydrogen-rich off-gases has been investigated in the Netherlands, this concept has not been commercially applied. This may be attributed to the limited availability of commercial fuel cell stacks and the limited track-record of fuel cells in industrial service which hampers acceptance by the chemical industry as 'proven technology'. Also the development-track selected by the fuel cell companies has been focused on packaged systems for stand-alone power generation. More important however, the economics of upgrading by-product hydrogen by applying fuel cells apparently are not good enough. Lance et al. [6], who investigated the use of hydrogen gas released in chlorine electrolysis, concluded that economically there is no point in the use of fuel cells for energetic upgrading of hydrogen in gas flows in the process industry. From a preliminary investigation of the use fuel cells in conventional ammonia production it was found that the application of a fuel cell to utilise off-gas is only attractive at a considerable electricity revenue and if a rather low cost of fuel cell equipment had been assumed [7]. In addition, pressure-swing-adsorption technology provides an economic solution for removal

of the greater part of the hydrogen from the syntesis-loop off-gases, allowing the hydrogen to be recycled to the ammonia process. Also the use of phosporus-oven off-gas, which is rich in carbon-monoxide proved to be only slightly more competitive compared to the case where the gas is fired in a gasturbine cogeneration system [8].

Process integrated appplication of fuel cells

A fuel cell stack not only converts hydrogen into water by electrochemical reaction with oxygen for the purpose of production of DC-currentis, but it also acts as an active device for hydrogen-removal, oxygen depletion of air etc. [2, 3]. Thus a fuel cell can be viewed as a multi-functional unit operation which is available for inclusion in chemical process system design: at the process system level, a chemical plant usually is designed as an interconnected set of unit operations, i.e., reactors, separators, compressors, pumps etc. This is equivalent to the 'balance-of-plant' calculations around fuel cell stacks.

An example is the system option developed for the much applied ICI Low-Pressure methanol process, which is based on steam reforming of methane. In this process synthesis gas is produced containing excess hydrogen. By integration of a fuel cell the syngas composition may be corrected. Excess hydrogen is converted by the fuel cell, and the system efficiency increases [9].

This kind of system designs involve the complete integration of a fuel-cell stack in a chemical plant. Usually these require only a fraction of the cost of a stand-alone fuel cell system because the amount of auxiliaries is limited. Moreover, by improving the performance of the chemical plant (e.g. increased plant efficiency or increased plant capacity) an additional competitive edge compared to stand-alone fuel cell systems is realized.

Factors which indicate that process integrated application of fuel cells could be favourable are the availability of process-off gases or synthesis gas to be used for fuel, the availability of pure cathode reactants (oxygen, CO_2), a high process power-to-heat ratio and a large of DC-power consumption [2].

Table 1: Characteristics of MCFC-stack and the fuel cell auxiliary system

	MCFC-stack	Auxiliary system
Primary function	produce DC-current	
Other functions	hydrogen depleting, CO_2-transporter, oxygen-depleting	
Inputs / Input processing	*anode*: hydrogen and/or carbon monoxide rich gas *cathode*: CO_2/air mixture	*fuel to anode*: production of H_2/CO (syngas) mixtures out of hydrocarbon fuel; removal of sulphur compounds; *oxydant to cathode*: air and CO_2 supply
Outputs / Output processing	*anode*: off-gas (CO_2, water, hydrogen, CO) *cathode*: off-gas (N_2, O_2, CO_2) 1-7 bar, 700°C	*anode off gas*: catalytic combustion of H_2/CO lean gas; CO_2 removal for recirculation; heat recovery. *cathode off gas*: heat recovery; off gases disposal to stack *DC output*: conversion to AC *shaft power*: electricity generator

These concepts have been formalized in the approach presented in [4], which serves to identify options for the integration of energy conversion devices in chemical plants. In this approach,

which may be used to identify novel market opportunities, the fuel cell stack is viewed as a multifunctional chemical unit operation, with specified functions, inputs and outputs. The approach comprises three steps. In the first step all functions of the fuel cell are described (the primary function is DC-power production, one of the secondary functions is hydrogen-depletion of a gas). The second step involves a description of all the functions of the auxiliary equipment present in a stand-alone fuel cell system (input processing, output processing etc.). The third and most elaborate step is the selection of chemical processes which can perform a number of functions of the fuel cell systems's auxiliary equipment. As stated preferably the chemical processes selected also benefit from the integration of the fuel cell, since this may provide the competitive edge required.

An example of such a fuel cell stack and fuel cell system description is given in above table (adapted from [4]).

Trigeneration processes

An option for the application of fuel cells in the chemical industry which yet goes one step further is the development of trigeneration systems: process systems designed for the combined production of power, heat and chemicals. Both chemical and power may be sold or such a system may be auxiliary to a plant utility system. The trigeneration system may be connected to a common grid where it is a part of a distributed power generation system.

An example involves the conventional synthesis of ammonia, a process which includes steam reforming. Use of the hydrogen-rich purge-stream is an option for fuel cell integration identified by Haldor Topsoe [5]. This option was evaluated together with a the design of an MCFC-based trigeneration system. In this case excess syngas production capacity is used to feed an arrangement of fuel cell stacks. Thus the trigeneration of ammonia, heat and power is realized. No special treatment of the fuel cell off-gases is required because they are sent to the primary reformer furnace as fuel and high temperature oxydant [7].

In a similar fashion a trigeneration system for methanol, heat and power could be developed. The synthesis gas could be taken from a variety of sources. Taking the example of methanol synthesis a step further, the combination of power production and methanol production/dissociation could be used for load-leveling purposes [10].

Evaluation fuel cell applications in the chemical industry

The application of fuel cells in the chemical industry is hampered by the status of the technology, which is not considered to be 'industrially proven' in the chemical industry, except for the PAFC. Any particular plant operator obviously would prefer proof of the technology in a similar or even the same application as in his plant. Power generation by process-integrated and trigeneration fuel cell systems, however, may be seen as advantageous compared to stand-alone fuel cell systems because of the reduced amount of auxiliary equipment required, which improves both power generation economics and system operational reliability. The economics of fuel cell applications, however, need to become more favourable which would be achieved. A reduction in stack cost and an increase in operational lifespan are desirable. The consequence of a limited lifespan obviously implies increased costs, both in capital and labor. These replacement costs may be capitalized, i.e. the net present capital cost be calculated. One way of calculating this amount is by determination of the amount of capital which needs to be set aside to allow the annuities required for replacement to be paid out of the capital and the interest earned. It is obvious that the total capitalized cost required for a fuel cell stack decreases incase its lifespan is lengthened. This effect is enforced in case interest-rates are low. Doubling the expected lifespan would yield a dramatic improvement in project economics.

In case trigeneration systems are considered, the added value of the power generated by the fuel cell needs to exceed that of the production of the chemical product. Often this is only the case if single-train syngas capacity installed exceeds single-train chemical reactor loop. In this case, both chemical production and power generation benefit from the reduction in capital per unit syngas produced.

Inclusion of fuel cells will increase the complexity and operational characteristics of the chemical process system. Thus the perceived risk of unintended plant shutdown increases. As mentioned, the integrated fuel cell system is expected to be more simple than a stand-alone system. In any case a system design which allows continued operation of the chemical plant in case the fuel cell shuts down is to be preferred. Also basic control preferably is straightforward .

The fuel cell stack may perform functions which could also be performed by other technology. To arrive at succesful commercial fuel cell development therefore it is desired the combination of functions offered by the fuel cell cannot be adequately competed with.

Concluding remarks

Not only simple application of fuel cells to utilize waste gases is an option, also more sophisticated applications can be developed which may be seen as options presenting market-niches unique to fuel cells. Proper design will result in high system operational reliability, which exceeds the reliability of stand-alone systems and which is accpetable to chemical plant operators.

The conceptual method introduced may help market-developers identify options for fuel cell application in the chemical industry. Also, trigeneration systems may be considered. Possibly this will help to bring a substantial fleet of commercial fuel cell systems on-stream, thereby entering a spiral of cost-reductions because of increased stack-volumes produced.

References

1. Hirschofer, J.H, Stauffer, D.B and Engleman, R.R., "Fuel Cells, A Handbook (revision 3)", US-DOE report METC-94/1006, Morgantown, 1994

2. Schinkel, J.N., Dijkema, G.P.J., Weijnen, M.P.C., "Novel opportunities for fuel cell commercialization: process integrated applications", Proc. Int. Conference "Bringing Fuel Cells Down to Earth", Los Angeles, 1994.

3. Yang, W.C., Westinghouse Electric Corporation, Personal Communication, 1996 ("trigeneration")

4. Dijkema, G.P.J., Luteijn, C.P. and Weijnen, M.P.C., "Process design for combined generation of power, heat and chemicals: process integrated applications of energy conversion systems in chemical plants", Proc. 5th World Congress of Chemical Engineering, Vol. III, pp. 28-34, San Diego, 1996

5. Frydenlund, F.A., EP. 0423177 to Haldor Topsoe 1993.

6. Lance J.R. et. al., Int. J. Hydrogen Energy 8, 219-224, 1984

7. Dijkema, G.P.J., Vervoort, J., Daniëls, R.J.E., Luteijn, C.P., Ammonia synthesis and er-mcfc-technology - a profitable combination?", Fuel Cell Seminar, Orlando, 1996 (to appear).

8. Goossens, J.C.J.M., "Conceptual design of a fuel cell system for an electrothermal phosphorus process", TwAIO study report, Faculty of Chemical Engineering and Material Science, Delft, 1995.

9. Dijkema, G.P.J., Veenstra, A.F., Vriesendorp, M. and de Lathouder, H.C., "Design of a MCFC-upgrade kit for a steam-reforming methanol plant", "1994 Fuel Cell Seminar, Program and abstracts", San Diego, 1994.

10. Mills, G.A., Fuel 8, 1243, 1994.

MARKETS AND COMMERCIALIZATION SCENARIOS FOR EMERGING FUEL CELLS IN EVOLVING ELECTRICITY MARKETS

Daniel M. Rastler
Electric Power Research Institute
3412 Hillview Avenue
Palo Alto, CA

Abstract

Electricity markets in the United States are undergoing unprecedented structural changes as a result of the confluence of regulatory, competitive, and technological forces. This paper introduces these structural changes and forces and discuss the implications, markets and commercialization scenarios for emerging fuel cells in evolving US electricity markets..

Evolving Electricity Structure and Markets

Electric industry restructuring is radically evolving to a new paradigm where customers will be able to purchase electricity as a commodity. New energy service providers will also emerge to "package" and offer a wide variety of energy service products to customers. Customers will have a landmark opportunity to choose their own energy providers. Structural changes, deregulation and the resulting competitive environment will significantly impact commercialization strategies and markets for fuel cell technology. The implications suggest there will be significant challenges and barriers to commercialization of fuel cells but there will also be new opportunities for the introduction of new products and services utilizing new technologies. The electric utility industry has been in a steady transition during the past 40 years (Table 1). The evolving transition can be generally described as movement from: "investments in infrastructure" to investments in customer services; regulatory guaranteed rates of return to performance based returns; a system focus perspective to a regional franchise, national and global competitive focus. Customers want more choices, lower electric bills and new and better services. Regulatory changes have opened up competition for wholesale power; competition at the retail level is expected by 2000-2002. . Market demands are driving utilities to develop strategic business responses.

Utility Response

Utilities are repositioning both their core and non-core businesses in response to market changes. The changing focus is from a vertically integrated managed utility to separate lines of business which include: production, transmission, and retail/energy services. In the core business, this involves becoming more cost competitive; creating a "customer service" environment; adding or dropping lines of business; adding or dropping assets; and changing the scale and scope of business. This could involve mergers, getting out of the new generation business, and creating both a national and global market reach. At least nine utility mergers have already occurred during the past two years enhancing the market reach and economy of scale of generation, transmission and distribution assets of the participants. International acquisitions in South America, England and Australia have also occurred providing new growth opportunities. Utility positioning outside of the core businesses includes growing revenues in energy related and non-energy related businesses. This includes establishing non-regulated energy service companies and taking equity investments in emerging technologies which enhance the core business. Table 2 illustrates the diversity of new business entities in the evolving electric utility structure.

Table 1: Electric Utility Industry in Transition

	Building Era 1950-Early 70's	Transition Era Late 70's-Early 90's	Services Era Post 90's
Generation	Build Power Plants	Buy Power	Restructure
Transmission	Interconnect Power Plants	Build Power Grid	Improve/ Optimize
Distribution	Install Wires	Manage Wires defer capital	Optimize
Energy Services	Not Utility Business	Not Utility Business	New Business Opportunities

Given the uncertainty of increased competition, electric utilities face a number fundamental issues:

- How to secure premier positions within the new industry?
- How does a company distinguish itself from the competition?
- What are the short-term and long-term growth strategies?
- What customer value-added products and services should be packaged with electricity?

Implications to Fuel Cells

In view of the structural changes outlined above, industry leaders are prioritizing their efforts on: restructuring and reengineering the organization; cost reduction; work force reduction; and increasing focus on marketing strategies and market analysis. These efforts coupled with a surplus of electrical capacity translates into a difficult business environment for the introduction of new emerging fuel cell technologies. While electric and gas utilities have historically pioneered the introduction of new technology, the associated risks were moderated by monopoly status and allowance for rate-based costs to be passed on to customers. New regulatory changes favor enhanced competition, lowest-cost providers, and differentiated services that deliver value to customers beyond traditional kilowatts. Utilities will not be able to provide the "market pull" support in the way previously envisioned for commercialization of fuel cells.

Competing technologies continue to place pressure on the performance and cost requirements for fuel cell products. Advancements in combustion turbines and combined cycles during the past decade have eroded the historic economy-of-scale advantage of long-payback large central station power plants. Compact aeroderivative turbines and proven heavy-frame (industrial) gas turbines are commercially available in 1 to 100 MW sizes, can be deployed on a one-year schedule and have lower operating costs than even a gas-fired boiler central station plant. Advanced designs available before the decade is out will have simple cycle thermal efficiencies of 45% and projected installed capital costs below $500/kW. In that regard, fuel cells are not expected to be competitive with bulk power generation resources for quite some time, if ever. That is, it will be very difficult for fuel cells to compete in a deregulated bulk power commodity market. Fuel cells, therefore, will most likely find applications in a variety of distributed generation/energy services applications. Competition is expected to increase market efficiency, decrease costs and decrease average retail

rates for both commercial and industrial customers. Lower rates could present a significant barrier to the use of on-site distributed fuel cells as discussed below.

Table 2: Stakeholders in Evolving Electric Industry

Stakeholder	Function
Integrated Utility	Provides all electric supply functions
Transmission & Distribution Utility	Provides all electric supply functions except generation
GENCO	Owns and operates generation assets
GRIDCO	Owns, and manages the transmission system
OPCO	Dispatches and manages the sale of electricity over the transmission system
LINECO	Owns and manages the distribution system
RETAILCO	Buys and sells electricity across the distribution system
Power Marketer	Arranges contracts among buyers and sellers of electricity
ESCO	Electric service company selling diverse solutions to consumers
Mini-Genco	Installs & Operates distributed resource services to distribution and transmission portions of the market

Markets for Fuel Cells

The restructured industry will create new opportunities for distributed generation and energy services. Distributed generation includes small gas turbines, micro-turbines, fuel cells, storage technologies, and a host of other novel hybrid concepts could play a significant role in the future of the electric power industry. The emerging competitive environment allows for greater opportunities for new players to use new technologies to offer energy services to industrial, commercial and residential customers. Energy Services Companies (ESCOs), Power Marketers, Mini-Gencos and other third parties will seek to use near-commercial and technically proven technologies as part of integrated energy services offerings.

Fuel cells systems offer a combination of performance and operating characteristics which makes them potentially ideal distributed resources (Table 3). EPRI market assessments imply that in the near term it will be *customer needs* for low electricity cost, reliability, power quality and load demand that will dictate the markets and applications for distributed power. These targeted distributed generation offerings can attract customers with their potential - depending on regulatory treatment - to avoid wheeling tariffs and possible stranded-assets-recovery wires charges. Therefore, a strong near-term competitive strategy would be to invest in distributed generation to provide direct access services for specific industrial, commercial and residential market segments. Whether the utility views this approach as an offensive strategy or one to be defended against depends on who is making the offer to the customer.

The most likely adopters of fuel cells will be non-regulated Energy Service Companies (ESCOs) offering packaged bulk power and valued added services to customers. ESCOs will favor fuel cell products in the 30 kW to 5,000 kW sizes. GENCOs and Mini-Gencos may adopt larger fuel cell products (e.g. 1 to 20 MW SOFC-CT and MCFC systems) if they can compete with bulk power or offer other quantifiable values. Fuel cell produced power will be used to augment bulk power most-likely through a premium service or cogeneration driven customer need. Near term applications could be in industrial and commercial cogeneration sites where electric and gas rates are high; in certain commercial sectors where high reliability and premium service will be valued high enough to off-set the high cost of fuel cell power. An EPRI market study estimated that small solid oxide fuel cells (15 kW to 1,000 kW) could serve most of the electric needs of over 900,000 existing US commercial buildings at lower costs than their current utility rates, assuming projected installed cost targets of <$1100/kW are realized. However, the extent to which such markets are realized will depend on what happens to retail rates as a result of competition, and on whether exit fees act as disincentives for customers to leave the utility system for a resource offering from another supplier.

Table 3: Markets for Fuel Cell Products

Stakeholder	Fuel Cell Type	Market
GENCO	SOFC-CT (large) MCFC	Wholesale producer Industrial cogeneration
Mini-Genco	SOFC-CT; MCFC PEMFC	Integrated services to LINECO or Retailco
LINECO	SOFC-CT (small) MCFC; PEMFC	Distribution Asset Management
Retailco	PAFC, SOFC-CT SOFC; PEMFC	Commercial, Industrial, Residential; premium power
ESCO	PAFC, SOFC, PEMFC	Commercial/industrial cogeneration; premium power

Conclusion

The electric utility industry is entering into a competitive era in which the business environment requires investments in new technology to provide an immediate as well as long term return. Because fuel cells are at least five years from commercialization, their impact on near-term utility business is not anticipated. New mechanisms for product introduction and commercialization of fuel cells is required in view of the poor success of past and current initiatives. Electric utilities seek to deploy new technologies that respond to customer needs and enhance their ability to compete. Therefore, fuel cell developers need to focus technology development toward products which can provide cost-effective "value added" services to customers. Because EPRI member utilities represent over 75% of the total kWh sold in the US, EPRI is in a unique position to assist fuel cell developers in defining/developing marketable products and in implementing their commercialization business plans in the evolving restructured electric power industry.

1. Strategic Market Assessment of Distributed Resources, EPRI, Dec. 1995
2. Commercial Sector Solid Oxide Fuel Cell Business Assessment, EPRI, Sept. 1996
3. Residential Fuel Cells: Technology Readiness Assessment, EPRI, June 1996
4. State of the Art of Fuel Cells Technologies for Distributed Power, EPRI, Sept. 1996
5 G.T. Preston, D.M. Rastler, "Distributed Generation: Competitive Threat or Opportunity", Public Utilities Fortnightly Vol. 134, No. 14, pp. 13, August 1996.

ADDED VALUE FOR ON-SITE FUEL CELLS THROUGH EQUIPMENT AND APPLICATION INTEGRATION

Rick Whitaker
ONSI Corporation
South Windsor, Connecticut 06074

Proven in the Marketplace: On-site fuel cell power plants are not an exciting new electricity generating technology. They are an economic and beneficial addition to the operating systems of commercial buildings and industrial facilities.

ONSI Corporation is part of International Fuel Cells Corporation and is jointly owned by United Technologies Corporation, Toshiba, and Ansaldo. ONSI has proven in the last three years that initial demand for packaged fuel cell power plants, like our 200 kW PC25™ fuel cell shown in Figure 1, comes from the commercial building sector. However, this sector and the companies which service it are only tangentially interested in fuel cells as an emerging electricity generating technology. What they are most interested in is how the PC25 can integrate into their building's system; how it can deliver energy efficient dollars to the bottom line; and how it can deliver operating benefits to their business.

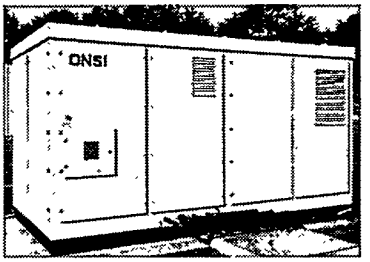

WCN-15162

Figure 1: PC25 200 Kilowatt Power Plant for On-site Service

The PC25 Fuel Cell

The 200 kW PC25 is a packaged power plant, fueled by either natural gas or propane. Its key characteristics are shown in Table 1.

Table 1
PC25 Power Plant Key Characteristics

Configuration Features	Output Characteristics	
Indoor/Outdoor Installation	Power Output	200kW
Grid Connected/Grid Independent Automatic, Unattended Operation	Heat Available	700,000 Btu/Hr 140°F Hot Water
Remote Monitoring	Electric Efficiency	40%
Direct Connection to City Gas Line	Overall Energy Efficiency	85%

Over 100 have been manufactured to date, on a fully automated, volume production line in South Windsor, CT. As of July, 1996, 70 have been installed and are operational in 12 countries in North America, Europe and Asia. These power plants together have accumulated over 1.1M hours of operational experience.

Product Experience

ONSI's PC25 Phosphoric Acid fuel cell power plant has proven the superiority of fuel cell power over conventional technologies in reliability, efficiency and ease of siting.

Reliability: The initial installations have averaged an adjusted 95% availability. This is due to their Mean Time Between Forced Outage of 2200 hours (2 1/2 months), compared to conventional technologies' 500 to 800 hours. It is also due to only one shutdown a year for scheduled maintenance. These units have been so reliable that three have already had continuous runs of greater than one year, a world's record.

Efficiency: The PC25's electrical efficiency of 40% has been tested in the factory and proven in the field. It is a third greater than conventional technology of similar size. Use of cogenerated heat has produced efficiencies of greater than 80% for some units in the field.

Siting: The PC25 has negligible emissions, and has been exempted by the South Coast Air Quality Management District in California (among other agencies) from all air permitting requirements. It has the noise and vibration level, at full power, of a window air conditioner. There are no special installation requirements.

Market Demand

With this bundle of benefits, the PC25 has found its initial market demand as a Premium Power addition to a building's operating systems.

We have found six applications to be most valuable for the PC25 in commercial and industrial buildings. These are described in Table 2.

Table 2
PC25 Fuel Cell Applications

	ON-SITE ENERGY	CONTINUOUS POWER		QUALITY POWER	INDEPENDENT POWER	
		Backup	Uninterrupted		Stand-alone	Remote
Condition	• More power • Lower cost	• No outages • Grid quality acceptable for short periods	• No break • Grid quality-acceptable for short periods	• No break	• No grid exposure allowed	• No grid
Example	• Hotel in constrained grid	Public buildings with critical services	Automated manufacturing	Casino	Financial trading floor	Rural resort
Present Solution	• Grid	• Grid Stand-by Diesel	• Grid UPS Stand-by Diesel	• Grid UPS Stand-by Diesel	• UPS Continuous redundant on-site turbine/ diesel generation	On-site Diesel generation

Figure 2 shows the system's integration and operating modes for the Continuous Power, Uninterrupted application, as an example. It is fairly straightforward and not excessively expensive.

Because the PC25's operating costs are very low and it delivers valuable dedicated power, the economics of these six applications are superior to conventional solutions, in most areas of the country today. This is shown in Figure 3.

Power Plant Operation

Normal

- Grid independent, but synchronized to the grid
- Dedicated source for critical load (① and ③ closed, ④ open)

Grid Outage

- No effect on load

PC25 Outage

- PC25 disconnects through static switch
  - Switch opens ③ and ④ closes
  - ① opens
- Switches–down to 1/4 cycle
- Grid powers load for short period

PC25 Returns

- PC25 reconnects through switch
  - ① closes
  - Switch opens ④, closes ③
  - No break

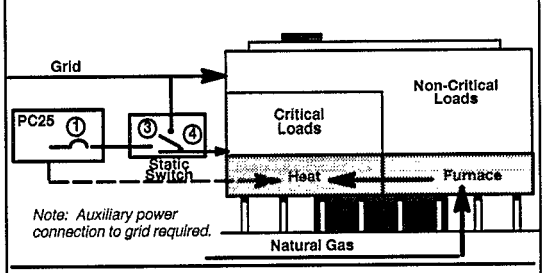

Building Types

- Data centers
- Testing centers
- Hospitals
- Industry
  - Continuous processes
  - Automated processes

Figure 2: Continuous Power, Uninterrupted – No Break; Grid Acceptable for Short Periods

End Use Application	Alternative	Key Components: Capital Cost	Key Components: Annual	Differential ROI*
ON-SITE ENERGY	• Grid	1.0M $ ALT PC25 -0-	0.5M $ ALT PC25	~10 %
CONTINUOUS POWER				
Backup	• Grid • On-site back-up generator	1.0M $	0.5M $	~20 %
Uninterrupted	• Grid • On-site back-up generator • UPS	1.0M $	0.5M $	>50 %
QUALITY	• Grid • UPS • On-site back-up generator	1.0M $	0.5M $	>50 %
INDEPENDENT POWER				
Stand-alone	• Multiple redundant, on-site conventional generators in continuous operation • UPS	5.0M $	1.0M $	>100 %
Remote	• On-site generators	5.0M $	1.0M $	~10 %

*8.0¢/kWh elec, $4.00 gas, 20 yr, $600K per power plant

Figure 3: PC25 Power Plant High Value Applications

Hotels, hospitals, large office buildings, high-tech manufacturing sites and institutions (universities, jails, etc.) have been the most common early customers of these applications. This is generally because of these buildings' size, thermal loads, and need for dedicated power.

New Applications

With Carrier, a sister subsidiary within United Technologies, we are currently exploring additional integrated applications with HVAC equipment. At present, the cogenerated heat from the PC25 can be used in certain types of Carrier's absorption chilling equipment. This system delivers not only cooling, but also Premium Power, at an unmatched level of energy efficiency and environmental cleanliness. A schematic of this system is shown in Figure 4.

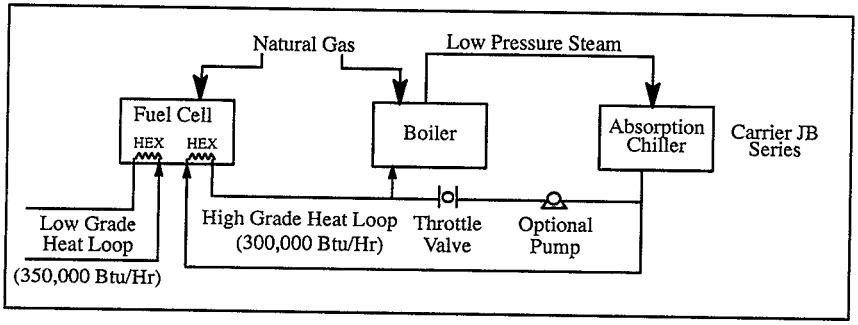

Figure 4: Basic Fuel Cell / Chiller Interconnection Schematic

Additional benefits: joint installation results in lower cost and, because of the PC25's reliability and remote monitoring, the same HVAC maintenance force can service the fuel cells. In some areas of the U.S. today, the payback on this integrated system can be as fast as 2 to 3 years.

We are also exploring integration with dehumidification systems in facilities.

Conclusions

In the hard, competitive business world of today, there are few people who will purchase equipment solely because of technological innovation, a history from NASA's space program, or "greeness". At ONSI, we are proving real dollar benefits from fuel cell power to building owners, as we begin initial penetration of the market. This requires integration of our equipment and installations with commercial facilities' operating systems and sites. More and more customers are accepting that we have the product that can do the job.

COMMERCIALIZATION OF THE 2.8MW DFC PLANT: THIS IS IT!

Donald R. Glenn
Fuel Cell Engineering Corporation
Washington, DC & Danbury, CT USA

Jeffrey Serfass
Fuel Cell Commercialization Group
Washington, DC USA

ERC's carbonate-based Direct Fuel Cell (DFC) program continues to be a model for the transition from R&D to commercial viability. While the ultimate conclusion, that of commercial product introduction and sales, remains just ahead, the public/private sector cooperative programs in place are effectively advancing the program to its planned completion. The five-year market development program with the Fuel Cell Commercialization Group (FCCG), a utility-led buyers group, remains strong despite the uncertainty of impacts associated with the changing electric utility industry. Starting in 1996, these buyers may initiate advanced orders for the first commercial units as called for in our program's commercialization plan and schedule. See figure at right ➢

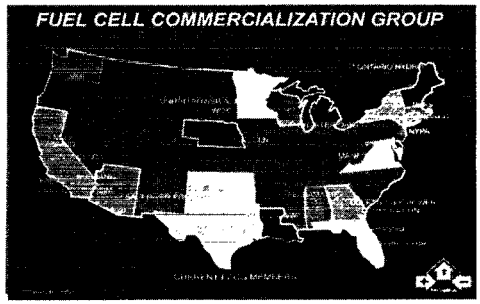

The Santa Clara Demonstration Project (SCDP)

In April 1994, ground was broken for the plant's construction; the balance-of-plant (BOP) was completely installed by June 1995. Historically, the BOP portion of fuel cell plants have been the primary source of plant trips and malfunctions. Consequently, the SCDP's BOP was pre-tested in advance of the DFC stack submodules being installed. This conservative approach lowers the risk that a faulty BOP operation causes the new technology stacks to perform below our expectations. During the pre-testing period, a moderate amount of rework was required, not unexpected for a first-of-a-kind new technology demonstration. BOP testing was completed in March 1996.

Full plant operation began in April 1996 and is planned to continue for up to a two-year period. The SCDP was formally commissioned on June 3rd. More details on this program are presented in another paper at this conference. The Santa Clara testing will build confidence that a proof-of-concept carbonate fuel cell power system can function on a utility site at a scale representative of numerous utility and industrial applications.

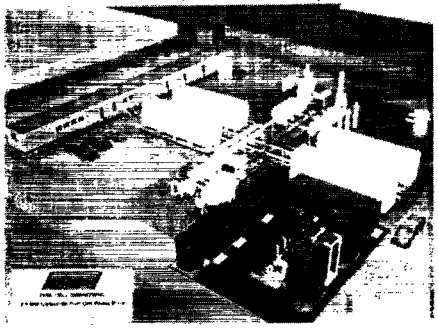

Moreover, the operation, resulting data and field experience gained, will be input to the ongoing commercial unit design effort. Succesfull operation of the SCDP is one of several keys to the FCCG buyers' advanced orders becoming firm orders. The SCDP test results and other findings are to be fedback to the commercial unit's final design and planned process development unit testing. The figure at left shows a significantly reduced footprint for the 2.8MW commercial unit.

Technology Development

The major thrusts of the R&D program are to optimize component designs by reducing material content and improving fuel cell performance features such as power density and cell voltage to lower costs. The results will effect finalizing overall stack and system designs for the commercial unit. Over 11,000 hours of testing have been compiled on stacks constructed with components representative of the SCDP, another important milestone toward validation of the direct carbonate fuel cell technology.

This five-year ERC-DOE cost-shared program comprises the remaining elements to essentially complete the DFC R&D initiative to produce a market entry position. The government's role is to fund the research and development of the full-size fuel cell stack and stack test facilities, power plant system design, and system verification tests. The private sector has concentrated on funding prototype manufacturing facilities, process equipment and balance of plant equipment.

The key objectives of the current effort are to develop a full-size stack design, improve fuel cell performance, and improve the endurance of fuel cell components. An important goal toward completing stack design development involves cell area scaleup. Significant design progress has been achieved through scaling up the cell area by 33% to 9 ft^2, reducing cell weight by 40%, and lowering component manufacturing costs. Progress was also made in tackling fuel cell endurance with a four-fold improvement in cathode strength and verification of several previously developed cell matrix strengthening approaches.

Efforts are targeted to improve fuel cell component performance and reduce materials content to further lower costs. These advances will also enhance fuel cell power density, component life and stack reliability. Additionally, ERC has achieved over 80,000 hours of cumulative testing of the carbonate fuel cell while its licensees reached 40,000 hours of testing, exceeding by far the most hours tested by any other advanced fuel cell technology.

Fuels flexibility remains one of the most attractive market features of the fuel cell, offering operational alternatives for power plant managers when fuel prices fluctuate. In the coordinated DOD/DOE program, co-sponsored by the Defense Advanced Research Projects Agency (DARPA), a capability to process diesel (DF-2) and jet (JP-8) logistics fuels for the DFC has been demonstrated. This capability, once proven, will allow military planners and energy systems designers to specify high efficiency, non-polluting fuel cell power plants for fixed military bases.

An East Coast demonstration power plant will be constructed at ERC's Danbury headquarters. It will be capable of supporting extensive testing of the prototypical commercial power plant as well as being adaptable for alternative fuels testing. This plant's design will incorporate improvements validated through the R&D effort, experience from the SCDP, and other findings. The unit and facility is expected to verify improved power plant performance, plant equipment cost reductions, and host field crew proficiency training courses for performing field operations- module handling and installation, plant start-up and acceptance operations, and O&M responses.

Product Development

The collaboration between the FCCG and FCE continues to follow the program plan established over six years ago. Interactions with the FCCG's Design and Engineering, Contracts, Marketing, and System Planning Committees, intensified as the conceptual and preliminary design milestones for the 2.8-MW commerical unit were accomplished. Along

with DOE, these committees are guiding the unit's design and economics to assure that cost effectiveness and performance features remain compatible with market requirements. During the period since the last seminar, FCE provided formal conceptual and preliminary design reviews of the commercial unit to the FCCG. These reports reflected continuing agreement with the performance and price targets set early in this collaboration as a prerequisite for the FCCG buyers' purchase commitment.

In response to DOE and industry guidance, and cost reduction studies, FCE revised the baseline direct fuel cell stack capacity for the commercial unit. The resulting plant design is more compact and simpler, both highly advantageous to the marketability of a new technology. Power plant and transformation specifications to standardize the plant's interconnection were developed from a nationwide survey covering 37 utilities' distributor substations.

The pre-commercial test unit construction phase will begin after receipt of the appropriate site permits. The unit will serve to qualify the commercial design of the stack module and BOP modules prior to firming up production quantity orders with FCE's subcontractors. This effort is coordinated with attaining firm orders from the FCCG buyers for their early production commercial units.

Commercialization Planning

During the year, the FCCG and ERC's commercial subsidiary, Fuel Cell Engineering Corporation (FCE), essentially completed the generic contract to be used for ordering their early production units (EPUs). This contract was developed to minimize the costs of contract preparation and negotiations between the supplier (FCE) and the FCCG buyers for what is intended to be a catalog-standard power generator. The present schedule, which is dependent on fully funding the cost-shared DOE-ERC PDI initiative, calls for FCE to begin deliveries of the first commerical units in late 1999. By April 1998, the FCCG buyers are to have executed their collective contracts with FCE, as advanced orders. These orders are expected to become firm upon the company's commitment to equip ERC's Torrington facility for commercial production of the EPUs.

The FCCG buyers of the EPU product are also considering other strategies including a broader business alliance with FCE, adding services to improve customer retention benefits, and utilization of alternative energy resources such as landfill and digester gas fuels. The DFC power plant is particularly well-suited to employ these fuels. The FCCG EPU buyers will be positioning their firms as leaders with the most environmentally friendly and energy efficient conversion technology of the coming decades.

ERC's other commercial subsidiary, the Fuel Cell Manufacturing Corporation (FCMC), is expanding its Torrington, Connecticut facility to prepare to produce DFC stacks and modules for the EPUs. The newly acquired manufacturing capability is also tied to the DOE-ERC cost-shared contract in that the commercial stacks are a scale-up from the SCDP stacks as was described above (see Technology Development). Through this approach, costs to all sponsors are contained as production equipment outlays are ERC's responsibility while the R&D to design and test the new stack configuration is covered by the DOE in their long-standing role in funding technology development.

ERC and its subsidiaries are seeking and entering various strategic alliances to present to the buying markets a strong and credible domestic and international team of capabilities. Though many of these alliances remain to be consummated, discussions with key subcontractor firms, architect/engineering organizations and power equipment purchasers continue. Many of the companies involved with the Santa Clara demonstration are considering positions in the cmmercial endeavors, leveraging their early experience with the SCDP. It is the company's intention to form whatever associations it deems important to assure a successful deployment and lasting future for the first and follow-on products based on DFC stack technology.

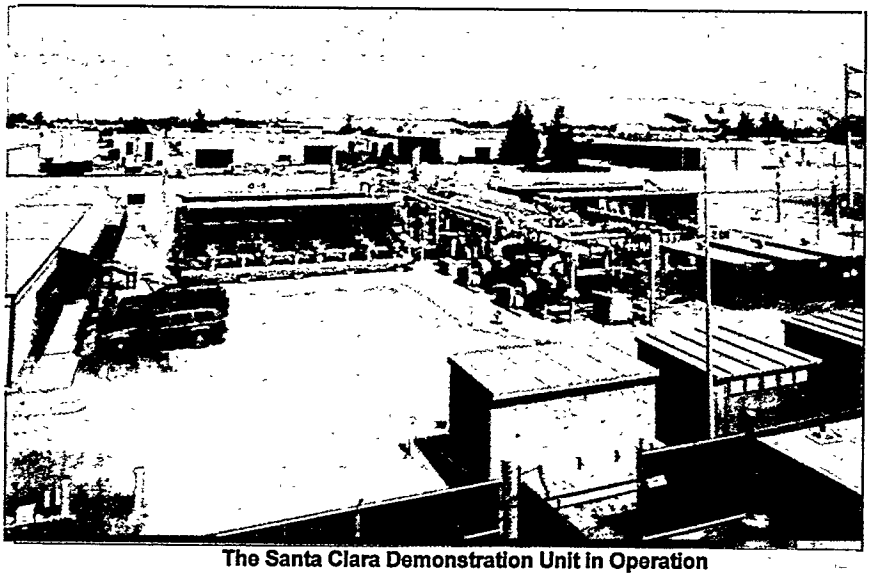

The Santa Clara Demonstration Unit in Operation

Perhaps of greatest importance, these fuel cell systems introduce a new industry bringing with their commercial success many new primary manufacturing and supporting jobs. Domestic and international demands for highly efficient, clean and easily sited smaller power generation schemes will assure realization of these jobs and favorably impact U.S. commerce and exports.

Much credit for the present aggressive program achievements are the result of the high technical competency and superior management capability provided by DOE's Morgantown Energy Technology Center's team.

INDUSTRY SUPPORT FOR MOLTEN CARBONATE FUEL CELL COMMERCIALIZATION

John T. Nimmons, J.D.
Managing Director
Alliance to Commercialize Carbonate Technology
Olympia, Washington USA 98510

The Alliance to Commercialize Carbonate Technology (ACCT®) is a working alliance of utilities and industry, created to help bring molten carbonate fuel cell (MCFC) technology into commercial markets by the year 2000. Its principal focus is the IMHEX® MCFC power plant under development by the team of M-C Power Corporation, the Institute of Gas Technology, The Bechtel Corporation, and Stewart & Stevenson Services, Inc. (the "Development Team"), although many ACCT members are also interested in other fuel cell technologies. This paper will describe ACCT's background, mission, approach and activities, as well as opportunities for those interested to join in ACCT's ongoing work toward MCFC commercialization.

ACCT's Background

ACCT was originally formed in 1991 by M-C Power Corporation, one of two leading American developers of MCFC technology. For the next several years, ACCT functioned simply as an informal utility and industry group that gathered periodically to follow the development of M-C Power's IMHEX® fuel cell technology. In 1994, as the technology neared the end of its development phase and approached the beginning of demonstrations and commercialization, M-C Power and ACCT participants agreed that the time was ripe for the Alliance to crystallize its mission and become a more formal, user-driven organization that could work closely with M-C Power's Development Team to help define the commercial power plant and support it into the market.

During 1994, representatives from utilities and industry worked intensively with the Development Team to define ACCT's new mission and design an approach and structure to achieve it. ACCT incorporated and began accepting formal memberships at the end of 1994. In just over a year and a half, its membership has grown to include twenty of the leading electric and gas utilities, natural gas pipelines, and other industries from all regions of the US, as well as from Canada and Sweden. In early 1996 ACCT increased its membership by over 30%, and it hopes to continue that trend for the next several years as MCFC power plant demonstrations create additional interest in the technology.

ACCT's Mission

ACCT's mission is:

1. To help its member companies understand MCFC technology and the regulatory and business environment in which it will compete, and evaluate early MCFC applications and markets;
2. To help focus and support IMHEX® MCFC development and demonstration efforts in areas of critical interest to potential purchasers and users;
3. To provide opportunities for members to shape commercial power plant design, participate in demonstrations, and learn from early MCFC experience;
4. To build industry confidence that MCFC power plant performance, reliability, and cost targets can be met; and
5. To work with the Development Team to establish a framework for early commitments to purchase the first IMHEX® commercial units by the year 2000.

ACCT's Approach

ACCT's approach is to pursue these purposes through an active collaboration, both *among* member organizations serving on its working committees and its governing body, and *between* member organizations and representatives of the Development Team, who serve on ACCT committees and participate as non-voting members of the organization. In addition to its paid membership of industry and utility companies, ACCT works closely with its advisory members representing government and industry research organizations, presently including the U.S. Department of Energy, the Electric Power Research Institute, and the Gas Research Institute.

As a user-driven group, ACCT appreciates that many of its members are interested not only in M-C Power's IMHEX® technology, but also in other emerging fuel cell technologies that might serve different types of applications and markets. A number of ACCT's member companies also belong to organizations that support other fuel cell technologies. ACCT in no way discourages such participation, and in fact tries to keep its members up to date on the progress of all fuel cell technologies at its regular membership meetings.

ACCT's Ongoing Activities

During 1996, ACCT has pursued three types of activities in support of MCFC commercialization. These include advocating continued MCFC funding; profiling early buyers for commercial MCFCs; and working with M-C Power to structure industry participation in future demonstrations and cost-sharing for the remaining stages of commercialization. The following briefly describes each of these initiatives.

This year as in the past, ACCT has actively supported efforts to ensure continued US government funding for MCFC development through the next few critical years. This year's activities come at an especially critical time. Accelerated moves toward competition and restructuring among US electric utilities have dramatically reduced the availability of industry research, development and demonstration funding just as MCFC technology moves into its most costly demonstration phase. For this reason, it has been especially critical to maintain public funding at levels that fuel cell developers need to meet schedules and achieve milestones previously announced to the industry they are counting on to buy and use their products. Toward this end, ACCT has appeared before US Congressional committees responsible for MCFC funding, and has facilitated its members' efforts to make their support for MCFC development known to key members of the US Congress.

Industry support for MCFC development itself depends on industry confidence that there will be viable applications and markets for the technology when it becomes commercial. Among the IMHEX® Development Team, Stewart and Stevenson Services will be responsible for North American distribution and sales of the commercial power plant. However, Stewart and Stevenson expects to work with companies interested in sub-distributorships or other arrangements that can help move the technology to market. ACCT member companies are among those with such interests, since they are not only prospective MCFC users, but potential sub-distributors, installers, and energy service providers for MCFC power plants. As a result, many ACCT companies have strong interests in understanding what markets are likely to develop for commercial MCFCs.

ACCT's Market Committee began addressing this question in mid-1995. It decided then that, given the rapid changes occurring in the US electric industry, a conventional market analysis conducted in 1996 would be of little value when the technology becomes commercial at the turn of the century. The Committee also recognized that early commercial markets are especially critical for fuel cell technologies, since necessary cost reductions depend in part on achieving early mass production economies. The Committee therefore chose not to proceed with a global assessment of long-term MCFC markets, but instead to focus on a more immediate and relevant inquiry: namely, who will be the "early adopters" of the technology, what distinguishes them from adopters in a more mature market, and what attributes of an MCFC power plant are of most interest to them?

To begin to answer these questions, ACCT and M-C Power have retained experienced energy and utility market consultants to survey key industrial and commercial market segments. The purpose of their study is to profile "early adopters" and to identify power plant attributes of special interest to them. Study results due this fall are expected not only to provide market intelligence for ACCT members interested in purchasing, distributing, installing, and servicing onsite power plants, but also valuable information on product design and definition for the Development Team as it proceeds to develop the first commercial units. Moreover, this "early adopter" study is proceeding in parallel with several other market analyses being performed independently for M-C Power. The results of these various studies should come together soon to provide a useful foundation for investment decisions by ACCT member companies as well as the Development Team.

A third area of activity for ACCT in 1996 has been to work with M-C Power to structure industry participation in future demonstrations, and to develop cost-sharing incentives for the remaining stages of commercialization. The next milestone for M-C Power's program is to demonstrate a 250 kW power plant at Naval Air Station Miramar in San Diego (see artist's rendering below).

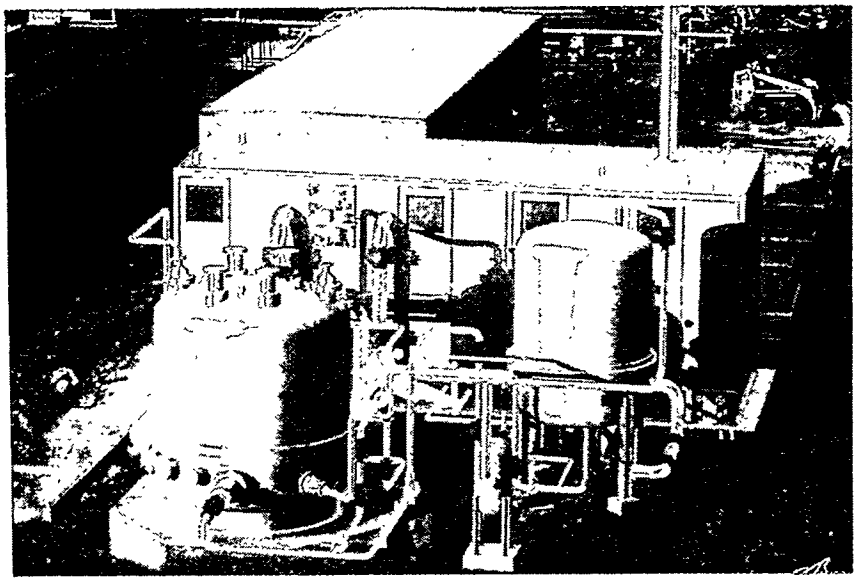

M-C Power 250 kW Miramar Demonstration Power Plant - Courtesy T. Bourke.

Once the Miramar plant is up and running, attention will turn to planning for the first 1 MW IMHEX® prototype power plant, expected to begin operation in 1998 or early 1999. Although funding for development of this plant is included in M-C Power's existing five-year contract with the US Department of Energy, the contract requires substantial industry cost-sharing. Accordingly, ACCT member companies have been working with M-C Power to define the needs of potential cost-sharing participants and the kinds of incentive structures needed to bring forth investment. These discussions are likely to continue through 1996 and into 1997. They are expected to provide a foundation for developing a framework for later commitments by individual ACCT member companies and others to purchase the first commercial MCFC power plants when they become available.

The types of collaborative efforts between ACCT and the Development Team described here are intended to continue during the next several years. If they establish confidence in early MCFC markets and succeed in generating continued federal support and increased industry investment, ACCT will have performed a valuable function for its members, and for the overall fuel cell commercialization effort. ACCT continues to welcome new members, whether they are new to fuel cell technology and simply wish to follow its development, understand its applications and participate in its progress, or whether they are already confident that it can meet their strategic business needs in the year 2000 and beyond and eager for the competitive advantages that early commitment can bring.

❑ ❑ ❑

COST PROJECTIONS FOR PLANAR SOLID OXIDE FUEL CELL SYSTEMS

Dr. Kevin Krist
Gas Research Institute
8600 West Bryn Mawr
Chicago, IL 60631

John D. Wright, Dr. Cecily Romero
TDA Research
12345 W. 52nd Avenue
Wheat Ridge, CO 80033

Dr. Tan Ping Chen
Bechtel Group, Inc.
50 Beake St.
San Francisco, CA 94119-3965

The Gas Research Institute (GRI) is funding fundamental research on solid oxide fuel cells (SOFCs) that operate at reduced temperature. As part of this effort, we have carried out engineering analysis to determine what areas of research can have the greatest effect on the commercialization of SOFCs. Previous papers have evaluated the markets for SOFCs and the amount which a customer will be willing to pay for fuel cell systems or stacks in these markets, the contribution of materials costs to the total stack cost, and the benefits and design requirements associated with reduced temperature operation (1,2). In this paper, we describe the cost of fabricating SOFC stacks by different methods. The complete analysis is available in report form (3).

In summary, we found little difference in the cost of stacks manufactured by traditional ceramic forming techniques (such as ball milling, tape casting, calendering and screen printing and sintering) atmospheric plasma spraying. The cost of putting down a layer of material of a given thickness is much higher in a process that must be carried out under vacuum (sputtering and vacuum plasma spraying). Even though vacuum processes are capable of making thin gas tight layers, their use still significantly increases the cost of the stack. Thus, vacuum processes are desirable only if their use can significantly increase the performance. In general, when a low cost metal interconnect is used (an interconnect stamped from a sheet of high alloy metal), a wide variety of ceramic and atmospheric plasma spraying processes can be used to make fuel cell stacks at a cost of \$500-600/m^2 (\$250-300/kW at a power density of 2 kW/m^2). In contrast, the addition of a single vacuum step to produce a 5μm thick electrolyte layer adds \$100/m^2 (sputtering) to \$150/m^2 (for vacuum plasma spraying). The use of a thick ceramic interconnect (2 mm thick with gas passages for the fuel and air) instead of a metal interconnect adds approximately \$500/m^2 to the cost of the stack.

To calculate the cost of manufacturing planar stacks, we defined complete manufacturing process flow sheets. The analysis included all the steps needed to fabricate a stack, starting with powders and ending with stacks that have been assembled and tested. We assumed the production of 200 MW of capacity per year. This is large enough that all of the equipment in the manufacturing facility can be used 24 hours per day; this facility is larger than the market entry facility (10 to 20 MW capacity per year), but costs could be reduced even further at greater production rates.

To calculate the SOFC stack manufacturing costs, we identified all of the steps needed to produce a stack. We specified the equipment and the number of units needed. The cost and throughput of the equipment was based on manufacturers specifications. The total fixed capital investment (which includes the cost of equipment, installation, land, site development, service facilities, and indirect costs such as engineering, construction overhead, contingency and contractors) was taken as 3.9 times the FOB equipment cost. Working capital was 20% of the fixed capital investment.

The annual direct operating costs include the cost of raw materials, utilities, labor and maintenance. Raw materials costs were taken from suppliers estimates, and generally account for 40% for the total stack cost (slightly less when expensive vacuum deposition processes are used). The major raw materials costs are those for the lanthanum strontium manganite cathode (LSM) at $40/kg, yttria stabilized zirconia (YSZ) electrolyte at $45/kg, YSZ stabilized nickel cermet anode ($24/kg) and the metal ($10/kg) or lanthanum strontium chromite (LSC) interconnect at $60/kg. The costs for these materials were manufacturers estimates of the price of these materials supplied to a large scale SOFC manufacturing facility, and are in general a factor of 2 to 10 less than the current cost of these materials in small scale production. The cost of solvents, binder and gases were also calculated explicitly, but have little effect on the results. Electricity was valued at 7.0¢/kWhr.

The direct costs also include utilities (which were calculated for each unit operation), maintenance (4% of fixed capital) general supplies (5% of fixed capital). However, the largest of the direct operating costs after raw materials is the labor needed to run the plant. Here we assume a workforce of 200 at an annual salary of $35,000/person. On average, direct labor accounts for 15% of the cost of manufacturing a fuel cell.

Indirect expenses are proportional to the direct expenses. Overhead (70% of labor) and administrative costs (25% of overhead) essentially double the effect of the labor costs (labor and expenses proportional to labor account for 30% of the stack cost). Other costs are proportional to the fixed capital investment; depreciation (10%), local taxes (2%), insurance (0.6% of fixed capital). Distribution (10%) and marketing and R&D (5%) are proportional to total expenses. Profit is calculated to provide a 20% rate of return, ie: (profit + depreciation)/(fixed + working capital) = 20%. In general, the direct cost of production account for 50% to 60% of the total manufacturing cost and indirect expenses account for 40% to 50%.

The cost of the unit operations needed to make a fuel cell are shown in Table I. The costs are given in terms of $/m^2. Each of these cost is the sum of three monthly costs (capital equipment * depreciation + maintenance + operation) divided by the number of m^2 of material the unit can process per month. In general, the traditional ceramic processing steps (ball milling, spray drying, screen printing, tape casting and calendering and laminating) and atmospheric plasma spraying are relatively inexpensive. The exception is the sintering steps, which cost several times as much as the forming steps. The cost of atmospheric plasma spraying is similar to that of the more traditional ceramic processes. The vacuum processes are much more expensive because of their high capital cost and low throughput.

Table I Processing characteristics and costs of the manufacturing steps.

Operation	Cap. Cost ($K)	Throughput m^2/d	Monthly costs ($K) capital + operating	Processing Cost $/$m^2$
Spray drying (130 μm layer)	200	1000	9.1 + .3 = 9.4	0.35
Ball mill (130 μm layer)	60	350	2.7 +1.6 = 4.3	0.42
Screen printing	150	670	6.8 + 0.1 = 6.9	0.43
Tape casting (150 cm/min by 0.3 m)	281	410	12.8 + 3.5 = 16.3	1.49
Tape calendering (1.5 m/min by 0.5 m wide)	500	635	22.8 + 5.0 = 27.8	1.71
Metal forming	300	400	13.7 + .4 = 14.1	1.62
Laminating	350	350	15.9 + 0.5 = 16.4	1.62
Atm plasma spray (25 μm layer)	260	290	11.8 + 3.0 = 14.8	1.77
Green machining	500	350	22.8 + .5 = 23.2	2.73
Cold isostatic pressing	800	400	36.4 + .3 = 36.7	3.17
Stacking	500		22.8 + 7.6 = 30.4	3.64
Inspection	750	300	34.1 + 7.6 = 41.7	5.00
Tunnel furnace (oxidizing, 6 hr)	1,000	286	45.5 + 102 = 148	17.92
Tunnel furnace (reducing, 6 hr)	2,000	286	91. + 121 = 212	22.66
Vacuum plasma spray (5 μm)	1,500	45	113 + 3.6 = 117	55
Sputtering (5 μm layer)	8,000	350	364 + 119 = 483	48

SOFCs manufactured by a wide variety of traditional ceramic methods and atmospheric pressure spraying cost $500 to $600/$m^2$ ($250-300/kW at 2 kW/$m^2$); the better raw material utilization of the ceramic processes offsets the faster rate of the plasma spray (Figure 1). Vacuum processes are considerably more expensive, increasing the cost of production by $200 to 300/$m^2$, while the use of a ceramic interconnect increases the costs by roughly $500/$m^2$. It is also important to note that the cost of manufacturing the fuel cell by a wide variety of conventional ceramic and atmospheric plasma spray technologies is low enough to make the systems competitive in co-generation and combined cycle applications (Figure 1) (2).

Perhaps the most important point to remember about the cost estimating process is that the cost of raw materials and processing scale with either the volume of material used or the number of square meters processed, even though the results are generally reported in terms of $/kW of capacity. In fact, the cost in $/kW is the cost in $/$m^2$ divided by the power density. Thus, by far the most effective means of reducing the cost of fuel cell fabrication is to increase the power density of the fuel cell.

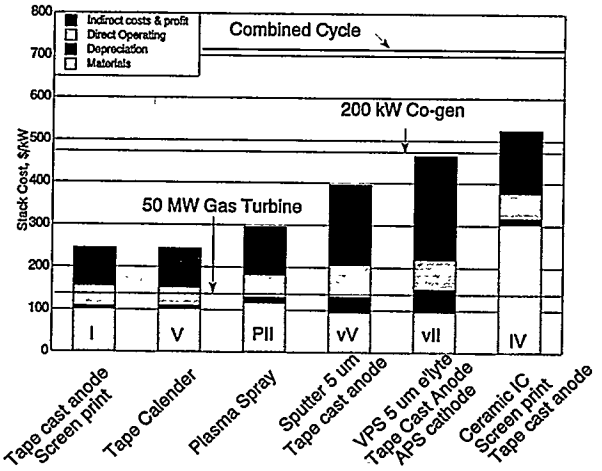

Figure 1 Summary of SOFC Stack Costs

I	Tape cast anode (200 μm) and electrolyte (25 μm), screen print
V	Tape calender anode (200 μm), electrolyte (25 μm) and cathode (25 μm), green machine, co-sinter, metal IC, stack
PII	Atmospheric plasma spray anode (200 μm), electrolyte (25 μm) and cathode (25 μm), co-sinter, metal IC, stack
vV	Tape cast anode (200μm), sputtered electrolyte (5 μm) and cathode (5 μm), sinter, metal IC, stack
VII	Tape cast anode (200 μm), VPS electrolyte (5 μm) and cathode (5 μm), sinter, metal IC, stack
IV	Tape cast anode (200μm) and electrolyte (25μm), screen print cathode (25 μm), sinter, green machine, LSC IC, stack

References

1 Krist, K and J.D. Wright, Fabrication Costs for Reduced Temperature Solid Oxide Fuel Cells, 1994 Fuel Cell Seminar. 1994.

2 Krist, K and J.D. Wright, "Manufacturing Costs for Planar Solid Oxide Fuel Cells" Proc. of the Fourth International Symposium on Solid Oxide Fuel Cells, Yokohama, Japan, Dokiya, M. et al., eds., The Electrochemical Society.

3 Romero, C and J.D. Wright, The Value and Manufacturing Costs of Planar Solid Oxide Fuel Cell Stacks, GRI Topical Report, July 1996

COMMERCIAL BALLARD PEM FUEL CELL NATURAL GAS POWER PLANT DEVELOPMENT

David S. Watkins, David Dunnison
Ballard Power Systems Inc.
9000 Glenlyon Parkway
Burnaby, British Columbia
Canada V5J 5J9

Ronald Cohen
FCP Engineering
21837 Reflection Lane
Boca Raton, Florida
USA 33428

Introduction

The electric utility industry is in a period of rapid change. Deregulation, wholesale and retail wheeling, and corporate restructuring are forcing utilities to adopt new techniques for conducting their business. The advent of a more customer oriented service business with tailored solutions addressing such needs as power quality is a certain product of the deregulation of the electric utility industry. Distributed and dispersed power are fundamental requirements for such tailored solutions. Because of their modularity, efficiency and environmental benefits, fuel cells are a favored solution to implement distributed and dispersed power concepts.

Ballard Power Systems has been working to develop and commercialize Proton Exchange Membrane (PEM) fuel cell power plants for stationary power markets. PEM's capabilities of flexible operation and multiple market platforms bodes well for success in the stationary power market. Ballard's stationary commercialization program is now in its second phase. The construction and successful operation of a 10 kW natural gas fueled, proof-of-concept power plant marked the completion of phase one.

In the second phase, we are developing a 250 kW market entry power plant. This paper discusses Ballard's power plant development plan philosophy, the benefits from this approach, and our current status.

Power Plant Development Plan and Benefits

The Power Plant development plan portion of our commercialization drive consists of:

1. Definition of market needs.
2. Establish a specification for the selected product with help from potential users.
3. Conduct system design and cost trade off studies to define the optimum combination of component technologies and designs in an integrated system to meet the specification.
4. Initiate the Power Plant development effort using available component designs and technologies.
5. Initiate component development and technology advancement programs guided by power plant needs.
6. Field test early power plants to mature reliability of the power plant in the real world of the customer.
7. Upgrade power plants with improvements to the system and components from parallel development and technology programs to enhance functionality, reliability and cost.
8. Periodically adjust vision and development/technology plans based on new information from field testing, design, development/technology programs, cost analysis, user input, and market needs.

The outstanding benefits of this development plan are:

1. A vision for the product at the power plant systems level is established based upon market information to guide technology and power plant development programs. This power plant level specificity prevents unfocused research and development efforts.

2. This vision communicates the product to customers, management, and investors.
3. A corporate vision including multiple product visions and attendant development plans helps to integrate technology and development efforts to improve the efficiency of the overall effort. Test equipment, manufacturing equipment, test and development activities, for example, can encompass a wider range of effect for a small additional effort. The net result is that the programs are less expensive and lead to better, more refined products in the shortest possible time.

250 kW Class Engineering Prototype Power Plant Development Status

The 10 kW proof of concept power plant has successfully demonstrated its key objectives. The power plant was packaged and incorporated all major design features of the commercial unit including pressurization, integral fin-fan cooling heat exchanger, natural gas fuel processor, high voltage stack, inverter, automatic controls, full turndown (0 to 10 kW net AC), load transients and multiple starts.

The 250 kW class engineering prototype power plant is scheduled for assembly with mechanical and electrical verification during the 1st quarter of 1997. Commissioning and initial testing will be completed during the 2nd quarter of 1997. Detailed design of the engineering prototype is now complete, and construction underway. This first unit is 8' x 8' x 24' and weighs 35,000 pounds. This developmental power plant is about 6 feet longer and weighs about 10,000 pounds more than the commercial power plant vision because it contains developmental components, extra hardware for flexibility to prevent component mismatch problems, significant engineering instrumentation, and additional space for access.

Successful operation of the Fuel Processing Subsystem (FPS) up to full power has been achieved. The data has verified the component and subsystem models and sub scale test results used to effect the scale up. Figure 1 shows the 250 kW reformer which is about 40 cubic feet. This is the smallest reformer for its capacity in existence.

Successful operation of the Air Pressurization Subsystem (APS) up to full power has also been achieved. Figure 2 shows the dual turbocharger assembly with inter-cooler attached as it is being constructed to the power plant configuration.

The power plant stack design is complete and short stack tests of full size cells are ongoing. Figure 3 compares a sub scale 0.38 ft^2 single cell to the full size 1.4 ft^2 single cell that will be used in the 250 kW power plant. Figure 4 shows a 20 cell short stack with the 1.4 ft^2 active area.

Final design of the inverter is complete and delivery scheduled for January 1997. The power plant test stand is essentially complete. Additional power plant components have been ordered. Suppliers for advanced and/or production components have been identified and discussions are in process.

In summary, the technology, advanced component designs, and development efforts are very encouraging. Based upon these results, we are confident that further refinement to a mature product meeting specification requirements is on track. We expect this mature product to weigh about 25,000 pounds and possibly less at about 8' x 8' x 18' in overall size. We expect it to have an efficiency of 40% LHV and to be capable of meeting the cost, emissions, noise and other benefits expected of mature fuel cell power plants.

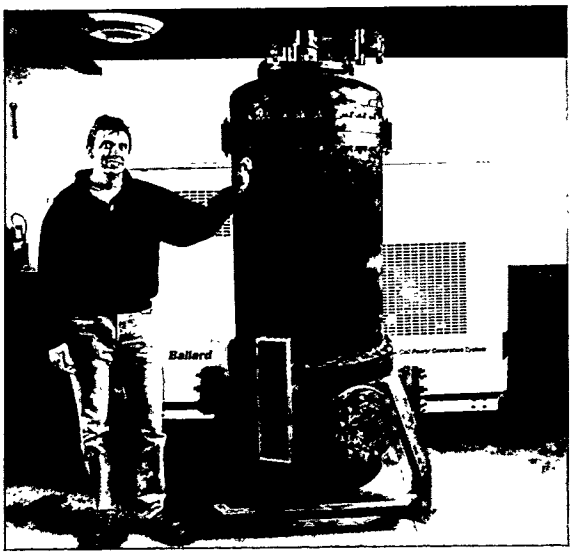

Figure 1: 250 kW Reformer

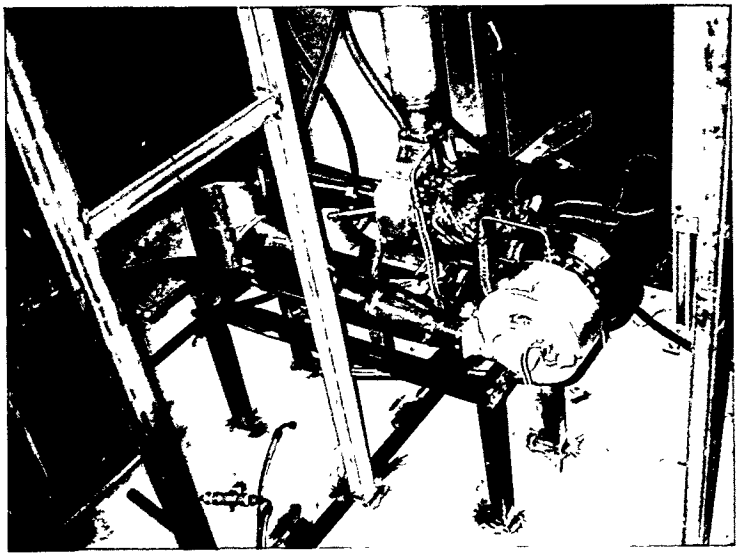

Figure 2: Dual Turbocharger Assembly

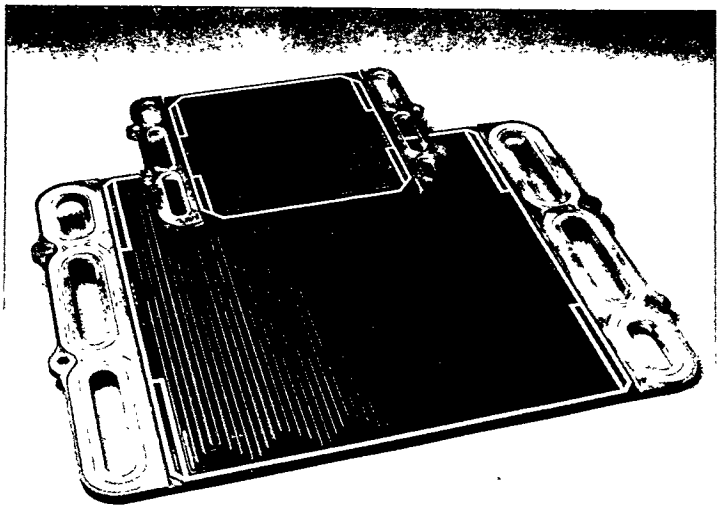

Figure 3: 0.38 ft^2 vs 1.4 ft^2 Cell

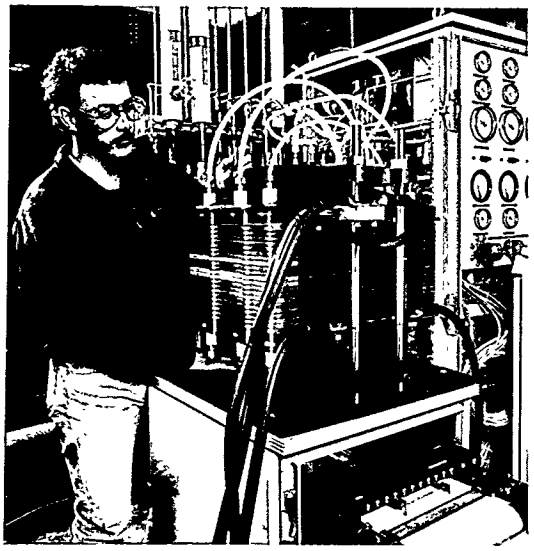

Figure 4: 20 Cell Short Stack

DEVELOPMENT OF A 10 kW HYDROGEN/AIR PEM FUEL CELL STACK

F. Barbir*, F. Marken*, B. Bahar† and J.A. Kolde†

*Energy Partners, Inc.
1501 Northpoint Pkwy. #102
West Palm Beach, FL 33407

†W.L. Gore & Associates, Inc.
101 Lewisville Road
P.O. Box 1100
Elkton, MD 21922-1100

PEM fuel cells have potential for meeting automotive industry's power density and cost requirements, such as 0.8 kW/kg, 0.8 kW/l and $30/kW. For automotive applications, the fuel cell power requirements are in the 10-100 kW range. As the first phase in reaching this power output, a 10 kW PEM fuel cell stack has been developed at Energy Partners [1].

The stack consists of 50 cells with relatively large active area of 780 cm^2. The main feature of the stack is the advanced membrane electrode assembly (MEA) developed by W.L. Gore & Associates, Inc. These novel MEAs consist of a thin composite perfluorinated polymer membrane with a catalyst layer with platinum loading of 0.3 mg/cm^2 on each side. The combination of reinforcement and thinness provides high membrane conductance and improved water distribution in the operating cell. In addition, the membrane has excellent mechanical properties (particularly when it is hydrated) and dimensional stability [2].

Two different gas diffusion layers were employed. A thin, soft, microporous, and hydrophobic gas diffusion material (GoreCarbel™) was applied directly on the back of the catalyst layer to protect the thin membrane as suggested by the MEA manufacturer. It provides much better electrical contacts at the surface of the catalyst layer, and may also contribute to water removal, as suggested by Wilson, *et al.*, [3]. A thicker, macroporous, Teflon-treated carbon fiber paper provides membrane support and makes contacts with the bi-polar collector plate.

The collector/separator plates are made of graphite in a proprietary two step compression molding process, thus avoiding expensive and time-consuming machining. The plates have the embedded hydrogen and air flow fields on opposite sides. Internal manifolds are placed around the perimeter of the plate. Cooling of the stack is provided by de-ionized water which circulates through cooling cells strategically distributed between the active cells. The current is drawn from the stack at two gold-plated copper bus plates placed at opposite ends of the stack. The stack is held together by two aluminum plates bolted together with tie-rods. All the connections for hydrogen, air and cooling water are provided on one of the end-plates. The stack weighs 69 kg (or 17.7 kg/m^2) and has a volume of 38 liters.

The stack normally operates on hydrogen/air at 300 kPa (although it has been successfully operated at 170 kPa). The prescribed operating temperature (defined as the temperature of the cooling water outlet) is 65°C. Nominal power output of the stack is 10 kW, but a peak of 11.4 kW has been achieved during testing. Figure 1 shows the stack polarization curve at standard operating conditions. Operation is very stable, even at high power levels. The stack was operated at 9.5 kW for three 8-hour periods. More than 100 operating hours have been accumulated during testing.

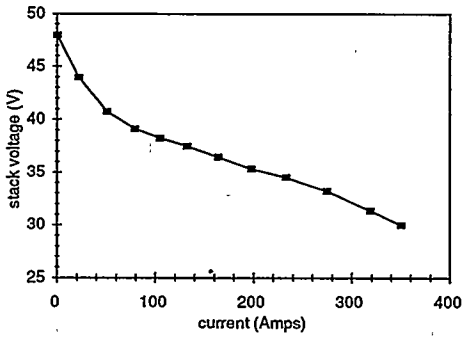

Figure 1 Performance of a 50-cell stack (H_2/Air, 300 kPa, 65°C)

The stack is capable of delivering >7 kW at cold start in less than two seconds, a feature of interest for automotive applications. The stack was also very responsive to load changes varying between 20% and 95% of the load (i.e., 2.0 and 9.5 kW). The responsivity of a fuel cell system in practical application will be limited by a compressor, not the fuel cell.

Due to a very thin membrane, water back-diffusion from the cathode to the anode may be higher than the electro-osmotic drag at certain current densities. During 2 hours of operation at 9.5 kW 11 kg of water accumulated at the cathode outlet, and 2.5 kg at the anode outlet, although hydrogen gas was not humidified prior entering the stack.

Nominal power (10 kW) is achieved at 410 mA/cm^2 and 31.3 V (corresponding to 0.626 V/cell). The performance of the entire stack appears to be limited by a few cells that seem to suffer from severe mass transport problems (Fig. 2). Figure 3 shows the individual cell potential distribution at different current densities. A majority of the cells are well above 0.65 V at 410 mA/cm^2, thus having potential of achieving much higher power densities (>0.36 W/cm^2).

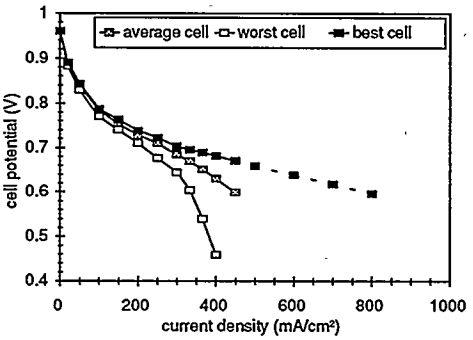

Figure 2 Performance of individual cells in 50-cell stack

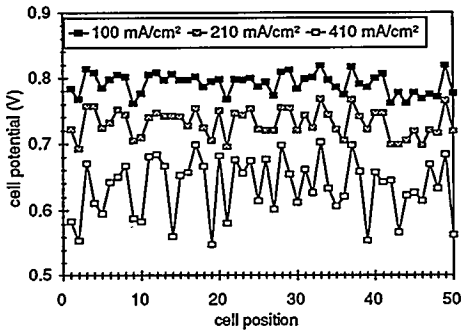

Figure 3 Cell potential distribution in 50-cell stack at different current densities

There is a big discrepancy in published data on the performance of PEM fuel cells in laboratories and in practical applications. Significant development efforts are needed to cross the gap from a small single cell in a controlled environment to a stack of large active area cells operating in a practical application, such as a fuel cell powered vehicle. A variety of technical problems must be addressed in developing a large fuel cell stack, such as:

- manifolding,
- sealing of the cells (particularly around the manifolds),
- uniform reactants supply to each cell,
- uniform reactants supply over large active areas inside each cell,
- product water removal,
- heat removal, and
- electrical contacts over large areas.

Development of the 10-kW stack was accompanied by the experiments with a 150 cm^2 single cell, using the same MEA (Gore PRIMEA™). As opposed to a cell in a multi-cell stack, the single cell experiment allows operation at controlled conditions, i.e., flow rate, pressure temperature and humidity of both reactant gases. Figure 4 shows the performance of a single cell (150 cm^2) with hydrogen/air at 60 °C and 300 kPa.

Power density of ~0.5 W/cm^2 was achieved at 0.6 V. When the hydrogen flow rate was increased the power density at 0.6 V increased up to >0.6 W/cm^2 (max. power density was 0.75 W/cm^2 but at lower voltage). It was also noted that the cell potential responded to the changes in hydrogen pressure much more than what should be expected just based on the Nernst equation. Such sensitivity to hydrogen flow rate and pressure indicates that the cell performance is affected by net water transport across the membrane from the cathode to the anode. Higher pressure on the hydrogen side apparently reduced the net water flux, and higher flow rate helped removing water from the anode. This was confirmed in operation of the 50-cell stack which needed constant purging of the hydrogen side.

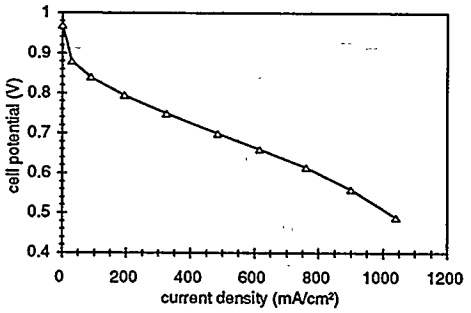

Figure 4 Performance of a single 150 cm^2 cell (H_2/Air, 300 kPa, 60°C)

With the performance currently achievable in single cell (i.e., >6 kW/m^2) the next generation Energy Partners' fuel cell stacks (with projected weight of <12 kg/m^2) will reach power density of >0.5 kW/kg and 0.8 kW/l, thus coming another step closer to the automotive industry requirements.

ACKNOWLEDGMENTS

Financial support for this work was partially provided by the Ford Motor Company and U.S. Department of Energy, under the Direct Hydrogen PEM Fuel Cell for Automotive Applications Program, subcontract No. 47-2-R31150.

GORE-PRIMEA™ series 5000 membrane electrode assemblies, GORE-SELECT™ membranes, and GORE-CARBEL™ gas diffusion layers were supplied under *Customer Sample Agreement* (No. 011704).

REFERENCES

1. F. Barbir, R&D of Direct Hydrogen Proton Exchange Membrane Fuel Cell for Automotive Applications, Phase I Final Report to DOE/Ford Motor Company, (subcontract No. 47-2-R31150), Energy Partners, Report No. 10539, 1996
2. J.A. Kolde, B. Bahar, M.S. Wilson, T.A. Zawodzinski and S. Gottesfeld, Advanced Composite Polymer Electrolyte Fuel Cell Membranes, in Proton Conducting Membrane Fuel Cells I, Proc. Volume 95-23, pp. 193-201, The Electrochemical Society, Pennington, NJ, 1995.
3. M.S. Wilson, J.A. Valerio, and S. Gottesfeld, Low Platinum Loading Electrodes for Polymer Electrolyte Fuel Cells Fabricated Using Thermoplastic Ionomers, *Electrochimica Acta*, Vol. 40, No. 3, pp. 345-363, 1995.

FLEMION®S AND PEFC

M. Yoshitake, N. Yoshida and T. Ishisaki
Fundamental Research Center, Asahi Glass Co., Ltd.
1150, Hazawa-cho, Kanagawa-ku, Yokohama-shi, KANAGAWA, JAPAN

INTRODUCTION

Asahi Glass Co., Ltd. (AGC) had commercialized chlro-alkali electrolysis process using perfluorinated ion exchange membranes (Flemion®). AGC participated in the PEFC project of NEDO (New Energy and Industrial Technology Development Organization) which started in the fiscal year 1992. In this program, AGC selected Flemion®S as one of the candidate membranes for PEFC. The properties of Flemion®S and Nafion®117 such as thermal stability, mechanical strength in dry and wet state, water content, AC specific resistance and gas permeability in dry and wet state, were evaluated and a new method of the preparation of membrane-electrode composites was developed (1-2).

EXPERIMENTAL

Membranes

Perfluorosulfonic acid type cation exchange membranes, Flemion®S (cation exchange capacity: 1.0 meq./g, thickness: 80 μ m, AGC) and Nafion®117 (0.91 meq./g, 175 μ m, du Pont), were studied. Figure 1 shows the chemical structure of these membranes.

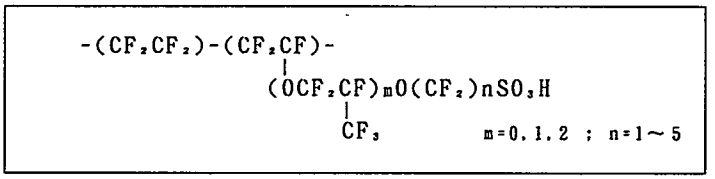

Fig. 1 Chemical structure of tested membranes: Flemion®S and Nafion®117

Gas permeability

Hydrogen and oxygen permeability were estimated by a measurement system in which wet gases were flowed on the both sides of the membrane in order to keep the membrane uniformly wet as shown in Fig. 2. Membranes were set in the ribbed cell made of PTFE after drying at 100℃ for 1 hour. Humidified test gas was flowed on one side of the membrane set in the cell and humidified inert gas was flowed on the other side. This inert gas was same as the carrier gas used in the gas chromatograph. The driving force for the permeation of the test gas (using

an inert gas as the carrier) through the membrane was the partial pressure difference between one side of the membrane and the another. Concentration of the test gas in the inert gas was measured by gas chromatograph. Nitrogen and helium were used as carrier gas of the gas chromatograph for the measurement of hydrogen and oxygen, respectively. Temperature of the cell and the humidifiers were changed in the range from 30℃ to 85℃ during the measurements. This method was used not only for the evaluation of gas permeation behavior of plain membranes but also for that of membrane-electrode composites.

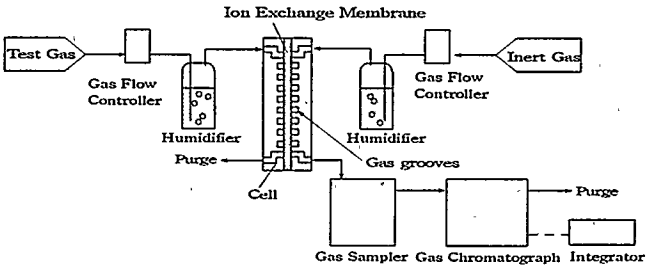

Fig. 2 Flow diagram of gas permeability measurement system

Preparation of membrane-electrode composites

Membrane-electrode composites (assemblies) were prepared by several methods such as hotpressing and "adhesion method" in which adhesives developed by AGC are used and the assembling is carried out by pressing slightly at room temperature. The latter method can afford smaller decrease in pore volume of gas diffusion electrode than the former one as shown in Fig.3. The adhesives contain fluorocarbon compounds and can be noninflammable.

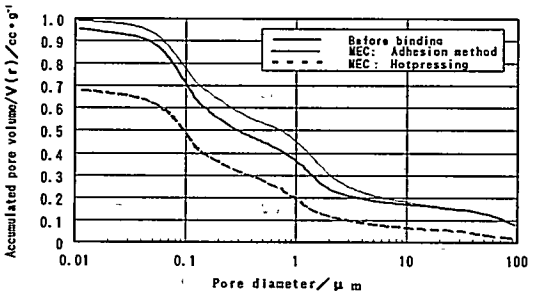

Fig.3 Pore distribution of the membrane-electrode composites

RESULTS

Basic properties of the membranes

Basic properties of the membranes are summarized in Table 1. It was examined that the area resistance of Flemion®S is about 43% of that of Nafion®117 and thermal stability and gas permeability of Flemion®S are almost equivalent to those of Nafion®117. It was also found that the gas permeability of the membrane-electrode composites were larger than that of the plain membranes.

Table 1 Characteristics of Flemion®S and Nafion®117

			Flemion®S	Nafion®117
Decomposition Temperature (℃)			287	275
Mechanical Properties		Dry	323/237	300/226
(70℃) TB/EB[1)]		Wet	183/252	183/265
Water Uptake(%) (70℃)			40	31
Specific Resistance (Ω·cm)			12.6	13.4
Area resistance (Ω·cm^2)			0.10	0.23
Gas Permeation coefficient	P[2)]	H_2	4.4×10^{-10}	4.6×10^{-10}
(25℃) (Dry)		O_2	5.3×10^{-11}	6.5×10^{-11}
Gas Permeation coefficient	P[2)]	H_2	3.8×10^{-8}	4.1×10^{-8}
(70℃) (Wet)		O_2	1.6×10^{-8}	1.8×10^{-8}
Gas Permeation rate	q[3)]	H_2	2.5×10^{-4}	1.2×10^{-4}
(70℃) (Wet)		O_2	1.1×10^{-4}	5.5×10^{-5}

1) TB : tensile strength at breakdown (kg/cm^2), EB : elongation at breakdown (%)

2) P:cm^3(STP)·cm/cm^2·sec·cmHg

3) q: cm^3(STP)/cm^2·sec

Performance of Flemion® S composites

The performance of Flemion®S-composites were evaluated using the labo-cells (10 cm^2) and the medium size cells (225 cm^2). It was examined that Flemion® composites gave smaller internal resistance than Nafion®117 composites as shown in Fig.4. Flemion®S composites gave the output voltage of 0.66V (labo-cell) in labo-cells and 0.60V in medium size cells, 0.5A/cm^2 at atmospheric pressure after the optimaization of test condition as shown in Fig.5.

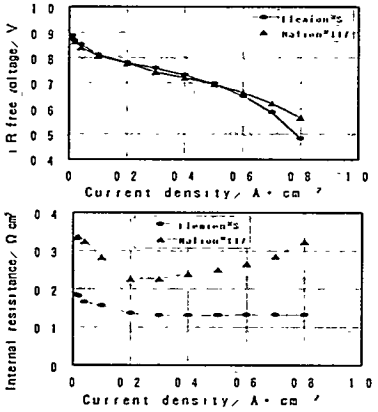

Fig.4 Performance of Flemion®S composite and Nafion®117 composite

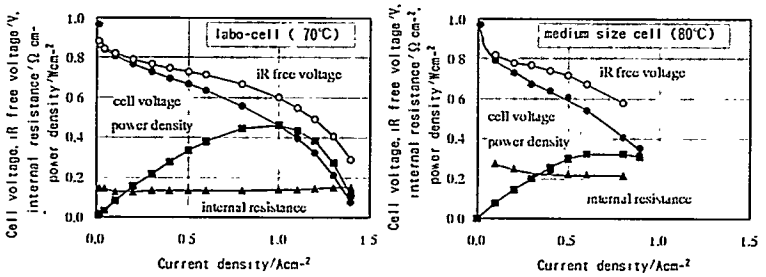

Fig.5 Single cell performance of Flemion®S-composites at atmospheric pressure
(Hydrogen utilization : 70% / air utilization : 40%, cathode Pt loading : 0.54 mg/cm^2)

REFERENCES

1. M. Yoshitake, M. Tamura and T. Ishisaki, FCDIC 1'st Symposium, (1994) 154.

2. M. Yoshitake, M. Tamura , N. Yoshida and T. Ishisaki, Denkikagaku, 64 (1996) 727.

ACKNOWLEDGMENT

This work was carried out under contract with the New Energy and Industrial Technology Development Organization (NEDO).

HIGH ENERGY DENSITY PROTON EXCHANGE MEMBRANE FUEL CELL WITH DRY REACTANT GASES

Supramaniam Srinivasan, Serguey Gamburzev, Omourtag A. Velev,
Frank Simoneaux, and A. John Appleby

Center for Electrochemical Systems and Hydrogen Research
Texas Engineering Experimental Station
Texas A&M University System
College Station, TX 77843-3402, USA

Introduction Proton exchange membrane fuel cells (PEMFC) require careful control of humidity levels in the cell stack to achieve a high and stable level of performance. External humidification of the reactant gases, as in the state-of-the-art PEMFCs, increases the complexity, the weight, and the volume of the fuel cell power plant. A method for the operation of PEMFCs without external humidification (i.e., self-humidified PEMFCs) was first developed and tested by Dhar at BCS Technology (1). A project is underway in our Center to develop a PEMFC cell stack, which can work without external humidification and attain a performance level of a current density of 0.7 A/cm^2 at a cell potential of 0.7 V, with hydrogen/air as reactants at 1 atm pressure. In this paper, the results of our efforts to design and develop a PEMFC stack requiring no external humidification will be presented. This paper focuses on determining the effects of type of electrodes, the methods of their preparation, as well as that of the membrane and electrode assembly (MEA), platinum loading and types of electrocatalyst on the performance of the PEMFC will be illustrated.

Optimization of Structures of Electrodes The traditional method of electrode preparation was significantly modified in order to retain the maximum amount of water in the active layer and hence to maintain the high ionic conductivity in the proton exchange membrane and the active layer in the electrode containing only the supported electrocatalyst and Nafion. The electrodes were fabricated by spreading an emulsion of platinum supported catalyst and Nafion 950EW onto teflonized substrate (carbon cloth)/diffusion layer (2, 3, 4). By this method of preparation perfluorosulfonic acid polymer was evenly distributed in the active layer of the electrode and thus provided the largest possible area of the electrocatalyst/electrolyte interface. Attaining this high interfacial area was confirmed by the very high electrochemical utilization of the platinum electrocatalyst, as determined using cyclic voltammetry. For the 20% Pt supported on Vulcan XC-72, this value was 48% (vs 10 - 20% obtained with the standard impregnation method). Another significant difference in the composition of the active layer was the elimination of Teflon which is a strong hydrophobic agent. In this way a better water balance was possible, as required for preventing drying-out of the membrane.

Experimental Procedure Experiments were carried out in 50 cm^2 PEMFC single cells at different temperatures and atmospheric pressure with H_2/air as reactants. The fuel cell electrodes were prepared *in-house* with Pt supported on Vulcan XC-72 carbon electrocatalysts (E-TEK Inc.). The Pt loading in the cathode was between 1.2 and 1.5 mg Pt/cm^2, and that in the anode between 0.3 and 0.4 mg Pt/cm^2. The proton exchange membranes, Nafion® 112 and GORE-SELECT™, were used as received. The reactant utilization was 95 % for hydrogen and 50 % for oxygen at all current densities.

PEMFC Performance with Dry Reactant Gases The data presented in Figure 1 illustrates the PEMFC (with a Nafion 112 membrane) performance with dry reactant gases. For comparison the performance of the PEMFC with 100% humidification of air and hydrogen is also presented. At low current densities there is hardly any difference in performance but at high current densities a lower hydration of the membrane is reflected in the ohmic controlled region of the cell potential vs. current density plot. In the PEMFC with the GORE-SELECT™ membrane, the difference in the performances for operation without and with external humidifications was considerably less than in the PEMFC with the Nafion membrane.

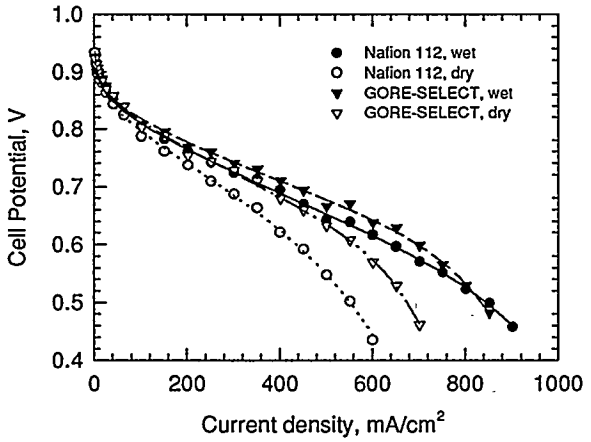

Figure 1 Cell potential vs. current density plots for cells with different membranes. 50 cm^2 cell, hydrogen/air reactants at atmospheric pressure, 50 °C. Anode electrocatalyst loading 0.4 mg/cm^2, cathode electrocatalyst loading 1.4 mg/cm^2. Reactant gas utilization - 95% for hydrogen and 50% for oxygen.

The dependence of the time on current density at a constant potential for the PEMFC operating with dry gases is shown in Fig. 2. Its performance was stable over a 200 h period. The current density at this potential obtained from the dynamically measured cell potential vs current density plot (Fig. 1) shows good agreement with its value, as obtained from the time study (Fig. 2). Such a result was obtained only when the operating temperature of the PEMFC was below 60° C. When the temperature was raised above this value, the PEMFC performance dropped drastically due to dehydration of the proton exchange membrane.

PEMFC Performance with only H_2 Gas Humidification If the restrictions on the operating conditions imposed by the low relative humidity of the reactant gases are not acceptable, a compromise may be reached by providing extra water only to the hydrogen side of the PEMFC. The data in Figure 3 shows that the PEMFC performance in this case is practically the same as in the PEMFC when both hydrogen and oxygen are humidified. Another advantage of this type of humidification is that it becomes easier to remove the product water as a vapor, which thereby reduces the amount of external cooling required to remove the heat generated in the PEMFC.

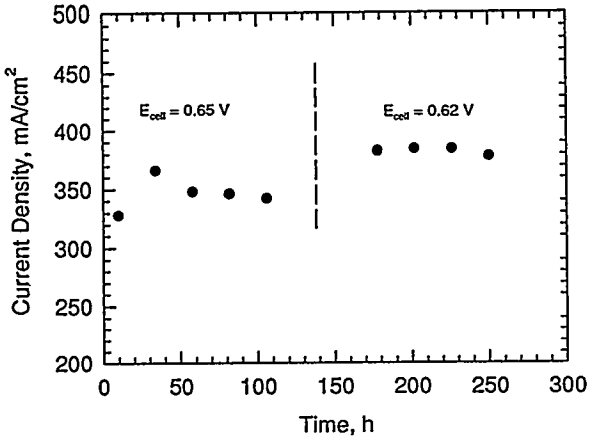

Figure 2 Current density as a function of time for cell operated with dry gases (H_2/air) at constant voltage. 50 cm^2 cell hydrogen/air reactant gases at atmospheric pressure. Anode electrocatalyst loading 0.3 mg Pt/cm^2, cathode electrocatalyst loading 1.1 mg/cm^2, Nafion 112 membrane. Reactant gas utilization - 95% for hydrogen and 50% for air.

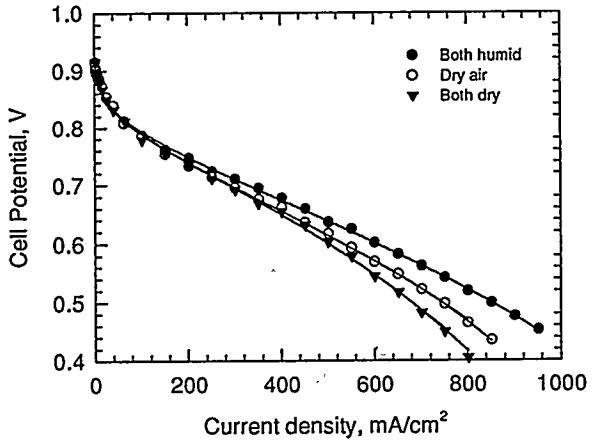

Figure 3 Cell potential vs. current density plots for PEMFCs with different humidification schemes. 50 cm^2 cell gases hydrogen/air reactants at atmospheric pressure, 50 °C. Anode electrocatalyst loading 0.3 mg Pt/cm^2, cathode electrocatalyst loading 1.4 mg/cm^2. Reactant gas utilization - 95% for hydrogen and 50% for air.

PEMFC Performance O_2 Enrichment Another method of increasing the cell performance is to use oxygen enriched air. The oxygen enrichment can be achieved by using a gas separation membrane. Oxygen enrichment is particularly valuable when the reactant gases are not humidi-

fied. Fig. 4 shows that when the oxygen content of the inlet air stream is close to 40%, the difference in PEMFC performance between dry and wet gases is minimal. Another advantage of oxygen enrichment is that it permits the operation of the PEMFC with the non-humidified reactant gases at a higher temperature than when using ambient air. By operation of the PEMFC at a higher temperature (say 80º C), its efficiency for the utilization of heat is increased and to some extent simplifies the heat removal sub-system.

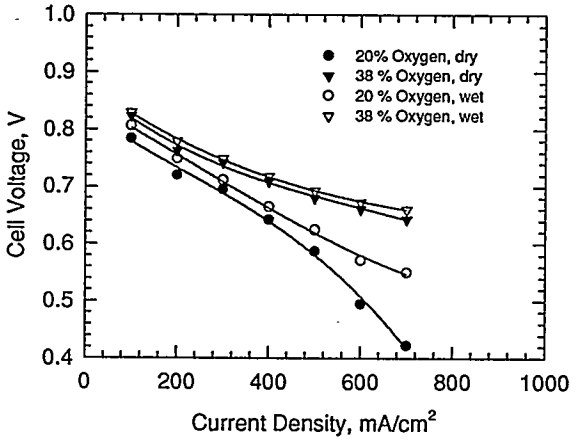

Figure 4 Beneficial effects of oxygen enrichment on H_2/air PEMFC performance for operation without humidification of reactant gases. 50 cm^2 cell area reactant gases at atmospheric pressure, 50 °C. Anode electrocatalyst loading 0.3 mg/cm^2, cathode electrocatalyst loading 1.4 mg/cm^2. Reactant gas utilization - 95% for hydrogen and 50% for air.

Conclusions By modifying the method of PEMFC electrode preparation we were able to operate cells without external humidification of reactant gases at relatively high power levels. The restriction on the operating temperature imposed by the removal of the humidification system may be alleviated by supplying extra water to the hydrogen stream only. Further optimization of the structure of the electroactive layer is needed to improve the performance of self humidified PEMFCs. Increasing the oxygen content of the air stream may be energetically favorable for achieving higher power density of the PEMFC power plant.

Acknowledgments The financial support of the Office of Naval Research (contract #N00014-95-1-0114) is gratefully acknowledged. Experimental samples of GORE-SELECT™ fluoroionomer composite membrane were provided by W.L. Gore&Associates, Inc. for a nominal charge to cover partial laboratory expenses under confidentiality agreement. GORE-SELECT™ is a trade mark of W.L Gore&Associates, Inc..

References

1 H.P. Dhar US Patent No. 5,242,764 (1993) and No 5,318,863 (1994)
2 M.S. Wilson and S. Gottesfeld, "J. of Applied Electrochem.", Vol. 22, p 1., 1992.
3 M. Uchida, Y. Aoyama, N. Eda, and A. Ohta, "J. Electrochem. Soc.", Vol. 142, p. 463, 1995.
4 S. Gamburzev, O.A. Velev, S. Srinivasan, and A.J. Appleby, 190th ECS Meeting, San Antonio, Texas, Oct. 6 - 11, 1996, Ext. Abstracts.

STUDY ON A PEFC PROPULSION SYSTEM FOR SURFACE SHIPS

Ryuta Ono
Ishikawajima-Harima Heavy Industries Co., Ltd.
2-1-1 Toyosu, Koto-ku, Tokyo 135, Japan

Syozo Tsuchiyama
The Shipbuilding Research Association of Japan
Senpaku Shinko Bldg., 1-15-16 Toranomon, Minato-ku,
Tokyo 105, Japan

This Abstract summarizes a series of presentations to the present Seminar, covering various aspects of a 1,000 kW PEFC system envisaged as propulsion system to equip a 1,500 DWT cargo vessel, reported under the following titles:-

- Performance Evaluation of 1kW PEFC
- Performance of Catalysts for CO Removal by Methanation Reaction
- Development of a Selective Oxidation CO Removal Reactor for Methanol Reformate Gas
- Experimental Investigation on a Turbine Compressor for Air Supply System of a Fuel Cell
- Dynamic Simulator for PEFC Propulsion Plant
- Power Feature Required for PEFC Powered Electric Propulsion Ship

The purpose of this study is to identify subjects requiring further development toward the realization of a practical fuel cell system to power ships.

(1) System composition

Methanol was adopted as fuel, for facilitating onboard storage; system pressure was set at 3 kgf/cm^2 abs. for enhancing thermal efficiency. Minimization of plant size and weight was sought through the adoption of a combined unit comprising plate-fin type heat exchangers, plate type reformer and shift converter. The system configuration is shown in Fig. 1.

The envisaged system performance parameters are:-

- Net power output (DC) : 500 kW x 2 units
- Operating pressure : 3 kgf/cm^2 abs.
- Fuel utilization : 80%
- Air utilization : 50%
- Thermal efficiency (HHV) : 45% at generator terminal.

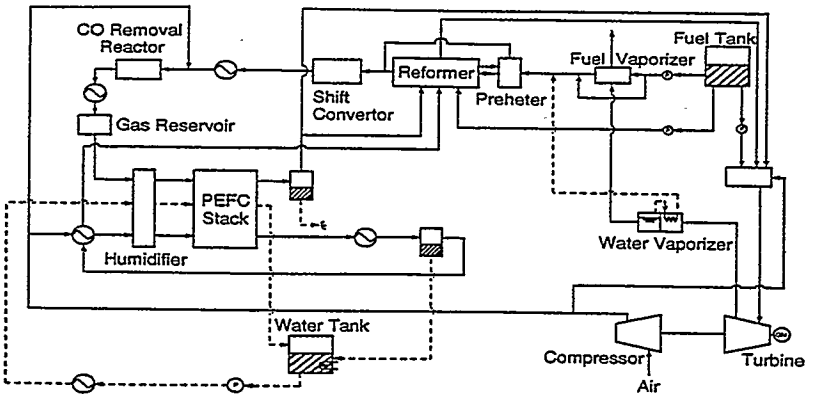

Fig. 1 System composition

(2) Characteristics of PEFC

In order to obtain basic data required for PEFC application to ship propulsion, tests were conducted on (a) a 1 kW PEFC stack and (b) a single cell, for determining system performance characteristics under static and dynamic load, and under operating conditions particular to ship propulsion (e.g. effects of hull inclination/pitching/rolling and of salinity).

The tests yielded V-I characteristics as reproduced in Fig. 2 together with curves for other types of fuel cell. Other findings of particular interest for application to ships included:-

- Ample load-following capability of PEFC stack
- Necessity of devising stack structure and shipboard arrangement to facilitate discharge of generated water when operating in inclined position brought by hull movement
- Need to provide adequate filtering of supplied air against saline atmosphere.

(3) CO removal

Tests for substantiating adequate CO removal were performed using a 1-kW class experimental unit, applying selective oxidation and methanation processes. Both processes were indicated to be capable of reducing CO content down to 10 ppm under static condition. Further tests are currently under way for determining the corresponding performances under dynamic load.

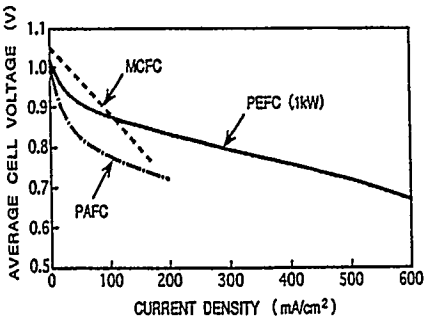

Fig. 2 V-I characteristics of different fuel cell types

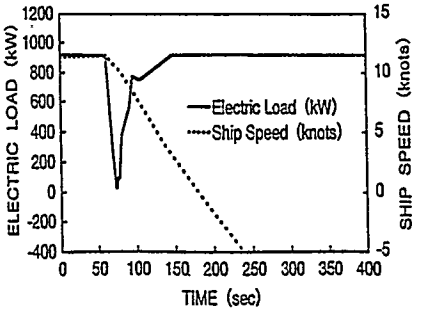

Fig. 3 Example of load change in maneuver (crash-stop astern)

(4) Air supply

An automobile exhaust gas turbocompressor was used for air supply to test unit, with which, data were acquired on the response characteristics under static, startup, and dynamic conditions. Other tests were conducted on the membrane-type humidifier requiring to equip PEFC systems, to obtain performance data covering also the case of operation in inclined position. Empirical characteristic performance equations were derived from the resulting data.

(5) Adaptation to load variations

While load variations in ship propulsion are quite moderate when navigating in open sea, consideration requires to be given to abrupt load changes occurring in the event of crash-stop astern maneuver (see Fig. 3), and upon actuation of bow thrusters for berthing and unberthing operations, as well as upon propeller racing in heavy sea. Another difference between marine and automobile applications is that the output for ship propulsion is too high for supplementation of power shortage by battery.

Load-following capability has been enhanced by providing the fuel supply circuit with advance control, and sharp drops of load are accommodated by diverting surplus anode effluent to the exhaust gas turbine combustor (catalyst combustor). A gas reservoir is installed to absorb excess reformate gas under lowering load and to supplement gas shortage under rising load. The turbocompressor is equipped with generator motor for enhancing load-following capability, and for absorbing the energy of superfluous anode effluent.

(6) Dynamic simulation

A dynamic simulator was devised for analyzing the load-following performance enhanced with the measures described in the preceding section. The simulator program covers most of the system components contained in Fig. 1, except for the water cooling circuit.

The response characteristics of the system as a whole, and the simulator programs to cover reformer and gas reservoir——both of which vitally influence the load-following capability——are being examined through integrated evaluation experiments currently under way.

(7) Trial design of engine room arrangement

The engine room arrangement was studied envisaging a 1,500 DWT cargo ship fueled with methanol (Figs. 4 and 5). The motor room is separated by bulkheads from the compartments for fuel cell and for methanol storage. For safety considerations, the fuel cell compartment is to be maintained at slightly negative pressure.

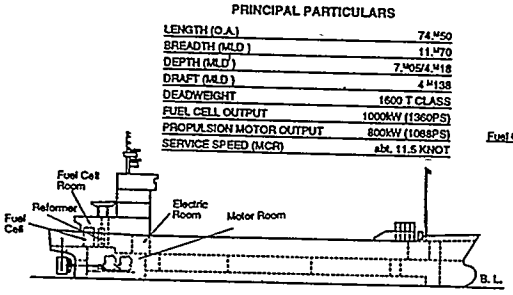

Fig. 4 General arrangement of ship

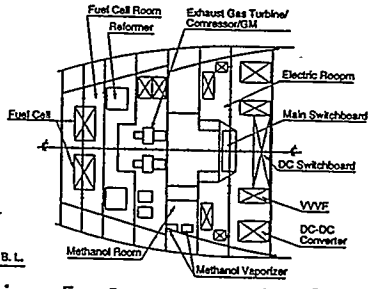

Fig. 5 Arrangement of engine room

(8) Integrated experiment on fuel supply circuit

For evaluating the dynamic characteristics of the fuel supply circuit, and for further verifying the measures adopted for enhancing load-following capability, an exeriment is currently under way on a model fuel supply system representing a 10-kW class PEFC unit fueled with methanol-water mixture, provided with combined plate type reformer and shift converter, and with CO removal ensured by selective oxidation process. The model is not equipped with fuel cell, and hydrogen gas consumption is simulated by adjusting the rate of gas discharge to system exterior.

POLYMER ELECTROLYTE DIRECT METHANOL FUEL CELLS: AN OPTION FOR TRANSPORTAION APPLICATIONS

S. Gottesfeld, S. J. C. Cleghorn, X. Ren, T. E. Springer,
M. S. Wilson and T. A. Zawodzinski
Materials Science and Technology Division, MS D429
Los Alamos National Laboratory, Los Alamos, NM 87545

Introduction

In the last few years polymer electrolyte fuel cell (PEFC) technology has advanced to the point of being considered a viable option for primary power sources in electric vehicles. The systems most frequently considered in this context have been based on either hydrogen carried on board the vehicle, or steam-reforming of methanol on board to generate a mixture of hydrogen and CO_2. Direct methanol fuel cells (DMFCs), which use a liquid methanol fuel feed, completely avoid the complexity and weight penalties of the reformer. Yet until recently DMFCs have not been considered a serious option for transportation applications, primarily because of the much lower power densities achieved compared with operation on hydrogen rich gaseous feeds. Recent advancements in DMFC research and development have been quite dramatic, however, with the DMFC reaching power densities which are significant fractions of those provided by the reformate/air fuel cell (RAFC). The use of established Pt-Ru anode electrocatalysts and Pt cathode electrocatalysts in polymer electrolyte DMFCs has resulted in very significant enhancements in DMFC performance particularly when such cells are operated at temperatures above 100°C and when catalyst layer composition and structure are optimized. The higher DMFC power densities recently achieved provide a new basis for consideration of DMFCs for transportation applications.

DMFC fabrication and testing at LANL

Thin film catalysts bonded to the membrane by the decal method [1,2] provided our best results in terms of catalyst utilization and DMFC performance. Unsupported Pt-RuO_x (Pt:Ru = 1:1) or supported PtRu/C catalysts were used for the anode catalyst and Pt-black or Pt/C was used for the cathode catalyst. Unsupported Pt-Ru anode catalysts yielded the highest overall anode performances. Catalyst inks were prepared by adding 5% Nafion solution to the water-wetted metal catalysts. To prepare the membrane/electrode assemblies (MEAs), appropriate amounts of anode and cathode inks were uniformly applied to Teflon decal blanks to give metal catalyst loadings of approximately 2 mg/cm^2. The single-cell fuel cell hardware, cell testing and high-frequency resistance measurement [3] systems have been described previously.

Figure 1 shows polymer electrolyte DMFC performances under conditions that take advantage of the significant increase in DMFC performance with temperature but may still be amenable to transportation applications. Air cathodes at 3 atm were used and the cell temperatures were set at 110°C. Figure 1 shows that, with the Nafion 112 MEA, a current of 370 mA/cm^2 at 0.5 V cell voltage was obtained with a 1M methanol feed. The low cell resistances measured at 110°C (Figure 1) are apparently brought about by the liquid anode feed in contact with the membrane. The polymer electrolyte DMFC may thus be easier to operate at temperatures above 100°C than the hydrogen/air PEFC. Figure 2 summarizes DMFC power outputs we obtained with oxygen and with air cathodes at 130°C and 110°C, respectively, and shows peak power outputs for this type of DMFC at almost 400 mW/cm^2 for the case of an oxygen cathode at 130°C and about 250 mW/cm^2 for the air cathode at 110°C.

DMFC vs. Reformer + RAFC: A Comparative Evaluation:

The significant increase in demonstrated DMFC performance, as shown above and by other research groups [4,5], has brought the peak power density of the polymer electrolyte DMFC to a

level which is only 2-3 times lower than that of a reformate/air fuel cell (RAFC). Consequently, at this point, some simple calculations reveal that the two options, (i) a DMFC stack and, (ii) a methanol reformer + RAFC stack, show comparable overall system characteristics.

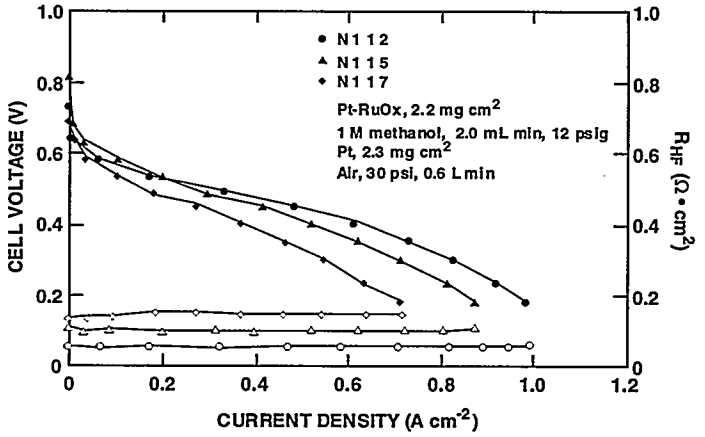

Figure 1. Polarization and high frequency resistance curves for a 110°C, 3 atm air cathode DMFC based on thin-film catalyzed membranes. Anodes: 2.2 mg/cm^2 Pt-RuO_x, 1 M methanol at 2 ml/min and 1.8 atm. Cathodes: 2.3 mg/cm^2 Pt-black.

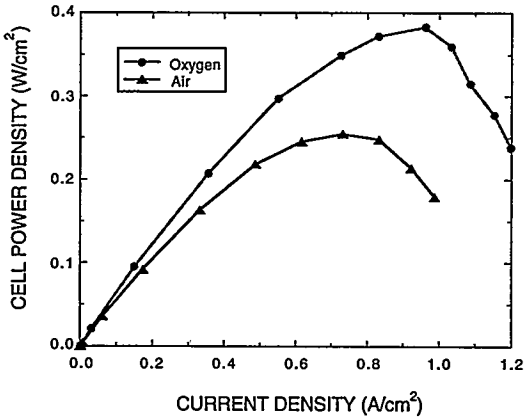

Figure 2. Power density curves for the thin-film catalyzed Nafion 112 assembly, operating at 130°C on oxygen and at 110°C on air.

Table I. Calculation of Energy Conversion Efficiencies for DMFC and RAFC Systems

Assumptions

- Methanol is either:
  (case 1) Converted directly in DMFC, or
  (case 2) Steam reformed to H_2 and converted in RAFC

Efficiency calculation

(case 1, DMFC)

Total Eff. $= \eta_v \cdot (\eta_{fuel\text{-}fc})_1 = [(V_{cell})_1/V^{*}MeOH/CO_2] \cdot (\eta_{fuel,fc})_1$

(case 2, RAFC)

Total Eff. $= \eta_{ref} \cdot \eta_{prox} \cdot \eta_v \cdot (\eta_{fuel,fc})_2$
$= [(V_{cell})_2/V^{*}MeOH/CO_2] \cdot (\eta_{fuel,fc})_2 \cdot \eta_{ref} \cdot \eta_{prox}$.

Conclusion

To achieve equal overall conversion efficiencies (MeOH to dc power):

$$(V_{cell})_1 = (V_{cell})_2 \cdot [(\eta_{fuel,fc})_2/(\eta_{fuel,fc})_1] \cdot \eta_{ref} \cdot \eta_{prox}.$$

Assuming $(\eta_{fuel,fc})_1 = 0.90$, $\eta_{ref} = 0.72$ and $\eta_{prox} = 0.97$, then

$$(V_{cell})_1 = 0.79\ (V_{cell})_2.$$

i.e., same overall energy conversion for DMFC operating at 0.55 V and RAFC at 0.70 V.

Subscripts: v = voltage, fuel.fc = fuel use in the fuel cell, ref = reforming + shift reactors, prox = preferential oxidation reformer.

Table I shows a comparison of overall system efficiencies. The calculation shows that the overall energy conversion efficiencies (methanol chemical energy to DC power) of the two systems are comparable (close to 40%) when the DMFC is operating at 0.55V and the RAFC is operating at 0.70V. This is true assuming:

(a) fuel efficiencies of 90% can be reached in the DMFC (100% fuel efficiency assumed for the RAFC),
(b) the methanol reformer efficiency (hydrogen energy out/methanol energy in), is 72%, and
(c) the overall energy efficiency of the preferential oxidation reactor (PROX) is 97%.

The main DMFC parameter that needs significant improvement to reach the DMFC performance level assumed in Table I is the fuel efficiency, which has been significantly smaller (around 50% at 80°C) in DMFCs employing Nafion® 1100 membranes. However, recent efforts to fabricate and evaluate DMFC membranes of significantly lower methanol "cross-over" rates (yet good protonic conductivity) have provided some promising results. The probability of reaching high DMFC fuel efficiencies following further similar efforts seems significant.

The conclusion of a comparable overall energy conversion efficiency for the two systems at the typical operation voltage per cell in each case (DMFC at 0.55V and RAFC at 0.70V) is significant yet obviously depends on the trade-off between the lower DMFC voltage efficiency and the efficiency losses of methanol reforming. Thus, the typically lower DMFC operation voltage is not to be taken as an immediate indication of an inferior overall system energy efficiency.

Table II. Projected DMFC and RAFC Stack And Systems Characteristics

	DMFC[a]	RAFC[b]
Stack Power Density (kW/kg)	0.25	1.0
Stack Materials Cost ($/kW)		
• Projected[c]	200	45
• Today	2500	1500
System Energy Density[d] (Wh/kg)	750	750

a) Advanced fuel cell stack is 50 - 75% of total weight. b) Advanced fuel cell stack is 10 - 30% of total weight. c) Assuming drop in PFSA membrane cost by order of magnitude. d) Assuming, in each case, a 50 kW; 300 kWh system of overall weight 400 kg and overall energy conv. efficiency 40%.

Table II uses some very rough estimates to compare three other key parameters for the two systems (DMFC and reformer + RAFC): the power densities, stack materials costs and system energy densities. The stack power density for the reformate/air fuel cell may be a factor of three higher, but the stack is only 10-30% of the total weight of the system vs. 50-75% of the weight expected in the case of the DMFC. The stack materials costs per kW are projected to be four times higher for the DMFC, mainly due to the lower power density, however, the DMFC stack cost is a much larger percentage of the total systems cost. The total system energy density for a 50 kW vehicle with a range of 300 miles assuming average speed of 50 mph (80 kph) is estimated to be similar for both options, around 750 Wh/kg. These estimates are very rough, but it seems that the DMFC could become a serious candidate for transportation applications, provided the following requirements are met:

(1) Catalyst loadings are further reduced,
(2) Long term stable performances are demonstrated, and
(3) Fuel efficiencies are actually increased to the 90% level.

ACKNOWLEDGMENT

This work was supported by the U. S. Dept. of Energy, Office of Transportation Technology.

REFERENCES

1. M. S. Wilson and S. Gottesfeld, "Thin-film Catalyst Layers for Polymer Electrolyte Fuel Cell Electrodes," J. Appl. Electrochem., Vol. 22, pp. 1-7, 1992.
2. M. S. Wilson, J. Valerio and S. Gottesfeld, "Low Platinum Loading Electrodes for Polymer Electrolyte Fuel Cells Fabricated Using Thermoplastic Ionomers," Electrochim. Acta, Vol. 40, p. 355, 1995.
3. T. E. Springer, M. S. Wilson and S. Gottesfeld, "Modelling and Experimental Diagnostics in Polymer Electrolyte Fuel Cells," J. Electrochem. Soc., Vol. 140, No. 12, pp. 3513-3526, Dec. 1993.
4. S. Surampudi, S. R. Narayanan, E. Vamos, H. Frank, G. Halpert, A. LaConti, J. Kosek, G. K. Surya Prakash and G. A. Olah, "Advances in Direct Oxidation Methanol Fuel Cells," J. Power Sources, Vol. 47, p. 377, 1994.
5. H. Grüne, G. Luft, K. Mund and M. Waidhas, "Research and Development of Low Temperature Fuel Cells at Siemens," Program and Abstracts, Fuel Cell Seminar, p. 474, San Diego, CA, Nov. 28 - Dec. 1, 1994.

RECENT ADVANCES IN HIGH-PERFORMANCE DIRECT METHANOL FUEL CELLS

S. R. Narayanan, W. Chun, T. I. Valdez, B Jeffries-Nakamura, H. Frank,
S. Surampudi and G. Halpert
Jet Propulsion Laboratory, California Institute of Technology,
4800 Oak Grove Drive, Pasadena, CA 91109

J. Kosek, C. Cropley and A. B. La Conti
Giner Inc., 14 Spring Street, Waltham, MA 02154

M. Smart, Quin-Ji Wang, G. Surya Prakash and G. Olah
Loker Hydrocarbon Research Center, Department of Chemistry,
University of Southern California, Los Angeles, CA 90089

Introduction

Direct methanol fuel cells for portable power applications have been advanced significantly under DARPA- and ARO-sponsored programs over the last five years. A liquid-feed direct methanol fuel cell developed under these programs, employs a proton exchange membrane as electrolyte and operates on aqueous solutions of methanol with air or oxygen as the oxidant. Power densities as high as 320 mW/cm^2 have been demonstrated. Demonstration of five-cell stack based on the liquid-feed concept have been successfully performed by Giner Inc. and the Jet Propulsion Laboratory. Over 2000 hours of life-testing have been completed on these stacks. These fuel cells have been also been demonstrated by USC to operate on alternate fuels such as trimethoxymethane, dimethoxymethane and trioxane. Reduction in the parasitic loss of fuel across the fuel cell, a phenomenon termed as "fuel crossover" has been achieved using polymer membranes developed at USC. As a result efficiencies as high as 40% is considered attainable with this type of fuel cell. The state-of-development has reached a point where it is now been actively considered for stationary, portable and transportation applications. The research and development issues have been the subject of several previous articles [1-5] and the present article is an attempt to summarize the key advances in this technology.

The Liquid-Feed Direct Methanol Fuel Cell

The heart of the fuel cell is a membrane-electrode assembly consisting of two catalyzed electrodes bonded to either side of a proton-exchange membrane similar to that used in the low-temperature hydrogen-oxygen fuel cells. Nafion 117 is an example of such a membrane. The anode employs platinum-ruthenium as the catalyst and sustains the electro-oxidation of methanol to carbon dioxide. The cathode employs platinum as the catalyst an sustains the electro-reduction of air/oxygen to water. During operation, an aqueous solution of methanol (about 3 v/v %) is circulated past the anode. The carbon dioxide produced at the anode is separated from the liquid stream and the solution is re-circulated. The fuel cell has been operated over between 15° and 120°C, the efficiency and power densities being higher at the higher temperatures. The typical operating point for many applications could be in the range of 50- 95°C. The fuel cell can operate at ambient pressure . The overall simplicity of this concept renders this fuel cell very attractive from a system perspective. A demonstration of the system concept for DARPA applications is now in progress at JPL and Giner Inc. Briefly, the performance of these fuel cells is determined by the activity of the anode catalyst, the methanol permeability and ionic conductivity of the membranes, cathode structures and method of preparation of membrane-electrode assemblies. Advances in each of these areas leading to the current levels of performance are summarized in the following.

Anode Performance:

Platinum-ruthenium is found to be the most efficient catalyst for the electro-oxidation of methanol. These catalysts usually consist of an alloy of platinum-ruthenium with small amounts of oxide in a reduced state and the best performance is found to be attained when the composition corresponds to a mole ratio of 50:50 (Pt:Ru). Catalysts separately prepared at the Jet Propulsion Laboratory and Giner Inc., by quite different methods have been found to have similar performance. Significant improvements in catalyst performance and utilization have been by modifications of preparation procedures. These catalysts are resistant to poisoning unlike pure platinum catalysts. The anode polarization curves for various concentrations of methanol have been derived from full cell performance data and demonstrate that very high current densities are possible at the anode using platinum-ruthenium catalysts. The typical operating electrode potential for the anode is in the range of 0.35-0.38 V for 400-500 mA/cm^2 at 90°C. Also, these results demonstrate that performance of the anode at high current densities is limited significantly by the mass transport of methanol rather than the activity of the catalyst. This situation presents a significant advance over the prior-art methanol fuel cells which could not operate at a tenth of the present power levels. Since mass transport of methanol and the kinetics of oxidation are enhanced by increasing temperature, higher performance can be attained by increasing the operating temperature of the fuel cell. The typical operating point for most applications is in the range of 55-95°C.

Cathode performance:

The cathode can be operated on air/oxygen. The fuel cells are capable of operating on air at ambient pressures. Figure 1 shows the typical performance differences for operation on air and oxygen.

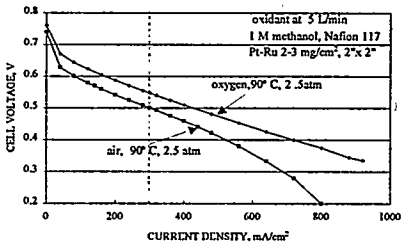

Figure 1. Performance of direct methanol fuel cell operating on air and oxygen

Current densities as high as 600 mA/cm^2 can be sustained on near-ambient pressure air. These results present significant improvement over the prior-art fuel cells based on methanol. From the point of the lowering overall system size and increasing system efficiency, the operability on ambient pressure air at stoichiometric rates of less than five is very important. The performance of the cathode is dependent on the flow rate of air. This performance characteristic is caused by the differences in the rate of removal of water produced at the cathode at various flow rates. The use of thin hydrophobic backing layers, ultra-thin catalyst layers and modified flow fields are found to have a beneficial effect on the performance of the cathode and are currently being pursued by JPL and Giner Inc.

Membrane-Electrode Assemblies:

The key step in the method of preparation of membrane-electrode assemblies for this type of fuel cell involves the formation of a catalyst-membrane interface that presents a large electrochemically active surface area and high protonic conductivity. Typically, the preparation of such membrane-electrode assemblies involve the formation of composite electrode layers

consisting of catalyst and proton-conducting material and hot-bonding of these layers to the proton-exchange membrane such as Nafion 117. Considerable differences in performance can arise from the methods employed. Enhanced performance of direct methanol fuel cells arising from the direct application of catalyst to the membrane are shown in Figure 2.

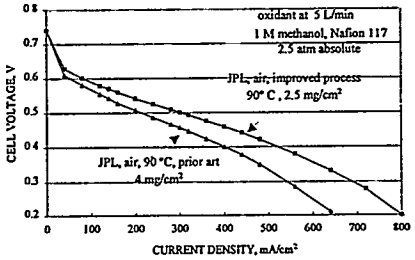

Figure 2 . Performance of direct methanol fuel cell with reduced loading and improved process for fabricating membrane electrode assemblies.

These new methods allow the formation of ultra-thin catalyst layers resulting in improved mass transfer and increased catalyst utilization.

Methanol Crossover:

Methanol crossover from the anode to the cathode results in consumption of fuel and also impacts the performance of the cathode causing the cell to operate at a lower overall efficiency. The crossover rate is largely determined by the permeability of the membrane and electrode structures to methanol. Nafion-117 present high ionic conductivity but is also highly permeable to methanol. Nafion membranes with higher equivalent weight have usually lower methanol permeability but also reduced ionic conductivity. Thus the development of membranes with low methanol permeability with high ionic conductivity has been an important effort. The recent results from USC demonstrate that such membranes can be developed. Figure 3 presents data on the relative methanol permeability of new membranes and Nafion 117. These new membranes also possess the high ionic conductivity of Nafion 117. The new membranes are expected to be less expensive than the state-of-art Nafion membranes. The implementation of these membranes into actual fuel cells is being currently pursued at JPL and the initial results show that the electrical performance approach that attained with Nafion.

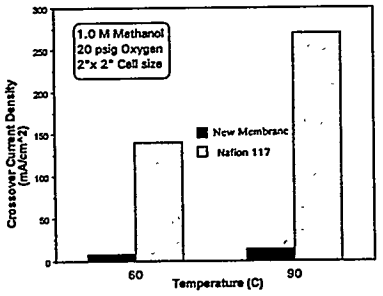

Figure 3. Relative methanol permeability and crossover rates observed with Nafion and newly developed membranes.

Stacks and Systems:

Five-cell stacks have been demonstrated at the 20 and 100 W level by JPL and Giner Inc., respectively with an aim to study stack designs and obtain parametric data on reactant flows and product management in order to be able to achieve a system concept demonstration at the end of December 1996. Performance data on five-cell stacks and membrane-electrode assemblies developed at JPL are presented in Figure 4.

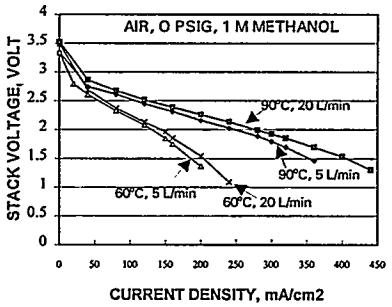

Figure 4. Performance of 5-cell JPL-built direct methanol fuel cell stack at ambient pressure

This data shows the scalability of single cell technology to multi-cell stacks. The development of a 22-cell 60 W stack is presently being pursued for portable power applications. System sizing and thermal management studies are currently underway at JPL and Giner Inc., and power densities in the range of 100W/ kg appear attainable for complete systems.

Life testing of fuel cells:

Operation of a five-cell stack over periods extending over 2400 hours has been carried out at Giner Inc. The performance does not show any significant decline over this period. Continuous operation at high power densities for 200 hours at 90°C also indicate no significant concern relating to short-term degradation.

Acknowledgment:

The work presented here was carried out with support from DARPA and ARO, under a contract with the National Aeronautics and Space Agency at the Jet Propulsion Laboratory, California Institute of Technology.

References:

1. S. R. Narayanan, T. Valdez, W. Chun, B. Nakamura, H. Frank and G. Halpert, Power Sources Conference 1996, Cherry Hill NJ.
2. S.Surampudi, S. R. Narayanan, E. Vamos, H. Frank and G.Halpert, J. Power Sources, 47(1994) 377-385.
3. J. Kosek, C.C. Cropley, A. B. La Conti, G. Wilson, S. R. Narayanan, E. Vamos, S. Surampudi and H. Frank, Proceedings of the IECEC 1993, Volume 1, p. 1209.
4. S. R. Narayanan, A. Kindler, B. Jeffries-Nakamura, W. Chun, H. Frank, M.Smart , S. Surampudi and G.Halpert, Proceedings of the First International Symposium on Proton Conducting Fuel Cells I, p261, The Electrochemical Society, 1995 (Eds. S. Gottesfeld, G. Halpert and A. Landgrebe)
5. S. R. Narayanan, A. Kindler, B. Jeffries-Nakamura, W. Chun, H. Frank, M.Smart, T. I. Valdez , S. Surampudi, J. Kosek and C. Cropley, " Recent Advances in PEM Liquid Feed Direct Methanol Fuel Cells," Proceedings of the Eleventh Annual Battery Conference on Applications an Advances, Long Beach, CA, January 1996.

PC25™ PRODUCT AND MANUFACTURING EXPERIENCE

Eugene W. Hall, William C. Riley and Gregory J. Sandelli
International Fuel Cells Corporation
South Windsor, Connecticut 06074

Product and manufacturing experience accumulated since the beginning of PC25 A production in 1991 provides a strong base of demonstration and experience for establishing future improvements to the PC25 power plant.

Field Experience

The PC25 power plant operating fleet now totals 67 power plants of the A, B and C models and additional units are being installed. As shown in Figure 1, total operating time for the fleet exceeds 1.1 million hours and individual units are now passing 30,000 hours total operating time with 27 units having operated for over 20,000 hours. This experience with fuel cell stacks or power plants including laboratory testing and extensive field testing of prior phosphoric acid power plants. Consequently it provides the first meaningful opportunity to assess the durability and reliability of any fuel cell technology in actual service conditions although it is most directly applicable to the phosphoric acid fuel cell.

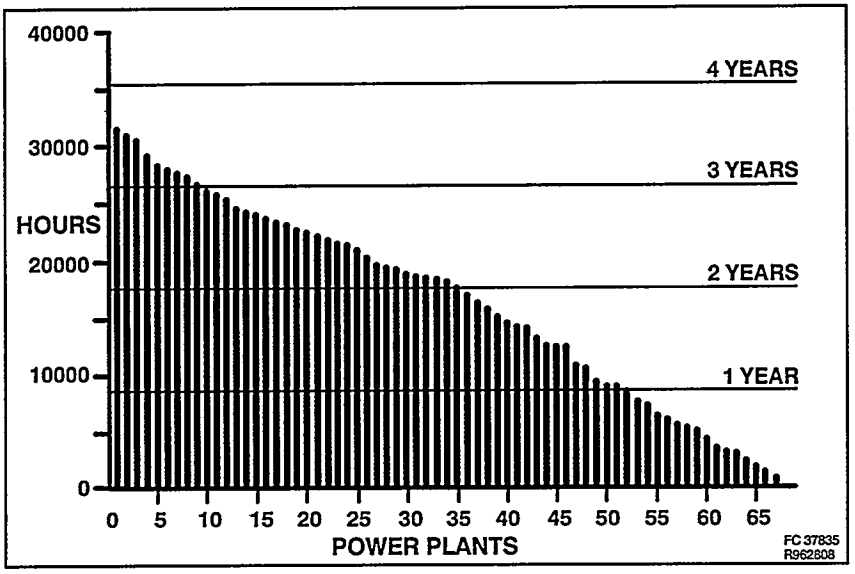

Figure 1: PC25 Power Plant Operating Time

The reliability and durability experience confirms the superiority of the phosphoric acid fuel cell technology compared to conventional equipment used for on-site service. Operation of many units in the initial fleet for periods in excess of the overhaul period for reciprocating engines and a mean time between forced outage which is more than double that of conventional equipment in this rating class and application demonstrates the phosphoric acid fuel cell power plant can provide superior availability and maintenance cost characteristics when product cost matures. This comparison is made at a time when the deployment of the product is still at an early stage, and before results of lessons learned from this deployment which have been applied to the latest power plant model, have had the opportunity to be demonstrated. IFC and ONSI expect the operating record of our new power plant model to show considerable improvement over the results obtained to date and also expect that model to continue to improve.

HP-311

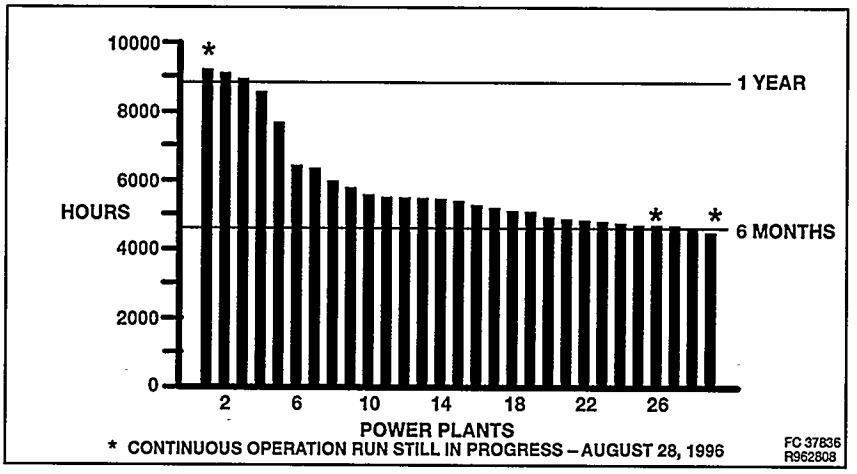

Figure 2: Continuous Runs in the PC25 Fleet

While mean time between forced outages is 2000 hours for the fleet, Figure 2 shows the fleet has experienced nearly 30 continuous runs greater than six months and three continuous runs greater than one year. This experience indicates the PC25 A design has potential for development to higher levels of reliability. Failures in the PC25 fleet are associated with ancillary components or with control decisions. To date, with proper system operating conditions, no failures have originated in the high technology elements of the power plant. As the causes for these failures are identified, improvements are instituted. For example, the first run of greater than one year was terminated by a broken fan belt. In the PC25 A and B fleets, an improved fan belt was identified which alleviates the problem. The PC25 C design alleviates or eliminates many of the failure causes in the PC25 A design. Direct drive fans were incorporated in the PC25 C to eliminate the problem. Sticking valves are another cause of failure which has been alleviated in the PC25 C through use of higher torque valve actuators. A number of changes have been incorporated into the controller to avoid shutdown and to avoid conditions which stress the cell stack or other components.

PC25 Production

IFC manufactured 74 PC25 A and PC25 B power plants in a facility in Middletown, Connecticut. That manufacturing experience and the smaller size of the PC25 C power plant provided the basis for a redesign of the manufacturing plant layout to improve material flow and production efficiency when the manufacturing operations were relocated to South Windsor, Connecticut.

Figure 3 shows IFC's new state-of-he-art 80,000 square foot production factory located at its South Windsor,Connecticut facility. The manufacturing processes employed were developed specifically for a low-cost, high-volume production of the PC25 C power plant. advantage was taken of the Model C's smaller size which allowed an increased use of subassemblies, directly insertable as complete units. Final manufacturing and assembly of the electric generating portion of the power plant – the fuel cell stack – is completely accomplished in this factory. The highly automated processes include robotic component handling and assembly of the PC25 200-kW cell stack. The cell component manufacturing lines are arranged in a modified "spoke" fashion to allow for individual manufacturing requirements of each of the cell parts while bringing them in a continuous flow to a central stacking elevator. This power section is assembled with components and subassemblies provided by suppliers to form a complete fuel cell power plant. Rigid acceptance tests are performed to specific quality control criteria on the cell stack assembly prior to its installation into the power plant and on the completed power plant prior to its delivery.

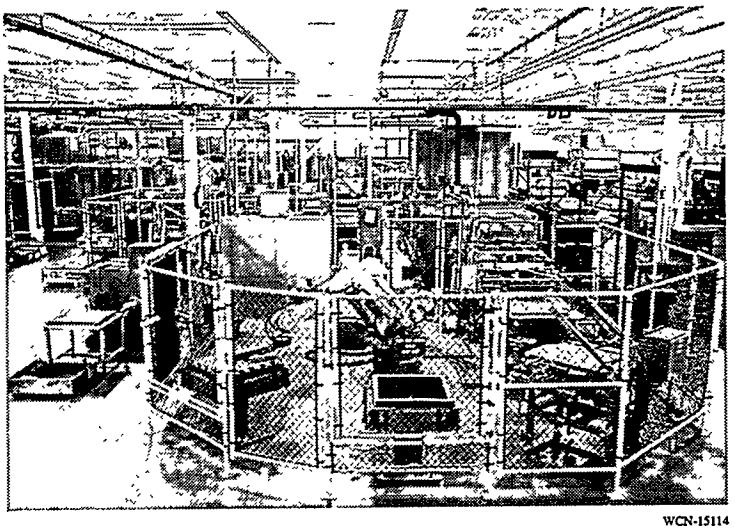

WCN-15114

Figure 3: Cell Stack Manufacturing

PC25 Product Support

A product support program was initiated even before the delivery of the first pre-production PC25 power plant to provide customers with the necessary expertise to install, operate and maintain their power plants and to provide customers with real-time technical back up. This provides ready identification and correction of any operating problems. A world-wide service network was put in place by ONSI and its international partners; Toshiba and CLC. The network provides around-the-clock response to customer needs through remote performance monitoring and diagnostics which maintains continuous surveillance of all power plant installations. There are presently over 100 power plants in the PC25 fleet located in 12 different countries around the world. The operation of each power plant, at the customer's option, is monitored on a daily basis. In addition, significant operating events automatically result in an annunciation and a data acquisition sequence at the monitoring center in South Windsor, Connecticut.

Acknowledgements

The results reported herein are based on efforts by many people at IFC, ONSI, our international partners; Toshiba and CLC, and the support personnel of many customers throughout the world.

STATUS OF MCFC STACK DEVELOPMENT AT HITACHI

S. Takashima, T. Kahara, M. Takeuchi,
Y. Amano, and T. Yoshida
Fuel Cell Development Center
Hitachi Works, Hitachi, Ltd.
1-1, saiwaicho 3-Chome, Hitachi-shi,
Ibaraki, 317, Japan

Introduction

Hitachi, Ltd. has been developing Molten Carbonate Fuel Cells in the New Sunshine project in Japan, and Hitachi is taking part in the development of a 1,000kW MCFC pilot plant at Kawagoe. Hitachi is engaged in system planning of the 1,000kW pilot plant, design and manufacturing of the reformer subsystem and the fuel cell subsystem, and design and manufacturing of the 250kW stacks for the 1,000kW plant.
The 250kW stacks are developed on the basis of the results of the 100kW stack in 1993 and the following 25kW stack in 1994.

In parallel to the stack development, Hitachi is also conducting researches for long endurance cells and stacks. In addition to the researches for anode, cathode, electrolyte, and electrolyte matrix, improvement of temperature distribution in stacks is investigated to extend the stack life.

This paper describes the planning status of the 250kW stacks for the 1,000kW MCFC plant and the developing status of stack cooling method for longer life.

Development of 250kW Stacks

Hitachi is developing 250kW stacks for the 1,000kW plant, and planning to install the two stacks at the plant in 1998. Table 1 shows the planning specification of the stack. Basic specifications such as the cell type and the electrode area are the same as the specifications of the

Table 1 Specification of the 250kW Stacks (2 sets)

No.	Item	Contents
1	Cell Type	Multiple Large Capacity Type
2	Flow Type	Cross Flow
3	Electrode Area	1.21 m^2
4	Stacked Cells	288 Cells
5	Block number	12
6	Module number	6
7	Power Output	263 kW (D.C.)

improved 25kW stack in 1994 [1]. The D.C. output of the unit stack is 263kW. The two stacks are connected in series to an inverter, and the A.C. output from the inverter is planned to be 500kW.

Fig. 1 shows the planning structure of the 250kW stack. The stack will consist of six modules and use bellows to compress the modules. Each module will be heated and checked separately at the work shop in Hitachi, and it will be transported after storage. The modules will be stacked to the full height at the testing site.

The 1,000kW plant is planned to be operated for 5,000 hours, and Hitachi is preparing additional 25kW stack test to confirm the specification and to demonstrate the performance under the equivalent operating condition to that of the plant.

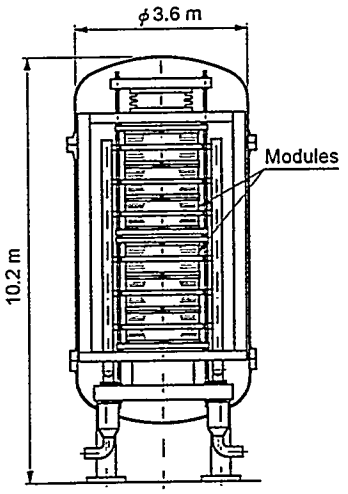

Fig. 1 250kW Stack Planning Structure

Development for long life stacks

Hitachi has adopted cross flow configuration from the view points of its structural simplicity and reliability of gas sealing between the anode and cathode gas, and Hitachi has developed Multiple Large Capacity Type to disperse hot spot which tends to yield in large stacks [2]. Since it was confirmed that the stack operating temperature and cell voltage drop rate had very close relation after the 100kW stack test, research and development to improve the stack temperature distribution are conducted. Fig. 2 shows a basic configuration of an improved flow pattern to moderate the hot spot in cell plane. The structure sets flow distribution in the cathode gas flow path, and introduce more flow at the anode gas inlet side where the current density is high in cross flow type. By this structure, the temperature distribution changes to a linear one in cross flow type, and the original hot spot vanishes.

In the actual application, as shown in Fig. 3, a suitable corrugated plate was selected and arranged to achieve an appropriate flow pattern. Fig. 4 shows test results of a stack with the flow regulated type structure. In the figure, the test results are compared to the calculated results at the same condition. The measured values are close to the calculated temperature distribution, and they show that the cathode gas temperature at anode inlet side is lower than that at the anode outlet side. This result shows that the flow pattern is effective for moderating the temperature distributions in cross flow type and a promising structure for longer life stack.

Conclusion

Hitachi, Ltd. is developing 250kW stacks and will complete the installation in 1998. Hitachi, Ltd. is also conducting research and development for long endurance MCFC stacks, and developed effective flow pattern in the field of stack cooling research.

Hitachi, Ltd. will continue to endeavor to develop large MCFC stacks and extend the MCFC stack endurance.

Acknowledgment

This work has conducted under a contract from NEDO (New Energy and Industrial Technology Development Organization) and MCFC Research Association (Technology Research Association for Molten Carbonate Fuel Cell Power Generation System). We appreciate their advice and support.

References

1. T. Kahara et al. "Status of MCFC Cell and Stack Technology at Hitachi", 1994 Fuel Cell Seminar, pp. 222-225, Nov. 1994.
2. T. Kahara et al. "Status of MCFC Cell and Stack Technology Development at Hitachi", The 2nd International Fuel Cell Conference, pp. 123-126, Feb. 1996.

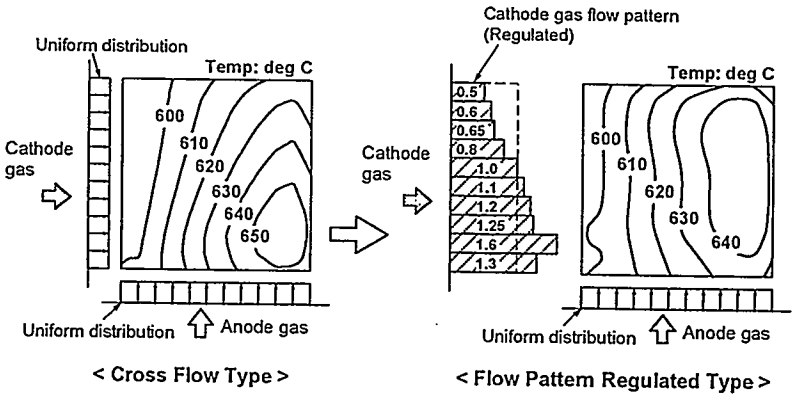

Fig. 2 Temperature distribution improvement by flow pattern regulated type structure

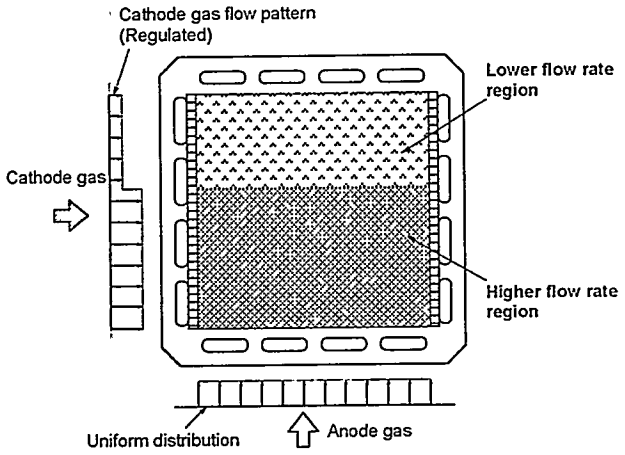

Fig. 3 Structure of cathode flow path for
flow pattern regulated type

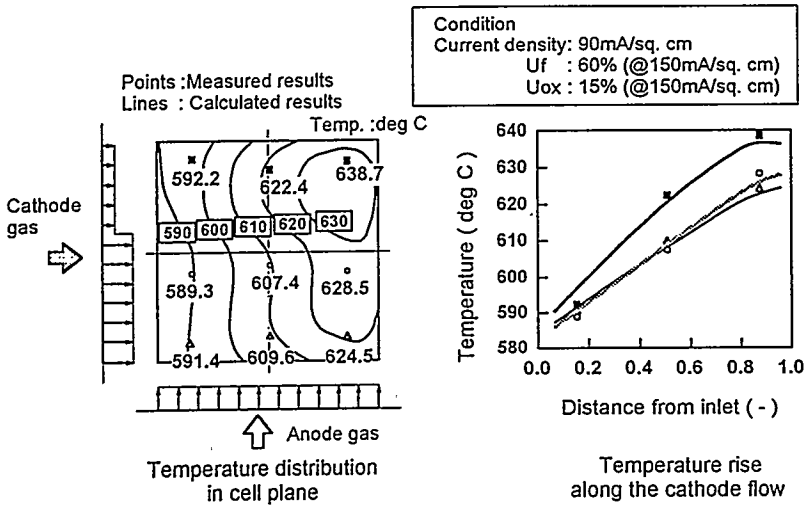

Fig. 4 Test results of the stack test
with cathode patten regulated type

BALANCE OF PLANT FOR SOFC
EXPERIENCES WITH THE PLANNING, ENGINEERING, CONSTRUCTION AND TESTING OF A 10 kW PLANAR SOFC PILOT PLANT

Kåre Kløv, Statoil Research Centre, Trondheim / Norway
and
Per Sundal, Tor Monsen and Arild Vik, Prototech AS, Bergen / Norway.

INTRODUCTION

The Statoil Solide Oxide Fuel Cell Research Program was started in January 1991. Some results from this Program were presented to the 1994 Fuel Cell Seminar in San Diego (1). The final technical milestone for the program was to design, engineer, construct and test a 10 kW pilot plant. From the very beginning, the importance of coordination and integration in the development of components, subsystems and systems, combined with basic research on cell and stack performance, were established as the guidelines for the program. In this way the progress towards the final goal was not a matter of making the best individual cell, the best stack or a superior balance of plant, but to build an efficient, reliable and operative pilot plant system, and thus make a further step towards a verification of commercial SOFC system technology.

SPECIFICATIONS

The following main specifications were given as the basis for the design of the SOFC pilot plant:

Electrical Power:	10 kW
Primary Fuel:	Natural Gas
Fuel Utilization:	80 %
Electrical Cell Potential:	0.60V/cell
Power Density:	0.25 W/cm^2
Electrical Efficiency:	40 %
Functional Lifetime:	5000 hours

The operability of the SOFC system should be verified by cycling of the plant from room temperature (25 degrees centigrade) up to 1000 degrees centigrade and back to room temperature two times. The plant should be fully operable at working temperature after each cycling, without detrimental degradatiton in electrical performance or structural integrity.

PROJECT PHILOSOPHY

The Statoil SOFC Pilot Plant is one of the very first constructions of this kind, therefore the existing basis for design, production and operations was, and still is, limited. The system design philosophy thus reflects this basic condition in such a way that every effort was made in order to reduce the uncertainty in system design, production and operation.
The project was planned to be a conventional construction project, but with associated required development and test activities. Design and construction based on proven technology was not always possible, but safe and reliable design was, if possible, chosen instead of risky new applications with potential higher performance. Optimalization of design therefore was not given priority, probably making the total construction costs higher but operational risks lower.

The system architecture also was influenced by this basic philosophy. In order to minimize electical losses, pressure drops and thermal losses as well as to achieve functional benefits, a compact centralized design was derived as the basis for detailed engineering. This concept includes major system components such as afterburner, heatexchangers and prereformer to be integrated in proper thermal zones of the fuel cell compartment. The heat from the electrochemical conversion in the fuel cell stacks are removed primarily through convection, and radiative heat flows were minimized. This thermal conceptual layout reduces thermal gradients in

stacks, as well as makes the entire construction easily adapted to later scaleup of electrical performance.

ENGINEERING AND CONSTRUCTION

The engineering activity was started when the feasibility and conceptual studies were completed. A detailed thermodynamic system analysis set the guidelines for the later design of heat exchangers, afterburner, electrical heaters and fuel cell chamber.This analysis concluded that the system would be self supplied, electrical heaters would be necessary only for the startup and close down of the pilot plant. By utilization of plate heat exchangers, a very compact design was found to be technical feasable. Mathematical modelling and simulations showed that a partial prereforming of the natural gas was beneficial, and thus a prereformer unit was designed as a part of the low temperarure heat excanger combined with a backup external prereformer.

The engineering work was performed according to experience, know how, rules and regulations given by Statoil and Norwegian authorities. Finite element analysis tools were used for detailed fluid, thermal and thermodynamic analysis of the details and the integrated system. The fuel cell stack operating temperature of 1000 degrees centigrade results in maksimum temperatures approaching 1100 degrees centigrade in the afterburner. This called for extensive studies of material properties and behaviour. The materials for the BOP were selected based on a series of dedicated tests of several alloys in both reducing and oxidizing environments.

Special attention was paid to the problem of thermoelastic deformations. Flexible joint elements were designed, tested and implemented in order to avoid destructive thermomechanical forces that would break metallic welds and destroy ceramic components. A specially designed suspension system for the heat exchangers had to be developed for the same reasons.

Sealing methods were developed, tested and implemented for metal/metal, metal/ceramic and ceramic/ceramic connections.

In order to minimize loss of produced electrical power in the stack system, a dedicated current collector system for SOFC stacks were developed and patented. The system performance is based on a combination of specially designed current collectors and pneumatic stack pressurizing elements, resulting in significant improved electrical performance with very low degradation rate.

Considering the SOFC pilot plant to be operating in a specific Statoil industrial environment, the possible risk and hazards involved in such an operation were carefully investigated throughout the engineering and construction phase. Risk analysis concluded that the SOFC pilot plant was more safe than conventional industrial petrochemical plants. Hazop studies as well confirmed the plant to be free from fatal design errors and set the standard for reliable operational prosedures. In this respect the pilot plant was given the required authorisation both by Norwegian authorities and Statoil.

The instrumentation of the plant, being the very first of its kind in Norway, was by intention made considerable more comprehensive than needed for the purpose of surveillance and process control. This was done due to the need of scientific and diagnostic data. The control and monitoring of the plant were decided to be partly manual and partly automated. The supply system is physically separated from the fuel cell compartment, while control and monitoring equipment of the plant are installed in a separate control room. This system layout was mainly determined by safety as well as operational and maintenance reasons. The control functions are handled by local controllers, operated from the control room.

The process monitoring and data aquisition are performed by dedicated computers, which will handle alarms and give warning signals to the operator. In stationary operations the plant will run unmanned at nights and manned in daytime.

TESTING

The testing procedure was divided in three phases:

Phase I: Functional test of all components according to given specifications.(Cold Test).
- Supply rates-functionality-electrical/electronical-flow control.

Phase II: System functional test without SOFC stacks. (Warm Test I).
-Thermal control -fuel management.

Phase III: System functional test including SOFC stacks.(Warm Test II).
- Start up-operation-close down- system control and monitoring.

Both test phase I and II were performed without major problems. However, the final system functional test suffered from mechanical problems related to inferior strength of the stack interconnect material. The final test was then postponed, in order to concentrate on the interconnect problem. As a result of this effort, the mechanical strength of the interconnect material has been raised by a factor of 1.7, thus resulting in mechanical properties well within the required specifications. The final system test will be restarted in late autumn this year.

The results from test phase I and II were very encouraging related to system performance. No fatal incidents occured, the control system performed well, and an emergency shut down during the first system functional test was properly handled without any damage to the plant. Nevertheless, small cracks in metallic weldings in the high temperature zone was found during the inspection of the plant after test. It has been established that these cracks were a result of the combination of inadequate welding procedures and constructional imperfections. This problem is now solved by new design and more experience in welding of these high temperature alloys.

Prior to the test, the possibility of soot and carbon formation in heat exchangers and afterburner was a concern. However, no indications of such reactions were found in later pilot test investigations, probably due to excellent behaviour of the prereformer and a system geometry which provided for the right temperature balances throughout the whole system.

COST

The relative cost between the different main elements for manufacturing and construction of the Pilot Plant is compared to the estimated target cost for a commercial plant of 1 MW. The target cost is based on industrial materials and commercial manufacturing.

Main Elements	Actual Cost	Target Cost
Stacks		
Materials	5%	25%
Production	15%	25%
BOP-system		
Materials	40%	30%
Production	40%	20%

The cost of the BOP system for the 10 kW plant is significant compared to the cost of the SOFC stacks. A commercial plant can only be realized through optimized design and construction with simple, reliable and cost efficient solutions.

CONCLUSIONS

The realization of the BOP system was performed according to the planned activities. However, the technical complexibility combined with operational requirements were to some extent more comprehensive than anticipated, causing some delay of the project milestones.
Several challenging engineering tasks related to high temperature materials, thermoelastic deformations and sealing were identified. The required effort was put on design, analysis and testing, resulting in satisfactory solutions.

The operational tolerances of stacks are basically low, leaving the instrumentation, control and monitoring of the system to be carefully designed in order to avoid fatal incidents. Risk analysis and hazop studies confirmed the safe design of the plant, and authorisation was given for contruction and operation of the pilot plant by Norwegian authorities and Statoil.

In our opinion there is no fundamental barrier prohibiting the realization of commercial SOFC plants. However, to reach this goal, elements of the present concept have to be changed or modified, and all manufacturing processes have to be industrially optimized in order to reduce cost.

Fig.1 Statoil 10 kW SOFC Pilot Plant.
View of the supply compartment.

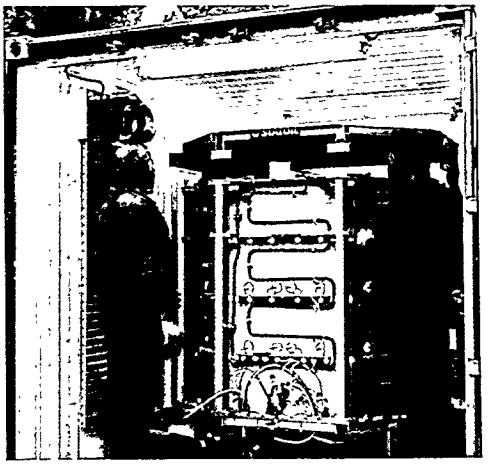

Fig.2 STATOIL 10 kW SOFC Pilot Plant.
View of the SOFC compartment.

References
1. R. Ødegård. Proceedings of the 1994 Fuel Cell Seminar, San Diego, California, 1994, p. 658.
2. F. Blaker. Proceedings of the First European Solide Oxide Fuel Cell Forum, Lucerne, Switzerland, 1994, p.49.

DEVELOPMENT OF 5 kW CLASS MOLB TYPE SOFC

M.Hattori, Y.Esaki and Y.Sakaki
Electric Power Research & Development Center
Chubu Electric Power Company, Inc. Nagoya, Japan
H.Miyamoto, Takasago Research & Development Center
F.Nanjo, T.Matsudaira and K.Takenobu
Kobe Shipyard and Machinery Works
Mitsubishi Heavy Industries, LTD., Japan

1. INTRODUCTION

Fuel cell development has been accelerated in recent years primarily due to its high efficiency and minimum environmental effect. Especially SOFC is receiving greater attention due to its excellent characteristics. Among several types of SOFC, MOLB (MOno block Layer Built) type SOFC provides following advantages for a large scale power plant;

1) Suitable for mass production, and 2) able to obtain high power density.

Chubu Electric Power Company, Inc.(CEPCO) and Mitsubishi Heavy Industries, LTD. (MHI) have jointly developed and evaluated the MOLB type SOFC on since 1990. This paper presents recent progress on it.

2. ELEMENTAL STUDY

To evaluate durability of MOLB type SOFC, a long term generation test of 75×75mm 2-cell stack has been performed in the 10W class generation test facility which has been installed in the laboratory of CEPCO. Fig. 1 shows the results. The accumulated hours of electric power generation exceeded on year. In the beginning stage, the electrical current density at the cell voltage of 0.7V was 329 mA/cm^2.

The deterioration rate was as small as 2.5% per 1000 hours, only a tenth of that established by the former stack in 1992.

3. 1 kW CLASS MODULE

In 1992, the maximum output of 1328W was recorded on 150×150mm 40-cell 3 stacks (1). Fig. 2 shows a 1 kW module of MOLB type SOFC in 1993. It consists of 4 stacks of 150×150mm 10-cells. The results of electric power generation test in 1993 are shown in Table 1. The maximum power was 1275W and the power at the cell voltage of 0.7V was 1132W. The maximum power density was 0.236 W/cm^2.

4. 5 kW CLASS MODULE

Now, we are testing the stack which consists of 200×200mm cells for the 5 kW class module. Fig. 3 is a 5 kW class generation test facility which has been installed in the laboratory of CEPCO. Fig. 4 is the first trial test stack of which expected power output is 1 kW in 1995. It consists of 200×200mm 20-cells. Table 2, Fig. 5 and Fig. 6 show the test results.

The maximum power output was 1059W and the stack electrical efficiency was 35.6% on HHV base and the power density was 0.187 W/cm^2 at the fuel utilization rate of 86.5%. The continuous operation was done in half load and 3/4 load and long term stable operation of 2,000 hours was verified.

In 1996, 2 kW class test was carried out. Fig. 7 shows the 2 kW class stack. It consists of 200×200mm 40-cells. Table 3 shows the test results. The maximum power output was 2418W by the hydrogen as a fuel. And by the reforming gas from a city gas, the power output of 2015W was obtained.

5. CONCLUSIONS

We improved the 1 kW class module by 150×150mm cell and then 200×200mm cell has been developed for 5 kW class module. In 1993, the power output of 1 kW class was generated by 150×150mm 10-cell 4 stacks. And in 1995, the power output of 1 kW class was generated by 200×200mm 20-cell stack and in 1996, the power output of 2.4 kW by 200×200mm 40-cells. The next milestone is 5 kW class test by 2 stacks of 200×200mm 40-cells.

6. REFERENCE

1. Kato et al "1 kW Generation Test of MOLB type SOFC", Proceedings of the 3rd int. Symp. on SOFC, Hawaii (1993), P.809.

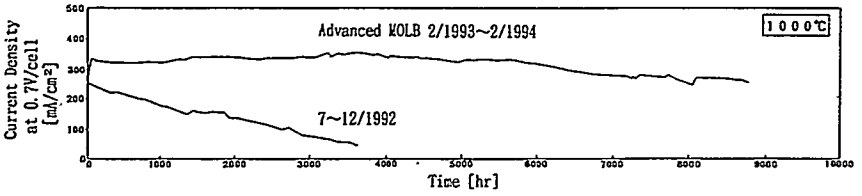

Fig. 1 Results of 75×75mm 2-cell MOLB type stack Continuous Electric Power Generation Test

Table. 1 Results of MOLB type SOFC 1kW Class Module Electric Power Generation Test (150×150mm 10-cell 4 stacks)

Flow Rate	H_2 [Nl/min]		60				
	Air [Nl/min]		150				
Electric Power Generation Performance	Stack No.		A	B	C	D	Total
	$P_{0.7V}$	W	266	259	323	284	1,132
		W/cm^2	0.171	0.166	0.207	0.182	0.181
	$I_{0.7V}$	mA/cm^2	244	273	296	260	259
	Pmax	W	279	294	368	334	1,275
		W/cm^2	0.179	0.188	0.236	0.214	0.204

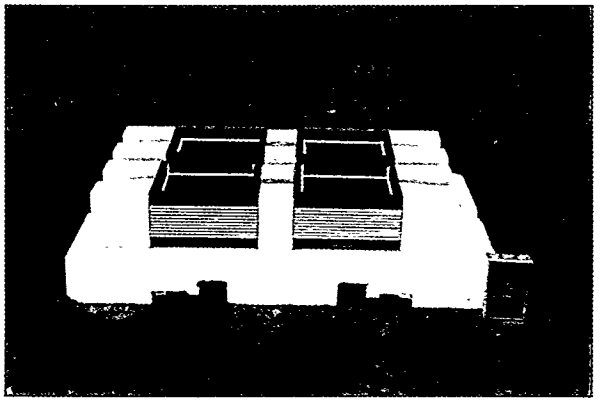

Fig. 2 MOLB type SOFC 1kW Class Module in 1993
(150×150mm 10-cell 4 stacks)

Fig. 3 MOLB type SOFC 5kW Class Module Test Facility

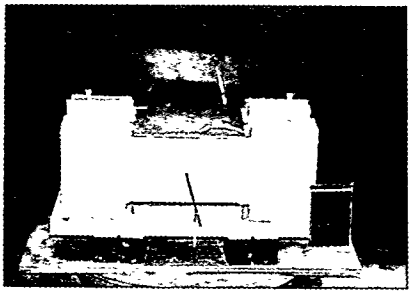

Fig. 4 MOLB type SOFC 1kW Class Stack in 1995
(200×200mm 20-cells)

Table. 2 Results of MOLB type SOFC 1 kW Class Stack Electric Power Generation Test in 1995
(200×200mm 20-cells)

OPERATION MODE	Power [W]	Efficiency [%]	Power density [W/cm^2]	U_F [%]	H_2 [Nℓ/min]
High Efficiency & High Power (27/4/'95)	997	33.5	0.176	86.3	14
(5/7/'95)	1059	35.6	0.187	86.5	14
High Efficiency & Continuous (28/4/'95) ～ (4/7/'95)	460	36.0	0.081	71.0	6
(5/7/'95) ～ (18/7/'95)	496	38.9	0.088	71.6	6
	844	33.1	0.149	70.4	12
	863	33.8	0.153	70.4	12

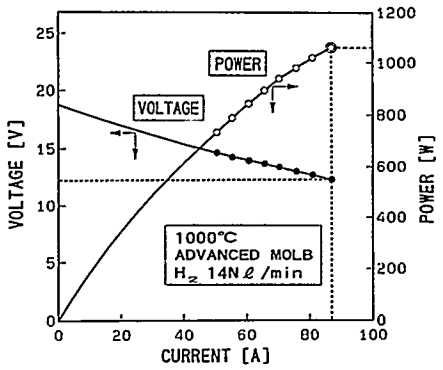

Fig. 5 Results of MOLB type SOFC 1kW Class Stack Electric Power Generation Test in 1995 (200×200mm 20-cells)

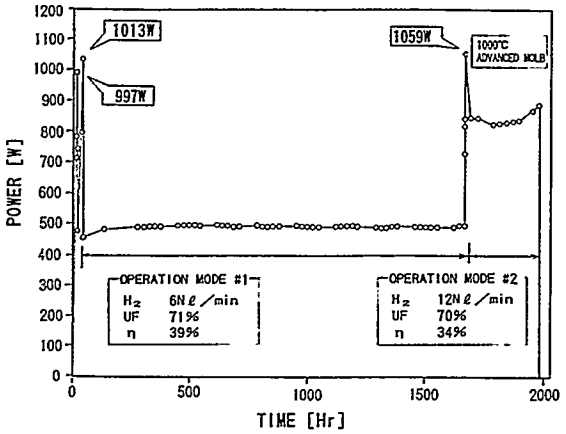

Fig. 6 Results of MOLB type SOFC 1kW Class Stack Electric Power Generation Test in 1995 (200×200mm 20-cells)

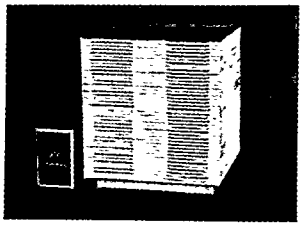

Fig. 7 MOLB type SOFC 2 kW Class Stack in 1996 (200×200mm 40-cells)

Table 3 Results of MOLB type SOFC 2 kW Class Stack Electric Power Generation Test in 1996 (200×200mm 40-cells)

OPERATION MODE	Power [W]	Efficiency [%]	Power density [W/cm²]	U_F [%]	H_2 [Nℓ/min]
High Power by H_2 (3/4/'96)	2418	27.2	0.214	80.8	41.7
Continuous by Reforming Gas (3～5/4/'96)	2015	29.0	0.178	68.8	32.7

LOW COST ELECTRODE DEVELOPMENT AND PERFORMANCE IN BALLARD ADVANCED STACK HARDWARE

G.A.Hards, T.R.Ralph
Johnson Matthey Technology Centre,
Blounts Court, Sonning Common,
Reading, U.K.

D.P.Wilkinson, S.A.Campbell
Ballard Power Systems,
Burnaby, B.C.
Canada.

Introduction

Cost reduction is a critical requirement for the widespread commercial application of proton exchange membrane fuel cell (PEMFC) technology. Significant stack cost savings are available through materials cost reductions and the development of low cost, high volume, manufacturing processes. This paper summarises progress made by Ballard Power Systems and Johnson Matthey in the development of lower cost stack component technology. Single cell performance in Ballard Mark V hardware, of membrane electrode assemblies (MEAs) employing volume manufactured electrodes with catalyst loadings below 1.0 $mgPtcm^{-2}$, are comparable to current stack MEAs comprising unsupported platinum based catalysts with loadings of 8.0 $mgPtcm^{-2}$. In the advanced stack hardware, under development for motive and utility applications, the low cost MEAs exhibit high performance and minimal voltage decays after over 3,000 hours of stack operation. Cell to cell reproducibility is excellent, highlighting the high consistency of product available from the manufacturing processes. The MEAs represent a significant progress in the commercialisation of PEMFC systems. Incorporation of the technology in commercial prototype stacks is underway.

MEA Fabrication

A high volume electrode manufacturing process has been developed based on printing technology. The process was selected based on its ability to meet several key criteria, including low capital investment, scaleability with increasing demand, low unit cost, flexibility to accommodate a wide range of formulations and structures, high yield and high product reproducibility. A pilot plant facility established at Johnson Matthey has the capability of meeting demand over the coming years as the PEMFC enters commercial production. The low precious metal loading electrodes comprise Pt/Ru catalyst based anodes (50:50 atomic ratio Pt:Ru), and pure Pt catalyst based cathodes, supported on Cabot Vulcan XC72R carbon black. To maximise the catalyst surface area available for reaction in the printed electrodes a soluble form of the proton conducting electrolyte is incorporated into the active catalyst region in a fashion that allows for mass production. Anode catalyst loadings from 0.1 - 0.4 $mgPtcm^{-2}$ and cathodes from 0.2 - 0.7 $mgPtcm^{-2}$ have been routinely manufactured.

Beginning of Life Performance

Figure 1 compares the performance of a low catalyst loading MEA (0.6 $mgPtcm^{-2}$) and a higher loading unsupported platinum black MEA (8.0 $mgPtcm^{-2}$). The beginning of life (BOL) data is from a standard Ballard Mark V single cell of 240.2 cm^2 active area, operating at 80°C on hydrogen/air at 30/30 psig and 1.5/2.0 stoichiometry. The membrane electrolyte was the Dow XUS-13204.10 experimental material. The BOL performance of the lower cost MEA is equivalent to the higher catalyst loading MEA employed in current demonstration Mark V stacks. There are no issues associated with the combination of carbon supported catalyst based anodes and cathodes in this cell hardware. At a cell voltage of 0.65 V, the low loading MEA generates 0.8 Acm^{-2}. This translates to a much reduced

platinum requirement of ca. 1.2 $gPtkW^{-1}$, which is compatible with the cost targets for PEMFC applications in both stationary power generation and heavy duty transportation such as transit buses.

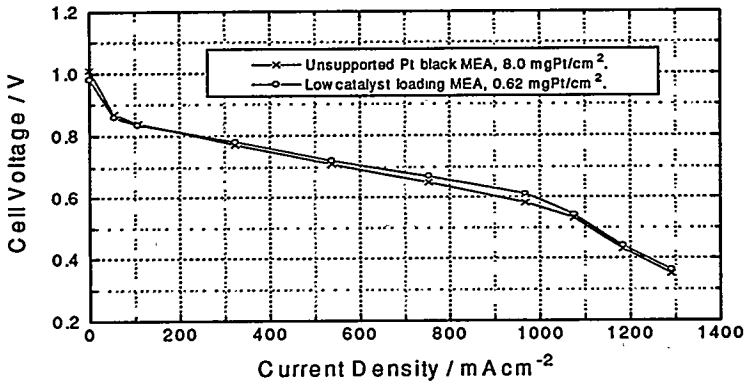

Figure 1: Ballard Mark V single cell performance of high catalyst loading (8.0 $mgPtcm^{-2}$) and low catalyst loading (0.62 $mgPtcm^{-2}$) MEAs.

These extremely encouraging results represent a successful demonstration of low catalyst loading MEA performance in large scale, practical PEMFC hardware functioning at practical operating conditions.

Durability in Advanced Stack Hardware

The durability of the low cost MEA technology has been evaluated in the range of latest generation Ballard stack technologies, currently under development for application in utility, submarine, bus and automotive applications. Excellent durability has been demonstrated on hydrogen fuel in sub-stack units of 4 to 8 cells and full sized stacks. For example, Figure 2 shows the performance of MEAs with the Dow membrane and anode and cathode catalyst loadings of 0.25 and 0.50 $mgPtcm^{-2}$ respectively, in a 4-cell stack representative of the second generation bus stacks. After operation for 1,000 hours at 0.65 Acm^{-2}, with approximately 5 hour excursions to 1.1 Acm^{-2}, the degradation rate of less than 4 μVhr^{-1} successfully meets the durability performance goal.

For stationary power plant and light duty vehicle applications it is likely that the anode fuel will be impure hydrogen (reformate) rather than pure hydrogen, produced via the reforming of hydrocarbon fuels such as natural gas or methanol. Demonstration of satisfactory performance and durability in this environment is much more demanding due principally to anode poisoning by trace levels of carbon monoxide, although carbon dioxide poisoning and dilution effects will also reduce performance levels. Figure 3 shows the long term performance of each cell in a 4-cell sub-stack, operating under stationary power plant testing conditions. The cells contain Du Pont Nafion® 117 membrane and are operating with air as oxidant and simulated reformate as fuel (70% hydrogen, 25% carbon dioxide and smaller quantities of contaminants including 10 ppm carbon monoxide). The MEAs comprise low catalyst loading electrodes with a total cell loading of 0.8 $mgPtcm^{-2}$. The stack was run for 3,000 hours at 0.54 Acm^{-2} on reformate fuel with intermittent control checks on pure hydrogen fuel to provide comparative decay rate data.

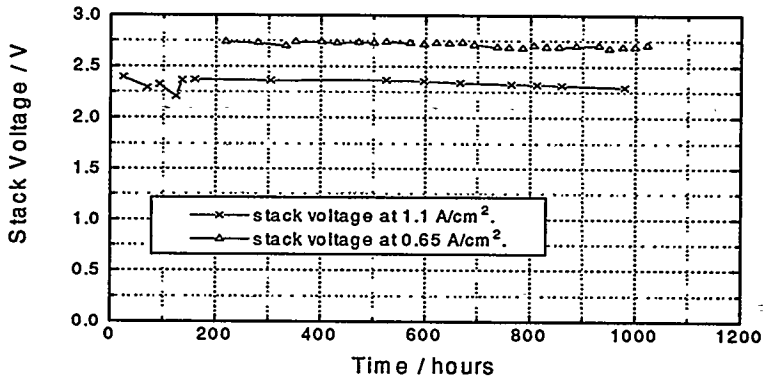

Figure 2: Sub-stack durability of low catalyst loading MEAs (0.75 mgPtcm^{-2}) operating on H_2/air under transit bus application conditions.

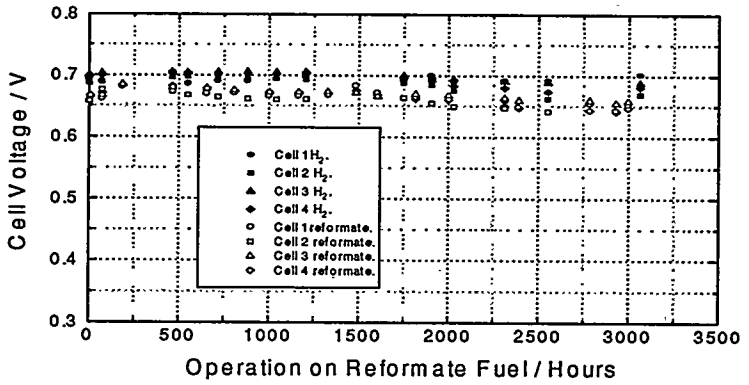

Figure 3: Durability of 4-cell sub-stack operating on simulated reformate/air under stationary power plant conditions - MEA loading 0.80 mgPtcm^{-2}.

The initial performance on reformate fuel is lower than with pure hydrogen but is close to the 30 mV expected for operation on hydrogen fuel diluted to 70% with inert components. The poisoning effects of carbon monoxide and carbon dioxide have been eliminated by the combined use of the more poison tolerant Pt/Ru anode catalyst, and a low level 2% air bleed passed directly into the anode chamber. After 3,000 hours of continuous operation on reformate fuel there was little degradation in the performance of the cells, with an acceptable decay rate of 4μVhr^{-1}measured for both reformate and pure hydrogen operation.

Cell Reproducibility

In addition to the high performance and durability the low catalyst loading MEAs also exhibit excellent cell to cell reproducibility. This has been retained on scale up from sub-stacks to full stack builds. Figure 4 shows the consistent cell voltages produced by the individual cells in an 80 cell stack built for the air independant propulsion (AIP) application. The MEAs comprise cathodes with 0.6 mgPtcm^{-2}, anodes with 0.25 mgPt cm^{-2} and Nafion® 117 membrane. The minimal variation in cell performance over a range of current densities on hydrogen/air operation is clearly evident. This highlights the high degree of consistency achieved in the MEA produced from the high volume manufacturing process and the efficient control of operating conditions throughout the stack.

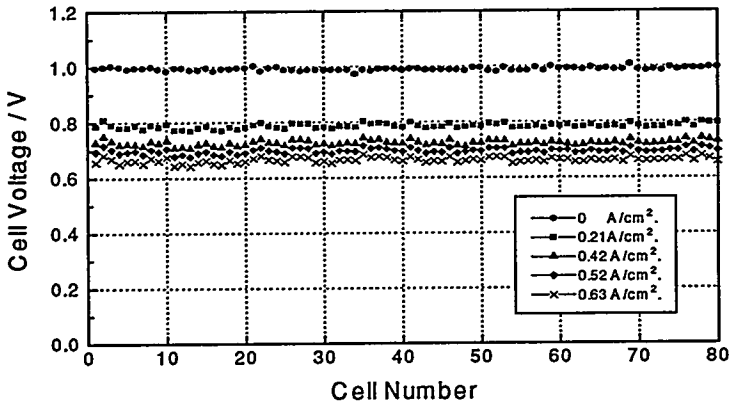

Figure 4: Performance of 80 cells in AIP stack build - MEA loading 0.85 mgPtcm^{-2}.

Conclusions

These results confirm that the low cost, high volume manufacturing process developed for low catalyst loading MEAs is providing good performance, high durability and excellent reproducibility under a wide range of practical operating conditions representative of the applications being targeted by the PEMFC. Additional cost reductions are anticipated through progressive reductions in the electrode catalyst loadings and performance enhancement through improved MEA and cell design.

Acknowledgement

The Johnson Matthey work on low catalyst loading MEA development has been supported by the UK Energy Technology Support Unit for the Department of Trade and Industry.

Development of Fuel Processors for Transportation and Stationary Fuel Cell Systems

William L. Mitchell, Jeffrey M. Bentley, and Johannes H.J. Thijssen
Arthur D. Little, Inc.
Acorn Park, Cambridge, MA, USA 02140

Five years of development effort at Arthur D. Little have resulted in a family of low-cost, small-scale fuel processor designs which have been optimized for multiple fuels, applications, and fuel cell technologies. The development activities discussed in this paper involve Arthur D. Little's proprietary catalytic partial oxidation fuel processor technology. This technology is inherently compact and fuel-flexible, and has been shown to have system efficiencies comparable to steam reformers when integrated properly with a wide range of fuel cell types.

Experimental Setup

The fuel processor hardware used in all of the experiments is shown in Figure 1. The fuel processor system includes a partial oxidation (POX) zone and a catalyst clean-up bed, high temperature shift (HTS) and low temperature shift (LTS) reactors, and an integrated air preheater and steam generator. As shown in the process flow diagram in Figure 2, the construction of the fuel processor is highly integrated with respect to fluid flow and heat transfer. When designed for operation with sulfur bearing fuels such as gasoline, JP-8, or natural gas, the fuel processor system also includes a compact de-sulfurization bed integrated inside the reactor vessel prior to the LTS.

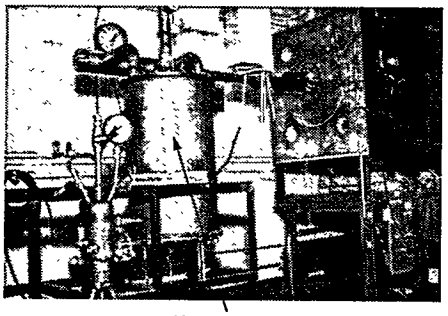

50 kWe Fuel Processor

Figure 1. Prototype Reformer

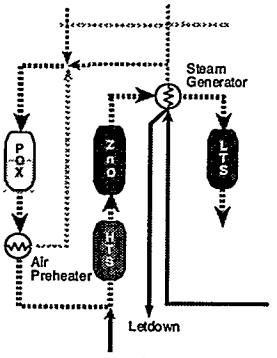

Figure 2. Flow Diagram

The POX zone consists of a pure gas-phase reaction zone which reacts the primary fuel with air and steam or water to form hydrogen, carbon monoxide, residual methane, water vapor, carbon dioxide, and nitrogen. This gas-phase front end effectively decouples the fuel structure from the remainder of the fuel processor, allowing multi-fuel operation. The POX reactor consists of fuel and air injectors arranged so as to rapidly mix the fuel and air and direct the mixture towards the entrance of the reactor. The reacting flow is then injected, forming a cyclonic vortex which promotes rapid and extensive product recirculation and entrainment of product into the incoming fuel/air mixture. The catalyst clean-up section downstream of the POX reactor uses a steam reforming catalyst in order to convert the residual methane from the POX effluent to additional carbon monoxide and hydrogen. Finally, the HTS and LTS reactors promote the

water-gas shift reaction which reacts water and carbon monoxide to form hydrogen and carbon dioxide.

Ethanol Fuel Processor Results

The ethanol fuel processor , sponsored by DOE and the State of Illinois, was designed to provide a hydrogen rich gas stream to support a 50 kWe fuel cell with an overall system efficiency of 43% at full power which translates into a thermal input capacity of approximately 120 kWth. Operating pressure of the reformer varied between 1 and 3 atm. Performance of the reformer was measured by determining the conversion efficiency and carbon monoxide outlet concentrations for various reformer equivalence ratios and steam to carbon ratios. Equivalence ratio (ϕ)is defined as the actual fuel/air ratio divided by the stoichiometric fuel/air ratio. Figure 3 shows a graph of conversion efficiency versus equivalence ratio. From the plot, it is apparent that non-catalytic POX operation yields low conversion efficiencies with carbon free operation to $\phi = 4.3$. Catalytic POX operation , also shown in Figure 3, exhibits conversion efficiencies approaching equilibrium values at $\phi < 3.0$ with somewhat less than equilibrium conversion as ϕ increases. This decreasing conversion with increasing ϕ is due to increased methane slip from the catalyst clean-up bed. Depending on the catalyst clean-up bed operating temperature, methane slip out of the bed can vary dramatically as shown in Figure 4. This variance is due in part to a very aggressively scaled catalyst bed. By carefully managing the bed operating temperature and/or decreasing the bed space velocity slightly, low methane slip has been achieved. Figure 5 shows the performance of the entire fuel processing system including the shift catalysts. When operating at proper conditions, carbon monoxide concentrations on the order of .4% on a wet basis are achievable at the outlet of the reformer.

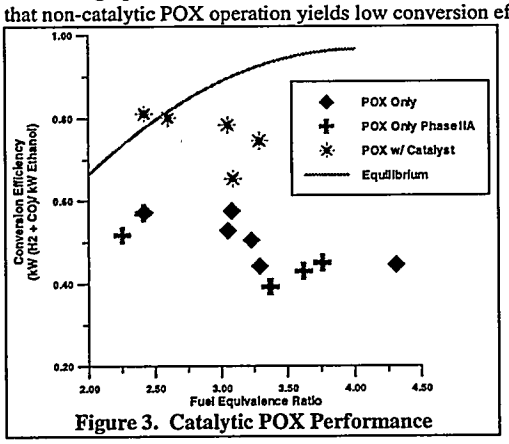

Figure 3. Catalytic POX Performance

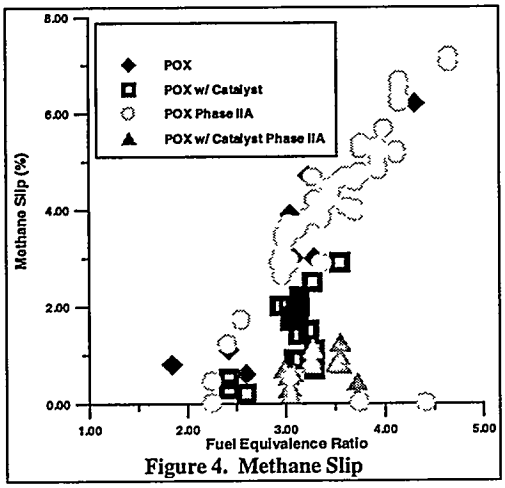

Figure 4. Methane Slip

Gasoline Fuel Processor Development

As a first step in the refinement of the ethanol fuel processor for gasoline use, a series of transient tests were performed at constant ϕ to determine the impact of transients on POX and catalyst performance. Figure 6 describes the transient response of the fuel processor during a 2:1 step turndown in thermal input, followed by a 1:2 step turn-up. During the power changes, ϕ and steam to carbon ratio were fixed at 3.5 and 2.0 respectively. The plot shows that due to the thermal stability of the shift catalyst beds, only the POX and

catalyst cleanup beds show any appreciable change in temperature. Due to the fact that the shift beds remain at constant temperature, one would expect the carbon monoxide levels exiting the reformer to remain constant throughout the transient. Figure 7 shows that for a 2 second step increase in thermal input from 31 to 62 kWth, CO concentration remains largely unaffected.

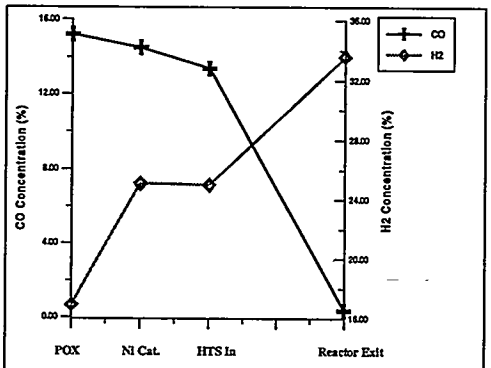

Figure 5. Concentration vs. Bed Location

The next step in evolution of the gasoline fuel processor was the development of an autonomous control system. The control system was developed by first constructing a fully dynamic model of the fuel processor including kinetic effects in the catalyst beds. Once the model was developed, simple single-loop controllers were designed and tested against the model. Output from the control system tests show that during a 1:4 step turn-up in reformer power, gas temperatures through the shift beds are expected to increase 120 °C with a corresponding increase in CO concentration at the reactor exit increase from .4 to 1.2%. However, the experimental results show that the gas phase temperature is less important than the catalyst bed temperature in determining CO conversion. Finally, the control system modeling shows that the reformer responds at a slew rate in excess of 100 kW/sec. The actual control system software is now complete and is being integrated on the testbed in conjunction with low cost automotive flow controllers and will be tested in the upcoming months.

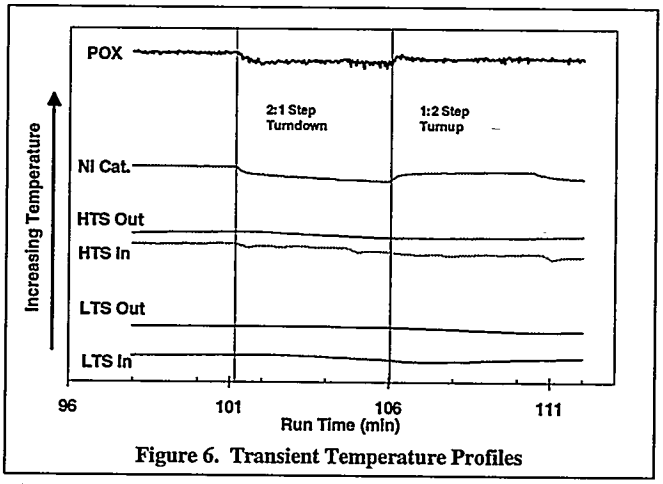

Figure 6. Transient Temperature Profiles

JP-8 Fuel Processor

A fuel processor capable of delivering sulfur-free reformate to a solid oxide fuel cell (SOFC) was developed and delivered to a client where it has undergone over 1200 hours of successful testing. During the development of the POX only fuel processor, the client dictated that the only acceptable fuel gases to the SOFC were hydrogen, carbon monoxide, and small amounts of methane. Hydrocarbons higher than methane are prone to form carbon inside the SOFC and therefore, were to be avoided. Figure 8 shows that conversions of 65 to 72 % were possible for $2.0 < \phi < 3.6$ with less than 1% of the fuel converted to carbon. An active carbon removal system and a gas-phase desulfurization system were developed to deliver particulate free, sulfur

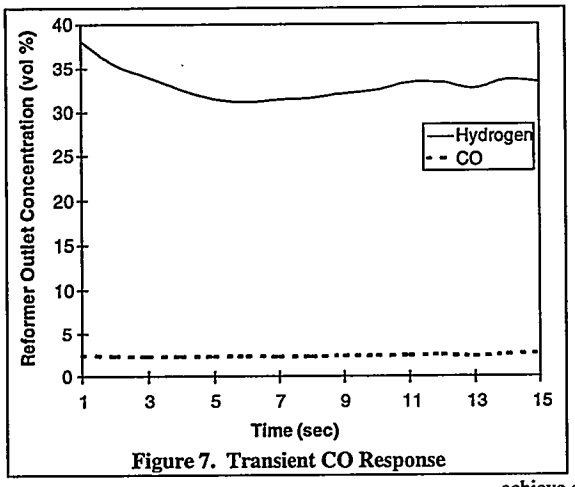

Figure 7. Transient CO Response

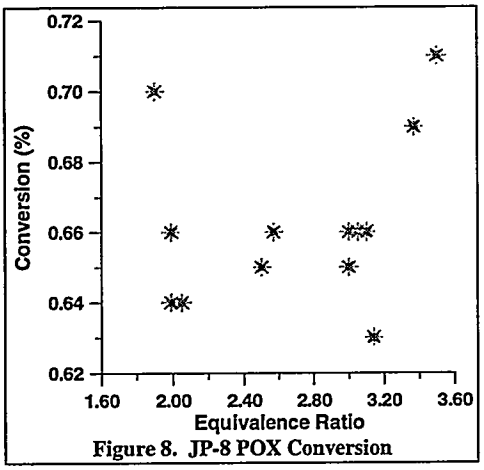

Figure 8. JP-8 POX Conversion

free reformate to the fuel cell. Under different operating parameters, the same fuel processor operated up to a ϕ of 3.8 without carbon formation. During operation at this condition, there were some C-2 hydrocarbons in the reformate stream.

CO Clean-up Technologies

Proton Exchange Membrane (PEM) anode catalysts are poisoned by carbon monoxide. The LTS converter in the ADL multi-fuel reformer is designed to achieve equilibrium concentrations of CO according to the equilibrium constant of the water-gas shift reaction. In practice, the CO concentration is reduced by the LTS to a range between 0.5 to 1.0% depending on the steam to carbon ratio and the bed operating temperature. However, depending on the PEM fuel cell anode catalyst composition and loading, significant performance degradation can occur at CO concentrations on the order of 10 to 100 ppm. Therefore, some sort of CO polishing device is needed between the fuel processor and the fuel cell. In support of the gasoline reformer program, ADL is working with Los Alamos National Lab (LANL) in order to integrate a LANL preferential oxidizer (PROX) into the reformer system. Along with this effort, ADL is also working with Johnson Matthey to integrate their proprietary PROX technology with the gasoline reformer. Finally, ADL is currently testing a proprietary PROX catalyst which features enhanced selectivity over normal platinum based PROX catalysts. This catalyst was tested in a temperature range between 150-270 °C with simulated reformate and has shown CO oxidation rates comparable to conventional PROX catalysts with significantly enhanced selectivity. As another approach to CO clean-up, ADL is also investigating the use of membrane technology to supply pure hydrogen to the fuel cell.

Conclusions

Five years of development effort at Arthur D. Little have resulted in a family of low-cost, small-scale fuel processor designs which have been optimized for multiple fuels, applications, and fuel cell technologies. When properly integrated, system efficiencies of 43% at rated power can be achieved as shown in Table 1, which are similar to reported system efficiencies using methanol steam reformers. Other achievements to date include:

- 2500 + hours of operating experience at 50 kWe on ethanol, gasoline, JP-8, methanol, and natural gas
- Demonstrated performance of .7 kw/l and .6 kW/kg compares favorably with PNGV targets.
- Simple, automotive-type control system developed.
- Difficult issues resolved with functioning hardware including:
  - Vaporization of aromatics
  - Catalyst thermal control
  - Sulfur Control
- Promising paths for CO control including:
  - Proprietary PROX catalyst with enhanced selectivity
  - Membrane technology

Table 1. System Performance -E95

Stack Efficiency (HHV) (1)	43.4%
Fuel Processor Efficiency (HHV) (2)	90.1%
Auxiliaries	
• Pumps & Compressors (kW)	-4.07
• Expander (kW)	4.4
E95 Fuel Input (kWth LHV)	54.9
Gross DC Power (kW)	23.7
Net Power (kW)	23.9
LHV Gross System Efficiency	43.0%
LHV Net System Efficiency	43.3%

(1) Fuel cell power out/total hydrogen to
(2) Total hydrogen to anode/total ethanol input to system.

Acknowledgements
This work has been funded in part by several different organizations including the Department of Energy, Office of Transportation Technologies, The Advanced Research Projects Agency, the Illinois Department of Commerce and Community Affairs, and the Illinois Corn Growers Association. Industry support for the development of the gasoline fuel processor has been provided by the Chrysler Corporation.

THREE FUEL CELL BUSES: DID THE PROMISE LIVE UP TO REALITY?

Donna Lee
U.S. Department of Energy
1000 Independence Avenue, SW
Washington, DC 20585

Introduction

A program, sponsored by the U.S. Department of Energy (DOE), the U.S. Department of Transportation's Federal Transit Administration (DOT/FTA), and South Coast Air Quality Management District (SCAQMD) has resulted in the delivery of three 30-foot, methanol-fueled, phosphoric acid fuel cell (PAFC)/battery-powered buses. Since 1987, the design and fabrication of these first-of-a-kind vehicles proceeded along a complex and difficult pathway. Issues remain on whether the actual performances of the buses lived up to the expectations, how the buses will be utilized, and how commercialization efforts will continue.

FUEL CELL BUS: 30-feet long, 25,000-pounds, 25-passenger capacity, air conditioning, wheelchair lift, 150-mile range, 0-to-40mph in 36 seconds (compared to the required 46 seconds), 62 mph maximum speed. The first bus has logged 2,300 miles and meets all transit bus requirements.

Program Overview

The objective of this program is to show the feasibility of a methanol-fueled PAFC/battery propulsion system for a small urban transit bus application and to advance the fuel cell and control technologies in an integrated fashion with available power train technology so as to provide an alternative for diesel-powered buses. The bus was selected as an entry point for application of fuel cells in

transportation because operation in urban areas will accentuate environmental benefits; the transit route structure is relatively fixed and permits evaluation under controlled conditions; the transit industry has an infrastructure in place to support operation and evaluation of the fuel cell bus; the long service life of transit buses allows amortization of higher acquisition cost over a reasonable time period; and the bus size could accommodate the first generation fuel cell designs. The overall program is divided into four phases:

Phase I: Proof-of-Concept (Design and Fabrication of Brassboard System)
Phase II: Demonstration (Design and Fabrication of Three Test Bed Buses)
Phase III: Test & Evaluation (In-Service Evaluation)
Phase IV: Commercialization (40-foot Bus Program)

Phase I, which began in 1987, was a system design and integration effort directed at demonstrating proof-of-feasibility of the fuel cell/battery propulsion system. Both air-cooled and liquid-cooled PAFC systems were evaluated in two separate cost-shared industrial contracts, one with a team led by Energy Research Corporation, and the other with a team led by Booz-Allen & Hamilton. Based on the results of the Phase I effort, it can be concluded that a fuel cell/battery powered urban bus is technically feasible and practical. The life cycle costs of the fuel cell bus can be economically competitive with the diesel and offers the additional benefits of improved acceleration, lower noise and very low emissions.

Phase II, which began in 1991, involved the design and construction of three 30-foot buses based on the liquid-cooled design from Phase I and the engineering assessment of a commercial 40-foot bus concept. The contractor team was led by H Power Corporation (system integration, fabrication, initial testing) with subcontracts with Fuji Electric Corporation, Ltd. (fuel cell system hardware), Bus Manufacturing Inc. (fabrication of bus structure), Soleq Corporation and Saminco Corporation (power electronics), Transportation Manufacturing Corporation (40-foot bus design concept and 30-foot bus design assistance), and Booz-Allen & Hamilton, Inc. (bus system analyses & integration assistance). The project management team consisted of representatives from DOE, Argonne National Laboratory, and Georgetown University. The first test bed bus was successfully completed and demonstrated in April 1994. The remaining two buses were completed in 1995.

Phase III, which began in 1995, involves in-service performance testing of the third bus at Georgetown University. Operational data such as required maintenance, fuel consumption, emissions and energy efficiency will be collected, analyzed and documented. Testing has been delayed while numerous system integration and design problems are corrected. The first bus is currently at Argonne National Laboratory in Chicago and the second bus is at Energy Technology Engineering Center in California.

Phase IV, which began in 1994, will result in one pre-production prototype 40-foot PAFC bus and one developmental 40-foot proton-exchange-membrane (PEM) fuel cell bus, both running on reformed methanol. The development team includes Booz-Allen & Hamilton, Kaman, NovaBUS, International Fuel Cells, and Ballard. This phase is managed by Georgetown University, funded solely by DOT/FTA, and scheduled to end in 1998.

Summary of Phase II Test Results

Fuel Economy

The fuel economy, as determined during acceptance testing of the first test bed bus, was 2.06 miles per gallon (mpg) of methanol, which is equivalent to 4.7 mpg of diesel (lower heating value basis). A standard diesel bus averages about 3.5 mpg.

Fuel Cell Efficiency Compared to Diesel Engine

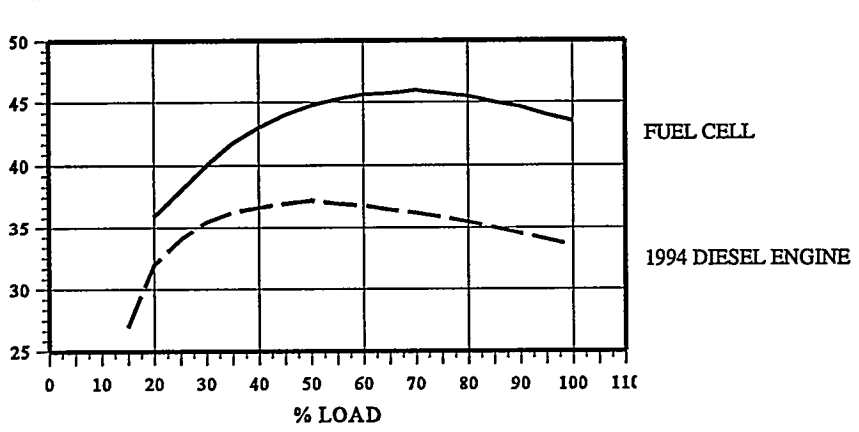

Fuel Cell Emissions Compared toVarious Bus Engines

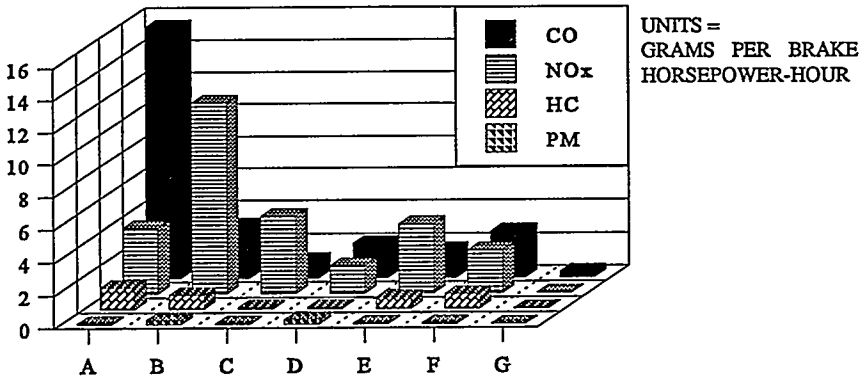

A = 1998 Urban Bus Federal Emission Standards
B = 1977 Detroit Diesel 6V71N MUI Bus Engine
C = 1995 Detroit Diesel Series 50 Bus Engine
D = Methanol M100 Bus Engine
E = Ethanol E95 Bus Engine
F = Compressed Natural Gas Bus Engine
G = Fuel Cell Bus Powerplant

Environmental, Safety & Health Issues

A report on the environmental, health and safety issues that may affect commercialization of the PAFC buses states that the in-use environmental impacts are insignificant compared to the diesel bus. Only minor amounts of air pollutants are produced during the steam-formation of methanol. The high noise level caused by vehicular traffic contributes considerably to urban stress and based on the initial test results, the fuel cell bus is projected to be much quieter than a diesel bus. In terms of the health and safety of bus maintenance personnel or passengers, the report concludes that the bus is as safe as a typical diesel bus. The intrinsic hazards include phosphoric acid, mineral oil, hydrogen gas, methanol, cadmium, nickel, high-power batteries and high-temperature exhaust from the reformer. The risks from these constituents were minimized in the design features which include hydrogen sensors, a fireproof wall between the passenger compartment and fuel cell compartment, an automatic fire-suppression system, and fuel cell and battery compartment ventilation fans.

Future Plans for the Test Bed Buses

The current plan for the first test bed bus is to leverage current DOE efforts in PEM fuel cell research and ethanol reformer development by replacing the current system with an ethanol-fueled PEM system and operating the bus in a region of the U.S. where ethanol is readily available. SCAQMD is still in the process of formulating a demonstration plan for the second bus. DOT/FTA plans on maintaining the third bus at Georgetown University to take advantage of the existing fueling set up, low overhead, and experience base. The experience gained at Georgetown will be applied to the 40-foot bus commercialization program.

Conclusion

The fuel cell bus has met or exceeded expectations with lower emissions (100 times lower than 1998 Federal standards), higher engine efficiency (25% better than diesel), higher fuel economy (25% better than diesel), lower noise (two times quieter than diesel), and equivalent operating performance (same as current diesel buses). The higher weight and higher capital cost projections are issues that need to be addressed in the commercialization phase where components will be optimized for weight, performance, and manufacturing cost reduction. Overall, this program is a success -- fuel cell technology in an urban transit application was demonstrated and validated with very good results. Completion of the test and evaluation of the 30-foot buses will be invaluable in avoiding past mistakes. A great deal of hands-on systems experience has been gained about this complex, integrated electric vehicle. With such a strong basis to build upon, the development of the next generation fuel cell bus looks very promising.

References

"Research and Development of A Phosphoric Acid Fuel Cell/Battery Power Source Integrated in A Test-Bed Bus," Final Report written by H Power Corporation for DOE Contract No. DE-AC02-91CH10447, May 30, 1996.

"Environmental, Health, and Safety Issues of Fuel Cells in Transportation, Volume 1: Phosphoric Acid Fuel-Cell Buses," Report written by Shan Ring of the National Renewable Energy Laboratory, December 1994.

FUEL CELL TRANSIT BUS DEVELOPMENT & COMMERCIALIZATION PROGRAMS AT GEORGETOWN UNIVERITY

R. Wimmer, J. Larkins and S. Romano
Georgetown University
37th & O Street
Washington, D.C. 20057

Fourteen years ago, Georgetown University (GU) perceived the need for a clean, efficient power systems for transportation that could operate on non-petroleum based fuels. The transit bus application was selected to begin system development. GU recognized the range and recharge constraints of a pure battery powered transit bus. A Fuel Cell power system would circumvent these limitations and, with an on board reformer, accommodate liquid fuel for rapid refueling.

Feasibility studies for Fuel Cell power systems for transit buses were conducted with the Los Alamos National Laboratory in 1983. Successful results of this investigation resulted in the DOT/DOE Fuel Cell transit bus development program. The first task was to prove that small Fuel Cell power plants were possible. This was achieved with the Phase I development of two 25 kW Phosphoric Acid Fuel Cell (PAFC) brassboard systems. A liquid cooled version was selected for the Phase II activity in which three 30-foot Fuel Cell powered Test Bed Buses (TBBs) were fabricated. The first of these TBBs was delivered in the spring of 1994. All three of these development vehicles are now in Phase III of the program to conduct testing and evaluation.

GU is conducting a thorough operational testing program on the Fuel Cell buses. This includes dynamic emission testing at West Virginia University, instrumented route operation in the Washington, DC area, and fuel efficiency monitoring. The results of this testing is being documented and is aiding the design decisions on the 40-foot bus commercialization project.

To date, every major question about Fuel Cell powered buses has been addressed in a methodical and thorough manner within these activities. The Los Alamos study verified that the concept was feasible; the 25-kW brassboard units showed that the technology could be engineered to the size required for transit buses, and the three TBBs proved that Fuel Cells could indeed power these vehicles. The remaining issue is whether Fuel Cell powered transit buses can be commercialized.

The Federal Transit Administration (FTA) awarded a Grant to GU in October of 1993 to commercialize a Fuel Cell powered transit bus. To achieve commercialization of the technology in the near term, the mature International Fuel Cells PAFC was selected for the initial program. The original FTA Grant has since been modified to accommodate a Proton Exchange Membrane Fuel Cell (PEMFC) manufactured by the Ballard Power Corporation. Two commercializable, liquid-fueled 40-foot transit buses are to be produced: one with each type of Fuel Cell. A team led by Booz-Allen & Hamilton (with Kaman and NovaBUS) was selected as the systems integration contractor. The Grant will also address the propulsion needs for FTA's Advanced Technology Transit Bus (ATTB).

This paper presents preliminary test results gained from the TBB testing program and how these are being applied to guide the 40-Foot Commercial Transit Bus Development Program. Of special interest is the high degree of interaction between the various subsystems of a true hybrid electric drive system. This is further complicated when the Fuel Cell must operate on reformed liquid fuel introducing a further degree of technical integration into the overall control scheme. It was only after the introduction of a detailed data acquisition package onboard TBB #3 that the problems introduced by this complexity could be properly understood and addressed.

The TBB test results are presented to illustrate these technical issues. Voltage matching of the two electrical power sources is critical in the hybrid propulsion train. The difficulty lies in achieving this match with subsystems that have vastly different transient responses and constantly changing loads. The techniques used on the TBBs include reactant flow control to adjust fuel cell output power and "current limiting" to maintain the battery voltage within the desired range. This paper will discuss difficulties inherent with these techniques and changes being considered for the 40-foot program. Additional data will be presented on battery performance, system efficiency, and water recovery to be used in the reforming process.

The data collected from testing and operating the TBBs has been invaluable in developing the system design and control strategy for the 40-Foot Commercial Transit Bus Development Program. Many of the "lessons learned" apply to not only future fuel cell buses, but to hybrid vehicles in general.

The 30-Foot TBBs are performing as expected and meets all transit industry and Americans with Disabilities Act requirements. These fully functional heavy-duty transit buses are providing engineering experience to guide the 40-foot commercialization effort. Two 40-foot Fuel Cell powered transit buses will be delivered in the 1997/1998 time frame to meet the Congressional edict to commercialize this highly competitive, environmentally beneficial technology.

TRANSPORTATION ENGINE COMMERCIALIZATION AT BALLARD POWER SYSTEMS

N. C. Otto and P. F. Howard
Ballard Power Systems Inc.
9000 Glenlyon Parkway
Burnaby, British Columbia
Canada V5J 5J9

Engine Commercialization Plan

Ballard is adapting its leading fuel cell technology for transit bus engines in three phases.

In the first phase, completed in 1993, Ballard developed and demonstrated a 125 HP fuel cell engine in a 32-foot light duty transit bus. This was the world's first zero-emission vehicle (ZEV) powered completely by PEM fuel cells. The bus is a reliable, smooth performing vehicle that clearly established the viability of Ballard Fuel Cells for zero-emission transit bus operation.

In the second phase, completed in 1995, Ballard refined its fuel cell technology, building a 275 HP fuel cell engine for a 40-foot heavy duty transit bus. The fuel cell engine fits in the existing engine compartment and meets the performance of a combustion powered vehicle, but with no pollution.

In the third phase, small fleets of ZEV buses will be tested with Chicago Transit Authority and BC Transit. These test fleets will provide the performance, cost and reliability data necessary for commercial production.

Commercial production of Ballard's environmentally clean engines will begin in the 1998-1999 timeframe.

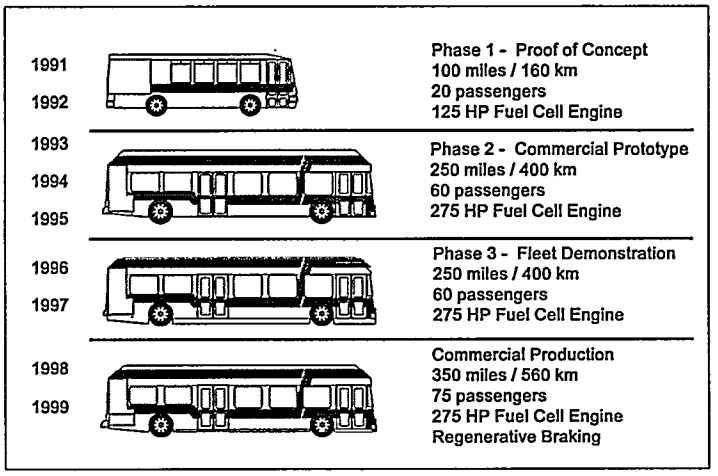

Figure 1: Bus Engine Commercialization Plan

Phase 1 - Proof of Concept

The first phase demonstrated the viability of Ballard Fuel Cell Engines for transit buses. The world's first fuel cell powered bus ran on the streets of Vancouver, British Columbia on January 27, 1993, proving the potential for Ballard Fuel Cell Engines. The engine for this vehicle was developed using 24 of Ballard's first generation 5 kW stacks connected in three series strings to deliver 120 kW gross power (160 Vdc @ 750 Amperes). The rest of the engine system was assembled from components commercially available "off-the-shelf". The engine was fueled by compressed hydrogen gas, stored at 3000 psig in standard DOT-approved fibreglass-reinforced aluminum cylinders. These cylinders are widely used on compressed natural gas-powered buses.

The bus demonstrated many important performance characteristics: startup takes less than four seconds; power is available for propulsion immediately; maximum power is available in less than one tenth of a second; low end torque is excellent, allowing the driver to pull away from the curb and into traffic quickly and safely. The Ballard Fuel Cell Engine demonstrated 46% fuel efficiency, compared to 20% efficiency for a conventional diesel engine. With improvement in subsystems, Ballard engines will exceed 50% efficiency.

The bus clearly demonstrated that a PEM fuel cell engine can meet vehicle performance criteria while creating no pollution. This bus continues to provide demonstrations of the future of pollution-free transportation in various cities across North America.

Figure 2: **World's First Fuel Cell Powered ZEV Bus**

Phase 2 - Commercial Prototype

The second phase improved the fuel cell engine, meeting the performance of a diesel engine in powering a full size 40-foot heavy duty transit bus.

A major increase in fuel cell power led to substantial increases in engine performance in phase two. Second generation fuel cells, two and one half times more powerful than their phase one counterparts, drove a 275 HP engine fitted into a fully functional transit bus.

New Flyer Industries model H40LF advanced low floor transit bus was used as the development and testing vehicle for the second phase engine. New Flyer built the coach and assisted with the engine and fuel storage installation.

The engine uses 20 of Ballard's second generation 13 kW stacks connected in two strings to deliver 260 kW gross power (650 Vdc @ 400 Amperes). Its cooling system is designed to operate at temperatures below freezing. Fuel for this bus is carried on the roof in advanced light-weight graphite/polymer composite cylinders which carry three times more fuel than the cylinders used in phase one, providing the bus with a range of over 250 miles (400 km).

The bus retained standard vehicle characteristics and met Urban Mass Transit Authority (UMTA) performance criteria:

Gradability	Start on 20% grade Maintain 20 mph (30 km/h) on 8% grade
Acceleration	0-30 mph (0-50 km/h) in 19 seconds
Top Speed	60 mph (95 km/h)

Table 1: **Commercial Prototype Performance Specifications**

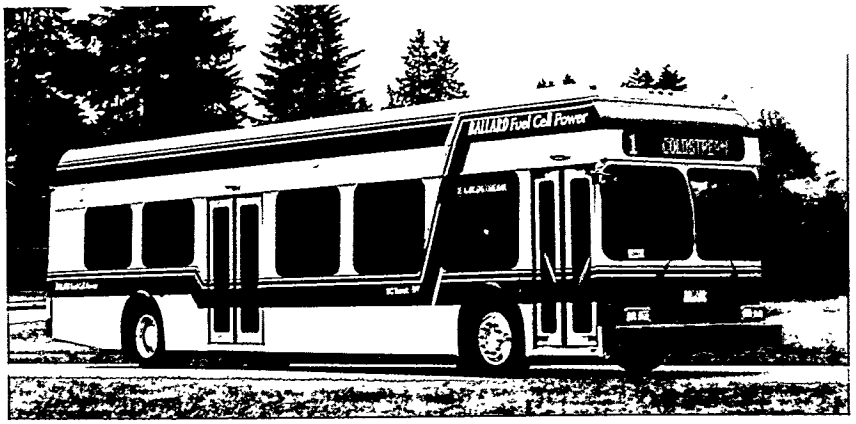

Figure 3: **Commercial Prototype ZEV Bus - New Flyer H40LF Low Floor Bus**

Performance testing, development and demonstrations of the commercial prototype bus have been ongoing since July 1995. The bus has passed all specified safety inspections as required by the BC Motor Vehicle Branch to carry a permanent motor vehicle license.

Phase 3 - Demonstration Fleets

The Chicago Transit Authority and BC Transit in Vancouver will each begin testing three bus fleets beginning in mid 1997. Operational data from this third phase will be used to further refine the production engine.

The production engine will be based on a third generation fuel cell which has five times more power than the first generation fuel cell. This makes the engine smaller and lighter. This engine will allow the transit bus to carry the industry standard of 75 passengers. The range of the bus will be extended to 350 miles (560 km) by increasing engine efficiency and by recovering energy generated from the braking system.

Refueling

For the initial three bus demonstration fleets, hydrogen will be produced off-site and delivered by truck in liquid form. At the bus depot, the hydrogen will be stored in an above ground tank. The liquid will be pumped to a vaporizer where its pressure increases as it changes to a gas. Refueling will be accomplished with a simple gas transfer which is fast and does not require a compressor. For large fleet use, hydrogen could be produced on-site or delivered through a pipeline. This is the most economical method to produce hydrogen today.

In the future, hydrogen may be produced from electrolysis of water using renewable clean electricity. In this way, the full cycle of fuel production to fuel use will be inexhaustible, sustainable and clean.

Multifuel Capability

In addition to operating on hydrogen directly either as a gas or liquid, Ballard is developing the capability to operate PEM fuel cells on alcohol-based fuels such as methanol and petroleum-based fuels such as natural gas, gasoline and diesel.

Ballard has developed a 40 kW sub-scale prototype powerplant to provide Air Independent Power (AIP) for submarine use. This power plant uses liquid methanol as the fuel and a steam reforming process to produce hydrogen. Hydrogen cleanup is accomplished with a palladium membrane separator. This system has been under development and test since 1994 and has established the capability to develop the full size 400 kW powerplant for military submarines.

Based on the experience gained from the AIP system, Ballard is building a 100 kW PEMFC Power System (FCPS) for a 40-foot hybrid transit bus using methanol as the fuel. The FCPS will include controls, fuel reforming, air delivery, cooling system, thermal integration, water recovery and water treatment system. This unit will be delivered to Georgetown University at the end of 1997 for integration into a 40-foot transit bus.

As part of the development effort, Ballard is evaluating multi-fuel fuel processors. Working with Energy and Environmental Research Corporation, Ballard will assess integrating "unmixed combustion" technology with the Ballard PEMFC and a palladium membrane hydrogen separator.

As part of Ballard's stationary program, Ballard has developed the capability to operate on natural gas and is building a 250 kW natural gas powerplant for delivery in 1997. This unit will operate on pipeline natural gas and deliver high quality ac power to the electrical grid.

Summary

Fuel cell engines are here. The noisy, polluting internal combustion engine can be a thing of the past. The question facing the Company is no longer "Does the technology work?" Ballard provied that it does. Today the Company is asked "How much and when?" Clean pollution free transportation using Ballard fuel cell engines will be running on the streets of North America before the year 2000.

PEM FUEL CELL STACK DEVELOPMENT FOR AUTOMOTIVE APPLICATIONS

Dr. William D. Ernst
Technology Division
Mechanical Technology, Inc.
Latham, NY 12110

Introduction

Presently, the major challenges to the introduction of fuel cell power systems for automotive applications are to maximize the effective system power density and minimize cost. The material cost, especially for Platinum, had been a significant factor until recent advances by Los Alamos National Laboratory and others in low Platinum loading electrode design has brought these costs within control. Since the initiation of its PEM stack development efforts, MTI has focused on applying its system and mechanical engineering heritage on both increasing power density and reducing cost. In May of 1995, MTI was selected (along with four other companies) as a subcontractor by the Ford Motor Company to participate in Phase I of the DOE Office of Transportation Technology sponsored PNGV Program entitled: "Direct-Hydrogen-Fueled Proton-Exchange-Membrane (PEM) Fuel Cell System for Transportation Applications". This Program was instituted to:

- Advance the performance and economic viability of a direct-hydrogen-fueled PEM fuel cell system,
- Identify the critical problems that must be resolved before system scale-up and vehicle integration, and
- Integrate the fuel cell power system into a sub-scale vehicle propulsion system.

The Phase I objective was to develop and demonstrate a nominal 10 kW stack meeting specific criteria. Figure 1 is a photograph of the stack used for these demonstrations. After completion of Phase I, MTI was one of only two companies selected to continue into Phase II of the Program. This paper summarizes Phase I stack development and results.

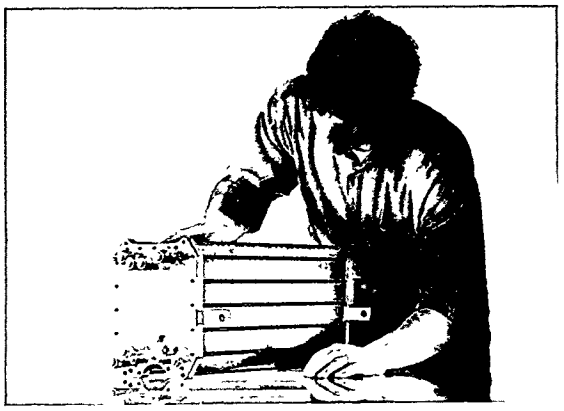

Figure 1 - MTI 10 kW Fuel Cell Stack

Performance Requirements - The objectives of Phase I were to advance the performance, power density and economic viability of direct-hydrogen-fueled PEM fuel cell stacks for automotive propulsion, and fabricate a 10 kW stack to demonstrate the improvements achieved. The fuel cell stack performance requirements included the following:

1. Fueled with hydrogen gas and air;
2. Stack gross power output of approximately 10 kW when operating at 0.6 V per cell;
3. Catalyst loading of 0.25 mg/cm^2 or less (total for cathode and anode together);
4. Stack power density of 3.63 kg/kW (8 lbm/kW), excluding auxiliary equipment, when operating with air supply pressure of 308 kPa (30 psig) or less.

The considerably more stringent requirements for the Phase II power system presently under development by MTI are indicative both of the near term state of the technology and eventual automotive requirements:

1. Fueled with hydrogen gas and air;
2. System net power output of 50 kW when operating at 0.6 V per cell;
3. Catalyst loading of 0.25 mg/ cm^2 or less (total for cathode and anode together);
4. System net power density of 1.82 kg/kW (4 lbm/kW), excluding auxiliary equipment (radiator, water pump, etc) when operating at air supply pressure of 308 kPa (30 psig)or less;
5. Specific operating voltage range.

Design and Performance Development The overall development approach was to evaluate new concepts in laboratory size hardware and then to scale up to the 10kW size where they would be verified. The overall 10 kW stack specification is shown in Table 1. The cost reduction efforts were focused on the implementation of low Platinum loading catalyst technology for the membrane electrode assembly (MEA) by a technique that could be utilized in volume production. This task resulted in a manufacturing capability with throughput adequate for pilot production and yielded cells of 50 cm^2 size with performance similar to that shown in Figure 2 for two different Platinum loadings.

The next step in the development process was to achieve comparable performance in much larger cells. As demonstrated in Figure 3, the overall cell performance target level of 800 ma/cm^2 at 250 cm^2 was easily reached. With the cell performance target reached, attention was turned to increasing the stack power density by increasing cell pitch. The final tested design was approximately 6 active cells per inch including the humidification and cooling/heating functions; however designs of 8 to 10 active cells per inch appear feasible in the near term.

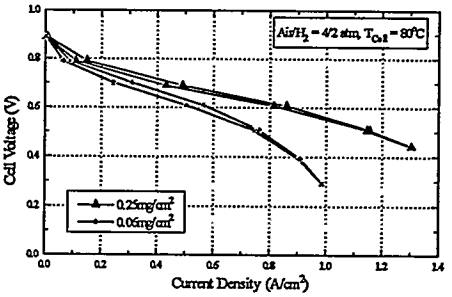

Figure 2 - Initial Single Cell Performance - 50 cm^2

Table 1: 10 kW Stack Design Specifications

PARAMETER	SPECIFICATION	PARAMETER	SPECIFICATION
Stack Power Density	3.63 kg/kW	Cell Platinum Loading	0.25mg/cm^2
Stack Construction	Filter Press	Cell Voltage	0.6 V
Air Pressure	308 kPa	Cell Construction	Modular
Air Stoichiometry	2.0	Cell Shape	Rectangular
H_2 Pressure	239-308 kPa	Cell Operating Temp.	85 °C
H_2 Stoichiometry	1.5	Humidification	Internal

Although internal humidification was not a requirement of the program, in the interest of obtaining the greatest possible power density, it was incorporated in the stack while greatly reducing the required volume. As shown in Figure 4, current density performance with internal humidification can equal or slightly better external humidification. The selected stack design used conventional filter press construction with all components designed and fabricated by MTI from raw materials.

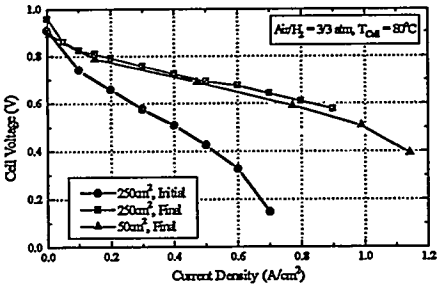

Figure 3 - Single Cell Performance
50 cm^2 vs. 250 cm^2

Stack Testing - MTI designed and built test stations were used for all testing. The larger stacks were tested using an 800 SLM scroll type air compressor, pressurized hydrogen gas, a closed loop heating/cooling system, and a custom designed load bank all controlled through LabVIEW. Four stacks of various power levels were built and tested using MTI internal funds including 1kW, 1.7kW, 5kW and 10kW versions each of which provided valuable learning experiences.

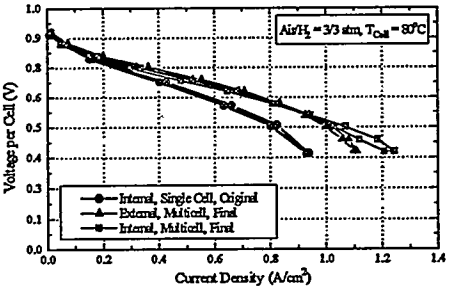

Figure 4 - Internal vs. External Humidification
50 cm^2

The first stack to be tested was the 1 kW version which verified the scale up from laboratory size to full size cells. The performance test results shown in Figure 5 compare single cell with stack results and indicate their good agreement. The tests also demonstrated that there was inadequate air supply capacity in the test station above the 1 kW level which was corrected in the design for a 10 kW test station.

Test results for the 10 kW stack are shown in Figure 6 which indicate that the target performance was reached at 0.6 volts per cell. While this performance was expected to have been reached with MEAs having 0.25 mg Pt/cm^2, independent assay of the MEAs demonstrated that it had been reached with a loading of only 0.17 mg Pt/cm^2. This result was unexpected and led to the decision to build another stack with the design Platinum loading.

A 1.7kW stack was then built using MEAs with Platinum loading of 0.25 mg/cm^2. This power level was selected because it would utilize available hardware and raw materials and was consistent with the modular configuration of the stack structure. Performance results for this stack when scaled to the number of modules in the 10 kW stack design indicated that a power level of 11kW would be reached. Thus, the additional 0.08 mg Pt/cm^2 provided an increase of approximately 10% in stack power level. The power density at 11 kW would be 3.54 kg/kW (7.8 lbm/kW) with internal humidification and 3.22 kg/kW (7.1 lbm/kW) without internal humidification. These results are consistent with the overall program requirements

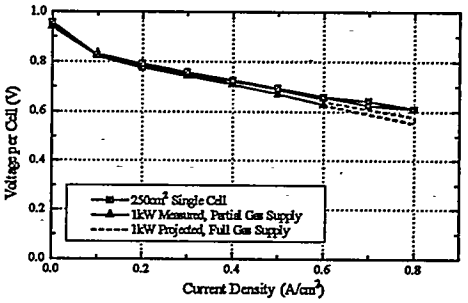

Figure 5 - Single 1kW cell

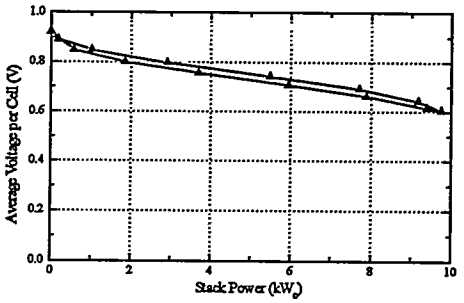

Figure 6 - MTI 10 kW Stack performance

Acknowledgment

This work was performed under contract from the Ford Motor Company as sponsored by the DOE Office of Transportation Technology with further support from the New York State Energy Research and Development Authority and MTI internal R&D funds. The author wishes to thank Steve Chalk of DOE, Dr. Djong-Gie Oei of Ford and Dr. Lawrence Hudson of NYSERDA for their guidance and encouragement.

DESIGN AND PERFORMANCE OF A PROTOTYPE FUEL CELL POWERED VEHICLE

Peter A. Lehman and Charles E. Chamberlin
Schatz Energy Research Center
Humboldt State University
Arcata, CA 95521
Phone: (707) 826-4345 / Fax: (707) 826-4347 / email: serc@axe.humboldt.edu

Introduction

The Schatz Energy Research Center (SERC) is now engaged in the Palm Desert Renewable Hydrogen Transportation System Project. The Project involves a consortium which includes the City of Palm Desert, SERC, the U.S. Department of Energy, the South Coast Air Quality Management District, and Sandia and Lawrence Livermore National Laboratories. Its goal to develop a clean and sustainable transportation system for a community will be accomplished by producing a fleet of fuel cell vehicles, installing a refueling infrastructure utilizing hydrogen generated from solar and wind power, and developing and staffing a fuel cell service and diagnostic center. We will describe details of the project and performance goals for the fuel cell vehicles and associated peripheral systems.

In the past year during the first stage in the project, SERC has designed and built a prototype fuel cell powered personal utility vehicle (PUV). These steps included:

- Designing, building, and testing a 4.0 kW proton exchange membrane (PEM) fuel cell as a power plant for the PUV.
- Designing, building and testing peripherals including the air delivery, fuel storage/delivery, refueling, water circulation, cooling, and electrical systems.
- Devising a control algorithm for the fuel cell power plant in the PUV.
- Designing and building a test bench in which running conditions in the PUV could be simulated and the fuel cell and its peripheral systems tested.
- Installing an onboard computer and associated electronics into the PUV
- Assembling and road testing the PUV.

PUV System and Fuel Cell Design

As the first step in the design and construction of the SERC prototype fuel cell PUV, we selected the E-Z-GO golf cart to serve as the platform because it was already established and accepted in the Palm Desert community and used an efficient motor and motor controller. We then acquired, instrumented, and tested an original, battery powered E-Z-Go Golf Cart.

The fuel cell stack developed for and used in the prototype was designed:

- to operate throughout the entire range of driving conditions at a voltage compatible with the E-Z-GO motor controller,
- to provide sufficient power to cruise at constant speed up a mild incline and still charge the batteries,
- to require low parasitic loads for auxiliary systems such as air supply, water circulation, control computer, solenoids, sensors, etc., and
- to operate efficiently.

To meet these demands, the resulting fuel cell stack contains 64 cells with 300 cm^2 active area and delivers more than 4.0 kW peak power. During cruising conditions, the stack operates at 0.71 volts/cell which corresponds to a 57% stack efficiency (LHV). The required stack air inlet pressure is less than 2 psig.

Figure 1 provides a simplified schematic diagram of the prototype system. All of the energy to power the cart comes from the hydrogen stored onboard in two compressed gas cylinders that together hold about 0.16 kg H_2. The hydrogen plus air from a low power, high efficiency blower combine in the fuel cell stack and provide power to the traction bus through a DC-to-DC converter. The power to the PUV's 1.5 kW series DC motor is controlled by the driver via the E-Z-GO motor controller. Power from the traction bus also charges the batteries during normal idling and cruising conditions and power is provided to the traction bus from the batteries during periods of acceleration and hill climbing. Only a small fraction of 30 amp-hr battery capacity is normally utilized. Power for all of the auxiliary systems is drawn from the traction bus through a small DC-to-DC converter. The control algorithm for the fuel cell power plant in the PUV manages the power demand on the fuel cell stack plus the air flow, battery charging/discharging, and system heat management.

PUV Construction and Testing

Following testing of the original, battery powered cart and the design of the PUV system and fuel cell, the fuel cell stack was constructed and tested and the individual PUV auxiliary or peripheral subsystems were designed and individually tested and calibrated. The PUV peripheral subsystems include 1) air delivery, 2) fuel storage, delivery, and refueling, 3) water circulation and cooling, 4) electrical systems, and 5) on-board computer hardware and software. In the design and testing of each of these subsystems, component safety, reliability, size, and parasitic power demands were important considerations.

After the lab evaluation was completed, the PUV was further tested at a nearby race track where the original cart trials had taken place. In a series of 0.25 mile runs, the SERC prototype PUV exhibited equal acceleration and slightly higher maximum speed in comparison to the original, battery powered E-Z-GO golf cart .

Figure 2 shows how the power demands to the motor controller and the parasitic loads are partitioned between the fuel cell and the battery during the test run. Before the start while the PUV is idling, the power is all coming from the fuel cell and is being used to support the parasitic loads and to recharge the battery. After the first 2 seconds of the run during which the sharply peaking power demands of the motor controller are met primarily by the battery, the fuel cell has ramped up and the contribution from the battery falls quickly to zero by 10 seconds into the run. For the remainder of the run, the fuel cell again provides all of the power to the motor controller and the parasitic loads and also recharges the battery.

Since one of the major objectives in the design of the fuel cell stack and the PUV subsystems was the minimization of parasitic loads, it was rewarding for us to

examine the parasitic load observed during the test runs. From idling conditions up to about 2000 W of power to the motor controller, the parasitic load is constant at approximately 80 W. Above 2000 W, the parasitic load is only about 4% of the power to the motor controller. Table 1 summarizes the specifications for the prototype fuel cell powered (PUV) as built and tested.

Conclusions

On November 1, 1994, SERC submitted to the City of Palm Desert a report comparing fuel cell battery, and gasoline powered golf carts and soon after agreed to design, build, and introduce a prototype fuel cell powered PUV at the November 5, 1995 Palm Desert Golf Cart Parade. The prototype PUV was completed on schedule and did debut on November 5, 1995 at the Palm Desert Golf Cart Parade. The cart performs well and meets our initial goals.

To date, we have installed an interim hydrogen refueling station and delivered the first PUV to the City of Palm Desert as part of the Palm Desert Renewable Hydrogen Transportation System Project. Within the next year, we will deliver two additional PUVs, be nearing completion of the first neighborhood electric vehicle (NEV), and be constructing the photovoltaic hydrogen production system.

Acknowledgments

The authors gratefully acknowledge generous grant funding from Mr. L.W. Schatz of General Plastics Manufacturing Co., Tacoma, WA, USA, and the assistance of Schatz Energy Research Center staff: P. Barger, A. Cohen, S. Ebers, R. Glover, R. Herick, T. Herron, A. Jacobson, A. La Ven, R. Mayberry, C. Parra, G. Pauletto, M. Rocheleau, L. Reid, R. Reid, and J. Zoellick.

Table 1. Specifications for Prototype Fuel Cell Powered PUV

Characteristic	Value
Fuel cell type	proton exchange membrane (PEM)
Fuel cell stack power	4.0 kW (5.4 hp)
Number of cells	64
Hydrogen energy consumption	0.34 kWh/mile
Mileage (gasoline energy equivalent)	110 mpg
Fuel cell system weight	200 lbs
Traction bus voltage	36 volts (nominal)
Electric motor size	1.5 kW (2.0 hp)
Hybrid battery size	30 amp-hrs
Cruising speed	12 mph
Fuel cell net power at cruising speed	1.8 kW
Hydrogen tank volume	14 liters
Hydrogen gas storage pressure	2000 psig
Range	20 miles
Refueling time	2 minutes

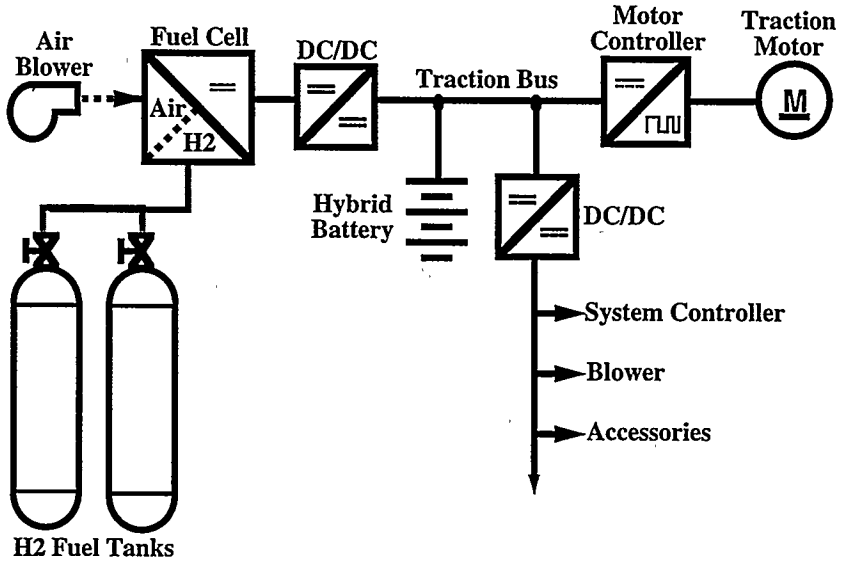

Figure 1: Schematic of SERC Prototype PUV

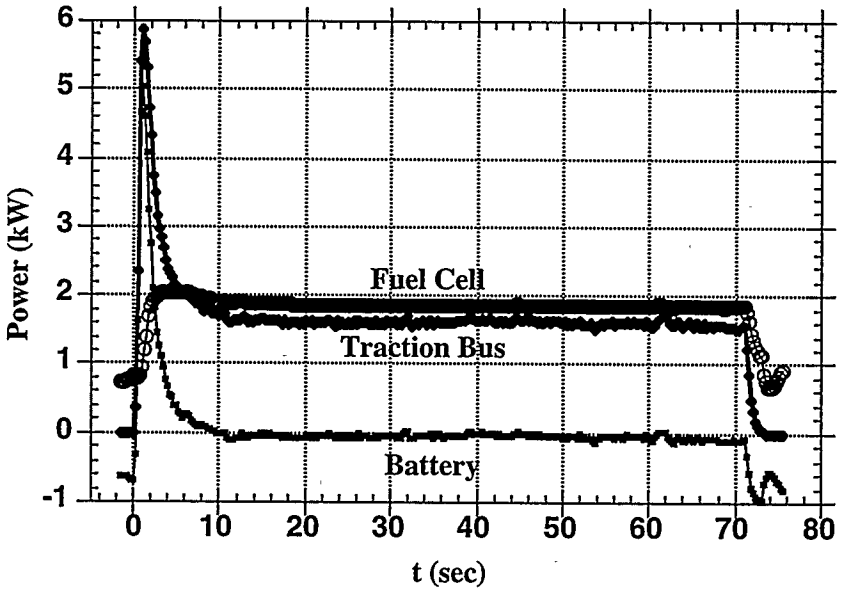

Figure 2: Response of Fuel Cell during Acceleration

FUEL CELL POWER SYSTEM FOR UTILITY VEHICLE

M. Graham, F. Barbir,
F. Marken, M. Nadal
Energy Partners, Inc.
1501 Northpoint Parkway, Suite 102
West Palm Beach, FL 33407

Based on the experience of designing and building the Green Car, a fuel cell/battery hybrid vehicle, and Genesis, a hydrogen/oxygen fuel cell powered transporter (Figure 1), Energy Partners has developed a fuel cell power system for propulsion of an off-road utility vehicle. A 10 kW hydrogen/air fuel cell stack has been developed as a prototype for future mass production. The main features of this stack are discussed in this paper. Design considerations and selection criteria for the main components of the vehicular fuel cell system, such as traction motor, air compressor and compressor motor, hydrogen storage and delivery, water and heat management, power conditioning, and control and monitoring subsystem are discussed in detail.

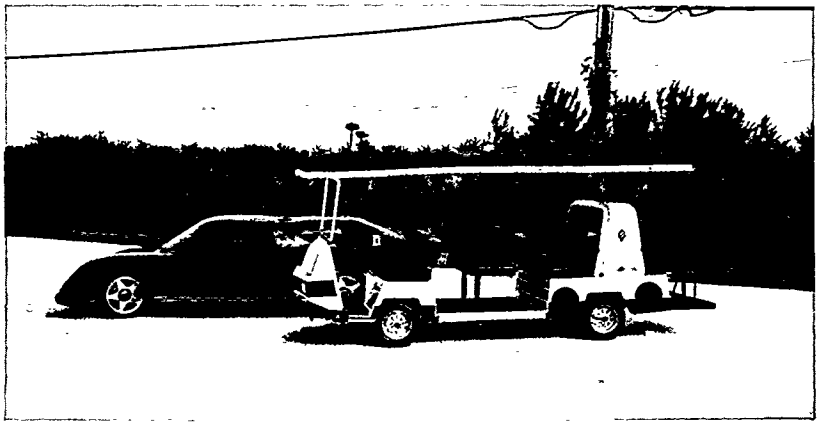

Figure 1. Green Car and Genesis
Fuel Cell Powered Vehicles

VEHICLE

Energy Partners, Inc. completed its most recent fuel cell conversion vehicle using the base platform of a John Deere Gator™ 6X4 chassis (Figure 2). Traditionally, the primary market areas for this vehicle have been in farming and grounds-keeping. This conversion expands that sales market by providing a nimble, nonpolluting vehicle for use in closed environments, as well as open areas with access to hydrogen fuel.

The chassis was received without the standard ICE powerplant and supporting equipment, such as the fuel tank and radiator. Early modifications to the vehicle included removal of engine mounts, as well as two drive wheels. The traction system was replaced with a DANA axle coupled to a series wound GE motor and a Curtis motor controller. These off-the-shelf components were chosen primarily for their widespread use in similar applications and excellent track records, but also because of favorable efficiency ratings.

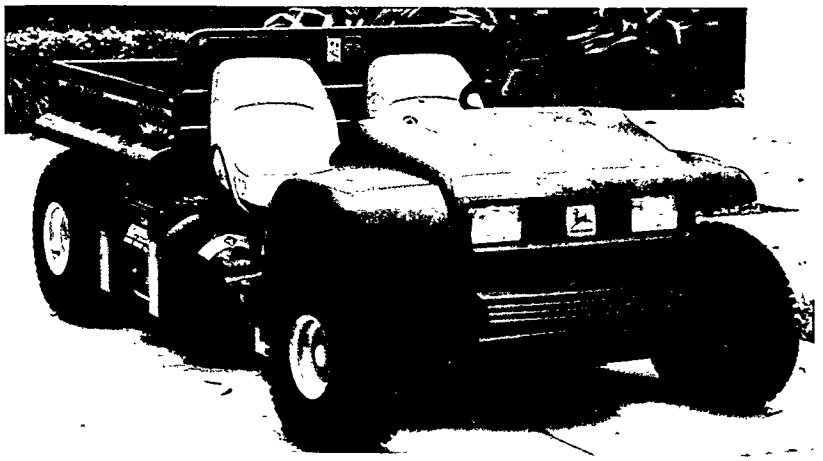

Figure 2. Gator™ Fuel Cell Powered Vehicle

FUEL CELL

The heart of the Gator™ fuel cell power system consists of an Energy Partners Model IB 10 kW fuel cell stack. The stack contains 60 advanced membrane electrode assemblies, with an active area of 780 cm^2/cell. This stack is a direct result of a grant from the Florida Energy Office for the commercialization of fuel cells, as well as Energy Partners' successful involvement in the DOE sponsored contract with Ford Motor Company, *PEM Fuel Cell for Transportation*. The stack uses collector plates which are manufactured by Energy Partners through a two-step compression molding process. Final machining of reactant headers and manifolds, as well as manufacture of end plates and bus plates, are also accomplished in our facilities, using a CNC milling machine.

SUPPORT SYSTEMS

Air Compressor and Compressor Motor

The most critical subsystem of the fuel cell support system is undeniably that of the air compressor. It was clear from the beginning of the program that an efficient, small and lightweight package would need to be identified. Several types and manufacturers of compressors were considered, and in the end, a modified screw compressor provided by VAIREX was selected. The compressor is directly coupled to a Uniq Mobility DC brushless permanent magnet motor/controller assembly, chosen for its high efficiency. Together, this combination delivers a maximum of over 20 cfm at 20 psig to the fuel cell stack.

Hydrogen Storage and Delivery

Early in the design of the vehicle, it was decided that range and run-time would meet or exceed the ability of the existing ICE powered vehicle. In support of this goal, two EDO LiteRider™ composite cylinders were chosen to carry the hydrogen fuel. Factors such as simplicity, weight, volume and cost were carefully considered prior to making this decision. The use of compressed

gas allows for a simple delivery method, controlled by the operation of solenoid valves on both of the cylinders. By using two of the model 60L cylinders, a maximum internal volume of 25,000 standard liters of hydrogen can be carried at 3000 psig, allowing for a minimum run-time of over 4 hours.

Water and Heat Management

The required humidification of the membrane is accomplished through the use of an Energy Partners designed and manufactured humidifier. This device is located on the air-side of the system, simply and reliably delivering de-ionized water from the cooling water reservoir into a chamber, where the entering air stream carries the humidifying mist into the fuel cell stack. The bulk of the excess water diffuses across the membrane and exits from the hydrogen side of the stack.

Cooling of the stack is accomplished by the circulation of de-ionized water through the stack. After exiting the stack, the water travels through a series of stainless steel heat exchangers which dissipate the heat. The degree of cooling is further controlled through the use of fans mounted on the radiators, which are individually operated by the microprocessor controller.

Power Conditioning

Several methods of power conditioning are employed in the Gator™ fuel cell power system. The air compressor motor controller allows a 30-100 V input voltage range, and a 42 V battery bank provides the initial power to start the system. Once fuel cell voltage rises above 50 V, the fuel cell contactor is engaged, powering the system and recharging the batteries. Two Curtis DC-DC converters are utilized to provide the 12 V required for operating the bed lift, pressure switches, solenoid valves, fans and water pump, as well as the microprocessor controller.

Additional power conversion is provided by the inverter, located in the bed of the vehicle. A Trace inverter delivers 120 VAC (modified sine wave) power for operation of hand tools at remote sites.

CONTROL AND MONITORING

Extensive efforts were directed towards developing a comprehensive controls system which would successfully initiate and operate the fuel cell system. Particular attention was paid to the monitoring and shutdown capability of the controls system. The result is an inherently safe vehicle, which is simply operated.

A microprocessor based controller, manufactured by Digitronics Sixnet, was chosen as the controls hardware. The main board is complemented by a 16-channel isolated analog input board, as well as two 8-channel digital I/O boards and RTUview, a user interface consisting of an integral keyboard and display unit. The controller is programmable in C, but many of the operating parameters of the vehicle are accessible through the user interface.

The controller monitors data such as reactant temperature and pressure, cooling water temperature, cell voltage and stack current. Using this data, functions such as initiating air compressor startup, engaging the fuel cell contactor and cooling fans, and shutting down the fuel cell system are accomplished. Any shutdown not initiated by the operator is recorded in controller memory, and the reason for shutdown is displayed on the user interface.

Aside from the stacks themselves, the critical difference between the hydrogen/air systems of the Green Car and the Gator™ lies in the respective air compressor operating strategies. The Green Car delivered a constant flow rate of air to the fuel cell stacks, whereas the Gator™ utilizes a more efficient strategy of varying the air flow to suit the imposed load. This is achieved by linking the compressor motor and traction motor potentiometers to the accelerator pedal.

PERFORMANCE

All performance expectations for the fuel cell powered Gator™ were met. Range, acceleration, speed, hill climbing and load carrying capacity match that of the ICE powered predecessor. A maximum speed of 23 mph was achieved in testing and a load of nearly 1200 lbs in passengers and payload was driven up a 22% grade. Noise from the compressor was reduced by acoustic insulation and isolation mounting of the compressor itself.

The model IB fuel cell stack demonstrates reliable performance with consistent, high cell voltages. The performance of the stack installed in the Gator™ is shown in Figure 3.

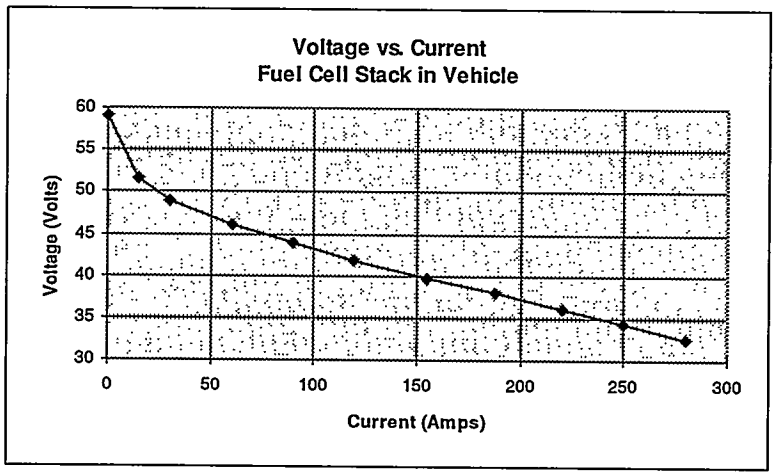

Figure 3. Polarization Curve for
Model IB Fuel Cell Stack Installed in Gator™

At maximum power, the fuel cell stack generates over 9.0 kW, of which, approximately 3.0 kW is required to operate the compressor and other ancillary equipment. At low and intermediate loads the efficiency is much higher, allowing vehicle operation for more than 4 hours.

Performance such as this indicates that the technology is available for introduction in specific applications. Utility vehicles are seen as a niche market which will create a greater demand for fuel cells. This demand will be met by industrial scale manufacturing, which in turn will reduce cost and aid fuel cell commercialization in other markets.

FUEL CELL DEVELOPMENT FOR TRANSPORTATION: CATALYST DEVELOPMENT

Narayan Doddapaneni and David Ingersoll
Sandia National Laboratories
Battery Research Department
Albuquerque, NM 87185-0614

Introduction

Fuel cells are being considered as alternative power sources for transportation and stationary applications. The degradation of commonly used electrode catalysts (*e.g.* Pt, Ag, and others) and corrosion of carbon substrates are making commercialization of fuel cells incorporating present day technologies economically problematic. Furthermore, due to the instability of the Pt catalyst, the performance of fuel cells declines on long-term operation. When methanol is used as the fuel, a voltage drop, as well as significant thermal management problems can be encountered, the later being due to chemical oxidation of methanol at the platinized carbon at the cathode. Though extensive work was conducted on platinized electrodes (1-3) for both the oxidation and reduction reactions, due to the problems mentioned above, fuel cells have not been fully developed for widespread commercial use. Several investigators have previously evaluated metal macrocyclic complexes as alternative catalysts to Pt and Pt/Ru in fuel cells (4). Unfortunately, though they have demonstrated catalytic activity, these materials were found to be unstable on long term use in the fuel cell environment. In order to improve the long-term stability of metal macrocylic complexes, we have chemically bonded these complexes to the carbon substrate, thereby enhancing their catalytic activity as well as their chemical stability in the fuel cell environment. We have designed, synthesized, and evaluated these catalysts for O_2 reduction, H_2 oxidation, and direct methanol oxidation in Proton Exchange Membrane (PEM) and aqueous carbonate fuel cells. These catalysts exhibited good catalytic activity and long-term stability. In this paper we confine our discussion to the initial performance results of some of these catalysts in H_2/O_2 PEM fuel cells, including their long-term performance characteristics as well as CO poisoning effects on these catalysts.

Experimental

Several metal phthalocyanine polymer complexes $(MPc)_n$ having the structure shown in Figure 1 were synthesized in our laboratory. These catalysts were synthesized by heating a mixture of 3,3',4,4'-benzophenone tetracarboxylic dianhydride, metal chloride(s), and urea at 200°C for 2 hours. The complexes prepared were $(CoPc)_n$, $(PtPc)_n$, $(Pt\text{-}RuPc)_n$, $(Pt\text{-}MoPc)_n$, and $(RuPc)_n$. In this study only $(CoPc)_n$ and $(Pt\text{-}RuPc)_n$ were evaluated. A detailed description of the synthetic procedure of the catalysts and their impregnation onto the carbon substrate has been previously described (5,6). When the carbon/catalyst mix is heat treated in an inert atmosphere to about 475°C, a covalent bond appears to form between the carbon substrate and the benzene ring of the complex, as shown in Figure 2. It should be noted that these complexes are soluble in common organic solvents and aqueous solutions of mineral acids, however, after heat treatment they become insoluble.

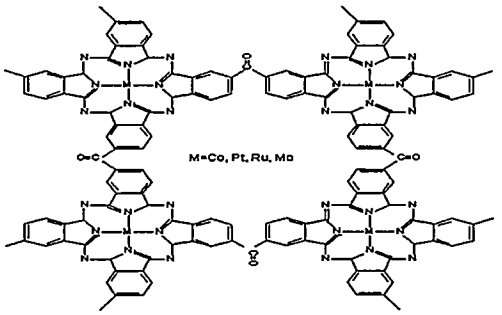

Figure 1

The membrane electrode assemblies (MEAs) used in this work were prepared by Giner, Inc., Waltham MA. All electrodes, exceept those composed of Pt-black, contain 20% Nafion 117, and were cast onto Teflonized carbon fiber paper. Fuel cells were constructed having cathodes composed of either Pt-black (4 mg Pt/cm^2) or 20% Pt/Vulcan (0.5 mg Pt/cm^2). The anodes used in these cells consisted of either Pt-black, 10% Pt/Vulcan (0.25 mg Pt/cm^2), 20%Pt/Vulcan (0.5 mg Pt/cm^2), or 15% (Pt-RuPc)$_n$/Vulcan (0.035 mg Pt/cm^2 and 0.018 mg Ru/cm^2). All MEAs had active areas of 40 cm^2 and were evaluated at 80°C with 30 psig H_2 and either 30 or 60 psig O_2. The electrochemical screening of these complexes for the oxidation of hydrogen and reduction of oxygen in acid media was carried out in our laboratory. In order to provide independent evaluation of the performance of these inexpensive catalysts, PEM fuel cell fabrication and testing was carried out at Giner, Inc.

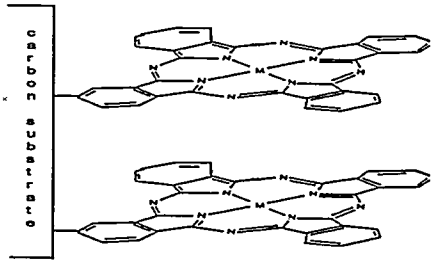

Figure 2.

Results and Discussion

Fuel cells of varying combinations of anodes and cathodes were evaluated using H_2 and these results are shown in Figure 3. As seen, the fuel cell having the (Pt-Ru Pc)$_n$/Vulcan anode had slightly lower voltage than the other electrode combinations. However, the initial performance of this system is very promising, considering the unoptimzed nature of this MEA and significantly lower noble metal loadings. At 500 mA/cm^2, this fuel cell with a Pt-black cathode exhibited a terminal cell voltage of 650 mV. A fuel cell built with an anode and a cathode both composed of 20% Pt/Vulcan exhibited

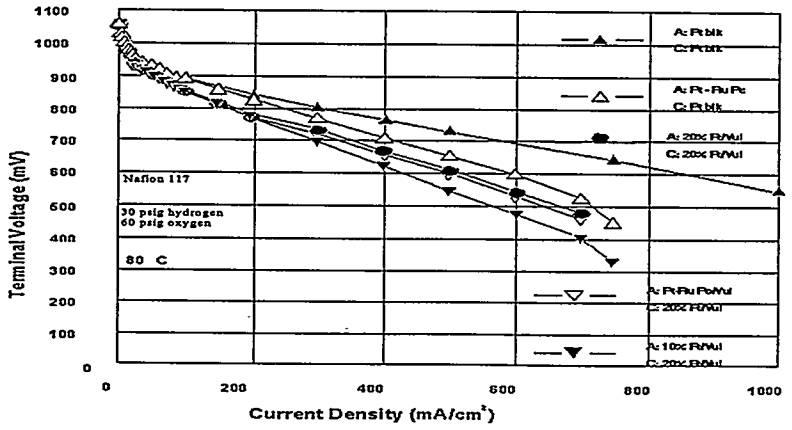

Figure 3. Comparison of PEMFC Performance of PtRuPc/vulcan with State-of-the-Art catalysts.

a terminal voltage of 610 mV. In comparison to this, the fuel cell built with a 15% $(Pt\text{-}RuPc)_n$ /Vulcan anode and a 20% Pt/Vulcan cathode has a terminal voltage only 60 mV lower, namely 550 mV *vs* 610 mV. We have also evaluated the performance of the cobalt transition metal phthalocycanine complex ($(CoPc)_n$) on heat treated Black Peal 2000. The catalyst exhibits good catalytic activity for hydrogen oxidation. Further studies of these nonprecious metal macrocyclic complexes are currently in progress and the data will be reported in future publications.

The stability characteristics of a PEM fuel cell using a 40 cm^2 MEA composed of a 15% $(Pt\text{-}RuPc)_n$/Vulcan anode and a 20% Pt/Vulcan cathode were evaluated at 80°C and 500 mA/cm^2. In Figure 4 the terminal voltage as a function of time for continuous operation over 800 hours is shown. As seen, the voltage observed is relatively constant at about 600 mV. The minor variations in voltage are attributed to changes in the degree of membrane hydration. A second cell was built and tested under similar conditions in order to evaluate the performance reproducibility. This cell was continuously operated at 500 mA/cm^2 for 102 hours and was then shut-down for 48 hours. The cell was then restarted and the testing continued for another 98 hours, for a total testing time of 200 hours. It should be noted that this discontinuous operation of the cell did not adversely affect its performance. The cell also displayed stable operating characteristics, and this can be seen in the polarization behavior of this cell measured before and after 200 hours of operation. These results are shown in Figure 5 on the following page. One thing that can be seen upon examination of this data is that fuel cell terminal voltage has increased after operation. This improved performance could be the result of increased hydration of the assembly.

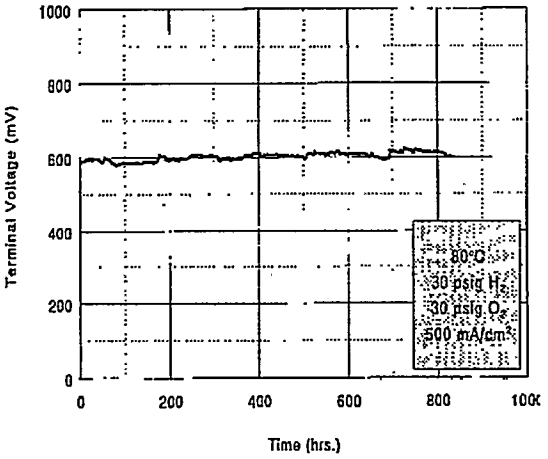

Figure 4. Life Test of Pt-RuPc/Vulcan Catalyst in PEMFC.

Studies of the effect of carbon monoxide contamination of the fuel have been initiated. Preliminary results have shown voltage drops of 25mV, 30mV, and 325mV for CO levels of 10ppm, 20ppm, and 100ppm in the H_2 fuel, respectively. Los Alamos National Laboratory (LANL) has reported (7) values of 90mV and 390-400mV for CO levels of 5ppm and 20ppm, respectively. No results were reported at higher CO levels. The LANL results were obtained using Pt/Vulcan anode formed into a thin-film having a Pt loading of 0.14 mg/cm^2. This is four times the noble metal loading of the $(PtRuPc)_n$/Vulcan. We believe that the voltage drop in the $(Pt\text{-}RuPc)_n$ /Vulcan can be reduced by optimization of the electrode, including removal of the small amounts of uncomplexed noble metal which could be present. Future work will be made on pure $(Pt\text{-}RuPc)_n$ complex catalyst.

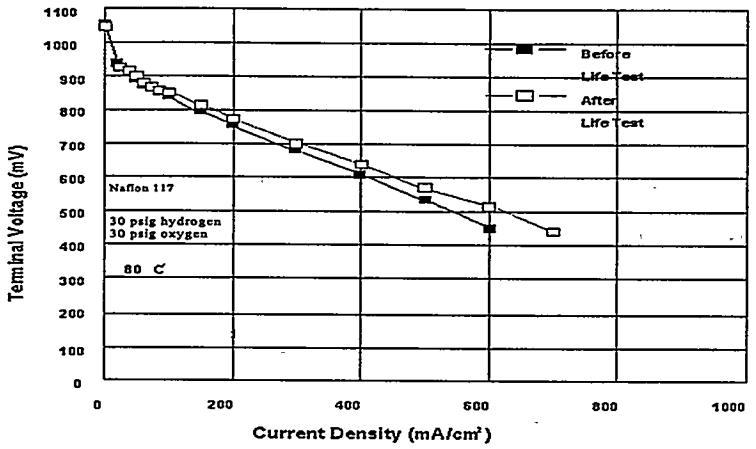

Figure 5. Polarization of Pt-RuPc/Vulcan Catalyst in PEMFC Before and After 200 hr LifeTest

Conclusions

Metal phthalocycanine complexes have been evaluated as alternate catalysts for Pt in H_2/O_2 PEM fuel cells. Preliminary results with $(Pt\text{-}RuPc)_n$ and $(CoPc)_n$ show very promising catalytic activity for H_2 oxidation. PEM fuel cells with unoptimized MEAs using these catalysts performed as well as MEAs containing Pt catalyst. The noble metal loading of the alternate catalysts evaluated in these studies is significantly lower than the precious metal catalyst loading presently being used in fuel cells. During 800 hours of continuous operation at 500 mA/cm² and 80°C, the fuel cell performance was stable. This vividly demonstrates the stability of the metal macrocyclic complex in the operating environment of the fuel cell. The tolerance of the $(Pt\text{-}RuPc)_n$ macrocyclic complex to the presence of CO is superior to the Pt catalyst, in spite of the fact that it contains 0.035 mg Pt/cm², compared to 0.14 mg Pt/cm² in the LANL work. Finally, long-term stability tests of PEM fuel cells with $(Pt\text{-}RuPc)_n$ catalyst and its tolerance to CO is in progress and the results will be reported in future publications.

References

1. Y. Kiras, J. Electrochem. Soc., 143, 2152, (1996) and references therein.
2. S. Mukerjee and J. McBreen, *ibid,* 143, 2285, (1996) and references therein.
3. M.K. Ravikumar and A.K. Shukla, *ibid,* 143, 2601, (1996) and references therein.
4. G. Lalande, G. Tamizhanani, R. Cote, L. Dignard-Bailey, M.L. Trudeau, R. Schulz, D. Guay, and J.P. Dodelet, *ibid,* 142, 1162, (1995).
5. N. Doddapaneni, US Patent 4,405,695, (1983).
6. N. Doddapaneni, Proceedings of the Symposium on Lithium Batteries, PV84-1, p 122, A.N. Dey editor, Electrochemical Society Inc., Pennington, NJ, (1984).
7. M.S. Wilson, C.R. Delouin, J.A. Valerio and S. Gottesfeld, 28th Proceedings Intersociety Energy Conversion Engineering Conf., 1, 1203, (1995).

Acknowledgements

We thank Dr. J. Kosek and Ms. C. Cropley of Giner, Inc for the PEMFC evaluations.

ELECTRODE POROSITY AND EFFECTIVE ELECTROCATALYST ACTIVITY IN ELECTRODE-MEMBRANE-ASSEMBLIES (MEAs) OF PEMFCs

A. Fischer, H. Wendt
Institut für Chemische Technologie
der TH Darmstadt, Petersenstr. 20,
D - 64287 Darmstadt, Germany

Introduction

New production technologies of membrane-electrode-assemblies for PEMFCs which ensure almost complete catalyst utilization by "wetting" the internal catalyst surface with the ionomeric electrolyte, (1) to (4), allow for a reduction of Pt-loadings from prior 4 mg cm^{-2} to now less than 0.5 mg cm^{-2}. Such electrodes are not thicker than from 5 to 10 µm.

Little has been published hitherto about the detailed micromorphology of such electrodes and the role of electrode porosity on electrode performance. It is well known, that the porosity of thicker fuel cell electrodes, e. g. of PAFC or AFC electrodes is decisive for their performance. Therefore the issue of this investigation is to measure and to modify the porosity of electrodes prepared by typical MEA production procedures and to investigate the influence of this porosity on the effective catalyst activity for cathodic reduction of oxygen from air in membrane cells. It may be anticipated that any mass transfer hindrance of gaseous reactants into porous electrodes would manifest itself rather in the conversion of dilute gases than in the conversion of pure gases (e.g. neat oxygen). Therefore in this investigation the performance of membrane cell cathodes with non pressurized air had been compared to that with neat oxygen at cathodes which had a relatively low Pt-loading of 0.15 mg cm^{-2}.

Experimental

The manufacturing procedures for MEAs initially developed by Wilson, Gottesfeld and coworkers (1) to (3) and by Srinivasan (4) and Escribano and coworkers (5) were used. Addition of (i) volatile but homogeneously dissolved pore forming materials (ammonium salts) or (ii) particles of sparcely soluble non volatile but leacheable fillers (lithium carbonate) allowed to adjust the fine porosity by method (i) and coarse porosity by method (ii) within the limits from 25 to 65 vol. %. Additionally to Wilson's and Gottesfeld's hot pressing method a hot spray method was used (2) to (4) by spraying the cold catalyst ink on a heated membrane. The immediate vaporization of the solvents, isopropanole and water, creates - depending on the process temperature - a fine-porosity of from 25 to 35 vol. %. The catalyst loading determined by the amount of 30 wt % Pt on Vulcan XC-72 was kept constant (0.15 mg Pt per cm^2) at the anode and cathode for all experiments. The porosity of the electrodes was determined pycnometrically by flooding the dry, symmetrically constructed MEA with toluene at reduced pressure and calculating from the weight gain the flooded void and porosity by accounting for the measured electrode thickness (~ 10 to 20 µm). Current voltage curves were measured under the following standardized conditions in 25 cm^2 cells:

H_2 flow rate:	300 Nml/min vapour saturated at 85 °C, corresponding to a limiting current density of 1.86 A cm^{-2},
oxygen flow rate:	150 Nml / min and
air flow rate:	300 Nml / min, corresponding to an O_2-supply limited current density of 0.74 A cm^{-2}.

Results

Table 1 collects the porosity data and the internal conductivities of the electrodes fabricated by five different production procedures, beginning with hot pressed electrodes proceeding to hot sprayed electrodes which had been produced with a catalyst ink containing the leachable filler, which produces coarser pores. One observes a steady increase of the porosity P, which varies from 20 up to 65 vol %. Simultaneously the electronic conductivity of the electrodes decreases from 2.4 to 0.44 S cm^{-1} by a factor of 5.5, which is more than proportional as (1-P) decreases only by a factor of 2.3.

Fig. 1 compares the current voltage curves of hot pressed electrodes with that of three different hot sprayed electrodes. Hot sprayed electrodes prepared without any additive are already better than hot pressed ones. But still the performance is improved by forming a more porous structure with up to 65 % void. At a cell voltage of 0,5 V the current density increases by a factor of 1.7 from 220 to 380 mA cm^{-2} and at 0.4 V from 300 to 380 mA cm^{-2} by a factor of approx. 1.3.

Discussion

Contrary to the general, little disputed, opinion that thin film MEA-cathodes are not really porous or that their porosity does not matter much, our results show that the porosity of MEA-cathodes which are operating on non-pressurized air is significant for obtaining high current and power densities. Simple model calculations show that the higher resistivity of the more porous electrodes cannot affect these data as the current is collected by relatively well conducting carbon paper, which covers the electrode evenly, so that the current has to pass through no more than several micrometers of the low conducting electrode matrix generating at current densities of 1 A cm^{-2} no more than 2 to 3 mV ohmic voltage losses. A detailed evaluation of our data shows, that increasing the porosity by a factor of three leads to an increase of the mass transfer limited current density by a factor of 1.3. The greater part of improved current and power densities in the cell voltage range of from 0.4 to 0.7 V, however, seems to be due to an increased utilization of the catalyst as it is manifested in increasing apparent i_o values up to values of approx. 3.7 $\mu A\ cm^{-2}$.

References

(1) M.S. Wilson, S. Gottesfeld, Thin film catalyst layers for polymer electrolyte fuel cell electrodes, J. Appl. Electrochemistry, 22 (1992), 1 - 7
(2) M.S. Wilson, Membrane catalyst layer for fuel cells, US Pat. 5, 234,777 (1993)
(3) M.S. Wilson, Membrane catalyst layer for fuel cells, US Pat. 5,211,984 (1993)
(4) M.S. Wilson, High performance catalyzed membranes of ultra low Pt loadings for polymer electrolyte fuel cells, J. Electrochem. Soc. 139 (1992) L28 - 30
(5) S. Srinivasan, A.C. Ferreira, R. Mosdale, S. Mukerjee, J. Kim, s. Hirano, S.-M. Lee, F.N. Buchi, A.J. Appleby, "Proton exchange membrane fuel cells for space and electric vehicle application" in Program and Abstracts, Fuel Cell Seminar 1994 San Diego, USA, p. 424-7
(6) S. Escribano, S. Miachon, P. Aldebert, "Low platinum loading wide electrodes for internal humidification hydrogen/oxygen polymer electrolyte membrane fuel cells" in New materials for fuel cell systems 1, Ed. O. Savadogo, P.R. Roberge, T.N. Veziroglu, Editions de l'École Polytechnique de Montréal, p. 135 - 43, Montreal 1995

Table 1

Porosity and intrinsic electronic conductivity of MEA-electrodes obtained by different productive procedures

procedure	1 hot pressed no additive	2 hot sprayed no additive	3 hot spray with low temp. vaporized add.	4 hot spray with high temp. vaporized add.	5 hot spray with leachable filler
Porosity %	20	35	42	48	65
κ/Scm^{-1}	2.35	1.64	0.83	1.04	0.44
i_o(app)/Acm^{-2}	$1.4 \cdot 10^{-6}$	$1 \cdot 10^{-6}$	$1.9 \cdot 10^{-6}$	$3.1 \cdot 10^{-6}$	$3.7 \cdot 10^{-6}$

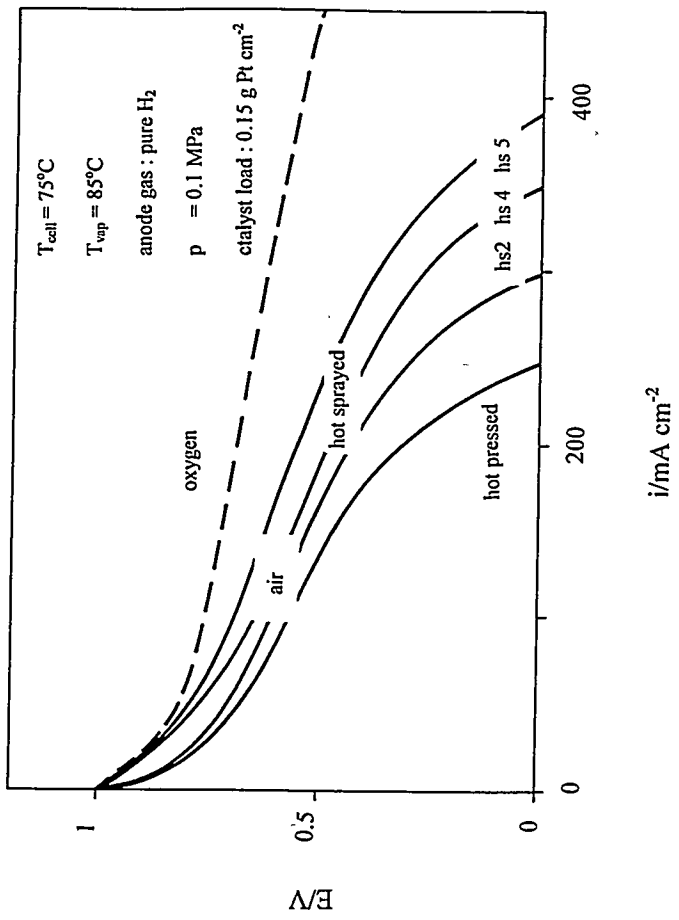

Fig. 1: current density / cell Potential correlation for PEMFCs with differently prepared cathodes (always loaded with 0.15 mg Pt per cm^2); hs2, hs4 and hs5 are hot sprayed electrodes of columns 2, 4 and 5 in Table 1.

SELF-HUMIDIFIED PROTON EXCHANGE MEMBRANE FUEL CELLS: OPERATION OF LARGER CELLS AND FUEL CELL STACKS

Hari P. Dhar, James H. Lee, and Krzysztof A. Lewinski
BCS Technology, Inc., 2812 Finfeather Road, Bryan, TX 77801, USA
Tel. (409)-823-7138, Fax. (409)-823-8475, E-mail. bcstech@cy-net.net

INTRODUCTION

The PEM fuel cell is promising as the power source for use in mobile and stationary applications primarily because of its high power density, all solid components, and simplicity of operation. For wide acceptability of this power source, its cost has to be competitive with the presently available energy sources. The fuel cell requires continuous humidification during operation as a power source. The humidification unit however, increases fuel cell volume, weight, and therefore decreases its overall power density. Great advantages in terms of further fuel cell simplification can be achieved if the humidification process can be eliminated or minimized. In addition, cost reductions are associated with the ease of manufacturing and operation.

At BCS Technology we have developed a technology of self-humidified operation of PEM fuel cells based on the mass balance of the reactants and products and the ability of membrane electrode assembly (MEA) to retain water necessary for humidification under the cell operating conditions. The reactants enter the fuel cell chambers without carrying any form of water, wheather in liquid or vapor form. Basic principles of self-humidified operation of fuel cells as practiced by BCS Technology, Inc. have been presented previously in literature [1, 2, 3]. Here, we report the operation of larger self-humidified single cells and fuel cell stacks. Fuel cells of areas up to 100 cm^2 have been operated. We also show the self-humidified operation of fuel cell stacks of 50 and 100 cm^2 electrode areas.

Attempts to introduce self-humidification to the fuel cell led to the introduction of the special membrane that was recast from the solubilized PEM electrolyte in the presence of SiO_2 or TiO_2 by Watanabe *et al.* [4]. This membrane was modified by deposition of Pt film (approx. 0.1 $mg{\cdot}cm^{-2}$) inside a bulk of the membrane via cation exchange followed by reduction. The self-humidification mechanism was based on the ability of such membrane to transport reactants, both hydrogen and oxygen, which then recombined on the embedded Pt film. The water, product of this reaction, directly humidified the membrane. Such mode of operation required very high stiochiometries of reactants, 5 and 10 for hydrogen and air, respectively. Other works on self-humidified operation of the fuel cell concentrated on conveying water from feed point to the membrane itself by introduction of some kind of transport mechanism. Cisar *et al.* [5] developed a membrane cast in the presence of special micro-tubing. The embedded micro-tubes provided internal water passages providing water for membrane humidification. Similar approach, also based on direct addition of water to the membrane was developed by Watanabe *et al.* [6].

EXPERIMENTAL

Two approaches have been developed to operate fuel cells self-humidified. The approaches differ in the way MEAs are prepared. In one approach, deposits of a solubilized proton exchange membrane is used as the electrolyte for the fuel cell. The deposits show different characteristics from the membrane they are produced from. The water absorption capability of the deposit is greater than that of the parent membrane. In this sense, a new class of proton exchange material is obtained from the solid form of the membrane. Two electrodes with the deposits are assembled with a plastic film placed around the edges of the electrodes. In the second approach, a regular membrane is used in combination with deposit of the solubilized membrane. The fuel cell performance is dependent, among others, on the amount of the deposit, thickness of the membrane

equivalent weight of the membrane and the deposit. Fuel cell reactants are hydrogen/air and hydrogen/oxygen.

RESULTS

The performance data were obtained in the form of current-potential relationships under various experimental conditions. All cells and stacks operate in self-humidified mode with dry reactants. Figure 1 shows the performance of a 50 cm^2 fuel cell operated with air at 2.35 atm at two different Pt loadings. The performance achieved was 0.716 V and 0.756 V at 0.5 $A \cdot cm^{-2}$ for 0.5 and 1.0 $mg \cdot cm^{-2}$ of Pt catalyst, respectively. This cell is based on Nafion 1100 electrolyte deposit technology. Other experimental conditions are given in the figure's caption. Figure 2 shows similar data obtained with larger, 108 cm^2 cell based on Nafion 115 membrane. Presented graph shows the performance of such cell with both, air and oxygen, at the atmospheric pressure. Figure 3 and Figure 4 show similar data to the above, but obtained for the three- and four-cell stacks, respectively. Complementing Figure 5 presents stability data collected from somewhat smaller cell of 25 cm^2 active area for few different current densities.

The presented data show that self-humidification phenomena is not limited to small fuel cell units, but can easily be incorporated into larger fuel cells and stacks. It's worth to note that performance is not sacrificed. On the contrary, the technology allows not only to take advantage of the cell simplification (the absence of humidification unit and associated auxiliaries) but also achieve very high performance levels.

1. H. P. Dhar. 29th IECEC Conference Proceedings, Monterey, CA, Aug. 7-11, 1994. Vol. 2, pp. 865-870.
2. K. A. Lewinski and H. P. Dhar , Report Submitted to National Science Foundation (NSF), Arlington, VA, Contract # DMI-9460292, 1995.
3. H. P. Dhar, U.S. Patent Nos. 5,242,764 (1993) and 5,318,863 (1994).
4. M. Watanabe, H. Uchida, Y. Seki, and M. Emori. Extended Abstract No. 606. Electrochemical Society Meeting. October 9-14, 1994. Miami Beach, FL.
5. A. Cisar, A. Gonzalez-Martin, O. J. Murphy, S. F. Simpson, and C. Salinas. 30th IECEC Conference Proceedings, Lake Buena Vista, FL, July 30-Aug. 4, 1995.
6. M. Watanabe, Y. Satoh, and C. Shimura. *J. Electrochem. Soc.* 140, (1993), 3190-3193.

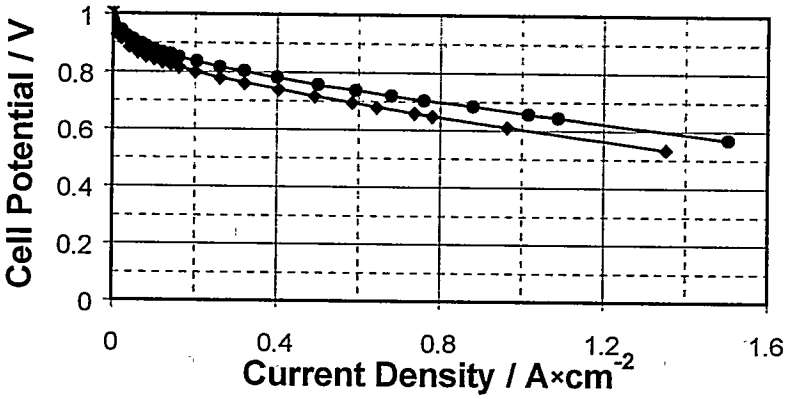

Figure 1. Fuel cell performance with Pt loading of 0.5 and 1.0 $mg \cdot cm^{-2}$ (lower and higher curve, respectively). Experimental conditions: electrolyte, Nafion 1100 deposit; electrolyte loading, 10 $mg \cdot cm^{-2}$; temperature, 50°C; electrode active area, 50 cm^2; air as the oxidant at 2.35 atm pressure.

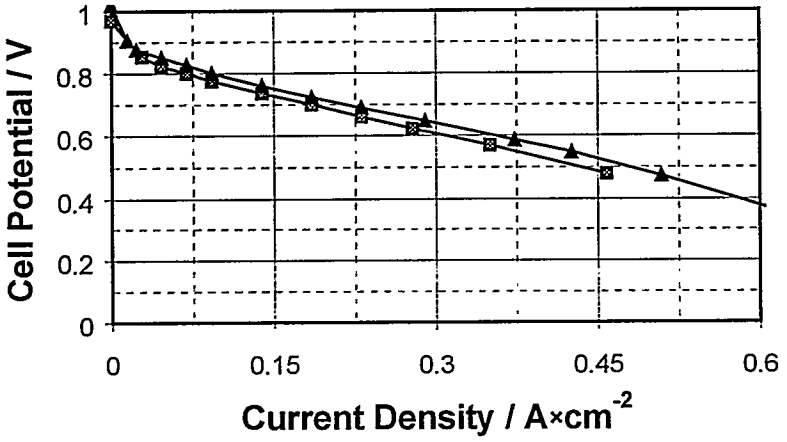

Figure 2. Fuel cell performance of a single cell of electrode area 108 cm^2. Experimental conditions: electrolyte, Nafion 115; Pt loading, 0.5 $mg \cdot cm^{-2}$; temperature, 50°C; reactants, H_2/air and H_2/O_2 at the atmospheric pressure (lower and higher curve, respectively).

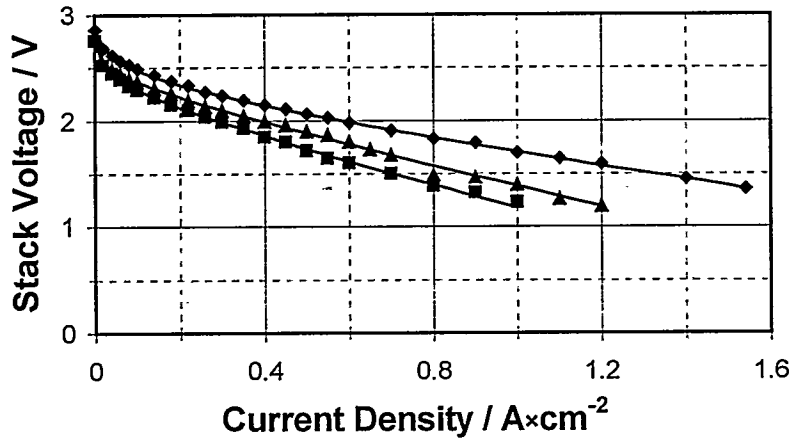

Figure 3. Performance data of three-cell stack of electrode area 50 cm^2 for each cell. Experimental conditions: electrolyte, Nafion 1100 deposit; electrolyte loading, 10 $mg \cdot cm^{-2}$; Pt loading, 0.5 $mg \cdot cm^{-2}$; temperature, 60°C; air at 1.0 and 2.35 atm pressure and oxygen at 1.0 atm of pressure were used as the oxidants (lowest to highest performance curve).

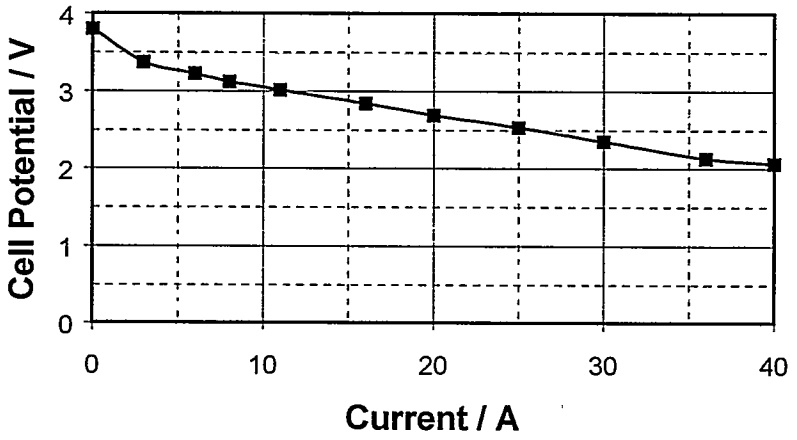

Figure 4. Performance data of four-cell stack of electrode area 108 cm^2 for each cell. Experimental conditions: electrolyte, Nafion 115; Pt loading, 0.5 $mg \cdot cm^{-2}$; temperature, 50°C; reactants, H_2/air at the atmospheric pressure.

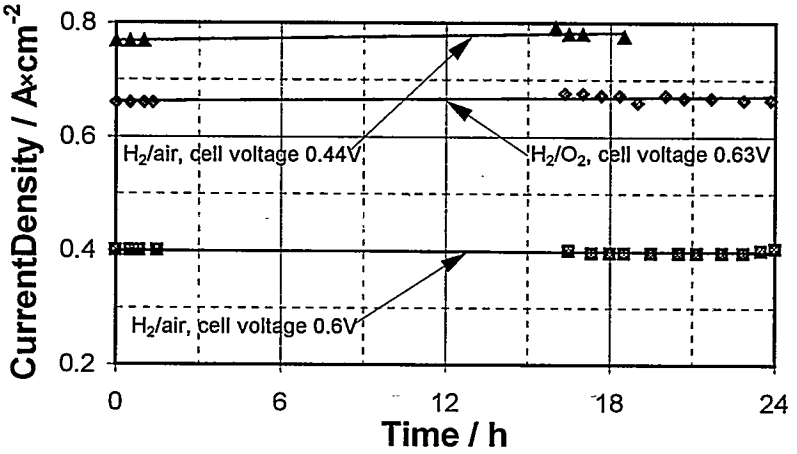

Figure 5. Stability test data plotted as current density at constant cell potential in time for fuel cell electrode with Nafion loading of 10 $mg \cdot cm^{-2}$ and Pt loading of 0.5 $mg \cdot cm^{-2}$. The electrolyte deposit, Nafion 1100; temperature, 50°C; electrode active area, 25 cm^2; air and oxygen were used as oxidants at the atmospheric pressure.

ACKNOWLEDGMENTS

The financial supports from the NASA-funded Center for Space Power, Texas A&M University, College Station, TX and NSF (SBIR grant DMI-9460292) are acknowledged with gratitude.

DEVELOPMENT OF A POLYMER FUEL CELL SYSTEM FOR NAVAL SURFACE SHIP APPLICATIONS

D. Schmal, C.E. Kluiters, I.P. Barendregt*
TNO Institute for Environmental Sciences,
Energy Research and Process Innovation
P.O. Box 6011, 2600 JA Delft, The Netherlands
*Royal Netherlands Navy
P.O. Box 20702, 2500 ES Den Haag, The Netherlands

Introduction

In the framework of the development of new generations of surface ships, the Royal Netherlands Navy is studying the option of the all-electric ship concept. Background is the growing demand of electric power on board of naval ships for various services (including weapons and sensors). Important features of such an all-electric ship concept are decentralised electric energy generation and storage.
In such an all-electric ship concept, fuel cells are expected to play an important role in the future, not only for reasons of energy efficiency and low emissions, but also because of their potential military advantages. Especially polymer electrolyte fuel cell systems appear to be very interesting for this application [1].

All-electric ship concept

Current naval ships like frigates generally have separated systems for propulsion and electric power generation. The propulsion engines (gas turbines and/or diesel engines) in these conventional concepts directly drive the propulsion shafts. For the on-board supply of electricity, separate diesel engines/generators are mostly applied.
Due to the development of systems, e.g. sensors and weapons, requiring more electrical energy, the ratio of electrical power to (mechanical) propulsion power will increase. In the current generation of frigates, with separated installations this ratio has a value in the order of 0.02, whereas in the future it is expected to rise to 0.2 or even higher. Taking into account that propulsion engines of naval ships run at part load during a significant percentage of the time at sea, it will be clear that an integrated power generation installation for propulsion and ship's services is a better solution than the state-of-art separated installations, with respect to:

- totally installed power,
- operational flexibility,
- engines will run at more optimal load which will have positive consequences for energy efficiency and maintenance of the power generation system,
- the possibility of decentralised power generation, resulting in lower vulnerability, an important aspect for frigates.

With respect to the energy efficiency it was shown in a previous study [1] that, with an all-fuel cell energy supply system in a frigate, compared to the gas turbine/diesel system, energy (fuel) savings of 25-30% could be reached.

A possible lay-out of an all-electric ship concept is given in Figure 1. Components for electricity generation and storage in such an all-electric ship concept are for example efficient gas turbine/generators in various power ranges, but also fuel cells as well as batteries for electric energy storage. The use of fuel cells will have a number of advantages:

- favourable part load performance,
- relatively little maintenance (no moving parts),

- low noise and vibration level (low underwater noise signature),
- low exhaust gas temperature (low infrared signature),
- low emissions,
- modular construction (flexibility in location).

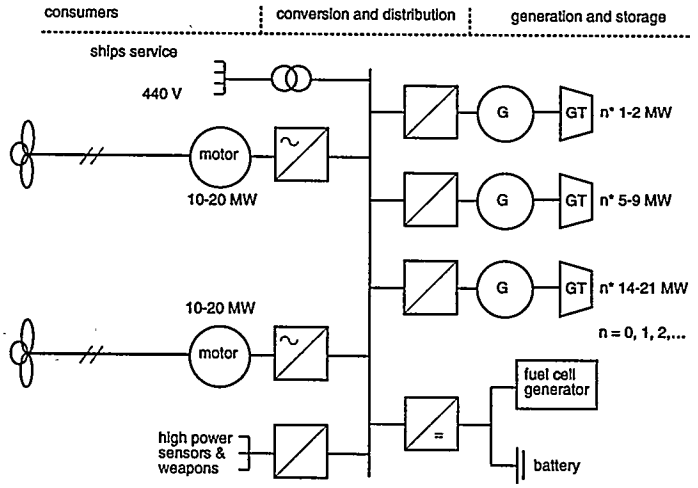

Figure 1 Schematic drawing of the all-electric ship concept

As mentioned, a fuel cell system has a high part load efficiency and it is expected that a fuel cell system which is integrated in the right way with gas turbines will have an even higher electric efficiency. For the long term it is even thinkable that the electric power generation plant on board of naval ships will completely consist of fuel cell generators or integrated fuel cell/gas turbine generators.

Fuel cell tests

Fuel cell stack

As part of a feasibility study, carried out by TNO for the Royal Netherlands Navy, a test programme is run with a polymer electrolyte fuel cell stack of De Nora in Italy. For this purpose a stack of 1 kW was chosen, containing 20 cells connected in series and having an active electrode area in the range of 200 cm^2 each. This stack is of the same type as the 8 stacks of 5 kW delivered by De Nora to Ansaldo (Italy) for construction in a fuel cell hybrid bus.
The stack is of a very robust design. However, as a consequence the power density is on the low side (about 100 W/kg). In more recent developments at De Nora, in the framework of European Joule projects (e.g the FEVER project with Renault and the recently started HYDRO-GEN project with PSA), significant improvements are made and expected.
In Figure 2 a picture of the 1 kW stack at the TNO laboratory is shown.

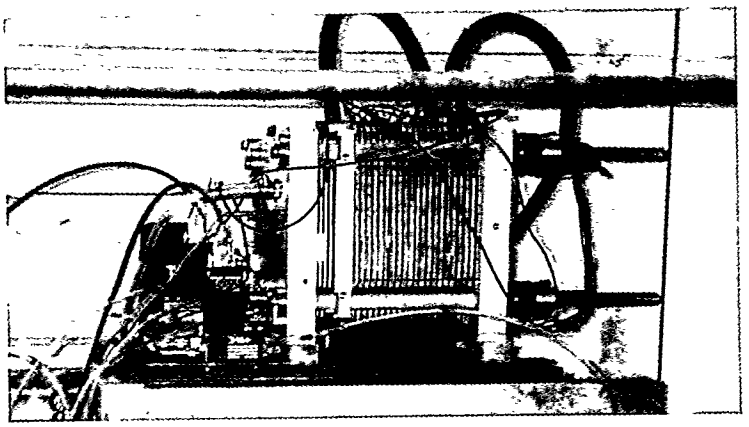

Figure 2 Picture of the 1 kW De Nora stack.

Test results so far

Tests with this stack, up to now using hydrogen as fuel and oxygen from the air, were started in the fall of 1995. The tests carried out so far are related to:

- acceptance (together with De Nora),
- static tests (I-V curves, power curves etc.),
- dynamic tests with programmed load and load related hydrogen and air supply (i.c. stoichiometry independant of power delivered), using Digatron equipment.

In the near future tests will be started with simulated ship conditions.

In Figure 3 the polarisation and power curve of the stack are given. The behaviour is conform expectations.

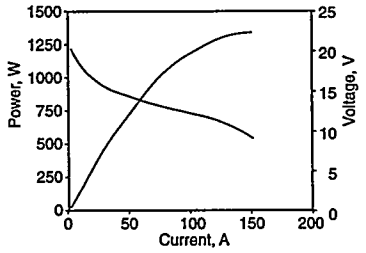

Figure 3 Polarisation and power curve of the 1 kW De Nora stack

Figure 4 gives the influence of hydrogen stoichiometry on voltage level at a current of 100 A. It can be seen that down to stoichiometries of 1.05 there is no influence on performance. An important practical consequence of this is that, when using hydrogen as a fuel, once-through flow should be possible (no recirculation pumps etc.). This makes the system relatively simple.

More detailed measurements at lower stoichiometries are currently carried out. Also measurements at air stoichiometries lower than 1.5 will be done.

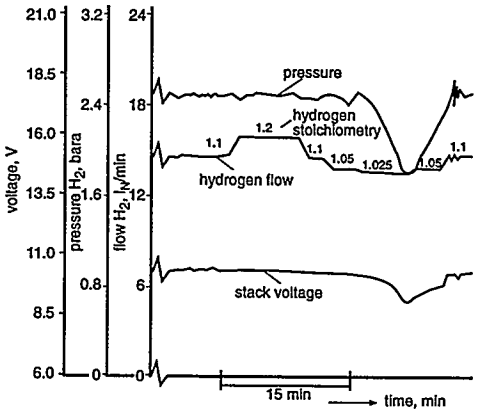

Figure 4 Influence of hydrogen stoichiometry on stack performance (100 A, 60°C).

Future tests and development

Future tests will include:

- low temperature and low pressure tests,
- lower hydrogen and lower air stoichiometry tests,
- dynamic load tests,
- cold start,
- dynamic load test according to a load profile that will simulate an operational profile of a naval surface ship.

There will also be an investigation into the fuel to be used.

A definition will be made of a demonstration project for on-board ship applications, possibly in co-operation with other navies.

Conclusions so far

After a few hundred hours of use at very different conditions with respect to temperature (including a number of cold start-ups) the behaviour of the stack is still very satisfying. Some minor problems have been found, especially at lower temperatures, with respect to water condensation, leading to a partial fall-out of single cells. However, after supplying dry gas for some time, this proved to be reversible.

At the seminar results will be shown of recent tests.

Acknowledgement

The project is carried out by TNO under contract A94/KM/133 with the Royal Netherlands Navy.

Reference

1. D. Schmal, M.J.E. Verschoor, I.P. Barendregt, "Future applications of fuel cells on naval ships related to energy savings", Abstracts 1994 Fuel Cell Seminar, Nov. 28 - Dec. 1 1994, San Diego.

Development and Properties of the "Stonehart" Humidity Stabilized Perfluoro-Polymer Membrane.

Paul Stonehart

Stonehart Associates Inc. PO Box 1220, 17 Cottage Road
Madison. Connecticut 06443-1220. U.S.A.
Tel : 203-245-7507 FAX : 203-245-9372

The purpose of this paper is to examine the role that water plays in the Polymer (or Proton) Electrolyte Membrane Fuel Cells (PEMFCs -- also called PEFCs). Since proton conduction is the main ionic charge carrier, it is worthwhile to examine how this happens and how the water interacts with the perfluoro-polymer structures; examining **the microstructure of the membranes** and how they have been modified to overcome the water transport limitations inherent in the PEMFC.

Background

Under fuel cell operating conditions, the ionic migration of the proton in the membrane causes the water molecules to move -- this is the so called "ion-drag" because the proton is too small to exist alone and so is solvated with the surrounding water. In effect, the anode is depleted of water and dries out and the cathode is flooded since that is where water production occurs. This phenomenon has been measured in excruciating detail *ad nauseam* but without any intent to influence the properties of the membranes. In each instance, only commercially available membranes have been measured. The ionic conductivity is then sensitive to the degree of solvation for the proton (expressed as the water content of the membrane).

The review of Zawodzinski et al.(11) covers most of the literature on this topic, and shows that there are differences in the number of moles of water associated with each proton, and that the ratios vary between 1.4 to 4.0. More recently, Sone et al. (12) have measured the proton conductivity in Nafion® 117 as a function of humidity and temperature, finding that the rate of change in membrane conductivity with water content switches from a singular regime when $\lambda < 4$ (λ=moles of water/moles of sulphonic acid) to another regime when $\lambda > 4$. This is exactly where a transition would be expected for rotational transport (or restricted Stokes-Einstein mobility) of the relatively rigid $H_9O_4^+$ complex formed by a central H_3O^+ with three molecules of water in the hydration shell where the excess proton is delocalised in the hydration structure allowing fast proton tunneling over the whole complex -- hence apparent proton transport. The "Gemini" programme overcame this water migration problem with fiber wicks, drawing the water back externally from the cathode to the anode in order to maintain a water balance. The "Stonehart" membrane overcomes the water migration problem by incorporating high surface area silica within the perfluoro-polymer structure to provide a route for back diffusion of the water from the cathode to the anode and maintain the water balance.

It was recognized long ago that one of the limiting factors for the use of non-fully fluorinated membranes was the attack of hydro-peroxy free radicals (HO_2°), produced

by the oxygen reduction reaction, on the -CH- sites. This limitation will still apply to alternative polymers with -CH- functional entities. The fully fluorinated polymer, Nafion®, was developed for the chlor-alkali industry and has been seconded to fuel cell technology, although at this time, there is insufficient volume of sales to justify any special developments for the latter application.

For a cell running at 1 Amp/sq.cm. at 0.7 Volts (terminal) then 1 kW of power requires a total cell area of 1,428 sq.cm. At an early entry membrane cost for sample volumes of between $700 and $1000/sq.m., the membrane cost is **$0.08/sq.cm.**; which is **$114.24/kW**. If we increase the design point to achieve a power density to **1.4W/sq.cm.** (see reference 7) and with present near term membrane costs of $300/sq.m. for pilot plant quantities, this membrane cost becomes **$21.42/kW**. which is certainly low enough to develop the market, especially since the membrane cost will decrease further with volume production. **Clearly the membrane cost is not a barrier to commercialization of PEMFCs.** So we must ask, **"Why is anyone trying to develop inferior membrane materials for PEMFCs with dubious commercial production, acceptability, lifetimes, or performances?"**

The conductivity of a perfluoro-membrane is influenced by the molecular structure, particularly since in the acid form it has a dual functionality. The perfluoro-portions of the polymer chain achieve a crystallinity akin to that of polytetrafluoroethylene (PTFE), and reflect the physical properties of that material; whereas the sulphonated regions of the polymers align in a non-crystalline manner and are associated with the water molecules. This gives rise to the concept of ionic clusters and of segregated core-shell structures within the polymer membrane, described respectively by Gierke et al.(9), and by Yeo and Eisenberg (10). For **1 g.mol** per litre, there are Avogadro's number of entities, which is 6.02×10^{23} per litre. Since there are 10^{-3} g.moles per cm^3 , and **6.02×10^{20} entities per cm^3**, then this translates to about **1 molecular entity in 2 nm^3** (this is 2,000 $Å^3$). Nafion® has a density of about 2 g/ml. in the dry-state and an equivalent weight of (say) 1100. This then translates to a concentration of **1.82 mol/litre.** (for EW = 1000 then it is 2 mol/l). **This suggests that there is 1 sulphonic acid group per cubic nanometer of membrane.**

The previous implication has been that the membrane structures are a continuum but in reality they contain a nano-dimensioned highly localized ionic interface with amorphous sulphonic acid rich regions of about 3nm in diameter, surrounded by the crystalline, water-proof, gas-permeable, "PTFE" regions of about 5nm in size. The sizes of the perfluoro-polymer shell and the ionic clusters are dependent upon the equivalent weights (EW) of the sulphonated perfluoro-polymer and the lengths of the perfluoro side-chains. The larger the EW, the larger the PTFE character of the membrane. For an EW of 1100, there must be, on average, about 17 $-CF_2-$ groups per EW in the "PTFE" region, acting as an annulus around the sulphonate groups inside the core.

Water Retention Properties of Silica.

In evaluating candidate approaches to improving the conductivity and water retention properties of perfluoro-polymer membranes it was decided that there was a greater chance for improving the properties of the membrane by developing a composite membrane structure rather than by modifying the perfluoro-polymer structure itself.

Considering inorganic additives, it is important to recognize that trace metals can act as ionic poisons to the perfluoro-polymer membrane, notably Group IIa (Ca, Ba) as well as Fe, Al, etc. At the same time, additives must be stable to the super-acid polymer environment and be compatible with the processing. This led to considering metal oxides of Groups IVa and b of the periodic table. When commercial availability at low cost in high surface area form was evaluated, the choice focussed upon fumed silica.

Silica in the form of silica gel is well known as a superior desiccant but this material depends upon an induced pore structure for some of the desiccant properties. Fumed silica is pore free with a micro-metric fibrous structure but water adsorbs strongly at the surface due to association as an hydrated oxide. The silicon oxides from Cabot Corporation (Cab-o-Sil is the trademark) have a non-porous fibrous morphology and are ideal for melding with the perfluoro-polymer sulphonic acid microstructures described previously. Although similar sizes of fumed silicas are available from Degussa AG Geschäftsbereich Anorganische Chemieprodukte, which licensed their preparation technology for fumed silica to Cabot Corp., it is our experience that, for whatever reason, the materials from Cabot seem to be more compatible to our perfluoro-membrane processing than those from Degussa.

Water retention for perfluoro-polymer membranes containing silica
A series of membranes were constructed by casting films from alcoholic solution using monomer solutions from Aldrich Chemical Company, Inc., who retail small quantities of Nafion® monomer from DuPont. The films were cast in the sodium form and then ion-exchanged after sintering and subsequently heat treated to remove residual moisture. Water contents were obtained after equilibrating the films in water vapour at 25°C.

The magnitudes of water uptake were surprising, especially at low levels of silica content. In all instances, it appeared that a steady water content was reached after 1.0% of silica loading, no matter the surface area of the silica; although the initial rates of water increase with silica content appeared to track the differences in surface area of the silica. Also, the plateaux for water uptake were lower with low surface area silica than with the high surface area silica.

Resistance measurements on composite membranes were obtained using a four-point probe, and expressed as resistance per square (dimensionless). The values were normalized to those resistance values of the Nafion® without silica.

It is surprising that the resistance values of the membranes decrease immediately on addition of the silica and go through a minimum around 1-5%. In real terms, the resistivity minimum of the composite Nafion® film with silica is halved from that base resistivity in the absence of silica. We may conjecture that in addition to providing greater water retention, the highly dispersed nature of the fibrous silica disrupts the ordered nature of the native Nafion®, providing greater mobility for the solvated proton, removing any electro-striction due to the sulphonic acid channels. At very high loadings of silica (>50wt%) the membrane is starved for the highly ionized sulphonated perfluoro-polymer and the resistance increases correspondingly. It can be seen that the composite membranes can accommodate up to 40% silica and still have the same conductivity as native Nafion® without silica added.

It is important to give credit to other work pursuing non-humidified perfluoro-membranes, and here the work of Dhar (13,14) should be mentioned. He used an approach of applying a very thin perfluoro-polymer membrane onto the electrode surface and relied on the self back-diffusion of water in the membrane. This membrane is highly permeable to gas molecules such as hydrogen and oxygen, leading to gas cross-over as the membranes become thinner, and providing thereby for an inherent limitation in the membrane thinness. Similarly, the Gore-Select membrane (15) is 12 micrometers (0.0005") thick comprising a PTFE porous web infiltrated with Asahi-Chemical's "Aciplex®" perfluoro-polymer, EW 900. This membrane is significantly more ionically resistive than the native Aciplex® due to the increased PTFE content, is more gas-permeable and, of course, there is no bonding between the perfluoro-polymer and the PTFE web, which we might expect will lead to the membrane developing the "bends" due to nitrogen gas-bubble nucleation from the fuel cell air electrode side. Patents have been filed by Stonehart Associates Inc. (SAI) on the use of silica in perfluoro-membranes for PEMFCs and are issuing (16).

References

1. W.T. Grubb in "Proc. 11th Annual Battery Res. Dev. Conference" PSC Publications Comm. Red Bank. NJ. p.5 (1957) and USP 2,913,511 (1959).
2. H. Gregor, US Army Contract # DA-36-039 SC-85384 30 Nov. 1960.
3. I. Raistrick, US Patent 4,876,115 (1989)
4. H.P. Gregor, in "15th Annual Power Sources Conference". PSC Publications Comm. Red Bank. NJ. pp.4-9 (1961)
5. R.B. Hodgdon Jr. et al., US Patent 3,341,366 Sept 12,1967 (Assigned to GE)
6. J. Wei et al., US Patent 5,422,411 June 6th 1995 (Assigned to Ballard Power)
7. K. Sakairi, K. Tsurumi, S. Kawaguchi, M. Watanabe, and P. Stonehart **"Advanced Catalyst Designs with Thin Membranes for PEMFC's"** in "National Fuel Cell Seminar Publication", U.S. Department of Energy, Tucson, Arizona, 1992. pp.153-156.
8. G.A. Olah, G.K.S. Prakash, and J. Sommer, "Superacids" J. Wiley & Sons., NY 1985. ISBN 0-471-88469-3
9. T.D. Gierke, G.E. Murn, and F.C. Wilson, J. Polymer Sci., Polymer Phys. Edit. 19, 1987 (1980)
10. S.C. Yeo and A. Eisenberg, J. Applied Polymer Sci. 21, 875 (1977)
11. T.A. Zawodzinski, J. Davey, J. Valerio, and S. Gottesfeld. Electrochim. Acta, 40, 297 (1995)
12. Yoshitsugu Sone, Per Ekdunge, and Daniel Simonsson J. Electrochem. Soc. 143, pp. 1254-1259 (1996)
13. H. Dhar, US Patent 5,242,764 Sep 7, 1993; and US Patent 5,318,863 Jun 7, 1994.
14. H. Dhar, in Extended Abstracts of the 1994 Fuel Cell Seminar San Diego, California pp.85-88.
15. J.A. Kolde, B. Bahar, M.S. Wilson, T.A. Zawodzinski, and S. Gottesfeld in "Proton Conducting Membrane Fuel Cells I" PV 95-23 pp.193-201. The Electrochem. Soc., Pennington. NJ. 1995. ISBN 1-56677-118-8
16. P. Stonehart and M. Watanabe, US Patent 5,523,181 Jun 4, 1996.

EFFICIENT Pt CATALYSTS FOR POLYMER ELECTROLYTE FUEL CELLS

J. Fournier, G. Faubert, J.Y. Tilquin, R. Côté, D. Guay, J.P. Dodelet
INRS-Énergie et Matériaux
C.P. 1020, 1650 boulevard Lionel-Boulet, Varennes, Québec, Canada, J3X 1S2

Introduction

Commercialization of polymer electrolyte fuel cells (PEFCs) requires an important decrease in their production cost. Cost reduction for the electrodes principally concerns the decrease in the amount of Pt catalyst necessary for the functioning of the PEFC without affecting cell performance. The first PEFCs used in the Gemini Space Program had a loading of 4-10 mg Pt/cm^2 (1). The cost of the electrodes was drastically reduced when pure colloïdal Pt was replaced by Pt supported on carbon (Pt/C) with a Pt content of 0.4 mg/cm^2 (2,3). Since the occurrence of that breakthrough, many studies have been aimed at further lowering the Pt loading. Today, the lowest loadings reported for oxygen reduction are of the order of 0.05 mg Pt/cm^2 (4,5).

The carbon support of commercial catalysts is Vulcan XC-72 from Cabot, a carbon black with a specific area of 254 m^2/g. Graphites with specific areas ranging from 20 to 305 m^2/g are now available from Lonza. The first aim of the present study was to determine the catalytic properties for O_2 reduction of Pt supported on these high specific area graphites. The second aim was to use Pt inclusion synthesis on these high area graphites, and to measure the catalytic performances of these materials. Lastly, this same Pt-inclusion synthesis was extended even for use with Vulcan and Black Pearls as substrates (two carbon blacks from Cabot). All these catalysts have been labelled Pt-included materials to distinguish them from the Pt-supported ones. It will be shown that the reduced Pt content Pt-included materials obtained with high specific area substrates a are excellent catalysts for oxygen reduction, especially at high currents. Therefore, Pt inclusion synthesis appears to be a new method to decrease the cathodic Pt loading.

Catalyst preparation

The graphites from Lonza were KS6, HS100-M6, and HS300-M6. Their specific surface areas are 20, 110, and 305 m^2/g, respectively. The carbon blacks were Vulcan XC-72R and Black Pearls 2000 with specific surface areas of 254 and 1475 m^2/g, respectively. Pt catalysts supported on graphites or on carbon blacks were prepared by the method described by Zeng and Hampden-Smith (6), using $PtCl_2$ and triethylborohydride. Pt catalysts were also obtained by using an intercalation procedure (7). Pt(IV) chloride was first intercalated in graphite or carbon blacks. The obtained materials were reduced by K-Naphthalene in tetrahydrofuran.

Analytical and electrochemical characterization

Elemental analysis was performed by neutron activation. For the electrochemical measurements in full cells, the anode consisted of a 1 cm^2 ELAT electrode (from E-TEK, Natick, Ma) catalyzed with 0.37 mg/cm^2 (20 wt%) Pt. For the cathode, the catalyst suspension was sprayed uniformly on a 1 cm^2 uncatalyzed ELAT electrode from E-TEK. The anode received one paint brush applied coating of 5 wt% Nafion recast solution. A single cell assembly was prepared by pressing a Nafion 117 membrane between the anode and the cathode under 2500 pounds per square inch of pressure at 140°C for 40 sec. All fuel cell measurements were performed at 80°C. The O_2 and H_2 gas pressures were 60 and 30 psig, respectively. The O_2 and H_2 gas flow rates were 402 and 127 cm^3/min, respectively. The two gases were humidified prior to admission into the fuel cell by passing them through stainless steel containers filled with distilled H_2O kept at 105°C. Before

performing any measurements, the fuel cell was left under open circuit for 0.5h with flowing O_2 and H_2, and then the fuel cell assembly was conditionned at 0.7V for 2.5h. Next, the impedance of the fuel cell assembly was measured. Typical values obtained varied from 0.3 to 0.5 Ω/cm^2. Cell resistances obtained for each fuel cell assembly was used to iR correct the cell potential. For the hydrogen electrosorption curves, the electrochemical measurements were conducted in an air-tight three compartment electrochemical cell at room temperature. The electrolyte was H_2SO_4 at pH 0.5. The working electrode was a thin layer of Nafion impregnated catalyst cast on a vitreous carbon disk held in a Teflon cylinder.

Results and Discussion

A list of all Pt-based catalysts used in this work appears in Table 1. The same table gives the Pt content for each material as well as the Pt loading at the cathode and the specific surface area of Pt catalysts determined by electroadsorption of hydrogen. Fig.1 displays the polarization curves of all graphite-based catalysts. The open symbols represent the included Pt materials while the dark symbols refer to the supported Pt ones. The broken and dotted lines are the polarization curves obtained with ETEK5 and ETEK20, respectively. These curves are given for comparison purposes. Fig.2 displays the polarization curves for all carbon black based catalysts. The open symbols represent the included Pt materials while the dark symbols refer to the supported Pt ones. The dash-dotted, broken and dotted lines are the polarization curves obtained with ETEK2, ETEK5 and ETEK20, respectively. These curves are given for comparison purposes.

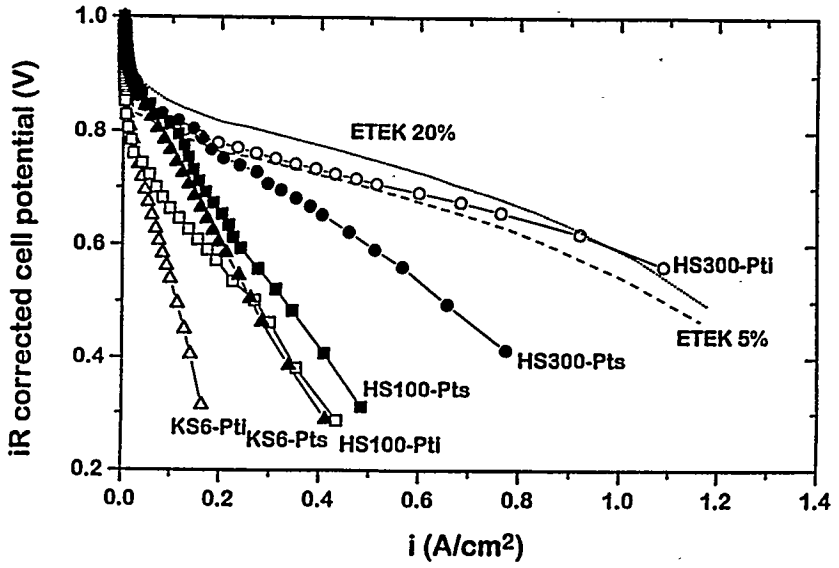

Figure 1: iR-corrected polarization curves, recorded at 80°C for H_2/O_2 , of all graphite-based catalysts. Open symbols: Pt-included materials; dark symbols: Pt-supported materials. Broken and dotted lines: ETEK5 and 20%, respectively.

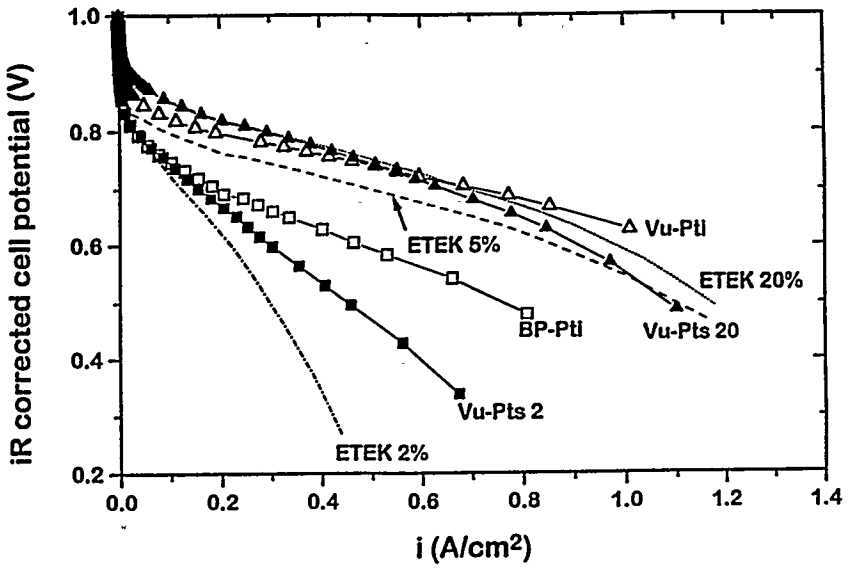

Figure 2: iR-corrected polarization curves, recorded at 80°C for H_2/O_2 , of all carbon black-based catalysts. Open symbols: Pt-included materials; dark symbols: Pt-supported materials. Broken and dotted lines : ETEK5 and 20%, respectively.

A quick examination of Figs. 1 and 2 shows that the major difference between catalyst samples, particularly in the high current region of interest to fuel cell developers, is the slope of the cathode polarization curves plotted on linear coordinates (E vs i). This linear region is typically controlled by resistive losses within the catalyst layer which are not removed by iR correction. These resistive losses are typically electrode structure related and may be either electronic (contact resistance between graphite or carbon support particles), ionic or both in nature.

From the linear region of the polarization curves plotted in Fig.1, one can deduce that: i) a higher support specific area yields higher performance for both supported or included-Pt catalysts; ii) the performance of the included Pt in KS6 (Δ) is lower than that of the supported Pt on the same material (▲). KS6 is a low specific area support (20 m^2/g). For HS300, a high specific area graphite (305 m^2/g), the contrary is true. Indeed, the catalytic activity of HS300-Pti (O) is much higher than that of HS300-Pts (●). At high current the polarization curve of HS300-Pti departs from that of ETEK5 and even crosses the polarization curve of ETEK20 above 1 A/cm^2. It is worth mentioning that HS300-Pti contains only 8.3 wt% Pt compared to 20 wt% Pt for ETEK20 (a 2.4 ratio in the Pt wt%), and that the Pt loading for HS300-Pti is 0.110 mg/cm^2 compared to 0.287 mg/cm^2 for ETEK20 (a 2.6 ratio in the Pt loading of the electrode).

From the linear region of the polarization curves plotted in Fig. 2, one can deduce that: i) considering the Pt loading of the various cathodes, Vu-Pti (Δ) displays a much better performance than either Vu-Pts (▲) or even ETEK20, especially at high currents. Indeed, Vu-Pti contains only 6.1 wt% Pt compared to 20 wt% Pt for ETEK20 (a 3.3 ratio in the Pt wt%); the Pt loading for Vu-Pti is 0.073 mg/cm^2 while it is 0.287 mg/cm^2 for ETEK20 (a 3.9 ratio in the Pt

loading of the electrode); ii) a similar observation can be made for BP-Pti (■). At equivalent Pt wt% and Pt loading on the cathode, BP-Pti performs much better performing than ETEK2. Analysis of Figs. 1 and 2 in this fashion of course assumes that the polarization of the hydrogen anode in the fuel cell is only a few mV.

Table 1
Pt content, Pt cathode loading and specific surface area of Pt-included and Pt-supported catalysts

Type of catalyst	Pt wt%	Pt at the cathode, mg/cm^2	Specific surface area m^2 of Pt/g of catalyst
Pt-included			
KS6-Pti	10.8	0.170	2.33
HS100-Pti	7.4	0.093	1.35
HS300-Pti	8.3	0.110	3.25
Vu-Pti	6.1	0.073	3.00
BP-Pti	2.4	0.025	-
Pt-supported			
KS6-Pts	20	0.280	7.31
HS100-Pts	10	0.128	5.24
HS300-Pts	10	0.129	5.39
Vu-Pts	2	0.023	1.11
Vu-Pts	20	0.240	10.21
ETEK2	2	0.024	1.33
ETEK5	5	0.075	3.40
ETEK10	10	0.128	6.37
ETEK20	20	0.287	11.33
ETEK30	30	0.377	15.10

The low current regions of Figs.1 and 2 are linear on a log i vs E plot. They are controlled by the catalyst activity. The mass and specific activities of Vu-Pti and HS-Pti are comprised between the mass and specific activities of ETEK20 and ETEK30. The low Pt content Vu-Pti and HS300-Pti catalysts are therefore active and perform well.

Bibliography

1 A. J. Appleby and E. B. Yeager in "Assessment of Research Needs for Advanced Fuel Cells", S. S. Penner, Editor, Energy II, Chap. 4 (1986).
2 W. Juda, 134th Meeting of the Electrochemical Society, Montreal, Canada, 1968.
3. S. Srinivasan, E. A. Ticianelli, C. R. Derouin and A. Redondo, *J. Power Sources*, **22**, 359 (1988).
4. A.J. Taylor, E. B. Anderson and N. R. K. Vilambi, *This Journal*, **139**, L45 (1992).
5. C. Ferreira and S. Srinivasan, in *Proceedings of the Symposium of Electrode Materials and Processes for Energy Conversion and Storage*, Edited by S. Srinivasan, D. D. Macdonald and A. C. Khandkar, The Electrochemical Society, 1994, p. 173.
6. Y. Tilquin, R. Côté, G. Veilleux, D. Guay, J. P. Dodelet and G. Dénès, *Carbon*, **33**, 265 (1995).
7. Zeng and M. J. Hampden-Smith, *Chem. Mater.*, **5**, 681 (1993).

THE CANADIAN FUEL CELL R&D PROGRAM

N. R. Beck and M. Hammerli
CANMET Energy Technology Centre
Natural Resources Canada (NRCan)
580 Booth Street, Ottawa, Ontario, Canada, K1A 0E4

ABSTRACT

This paper gives an overview of the Canadian Fuel Cell R&D Program (CFCP). The program includes both mobile and stationary applications. It is based on Canadian as well as other fuel cell technologies. The Canadian fuel cell technologies comprise the development of the Polymer Electrolyte Fuel Cell (PEFC) of Ballard Power Systems Inc., as well as the Alkaline Fuel Cell of Astris Inc. Materials development issues are an important element of the Program. An outstanding example is the creation of the new BAM3G membrane technology of Ballard Advanced Materials in support of the Canadian PEFC technology. Finally, some system successes will be highlighted.

1. INTRODUCTION

The objective of this paper is to present an overview of the Canadian Fuel Cell R&D Program with special emphasis on Canada's PEFC bus and the PEFC 200 kW Class Power Generator for distributed electricity/heat co-generation applications.

2. THE CANADIAN FUEL CELL TECHNOLOGIES

2.1. The Ballard PEFC

The main Canadian expertise in the PEFC technology rests with Ballard Power Systems. Its PEFC technology is considered by many to be the world-leading technology. The two main disadvantages of the PEFC, which are being addressed, are its high cost per kilowatt and its sensitivity to poisons in hydrogen, such as carbon monoxide in reformed natural gas or methanol, etc. Ballard recognized early in their development that the high cost is mainly due to:

(a) the relatively high platinum/precious metal electrocatalyst loadings;
(b) the relatively expensive DuPont "NafionTM" 117, and the more recent Dow Chemical perfluorinated polymer electrolyte membranes.

A research program was initiated in 1988 at Ballard Advanced Materials to address the polymer electrolyte cost issue. Five years later, a prototype of a new polymer electrolyte, designated BAM3G, has been produced by the contractor. Membrane-Electrode-Assemblies (MEA's), incorporating the new BAM3G proton exchange membrane, were fabricated using standard Ballard fuel cell electrodes. Single-cell tests of the BAM3G in a Ballard MK4 test station gave performances better than those obtained with Nafion™ 117 under identical conditions over the entire current density range, and better than those obtained with the DOW polymer electrolyte at the higher current densities. Furthermore, this performance has been maintained, within an acceptable "ageing" factor, for up to 5,000 hours at a current density of 500 ASF (amperes per

square foot). Based on these encouraging results, the monomer and polymer syntheses were recently scaled-up to produce MEA's suitable for the MK-5 Ballard stack. Longevity tests were begun with BAM3G MEA's in a six-cell commercial-size MK-5 Ballard stack in 1994 and are continuing, with encouraging results to date. Efforts are continuing to reduce the cost of producing and processing these new polymers as well as at scaling-up to kilogram quantities.

Other cost problems, such as bi-polar plates, were also identified early on in the development program and are being addressed systematically, in both Phase 2 of the Ballard Bus Program (a 40 foot/60 passenger transit bus) and stationary power plant projects, by Ballard Power Systems.

The problem of electrocatalyst poisoning is being addressed with encouraging results. Anode catalysts which are more tolerant to carbon monoxide poisoning are being investigated in conjunction with Johnson Matthey, as are methods for in-situ regeneration. *While work remains to be done in all of these areas, there do not appear to be any technical reasons why these issues cannot be solved to meet the time, performance and cost goals in the respective markets.*

2.2 The Alkaline Fuel Cell

Canada has identified possible niche markets for alkaline fuel cells for portable power systems of the order of 1 to 5 kW. Astris Inc. has been receiving R&D support for this development over the last few years. More recently, Fuel Cell Technologies are also working towards this goal.

3. OTHER FUEL CELL PROJECTS

3.1 Projects with US Fuel Cell Technologies

A 3-year project, which ends in 1996, was initiated to evaluate Westinghouse Electric's Solid Oxide Fuel Cell (SOFC) technology under modest pressures, e.g. 10 atmospheres, using Canadian natural gas as the feed. Two identical test stands have been built and commissioned at Ontario Hydro, the contractor in this Project. Each has been designed to accept SOFC tubes up to 200 cm in length. All SOFC Test Articles are supplied by Westinghouse U.S.A. free of charge to the Project and all are operated first at 1 atmosphere by Westinghouse prior to shipping and installation at Ontario Hydro. This provides valuable baseline data between the two test sites. Excellent results have been obtained to date and discussions for a possible Phase 2 are now underway as a result.

A 200 kW Phosphoric Acid Fuel Cell (PAFC) Demonstration Plant (PC-25A) from ONSI, USA was installed in late 1993 at Ontario Hydro's Central Regional Office, in Markham, (Toronto) Ontario. Commissioning started in February 1994. The fuel cell uses pure hydrogen derived from Canadian natural gas. AC electricity is fed directly into the building grid in a load-following mode. No difficulties have been observed with the plant's ability to load-follow. By-product heat at about 80 °C is delivered to the building's heating system as required, thus demonstrating co-generation. Sponsors of this project are: the Canadian Electrical Association, Consumers Gas, Natural Resources Canada, Ontario Hydro and the Ontario Ministry of Environment and Energy. The unit is expected to be moved to another potential user location by the end of December, 1996.

3.2 Hydrogen Fuel-Cell-Powered Transit Buses

The Ballard PEFC Fuel Cell Bus Program consists of four phases:

Phase 1: Proof of Concept with a 20 passenger transit bus, with traction power from fuel cells only, and with a 160 km/100 mile range. The on-board fuel is compressed hydrogen gas.

Status: Project completed in March 1993; road tests begun in February of 1993 and continuing in Phase 2.

Phase 2: A Prototype 60 passenger transit bus (standard 40-foot low floor design) with a 280 km/175 mile range. The on-board fuel is compressed hydrogen gas.

Status: The Project commenced in July 1993 and continues with testing of the 40-foot bus. The performance is equal to or better than that of an equivalent diesel powered bus with 60 passengers on-board. All traction power is supplied by the fuel cell stacks.

Phase 3: A Demonstration Fleet, based on a 75 passenger bus with fuel cell traction power only, and with a 400 km/250 mile range. The on-board fuel is compressed hydrogen gas.

Status: Began in October, 1995 and will be completed in 1997. Transit operators will be testing buses in 1997-1998 .

Phase 4: Commercial Production of a 75 passenger bus with a 560 km/350 mile range. The on-board fuel will be compressed hydrogen gas.

Status: Expected to start in 1997 with the first units available in 1998.

The Phase 1 Transit Bus, the world's first fuel-cell powered ZEV (Zero Emission Vehicle) bus, was completed on schedule and within budget. This proof-of-concept vehicle is meeting its performance targets and is providing valuable data for the subsequent phases. The fuel cell engine was designed and built by Ballard Power Systems and SAIC Canada did the systems integration, with valuable assistance from BC Transit. *Note that this bus relies solely on the Ballard PEFC stacks (24x5 kW = 120 kW) for its motive power.* Hydrogen gas, stored at 3000 psig in fibreglass-wrapped aluminum cylinders, is the on-board fuel. This storage option does, however, result in a limited but still useful range of about 160 km/100 miles. The bus has been and is operating on city streets in and around Vancouver and has been on display in several North American cities.

In Phase 2, the range is increased by using lighter hydrogen storage cylinders (all-composite construction, supplied by EDO Canada) and lighter construction materials where possible. Further, the Phase 2 bus incorporates fuel cell stacks (FCS) which are lighter and smaller per kW. Thus, the FCS for Phase 2, which are rated at 13 kW compared to 5 kW in Phase 1, require only about one half the volume. *The net result is that the Phase 2 Fuel Cell Engine fits directly into the diesel engine cavity and is mounted on tracks for easy servicing.* Much of this improvement involves materials R&D into fuel cell stack component as well as peripherals. The

trend towards larger power ratings per FCS is driven by the necessity to reduce the cost as well as volume and weight per kW. The Phase 2 bus is now undergoing street testing and is serving well as a live display. Phase 2 was sponsored by the government of British Columbia, California's South Coast Air Quality Management District and Natural Resources Canada.

Phase 3 is now also underway. The City of Chicago announced recently its intention to purchase three Phase 3 buses from Ballard Power Systems. The B.C. Transit Authority will also participate in Phase 3. It is anticipated that at least one more North American city/municipality will join Phase 3. Direct experience by transit bus operators will provide Ballard with a feed-back loop for fine tuning technical issues as well as for addressing operational issues, such as refuelling. Electrolytic hydrogen, produced on the transit bus operator's site using off-peak electricity at night is an attractive hydrogen fuel supply option. This option, as well as others, will be a small but important part of Phase 3.

3.3 The PEFC As A Stationary Power Source

Based on its success in the transportation sector, Ballard concluded that its PEFC technology is also suitable for stationary applications in the "distributed power" world-wide markets. However, to meet the cost projections, automated manufacturing, further improvements in the fuel cell stacks, improvements in natural gas processing, and systems integration would be necessary. Thus, Phase 1 of the "Utility Demonstration Project", included the construction of two prototype power plants (one based on hydrogen, the other on natural gas as the feed). Phase 1 was initiated in June, 1991 and finished on June 30, 1994. Funding for Phase 1 was provided by Western Economic Diversification (a federal agency), the Province of British Columbia and Ballard Power Systems. NRCan/CANMET provided technical advice and assistance on behalf of the federal and provincial government funding agencies of this Project.

The main deliverables from Phase 1 were a 30 kW PEFC Power Plant fed with by-product hydrogen from a chloralkali plant, and a 10 kW Subscale Engineering Plant fed with natural gas. Co-generation, load following, etc., were demonstrated on the 10 kW plant. Phase 2 consists of constructing a "Product Development 250 kW Commercial Prototype" Ballard PEFC Power Plant with natural gas as the source of hydrogen. The main focus in Phase 2, underway since mid-1994 and expected to be completed in 1997, is weight and volume reduction in order to reduce costs and decrease the foot-print.

Many technical aspects in Ballard's stationary applications program feed directly into the mobile applications program and vice-versa. Also, Ballard has allied itself with Daimler-Benz for the development of mobile applications. It has also been associated with Johnson Matthey to investigate the best manufacturable processes for the mass production of MEA's with low platinum loading but high utilization. These alliances are mutually beneficial. There is a lot of proprietary R&D on-going in both programs, much of it involving materials R&D.

4. SUMMARY

For Canada the major fuel cell activity will continue to be focussed on the Ballard PEFC "ZERO EMISSION VEHICLE" Transit Bus development. While the ZEV Bus projects were highly successful, work remains to be done to reduce the cost of the fuel cell stacks. Hydrogen

storage options for transit buses require more R&D. The compressed gas option can benefit from our experience with new compressed natural gas cylinders. Also, the development of the Ballard PEFC for stationary "distributed power" applications feeds directly into the mobile applications' program and vice-versa. The Alkaline Fuel Cell appears to be attractive as a mobile power source in the 1 to 5 kW range. R&D support to Canadian contractors for evaluating foreign fuel cell technologies is a sound investment for potential Canadian users of these technologies. This activity also creates development and business opportunities for Canadian companies in fuel cell plant sub-systems.

5. ACKNOWLEDGEMENTS

The dedication and support received from all contractors participating in the CFCP are gratefully acknowledged. Westinghouse Electric are acknowledged with thanks for their vital role in the SOFC Project, as is the South Coast Air Quality Management District for their interest in the Ballard fuel cell and for financial support of the Phase 2 Bus Project. Other co-sponsors of various projects include: BC Transit, the Canadian Electrical Association, Consumers Gas, Gas Technology Canada and its members, the Government of British Columbia, and the Ontario Ministry of Environment and Energy.

PROCESS SIMULATION OF A PEM FUEL CELL SYSTEM

K. Ledjeff-Hey[1,2], J. Roes[1], V. Formanski[1], J. Gieshoff[2], B. Vogel[2]

[1]Gerhard-Mercator-Universität - Gesamthochschule Duisburg
Fachbereich Maschinenbau, Fachgebiet Energietechnik
D-47048 Duisburg / Germany

[2]Fraunhofer Institute for Solar Energy Systems
Oltmannsstrasse 5
D-79100 Freiburg / Germany

ABSTRACT

The thermodynamic performance of a PEM fuel cell system for producing electrical power from natural gas is investigated by considering the flows of energy and exergy through the various steps of the whole system. The flows of energy are evaluated using a computer code for energy and exergy analyses. The fuel cell system is designed to produce a hydrogen volumetric flow of nearly 5.0 m^3_{NTP}/h, provided to the fuel cell at an absolute pressure of 2.9 bar. The fuel cell itself is working with an efficiency of about 60 % at an operating temperature of 65 - 75 °C with an air ratio of four and provides a maximum electric power of 9 kW. Taking into consideration only the produced electric power as useful output of the fuel cell system a total efficiency of 42.2 % is calculated using the simulation results.

INTRODUCTION

Proton Exchange Membrane (PEM) fuel cell systems offer a new and very interesting option to convert fossil fuels to electric energy with high efficiency and high power density, for example as a heat and power system or for mobile applications. Normally the fuel gas of such a low temperature fuel cell is hydrogen. Hence, a PEM fuel cell system contains a fuel gas production and purification unit, beside the fuel cell. When hydrogen is produced by natural gas steam reforming, the product gas contains fractions of carbonmonoxide, carbondioxide, unconverted hydrocarbons and other impurities beside hydrogen. Particularly carbonmonoxide poisons the catalyst layer of the fuel cell membrane. Thus, the CO fraction in the hydrogen gas must be less than 10 ppmv to properly fulfil the requirements of a PEM fuel cell. Therefore an effective gas purification is of prime importance for the proper functioning of a fuel cell system.

A PEM fuel cell needs to be supplied by fuel gas and reaction air. Also a cooling system is required. The principle processes of a PEM fuel cell system consist of the hydrogen production, the hydrogen purification and the air compression. For the production of hydrogen an integrated natural gas burner is used. The principle objective of this study is the theoretical description of each process step and the combination of both, heat and mass flow, to optimise the over all efficiency. For the above description the balances of energy and mass, and mathematical formulations for the chemical reaction kinetics are used.

PROCESS DESCRIPTION

The process flow sheet of the calculated fuel cell system is shown in Figure 1. In the first step the natural gas used for the steam reforming is compressed to an absolute pressure of 3.8 bar (K1). Catalysts are used for steam reforming and carbonmonoxide conversion. To avoid damaging of these catalysts a ZnO bed for the desulphurization has been integrated in the fuel cell system after the natural gas compressor. The steam reforming of the natural gas takes place in the reformer unit after adding the overheated process steam. The volumetric flow of the natural gas for the reforming is set to 1.3 m^3_{NTP}/h. The steam to carbon ratio is set to S/C = 3.1. The requirements described above are necessary to offer the fuel cell a hydrogen flow of 5.0 m^3_{NTP}/h. The reaction temperature

in the reformer is set to 800 °C for the calculation. The principle chemical reactions for the steam reforming are:

$$CH_4 + H_2O \Leftrightarrow CO + 3H_2 \quad , \quad \Delta_R\overline{H}^{\varnothing} = 206\ kJ/mol, \qquad (1)$$

$$CO + H_2O \Leftrightarrow CO_2 + H_2 \quad , \quad \Delta_R\overline{H}^{\varnothing} = -41\ kJ/mol. \qquad (2)$$

The posterior conversion of carbonmonoxide (2) is carried out in a high temperature step (shift 1, 320°C) and in a low temperature step (shift 2, 220 °C) and is used to increase the ratio of hydrogen and to decrease the ratio of carbonmonoxide in the product gas. In the shift reactor also a slight methanation reaction takes place. The carbondioxide scrubbing in the absorber column is carried out at an absolute pressure of 3.1 bar with an activated 40 % methyldiethanolamine solution (MDEA). This purification step correspond to a patent of the BASF AG, Ludwigshafen Germany /5/, using piperazin as activator. The overall reaction for the CO_2-scrubbing with an aqueous solution of MDEA is described by:

$$CO_2 + H_2O + R_3N \Leftrightarrow R_3NH^+ + HCO_3^- , \qquad (3)$$
$$R = C_2H_4OH .$$

The final gas purification step in this fuel cell system is the methanation to convert the residues of carbonmonoxide and carbondioxide, with hydrogen as reactant.

In addition to the purified hydrogen, the PEM fuel cell needs to be supplied with reaction air (air ratio 2 - 4). The calculations of the process in this study are based on an absolute working pressure of the fuel cell of 2.9 bar. Apart from the production of electricity the PEM fuel cell produces a significant quantity of heat. Thus, a suitable cooling system is necessary. A separate flow of cooling water is used as a heat transport medium. The process water for the steam reforming is taken out of this water stream. The reaction heat for reforming offers a natural gas burner, additionally utilising the off gas from the fuel cell.

SIMULATION METHODOLOGY

The computer code Aspen Plus® from Aspen Technology Inc. Cambridge, Mass. USA is used for the process simulation of the fuel cell system. The simulation employs definitions of the system components, data of incoming mass flows and their heat and mass linkage. The simulation methodology of the fuel cell system follows the flowsheet configuration shown in Figure 1.

The reformer furnace is modelled by an 'Equilibrium Reactor', where an isothermally reaction occurs, and a heater in which heat is transformed from the burner flue gas. The shift section is also modelled by an 'Equilibrium Reactor', where the water gas shift reaction occurs isothermally. Conversion rates and kinetic data for the parallel methanation in the shift reactors and the water gas reaction are estimated in own measurements. The estimated parameters were integrated into the computer simulation. The CO_2-scrubbing and the regeneration of the MDEA solution are modelled as a 'Rigorous Distillation' columns. The methanator is modelled as 'Equilibrium Reactor', where the methanation occurs isothermally. The compression of the natural gas and the fuel cell air is calculated as polytropic with an efficiency of 72 % (K1, K2). The efficiency of the fuel cell is determined to be 60 %. This describes the conversion of the hydrogen energy flow to electricity. The fuel cell system is calculated based on fifteen heat exchangers to consider a nearly optimised heat integration of the system.

RESULTS AND DISCUSSION

The main results of the energy and mass analyses are presented below. The computed compositions of the hydrogen gas with the volumetric flow are shown in Table 1. The energy inputs of the calculated fuel cell system are the natural gas for reforming, the natural gas for the burner, the electrical power for the air compressor, the natural gas compressor and the MDEA pump. The calculation results show a volumetric flow of 0.71 m^3_{NTP}/h for the burner fuel gas. The energy effort of the steam reforming conversion is calculated to 3.36 kJ/s, the CO shift step sets free 2.31 kJ/s and the methanator dismisses 0.07 kJ/s. The CO_2 absorption is calculated on the basis of a packed tower with five theoretical stages, operating with an absorbent circulation rate of 0.0374 m^3_{NTP}/h. 2.0 kJ/s thermal power is needed to achieve a regeneration of the aqueous solution of activated MDEA of 95 %. The necessary quantity of electrical power for the fuel cell system described as above is calculated to be 1.9 kJ/s.

Table 1: Calculated gas compositions after each process step

reaction step	product gas composition				total volumetric flow
	H_2/vol.%	CH_4/vol.%	CO /vol.%	CO_2/vol.%	m^3_{NTP}/h
steam reforming	54.03	0.44	10.35	5.74	7.860
CO conversion	64.03	0.48	0.35	15.74	7.860
CO_2 absorption	97.63	0.56	0.52	0.11	5.154
methanation	97.08	1.11	-	-	5.099

The PEM fuel cell has a maximum output of 9 kJ/s electric power. This is based on a determined efficiency of 60 % and a calculated hydrogen volumetric flow of 4.95 m^3_{NTP}/h. The over all efficiency of the PEM fuel cell system is computed to be 42.2 %. For the latter electric power is the only considered system output. The results of this study are based on the conditions described above.

References

Journal Articles

/1/ Casper, M.S. ed.; Hydrogen Manufacture by Electrolysis, Thermal Decomposition and Unusual Techniques; Park Ridge, N.Y.; Noyes Data Corp; 1978.

/2/ Glasscock, D. A.; Rochelle G.T.; AIChE Journal. Vol. 39. No. 8. 1389 - 1397; 1993.

/3/ Xu, G.; Zhang, C.; Qin, S.; Wang, Y.; Ind. Eng. Chem. Res., Vol. 31, 921 - 927; 1992.

Reports

/4/ Aspen Technology, Inc.; Aspen Plus Introductory Manual, Release 9, Volume 1; Cambridge, Mass.; 1994.

/5/ Küßner, K.; Henrici, H.; Appl, M.; Auslegungsschrift 25 51 717; Deutsches Patentamt München, 1980.

Books

/6/ Kent, J. A., ed.; Riegel's Handbook of Industrial Chemistry; 8 th ed.; Toronto, Van Nostrand Reinhold; 1983.

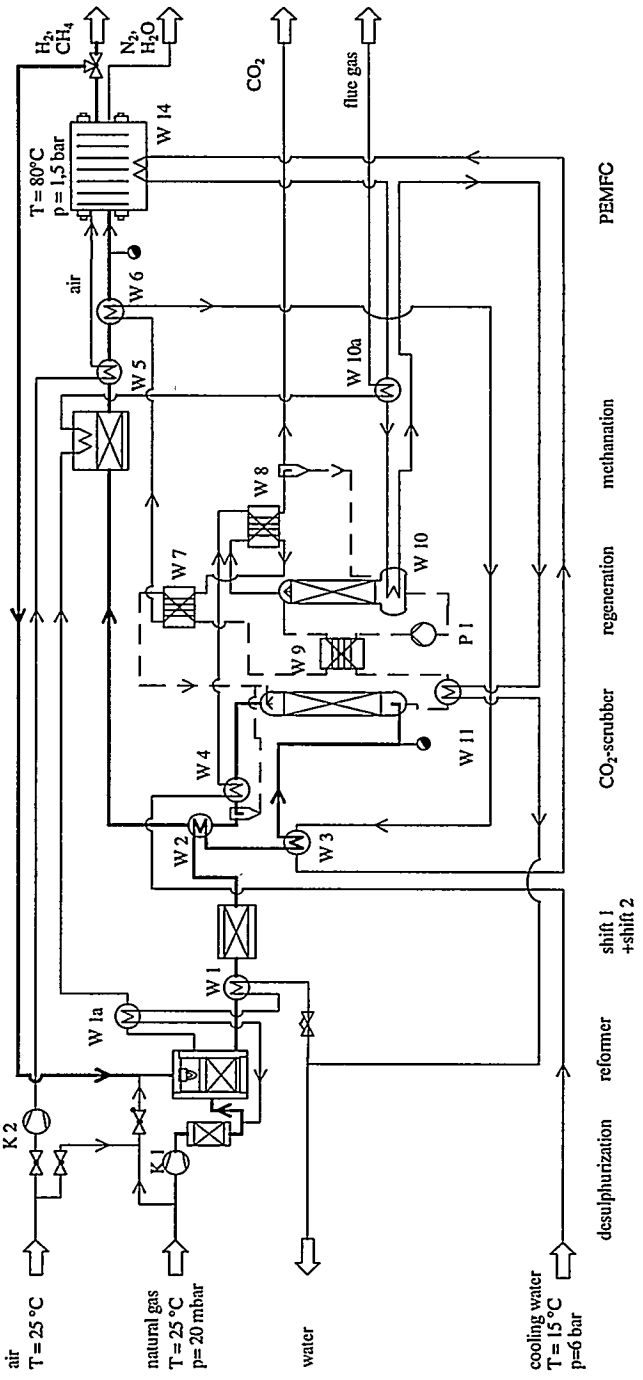

Figure 1: Process flow sheet for the simulation of the fuel cell system

DEVELOPMENT OF SMALL POLYMER ELECTROLYTE FUEL CELL STACKS

V. A. Paganin, E. A. Ticianelli and E. R. Gonzalez
Instituto de Química de São Carlos, USP
CP 780, 13560-970 São Carlos, SP, Brazil

INTRODUCTION

The polymer electrolyte fuel cell (PEFC) has been one of the most studied fuel cell systems, because of several advantages for transportation applications. Research involve fundamental aspects related to the water transport and the fuel cell reactions (1,2), the practical aspects related to the optimization of the structure and operational conditions of gas diffusion electrodes (1-6), and technological aspects related to water management and the engineering of operational sized fuel cell modules (7-13). In many of these works it is observed that very satisfactory results regarding the performance of low catalyst loading electrodes (0.15 to 0.4 mg Pt/cm^2) have been obtained in single cells (2-6). However, the use of such electrodes is not yet being considered for building fuel cell stacks and, although not usually mentioned (7-13), fuel cell modules are assembled employing electrodes presenting catalyst loadings in the range of 2 to 4 mgPt cm^{-2}.

In this work the results on the research and development of small polymer electrolyte fuel cell stacks employing low catalyst loading electrodes are described. The systems include the assembly of single cells, 6-cell and 21-cell modules. Testing of the stacks was conducted in a specially designed test station employing non-pressurized H_2/O_2 reactants and measuring the individual and the overall cell voltage versus current characteristics under several operational conditions for the system.

EXPERIMENTAL

The working electrodes were prepared by a combined filtration/brushing procedure using platinum-on-carbon (Pt/C) catalysts (E-Tek), carbon powder (Vulcan XC-72, Cabot), a carbon cloth substrate (PWB-3, Stackpole), a Polytetrafluoroethylene (PTFE) suspension (Teflon T-30, Du Pont) and a Nafion® solution (Aldrich, 5 wt.% in 10% water/low aliphatic alcohols). Except where mentioned, the electrodes employed in the modules were made with 20 wt.% Pt/C, 1.1 mg Nafion® cm^{-2}, 0.4 mg Pt cm^{-2} in the catalyst layer and with 30 % PTFE and 50μm thickness in the diffusion layer. All the details regarding the procedures for the membrane & electrode assembly preparation were presented previously (6).

The main characteristics of the fuel cell stacks are summarized in the scheme presented in Figure 1. The bipolar and end plates were fabricated using a non porous furfural impregnated graphite material in which a series/parallel flow field was machined out. The gaskets were cut out from a silicon rubber fiberglass cloth. The cells with an active electrode area (geometric) of 20 cm^2 were clamped between aluminum plates. The distribution of gases to the cells was done using an external parallel manifolding system made with stainless steel and containing individual needle valves for the control of the gas flow rates for each cell.

The cooling system was tested employing water cooling plates distributed every three cells throughout the stack. The temperature control is conducted using thermocouples inserted in pre-determined places in the 6 and 21 cells stacks. The principle of operation is based in a constant coolant flow on/off concept, set to establish a maximum range of ± 3 °C in the highest point of the fuel cell operating temperature.

Humidification of the reactants was carried out by bubbling the gases through water contained in stainless steel bottles thermostated to the desired temperature. Measurements of the cell potential

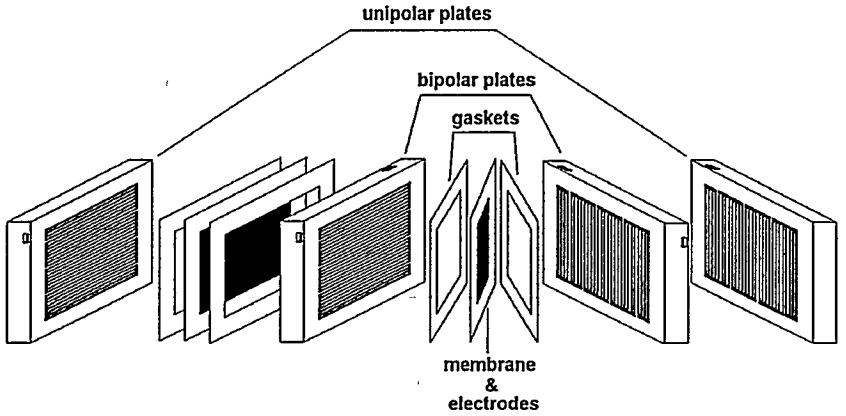

Figure 1 - Scheme of the configuration of the multi-cell stacks.

as a function of the current density were made galvanostatically using an electronic load (HP-6050A, Hewlett Packard) and an IBM-PC compatible microcomputer equipped with a digital I/O and multiplexer plate (DAS-1600, Keithley). Testing of the stacks was conducted in a specially designed test station (14) employing non-pressurized H_2/O_2 reactants.

RESULTS AND DISCUSSION

Figure 2 shows the cell potential vs. current density characteristics obtained at several cell and humidification temperatures for the single cells with 5 and 20 cm^2 electrodes assembled with Nafion 117 membrane. The results obtained at a cell temperature of 80 °C with the humidifiers at T_{H2} = 95 °C and T_{O2} = 85 °C show that the increase in the electrode area from 5 to 20 cm^2 resulted in a small diminution in the performance of the system. Fig. 2 also shows that for T = 80 °C a pronounced decrease in the performance is observed when the humidification of the reactant gases is carried out at the same temperature of the cell. However, the situation is less critical for lower temperatures, although a leveling of the performance occurs for temperatures below 70 °C.

The average cell potential vs. current density characteristics at 80 °C of the single cells with 5 and 20 cm^2 electrodes and of the 6 cell stack with 20 cm^2 electrodes assembled with Nafion 115 membrane are presented in Figure 3. It is observed that in the case Nafion 115, there is also a diminution of the single cell performance when the electrode area is increased from 5 to 20 cm^2, although the performance of the 20 cm^2 cell presents better characteristics with Nafion 115 than with Nafion 117. On the other hand it is seen that, for current densities up to 0.5 A/cm^2, the increase in the number of cells from 1 to 6 introduces only a small decrease in the cell performance.

Figure 4 presents the effect of temperature on the performance of the 21 cell stack assembled using Nafion 115 membrane and electrodes with 20 cm^2. It is observed that the average performance of the individual cells is smaller than those of the single cell or those of the 6-cells stack. It is also seen that the increase of temperature presented a positive effect only up to 50 °C, after which a leveling occurs in the system performance.

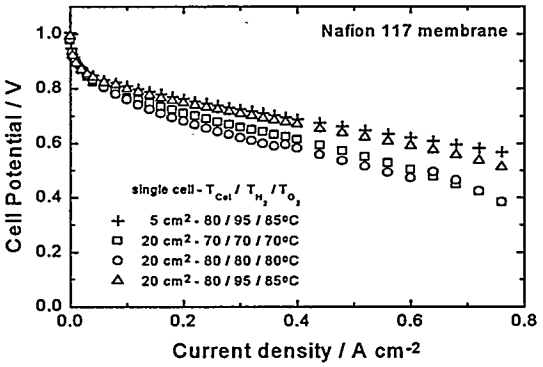

Figure 2 - Cell potential vs. current density plots for the single cells with 30 wt.% Pt/C, 0.8 mg Nafion/cm^2 electrodes.

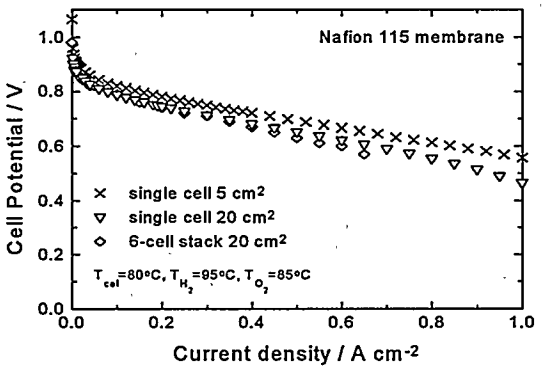

Figure 3 - Average cell potential vs. current density plots for the single cells and 6-cells stack.

The following observations can be made from the results of this work: (i) for Nafion 117, the scale-up of the electrodes from 5 to 20 cm^2 introduced a small increase in the slope of the linear region of the polarization curves which is an indication of an increase of electrolyte resistance probably associated with the water balance; (ii) for Nafion 115, the effect of the electrode scale-up is related to a parallel shift of the curves, probably associated with some gas cross-over and/or a diminution of platinum effective area; (iii) the increase in the number of cells in the stack leads to a increase in the slope of the linear region indicating problems regarding the water management; (iv) the performance of the several stacks assembled in this laboratory with low catalyst loading electrodes showed that the power generation is of the order of 0.35 kW/gPt at 0.5 A/cm^2. In the same region of current densities, the values reported for high platinum loading electrodes are in the range of 0.05 to 0.1 kW/gPt (7-13) thus showing that utilization of low catalyst loading electrodes provides a better situation with respect to platinum utilization.

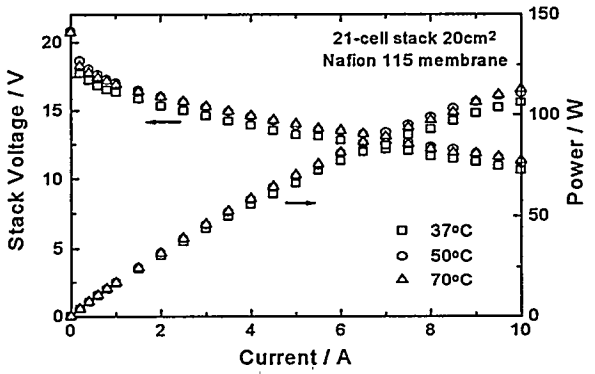

Figure 4 - Voltage and Power of the 21-cells stack as a function of current. Hydrogen humidified at 15 °C and oxygen humidified at 5 °C above the cell temperature.

ACKNOWLEDGMENTS

The authors wish to thank the Fundação de Amparo à Pesquisa do Estado de São Paulo (FAPESP), Conselho Nacional de Desenvolvimento Científico e Tecnológico (CNPq), and Financiadora de Estudos e Projetos (FINEP) for financial assistance.

REFERENCES

1. S. Gottesfeld, G. Halpert and A. Landgrebe (Eds.), *Proton Conducting Fuel Cells*, The Electrochemical Society, NJ, (1995).
2. M. Uchida, Y. Aoyama, N. Eda, and A. Ohda, *J. Electrochem. Soc.*, **142** (1995) 463.
3. P. G. Dirven, W. J. Engelen, C. J-M. Van Der Poorten, *J. Applied Electrochem.*, **25** (1995) 122.
4. S. Miachon and P. Aldebert, *J. Power Sources*, 56 (1995) 31.
5. T. N. Veziroglu, C. L. Winter, J. P. Baselt, and G. Kreysa (Eds.), *Hydrogen Energy Progress XI*, International Association of Hydrogen Energy, Vols. 1-3 (1996).
6. V. A. Paganin, E. A. Ticianelli, and E. R. Gonzalez, *J. Applied Electrochem.*, 26 (1996) 297.
7. D. P. Wilkinson, H. H. Voss and K. Prater, *J. Power Souces*, 49 (1994) 117.
8. D. R. Brighton, G. A. Clark, M. J. M. Rowan, and P. L. Mart, *1994 Fuel Cell Seminar Abstracts*, San Diego, CA, 1994, p. 547.
9. S. Galli and L. Barberini, *1994 Fuel Cell Seminar Abstracts*, San Diego, CA, 1994, p.527.
10. W. Urabe, S. Maruyama, A. Kusunoki, and J. Ohtuki, 1994 Fuel Cell Seminar Abstracts, San Diego, CA, 1994, p. 311.
11. F. Vermeulen, *1994 Fuel Cell Seminar Abstracts*, San Diego, CA, 1994, p. 635.
12. C. Mantegazza and A. Maggiore, in *Hydrogen Energy Progress XI*, T. N. Veziroglu, C. L. Winter, J. P. Baselt, and G. Kreysa (Eds.), International Association of Hydrogen Energy, Vol. 2 (1996) 1647.
13. J. Scholta, M. V. Lüttichau, and B. Rohland, in *Hydrogen Energy Progress XI*, T. N. Veziroglu, C. L. Winter, J. P. Baselt, and G. Kreysa (Eds.), International Association of Hydrogen Energy, Vol. 2 (1996) 1957.
14. V. A. Paganin, T. J. P. Freire, E. A. Ticianelli and e. R. Go nzalez, *Int. J. Hydrogen Energy*, submitted.

EFFECTS OF MICROSTRUCTURE ON CARBON SUPPORT IN THE CATALYST LAYER ON THE PERFORMANCE OF POLYMER ELECTROLYTE FUEL CELLS

Makoto Uchida, Yuko Fukuoka, Yasushi Sugawara, Nobuo Eda, and Akira Ohta
Technology Laboratory, Matsushita Battery Ind. Co., Ltd.
1, Matsushita-cho, Moriguchi, Osaka, 570, Japan

INTRODUCTION

In the case of the Polymer-electrolyte fuel cells (PEFCs), the reaction sites exist on the platinum (Pt) surface covered with PFSI. Though PFSI membrane is used as an electrolyte of the PEFC, the membrane does not soak deeply into the electrodes as a liquid electrolyte does. Therefore, PFSI solution was impregnated into the catalyst layers to increase the contact areas between Pt and PFSI. In our previous work [1] we proposed a new preparation method of the M&E assembly which emphasized the colloid formation of the PFSI to optimize the network of PFSIs in the catalyst layer and also to simplify the fabrication process of the M&E assembly. Following this work, we focused on the microstructure of the catalyst layer. The importance of the morphological properties of the gas-diffusion electrodes on performance has been reported in several papers. The catalyst layer was claimed to have had two distinctive pore distributions with a boundary of ca. 0.1 μm. The smaller pore (primary pore) was identified with the space in and between the primary particles in the agglomerate of the carbon support and the larger one (secondary pore) was that between the agglomerates. [2] In our recent work, [3] we reported that the PFSI was distributed only in the secondary pores, and the reaction sites were therefore limited to that location. The results indicated that the PEFC system required a particular design rather than a conventional one [2] for the fuel cells with liquid electrolytes. We proposed that novel structure and/or preparation methods of the catalyst layer were keys to higher utilization of Pt.

EXPERIMENTAL

Twelve carbon supports with different specific surface areas (Sc) were chosen as electroconductive carbon blacks. The carbon blacks were produced by the oil-furnace process or acetylene process. The supported Pt catalysts (Pt-C) were prepared according to a colloidal method in the literature. [4] The PFSI solution: an experimental Flemion® solution (Asahi Glass) was used and poured into butyl acetate. The mixture changed immediately to a colloidal state. Then the Pt-C made of various carbon blacks were mixed with the PFSI colloidal solution. As a result of cross-linking among the PFSI chains adsorbed on the carbon supports by ultrasonic treatment, the mixture was transformed to a paste. The paste was uniformly spread over the wet-proofed carbon paper (Toray) for a gas-diffusion layer. The electrodes layered with the paste were hot pressed on both sides of a PFSI membrane. The membrane thickness of Flemion A (experimental membrane, Asahi Glass) was 80 μm in a dry state, and the equivalent weight value was 900. Identical electrodes were used for an anode and a cathode. The Pt-loading was 0.5 mg/cm^2 per electrode, and the PFSI content ranged from 0.1 to 2.0 mg/ cm^2 per electrode. A single cell was constructed with the M&E assembly, two porous carbon plates with rib-channel patterns on one side for gas supply, two glassy carbon frames, and two copper current collectors. The cell was compressed between two stainless steel end plates. The cell temperature was held at 50 °C throughout the experiment. The geometric reaction-area of the cell was 25 cm^2. The reactant gases (hydrogen/oxygen) were fed to the cell at a flow rate of 350 ml/min. The gas-outlets from the cell were opened to the atmosphere. The anode gas and the cathode gas were humidified by being flowed through water held at 60 °C in glass bottles under atmospheric pressure prior to being provided to the cell. Electrochemical measurements of the single cell were done galvanostatically. The current was increased stepwise every 15 minutes, and the potential was logged in the steady state. All of the denoted polarization curves contained IR resistance. The resistance of the cell was measured at 1 kHz under load by a digital ac milliohmmeter. The pore-size distribution and the specific pore volume were calculated from an intrusion curve obtained by a mercury pore sizer. The specific surface area (Sc) and the pore volume distribution of the carbon blacks were measured by an N_2 adsorber and calculated by the Brunauer-Emmet-Teller (BET) and Barrett-Joyner-Halenda (BJH) equations. The Pt mean diameter and the Pt surface area of the Pt-C were

measured by a CO adsorber. A particle-size distribution of the PFSI colloid made from the Flemion solution and butyl acetate was measured by a dynamic light-scattering spectrophotometer with Ar laser.

RESULTS AND DISCUSSION

Effects of the PFSI content on the pore volume distribution in the membrane/electrode assemblies and modeling the internal structures of the catalyst layer. —The specific pore volume distributions of the M&E assemblies with various PFSI content and an experimental acetylene black (AB18, Sc 835 m^2/g, Denkikagaku Kogyo) showed three pore zones which had critical boundaries at ca. 0.04 and 1.0 μm, and had peaks in pore-size distribution from 0.02 to 0.04 μm. The specific pore volume from 0.04 to 1.0 μm decreased with an increase of the PFSI content. Pores larger than 1.0 μm are from the carbon paper. We define the pores f rom 0.02 to 0.04 μm to be the "primary pores", and the pores from 0.04 to 1.0 μm, the "secondary pores" in the PEFC. The volume of the secondary pores linearly decreased with the increase of the PFSI content but that of the primary pores remained unchanged. The particle size distribution of the PFSI colloid consisted chiefly of the primary particles with a mean diameter about 0.043 μm. The schematic internal structures of the catalyst layer with Pt-C agglomerate are illustrated in Fig. 1, one with a liquid electrolyte (Fig. 1a) and the other with a polymer electrolyte (Fig. 1b). From these results, it should be emphasized that the PFSI added to the catalyst layer exists only in the secondary pores and not in the primary pores (Fig. 1b). We proposed that the secondary pores behaved as reaction sites in the PEFC, because the electrolyte (PFSI) existed only in there. Watanabe *et al.* [2] reported that the primary pores work as a "reaction volume" and the secondary pores as main gas channels in fuel cells with liquid electrolytes (e.g. PAFC) (Fig. 1a). As for this difference between our results and Watanabes', the former was a polymer and the latter liquid. It seemed that the PFSI was not able to penetrate into the primary pores (< ca. 0.04 μm) in contrast to phosphoric acid, because a particle size of the PFSI (ca. 0.04 μm) was larger than a molecular size of phosphoric acid. This suggested that the Pt particles loaded inside the agglomerate did not take part in the reaction, since the inside Pt particles were out of contact with the polymer electrolyte.

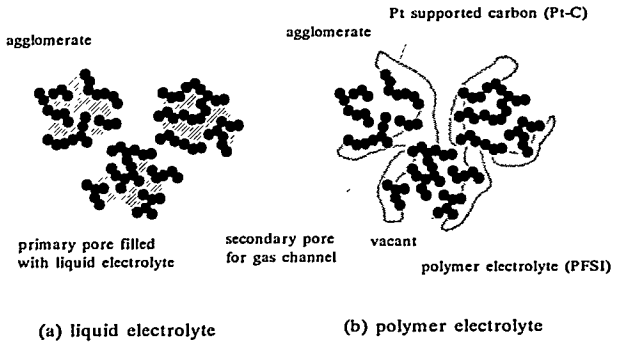

Fig. 1. Schematic of the internal structure of the catalyst layer.

Effect of the carbon supports on the cell performance. —The effects of the carbon supports on the polarization curves are shown in Fig. 2. The influence of the carbon blacks on PEFC performance was remarkable. Cells with acetylene blacks had better performance than those with

oil-furnace blacks. Differences in the electrochemical characteristics of the cells with the furnace blacks were large; cells with Ketjen black 600JD, N330, #3950, and Black pearls 2000 hardly discharged. Their adhesive strengths between membrane and electrode were very weak; some electrodes peeled off the membrane. Those electrodes simultaneously caused floodings in their gas channels.

Effects of the carbon supports on the pore-volume distribution in the catalyst layer. — The relationship between the specific pore volume in the pore zone of from 0.04 to 1.0 μm and the current densities of the cells at 850 mV (IR-free) in a charge transfer control region are shown in Fig. 3. Data with the PFSI content 1.0 mg/cm^2 were plotted with the legend ●, and the data with increased PFSI content (shown in figure) were with the legend ⊙. Performance of the cells with the PFSI content of 1.0 mg/cm^2 increased with the specific pore volume up to 0.070 cm^3/g, and then decreased, while performance with the PFSI content from 1.2 to 2.0 mg/cm^2 increased with specific pore volume. Current density increased linearly with specific pore volume. It seems that the reaction area comprised of PFSI and Pt increased ordinarily with pore volume, but excessive pore volume caused shortage of PFSI even when the content was 1.0 mg/cm^2. A proper addition of PFSI to the catalyst layer regained the continuity of PFSI and thus the interface between the PFSI and the Pt, and then the reaction area increased. From these results, it should be emphasized that the improvement of the PEFC performance was achieved by the optimal carbon support with larger pore volume able to distribute the PFSI over the Pt inside the agglomerate. [5]

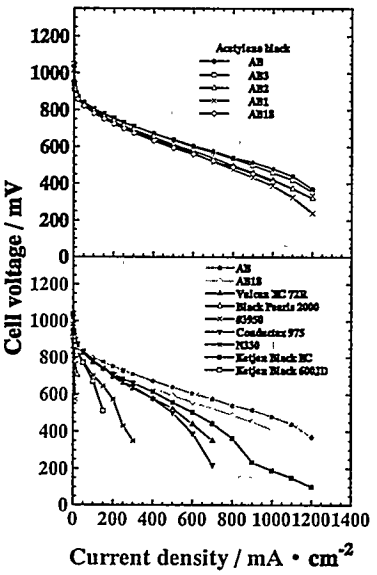

Fig. 2. Effects of the carbon supports on the polarization curves of the cells comprised of Flemion PFSI 1.0 mg/cm^2.

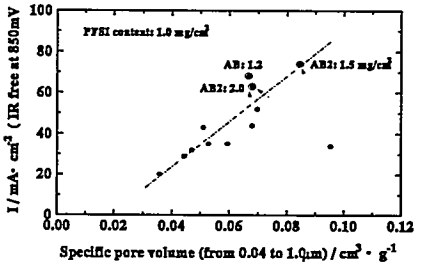

Fig. 3. Relationship between the specific pore volume in the pore zone (0.04 to 1.0 μm) and the current densities at 850 mV : (●) PFSI content 1.0 mg/cm^2 and (⊙) 1.2, 1.5, 2.0 mg/cm^2.

Effect of the carbon supports on the pore-volume distribution on the surface of the carbon blacks. — The specific pore volume distributions of the carbons were measured by N_2 adsorption and were calculated by the BJH method. Pore volumes of the carbon blacks consisted chiefly of pores smaller than 8 nm. The primary particle diameter of the carbon blacks ranged from 10 to 40 nm. Almost all the pores of the carbons seemed to be in the primary particles. Pore volume increased with the surface area of carbon black. Most of their surface area was in pores smaller than 8 nm. The Pt in these pores (< 8

nm) is considered not to contribute to the reaction for the PEFC stated above, because the particles of the PFSI are larger than the pore diameters and Pt can not contact the PFSI. The relationship between the specific pore volume in the pores smaller than 8 nm of the carbon blacks and the current densities of the cells with those carbons at 850 mV (IR-free) are shown in Fig. 4. Current density at 850 mV decreased with an increase of specific pore volume (< 8 nm). A tendency for the reaction area of the cell to decrease with increase the specific pore volume seems real. AB had both the smallest specific pore volume and the smallest specific surface area. The Pt particles were smaller than the pore diameter (< 8 nm) at the entrance could be adsorbed on the very surfaces of the pores. The rate of Pt in the pores seemed generally to increase with the specific pore volume, because the Pt loading was fixed at 0.5 mg/cm^2. Consequently, it should be emphasized that improvement of the PEFC performance was achieved by optimal carbon support with smaller pore volume on the surface of the carbon primary particles, like acetylene blacks, so as to decrease the Pt absorbed in the small pores which the PFSI could not soak into. [5]

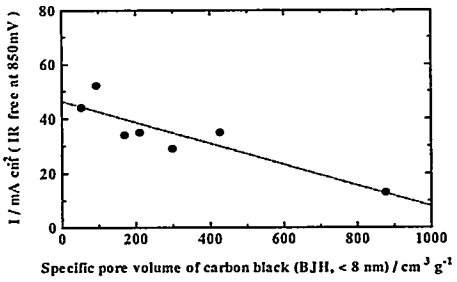

Fig. 4. Relationship between the specific pore volume of pores smaller than 8 nm in the carbon blacks and current densities at 850 mV.

CONCLUSIONS

In the pores (0.04 to 1.0 μm) where PFSI existed, specific pore volumes of the M&E assemblies with acetylene blacks were larger than those with furnace blacks. The reaction areas of the cells with the proper PFSI content increased linearly with specific pore volume. Improvement of PEFC performance was achieved by optimal carbon support with a larger pore volume able to distribute the PFSI over Pt inside the agglomerate.

Current density at 850 mV decreased with an increase of specific pore volume (< 8 nm). This tendency means that the reaction area of the cell to decrease with an increase in specific pore volume. Improvement of PEFC performance was achieved by optimal carbon support with smaller pore volume (< 8 nm) on the surface of the carbon primary particles so as to decrease Pt absorbed in the small pores where PFSI could not be absorbed.

REFERENCES

1. M. Uchida, Y. Aoyama, N. Eda, and A. Ohta, "New Preparation Method for Polymer-Electrolyte Fuel Cells," J. Electrochem. Soc., Vol. 142, No. 2, pp. 463-468, Feb. 1995.
2. M. Watanabe, M. Tomikawa, and S. Motoo, "Experimental Analysis of the Reaction Layer Structure in a Gas Diffusion Electrode," J. Electroanal. Chem., Vol. 195, pp. 81-93, 1985.
3. M. Uchida, Y. Aoyama, N. Eda, and A. Ohta, "Investigation of the Microstructure in the Catalyst Layer and Effects of Both Perfluorosulfonate Ionomer and PTFE-Loaded Carbon on the Catalyst Layer of Polymer Electrolyte Fuel Cells," J. Electrochem. Soc., Vol. 142, No. 12, pp. 4143-4149, Dec. 1995.
4. G. Petrow and R. J. Allen, U. S. Patent, No. 4044193 (1977).
5. M. Uchida, Y. Fukuoka, Y. Sugawara, N. Eda, and A. Ohta, "Effect of Microstructure of Carbon Support in the Catalyst Layer on the Performance of Polymer-Electrolyte Fuel Cells," J. Electrochem. Soc., Vol. 143, No. 7, pp. 2245-2252, July 1995.

PREPARATION METHOD OF ULTRA LOW PLATINUM LOADING ELECTRODES FOR POLYMER ELECTROLYTE FUEL CELLS

Yuko Fukuoka, Makoto Uchida, Yasushi Sugawara, Nobuo Eda, and Akira Ohta
Technology Laboratory, Matsushita Battery Ind. Co., Ltd.
1, Matsushita-cho, Moriguchi, Osaka, 570, Japan

Polymer electrolyte fuel cells (PEFCs) necessitates platinum (Pt) catalyst for its operating temperature. It is important to enhance the utilization of Pt for the cost. The reaction sites exist on the Pt surface covered with perfluorosulfonate ionomer (PFSI) in PEFC. PFSI solution was usually impregnated into the catalyst layers to increase the contact areas. We proposed a preparation method of the M&E assembly which emphasized the colloid formation of the PFSI to optimize the network of PFSIs in the catalyst layer.[1] After this work, we focused on the microstructure of the catalyst layer. We recently reported that the PFSI was distributed only in the pores formed between the agglomerates, and the reaction sites were therefore limited to that area.[2] The results indicated that the PEFC system required a particular design compared with a conventional one [3] with liquid electrolytes. We proposed novel structure and/or preparation methods of the catalyst layer to be key issues to get higher Pt utilization. We studied the effect of the carbon support on the cell performance. [4] The performance was improved by an optimal carbon support : that has (*i*) a larger pore volume (0.04 to 1.0 μm in diameter) able to be distributed the PFSI and (*ii*) smaller pore volume (< 8 nm in diameter) on the surface of the carbon primary particles. We report here the high dispersion method of the PFSI colloid to lower Pt loading with optimal carbon support.

EXPERIMENTAL

The supported Pt catalysts (Pt-Cs) were prepared according to a colloidal method in the literature. [5] The PFSI solution: an experimental Flemion® solution (Asahi Glass) was poured into butyl acetate. The mixture changed immediately to a colloidal state. Then the Pt-Cs of various acetylene blacks (Denki Kagakukogyo) were mixed with the PFSI colloidal solution. As a result of cross-linking among the PFSI chains adsorbed on the carbon supports by ultrasonic treatment, the mixture was transformed to a paste. The paste was uniformly spread over the wet-proofed carbon paper (Toray) for a gas-diffusion layer. The electrodes layered with the paste were hot pressed on both sides of a PFSI membrane. The membrane thickness of Flemion A (experimental membrane, Asahi Glass) was 80 μm in a dry state, and the equivalent weight value was 900. Identical electrodes were used for an anode and a cathode. The new method for preparation of electrodes was improvement of the previous one. The PFSI solution was dropped into the mixture of Pt-C and butyl acetate while stirring. After that, the mixture was treated with ultrasonication and M&E assembly was made in the same way as the previous method. A single cell was constructed with the M&E assembly, two porous carbon plates with rib-channel patterns on one side for gas supply, two glassy carbon frames, and two copper current collectors. The cell was compressed between two stainless steel end plates. The cell temperature was held at 50 °C throughout the experiment. The geometric reaction-area of the cell was 25 cm^2. The reactant gases (hydrogen/oxygen) were fed to the cell at a flow rate of 350 ml/min. The gas-outlets from the cell were opened to the atmosphere. The anode and the cathode gases were humidified by being flowed through water held at 60 °C in glass bottles under atmospheric pressure prior to being provided to the cell. Electrochemical measurements of the single cell were done galvanostatically. The current was increased stepwise every 15 minutes, and the potential was logged in the steady state. All of the denoted polarization curves contained IR resistance. The resistance of the cell was measured at 1 kHz under load by a digital ac milliohmmeter. The pore-size distribution and the specific pore volume were calculated from an intrusion curve obtained by a mercury pore sizer.

RESULTS AND DISCUSSION

Modeling the internal structures of the catalyst layer. — The cells with acetylene blacks gave good performance in our study of the carbon supports. [4] The specific pore volume distributions of the

M&E assemblies with various acetylene blacks are shown in Fig. 1.AB is commercial acetylene black and the others are experimental ones. The peak diameters of the pores of M&E assemblies with AB2, AB3, and AB were ranged from 0.04 to 1.0 μm where the PFSI was distributed. [1] And those with AB1 and AB18 were on the boundary and out of the range, respectively. Peak diameter depends on the size of the pores formed on and between the primary particles in the agglomerate of the carbon support (the primary pore). [3] This result means that the PFSI was distributed both inside and outside the agglomerates with AB1, AB2, AB3, and AB, but it was distributed only outside the agglomerates with AB18. The schematic internal structure of catalyst layer is illustrated in Fig. 2, one with AB18 and the other with AB. AB18 was the carbon support in our study of the PFSI distribution in the catalyst layer.[2] The best performance was achieved with AB on the effect of carbon supports. The Pt particles inside the agglomerates of AB18 did not take part in the reaction in the catalyst layer because the PFSI was not distributed there. On the other hand, AB has large primary pores able to be distributed the PFSI. The Pt particles both inside and

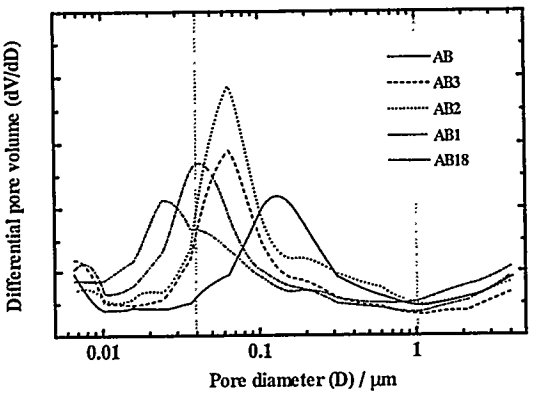

Fig. 1 Specific pore volume distributions of various acetylene blacks.

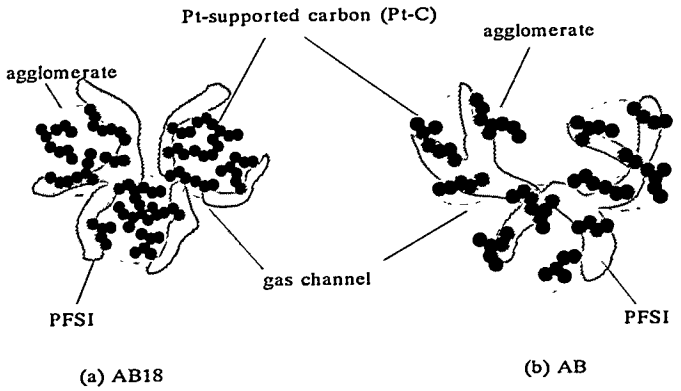

Fig.2 2D-Schematic internal structure of the catalyst layers.

outside the agglomerates of AB were covered with the PFSI in the catalyst layer. Furthermore, AB has smaller pore volume on the surface of carbon primary particles. [4] Pt particles in those pores are out of contact with the PFSI. The active surface area and the Pt utilization of the cell with AB were higher than that with AB18.

Effect of the preparation method of the catalyst layer on the cell performance. — The polarization curves of the cells in table 1 are shown in Fig. 3. The performance of the cell C was inferior to that of the cell A. Though the carbon support was optimized, the cell with lowered Pt loading did not achieve the sufficient performance. The preparation method was improved with AB in order to increase the reaction area. The performance of the cell D was superior to that of the cell A. The current densities at 850 mV(IR free) of the cell C and D were 9 mA/cm^2 and 11.5 mA/cm^2, respectively. Furthermore, the voltage at 1200 mA/cm^2 of the cell D was equal to that of the cell B. In the EPMA line analysis of the cross section of M&E assemblies, the thickness of the catalyst layer of the cell B and D were about 45 and 50 μm. The Pt content of Pt-C with 0.1 mgPt/cm^2 was lower than that with 0.5 mgPt/cm^2 . The reaction area increased and the supply of the reaction gases to the reaction sites were improved even the thickness of the catalyst layer kept unchanged. In the previous method the PFSI colloid coagulated before being adsorbed immediately on Pt-C. While in the improved method the PFSI solution was dropped into the mixture of Pt-C and butyl acetate. The PFSI colloid right after formation was adsorbed on Pt-C before coagulation and dispersed on Pt-C finely. The thickness of the PFSI on Pt particles got thinner due to the high dispersion of the PFSI on Pt-C. Consequently, the high performance of the cell with ultra low Pt loading was achieved.

Table 1 Specification of the cells.

cell	Pt loading mg/cm^2	carbon support	preparation method
A	0.5	AB18	previous
B	0.5	AB	previous
C	0.1	AB	previous
D	0.1	AB	improved

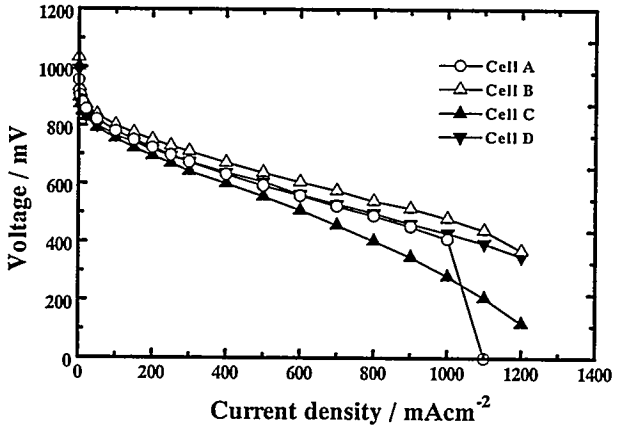

Fig. 3 Polarization curves of various cells.

CONCLUSION

The performance of PEFC with 0.1 mgPt/cm^2 was superior to that with 0.5 mgPt/cm^2 by the followings reasons: (i) optimized carbon support and (ii) improvement of the preparation method of the M&E assembly. In the improved method, the PFSI colloid right after formation was adsorbed immediately on Pt-C before coagulation of the colloids. The PFSI was dispersed on Pt-C finely and the thickness of the PFSI on the Pt particles got thinner. Consequently, the reaction area increased and the supply of the reaction gases was improved.

REFERENCES

1. M. Uchida, Y. Aoyama, N. Eda, and A. Ohta, "New Preparation Method for Polymer-Electrolyte Fuel Cells," J. Electrochem. Soc. , Vol. 142, No. 2, pp. 463-468, Feb. 1995.
2. M. Uchida, Y. Aoyama, N. Eda, and A. Ohta, "Investigation of the Microstructure in the Catalyst Layer and Effects of Both Perfluorosulfonate Ionomer and PTFE-Loaded Carbon on the Catalyst Layer of Polymer Electrolyte Fuel Cells," J. Electrochem. Soc. , Vol. 142, No. 12, pp. 4143-4149, Dec. 1995.
3. M. Watanabe, M. Tomikawa, and S. Motoo, "Experimental Analysis of the Reaction Layer Structure in a Gas Diffusion Electrode," J. Electroanal. Chem. , Vol. 195, pp. 81-93, 1985.
4. M. Uchida, Y. Fukuoka, Y. Sugawara, N. Eda, and A. Ohta, "Effect of Microstructure of Carbon Support in the Catalyst Layer on the Performance of Polymer-Electrolyte Fuel Cells," J. Electrochem. Soc. , Vol. 143, No. 7, pp. 2245-2252, July 1996.
5. G. Petrow and R. J. Allen, U. S. Patent, No. 4044193 (1977).

HIGH PERFORMANCE RADIATION-GRAFTED MEMBRANES AND ELECTRODES FOR POLYMER ELECTROLYTE FUEL CELLS

Shinji Nezu , Hideo Seko, Masaki Gondo, and Naoki Ito
IMRA Materials R&D Co., Ltd.
5-50 Hachiken-cho
Kariya, Aichi 448 JAPAN

INTRODUCTION

Polymer electrolyte fuel cells (PEFC) have attracted much attention for stationary and electric vehicle applications. Much progress has been made to improve their performance recently. However there are still several problems to overcome for commercialization. Among them, the cost of polymer electrolyte membranes seems to be rather critical, because a cost estimate of a practical fuel cell stack shows that the membrane cost must be reduced at least by two orders of magnitude based on current perfluorosulfonic acid membranes eg. Nafion®. Thus the development of new membrane materials is strongly desired. Styrene grafted tetrafluoroethylene-hexafluoropropylene copolymer (FEP) membranes have been studied for a fuel cell application by G. Scherer et al. (1). These authors showed that membranes obtained by radiation grafting served as an alternative membrane for fuel cells although there were several problems to overcome in the future. These problems include shorter life time which was concluded to result from the decomposition of grafted polystyrene side chains. We report here the performance of our fuel cells which were fabricated from our radiation grafted membranes (IMRA MEMBRANE) and gas diffusion electrodes.

EXPERIMENTAL

Membrane synthesis

The following four different types of membranes were prepared by radiation graft polymerization:
sulfonated styrene grafted polytetrafuloroethylene (PTFE)
sulfonated styrene grafted tetrafluoroethylene-perfluoroalkylvinylether copolymer (PFA)
sulfonated styrene grafted tetrafluoroethylene-hexafluoropropylene copolymer (FEP)
sulfonated styrene grafted terafluoroethylene-ethylene copolymer (ETFE).

A matrix film (PTFE, PFA, FEP, or ETFE) of 50 μm in thickness was irradiated by gamma ray (^{60}Co). The irradiated film was contacted with styrene for graft polymerization. The styrene grafted film was sulfonated using a chlorosulfonic acid solution and then hydrolyzed with a potassium hydroxide solution.

Gas diffusion electrodes and cell assembly

A carbon black/PTFE composite sheet of 100 μm in thickness was used for an electrode substrate. The sheet of 36.5mm in diameter ($10cm^2$) was dipped with a H2PtCl6 solution, dried, and then reduced in H2 gas flow to form a platinum catalyst layer. Platinum loading amount was $0.5mg/cm^2$. A Nafion solution was impregnated onto the catalyst layer. A cell assembly was prepared by hot pressing of a electrolyte membrane, gas diffusion electrodes, and electricity collectors (230μm carbon paper with PTFE).

Ceil operation

Fuel cells were operated with either H2/O2 gases or H2/Air gases at the pressures of 1.0 to 1.5 atm. The gases were humidified with water bubblers. The cell temperatures ranged between 55 and 75 °C depending on other conditions. Current density and cell voltage characteristics were recorded to evaluate cell performance.

RESULTS AND DISCUSSION

Among four different matrix films employed for styrene grafting, only ETFE matrix films gave electrolyte properties necessary for fuel cells, resulting in cell performance which was comparable or superior to conventional perfluorosulfonic acid membranes. The most difficult problem we encountered with other matrix films PTFE, FEP, and PFA is the lack of mechanical strength. With PTFE and PFA, we could not prepare electrolyte membranes which had both electrical conductivity as high as the conventional membranes and enough mechanical strength enabling cell fabrication. Appreciable decrease in strength was found for these matrix films after gamma ray irradiation of even 20 kGy, followed by the increase in brittleness after subsequent reactions. Although the above problem was relatively lightened with FEP, we often encountered the difficulties such as membrane tearing during hot pressing or cell operation, and rapid increase in electrical resistance in the time range of several tens of hours. Thus we chose ETFE as a matrix film for further work. Table 1 shows some of properties of IMRA MEMBRANE.

Table 1. Properties of IMRA MEMBRANE

Thickness (μm)	75 μm in dry
Ion exchange capacity	2.1 meq/g (EW: 480)
Resistance	0.3 $\Omega \cdot cm^2$ in 1M NaCl at 25 °C at 1000 Hz
Water content	80 % at 25 °C

Figure 1 shows the comparison in polarization characteristic between IMRA MEMBRANE and a conventional perfluorosulfonic acid membrane.

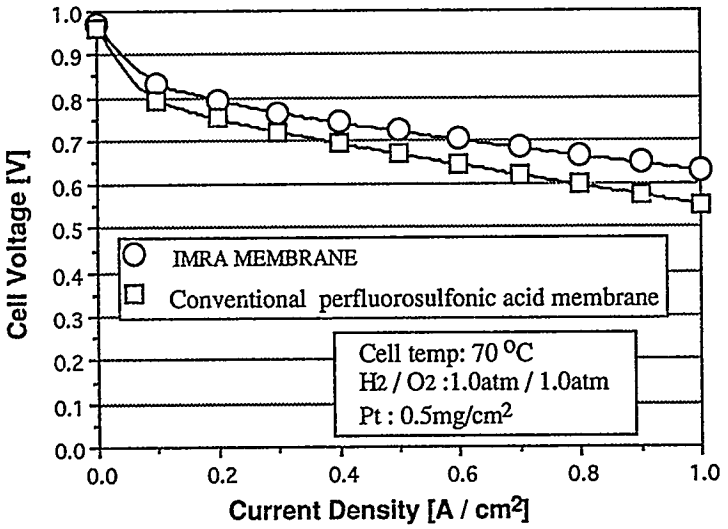

Figure 1. Comparison between IMRA MEMBRANE and a conventional membrane in fuel cell performance.

As shown in Fig.1, it was possible to make a fuel cell with IMRA MEMBRANE and electrodes which shows higher performance than that with a conventional membranes. It should be noted that IMRA MEMBRANE used in this experiment was slightly thicker than the conventional membrane. The gas diffusion electrodes were taken from the same lot for both the experiments to ensure that catalytic activity does not make a difference.

Figure 2 shows polarization curves obtained with IMRA MEMBRANE and electrodes at various running conditions. In the case of hydrogen/oxygen feed gases, the cell could be run at broad temperature range for the cell and humidification bubbler. On the other hand, the cell with air feed gas tended to dry up unless the running condition was carefully chosen. The cell temperature was lowered or the amount of water vapor supplied with gases was increased compared with the case of hydrogen/oxygen feed gases so that the cell could keep constant performance.

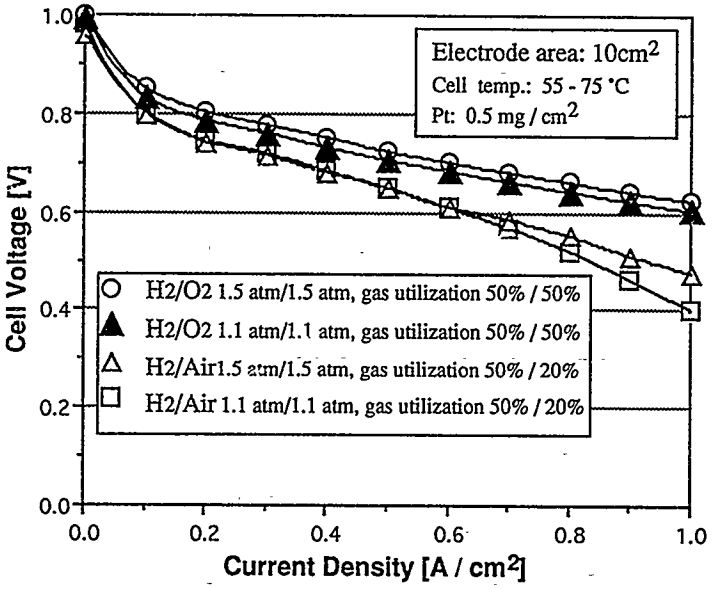

Figure 2. Polarization curves obtained at various operating conditions.

In order to evaluate the durability of IMRA MEMBRANE, the cell was run continuously for about 250 hours. As shown in Figure 3, the cell voltage was stable during this period at the constant current operation. The difference in ion exchange capacity between before and after the run was within experimental error. Thus we concluded that no appreciable decomposition of the membrane occurred in this time range. We are now attempting another life time test for a longer period. It has been reported that sulfonated styrene grafted FEP is subjected to decomposition, when it is used as an electrolyte for a fuel cell, showing the increase in electric resistivity just after the start of cell operation (1). This decomposition has been ascribed to the scission of the grafted polystyrene side chains (1). We also confirmed the similar phenomenon with FEP matrix films. However, the membrane made from ETFE showed different characteristics: higher mechanical strength and chemical stability. If the styrene side chains were subjected to decomposition, the membrane made from ETFE would behave the same way. Thus we postulate another mechanism for the decomposition as follows:

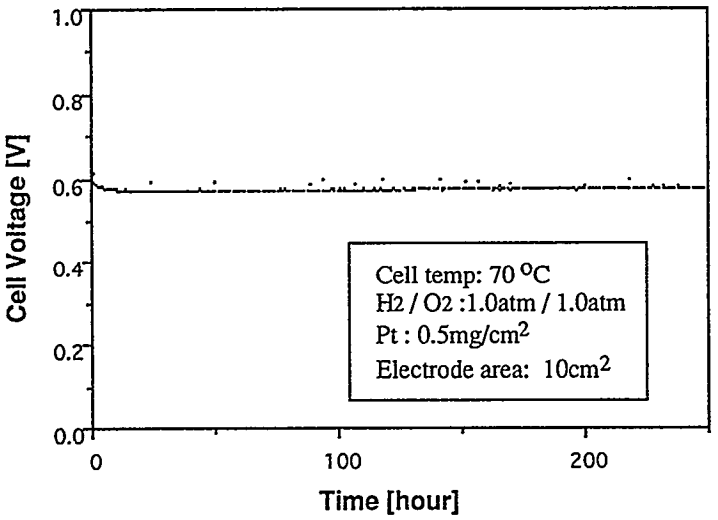

Figure 3. Cell voltage vs. time of operation of H2/O2 fuel cell at the current density of 0.7 A/cm^2.

It is likely that the main chains of perfluorinated polymers such as FEP, PFA, and PTFE are subjected to chain scission at carbon-carbon bonding rather than the carbon-fluorine bonding upon the irradiation by gamma rays to form radicals, considering the bonding energies. Upon grafting reaction, styrene is grafted onto the low molecular weight fragments resulting from the chain scission for these perfluorinated matrix polymers. Thus resultant membranes lose mechanical strength and the low molecular main chain fragments connected with sulfonated polystyrene might be dissolved into water during cell operation. ETFE contains polyethylene structures in the main chain. It is well known that polyethylene is subjected to crosslinking upon the irradiation by gamma rays. Therefore, even if fluorinated portions in ETFE are subjected to chain scission, the main chains are interconnected through crosslinking at polyethylene portions. This gives better mechanical strength and stability in fuel cell operation.

CONCLUSIONS

1. Using radiation grafted membranes, superior fuel cell performance which exceeds conventional perfluorosulfonic acid membranes can be obtained without appreciable initial degradation of membranes.

2. Selection of matrix films are of critical importance in radiation graft polymerization for fuel cell membranes.

REFERENCES

1. G. Scherer et al., "Study of Radiation-grafted FEP-g-Polystyrene Membranes as Polymer Electrolytes in Fuel Cells", Electrochimica acta, Vol. 40, No.3, pp. 345-353, 1995

PEM Fuel Cell Stack Performance Using Dilute Hydrogen Mixture. Implications on Electrochemical Engine System Performance and Design

Michael A. Inbody, Nicholas E. Vanderborgh, James C. Hedstrom and Jose I. Tafoya
Engineering Sciences and Applications Division
Los Alamos National Laboratory
Los Alamos, New Mexico 87545

Introduction

Onboard fuel processing to generate a hydrogen-rich fuel for PEM fuel cells is being considered as an alternative to stored hydrogen fuel for transportation applications. (1) If successful, this approach, contrasted to operating with onboard hydrogen, utilizes the existing fuels infrastructure and provides required vehicle range. One attractive, commercial liquid fuels option is steam reforming of methanol. However, expanding the liquid methanol infrastructure will take both time and capital. Consequently technology is also being developed to utilize existing transportation fuels, such as gasoline or diesel, to power PEM fuel cell systems.(2)

Steam reforming of methanol generates a mixture with a dry gas composition of 75% hydrogen and 25% carbon dioxide. Steam reforming, autothermal reforming, and partial oxidation reforming of C_2 and larger hydrocarbons produces a mixture with a more dilute hydrogen concentration (65%-40%) along with carbon dioxide (≈20%) and nitrogen (≈10%-40%). Performance of PEM fuel cell stacks on these dilute hydrogen mixtures will affect the overall electrochemical engine system design as well as the overall efficiency.(3) The Los Alamos Fuel Cell Stack Test facility was used to access the performance of a PEM Fuel cell stack over the range of gas compositions chosen to replicate anode feeds from various fuel processing options for hydrocarbon and alcohol fuels. The focus of the experiments was on the anode performance with dilute hydrogen mixtures with carbon dioxide and nitrogen diluents. Performance with other anode feed contaminants, such as carbon monoxide, are not reported here.

Experimental:

Fuel Cell Stack: A Ballard Power Systems Mk. V Fuel Cell Stack (Serial No. 212), nominally rated at 5 kW when operated on 100% hydrogen, was used for these measurements. This stack has 35 fuel cells with an active cell area of 232.8 cm^2. This deionized water-cooled stack also includes internal membrane humidification units for both the anode and cathode feeds so that external humidification of the gas feed is not necessary at the design operating conditions. In normal operation, the reactants traverse the stack length, enter the humidification section, and are then distributed to the individual cells.

Test Instrumentation: A test instrument of unique design (Figure 1) was used for these measurements. The gas feeds to the anode and cathode of the fuel cell stack are controlled by MKS 1559A mass flow controllers. Hydrogen, nitrogen, and carbon dioxide are mixed to generate the anode reaction at flows up to those required for a 20 kW fuel cell stack. Air injection, controlled using another mass flow controller, can be set up to 2% by volume of the total anode flow. Anode air injection has been used to prevent degradation of fuel cell performance observed when carbon dioxide is in the anode feed, and to decrease adverse effects of carbon monoxide.(1) The cathode feed is air.

The test instrument includes 4- kW computer-controlled vaporizers to add controlled quantities of steam to both cathode and anode feeds up to 100% relative humidity at the stack operating temperature. Because the Ballard test hardware includes internal humidifiers, the vaporizers were not normally used for the experiments in this study. However, the effect of inlet stream humidification was investigated for the higher flow rates with dilute hydrogen at high anode stoichiometry.

The anode and cathode exhaust flows traverse water-cooled condensers before passing through back-pressure regulators to the exhaust vents. The dome-loaded back-pressure regulators

maintain the anode and cathode operating pressures. PID pressure controllers on these back pressure regulators allow the gas flow rates to be changed over the full experimental range without user-adjustment.

Heat generated by the fuel cell stack is removed by a deionized water cooling loop through a temperature-controlled heat exchanger to a building chilled-water loop. The deionized water cooling loop was pressurized with the nitrogen supply to within 10 psi of the stack gas operating pressures. Cooling water flow rates through the stack are controlled by bypass valves. Two 1 kW heaters are included in the cooling loop so that the cooling loop can be used to warm up the fuel cell stack to its operating point and to augment heat input at low current density operation.

The fuel cell stack electrical energy is fed to a current-controlled electrical load (PWM). Load output is fed to a water-cooled resistor. A software-based PID controller maintained the current set-point on the fuel cell stack.

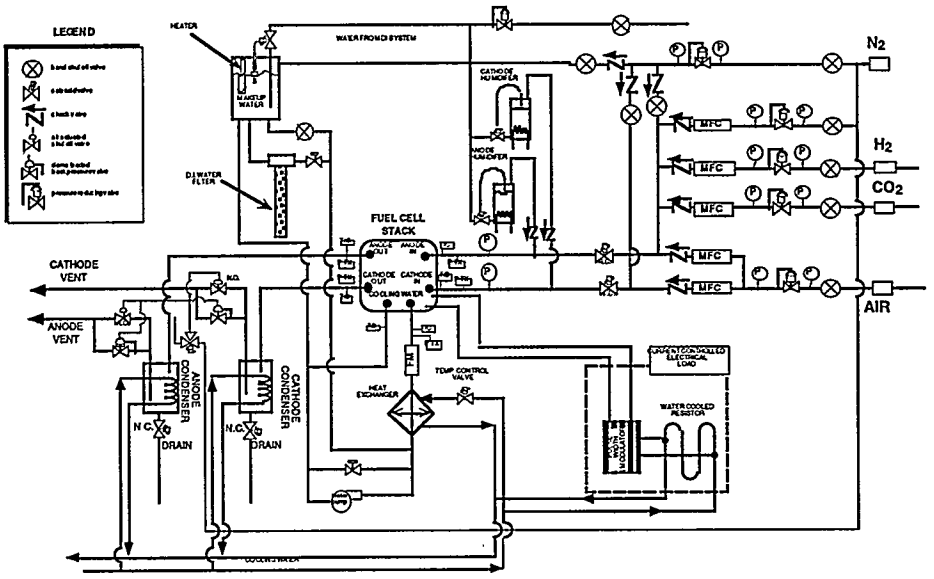

Figure 1. Schematic of the PEM Fuel Cell Stack Test Hardware.

Testing is accomplished with VME-based data acquisition system using an embedded computer controlled by EPICS control software.

Results

Figure 2 shows performance with hydrogen nitrogen mixtures. These data were taken with a stack temperature of 80 °C, pressures of 300 kPa, and with cathode stoichiometry of 2.5 and anode of 1.2 (based on hydrogen flow). As is apparent. although relative small voltage loss is apparent at low current density, at higher current density voltage losses of > 100 mV appear when 60% N_2 is fed to the anode, contrasted to 100% hydrogen data.

Figure 3 shows the effect of variable stoichiometry showing hydrogen-carbon dioxide-nitrogen data. These data are all at 500 ma/cm^2, an intermediate current density. Data were taken with 2% air injection, one standard condition that has been successful in eliminating voltage loss found on platinum anodes with carbon dioxide mixtures. Although data were taken below a stoichiometry of 1.05, individual cells tend to show large voltage loss, and that data is not time

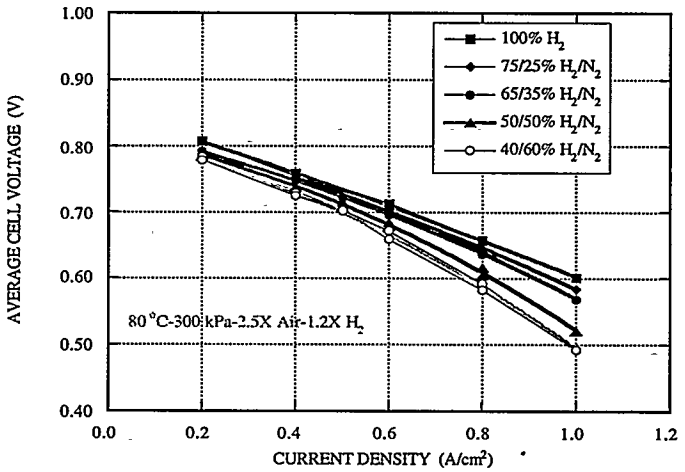

Figure 2: Effect of Nitrogen Dilution on PEM Stack Performance. Polarization curves (constant stoichiometry) for five hydrogen/nitrogen mixtures.

independent. At lower stoichiometry levels, individual cells tend to show unstable performance. The data control system is programmed to abort tests when individual cell voltages reach unacceptably low values, thus preserving stack integrity.

Conclusions:

Demonstrated voltage losses with nitrogen and/or carbon dioxide dilution are larger than predicted by the Nernst equation. Operating contemporary stacks with dilute hydrogen mixtures involves voltage penalties, especially at lower stoichiometry values. The exact explanations for these losses remain under investigation and may involve moisture content, formation of surface contaminants, and electrode flooding. Indeed, some performance loss may even result from pore flooding, leading to mass transport limitations within the *cathode* electrode; however most of the losses are probably within the anode structure. Most likely hydrogen solubility in the Nafion™ solution (encapsulating the Pt catalyst particles) is displaced by nitrogen and carbon dioxide.(4) These data tend to suggest that earlier performance loss noted with CO2 may be this result, contrasted to a reverse shift generation of CO.(1) These results point to the need for both improved electrode structures for these fuel processing product mixtures and improved techniques for handling

two-phase flow within these stacks. With improved stack designs however, robust and efficient performance should prove technically feasible.

Acknowledgment:

These studies are supported by the Office of Transportation Technology, the United States Department of Energy.

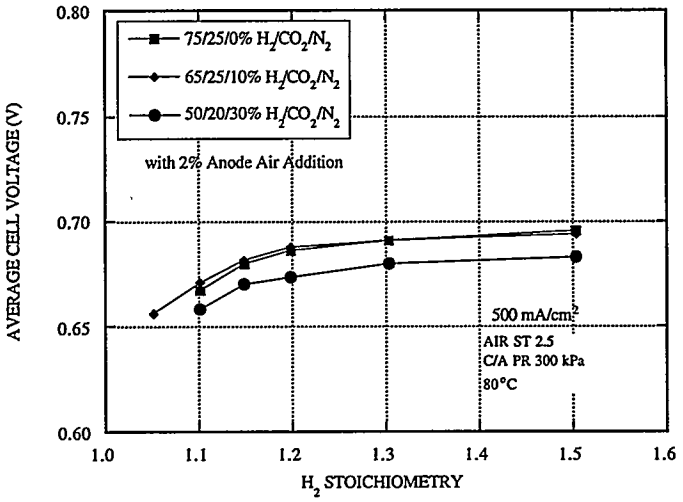

Figure 3: Effect of Anode Stoichiometry on PEM Stack Performance. Data at 500 ma/cm^2 for hydrogen-carbon dioxide-nitrogen mixtures. Based on hydrogen stoichiometry. Data below a stoichiometry of 1.1 become unstable, with individual cells demonstrating severe voltage loss.

References:

1. anon, "Research and Development of Proton-Exchange-membrane (PEM) Fuel Cell System for Transportation Applications," The United States Department of Energy, Phase I, Final Report, Contract no. DE-AC02-90CH10435, January 1996.

2. J. M. Bentley, W. L. Mitchell, J. Thijssen, "Reformer and Hydrogen Storage Development for Fuel Cell Vehicles," Annual Automotive Technology Development Contracts' Coordination Meeting, Dearborn, MI, October 1995.

3. L. F. Brown, "A Survey of Processes for Producing Hydrogen Fuel From Different Sources for Automotive-Propulsion Fuel Cells", Los Alamos National laboratory, LA-113112-MS, March 1996.

4. K. R. Weisbrod, S. A. Grot, and N. E. Vanderborgh, Through-the-Electrode Model of a Proton Exchange membrane Fuel Cell," Electrochemical Society Proceedings, Volume 95-23, p. 152.

PERFORMANCE EVALUATION OF PEFC STACK

Jun-ichi Fujita, Jitsuji Ohtsuki
Technical Research Center,
The Kansai Electric Power Co., Inc.
3-11-20 Nakoji Amagasaki, 661, Japan

Yoshihiko Shindo, Yoshiaki Enami, Shinji Kinoshita, Kyoichi Urabe
New Energy Laboratory,
Fuji Electric Corporate Research & Development, Ltd.
2-2-1 Nagasaka Yokosuka, 240-01, Japan

INTRODUCTION

Polymer electrolyte fuel cells (PEFCs) have many advantages such as high current density, short start-up time and endurance for start-stop cycles. Making use of these advantages, Fuji Electric has been working with the Kansai Electric Power Co., Inc. to explore practical applications of PEFCs for an electric utility use. Since large-sized electrodes are required in the electric utility applications, we have fabricated 600cm^2 membrane-electrode assemblies by using hot-press method. We have also designed a cell stucture to realize a uniform reaction over the electrodes. The structure includes a properly-shaped gas flow channel, a temperature-gradient cooling system. Using the 600cm^2 (25x24cm) electrodes, a 30-cell stack (5kW) were constructed and tested.

EXPERIMENTAL

Specifications of the 5kW stack are shown in Table 1. Water management is an important factor to operate PEFCs stably for a long time, especially in the case of large-area electrodes. We have developed a method that intentionally maintains large temperature difference between gas inlet and outlet in a cell, so that the outlet temperature is higher than the inlet temperature. This prevents condensation of water and allows successful water removal even at the gas outlet where water vapor content increases. The temperature distribution can be changed in electrodes by controlling the temperature and the flow rate of cooling water. The stack was operated with 0.1MPa abs. H_2/air at 70℃. Hydrogen gas and air were humidified externally by passing them through water in a vessel maintained at constant temperature. Air utilization was 25% and H_2 utilization was 75%.

Table 1. Specifications of 5kW Stack

Electrode Area	**600 cm^2**
Number of Cells	**30 cells**
Rated Power	**5 kW**
Rated Voltage	**21V**
Rated Current Density	**0.4 A/cm^2**

RESULTS

Figure 1 shows the dependence of the stack voltage on the dew point of air at 0.4A/cm^2. The dew point of hydrogen gas at the inlet of the stack was 60℃. Cell temperature difference between gas inlet and outlet was fixed at 5℃. When the dew point was higher than 70℃, the voltage was costant. It shows that water in the cell was effectively removed by the temperature difference. When the dew point was lower than 70℃, the voltage gradually decreased. Electrolytes dry at the low dew point, which increases cell resistance. Therefore it is necessary for electrolyte to maintain appropriate water content to obtain good performance. Figure 2 shows I-V and I-P characteristics of the stack operated at 70℃. At the rated current of 240A, the stack showed a voltage of 21V with output power of 5.0kW.

CONCLUSIONS

We have developed a 5kW stack with 600cm^2 electrodes. The total output power was 5.0 kW at the rated current of 240A (0.4A/cm^2). At the high dew point of air , the cell voltage was stable. The temperature difference method showed an effect for removing product water from cathodes.

REFERENCES

[1] M. S. Wilson et al., Electrochimica Acta, Vol.40, No.3, p.355, 1995
[2] H. H. Voss et al., Electrochimica Acta, Vol.40, No.3, p.321, 1995
[3] Y. Enami et al., Proceedings of the 2nd International Fuel Cell Conference, Japan, p.529, 1996

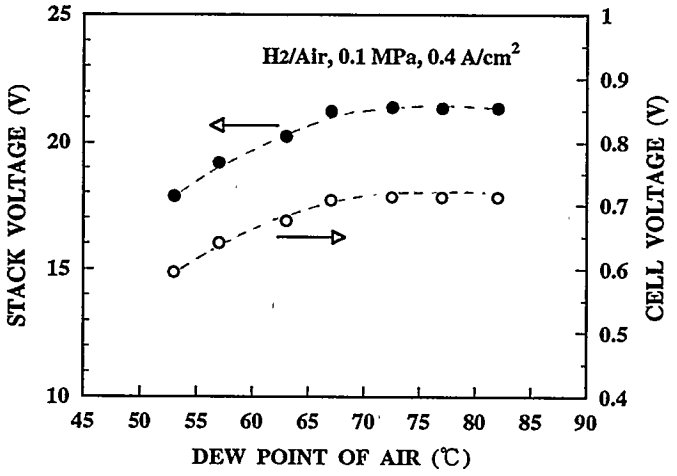

Figure 1. Dependence of Voltage on Dew Point of Air

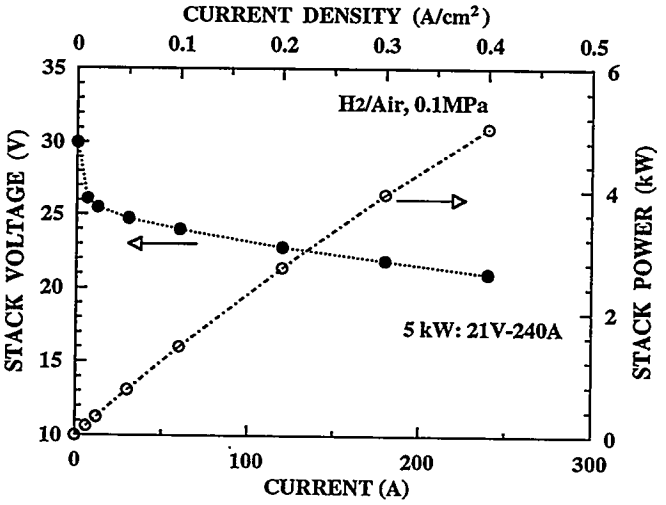

Figure 2. I-V, I-P Characteristics of 5kW Stack

AN OPTIMIZATION STUDY ON PEFC DRIVE ELECTRIC VEHICLE

K.Kishida, M.Tanaka, K.Kanai, Y.Iwahashi, K.Tsumura
Fukui University of Technology, 3-6-1 Gakuen, Fukui City
Fukui Prefecture, 910 Japan

1. Fuel Cells for Electric Vehicle

Efforts have been made to develop fuel cell powered EVs (electric vehicles) in several countries and to demonstrate its high potential. Since 1990 fuel cell research has been conducted at FUT (the Fukui University of Technology) beginning with PAFC. Research effort is now being focused upon the application of fuel cells to the EV drive as this technology shows great future potential, particularly in the area concerning environmental protection.

PEFC (Polymer Electrolyte Fuel Cell) has been chosen as the fuel cell for the EV power source because it possesses an inherent high power density and it also has another important feature ; operation can be started under ambient temperature without preheating.

The principal objective of this research is to pursue the optimum system of a PEFC drive EV. The size of the prototype vehicle in the university project is limited to a certain range and the capacity of the PEFC stack is also limited, for the time being anyway, as the PEFC technology is still under developmental stage in Japan. A 1.5 kW class PEFC stack has become available for the research at FUT by courtesy of a PEFC developer.

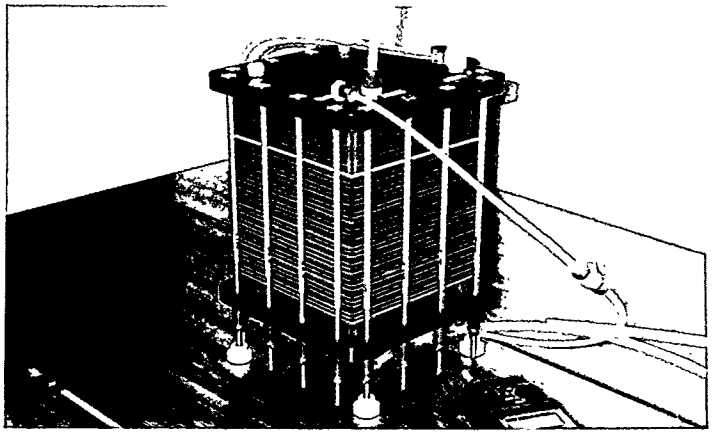

Fig.1 A 1.5kW PEFC Stack

In order to design an optimum system of a PEFC drive EV, thorough studies on the PEFC stack characteristics have been undertaken to clarify and to optimize the interface conditions.

Fundamental characteristics of the PEFC stack are discussed first. With this knowledge, the power conversion and transmission system should be designed taking into account the compatibility between the fuel cell stack performance and the power demand of the vehicle.

2. Characteristics of PEFC Stack

The vehicle's PEFC stack is one of the prototype stacks in the stage of research and development. The stack consists of 25 cells having the effective cell area of 225 cm^2. An internal humidifier is integrated in the stack to control the humidity of the gases, both fuel and oxidant. The exterior view of the stack is shown in Fig.1. The performance of the stack has been measured under various operating conditions.

The stack voltage characteristics and the resultant output power, with change in current (current density), are shown in Fig.2. and Fig.3.

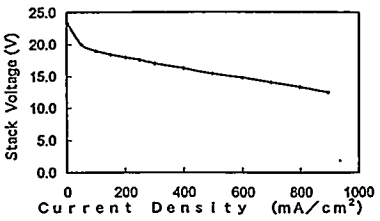

Fig.2 Voltage vs. Current Density Characteristics

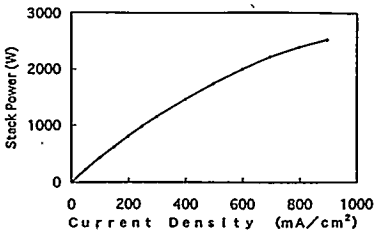

Fig.3 Power vs. Current Density Characteristics

A test to confirm the response characteristics of power supply build-up for a sudden increase in power demand shows a satisfactorily quick response in power increase from the stack as is shown in Fig.4. Frequent power change for a short time duration, which would take place during vehicle operation, is simulated in a typical form seen in Fig.5. This resulted in a slight change of the average cell voltage, but this should not affect vehicle operation.

Although the data are not shown for the characteristics that depend on different gas utilization factors, tests have been

conducted to monitor any effect or change in performance. There were no noticeable change within the range of possible operating conditions.

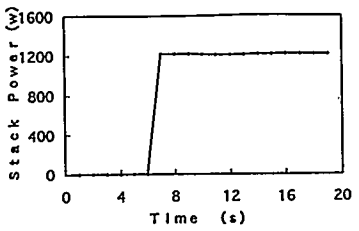

Fig.4 Stack Power Build-up Characteristics

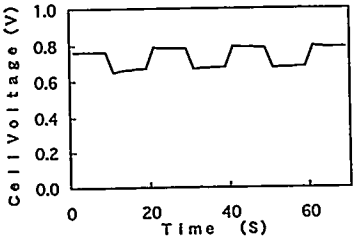

Fig.5 Average Cell Voltage Change with Change in Load Current

For system designers, it is important to know the equivalent electrical circuit of the power source in advance to execute the design particularly for the dynamic response of the overall system. A simplified equivalent electrical circuit (a first order approximation) of a fuel cell can be expressed as is shown in Fig.6, consisting of an electrolyte resistance [R_r], a charge transfer resistance [R_e] and a capacitance [C] representing the electrical double layer capacity.

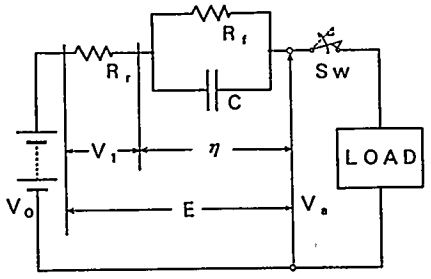

Fig. 6 Equivalent Electrical Circuit of a Fuel Cell

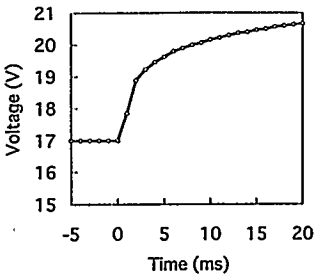

Fig.7 Voltage Transient at Abrupt Current Break

To determine the values of the individual elements, an analysis by means of electrical transient has been applied. An abrupt break of the load current of the fuel cell stack gives a step

change in the stack voltage, which is then followed by an exponential decay of the voltage. This phenomenon is seen in Fig.7, from which R_r, R_e and C have been calculated. For example, the time constant of the circuit is given as about 360 ms. Thus, the equivalent electrical circuit of the stack has been confirmed.

3. Power Conversion System

One of the fundamental problems during the vehicle design was the selection of the drive motor. A few kW order fuel cell stack usually generates the stack voltage at around 10-20 V at full load under reasonable design conditions. Low voltage d-c motors are available for small capacity vehicles, however, d-c motor drive is no longer advanced technology in view of cost, maintenance and operability for larger capacity vehicles.

The first prototype EV being built at FUT is small and it is no problem to adopt a d-c motor for drive, but in the standpoint of pursuing an optimum design for FC drive EVs for the next stage, a-c motor drive systems are being studied.

Mock-up tests of an induction motor drive system consisting of a d-c to a-c converter, voltage step-up units and a variable frequency controller are conducted. It is working reasonably well but the sophisticated system resulted in lower efficiency of the power conversion process.

An alternative method is the d-c brushless motor drive concept (by means of synchronous motor control). This technology has recently been widely used and well designed components are available in a certain range of the capacity. In-wheel type of the brushless motor will be tested shortly. Comparison of these different power conversion systems will be discussed at the Seminar.

4. Conclusion

Fundamental characteristics of a PEFC stack have thoroughly been studied first to clarify the operational conditions taking into account the interfacial compatibility with the motor drive system. In conclusion, it has been proved that the PEFC has appropriate characteristics as the power source of EVs. In the meantime, the power conversion and transmission system to drive the vehicle is being studied using several different types so as to assess compatibility. The approach to pursue an optimal design for FC powered EVs will be discussed at the Seminar.

MODELING OF GASEOUS FLOWS WITHIN PROTON EXCHANGE MEMBRANE FUEL CELLS

Kirk R. Weisbrod, Nicholas E. Vanderborgh
Energy and Process Engineering Group
Los Alamos National Laboratory,
Los Alamos, New Mexico · 87545

Stephen A. Grot
Delphi Energy and Engine Management Systems
Rochester, NY 14602

Introduction

Development of a comprehensive mechanistic model has been helpful to understand PEM fuel cell performance. Both through-the-electrode and down-the-channel models have been developed to support our experimental effort to enhance fuel cell design and operation (1).

The through-the-electrode model was described previously. This code describes the known transport properties and dynamic processes that occur within a membrane and electrode assembly (1). Key parameters include transport through the backing layers, water diffusion and electro-osmotic transport in the membrane, and reaction electrochemical kinetics within the cathode catalyst layer. In addition, two geometric regions within the cathode layer are represented, the first region below saturation and second with liquid water present. Although processes at high gas stoichiometry are well represented by more simple codes, moderate stoichiometry processes require a two dimensional representation that include the gaseous composition and temperature along flow channel. Although usually PEM hardware utilizes serpentine flow channels, this code does not include such geometric features and thus the flow can be visualized along a single channel.

This paper describes the "down-the-channel model" which also incorporates all components of the earlier through-the-electrode model. The model proceeds by solving localized "through the electrode model" arithmetic, and uses those new conditions to set initial conditions for the next cell "down the channel." The model is first validated by comparison to a series of single cell tests under varying conditions. The effect of membrane thickness is explored. The impact of anode and cathode gas humidification, operating temperature and pressure are predicted.

Model Description

The model calculates the water and gas fluxes in the membane electrode assembly (MEA) and obtains the current density at each step along the flow channel. Components of the through-the-membrane model are summarized first, followed by the down-the-channel formulation.

Primary components of the model include gas transport, water and ionic transport in the membrane, and catalytic layer diffusion and reaction.

1. The transport of all gaseous components are represented by the Stefan-Maxwell equation. Often, at some location in the cathode backing, liquid water from the cathode catalyst layer is vaporized and travels to the cathode channel as vapor. For the region where liquid water is present, the effective diffusion coefficient is decreased further because some porosity in the backing layer is water filled.
2. Net water transport through the membrane is the sum of electro-osmotic drag and diffusion processes. It is defined as positive from anode to cathode. Depending upon conditions in the anode and cathode channels, diffusion may be transporting water either toward or away from the anode catalyst layer. The model assumes liquid water is not transported through the anode backing. Because of this vapor transport , at the anode catalyst layer - membrane interface the membrane is at equilibrium with saturated vapor as long as *liquid* water is present (two phase) in

the anode channel. Relationships for the expansion of the membrane as a function of water content are also included. Membrane transport rates, water diffusion and proton conductivity, agree with those published previously (2).

3. Oxygen reduction in the cathode catalyst layer is described by four main equations. (a) Butler-Volmer reaction kinetics are used with reaction coefficients derived from Parthasarathy et al. (3,4). (b) Potential drop through the porous catalyst layer was calculated by ohms law with an effective resistivity dependent upon bulk conductivity at a given water saturation and porosity of the layer. (c) Flux of oxygen is related to local current density. (d) Finally, the change in oxygen concentration with position is related to oxygen flux and the effective oxygen diffusion coefficient. As in other models, it is assumed that the cathode dynamics are rate limiting, and thus hydrogen oxidation rate terms are not included. In anode-limited electrochemical cases other models would be required.

The down the channel section of the model solves for the change in gas temperature and compositions for the anode and cathode channels. In the calculations shown here, that anode and cathode gases flow in parallel. While the gas streams can enter at any temperature, all solid components including backing layers are at uniform temperature at any one point along the flow channel. The differential equations used to describe the down the channel behavior are similar to those given by Nguyen et al (5). Ten equations are solved for the following 10 unknowns: five at the anode

$$M_{H_2}, M_{CO_2}, M^{v}_{w,a}, M^{l}_{w,a}, T_a$$

and five for the cathode

$$M_{O_2}, M_{N_2}, M^{v}_{w,c}, M^{l}_{w,c}, T_c$$

where M represents moles of a given component.

Experimental

A unique single cell fixture and test stand were designed and constructed to provide tight control on all testing parameters, including mass flow control of gas streams, active humidification control using computer controlled liquid chromatography pumps with constant temperature vaporizers. Both the anode and cathode exhaust streams were condensed and the total water content measured gravimetrically. Water mass balances were obtained with 2% accuracy. Cell temperature was controlled using circulation of a constant temperature fluid through heat exchangers built into the single cell. A data acquisition and control system allowed unattended operation with programmed gas stoichiometries and humidification (6,7). High frequency resistance of the MEA, the "membrane resistance", was measured at 1 kHz by a 4 probe method.

Membrane electrode assemblies (MEAs) were assembled by a procedure similar to that described by Wilson et. al. (8). Two decals were coated with a carefully controlled thickness of catalyzed ink in the tertiarybutyl amine form and dried in an oven. One decal was placed on each side of the membrane and pressed under controlled conditions. The catalyzed membrane was then sandwiched between two pieces of wet-proofed graphite paper and placed in the test cell. Active area was 46 cm^2.

Model Validation

A series of PEM fuel cell tests provided a data base for validating the model. While the test stand was designed with the ability to perform constant stoichiometry polarization curves, the tests shown here were operated at constant flow to minimize the scan time. At high flow rate with saturated gas streams, Fig. 1(a) shows that a good fit between the model and data is obtained. Two adjustable parameters are required to obtain this match: 1.) pore volume occupied by water in the catalyst layer and 2.) water in the saturated region of the cathode backing layer. At lower flow

with an unsaturated cathode feed, performance near the mass transfer limiting current is over estimated by the model (Fig. 1(b)). Apparently, flow distribution, flow field lands, or partial flooding at the backing-membrane interface occurs. These processes are not accounted for in the model at lower stoichiometries.

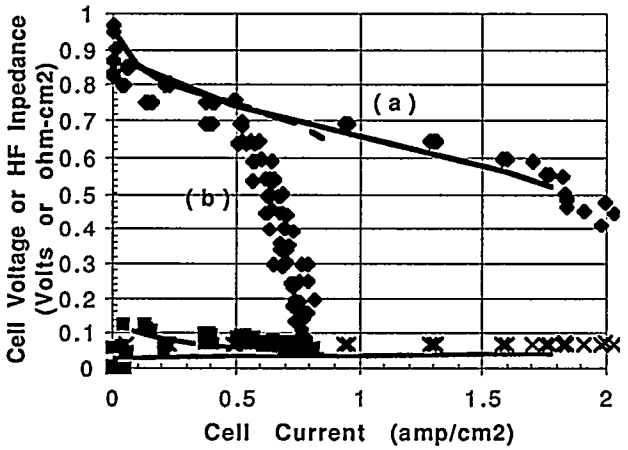

Figure 1. Single Cell Validation: (a) 85°C, Anode: H2, 2.5 atm, 100% RH, 1.0 slpm, Cathode: Air, 2.5 atm, 100% RH, 5.0 slpm (b) same except Anode: 0.34 slpm Cathode: 0.77 slpm, 50% RH (flow rate corresponds to a Stoichiometry of 1 @ 1 amp/cm^2).

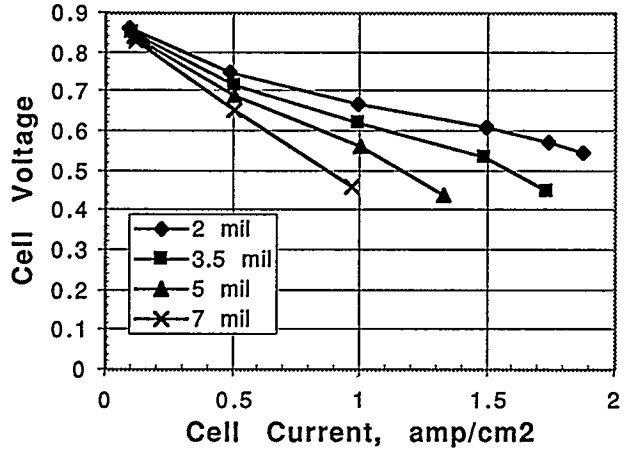

Figure 2. Effect of thickness of NAFION™ 1100 equivalent weight membrane upon predicted performance; 80°C, Anode: H2, 2.5 atm, 95 % RH, 1.5 stoich., Cathode: Air, 2.5 atm, 50% RH, 2.0 stoich.

Net water transport measurements are usually not definitive. It is difficult to properly represent irreversible processes at the membrane interfaces. In the first case with an inlet cathode relative humidity of 100%, anode inlet was controlled at 80%. Measured and calculated net water transport

numbers agreed well and varied from -2.5 to 0.0 moles H_2O/H^+, indicating water transport from the cathode to the anode. For an anode relative humidity of 100%, less than 0.1 moles H_2O/H^+ was measured in either direction when the current density is varied from 0.1 to 1.5 amp/cm^2. The model predicts -1.1 to +0.3 moles H_2O/H^+ . This difference could be explained by the interface containing higher resistance to water transport than included in the model.

Predicted Performance

The impact of thickness upon performance was explored for NAFION™ 1100 equivalent weight. Fig. (2) illustrates the decrease in performance which arises from the combined effects of higher resistance which is made worse by slower diffusion of water in the direction cathode-to-anode. The high current data tend to indicate where mass transfer limitations become predominant and performance drops rapidly. As this limit is approached, the model is highly unstable.

Other parameters to be explored at the meeting include anode and cathode humidification, and the influence of cell temperature and pressure.

Conclusion

A through-the-electrode model, based upon independently measured or calculated parameters, was combined with down-the-channel subroutines to obtain improved predictions of PEM cell performance. Modeling the down-the-channel vector is necessary to obtain an improved cell representation when water accumulation and transport are important. After model validation with experimental data, predictions were made for parameters dependent upon water balance in the flow channels and transport through the membrane.

Acknowledgment

This work was performed as part of the Electrochemical Engine Project supported by General Motors and the US Department of Energy, Office of Transportation Technology.

References

1. K. R. Weisbrod, S. A. Grot and N. E. Vanderborgh, "Through-the-Electrode Model of a Proton Exchange Membrane Fuel Cell with Independently Measured Parameters," Extended Abstract for paper presented at the 188th Meeting of the Electrochemical Society, Chicago, Ill., October 8-13, 1995.
2. T. A Zawodzinki, T. E. Springer, J. Davey, R. Jestel, C. Lopez, J. Valerio and S. Gottesfeld, *J. Electrochem. Soc.* 140, 1981 (1993).
3. A. Parthasarathy, S. Srinivasan and A. J. Appleby, *J. Electrochem. Soc.* 139, 2530 (1992).
4. A. Parthasarathy, S. Srinivasan, A. J. Appleby and C. R. Martin *J. Electrochem. Soc.* 139, 2856 (1992).
5. T. V Nguyen and R. E White, *J. Electrochem. Soc.* 140, 2178 (1993).
6. DOE/GM Phase I Final Report, Research and Development of Proton Exchange Membrane Fuel Cell System for Transportation Applications, (Contract DE-AC02-90CH10435).
7. S. A. Grot, J. C. Hedstom and N. E. Vanderborgh, Paper W3.5, Materials Research Society Spring Meeting, San Francisco, Ca, April 17-21 (1995).
8. M. S Wilson, J. A Valerio and S. Gottesfeld, *Electrochim. Acta*, 40, p 355 (1995).
9. M. Thomas, Mescoubes, and M Pineri, "Pervaporation and Permeation of Water Through a Perfluorinated Ionomer Membrane: Determination of the Permeant Concentration Profiles to Explain the Transport Properties," Proceedings of Third International Conference on Pervaporation Processes in the Chemical Industry, Nancy, France, September 1988.

NOVEL, LOW-COST SEPARATOR PLATES AND FLOW-FIELD ELEMENTS FOR USE IN PEM FUEL CELLS

D.J. Edlund
Northwest Power Systems, LLC
Bend, OR

PEM fuel cells offer promise for a wide range of applications including vehicular (e.g., automotive) and stationary power generation. The performance and cost targets that must be met for PEM technology to be commercially successful varies to some degree with the application. However, in general the cost of PEM fuel cell stacks must be reduced substantially if they are to see widespread use for electrical power generation.

A significant contribution to the manufactured cost of PEM fuel cells is the machined carbon plates that traditionally serve as bipolar separator plates and flow-field elements. In addition, carbon separator plates are inherently brittle and suffer from breakage due to shock, vibration, and improper handling. Alternatives to machined carbon bipolar plates that have been disclosed include woven wire mesh or expanded metal mesh composed of corrosion resistant metals (1,2); molded composites consisting of powdered carbon (graphite) suspended in a polymer matrix (3); flexible graphite sheets that contain grooves much like the machined carbon plates (4); and flexible graphite stenciled with discontinuous flow channels (5). These alternative approaches suffer from drawbacks including relatively high electrical resistance, poor performance, and/or high manufacturing costs.

Northwest Power Systems is developing a separator plate (called a bifurcated separator device) that promises to offer low electrical resistance, low manufacturing cost, compact size, and excellent durability. Our approach is to separate the functions of current collection and gas flow distribution and then to design two separate elements to achieve the desired performance characteristics. Thus, the bifurcated separator plate consists of two discrete members; the current collector and the flow-field element. For instance, current collection is achieved using a thin graphite-clad metal sheet, either perforated or slotted. Gas flow distribution is achieved using a mesh fabricated from plastic or metal that has the desired chemical durability within the PEM environment. Combining these two separate elements into a single device yields a bifurcated separator device that performs as a bipolar separator plate.

An advantage of this alternative approach to making bipolar plates is that the current collector and the flow-field element can be independently optimized for performance, durability, and low cost. The result is a non-brittle and thin device that has low electrical resistance, good chemical resistance, and is inexpensive to manufacture. The chemical resistance of the bifurcated separator device is a direct result of the graphite cladding employed with the current collector and the use of chemically robust plastic or metal mesh for the flow-field element.

Manufacturing the bifurcated separator device is simple--no machining is required. The components are punched from sheet stock and pressed into the final shape. In volume, manufacturing costs are expected to be <$1/ft^2.

This poster will present 1) the key features of the bifurcated separator plate; 2) performance data obtained with prototype bifurcated separator plates; and 3) manufacturing economics.

References

1. A. Leonida, "Hydrogen/Oxygen SPE Electrochemical Devices For Zero G Applications," Proceedings of the European Space Power Conference, Madrid, Spain, pp. 227-231, October 2-6, 1989

2. J.F. McElroy, "SPE Regenerative Hydrogen/Oxygen Fuel Cells For Extraterrestrial Surface Applications," 24th IECEC, Volume 3, pp. 1631-1636, August 1989

3. R.J. Lawrence, "Low Cost Bipolar Current Collector-Separator For Electrochemical Cells," U.S. Patent No. 4,214,969, July 29, 1980

4. D.P. Wilkinson, G.J. Lamont, H.H. Voss, and C. Schwab, "Embossed Fluid Flow Field Plate For Electrochemical Fuel Cells," WO 95/16287, June 15, 1995

5. K.B. Washington, D.P. Wilkinson, and H.H. Voss, "Laminated Fluid Flow Field Assembly For Electrochemical Fuel Cells," U.S. Patent No. 5,300,370, April 5, 1994

PEM FUEL CELL APPLICATIONS AND THEIR DEVELOPMENT AT INTERNATIONAL FUEL CELLS

Thomas F. Fuller, Michael E. Gorman and Leslie L. Van Dine
International Fuel Cells Corporation
South Windsor, Connecticut 06074

International Fuel Cells (IFC) is involved with the full spectrum of fuel cell power plants including the development of Proton Exchange Membrane (PEM) fuel cell systems. The extensive background in systems, design, materials and manufacturing technologies has been brought to bear on the development of highly competitive PEM power plants. IFC is aggressively pursuing these opportunities and is developing low-cost designs for a wide variety of PEM fuel cell applications with special emphasis on portable power and transportation. Experimental PEM power plants for each of these applications have been successfully tested.

IFC brings to PEM fuel cell development two distinct design features: (1) IFC's Passive Water Management (PWM) design concept and (2) graphite construction benefits from our extensive experience in manufacturing. PWM, with its inherent internal saturation, greatly simplifies the power plant supporting systems leading to reduced cost, weight and volume and makes ambient pressure operation practical. The PWM concept is illustrated in Figure 1. Only one circulator, the water pump, is needed for thermal and water management. Recycle of reactants is not required, thereby improving reliability and durability of the system. Because the liquid water is contained by capillary forces, the system can be attitude and gravity independent.

Underwater Application

Figure 2 is a photograph of the prototype Unmanned Underwater Vehicle (UUV) PEM 10-kW power plant developed and tested by IFC under a program sponsored by the Defense Advanced Research Projects Agency of the U.S. Department of Defense. This was IFC's first full-size stack incorporating the PWM concept. The power plant, which consisted of two 80-cell stacks, ran for more than 500 hours in a simulated mission profile.

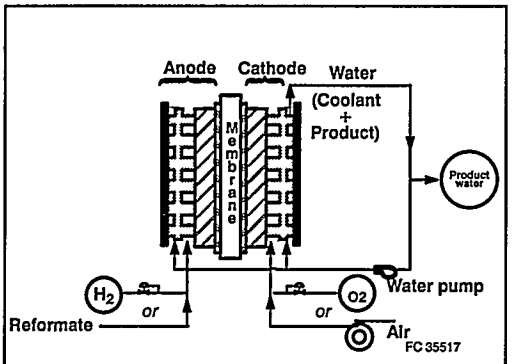

Figure 1: PWM Concept

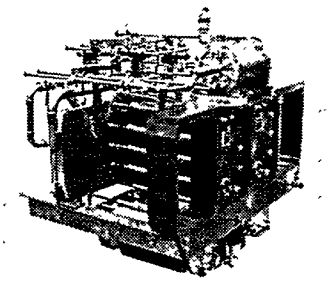

WCN-14922

Figure 2: UUV 10-kW Power Plant

HP-309

Vehicle Application

In automotive applications both pressurized and ambient pressure power plant designs benefit from PWM. Of the two, ambient pressure design is considered to be the less costly and more reliable approach. IFC has been selected by Ford Motor Company to demonstrate a 50-kW PEM power plant for vehicle application under a U.S. Department of Energy program. Figure 3 illustrates the PWM, ambient pressure design concept of this power plant, which consists of two 25 cell stack modules and appropriate ancillaries. Figure 4 is a photograph of a 25-kW cell stack module mockup. The estimated characteristics of this power plant for operation in 1997 are shown in the Table. This 50-kW hydrogen-air power plant design includes all ancillary components to provide and distribute the reactants and meets the design criteria established by Ford for their vehicle application.

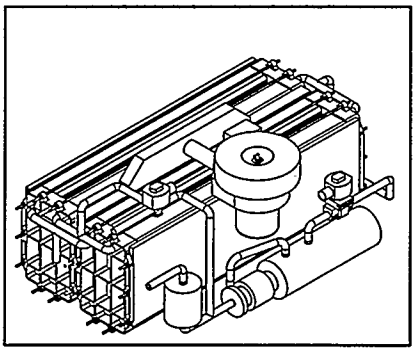

CA180

Figure 3: 50-kW Automotive Power Plant

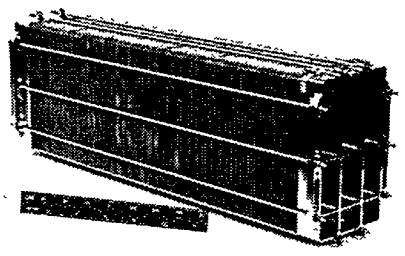

WCN-15361

Figure 4: 25-kW Automotive Module Mockup

Table
Automotive Power Plant Characteristics

Rating	50 kW
Weight	370 W/kg (6 lbs/kW)

IFC is currently engaged in two additional fuel cell programs for light duty transportation applications. These are also sponsored by the Department of Energy. In the first, IFC is teamed with Texas A&M University and BCS Technology to increase the power density of the power plant to 1100 W/kg (2 lb/kW), significantly beyond the Ford Phase II goals. The fuel cell will operate on hydrogen and air at ambient pressure. This increase in specific power will be accomplished by using advanced light weight materials, improved catalysts, and better system integration. In the second program, IFC is teamed with the University of Connecticut and the University of Southern Mississippi to advance the viability of direct methanol fuel cells for light duty transportation applications. The key development areas are methanol impermeable membranes, improved catalysts, and system integration and design.

Portable Power Application

To the U.S. Army, PEM portable power systems offer attractive logistic characteristics with the opportunity for extended mission capabilities. In a PEM portable power system application, IFC's PWM concept increases system efficiency, reduces the quantity of reactants that must be carried, reduces the weight of the fuel cell stack and eliminates other system components. All increase power system portability and soldier mission effectiveness and reduce system cost. Figure 5 is a photograph of a 150-Watt hydrogen/oxygen "Soldier Cooling Power Module" under development by IFC for the U.S. Army. The complete system consists only of the PEM stack and the hydrogen and oxygen tanks with their regulators. The total weight of the entire delivery package is less than 4.5 kg (10 pounds) with gas supplies for 1200 watt-hours of operation. IFC has been selected to develop a derivative hydrogen air system.

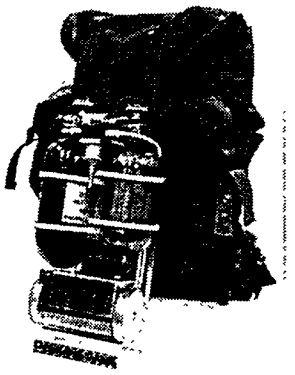

WCN-15356

Figure 5: 150 Watt Portable Power System

Direct methanol PEM fuel cell designs are in the early development stage. At IFC, a DARPA funded program is directed at a 150-Watt, 600 Watt-hour person portable power module. The need is for individual soldier cooling and electronic warfare devices operational on logistic fuel. In this application, the primary driver is low system weight. Successful development may open broader applications in transportation and portable power. Figure 6 is a rendering of the methanol system. The program focuses on developing an understanding of critical operating issues. These issues include methanol cross-over and anode performance.

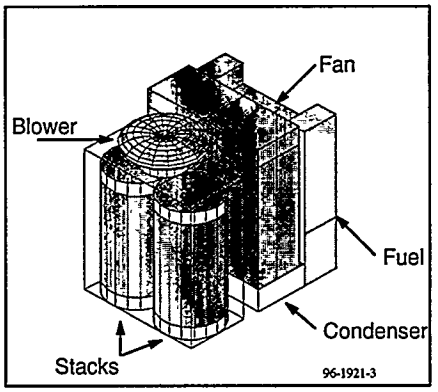

Figure 6: 150-Watt Direct Methanol System

Acknowledgements

IFC wishes to thank the U.S. Department of Energy, the U.S. Army, the Ford Motor Company, Texas A&M University, and the Defense Advanced Projects Agency and the Office of Naval Research for their continued support of our PEM power plant development programs.

HP-309

THE EFFECT OF OPERATION AND DESIGN PARAMETERS ON THE PERFORMANCE OF THE DIRECT METHANOL FUEL CELL

S. F. Simpson, A. Cisar, K. Franaszczuk, H. Moaddel, D. Brejchova,
C. Salinas, D. Weng, and O. J. Murphy
Lynntech, Inc.
7610 Eastmark Drive
Suite 105
College Station, TX 77840

Fuel cell technology continues to receive considerable attention as a potential replacement for fossil fuels as a primary source of terrestrial power. Ideally, such power systems would operate at relatively low temperatures (< 100°C) which suggests strongly the use of cell technology based upon the proton exchange membrane (PEM). Without question, hydrogen is a very desirable fuel choice for these types of systems, because of its high energy density. However, the difficulties associated with the production and routine handling of hydrogen limit severely its commercial use at present. The direct methanol fuel cell (DMFC) is a particularly attractive alternative to the use of the hydrogen/oxygen cell. Although not as high as hydrogen, the energy density of methanol is the highest among the organic fuels. Furthermore, because of the similarity in liquid handling requirements between methanol and gasoline, a significant portion of the infrastructure necessary for the marketing and distribution of the fuel is already in place. Other inherent attributes of the DMFC which include rapid start-up and operation with little or no emission or noise signature have led to an intense DMFC research effort over the past twenty years and, indeed, the DMFC has even been referred to as "the electrochemist's dream".[1]

Despite these advantages and the overall allure of the DMFC, a number of technical challenges must be overcome before the DMFC can become practical. These challenges pertain primarily to performance limitations of the cell that are the result of a number of factors such as the methanol crossover that occurs across the PEM and relatively poor electrocatalysis at the anode. As might be expected, these limitations and their causes will impose significant design restrictions and requirements on a DMFC stack, and an understanding of these constraints is of paramount importance to DMFC commercial development. Thus, the purpose of this work is twofold. Initially, a series of experiments were performed to characterize DMFC performance as a function of a number of experimental

[1] S. Srinivasan, J. Electrochem. Soc., 136, 41C (1989).

parameters such as reactant backpressure, concentration, and flow rate. Following this characterization, various experimental techniques and component design approaches were evaluated in an attempt to overcome the aforementioned limitations and improve the overall performance of the DMFC.

To appreciate the unique behavior of the DMFC, one need not look further than the nature of the fuel itself. As an example of how the cell reacts to different fuel conditions, the effect of methanol concentration on DMFC performance is presented in Figure 1. In addition, cell potential data obtained from both high and low current density cell operation are shown plotted as a function of fuel concentration in the inset in the figure. As the data in both the figure and the inset illustrate, cell performance and fuel efficiency at low current density decreases monotonically with increasing methanol concentration, and this effect is undoubtedly the result of methanol crossover through the PEM. In contrast, the cell voltage / fuel concentration profile for cell operation at high current density exhibits a maximum. Here, voltage decreases observed for solutions of low methanol concentration under high current conditions are the result of mass transport limitations within the electrode. From this relatively simple and straightforward experiment, it becomes clear that DMFC stack design must involve consideration of both the desired power output level and fuel efficiency which ultimately will be governed by the constraints of the application at hand.

Because the methanol fuel in the low temperature DMFC is supplied and utilized in the liquid state, it is to be anticipated that electrode designs implemented and used successfully in the familiar hydrogen/oxygen fuel cell will not be optimum for the DMFC. To illustrate the effect of electrode structure on DMFC performance, polarization curves were collected for a series of membrane and electrode assemblies in which all experimental and design variables were held constant except for the structure of the anode. The resulting curves are shown in Figure 2 and demonstrate clearly the critical dependence of DMFC performance on anode structure. As the data in the figure show, the cell performance level ranges from the very poor performance of structure 5 to the acceptable performance of structure 4. Significantly, it should be noted that some of the differences in the electrode structures represented by the curves in Figure 2 are the result of small, subtle changes in electrode fabrication technique.

As shown by these two examples, DMFC performance depends critically upon a number of experimental factors, and results will be presented which explore the effects of some of these variables. In addition, recent results will be presented regarding work in the area of catalyst development for use at both the anode and the cathode of the DMFC.

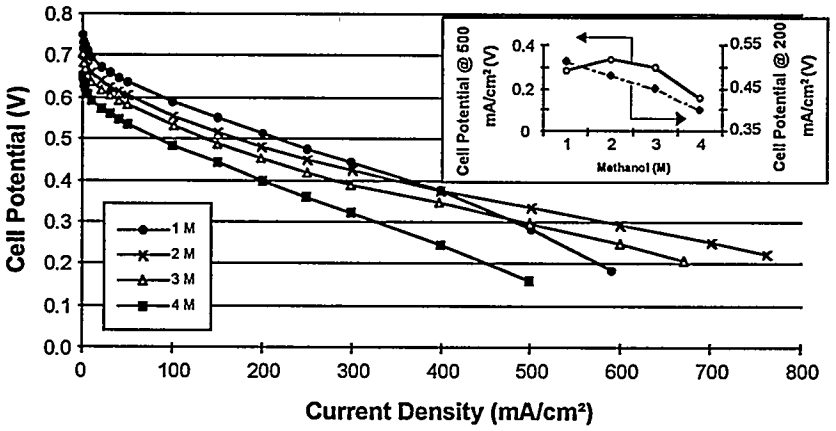

Figure 1. The Effect of Methanol Concentration on Fuel Cell Performance. The active electrode area was 25 cm^2, and the cell temperature was 110°C. Other experimental conditions follow. Membrane: Nafion® 117; anode: 4 mg/cm^2 unsupported Pt-Ru; cathode: 4 mg/cm^2 Pt black; O_2 flow rate: 3.9 L/min; O_2 backpressure: 30 psi; MeOH flow rate: 8 mL/min; MeOH backpressure: 30 psi; MeOH concentration: 2 M.

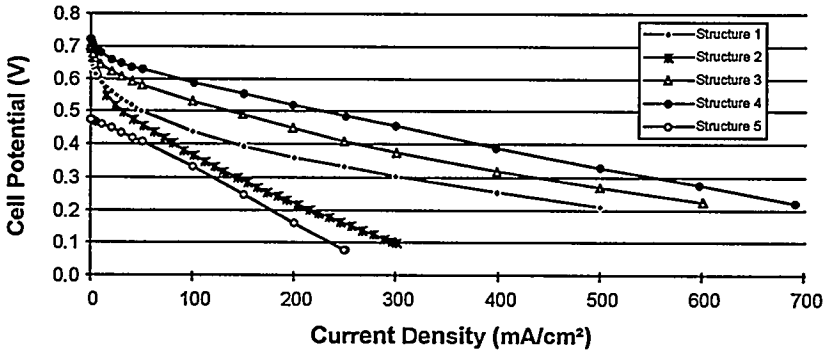

Figure 2. The Effect of Anode Electrode Structure on DMFC Performance. The cell temperature was 80°C. Other experimental conditions were the same as described in the caption of Figure 1.

THE IMPORTANCE OF WATER CONTROL TO PEM FUEL CELL PERFORMANCE

Alan Cisar, Oliver J. Murphy, and Stanley F. Simpson
Lynntech, Inc.
7610 Eastmark Dr., Suite 105
College Station, TX 77840

All membranes currently in use in polymer electrolyte membrane (PEM) fuel cells have sulfonate ($-SO_3^-$) groups as the anionic functionalities attached to the backbone of the polymer electrolyte. As a consequence of this fact, all PEM membranes depend on the presence of water in the electrolyte to facilitate proton transport. This includes perfluorinated membranes, such as Nafion® (DuPont) (1), and Gore Select™ (W. L. Gore) (2), partially fluorinated membranes, such as the Ballard membrane, which is a derivatized trifluorostyrene (3), non-fluorinated membranes, including both sulfonated polyparaphenylene (Maxdem's Poly-X™) (4) and sulfonated styrene-butadiene (DAIS) (5), and the various grafted materials that have been described in the literature (6 ,7). In every case, without water, the proton conductivity of the membrane is insufficient to support fuel cell operation.

Since in every case currently reported increasing the water content of the membrane reduces the resistance to proton conduction (8 ,9), there is a clear advantage to maintaining the membrane in a state of complete saturation. Maintaining the membrane in a state of saturation requires that either the gas in contact with the membrane is saturated with the water vapor, or that the membrane is in contact with liquid water. The presence of liquid water within the cell is not desirable, since the water can cover the surface of the electrocatalyst, blocking access for gases and water droplets in small passages can cause pressure fluctuations.

As a result of this factor, water management has been a major concern to PEM fuel cell developers from the beginning of the technology. Over the last three decades a variety of methods have been developed for controlling the amount of water in a fuel cell stack, each with its own advantages and disadvantages. As the dual drivers of cost and performance continue to push improvements, this problem has become more important. This paper reviews the full range of recorded techniques, from the simplest sparging bottle systems to the most sophisticated internal transfer systems that use water permeable separators to permit the transfer of water from cathode to anode or the back diffusion of waterfrom the cathode to the anode through exceedingly thin membranes.

Humidification techniques can be broadly categorized into two categories, internal to the stack and external from the stack. Internal, or in-the-stack methods, typically limit the gas dew point to the operating temperature of the stack. External methods permit greater flexibility in gas dew point, but require the system to have additional controls as well and generally a significantly to the size of the stack as well.

The most commonly used in-stack humidification method is the "Dummy cell". A dummy cell humidifier, as shown in Figure 1, has separate chambers for gas and water with a water permeable membrane between them. The water is heated to the stack temperature, typically by circulating through the stack as cooling water. The gas is humidified by water evaporating from the membrane. (10) In one variation of this method the gas stream inside the stack passes repeatedly over a cell, and then over a short section of humidifier, with each cell in the stack having its own humidification section, instead of using a common humidifier section at one end of the stack, as is the more general practice. (11)

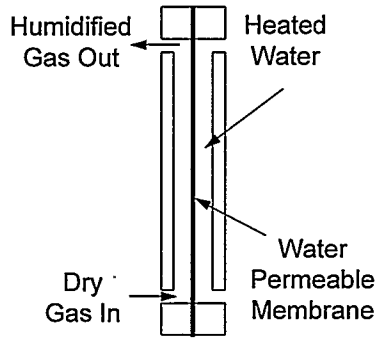

Figure 1. Cross section view illustrating the function of a "Dummy Cell" type humidifier.

Another method of internal humidification involves the use of membranes with internal passages for water flow. This method permits the direct humidification of the electrolyte membrane, and the use of completely dry gases. This approach is especially useful for regenerative fuel cells, which function both as fuel cells and electrolyzers. (12) Direct injection of water as a fine mist into the gas manifolds of a fuel cell stack is another means for humidifying gas inside a fuel cell stack. For multikilowatt systems this can be a compact, volume efficient method. This method, like all in-stack methods, utilizes the phase change enthalpy of evaporation to cool the stack while humidifying. One recent patent reveals a method for fabricating hydrophilic microporous bipolar plates with internal cooling channels. By proper control of pressures within the stack, liquid water formed in the cathode compartment can be forced into the cooling water channels for removal and water from the cooling channels can be forced into the anode chamber to humidify the fuel. (13)

Still another approach to humidification is the use of thin membranes. These membranes are sufficiently thin that the water made by the fuel cell can diffuse from the cathode to the anode along the concentration gradient at a rate comparable to the electro-osmotic flow and keep the membrane sufficiently saturated to support good conductivity. (14) While this approach is a simple and elegant solution to the humidification problem, this is also a solution that requires careful control of the stack produce stable operation.

The simplest external humidification system is the sparger. In a sparger the gases entering the fuel cell are dispersed as fine bubbles and the bubbles permitted to rise through a volume of heated water. As the bubbles rise, the gas quickly becomes saturated with water vapor, reaching equilibrium with the liquid phase. While spargers offer good control of the water content of the gas stream, the required contact time for humidification produces humidifiers that are generally larger than the stack for which they humidify gas.

More recent developments include the use of water permeable tubes surrounded with water to supply a large evaporation surface for the gas passing through the tubes. This approach, which is illustrated in Figure 2, has proven quite flexible and efficient. One variation on this method uses this tube structure in manner more like the one for which it was designed; gas drying. (15) In this approach the wet air exiting the fuel cell passes through the tubes where the gas

is indicated in Figure 2, while the fuel gas passes through the section of the device labeled hot water reservoir in the figure. (There is no heating element used in this configuration.) This leads to the transfer of part of the fuel cell's product water from the exiting air stream to the incoming fuel stream.

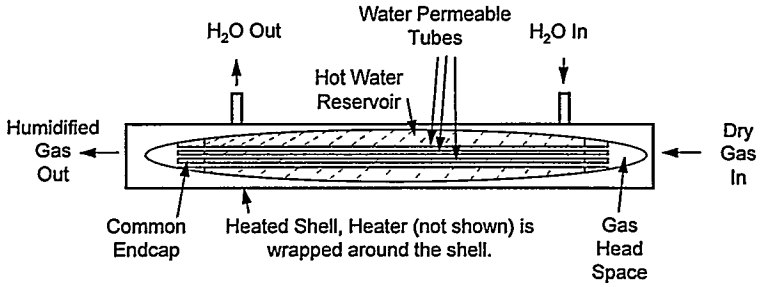

Figure 2. Cut-away view of a parallel tube type humidifier, illustrating the function of this compact device.

Many other methods have been proposed and tested for humidifying feed gases for fuel cells, some of which will also be discussed. (16) Fuel cells are not the only devices requiring gas humidification. There are many varieties of medical equipment that require precise control of humidity, and an even wider variety of methods have been developed to humidify gases. This area can offer many potential approaches to fuel cell humidity control, some of which will be considered here.(17 ,18)

REFERENCES

1. H. L. Yeager, "Transport Properties of Perfluorosulfonate Polymer Membranes," ACS Symposium Series, Vol. 180, pp. 41-63, 1982.
2. J. A. Kolde, B. Bahar, M. S. Wilson, T. A. Zawodzinski, and S. Gottesfeld "Advanced Composite Polymer Electrolyte Fuel Cell Membranes," Proc. Electrochem. Soc., Vol. 95-23, pp. 193-201, Oct. 1995.
3. A. E. Steck, "Membrane Materials in Fuel Cells," Proc. 1st Int. Symp. on New Mat. for Fuel Cell systems, pp. 74-94.
4. R. R. Gagné, S. A. Harding, M. Marrocco, M. Trimmer, and Y. Wang, "Poly-X™ Polyparaphenylenes: A New Family of Processible Amorphous Thermoplastics with Extraordinary Mechanical Properties." Polymer Preprints, Japan, Vol. 42, No. 1, pp. 138-141, 1993.
5. G. E. Wnek, J. N. Rider, J. M. Serpico, A. G. Einset, S. G. Ehrenberg, T. N. Tangredi, and L. A. Raboin, "New Hydrocarbon Proton Exchange Membranes Based on Sulfonated Styrene-Ethylene/Butylene Styrene Triblock Copolymers," Proc. Electrochem. Soc., Vol. 95-23, pp. 2247-251, Oct. 1995.
6. F. N. Büchi, B. Gupta, O. Haas, and G. G. Scherer, "Study of Radiation-Grafted FEP-g-Polystyrene Membranes as Polymer Electrolytes in Fuel Cells," Electrochim. Acta, Vol. 40, No. 3, pp. 345-353, March 1995.

7. A. G. Guzman-Garcia, P. N. Pintauro, M. W. Verbrugge, and E. W. Schneider, "Analysis of radiation-grafted membranes for fuel cell electrolytes," J. Appl. Electrochem., Vol. 22, pp. 204-214, 1992.
8. Y. Sone, P. Ekdunge, and D. Simonsson, "Proton Conductivity of Nafion 117 as Measured by a Four-Probe AC Impedance Method," J. Electrochem. Soc., Vol. 143, No. 4, pp. 1254-1259, Apr. 1996.
9. T. A. Zawodzinski, J. Davey, J. Valerio, and S. Gottesfeld, "The Water Content Dependence of Electro-osmotic Drag in Proton-Conducting Polymer Electrolytes," Electrochim. Acta, Vol. 40, No. 3, pp. 297-302, March 1995.
10. C. Y. Chow and B. M. Wozniczka, "Electrochemical Fuel Cell Stack with Humidification Section Located Upstream from the Electrochemically active Section," **U.S. Patent 5,382,478**, January 17, 1995.
11. N. E. Vanderborgh and J. C. Hedstrom, "Fuel Cell Water Transport," **U.S. Patent 4,973,530**, November 27, 1990.
12. A. Cisar, A. Gonzalez-Martin, and O. J. Murphy, "Internally Humidified Membranes for use in Fuel Cells," Proc. 1st Int. Symp. on New Mat. for Fuel Cell systems, pp. 104-114, 1995.
13. A. P. Meyer, G. W. Scheffler, and P. R. Margiott, "Water Management System for Solid Polymer Electrolyte Fuel Cell Power Plants," **U.S. Patent 5,503,944**, Apr. 2, 1996.
14. H. P. Dhar, "Internally Humidified High Performance Proton Exchange Membrane Fuel Cells", Extended Abstracts, 1994 Fuel Cell Seminar, pp. 85-88, 1994.
15. J. Kertzman, "Fluid Drying Tube," **U.S. Patent 4,705,543**, Nov. 10, 1987.
16. R. A. Sederquist, "Process for Humidifying a Gaseous Fuel Stream," **U.S. Patent 4,530,886**, Jul. 23, 1985.
17. G. J. LaTorraca, "Humidifier Module for Use in a Gas humidification Assembly," **U.S. Patent 4,921,642**, May 1, 1990.
18. K. G. Miller, "Heated Respiratory Therapy Humidifier," **U.S. Patent 4,657,713**, Apr. 14, 1987.

PERFORMANCE OF DIRECT METHANOL POLYMER ELECTROLYTE FUEL CELL

Dong Ryul Shin, Doo Hwan Jung, Chang Hyeong Lee, Young Gab Chun
Fuel Cell Research Team, Korea Institute of Energy Research 71-2, Jang -dong,
Yusong-Ku, Taejeon, 305-343, Korea

INTRODUCTION

Direct methanol fuel cells(DMFC) using polymer electrolyte membrane are promising candidate for application of portable power sources and transportation applications because they do not require any fuel processing equipment and can be operated at low temperature of 60°C - 130°C.[1] Elimination of the fuel processor results in simpler design, higher operation reliability, lower weight volume, and lower capital and operating cost.

However, methanol as a fuel is relatively electrochemical inert, so that kinetics of the methanol oxidation is too slow. Platinum and Pt-based binary alloy electrodes have been extensively studied for methanol electro-oxidation in acid electrolyte at ambient and elevated temperatures. Particularly, unsupported carbon Pt-Ru catalyst was found to be superior to the anode of DMFC using a proton exchange membrane electrolyte(Nafion).[2]

The objective of this study is to develop the high performance DMFC. This paper summarizes the results from half cell and single cell tests, which focus on the electrode manufacturing process, catalyst selection, and operating conditions of single cell such as methanol concentration, temperature and pressure.

EXPERIMENTAL

Half cell tests were carried out in an air-sealed glass that had three separate compartments for the working, counter, and reference electrode. Teflon-bonded carbon supported electrodes with 10w/o Pt, 20w/o Pt, and 20w/o Pt-10w/o Ru catalysts coated on carbon paper (Toray T-90)was used for working electrodes having geometric area of 0.9cm^2 in this study. A platinum gauze(99.999%) was used as the counter electrode. A saturated calomel electrode(SCE) was used for the reference electrode. Potentiodynamic polarization and cyclic voltammetry experiments were performed in 1M H_2SO_4 at constant temperature of 60°C using an EG&G potentiostat/galvanostat.

For single cell performance tests, carbon supported Pt-Ru and unsupported Pt-RuO_x binary metal powders were used for the anode catalyst. Carbon supported anode electrode was prepared with 20w/o Pt-10w/o Ru(Johnson-Matthey) mixed homogeneously with 20w/o of FEP (Fluoethylene propylene) solution and solvent(Micsol). The mixed paste was coated on carbon paper, then, was dried in the oven under nitrogen atmosphere at 100°C for 1hour. The cathode catalyst layer was prepared with 20w/o Pt/C(Johnson-Matthey) employing the same preparation method as anode catalyst layer.

Pt-RuO_x metal powder(atomic ratio Pt:Ru=1:1, E-TEK) was used for the unsupported anode catalyst and Pt-black(20 m^2/g, Johnson-Metthey) was used for the cathode catalyst. The catalyst inks were prepared by adding 5% Nafion solution(Aldrich Inc.) to water-wetted metal catalysts. Compositions of dry ink were 85w/o Pt-RuO_x with 15w/o Nafion for anode ink, and 93 w/o Pt-black with 7w/o Nafion for cathode ink.[3] To prepare the catalyst layer, appropriate amounts of anode and cathode ink were uniformly applied to carbon paper of 8.4 cm^2 area to give metal catalyst loading of approximately 4mg/ cm^2, then, dried as mentioned above. Nafion membrane(117) was cleaned and converted into the acid form by boiling the membrane in 3% H_2O_2, DI water,5% H_2SO_4, and then DI water again for over 1 hour each step. Membrane and electrode assembly(M&EA) was made by hot pressing at 120 °C with 100 kg/ cm^2 for 120 seconds after applying about 0.6 mg/ cm^2 of Nafion solution on the surface of anode and cathode electrodes. M&EA was inserted into fuel cell hardware consisted of graphite block with machined serial flow channel, copper current collectors, and

stainless steel for compression plates.

The single cell was adopted gas feed design. Methanol solution with a pure water as a fuel was pumped into the vaporizer, and then the fuel gas was introduced to the anode channel of the cell, and pure oxygen gas was supplied into the cathode channel. Heater was located on the outside surface of the cell. Cell performances were evaluated over the temperature ranges of 30-130°C, pressure ranges of 0 - 3 kg/cm^2 , and concentration ranges of 0.5 - 4 M methanol as a fuel.

RESULTS AND DISCUSSION

Fig. 1 shows cyclic voltamogram for carbon supported anode electrodes with 20w/o Pt and 20w/o Pt - 10w/o Ru obtained at a scan rate of $20mVs^{-1}$ in 1M H_2SO_4 + 1M CH_3OH solution at 60°C. As applied potential increases, anodic reaction current peaks are observed in the range 0.95 V vs. SCE and 0.7 V vs SCE. As the potential scan reverses, the current peaks are also observed at about of 0.5V vs SCE and 0.4 V vs SCE. It is known that the anodic reaction peaks on the positive potential scan are related to the oxidation of CH_3OH and other peaks on the negative-going sweep are the reduction of oxygen-containing species on the platinum catalyst.[4] As shown in the figure, when the carbon supported Pt - Ru catalyst is used for an anode electrode, the reaction current peaks of methanol are appeared at lower potential than that of the carbon supported Pt electrode. These seem to be related with that Ru plays an important role in accelerating the reaction rate of CH_3OH electro-oxidation. Several mechanisms have been postulated including modification of the electronic nature of the surface, blocking of the poison formation reaction, and co-adsorption of oxygen containing species which can then take part in the main oxidation reaction. The adsorption and dehydrogenation of methanol on Pt surface atom ensembles are followed by the oxidative removal of methanol dehydrogenation fragments via oxygen-containing species on adjacent Ru atoms.

Fig. 2 shows the performance of the single cell using carbon supported Pt-Ru catalyst as an anode electrode and carbon supported Pt catalyst as a cathode electrode for various methanol concentrations at a constant temperature of 130°C. Each datum represent typical steady state voltage which was taken after continuous operation for 5 minutes at the indicated current density. The results show that at high operating current densities, the highest cell voltage is obtained with 2.5M methanol, while relatively lower voltages are obtained with 4M and 0.5M methanol concentration. The poor performance of the cell at highest methanol concentration is seems to be attributed to the methanol cross-over from anode side to cathode side.

Fig. 3 shows the performance of the single cell using unsupported Pt-Ru binary metal catalyst as an anode electrode and a platinum black as a cathode catalyst at the temperature ranges of 60 - 130°C with 2.5M methanol as an anode fuel. As shown in the figure, at potential of 0.4V at the temperature ranges of 100, 110, 120 °C, and 130°C, the current densities are 160, 210, 230 mA/cm^2 and over than 250 mA/ cm^2 , respectively. From the experimental, it shown that anode electrode made of unsupported Pt-Ru catalyst was superior to the electrode made of supported Pt-Ru catalyst. At high temperature, the high performance is attributed to the combined effects of a reduction of ohmic resistance and polarization.

Fig. 4 shows the performance of single cell at various operating pressures.The pressure of anode side is constant at 0 kg/cm^2(gauge) whereas the cathode side vary from 0 to 3 kg/ cm^2. As shown in the figure,The higher cell voltage and open circuit voltage were measured when the cell was operated at the pressure difference of 2 and 3 kg/cm^2 than at the pressure difference of 0 kg/ cm^2. It seems that if the pressure of cathode side was higher than the anode side, it could prohibit effectively the cross-over of methanol from anode side to cathode side, and easy to some extent to eliminate water formed at cathode by electrochemical reaction and increase the reaction activity of catalyst in the electrode.

CONCLUSION

This study was a preliminary stage for developing DMFC. The obtained results will be extended for next work. This study showed that unsupported Pt-Ru catalyst was superior to supported Pt-Ru catalyst for a direct methanol polymer electrolyte fuel cell.

The single cell using unsupported carbon Pt-RuO_x binary metal powder as an anode catalyst and Pt black as a cathode catalyst was shown to be high performance. The performance of single cell was enhanced with increasing cell temperature. High operation temperature attributed to the combined effects of the reduction of ohmic resistance and polarization at high temperature. The higher cell voltage at constant current density were obtained when the cell was operated at cathode side pressure of 2 - 3 kg/ cm^2 with anode side of atmosphere than the pressure of both sides were atmosphere. High cell voltage was obtained from the concentration of 2.5M methanol.

REFERENCES

1. A.K. Shukla, P.A.Christensen, A.Hamnett, and M.P.Hogarth, "A vapor-feed direct-methanol fuel cell with proton - exchange membrane electrolyte", *J. Power Sources*, 55, 87(1995)
2. J.B.Goodenough et.al. "Methanol oxidation on unsupported and carbon supported Pt-Ru anode", *J. Electronal. Chem*, 240, 133(1988)
3. X.Ren, M.S.Wilson, S.Gottesfeld, "High performance direct methanol polymer electrolyte fuel cells", *J. Electrochem. Soc.*, 143, L12(1996)
4. N.A.Hampson, M.J.Wilars, "The methanol - air fuel cell : A selective review of methanol oxidation at platinum electrode in acid electrolyte", *J.Power Sources*, 4, 191(1979)

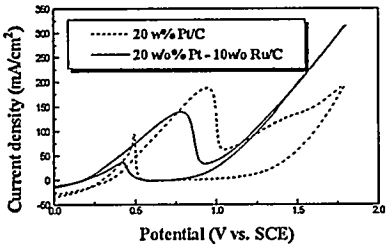

Fig. 1 Cyclic voltammogram for carbon supported Pt and Pt-Ru electrode obtained at a scan rate of $20mVs^{-1}$ in H_2SO_4 + 1M CH_3OH.

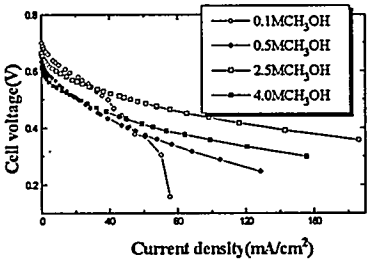

Fig. 2 The performance of single cell using by carbon supported Pt-Ru electrode for various methanol concentrations at 130°C. anode : 20 w/o Pt-10w/o Ru/C(1.5 mg Pt/cm^2), and atmosphere, and 2.5M methanol at 9ml/min. cathode : 20w/o Pt/C(0.4mg Pt/cm^2), and $3Kg/cm^2$ O_2 at 105 sccm.

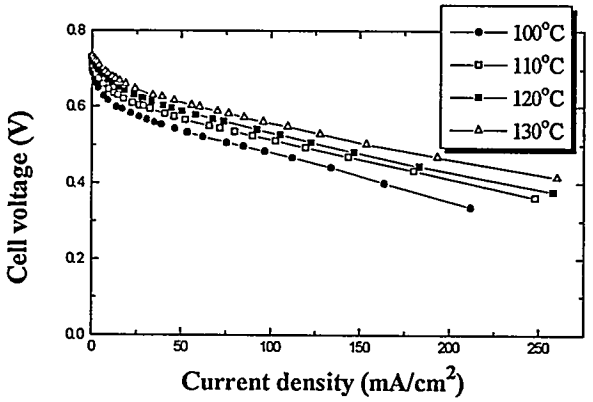

Fig. 3 The performance of single cell by using unsupported Pt-RuO_x electrode. anode : 4.0mg/cm^2 Pt-RuO_x, 1kg/cm^2, and 2.5M methanol at 9ml/min. cathode : 4.0mg/cm^2 Pt-black, 3 kg/cm^2 , O_2 at 105 sccm.

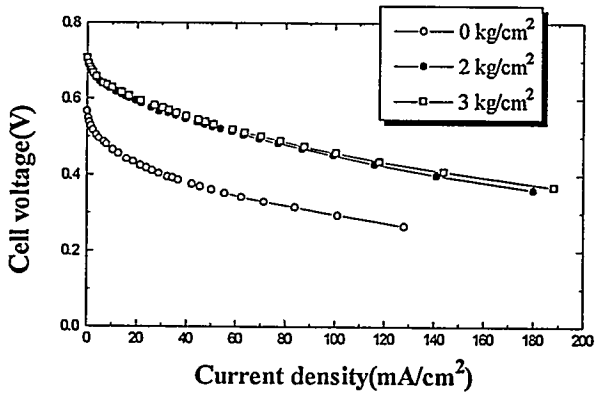

Fig. 4 The performance of single cell using by carbon supported Pt-Ru electrode for various operating pressure at 130°C. anode : 20 w/o Pt-10w/o Ru/C(1.5 mg Pt/cm^2), atmosphere, and 2.5M methanol at 9ml/min. cathode : 20w/o Pt/C(0.4mg Pt/cm^2), and 3Kg/cm^2 O_2 at 105 sccm.

PERFORMANCE IMPROVEMENT OF PEFC MODULES WITH CELLS CONTAINING LOW AMOUNT OF PLATINUM

*Y.Miyake, M.Kadowaki, A.Hamada, M.Kaneko, T.Nakaoka,
T.Matsubayashi and K.Nishio
New Materials Research Center, SANYO Electric Co., Ltd.
1-1 Dainichi-higashimachi, Moriguchi-shi, Osaka 570, Japan

M.Enami and K.Takasu
New Energy and industrial Technology Development Organization (NEDO)
Sunshine 60, 3-1-1, Higashi-ikebukuro. Toshima-ku, Tokyo 170, Japan

ABSTRACT

Cell components of the PEFC module were studied to improve the module performance. The cell performance in a high air utilization region was improved by selecting an air channel design of the separator in which high air flow speed was obtained. Optimization of Teflon® amount on the cathode backing carbon paper also contributed the cell performance.

Modifications of the gas channel design and the backing carbon paper were carried out in a 200 cm^2 × 20-cell module and 36-cell module. Dependence of air utilization on module performance was remarkably improved and power density of more than 0.3 W/cm^2 was achieved in spite of the platinum amount in the cells was decreased to 1.1 mg/cm^2.

INTRODUCTION

Polymer electrolyte fuel cells (PEFCs) offer many advantages, such as low operating temperature and a high power density. Taking these advantages, PEFCs have been paid much attention as a promising power source for transportation use and stationary use in recent years. SANYO has been developing PEFCs as an R & D project of NEDO under the New Sunshine Project from FY 1992.

In PEFCs, a precious metal, platinum is used as the electrode catalyst. Therefore, reducing the electrode catalyst is one of the important subjects for practical application. We have developed an electrode with a new structure which has already reported[1),2)], called "High ion conductive electrode". We have developed 1 kW class module (1st model, 200 cm^2 × 20-cell module) with this unique electrode in last year. The output power density of more than 0.3 W/cm^2 was achieved at a pressure of 3 atm and current density of 0.5 A/cm^2 (this performance met the projected target) in this module, but the large voltage drop occurred when the air utilization was higher than 20 %. To solve this problem and to develop higher performance modules, we examined the cell components of the PEFC module, mainly concerning with air channel configuration of the gas separator and the current collector of the electrode.

In this paper, results of the study and the operating tests of 200 cm^2 × 20-cell module (2nd model) and 200 cm^2 × 36-cell module in which cell components were modified are described.

EXPERIMENTAL

(1)Influence of air flow speed through the air channel on the cell performance

The relationship between cell performance and air flow speed through the air channel of the separator was examined by 200cm² single cells. Fabrication method of the test cell units was previously described [3]. Four kinds of the gas separators, in which the air channels were designed so that air flow speed became 1, 3, 5, 7 times that of separator adopted in 1 kW class module (1st model), were designed for the test cells.

(2)Effect of Teflon® amount on the carbon backing paper on the cell performance

The relationship between cell performance and Teflon® amount on the carbon backing paper was examined. Property of the backing carbon paper and cell performance were measured when the Teflon® amount on the backing carbon paper was changed. 25 cm² single cells were used to measure the cell performance.

(3)Module operating test

The specification of 200 cm² × 20 cell module (2nd model) and 200 cm² × 36-cell module were listed in table 1. Photograph of 200 cm² × 36-cell module is shown in figure 1. Water cooling was adopted and the cooling plate was placed in every two cells. Platinum amount of the cathode and the anode were controlled to 0.6 mg/cm² and 0.5mg/cm². Nafion® 115 was adopted as a membrane of the cell unit. Cell components were modified in both modules from the results of above experiment.

These modules were tested using pure hydrogen as a fuel and air as an oxidant. The output characteristics and the influence of reactant gas utilization on the module performance were measured. These results were compared with that of 200 cm² × 20-cell module (1st model).

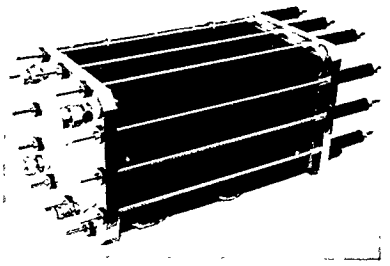

Fig.1 Photograph of 200 cm2 × 36-cell module.

Table 1 Specifications of the test modules

Module	200cm².20-cells(2nd model)	200cm², 36-cells
Output power Cooling method	1 kW class Water cooling	2 kW class Water cooling
Relative air flow speed through air channel	5 (vs. 1st model)	5 (vs. 1st model)
Pt amount of the electrodes Cathode(mg/cm²) Anode (mg/cm²)	 0.6(1st model: 0.7) 0.5(1st model: 0.7)	 0.6 0.5
Membrane	Nafion® 115	Nafion® 115

RESULTS AND DISCUSSIONS

(1)Influence of air flow speed

Figure 2 shows relationship between cell voltage and air flow speed through the air channel of 200 cm^2 single cells. When the relative air flow speed was less than 5, no cell voltage change was observed at the air utilization of 20 %. But in case of air utilization of 46 %, higest voltage was obtained when the relative air flow speed was 5. It was considered that air channel closing by the product water was restricted by increasing the air flow speed. It was found that better cell performance was obtained even at high air utilization by increasing the air flow speed.

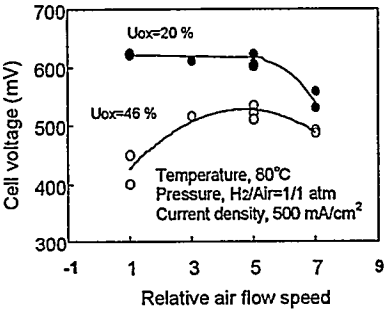

Fig. 2 Relationship between cell voltage and air flow speed through th air channel of 200 cm^2 single cells.

(2)Influence of Teflon® amount on the carbon backing paper

Figure 3 shows relationship between cell voltage and Teflon® amount on the carbon backing paper. When air utilization was 40 %, cell voltage tended to lower with increasing Teflon® amount on the carbon backing paper. Wetproofing property of the backing carbon paper becomes distinct when the Teflon® amount increases. However, excess wetproofing property leads to lower water drawing from the cathode. That seemed to be why the cell voltage with large Teflon® amount on the backing carbon paper lowered at air utilization of 40 %. It was found that less than 15 wt% of Teflon® amount was desirable for the cathode backing carbon paper.

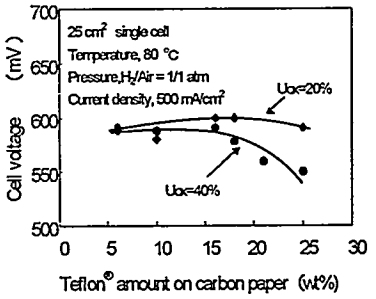

Fig. 3 Relationship between cell voltage and Teflon® amount on the carbon backing paper.

(3)Module operating test

Figure 4 shows the relationship between module voltage and air utilization. The dependence of air utilization on module voltage was remarkably improved and good performance was obtained even at high air

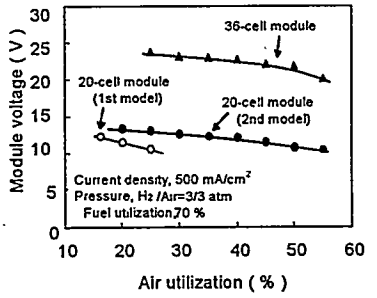

Fig. 4 Relationship between module voltage and air utilization.

utilization of 50 %. It was confirmed that modification of the air channel design and change in the Teflon® amount of the backing carbon paper was effective to improve the module performance in a higher air utilization.

Figure 5 shows output characteristic of 200 cm^2 × 36-cell module. The output power of 2.22 kW, power density of 0.31 W/cm^2 was obtained at a current density of 500 mA/cm^2, a pressure of 3 atm and a air utilization of 40 %. Uniform cell voltage distribution of about 20 mV was observed.

Figure 6 shows the result of daily start-shut-down operation test of 200 cm^2 × 36-cell module. The test continued for a 3700 hours and about 40 cycles of operation was achieved. The module voltage was almost constant at a current density of 300mA/cm^2, but The cell resistance tended to increase slightly in this period.

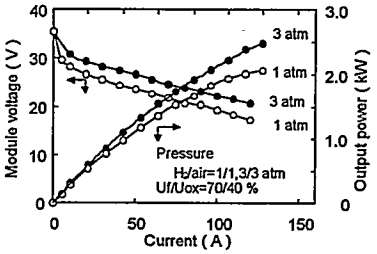

Fig. 5 Output characteristics of 200 cm^2 × 36-cell module.

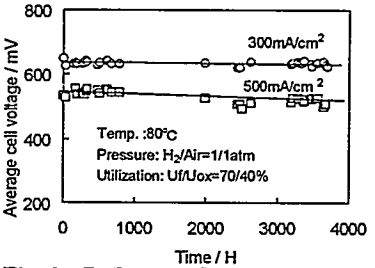

Fig. 6 Daily start-shut-down test of 200 cm^2 × 36-cell module.

CONCLUSION

Cell components of the PEFC module were studied to improve the module performance. Modifications of the gas channel design and the backing carbon paper were carried out in a 200 cm^2 × 20-cell module and 36-cell module from the results of the study. Dependence of air utilization on module performance was remarkably improved and power density of more than 0.3 W/cm^2 was achieved

ACKNOWLEDGMENT.

Part of this work was performed as an R & D project of the New Energy and Industrial Technology Development Organization (NEDO) under the New Sunshine Project of MITI.

REFERENCES

1) A. Hamada et. Al., Proceedings of the 1st FCDIC Fuel Cell Symposium, p.174(1994)
2) T. Matsubayashi et. Al., Proceedings of the 1994 Fuel Cell Seminar, p.158(1994)
3) T. Matsubayashi et. Al., Proceedings of the 2nd International Fuel Cell Conference, p.371(1996)

STAINLESS STEEL WIRE MESH FLOW-FIELDS FOR POLYMER ELECTROLYTE FUEL CELLS

Christine Zawodzinski, Mahlon S. Wilson and Shimshon Gottesfeld
Electronic and Electrochemical Materials and Devices Research Group, MS D429
Los Alamos National Laboratory, Los Alamos, N.M. 87545

Introduction

The advantages offered by the PEM fuel cell, efficient power generation with little or no environmental emissions, low operating temperature, and non-liquid/non-corrosive electrolyte, make it attractive as a potential power source for transportation and for portable and stationary power generation applications. Fuel cells have been successfully demonstrated in a number of aerospace, utility and military applications, however, the high cost of fuel cells compared to conventional power generation technologies has delayed their potential widespread use. Stack manufacturers have historically used high-platinum loading membrane/electrode assemblies (MEAs) and intricately machined graphite bipolar plates, which have made the cost too high for most commercial applications. We have thus focused our efforts on decreasing the cost of these components in order to demonstrate an inexpensive, yet high performance PEM fuel cell. Here, we describe the design and demonstration of a 100 cm^2 (active area) cell that utilizes ultra-low platinum loading MEAs and inexpensive, stainless steel wire screen flow-fields.

Membrane/Electrode Assembly

Our efforts in the design of this cell involved adapting ultra-low platinum loading technology developed at Los Alamos [1] to reproducibly fabricate larger-scale, high performance MEAs. This was achieved using a computer-controlled chart-recorder process that has been previously described [2]. A typical MEA consists of a 100 cm^2 active area catalyzed Nafion™ membrane (Nafion 112 from DuPont) and two E-TEK (Natick, MA) carbon cloth backings. The platinum loading is approximately 0.14 mg Pt/cm^2/electrode, which corresponds to a dramatic decrease in total stack platinum content and significantly reduces the cost of the MEA.

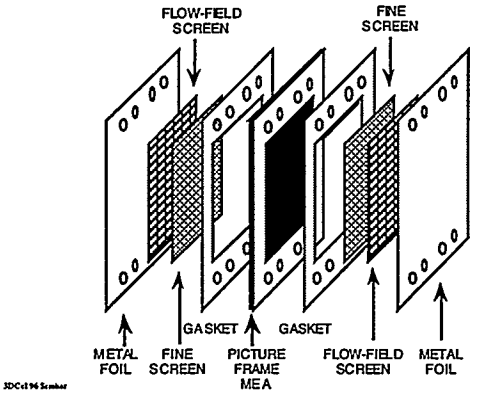

Figure 1. Components of a unit cell utilizing wire-screen flow-fields, metal foil separators, and a Picture Frame MEA.

Wire Screen Flow-Fields and Unit Cell Configuration

More recently, we have focused on replacing machined graphite or machined metal flow-fields with inexpensive, off-the-shelf wire screens and foils [2]. The flow-fields are based on simple woven wire-mesh screens of various stainless steels, which can be sandwiched around a thin metal plate of the same material to create a bipolar plate/flow-field configuration for use in a stack. Major

advantages of using stainless steel wire screens include the elimination of expensive raw materials as well as machining and/or other special fabrication costs. Many types of screens are readily available in a variety of thicknesses and mesh sizes. The screens are also relatively light-weight in comparison to thick graphite or solid metal plates. Another advantage of metal screen hardware is that the screens and foils are not brittle, thus very thin unit cells may be possible. The wire screen flow-field consists of a sandwich of two screens, a coarse mesh and a fine mesh, that sit within a compressible gasket "frame" backed by a thin, metal foil (Figure 1). The fine mesh screen, which is situated between the coarse mesh screen and the MEA, allows adequate reactant access to the MEA while protecting the carbon cloth backing from squeezing into the coarser screen. The MEA is encased within a thin metal "picture frame" which simplifies sealing and manifolding and has the added benefits of making the MEA easy to handle and align within the cell during assembly. Cooling plates (not depicted in the figure) can be provided as well by sandwiching two unit cells around a wire-screen flow-field.

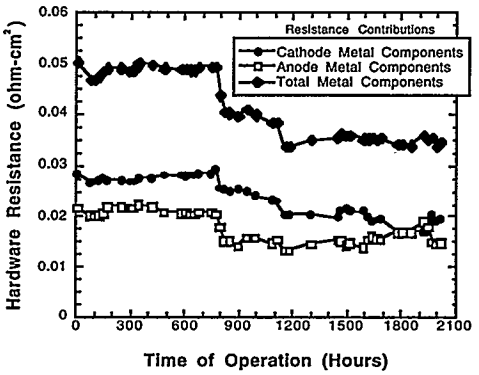

Figure 2. Measured contributions of the 316 SS metal components to the cell resistance on the anode and cathode sides and the total contribution over the life of a cell.

100 cm^2 Single Cells

The first screen flow-fields tested were made of untreated 304 stainless steel (SS), however, it became necessary to acid-etch the screens and foils to remove surface oxide layers that decreased their conductivity. A typical 100 cm^2 single cell utilizing the acid-etched 304 SS flow-fields and operating on humidified, pressurized H_2/air provided about 0.5 W/cm^2 at 0.62 V (50% LHV voltage efficiency). Both the hydrogen and air gas streams were pressurized at 3 atm and flow rates were maintained at approximately 2 and 4 L/min., respectively. These flows are slightly greater than the 1 and 2X the stoichiometric amount of flow required to operate the cell at 1 A/cm^2. Typical pressure drops across the cathode flow-field were about 0.13 atm (2 psi). The high frequency cell resistance (HFR) was close to 0.15 Ω cm^2, which is somewhat high compared to small cells, but not unreasonable considering the numerous components and interfaces involved and the size of the active area. With time, the 304 SS cells demonstrated loss of component conductivity. It was anticipated that the use of 316 SS instead of 304 would improve the stability of the metal structures. Thus, cells were assembled using 316 SS components that were not surface treated beyond a simple cleaning. The latter cells performed as well as the etched 304 SS cells and showed no appreciable performance losses over time.

One such 316 SS single cell was operated for 2000 h at a constant voltage of 0.5 V. The long-term performance of the cell was monitored in a number of ways: by measuring voltage drops across the cell components, measuring the HFR, and by periodically obtaining polarization curves. With the cell set to operate at a fixed current, the voltage drops were measured between the various components, which allows the calculation of the contribution of the metal components to the cell resistance. The 2000 hour life test results are shown in Figure 2.

The anode and cathode metal component contributions in Figure 2 consist of the resistances of all components and interfaces between a fine screen (positioned against the MEA) and its respective current collector plate. Thus, the current traverses 1) the SS fine screen, 2) the SS flow-field screen, 3) an SS foil separator plate, and 4) the current collector plate, a total of four components and three interfaces. Also shown in this figure is the total contribution of the metal hardware, calculated from the measured voltage difference between the fine wire sense leads and the current collector plates at a fixed current. The curves in Figure 2 demonstrate that the contribution of the metal hardware is relatively stable during the 2000 hour test. The exception occurs at about 800 h, whereupon the tie-bolts holding the cell together were re-torqued, which brought the components together more forcefully and substantially improved the conductivities across the interfaces. The improvement in cell performance is demonstrated in Figure 3. From the improvement in the low-current density region of the curves, it is evident that the performance enhancement upon tightening the cell was also due to realizing more effective electrode performance.

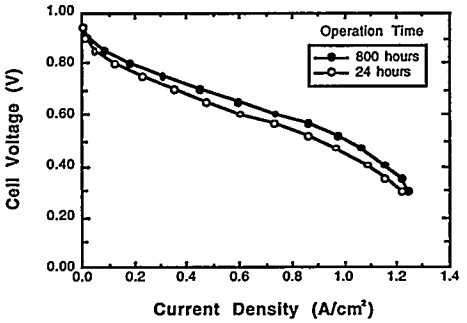

Figure 3. Polarization curves of a cell using 316 SS wire screen and foil components after 24 and 800 h. The improvement is primarily due to re-torqueing of the tie-bolts.

If the stainless steel in the cell was corroding or passivating, the resistance of the metal components would tend to increase over time. This is not observed in Figure 2, which either suggests that corrosion was minimal or that residual corrosion did not cause any appreciable surface passivation. Polyvalent metal ions liberated by residual dissolution of the metal hardware could conceivably enter into the polymer electrolyte membrane and tie up active sites, thus adversely affecting the protonic conductivity of the ionomer. Samples of the MEA were analyzed by EDS (Energy-Dispersive X-Ray Spectroscopy) for the presence of molybdenum, a component unique to 316 SS. No molybdenum was found, though it should be stressed that the detection levels are only in the parts per thousands. Further analyses are underway. In any case, loss of conductivity by ionic inclusion should have been observed by an increase in cell HFR. From Figure 4, the HFR did fluctuate with time, which may only be a reflection of the changes in hydration state of the membrane.

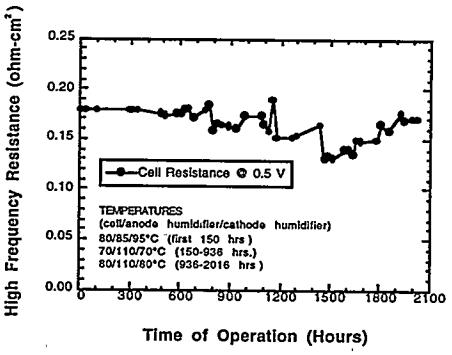

Figure 4. High Frequency Resistance (HFR) of a cell using 316 SS wire screen and foil components over 2000 h.

The 316 SS hardware was clearly superior to the 304 SS in terms of long-term stability. Disassembly after 2000 hours of the 316 SS cell revealed no visible corrosion of the metal components. Perhaps 316L SS could be even more stable than 316 SS because of its lower carbon content and corresponding lower corrosion susceptibility [3].

The long-term performance and stability obtained with the use of untreated metal alloy screens/foils in combination with low platinum loading MEAs are encouraging because these components could provide the basis for a very low-cost PEM fuel cell stack technology.

Acknowledgment
This work was supported by the Hydrogen Program of the Department of Energy, Office of Utility Technologies.

References
1. M. S. Wilson, J. Valerio and S. Gottesfeld, "Low Platinum Loading Electrodes for Polymer Electrolyte Fuel Cells Fabricated Using Thermoplastic Ionomers," Electrochim. Acta, Vol. 40, p. 355, 1995.
2. C. Zawodzinski, M. S. Wilson, and S. Gottesfeld, "PEM Fuel Cell Stack Development Based on Membrane-Electrode Assemblies of Ultra-Low Platinum Loadings," in "Proton Conducting Membrane Fuel Cells I," S. Gottesfeld, G. Halpert, and A. Landgrebe, Eds., The Electrochemical Society Proceedings Series, Vol. 95-23, p. 57, 1995.
3. R. K. A. M. Mallant, F. G. H. Koene, C. W. G. Verhoeve and A. Ruiter, "Solid Polymer Fuel Cell Research at ECN," Program and Abstracts of the Fuel Cell Seminar, p. 503, Nov. 28 - Dec. 1, San Diego, CA, 1994.

CHARACTERIZATION AND BASIC RESEARCH INVESTIGATIONS AT PEFC ELECTRODES AND MEA

M. Schulze, N. Wagner, G. Steinhilber, E. Gülzow, M. Wöhr, K. Bolwin

Institut für Technische Thermodynamik
Deutsche Forschungsanstalt für Luft- und Raumfahrt (DLR)
Pfaffenwaldring 38-40, D-70569 Stuttgart, Germany

Introduction

For the study of electrochemical and transport mechanisms in polymere electrolyte fuel cells (PEFC) electrodes and for a further development of PEFC electrodes it is important to characterize these electrodes. The characterization of the electrodes was performed by electrochemical analytical as well as physical methodes on both single electrodes and electrode-membrane assemblies (MEA). In addition to voltage-current characteristics the electrodes were electrochemically measured by cyclic voltammetry, electrochemical impedance spectroscopy and chronopotentiometry. To determine the pore systems nitrogen adsorption and mercury porosimetry were used. Chemical composition and microstructure of the electrodes were studied by surface science methodes like scanning electron microscopy or X-ray induced photoelectron spectroscopy. The results of characterization are the base for theoretical simulation of fuel cells and fuel cell stacks.

Surface Science Methods

The X-ray Photoelectron Spectroscopy yields quantitive informations on concentration of elements on surfaces and the binding states of these elements. Up to 100nm depth profiles can be recorded by measuring XP-spectra and ion etching the surface alternatingly. We have studied gas diffusion electrodes which were produced by DLR [1, 2] and commercial E-TEK electrodes. The main components of the surface are carbon and fluorine from carbon black and PTFE. Additional platinum from the platinized carbon black, oxygen and sulfur are detected in the XP-spectra of the electrodes. In the electrode produced by DLR the platinum concentration is equal to the platinum concentration in the used carbon black and keeps constant during depth profiling. In depth profiles of DLR produced electrodes XP-spectra show only a decomposition of the polymers [3], which is induced by X-ray exposure and ion bombardment. E-TEK electrodes show different results in depth profiling. The surface of E-TEK is covered by a PTFE-film with a thickness of 3 nm; so the platinum concentration in these electrodes increases at the begining of depth profile measurements.

In all electrodes sulfur can be observed in a concentration of 0.2 - 0.4 %. This sulfur concentration is also measured in the carbon black; sulfur from Nafion in these electrodes gives only a minor portion of the total sulfur signal.

In polymer electrolyte fuel cells (PEFC), Nafion is used as the electrolyte. Its contact with the cell electrode also enlarges the three-phase boundary between the catalyst, gas and proton-conducting membrane. Nafion is inserted in electrodes to enlarge the three phase boundary, which is relevant for the reaction [4-6]. The distribution of Nafion is critical to optimize the electrodes. Addition of Nafion powder to the electrode during preparation is an solvent free procedure [7]. The electrodes are produced by a rolling process, which is described in literature [2, 8-12]. These electrodes consist of platinated carbon black, polytetrafluorethylene (PTFE) as an organic binder and Nafion. The particle size of the used pulverized Nafion is some μm [13].

The distribution of the different components of the electrodes is important for their operation behavior. The structure of electrodes was investigated by Scanning Electron Microscopy (SEM). The SEM images provide no information about the materials of the particles. The Energy Dispersive X-ray spectroscopy (EDX) allows to study the element distribution on the electrode surface.

Since Nafion is chemically related to the polytetraflourethylene (PTFE) used as binder in the electrode, distinction between both is only possible through observation of sulfur peaks, obtained by analysis of the electrodes using surface science methods. By means of EDX analysis one is able to determine the local distribution of elements. Using these methods however, platinum in

the electrodes give an X-ray signal, which is superposed to the sulfur signal. Therefore it is a problem to distinguish the two elements. Sulfur seems to be detected at those places where platinum is present. The second problem of Nafion detection by the sulfur signal is, that the sulfur concentration in Nafion is not significantly higher then in the carbon black. Figure 1 shows a micrograph of the cross section and the EDX mappings for carbon, sulfur, platinum and fluorine of a Nafion powder containing electrode. Light areas in the element maps indicate a high concentration of the elements, dark areas a low concentration. Thus sulfur can not be used to distinguish Nafion from PTFE. Further Scanning Auger Electron Spectroscopy (SAES) is not able to distinguish between Nafion and PTFE, since the same problem arises- the superposition of Auger electrons from sulfur and platinum.
In order to investigate the electrodes by these methods, the Nafion must be marked somehow. One possibility is to exchange the conducting protons in the Nafion with alkali ions. Through the choice of alkali ions, one is able to choose a specific area of the spectra which does not coincide with signals from other electrode components; sodium is a good tracer-candidate for the surface science methods. Having marked Nafion with alkaline ions the distribution of Nafion in a fuel

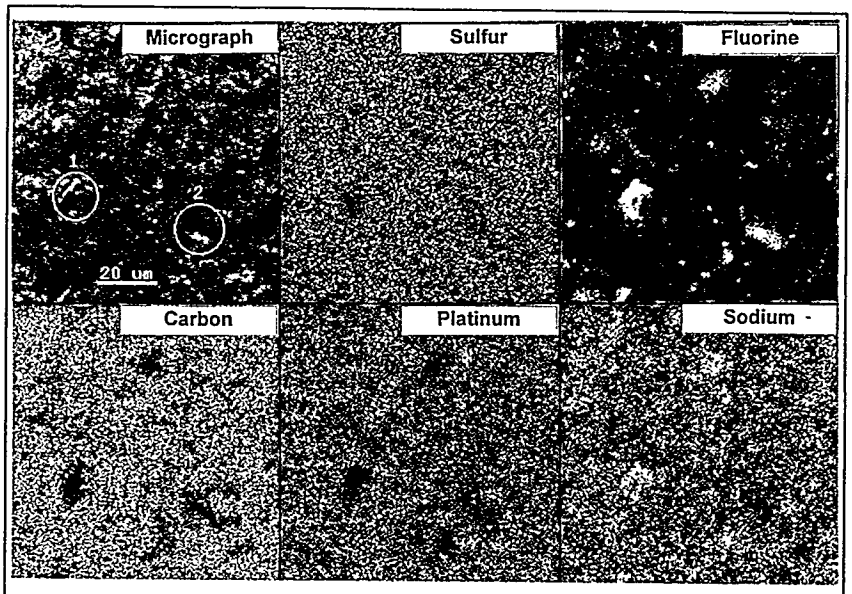

Fig. 1: SEM-image of a gas diffusion electrode for PEFC and EDX-mappings for the elements: C, S, Pt, F and Na after marking Nafion by Na

cell electrode can be measured. For this, the element distribution of fluorine and the alkaline metal must be determined.
Secondly the membrane was characterized by XPS to determine the element composition. Sulfur can be identified by XPS measurements, however the spatial element distribution on the surface can not be determined. After ion exchange sodium produces the Na1s-signal at a binding energy of about $E_{b,Na1s}$ = 1075 eV in the XP-spectrum. The sulfur signal is observed at a binding energy of $E_{b,S2p}$ = 170 eV.

Figure 1 also shows the element distribution of sodium on the electrode after ion exchange additionally. In the SEM image a Nafion particle is labeled with a. At this position a concentration of fluorine and sodium is detected. The particle labeled with b consists of PTFE; a concentration of fluorine is found, but no concentration of sodium. By marking Nafion with alkaline ions, Nafion and PTFE in an electrode can be distinguished by the sodium concentration using EDX mapping. However sodium concentrations not only exist on Nafion particles. Sodium is also concentrated at platinum particles. For a reliable identification of Nafion the distribution of sodium and fluorine has to be measured.

Porosimetry

For the transport mechanism and the structure of the electrodes the pore systems are significant. Using nitrogen adsorption and mercury porosimetry [15, 16] the pore systems of membrane electrode assemblies, single electrodes and of their components are measured. The electrodes consist of the catalyst supported carbon black and a carbon backing. Electrodes produced by a rolling process at DLR [1, 2, 7], wet chemically prepared electrodes and commercial electrodes from E-Tek and GDE have been measured. In addition the pore system of membrane-electrode-assemblies (MEA) was measured.

Two different pore systems have been found; the carbon backing has a porosity with a pore radius of about 10 to 30 µm, the catalyst supporting carbon black has a pore system in the range of 7 to 30 nm pore radius. The porosimetry measurement of the supporting carbon black shows two maxima in the pore size distribution. The maxima in the pore size distribution for the supporting carbon black are at pore radii of about 10 nm and 20 nm.

For all electrodes the pore systems of the carbon backing and the catalyst supporting carbon black can be observed. Preparing the electrodes wet chemically or by the rolling process the pore system of the carbon backing in not changed. The pore system of the carbon black is unchanged at wet chemical preparation, but the pore size of the carbon black decreases at the rolling process.

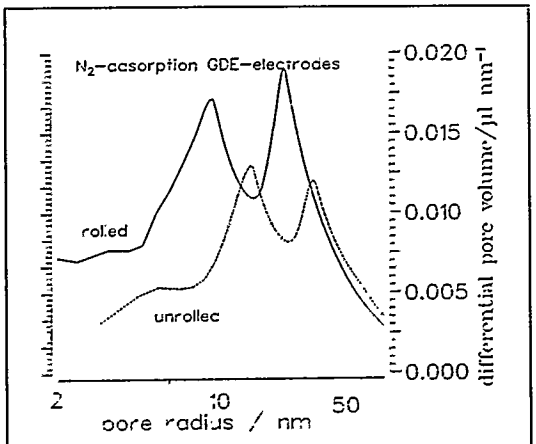

Fig. 2: Pore size distribution of a rolled electrode and an unrolled electrode

A rolled electrode has more narrow pores then the catalyst supporting carbon black. The two maxima in the pore size distribution of the carbon black shift 2-4 nm to lower pore radii. This compression of the pores is been observed also on commercial electrodes, which were rolled at DLR to study the influence of the rolling process.

BET measurements on MEA shows the pore systems of the applied electrodes. The protonic conducting polymere yields no additional porosity, so only the pore system of the electrode is determined by the porosimetric measurements. The porosimetry allows to measure the pore size distribution of electrodes in a MEA structure as well as that of single electrodes.

Electrochemical investigations

Electrodes were characterized electrochemically using Electrochemical Impedance Spectroscopy (EIS), Cyclic Voltammetry (CV) and measurements on a rotating disc electrode [17]. These measurements were performed in a half cell configuration with a 1 mol H_2SO_4 electrolyte. Also the MEA was measured using EIS.

Cyclic voltametric measurements on polished platium yields two hydrogen adsorption peaks and the potential ranges of hydrogen and oxygen evolution. Measuring the commercial ElectroChem electrodes the hydrogen adsorption peaks are not observed. At a potential more negative than 700 mV the current density shifts to more negative values if one changes from an inert gas saturated electrolyte to a oxygen saturated electrolyte. In this potential range below 700 mV a current caused by the oxygen reduction und limited by diffusion processes, leads to this shift in the current density.

At porous electrodes the electrochemically active surface is higher than the geometric surface. The geometric factor as the ratio of active and geometric surface was determined to be about 40 by EIS measurement using the half cell configuration with sulfur acid

The kinetics of the oxygen reduction and the hydrogen oxidation was studied. For the oxygen reduction on an ElectroChem electrode the kinetic parameters are determined: the exchange current density is about 2 $\mu A/cm^2$ and the Tafel slope is 92 mV/decade. The kinetic inhibition of the hydrogen oxidation is 3 decades lower, so the anode in a MEA can be used as reference and counter electrode.

For the interpretation of the EIS measurement of the porous electrodes a model is used, which takes cylindric pores into account [18,19]. At current densities lower than 100 mA/cm^2 the current-voltage characteristics is dominated by kinetic inhibitions, above 100 mA/cm^2 the resistance of the electrolyte leads to a linear increase of the characteristics in addition to a constant amount from the kinetic inhibition.

Conclusions

The platinum concentration in gas diffusion electrodes produced by DLR is constant in the examined depth range and equal to the platinum concentration in the catalyst supporting carbon black. In contrast commercial E-TEK electrodes are covered by a 3 nm PTFE-film. The catalyst supporting carbon blacks contains sulfur, which can be detected by XPS.

Laterally resolved surface science methods allow to determine the distribution of the different components of electrodes. The sulfur signal from Nafion is superposed by a platinum signal, so the sulfur concentration does not allow a distinction of Nafion and PTFE in an electrode.

Nafion can be marked by ion exchange with alkaline ions. In order to identify Nafion and PTFE unambigously, the concentration of fluorine and the tracer alkaline must be measured. Thus the distribution of Nafion and PTFE in an electrode can be determined by EDX.

Porosimetry measurements yield two pore systems in the electrode, one from the carbon backing and one from the catalyst supporting carbon black. At a rolling process the pore size of the carbon black decreases and the pore size distribution shifts to lower pore radii.

The porosimetry allows to determine the pore size distribution of electrodes in a MEA structure as well as that of single electrodes. The protonic conducting polymere yields no additional porosity, so only the pore system of the electrode is determined by the porosimetric measurements. This allows to investigate degradation processes of the electrodes under electrochemical operation.

Electrochemical investigations yield insight into informations on the electrochemical kinetics, the active surface and the degree of utilization of the electrodes and the electrochemically relevant pore structure. Additionally it is possible to separate infuences of different parameters on the overvoltage in fuel cells.

Acknowledgements
The authors gratefully acknowledge the financial support of Deutsche Forschungsgemeinschaft (DFG). The surface science studies in this work were performed as part of the Sonderforschungsbereich 270. Further the authors acknowledge the financial support of the State of Baden Württemberg (Wirtschaftsministerium, Fuel Cell Program of Baden Württemberg). The authors thank their collegues for experimental support, mainly D. Bevers for the preparation of the electrodes and Dr. M. v. Bradke for the EDX measurements.

Literature References

1. D. Bevers, E. Gülzow,. A. Helmboldt, B. Müller,.Innovative Production Technique for PEFC Electrodes, Proc. Fuel Cell Seminar Orlando (1996)
2. D. Bevers, N. Wagner, M. von Bradke; Innovative Production Procedure for Low Cost PEFC Electrodes and Electrode Membrane Structures; Proc. 11th World Hydrogen Energy Conf.-Stuttgart, 1996 Germany
3. M. Schulze, K. Bolwin, E. Gülzow, W. Schnurnberger, Fresenius J. Anal. Chem. 353 (1995); p778
4. S. Srinivasan, E. A. Ticianelli, C. R. Derouin, A. Rodondo; J. Power Sources (1988) 22; p 359
5. K. Petrov, Ke Xiao, E. R. Gonzales, S. Srinivasan, A. J. Appleby, O. J. Murphy; Int. J. Hydrogen Energy (1993) 18; p907
6. E. A. Ticianelli, C. R. Derouin, A. Redondo, S. Srinivasan; J. Electrochem. Soc. (1988) 135; p2209
7. K. Bolwin, E. Gülzow, D. Bevers, W. Schnurnberger; Solid State Ionics (1995) 77; p324
8. H. Sauer: Verfahren und Vorrichtung zur Herstellung einer kunststoffgebundenen Aktivkohleschicht für dünne Gasdiffusionselektroden; DBP 2941 774 C2 (1985)
9. A. Winsel; DECHEMA Monographie (1985) 98; p181
10. E. Gülzow, K. Bolwin, W. Schnurnberger; DECHEMA Monographie (1989) 117; p365
11. E. Gülzow, W. Schnurnberger, Preparation and characterization of gas diffusion electrodes for alkaline fuel cells; Proc. Fuel Cell Seminar, Phoenix 1990; p453
12. E. Gülzow, B. Holzwarth, W. Schnurnberger, M. Schulze, G. Steinhilber, N. Wagner; PTFE bonded gas diffusion electrodes for alkaline fuel cells; Proc. 9th World Hydrogen Energy Conf., Paris 1992; p1507
13. D. Bevers, G. Bacsur, N. Wagner, K. Bolwin; Powder Technology (1995) 84; p269
14. M. Schulze, N. Wagner, M. v. Bradke, W. Schnurnberger, E. Gülzow; Proton Exchange with Alkaline Ions in Nafion; Proc. 11th World Hydrogen Energy Conf. - Stuttgart, (1996) Germany, p 2625
15. Carlo Erba Microstructure Line No 5 (1987), p 1
16. Carlo Erba Microstructure Line No 19 (1987), p 2
17. P. Delahay, New Instrumental Methods in Electrochemistry; Interscience, New York (1954)
18. H. Göhr, C. A. Schiller, Poster, 34th I.S.E. Meeting, Erlangen (1983)
19. C. A. Schiller, Thales Software Guide, Kronach (1994)

INNOVATIVE PRODUCTION TECHNIQUE FOR PEFC ELECTRODES

D. Bevers, E. Gülzow; A. Helmbold, B. Müller

DLR, Institut für Technische Thermodynamik
Pfaffenwaldring 38-40
D-70569 Stuttgart, Germany
Tel. +49 711 6862 324
Fax. +49 711 6862 747
e-mail erich.guelzow@dlr.de

Abstract

Fuel cells are high efficient and low polluting energy conversation devices. Using hydrogen as a fuel gas they are applicable to solve environmental problems e.g. CO_2 impact on the climate. Thus international research efforts have been increased in recent years. Low temperature fuel cells e.g. the PEFC are specially applicable for future transportation and stationary energy supply systems. Application and economics success of his technology is obstructed by the high investment costs with respect to conventional energy conversion devices.
The intent of our activities is the improvement of electrodes and membrane-electrode-assemblies as used in PEFC. Commercial and technical aspects of electrode manufacturing have been considered in early stages of the development of the production procedure.
Two different techniques are developed at DLR. The first is a rolling procedure as used for production for batteries and alkaline fuel cells which has been modified and adapted to the specific demand of PEFC electrodes. [1] The second technique is a new printing process to produce ultra thin layers of catalyst directly on the electrolyte.
In this paper we will show the first results of the first electrode technique which have been tested in fuel cells and a short description of the second very new method.

Production of electrodes

The technique to produce low temperature fuel cell electrodes by reactive mixing of the components and rolling an endless electrode strip has been developed at the VARTA AG [2,3] together with the University of Kassel. The principle technique is shown in Fig. 1. The components of the catalytic layer (e.g. Vulcan XC-72 with different Pt/C loadings supplied by E-Tek and PTFE powder Hostaflon TF 2053 supplied by Hoechst) are mixed in a fast running knife mill for a short time and water cooling. This mixture is then applied under two different conditions onto a support which consists of an in house hydrophobed carbon cloth (e.g. E-Tek Cloth Type „A"), the powder mixture is either supplied vertical via line fummel under gravity influence (Fig.1) or it is supplied horizontally by sieving it through a silver mesh onto the support just before it enters the calander (Fig.2). The carbon cloth has been made hydrophobic by appling carbon (Vulcan XC-72) / PTFE suspension (Hoechst Hostaflon TF 5032) to both sides of the carbon cloth. This treatment has shown the best result yet concerning the compromise

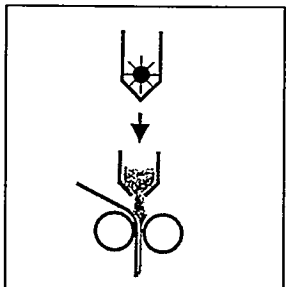

Fig 1. powder supply under gravity influence

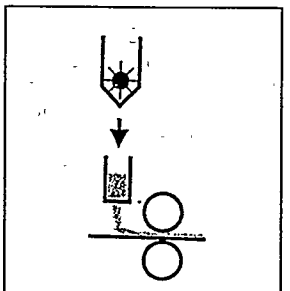

Fig. 2. horizontal powder supply

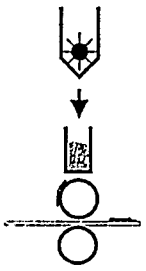

Fig. 3 Printing Method

between gas and water transport. The pretreatment of the carbon cloth is necessary to avoid loosing too much catalytic material in the roughness of the paper and improves the gas and water transport properties of the carbon cloth with regard to unhydrophobed cloth or cloth thatwas directly hydrophobed in PTFE suspension.

The third very new technique to produce PEFC electrodes is an printing method. The catalyst mixture is deposit onto an electrostatic load charged roll. From this roll the catalyst mixture is rolled onto the polymer electrolyte directly, that is like a real printing process. A schematic picture is shown in Fig. 3. With this very new technique it is possible to prepare thin layers of catalyst which allow a very good contact to the electrolyte. We did not investigate the electrochemical performance in full fuel cells yet.

Test facility

As a result of our research we found, that fuel cell conditions and periphery has a major impact on the fuel cell performance. Therefore it will be described more detailed, to enable a comparison of our results to measurements of other labs. All measurements are performed with pure hydrogen (2.3 bar) and pure oxygen (2.5 bar). Hydrogen is humidified at 80°C and keeping the gas at this temperature until it reaches the fuel cell. Oxygen passes through the humidifier at 20°C an then heated up to 30°C before it enters the cell. The hydrogen flow is „dead end" whereas the oxygen flow is adopted to the certain electrodes and its characteristics. Fuel cell temperature itself is 80°C. The electrode area is about 25 cm^2. As „standard EME unit" we use a E-Tek electrode on Nafion 117 - without impregnating and hot pressing to minimize the influencing parameters for the sake of system verification. The characterization methods are described in the second paper of DLR at this meeting.

Fig. 4 SEM picture of an EME unit with in house prepared electrodes (DLR) —— 125 µm

Results

We decided to use a commercial E-Tek electrode (0,4 mg Pt/cm^2, 20% Pt/C) as a standard reference for comparison reasons. The electrode is used as anode and cathode and is simply laid on Nafion 117 and fixed in the test facility. This was done to minimize the influencing parameters such as impregnating with Nafion suspension or hot pressing. The resulting reference I/U curve is shown in Fig. 5. Preparing the electrodes by supplying the powder mixture vertically via a line funnel under gravity influence resulted in electrodes. It can be seen clearly that this electrode is much to thick to allow effective gas transport. This was confirmed in the electrochemical fuel cell measurements. In the characteristics the hinderance for gas diffusion can clearly be seen.

Changing the rolling parameters did not influence the thickness of the electrode. We attribute this to the fact that the amount of powder retracted into the calandar has its minimum value determined by the retraction angle which is set by the roller diameter and its material. Preparing the electrodes

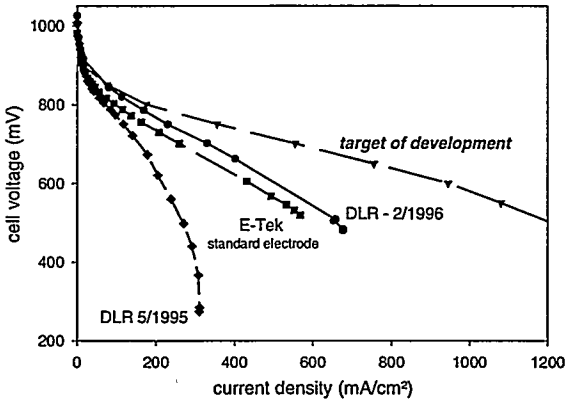

Fig. 5 characteristics of rolled and commercial electrodes
(E-Tek curve on Nafion 117 without impregnation and hot pressing to minimise the influencing parameters)

in a second manner resulted as dipicted in Fig. 4. The thickness of the reaction layer is in the range of the commercial standard electrode. The power output is essentially the same as with the commercial electrode. The measurements are carried out without hotpressing the electrode membrane structures before. The exchange current-density can be calculated to be in the order of $i_0 = 4\ 10^{-4}$ A/cm^2 from the characteristics. First experiments of long time behavior shows no degradation effect during a period of 320 hours. [4]

Conclusions

We developed a rolling process which allows the production of electrodes to be used in PEFC which have the same power density characteristic as commercial electrodes. This process offers a possibility to produce electrodes on a large scale base with reproducible characteristics. After having optimized the rolling process to the special requirements of PEFC electrodes, the task is now to include advanced electrode preparation steps into this production process as there is enlargement of the three-dimensional reaction area.
In contrast to the well-known process of impregnating electrodes with solved Nafion we will try to mix solid electrolyte powder into the powder which is rolled onto the support [5]. This will avoid hazardous solvents in the before mentioned process.
A second new technique is developed to prepare layers of catalysts directly onto the polymer membrane. Now we have to investigate the electrochemical behavior of these catalyst layers and the electrochemical performance in a fuel cell.

Acknowledgements

The authors thank their collegues for experimental support, mainly Dr. N. Wagner for the electrochemical measurement (EIS) and Dr. M. von Bradke for the SEM pictures. The authors gratefully acknowledge the financial support of the State of Baden Württemberg.

Literature References

[1] Preparation of pours electrodes and laminated electrode-membrane structures for polymer electrolyte fuel cells; K. Bolwin, E. Gülzow, D. Bevers, W. Schnurnberger; Solid State Ionics, 77 (1995) 324-330

[2] Apparatus and method for a plastic-bound activated carbon layer for thin gas-diffusion electrodes; H. Sauer (VARTA AG); Ger. Offen. 2 941 774 (CI H01M4/88); Apr. 30, 1981, Appl. Oct. 16, 1976; 9pp

[3] Porous gas electrodes; A.Winsel (VARTAAG); Ger. Offen. DE 3 342 969 (CI. C25B11/06), Jun. 5, 1985, Appl. 28, 1983; 12pp

[4] Characterization and basic research investigations at PEFC electrodes and MEA; M. Schulze, N. Wagner, G. Steinhilber, E. Gülzow, M. Wöhr, K. Bolwin; Proc. Fuel Cell Seminar Orlando (1996)

[5] Preparation and Characterization of Nafion powders for low cost PEFC electrode production; D. Bevers, G. Bacsur, N. Wagner, K. Bolwin; Powder Technology, 84 (1995) 269-276

OPPORTUNITIES FOR PORTABLE BALLARD FUEL CELLS

H. H. Voss and J. R. Huff
Ballard Power Systems Inc.
9000 Glenlyon Parkway
Burnaby, British Columbia, Canada V5J 5J9

Introduction

With the increasing proliferation and sophistication of portable electronic devices in both commercial and military markets, the need has arisen for small, lightweight power supplies that can provide increased operating life over those presently available. A solution to this power problem is the development of portable Ballard Fuel Cell power systems that operate with a hydrogen fuel source and air. Ballard has developed PEM fuel cell stacks and power systems in the 25 to 100 watt range for both of these markets.

For military use, Ballard has teamed with Ball Corporation and Hydrogen Consultants, Inc. and has provided the Ballard Fuel Cell stack for an ambient PEM fuel cell power system for the DoD. The system provides power from idle to 100 watts and has the capability of delivering overloads of 125 watts for short periods of time. The system is designed to operate over a wide range of temperature, relative humidity and altitude. Hydrogen is supplied as a compressed gas, metal hydride or chemical hydride packaged in a unit that is mated to the power/control unit. The hydrogen sources provide 1.5, 5 and 15 kWh of operation, respectively. The design of the fuel cell power system enables the unit to operate at 12 volts or 24 volts depending upon the equipment being used.

For commercial applications, as with the military, fuel cell power sources in the 25 to 500 watt range will be competing with advanced batteries. Ambient PEM fuel cell designs and demonstrators are being developed at 25 watts and other low power levels. Goals are minimum stack volume and weight and greatly enhanced operating life with reasonable system weight and volume.

This paper will discuss ambient PEM fuel cell designs and performance and operating parameters for a number of power levels in the multiwatt range.

Military Applications

The team of Ballard, Ball Aerospace and Technologies Corporation, and Hydrogen Consultants, Inc. has developed a 100 watt PEM fuel cell based power system that operates on hydrogen and air. The power system is comprised of two separate parts; a power module containing the fuel cell system and controls and a fuel module containing the hydrogen fuel supply system. The power module utilizes a 100-watt nominal Ballard hydrogen/air fuel cell stack that is configured to provide either 12 or 24 volt operation, as required, over a wide range of operating conditions; including from 0° to 50°C, from 0 to 95% relative humidity, and from sea level to 8000 feet elevation. The fuel cell uses air as the oxidant and coolant; supplied and controlled by small fans. Hydrogen energy storage options include a metal hydride storage vessel (1.3 kWh); a high pressure, composite gas cylinder (5 kWh); or a chemical hydride system, which is under development (15 kWh). The complete power system is man-portable and fits into a standard military backpack. (The unit's volume is less than 1 ft^3 with any of the hydrogen storage options and the weight of the unit is approximately 27 pounds.) The power system can deliver 2 to 100 watts continuous power and short duration peak power of 125 watts. It is also capable of up to 15 kWh of energy storage at 10 watts continuous power. The electrical interface characteristics

of voltage, voltage overshoots, settling time, and response to load changes are well within normal specifications.

The portable fuel cell power system has been thoroughly tested and has successfully met the required electrical characteristics. The system also has been operated at the four extreme points defined by combinations of the required operating conditions. In addition, the system has undergone shock and vibration testing. Units have been successfully field tested by military personnel using both 12 and 24 volt equipment.

Commercial Applications

Ballard has begun development of portable hydrogen/air PEM fuel cell systems for commercial applications that require power in the 25 to 500 watt range. Ambient PEM fuel cell designs and demonstrators are being developed at 25 watts and other power levels at the lower end of this range. The goals for these efforts are minimum stack volume and weight, greatly enhanced operating life, and reasonable system weight and volume. These designs use ambient air as the source of reactant oxygen and for cooling. Metal hydrides are used for hydrogen fuel storage. An initial 25 watt prototype is shown in Figure 1.

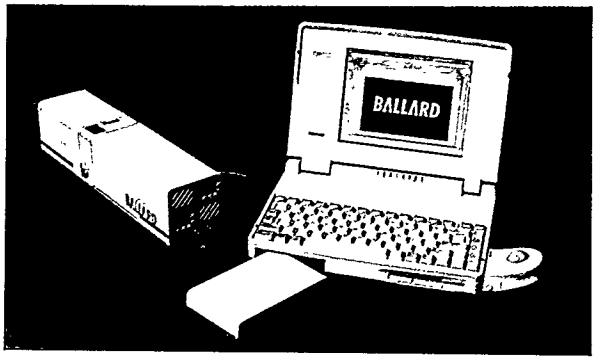

Figure 1: **25 Watt Prototype**

This system contains a 16-cell fuel cell stack and has a 12 VDC nominal output. The hydrogen storage capability is sufficient to provide 300 Wh of operation at 25 watts. The metal hydride and power unit plus controls are packaged separately; therefore, it is possible to increase the energy storage of the system by increasing the size of the hydride hydrogen storage module. This prototype has demonstrated the feasibility of portable hydrogen/air PEM fuel cells systems for providing power in the lower end of the power range being evaluated. Design and development of the system for commercial applications is continuing.

Acknowledgment

The 100 watt power plant system for military applications effort was supported by the U.S. Department of Defense.

X-RAY ABSORPTION AND ELECTROCHEMICAL STUDIES OF DIRECT METHANOL FUEL CELL CATALYSTS

Deborah J. Zurawski, Antonio J. Aldykiewicz, Jr., Shannon F. Baxter, and Michael Krumpelt
Electrochemical Technology Program
Argonne National Laboratory
9700 South Cass Avenue
Argonne, Illinois 60439

Introduction

In order for polymer electrolyte fuel cells to operate directly on methanol instead of hydrogen, a distinct advantage for portable applications, methanol oxidation must be catalyzed effectively in the acidic environment of the cell. Platinum-ruthenium and platinum-ruthenium oxide are generally considered to be the most active catalysts for this purpose. The presence of ruthenium significantly enhances the activity of platinum in these catalysts, for reasons not yet fully understood. We are using X-ray absorption spectroscopy (XAS) and electrochemical techniques to evaluate the mechanisms proposed to account for this enhancement in order to further improve the catalyst's activity.

We are considering three enhancement mechanisms. An intermediate in the oxidation of methanol on platinum is carbon monoxide and its oxidation is the rate-determining step in the overall oxidation mechanism [1]. It has been proposed that ruthenium facilitates the removal of carbon monoxide from the platinum surface [2]. First, it has been proposed that ruthenium decreases the strength of the platinum-carbon monoxide bond. Carbon monoxide bonds to the catalyst by interacting with the d-band of platinum [3], therefore a change in the d-band occupancy of platinum as a result of alloying may influence the bond strength of carbon monoxide. Another proposed enhancement mechanism involves lowering of the potential for the formation of the CO-oxidizing species [2]. Finally, the binary catalysts may have a structure which is more conducive to the methanol dehydrogenation and carbon monoxide reactions [4]. Based on these three proposed enhancement mechanisms, a goal of this study is to correlate catalyst electronic properties, structure, and oxidation state with the performance of proton-exchange membrane (Nafion) direct methanol fuel cells.

Experimental

We have used XAS to determine the effect of carbon support and ruthenium concentration on the d-band occupancy, structure, and oxidation state of platinum-ruthenium. We also determined the effect of electrode fabrication [5] (mixing with solubilized Nafion and hot-pressing to a Nafion membrane) on the platinum-ruthenium oxide and platinum-ruthenium catalysts. The activity of the platinum-ruthenium catalysts for methanol oxidation was determined using steady-state galvanostatic measurements on the catalysts incorporated in full membrane-electrode assemblies (MEAs).

Unsupported and carbon-supported (Vulcan XC-72R, Cabot) platinum and platinum-ruthenium alloy catalysts were synthesized by reduction from an aqueous solution of the metal chlorides. The resulting catalyst particles were dried, and heat-treated at 250°C in a reducing atmosphere. The compositions tested range from 0 to 42 mol% ruthenium. X-ray diffraction (XRD) analysis verified that the platinum and ruthenium are alloyed. An unsupported metal oxide catalyst of nominal composition $PtRuO_x$ was provided by an outside vendor. XRD analysis showed this material to consist of a mixture of platinum and ruthenium oxide.

XAS measurements were made of the catalyst powders supported on X-ray transparent tape, supported in Nafion (EW=1100, DuPont), and in MEAs. These experiments were performed at beamlines X-19A and X-23A2 at the National Synchrotron Light Source at Brookhaven National Laboratory.

The scanned X-ray energy ranges covered the Pt L_3 and L_2 edges and the Ru K edge (X-23A2 only). Absorption measurements of a platinum foil and ruthenium black pellet were made simultaneously with those of the catalyst samples to calibrate the monochromator. The coordination numbers and Pt-Pt bond distances were calculated from fits to the EXAFS portion of the L_3 absorption edge following published procedures [6,7]. The d-band occupancy of platinum was determined from the height of the L_3 absorption edge [8]. Oxidation states of ruthenium and platinum in the catalysts were determined by comparing the XAS spectra of the catalysts with those obtained for platinum and ruthenium compounds with known oxidation states.

The electrochemical activity of the catalysts for the oxidation of methanol was evaluated in full MEAs fabricated by the ink technique [5]. Catalyst loadings were approximately 4 mgPt/cm²/electrode. The MEA test apparatus consists of two graphite blocks with machined reactant flow channels and carbon cloth (E-Tek) or carbon paper (Spectracorp) flow fields. The anode and cathode were supplied with deaerated 2 M methanol and hydrogen,respectively, both at 0 psig. Using this configuration, the cathode acted as both the counter and reference electrodes and allowed measurement of the anode overpotential. The cell temperature was maintained at 90°C.

Results and Discussion

The Pt L_3 X-ray absorption promotes electrons to 5d orbitals. The height of the L_3 absorption edge is a measure of the probability of this transition and therefore is proportional to the number of vacancies in the 5d orbitals. The normalized height of the Pt L_3 absorption edge is compared in Fig. 1 for the supported and unsupported platinum catalyst particles and in Fig. 2 for catalyst particles with ruthenium compositions ranging from 0 to 42 mol%. As seen from these figures, both the carbon support and the presence of ruthenium increase the number of platinum d-band vacancies (i.e., withdraw electrons). The electron-withdrawing effect of ruthenium observed here is in agreement with the results of McBreen and Mukerjee [9].

The activity for methanol oxidation was found to increase with addition of ruthenium to the catalyst. This increase in activity is illustrated in Fig. 3 as an increase in the total methanol oxidation current (normalized to the total weight of platinum in the anode) at a given overpotential. The 58 mol% platinum/42 mol% ruthenium alloy was found to be the most active for methanol oxidation of the four catalysts tested.

The alloy catalysts were found to consist of platinum and ruthenium, whereas the nominal $PtRuO_x$ was a mixture of platinum oxide and ruthenium oxide. No change was observed in the oxidation state of the alloys when they were supported in Nafion. The electrode fabrication procedure reduced the oxidation state of platinum in the $PtRuO_x$ catalyst, but not the oxidation state of ruthenium.

Our preliminary results indicate that ruthenium does effect the d-band occupancy of platinum, which in turn may effect the kinetics of the methanol oxidation reaction on this metal by altering the strength of the platinum-carbon monoxide bond. Futher research is needed to clarify the effect of ruthenium concentration on platinum's d-band occupancy, to establish the optimum d-band occupancy for the methanol oxidation reaction, and also to determine the oxidation states of platinum and ruthenium during methanol oxidation.

Acknowledgment

The authors gratefully acknowledge the collaboration of Professors Carlo Segre, Grant Bunker, and Eugene Smotkin of the Illinois Institute of Technology. This research was sponsored by the

U.S. Army Research Office, Research Triangle Park, NC, through the Fuel Cell/Battery Research Hub at the Illinois Institute of Technology. This research was conducted at Argonne National Laboratory which is operated by the University of Chicago for the U.S. Department of Energy under Contract No. W-31-109-Eng-38. X-Ray experiments were performed at the National Synchrotron Light Source at Brookhaven National Laboratory, Upton, NY.

References

1. B. Beden, C. Lamy, A. Bewick, K. Kunimatsu, *J. Electroanal. Chem.*, Vol. 121, pp. 343-347, 1981.
2. R. Parsons and T. VanderNoot, *J. Electroanal. Chem.*, Vol. 257, pp. 9-45, 1988.
3. G. Blyholder, *J. Phys. Chem.*, Vol. 68, p. 2772, 1964.
4. H. Gasteiger, N. Markovic, P.N. Ross, Jr., and E. Cairns, *J. Phys. Chem.*, Vol. 97, pp. 12020-12029, 1993.
5. M.S. Wilson and S. Gottesfeld, *J. Appl. Electrochem.*, Vol. 22, pp. 1-7, 1992.
6. J.J. Rehr, R.C. Albers, and S.I. Zabinsky, *Phys. Rev. Lett.*, Vol. 69, p. 3397, 1992.
7. J.J. Rehr, *Jpn. J. Appl. Phys.*, Vol. 32, p. 8, 1993.
8. A.N. Mansour, J.W. Cook, Jr., and D.E.Sayers, *J. Phys. Chem.*, Vol. 88, pp. 2330-2334, 1984.
9. J. McBreen and S. Mukerjee, *J. Electrochem. Soc.*, Vol. 142, pp. 3399-3404, 1995.

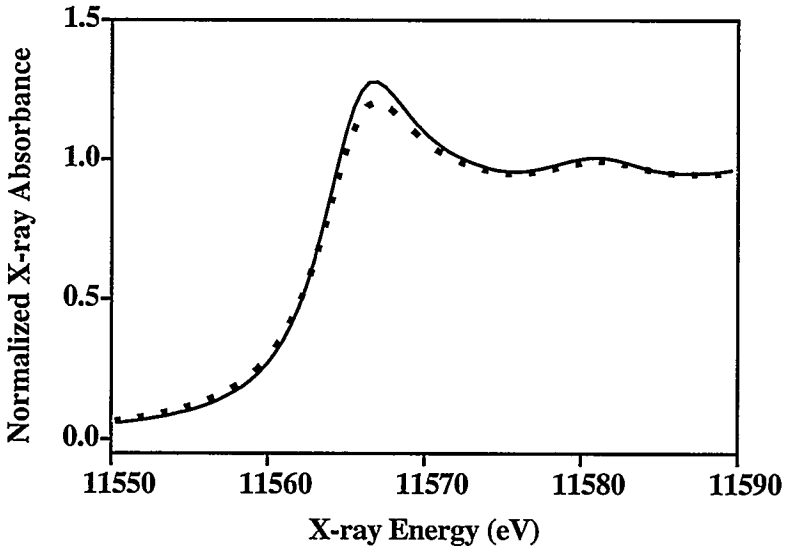

Figure 1. Pt L_3 X-ray absorption for 50 mol% PtRu catalyst, unsupported (dashed line) and supported on carbon (solid line).

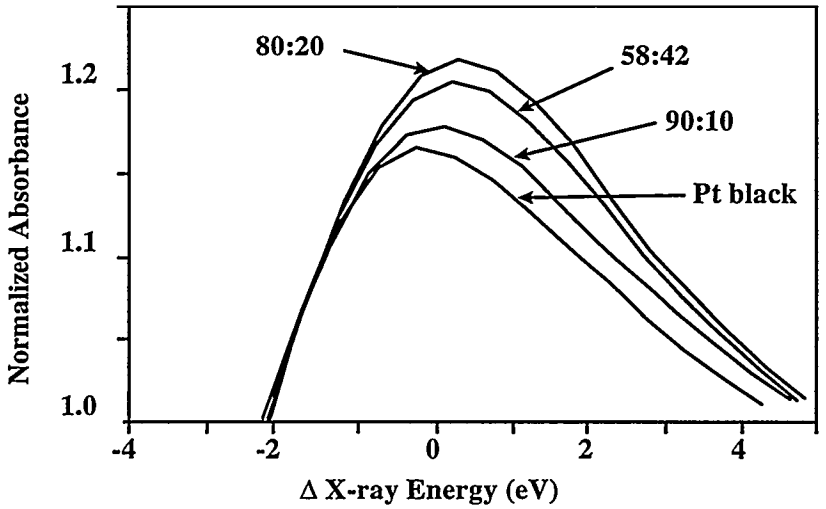

Figure 2. Pt L_3 X-ray absorption for unsupported Pt and PtRu catalysts. Indicated ratios are mole% Pt : mol% Ru for the alloy catalysts.

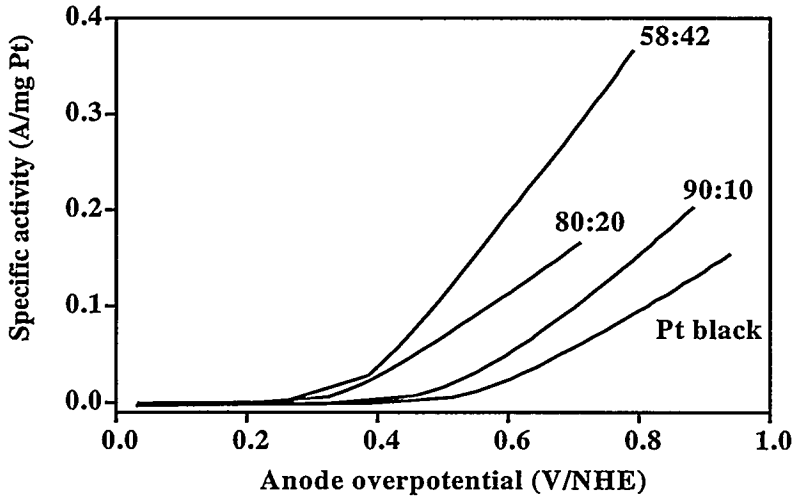

Figure 3. Specific activity for methanol oxidation of unsupported Pt and PtRu catalysts. Indicated ratios are mol% Pt : mol% Ru in the alloy catalysts.

ANALYSIS OF THE ELECTROCHEMICAL CHARACTERISTICS OF A DIRECT METHANOL FUEL CELL BASED ON A Pt-Ru/C ANODE CATALYST

A.S. Aricò[1], P. Creti[1], R. Mantegna[1], P. L. Antonucci[2], N. Giordano[1] and V. Antonucci[1]

1) C.N.R. Institute for Transformation and Storage of Energy, Salita S. Lucia sopra Contesse 39, 98126 S. Lucia, Messina, Italy

2) Institute of chemistry, Faculty of Engineering, University of Reggio Calabria, Via Cuzzocrea 48, 89100 Reggio Calabria, Italy

INTRODUCTION

This paper deals with a vapour-feed direct methanol fuel cell (DMFC) based on a Nafion 117® solid polymer electrolyte. Pt-Ru/C and Pt/C catalysts were employed for methanol oxidation and oxygen reduction, respectively. Structure and surface chemistry of catalysts were investigated by X-ray powder diffraction (XRD) and X-ray photoelectron spectroscopy (XPS). Membrane /electrode assembly (M&E) was prepared by using a "paste process" method. Electrical power densities of about 150 mW cm^{-2} were obtained at 95 °C with Pt loadings of 0.8 and 0.5 mg cm^{-2} at anode and cathode, respectively.

EXPERIMENTAL

Catalysts. — 20% Pt/C and 20% Pt - 10% Ru/C catalysts were purchased from Electrochem. Inc. (Woburn, MA) and used for the oxygen reduction and methanol oxidation reaction in DMFC, respectively.

Fabrication of the membrane/electrode assembly.— The M&E assemblies were prepared according to a "paste process" procedure already developed for SPE fuel cells [1]. Catalysts were directly mixed with a colloidal suspension of Nafion® in butyl acetate solution in an ultrasonic bath. The obtained paste was spread on carbon cloth backings. Pt loadings were 0.8 mg cm^{-2} in anode and 0.5 mg cm^{-2} in cathode. Nafion® loading was 1 mg cm^{-2} in both electrodes. The electrodes were pressed onto a purified Nafion® 117 membrane at 150 °C and 90 atm for 1.5 min.

Single cell. — Electrode/membrane assemblies having 50 cm^2 geometrical electrode area were loaded into a single cell test fixture. The cell was operated at 95 °C. Gaseous CH_3OH solutions of various concentrations were supplied to the anode (1 atm). Humidified oxygen (100° C) was fed to the cathode at 3.5 atm.

RESULTS

X - ray diffraction analysis. — Fig. 1 shows the X-ray diffraction patterns of 20% Pt - 10% Ru/C and 20% Pt/C catalysts. Both catalysts exhibit the characteristic diffraction peaks of the Pt fcc structure. The diffraction peaks in the Pt-Ru catalyst slightly shift to higher two-theta values with respect to the same reflections of Pt in the JCPDS card. Such evidence accounts for the presence of a Pt-Ru alloy in the catalyst. a_{fcc} values of 3.921 and 3.905 Å for Pt/C and Pt-Ru/C catalysts, respectively, were obtained from the 220 peak profile fitting. According to the variation of fcc lattice parameter with composition for Pt-Ru bulk alloys an atomic fraction of about 20% Ru should be present in the carbon supported alloy. The average particle size in the two catalysts was determined from the broadening of the (220) reflection of the fcc lattice by using the Debye-Sherrer equation. The average particle size in Pt/C catalyst was 23 Å. A larger particle size was determined for the Pt-Ru catalyst i.e. 38 Å as clearly evidenced by the increase in sharpness of the diffraction peaks in this sample (Fig. 1).

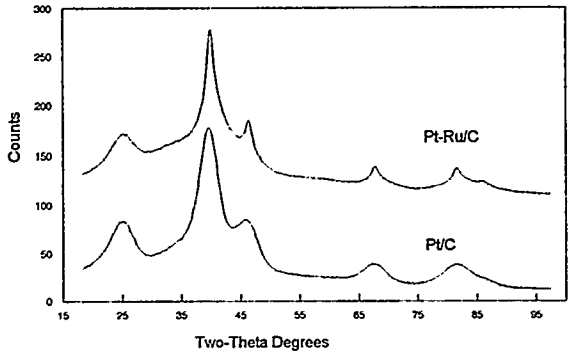

Fig. 1. X-ray diffraction patterns of carbon supported catalysts.

XPS analysis. — The nature of surface species of Pt/C and Pt-Ru/C catalysts was investigated by XPS analysis. The Ru $3p_{3/2}$ line in the Pt-Ru/C catalyst (Fig. 2a) derives from the contributions of two components with B.E. of 463.37 and 466.90 eV. These peaks could be attributed to RuO_2 and RuO_3 species. Yet, the width of ca. 4 eV of the main peak suggests that this component could derive from the contributions of more than one species with similar B.E. In order to understand the nature of the electronic effects that Ru could cause on the Pt in the present catalyst, we have investigated the Pt 4f region (Fig. 2b). To achieve a consistent fit of the spectral data three components were needed for the Pt $4f_{7/2}$ at B.E. 71.78 (Pt°), 73.20 (Pt^{2+}) and 74.65 (Pt^{4+}). It is noteworthy that the peak position of zerovalent Pt in the Pt-Ru/C sample shifts by 0.23 eV to higher B. E. with respect to the Pt/C sample.

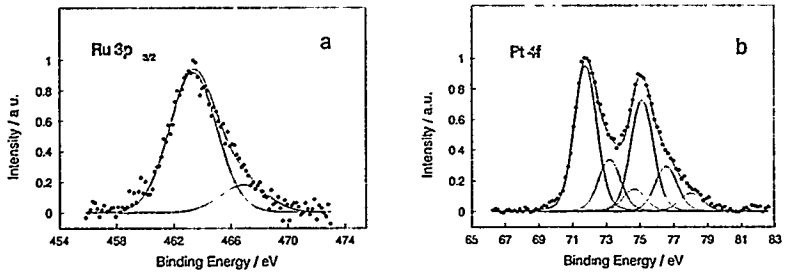

Fig. 2 a-b. X-ray photoelectron spectra of the Pt-Ru/C catalyst

SEM-EDAX analysis. — The "paste process" method introduces new features with respect to the conventional procedures employed in the realization of a M&E assembly. In the present assembly the ionomer is distributed through the overall catalyst region. As opposite, in the conventional method, the ionomer is localized at the electrode - electrolyte interface. It is pointed out that the colloidal ionomer chains, in the "paste process", establish links between catalyst particles improving the structural integrity of the catalyst layer and supplying a net- work for proton conduction. Microprobe analysis was carried out on various portions of

the catalyst layers. The relative intensities of platinum and sulfur signals did not significantly change along the catalyst layers accounting for a homogeneous distribution of the ionomer in the two catalysts. It is observed that the "paste process" preparation method allows a significant increase of the three-phase reaction zone at the electrode-electrolyte interface.

Electrochemical analysis. — Fig. 3 shows a comparison of the galvanostatic polarization data with 2 M and 1.5 M methanol concentration together with the corresponding power density curves obtained upon correction for ohmic drop (0.22 ohm cm^2). It can be observed that the open circuit potential is close to 0.9 V. Significant potential losses are observed in the activation and diffusion controlled regions of the polarization curves. At low current densities, a sudden decrease of about 0.2 V of cell potential is recorded when a slight current is allowed to pass through the cell (Fig. 3). The polarization curve obtained in 1.5 M methanol solution showed a lower deactivation at intermediate currents. Power densities of about 150 mW cm^{-2} are obtained at 95 °C with low Pt loadings in the electrodes.

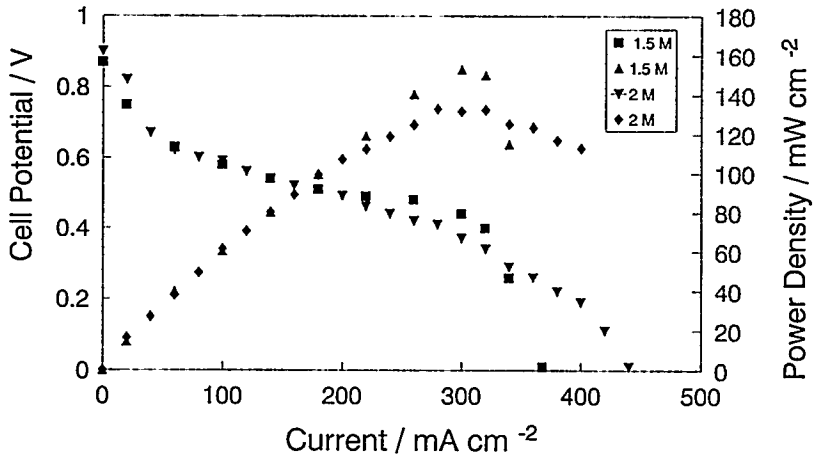

Fig. 3. Comparison of the raw polarizations and IR-free power density curves for the DMFC with 1.5 and 2 M methanol concentrations (3.5 atm O_2; cell temperature 95 °C).

DISCUSSION

The polarization behavior of the present DMFC appears to be mainly affected by the methanol oxidation process. It is known that the chemisorption of methanol on Pt occurs at potential values below 0.2 V vs. NHE. On the other hand, the chemisorption process of methanol on Ru sites is significantly less favored than on Pt sites but it is strongly activated by the temperature [2]. Besides, the water displacement reaction producing oxygen species chemisorption on Ru sites occurs at potentials as low as 0.2 V vs. NHE [2]. From these

evidences, it is thought that at 95° C a significant fraction of Ru sites can suitably chemisorb OH groups, as the overpotential slightly increases. The polarization curves of the present DMFC show a potential drop of about 0.2 V at very low current density. Afterwards, the current increases steeply with potential. This behavior could be related to a mechanism involving a first dehydrogenation step followed by oxidation of chemisorbed residues as the anode overpotential becomes sufficiently high for a fast water displacement on Ru sites.

As described above, a lower Ru content (20%) was experimentally determined for the Pt-Ru alloy in the present catalyst with respect to the nominal composition (50%). This suggests that the remaining Ru atoms are present as RuO_x species as accounted by XPS analysis. Accordingly, it could be suggested that the formation of RuO_x species occurs at the surface of the catalyst. It is observed that formation of "labile" oxygen groups on Ru sites being not directly alloyed with Pt but close enough to Pt sites, can allow the chemical interaction between these groups and the adsorbed methanolic residues to produce CO_2. It is thought that both mechanisms involving Pt-Ru alloy and RuO_x species could actively participate to the methanol oxidation reaction. RuO_x species are probably less poisoned by adsorbed methanolic residues with respect to Ru sites in the Pt-Ru alloy at high temperatures. Yet, it is likely that the absence of an atomic mixing of Pt with RuO_x species imposes an activation barrier for the migration of adsorbed intermediates reducing the activity of the Pt-Ru/C catalyst.

AKNOWLEDGEMENT

The authors gratefully acknowledge the contribution of Professor Nicola Giordano who left us on May 10th 1996, at the height of his scientific insight.

REFERENCES

1. M. Uchida, Y. Aoyama, N. Eda, and A. Ohta, *J. Electrochem. Soc.*, 142, 463 (1995).

2. H. A Gasteiger, N. Markovic, P. N. Ross, Jr., and E. J. Cairns, *Electrochim. Acta*, 39, 1825 (1994).

COMPARISON OF Pt-BASED BINARY AND TERNARY ALLOY ANODE CATALYSTS FOR POLYMER ELECTROLYTE DIRECT METHANOL FUEL CELLS

Renxuan Liu, K. L. Ley, Cong Pu, E. Reddington, K. Triantefillou,T.E. Mallouk, E. S. Smotkin
Department of Chemical and Environmental Engineering
Illinois Institute of Technology, Chicago, IL 60616

INTRODUCTION:

As an anode catalyst, Pt is highly active for the adsorption and dehydrogenation of methanol, however, the surface is poisoned by CO.[1] To oxidize CO to CO_2, a second oxygen atom is required from an adjacent adsorbed water molecule.(see Figure 1) Bifunctional alloys composed of Pt and a second metal M, able to activate H_2O (forming $-OH_{ads}$) at low potentials, are candidate materials for methanol electro-oxidation catalysts.[2] A proposed mechanism is:

$Pt + CH_3OH \rightarrow Pt\text{-}CH_3OH_{ads}$ [1]

$Pt\text{-}CH_3OH_{ads} \rightarrow Pt\text{-}CO_{ads} + 4H^+ + 4e^-$ [2]

$M + H_2O \rightarrow M\text{-}H_2O_{ads}$ [3]

$M\text{-}H_2O_{ads} \rightarrow M\text{-}OH_{ads} + H^+ + e^-$ [4]

$Pt\text{-}CO_{ads} + M\text{-}OH_{ads} \rightarrow Pt + M + CO_2 + H^+ + e^-$ [5]

Figure 2 shows that metals which enhance methanol oxidation activity when alloyed with Pt have similar M-O bond strengths (see bold print), suggesting that the best binary alloy catalysts have second metals that are optimized with respect to the ability to oxidatively adsorb water (affecting steps [3]&[4]), *and* the ability to dissociate M-O bonds to yield CO_2 (step [5]).[3]

BIFUNCTIONAL CATALYSTS

APPROACH: DEVELOP TERNARY $Pt\text{-}M_1\text{-}M_2$ ALLOYS (M_1, M_2 = Ru, Os) WITH MODIFIED METHANOL AND H_2O ADSORPTION PROPERTIES[4]

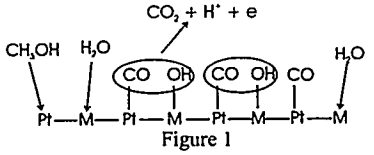

Figure 1

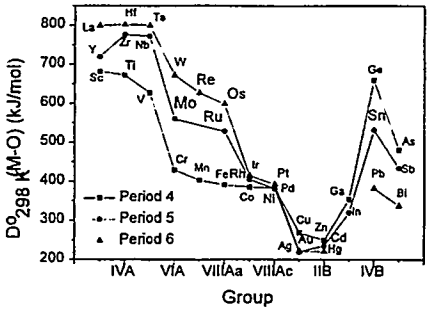

Figure 2

EXPERIMENTAL:

Smooth electrodes: Polycrystalline Pt and Pt based alloys of selected compositions in the Pt-Ru-Os system (Figure 3) were prepared by arc-melting. All electrodes were prepared for voltammetric studies using the following regime: (1) Polish to 0.25μm; (2) Ultrasonically clean in Nanopure™ water; (3) Etch in aqua regia for 10 seconds; (4) Ultrasonically clean in Nanopure™ water and transfer to the electrochemical cell.

The potential vs. time program shown in Figure 4 was applied to each electrode in 0.5M H_2SO_4 solution to investigate the CO tolerance of each electrode.

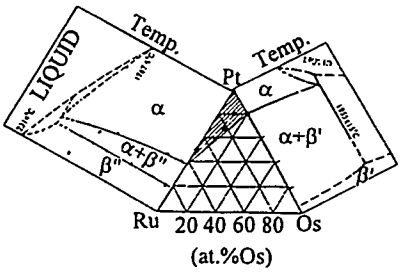

Figure 3

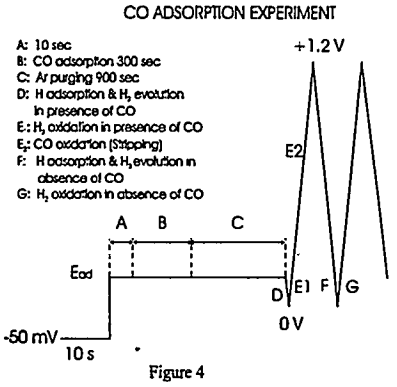

Figure 4

Steady-state methanol oxidation studies were done in 2M MeOH/0.5M H_2SO_4 solution. An initial step to -50mV was performed to reduce surface oxides and then each electrode was subjected to a series of potentiostatic steps; a 10 minute time period was used to reach the steady-state current of methanol oxidation at each potential.

Dispersed catalysts:

Pt, Pt-Ru(50:50) and Pt-Ru-Os(65:25:10) catalysts were prepared by reduction of aqueous H_2PtCl_6, $RuCl_3$, $OsCl_3$. All catalysts showed single phase FCC XRD patterns. Membrane electrode assemblies were fabricated with the catalysts and tested in liquid feed direct methanol fuel cells.

RESULTS:

Figure 5 shows the CV obtained on a Pt-Ru-Os(65:25:10) electrode as the potential was swept to 0 V and then to 1.2V after dosing CO at 0.3V. On the first scan, the hydrogen oxidation charge (Q_H^{CO}) is limited by the presence of adsorbed CO. On the second scan, the maximum hydrogen oxidation charge (Q_H^H) is obtained since the CO_{ads} is oxidized during the first scan. In Figure 6 the value of $\Psi=(Q_H^H-Q_H^{CO})/Q_H^H$ ($0\leq\Psi\leq1$) is used as a measure of CO poisoning for each electrode. Based on Ψ, the ternary alloy Pt-Ru-Os(65:25:10) is the most resistant to CO

poisoning. with Pt-Ru(50:50) and Pt-Os(80:20) slightly worse. As shown in the Figure 7, Pt-Ru(50:50) and Pt-Ru-Os(65:25:10) exhibited the lowest potentials for methanol oxidation and the highest steady-state currents: below 0.6V. the steady-state activity was similar for Pt-Ru(50:50) and Pt-Ru-Os(65:25:10) with the latter exhibiting better performance at overpotentials above 0.6V. Pt had the highest onset potential for methanol oxidation and lowest methanol oxidation currents.

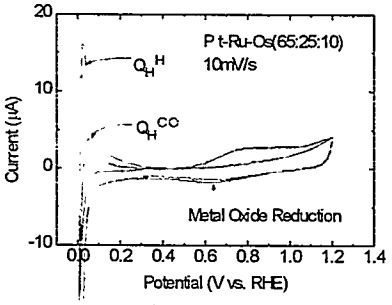

Figure 5

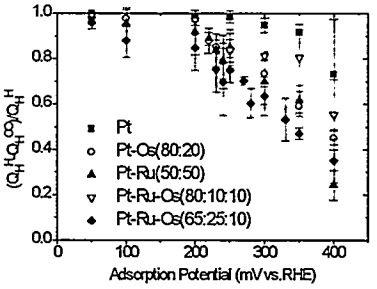

Figure 6

The single cell measurements for methanol oxidation in a liquid feed DMFC for the dispersed catalysts showed that under the same experimental conditions the catalytic activity for methanol oxidation is in the order: Pt-Ru-Os(65:25:10) > Pt-Ru(50:50) >>Pt. (Figure 8)

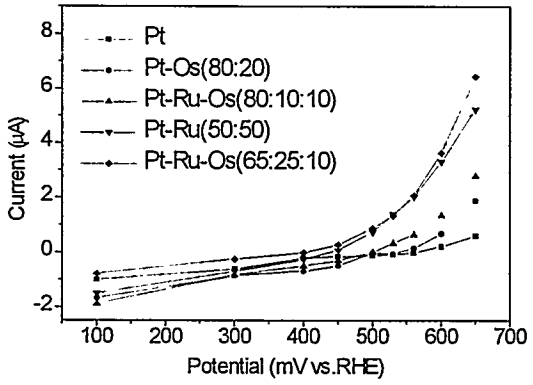

Figure 7

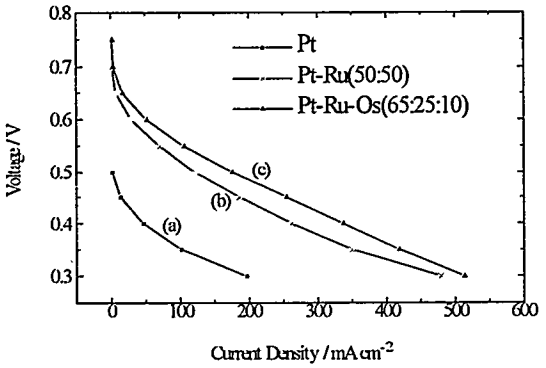

Figure 8

CONCLUSIONS:

CO tolerance and methanol oxidation studies on single phase smooth electrodes, as well as methanol oxidation studies on dispersed fuel cell electrodes indicate that bifunctional ternary catalyst in the Pt-Ru-Os system is superior to binary Pt-Ru catalyst for DMFC anode. A rational methodology is presented for the development of improved DMFC anode catalyst.

ACKNOWLEDGMENTS:

Financial support from the U.S. Army Research Office and the Advanced Research Projects Agency is gratefully acknowledged.

[1] R. Parsons, and T. VanderNoot, *J. Electroanal. Chem.*, 257, 9, (1988).
[2] D.F.A. Koch. Australian Patent 46123, 1964.
[3] N.I. Il'chenko, and G.I.Golodets, *J. Catal.* 39,73, (1975).
[4] Renxuan Liu, K.L: Ley, Cong Pu, Qinbai Fan, N. Leyarovska, C. Segre, and E. S. Smotkin, "Bifunctional Pt-Ru-Os Ternary Alloys: Improved Platinum-based Anodes for Direct Methanol Fuel Cells", in "**Electrode Processes VI**", A. Wieckowski and K. Itaya, Editors, PV 96-8, pp 341-355 Electrochemical Society Proceedings, Pennington, NJ (1996)

DISCOVERY OF METHANOL ELECTRO-OXIDATION CATALYSTS BY COMBINATORIAL ANALYSIS

T.E. Mallouk*[1], E. Reddington[1], C. Pu[2], K. L. Ley[2], and E.S. Smotkin*[2]
[1]Deparment of Chemistry
The Pennsylvania State University, University Park, PA 16802
and
[2]Department of Chemical Engineering
Illinois Institute of Technology , Chicago, IL 60616

Hydrogen fuel cells are likely to become a major energy source in the next century, but they are not ideal for all applications. A safe alternative fuel with a high energy density will be necessary for transportation and mobile applications. Direct methanol-air fuel cells (DMFCs) are an attractive alternative to hydrogen fuel cells because of the high energy density and low cost of methanol as a fuel [1]. However, in order for DMFCs to become commercially viable, better electrocatalysts for the anode reaction need to be developed.

In a DMFC, methanol and water undergo a six electron oxidation [2] at the anode to produce carbon dioxide and protons (1),

$$CH_3OH(aq) + H_2O(l) \text{ -----> } 6H^+(aq) + CO_2(g) + 6e^-,\ E^\circ = +0.04 \text{ V vs. NHE} \quad (1).$$

Platinum is the most efficient single metal catalyst for this reaction. The generally accepted reaction mechanism [3], (2)-(4),

$$CH_3OH_{ads} \text{ -----> } CO_{ads} + 4H^+(aq) + 4e^- \quad (2)$$
$$H_2O_{ads} \text{ -----> } OH_{ads} + H^+(aq) + e^- \quad (3)$$
$$CO_{ads} + OH_{ads} \text{ -----> } CO_2(g) + H^+(aq) + e^- \quad (4),$$

involves adsorption and partial oxidation of methanol on the surface of the electrode (2). Adsorbed OH from hydrolysis of water (3) reacts with the adsorbed CO to produce carbon dioxide and a proton. At low overpotentials, the slow step in the sequence is (3). Platinum electrodes suffer from many drawbacks, such as expense, low current density, and rapid formation of a CO poisoning layer.

It has been shown that a ruthenium/platinum alloy electrochemically oxidizes methanol more efficiently than pure platinum [4]. Ru improves the kinetics of the slow step of the reaction (3) by dissociating water at a lower overpotential than Pt. Alloying ruthenium with platinum also improves the catalyst resistance to CO poisoning. In addition to ruthenium, many alloys of Pt and different metals have been tested for catalytic ability, including Ag [5], Au [5], and Pd [6]. Ad-atoms of different elements[7], such as Bi [8], Sn [9], and Ru [10], on Pt have also been tested for catalytic ability. In general, these modifications only slightly improve the kinetics of electrochemical oxidation of methanol, if at all. The best known catalysts at present are Pt(50)/Ru(50) (mole ratio) [11] and a recently developed Pt/Ru/Os ternary composition [12].

There is at present no way to calculate the chemical composition of different metals that will afford the best catalyst for this reaction, although knowledge of phase equilibria and heuristic bond strength/activity relationships do provide some guidance in the search for effective ternary compositions [12]. In the absence of a more general and predictive model, an Edisonian approach to the problem is appealing. Combinatorial methods, which have been used extensively in bio-organic systems, provide a way to screen a very large number of multi-component catalysts simultaneously. Binary systems of platinum

and other metals have been well studied, but with one exception [12], ternary and higher systems have not been investigated, and offer a ripe area for combinatorial discovery.

There are only a few examples in the literature of combinatorial approaches to materials discovery. Schultz and co-workers searched for magnetoresistive [13] and superconducting [14] properties of different mixtures of metal oxides, and Natan and co-workers [15] developed a way to deposit colloidal gold and silver on a substrate with varying densities. The area is currently undergoing rapid growth, as combinatorial libraries of thermal catalysts and other materials are now being prepared. However, there has been to our knowledge no previous application of combinatorial methods to problems in electrocatalysis.

This combinatorial technique involves generating an array of electrodes with varying metal compositions, on a conductive substrate. Generally, to test the effectiveness of an electrocatalyst, one measures the current as a function of potential. This would be a time-consuming, serial process for arrays containing many electrocatalyst compositions, and would not have the combinatorial advantage of parallel screening. Instead, an indirect measurement was used which allows optical imaging of the activity of an array of electrocatalysts. The electrochemical oxidation of methanol (or any other organic molecule) involves the generation of protons at the electrode. Therefore, the local pH in the diffusion layer at the electrode surface drops considerably. When the potential of an array electrode is swept slowly from cathodic to anodic potential, the best catalyst compositions (those that oxidize methanol at lowest overpotentials) generate acid first. A solution phase, fluorescent pH indicator can then be used to detect catalysts that most efficiently oxidize methanol.

We report here a proof of concept of the application of combinatorial methods, to the discovery of optimized ternary catalysts for methanol electro-oxidation. Toray carbon paper was used as a substrate for the electrode arrays because it is electrically conductive, but not catalytic. It is composed of thin carbon fibers that help to hold the catalyst on its surface. These substrates were cut into triangular shapes, and solutions of metal salts were applied with a microliter syringe such that each spot contained the appropriate molar ratio of three different metals. The salts were then reduced to zero-valent metals by addition of a sodium borohydride solution [16]. After rinsing and drying, a ternary array of three metals has been prepared, with a simple map (much like a ternary phase diagram) describing the chemical composition of each spot. Ternary combinations of five transition elements (Pt, Ru, Os, Rh, Pd) were studied. When the metal salts were reduced individually by borohydride, only platinum showed a powder x-ray diffraction pattern. The individual particles produced in this way are therefore either amorphous, or the size of the crystalline domains is too small to give an x-ray pattern. The individual metals were also characterized by comparing their cyclic voltammograms (CVs) in sulfuric acid to crystalline samples. All CVs of the amorphous metals appeared similar to that of the microcrystalline metals, except for Os. An element map performed by SEM/EDAX shows that the three metals are mixed intimately on the 200 nm scale.

The oxidation of methanol produces protons according to reaction (1). At the concentrations and current densities used in this study, the local pH around the electrode is calculated to drop considerably (to about -0.5 or 0.5) with efficient catalysis. A fluorescent pH indicator that is not fluorescent in base, but strongly fluorescent in acid is the ideal molecular probe for this reaction.

Efficient catalysts were detected experimentally as follows. The electrode array was electrically contacted and, the contacts were insulated with epoxy resin. The triangular array was then immersed, face-up, into an aqueous solution of methanol, electrolyte, and fluorescent indicator. The electrode array is the working electrode in a typical three electrode cell, with a platinum counter electrode and an SCE reference electrode. The pH of the indicator solution was adjusted to be slightly higher than the indicator pKa, i.e.,

the intial state is non-fluorescent. A hand-held UV lamp was used to generate UV (354 nm) light. A single potential sweep was conducted, starting at cathodic and ending at anodic potentials, where all the electrodes in the array oxidize methanol. Efficient catalysts are those that cause the solution directly above the electrode to fluoresce at lowest overpotential, and were detected by visual inspection. The chemical composition of the most efficient catalyst in an array was known from its location, and larger individual electrodes of the same composition were then prepared. The i-V characteristics of these individual electrodes were then compared with those of Pt(50)/Ru(50), and apparent heterogeneous rate constants were determined by rotating disk voltammetry.

Initial results using acridine as the indicator were quite promising. Acridine, pKa = 5.0, fluoresces a weak violet in base, and fluoresces bright green in acid. Quinine, pKa = 5.5,

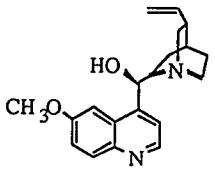

quinine

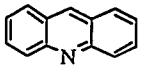

acridine

also fluoresces brightly in acidic solutions. Electrode arrays that each contained 15 different ternary compositions were prepared from the five metals studied. The binary "edges" of each ternary phase diagram were eliminated in order to allow more thorough evaluation of ternary compositions. Assessment of the possible ternary compositions of Pt, Ru, Os, Rh, and Pd required 9 arrays and a total of 135 unique compositions. Some compositions of Pt/Os/Rh oxidized methanol very effectively at low overpotentials. Individual electrodes were prepared for the most promising compositions, and the i-V curves were then compared with those of Pt(50)/Ru(50). At high pH, the Pt(60)/Os(25)/Rh(15) catalyst (Figure 1) oxidizes methanol more efficiently than the

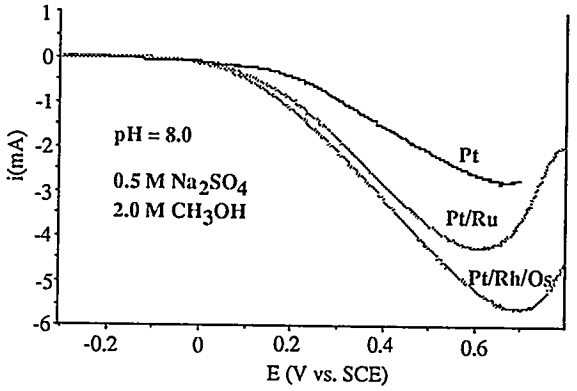

Figure 1: Current-voltage curves for methanol electro-oxidation at pH 8, using colloidal metal catalysts supported on carbon. Electrode compositions are Pt, Pt/Ru (50/50), and Pt/Rh/Os (60/15/25). The optimum composition was found by combinatorial screening of ternary combinations of Pt, Ru, Os, Rh, and Pd, using acridine as a fluorescent indicator.

Pt(50)/Ru(50) catalyst. At lower pH, the performance of Pt(60)/Os(25)/Rh(15) is slightly inferior to that of Pt(50)/Ru(50), but still much better than that of pure platinum. The performance of the electrodes at low pH is crucial, because real DMFC's operate at low pH. The combinatorial screening was intially done at a pH of 8 because of the high pKa of the indicator. Nevertheless, these initial results are encouraging because they vindicate the combinatorial method; that is, under conditions where the screening was done (high pH), the best catalyst was quickly identified.

In order to identify the best anode catalysts for conditions under which DMFC's normally operate, a low-pH fluorescent indicator was identified and synthesized by a modification of literature methods. PTP (pKa = 3.0) forms metal complexes with many transition metal ions. The coordinated dication withdraws electron density from PTP, so that protonation becomes more difficult. This effect lowers the pKa by another unit, to ~1.8. Although the copper complex of PTP is known in the literature, Cu^{2+} could interfere electrochemically at potentials used in the voltammetric scans. Ni^{2+} was therefore used instead, and did not interfere with the electrode reaction.

With this improved indicator, the arrays were re-evaluated at low pH. This investigation, which is still in progress, involves more components (Pt, Rh, Os, Ru, Pd and Ag), and a larger number of ternary compositions per array (28). Upon completion of this study, 20 arrays will have been tested, and a total of 560 individual electrodes assessed. A Pt(50)/Ru(50) spot is fabricated on all arrays for purposes of in-situ visual comparison. Preliminary data acquired at low pH indicate that Pt/Rh/Os electrodes and Pt/Ru/Os electrodes perform most efficiently. Quantitative comparisons of conventional binary catalysts with these new compositions will be reported at the meeting.

The authors thank Anthony Czarnik and Peter Schultz for helpful discussions. This work was supported by the Office of Naval Research (LBL Molecular Design Institute).

Literature Cited:

[1] Parsons, R.; and VanderNoot, T *J. Electroanal.Chem.* ,1988, *257*, 9.
[2] Leger, J.-M.; Lamy, C. *Ber. Bunsenges. phys. Chemie*, 1990, *94*, 1021.
[3] Markovic, N.M.; Gasteiger, H.A.; Ross, P.N.; Jiang, X.; Villegas, I.; Weaver, M.J. *Electrochim.Acta*, 1995, *40*, 91; Lamy, C. *Electrochim. Acta*, 1984, *29*, 1584.
[4] Bockris, J.O'M.; Wroblowa, H. *J. Electroanal.Chem.* , 1964, *7*, 428; Dahms, H.; Bockris, J.O'M.; *J. Electrochem. Soc.* 1964, *111*, 728.
[5] Stelmach, J.; Holze, K.; Beltowska-Brzezinska, M. *J. Electroanal.Chem.* , 1994, *377*, 241.
[6] Kadirgan, F.; Beden, B.; Leger, J., Lamy, C. *J. Electroanal.Chem.*, 1981, *125*, 89.
[7] Janssen, M.M.P.; Moolhuysen, J. *Electrochim. Acta*, 1976, *21*, 869; Guha, P.K.; Bhattacharya, A.; Kundu, K.K. *Indian J. Chem. A*, 1989, *28*, 267.
[8] Adzic, R.R.; O'Grady, W.E.; Srinivasan, S. *J. Electrochem. Soc.*, 1981, *128*, 1913.
[9] Watanabe, M.; Furuuchi, Y.; Motoo, S. *J. Electroanal.Chem.* , 1985, *191*, 367
[10] Shibata, M.; Motoo, S.; *J. Electroanal.Chem.* 1986, *209*, 151; Szabo, S.; Bakos, I. *J. Electroanal.Chem.* , 1987, *230*, 233.
[11] Gasteiger, H.A.; Markovic, N.; Ross, P.N. Jr.; Cairnes, E.J. *J. Phys.Chem.*, 1994, *98*, 617; Watanabe, M.; Uchida, M.; Motoo, S. *J. Electroanal.Chem.*, 1987, *229*, 395.
[12] Liu, R.-C.; Ley, K. L.; Pu, C.; Leyarovksi, N.; Segré, C.; Smotkin, E. S. *J. Electrochem. Soc.*, in press.
[13] Briceño, G.; Chang, H.; Sun, X.; Schultz, P.G.; Xiang, X.-D. *Science*, 1995, *270*, 273.
[14] Xiang, X.-D.; Sun, X.; Briceño, G.; Lou, Y.; Wang, K.A.; Chang, H.; Wallace-Freedman, W.G.; Chen, S.-W.; Schultz, P.G. *Science*, 1995, *268*, 1738.
[15] Baker, B.E.; Kline, N.J.; Treado, P.J.; Natan, M.J. *J. Am. Chem. Soc.* in press.
[16] McKee, D.W.; Norton, F.J.; *Journal of Catalysis*, 1964, *3*, 252; McKee, D.W. *Journal of Catalysis*, 1969, *14*, 355.

REMOVAL OF SULFUR CONTAMINANTS IN METHANOL FOR FUEL CELL APPLICATIONS

S. H. D. Lee and R. Kumar
Electrochemical Technology Program
Argonne National Laboratory
9700 South Cass Ave.
Argonne, IL 60439

and

R. Sederquist
International Fuel Cells
195 Governors Highway
P.O. Box 739
South Windsor, CT 06074

INTRODUCTION

Fuel cell power plants are being developed for transit bus and passenger car applications that use methanol as the on-board fuel. Commodity methanol by itself contains very little sulfur; however, it may occasionally be contaminated with up to about 1% diesel fuel or gasoline in current liquid-fuel distribution systems, leading to the presence of sulfur in the methanol fuel. This sulfur must be removed because of its deleterious effect on the reforming catalysts. International Fuel Cells has set the allowable sulfur limit in the methanol fuel at less than 1 ppm.

RESULTS AND DISCUSSION

Sulfur compounds present in a typical diesel fuel were identified by a gas chromatograph coupled to a mass spectrometer (GC/MS) and a gas chromatograph with a flame photometric detector (GC/FPD) operated in the sulfur mode; they were found to be essentially C1-C4 alkyl-substituted benzothiophenes, 0-C3 alkyl-substituted dibenzothiophenes, and their isomers. Table 1 summarizes the estimated relative amount of each sulfur group in diesel fuel. The totals are 33~35% benzothiophenes and 65~67% dibenzothiophenes.

Table 1. Estimate of Relative Amount of Sulfur Groups in Diesel Fuel

Compound Class	Approximate Percentage of Total Organic Sulfur	
	GC/MS	GC/FPD
C1-Benzothiophenes	6.4	1.3
C2-Benzothiophenes	9.9	9.7
C3-Benzothiophenes	11.8	14.9
C4-Benzothiophenes	6.9	7.4
Total Benzothiophenes	**35.0**	**33.3**
Dibenzothiophene	7.8	8.1
C1-Dibenzothiophene	19.9	27.4
C2-Dibenzothiophene	24.4	21.9
C3-Dibenzothiophene	12.9	9.3
Total Dibenzothiophenes	**65.0**	**66.7**

Next, activated alumina, activated bauxite, activated carbon, attapulgite clay, and diatomaceous earth were experimentally evaluated for their sulfur adsorption capabilities from methanol that had been doped with 1 vol% diesel fuel (containing 0.29% S). Activated carbon (AC) was found to be the most effective. Subsequently, several commercially available activated carbons (Table 2) made with different starting materials and activation processes were screened. In general, the coconut-based carbons activated by high-temperature steam were found to be more effective than the coal-based activated carbons in removing sulfur compounds from the contaminated methanol.

Table 2. List of Activated Carbons Tested for the Adsorption of Sulfur in Methanol

Carbon Type	Raw Material	Activation Process	Surface Area,[a] m^2/g
Filtrasorb 400[b]	Bituminous Coal	High Temp. (HT) Steam	950-1050
Type ADP[b]	Bituminous Coal	HT Steam and Acid Washing	1500
Centaur[b]	Bituminous Coal	Patented Process	800-850
Type CPG LF[b]	Bituminous Coal and Binder	HT Steam	950-1050
Type PCB[b]	Coconut Shell	HT Steam	1150-1250
Type MI[c]	Coconut Shell	HT Steam	1300
Type SE[c]	Coconut Shell	HT Steam	1200
Type COC/AW L60[d]	Coconut Shell	HT Steam	1150-1200
Type COL/P L60	Bituminous Coal	HT Steam and Acid Washing	950-1000
Nuclear SA-20[e]	Wood	HT Steam	1400-1800
Ambersorb No. 572[f]	Ion Exchange Resin	Patented Process	1100

[a]Measured by the N_2 BET method.
[b]Calgon Carbon Corp., P.O. Box 717, Pittsburgh, PA 15230.
[c]Barnebey & Sutcliffe Corp., P.O. Box 2526, Columbus, OH 43216.
[d]Carbon Activated, 1662 W. 139th Street, Gardena, CA 90249.
[e]Westvaco Corp., Carbon Department, Coventon, VA 24428.
[f]Rohn and Haas Co., 5000 Richmond Street, Philadelphia, PA 19137.

The adsorption capacity of an adsorbate on activated carbon is related to the adsorbate's concentration in solution. Equilibrium adsorption isotherm tests were conducted to determine the relationship between the concentration of sulfur in methanol and the activated carbon dosage. These tests used the coal-based Calgon Filtrasorb 400 AC and three coconut-based carbons: Calgon Type PC and B&S Types SE and MI. As expected, the sulfur concentration in the AC-treated methanol decreased with increasing dosage. At 1-g carbon per 100-mL methanol, AC removed approximately 45% of the benzothiophenes and approximately 97% of the dibenzothiophenes. This value increased to 97-99% for benzothiophenes and essentially 100% for dibenzothiophenes at a dosage of 4-g AC/100-mL methanol.

The data obtained from the equilibrium adsorption isotherm tests were interpreted by using the empirical Freundlich equation (1):

$$X/m = KC^{1/n}, \text{ or } \log (X/m) = \log K + 1/n \log C$$

where X = amount of sulfur impurity adsorbed, g
m = mass of activated carbon, g
C = sulfur concentration in methanol after equilibrium, mg/L
K, n = constants

All four adsorption isotherms (Fig. 1) in the plots of log (X/m) versus log C show two linear regions. Adsorption characteristics of a solution containing two solutes measured by a gross concentration parameter are reflected in an isotherm plot consisting of two straight lines (2). The adsorption isotherms in Fig. 1 suggest that the benzothiophene group in methanol has different adsorptivity on activated carbon from the dibenzothiphene group, and the two types of sulfur species compete for adsorption sites in the pore structure of the activated carbon.

Figure 1 also shows that the coal-based Filtrasorb 400 AC has higher sulfur adsorption capacities than the coconut-based ACs for methanol solutions that have sulfur concentrations greater than about 4.0 mg/L (5 ppmW). However, the reverse is true for sulfur concentrations less than 4.0 mg/L. Among the three coconut-based ACs tested, B&S Type MI has the highest sulfur adsorption capacity.

A preliminary assessment of the dynamic performance of these ACs was obtained in a bench-scale, dynamic batch test. In this test, Calgon Filtrasorb 400 and B&S Type MI activated carbons were packed in a Pyrex glass column of 1.77-cm ID x 91.44-cm length (0.5-in. ID x 36-in. length). The carbon has a particle size of 1.64 x 0.84 mm (-12 +20 U.S. Standard Testing Sieve No.) and was tested with diesel-fuel-contaminated methanol (containing 30 ppmW sulfur) at a flow rate of 5 mL/min. The empty bed contact time was 24 min. A 5-mL effluent sample was collected at the end of the column for every time interval tested. The test with Filtrasorb 400 lasted 16 hours, and the test with Type MI lasted 30 hours.

The sulfur breakthrough curves for both tests are shown in Fig. 2. Within experimental and analytical errors, both ACs behave similarly in terms of their breakthrough characteristics. During the first 3.0 h of continuous flow testing, they removed 100% of the 30 ppmW sulfur in the methanol feed. The breakthrough curve levels off at an effluent sulfur concentration of 24 ppmW, which is 80% of the sulfur concentration in the methanol feed. Apparently, the sulfur compounds in the feed had not totally broken through the column after the 30-h test (i.e., the column has not reached dynamic equilibrium with the feed). A GC/MS analysis of the effluent sample collected at 29 h showed approximately 89% of total benzothiophenes and approximately 29% of total dibenzothiophenes in the methanol feed.

The breakthrough data shown in Fig. 2 were mathematically analyzed by the LUB/equilibrium section concept (3). On the basis of this concept, the dynamic adsorbate loading (or adsorption capacity) of the activated carbons was estimated to be 0.79 mg S/g AC for the 80% adsorption capacity level. By extrapolation, the dynamic adsorption capacity of these two ACs would be 1.0 mg S/g AC if these activated carbons were tested until the complete breakthrough of sulfur from the column. Figure 1 indicates that the equilibrium isotherm adsorption capacity for Calgon Filtrasorb 400 and B&S Type MI activated carbons is 3.5 and 2.8 mg S/g AC, respectively. Therefore, the dynamic adsorption capacity of 1.0 mg S/g AC for these two activated carbons is about one-third of their equilibrium isotherm adsorption capacities.

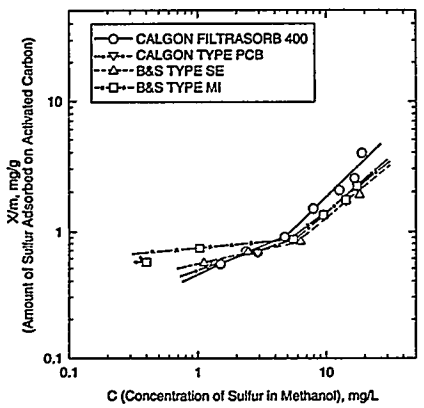

Fig. 1. Adsorption Isotherm of Activated Carbon for Sulfur in Methanol

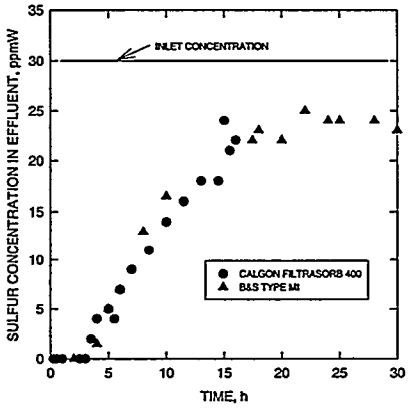

Fig. 2. Breakthrough Curve of Activated Carbon for Sulfur in Methanol

CONCLUSION

The equilibrium adsorption isotherm and breakthrough data were used to assess the feasibility of developing a granular activated carbon (GAC) adsorber for use as a sulfur removal subsystem in transportation fuel cell systems. Results of this analysis suggest that an on-board GAC adsorber may not be attractive due to its size and weight constraints. However, it may be feasible to install this GAC adsorber at methanol distribution stations, where space and weight are not a critical concern. A preliminary economic analysis indicated that the GAC adsorber concept will be attractive if the spent AC can be regenerated for reuse. It should be emphasized here that these preliminary analyses were made on the basis of the very limited breakthrough data obtained from the bench-scale testing. More detailed optimization on the dynamic testing parameters and the study on regeneration of the spent AC are needed.

ACKNOWLEDGMENTS

This work is supported by the U.S. Department of Transportation.

REFERENCE

1. "Laboratory Evaluation of Granular Activated Carbon for Liquid Phase Applications," Application Bulletin AB-002-12/93, Calgon Carbon Corporation, Pittsburg, PA, 1993.
2. F. E. Bernardin, "Experimental Design and Testing of Adsorption and Adsorbates," Adsorption Technology, ed, Frank L. Slejko, Marcel Dekker, Inc., New York, 1985.
3. J. J. Collins, "The LUB/Equilibrium Section Concept for Fixed-Bed Adsorption," Chem. Eng. Prog. Symp. Series No. 74, Vol. 63, pp. 31-35 (1967).

EVALUATION AND PERFORMANCE OF AN UNCONVENTIONAL AFC-DESIGN

Stephan Schwartz, Olle Lindström
Department of Chemical Engineering and Technology
Royal Institute of Technology (KTH), S-100 44 Stockholm, Sweden

Introduction

Alkaline fuel cells, AFC, now play a Cinderella role after their successes in space. There are signs that the "CO_2 syndrome" at last will have its cure. The argument that removal of CO_2 from air and hydrogen should be so expensive that AFC has to be ruled out for terrestrial applications is no longer true. Its low stack cost will be the decisive feature.

The AFC could easibly be developed to a mature, industrial product for a large number of applications.We and a few other groups have tried to keep the AFC technology alive in a hostile climate, preparing for a rebirth as happened to its notorious rival the PEFC.
We have concentrated our efforts on two designs characterized by external or internal manifolding. Both designs rely on an electrolyte chamber giving a constant pressure between the gas space and the the electrolyte over the whole electrode surface. Hoechst has developed another cell design for the same purpose. We shall here decribe the design of such a module with external manifolding.

Experimental

The new AFC-stack developed at KTH has recently been tested in a 7-cell module size, Fig. 1. The stack is of the bipolar type with external manifolding. Emphasis is on stacks with big electrode areas with minimized parasitic currents in the system.

The module consists of seven cells. A stack will use several modules with cooling plates located between the modules.

The gas system, Fig.2, for a full stack shall not only feed the electrodes with hydrogen and oxygen (air) but also take care of the reaction water. Water vapor is condensed in a condenser and returned to the electrolyte system to adjust the electrolyte concentration. In our present tests, however, a simple gas flow through system is used.

The electrolyte system is a combined "wetted and falling" system and gives no pressure gradient against the electrodes. The differential pressure on every point over the electrodes is constant. The matrix consists of two parts, one microporous membrane against the hydrogen electrode and one non-woven cloth against the oxygen electrode.Vertical thin channels in the wetted cloth permit the electrolyte to fall freely downwards. A falling electrolyte scheme has been described by Tetzlaff, et al (1).

The electrolyte is pumped from a sump up to a distribution chamber from which thin tubes distribute the electrolyte to basins above each cell compartment, Fig.3. In the bottom of the stack the electrolyte drops from each cell compartment down to an assembly box and is then sent back to the sump again. The thin pipes together with the "dropping" gives a very low parasitic current.

A stack module consists mainly of two repeating units: the centrum unit and the matrix unit. Fig. 4 shows a cross section of an enlarged centrum unit and a matrix unit. The centrum unit consists of a separator plate or collector, which serves a gas distributor for the oxygen and hydrogen electrodes. To secure the electrical contact and to minimize ohmic losses the components are spotwelded together through the whole package by current collector disks.

The constant differential pressure electrolyte system and the spotwelded collectors permit big electrode areas.

The electrodes consist of a porous gas diffusion layer with 60 wt% PTFE on carbon, a nickel wire mesh and an active layer of 12,24 wt% CoTPP and 12 wt% PTFE on carbon for the oxygen electrodes. The active layer for the hydrogen electrode consists of 8.3 wt% Pt and 8.3 wt% Pd and 17 wt% PTFE on charcoal.

Test results

Since the end of February 1996 a seven cell module (7*200 cm^2) has been tested at KTH. Fig. 5 shows polarization curves with and without ohmic drop. Pseudoresistances are 1.1 and 0.6 ohm cm^2 respectively.The tests were performed at 35-40°C, pure hydrogen and oxygen and 6-M KOH. Most of the ohmic drop is due to losses in the matrix system. A comparison between different gas compositions, Fig. 6, shows significant performance and the importance of high gas concentrations. Fig. 7 shows the performance characteristics of each cell at different loads and Fig. 8 shows the module potential v.s. time at a load of 10 A, i.e. 50 mA/cm^2. The potential drop is 40 uV/h per cell.

Acknowledgement

Financial support by the Swedish Agency for Research Cooperation with Development Countries (SAREC) is gratefully acknowledged.

REFERENCE

1, K.-H. Tetzlaff, W. Wendel:
DECHEMA, Monogr. 112 (1988) 325.

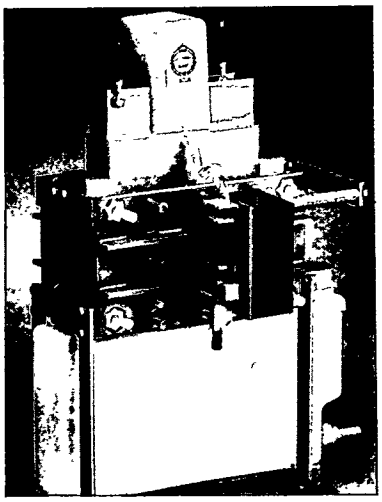

Fig. 1 The 7-cell module system.

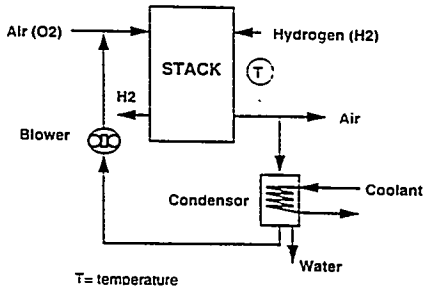

Fig. 2 Flow sheet. The gas system.

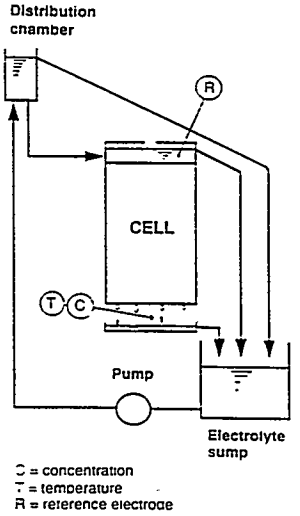

Fig.3 Flow sheet. The electrolyte system.

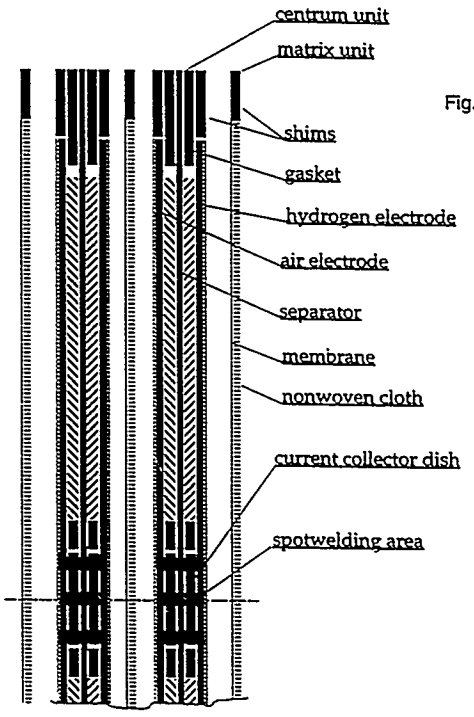

Fig. 4 Cross section of outspread centrum units and matrix units

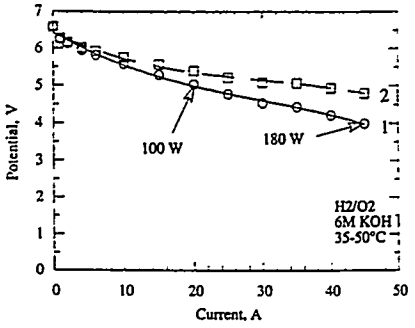

Fig. 5 Polarizatuon curves with (1) and without (2) ohmic drop.

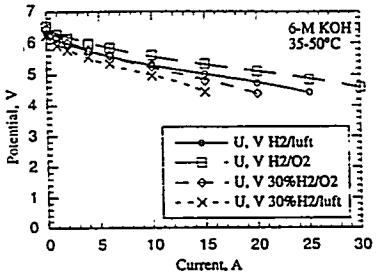

Fig. 6 Polarizatuon curves for different gas combinatuons.

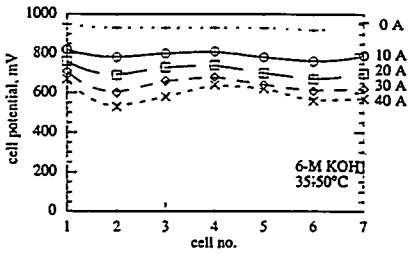

Fig. 7 The performance characteristucs of each cell at different loads.

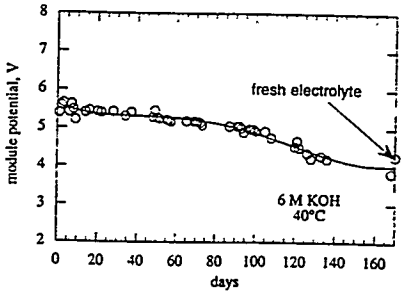

Fig. 8 The module potential v.s. time at a load of 10 amperes

PERFORMANCE OF Pt-Co ALLOYS AND CoTPP CATALYSTS FOR THE REDUCTION OF OXYGEN IN AFC

Y. Kiros
Royal Institute of Technology, Department of Chemical Engineering and Technology, Chemical Technology, S-100 44 Stockholm, Sweden

A. Sampathrajan, and M. Ramanathan
Tamil Nadu Agricultural University, College of Agricultural Engineering, Department of Bio-Energy, Coimbatore 641 003, India

INTRODUCTION

One of the primary problems of the oxygen reduction reaction (ORR) for especially low and medium temperature fuel cells such as AFC, PEFC and PAFC is the high activation overpotential. This high overpotential is due to the complicated nature of the ORR and the morphological properties of the catalyst particles. High catalyst dispersion on the carbon support and small particle sizes, non-agglomeration and/or non-dissolution of the electrocatalyst is desired for the long-term operation of the electrodes.

In this study electrodes were tested at different temperatures and concentrations in order to substantiate their influences on the activity and stability of the electrocatalysts, i.e; cobalt tetraphenylporphyrin (CoTPP) and alloys of platinum and cobalt.

EXPERIMENTAL

The CoTPP catalysts were prepared and impregnated on carbons of 1:1 ratio of Vulcan XC-72 and Ketjenblack EC with a total surface area corresponding to 585 m^2/g. Cobalt acetate was dissolved in methanol and homogenized with the carbon support, dried and then mixed again with meso-tetraphenylporphyrin in concentrated formic acid. Following the drying, mixing and homogenization steps, the catalyst material on support underwent pyrolysis at 700 °C under nitrogen atmosphere for 5 hours (1). The total surface area after the heat-treatment was found to be 202 m^2/g. The support material for the preparation of the alloys was the same as for the CoTPP. Chloroplatinic acid dissolved in deionized water with 5% non-ionic surfactant was added under ultrasonic agitation to the cobalt acetate and carbon mixture. The atomic ratio of platinum to cobalt was 1:3. The mixture was finally heat-treated at 900 °C under a flow of 1:1 volume ratio of nitrogen and hydrogen gas mixtures for 2 hours. The BET-surface area of the catalyst and carbon mixtures was 540 m^2/g.

PTFE-bonded gas diffusion electrodes were prepared by rolling the active (catalyst) layer and diffusion layer separately. The layers were then rolled together on a nickel screen (100 mesh) to obtain an electrode with a total thickness of 0.55-0.60 mm after compacting, drying and sintering. The carbon support on the diffusion layer was wet-proofed with a higher amount of PTFE than the catalyst layer. The electrodes were then assembled and tested galvanostatically at a constant load of 100 mA/cm^2 in 6M KOH and at 80 °C. The deterioration or decay rate of the electrode was measured versus a Hg/HgO reference electrode and recorded over a period of time until the potential reached -200 mV.

RESULTS AND DISCUSSION

The role of macrocycles or N_4 chelates in oxygen reduction in alkaline electrolytes has been extensively studied. The activity and stability of the macrocycles impregnated on carbon supports

are improved by thermal treatment at higher temperatures. Fig. 1 and Fig. 2 show the potential versus current density characteristics of the gas diffusion electrodes, prepared from CoTPP with loadings of approximately 1.5 mg/cm^2. As shown in the figures, 6M KOH and 80 °C gives a higher performance improvement than the other concentrations and temperatures studied. This is due to the influence of temperature on the electrode kinetics and the characteristics of the electrolyte where higher ionic conductivity and lower diffusion coefficient depend on the strength of the bulk concentration (2). However, the high performance of the CoTPP-based electrode is not sustainable due to factors mainly such as dissolution of cobalt (3), wetting-in properties of the electrode (4) or corrosion of the electrode materials (5). Atomic absorption spectrophotometer (AAS) analysis of the electrolyte after 200 hours of electrochemical operation of the electrode showed an almost 60% loss of cobalt, which together with the charred residue of the macrocycle constitute the active component in the reduction of oxygen.

Fig. 3 shows polarization curves for electrodes catalyzed by CoTPP, platinum-cobalt alloy and platinum. CoTPP shows superior activity among the electrocatalysts considered. Surface, structural, chemical and electrochemical characterizations of the Pt-Co electrocatalysts have been reported elsewhere (6). The Pt-Co alloy catalyzed electrode was superior by approximately 20 mV than the pure platinum-based electrode. Jalan et al (7) suggested that the smallest nearest-neighbor distance of platinum atoms with the transitional metals would be ideal for the dual site adsorption of oxygen or peroxide. Paffett et al (8) proposed that surface roughness effects due to dissolution of the base metal gives surface area effect and hence improvement of the oxygen reduction activity.

Fig. 4 shows comparison of the long-term operation of the Pt-Co and CoTPP-based electrodes. At higher temperatures, the decay rates of the CoTPP-based electrode are higher than lower temperature operation, where small decay rates after 7000 hours of operation of the CoTPP-based electrodes were reported (3). The operation time of the Pt-Co electrocatalyst increased approximately four-fold compared to the CoTPP-based electrode. TEM analysis of a fresh and used electrode after 670 hours of electrochemical operation has shown agglomeration of the catalyst particles, which is the main factor for the deterioration of the electrode performance (9).

Acknowledgement-The authors wish to thank Professor Olle Lindström for discussions. Financial support by the Swedish Agency for Research Cooperation with Developing Countries (SAREC) is gratefully acknowledged.

REFERENCES

1. Y. Kiros and S. Schwartz, J. Power Sources, 36 (1991) 547.
2. M. Viitanen and M.J. Lampinen, Journal of Power Sources, 32 (1990) 207.
3. Y. Kiros, O. Lindström and T. Kaimakis, J. Power Sources, 45 (1993) 219.
4. A. Lundblad and P. Björnbom, J. Electrochem. Soc., 141 (1994) 1503.
5. K. Tomantschger, R. Findlay, M. Hanson, K. Kordesch and S. Srinivasan, J. Power Sources, 39 (1992) 21.
6. Y. Kiros, J. Electrochem. Soc., 143 (1996) 2152.
7. V. Jalan and E. J. Taylor, ibid., 130 (1983) 2299.
8. M. T. Paffett, J. G. Beery and S. Gottesfeld, ibid., 135 (1988) 1431.
9. Y. Kiros, Asian Seminar on Fuel Cells, Apr. 25-26, Coimbatore; Tamil Nadu, India.

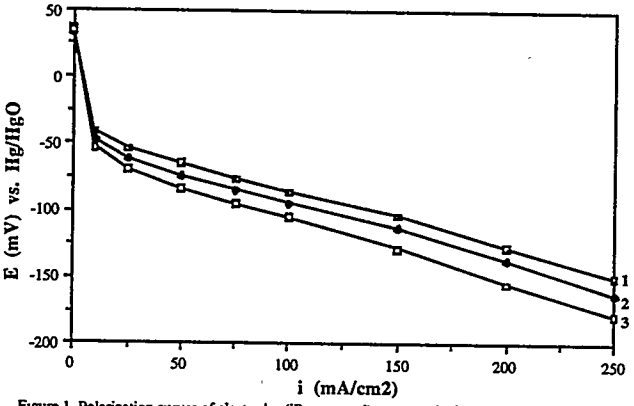

Figure 1. Polarization curves of electrodes (iR-corrected), promoted with CoTPP and tested at 20 °C and KOH concentrations of 1) 6M 2) 9M and 3) 12M

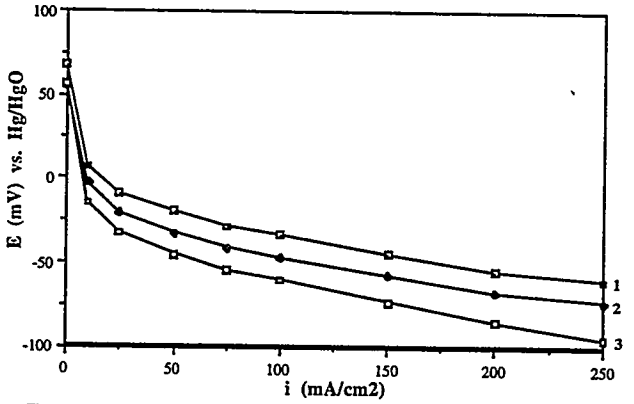

Figure 2. Polarization curves of electrodes (iR-corrected), promoted with CoTPP and tested at 80 °C and KOH concentrations of 1) 6M 2) 9M and C) 12M

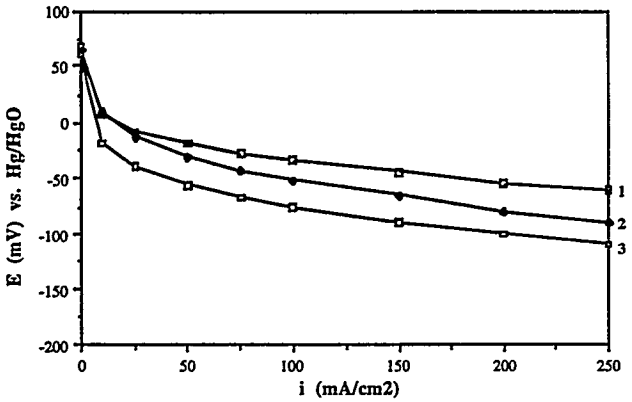

Figure 3. Comparison of polarization data among electrodes (iR-corrected), catalyzed by 1) CoTPP 2) Pt-Co alloy and C) Pt

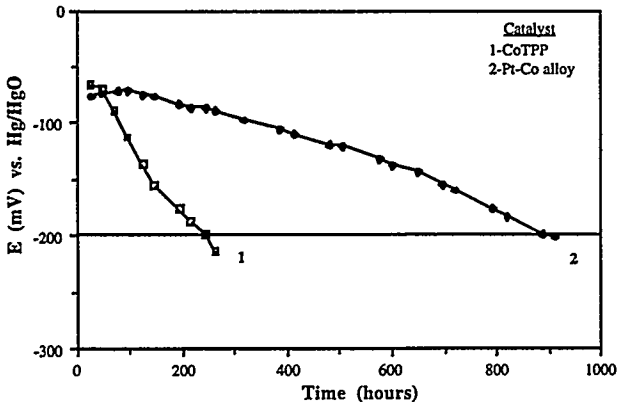

Figure 4. Potential versus time of the CoTPP and Pt-Co catalyzed electrodes.

FCPP APPLICATION TO UTILIZE ANAEROBIC DIGESTER GAS

Yoshio Nakayama
Environment & Urban System Engineering Division
Toshiba Corporation
1-1 Shibaura 1-chome, Minato-ku, Tokyo 105, Japan

Nobuyuki Kusama
Fuel Cell Systems Division
Toshiba Corporation

Katsuya Wada
Heavy Apparatus Eng. Laboratory
Toshiba Corporation

1. INTRODUCTION

Toshiba and a municipal organization of Yokohama city are jointly conducting a program to utilize ADG (Anaerobic Digester Gas) more effectively. ADG which contains about 60% methane is produced by anaerobic digestion of waste water treatment sludge and has been used as an energy source for heating digestion tanks in sewage treatment plants and/or for combustion engine fuel. This program is focused on operating a commercial Phosphoric Acid Fuel Cell(PAFC) power plant on ADG because of its inherently high fuel efficiency and low emissions characteristics.

According to the following joint program, we have successfully demonstrated an ADG fueled FCPP. The success of this study promises that the ADG fueled FCPP, an environment-friendly power generation system, will be added to the line-up of PC25™C applications.

The joint program consists of three phases as follows:

Phase-1 (August, 1994 - October, 1995)
- Evaluation of ADG composition
- Small scale verification tests of the ADG pretreatment system characteristics and Fuel Processor System(FPS) performance

Phase-2 (November, 1995 - March, 1996)
- Installation of demonstration plant (a 200 kW FCPP and an ADG pretreatment unit)

Phase-3 (April, 1996 - March, 1997)
- Parametric tests on three cases of methane concentration (90%, 75% and 60%)
- Continuous operation on 60% methane
- Evaluation of capability to operate on 60% methane
- Definition of the optimum system for the ADG fueled FCPP application

2. EXPERIMENTAL PROGRAM

The system flow diagram for this study is shown in Figure 1. This system consists of a standard 200 kW FCPP designed to operate on pipeline natural gas and an ADG pretreatment unit which containing several sub-units as shown in Figure 1.

The desulfurizer operates at ambient temperature and pressure and reduces hydrogen sulfide ($Fe_2O_3 + 3H_2S \rightarrow Fe_2S_3 + 3H_2O$). ADG contaminants are adsorbed by an activated carbon bed. A compressor is utilized to convey the ADG through a pressure swing adsorption unit (PSA) at the required pressure. The PSA consists of 2(two) beds in series with automatically reversing capability.

The design also provides the capability to adsorb CO_2 (methane concentration) on one bed while the other bed is desorbing CO_2 by using a vacuum pump. The product gas ,concentrated methane by the PSA, is delivered to the 200 kW fuel cell power plant .And the gas which is not concentrated methane (removed only contaminants from the ADG feed gas) is also usable by using the PSA by-pass line.

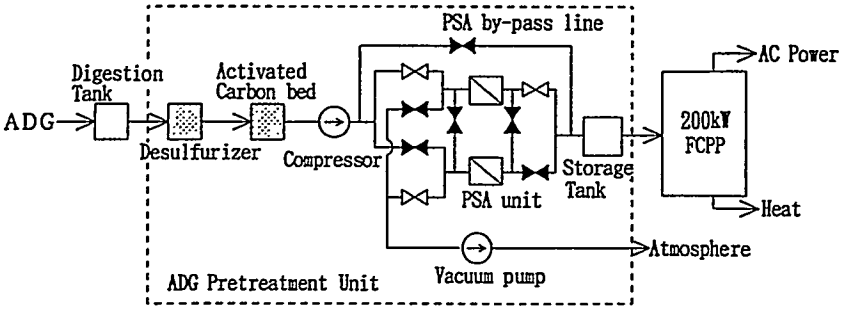

Figure 1. System flow diagram

In Phase-1, the verification tests of ADG pretreatment and FCPP Fuel Processor System(FPS) performance on ADG which contains up to 40 % diluents (CO_2) were performed. An analysis of seasonal ADG composition at the Yokohama city facility was also carried out. A small scale test unit was used in this phase. A small scale test unit consists of an ADG pretreatment unit and a FPS unit which contains a reformer, a steam tank to supply the steam for reforming, an electrical heater to provide the heat for reforming and a low temperature shift converter (LTS).

In Phase-2, a standard 200 kW FCPP (PC25™B) which was designed to operate on pipeline natural gas and a full-scaled ADG pretreatment unit were installed at Hokubu Sludge Treatment Center of Yokohama city. A complete view of this plant is shown in Figure 2.

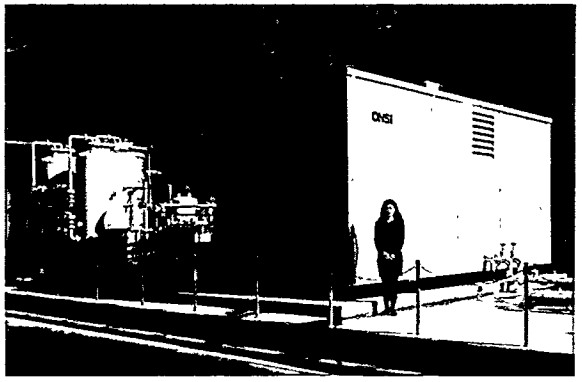

Figure 2. Complete view of the demonstration plant

In Phase-3, the parametric test for each methane concentration (90%, 75% and 60%) was performed. The plant operation data for each test was collected by means of gas analyses in the FCPP and supplied ADG flow rates which was measured by the external flow meter. The main technical approach in this phase was to evaluate the capability to operate on 60% methane.

3. RESULTS AND DISCUSSION

(1)*PHASE-1*

Table 1 presents the seasonal ADG composition. The data shows that the methane constituent is almost 60 vol% for all season and its seasonal fluctuations are small. It is noted that a small amount of oxygen (less than 1 vol%)is also present.

The FPS test results are shown in Figure 3. The methane conversion is lower than what was experienced in the natural gas fueled FCPP. And the methane conversion shows a tendency to decrease as the methane concentration reduces. The reason is estimated that the heat to be given for reforming of methane was not sufficient since a part of heat source was consumed for heating the diluent as CO_2 ,which provided by an electrical heater and is constant in this test.

The CO conversion for each methane concentration is the same as what was experienced in the natural gas fueled FCPP. The CO concentration at the FPS outlet gas is less than 1.0 vol% which meets the FCPP requirements. These results confirm FPS operability on 60% methane.

In addition, the following results were obtained:

(a) The period of PSA bed Adsorption/Desorption was 140 seconds.
(b) The Hydrogen Sulfide varies irregularly with peaks to 50 ppmv for a short time.
(c) ADG contaminants are sufficiently removed by the pretreatment unit confirming its design satisfies FCPP requirements.
(d) A part of the CO_2 in the ADG contributes to the reforming as a substitute for H_2O, judging from the CO_2 concentration at the reformer outlet gas shown in Figure 3.

Table 1 Seasonal ADG composition

	Spring	Summer	Autumn	Winter
Methane (vol%)	N/M	59.6	64.0	63.2
Carbon Dioxide (vol%)	N/M	38.2	35.4	35.2
Nitrogen (vol%)	2.1	3.0	0.8	1.5
Oxygen (vol%)	0.06	1.0	0.3	0.3
Hydrogen Sulfide (ppmv)*1	N.D	N.D	2.7	2
Chlorine (ppmv)	N.D	N.D	N.D	N.D
Hydrogen Chloride (ppmv)	N.D	N.D	4	23
Ammonia (ppmv)	N.D	N.D	N.D	N.D
H_2O (vol%)	N/M	1.4	2.5	1.3

N.D:Not Detected N/M:Not Measured
*1: Hydrogen Sulfide is reduced previously at the digester tank inlet.

(2)*PHASE-3*

Table-3 presents the data from the parametric tests and the estimated value at 200kW electrical output on 60% methane. In this test plant, the maximum load on 60% methane was 137 kW due to the increased pressure drop in the ADG piping which was the ADG inlet piping of FCPP and the piping between FCPP and the ADG pretreatment unit.

The parasite power of the ADG pretreatment unit was 7 kWh, consumed by the compressor. It is noted that the CO concentration at LTS outlet gas has a tendency to increase as methane concentration becomes low, due to the conversion a part of CO_2 into CO in the reformer. It is estimated that the optimum S/C would be 3.5 with 200 kW on 60% methane.

For the maximum load , it is confirmed that the standard PC25 B would be able to achieve 200kW electrical output on 75% methane. However, due to an increase in the amount of volume flow, maximum load on 60% methane would be 160 kW.

From the above results, it is confirmed that an ADG fueled FCPP can be designed by modifying the standard FCPP on natural gas without any special technology developments which require the system and component design, verification testing etc.

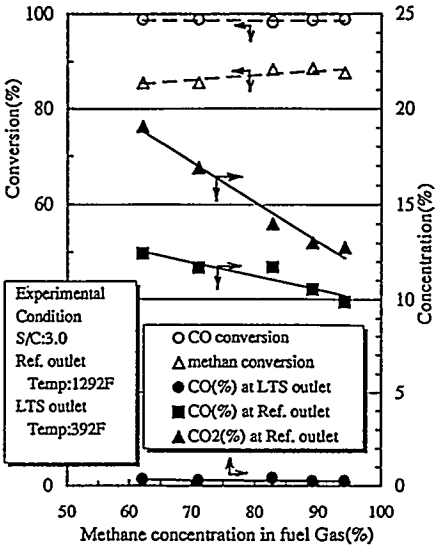

Figure 3. FPS test results in Phase-1

The modifications necessary to achieve 200kW electrical output on 60% methane are as follows:

(1) Increase the size of ADG feed gas flow piping.
(2) Increase the capacity of the valves on this pipingline.
(3) Define the ejector specification to reduce the parasite power for the ADG pretreatment unit.

Table-3 Parametric test results

Methane Concentration(%)	90%	75%	60%	
Electrical Output(kW)	200kW	150 kW	137 kW	200kW(Estimate)
Electrical Efficiency (LHV%)	37.8	36.8	35.4	37.6
ADG Fuel Flow (pph)	108.5	110.6	154.4	239.6
Ejector Position (%)	63	52	35	65
Methane Conversion. (%)	92.1	91.1	92.9	91.6
CO Conversion (%)	97.9	97.2	96.8	97.3
CO Concentration at LTS outlet gas (vol%)	0.3	0.6	0.5	0.3
S/C ratio(-)	3.6	3.0	3.0	3.5

4. CONCLUSION

From the success of this study, it is confirmed that the ADG fueled FCPP can be practically designed by slightly modifying the standard FCPP on natural gas so that the FCPP can be operated on ADG which contains about 60% methane.

Toshiba believes that the ADG fueled power plant ,which can be a highly effective use of anaerobic digester gas, is an influential application for FCPP and will be added to the line-up of PC25 C applications.

LOCAL BIOFUELS POWER PLANTS WITH FUEL CELL GENERATORS

O. Lindström
Department of Chemical Engineering and Technology
Chemical Technology
Royal Institute of Technology
S-100 44 Stockholm, Sweden

The fuel cell should be a most important option for Asian countries now building up their electricity networks. The fuel cell is ideal for the schemes for distributed generation which are more reliable and efficient than the centralized schemes so far favoured by the industrilized countries in the West. Not yet developed small combined cycle power plants with advanced radial gas turbines and compact steam turbines will be the competition. Hot combustion is favoured today but cold combustion may win in the long run thanks to its environmental advantages.

Emission standards are in general determined by what is feasible with available technology. The simple conclusion is that the fuel cell has to prove that it is competitive to the turbines in cost engineering terms. A second most important requirement is that the fuel cell option has to be superior with respect to electrical efficiency.

The primary energy sources for a world population of say 10 billion people consuming a total of 250 000 Twh are limited. Only photovoltaics, biofuels and fusion are able to meet the requirements in particular with respect to quantity and quality. Biofuels and fuel cells seem to be a very good solution together with photovoltaics of the energy dilemma facing the world during the next century. Cold combustion has to be given a fair chance in the competition with hot combustion.

Sweden and India have carried out a six year program for development and evaluation of fuel cell power plants for biofuels on the grounds indicated above. Figure 1 shows the per capita consumption of electricity as a function of time in Sweden and India. The Utopia of the next century (what is the alternative?) may exhibit about the same per capita consumption of electricity in Sweden and in India with half of their shares of the assumed 250 000 Twh being electricity. Sweden must then reduce its electricity consumption to the level of the early eighties whereas India has to step up manifold.

Sweden should be able to follow the route in Figure 1 simply by living up to the political decision to shut down the nuclear power reactors now supplying almost half of the Swedish electricity. This is easy to say but very difficult in practice. The energy scene has, however, so far seen very great changes. The changes may take place more rapidly in the future than in the past. The development curve for India in Figure 1 should become reality, Sweden's built up curve is already history. There will be irregularities and the average, annual increase may be somewhat slower than the 10 % used here. The big uncertainty is *what kind of power plants* will supply the electricity to the Indian people.

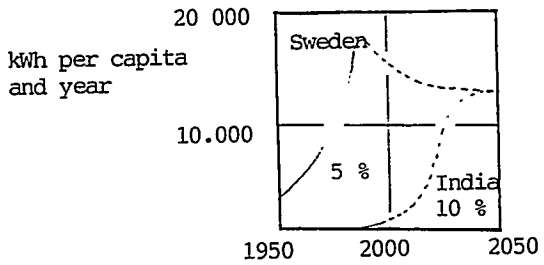

Figure 1. Electricity scenarios for India and Sweden

Today, advanced coal power plants and nuclear power plants !? Tomorrow, photovoltaics and fuel cell power plants for biofuels!? There will of course also be room for windpower and hydropower. We shall not here make a forecast regarding the composition of India´s future power plant box. Cost engineering criteria will become more and more important also for power plant investments.

Indian Council of Agricultural Research, ICAR, with Dr. G. Singh as responsible director (now Dr. Bhattacharya) and Swedish Agency for Research Cooperation, SAREC, with Dr. M. Bhagavan as responsible director therefore initiated and directed a joint program for demonstration and evaluation of the fuel cell option for India´s energy. The work to be summarized here was carried out in Sweden at KTH (Lindström, Sara Thyberg Naumann, Carin Myrén, Schwartz, Kiros, Gustafsson, Ömlin and Ganemi) and by the Indian teams at PAU, Ludhiana (Bhatnagar - now retired, C.P. Singh, Panesar, Jain, Jindal and others); CIAE, Bhopal (Srivastava - now retired, G. Singh - earlier ICAR, Nema and Dubey) and TNAU, Coimbatore (Swaminathan - now retired, Ramanathan and Sampath Rajan).

The Swedish group has a long fuel cell history, beginning with a 200 kW AFC power plant for submarines developed at Swedish ASEA (now ABB). All four groups have a vast experience from biofuels and biofuels processing. Emphasis was from the beginning on biofuels processing. Fuel cell hardware was to be purchased. It had to be produced within the project when Swedish agencies decided to drop AFC work at KTH following the international trend due to what we call the CO_2 syndrome. (The common misbelief that AFC is not suitable for terrestrial applications since CO_2 cannot be eliminated from air and hydrogen at acceptable cost).

After evaluation of available schemes the practical work was concentrated on two laboratory development units, LDU. LDU 1 for biogas used a 2.5 kW PAFC generator from Energy Research Corporation. The system was put up at PAU in Ludhiana. The other scheme shown in Figure 2, LDU 2, was demonstrated and operated at the Asian Seminar on Fuel Cell Technology for Rural Electrification (INDO-SAREC) in Coimbatore April 25-26 this year. Carbon dioxide was removed by a solid bed absorber and a final scrubber. Noble metal catalyzed anodes were found to be very sensitive to carbon monoxide as in the PEFC. We used a PROX reactor to bring down the carbon monoxide to a level below 5 ppm as in the PEFC schemes. Traces of oxygen from the gasification were removed in an "oxidizer".

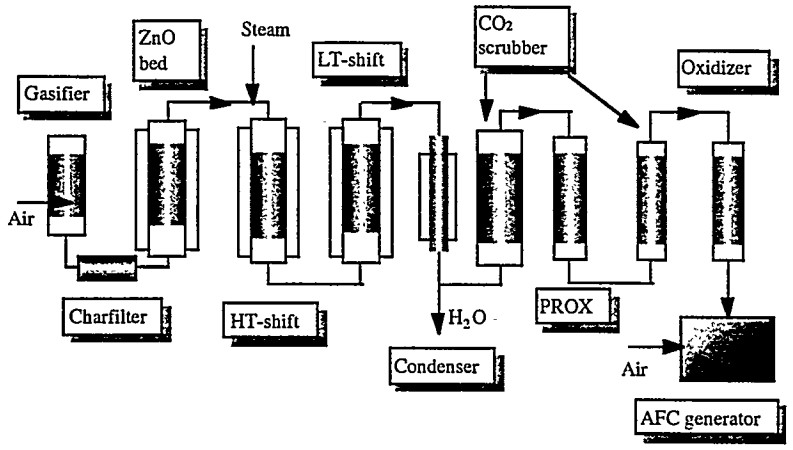

Figure 2. LDU-2, the first (small) power plant of its kind for solid biofuels

An attempt will be made to introduce a palladium diffuser now subject to development by the group Delta Power in Sweden which would simplify the system a great deal. Pure hydrogen instead of the nitrogen mixture is expected to pay for the expensive compressor. Cost of the palladium diffuser with a 1 μm thick palladium layer is acceptable.

The production capacity of AFC stacks is limited at KTH. We were, however, able to purchase four Elenco standard stacks intended for the Elenco bus project which were delivered to the Indian partners.

Free electrolyte as in the Elenco stacks is a risk, which we certainly learnt with the 200 kW system in Västerås. Emphasis in the AFC work at KTH and the fuel cell laboratory of TNAU in Coimbatore is therefore devoted to reliable electrolyte systems. We have modified a design developed by Hoechst which gives a constant pressure drop between the gas and electrolyte sides of the electrode . One design relying on external manifolding is now subject to life test in a 7 cell module as reported in the paper by Schwartz and Lindström to this seminar. The design with internal manifolding, "I-cell", is somewhat related to present MCFC and PEFC designs, which look like modern plate heat exchangers. Figure 3 shows a plate heat exchanger modified for AFC electrodes. Small double cell stacks were built and tested using components from plate heat exchangers (for beer cooling!). Cathodes used pyrolyzed macrocycles.

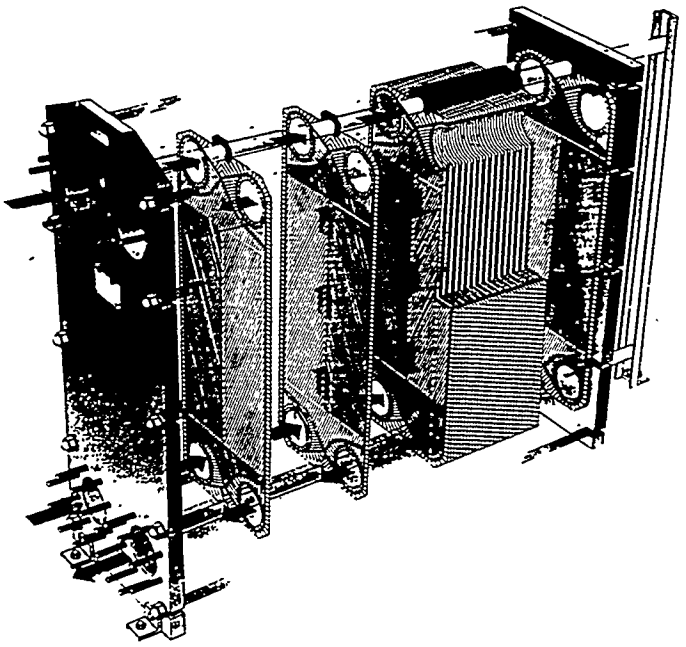

Figure 3. Delta Power's AFC stack concept designed as a plate heat exchanger like present MCFC and PEFC stacks

Analysis of these stack designs indicate a price around 100 USD/kW for the naked fuel cell module. This permits a life of 10 000 hours, which is the present target. Most of the components used in I-cell design can be recycled after service.

This program is now in its seventh year. At KTH emphasis is on life improvement whereas the Indian partners will continue to work on fuel processing and testing of LDU 2 with domestic AFC stacks and Elenco stacks.

The four teams wish to express their great gratitude to ICAR and SAREC for deep involvement and support.

INTEGRATED ANALYSIS OF THE 'SPONGE IRON REACTOR AND FUEL CELL SYSTEM'

J. Lehrhofer, M. Ghaemi, H. Wernigg, K. Friedrich and K. Kordesch
Graz University of Technology
Department of Electrotechnical Management and Energy Innovation
Krenngasse 37/1
8010 Graz, Austria

1. Introduction

The system Sponge Iron Reactor/Fuel Cell (SIR/FC) is investigated from the ecological and technical aspects and also the pre-conversion energy chain as a part of the natural gas fuel cycle is analysed. What are the decisive characteristics of a sponge iron reactor or the basic process cycle sponge iron/hydrogen/ iron oxide? This process cycle offers a simple possibility to store the energy of synthesis gases in the form of sponge iron and at the same time to reform and condition these synthesis gases. As 'product' of this energy storage one receives pure hydrogen which is intended for the running of fuel cells.

2. Natural Gas fuel cycle (Precombustion chain) for Austria

The supply of natural gas in Austria in 1994 was made up of imported gas from the former Soviet Union (Community of Independent States - CIS) with 71%, Norway and Germany each with 4% and domestic production of 21% (1). According to the country of origin the national different process chains for natural gas are taken into account. The provision of natural gas down to the low pressure consumer in Austria essentially requires the process steps shown in Fig.1. In the sense of Life cycle analysis the direct and indirect environmental pollution was determined for each process step.

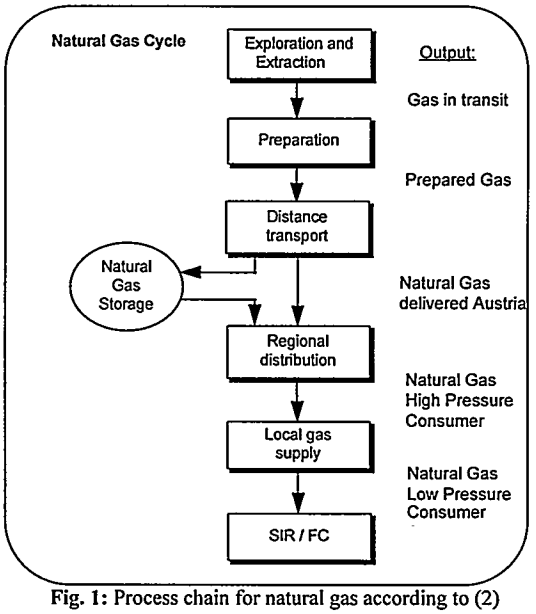

Fig. 1: Process chain for natural gas according to (2)

2.1 Exploration and Extraction

This process step includes the exploration of reserves and trial drilling and also the subsequent extraction of the natural gas. The natural gas from Austria, CIS and Germany comes only from onshore production, whereas that from Norway is produced only by offshore rigs (2). Generally 1% of the natural gas is used for extraction. This figure includes the compression expended for the collection of the natural gas, transport to the preparation plant and for compensation of the pressure loss. Emissions in to the atmosphere originate from the provision of energy, from the burning off of the natural gas, from gas leaks in plant and leaks during aeration or repairs.

2.2 Preparation

Before being fed into the transport and supply network the crude gas must be prepared in order to meet the quality requirements for final consumption. In principle one differentiates between four to five preparation steps (2):

- the separation of free water and oil
- the separation of higher hydrocarbons and gas drying
- desulphuration and recovery of sulphur by means of Claus plant
- final drying of higher hydrocarbons

In particular the preparation of sulphurous acid gas requires a relatively high energy expenditure, approximately 3% of the natural gas produced.

2.3 Distance transport and natural gas storage

In western Europe there is a well-developed network for the long distance conveyance of the prepared natural gas in operation which together with the seasonal storage provides for compensation of peak demand and permits national supply by imported gas of various origin. Austria is in a position to cover domestic natural gas consumption for a period of six months from stored natural gas (3). At distances of 100 to 200 km turbo-compressors with gas turbine drive compensate the loss of pressure and draw natural gas direct from the main to cover their energy requirements. Gas turbines with a performance of 5 to 15 MW and an annual efficiency of 30% are employed. Taking into account a specific gas consumption of the compression stations of 2% per 1000 km for Germany (distance 800 km), Norway (distance 1500 km) and 3% per 1000 km for the CIS countries (distance 6000 km) there results a considerable energy consumption for distance transport of between 2% and 18 % of the natural gas transported depending on the country of origin (2). Leakages in the network in western Europe are about 0.01 to 0.02 vol.-% per 1000 km. For the network in the CIS a probable leakage of 1.5 vol.-% per 1000 km is given (2).

2.4. Regional distribution

For feeding into the regional distribution the share in the incidence of gas in Austria is correspondingly taken into account, whereby German conditions are applied for conveyance within Austria. Natural gas leakage in regional distribution is about 0.07 vol.-% and consumption for compression is rated at 0.2 % (2).

2.5 Local gas supply

Leakages in local gas supply are markedly higher at about 0.95 vol.-% since in part old town gas mains are still in use.

Waste heat produced - emissions thereby produced in process steps						
process steps:		Exploration/ Extraction	Preparation	Distance transport	Regional distribution	Local gas supply
Emissions	Unit	[Unit/$TJ_{low\ pressure\ consumer}$]				
CH4	[g]	35471	43931	246491	1819	186964
CO	[g]	3234	246	6059	261	1048
CO2	[kg]	1269	627	7794	123	453
N2O	[g]	20	12	140	2	8
NMVOC	[g]	3698	160	1411	4963	1947
NOx	[g]	8936	1026	27978	1046	1779
Particles	[g]	6996	2926	4614	2462	6898
SOx	[g]	6936	27485	5480	1062	1998
Waste Heat	[TJ]	0,02	0,012	0,154	0,001	0,006

Table 1: Waste heat and emissions for provision of natural gas to low pressure consumers

3. Employment of natural gas or synthesis gas in the sponge iron process cycle

Among the various applications of sponge iron, its application as an alternative for gas purification or conversion is considered.

3.1 Direct employment of natural gas

Beside the employment of various industrial gases such as biomass gas, synthesis gas or water gas a direct and indirect employment of natural gas is also possible for the reduction process:

$$Fe_3O_4 + 4CH_4 \rightarrow 3Fe + 8H_2 + 4CO$$

Investigations are necessary to determine the influence of the main and subsidiary components of natural gas on the reduction process. The following oxidation process of the sponge iron with water vapour produces pure hydrogen:

$$3Fe + 4H_2O \rightarrow Fe_3O_4 + 4\ H_2$$

The applicability of sponge iron is determined by its cycle behaviour. A low tendency to sintering (for example at low temperatures) and minimal side reactions (for example carbonization and pore clogging of the Fe pellets through carbon containing gas) are the preconditions for good cyclability of the sponge iron. With not too high carbon precipitation, regeneration of the sponge iron with steam at a high temperature can provide a higher number of cycles of the sponge iron. The higher stability of methane as main component of natural gas compared to CO in the lower temperature range of 400 - 600 °C leads to lower precipitation of carbon and therefore conforms to the above-mentioned pre-conditions. The following kinetic factors can contribute to the optimisation of the reaction process and are the basis for further enquiry:
- the employment of catalysts
- raising the speed of the reaction through the conversion of the pellets into powder.

Optimation of the sintering process and further improvements in the basic material for the structural substances to maintain porosity are also undertaken.

3.2 Employment of natural gas according to the steam fission method

For an indirect employment of natural gas a conversion of the gas should be carried out according to the steam fission method (4). Synthesis gas generation from natural gas in the presence of steam is based on a coupling of exotherm and endotherm gasification reactions. A number of different processes are available for the purification of synthesis gas from the components H_2S, COS and CO_2. In the presence of catalysts, after a desulphuration process natural gas can be cracked. The gas produced contains a predominate proportion of methane which with steam at high temperature can be converted to CO and H_2 in the presence of high temperature resistant Ni catalysts. Part of the product gas is burnt with addition of air or oxygen and the gas mixture thus heated to above 1200°C. At this temperature the methane is converted down to a proportion of 0.2-0.3 vol.-% with too large a proportion of CO the desired CO/H_2 relation can be set by a partially catalysed conversion. The CO/H_2 mixture produced can be employed for reduction of the iron oxide at temperatures over 800°C. Extended conversion of CO to CO_2 through the reduction process and production of pure hydrogen through the subsequent oxidation will thus be possible.

3.3 CO-conversion

In the low temperature range from 400-600°C the employment of the gas mixture mentioned is not possible or not satisfactory because of unstable behaviour and the disproportion of CO which results in heavy precipitation of carbon and clogging of the pores of the pellets. Therefore conversion of this gas should be carried out. The sponge iron reactor can offer a favourable alternative to CO shift conversion. The conversion of this gas can be carried out with steam at 200 - 400°C with catalysts. Conversion catalysts consist of sponge iron Fe_3O_4 and Cr oxide mixtures which are used at 350-400°C. with them the CO content can be reduced to 3-4 vol.-% . In this phase the employment of the gas mixture generated and the CO residue's disturbance of the reduction process should be investigated. The gas generated will be employed for the reduction after condensation of the superfluous water. A second catalytic conversion can be introduced in the case of the cycle behaviour of the sponge iron being influenced by the CO residue. In this phase effective low temperature catalysts can be used, for example G66 from Girdler on the basis of Cu-Zn oxide, whose operating temperature is about 190-260°C. At this temperature there is a small amount of CO in the water gas equilibrium. As mentioned , completely pure production of hydrogen can be carried out through the subsequent oxidation process with steam.

(1) ÖSTAT, "Energieversorgung Österreichs: Jahresheft 1994", Österreichische Staatsdruckerei, Wien, 1994.
(2) R. Frischknecht, P. Hofstetter, I. Knoepfel, R. Dones, E. Zollinger, "Ökoinventare für Energiesysteme: Grundlagen für den ökologischen Vergleich von Energiesystemen und den Einbezug von Energiesystemen in Ökobilanzen für die Schweiz", ETHZ, PSI, Schlußbericht des BEW/NEFF-Forschungsprojektes 'Umweltbelastung der End- und Nutzenergiebereitstellung',1994.
(3) G. Mauschitz, "Emissionen von Methangas und Kohlendioxid aus der Bereitstellung und Verfeuerung fossiler Energieträger für die österreichische Brennstoffversorgung", Technische Universität Wien, 1995.
(4) K. Wissermel, H. J. Arpe, Industrielle Organische Chemie, pp. 17-30, VCH, Frankfurt, 1988.

ONBOARD FUEL REFORMERS FOR FUEL CELL VEHICLES: EQUILIBRIUM, KINETIC AND SYSTEM MODELING

Thomas G. Kreutz, Margaret M. Steinbugler, and Joan M. Ogden

Center for Energy and Environmental Studies
School of Engineering and Applies Science
Princeton University, Princeton, New Jersey 08544

Introduction

On-board reforming of liquid fuels to hydrogen for use in proton exchange membrane (PEM) fuel cell electric vehicles (FCEVs) has been the subject of numerous investigations (1-10). In many respects, liquid fuels represent a more attractive method of carrying hydrogen than compressed hydrogen itself, promising greater vehicle range, shorter refilling times, increased safety, and perhaps most importantly, utilization of the current fuel distribution infrastructure. The drawbacks of on-board reformers include their inherent complexity [for example a POX reactor includes: a fuel vaporizer, a reformer, water-gas shift reactors, a preferential oxidation (PROX) unit for CO cleanup, heat exchangers for thermal integration, sensors and controls, etc.], weight, and expense relative to compressed H_2, as well as degraded fuel cell performance due to the presence of inert gases and impurities in the reformate.

Of the numerous liquid fuel reforming strategies, steam reforming of methanol (SRM) has long been considered a top contender for on-board generation of hydrogen. An alternative that has received recent attention is partial oxidation (POX) of automotive fuels such as gasoline and diesel fuel. POX has a number of important advantages over SRM:

- it typically involves a shorter startup time and has better transient behavior,
- it is potentially lighter weight and less expensive,
- POX reformers potentially have the capability to reform many different fuels, e.g. gasoline, diesel fuel, ethanol, methanol, various blends, etc.,
- gasoline and diesel fuel have roughly twice the volumetric energy density of methanol,
- reforming automotive fuels avoids complex fuel distribution infrastructure issues.

However, gasoline POX also suffers from some disadvantages with respect to SRM:

- N_2-diluted POX reformate results in lower fuel cell performance relative to SRM reformate,
- hydrogen in the fuel cell anode exhaust is not readily integrated in a POX system,
- both catalyzed and uncatalyzed POX systems are exothermic and involve significantly higher temperatures; thus, they may be subject to greater thermal losses,
- automotive fuels are ever-changing distillate blends and contain contaminants such as sulfur which must be removed by the fuel processor.

Both approaches are being vigorously pursued by a number of different groups (3-10).

In this work, we have analyzed POX fuel reformers in detail, and have further integrated these results into a FCEV model that compares the fuel economy of FCEVs powered by on-board POX and SRM fuel processors with the fuel economy of a direct hydrogen vehicle. In the first portion of the study, partial oxidation of a number of different fuels has been examined from a fundamental viewpoint using both equilibrium calculations and detailed kinetic modeling with complex chemical reaction mechanisms. The effects upon reformer conversion efficiency of temperature, pressure, stoichiometry, water addition, reactant preheating, and residence time have been examined in detail. In the second portion of the study, the results have been integrated into a FCEV model that enables us to predict fuel economy for different types of vehicles under varied driving schedules. This latter work provides a point of comparison with a recent study from Directed Technologies (11) of estimated FCEV performance when using compressed H_2 storage versus on-board reforming of liquid fuels which indicated that the former approach might yield twice the fuel economy of the latter.

Results of Equilibrium and Kinetic POX Modeling

Some results of our modeling are summarized here. Reformer temperature is critical to the efficiency of converting hydrocarbon fuels to $CO+H_2$, from both equilibrium and kinetic standpoints. Above ~800 C, the conversion efficiency (defined here as the moles of $CO+H_2$ produced divided by the maximum possible moles of $CO+H_2$, which for POX is equal to the number of moles of C plus one half of the moles of H) at equilibrium is essentially unity and temperature independent; below this temperature, the conversion efficiency falls dramatically. In an uncatalyzed POX reactor, the time required for near-equilibrium conversion decreases exponentially with increasing temperature at a rate of roughly an order of magnitude per 100 C. Increasing the reformer pressure has only a weak effect on the equilibrium conversion efficiency, but dramatically increases the rate of soot production. Reactant stoichiometry plays a critical role in the conversion efficiency, which rises with increasing equivalence ratio (i.e. decreasing O_2) to unity at an optimal value, Φ_{opt}, where there is just enough oxygen to oxidize the carbon in the fuel to CO. Above this value, the conversion efficiency falls as equilibrium carbon is formed instead of CO. The time required for near-equilibrium conversion is also found to peak sharply at Φ_{opt}. In practice, the maximum conversion efficiency is limited by soot formation which typically occurs at an equivalence ratio, Φ_{max}^{soot}, that is often substantially below Φ_{opt}. Similar to the presence of excess water in a steam reformer, water addition to a POX reactor is sometimes found to push up the sooting limit to higher equivalence ratios and thus enable higher conversion efficiencies (1,12). The downside of this practice is the energetic cost of raising steam. Reactant preheating is also a key consideration in these fuel rich systems where the chemical heat release alone is usually too small to yield sufficient reaction temperatures. Effective preheating of cold reactants by hot products is particularly important in uncatalyzed POX reactors where temperatures need to be as high as 1600 C for good conversion efficiency of 'refractory' fuels such as methane (9). Accurate calculation of sooting limits is beyond the present state-of-the-art, even for the simplest of hydrocarbon fuels. Nevertheless, empirical sooting limits and maximum conversion efficiencies have been measured for most fuels of interest. Typical results are given in Table I.

Table I. Optimal (dry) and maximum practical equivalence ratios for POX reactors, and measured maximum conversion efficiency and energy efficiency [defined as the heating value (HV) of the post-shift H_2 divided by the HV of the fuel) given both on a lower heating value basis (i.e. LHV H_2/LHV fuel) and a higher heating value basis (HHV H_2/HHV fuel).

Fuel (refs.)	Φ_{opt} (dry)	~Φ_{max}^{soot}	Conversion Efficiency	Energy Efficiency (LHV/HHV)
Gasoline (1-2,12)	2.9	3.5	0.97	0.78/0.87
Diesel fuel/JP7 (9)	2.9	2.9	0.88	0.67/0.74
Methane (9)	4	2.9	0.83	0.75/0.80
Ethanol (4,5)	6	4.3	0.82	0.80/0.86

Vehicle Fuel Efficiency Modeling

The results of the reformer analysis were integrated with a fuel cell electric vehicle model in order to assess the effect of reformer efficiency, reformer weight, and reformate quality upon the fuel economy of the vehicle. The model, recently developed by Steinbugler (13), determines the power required for a given vehicle to cover an arbitrary driving cycle. It determines the size and weight of the fuel cell, fuel storage, and peaking device (if included) necessary to achieve a given performance specification. For this preliminary analysis, we have chosen parameters corresponding to a midsize vehicle having 1) a traditional steel chassis (Ford Taurus; 1050 kg glider weight) , or 2) a lightweight body (aluminum-intensive Sable; 750 kg glider weight). The weight of two passengers (136 kg) was also included. A fairly high power-to-weight ratio (~0.06 kW/kg) was required to obtain performance comparable to contemporary automobiles, in particular the ability to accelerate 3 mph per second at 65 mph. City and highway driving were modeled using

the federal urban and federal highway driving schedules (FUDS and FHDS, respectively). A peaking device, which can significantly alter the vehicle design and performance, was not employed in this initial analysis but is actively being studied.

The vehicle model was used to compare FCEV performance using 1) direct (compressed) hydrogen, 2) methanol steam reforming, and 3) gasoline/diesel POX. The reformers and fuel cell (both anode and cathode) were operated at 3 atm and a cathode stoichiometry of 2.0. The fuel cell polarization curve (14) was modified using the calculated anode overpotentials of Gottesfeld (15) to account for the effects of hydrogen dilution by CO_2 and N_2. These effects are significantly larger than simple Nernst corrections, particularly at high current densities where mass transport effects are important. For example, at 1 A/cm^2, the fuel cell potential drops by an estimated 9.4% on SRM reformate and 20% on POX reformate. It was assumed that loss of fuel cell performance due to the presence of CO_2 could be prevented by the addition of a small amount (~2%) of air to the reformate (7). In the direct H_2 system, the weight of the hydrogen storage (7.5% H_2 by weight) was chosen as 50 kg, corresponding to a range of 200-300 miles. The specific power of the ADL POX reformer (4), 0.6 kW_e/kg, is roughly equal to projections by General Motors (6) for SRM. Therefore, both processors are assumed to have the same weight, calculated by scaling up 0.6 kW_e/kg to obtain the required power and adding 15 gal of fuel. With a steel chassis, the vehicle requires a 150 kW_e, 320 kg fuel processor/storage system; only 130 kW_e, 270 kg are needed by the aluminum-intensive vehicle. It is assumed that the reformers can follow the load with an efficiency that is load-independent; furthermore, the shift reactors are assumed to convert all CO to H_2 and CO_2. The energy efficiency of the fuel processors, defined as the HV of H_2 used by the fuel cell divided by the HV of the incoming fuel, is taken to be 0.76/0.79 (LHV basis/HHV basis) for SRM (10) and 0.71/0.78 for gasoline POX (12). In the highly endothermic SRM process, the system efficiency is only weakly dependent on fuel cell utilization (80%) because the anode exhaust is profitably used as fuel in the steam reformer burner. In the exothermic POX process, however, the assumed 90% H_2 utilization directly yields a 10% reduction in system efficiency because the anode exhaust, while useful for vaporizing fuel, for example, should not significantly increase the efficiency of a POX reformer having good thermal integration.

Table II. Preliminary estimates of fuel economy, in miles per equivalent gallon of gasoline (MPEG) for combinations of glider weight, hydrogen source, and driving cycle.

Glider Weight (kg)	H_2 Generation / Storage System	Curb Weight of Vehicle (kg)	Peak Power (kW_e)	FUDS MPEG (LHV/HHV)	FHDS MPEG (LHV/HHV)
750	Direct H_2	1553	105	63.0/59.0	74.8/70.0
	Methanol SR	1934	126	40.8/39.6	51.2/49.8
	Gasoline POX	1989	129	36.6/36.6	46.9/46.9
1050	Direct H_2	2023	131	51.5/48.2	65.6/61.4
	Methanol SR	2485	156	33.2/32.3	44.4/43.2
	Gasoline POX	2560	160	29.9/29.9	40.8/40.8

Results of the preliminary vehicle modeling are shown in Table II where the total vehicle curb weight, peak power, and the estimated fuel economy were calculated for each combination of glider weight, hydrogen source, and driving schedule. A large disparity in fuel economy can be seen between the direct H_2 and reformer systems. It is caused first by reformer efficiency; roughly 20-25% of the energy of the fuel is lost in reformation. Second, the reformers add significantly (21-22%) to the final curb weight of the vehicle, further reducing the fuel economy by 14% on FUDS (10% on FHDS). Third, the POX system loses 10% of the H_2 in the anode exhaust. Finally, poor reformate quality penalizes the SRM system by ~2% on FUDS (~1% on FHDS), and twice that for the POX system. Note that this last effect can be significantly exacerbated during more aggressive driving cycles that require higher average and peak power from the fuel cell.

Conclusions

Our preliminary estimates of FCEV fuel economy are consistent with the Directed Technologies' assessment (11), indicating that FCEVs with on-board gasoline POX and methanol steam reformers have significantly lower fuel economy than vehicles using compressed H_2 storage. This loss of efficiency may be the cost of enabling FCEVs to achieve modest near-term market penetration without requiring significant changes in the transportation fuel distribution infrastructure. It must be emphasized that there are large uncertainties in many of the parameters used in this initial analysis. Nevertheless, the basic trends are not likely to change significantly as the modeling becomes more refined or the parameters more tightly determined, particularly if they are based on current technology. The results clearly indicate areas where technological advances will have the largest impact, for example, increasing the efficiency and decreasing the weight of the fuel processor. Future work will examine the effect of peaking devices as well as economic considerations.

References

1. J. Houseman and D. J. Cerini, "On-Board Hydrogen Generator for a Partial Hydrogen Injection Internal Combustion Engine", SAE Paper No. 740600, The Society of Automotive Engineers, 1974.
2. J. Houseman and D. J. Cerini, "On-Board Hydrogen Generation for Automobiles", Proceedings of the Eleventh Intersociety Energy Conversion Engineering Conference, 769001, Stateline, Nevada, 1976.
3. "Multi-Fuel Reformers for Fuel Cells Used in Transportation", U.S. Department of Energy Report No. DOE/CH/50343-2, Arthur D. Little, Inc., Cambridge, MA, 1994.
4. W. L. Mitchell, J. H. J. Thijssen, J. M. Bentley, and N. J. Marek, "Development of a Catalytic Partial Oxidation Ethanol Reformer for Fuel Cell Applications", SAE Paper No. 952761, The Society of Automotive Engineers, 1995.
5. W. L. Mitchell, "Development of a Partial Oxidation Reformer for Liquid Fuels", presented at the Society of Automotive Engineers TOPTEC: Fuel Cells for Transportation, Alexandria, VA, April 2-4, 1996.
6. "Initial Conceptual Design Report", U.S. Department of Energy Report No. DOE/CH/10435-01, Allison Gas Turbine Division, General Motors Corporation, 1993.
7. "Research and Development of Proton-Exchange-Membrane (PEM) Fuel Cell System for Transportation Applications", U.S. Department of Energy Report No. DOE/CH/10435-02, Allison Gas Turbine Division, General Motors Corporation, 1996.
8. R. Kumar and S. Ahmed, "Fuels Processing for Transportation Fuel Cell Systems", Argonne National Laboratory Report No. ANL/CMT/CP--84932, presented at the First International Symposium on New Materials for Fuel Cell Systems, Montreal, Canada, July 9-13, 1995.
9. D. Moard and B. Bhatt, Hydrogen Burner Technology, Inc., personal communication, February, 1996.
10. S. Kartha and S. Fischer, "Analysis of On-board Fuel Processing Designs for PEM Fuel Cell Vehicles", presented at the 1996 Fuel Cell Seminar, Kissimmee, FL, November 17-20, 1996.
11. C. E. Thomas, "Overview of Onboard Liquid Fuel Storage and Reformation Systems", presented at the Society of Automotive Engineers TOPTEC: Fuel Cells for Transportation, Alexandria, VA, April 2-4, 1996.
12. Ryan Katofsky, Arthur D. Little, Inc., personal communication, August, 1996.
13. M. M. Steinbugler, "How Far, How Fast, How Much Fuel: Evaluating Fuel Cell Vehicle Configurations," presented at the Commercializing Fuel Cell Vehicles Conference, Chicago, IL, September 17-19, 1996.
14. S. Srinivansan, A. C. Ferreira, M. Wakizo, J. Kim, A. J. Appleby, J. McBreen, "Methods to Attain High Energy Efficiencies and Long Lifetimes in Polymer Acid Fuel Cells", Final Report to NASA Lewis Research Center, NASA Lewis Grant No. NAG3-1225, July, 1993.
15. S. Gottesfeld, Los Alamos National Laboratory, personal communication, August, 1996.

ANALYSIS OF ON-BOARD FUEL PROCESSING DESIGNS FOR PEM FUEL CELL VEHICLES

S.Kartha, S.Fischer, and T.Kreutz
Center for Energy and Environmental Studies
School of Engineering and Applied Science
Princeton University, Princeton, NJ 084544

As a liquid fuel with weight and volume energy densities comparable to those of gasoline, methanol is an attractive energy carrier for mobile power systems. It is available without contaminants such as sulfur, and can be easily reformed at relatively low temperatures with inexpensive catalysts. This study is concerned with comparing the net efficiencies of PEM fuel cell vehicles fueled with methanol and hydrogen, using fuel cell system models developed using ASPEN (1) chemical process simulation software. For both the methanol and hydrogen systems, base case designs are developed and several variations are considered that differ with respect to the degree of system integration for recovery of heat and compressive work. The methanol systems are based on steam reforming with the water-gas shift reaction and preferential oxidation, and the hydrogen systems are based on compressed hydrogen. This analysis is an exercise in optimizing the system design for each fuel, which ultimately entails balancing system efficiency against a host of other considerations, including system complexity, performance, cost, reliability, weight and volume.

HYDROGEN SYSTEMS: For each fuel, we considered a "no frills" base case upon which we made incremental changes to help illuminate the point at which marginal efficiency improvements might not justify the added design complexity. This preliminary analysis considers only steady-state operation for a nominal 50 kW net fuel cell output, accounting for the main parasitic loads (i.e. compressive requirements) but not for other loads (e.g., pumping, power conditioning etc) that can be expected to be constant across all the cases considered here. In the case of hydrogen-fueled FCVs, the base case consisted of a simple system in which tanked hydrogen was stored at 5000 psi, and the fuel cell was operated(2) at 0.6 V at a temperature of 90°C, and the anode and cathode feeds were pressurized to 3 atmospheres with a pressure drop across the stack of 5 psi. The cathode stoichiometry was taken to be 2:1. The adiabatic efficiency of compressors and expanders was taken to be 75%.

As shown in Table 1, the base case included a single stage compressor for the air supply to the cathode, and included no recovery of compressive work from either the fuel cell exhaust or the high-pressure hydrogen, yielding a net system efficiency (defined as electrical power out relative to higher heating value of fuel supplied) of 32.6%. Case A upgrades the air compressor to a 2-stage compressor with intercooling to ambient temperature. The improvement in efficiency is a nominal 0.5%, notwithstanding the relatively significant increase in cost and complexity associated with an intercooled two stage compressor. Case B includes expansion of the fuel cell cathode exhaust (after condensation of water vapor) from 3 atm to 1 atm, allowing the recovery of roughly 40% of the mechanical work embodied in the compressed stream and a system efficiency gain of almost 3%. Case C upgrades the exhaust expander to a 2-stage expander with a reheat using fuel cell waste heat, but yields only a marginal improvement over the single stage expander. Cases D, E, and F consider increasing degrees of recovery from the compressed hydrogen, considering single stage expansion from 5000 psi, single stage expansion from 8000 psi, and 2-stage expansion from 5000 psi respectively, with efficiency improvement increasing from 1.5% to 1.7% to 2.2%. While storage at 8000 psi might be attractive from the standpoint of improved vehicle range, there is no incentive from the standpoint of vehicle efficiency, since the minor improvment in recovery of compressive work is more than offset by additional compressive requirements at the refilling station. The minor benefit derived from using a 2-stage expander is unlikely to be justified by the difficulty of providing safe on-board high pressure heat exchangers for reheating the hydrogen stream between expansion stages.

This analysis suggests that there is incentive for considering a single stage expanders for the

cathode exhaust and perhaps for the compressed hydrogen in light of the efficiency gains, but that double stage expanders or higher hydrogen storage pressures are probably not indicated in view of added system complexity.

Table 1. Effect of design variations on net system efficiency of 50 kW hydrogen FCV.

	air compression	exhaust expansion	hydrogen expansion	net efficiency
base case	+8.6 kW 1-stage	-0.0 kW (no recovery)	-0.0 kW (no recovery)	32.6 %
A	+8.0 kW 2-stage	*	*	+0.5 %
B	*	-3.7 kW 1-stage	*	+2.9 %
C	*	-3.9 kW 2-stage	*	+3.1 %
D	*	*	-1.9 kW 5000 psi, 1-stage	+1.5 %
E	*	*	-2.1 kW 8000 psi, 1-stage	+1.7 %
F	*	*	-2.8 kW 5000 psi, 2-stage	+2.2 %

* same value as in base case.

METHANOL SYSTEMS: The base case for the methanol-fueled FCVs consists of a steam reformer operating at 260°C and 3 atm using Cu-Zn catalysts, with a steam to carbon ratio of 1.5:1, generating a total yield of 2.87 moles of hydrogen for each mole of methanol(3). The fuel cell is conservatively assumed to operate economically at no greater than 78% utilization, with a voltage penalty due to reformate dilution of 3%(4). This also assumes that CO is reduced to tolerable ppm levels by addition of 2% oxygen in a preferential oxidation stage following reforming reactions and the water-gas shift reactions.

In such a system, fuel processing constitutes a significant heat load, roughly 12 kW_{th} for the reforming reactions and 27 kW_{th} for the evaporation and preheat of the methanol/water mixture, so the degree of thermal integration will dramatically affect overall system efficiency. In the cases considered, the efficiency of heat exchangers was assumed to be 87%. As displayed in Table 2, the base case assumes that hydrogen remaining in the anode exhaust is combusted to provide heat for the evaporator and reformer, but that no compressive work is recovered in an expander. In order to provide sufficient heat, the hydrogen utilization is set at 64%. In case A, a combustor and turbo expander (operating at an inlet temperature of 1100 K) recover compressive work from the anode and cathode exhaust streams, satisfying the compressive requirements of the air stream and providing additional power. Because energy in the exhaust is converted to mechanical work in the expander, less remains for providing heat to other processes and the utilization must be reduced to

59% in order to meet heat requirements. The net affect is a 7.0% improvement in system efficiency, despite the decreasing hydrogen utilization. In case B, the fuel utilization is set at the maximum value of 78%, and methanol is burned directly to supply heat. The anode exhaust is then combusted without supplying heat to other processes and expanded through a higher temperature turbo expander (≈1400 K). This yields an additional 2.8% efficiency gain over case A. Case C attempts to exploit the turbo expander further, recompressing the exhaust streams to 5.5 atm before combusting in order to produce more power, but yields only an additional 0.9% efficiency gain.

Modelling of the methanol-fueled systems suggests that recovery of compressive power from the fuel cell exhaust is likely to be desireable, and that the expander technology (inlet temperatures, size, cost, efficiency etc) may determine the optimal operating point with respect to apportioning the energy in anode exhaust for heat vs power.

Table 2. Net system efficiencies for base case and variations of 50 kW methanol FCV.

	fuel cell power	air compression	exhaust expansion	fuel consumed	net efficiency
base case	61.8 kW	-11.8 kW	0.0 kW	219.7 kW	22.8%
A turbo-expander	44.0 kW	-7.3 kW	13.3 kW	167.6 kW	+7.0%
B methanol combustor, high-temp turbo-expander	42.2 kW	-7.0 kW	14.8 kW	153.2 kW	+9.8%
C methanol combustor, recompression, high-temp turbo-expander	38.2 kW	-11.4 kW	23.2 kW	149.2 kW	+10.7 %

To compare the efficiencies of the hydrogen and methanol systems we take cases that are likely to approximate the optimal designs. For hydrogen, this might be the 37% efficient system with single stage expansion of fuel cell exhaust and compressed hydrogen. For methanol, a compromise might be struck between methanol-fueled systems A and B (which would satisfy heat requirements with combustion of anode exhaust in addition to some methanol, with the relative amounts determined in part by performace of expander technologies) that would have an efficiency of roughly 31%. The methanol-fueled system then has an efficiency relative to the hydrogen system of 84%. (As far as the full fuel cycle, this difference is widened by the lower efficiency with which natural gas or biomass is converted to methanol compared to hydrogen, roughly 92% in relative terms including hydrogen compression at the refilling station(5).) On the other hand, there are the obvious benefits of a less dramatic change in fuel infrastructure required by methanol compared to hydrogen.

1. The simulations were carried out using Aspen Plus, a software package for simulating chemical and industrial processes .

2. This is consistent with typical figures in the literature, for example, James, Brian D., George N. Baum, and Ira Kuhn, "Technology Development Goals for Automotive Fuel Cell Power Systems." Final Report, Contract No. 22822402, 1994, Argonne National Laboratory.

3. This is consistent with typical figures in the literature, for example, Arthur D. Little, "Multi-Fuel Reformers for Fuel Cells Used in Transportation." Final Report, 1994, USDoE, Office of Transportation Technologies.

4. Weisbrod, K. and N. Vanderborgh, "Effect of perating Parameters and Anode Gas Impurities Upon Polymer Electrolyte Fuel Cells." 29th IECEC, 1994, American Institute of Aeronautics and Astronautics. also, personal communication, S. Gottesfeld, Los Alamos National Laboratory, 1996.

5. Derived from R. Williams, E. Larson, R. Katofsky, and J. Chen, "Methanol and Hydrogen from biomass for Transportation" Energy for Sustainable Development, January, 1995.

DEMONSTRATION TEST OF A REFORMER EMPLOYING THERMAL RADIATION MEDIA FOR MULTI-MEGAWATT FUEL CELL APPLICATIONS

Y. Morita*, M. Ogawa**, T. Horie*, Y. Mizumoto***
* Chiyoda Corporation, Yokohama 230 Japan
** Kansai Electric Power Co., Amagasaki 661 Japan
*** Mitsubishi Electric Corp., Kobe 652 Japan

Introduction

The authors made presentation of functions and roles of the thermal radiation media[1], extensive test results on the thermal radiation media sample[2] and characteristics of an atmospheric 500kw PAFC model facility together with perspective to a 5MW class dispersed-use plant[3].
This paper outlines the specifications and features of a prototype reformer having a capacity of 650kw class PAFC and configuration of atmospheric 500kw PAFC demonstration plant.

Prototype Reformer

A prototype reformer employing the thermal radiation media having a capacity of 673Nm³/H Hydogen production equivalent to a 650kw class PAFC has been manufactured. Table-1 and Figure-1 illustrate its specifications and configuration respectively.
This prototype is characterized by the following functional and structural features.

1) It is equipped with five bayonet type catalyst tubes each of which is composed of an outer tube of 88 OD and an inner tube of 150ϕ OD having an effective length of 2.8m respectively, and loaded with reforming catalysts of 5ϕ for the upper part and 8ϕ for the lower part. Such specifications of the catalyst tube and catalyst should be kept identical in the scale-up to a multi-megawatt reformer.
2) Within the shell, three kinds of the thermal radiation media are arranged so as to envelop each of the catalyst tubes aimed at enhancement of heat transfer, suppression of wall ratiation effects and prevention of uneven flow of the flue gas.
3) Three kinds of fluid, i.e., the process feed, the reformed gas and the flue gas are sealed one another in

three manifolds, resulting in low pressure drop both in the process and flue gas sides.

4) Outer catalyst tubes and catalysts are supported by a double-tubesheet composing a part of the process feed manifold and inner catalyst tubes are supported by the outer tube wall, and all the internals except heat transfer enhancement members within the shell are supported by a conical plate being welded to the shell wall, thereby preventing thermal distortion of every hot part.
5) Except for the connecting part to burner and reformed gas manifold, major parts of hot insulation are composed of ceramic fibre module having lower density and heat capacity than castables aimed at a short heating up time of less than four hours.
6) Burner is of horizontal short flame type having a dual tip, one for AEXG (anode exhaust gas) in the normal operation, another for the natural gas in the start-up operation.
   Combustion air and AEXG are sufficiently swirled and mixed to reach complete combustion within a short flame length under the NO_x emission level of not greater than 10ppm.

Demonstration Plant

An atmospheric 500kw PAFC demonstration plant incorporating the prototype reformer has been constructed.
Figure-2 shows the flow scheme and major operating conditions for the rated 500kw (DC) case.
This plant is principally to verify the performance of the cell stack and reformer through extensive test operation.
Such test results shall be presented in the poster session.

References

1) Y.Morita et al:2nd FCDIC FC Symp., May 1995, Tokyo, Japan
2) Y.Morita et al:2nd IFCC, Feb. 1996, Kobe, Japan
3) M.Ogawa et al:3rd FCDIC FC Symp., June 1996, Tokyo, Japan

TABLE-1 Major Specifications of Prototype Reformer

Capacity	H_2 Production	673 Nm^3/H
Operating Conditions	Temperature	: 775 °C
	Pressure	: 0.27 kg/cm^2G
	Steam to Carbon Ratio	: 2.5
Pressure Drop	Process Side	: 0.65 kg/cm^2
	Flue gas Side	: 700 mmH_2O
Design Temperature	Catalyst Tube	: 1,100 °C
	Inner Tube	: 850 °C
	Process Feed Manifold	: 600 °C
Design Pressure	Process Side	: 0.99 kg/cm^2G
Material	Catalyst Tube	: 25Cr-35Ni-Nb-Ti
Thermal Radiation Media	: Ceramic Foam + Wire Mesh Stack	
Catalyst	: 5Ø (Upper 0.95 m) + 8Ø (Lower 1.9 m)	
Burner	Horizontal Short Flame Type	
	Heat Release	: 486 Mcal/H
	Fuel Gas	: Anode Exhaust Gas (Normal) Natural Gas (Start up)
	Air Ratio	: 1.4 - 2.0
	Combustion Temp.	: 1,300 - 1,470 °C
	NOx	: Not greater than 10 ppm @ O_2 7%

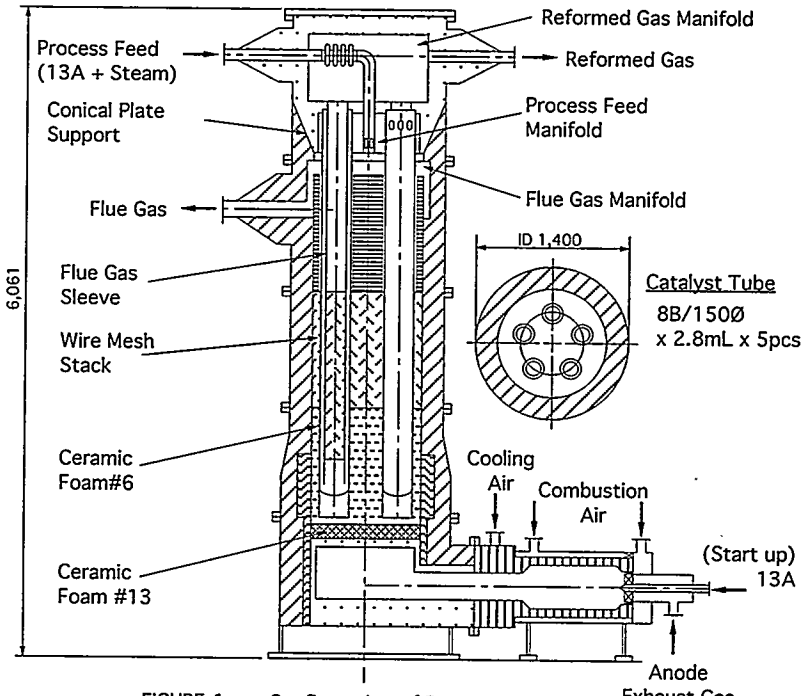

FIGURE-1 Configuration of Prototype Reformer for 650 kw Class PAFC

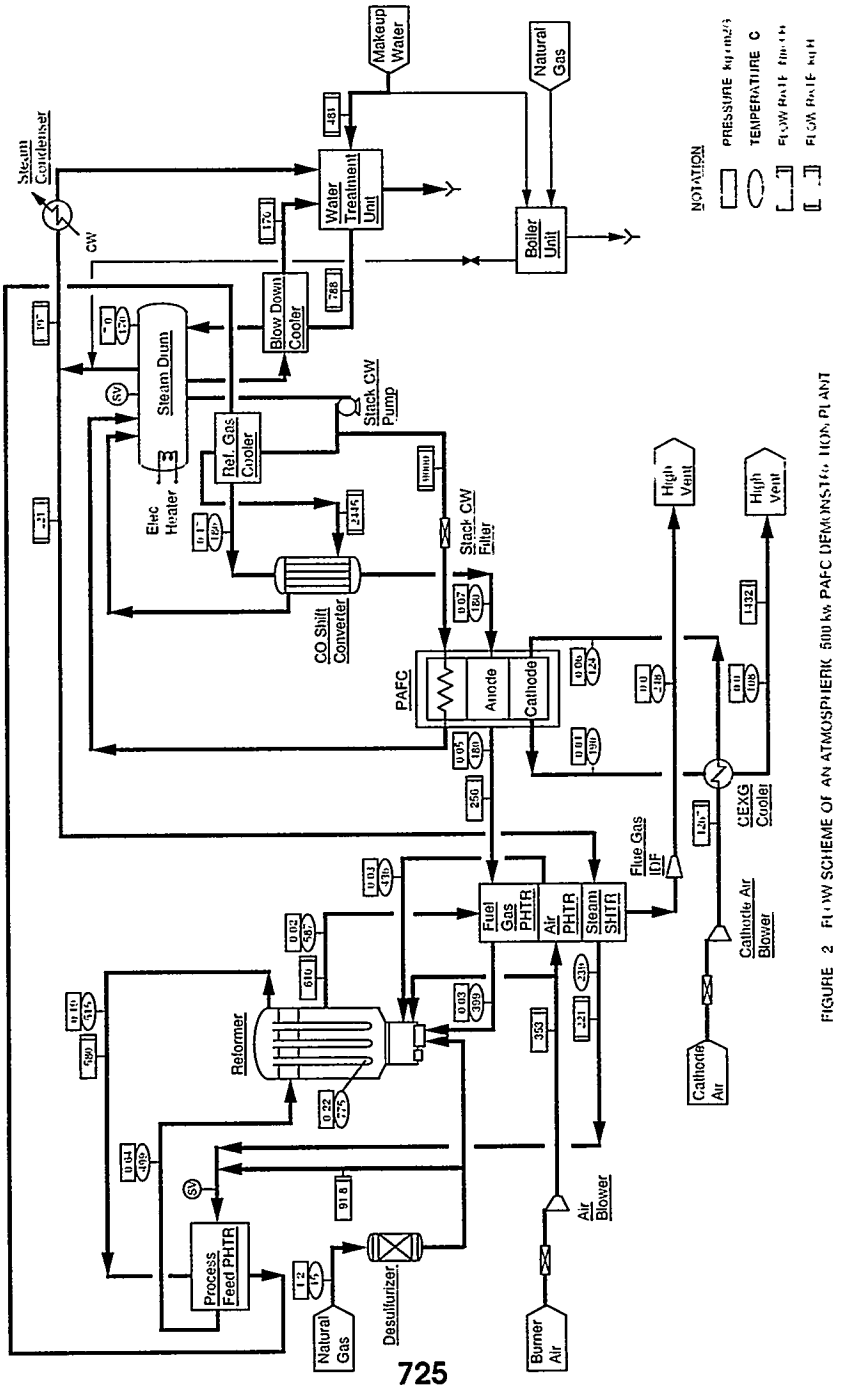

FIGURE 2 FLOW SCHEME OF AN ATMOSPHERIC 500 kW PAFC DEMONSTRATION PLANT

DEVELOPMENT AND LIFE EVALUATION OF A STEAM REFORMING PROCESS FOR PAFC

S. Nagase, S. Takami, M. Masuda, N. Shinke and N. Iwasa
Osaka Gas Co. Ltd.,Osaka, Japan

ABSTRACT

This paper reports a life evaluation method for a CO shift process in the steam reforming process for PAFC. A CO shift reactor simulation was developed to evaluate the whole performance of the CO shift process. The calculation results of the simulation almost coincide with the experimental data obtained from a demonstration plant. By evaluating and grasping the sintering trend of the catalyst, and by simulation calculation of the reactor, it became possible to evaluate the performance at targetted operation hours.

INTRODUCTION

A steam reforming process is one of the important composing elements of PAFC. It is desired that the process should become more compact and can supply hydrogen stably to cells for long periods (for example 40,000 hours) without exchanging catalysts. To meets these requirements, we have been developing an advanced steam reforming process for PAFC (1)(2).

Up to the present, the performance and the durability of the steam reforming process for more than twenty thousand hours have been confirmed by field monitor tests at 50 kW demonstration plants. Figure 1 shows the CH_4 concentration at the steam reformer outlet and CO concentration at the CO shift reactor outlet of the 50 kW plant. The CH_4 concentration is held at 1% or less even after 20,000 hours. The CO concentration is steadily maintained the desired value of 1.0% or less even after 20,000 hours. However, an evaluation of the catalyst for longer periods is necessary for practical use of PAFC.

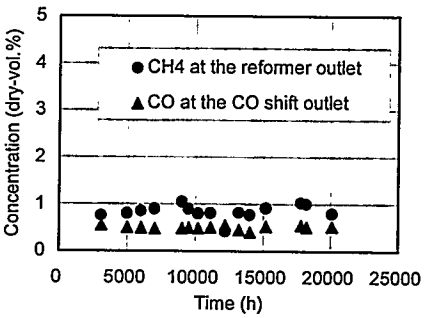

Figure 1. Performance of a demonstration plant

As for the desulfurization process, we have already established to evaluate the life and to design the method and confirmed the required amount of desulfurization catalyst (2). This time we investigated a life evaluation method of the CO shift process which largely depends on the activity of catalyst and is essential to make a compact steam reforming process.

LIFE EVALUATION OF THE CO SHIFT CATALYST

It is said that chlorine poisoning, sulfur poisoning and sintering by heat are major factors of deactivation in a Cu-Zn type CO shift catalyst (3). Chlorine poisoning is excluded, because this process gas is not contaminated with chlorine. With our unique high performance desulfurization process, the steam reforming catalyst is not subjected to sulfur poisoning. Since the CO shift process is a downstream of the steam reforming process, it is almost unnecessary to consider sulfur poisoning of CO shift catalyst.

Accordingly, only sintering has to be taken into consideration as a main factor of deactivation. Thus it is important to accurately evaluate the elapsed time changes in the sintering level and the level of sintering required to satisfy the necessary performance of the

process.

Elapsed time changes in sintering level

In general, it is known that the activity of the CO shift corresponds to the surface area of Cu metal (4). Therefore the surface area of Cu is used as an index of sintering level.

Figure 2 shows the analysis results of surface area of Cu on the CO shift catalyst extracted from 50 kW PAFC demonstration plants. The surface area of active metal on the catalyst generally decreases largely in the initial phase, and then decreases gradually. If this tendency could be analyzed precisely, a sintering level after a target operation period can be estimated by extrapolating this tendency to extended operation hours.

The decrease in the surface area of the active metal on a catalyst can be expressed in the form of an equation

$$\frac{dS}{dt} = -kS^n \quad (S\ ;\ \text{active metal surface area, } k\ ;\ \text{rate constant})$$

This equation is transformed into

$$\ln S = -kt + \ln S_0 \qquad (n=1)$$

$$\frac{1}{S^{n-1}} = \frac{k}{n-1} \cdot t + \frac{1}{S_0{}^{n-1}} \qquad (n \neq 1)$$

Applying this equation to the analysis results of the used catalysts, this equation is best fitted to the results in case of n=1. This regressed linear line (n=1) is shown in figure 2. By extrapolating this line to extended operation hours based on the analysis results of the catalysts used in demonstration plants, the sintering level in operation time can be estimated.

By the catalytic activity test of the CO shift catalyst in the estimated sintering level, the life evaluation is possible. However, it is necessary to consider the following points when the whole performance of the CO shift process is evaluated.

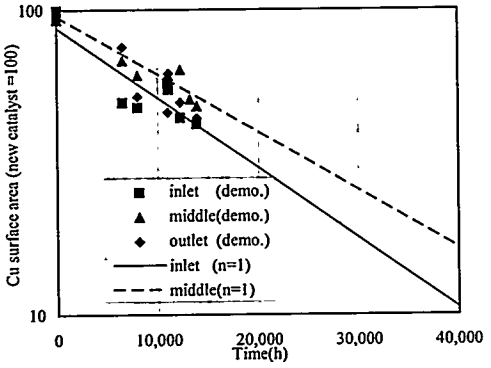

Figure 2. Elapsed time changes in surface area of Cu on CO shift catalyst

Performance evaluation of the process

The CO shift reaction ($CO + H_2O \rightarrow CO_2 + H_2$) is an exothermic reaction and low temperature is advantageous in chemical equilibrium. On the other hand, high temperature is advantageous in reaction rate. Consequently, a trade-off relation must be considered between reaction rate constant and chemical equilibrium in regard to the reaction temperature in CO shift reaction.

Cooling coils are equipped with our CO shift reactor and cooling water flows inside the coils. This cooling water removes the reaction heat of the CO shift reaction and also decreases the reaction temperature towards the exit, which is favorable for the point of chemical

equilibrium. As the result, a temperature distribution is determined by a delicate affair between reaction heat and cooling in the CO shift reactor.

Because of the above mentioned reason, it is difficult to make a simple estimate of the performance of the CO shift process and also difficult to reproduce this temperature distribution by a labo-scale experiment. The help of a reactor simulation is necessary to evaluate the process performance.

Reactor simulation

There exist complex radial and axial temperature distributions by reaction heat and cooling water in the CO shift reactor. Moreover, radial and axial concentration distributions of gas components occur. Therefore, we need two-dimensional simulation model taking radial and axial distributions into account.

A calculation of the amount of the reacted CO can be expressed in the form of an equation

$$-\Delta[CO]=k(T)\cdot catv\cdot([CO][H_2O]-[CO_2][H_2]/Kp)$$

k(T) ; reaction rate constant, catv ; catalyst volume
Kp ; equilibrium constant

As regards a calculation of heat balance, the following conditions are assumed.

- It is steady state.
- Flow direction of fluid is only axial direction.
- Flow rate is uniform in the whole reactor.
- Heat conductivity of axial direction can be ignored.
- Heat of reaction exists.

On the assumption, the calculation of heat balance can be expressed in the form of an equation

$$\frac{\partial T}{\partial z}=\frac{k}{\rho c}\cdot\frac{1}{v_z}\left[\frac{1}{r}\cdot\frac{\partial T}{\partial r}+\frac{\partial^2 T}{\partial r^2}\right]+\frac{\delta q}{\rho c}\cdot\frac{1}{v_z}$$

T ; temperature z ; length along axis k ; heat conductivity
ρ ; density of gas c ; specific heat at constant pressure
v_z ; flow rate r ; radius δq ; heat of reaction

By solving this differential equation, temperature distribution is calculated.

Figure 3 shows the results of the simulation of temperature and CO concentration distributions. The vertical axis shows the direction of gas flow. The horizontal axis shows the radius of the reactor. At the entry section of the reactor, temperature rises by the reaction heat and thereafter temperature decreases gradually by cooling. Temperature at center is highest as regards distribution of radius direction. On the other hand temperature near cooling coil are low. The CO concentration decreases greatly at the entry section and thereafter decreases slowly.

To verify the simulation, detailed data were obtained from actual plants. Figure 4 shows the result of simulation and a part of detailed data from an actual plant. The temperature profile of simulation almost coincides with the actual data. The CO concentration at the outlet of the actual plant was 0.90%, and was nearly equal to the calculated value obtained 0.95%. Hence, it is proved that the calculated result by simulation agreed with the actual data, and that the performance of CO shift process can be predicted by using this reactor simulation.

Since sintering level at the targetted operation hours could be evaluated, it is now possible to evaluate the process performance by making simulation calculation using the reaction rate constant of the catalyst at that sintering level.

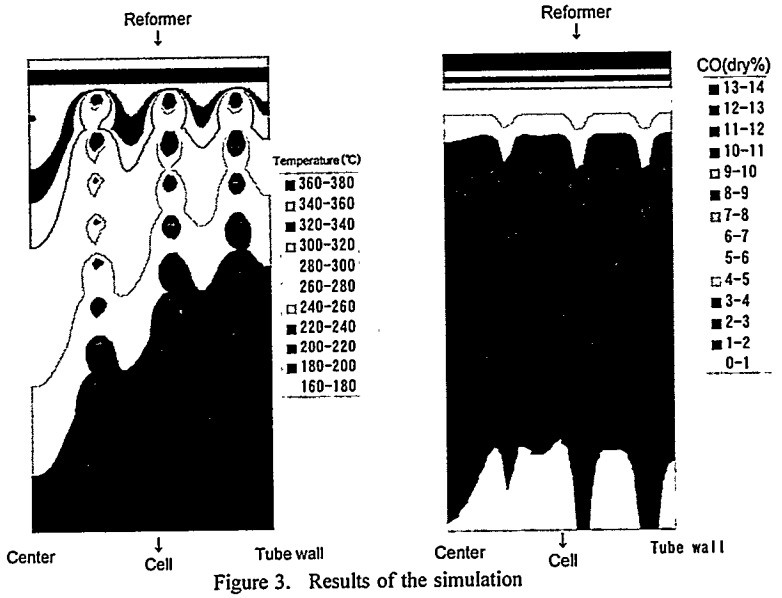

Figure 3. Results of the simulation

SUMMARY

From the analysis results of the catalysts used in demonstration plants, the trend of the sintering level was estimated. By calculating the reaction rate constant at that sintering level using developed simulation method, it became possible to evaluate the performance of the CO shift process at targetted operation hours.

At present, studies are being carried out for accurate estimating of the sintering level. It is believed that further reliability in life evaluation will become possible.

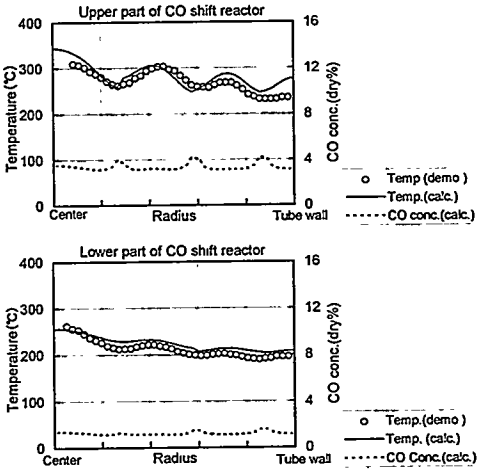

Figure 4. Comparison of the simulation results with the experimental data

REFERENCE

1) O. Okada, T. Tabata, S. Takami, K. Hirao, M. Masuda, H. Fujita, N. Iwasa and T. Ohama, Prep. 1992 Int. Gas Research Conf., Orlando(1992)
2) S. Nagase, S. Takami, M. Masuda, O. Okada, N. Iwasa and M. Hamada, Prep. 1995 Int. Gas Research Conf., Cannnes(1995)
3) Martyn V. Twigg, Catalyst Handbook second edition, p324-327, Wolfe Publishing Ltd., England(1989)
4) ibid.,p.310

DEVELOPMENT OF A HYDROGEN GENERATOR FOR FUEL CELLS BASED ON THE PARTIAL OXIDATION OF METHANE

V. Recupero, T. Torre, G. Saija and N. Giordano
Institute CNR-TAE, via S.Lucia sopra Contesse 39, 98126 S. Lucia, Messina, Italy.

Introduction

As well known, the most acknowledged process for generation of hydrogen for fuel cells is based upon the steam reforming of methane or natural gas (SRM). The reaction is endothermic (ΔH_{298}= 206 kJ/mole) and high H_2O/CH_4 ratios are required in order to limit coke formation at T higher than 1000 K. Moreover, it is a common practice that the process's fuel economy is highly sensitive to proper heat fluxes and reactor design (tubular type) and to operational conditions. Efficient heat recovery can be accomplished only on large scale units (> 40,000 Nm^3/h), far from the range of interest of "on-site" fuel cells. Even if, to fit the needs of the fuel cell technology, medium sized external reforming units (50-200 Nm^3 H_2/h) have been developed and/or planned for integration with both the first and the second generation fuel cells, amelioration in their heat recovery and efficiency is at the expense of an increased sophistication and therefore at higher per unit costs. In all cases, SRM requires an extra "fuel" supply (to substain the endothermicity of the reaction) in addition to stoichiometric requirements ("feed" gas).
A valid alternative could be a process based on catalytic partial oxidation of CH_4 (CSPOM), since the process is mildly exothermic (ΔH_{298}= -35.6 kJ/mole) and therefore not energy intensive. Consequently, great interest is expected from conversion of methane into syngas, if an autothermal, low energy intensive, compact and reliable process could be developed.

Experimental

The experimental work, carried out by the Institute CNR-TAE of Messina, in the framework of the JOULE II Programme Fuel Cell (fundend in part by the Commission of the European Communities), coverered the following approaches:

- Screening and evaluation of commercially available Ni-supported catalysts. Catalytic tests and characterization.
- Modelling of the catalyst's kinetics and of the reactor geometry in order to provide a basis for an explanation on the reaction mechanism involved, and a rigorous calculation of the temperature-conversion profiles.
- Design and construction of an adiabatic reactor prototype of 5 Nm^3 H_2/h.
- Experimental tests on the prototype, in order to define the optimized reaction conditions and to evaluate the endurance of catalysts.
- Balance of plant analysis in order to make an assessment of the requirement for gas clean-up and of the basic design of the integrated system "fuel processor-fuel cell".
- Techno-economic evaluation based upon advantages and proven and/or expected savings, from introduction of the CSPOM concept in combination with different categories of fuel cells (i.e.SOFC, MCFC, PAFC, SPE).

Results and discussion

A series of experiments on commercial catalysts have been done by operating at extremely high space velocities in order to get reliable kinetic data on the pathway of the title reaction on different supported Ni catalysts [1, 2].
Catalytic measurements were performed in a conventional fixed by continuous flow reactor operated under atmospheric pressure, using pure O_2 as the oxidant.
The influence of reaction temperature (773-973 K) and gas hour space velocity (GHSV = 1.3 E6 - 3.9 E6 h-1) on activity and selectivity of the different catalytic systems was investigated. The difference of temperature between the catalytic bed and the wall reactor (ΔT), has been careful measured during the runs.
It has been observed that even at very high GHSV (2.6 E6 h-1) the CH_4 conversion in the temperature range investigated is substantially high (> 50 %) although lower than that estimated by the termodynamic equilibrium. The CH_4 conversion increases with the reaction temperature even after total O_2 conversion is reached (ca. 550 C). This finding indicates that the endothermic reaction ($CH_4 + H_2O$ - CO + 3 H_2; $CH_4 + CO_2$ - 2CO + 2H_2) occur at higher temperature (> 550 C). The CRG-B, CRG-F (British Gas) and Nissan Girdler GP65 catalysts show the best performance while GIrlder G91-B and ICI 57-3 catalysts possess a very low activity. The CO and H_2 selectivities, as a function of the reaction temperature, have been identified, also.
Besides, the relationship between ΔT and the reaction temperature has been investigated: it is very interesting that, on CRG-B and CRG-F catalysts, the contributions of endothermic reactions is more consistent at higher reaction temperatures. In fact, at a $\Delta T < 575$ C, the ΔT is extremely high (> 100 C) indicating that the reforming reactions are inhybited.
TPR and XPS characterization of Ni catalysts, supported on magnesium oxide, alumina and calcium-aluminate, have been carried out [1]. XPS experiments on different catalysts have been finalized in order to obtain respectively the metal-support surface composition. A clear influence of the surface availability of metal Ni upon the extent of the reaction (expressed by the T to reach 50 % conversion) has been disclosed.

An hydrogen generation system (mod. CSPOM1/01) able to produce hydrogen and carbon monoxide, starting from a mixture formed by air and methane, has been designed and realized (Fig. 1).
The main key features, upon which the prototype was based [2] were the following:
* Simple design;
* Easy construction;
* High compactness;
* Good flexibility;
* High reliability;
* Low cost;
* Low maintenance;
* High safety.

The CSPOM1/01 reactor is a fixed bed reactor. To overcome temperature gradients (hot spots) the catalyst is diluted with a inert (Alumina, catalyst/alumina ratio = 1/3). The internal reactor volume is 637 cm^3; the reactor weight (including catalyst and alumina) is ca. 2000 g; this reactor is able to produce 5 Nm^3/h of syngas (H_2 + CO).

On the basis of the procedure identified during the microscale tests, the foreseen runs have been carried out. The prototype has well performed and the results have been satisfactory.
The working conditions of the firstst series of tests has been the following:
- catalyst CRG-F, size 3x3 mm (pellets);

- P = 1 bar;
- T = 1073-1173 K;
- O2/CH4 = 0.50-0.55;
- G.H.S.V. = 80000 h-1;
- Linear velocity = ca. 1 m/sec.

The main features, following the results [3], have been:

- Conversion of the methane close 97 %, stable during the run time (Fig. 2);
- Conversion of the oxygen close 100 %;
- Selectivity to carbon monoxide close 99 % (Fig. 3);
- Selectivity to hydrogen close 87 % (Fig. 4).

Conclusions

The following main conclusions can be drawn from the work performed:

- A commercial Ni/Al2O3 catalyst (CRG-F by British Gas) has been selected for catalytic tests.
- A semiautomatic test facility (microreactor scale), for the methane partial oxidation, has been realized.
- Activity measurements, in microreactor scale on different commercial catalysts, have been carried out: by using the CRG-F catalyst, very high CH_4 conversions and H_2 yields are found (at temperature ca. 1073 K and O_2(air(/CH_4 ratios of 0.50-0.55, methane conversion and hydrogen selectivity are close to 100 %).
- Structural and surface characterization of various commercial catalysts has been accomplished.
- The 5 Nm^3/h of syngas prototype has been designed and assembled.
- The check tests and preliminary experiments have been succesfully carried out;
- The working run have been succesfully carried out.
- Main results: Methane conversion close 97 %, Oxygen conversion close 100 %, Selectivity to carbon monoxide close 99 %, Selectivity to hydrogen close 87 %.
- Distribution of the temperature sufficiently uniform along the catalytic bed has been obtained.

Work in progress has been addressed to analyse some main aspects: particularly, the use of natural gas, instead of methane (stability of the catalyst to sulfur); the rigeneration of the catalyst, the materials compatibility, etc.; are under progressing.

References

[1] V. Recupero et al. " Theoretical and experimental studies for a compact H_2 generator, via catalytic partial oxidation of CH_4, integrated with second generation fuel cells". Contract JOU2-CT93-0290, First periodic report covering the period from February 1st to July 31, 1994.

[2] V. Recupero et al. " Theoretical and experimental studies for a compact H_2 generator, via catalytic partial oxidation of CH_4, integrated with second generation fuel cells". Contract JOU2-CT93-0290, First periodic report covering the period from August 1st, 1994 to January 31, 1995.

[3] V. Recupero et al. " Theoretical and experimental studies for a compact H_2 generator, via catalytic partial oxidation of CH_4, integrated with second generation fuel cells". Contract JOU2-CT93-0290, First periodic report covering the period from February 1st, 1995 to July 31, 1995.

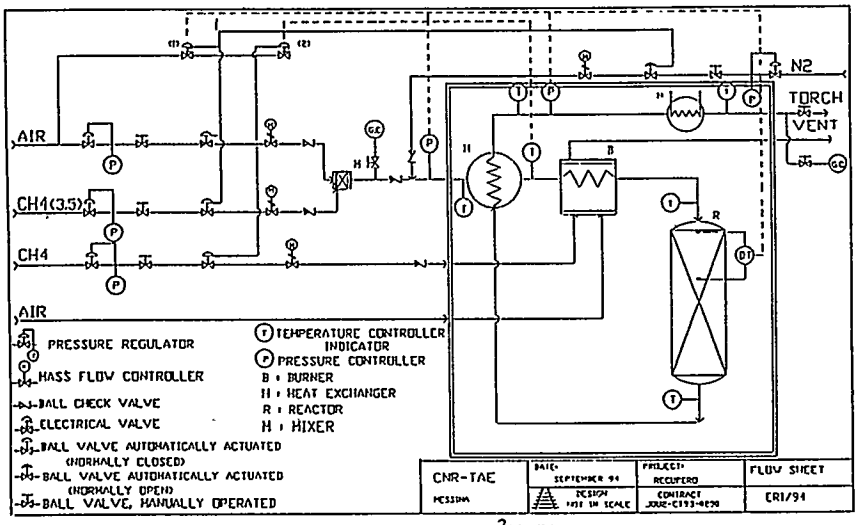

Fig. 1: Flow sheet of the CSPOM1/01 prototype,(5 Nm^3H_2/h).

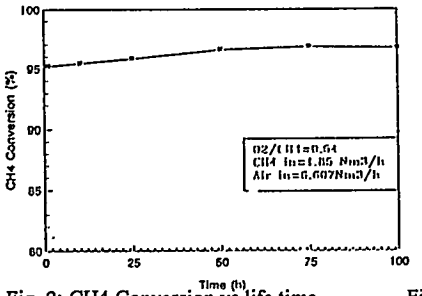

Fig. 2: CH4 Conversion vs life time. CSPOM1/01 prototype (5 Nm^3H_2/h).

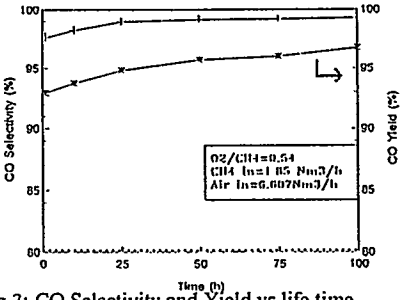

Fig.3: CO Selectivity and Yield vs life time. CSPOM1/01 prototype (5 Nm^3H_2/h).

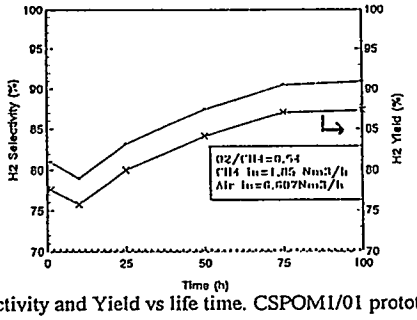

Fig. 4: H2 Selectivity and Yield vs life time. CSPOM1/01 prototype (5 Nm^3H_2/h).

TECHNO-ECONOMICAL ANALYSIS OF AN INTEGRATED HYDROGEN GENERATOR - FUEL CELL SYSTEM

V. Recupero, G. Maggio, R. Di Leonardo, M. Lagana'
Istituto CNR-TAE, via S.Lucia sopra Contesse 39, 98126 S. Lucia, Messina, Italy.

Introduction

As well known, the most acknowledged process for generation of hydrogen for fuel cells is based upon the steam reforming of methane or natural gas (SRM). The reaction is endothermic (ΔH_{298}= 206 kJ/mole) and high H_2O/CH_4 ratios are required in order to limit coke formation at T higher than 1000 K. Moreover, a common practice indicates that the process fuel economy is highly sensitive to proper heat fluxes, reactor design (tubular type) and to operational conditions. Efficient heat recovery can be accomplished only on large scale units (> 40,000 Nm^3/h), far from the range of interest for "on-site" fuel cells. Even if, to fit the needs of the fuel cell technology, medium sized external reforming units (50-200 Nm^3 H_2/h) have been developed and/or planned for integration with both the first and the second generation fuel cells; amelioration in their heat recovery and efficiency is at the expense of an increased sophistication and therefore an higher per unit costs. In all cases, SRM requires an extra "fuel" supply (to substain the endothermicity of the reaction) in addition to stoichiometric requirements ("feed" gas).
A valid alternative could be a process based on catalytic selective partial oxidation of CH_4 (CSPOM), since the process is mildly exothermic (ΔH_{298}= -35.6 kJ/mole) and therefore not energy intensive. Consequently, a great interest is expected on conversion of methane into syngas, if an autothermal, low energy intensive, compact and reliable process should be developed.
In this respect, the work, carried out by the CNR-TAE Institute of Messina, in the framework of the JOULE II Programme Fuel Cell (funded in part by the Commission of the European Communities) regarded the development of a Hydrogen Generator for Fuel Cells, based on the CSPOM concept. An assessment of the requirements for clean-up of gases, according to the category of fuel cells has been made. Based upon the results of this evaluation, a balance of plant analysis, , has also been made to: *a*) gather a basic design scheme of the integrated system, *b*) identify further peripherical subsystems (if any), and envisage the optimal configuration for the integrated system, *c*) assess overall thermodynamic, thermal and electrical efficiencies, specifying (for each type of fuel cell) operating conditions, as well as most proper integration of heat and mass flows between fuel processor and electrochemical generator.

Results and Discussion

As a part of the work performed [1,2], in order to make an assessment of the requirement for gas clean-up and of the basic design of the integrated system "fuel processor - fuel cell", a balance of plant analysis has been developed [3]. Particularly, the requirements for clean-up of gases has been identified according to the category of fuel cells, as follows. For both SOFCs and MCFCs which can accept CO, no clean-up is necessary. For PAFCs, a reactor for WGSR will be necessary. For the SPEFCs, besides the WGSR, a catalytic reactor for the total abatment of CO will be further considered in cascade. Other key features concerned: *a*) hydrogen that is not consumed in the anode has to be utilized in other sections of the integrated system to maximize thermal efficiency; *b*) utilization of energy of every stream in the system must, also, be maximized, : therefore, a considerable effort goes into the optimum use of heat exchangers, condenser, and other energy exchange devices. As regards point a), in the steam reforming fuel processor the un-reacted hydrogen is fed to the reformer furnace and supplies most, if not all, of the energy requirements for the endothermic steam-hydrocarbon reactions. In systems that do not require energy to process the fuel (such as autothermal reforming and partial oxidation)

other uses must to be found for this anode exhaust to maximize the efficiency (i.e the use of a membrane to separate hydrogen and carbon dioxide in order to recycle the same hydrogen in the fuel cell).
Only by evaluating the total system, the feasibility of various fuel-processing schemes can be assessed and compared.
On the other hand, the perceived potential which makes the CSPOM a pursuable alternative to the methane steam reforming (SRM) is implicit whenthe "overall" fuel specific consumption, for the two processesare compared. For the SRM:

$$CH_4 + 2H_2O \Leftrightarrow CO_2 + 4H_2$$

stoichiometric ("feed") requirement is 0.28 Nm^3 CH_4/Nm^3 H_2 (90% conv. of CH_4). Because of its high endothermic character (ΔH_{298}= 206 kJ/mole) and other inefficiencies, an extra amount of CH_4
"fuel") is needed. A survey of released information shows that for typical medium sized plants (1,500 Nm^3 H_2/h), the total "feed" + "fuel" requirement is in the order of 0.45 Nm^3CH_4/Nm^3H_2 (Table I).

Table I: Performance data per 1000 SCF (26.8 Nm^3) hydrogen based on a typical medium-sized plant (1500 Nm^3 H_2/h), [4].

	1	2	3	4	5
Feed and fuel (MBTU)	430	434	448	430	589
Specific consumption (Nm^3 CH_4/Nm^3 H_2)	0.45	0.455	0.47	0.45	0.62
Case 1: Standard hydrogen plant, reforming without air preheat using only HT shift reactor.					
Case 2: Case 1, including LT shift reactor.					
Case 3: case 1, including gas turbine exhaust as combustion air (enthalpy of air included).					
Case 4: Case 1, generating electricity with the available (exported) steam.					
Case 5: Case 4, with auxiliary firing in the convection section.					

Because of scale's economy, larger units (> 40,000 Nm^3H_2/h) allow a lower consumption down to 0.41 Nm^3 CH_4/Nm^3H_2 . However since H_2 for fuel cells is a commodity not available "over the fence", a comparison with figures for typical small sized plants (200 or ever 500 Nm^3H_2/h) like those marketed for the 50-200 kW PAFC is compulsory. According to specifications given by Companies, "minimum" specific consumption on such plants is in the order of 0.45 Nm^3CH_4/Nm^3H_2 or 4,000 kcal/Nm^3H_2 (based upon LHV) which should thus be taken as a reference for the comparison.
Conversely, as the CSPOM is mildly exothermic:

$$CH_4 + 1/2\ O_2\ (air) \xrightarrow{1000\ K} CO + 2H_2$$

the total net specific consumption is exclusively dictated by stoichiometry (0.33 Nm^3CH_4/Nm^3H_2) which for a specific CH_4 conversion of 90% turns to be 0.36 Nm^3 CH_4/Nm^3H_2. Moreover, it is important to stress that this specific consumption is, by definition, insensitive to the size and this allows to anticipate a flexibility, as to the size of the fuel processor modules required, totally lacking in conventional steam reforming.
From the above it is evident that the CSPOM allows a saving with respect to conventional SRM, varying, depending upon the size, from 12 to 20 % in the fuel consumption per unit CO and H_2. If the comparison is restricted to the small sized plants (50-200 Nm^3/h), a sound estimate is, at least, a 15 % saving .
The comparison in terms of productivity is also in favour of the CSPOM. As typical contact times for total conversion of CH_4 are in the order of 0.04 sec, a productivity of 0.3 - 0.5 mol CH_4 conv./kg cat sec is expected, which is at least one order of magnitude higher of that

reported for most efficient SRM plants. Therefore it could be anticipated that CSPOM will demand reactor's sizes at least one order of magnitude smaller, with inherent savings in investments which preliminary estimates assume to be in the order of 30 %.
Technical benefits, as above, should be weighted, in turn, in terms of a lower, likely 20 % lesser emission of CO_2 per unit energy produced and, on the side of investments, in lower amortization rates with the added benefits of an easier workability and a more compact assembly bound to the adiabatic vs. the tubular configuration.
Besides, because of its lower heat entalpy, promptness to start-up and shut-down in CSPOM is expected to be higher and to follow better the changes in the load of the fuel cell subsystem. It should be noted that the theoretical debit for using 50 % syngas rather than 100 % (due to the use of air) results in a loss of only 15 mV in open circuit potential, a trivial disadvantage. Furthermore, as the adiabatic characteristics of a CSPOM reactors would demand less stringent engineering geometry and regulations, a wide "degree of freedom" in the modularity of use is expected, making possible to respond to whatsoever site-specific needs.
Summing up main features, the advantages of CSPOM vs SRM could be anticipated as following (Table II).

Table II: Synoptical view of advantages and saving in CSPOM vs SRM (in arbitrary units).

	Ref. [5]	Ref. [6]	Ref. [7]
Specific consumption of fuel per unit H_2			
SRM	100		
CSPOM	80-90		
Investment costs for a 2000 STPD - Methanol Plant			
SRM	100	100	
CSPOM with the O_2 separation unit	53	78	
without the O_2 separation unit	n.a.	55	
Unitary costs of H_2			
SRM	100	100	100
CSPOM with the O_2 separation unit	n.a.	71*	40**
without the O_2 separation unit	50-70**	n.a.	n.a.

* Calculated on the basis of a 20 % ROI + 10 % amortization on investment costs
** Depending upon the size
*** Calculated on the basis of 100 Nm^3 H_2/h
n.a Not Available

Altogether, volume, unit costs, reliability, committement to user's requirements add in anticipating the high competitiveness of a CSPOM based fuel economy with respect to most traditional means of a syngas and/or H_2 generation. As with addition of some proper gas cleanup processes, the quality of gas can be adjusted to fit the requirements of even the most demanding fuel cells (PAFCs, SPEFCs), the "as claimed" CSPOM concept should be considered of a more general validity and strategical importance. Table III summarizes the main advantages (and disadvantage) of the Methane Partial Oxidation System versus the various fuel cell generations.

Conclusions

In the framework of the JOULE II Programme, the CNR-TAE Institute , Messina, developed a Hydrogen Generator for Fuel Cells based on the Catalytic Partial Oxidation of Methane (CSPOM). In this respect an analysis, to provide background for applications of the CSPOM

Table III: Main advantages and disadvantages of the Hydrogen Generator via Methane Partial Oxidation System versus different Fuel Cells.

Fuel Cell	Adantages	Disadvantages
Solid Polymer Electrolyte	* Very fast answer to the load variations * Compactness * Reliability * Low Cost	* Need of the WGSR and CO Selective Oxidation subsystem * Need to optimize the exhaust hydrogen of the fuel cell * Need to optimize the thermal balance
Phosphoric Acid	* Very fast answer to the load variations * Compactness * Reliability * Low Cost	* Need of the WGSR subsystem * Need to optimize the exhaust hydrogen of the fuel cell * Need to optimize the thermal balance
Molten Carbonate and Solid Oxide	* Direct use of the gas outgoing from the CSPOM * Very fast answer to the load variations * Compactness * Reliability * Low Cost	* Need to optimize the thermal balance

concept to the fuel cell technology, has been carried out. Particularly, different hydrogen generators have been analyzed to identify the better system to be integrated with the different generations of fuel cells; an economic comparison has, also, been accomplished between the methane partial oxidation system and the methane steam reforming. The basic schemes and the detailed configuration of the Hydrogen Generator-Fuel Cell (Solid Polymer Electrolyte, Phosphoric Acid, Molten Carbonate, Solid Oxide) have been identified. The analysis gave an indicative, although firm, estimate of savings in investments and utility consumption per unit energy produced by such integrated systems, confirming the technical and economical advantages of the Catalytic Partial Oxidation System versus the classic Steam Reforming.

References

[1] V. Recupero et al. " Theoretical and experimental studies for a compact H_2 generator, via catalytic partial oxidation of CH_4, integrated with second generation fuel cells". Contract JOU2-CT93-0290, First periodic report covering the period from February 1st to July 31, 1994.

[2] V. Recupero et al. " Theoretical and experimental studies for a compact H_2 generator, via catalytic partial oxidation of CH_4, integrated with second generation fuel cells". Contract JOU2-CT93-0290, Second periodic report covering the period from August 1st, 1994 to January 31, 1995.

[3] V. Recupero et al. " Theoretical and experimental studies for a compact H_2 generator, via catalytic partial oxidation of CH_4, integrated with second generation fuel cells". Contract JOU2-CT93-0290, Third periodic report covering the period from February 1st, 1995 to July 31, 1995.

[4] KTI, Mannesmann Group, Private Communication (1994).

[5] T. Sudset, J. Sogge and T. Strom, Proc. 4th European Workshop on Methane Activation, Eindhoven, The Nederlands, May 16-17 (1994).

[6] CNR-TAE, Internal Report (1994).

MODELLING STUDIES TO PROPER SIZE A HYDROGEN GENERATOR FOR FUEL CELLS

G. Maggio, V. Recupero, R. Di Leonardo, M. Laganà
Istituto CNR-TAE, via S.Lucia sopra Contesse 39, 98126 S. Lucia, Messina, Italy.

Introduction

Based upon an extensive survey of literature [1-3] a mathematical model has been developed to study the temperature profile along the catalytic bed of a reactor for the methane partial oxidation. The model allowed a preliminary design of a 5 Nm^3 syngas/h prototype to be integrated with second generation fuel cells as hydrogen generator (in the framework of the EC-JOU2 contract). This design was based on some target features, including the choice of a GHSV (gas hour space velocity) equal to 80000 h^{-1}, a catalyst particle size of 1/8", a molar air/methane ratio of 2.7 (i.e. O_2/CH_4=0.53), a linear velocity in the catalytic bed of about 2 m/sec, and an inert/catalyst ratio 3:1. Starting from this data, the work has been concerned with the identification of the controlling regime (kinetic or diffusional), and then with the estimation of the gas composition and temperature profiles along the reactor. A comparison between experimental and model results has also been accomplished.

Modelling approach

Identification of the controlling regime is paramount for calculating the basic dimensions of the reactor and for determining the degree of partition of the inert diluent solid alongside the whole length of the catalytic bed to assure quasi-isothermal conditions, in order to avoid *hot spots*. As it is generally agreed [1-4] that the catalytic selective partial oxidation of methane (CSPOM) reaction is very fast, i.e. the reaction is said to be at equilibrium even at very high space velocity (in the order of 10^4 - 10^5 h^{-1}), the overwhelming influence of mass and heat transfer effects is likely expected. Our results, derived from well known equations [5-6] and based on data reported in Tab.I, confirmed this statement and the targeted GHSV upper limit of 80000 h^{-1} should be seen as a compromise between productivity and detrimental effects by local overheating.

Tab.I: 5 Nm^3 syngas/h reactor data.

Temperature	800°C=1073 K
Pressure	2 ata
Inlet total gas flow rate	6.85 m^3/h= 305.61 mol/h
Inlet gas composition	CH_4=27.0%, O_2=14.6%, N_2=58.4%
Reactor internal diameter	5.0 cm
Catalytic bed length	17.3 cm
Mean particle diameter	1/8 inch
Bed void fraction	0.35
Catalyst particle density	1.23 g/cm^3
Catalyst bulk density	0.8 g/cm^3
GHSV	80000 h^{-1}
Catalyst volume	85 cm^3
Inert/catalyst ratio	3:1
Particle geometry	Cylinder

To obtain a careful estimation of the longitudinal temperature and composition profiles, various partial methane oxidation reaction models, derived from literature [7-8], have been considered and analyzed. However, the model results seem to confirm [7] that the reaction pathway involves initial conversion of some CH_4 to CO_2 and steam, followed by a sequence of steam reforming and water gas shift reactions, to give equilibrium product yields.

Having assumed and proved that the reaction is controlled by external mass transport, it was further supposed that the composition of the reaction mixture at the catalyst surface is in thermodynamic equilibrium with the mixture in the bulk flow.

An original simulation model, based upon these assumptions, has been usefully developed. Equilibrium relationships in terms of molar flows have been derived, introduced into the model and solved simultaneously by an iterative procedure (the well-known Newton method for non-linear equations). As first approximation, a simplified version of the model has been realised, assuming negligible axial temperature profile and thermal dispersion.

Based upon an elementary material balance and its stoichiometry, the extent of each reaction for the selected set of reactions, was calculated and used for the prediction of the overall reaction enthalpy in a volumetric reactor element according to the equation

$$Q = \sum_{i=1}^{N} \Delta H_r^i \frac{dF_i}{dz} = \sum_{i=1}^{N} \Delta H_r^i \Delta F_i \qquad (1),$$

where the summation is extended to all reactions of the assumed reaction model; Q is the heat generated at the specific axial element of the reactor, ΔH_r^i the standard heat of reaction for the reaction r, and ΔF_i the number of moles of component i reacted according to reaction r.

Temperature gradient in the reactor at the selected axial coordinate was calculated as

$$\frac{dT}{dz} = \frac{Q}{\sum_{i=1}^{n} F_i C_P^i} \qquad (2),$$

where dT is the temperature change, dz the length of the differential element of the reactor, F_i the molar flow of component i and C_P^i its heat capacity in the stream.

To take into account the influence of the relative weight of the reaction rate controlling regime a corrective factor of unsteady conditions was introduced according to the equation

$$\Delta F_{CH4}^c = \Delta F_{CH4} (1+\varphi) \qquad (3),$$

where ΔF_{CH4}^c is the total amount of consumed methane in the differential reactor element, ΔF_{CH4} is the amount of methane reacted at the catalyst surface by mass transport, and φ is a corrective factor which accounts for the reaction rate (φ=0 only mass transfer, φ>0 faster reaction, φ=∞ the reactant is completely consumed in the differential element of reactor).

A more sophisticated version of the model has also been developed and compared with the approximate one. On this purpose, without changing its original *philosophy*, the model has been generalized considering the different effects associated with the heat transfer in packed beds, and expressing the effective thermal conductivity as a function of these effects [1, 9]. In particular, some more realistic assumptions have been introduced in the complete model, as specified in the following:

- evaluation of mass transfer coefficient for each component, instead of constant value used before;
- both temperature and concentration variations have been calculated in the radial as well as in the longitudinal direction;
- thermal dispersion and irradiation effects have been considered.

Results and discussion

The results obtained by the model are represented in Figs.1-3. In particular, Fig.1 shows the behaviour of the concentration and temperature profiles along the longitudinal direction of the reactor relatively to the case when the radial effects are neglected (approximate model). Fig.2 shows the profiles obtained by the model when the radial effects are taken into account (complete model). At last, in Fig.3 the longitudinal temperature profiles obtained by the two versions of the model are compared with experimental results.

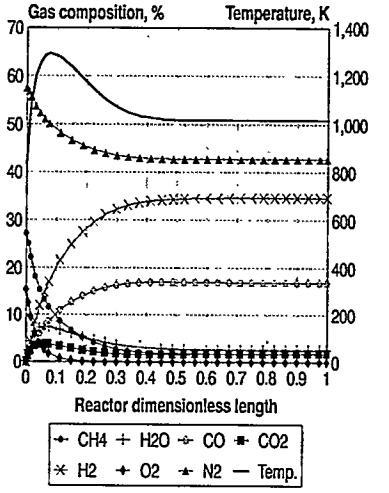

Fig.1: Temperature and concentration profiles calculated by the model version which doesn't take radial effects into account (approximate model).

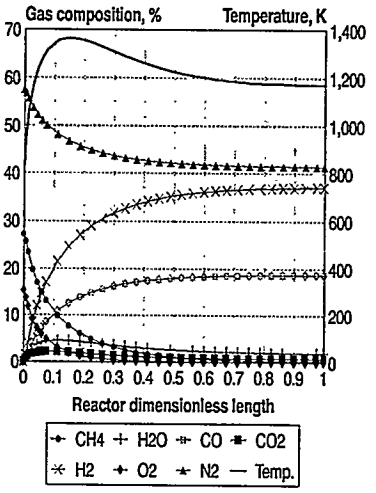

Fig.2: Temperature and concentration profiles calculated by the model version which takes radial effects into account (complete model).

Inspection of these figures reveals that the modifications introduced into the final version of the model affected the results with dissimilar influences on the concentration and temperature profiles. Main results can be summarized as follows:

- all modifications showed a negligible influence on the concentration profiles, which do not vary significatively in comparison with the values of the previous model version;
- the introduction of different mass transfer coefficients resulted in a negligible effect on the temperature profile, providing temperatures slightly higher with respect to the approximate version of the model but without any change in the shape;
- the irradiation and dispersion contributions influenced the shape of the temperature profile; in fact, the temperature increased in the first part of the catalytic bed in comparison with the results obtained when these effects were neglected (the peak is about 70°C higher than the value of the approximate model, and its localization is slightly shifted). Otherwise it decreased more gradually in the last part of the catalytic bed;
- the agreement between the simulation results and the experimental ones has been further improved (Fig.3).

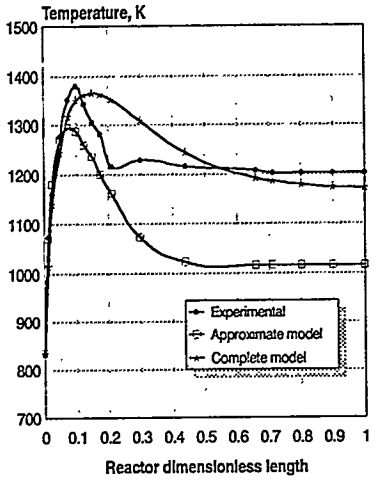

Fig.3: Comparison between experimental and calculated, without (approximate model) and with radial effects (complete model), temperature profiles.

Conclusions

A model to calculate the gas composition, the adiabatic temperature and its longitudinal profile along a reactor for the CSPOM has been developed, in order to design a 5 Nm^3 syngas/h reactor, and thereafter to scale-up towards larger units of a size typically needed to supply gases to a 50-200 kW Fuel Cell Power Plant. The model allows sensitivity studies to be performed for a variety of reactor designs in the capacity range of 1-200 Nm^3 syngas/h or so. These sensitivity analyses have two significant design implications: (i) to provide the reactants and products composition profile in the catalytic bed and (ii) to provide the operating conditions (preheating temperature, pressure, GHSV, catalyst particle size, air/methane ratio, inert/catalyst ratio, etc.). Thereafter the optimal reactor configuration, to assure quasi-isothermal conditions, higher methane conversion and H_2 and CO selectivities, may be consequently individualised.

The proposed approximate version of the model provides useful information in this regard; the complete model takes radial effects into account and better fits the experimental values.

References

[1] E.Singer and R.H.Wilhelm, *Ind.Eng.Chem.*, 46 (1950), 343.
[2] K.Hashimoto, N.Taneda, Y.Horiguchi and S.Nagata, *J.Res.Inst.Catalysis, Hokkaido Univ.*, (1968), 541-563.
[3] W.B.Argo and J.M.Smith, *Chem.Eng.Progr.*, 50, No.10 (1954), 504-510.
[4] A.K.Bhattacharya, J.A.Breach, S.Chand, D.K.Ghorai, A.Hartridge, J.Keary and K.K.Mallick, *Applied Catalysis A: General*, 80 (1992), L1.
[5] O.A.Hougen and K.M.Watson, Chemical Process Principles, John Wiley & Sons Ed., New York, 1957.
[6] P.B.Weisz, *Z.Physik.Chem.*, Neve Folge, II, 1-15, 1957.
[7] W.J.M.Vermeiren, E.Blomsma and P.A.Jacobs, *Catalysis Today*, 13 (1992), 427-436.
[8] J.K.Hockmuth, *Applied Catalysis B: Environmental*, 1 (1992), 89-100.
[9] H.Vershoor and G.C.A.Schuit, *Appl.Scientific Research* 42, A2, No.2, (1950), 97.

OPERATION OF THE 25 kW NASA LEWIS SOLAR REGENERATIVE FUEL CELL TESTBED FACILITY

G. E. Voecks. N. K. Rohatgi, S. H. Moore, D. L. Jan. and N. W. Ferraro
Jet Propulsion Laboratory
4800 Oak Grove Dr.
Pasadena, CA 91109
M. Warshay and P. R. Prokopius (Consultant)
NASA Lewis Research Center
28000 Brookpark Road
Cleveland, OH
H. S. Edwards, G. Smith
Naval Air Weapons Center
China Lake, CA 93555

Assembly of the NASA Lewis Research Center Solar Regenerative Fuel Cell Testbed Facility has recently been completed and system testing is in progress. This facility includes the integration of 50 kW photovoltaic solar cell arrays, a 25 kW proton exchange membrane (PEM) electrolysis unit, four 5 kW PEM fuel cells, high pressure hydrogen and oxygen storage vessels, high purity water storage containers, and computer monitoring, control and data acquisition. The purpose of this facility is multi-faceted, but was originally intended to serve as a testbed for evaluating a closed-loop powerplant for future NASA extended life support operations, such as a Lunar outpost, and also as a terrestrial powerplant example for remote or continuous back-up support operations. The fuel cell and electrolyzer subsystems' design and assembly were conducted by the Jet Propulsion Laboratory (JPL), the photovoltaic arrays and electrical interconnect to the electrolyzer were provided by the U. S. Navy/China Lake Naval Weapons Center, and testing and operations are being carried out by JPL.

This testbed facility allows for separate operation of each subsystem, i.e., photovoltaic arrays, electrolyzer, fuel cells, support equipment, as well as integrated operation to simulate expected electrical demand profiles. During the course of operations, many important technical points have been learned. The interconnect between the photovoltaic arrays and the PEM electrolyzer, which can deliver both hydrogen and oxygen at nearly 20,600 kPa (3000 psi), has been designed to allow operation of the electrolyzer (1) separately from the grid, (2) entirely from the photovoltaic arrays, or (3) from the grid in a back-up mode. The four fuel cells have been connected in such a manner that they may be operated separately or combined to evaluate their performance coincidentally with duty cycles commensurate with different demands to reflect NASA requirements for isolated operations. All the operating data and energy and mass balances are being performed in order to determine where system and subsystems inefficiencies exist, what technical improvements are most important, and how such a system can best be integrated for future NASA missions where thermal and electrical energy conservation are of extreme importance.

From operating data and experience, control strategies and equipment design will be determined that will enable automated operation, a key goal for both NASA and terrestrial users. Start up, shut down, and load following to efficiently meet prescribed duty cycles impact the choice of equipment and the system design as well as the control strategy.

The system description and performance data constitute Phase I of multiple activities planned to take place in the next few years. System modeling is being performed in parallel with the experimental testing and will be used to determine the most efficient system design, from the standpoint of weight, volume and cost of electrical power.

In addition to detailed facility and system layout and operations, performance data, mass and energy determinations and modeling analyses will be presented to illustrate the capabilities of the testbed facility and basis for advanced designs.

LIGHTWEIGHT PRESSURE VESSELS AND UNITIZED REGENERATIVE FUEL CELLS

F. Mitlitsky, B. Myers, and A.H. Weisberg
Lawrence Livermore National Laboratory
7000 East AVE, P.O. Box 808, L-045
Livermore, CA 94551-0808

High specific energy (>400 Wh/kg) energy storage systems have been designed using lightweight pressure vessels in conjunction with unitized regenerative fuel cells (URFCs). URFCs produce power and electrolytically regenerate their reactants using a single stack of reversible cells. Although a rechargeable energy storage system with such high specific energy has not yet been fabricated, we have made progress towards this goal. A primary fuel cell (FC) test rig with a single cell (0.05 ft^2 active area) has been modified and operated reversibly as a URFC. This URFC uses bifunctional electrodes (oxidation and reduction electrodes reverse roles when switching from charge to discharge, as with a rechargeable battery) and cathode feed electrolysis (water is fed from the oxygen side of the cell). Lightweight pressure vessels with state-of-the-art performance factors (burst pressure * internal volume / tank weight = P_b V / W) have been designed and fabricated.[1] These vessels provide a lightweight means of storing reactant gases required for fuel cells (FCs) or URFCs. The vessels use lightweight bladder liners that act as inflatable mandrels for composite overwrap and provide the permeation barrier for gas storage. The bladders are fabricated using materials that are compatible with humidified gases which may be created by the electrolysis of water and are compatible with elevated temperatures that occur during fast fills.

Lightweight vessels have been designed and fabricated to react purely pressure loads or hybridized pressure and structural loads. Use of these hybridized vessels can result in lower system mass for various vehicles, such as high altitude long endurance (HALE) solar rechargeable aircraft (SRA).[2] We have designed, fabricated, and load tested to failure (in bending) a series of prototype hybridized vessels that can withstand the structural loads expected in a HALE SRA, in addition to storing the reactant gases required by a URFC energy storage system.

URFC systems with lightweight pressure vessels were designed for zero emission vehicles (ZEVs). Such systems are shown to be cost competitive with primary FC powered vehicles that operate on hydrogen/air with capacitors or batteries for power peaking and regenerative braking. URFCs are capable of regenerative braking via electrolysis and power peaking using low volume/low pressure accumulated oxygen for supercharging the power stack.[3] URFC ZEVs effectively carry their infrastructure on-board, enabling electrical recharge at home, work, or the highest power electric vehicle charging stations under consideration (by virtue of the large active area of cells that are sized for power production). URFC ZEVs can be safely and rapidly (< 5 minutes) refueled from high pressure hydrogen sources, when available, to achieve driving ranges in excess of 350 miles. URFC ZEVs can be refueled using home electrolysis units, but procurement of such units becomes an option, rather than a requirement, as is the case of other hydrogen powered vehicles prior to the existence of a widespread hydrogen infrastructure.

A single cell cycle life test for a URFC showed that reversible operation of cell membrane and catalyst is feasible without significant degradation,[4] thus refuting comments to the contrary made at the 1994 Fuel Cell Seminar. This test was performed in the early 1970s at ambient temperature using a membrane that is similar to DuPont's Nafion 120. The catalyst (E-5™) is a proprietary General Electric mixture of Pt, Pt-group metals, and their oxides. This test was a proof-of-principle energy storage system for a long life (7-10 yr) geosynchronous satellite, that was required not to use mechanical pumps (for reliability). The cell used a wicking cloth (typically quartz or Dacron) to feed water to the cell in zero-gravity. Upon disassembly of the cell, the initially hydrophilic wicks had become hydrophobic which degrades wicking and may well account for most of the limited cell degradation (<40 mV) shown in figure 1. It should be noted that other substitutes for wicks exist for zero-gravity operation, and wicks are clearly not required for terrestrial applications. Since this early data is sparse and masked by the unnecessary wicking cloth, we plan to perform a series of lifetime tests to show that high cycle life URFCs are feasible.

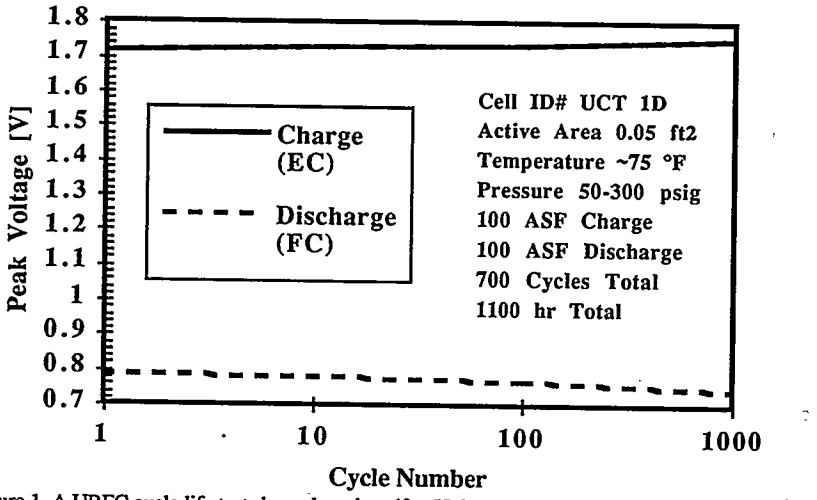

Figure 1. A URFC cycle life test shows less than 40 mV degradation over 700 cycles (1100 hr)[4].

Battery/URFC System	Theoretical Specific Energy [Wh/kg]	Packaged Specific Energy [Wh/kg]	Comments
H_2/O_2 URFC	3660	400-1000	URFCs with lightweight pressure vessels
Zn/O_2	1035	250	Excess Zn required, poor cycle life, dry-out
Li-SPE/MO_x*	735	220	Novel packaging for unmanned system
Ag/Zn	450	200	Excess Zn required, low charge rate
$Li/LiCoO_2$	735	150	Poor cycle life, high capacity fade
$Li/AlFeS_2$	515	150	≥400°C thermal management
Na/S	1180	150	~350°C thermal management
Li/TiS_2	470	130	~50% DOD for high cycle life (900 cycles)
Li/ion	700	100	Marginal improvement for larger cells
Ni/Zn	305	90	Excess Zn required, low specific energy
Ni/MH_x	470	70	MH_x is metal hydride
Ni/H_2	470	60	Low specific energy
Ni/Cd	240	60	Low specific energy
Pb/acid	170	50	Low specific energy

Figure 2. Theoretical and packaged specific energy for URFCs and rechargeable batteries.[2]
*Li-SPE/MO_x is Li-solid polymer electrolyte/metal oxide system packaged for unmanned systems.

A variety of hydrogen storage technologies are being considered for vehicular applications, including: physical storage, chemical carriers, gas-on-solid adsorption, and metal hydrides. These techniques have been compared in terms of weight, volume, complexity, cost, dormancy, and safety.[5,6] By the criteria discussed in those references, compressed gas storage using carbon fiber composite pressure vessels wound onto metal or plastic liners has been identified as one of the best near-term technologies.

The development of lightweight composite storage tanks using polymeric bladders as the inflatable mandrel and integral liner has been partially performed under a program funded by the DOE, Office of Transportation Technologies, in conjunction with Ford Motor Company. Tanks fabricated using this technology have advanced the state-of-the-art in tank performance factors, while achieving the high cycle life capability of thick metal or polymeric liners. Since the liners are thin and lightweight, the weight and volume penalties associated with packaging tanks into multiple units is reduced. The performance factor of a bladder lined tank using lower strength/less expensive carbon fibers (such as T700S or Panex 33) can match the performance factor of similar tanks with thick liners using higher strength/more expensive carbon fiber (such as T1000G). This is important because tank cost is dominated by fiber cost and the fiber cost per tank for T1000G is currently a factor of three-four times that of T700S or Panex 33.

Vehicles using rechargeable batteries have limited range per charge (<200 miles) due to low specific energy as shown in figure 2. Vehicles using lightweight pressure vessels for the onboard storage of hydrogen, combined with lightweight primary fuel cells can have greater than 350 mile range, could be rapidly refueled by sources of high pressure hydrogen (when available), and will be compatible with home electrolysis units. Such systems will require a hydrogen infrastructure or procurement of home electrolysis unit. Vehicles using lightweight pressure vessels and lightweight regenerative fuel cells will have the features of primary fuel cells and a rechargeable specific energy that is greater than 400 Wh/kg. Such systems would be dual-fueled vehicles that can use the existing electrical infrastructure, can utilize hydrogen infrastructure for rapid refueling (when available), enable regenerative braking by electrolysis, enable power peaking by oxygen supercharging, and will be cost competitive with primary hydrogen fuel cell vehicles.

ACKNOWLEDGMENTS

P.J. Regna (Aero Tec Laboratories), C.J. Anderson, G. Kendall, W.M. Parks, and D.H. Swan (AeroVironment), B.D. James and I.F. Kuhn, Jr. (Directed Technologies), S. Chalk and J. Milliken (DOE), R.C. Haddock and R. Willardson (EDO Fiber Science), G.H. Purnell and R.I. Sims (Ford), J.F. McElroy, T.M. Molter, L. Moulthrop, and R. Zhang (Hamilton Standard), M.L. Dickerson, M.J. Eckart, W. Jensen, and J.C. Whitehead (LLNL), J. Baer-Reidhart (NASA Dryden). This work was performed under the auspices of the U.S. DOE by LLNL under contract number W-7405-Eng-48.

REFERENCES

1. F. Mitlitsky, B. Myers, and F. Magnotta, "Lightweight bladder lined pressure vessels," *Disclosure and Record of Invention*, DOE Case No. IL-9722, 1995.

2. F. Mitlitsky, N.J. Colella, B. Myers, and C.J. Anderson, "Regenerative Fuel Cells for High Altitude Long Endurance Solar Powered Aircraft," Proc. 28th IECEC, Vol. 1,. pp. 1255-1262, Aug. 8-13, 1993 (UCRL-JC-113485).

3. F. Mitlitsky, N.J. Colella, and B. Myers, "Unitized Regenerative Fuel Cells for Solar Rechargeable Aircraft and Zero Emission Vehicles," 1994 Fuel Cell Seminar, pp. 624-627, Nov. 28-Dec. 1, 1994 (UCRL-JC-117130 and UCRL-MI-117130).

4. P.J. Chludzinski, I.F. Danzig, A.P. Fickett, and D.W. Craft, "Regenerative fuel cell development for satellite secondary power," General Electric Company, Technical Report AFAPL-TR-73-34, Jun. 1973.

5. F. Mitlitsky and B. Myers, "Development of an advanced, composite, lightweight, high pressure storage tank for on-board storage of compressed hydrogen," *Fuel Cells for Transportation TOPTEC: Addressing the Fuel Infrastructure Issue,* Alexandria, VA, April 1-2, 1996 (UCRL-MI-123802).

6. B.D. James, G.N. Baum, F.D. Lomax, Jr., C.E. Thomas, and I.F. Kuhn, Jr., "Comparison of onboard hydrogen storage for fuel cell vehicles," Ford Motor Company/DOE, February, 1996.

HYDROGEN FUEL CELLS IN CHEMICAL INDUSTRY: THE ASSEMINI PROJECT

G. Caserza, T. Bozzoni — Ansaldo CLC s.r.l.
Via D'Annunzio 105, 16121 Genova (Italy)

G. Porcino, A. Pasquinucci — Enichem s.p.a.
Via Taramelli 26, 20124 Milano (Italy)

Introduction

Chemical and petrochemical industries generate large quantities of hydrogen-rich streams, in the range 50%-100% H2 concentration by volume, as by-products of electrochemical or de-hydrogenation processes, or exhausts/purging in hydrogenation processes. Due to safety aspects, and because of the low density, which makes difficult transportation and storage, such streams often constitute a problem for plant managers. In most cases recycling within the plant processes is not possible, and transportation to other sites, generally by truck after compression in cylinders, is not economical. Many of these streams are therefore simply co-burned in plant boilers, and in some cases even wasted by venting or flaring. Their value ranges from zero (if vented), to the value of the fuel used in the boiler where they are co-burned.

Hydrogen fuel cell units would offer an easy and safe way to manage such streams, getting revenues from generated electricity and heat. Working with hydrogen would make fuel cells reach their best in terms of electrical efficiency, high grade heat generation, availability, flexibility for installation and operation, and easy of licensing, thanks to their null or negligible environmental impact. Considering both technical and economic aspects, the installation of hydrogen fuel cells in chemical industry results practically interesting in many circumstances, even with present high investment cost.

Typical hydrogen quantities in chemical and petrochemical plants are sufficient to power fuel cells from some hundreds kWs to several MWs. Rough estimates, based on chlor-alkali industry alone, give hydrogen by-product availability sufficient to install up to 600 MW fuel cell power in Europe, which could double or more if chemical and petrochemical sectors are considered. Even if only a part of that hydrogen would be conveniently employed in fuel cells, this constitutes a niche market, which involves consistent volumes in the immediate.

Hydrogen Plants Concept

Hydrogen plants will be based on the 900 kW d.c. capacity module concept, developed by CLC from the phosphoric acid fuel cell ONSI PC25 C (TM) natural gas plant concept. The module is conceived as a shop made package, adopting four phosphoric acid fuel cell stacks identical to the ones installed into the PC25 C (TM) plant. It is designed as an independent operating, self controlled unit, suitable for unattended operation in single or multiple units installations. Package dimensions will be approximately equivalent to a standard commercial container.

Preliminary module characteristics are:

Power Output	900 kW d.c.
Steam production (140 °C, 4 bar steam)	780 kg/h
Maximum Hydrogen Consumption	630 Nm3/h
Gross Electrical Efficiency (d.c.)	47% LHV
Gross Thermal Efficiency	30% LHV
Global Conversion Efficiency	77% LHV
Operation	more than 8000 h/year

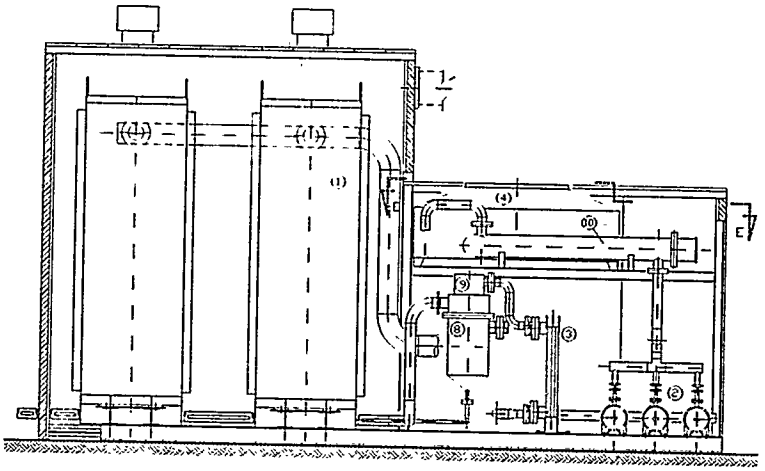

Study of the 900 kw fuel cells hydrogen module - longitudinal section

To get the maximum flexibility for different site specific interface requirements, separate service systems will be provided, specifically designed for the management of process and electric interfaces between module and site facilities. Typical service system functions will be hydrogen feed pressure control and purification, steam distribution to utilisation, condensate treatment, power voltage elevation and line connection, etc.. Remote operator interface will be provided, generally to be located in the existing plant control room, to supervise and control module. Specific functions will be provided to co-ordinate module(s) operation, according to actual site operating requirements. The typical hydrogen fuel cell plant operating mode will be to modulate automatically electric power, in order to consume a fixed portion (or all) of the hydrogen feed.

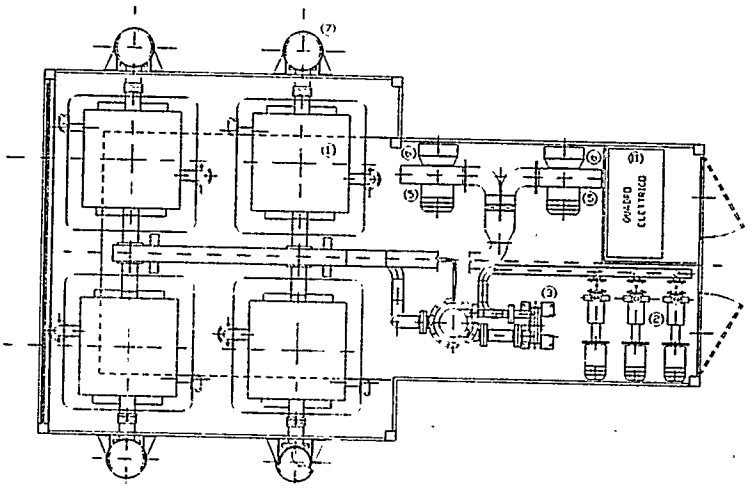

Study of the 900 kw fuel cells hydrogen module - top section

Chlor-alkali Industry and the Assemini Project

Chlor-Alkali Industry, produces chlorine, caustic soda and hydrogen by electrolysis of brine, a sodium chloride water solution. It provides ideal conditions for fuel cell integration (see fig 2), since very pure hydrogen is produced (especially from modern membrane electrolysers), at low pressure and temperature, which can be fed almost directly to the fuel cells. Fuel cell can generate up to 20% of the electric energy consumed by the electrolytic process, and steam to be used for caustic soda concentration. The conditioned d.c. energy generated by fuel cells can be supplied directly to the electrolytic process, thus avoiding the d.c. to a.c. electricity conversion, with equipment cost reduction and increase of efficiency.

INTEGRATION of CHLOR-ALKALI and FUEL CELLS

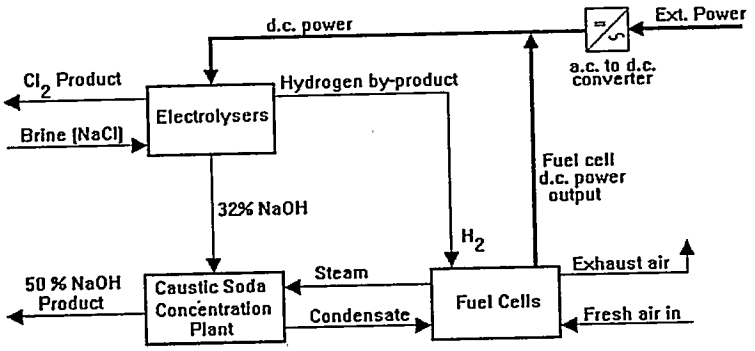

For the above reasons, the chlor-alkali plant of Assemini was identified, among other Italian by-product-hydrogen sources suitable for application of fuel cells, as the most appropriate site for a first demonstration.

The Assemini chlor-alkali plant, located in the island of Sardinia (Italy), is owned by EniChem, the greatest Italian chemical company. It adopts monopolar membrane electrolysers, with a total capacity of 170.000 t/year chlorine, 150.000 t/year caustic soda, with by-product hydrogen production around 6300 Nm3/h, now almost totally burned in the plant boiler.

Basing on such hydrogen flowrate, fuel cell capacity is dimensioned to 9 MW d.c., constituted by 10 x 900 kW d.c hydrogen modules. The Assemini Fuel Cell Plant is planned to generate yearly about 68 GWh electricity, and 62.000 t of steam from 48 million Nm3 of hydrogen.

The project cost is estimated around 28 million USD. It will be founded by private capital and banking, and partially by government subsidies. First fuel cell modules are scheduled for delivery in early 1998, with immediate start-up and operation of each module, after installation and a short testing period. The plant will be completed in 1999, when full capacity will be reached.

THE LOW-TEMPERATURE PARTIAL-OXIDATION REFORMING OF FUELS FOR TRANSPORTATION FUEL CELL SYSTEMS

R. Kumar, S. Ahmed, and M. Krumpelt
Electrochemical Technology Program
Chemical Technology Division
Argonne National Laboratory
Argonne, IL 60439

Introduction

Passenger cars powered by fuel cell propulsion systems with high efficiency offer superior fuel economy, very low to zero pollutant emissions, and the option to operate on alternative and/or renewable fuels. Although the fuel cell operates on hydrogen, a liquid fuel such as methanol or gasoline is more attractive for automotive use because of the convenience in handling and vehicle refueling. Such a liquid fuel must be dynamically converted (reformed) to hydrogen on board the vehicle in real time to meet fluctuating power demands [1]. This paper describes the low-temperature Argonne partial-oxidation reformer (APOR) developed for this application. The APOR is a rapid-start, compact, lightweight, catalytic device that is efficient and dynamically responsive. The reformer is easily controlled by varying the feed rates of the fuel, water, and air to satisfy the rapidly changing system power demands during the vehicle's driving cycle.

Reforming Processes

Hydrogen may be produced from fuels by either steam reforming or partial-oxidation reforming. In a steam reformer, the fuel (hydrocarbon, alcohol, etc.) is reacted with steam over a catalyst at a high temperature and pressure. The reaction is endothermic, and the heat of reaction is provided by the combustion of fuel and transferred to the process gas across a metal wall. Because of the indirect heat transfer, steam reformers are heavy, bulky, slow to start, and slow to respond to load changes. In a partial-oxidation reformer, part of the fuel is oxidized to provide the energy for the reforming reaction within the process gas. The direct heat transfer makes such a reformer compact, lightweight, and dynamically responsive. The addition of a suitable catalyst can be used to influence the product gas composition. The steam reformer is relatively complex, since it contains burners, extended heat transfer surfaces, and combustion air and exhaust duct work. The partial-oxidation reformer is mechanically simple due to the absence of these components.

Fuel Cell Systems

Figure 1 shows greatly simplified schematic diagrams for two fuel cell systems, one with a steam reformer and one with an APOR [2]. In the system with a steam reformer, the fuel and water are fed to the reformer, the temperature, humidity, and contaminant levels in the reformate are adjusted (not shown), and the fuel gas is then fed to the fuel cell stack, where 80–85% of the hydrogen is electrochemically oxidized to generate electricity. The exhaust fuel gas is recycled to the burner to provide the energy for fuel reforming. In the system with the APOR, the fuel, water, and air are fed to the reformer, and the reformate (after appropriate conditioning) is fed to the fuel cell stack; the spent fuel gas is not recycled to the reformer, although a catalytic burner (not shown) is used to avoid venting hydrogen to the environment.

The dynamic response of a steam-reformed, methanol-fueled, polymer electrolyte fuel cell system has been analyzed [3]. Different turn-down scenarios (from steady-state at the design point) were analyzed. In one, the flow rates of the fuel gas and air were ramped down while maintaining fuel utilization (u_f) constant at 85%. For a 50% reduction in power level, the simulation showed that the reformer catalyst overheated within a few seconds. One solution to alleviating this problem is to inject additional water into the process gas just ahead of the reformer. However, if the fuel gas flow rate is not decreased in concert with the decrease in fuel cell power, combustion of the excess hydrogen in the spent fuel gas at the reformer burner rapidly leads to unacceptably high reformer catalyst temperatures. These scenarios are discussed in detail in reference [3].

The dynamic response of the APOR is excellent. Power transients are accommodated simply by varying the feed rates of fuel, water, and air to the APOR. The product gas flow rate responds almost instantaneously, while its composition remains essentially constant. The reactor temperatures (and, therefore, the reaction chemistries and kinetics) are not significantly affected by changes in the fuel processing rate. Thus, the process control for the APOR is analogous to that of the fuel injection systems used in today's cars.

The calculated steady-state efficiencies of the two systems (fueled with methanol) are shown in Fig. 2. At a u_f of 85% or greater, the efficiency of the system with the APOR exceeds that of the steam reformer system. In automotive applications, the APOR system will be more efficient even at a lower u_f because the efficiency of the steam-reformer system decreases under fluctuating power demands [1]. The efficiency of the fuel cell system with the APOR is largely unaffected by power transients.

Argonne's Partial-Oxidation Reformer for Methanol

In the methanol APOR, hydrogen is generated by a combination of the exothermic partial-oxidation reaction, the endothermic decomposition and steam-reforming reactions, and the water-gas shift reaction:

$$CH_3OH(\ell) + \tfrac{1}{2}O_2 \rightarrow 2H_2 + CO_2 \qquad \Delta H_{298} = -155\ \text{kJ} \qquad (1)$$

$$CH_3OH(\ell) \rightarrow 2H_2 + CO \qquad \Delta H_{298} = +128\ \text{kJ} \qquad (2)$$

$$CH_3OH(\ell) + H_2O(\ell) \rightarrow 3H_2 + CO_2 \qquad \Delta H_{298} = +131\ \text{kJ} \qquad (3)$$

$$CO + H_2O(\ell) \rightarrow H_2 + CO_2 \qquad \Delta H_{298} = +3\ \text{kJ} \qquad (4)$$

The overall methanol-reforming reaction in the APOR may be written as:

$$CH_3OH + x(O_2 + 3.76N_2) + (1-2x)H_2O \rightarrow (3-2x)H_2 + CO_2 + 3.76xN_2 \qquad (5)$$

where x is the oxygen-to-methanol molar ratio, and $(1-2x)$ is the theoretical amount of water required to completely convert CO to CO_2. The energy released (or absorbed) by reaction (5) depends on the value of x. At $x = 0$, reaction (5) becomes the endothermic steam-reforming reaction (3); at $x = 0.5$, reaction (5) becomes the exothermic partial-oxidation reaction (1). Reaction (5) becomes thermally neutral at $x \approx 0.23$. To provide for the sensible heat in the reformate and the heat loss from the reactor, the operating oxygen-to-methanol ratio is a little higher than that needed for thermal neutrality.

The bench-scale APOR built and tested in our laboratory is shown schematically in Fig. 3 [4]. It consists of a cylindrical reactor packed with a copper-zinc oxide catalyst (both pellet and honeycomb catalyst structures have been tested). Methanol and water are injected as a fine spray (by using an ultrasonic nozzle) into a down-flowing air stream. The fuel-water-air mixture flows past a nichrome wire "igniter," which vaporizes a small amount of the methanol. The methanol is oxidized on the surface of the catalyst, and the heat generated rapidly raises the temperature near the inlet end of the catalyst bed to ≈500°C; methanol decomposition, steam-reforming, and the water-gas shift reactions then decrease the temperature to ≈200°C at the reactor exit. The reformate contains ~50% H_2, ~1% CO, and no CH_4 (see Fig. 4). The APOR needs no external heating or cooling. The reformate from the APOR can be fed to a phosphoric acid fuel cell as is, but it must be conditioned (e.g., preferential oxidation to reduce CO plus water injection to cool and humidify) before being fed to a polymer electrolyte fuel cell.

Discussion

A big advantage of the APOR over the more conventional steam reformer arises from the absence of indirect heat transfer, thus avoiding the weight and volume of the heat exchange components in a steam reformer. For example, the weight and volume of the methanol steam

reformer in the transit bus powered by a 50-kW phosphoric acid fuel cell are 266 kg and 415 L, respectively [5]; the corresponding values for the APOR are less than 35 kg and 25 L.

Because the mass (and the corresponding thermal mass) of the APOR is lower than that of the steam reformer, the time and fuel consumed during reformer start-up are reduced by at least one order of magnitude. Figure 5 shows that in the APOR, significant hydrogen is produced in less than two minutes; the steam reformer on the fuel cell bus requires at least 30 minutes.

The reformate from the APOR does have a lower H_2 concentration than that from a steam reformer (50% rather than 70–75%), leading to a small decrease (~10 mV) in cell voltage. Another disadvantage of the APOR is that the fuel cell anode must accommodate a 50% greater flow rate, requiring wider flow passages and leading to a decreased power density of the fuel cell stack. The reduced power density is offset, however, by the comparative simplicity of the fuel cell system using the APOR instead of a steam reformer. Simplifications include elimination of the recycle loop and the reformer burner, as well as the air and fuel preheater and/or vaporizer.

The APOR uses the copper-zinc oxide catalyst in the oxidized form, which does not sinter easily and can withstand high temperatures without degradation. The catalyst needs no activation before use, nor sequestration between uses, and may routinely be heated to 500°C or greater. The steam reformer uses a similar catalyst, but in a reduced form; the catalyst must be kept isolated from air, which would reoxidize it and render it ineffective. Also, the reduced catalyst sinters readily, and temperatures above ~280°C must be avoided.

Hydrocarbon Reforming

There is a great deal of interest in operating fuel cell vehicles on conventional gasoline and diesel fuels. The APOR concept has been used to reform the simple hydrocarbons octane and pentane as surrogates for such fuels. Preliminary tests with selected catalysts have yielded H_2 concentrations >40%. Research to develop improved catalysts is continuing.

Conclusion

Argonne's partial-oxidation reformer is a compact, lightweight, rapid-start, and dynamically responsive device to convert liquid fuels to H_2 for use in automotive fuel cells. An APOR catalyst for methanol has been developed and tested; catalysts for other fuels are being evaluated. Simple in design, operation, and control, the APOR can help develop efficient fuel cell propulsion systems.

Acknowledgment

This research was supported by the U.S. Department of Energy, Office of Advanced Automotive Technologies in the Office of Transportation Technologies, under contract number W-31-109-Eng-38.

References

1. "Reformers for the Production of Hydrogen from Methanol and Alternative Fuels for Fuel Cell Powered Vehicles," R. Kumar, S. Ahmed, M. Krumpelt, and K. M. Myles, Argonne National Laboratory Report ANL-92/31, 1992.
2. "Fundamentals of Fuel Cell System Integration," M. Krumpelt, R. Kumar, and K. M. Myles, *Journal of Power Sources*, 49, 37–51 (1994).
3. "Dynamic Response of Steam-Reformed, Methanol-Fueled, Polymer Electrolyte Fuel Cell Systems," H. K. Geyer, R. K. Ahluwalia, and R. Kumar, *Proceedings of the 31st Intersociety Energy Conversion Engineering Conference IECEC 96*, August 11–16, 1996, Washington, DC, Vol. 2, pp. 1101–1106.
4. "Fuels Processing for Transportation Fuel Cell Systems," R. Kumar and S. Ahmed, *Proceedings of the First International Symposium on New Materials for Fuel Cell Systems*, July 9–13, 1995, Montreal, Canada, pp. 224–238.
5. "Research and Development of a Phosphoric Acid Fuel Cell/Battery Power Source Integrated in A Test-Bed Bus," Phase II Final Report HPC-0144, H-Power Corp., Belleville, NJ, May 30, 1996, p. 24.

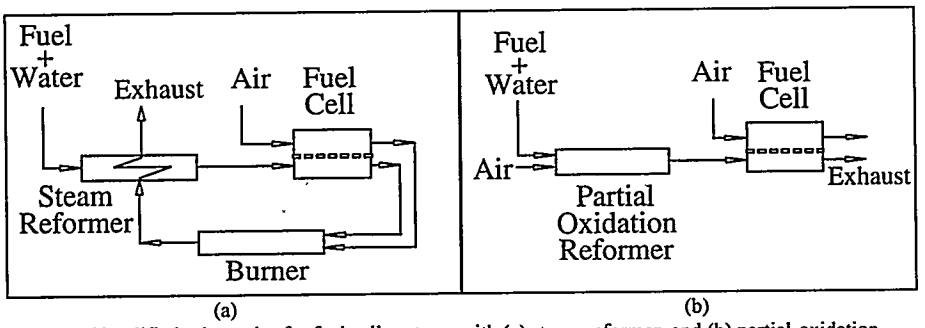

Fig. 1. Simplified schematics for fuel cell systems with (a) steam reformer, and (b) partial-oxidation reformer to convert liquid fuel to hydrogen for use in the fuel cell stack.

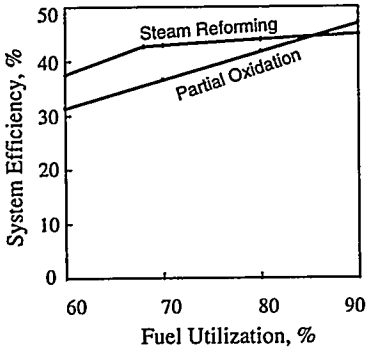

Fig. 2. Effect of fuel utilization on efficiencies of the two systems shown in Fig. 1.

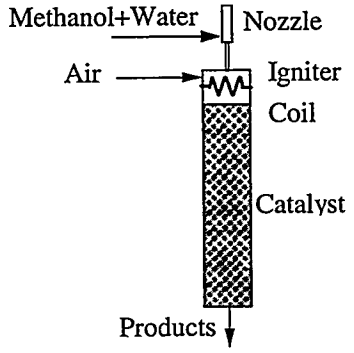

Fig. 3. Schematic of the APOR.

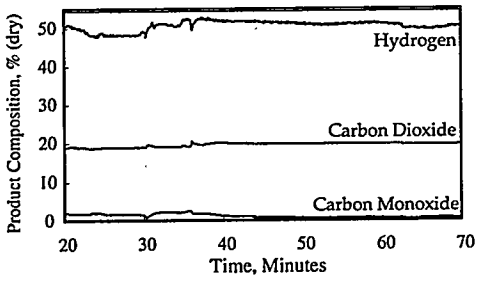

Fig. 4. Typical reformate composition from the APOR.

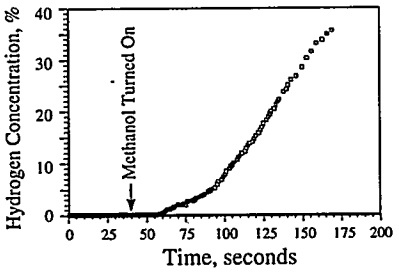

Fig. 5. Hydrogen production from the APOR during cold-start.

A POUND OF PREVENTION: AIR POLLUTION AND THE FUEL CELL

Barry L. Johnson
Agency for Toxic Substances and Disease Registry
Atlanta, GA
and
Robert Rose
Fuel Cells 2000
Washington, DC

The expanded use of fuel cells in transportation and power generation is an exciting proposition for public health officials because of the potential of this technology to help reduce air pollution levels around the globe. Such work is about prevention -- prevention of air emissions of hazardous substances. Prevention is a key concept in public health. An example is quarantine, which aims to prevent the spread of a disease-causing organism. In the environmental arena, prevention includes cessation of pollution.

Air pollution prevention policies also have a practical impact. Sooner or later ideas on technology, especially new technology, must be sold to policy makers, legislators, and eventually the public. Advocating technologies that will improve human health and welfare can be an effective marketing strategy.

We believe that the health and environmental potential of fuel cells is substantially underestimated by most analysts. While our focus is on the motor vehicle, an analysis similar to the one that follows is possible for stationary power generation, where "nontraditional" pollutants such as mercury are emerging as substantial public health concerns.

The air pollution story developed with considerable uncertainly about whether health effects might manifest. There were plenty of doubters -- especially in the automobile industry, which argued that their emissions could not be a problem to human health, or could be ameliorated, by taking advantage of the dilution effect of ambient air. Of course, these arguments were advanced in the mid-1960s, when there were only 90 million cars and trucks in the U.S. Today, there are 200 million, and we drive 2.3 trillion miles every single day. Given the trend, the new fuel cell technology appears to us to be the savior not only of our air quality but of our auto industry.

The argument of regulated industries can be summarized as The Solution to Pollution is Dilution. This fallacious maxim has had incalculable adverse consequences. Pollutants are still being dumped into waterways, the air, and soil. We and the other species on the planet continue to suffer the consequences. Our maxim must change: The Solution to Pollution is Diminution.

THE CAR CONUNDRUM. Access to personal transportation has characterized much of human endeavor. Today, even in the remotest corners of the world, internal combustion engines provide unprecedented personal mobility and demand continues to increase. In 1965 there were 178 million vehicles worldwide. Today, there are well more than 600 million; nearly 50 million new vehicles are produced every year. From the public health perspective, that means 50 million new pollution sources, and an exploding infrastructure that adds additional poisons to the environment. A new car built to U.S. emission standards will emit a ton of pollution during its life. An uncontrolled car will emit two to three times that. Many diseases or conditions involving various organ systems are affected by motor vehicle related pollution.

1. **"Criteria" pollutants** (see chart). While many inhaled pollutants have direct respiratory consequences, others affect the heart or nervous system. Pollutant exposure may alter normal activities and life-style. Within the respiratory tract itself, pollutants derived from motor vehicle emissions have the potential to induce bronchoconstriction, reduce pulmonary function, increase susceptibility to

respiratory infections, and contribute to tumor formation. The health significance of short-term effects is not well understood, and the contribution of repeated, reversible acute effects to chronic damage is not known. Low-level exposures may initiate an inflammatory process leading, for example, to production of excess connective tissue and ultimately to the development of chronic pulmonary disease.

Under the Clean Air Act of 1970, EPA has set national air quality standards for the criteria pollutants and established cleanup programs that have made the worst pollution days better, and accommodated substantial economic growth. But problems remain, and EPA's Clean Air Science Advisory Committee has recommended, based on the latest health studies, that the standards be stronger for ozone smog and fine particulate. Regulated industry is resisting, arguing that the air is "clean enough." Yet approximately 62 million people lived in counties where pollution levels exceeded the national standards for at least one of the six principal pollutants in 1994. That means one of four Americans experienced officially "unhealthful" levels of one or more air pollutants. At the most restrictive end of the CASAC recommended range, closer to 200 million would live in areas classified as unhealthful for ozone smog.

Urban Air Pollutant and Air Quality Standards

Pollutant	Sensitive Population	Effects	Prim. NAAQS	Aver. Time
Ozone (ppm)	Exercising children and young adults	Respiratory symptoms, lung function decrement, decreased exercise capacity	0.12	1 hr
CO (ppm)	Individuals with coronary artery disease	Myocardial ischemia (including angina) during exercise	35 9.5	1 hr 8 hr
NO2 (ppm)	Children, asthmatics	Respiratory symptoms, lung function decrements, increased airway reactivity	0.053	1 yr
SO2 (ppm)	Asthmatics	Respiratory symptoms, decrements in lung function	0.14 0.03	24 hr 1 yr
PM10 (ug/m3)	Respiratory disease sufferers	Increased mortality, respiratory symptoms, decrements in lung function	150 50	24 hr 1 yr
Lead (ug/m3)	Fetuses and young children	Impairment of neural development	1.5	3 mo.

Utell et al., Ann. Rev. Public Health, 15: 157, 1994.

2. Carcinogens. Ambient compounds derived from or related to motor vehicle emissions may cause mutations, result in DNA-adduct formation, and may ultimately be carcinogenic. The mobile air toxics specified in the CAA amendments (acetaldehyde, benzene, butadiene, formaldehyde, and polycyclic organic matter) are of concern mainly because of their potential carcinogenicity. There is a great deal of uncertainty both about the human unit risk estimate and the exposures. IARC concluded that there was sufficient evidence of carcinogenicity in experimental animals of whole diesel exhaust and of extracts of diesel exhaust particles, but limited evidence for the carcinogenicity of diesel exhaust in humans. Overall, diesel engine exhaust was probably carcinogenic to humans, even though epidemiologic evidence has provided only weak support for this proposition. Fuel production and distribution, and secondary products of vehicle exhaust (PAH, fine PM) and driving (e.g. cadmium from tires) add to the toxic brew.

3. Carbon Dioxide. The CO_2 in vehicle exhaust introduces us to a new, and qualitatively different, public health problem. In the long run, it could overshadow all the other air pollution problems (McMichael et al. 1993). In the 1990s there has come a rising awareness of the problems of climate change. Although health researchers have been slow to recognize that these are potential major public health problems, the eco-equation is quite simple: disruption of ecosystems leads to impairment of life-support systems, which threatens the health and survival of all species, including our own species, Homo sapiens. Our good health depends, finally, on those things we most take for granted--clean air, safe water, adequate food, tolerable temperature, stable climate, biodiversity and protection from solar UV radiation.

Much of our traditional environmental health concern has focused on the direct effects of toxicants like sulfur dioxide, nitrogen dioxide, organochlorine pesticides and heavy metals. By contrast, factors like carbon dioxide, methane, and CFC's are not toxic to humans. Nevertheless, in today's overloaded biosphere, the atmospheric accumulation of these factors portends widespread ecological disruption. The ramifications of climate change and of ozone layer depletion are many and varied, and will in turn cause a wide variety of indirect, longer term, effects upon human health and well-being.

It has been said that, globally, motor vehicles generate more air pollution than any other human activity (Walsh 1990). Whereas CO_2 accounts for around 20 percent of the planet's natural greenhouse effect it currently accounts for 60 percent of the superimposed man-made greenhouse effect (WHO 1991). The International Panel on Climate Change has calculated that, to stabilize atmospheric concentrations at 1990 levels, the rate of CO_2 emissions would need to be reduced by 60 percent and that of methane by 15 percent. The IPCC predicts that if emissions continue to grow at the current rate, a temperature rise of about 0.3. degrees C per decade would occur. Some forecast effects of global warming include:

- Direct thermal effects. During the next century, the number of heat wave days in temperate and sub-tropical climates is forecast to double.
- Stronger winds and cyclones from greater heat differentials. Increased floods and ocean storm surges.
- Change in the distribution of insects and other vectors for infectious diseases. Many species of mosquito will tend to spread as higher latitudes become warmer and wetter.
- Weather- and temperature-related damage to crop germination and growth. Increases in background temperature, and altered season rainfall are expected to reduce the yield of some of the world's most productive grain-growing temperate regions.

Our global dependence on fossil fuels must abate if CO_2 levels are to be significantly lowered. A less polluting form of transportation must replace fossil fuel-powered vehicles. The electric vehicle offers great promise if developed in ways that acknowledge environmental goals.

THE FUEL CELL OPTION. Electric vehicles, for many reasons, offer the promise that we can avoid a doomsday scenario where we can maintain our personal mobility only at the sacrifice of public health. Electric vehicles once led the race to provide personal mobility. By the turn of the 20th century, electric cars had found wide favor, especially among women, as a choice for transportation. Women, it is alleged, found the electric car to be clean, reliable, and relatively easy to operate. Yet the electric car was soon to be doomed. The internal combustion engine, even though far less reliable than the electric car, permitted longer range transportation and the promise of greater power and speed. And that is essentially where we are today.

"Greener fuels" are becoming increasingly common in the industrialized countries as a means to combat air pollution. But will changes in fuel provide the improvement in air quality that is needed? It is likely not to be THE answer, but part of a larger environmental strategy that will combine several methods to reduce pollution emitted from vehicles. We believe electric vehicles must be part of the

environmental improvement calculus, and that fuel cells are likely to win the EV power train competition.

Hydrogen fueled fuel cell vehicles are truly zero emission. Fuel cell vehicles with on-board equipment to convert fuel such as methanol to hydrogen do yield emissions, but these are expected to be small. Tests in California are under way to quantify them. Both fuel cell vehicles and battery electric vehicles have a large advantage over even the cleanest conventional vehicles. And while the difference between battery electric vehicles and fuel cell vehicles may seem small, it would mean a difference of more than 13,000 tons of NOx annually if calculated based on the Los Angeles Basin's nine million cars, and Los Angeles has a very low-polluting electricity generation infrastructure. Elsewhere in the U.S. the difference would be larger by a factor of two or three.

PREMIER EXAMPLE OF ENVIRONMENTAL DISEASE PREVENTION. This paper is about pollution, prevention, and public health. There is no better example of a situation that unites these themes than the removal of lead from gasoline. Tetra alkyl lead compounds as fuel additives to reduce engine knock produce lead oxide particulates. An unequivocal success in motor vehicle emissions control has been the near elimination of these emissions. Unleaded gasoline was essential to the introduction of catalyst control technology. The use of tetra alkyl lead compounds in motor fuel ended completely in 1993. The concomitant reduction of ambient lead levels and blood lead levels in the U.S. population is, we think, a classic in the environmental health literature. The data show quite dramatically that lead in people declines as lead is reduced in the environment, primarily from banning lead in gasoline.

What are the prevention benefits of all this? Quite simply, there is overwhelming evidence that low levels of lead in young children will reduce intelligence, impair the synthesis of heme, impair hearing ability, and cause developmental and cognitive delays. There is also published literature that associates children's lead exposure with later-life social dysfunction. Preventing these serious health and social consequences of lead is both cost and socially beneficial.

Prevention of lead exposures has become an international imperative. The environment ministers of 26 nations have committed their governments to fight the noxious effects of lead through cutting back use, tightening regulations and working with industries. The agreements signed include a political statement and a plan for action, but they are not legally binding and depend on the voluntary cooperation of industry. Many industrialized countries, including the U.S., have phased out lead as a gasoline additive. But in many developing nations, including China and India, traffic is now the largest source of lead dust. Fuel cell vehicles have a role to play even here, because they operate on lead-free fuels.

CONCLUSION. There is ample evidence that environmental quality, particularly air quality, is being degraded by pollution from internal combustion vehicles. The known adverse health effects of air pollutants and the damage to the ecosystem compel us to seek ways to improve environmental quality. The use of the fuel cell as a means for powering transportation vehicles holds great promise as part of a larger effort to reduce pollution levels globally.

FUEL CELLS FOR TRANSPORTATION: STATUS, OPPORTUNITIES AND CHALLENGES

Alan C. Lloyd, Ph.D.
Desert Research Institute, Energy and Environmental Engineering Center
P.O. Box 60220, Reno, Nevada; 89506-0220
Jonathan H. Leonard
South Coast Air Quality Management District, Technology Advancement Office
2185 Copley Drive, Diamond Bar, California 91765-4182.

Overview

Environmental issues will become important drivers influencing technology in the years ahead. For example, air quality legislation and regulation - locally, regionally, and globally - will continue to play an increasing role in influencing decisions made in choosing a particular energy source. Health concerns related to ambient fine particles (1) and the ongoing debate on global climate change and the need to reduce CO_2 emissions are two examples of the nexus between energy and the environment. Additionally, as conventional sources of energy and petroleum become depleted and as political issues remain, desires for energy diversity and energy security will require a menu of technologies and fuels.

It is recognized that many of the renewable and environmentally benign fuels and energy sources are expensive and that economics will play a key role in dictating which of these is going to be most successful. For example, generating hydrogen from wind or solar is expensive compared to conventional technologies and price competition is likely to be more intense in the area of electricity de-regulation (2). However, the cost of conventional fuels are also increasing because of a desire to clean them up or a desire to change their chemical and physical properties through partial oxidation or steam reforming. These additional treatments lead to increased costs so that the gap between the "clean" fuels and cleaning up conventional fuels becomes much narrower.

Practical Experience for Fuel Cells for Transportation

During the last two years, it is fortunate that some real world experience has been gained with fuel cells in the transportation sector. The majority of this information has been obtained from transit bus operations. Specifically, from two bus programs. First, the phosphoric acid fuel cell (PAFC) bus program developed under funding by the Department of Energy, Department of Transportation and the South Coast Air Quality Management District. This program featured a wetland reference coupled to the fuel cell, both developed by Fuji Electric Corporation. The 50-kilowatt PAFC stack for these three 30-foot buses operates on methanol reformate and is hybridized with a nickel-cadmium battery pack for peak power assistance and regenerative braking. This "near-zero-emission" technology is taken to the next level of development by a team led by Georgetown University International Fuel Cells using new federal funding.

The second program is the one conducted by Ballard Power Systems. They have developed aggressive commercialization expectations for fuel cell buses, having successfully demonstrated a 120 kW zero-emissions pure-hydrogen PEMFC shuttle bus. They have successfully developed a Phase II bus which is a 40-foot New Flyer bus with an improved and more powerful (250 kW) PEMFC stack. Several 40-foot buses are being built for demonstration programs in at least two cities, Vancouver and Chicago. Other cities are being explored. Progress between phase-one and phase-two of the Ballard program has been impressive and has led to application in a light-duty van being developed by Daimler-Benz. The progress on the Ballard bus technology gives every indication that transit fuel cell buses can be developed in the competitive range within the next three to five years provided costs continue to decrease to the ~ $500 per kW target set by Ballard. This time frame should be sufficient to meet the demands for clean buses in many inner cities, national parks, etc., to reduce public exposure to diesel particulate.

A major challenge facing the development of fuel cell buses in transit operation is to provide the fuel for the fuel cells. The choice offered continues to be a significant issue in talking about fuel cells for transportation. As has been seen with the alternative fuels arena, infrastructure can be the "Achilles heel" in getting technology into the market place. Thus, there is a significant dilemma: - should one concentrate on a fuel which has a readily available distribution network but which does not lead to true zero emissions compared with a very limited network for a fuel (e.g., H_2) which leads to a truly zero emission technology? There continues to be significant debate on the merits of both approaches. It appears that work is being pursued in both of these areas so that real world experience and the market place will dictate the most likely approach.

Applications of fuel cells in the light-duty vehicles are very limited. Daimler-Benz has successfully tested a prototype van using the Ballard fuel cell. The demonstration vehicle uses hydrogen while the production vehicles are expected to use an on-road methanol reformer. It appears that Toyota is also active in full-size fuel cell in a vehicle.

The major focus in the United States on fuel cells has been through the PNGV program in which the major auto manufacturers are adopting different approaches to fuel cells. The status of this program is discussed elsewhere (3).

The choice of fuel for the vehicle is also critical in the light-duty section where the DOE is placing large emphasis on partial oxidation of conventional fuels. This does not address the pressure to reduce CO_2 emissions into the atmosphere. If this becomes a major issue, then every effort should be focused on developing improved methods for the generation, storage and distribution of hydrogen.

California's Requirement for Zero Emission Vehicles

A major impetus for the world wide effort to develop zero emission vehicles was the requirement by the California Air Resources Board (CARB) that two percent of new vehicle sales in 1998 be zero emission. This requirement increased to ten percent by the year 2003. This regulation was changed in 1996 when the 1998 mandate was eliminated but the 2003 requirement was maintained. This decision was made in part because of the lack of the availability of adequate numbers of advanced battery vehicles which would meet the requirements of the general public for their automobiles. This finding is consistent with the comments by Williams (4) in which he indicated that technical progress had not kept pace with the dollars devoted to developing the technology.

While this delay was adversely received by the electric vehicle community and the environmental groups, it could be a positive development for fuel cell vehicles and technology. The additional time until 2003 can be utilized by the fuel cell developers to demonstrate that advances in the technology will provide the range and performance capabilities that the general public expect from their vehicles. Thus, opportunities exist to provide decision makers with evidence that fuel cells technology can compete with battery technology in this arena. Indeed, the CARB has responded to the comments by the fuel cell community and officially includes fuel cells in their menu of likely technologies to meet their zero emissions mandate. Fuel cells vehicles would also overcome the negative comments on battery powered electric vehicles by Lave and colleagues at Carnegie Mellon University (5). These authors argue that the emissions benefits from EV's are negligible and that the use of lead acid batteries may lead to unacceptably high levels of lead in the environment. Such was not the case when the original requirement was set forth in 1990.

Meeting the health related air quality standards is the reason for the CARB EV requirement. It is anticipated that with the expected promulgation of a fine particle standard ($PM_{2.5}$). The expected EPA action will provide the stimulus for various communities to look at every way possible to reduce emissions to attain the standard. Therefore, the potential to utilize truly zero emission technologies is expected to be readily embraced if this technology performs well and can be cost competitive. Reducing, manufacturing costs is a major focus of the DOE and U.S.CAR and various recommendations have been put forward (6). Combined market opportunities will increase volume production and also reduce costs.

In summary, the opportunities and future for fuel cells in the transportation sector appear good. Cost per kW and fuel availability will dictate whether these opportunities can be realized.

1. D.S. Sprentz, et al., Natural Resources Defense Council (1996). *Breath-Taking: Premature Mortality Due to Particulate Air Pollution in 239 American Cities,* Natural Resources Defense Council, New York, NY, 154 pp.

2. Federal Energy Regulatory Commission (FERC), Order 888, April 1996.

3. PNGV Technical Accomplishments, Partnership for a New Generation of Vehicles, United States Council for Automotive Research, July 1996.

4. R. H. Williams, Consumer Reports, September, 1996.

5. Lave, et al., *Environmental Science & Technology,* September, 1996,

6. Proceedings of Fuel Cell Manufacturing Workshop, Dearborn, Michigan, July, 1996,

LEGAL & REGULATORY ISSUES AFFECTING PARTICIPATION IN DISTRIBUTED RESOURCE MARKETS

John T. Nimmons, J.D.
President, John Nimmons & Associates
Olympia, Washington USA 98501

This paper describes recent research co-sponsored by the National Renewable Energy Laboratory and four investor-owned utilities. Its purpose was to investigate how legal and regulatory factors will shape strategic decisions on the roles of utilities and others in the development of distributed resources. The work was performed during 1995 and early 1996 by John Nimmons & Associates, with support from Thomas J. Starrs, Energy & Environmental Economics, and Awad & Singer.

Background

For several years, leading electric, gas and combination utilities in the US and Canada have been evaluating the use of distributed resources ("DR") as a way to reduce utility costs, make better use of utility plant, deliver energy to customers more efficiently, and achieve environmental benefits. Most recently, companies interested in DR have shifted their focus to its potential strategic uses in the competitive environment that is supplanting traditional energy markets in the US and abroad.

The DR concept envisions that traditional utility central station generation, transmission, and distribution will increasingly be supplemented with small, decentralized or "distributed" generation, storage, and demand-side management technologies. In the near term these will include gas and diesel generators and load management devices and, in more remote applications, wind turbines, photovoltaics and possibly other renewables. In the longer term DR will also include fuel cells and batteries. Depending on the technology and the need, distributed facilities might be installed on customer premises, or at substations or other locations on the utility's distribution system. In any case they will be *strategically sited and operated to add value to the utility system beyond traditional energy and capacity.* The added values that make DR attractive can include some combination of customer retention; reduced investment risk; deferred transmission and distribution (T&D) investment; reduced T&D losses; increased system reliability; local environmental benefits; overall system efficiencies; and site-specific economies such as thermal use from cogeneration.

Utility case studies have shown that DR can offer substantial, quantifiable benefits where distributed technologies are carefully selected and placed to match special site characteristics and local T&D needs. Most of those studies have addressed DR economics, evaluation, and planning. They have focused on how to locate valuable sites; whether distributed technologies can yield the benefits hypothesized; how these benefits can be quantified and their value established relative to other investments; and how planning and modeling tools can facilitate DR decisions.

The work described here adds another dimension to these inquiries. It represents a first systematic look at legal, regulatory, and institutional factors that will influence whether DR benefits can be realized in practice; who will capture them; and how DR participants can structure their activities to take advantage of business opportunities in emerging competitive markets.

Why Legal & Regulatory Issues Matter for Distributed Resources

The DR concept departs radically from the central station natural monopoly paradigm on which traditional utility regulation is based. DR benefits do not depend on economies of scale or scope that historically have justified the franchised monopoly and the regulatory system built around it. Instead, they depend on what might be called economies of dispersion, integration, standardization,

and mass production. These economies are available through the use of small modular systems placed close to the loads they serve, selectively matched to site conditions, and easily transported, installed, and operated. These fundamental differences from central station resources alone mean that DR does not fit easily within a legal and regulatory system built on natural monopoly concepts, and that widespread DR implementation will have far-reaching legal and institutional implications for the energy and utility industry.

Beyond that, DR has emerged at a time when federal and state utility law is rapidly shifting from traditional monopoly concepts toward a fully competitive environment for electricity supply. Non-utility power producers and energy service companies serve increasing percentages of markets once served exclusively by regulated utilities. In the US, generation is now recognized as a competitive function. Transmission has been similarly transformed through recent federal initiatives requiring non-discriminatory access to utility transmission and comparable pricing as between transmission owners and others using their systems. State legislators and regulators in more than 45 states are also addressing competition, restructuring, and/or alternative forms of regulation for electric utilities. Some states are already transitioning to "direct access" or retail wheeling regimes, which will allow retail electricity customers to abandon their local distribution utility in favor of other suppliers who offer cheaper, more flexible, and/or higher quality service. These developments are accelerating, so anyone interested in fuel cells or other DR technologies needs to understand their strategic implications for any DR activities they might be considering.

Research Objective & Scope

The research was essentially exploratory. Its objective was to identify and describe key elements of the legal and institutional framework likely to affect DR development. This framework includes barriers, incentives, constraints, and opportunities established by federal and state laws, regulations and agency practices, as well as relations among key stakeholders interested in DR development.

The research scope included federal and state energy and utility legislation, regulations, administrative practices, and judicial decisions. Specifically, it addressed federal and state jurisdiction over DR-related issues; recent federal initiatives on transmission access and pricing and state moves toward performance-based ratemaking; traditional state law and regulatory policies that continue to govern notwithstanding the current restructuring ferment; and federal and state antitrust issues of fundamental importance for DR implementation.

Research Findings

The research found that virtually all of these areas of law and regulation have the potential to impact DR development in important ways. Some of these are highlighted below.

Federal and State Jurisdictional Issues. Federal and state jurisdiction over matters affecting DR is multi-tiered, and jurisdictional boundaries are often uncertain. In general, federal regulators oversee wholesale power sales and transmission by public utilities in interstate commerce (broadly defined) and the facilities used for those purposes, while state regulators supervise retail energy sales and local distribution of energy commodities and services to the public. DR activities may be subject to both federal and state regulation depending on who owns them, what facilities they employ, who their customers are, and how their delivery contracts are structured. In any case, antitrust and anticompetitive principles will overlay many DR activities at both the federal and the state level, and will become more important as competition supplants regulation in the electric industry.

Transmission Access & Pricing. Threshold questions for many considering DR are whether it makes economic sense, and whether it can provide value for energy customers and competitive advantages for energy suppliers. The answers to these questions will be strongly influenced by new federal requirements for non-discriminatory transmission access to be achieved by separating (or "unbundling") the costs of generation, transmission and distribution, and by state moves toward retail access, also involving some form of unbundling.

The research suggested that unbundling can create valuable opportunities for DR to compete with the various unbundled utility functions, and that different forms of unbundling are likely to induce different levels of DR applications. Full retail access in which customers would see completely unbundled rates based on area- and time-specific utility costs, perhaps including environmental costs, could provide the greatest financial incentive for DR implementation by end users.

Performance-Based Ratemaking. A number of state utility commissions have recently taken steps to replace traditional cost-of-service ratemaking with performance-based (or "incentive") ratemaking ("PBR"). The research suggested that PBR in general can offer utilities more powerful incentives for DR than cost-of-service regulation. However, current PBR proposals vary considerably from state to state and utility to utility, and their eventual impact on DR development will depend greatly on how individual commissions and utilities choose to implement them.

Antitrust & Anticompetitive Considerations. Research in this area focused on the extent to which antitrust and anticompetitive concerns might dictate the nature and form of utility participation in DR markets. Because DR does not fit easily within conventional natural monopoly concepts, some have questioned whether regulated utilities should be involved in DR development and deployment at all; and if they should, how to prevent cross-subsidies from monopoly activities or unfair use of monopoly assets to disadvantage competitors. These questions have arisen in analogous situations involving other types of utility activities. The research suggests that the application of antitrust principles to these situations offers important lessons for utility DR participation, and that these principles will fundamentally shape the roles and business strategies available to utilities, their affiliates, and their competitors in DR development.

Federal antitrust laws, and many state laws patterned after them, apply to utilities as they do to other commercial entities. Historical doctrines immunizing regulated utilities from antitrust exposure offer protection only where the challenged activities are undertaken pursuant to state legislative or regulatory policy that is clearly articulated and affirmatively expressed, and are subject to active supervision by state regulators. Immunity is unlikely where utilities voluntarily initiate activities in markets that are or can be essentially competitive, and that extend beyond conventional natural monopoly markets.

This suggests that antitrust immunity is more likely for certain kinds of DR applications than others. DR applications more likely to be immunized are those that can be characterized as distribution system investments rather than generation, since the distribution system is expected to remain part of the regulated monopoly franchise under most restructuring scenarios. Examples might include a fuel cell installed at a substation operating near capacity that allows the utility to provide additional effective capacity while deferring or avoiding the cost of upgrading the substation, or a photovoltaic system installed on residential rooftop that reduces the customer's effective peak demand. Although these applications involve technologies that generate electricity, they provide substantial value to the distribution system and can reasonably be treated as monopoly distribution rather than competitive generation investments.

Where immunity is unavailable, courts and regulators have invoked antitrust law and anti-competitive principles to guard against two principal concerns. One is to protect utility ratepayers against the use of monopoly assets to cross-subsidize the utility's competitive activities at ratepayer expense. The other is to protect competitive markets against the unfair effects of such abuses. Both concerns can give rise to antitrust claims, usually under the federal Sherman Antitrust Act, but also under other federal and state laws designed to preserve competition.

Conventional Sherman Act claims of monopolization and attempted monopolization will be hard for challengers to establish during the early stages of any utility DR implementation. However, the theory of "monopoly leveraging", where courts have accepted it, requires a lower standard of proof, increases potential exposure to claims, and creates additional uncertainty over the permissible extent of utility participation in competitive markets. Even where leveraging has been rejected as a basis for Sherman Act liability, its underlying principles may be invoked in regulatory proceedings to constrain utility DR activities.

The research found that in analogous telecommunications cases, courts and regulators have responded to the use of monopoly power in a utility's core markets to erect barriers in competitive markets, by requiring strict separation of monopoly from competitive activities. At a minimum they have required separate accounting. In some cases they have required structural separation into legally distinct corporate entities operating independently and at arms' length from each other. Whether and under what conditions such requirements might be applied to energy utilities engaging in DR activities are open questions at this point, but they deserve serious consideration when developing business strategies for DR implementation.

State Public Utility Law Issues. The research found that state public utility laws may dictate results quite at odds with antitrust doctrines favoring separation of DR activities from the regulated utility, and could actually result in commission regulation of entities pursuing DR activities that are arguably competitive. These laws are especially relevant to DR facilities located on customer sites, and those furnishing energy offsite to someone other than the facility owner.

State utility laws will determine whether entities that own, control, manage, and/or operate DR facilities will be treated as public utilities subject to state commission regulatory jurisdiction. These laws specify what commodities and services are covered; they require service "to the public" to trigger regulatory jurisdiction; and they establish exemptions for specified resources and service configurations. Statutory, administrative and judicial definitions on each of these subjects vary considerably from state to state, and such variations often determine whether those who engage in DR activities will or will not be subject to the burdens and benefits of public utility regulation.

State law sometimes affords considerable flexibility to structure DR projects in ways that either invite or avoid regulation (for example, through the choice of resources and/or customers, the scope of distribution, the nature of contractual arrangements between the supplier and its customers, etc.). It is therefore important to carefully analyze individual state laws governing specific DR facilities and service configurations to ensure the desired outcome in particular cases.

Conclusion

A wide range of legal and regulatory factors will directly impact utility participation in DR markets and the opportunities available to utilities and others to compete in those markets. Understanding these factors is critical to structuring successful DR ventures.

DOD FUEL CELL DEMONSTRATION PROGRAM

Franklin H. Holcomb, Michael J. Binder, and William R. Taylor
U.S. Army Construction Engineering Research Laboratories
Champaign, IL 61826-9005

INTRODUCTION

The supply of reliable, cost-effective electric power with minimal environmental impact is a constant concern of Department of Defense (DOD) installation energy personnel. Electricity purchased from the local utility is expensive and represents only about 30% of the original energy input at the generating station due to generation and distribution inefficiencies. Because of master metering and large air conditioning loads, the demand portion of the installation's electric bill can be in excess of 50% of the total bill.

While the electric utilities in the United States have a very good record of reliability, there is significant potential for improving the security of electrical power supplied by using on-site power generation. On-site, dispersed power generation can reduce power outages due to weather, terrorist activities, or lack of utility generating capacity. In addition, as increased emphasis is placed on global warming, acid rain, and air pollution in general, the development of clean, highly efficient power producing technologies is not only desirable, but mandatory. Since the majority of central heat plants on U. S. military installations are nearing the end of their useful life, there is an opportunity to replace outdated existing equipment with modern technologies.

THE TECHNOLOGY

Fuel cells are electrochemical power generators with the potential for attaining very high electrical energy conversion efficiencies while operating quietly with minimal polluting emissions. In addition, by-product thermal energy generated in the fuel cell is available for use for cogeneration of hot water or steam, bringing the overall potential conversion efficiency (electrical plus thermal) to approximately 85%. Air emissions from fuel cells are so low that several Air Quality Management Districts in the United States, including several in California which has the nation's strictest limits on air pollutants, have exempted them from requiring a permit to operate.

Phosphoric Acid Fuel Cells (PAFCs) are in the initial stages of commercialization. While PAFCs are not economically competitive with other more conventional energy production technologies at the present time, current cost projections predict that PAFC systems will become economically competitive within the next few years as market demand increases.

THE FY 1993 DOD FUEL CELL DEMONSTRATION PROJECT

The FY 1993 Defense Appropriations Act provided $6.0M worth of equipment procurement funds per Service for the implementation of "non-developmental item natural gas fuel cells currently in production in the United States ... for power generation at military installations ... " with the recommendation that "... some of the cells be installed at locations in need of enhanced air quality ...". The purposes of this demonstration project are to stimulate growth in the fuel cell industry, which will lower costs through economies of scale and competition, and to determine the role fuel cells should play in DOD long-term energy supply strategy. The three Services, acting through the Defense Utilities Energy Coordinating Council (DUECC), requested that the U. S. Army Construction Engineering Research Laboratories (USACERL), a U. S. Army Corps of Engineers research laboratory affiliated with the University of Illinois at Urbana-Champaign, coordinate this fuel cell demonstration program for all three Services. Specific tasks associated with USACERL's coordination role in this program include the following: (1) Procurement of turnkey Phosphoric Acid Fuel Cell Power Plant packages: (2) Evaluation of potential DOD site installation candidates

in order to identify the specific sites where the PAFCs will be installed; (3) Monitoring of the electrical generation efficiency, degree of thermal utilization, air emission characteristics, and overall system reliability of the PAFCs to determine the economic and environmental benefits of owning and operating these systems: (4) Development of application guidelines based on the results of this project for the implementation of PAFC technology at DOD facilities; and (5) Documentation of all aspects of the entire DOD Fuel Cell Demonstration Project.
A solicitation was prepared for the purchase of turnkey Phosphoric Acid Fuel Cell Power Plant packages, to include purchase, site engineering, installation and startup, operation and maintenance training, and a five year warranty, maintenance and repair period. Following a negotiation period, ONSI Corporation was awarded a contract for the purchase of these turnkey PAFC systems. The terms of this contract involve cost-sharing on the part of ONSI Corporation and calls for partnering with the local utility serving the selected posts. A total of 12 200-kW PAFCs were purchased with the FY 1993 Appropriations and have been, or will be, installed at DoD installations, with specific installation sites being identified through contract modifications.

SITE SELECTION CRITERIA

Initial candidate sites were identified by Army, Air Force, and Navy/Marine Corps Headquarters through solicitation of their respective Major Commands/Major Claimants. As awareness of the program grows, individual installations are requesting to become a part of this program. Initial screening of candidate sites is performed through an economic analysis based on total electricity and natural gas usage and average unit costs as provided by the Defense Energy Information System(DEIS). This economic analysis considers the electrical savings available through operation of a fuel cell power plant. the associated natural gas costs to operate the system, and the natural gas savings obtainable through recovery of the by-product thermal energy.

Installations which appear to be good potential candidates as a result of this initial screening are then asked to submit copies of their actual past utility bills for a twelve month period in order that the economic analysis can be refined through the use of actual monthly energy consumption and utility rate schedule data. In addition, each candidate installation is asked to provide information regarding the degree of air quality attainment for the region in which they are located, as well as a description of the intended application for the recovered by-product thermal energy and an estimate of the amount of this recovered thermal energy which they could use. At the same time, potential opportunities for financial leveraging through cost sharing and/or rebates by the local utilities providing service to these candidate sites are investigated. Efforts are also made to insure equal distribution of fuel cell installation sites among the three Services, and to provide as wide a geographical and climatic distribution as feasibility allows.

Site visits are then made to those installations which still appear to be good potential candidate sites at the end of this evaluation process. These site visits allow for refinement of the estimate of by-product thermal energy usage, an analysis of the logistical factors surrounding potential fuel cell installation (e.g. distance from gas line, lengths of pipe and wiring runs, availability of sufficient land space for siting, etc.), and the development of a conceptual design package. The successful candidate sites are then identified to the ONSI Corporation to be selected installation sites through individual contract modifications. A kickoff meeting is held on site shortly after each contract modification to initiate the design and installation process.

CURRENT STATUS

PAFCs have been installed and are operational at Vandenberg Air Force Base, CA, Natick

Research, Development and Engineering Center, MA. Newport Naval Education Training Center, RI, the 934th Tactical Air Group, Minneapolis, MN, Kirtland Air Force Base, NM, Twenty-Nine Palms Marine Corps Base, CA, Nellis Air Force Base, NV, Camp Pendleton, CA, Ft Eustis, VA, U. S. Military Academy, West Point, NY, and Picatinny Arsenal, NJ. A PAFC is also slated for installation at the Galley at the U. S. Naval Academy, Annapolis, MD during 1996 as part of an overall building renovation project.

Of the 10 operational fuel cells being monitored, the first came on-line in February 1995 and the last in December 1995. As of 31 January 1996 (after nearly one year), the fleet had logged over 40,000 hours of operation. The unadjusted fleet availability was 89%. In early 1996 after one unit experienced water chemistry problems related to local conditions, some units were intentionally shut down while the problem was being investigated. Adjusting for these intentional shutdowns, the fleet of 10 units has an adjusted fleet availability of approximately 88% as of 30 June 1996; with over 52,000 hours of operation.

THE FY 1994 DOD FUEL CELL DEMONSTRATION PROJECT

The FY 1994 Defense Appropriations Act provided $6.25M worth of equipment procurement funds per Service "to continue procurement of nondevelopmental item (NDI) 200 kW phosphoric acid natural gas fuel cells currently in production in the United States". USACERL was again requested to coordinate this demonstration program for all three Services. Negotiations were conducted with ONSI Corporation leading to a contract for the purchase of 15-25 turnkey Phosphoric Acid Fuel Cell Power Plant packages similar to those which were purchased with the FY 1993 Appropriation. The following sites have been selected for PAFCs: 911th Airlift Wing, Pittsburgh, PA; Naval Air Station (NAS), Jacksonville, FL; NAS Fallon, NV; Laughlin AFB, TX; Watervliet Arsenal, NY; Fort Huachuca, AZ; Fort Richardson, AK; Westover ARB, MA; Little Rock AFB, AR; Stennis Space Center, MS; Davis-Monthan AFB, AZ; Edwards AFB, CA; Fort Bliss, TX; Pine Bluff Arsenal, AR; Port Hueneme, CA; Barksdale AFB, LA; and NDCEE, PA. Installation of these PAFCs are expected in 1997.

Congress has also appropriated $1.25M worth of FY 1994 research and development funds through the Advanced Research Projects Agency (ARPA) to accelerate research efforts focusing on technological improvements to reduce PAFC production costs on a cost-sharing basis. This program is also being managed by USACERL. A Broad Agency Announcement (BAA) was issued soliciting proposals for research activities which address improved component development, system integration, and/or manufacturing processes leading to reduced production costs for phosphoric acid fuel cells which operate on pipeline natural gas. A contract was awarded in December, 1994 to International Fuel Cells Corporation to support research activities which they proposed in response to this BAA. This effort is currently ongoing.

DEMONSTRATION OF 5MW PAFC POWER PLANT

Yutaka Usami
Phosphoric Acid Fuel Cell Technology Research Association (PAFC-TRA)
3-3-3, Tenjinbashi, Kita-ku, Osaka 530, Japan

Toshio Takae
New Energy and Industrial Technology Development Organization (NEDO)
3-1-1, Higashiikebukuro, Toshima-ku, Tokyo 170, Japan

Introduction

Phosphoric Acid Fuel Cell Technology Research Association, established in May 1991 by Japanese 10 electric power and 4 gas companies, started a new project in 1991FY, with the object of PAFC realization and aiming the development of 5MW-class PAFC power plant for urban energy center and 1MW-class power plant for onsite use. This project is carried out as 6 years plan jointly with New Energy and Industrial Technology Development Organization. The targets of the project are to evaluate and resolve the development task, such as a high reliability, compactness and cost reduction throughout the engineering, manufacturing and field testing of PAFC power plants.

PAC tests and power generating test operations of 5MW plant were completed in 1994. Conducting the 2 years continuous operations and studies since 1995, the plant operational performance, system control characteristics, waste heat recovery and environmental advantage will be demonstrated.

Development of 5MW Plant

Engineering of 5MW plant, manufacturing and installing of the major components except the cell stack assemblies and inverter were completed in 1991 and 1992, respectively. Inverter was produced and set up in 1993, cell stack assemblies were also made in 1993 and introduced in January 1995, after the PAC tests completion. In PAC tests, carried out since August 1994, temperature, pressure, flow rate and compositions at each location were tuned with the components in operation.

The initial power generation was performed in February 1995, 5MW plant passed the Japanese MITI inspection at rated load in March 1995 after the control system adjustment tests. Demonstrational operations and studies have been continueing from April 1995.

Concept and Structure of 5MW Plant

Considering a dispersed power source placed in an urban energy center, 5MW plant was developed based on the following concept:

- Dispersed power source settled in urban areas
- High efficiency power plant
- An advantage in environment
- Effective use of waste heat

Major structual features of 5MW plant were listed next:

- Adopted large capacity, area and high current density cell stacks
- A large axi-symmetric mono tube type reformer was chosen
- Air compressor and gas turbine were separatedly used

Process flow diagram of 5MW plant was shown in Fig. 1. Plant specifications were listed in the previous abstract. Regarding an urban area application, most part of components were

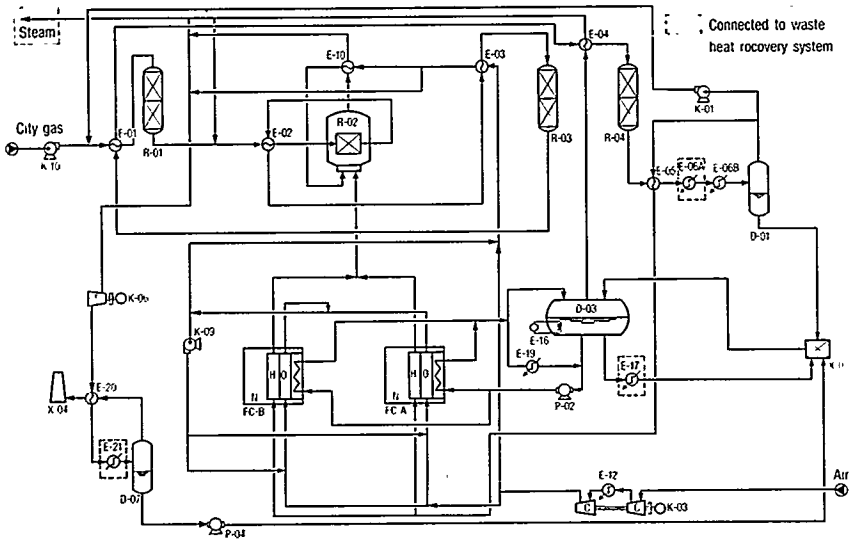

Fig. 1 Process flow diagram

assembled within doors, which had three hierarchical structure. Foot prints were reduced by means of adopting plate-fin type heat exchanger, etc. Exhaust chimney, cooling tower, water treatment system and nitrogen supply system were installed outside for their useful management.

Pressurized high performance cell stacks were taken up to achieve a high generating efficiency, also a short stack testing was carried out to prove the characteristics and reliability of the cell prior to a practical use. Aiming the growth of methane conversion rate and thermal efficiency in fuel processing system, the mono tube type reformer was selected. Three dimensional impellers were introduced to the separated air compressor and gas turbine to accomplish a more higher efficiency, on the other hand, direct steam injection to the gas turbine was planned to increase the generating efficiency.

The separated air compressor and gas turbine afford an advance in plant controllability and the limitation of direct fuel combustion only to a spent fuel, so as to the lower NOx emission simillar to the level at the convensional cogeneration system de-NOx outlet was performed. In the waste heat recovery system, surplus steam (174℃) and hot water (48-92℃) were recovered in each stage to adequately respond to the cooling, heating and hot water demands.

Demonstration of 5MW Plant

Cumulative generating hours and generated electric energy from the initial power generation to August 1996 are 3061hours and 6899MWh, respectively. Cell voltage was unexpectedly decreased in some parts of cell stack assemblies, the reformer tube pressure drop was coincidentally increased, so that the disassembled inspection of cell stack assemblies and reformer was carried out from June 1995. Three damaged cell stacks were

Item	Contents	Designed	Measured
Load kW (gross)		5000	4714
Efficiencies	generating, AC gross %	46	45.0
	generating, AC net %	42	37.3
	FPS %	100	99.7
	inverter %	97	97.5
Start up time, cold start h		6	8
NOx emissions ppmv, 7%O_2		≦10	3
Current harmonic distortion	overall %	≦5	1.7
	each %	≦3	1.1

Table 1 Performance of 5MW plant

replaced to the improved type to restore the performance, as well as the reformer packed material was increased to prevent a catalyst powdering. Plant operation was restarted in October 1995, a periodic inspection was executed from February to March 1996. Plant operation has been continuing since April 1996.

A summary of performance test carried out at around 1800hours operation was shown in Table 1. The maximum load was stayed in 94% of rated load, because of cell stack performance unbalance. Gross generating efficiency was decreased approximately 1% as compared with planned efficiency. For FPS efficiency and inverter efficiency were almost satisfied the designed rate, cell stacks voltage time decay supposed to be a major factor of plant efficiency decrease. In particular, 18 times starts/stops conducted in the adjusting test

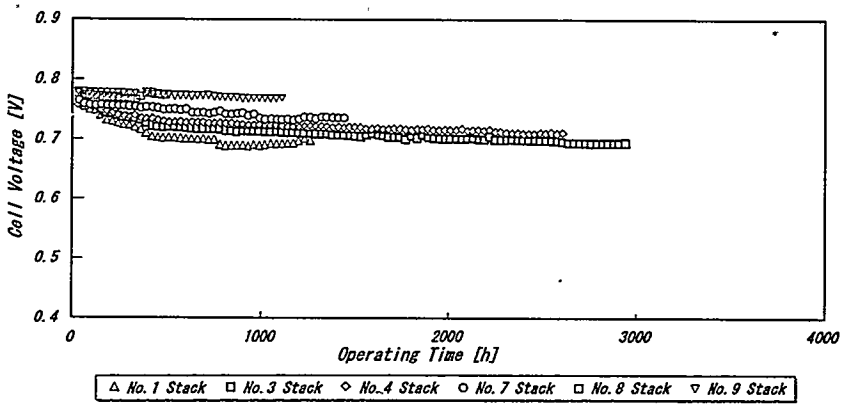

Fig. 2 Cell voltage time deterioration

made the cell voltage deterioration accelerated. Regarding the parasite power increase, the air compressor/gas turbine internal efficiencies were shorten and mechanical loss were unexpectedly larger. NOx emmision was 3ppmv, indicated the environmental advantage of PAFC power plant. Heat recovery, load change characteristics and special operation tests such as low S/C operation will be conducted in the second half of 1996.

The cell voltage time deterioration was illustrated in Fig. 2. Cell voltages shown in this Fig. were modified to the rated load state, that is the current density is as of 300mA/cm^2. Average cell voltage decay in 2500hours operation was around 50mV. Although, a gradual voltage deterioration was shown in ordinary operation after the initial frequent start/stop, the voltage decay was larger than expected. On the other hand, only a little cell voltage decrease was confirmed in more than 8000hours short stack test operation. Observing the further transition of cell voltage deterioration in the hereafter operation, the improvement of cell stack strength against the start/stop will be studied.

Cause of plant shutdown were shown in Table 2. Increase of differential pressure between anode and cathode or auxiliary machineries trips which triggered the emergency shutdown, and growth of pressure drop in the reforming process or exhaust gas blockade that caused the normal shutdown, were major factors of plant shutdown, excluding the result with operational plan and adjusting test. As the whole operation hours are inadequate, hereafter continueing the plant operation, extracting and overcoming the subjects, plant overall technologies will be established.

Cumulative start and stop	50
Normal shutdown	18
Operational plan	6
Increase of Δp in reforming process	4
Blockade in exhaust gas	4
Cell voltage decay	3
Auxiliary machinery failure	1
Emergency shutdown	32
Adjusting test	18
Increase of Δp between anode and cathode	5
Auxiliary machineries trips	3
Transmission system failure	3
Direct current ground fault	2
Increase of Δp in reforming process	1

Table 2 Cause of plant shutdown

Conclusion

5MW plant operation and testing will be continued untill March 1997, short stack test and evaluation studies will be kept going in parallel. The reliability, durability, maintenance and economy of PAFC plants and components will be grasped in these studies, so that the R&D on urban energy center-type PAFC power plants for practical use will be promoted.

EXPERIMENTAL ANALYSIS OF ELEMENTAL FACTORS CONTROLLING THE LIFE OF PAFCs

Masahiro Watanabe[1], Hideaki Miyoshi[2], Hiroyuki Uchida[1], Noriyuki Nakajima[3], Takashi Kitai[4], and Kunihiro Nishizaki[5]
Cooperative Research & Development Center, Yamanashi University,
Takeda 4-3, Kofu 400, Japan
1; Yamanashi University, 2; Mitsubishi Electric Co., 3; Fuji Electric Co.,
4; Toshiba Co., 5; Tokyo Gas Co. Ltd.

INTRODUCTION

Since 1991, 5MW-class and 1MW-class PAFC power plants have been demonstrated with the objective of accelerating development and commercialization by the Phosphoric Acid Fuel Cell Technology Research Association (PAFC-TRA) jointly with NEDO as one of MITI's fuel cell programs. As a complimentary research project to the demonstration project, the mechanism and rate of deterioration of the cells and stacks have been studied from 1995 FY, with the objective of establishing an estimation method for the service life-time of the cell stacks. Our work has been performed in the Basic Research Project, as part of that project on PAFCs, with the cooperation of Yamanashi University supported by the Ministry of Education, Science and Culture, PAFC-TRA supported by NEDO and three PAFC makers. We have selected the following four subjects as the essential factors relating to the life-time, after a year-long study of the literature and the accumulation of a large number of data as to the practical operations of the cells, cell stacks and plants of PAFCs; i.e.,

1) Mechanism of the degradation of electrocatalysts and the effect of the degradation on the electrode performances.
2) Effect of the electrolyte fill-level on the electrode performances.
3) Corrosion of cell constructing materials and the effect of the corrosion on the electrode performances.
4) The rate and mechanism of electrolyte loss under various operating conditions of a model cell.

The paper briefly introduces the interim results which have been found on the above subjects at this time.

ESSENTIAL CONCEPT OF THE EXPERIMENTAL APPROACH

In a time course of the practical operation of PAFCs, all of the factors mentioned above may change simultaneously, even in the small model cell used in the project as the standard (10×10 cm^2), attributable to the degradation of the cell performance and the life-time. Therefore, it is very difficult to separate the degree of their contribution to the degradation just by post-analysis of changes of the constructing materials or by the performance measurements such as cell voltage, O_2 gain, internal resistance or polarization curves. In order to clarify which factor may be attributed predominantly to the degradation and which factor may require further improvement through

future R&D, we have been challenged to evaluate the independent contribution of each factor (i) to the degradation of cell performance (ΔE), typically the cell voltage (E), at the cells which have had alloy catalysts at different corrosion-levels prepared under various corrosion conditions and had gas-diffusion electrodes at well-defined filling-levels with phosphoric acid electrolyte. We tried to change each factor independently within a short time by applying a more severe experimental condition or using specially designed experimental cells. The results can be combined with each other and can serve to isolate the dominant factor to the degradation and in the principle to evaluate the overall degradation rate of the model cell performance (dE/dt) as in the following:

$\Delta E = \Sigma(\partial E/\partial i)di$ (1), $dE/dt = \Sigma(\partial E/\partial i)(\partial i/\partial t)$ (2),

where the practical degradation rate of each factor ($\partial i/\partial t$) can be obtained from post-analysis for the model cell operated under a fixed condition of temperature, pressure and current density.
Details of the experimental or the experimental results are described in the other pages of the proceedings for our poster papers.

RESULTS AND DISCUSSION

1) In-situ X-ray diffraction analysis of the degradation process of alloy catalysts.

In order to monitor the whole corrosion process of alloy catalysts and also to get the catalysts at any corrosion levels, a specially designed cell was prepared, which is similar to a conventional single cell consisting of graphite plates with gas flow channels but added a window covered with a polyimide film on one of the plates for the X-ray diffraction. The paste (Pt/Co/Ni alloy supported on carbon black + 100% H_3PO_4) sandwiched between thin carbon papers was mounted to the window side of the cell as a working electrode, which was paired with the conventional gas-diffusion electrode supplied H_2 gas, across a SiC matrix electrolyte layer filled with H_3PO_4. The corrosion of the alloy catalysts was performed under controlled potential, temperature and humidity conditions. The results were discussed in combination with the post-analysis, such as the chemical analysis of their compositions or TEM and EPMA analysis of the catalyst particles. The following results have been found;

a) The whole corrosion process under any condition can be monitored by in-situ X-ray diffraction and samples at any corrosion levels can be obtained.

b) Under the condition near the practical PAFC operation, the dominant factor affecting the catalyst degradation is the temperature; e.g., the effect by the elevation of temperature from 200°C to 240°C is equivalent to that of the potential elevation from 0.7V to 0.9V.

c) The degradation appeared both in the non-noble metal components loss at the gross alloy composition and the surface area loss by the growth of the particle size.

d) Accompanied with the corrosion, a Pt single phase increases with the decrease of the original Pt/(Co+Ni)=1/1 phase of fcc, but intermediate phases with some distributions, which are simply abbreviated as Pt/(Co+Ni)=3/1 phase of fcc, are kept constant at the integrated intensity of the diffraction peaks and also the mean particle size. The corrosion mechanism is under clarification in combination with other analytical methods [1].

2) Effect of the electrolyte fill-level on electrode performance.

A conventional gas-diffusion electrode at PAFCs is composed of a mixture of fine particles of catalyst supported carbon black, abbreviated as Pt/CB, and polytetrafluoroethylene (PTFE), which forms the electrolyte- and gas-network, respectively. Both the gas permeability and utilization of the catalyst are controlled by a fill-level of electrolyte in the electrode. It has been recognized that optimization of the catalyst utilization is essential for high cell performance and over-filling brings about a shorter life-time. However, due to the lack of an appropriate and convenient method to evaluate the fill-level experimentally, there have been few reports [2,3] dealing with the relationship. We have proposed a new evaluation method of the fill-level, or the degree of Pt/CB wetted with the electrolyte [4], based on a double layer capacitance at the surface of CB itself by masking Pt surface with CO poisoning, because the former is considered to be much more stable than the latter during the long term operation of PAFCs. A cell, which can introduce the electrolytes of different concentrations and different reactant gases, was specially designed. The cell is not only use for the measurements of conventional polarization curves or O_2 gain at high temperature in 100% H_3PO_4 but also for the measurements of the double layer capacitance as well as the Pt surface area by the conventional hydrogen adsorption method at room temperature in 40% H_3PO_4. By repeating the process, the electrolyte fill-level was substantially accelerated. All of the measurements are performed automatically by a computer controlled system. The major results found so far are:

a) The double layer capacity for CB becomes a good measure for the electrolyte fill-level evaluation.

b) Each contribution of the gas-diffusion loss and the catalytic activity loss to the cell performance losses during the cell operation could be separated clearly by the proposed experimental method.

c) The critical fill-level leading to the life-time has been found at the standard electrode, where the gas-diffusion loss becomes predominant; the primary pores ($<$ca. 0.09 μ) formed between the primary CB particles were filled with electrolyte by 45% but the secondary pores ($\geqq$ca. 0.09 μ) formed between the CB agglomerates and acting as gas-networks were filled

up to 70%, although those at the optimum condition were 44% and 16%, respectively.

3) Corrosion of cell constructing materials and the effect on the electrode performances.
In this project, we focused our attention on the corrosion of CB substrate in Pt/CB under various conditions in comparison with that of Pt alloy particles supported. Electrochemical and physical methods have been used to separate the changes in the surface areas of CB and Pt, respectively.

4) The rate of electrolyte loss under various operating conditions of the model cell.
At the model cell, the electrolyte (PA) loss into exhaust gases of the anode and cathode has been measured by condensing it in cold traps and analyzing the amounts as a function of the operating temperature, utilization of reactant gases or current density. We are also going to identify species of phosphoric acids in the exhausting gases with a mass-spectrometer of ultra-high sensitivity. The following have been found:

a) The amount of electrolyte loss increases with an increase of the operating temperature at a constant utilization of each anode and cathode reactant gases and can be characterized with a mean linear velocity of the gas flow in ribs of the cell plates, e.g., at the cell operation of 220°C, U_{air}=60% and U_{H2}=80%, the concentration of PA in the cathode exhausting gas was nearly constant (ca. 27mg/Nm^3) in the region of 7-60 cm/s but that of the anode reaches nearly to the equilibrium concentration (ca. 57mg/Nm^3) at 1 cm/s and decreases with an increase of the velocity and coincides with that of the cathode in the region larger than 13 cm/s. These precise data must be very useful for the simulation of the amount of PA loss during the practical operation of large size PAFCs and for the cell operation or the cell design taken into account better electrolyte management.

ACKNOWLEDGMENT
This work has been supported by the Ministry of Education, Science and Culture, NEDO and PAFC-TRA.

REFERENCES

1) M. Watanabe *et al.*, *J. Electrochem. Soc.*, **141**, 2659 (1994).
2) M. Watanabe *et al.*, *J. Electroanal. Chem.*, **195**, 81(1985); *ibid.*, **197**, 195 (1986).
3) T. Mori *et al.*, *J. Electrochem. Soc.*, **133**, 896 (1985); *ibid.* **135**, 1104 (1988).
4) M. Watanabe *et al.*, *Denki Kagaku* (English issue), **64**, 460 (1996).

TUBULAR SOFC AND SOFC/GAS TURBINE COMBINED CYCLES--STATUS AND PROSPECTS

S.E. Veyo and W.L. Lundberg
Westinghouse Science & Technology Center
1310 Beulah Road
Pittsburgh, PA 15235-5098

Presently under fabrication at Westinghouse for EDB/ELSAM, a consortium of Dutch and Danish utilities, is the world's first 100 kWe Solid Oxide Fuel Cell (SOFC) power generation system. This natural gas fueled experimental field unit will be installed near Arnhem, The Netherlands, at an auxiliary district heating plant (Hulp Warmte Centrale) at the Rivierweg in Westervoort, a site provided by NUON, one of the Dutch participants, and will supply ac power to the utility grid and hot water to the district heating system serving the Duiven/Westervoort area. The electrical generation efficiency of this simple cycle atmospheric pressure system will approach 50% [net ac/LHV]. The analysis of conceptual designs for larger capacity systems indicates that the horizon for the efficiency of simple cycle atmospheric pressure units is about 55%.

An increase in operating pressure to ten atmospheres will yield about a ten percent increase in cell voltage, hence efficiency. At three atmospheres, the voltage increase is about half that at ten atmospheres. Previously reported conceptual design activity (1,2) for pressurized 3 MW and 5 MW SureCELL™ SOFC/Gas Turbine (PSOFC/GT) power plants operating at a pressure ratio of 8.8 and utilizing a highly efficient two shaft intercooled and recuperated gas turbine yielded combined cycle efficiencies of 61% and nearly 70%, respectively. The performance estimates for these plants have been refined, considering a reduction in SOFC power lead losses that is based upon recent experimental data, and a higher recuperator effectiveness of 93%. In addition, for the 3 MW plant, performance has been estimated for the case in which the reheat combustor at the power turbine inlet is not fired.

The objectives of the analyses reported herein were fourfold. The first was to document the improved performance potential of the two shaft turbine cycle given access to a better recuperator and lower lead losses, and the second objective was to assess the performance of PSOFC/GT combined cycles in the 3 MW plant application that are based on the use of a simple single shaft gas turbine having a design-point turbine inlet temperature that closely matches the temperature of the SOFC exhaust gas, about 850 C. The third objective was to estimate the performance potential of smaller combined cycle power plants employing a single SOFC submodule, and the fourth objective was to evaluate the cogeneration potential of such systems.

As in the previously reported analyses, the basic building block for an SOFC system is the 100 kW (atmospheric pressure) SOFC generator module (1152 cells, each 22 mm diameter by 1500 mm active length), now in manufacture. Using two such building blocks, each with an additional cell row (96 cells), an SOFC submodule was configured with 2496 tubular AES SOFCs in a common canister. This submodule has a nominal capacity of 600 kW dc at nine atmospheres pressure, and pressurized SOFC modules housing one, three, or four such submodules comprise the SOFC systems in the PSOFC/GT power plants that are discussed below.

Two cycles for pressurized SOFC/GT power plants based on a two-shaft gas turbine were described previously (2). In that gas turbine, the first shaft functions as a zero-net-power hot-gas generator, and ac power (1.4 MW) is produced by the power turbine on the second shaft. The gas generator is equipped with two stages of intercooled compression, and the compressor turbine has an inlet temperature requirement (861 C) that is very close to the temperature that is available at the exhaust of an SOFC module. The power turbine design inlet temperature is 863 C, and it is

normally achieved by burning natural gas fuel at a reheat combustor. An 88%-effective recuperator in this regenerative gas turbine cycle contributes to its high operating efficiency (43%, LHV).

When a pressurized SOFC module with three SOFC submodules is placed ahead of the high pressure combustor in this cycle, the SOFC operating point can be selected such that no fuel is required by the combustor. This leads to a PSOFC/GT plant rating of approximately 3 MW net ac. Similarly, a second module of identical design can be installed ahead of the low pressure reheat combustor and operated such that the flow of fuel to that combustor is also zero. In that case, a plant of nominal 4.5 MW rating results. Equipping each SOFC module with a fourth submodule results in more power from the plant, in excess of 5 MW, and higher efficiency. Updated performance estimates for the 3 MW and 5 MW power plants are summarized in Table 1; the estimates are based on the reduced lead losses and a 93% effective recuperator.

Table 1. PSOFC/GT (Two-Shaft) Power Plant Performance Estimates

Plant	3 MW-class	5 MW-class	3 MW-class, Unfired Power Turbine
Current Density, mA/cm2	496	410/344 *	582
SOFC Fuel Utilization, %	90	90	80
SOFC Power, MW ac	1.82	3.98	2.01
Gas Turbine Power, MW ac	1.41	1.40	1.15
Plant Net ac Power, MW	3.21	5.36	3.15
Plant Efficiency, Net ac/LHV	63.1	71.5	64.5

* HP module/LP module

The table also presents performance estimates for the case in which the power turbine in the 3 MW-class plant is not fired. To maintain the design inlet temperature at the compressor turbine inlet without the need to fire the HP combustor, the selection of a new SOFC operating point at a higher cell current is required. With this relatively high current, the best plant efficiency is achieved with a reduced utilization.

In another conceptual design approach to achieving a PSOFC/GT power plant of approximately 3 MW capacity, a single-shaft gas turbine of nominally 1.2 MW rating has been applied. The design pressure ratio for this turbine is 6.36, and the turbine inlet temperature is 868 C. The SOFC module was configured using three 600 kW submodules as in previous analyses. To integrate the SOFC module and the gas turbine, the gas turbine inlet temperature and pressure ratio values were retained, but the system mass flow was reduced about 14%. The gas turbine has no intercooler, but it is recuperated. and the plant performance estimates summarized in Table 2 were done for a recuperator effectiveness of 93%. The estimates indicate that a plant based on a single-shaft gas turbine can achieve power and efficiency performance that is similar to that for the two-shaft power plant.

Table 2. PSOFC/GT (Single-Shaft) Power Plant Performance Estimates

Current Density, mA/cm2	550
SOFC Fuel Utilization, %	80
SOFC Power, MW ac	1.95
Gas Turbine Power, MW ac	1.03
Plant Net ac Power, MW	2.93
Plant Efficiency, Net ac/LHV	63.7

Again utilizing a single-shaft gas turbine basis, but with a lower power rating, and a pressurized SOFC module housing only one submodule, a MW-class PSOFC/GT power plant can be configured that will also achieve very attractive performance. Figure 1 shows design-point performance for the plant operating with an SOFC fuel utilization of 85%, and for a low pressure ratio that may permit indoor installation. At each point on the curve the SOFC system configuration is fixed as indicated above, but the gas turbine sizing is allowed to change from point to point in response to changes in the SOFC operating point and the air mass flow requirement. Given a cell current density at each point on the curve, the SOFC stoichs requirement (3.5 minimum) was adjusted to maintain the recuperator effectiveness at 93%. The selection of a particular design-point on the curve for a specific application will of course depend on economic considerations.

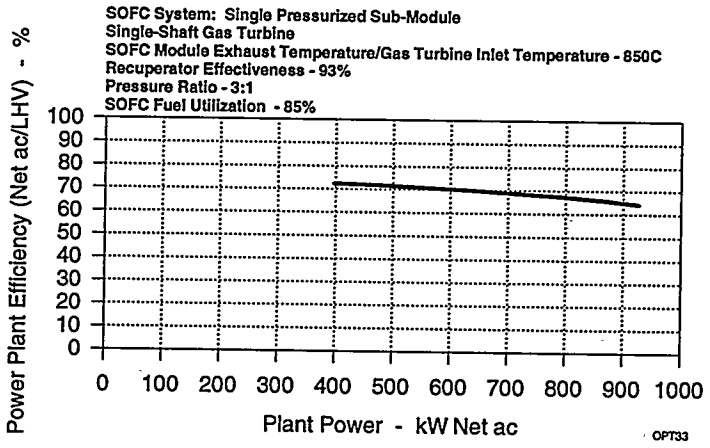

Figure 1. MW-class PSOFC/GT power plant performance estimates.

For the Figure 1 analysis, the distribution between SOFC power and gas turbine power range from 81%/19% at the low-power point, to 66%/34% at the highest power.

This same small power plant could also be equipped with a heat recovery steam generator (HRSG) and a hot-water heater for cogeneration application. Plant performance estimates are provided in Figure 2 for the case in which the HRSG/water-heater combination is positioned at the recuperator exhaust exit. Again, these estimates are the result of a design-point analysis in which the SOFC system consists of a single SOFC submodule, but the gas turbine and heat recovery system sizing is variable. The features of a fixed plant design would depend on economics. HRSG steam conditions at each point on the curves were fixed at 10 atm (abs), 10 C superheat, and the exhaust temperature at the water heater exit at 70 C. Hot water temperatures in the 120-140 C range will be achieved depending upon the water mass flow rate. It is noted that the thermal performance of the heat recovery system is affected by the arrangement of equipment. For example, higher steam temperatures could be achieved by placing the superheater ahead of the recuperator. An air bypass around the recuperator would also affect thermal performance.

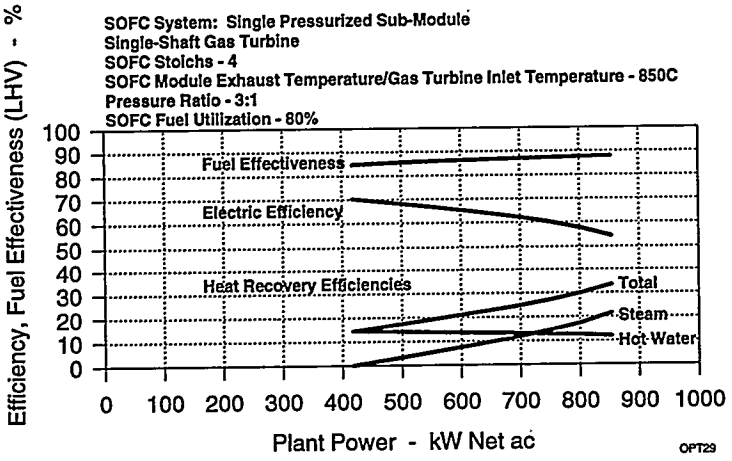

Figure 2. MW-class PSOFC/GT cogeneration system performance estimates.

Since the PSOFC/GT combined cycle can be configured to achieve very high levels of efficiency at capacity levels two orders of magnitude smaller than non fuel cell systems, the SureCELL™ PSOFC/GT is the ideal distributed power generator, and the concept has attractive cogeneration potential. Widely dispersed and located near load centers, SureCELL™ systems could contribute to a world wide reduction in carbon dioxide production because of their inherent efficiency. Using desulfurized fuel, and with minimal fuel combustion, the SureCELL™ system would also produce significantly less NOx and SOx than non fuel cell alternatives. The addition of the gas turbine as the bottoming cycle to the SOFC adds an increment of output without the consumption of additional fuel thereby yielding the higher efficiency. More importantly perhaps, the relatively low technology level of the turbine required results in the addition of this capacity and efficiency increment at far less cost than would be possible with fuel cells alone.

Tubular SOFC development is sponsored by Westinghouse and the United States Department of Energy, Morgantown Energy Technology Center, under cooperative agreement DE-FC21-91MC28055. Pressurized SOFC testing is supported by: DOE-METC; Westinghouse; and Ontario Hydro Technologies and their Canadian funding partners. In addition, analysis of pressurized cell test data is sponsored by the preceding plus the New Energy and Industrial Technology Organization (NEDO) of Japan and their participating Japanese Electric Power Companies.

References

1. F.P. Bevc and W.G. Parker, "SureCELL™ - Integrated Solid Oxide Fuel Cell Power Plants for Distributed Power Applications", PowerGen 1995 - Americas, Anaheim, CA, December, 1995.

2. F.P. Bevc, W.L. Lundberg, and D.M. Bachovchin, "Solid Oxide Fuel Cell Combined Cycles", ASME International Gas Turbine and AeroEngine Congress & Exhibition, Birmingham, UK, June, 1996.

HYDRODESULFURIZATION AND PREREFORMING OF LOGISTIC FUELS FOR USE IN FUEL CELL APPLICATIONS

M. M. Piwetz, J. S. Larsen, and T. S. Christensen
Haldor Topsoe, Inc. Houston, TX
Haldor Topsoe, A/S Lyngby, Denmark

Introduction

Fuel cell development programs have traditionally emphasized the use of natural gas as the primary fuel. However, to meet strategic requirements for fuel cells in military use, the fuel of choice must be accessible throughout the world, easily transported and stored, and compatible with other military uses. The United States military's logistic fuels (DF-2 diesel or JP-8 jet fuel) meet these requirements. The objectives of this program were to design and construct a fuel processing system (FPS) and by connecting the FPS with a SOFC and MCFC fuel cell, respectively, to demonstrate that such a system can be used to convert diesel or jet-fuel into a feed stream compatible with the fuel cell.

Project Description

ARPA (Advanced Research Projects Agency) of the U. S. Government provided funding for the program. Two prime contractors, Energy Research Corporation (ERC), and Westinghouse Electric Corporation (WEC) were selected to provide the fuel cells and test facilities. The project was administered by the NASA Lewis Research Center.

Haldor Topsoe Inc. (HTI) was contracted by ERC and WEC to provide laboratory testing, engineering design, construction and operational assistance for two 32 kW Brassboard fuel processors producing the feed for both a MCFC and a SOFC fuel cell. HTI's parent company, Haldor Topsoe A/S, provided the laboratory and pilot plant testing to determine optimal operating parameters.

Fuel Processing System

Requirements for the fuel processor were as follows:

- Skid mounted and as simple as possible.
- Operation on logistic fuels: diesel and jet-fuel.
- Maximize methane content in the fuel cell feed.
- Provide a feed to the fuel cell containing no higher hydrocarbons and no sulfur.

To meet these requirements, the lay-out selected for the fuel processing system consisted of three process steps, as shown on Figure 1:

- one-stage hydro-desulfurization (HDS)
- sulfur absorption of hydrogen sulfide on zinc-oxide
- adiabatic prereforming

Laboratory and Pilot Plant Testing

A laboratory and pilot plant testing program was carried-out by Haldor Topsoe A/S to demonstrate the desulfurization and adiabatic prereforming steps of the fuel processing system for operation on diesel and jet-fuel.

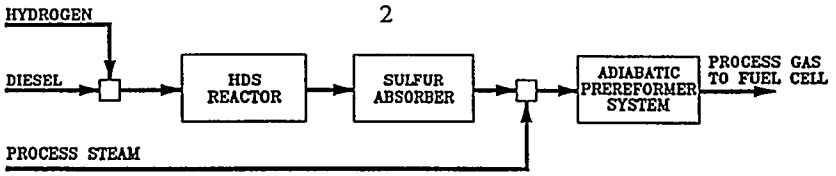

Figure 1 FPS Process Layout

The aim of the testing was to select the optimum operating conditions and catalyst volumes as well as to demonstrate the operability of the individual steps.

A 1200-hour laboratory study on deep desulfurization was carried out. The effect of temperature and space velocity on the HDS-degree was measured and kinetic parameters in a mixed order HDS kinetics were established, enabling performance prediction at other operating conditions. The degree of saturation of aromatics in the diesel was investigated and it was determined that 20-50% saturation of the di-aromatics and 50-80% saturation of tri-and poly-aromatics was obtained in the temperature range of 350-380°C.

Demonstration tests with a total duration of 600 hours on the desulfurization section were carried out, including both HDS and sulfur absorption on ZnO. The tests were carried out in a pilot plant with both diesel feed (DF-2 type) and jet-fuel (JP-8 type) at the operating conditions listed in Table 1. Deep desulfurization of DF-2 from 0.2 wt. % to below 1 wt ppm has been obtained in a one-stage HDS using the Topsoe TK-525 and HTZ-3 catalyst.

Adiabatic prereforming was investigated through a series of tests with a total duration of 2400 hours (1900 hours on diesel and 500 hours on jet-fuel) using the Topsoe RKNGR catalyst. The hydrocarbons in the diesel are completely converted into a methane-rich gas which contains no higher hydrocarbons and no sulfur.

Demonstration tests were then performed in a prereformer pilot plant unit at the operating conditions of Table 1. A 1000-hour test on diesel feed (1.0 wt ppm S) and a 500-hour on jet-fuel (0.7 wt ppm S) confirmed that stable operation with diesel as well as jet-fuel is obtainable. The catalyst volume of the adiabatic prereformer is determined by the poisons in the feed stream (mainly sulfur), but in case of diesel feed, some deactivation due to gum formation also takes place. A longer catalyst lifetime is obtained with jet-fuel at the same space velocity because the deactivation rate is lower and the reaction rates for steam reforming are faster for jet-fuel than for diesel.

The test program on both diesel feed and jet-fuel confirmed that a fuel processing system for logistic fuels can be designed and operated satisfactorily.

Table 1 **FPS Operating Conditions**

	HDS	ADIABATIC PREREFORMING
Pressure (barg)	45	25
Inlet temperature (°C)	380	480
H_2/Feed Ratio (Nm^3/kg)	0.5	0.5
H_2O/C Ratio	N/A	2.5

32 kW Fuel Processor

Based on the operating parameters acquired during the laboratory and pilot plant work, HTI began the basic engineering required to construct two 32 kW Brassboard units, one each for WEC and ERC. The basic engineering package included Process Flow Diagrams, P&ID's, Equipment Specifications and Logic for Safety and Control Systems. This information was then given to fabricators for competitive bidding. The successful bidder, Texas Systems and Controls, Inc. (Houston, Texas) began detailed engineering in December 1994.

The brassboard fuel processor was a completely self contained skid. Major equipment on the skid included reactors, air cooled condensers, and control system. A remotely located personal computer provided the interface between the operator and the control system. Heating for the unit, including both process heaters and heat loss compensation heaters, utilized electric heating elements. Feedstock and utility storage were provided off skid. Commercially available catalysts from Haldor Topsoe were used in the FPS.

The WEC skid was shipped to the Southern California Edison Fuel Cell Test Facility in Grand Terrace, California. It was installed and commissioned during the summer of 1995. The skid for ERC was shipped in August, 1995 and installed and commissioned in the fall of 1995.

Unit Operations - WEC

Start up on commercial grade JP-8 began on August 24, 1995. Initially, the unit met operating conditions but was limited to a maximum flowrate of approximately 70% of design capacities, due to electric heater limitations. Additional heater capacity was added, and the unit completed 766 hours delivering jet fuel reformate to the SOFC on October 11, 1995. During the run on jet fuel, the feed was desulfurized to less than 1 ppm (wt). Inlet sulfur concentration, present in the purchased JP-8, was 80 ppm (wt).

The unit processed 5.3 kg/hr jet fuel with a hydrogen to fuel ratio of 0.5: 1, and a steam to hydrocarbon ratio of 2.5:1. Reformate composition was nearly identical to the design basis, with a stream of approximately 50% methane (CH_4) on a dry basis. See Table 2.

When the jet fuel supply was nearly exhausted, diesel fuel was added and the unit continued operating. From October through February 1996, the fuel processor achieved the requisite 1500 hours delivering fuel to the SOFC. However, during this period, the fuel processor was actually operating 1918 hours, achieving an on line factor of 75%.

Again, the fuel processor met the goals of the diesel portion of the established test program. Exit sulfur levels remained below 1 ppm (wt) during the commercial diesel (DF-2) run (360 ppm (wt) total sulfur inlet). Reformate composition did not vary between the jet fuel test and the diesel test. Design flowrates of 5.75 kg/hr were achieved as necessary.

Some mechanical difficulties were encountered, consisting mainly of electric heater problems. High operating temperatures and low flowrates combined to require high heat densities in the heaters. This made them susceptible to failure. One control system failure was also recorded. The repair of the failed elements resulted in an on-line factor of 75%. However, no significant difficulties were encountered in the operation of the unit. The unit achieved the contracted 2000 hour runtime with the SOFC, and was subsequently shutdown for catalyst inspection.

Unit Operations - ERC

The successful startup of the ERC fuel processor began on October 2, 1995. Once the fuel processor achieved stabilized operating conditions on October 7, the unit was shut down to install the MCFC. Minor problems occurred in November and December, including a heater failure and flow control problems. These challenges were corrected and the unit was prepared in December for jet fuel and diesel, scheduled for January and February 1996.

Reformate from the fuel processor was delivered to the MCFC on January 23, 1996. The fuel processor continued operation on both jet fuel and diesel into February at which time the testing requirements of 400 hours combined run time (200 hours each on jet fuel and diesel) were accomplished. Total runtime logged with the MCFC was 560 hours. The deviations from design seen in reformate composition were due to slightly different conditions inlet the prereformer.

Table 2 **Reformate Composition (Dry Basis)**

Compound	Design	ERC Jet Fuel	ERC Diesel	WEC Jet Fuel	WEC Diesel
CO_2	19.0	19.0	17.8	19.6	19.6
Hydrogen	30.9	24.0	24.8	29.6	28.5
Methane	49.1	56.4	56.8	49.9	50.8
CO	1.0	0.6	0.6	0.9	1.1

Summary

The brassboard fuel processor achieved all goals set forth at the outset of the ARPA program. Selection of optimal operating conditions for deep-desulfurization and adiabatic prereforming of logistic fuels as well as demonstration of the operability of each process step were made by laboratory and pilot plant testing.

By using those test results, basic and detailed engineering of a fuel processing system was made and this system was implemented in two 32 kW fuel cell power plants (SOFC and MCFC). Neither the MCFC nor the SOFC showed any deleterious effects in processing this reformate. The 2200-hour operation of the fuel processing system connected to the WEC 32 kW SOFC unit confirmed that minimal catalyst poisoning can be obtained during long term operation as predicted. The combined fuel processing system and the fuel cells demonstrated the feasibility of fuel cell power production from logistic fuels in large scale.

Acknowledgment

This work was performed by Haldor Topsoe Inc. and its subcontractors as part of the ARPA Fuel Cell Power Plant Initiative. The prime contractors were Energy Research Corporation and Westinghouse Electric Corporation. Technical and management direction is being provided by the NASA Lewis Research Center under contract numbers NAS3-27021 and NAS3-27022.

STATIONARY MARKET APPLICATIONS POTENTIAL OF SOLID OXIDE AND SOLID POLYMER FUEL CELL SYSTEMS

J.N.Baker and W.H.Fletcher,
EA Technology,
Capenhurst,
Chester,
United Kingdom.
CH1 6ES.

1. Introduction

The UK DTI's Advanced Fuel Cells Programme currently focuses on two main fuel cell technologies, namely the solid oxide and solid polymer systems (SOFC and SPFC, respectively). The provision of accurate and timely market data is regarded as an important part of the overall programme objectives, such as to assist both Government and industry in their appraisals of the technologies. The present study was therefore commissioned against this background, with a complementary study addressing transportation and mobile applications. The results reported herein relate to the stationary market applications potential of both SOFC and SPFC systems.

2. Market Overview

The overall applications potential in the stationary applications sectors is strongly related to the global demand for new power generation and cogeneration capacity. Various independent market forecasts show very significant demand growths here, with world wide sales of power generation equipment approaching 100 GWe pa, by the turn of the century.

Access to just a small percentage of this market would provide an annual sales potential of several thousand MWe pa. However, to determine the primary market applications areas for fuel cell power plant requires a more in-depth investigation of both the likely performance characteristics of future fuel cell systems and also the performance of competitive plant, over this same time period. It also requires the features and characteristics of the individual market sectors, to be examined in detail. These various points are addressed below.

2.1 Central Power Generation

For large scale central power plant, at sizes of in excess of say 25 MWe, the market is presently satisfied by a mix of coal, hydro, natural gas and nuclear power plant, with that fired by natural gas forecast to take an increasing market share, up to the year 2010, if not beyond. The availability of a considerable range of gas turbine based power plant, offering high efficiencies, low emissions and reliable operation, all at attractive price levels, is believed to preclude any significant market entry by high temperature fuel cell power plant on timescales of up to 2010.

2.2 Distributed Generation

A combination of circumstances is developing, such that utilities are re-examining the case for distributed generation systems. Such factors include:-

- a general de-regulation of the utilities sector, with increased competition, and a general trend towards smaller power plant

-rapidly increasing costs of transmission and distribution (T&D) capacity

- increasing difficulties in securing wayleaves, (tracts of land underneath overhead power lines) mitigating against overhead power line systems.

- increased emphasis on energy efficiency and a desire to minimise T&D losses, which may typically amount to 5-10%

Utility ownership and operation of advanced SOFC power plant is likely to offer significant advantages in terms of asset optimisation, avoidance of additional T&D costs, enhanced security of supply, and system and energy efficiency benefits. It is also complementary to the demand side management (DSM) programmes, being pursued by many utility companies.

2.3 Cogeneration, or Combined Heat and Power (CHP)

An in-depth analysis of the cogeneration sector showed that market uptake in this sector is highly dependent on the underlying national legislative/regulatory frameworks and the often complementary financial and tariff regimes in force. Opportunities for cogeneration equipment as a whole can therefore be highly country, site and situation specific.

The applicability, to this sector, of both SOFC and SPFC systems was examined. For the larger scale, industrial sector, the market prospects for SOFC power plant are believed to be severely limited by the poor match of the heat to power ratios demanded by industry vs. those available from high efficiency (55% plus) SOFC plant, with heat to power ratios significantly below unity. Cogeneration schemes in such industrial sectors are typically heat demand led and achieve their financial sanction primarily on the revenue savings arising from displaced imported power. Any moves towards export based schemes are often inhibited by the unfavourable tariff structures for such schemes and the necessity to secure satisfactory long term export contracts. One exception to this rule could however occur in the form of utility owned and essentially straight generation plant, such as discussed under *distributed generation*, above. Here, the off take of a relatively small amount of heat, to service a local heat demand, could enhance the economics of what may already be a good straight generation scheme.

Within the smaller scale, commercial sector, considerable potential is believed to exist for SPFC systems, where their overall performance characteristics closely match those of existing reciprocating engine based systems. Solid polymer based systems are likely to possess considerable performance advantages in terms of their low noise and vibration, favourable emissions characteristics and reduced O&M costs.

3. Market Quantifications

3.1 SOFC Distributed Generation Systems

The multi-MWe distributed generation market is believed to represent an attractive market entry point for SOFC systems, for the various reasons discussed above. Three scenarios were

considered for the uptake of SOFC systems in this market sector, defined as high, central and low.
The development of the market for SOFC power plant is then predicted to follow the trends shown in Figures 1, shown in terms of the average annual sales in MWe , in each of seven successive five yearly periods, spanning the time frame 1995 to 2029.

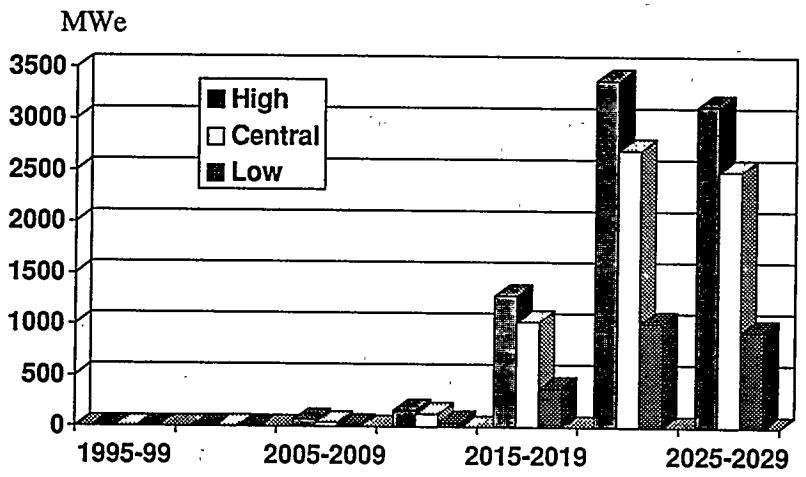

Figure 1:- **Average Annual Sales of SOFC Distributed Power Plant (MWe pa)**

3.2 SOFC Cogeneration Systems

A secondary market for SOFC systems may lie in the medium scale cogeneration market sector, with typical unit sizes here being some 500 kWe and with a small, but significant market sub-sector of micro-CHP units, at a typical size level of 10 kWe. The latter sub-sector could account for some 2.5% of overall SOFC cogeneration capacity. Again, various market scenarios were considered against the background of predicted demand growths for both electricity supply and cogeneration.

The central and low scenarios are believed to be far more realistic estimates in this market sector, noting the various considerations of heat to power ratio mis-matches and the commercial implications of export contracts. Under the central scenario, power plant sales are predicted to rise to in excess of 700 MWe pa, in the year 2025 to 2029 timeframe, i.e. some 20% of the level achieved in the high scenario for multi-MWe distributed generation systems.

3.3 SPFC Cogeneration Systems

The small scale cogeneration market sector forms an attractive market entry point for packaged SPFC cogeneration systems, with market share here being predominantly at the expense of existing gas engine systems. Figure 2 shows the predicted market growth for solid polymer systems in this sector, in MWe pa..

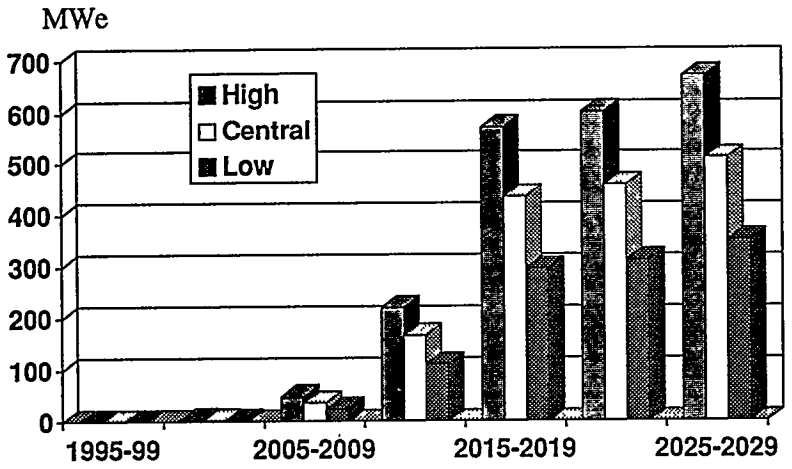

Figure 2:- (MWe pa) **Average Annual Sales of SPFC Cogeneration Power Plant**

4. Conclusions

4.1 The primary market entry point for solid oxide systems has been identified as the multi-MWe distributed generation sector, with typical unit sizes being in the range 5 to 25 MWe.

4.2 The market opportunities for SOFC cogeneration plant are believed to be highly country, site and situation specific, with the underlying national regulatory/legislative regimes, with respect to cogeneration, being the principal determinants of success.

4.3 The primary market entry point for solid polymer fuel cell systems, in the stationary applications sector, is believed to be in small scale (circa 50 kWe) cogeneration power plant.

AUTHOR INDEX

*Abstract not available at time of publication.

*Abstract not available at time of publication.

*Abstract not available at time of publication.

*Abstract not available at time of publication.

*Abstract not available at time of publication.

*Abstract not available at time of publication.

*Abstract not available at time of publication.